

Vol. 21, No. 3, September, 2022

ISSN (Print): 0972-6268; ISSN (Online) : 2395-3454

# NATURE ENVIRONMENT & POLLUTION TECHNOLOGY

*A Multidisciplinary, International Journal  
on Diverse Aspects of Environment*



**Technoscience Publications**

website: [www.neptjournal.com](http://www.neptjournal.com)





# Technoscience Publications

A-504, Bliss Avenue, Balewadi,  
Opp. SKP Campus, Pune-411 045  
Maharashtra, India

[www.neptjournal.com](http://www.neptjournal.com)

## Nature Environment and Pollution Technology

(An International Quarterly Scientific Research Journal)

### EDITORS

**Dr. P. K. Goel (Chief Editor)**

Former Head, Deptt. of Pollution Studies  
Y. C. College of Science, Vidyanagar  
Karad-415 124, Maharashtra, India

**Dr. K. P. Sharma**

Former Professor, Deptt. of Botany  
University of Rajasthan  
Jaipur-302 004, India

**Managing Editor :** Mrs. Apurva Goel Garg, C-102, Building No. 12, Swarna CGHS,  
Beverly Park, Kanakia, Mira Road (E) (Thane) Mumbai-401107,  
Maharashtra, India

**Published by :** Mrs. T. P. Goel, Technoscience Publications, A-504, Bliss  
Avenue, Balewadi, Pune-411 045, Maharashtra, India

**E-mail :** [contact@neptjournal.com](mailto:contact@neptjournal.com); [operations@neptjournal.com](mailto:operations@neptjournal.com)

### INSTRUCTIONS TO AUTHORS

#### Scope of the Journal

The Journal publishes original research/review papers covering almost all aspects of environment like monitoring, control and management of air, water, soil and noise pollution; solid waste management; industrial hygiene and occupational health hazards; biomedical aspects of pollution; conservation and management of resources; environmental laws and legal aspects of pollution; toxicology; radiation and recycling etc. Reports of important events, environmental news, environmental highlights and book reviews are also published in the journal.

#### Format of Manuscript

- The manuscript (*mss*) should be typed in double space leaving wide margins on both the sides.
- First page of *mss* should contain only the title of the paper, name(s) of author(s) and name and address of Organization(s) where the work has been carried out along with the affiliation of the authors.

*Continued on back inner cover...*

# Nature Environment and Pollution Technology

Vol. 21, No. (3), September 2022

## CONTENTS

1. **Zoyem Gouafo Mathurin, Talla Pierre Kisito, Ngapgue Francois and Médard Fogue**, Risk Assessment of Chemical Pollution of Industrial Effluents from a Soap Production Plant 931-940
2. **S. Isworo, S. Febrianto, T. Aji, P. S. Oetari and E. Jasmienne**, The Study of Air Quality and Risk Assessment at the Location of the Planned Railroad Between Makassar-Parepare, South Sulawesi, Indonesia 941-950
3. **Rohan Jeffrey Robert and C. R. Girish**, Pork Lard Derived Biodiesel Production: Characterization, Engine Performance and Emission Analysis 951-970
4. **G. C. Saha, M. A. Hasanath, M. N. Uddin and M. Hasan**, Sustainable Utilization of Textile Dyeing Sludge and Coal Fly Ash by Brick Production Through Traditional Kilns 971-980
5. **P. P. Nandusekar, U. S. Mukkannawar, R. G. Jaybhaye, U. D. Kulkarni and P. N. Kamble**, Evaluation of Source Emissions Dispersion Potential Near a Coastal Village of Maharashtra, India 981-992
6. **Yeshi Choden, Kinley Pelzang, Abeshik Dev Raj Basnet and Krishna Bdr Dahal**, Modeling of Leachate Generation from Landfill Sites 993-1002
7. **K. Harshala and N. D. Wagh**, Use of Agricultural Waste-Based Biosorbents for the Removal of Heavy Metals from Aqueous Solution: A Review 1003-1014
8. **Kai Su, Hongyun Chen and Cuili Gan**, Spatial Differentiation and Dynamic Evolution of Agricultural Carbon Emissions in Fujian Province of China 1015-1025
9. **Xiaoping Yan, Leixiang Wu, Jun Xie, Yongqian Wang, Chencheng Wang and Bing Ling**, Dynamic Changes and Precision Governance of Soil Erosion in Chengde City Using the GIS Techniques and RUSLE Model 1027-1037
10. **Abhinav Joseph, Pawan Gupta, Gahin De, Manohar Lal, Mukesh Kumar Meena, Laliteshwar Pratap Singh and Jyotsna Rattan**, Biodegradation of Natural Rubber by Fungi and Bacteria 1039-1048
11. **Fangbo Zhang, Zhiqin Li, Lei Tang, Jingting Wang, Chao Shen, Xiaojia He, Ran Li, Jingjie Feng and Naiwen Li**, Effects of Submerged Macrophyte Decomposition on Water Quality 1049-1058
12. **S. Saha, A. K. Bhagabati and R. Thakur**, Assessment of Drinking Water Accessibility and Quality in the Indo-Bhutan Himalayan Foothill Region of Assam, India 1059-1071
13. **Da Li, Zhonghua Yang, Junjie Zheng, Fangping Liu and Gang Ge**, The Influence of Floodplain Vegetation Patches on Hydrodynamic Characteristics: A Case Study in the Old Course of Fuhe River 1073-1085
14. **P. Devesh, B. Aishwarya and R. Gyana Prasuna**, Studies on the Isolation of Lipids from Mangrove Isolated Cyanobacterial Species 1087-1096
15. **Akhilesh Kumar Dewangan, Isham Panigrahi and R. K. Paramguru**, An Investigation of a Hybrid Plasma Gasification System for Various Waste Plastics Thermochemical Degradation in the Fuel Extraction Process 1097-1112
16. **Yang Hu and Zhongqiu Sun**, Assessing the Capacities of Different Remote Sensors in Estimating Forest Stock Volume Based on High Precision Sample Plot Positioning and Random Forest Method 1113-1123
17. **Wenjie Yu, Biao Qian, Beifeng Lv, Haibo Kang, Ping Jiang, Wei Wang and Na Li**, Efficient Adsorptive Performance of Graphene Oxide by Nano Clay 1125-1135
18. **A. Choudhary, P. Kumar, S. K. Sahu, C. Pradhan, S. K. Singh, M. Gašparovi, A. Shukla and A. K. Singh**, Time Series Simulation and Forecasting of Air Quality Using In-situ and Satellite-Based Observations Over an Urban Region 1137-1148
19. **Ramzi H. Amran, Mamdoh T. Jamal, Arulazhagan Pugazhendi, Mamdouh Al-Harbi, Mohammed Ghandourah, Ahmed Al-Otaibi and Md Fazul Haque**, Biodegradation and Bioremediation of Petroleum Hydrocarbons in Marine Ecosystems by Microorganisms: A Review 1149-1157
20. **R. Megha, Divya Murali, S. Amblikuttan, Rajesh Reghunath and K. Anoop Krishnan**, Palaeoclimatic Studies of the Late Quaternary Sediments from Chirakkara, Kollam District, Kerala, India 1159-1165
21. **C. P. Del Río-Galván, R.C. Hernández-León, M.O. Franco-Hernández and J. Meléndez-Estrada**, Primary Sewage Sludge Treatment Using A Spiral Support System 1167-1174
22. **Deepali Rajwade, Sadhana Jaiswal, Vinit Singh Baghel and Hemant Kumar**, Isolation, Identification and Characterization of Novel Azo Dye Degrading Bacteria from the Industrial Effluents of Raipur City, Chhattisgarh 1175-1182
23. **M. M. Sari, I. W. K. Suryawan, B. S. Ramadan, I. Y. Septiariva and S. Notodarmojo**, Marine Debris Management in the Parangtritis Beach Tourism Area, Yogyakarta During Covid-19 Pandemic 1183-1190
24. **Quratulain Maqsood, Esha Ameen, Muhammada Mahnoor, Aleena Sumrin, Muhammad Waseem Akhtar, Riya Bhattacharya and Debajyoti Bose**, Applications of Microbial Fuel Cell Technology and Strategies to Boost Bioreactor Performance 1191-1199
25. **Sudhir Kumar Chaturvedi**, Landslide Assessment Using Sentinel-1 SAR-C Interferometry Technique 1201-1207
26. **T. R. Shanthi, Mohammed Hatha and T. R. Satyakeerthy**, A Study on the Diversity of Pesticide-Resistant Bacterial Population from Different Agricultural Fields of Manjoor 1209-1216
27. **I. Benali, M. Bouderbala and N. Chèvre**, Study on the Establishment of the Gastropod *Lymnaea stagnalis* (Linné, 1758) as a Bio-sentinel to Monitor the Water Quality of North Algerian Rivers: Case of the El-Malah River 1217-1225

28. **Rajiv V. Shah**, Financial Incentives for Promotion of Electric Vehicles in India- An Analysis Using the Environmental Policy Framework 1227-1234
29. **Pradeep Khyalia, Jyoti Dangi, Sheetal Barapatre, Geeta Dhania, J.S.Laura and Meenakshi Nandal**, Comparative Analysis of Compost Quality Produced from Fungal Consortia and Rice Straw by Varying C/N Ratio and its Effect on Germination of *Vigna radiata* 1235-1242
30. **Zheng Ennan, Yin hao Zhu, Jianyu Hu and Tianyu Xu**, Effects of Humic Acid Organic Fertilizer on Soil Environment in Black Soil for Paddy Field Under Water Saving Irrigation 1243-1249
31. **Loay Alzriqat, Sana'a Odat and Ismaiel Abuamoud**, Main Characteristics of Trails on Yarmouk Forest Reserve, A Quantitative Approach to Trails Assessment 1251-1257
32. **K. Kalaivanan and J. Vellingiri**, Survival Study on Different Water Quality Prediction Methods Using Machine Learning 1259-1267
33. **G. Dhanya, T. S. Pranesha, Kamsali Nagaraja, D. M. Chate and G. Beig**, Comprehensive Modeling of Seasonal Variation of Surface Ozone Over Southern Tropical City, Bengaluru, India 1269-1277
34. **Kaizar Hossain, Mohd Talha Anees, Ahmad Farid Bin Abu Baker, Mohammad Muqtada Ali Khan, Amin E. Khalil, K. S. Ishola, Abdullah K., Mohd Nawawi M. N. and Mohd. Omar A. K.**, Application of Geoelectrical Methods for Estimating Water Infiltration in Soils 1279-1288
35. **E. Morales, S. Chávez, L. García, A. C. Caetano, J. Veneros, M. Á. Barrena and M. Oliva**, Variation in the Alcohol Components of *Coffea arabica* L. Wastewater Distillate Fermented Under Different Conditions 1289-1295
36. **Asad Ashraf and Izharul Haq Farooqi**, Investigation on the Treatment of Slaughterhouse Wastewater in a Sequential Batch Reactor 1297-1305
37. **Amarnath Bose and Devender Kumar Saini**, Biomass Fired Thermal Power Generation Technology- A Route to Meet Growing Energy Demand and Sustainable Development 1307-1315
38. **A. S. Nur Chairat, L. Abdullah, M. N. Maslan and H. Batih**, Applications of Marginal Abatement Cost Curve (MACC) for Reducing Greenhouse Gas Emissions: A Review of Methodologies 1317-1323
39. **H. P. Suseno and A. D. Warisaura**, Immobilization of Humic Acid on Bentonite and Its Application for Adsorption of Cs<sup>137</sup> and Am<sup>241</sup> 1325-1331
40. **P. Jayakumar, S. Padmanabhan, R. Lilly and K. Suthendran**, Bio-medical Waste Remediation by Environmental Safe Gelatin Coated Blood Sample Paper and its Effective Utilization 1333-1340
41. **B. K. Das, P. K. Das and P. Dash**, Evaluation of Phenotypic Responses of Selected Rice (*Oryza sativa* L.) Cultivars to Hexavalent Chromium Stress in Soil 1341-1347
42. **J. M Nyika and M. O Dinka**, A Mini-Review on the Use of Constructed Wetland Systems for Water Treatment in Developing Countries 1349-1356
43. **Xingjiang Song, Lin Zhou, Haibo Kang, Na Li, Wei Wang and Ping Jiang**, Study on Adsorption Properties and Mechanism of Graphene Oxide (GO) by Kaolin 1357-1365
44. **Simranjeet Singh, Anubha Kaushik and Bhoopesh Kumar Sharma**, A Study of Nutrient Removal Efficiency from Simulated Agriculture Run-off (SAR) Using Constructed Wetland Technology 1367-1374
45. **Arun Kalia and M. S. Dhanya**, Evaluation of Biodegradation Efficiency of Xylene Pretreated Polyethylene Wastes by Isolated *Lysinibacillus fusiformis* 1375-1380
46. **Priyanka Mary Sebastian and K. V. Bhaskara Rao**, Approaches in Bioremediation of Dioxins and Dioxin-Like Compounds – A Review on Current and Future Prospects 1381-1387
47. **Haifu Li, Chengjiu Guo, Fangli Su and Lifeng Li**, Effects of Cadmium on Superoxide Dismutase Activity in Reed Leaves 1389-1393
48. **Akshata Bandi H. and Nagraj S. Patil**, Estimation of Water Balance Components for the Watershed of Ghataprabha Sub-Basin 1395-1400
49. **Jie Li, Da Yao, Zhongyu Shi and Kaiyue Song**, Changes in Carbon, Nitrogen and Phosphorus Stoichiometry of Leaf-Litter-Soil in Differently Stands Under 'Plain Afforestation Program' in China 1401-1409
50. **N. A. Hemali and A. A. P. De Alwis**, Application of Material Flow Analysis to Municipal Solid Waste in Urban Areas in Developing Countries and Possible Solutions Under Circular Economic Framework 1411-1419
51. **Mahmuda Akter Khuky, Law Siong Hook, Lee Chin and Mohd Yusof Bin Saari**, The Impact of Textile and Clothing Export on Environmental Quality in Bangladesh: An ARDL Bound Test Approach 1421-1430
52. **Khan Md. Rabbani Rasha**, Salinity Prediction at the Bhairab River in the South-Western Part of Bangladesh Using Artificial Neural Network 1431-1438
53. **Vyacheslav M. Krayev, Alexey I. Tikhonov and Irina Kuzmina-Merlino**, Perspectives for the Use of Hydrogen Energy in European Countries 1439-1444
54. **N. P. A. Widjanarko and A. P. Siregar**, How Livestock and Industrial Energy Affect Indonesia's Surface Temperature 1445-1454
55. **Guanhua Zhang, Baoyang Sun, Feipeng Ren and Hao Li**, Response and Environmental Adaptation of Plant Community to Periodic Flooding in the Riparian Zone of Three Gorges Reservoir, China 1455-1462
56. **Ping Jiang, Xuhui Zhou, Jiandong Yang and Lin Zhou**, Strength Characteristics of Cement-Modified Iron Tailings and Their Adsorption on Graphene Oxide 1463-1470



The Journal  
is  
Currently  
Abstracted  
and  
Indexed  
in:

CAB Abstracts, U.K.

Ulrich's (Refereed) database

Zetoc

J-Gate

Centre for Research Libraries

Connect Journals (India)

Research Bible (Japan)

Elektronische  
Zeitschriftenbibliothek (EZB)

CNKI Scholar (China National  
Knowledge Infrastructure)

AGRIS (UN-FAO)

CNKI Scholar (China National Knowledge Infrastructure)

Scopus CiteScore (2020) 0.60

Scopus®, SJR (0.154) 2020

Index Copernicus (2020) = 119.70

Chemical Abstracts, U.S.A.

Indian Science Abstracts,  
New Delhi, India

Pollution Abstracts, U.S.A.

Elsevier Bibliographic  
Databases

Paryavaran Abstract,  
New Delhi, India

Zoological Records

Electronic Social and Science  
Citation Index (ESSCI)

Indian Citation Index (ICI)

CrossRef (DOI)

EBSCO: Environment Index™

Google Scholar

DOAJ

Environment Abstract, U.S.A.

ProQuest, U.K.

WorldCat (OCLC)

British Library

Indian Science

JournalSeek

SHERPA/RoMEO

Directory of Science

CSA: Environmental Sciences and Pollution Management

Access to Global Online Research in Agriculture (AGORA)

Present in UGC-CARE List (Group II)

UDL-EDGE (Malaysia) Products like *i*-Journals, *i*-Focus and *i*-Future

[www.neptjournal.com](http://www.neptjournal.com)

# Nature Environment and Pollution Technology

## EDITORS

### Dr. P. K. Goel (Chief Editor)

Former Head, Deptt. of Pollution Studies  
Yashwantrao Chavan College of Science  
Vidyanagar, Karad-415 124  
Maharashtra, India

### Dr. K. P. Sharma

Former Professor, Ecology Lab, Deptt. of Botany  
University of Rajasthan  
Jaipur-302 004, India  
Rajasthan, India

**Managing Editor:** Mrs. Apurva Goel Garg, C-102, Building No. 12, Swarna CGHS, Beverly Park, Kanakia, Mira Road (E) (Thane) Mumbai-401107, Maharashtra, India (**E-mail: [operations@neptjournal.com](mailto:operations@neptjournal.com)**)

**Business Manager:** Mrs. Tara P. Goel, Technoscience Publications, A-504, Bliss Avenue, Balewadi, Pune-411 045, Maharashtra, India (**E-mail: [contact@neptjournal.com](mailto:contact@neptjournal.com)**)

## EDITORIAL ADVISORY BOARD

1. **Dr. Prof. Malay Chaudhury**, Department of Civil Engineering, Universiti Teknologi PETRONAS, Malaysia
2. **Dr. Saikat Kumar Basu**, University of Lethbridge, Lethbridge AB, Canada
3. **Dr. Sudip Datta Banik**, Department of Human Ecology Cinvestav-IPN Merida, Yucatan, Mexico
4. **Dr. Elsayed Elsayed Hafez**, Deptt. of of Molecular Plant Pathology, Arid Land Institute, Egypt
5. **Dr. Dilip Nandwani**, College of Agriculture, Human & Natural Sciences, Tennessee State Univ., Nashville, TN, USA
6. **Dr. Ibrahim Umaru**, Department of Economics, Nasarawa State University, Keffi, Nigeria
7. **Dr. Tri Nguyen-Quang**, Department of Engineering Agricultural Campus, Dalhousie University, Canada
8. **Dr. Hoang Anh Tuan**, Deptt. of Science and Technology Ho Chi Minh City University of Transport, Vietnam
9. **Mr. Shun-Chung Lee**, Deptt. of Resources Engineering, National Cheng Kung University, Tainan City, Taiwan
10. **Samir Kumar Khanal**, Deptt. of Molecular Biosciences & Bioengineering, University of Hawaii, Honolulu, Hawaii
11. **Dr. Sang-Bing Tsai**, Zhongshan Institute, University of Electronic Science and Technology, China
12. **Dr. Zawawi Bin Daud**, Faculty of Civil and Environmental Engg., Universiti Tun Hussein Onn Malaysia, Johor, Malaysia
13. **Dr. Srijan Aggarwal**, Civil and Environmental Engg. University of Alaska, Fairbanks, USA
14. **Dr. M. I. Zuberi**, Department of Environmental Science, Ambo University, Ambo, Ethiopia
15. **Dr. Prof. A.B. Gupta**, Dept. of Civil Engineering, MREC, Jaipur, India
16. **Dr. B. Akbar John**, Kulliyyah of Science, International Islamic University, Kuantan, Pahang, Malaysia
17. **Dr. Bing Jie Ni**, Advanced Water Management Centre, The University of Queensland, Australia
18. **Dr. Prof. S. Krishnamoorthy**, National Institute of Technology, Tiruchirapally, India
19. **Dr. Prof. (Mrs.) Madhoolika Agarwal**, Dept. of Botany, B.H.U., Varanasi, India
20. **Dr. Anthony Horton**, Envirocarb Pty Ltd., Australia
21. **Dr. C. Stella**, School of Marine Sciences, Alagappa University, Thondi -623409, Tamil Nadu, India
22. **Dr. Ahmed Jalal Khan Chowdhury**, International Islamic University, Kuantan, Pahang Darul Makmur, Malaysia
23. **Dr. Prof. M.P. Sinha**, Dumka University, Dumka, India
24. **Dr. G.R. Pathade**, H.V. Desai College, Pune, India
25. **Dr. Hossam Adel Zaqoot**, Ministry of Environmental Affairs, Ramallah, Palestine
26. **Prof. Riccardo Buccolieri**, Deptt. of Atmospheric Physics, University of Salento-Dipartimento di Scienze e Tecnologie Biologiche ed Ambientali Complesso Ecotekne-Palazzina M S.P. 6 Lecce-Monteroni, Lecce, Italy
27. **Dr. James J. Newton**, Environmental Program Manager 701 S. Walnut St. Milford, DE 19963, USA
28. **Prof. Subhashini Sharma**, Dept. of Zoology, University of Rajasthan, Jaipur, India
29. **Dr. Murat Eyvaz**, Department of Environmental Engg. Gebze Inst. of Technology, Gebze-Kocaeli, Turkey
30. **Dr. Zhihui Liu**, School of Resources and Environment Science, Xinjiang University, Urumqi, China
31. **Claudio M. Amescua García**, Department of Publications Centro de Ciencias de la Atmósfera, Universidad Nacional Autónoma de México
32. **Dr. D. R. Khanna**, Gurukul Kangri Vishwavidyalaya, Haridwar, India
33. **Dr. S. Dawood Sharief**, Dept. of Zoology, The New College, Chennai, T. N., India
34. **Dr. Amit Arora**, Department of Chemical Engineering Shaheed Bhagat Singh State Technical Campus Ferozepur -152004, Punjab, India
35. **Dr. Xianyong Meng**, Xinjiang Inst. of Ecology and Geography, Chinese Academy of Sciences, Urumqi, China
36. **Dr. Sandra Gómez-Arroyo**, Centre of Atmospheric Sciences National Autonomous University, Mexico
37. **Dr. Manish Sharma**, Research and Development Cell, Bahra University, Shimla Hills, Shimla, India
38. **Dr. Wen Zhang**, Deptt. of Civil and Environmental Engineering, New Jersey Institute of Technology, USA



# Risk Assessment of Chemical Pollution of Industrial Effluents from a Soap Production Plant

Zoyem Gouafo Mathurin<sup>\*(\*\*)</sup>†, Talla Pierre Kisito\*, Ngague Francois<sup>\*(\*\*\*)</sup> and Médard Fogue\*

\*University of Dschang, Laboratory of Mechanics and Modeling of Physical Systems, Dschang, Cameroon

\*\*University of Dschang, Industrial Systems and Environmental Engineering Laboratory (IUT-FV), Bandjoun, Cameroon

\*\*\*Department of Civil Engineering, IUT-FV, Bandjoun, Cameroon

†Corresponding author: Zoyem Gouafo Mathurin; zoyemm@gmail.com

Nat. Env. & Poll. Tech.  
Website: [www.neptjournal.com](http://www.neptjournal.com)

Received: 24-09-2021

Revised: 02-12-2021

Accepted: 15-12-2021

## Key Words:

Water and environmental pollution

Mewou river

Industrial effluents

Soap factory

## ABSTRACT

The MEWOU river, which crosses the town of Bafoussam, is one of the main sources of drinking water and irrigation for the populations who live there. It is subject to intense agricultural and industrial activity all along its banks. Soap and refined oil factories generate pollution in the form of liquid effluents which are discharged without any form of treatment. The objective of this study is to assess the impact of soap factory effluent discharges on the quality of the surrounding water. In total, seven samples were analyzed during March, April, and May of the year 2021. The results we obtained were analyzed according to the regulatory requirements recommended by the Directives for the quality of drinking water and the Algerian standard relating to the limit values of the physico-chemical parameters. The results we obtained showed signs of significant pollution in particular: chemical oxygen demand (COD: 125.32-959 mg.L<sup>-1</sup>), 5 days-biochemical oxygen demand (BOD<sub>5</sub>: 2.3-99 mg.L<sup>-1</sup>), turbidity (2-520 NTU), TDS (130-13430 mg.L<sup>-1</sup>), Nitrite (4.96-21327.44 mg.L<sup>-1</sup>) and many other parameters greatly exceed those required by the international standard, we also noted strong pollution with heavy metals: chromium (35.76-1381.08 mg.L<sup>-1</sup>), lead (0.21 - 2.49 mg.L<sup>-1</sup>), iron (0.28- 17.82 mg.L<sup>-1</sup>), and cadmium (0.03-0.19 mg.L<sup>-1</sup>) which are above the values prescribed by the WHO. These highly polluted effluents released into the natural environment are harmful to the environment, biodiversity, and human health. This state of affairs requires urgent intervention to preserve the ecological balance. Otherwise, it can constitute a risk for public health in the short term by deteriorating the quality of the underground reservoir known as the main source of water supply for neighboring populations.

## INTRODUCTION

Water pollution results from the introduction of foreign matter capable of deteriorating the quality of the water in a body of water, thus posing negative effects on human life and health. Industrial effluents represent a point source of water pollution (Awomeso et al. 2010). While strict waste management and control policies have existed for years in developed countries, the implementation of the same model Regulation is struggling to take effect in developing countries like Cameroon, thus making it difficult to assess the current situation or compare and contrast its performance with other places/nations.

Based on a 2005 analysis of global urbanization prospects (INS 2004, ONU 2006) more than half of Africa's population is expected to live in cities by 2030. In Cameroon, 50% of the population lives in cities; The urban population increased from 28.5% of the total population to 52.8% between 1976 and 2003. By 2030, it is expected to reach over

70% of the population. During the same 1976 – 2003 period, the population density in Cameroon increased from 16.4 to 35.7 inhabitants per km<sup>2</sup> (INS 2004). In the large urban centers of the city of Bafoussam, the population density per square kilometer is high, the same is true for the cities of Douala, Yaoundé, and Garoua. This increase in the demographic pressure of cities like Bafoussam combined with the increase in population and the intensification of industrial activities makes the issue of controlling industrial effluents even more important.

In the town of Bafoussam, rivers are one of the main sources of freshwater supply, however, they are also vulnerable to both point and diffuse types of pollution. Wastewater discharges from industries around the town of Bafoussam deteriorate the quality of surface and underground water and soils (Gouafo & Yerima 2013). The effects of water pollution are often different depending on the mode of contamination. For humans, this is done by ingestion, contact, or consumption of contaminated fish from polluted waters. For example,



fish contaminated with biogenic elements such as copper and cadmium are highly toxic to humans. The presence of chromium and cadmium makes water unsuitable for domestic and agricultural use due to their toxicity (Kankou 2004).

The presence of toxic chemicals in industrial effluents can pose a threat to human and animal health as well as contaminate water quality (WHO 2008). The objective of this study is to assess the impacts of effluent discharges from soap production on the quality of nearby water by analyzing certain physicochemical parameters of the discharge water leaving this soap factory.

**MATERIALS AND METHODS**

The physico-chemical parameters analyzed in this study were the following: pH, temperature, turbidity (NTU), Electrical conductivity ( $\mu\text{S}\cdot\text{cm}^{-1}$ ), TDS, calcium, magnesium, potassium, sodium, bicarbonates, carbonate, nitric nitrogen, nitrate, nitrogen ammoniacal, ammonium, nitrite, chlorine, sulphate, sulfur, soluble phosphorus, aluminum, cadmium, copper, chromium, iron, lead, zinc, dissolved oxygen ( $\text{mg}\cdot\text{L}^{-1}$ ), chemical oxygen demand (COD) and 5 days of biochemical demand in oxygen, required by national standards, to qualify the sources of pollution with a global view of the chemical quality of the effluents discharged. The analysis

of the physico-chemical parameters was carried out at the Soil Analysis and Environmental Chemistry Research Unit, FASA, University of Dschang (Cameroon)

**Presentation of the Soap Production Plant (Cameroonian Company of Soap Factory)**

This is a large soap production plant located in Bafoussam, Kamkop (in the western Cameroon region). The western region has the city of Bafoussam as its capital. It is located in the mountainous region of West Cameroon, in the Mifi Sud watershed, between  $9^{\circ}30'$  and  $10^{\circ}35'$  East longitude and between  $5^{\circ}$  and  $6^{\circ}$  North latitude. It is at an average altitude of 1450 meters and extends over the highlands of the western mountain range. The expansion of the SCS plant in 2013 also boosted its production to 500 tonnes of refined oils every day. The SCS soap production plant releases a volume of raw polluted effluents of between  $80$  and  $100 \text{ m}^3/\text{day}$  into the environment

**Sampling and Physico-Chemical Analyses**

*Sampling Conditions*

For the results to be valid, special care must be taken when taking a water sample. First, the sample taken must be homogeneous, representative, and obtained without altering its

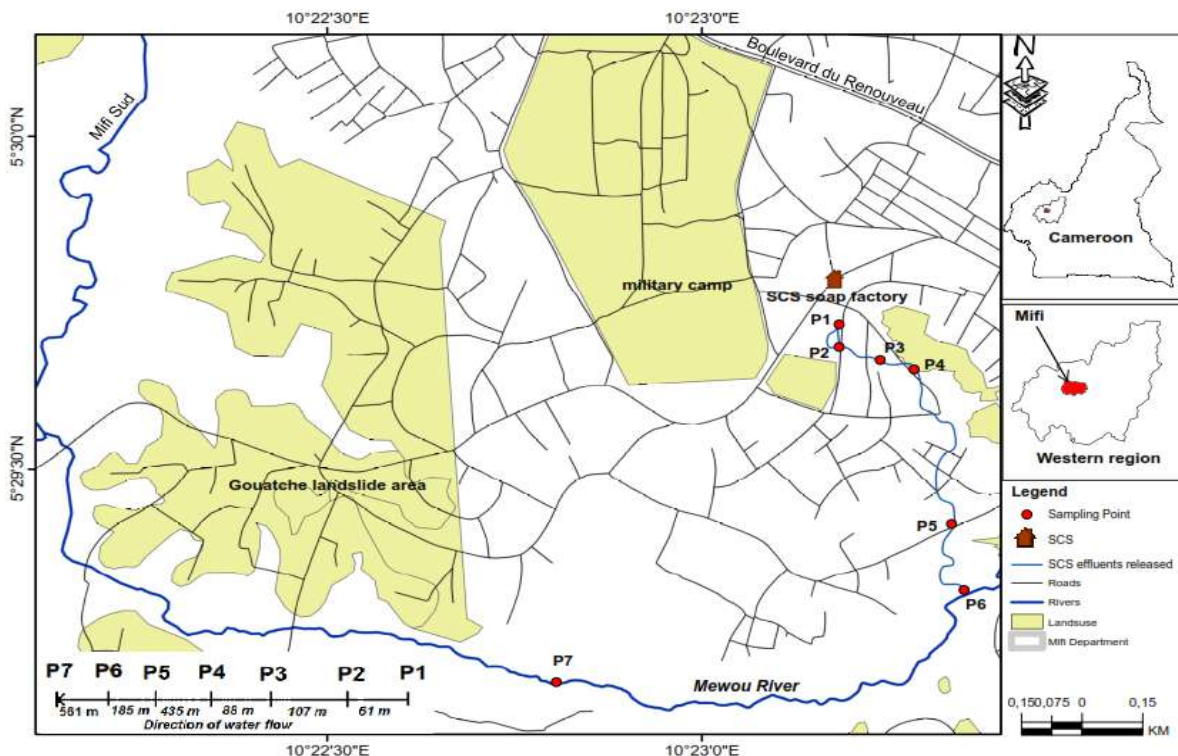


Fig. 1: Partial hydrographic network of the southern Mifi showing the location of the sites of the SCS (Cameroonian company of Soap factory).

microbiological or physicochemical characteristics. (Rodier et al. 2009).

The water samples used for the physico-chemical analysis were taken according to the method described by Rodier et al. (2009) in sterile disposable plastic bottles and stored at + 4 °C, then to be analyzed within 24 h following sampling, with the exception of two parameters, pH and temperature, which were measured on-site.

Samples were taken in the morning, and the used vials were held directly and extended to a depth of 30 to 50 cm from the surface of the polluted effluent of the SCS, a total of 7 samples were collected and analyzed (Table 1).

### *Physico-Chemical Analyses*

All the physico-chemical parameters analyzed were based on the standard methods given by the American Public Health Association (Rice et al. 2017) as follows:

- The temperature and the hydrogen potential (pH) were measured respectively by a thermometer and a pH-meter (Thermo-scientific ORION STAR 225)
- The electrical conductivity was determined using a conductivity meter. The result was expressed in micro siemens per centimeter ( $\mu\text{S}\cdot\text{cm}^{-1}$ );

### **Assessment of Organic Pollution of SCS Effluents**

For a better evaluation of the organic pollution of the discharged water, the parameters that indicate biodegradabilities such as the ratio BOD5 / COD, and the coefficient  $K = \text{COD} / \text{BOD5}$ , are of great importance. The use of these characterization

parameters is an excellent way to estimate the level of pollution of the raw effluents discharged and also to optimize the physicochemical parameters of these industrial effluents to propose a suitable wastewater treatment method.

### **Interpretation of Physicochemical Results**

Thanks to the analysis of physico-chemical and bacteriological parameters, it is possible to determine the sources and the pollutant load of wastewater. Before being released into the natural environment, they must meet the standards established to protect the receiving environment against pollution. The limit values are given in the Official Journal of the Algerian Republic and by those of (OJAR n.26, 2006, WHO 2008).

### **Statistical Analyses**

The experiment was repeated three times where the results obtained were presented as the mean  $\pm$  SD, calculated using the MATLAB software from whose representations have been given in the form of curves.

## **RESULTS AND DISCUSSION**

### **Physico-Chemical Analyses**

#### **Temperature**

Water temperature is an important factor as it governs the types of aquatic organisms that inhabit it. Its role is, among other things, to dissolve the gases in water, and to separate the dissolved salts, its measurement is necessary. Here the



(a)



(b)

Fig. 2: (a) Effluents released by the Cameroonian company of Soap factory in Bafoussam, Kamkop (Mathurin et al. 2022) (b) one of the meeting areas between the effluents and a watercourse in the town of Bafoussam.

Table 1: Description of study sites.

Sampling Point	Districts	Characteristics	Geographical locations	
			Longitude	Latitude
P1	Kamkop	Effluent discharge point	10°23'11"	5°29'43"
P2	Kamkop	Furnished, proximity Dwellings	10°23'15"	5°29'41"
P3	Kamkop	Points of contact between a river and effluents	10°23'14"	5°29'39"
P4	Kamkop	Unfinished, nearby dwellings used as laundry point	10°23'17"	5°29'39"
P5	Kamkop	Under a scupper	10°23'20"	5°29'25"
P6	Kamkop	Meeting with the MEWOU river	10°23'21"	5°29'19"
P7	Kamkop	MEWOU river	10°22'48"	5°29'10"

temperature of the industrial SCS discharges analyzed shows a variation from one sampled point to another (Fig. 3). The highest value was recorded for sample P1 (24.8°C) and the minimum value for sample P4 (22.8°C), with an average value for all samples, analyzed equally to 23.61 ° vs. These values are lower than the limit set by the Algerian standard (Table 2).

The effluent temperature varied from 22.9 to 24.8°C. This factor plays a very important role in the solubility of salts and gases (in particular O<sub>2</sub>) in water as well as the determination of the pH and the speed of chemical reactions. High temperatures induce additional pollution, thus affecting biological cycles (Gueddah 2003) by reducing the activities of dissolved oxygen, which can cause serious sewage disposal problems (Shivsharan et al. 2013). These values are the result of using hot water. The water produced by the pre-rinsing and washing operations is carried out at very high temperatures up to 70°C (Sayad 2015).

### Turbidity

The chemical and biological particles in suspension, which are the causes of turbidity, can have implications for both the aesthetics and the safety of the drinking water supply. Alone Turbidity does not systematically represent a direct risk to public health; however, it does highlight the presence of pathogenic microorganisms and is an effective indicator of potentially hazardous events throughout the water supply system, from abstraction to point of use. For example, high turbidity of water sources can harbor microbial pathogens, which can attach to particles and interfere with disinfection; high turbidity in filtered water may indicate poor elimination of pathogens; And an increase in turbidity in distribution systems may indicate flaking of biofilms and oxide scales or the penetration of contaminants through faults such as power outages (WHO 2017).

The effluents studied have turbidity values ranging from 2 to 520 NTU, due to the presence of colloidal materials from palm oil used for soap production. These results are close to those found by (Gouafo & Yerima 2013) which were from 37.4 to 105.5 NTU.

### Hydrogen Potential (pH)

The hydrogen potential (pH) of water provides information on its acidity or alkalinity (Rodier 1998). The pH of the industrial effluents studied reveals a high value for sample P3 (13.2), and a minimum value for the sample P7 (7.4); with an average value for all the samples analyzed equally to 10.53; which exceeds the range required by the national and international regulations.

The industrial effluents analyzed were characterized by a hydrogen potential (pH) ranging from 7.4 to 13.2 very alkaline, and located beyond the recommended standard (OJAR n.26 2006, WHO 2008). These variations in pH are

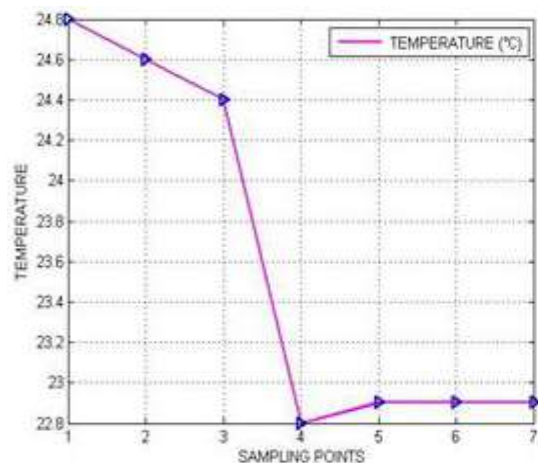


Fig. 3: Average effluent temperature values.



Table 2: Limits of the physicochemical parameters of industrial liquid effluent discharges from the SCS.

Parameters	Limit	Reference	Physicochemical analysis results		
			Minimum value	Maximum value	Mean $\pm$ SD
pH	8,5- 6,5	(OJAR n.26 2006)	7.4	13.2	10.53 $\pm$ 2.67
Temperature [°C]	30	(OJAR n.26 2006)	22.9	24.8	23.61 $\pm$ 0.86
Turbidity [NTU]	-	-	2	520	201.86 $\pm$ 201.83
Electrical cond [ $\mu$ S.cm <sup>-1</sup> ]	-	-	320	19980	9490.00 $\pm$ 9054.89
TDS [mg.L <sup>-1</sup> ]	0.2	(WHO 2008)	130	13430	5362.86 $\pm$ 4597.07
COD [mg.L <sup>-1</sup> ]	120	(OJAR n.26, 2006)	125.32	959	414.85 $\pm$ 259.216
BOD5 [mg.L <sup>-1</sup> ]	35	(OJAR n.26, 2006)	23	99	48.43 $\pm$ 26.19
COD / BOD5	-	-	3.79	19.67	9.42 $\pm$ 5.22
BOD5 / COD	-	-	0.0508	0.26	0.14 $\pm$ 0.07
Calcium [mg.L <sup>-1</sup> ]	-	-	2.4	26.4	7.09 $\pm$ 7.98
Magnesium [mg.L <sup>-1</sup> ]	-	-	3.4	10.21	4.93 $\pm$ 2.23
Potassium [mg.L <sup>-1</sup> ]	-	-	13.31	26.53	22.02 $\pm$ 4.75
Sodium [mg.L <sup>-1</sup> ]	-	-	3.8	452.06	167.46 $\pm$ 180.94
Bicarbonates [mg.L <sup>-1</sup> ]	-	-	2135	75640	24948.13 $\pm$ 31917.52
Carbonate [mg.L <sup>-1</sup> ]	-	-	6	13134	2250.00 $\pm$ 4511.40
Nitric nitrogen [mg.L <sup>-1</sup> ]	-	-	1.12	4814.32	1137.04 $\pm$ 1849.77
Nitrate [mg.L <sup>-1</sup> ]	50	(WHO 2008)	4.96	21327.44	5037.09 $\pm$ 8194.50
Ammoniacal nitrogen [mg.L <sup>-1</sup> ]	-	-	1.12	4.48	2.56 $\pm$ 1.15
Ammonium [mg.L <sup>-1</sup> ]	-	-	3.7	14.78	8.45 $\pm$ 3.81
Nitrite [mg.L <sup>-1</sup> ]	3	(WHO 2008)	3,67	15782.3	3727.44 $\pm$ 6063.93
Chlorine [mg.L <sup>-1</sup> ]	5	(WHO 2008)	39.05	223.65	112.08 $\pm$ 62.79
Sulphate mg L-1 [mg.L <sup>-1</sup> ]	1000~1200	(WHO 2008)	1049.6	9725.2	5046.51 $\pm$ 3368.62
Sulfur [mg.L <sup>-1</sup> ]	-	-	346.37	3209.32	1665.35 $\pm$ 1111.65
Soluble Phosphorus [mg.L <sup>-1</sup> ]	10	(OJAR n.26 2006)	5.64	1700.05	1113.11 $\pm$ 692.77
Aluminum [mg.L <sup>-1</sup> ]	3	(OJAR n.26 2006)	0	0.03	0.01 $\pm$ 0.01
Cadmium [mg.L <sup>-1</sup> ]	0.003	(WHO 2008)	0.03	0.19	0.10 $\pm$ 0.05
Copper [mg.L <sup>-1</sup> ]	0,5	(OJAR n.26 2006)	0	0.04	0.01 $\pm$ 0.01
Chromium [mg.L <sup>-1</sup> ]	0.7	(WHO 2008)	35.76	1381.08	717.47 $\pm$ 412.30
Iron [mg.L <sup>-1</sup> ]	3	(OJAR n.26 2006)	0.28	17.82	7.13 $\pm$ 5.86
Lead [mg.L <sup>-1</sup> ]	0.01	(WHO 2008)	0.21	2.49	0.68 $\pm$ 0.75
Zinc [mg.L <sup>-1</sup> ]	3	(OJAR n.26 2006)	0.51	1.98	1.72 $\pm$ 1.97
Dissolved oxygen [mg.L <sup>-1</sup> ]	-	-	0.32	1.92	1.10 $\pm$ 0.48

strongly influenced by the use of palm oil, chemicals such as nitric acid, and caustic soda (NaOH) in the operations of soap production, cleaning, and disinfection of equipment and facilities. industrial piping circuits, which can influence the pH of the receiving environment (Rodier 2005).

### Electrical Conductivity (EC)

The electrical conductivity of water is a direct indicator of

its salinity. This is an essential factor to follow when considering the reuse of wastewater for irrigation (agricultural fields) (Shilton 2006). A maximum value of the electrical conductivity of the effluents was recorded for the sample P4 (19980  $\mu$ S.cm<sup>-1</sup>), and a minimum value of 320  $\mu$ S.cm<sup>-1</sup> for the sample P7 (Fig. 6), with an average value for all the samples. samples analyzed equally to 9490  $\mu$ S.cm<sup>-1</sup> (Table 2).

The ability of water to conduct an electric current

corresponds to its conductivity, which is an indirect measure of the ionic content of the water. In reality, dissonant measurements of an environment highlight the existence of zones of pollution, infiltration, or mixing. (Ghazali 2013). The electrical conductivity of the industrial effluents studied was between 320 and 19980  $\mu\text{S}\cdot\text{cm}^{-1}$ , which can be explained by the mineral composition of the soap and also by the use of NaOH. These values were higher than those cited by (Gouafo & Yerima 2013), for industrial effluents from the SCS, with turbidity values ranging from 355 to 1859  $\mu\text{S}\cdot\text{cm}^{-1}$ .

### Total Dissolved Solids Content (TDS)

Total Dissolved Solids (TDS) is the parameter used to describe inorganic salts and very small amounts of organic matter that are present in the water. The main building blocks are essentially cations, anions, potassium, hydrogen carbonate,

magnesium, sodium, potassium, carbonate, chloride nitrate, and sulfate (WHO 2008).

The TDS parameter of the effluents analyzed showed a significant Variation from one sample to another (Fig. 7), where the highest value indicated a TDS content of 13430  $\text{mg}\cdot\text{L}^{-1}$  for sample P2, and content in the lowest TDS was equal to 130  $\text{mg}\cdot\text{L}^{-1}$  for sample P7. The mean TDS value of all samples analyzed was 5362.86  $\text{mg}\cdot\text{L}^{-1}$ .

### Nitrate Content ( $\text{NO}_3^-$ )

Nitrate concentrations in surface water can change rapidly due to surface runoff, uptake by phytoplankton, and denitrification by bacteria, but groundwater concentrations generally show relatively slow changes (WHO 2008). The nitrate

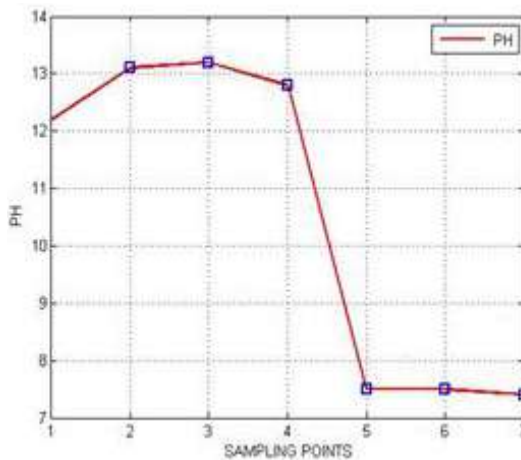


Fig. 4: Average pH values of effluents.

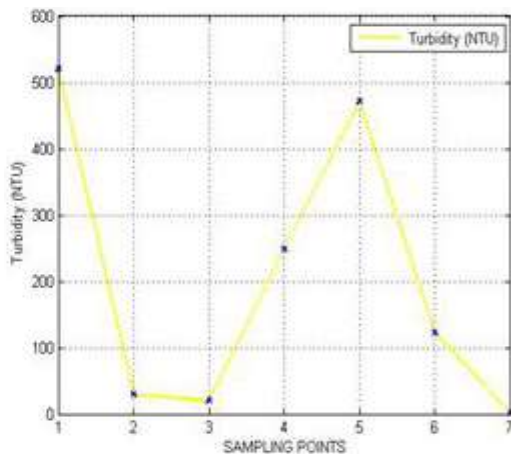


Fig. 5: Average effluent turbidity values.

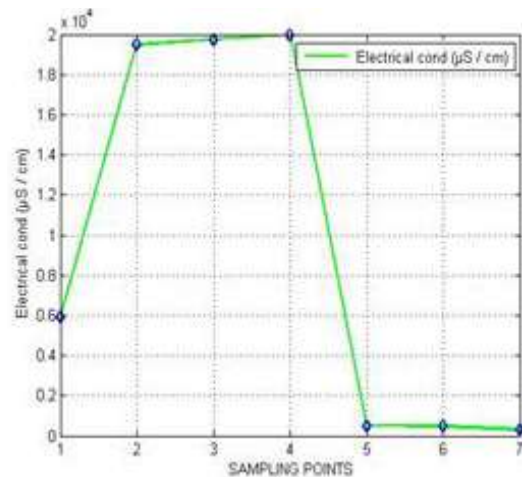


Fig. 6: Average electrical conductivity values of effluents.

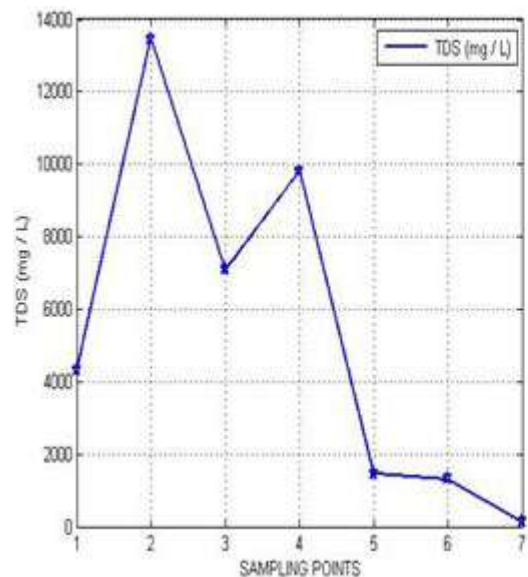


Fig. 7: Average values of TDS of effluents.

content of the SCS effluents varies from 4.96 to 21327.44 mg.L<sup>-1</sup> with an average content of 5037.09 mg.L<sup>-1</sup> (Fig. 7).

In surface water, Nitrate concentrations can vary rapidly due to uptake by phytoplankton, denitrification by bacteria, and surface runoff, but concentrations in groundwater generally show relatively slow changes. Some groundwater can also be contaminated with nitrates due to the leaching of natural vegetation (WHO 2008). The nitrate content ranged from 4.96 to 21327.44 mg.L<sup>-1</sup>; this is probably due to the use of nitric acid as a chemical disinfectant for closed pipeline circuits (Hamdani et al. 2005), by the nitrification reaction of the organic nitrogen present in industrial effluents at the basin level. In reality, nitrification is a two-step reaction in which ammoniacal nitrogen is oxidized to nitrites (NO<sub>2</sub><sup>-</sup>) and then to nitrates (NO<sub>3</sub><sup>-</sup>) (Chachuat 2001).

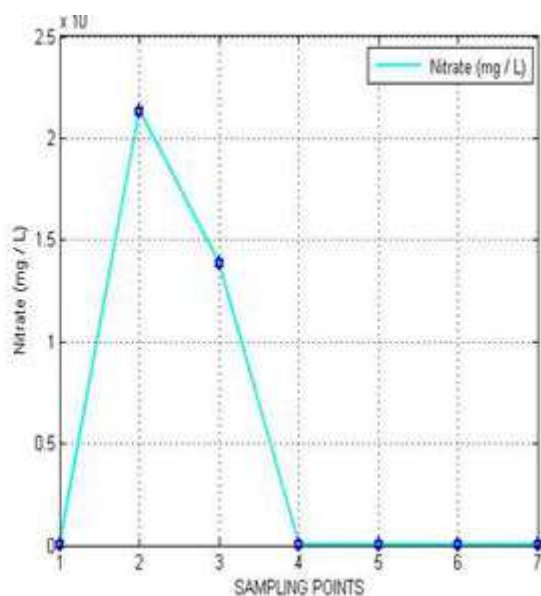


Fig. 8: Average values of nitrate of effluents.

### Nitrite Content (NO<sub>2</sub><sup>-</sup>)

The nitrite ion is considered to be the intermediate between ammoniacal nitrogen and nitrate, which justifies its low content in aquatic environments (Rodier et al. 1978). The nitrite contents were between 4.96 and 21327.44 mg.L<sup>-1</sup>, with an average content of 3727.44 mg.L<sup>-1</sup> (Table 3; Fig. 9).

The origin of the accumulation of nitrite may be linked to the inhibition of nitrification, incomplete denitrification or even decoupling of the activities of the various reducing enzymes in the denitrification (Philips et al. 2002). The values obtained which ranged from 3.67 to 15782.3 mg.L<sup>-1</sup> were 5,000 times higher than the prescribed standards (WHO 2008).

### Sulfate Content (SO<sub>4</sub><sup>2-</sup>)

Sulfates occur naturally in many minerals and are used commercially, primarily in the chemical industry. They are released into the water in industrial wastes and by atmospheric

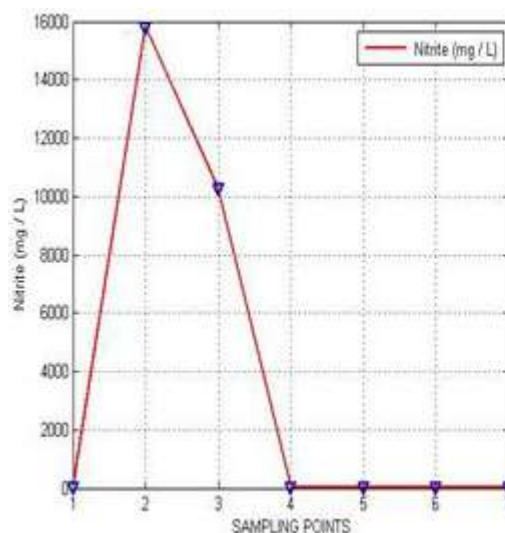


Fig. 9: Average nitrite values in effluents.

Table 3: variation of organic pollution indicators in the MEWOU river.

samples	Organic indicators		
	DO [mg.L <sup>-1</sup> ]	COD [mg.L <sup>-1</sup> ]	BOD5 [mg.L <sup>-1</sup> ]
P1	1.92	959	71
P2	1.28	555.3	99
P3	1.28	217.5	34
P4	1.28	333.5	55
P5	0.96	260.85	24
P6	0.64	452.52	23
P7	0.32	125.32	33



deposition (WHO 2008). The sulfate content of the industrial effluents analyzed varied from one sample to another (Fig. 10). The highest content is revealed for sample P3 (9725.2 mg.L<sup>-1</sup>) and a minimum value for sample P7 (79.38 mg.L<sup>-1</sup>), with an average value of all the samples, analyzed equally to 1049.6 mg.L<sup>-1</sup> (Table 2).

The sulfate content of the discharged industrial effluents was between 1049.6 and 9725.2 mg.L<sup>-1</sup>, these values are not tolerable because the WHO suggests that the sulfate content limit should not be higher than 1000-1200 mg.L<sup>-1</sup> (WHO 2008).

### Chemical Oxygen Demand (COD)

The chemical oxygen demand (COD) is an important parameter for determining the organic load in the water. In particular, for the operation of wastewater treatment plants, as well as for the characterization of water quality, this parameter is used worldwide and is one of the many directives relating to water quality. (Kolb et al. 2017). The COD values of the liquid effluents analyzed showed high concentrations ranging from 125.32 to 959 mg.L<sup>-1</sup> (Fig. 11), with an average value of 414. mg.L<sup>-1</sup>. These results exceed the recommendations of (OJAR n.26 2006).

The COD values ranged from 125.32 to 959 mg.L<sup>-1</sup>, these values were much too high compared to the limits prescribed by the regulations (OJAR n.26 2006). These high concentrations were due to the high pollutant loads of organic matter released by the water since the production of soap involves the use of large quantities of palm oil (Félix et al. 2017). These results are similar to those reported by (Gouafo & Yerima 2013) 122-958 mg.L<sup>-1</sup>. An industrial effluent with such a high COD can pose seri-

ous problems with reducing the oxygen concentration in waterways.

### Biochemical Oxygen Demand (BOD5)

The need for the oxygenation factor of water is very clear as the presence of oxygen modulates the aerobic decomposition reaction of organic matter and more generally affects the biological balance of aquatic environments. The organic pollution values expressed in BOD5 show significant variations from one sample to another (Fig. 12). The recorded BOD5 values vary from 33 mg.L<sup>-1</sup> (minimum value) to 99 mg.L<sup>-1</sup> (maximum value) with an average value of 48.43 mg.L<sup>-1</sup> (Table 2).

The BOD5 values obtained by the analysis of industrial effluents indicated an average value of 48.43 mg.L<sup>-1</sup>. This result is close to that found by (Gouafo & Yerima 2013) which ranged from 34 to 71 mg.L<sup>-1</sup> whose high BOD5 values could be explained by the abundance of organic matter. The chemical oxygen demand is the quantity of oxygen used by the materials present in the water which, under defined operating conditions, will oxidize. Indeed, its determination corresponds to an estimate of the oxidizable matter present in the water since its origin (Rodier 2005).

### Organic Pollution Assessment

Biodegradability provides information on the ability of an effluent to be decomposed or oxidized by microorganisms involved in the biological process of water purification. It is expressed by the coefficient K.

- If (K < 1.5): This means that the oxidizable materials are largely made up of highly biodegradable materials.

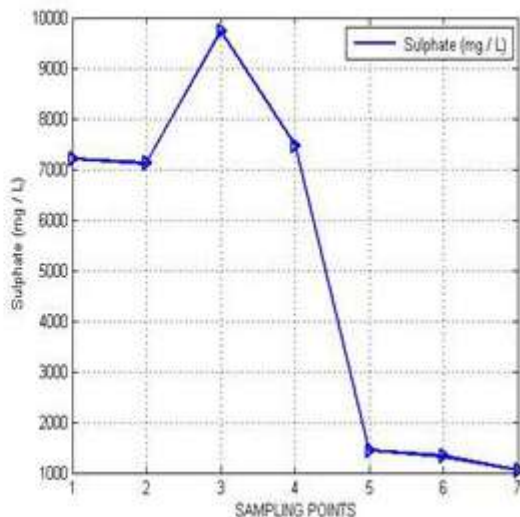


Fig. 10: Average sulfate values in effluents.

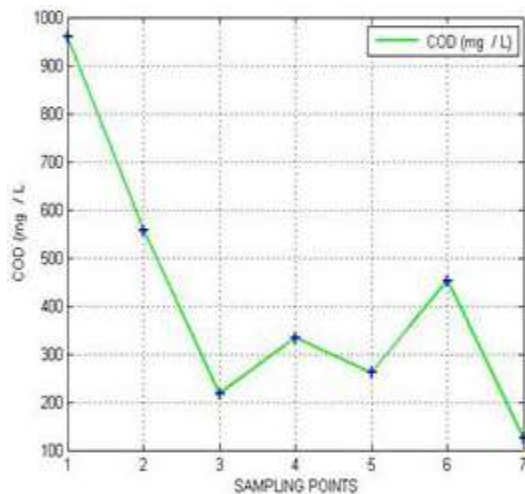


Fig. 11: Average COD values of effluents.

- If  $(1.5 < K < 2.5)$ : This means that oxidizable materials are moderately biodegradable.
- If  $(2.5 < K < 3)$ : This means that oxidizable materials are not very biodegradable.
- If  $K > 3$ : This indicates that oxidizable materials are not biodegradable. A very high K coefficient implies the presence of elements in the water that prevent bacterial growth, such as detergents, metal salts, hydrocarbons, phenols, etc. (Nabbou et al. 2020).

The industrial effluents studied have a K coefficient that varies from 3.79 to 19.67, which corresponds to that of industrial wastewater having a COD/BOD5 ratio greater than 3 (Rodier 1998). In addition, the average BOD5 / COD ratio of 0.14 reflects the low biodegradability of the substances contained in these effluents.

The COD / BOD5 ratio according to (Messrouk et al. 2014, Tardat-Henry & Beaudry 1992) Can make it possible to deduce whether the effluents are directly discharged into the receiving environment have the characteristics of domestic wastewater. this COD / BOD5 ratio is greater than 3 in our case, which means that the oxidizable materials thus released are not biodegradable. It can be deduced that the low biodegradability of this industrial wastewater from SCS may be associated with the presence of certain inhibitor products, such as palm oil heavily used for soap production, or with a high load of organic matter.

### Metal Concentrations

The values of the metals in the sample stream varied as follows: chromium (35.76-1381.08 mg.L<sup>-1</sup>), zinc (0.51-1.98 mg.L<sup>-1</sup>), lead (0.21-2.49 mg.L<sup>-1</sup>), potassium (13.31-26.53

mg.L<sup>-1</sup>), iron (0.28-17.82 mg.L<sup>-1</sup>), copper (0-0.04 mg.L<sup>-1</sup>), and cadmium (0.03-0.19 mg.L<sup>-1</sup>); the presence of lead is noted here with values greater than the WHO prescription, i.e. 0.01 mg.L<sup>-1</sup> in drinking water. The health risks of an elevated lead concentration include kidney damage, anemia, and brain edema (WHO 2008). Only the values of copper and Zinc were within the admissible standards; other heavy metals were clearly and unequivocally above allowable standards; which allowed us to establish a definite link between the contamination of the Mewou River with heavy metals and the discharge of industrial effluents from the SCS.

### CONCLUSIONS AND RECOMMENDATIONS

In view of the results that we obtained, it is clear that the industrial effluents of the SCS analyzed were highly polluted,

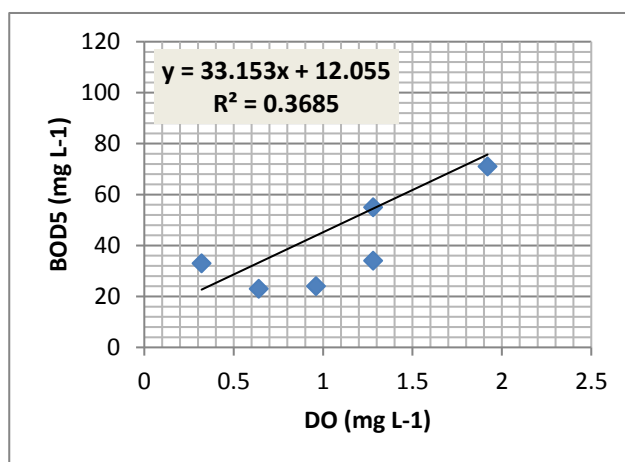


Fig.13: BOD against DO for River Mewou.

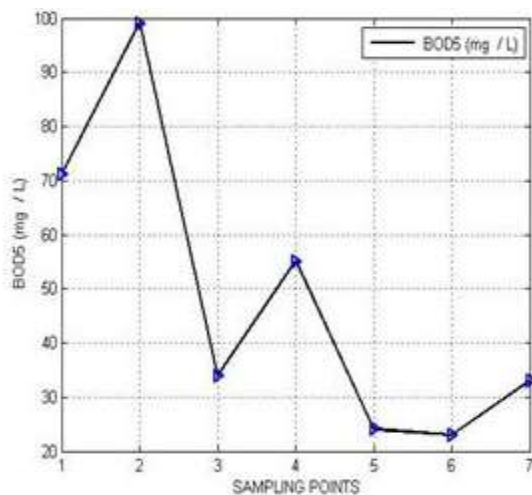


Fig. 12: Average values of BOD5 of effluents.

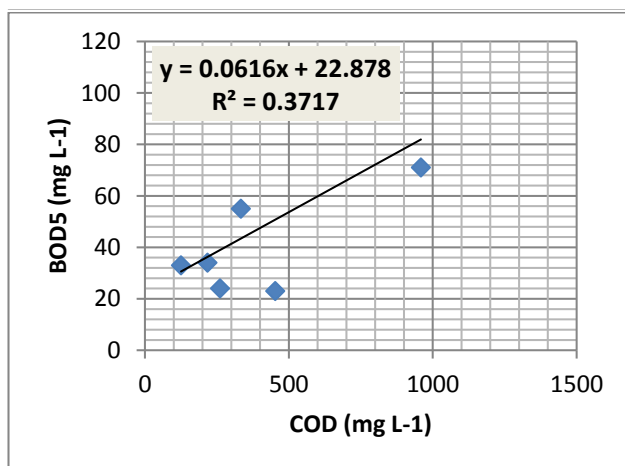


Fig.14: BOD5 against COD for River Mewou.

in particular in heavy metals (lead, chromium, and cadmium), and in organic matter, underlined in particular by high values of turbidity, COD and BOD<sub>5</sub>. All these indicators, witnesses of undeniable pollution, indicate that these effluents constitute a source of contamination of the receiving environment and present a threat to the ecosystem and public health.

This situation is caused by the lack of an industrial effluent treatment procedure at the production site. Finally, the following practices are recommended to limit the volume as well as the polluting load of liquid effluents:

- Beyond its position as a major economic actor (employers and producers of goods) that the soap production company SCS plays in the city of Bafoussam, these managers must become aware of the social responsibility incumbent on them and set up an effluent treatment unit.
- Develop practices that will make it possible to minimize discharged effluents as much as possible, in an approach of “Cleaner production techniques”, focused on the use of good practices to minimize water consumption;
- Set up anaerobic basins much more adapted to hot climates With relatively short retention times of only a few days, which can reduce the organic load by 40 to 70% (Shilton 2006).

## REFERENCES

- Awomeso, J.A, Taiwo, A.M, Gbadebo, A.M. and Adenowo, J.A. 2010. Studies on the pollution of a waterbody by textile industry effluents in Lagos, Nigeria. *J. Appl. Sci. Environ. Sanit.*, 5(4): 353-359.
- Chachuat, B. 2001. Optimal design and operation of activated sludge processes: State-of-the-art. *Chem. Eng. J.*, 281: 900-920.
- Félix, S., Araujo, J., Pires, A.M. and Sousa, A.C. 2017. Soap production: A green perspective. *Waste Manag.*, 66: 190-195. <https://doi.org/10.1016/J.Wasman.2017.04.036>
- Ghazali, Z. 2013. Study of the physico-chemical and bacteriological quality of the waters of the Ain Salama-Jerri spring (Region of Meknes-Morocco). *Larhyss*, 12: 25-36.
- Gouafo, C. and Yerima, B.P.K. 2013. Evaluation and mitigation of industrial wastewater pollutants from soap factories and breweries in the Bafoussam City Vicinity (Western Highlands of Cameroon). *Res. J. Environ. Earth Sci.*, 5: 529-536. <https://doi.org/10.19026/Rjees.5.5683>
- Gueddah, D. 2003 Assessment of industrial and urban pollution in the eastern region of Algeria. *Water Manag. Environ.*, 6: 1-25.
- Hamdani, A., Moufti, A., Mountadar, M. and Assobhei, O. 2005. Evolution of the physico-chemical and bacteriological quality of a dairy effluent over an annual cycle. *Waste Sci. Tech.*, 51: 414-425. <https://doi.org/10.4267/Dechets-Sciences-Techniques,1880>
- INS. 2004. Cameroon - Third Demographic and Health Survey, 2004, Cameroon.
- Kankou, M.O.S.O. 2004. Vulnerability of Waters and Soils of the Right Bank of the Senegal River in Mauritania: Laboratory Study of the Behavior of Two Pesticides. Ph.D. Thesis, University of Limoges France, France.
- Kolb, M., Bahadir, M. and Teichgräber, B. 2017. Determination of chemical oxygen demand (Cod) using an alternative wet chemical method free of mercury and dichromate. *Water Res.*, 122: 645-654. <https://doi.org/10.1016/J.Watres.2017.06.034>
- Mathurin, Z.G., Casimir, G., Kisito, T.P., 2022. Prediction of the compressive strength of concrete made with soap factory wastewater using machine learning. *Model. Earth Syst. Environ.* <https://doi.org/10.1007/s40808-022-01445-z>
- Messrouk, H., Mahammed, M., Hadj, T.Y. and Amrane, A. 2014. Physico-chemical characterization of industrial effluents from the town of Ouargla (South East Algeria). *Energy Proced.*, 50: 255-262. <https://doi.org/10.1016/J.Egypro.2014.06.031>
- Nabbou, N., Benyagoub, E., Mellouk, A. and Benmoussa, Y. 2020. Risk assessment for chemical pollution of dairy effluents from a milk processing plant located in Bechar (Southwest Of Algeria). *Appl. Water Sci.*, 10: 229. <https://doi.org/10.1007/S13201-020-01309-W>
- Ojar, N.26. 2006. Executive Decree No. 2006-141 Of 20 Rabie El Aouel 1427 Corresponding To April 19, 2006, Defining The Limit Values Of Industrial Liquid Effluent Discharges.
- ONU, 2006. World Urbanization Prospects, The 2005 Revision.
- Philips, S., Laanbroek, H.J. and Verstraete, W. 2002. Origin, causes, and effects of increased nitrate concentrations in aquatic environments. *Rev. Environ. Sci. Biotechnol.*, 1: 115-141. <https://doi.org/10.1023/A:1020892826575>
- Rice, E.W., Baird, R.B., Eaton, A.D. and Bridgewater, L.L. 2017. Standard Methods for the Examination of Water and Wastewater. 23rd Edition. Ed. American Public Health Association, Washington, DC.
- Rodier, J. 2005. *Water Analysis - Natural Water, Residual Water, Sea Water*. Dunod, Paris, France
- Rodier, J. 1998. *Water Analysis: Natural Waters, Residual Waters, Sea Waters, Chemistry, Physicochemistry, Microbiology, Biology, Interpretation of Results*. Eight Edition. Dunod, Paris, France.
- Rodier, J., Geoffray, C. and Kovacsik, G. 2009. *Water Analysis. Natural Waters, Residual Waters, Sea Water. Chemistry, Physico-Chemistry, Bacteriology, Biology*. Dunod, Paris, France.
- Rodier, J., Kovacsik, G. and Geoffray, C. 1978. *Water Analysis. Natural Waters, Residual Waters, Sea Water. Chemistry, Physico-Chemistry, Bacteriology, Biology*. Dunod, Paris, France.
- Sayad, L. 2015. The Self-Purifying Power of the Seybouse Wadi on Discharges from the Edough Annaba Algeria Dairy and the Environmental Objectives of Discharges Universite Mokhtar Badji Annaba (Algeria), pp. 203.
- Shilton, A.N. (Ed.) 2006. *Pond Treatment Technology*. Reprint. Ed. Integrated Environmental Technology Series, Iwa, London.
- Shivsharan, V.S., Kulkarni, S.W. and Wani, M., 2013. Physicochemical characterization of dairy effluents. *Pharm. Res.*, 12: 65.
- Tardat-Henry, M. and Beaudry, J.P. 1992. *Water Chemistry*. Modulo, France.
- WHO 2017. *Water Quality And Health: Review Of Turbidity: Information For Regulators And Water Suppliers*. Geneva, Switzerland.
- WHO 2008. *Guidelines For Drinking-Water Quality*. Geneva, Switzerland.





# The Study of Air Quality and Risk Assessment at the Location of the Planned Railroad Between Makassar-Parepare, South Sulawesi, Indonesia

S. Isworo\*†, S. Febrianto\*\*, T. Aji\*\*, P. S. Oetari\*\* and E. Jasmieni\*\*\*

\*Department of Environmental Health, Dian Nuswantoro University Semarang, Indonesia

\*\*Department of Environmental Impact Assessment, Mitra Adhi Pranata Inc., Semarang, Indonesia

\*\*\*Departement of Urban Regional Planning, Diponegoro University, Semarang, Indonesia

†Corresponding author; S. Isworo: slamet.isworo@dsn.dinus.ac.id

## Nat. Env. & Poll. Tech.

Website: [www.neptjournal.com](http://www.neptjournal.com)

Received: 06-07-2021

Revised: 24-09-2021

Accepted: 03-10-2021

### Key Words:

Air quality

Risk analysis

Total suspended particulates

Air pollutants

Hydrocarbons

Makassar-Parepare railway

## ABSTRACT

The National Railway Master Plan, it is stated that the target of developing the railway network in South Sulawesi Province is to connect areas that have the potential for transporting passengers and goods to support the development of integration between districts. The construction of the railway line has the potential to reduce air quality and health risks to the community around the location. This study aims to assess air quality and its risks during the construction of the railway line from Makassar to Parepare as a reference for environmental management and monitoring plan documents. Air sampling was made using multiple impinger and dust with a hi-volt dust sampler and then analyzed in the laboratory and compared with the Air Pollution Standard Index. Analysis of potential pollutants on health was carried out using the Environmental Health Risk Assessment method. The results showed that the air quality at the time of the study was still below the threshold value, and the environmental health risk assessment was still below the value with  $RQ > 0.1$  except for  $SO_2$  in adults. The conclusion of the study shows that the air quality at the time of the construction of the railway line is still relatively good, and environmental management and monitoring have been carried out quite well based on the direction of the environmental management and monitoring plan including implementing a green open space management program.

## INTRODUCTION

Rail transportation is a cheap and safe mode of land transportation, so it is very suitable for developing economic countries such as Indonesia, but in reality, in the land transportation system, the current rail transportation mode is relatively underdeveloped compared to other land transportation modes, this is due to inadequate supporting infrastructure (Saremi 2020). The development of railway infrastructure in Indonesia needs to be developed in all parts of Indonesia so that economic development can develop properly and evenly to all corners of the region which will have a significant impact. have impact on the condition of the national economy (Siagian 2017). Based on the South Sulawesi provincial government regulation number 0003/P2T-BKPM/9.24.N/VII/04/2015 in the implementation of the construction of the railway line, it is necessary to study the monitoring and management of the Makassar-Parepare railway line referring to the Environmental Impact Analysis document. which has been compiled. and declared worthy (Isworo 2019). Refers to environmental monitoring and management documents, especially in assessing the impact of air quality and health risks around the construction site (He et al. 2009).

The government regulation concerning the Air Pollutant Standard Index is officially used for determining air quality standards, this is in accordance with the decree of the Minister of the Environment number: KEP 45/MENLH/10/1997 concerning Indonesia's Air Pollutant Standard Index. The parameters used are particulates ( $PM_{10}$ ), sulfur dioxide ( $SO_2$ ), carbon monoxide (CO), ozone ( $O_3$ ), and nitrogen dioxide ( $NO_2$ ) (Istiqomah & Marleni 2020)

The studies on the impact of air quality on the construction of the Makassar-Parepare railways need to be supported by a study of environmental health risk analysis as one of the environmental management tools used to protect the public health due to the effects of poor air quality. The Environmental health risk analysis is used as an environmental impact approach which is a tool to identify, understand, and predict the conditions and characteristics of pollutants that have the potential to pose health risks (Khan 2018)

This study aims to determine the condition of air quality and the level of health risk of residents living at the construction site of the Makassar-Parepare railway so that it can be input for stakeholders in formulating environmental management and health risk control.

**MATERIALS AND METHODS**

The air quality parameters measured are: Total Suspended Particulate, Sulfur Dioxide (SO<sub>2</sub>), Nitrogen dioxide (NO<sub>2</sub>), Carbon monoxide (CO), Pb (Lead), and Hydrocarbons (HC) based on the predetermined Air Pollutant Standard Index parameters by the Ministry of Environment and Forestry of the Republic of Indonesia (Putra & Sitanggang 2020)

Sampling locations and air quality sampling were carried

out at location points covering 5 districts in South Sulawesi Province. Sampling locations that represent the location of settlements, public facilities, as well as trade, and services are given in Table 1.

Fig. 1 is the sampling location. Primary data on ambient air quality was collected by air sampling, measurement, and laboratory analysis. Air samples were taken with the Multiple Impinger tool. This air sample is then given a preservative

Table 1: Data collection methods and justification for air quality sampling period 1 (August 2019) and period 2 (October 2019).

Location	Coordinate	Number of measurement points	Method	Technical justification
Makassar	S: 05°06'40.72" E: 119°26'18.49"	1 sample point at the location of New Port Makassar	24 hours sampling, laboratory analysis	Air quality sampling locations are representative:
Maros	S: 05°02'19.32" E: 119°32'24.15" (Period 1) and S: 05°00'54.35" E: 119°32'57.49" (Period 2)	2 sample points at Marussu and Mandai locations	24 hours sampling, laboratory analysis	a) Location of paths traversed by equipment and material mobilization vehicles
Pangkep	S: 04°52'22.74" E: 119°35'04.35" (Period 1) and S: 04°49'54.64" E: 119°34'11.65" (Period 2)	2 sample points in Minasa Te'ne and Pangkajene locations	24 hours sampling, laboratory analysis	b) Residential settlements around the project site
Barru	S: 04°49'54.64" E: 119°34'11.65" (Period 1) S: 04°24'07.32" E: 119°37'48,52"(Period 2)	2 sample points on Baru and Sepee locations	24 hours sampling, laboratory analysis	
Parepare	S: 03°59'26.37" E: 119°38'45.65"	1 sample point in the location area of Soreang	24 hours sampling, laboratory analysis	

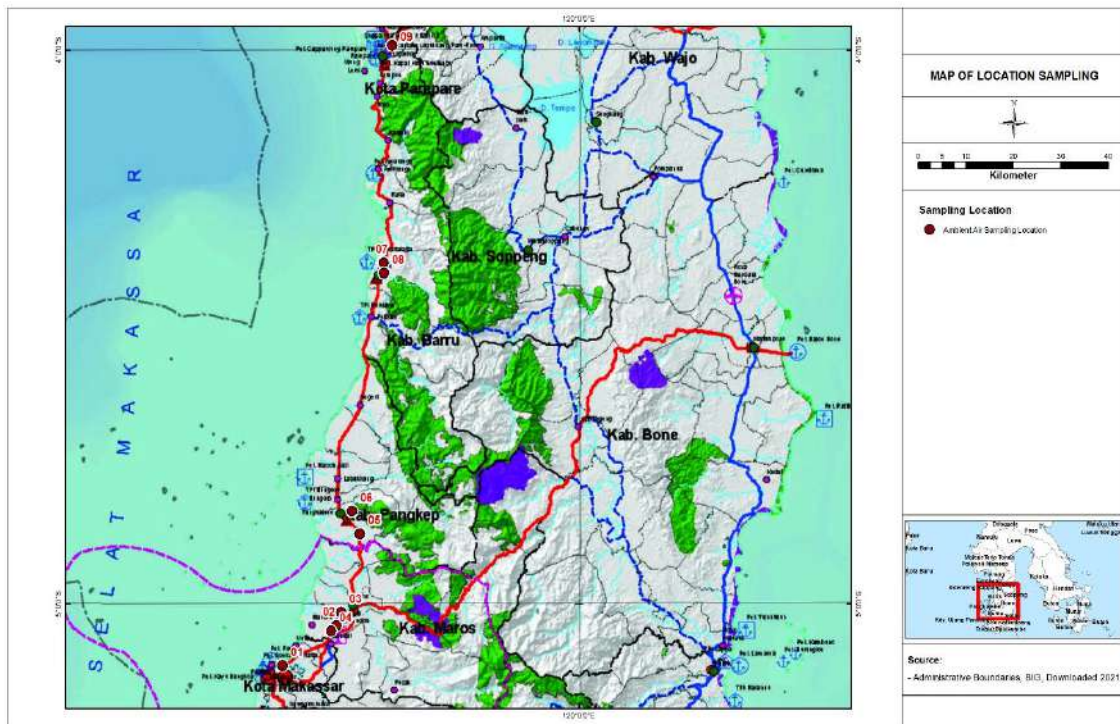


Fig. 1: Sampling location.

(H<sub>2</sub>SO<sub>4</sub> or HgCl<sub>2</sub>) and then analyzed in the laboratory, for dust particles, samples are taken with a dust sampler (hi-volt tool) and then analyzed in the laboratory (Sahu & Sahu 2019) The air quality parameter analysis methods are presented in Table 2.

Analysis of air quality parameter data by comparing the data from the sample analysis with the applicable ambient air quality standards, while the calculation of health risks refers to the Environmental Health Risk Assessment guidelines of the Indonesian Ministry of Health (Gusti & Yurnal 2019). Risk calculation is performed on the elements Total Suspended Particulate, NO<sub>2</sub>, SO<sub>2</sub>, and Pb as follows (Licina et al. 2017):

$$I = \frac{C \times R \times tE \times fE \times Dt}{Wb \times tavg}$$

Where:

I: Intake

C: Concentration

R: Intake rate (m<sup>3</sup>.hour<sup>-1</sup>)

tE: Exposure time per day (hour.day<sup>-1</sup>)

fE: Frequency of exposure in a year (day.year<sup>-1</sup>)

Dt: Duration of exposure, realtime (30 years projection)

Wb: Weight (kg)

t<sub>avg</sub>: average period, 30 years × 365 days/year (non carcinogenic) or 70 years × 365 days/year (carcinogenic)

The level of risk of non-carcinogenic effects is expressed in the notation Risk Quotient (RQ) which is obtained through the following equation (Das 2020). The Table 3 provides information on non-carcinogenic risk rate.

$$RQ = \frac{Ink}{RfC}$$

Table 2: Air sample collection and analysis methods.

No	Parameter	Data collection	Analysis method	Quality standards (Azis 2011)
1	Total Suspended Solids	Sampling, laboratory analysis	Gravimetry (Hamiresa et al. 2006)	230 µg.Nm <sup>-3</sup>
2	NO <sub>2</sub>	Sampling, laboratory analysis	Saltzman (Ramadhani 2018)	150 µg.Nm <sup>-3</sup>
3	SO <sub>2</sub>	Sampling, laboratory analysis	Spectrophotometer (Ashadi 2020)	365 µg.Nm <sup>-3</sup>
4	Pb	Sampling, laboratory analysis	Atomic Absorption Spectrophotometer (Ferreira et al. 2018)	0.5 µg.Nm <sup>-3</sup>
5	CO	Sampling, laboratory analysis	Titrimetric (Wu et al. 2019)	10.000 µg.Nm <sup>-3</sup>
6	HC	Sampling, laboratory analysis	Gas chromatography (Johnsen 2017)	160 µg.Nm <sup>-3</sup>

Table 3: Information on non-carcinogenic risk rate.

Notation	Information
Non-carcinogenic intake	The intake is calculated using the formula of non-carcinogenic intake exposure through the inhalation tract
RfC (Reference of Concentration)	The reference value of risk agents in exposure to the inhalation tract is contained in the literature. <a href="http://www.epa.gov/iris">www.epa.gov/iris</a> (Dourson 2018)

Where,

RQ > 1, so the concentration of risk agents will have an impact on health.

RQ ≤ 1, so concentration is not yet at risk of causing health effects.

## RESULTS AND DISCUSSION

The study was conducted on the existing condition of the Makassar-Parepare railway line which includes several segments, namely the ongoing segment and the completed segment. Segment 1: The construction of railroad crossings in Barru Regency, with a length of ± 20 km KM 76+200 to KM 92+300 has been completed. Segment 2: The construction of the railway line that crosses Barru-Palanro Regency along ± 40 Km, in the process of completion at KM 73+600 to KM 76+200 and KM 92+300 to KM 119+150 along 28 km. Segment 3: The construction of a 62.95 km railway crossing in the Barru-Mandai district in the development plan. Management and monitoring studies are carried out periodically so that the construction of the railway line is completed.

### Air Quality

Based on a review of the environmental impact analysis document that during the construction phase of the railway line construction, especially in land clearing, material transportation, excavation, or soil stockpiling, the construction of flyovers can cause a decrease in ambient air. Fig. 2 is the source of the impact of activities that cause a decrease in air quality.

Table 4 shows the results of the comparison between air



quality during the preparation of the environmental baseline for the 2014 environmental impact analysis activity and the results of monitoring period I (1 August 2019) and period II (17 October 2019) and then carried out health risk analysis on Pb, Total Suspended Solid, SO<sub>2</sub> and NO<sub>2</sub> (Table 5). Environmental Management standard indicators, based on government regulation no. 41 of 1999 concerning air pollution control (Maryati 2012), and regulation of the governor of South Sulawesi No. 69 of 2010 concerning quality standards for environmental damage criteria (Zakaria & Aly 2020) and air quality index EPA (Bishoi et al. 2009). Fig. 3 is the air quality measurement activity.

Air quality monitoring activities were carried out in Barru Regency as a sampling location to monitor construction activities that have been carried out since 2018 and the construction of the “fly over” railroad since 2019, while air quality monitoring activities were carried out in Maros regency, Pangkep regency, Makassar city, and Parepare regency aim to monitor pre-construction stage activities since 2019.

The results of the comparison of air quality measurements during the preparation of the initial environmental assessment environmental impact analysis (2014) and environmental monitoring periods 1 and 2 (2019) in Makassar, Maros, Pangkep, Maros, Baru, and Parepare, for the parameters of Total Suspended Particulate, Carbon Monoxide (CO), Sulfur Dioxide (SO<sub>2</sub>), Nitrogen Dioxide (NO<sub>2</sub>), Hydrocarbon (HC), Lead (Pb) the results are below the quality standard

index, even the results of air quality measurements in environmental monitoring activities are lower than the results of measurements in when preparing environmental baselines for environmental impact analysis activities (Istiqomah & Marleni 2020)

Temperature is one of the meteorological factors that affect the dispersion of pollutants in the ambient air. The temperature range at the location of the air quality sampling ranged from 28.1°C-36.2°C. This condition is relatively in the uncomfortable zone > 27.1°C (Indonesian Thermal Comfort Standard SNI T-14-1993-03). However, all workers involved in the construction of the railway line have used protective equipment to deal with thermal discomfort due to temperature, while the community around the project location has adapted to the tropical temperature (Ussiri & Lal 2017). Wind speed is also one of the meteorological factors that affect the dispersion of pollutants in the ambient air. The measurement results based on table 4, the wind speed values at the study site ranged from 0.5 m.s<sup>-1</sup> - 4.9 m.s<sup>-1</sup>, including the rather calm category (Beaufort scale) so they are relatively unobtrusive (Hasan et al. 2017). Air humidity affects the dispersion of pollutants in the ambient air. Sampling results show that humidity ranges from 36.2% - 58.98% (warm comfortable category). Standard Procedures for Energy Conservation Technical Planning in Buildings is 60% still meets the requirements (Huang et al. 2020). The results of CO measurements at the sampling locations ranged



Fig. 2: Activities of land clearing, material transportation, flyover construction, excavation or stockpiling of soil and excavators.



Fig. 3: Measurement of air quality for period 1 and period 2.





from  $755.73 \text{ g.Nm}^{-3}$  -  $5230 \text{ g.Nm}^{-3}$ , this value is still below the threshold value of the Air Pollution Standard Index, which is  $10.000 \text{ g.Nm}^{-3}$ . Carbon monoxide (CO) gas above the threshold value is an inhibitor of the respiratory chain, an inhibitor of oxidative phosphorylation, and breaks the oxidative phosphorylation circuit in cells (Stucki & Stahl 2020).  $\text{NO}_2$  and  $\text{SO}_2$  levels in the air if they are above the Air Pollution Standard Index will have a negative impact, which can cause respiratory tract irritation and increased mucus secretion in the lungs. The  $\text{NO}_2$  measurement results ranged from  $0.4 \text{ g.Nm}^{-3}$ - $38.11 \text{ g.Nm}^{-3}$  below the threshold value of  $150 \text{ g.Nm}^{-3}$  and the  $\text{SO}_2$  measurement results ranged from  $8.28 \text{ g.Nm}^{-3}$ - $150 \text{ g.Nm}^{-3}$  (threshold value of  $230 \text{ g.Nm}^{-3}$ ) (Agus 2020). Exposure to total suspended particulate in humans for a long time can irritate the respiratory system and can even enter the lungs, depositing in the alveoli, causing a chronic obstruction. The measurement results at the sampling location ranged from  $56 \text{ g.Nm}^{-3}$  -  $209 \text{ g.Nm}^{-3}$ , this value is below the threshold value of  $230 \text{ g.Nm}^{-3}$  (Gusti & Yurnal 2019). Pb levels can cause lead poisoning caused by the accumulation of these substances in human body tissues, even Lead (Pb) can be biomagnified in food web systems and is carcinogenic. The measurement results ranged from  $0.01 \text{ g.Nm}^{-3}$  -  $0.004 \text{ g.Nm}^{-3}$  below the threshold value of  $0.5 \text{ g.Nm}^{-3}$  (Ali et al. 2019).

### Environmental Health Risk Analysis

Environmental Health Risk Analysis is one of the risk man-

agement tools used to protect public health due to the impact of poor air quality (Glasson & Therivel 2019). The legal basis for Environmental health risk analysis in the study of environmental impacts is the Minister of Environment Regulation No. 05 of 2012 (Susanto & Mulyono 2018). Environmental health risk analysis used as an environmental impact assessment approach is a tool to identify, understand, and predict environmental conditions and characteristics that have the potential to pose health risks (Cohrssen & Covello 1999) The results of a public health survey of 80 residents in the study area showed that in the last 6 months as many as 25% of the population had complaints of health problems, while the remaining 75% said they had no complaints of illness. Most complaints related to influenza (10.0%), cough (8.75%) and fever (6.25%). Incidents of flu and cough symptoms specifically related to construction activities occurred in Barru Regency, where residents lived around the flyover construction site. Further evidence is needed on the correlation between improved air quality and public health conditions around the railway line construction site by conducting an environmental health risk analysis (Glasson & Therivel 2019).

Based on Tables 5 and 6, the health risk assessment is still in the good category, at the Risk Level Value  $< 1$  ( $\text{RQ} < 1$ ), and the impact of air quality does not need to be controlled. The possible health risk in a small population is the  $\text{SO}_2$  parameter that indicates the potential risk to the adult population (Irianto & Kusumayati 2020)



Fig. 4: Air quality management activities.

Table 5: The results of the risk analysis at the Makassar-Parepare railway construction site in the monitoring period 1.

Period I	Makassar			Mandai, Maros			Marusu, Maros			Minasatene, Pangkep					
	Parameters	Concentration [ $\mu\text{g}\cdot\text{Nm}^{-3}$ ]	Intake [ $\text{mg}\cdot\text{kg}^{-1}\cdot\text{day}^{-1}$ ]	Risk Level	Concentration [ $\mu\text{g}\cdot\text{Nm}^{-3}$ ]	Intake [ $\text{mg}\cdot\text{kg}^{-1}\cdot\text{day}^{-1}$ ]	Risk Level	Concentration [ $\mu\text{g}\cdot\text{Nm}^{-3}$ ]	Intake [ $\text{mg}\cdot\text{kg}^{-1}\cdot\text{day}^{-1}$ ]	Risk Level	Concentration [ $\mu\text{g}\cdot\text{Nm}^{-3}$ ]	Intake [ $\text{mg}\cdot\text{kg}^{-1}\cdot\text{day}^{-1}$ ]	Risk Level		
Period I	Man	Pb	0.01	0.00	0.00	0.00	0.00	0.00	0.00	0.00	0.00	0.00	0.00		
	Woman	Pb	0.01	0.00	0.00	0.00	0.00	0.00	0.00	0.00	0.00	0.00	0.00		
	Children	Pb	0.01	0.00	0.00	0.00	0.00	0.00	0.00	0.00	0.00	0.00	0.00		
	Man	TSP	212	0.06	0.02	209	0.06	0.02	204	0.06	0.02	184	0.05	0.02	
	Woman	TSP	212	0.07	0.03	209	0.07	0.03	204	0.07	0.03	184	0.06	0.03	
	Children	TSP	212	0.03	0.01	209	0.03	0.01	204	0.03	0.01	184	0.03	0.01	
	Man	SO <sub>2</sub>	8.28	0.00	0.09	8.28	0.00	0.09	8.28	0.00	0.09	8.28	0.00	0.09	
	Woman	SO <sub>2</sub>	8.28	0.00	0.11	8.28	0.00	0.11	8.28	0.00	0.11	8.28	0.00	0.11	
	Children	SO <sub>2</sub>	8.28	0.00	0.05	8.28	0.00	0.05	8.28	0.00	0.05	8.28	0.00	0.05	
	Man	NO <sub>2</sub>	6.50	0.00	0.09	6.50	0.00	0.09	6.50	0.00	0.09	6.50	0.00	0.09	
	Woman	NO <sub>2</sub>	6.50	0.00	0.11	6.50	0.00	0.11	6.50	0.00	0.11	6.50	0.00	0.11	
	Children	NO <sub>2</sub>	6.50	0.00	0.05	6.50	0.00	0.05	6.50	0.00	0.05	6.50	0.00	0.05	
Period I	Parameters	Pangkajene, Pangkep			Baru, Barru			Soreang, Parepare							
		Concentration [ $\mu\text{g}\cdot\text{Nm}^{-3}$ ]	Intake [ $\text{mg}\cdot\text{kg}^{-1}\cdot\text{day}^{-1}$ ]	Risk Level	Concentration [ $\mu\text{g}\cdot\text{Nm}^{-3}$ ]	Intake [ $\text{mg}\cdot\text{kg}^{-1}\cdot\text{day}^{-1}$ ]	Risk Level	Concentration [ $\mu\text{g}\cdot\text{Nm}^{-3}$ ]	Intake [ $\text{mg}\cdot\text{kg}^{-1}\cdot\text{day}^{-1}$ ]	Risk Level					
		Man	Pb	0.00	0.00	0.00	0.01	0.00	0.00	0.00	0.00	0.00	0.00	0.00	
		Woman	Pb	0.00	0.00	0.00	0.01	0.00	0.00	0.00	0.00	0.00	0.00	0.00	
		Children	Pb	0.00	0.00	0.00	0.01	0.00	0.00	0.00	0.00	0.00	0.00	0.00	
		Man	TSP	194	0.05	0.02	225	0.06	0.03	226	0.06	0.03	226	0.06	0.03
		Woman	TSP	194	0.07	0.03	225	0.08	0.03	226	0.08	0.03	226	0.08	0.03
		Children	TSP	194	0.03	0.01	225	0.03	0.01	226	0.03	0.01	226	0.03	0.01
		Man	SO <sub>2</sub>	8.28	0.00	0.09	8.28	0.00	0.09	8.28	0.00	0.09	8.28	0.00	0.09
		Woman	SO <sub>2</sub>	8.28	0.00	0.11	8.28	0.00	0.11	8.28	0.00	0.11	8.28	0.00	0.11
		Children	SO <sub>2</sub>	8.28	0.00	0.05	8.28	0.00	0.05	8.28	0.00	0.05	8.28	0.00	0.05
		Man	NO <sub>2</sub>	6.50	0.00	0.09	6.50	0.00	0.09	6.50	0.00	0.09	6.50	0.00	0.09
Woman	NO <sub>2</sub>	6.50	0.00	0.11	6.50	0.00	0.11	6.50	0.00	0.11	6.50	0.00	0.11		
Children	NO <sub>2</sub>	6.50	0.00	0.05	6.50	0.00	0.05	6.50	0.00	0.05	6.50	0.00	0.05		

Table 6: The results of the risk analysis at the Makassar-Parepare railway construction site in the monitoring period 2.

Period 2	Makassar				Palantikang, Maros				Mandai, Maros				Pangkep							
	Category	Parameters	Concentration [ $\mu\text{g}\cdot\text{Nm}^{-3}$ ]	Intake [ $\text{mg}\cdot\text{kg}^{-1}\cdot\text{day}^{-1}$ ]	Risk Level	Concentration [ $\mu\text{g}\cdot\text{Nm}^{-3}$ ]	Intake [ $\text{mg}\cdot\text{kg}^{-1}\cdot\text{day}^{-1}$ ]	Risk Level	Concentration [ $\mu\text{g}\cdot\text{Nm}^{-3}$ ]	Intake [ $\text{mg}\cdot\text{kg}^{-1}\cdot\text{day}^{-1}$ ]	Risk Level	Concentration [ $\mu\text{g}\cdot\text{Nm}^{-3}$ ]	Intake [ $\text{mg}\cdot\text{kg}^{-1}\cdot\text{day}^{-1}$ ]	Risk Level	Concentration [ $\mu\text{g}\cdot\text{Nm}^{-3}$ ]	Intake [ $\text{mg}\cdot\text{kg}^{-1}\cdot\text{day}^{-1}$ ]	Risk Level			
Period 2	Man	Pb	0.01	0.00	0.00	0.00	0.00	0.00	0.01	0.00	0.00	0.01	0.00	0.00	0.01	0.00	0.00			
	Woman	Pb	0.01	0.00	0.00	0.00	0.00	0.00	0.01	0.00	0.00	0.01	0.00	0.00	0.01	0.00	0.00			
	Children	Pb	0.01	0.00	0.00	0.00	0.00	0.00	0.01	0.00	0.00	0.01	0.00	0.00	0.01	0.00	0.00			
	Man	TSP	153	0.04	0.02	60.0	0.02	0.01	0.01	56.0	0.02	0.01	63.0	0.02	0.01	63.0	0.02	0.01		
	Woman	TSP	153	0.05	0.02	60.0	0.02	0.01	0.01	56.0	0.02	0.01	63.0	0.02	0.01	63.0	0.02	0.01		
	Children	TSP	153	0.02	0.01	60.0	0.01	0.00	0.00	56.0	0.01	0.00	63.0	0.01	0.00	63.0	0.01	0.00		
	Man	SO <sub>2</sub>	150	0.04	1.58	35.0	0.01	0.37	0.37	65.0	0.02	0.69	113	0.03	0.69	113	0.03	1.19		
	Woman	SO <sub>2</sub>	150	0.05	2.01	35.0	0.01	0.47	0.47	65.0	0.02	0.87	113	0.04	0.87	113	0.04	1.52		
	Children	SO <sub>2</sub>	150	0.02	0.89	35.0	0.01	0.21	0.21	65.0	0.01	0.38	113	0.02	0.38	113	0.02	0.67		
	Man	NO <sub>2</sub>	2.00	0.00	0.03	0.40	0.00	0.01	0.01	0.40	0.00	0.01	0.40	0.00	0.01	0.40	0.00	0.01		
	Woman	NO <sub>2</sub>	2.00	0.00	0.03	0.40	0.00	0.01	0.01	0.40	0.00	0.01	0.40	0.00	0.01	0.40	0.00	0.01		
	Children	NO <sub>2</sub>	2.00	0.00	0.02	0.40	0.00	0.00	0.00	0.40	0.00	0.00	0.40	0.00	0.00	0.40	0.00	0.00		
Period 2	Category	Parameters	Pangkajene, Pangkep				Baru, Barru				Soreang, Parepare									
			Concentration [ $\mu\text{g}\cdot\text{Nm}^{-3}$ ]	Intake [ $\text{mg}\cdot\text{kg}^{-1}\cdot\text{day}^{-1}$ ]	Risk Level	Concentration [ $\mu\text{g}\cdot\text{Nm}^{-3}$ ]	Intake [ $\text{mg}\cdot\text{kg}^{-1}\cdot\text{day}^{-1}$ ]	Risk Level	Concentration [ $\mu\text{g}\cdot\text{Nm}^{-3}$ ]	Intake [ $\text{mg}\cdot\text{kg}^{-1}\cdot\text{day}^{-1}$ ]	Risk Level									
			Man	Pb	0.01	0.00	0.00	0.01	0.00	0.00	0.01	0.00	0.00	0.01	0.00	0.00	0.01	0.00	0.00	
			Woman	Pb	0.01	0.00	0.00	0.01	0.00	0.00	0.01	0.00	0.00	0.01	0.00	0.00	0.01	0.00	0.00	
			Children	Pb	0.01	0.00	0.00	0.01	0.00	0.00	0.01	0.00	0.00	0.01	0.00	0.00	0.01	0.00	0.00	
			Man	TSP	66.0	0.02	0.01	76.0	0.02	0.01	0.01	27.0	0.01	0.00	27.0	0.01	0.00	27.0	0.01	0.00
			Woman	TSP	66.0	0.02	0.01	76.0	0.03	0.01	0.01	27.0	0.01	0.00	27.0	0.01	0.00	27.0	0.01	0.00
			Children	TSP	66.0	0.01	0.00	76.0	0.01	0.01	0.01	27.0	0.00	0.00	27.0	0.00	0.00	27.0	0.00	0.00
			Man	SO <sub>2</sub>	56.0	0.02	0.59	120	0.03	1.26	1.26	27.0	0.01	0.29	27.0	0.01	0.29	27.0	0.01	0.29
			Woman	SO <sub>2</sub>	56.0	0.02	0.75	120	0.04	1.61	1.61	27.0	0.01	0.36	27.0	0.01	0.36	27.0	0.01	0.36
			Children	SO <sub>2</sub>	56.0	0.01	0.33	120	0.02	0.71	0.71	27.0	0.00	0.16	27.0	0.00	0.16	27.0	0.00	0.16
			Man	NO <sub>2</sub>	0.40	0.00	0.01	0.40	0.00	0.01	0.01	0.40	0.00	0.01	0.40	0.00	0.01	0.40	0.00	0.01
Woman	NO <sub>2</sub>	0.40	0.00	0.01	0.40	0.00	0.01	0.01	0.40	0.00	0.01	0.40	0.00	0.01	0.40	0.00	0.01			
Children	NO <sub>2</sub>	0.40	0.00	0.00	0.40	0.00	0.00	0.00	0.40	0.00	0.00	0.40	0.00	0.00	0.40	0.00	0.00			



Policymakers will carry out air quality management activities by implementing a green open space management program with a minimum area of 10% (Maryanti et al. 2017). Some references that the Angsana plant (*Pterocarpus indicus*) can reduce CO<sub>2</sub> up to 70% SO<sub>2</sub> up to 50% (Laksono & Damayanti 2015) and; the Tamarind plant (*Tamarindus indica*) can reduce CO<sub>2</sub> up to 80% and SO<sub>2</sub> up to 90% and the umbrella plant Tiara (*Felicium decipiens*) can reduce CO<sub>2</sub> up to 70% and SO<sub>2</sub> up to 60% (Kusminingrum 2008).

### Air Quality Management

Air quality management at the Makassar-Parepare railway construction site has been carried out properly through compliance evaluation so that all air quality parameters are below the threshold value. Management is carried out by regularly watering locations that have the potential to generate dust, limiting vehicle speed to a maximum of 40 km.h<sup>-1</sup>, especially when passing through residential areas, installing traffic signs for speed limiting, avoiding material spills during the transportation process by covering the material with tarpaulins and every wheel of the vehicle that will leave the project site is cleaned in the cleaning pool (Fig. 4).

Caption: a) Periodic watering in potential locations. b) Installation of traffic signs around construction activity sites c) Material transport trucks have used tarpaulin covers on the tailgates, d) Cleaning up spilled material. e) Placing traffic control officers when transporting materials

### CONCLUSIONS

Parameters Total Suspended Particulate, Carbon Monoxide (CO), Sulfur Dioxide (SO<sub>2</sub>), Nitrogen Dioxide (NO<sub>2</sub>), Hydrocarbons (HC), Lead (Pb) are below the quality standard Air Pollution Index, and the level of health risk (RQ) < 1.

### ACKNOWLEDGMENTS

The author is very grateful to the management of the East Java Regional Railway Engineering Center and environmental consultant PT. Mitra Adi Pranata Consultant so that this research can run well.

### REFERENCES

Agus, R.M. 2020. The ambient air quality of SO<sub>2</sub> and NO<sub>2</sub> in settlements around the industrial area of Makassar 2019. *Enferm. Clinic.*, 30: 328-332.

Ali, H., Khan, E. and Ilahi, I. 2019. Environmental chemistry and ecotoxicology of hazardous heavy metals: environmental persistence, toxicity, and bioaccumulation. *J. Chem.*, 14: 1-15

Ashadi, A. 2020. Utilization of Mendong plant activated charcoal as SO<sub>2</sub> gas adsorbent: a preliminary study. *IOP Conf. Series Mater. Sci. Eng.*, 141: 12040.

Azis, M. 2011. Measuring air pollutant standard index (ISPU) with photonic crystal sensor based on wireless sensor network (WSN). 2nd International Conference on Instrumentation, Communications, Information Technology, and Biomedical Engineering, 8-9 November 2011, Bandung, West Java, Indonesia, IEEE, Manhattan, NY, pp. 348-351

Bishoi, B., Prakash, A. and Jain, V.K. 2009. A comparative study of air quality index based on factor analysis and US-EPA methods for an urban environment. *Aerosol Air Qual. Res.*, 9(1): 1-17.

Cohrssen, J.J. and Covello, V.T. 1999. *Risk Analysis: A Guide to Principles and Methods for Analyzing Health and Environmental Risks*. Diane Publishing Company, Pennsylvania, US.

Das, A. 2020. Non-carcinogenic and carcinogenic risk assessment of trace elements of PM<sub>2.5</sub> during winter and pre-monsoon seasons in Delhi: A case study. *Exp. Health*, 12(1): 63-77.

Dourson, M.L. 2018. Let the IRIS Bloom: Regrowing the integrated risk information system (IRIS) of the US Environmental Protection Agency. Elsevier, Netherlands, pp. A4-A5

Ferreira, S.L., Bezerra, M.A., Santos, A.S., dos Santos, W.N., Novaes, C.G., de Oliveira, O.M., Oliveira, M.L. and Garcia, R.L. 2018. Atomic absorption spectrometry—A multi-element technique. *TrAC Trends in Analytical Chemistry*, 100: 1-6.

Glasson, J. and Therivel, R. 2019. *Introduction to environmental impact assessment*. Routledge, London, UK.

Gusti, A. and Yurnal, R.A. 2019. Health risk assessment of total suspended particulate exposure to the employee of PT Semen Padang, Indonesia. *Iran. J. Public Health*, 48(8): 1535.

Gusti, A. and Yurnal, R.A. 2017. Environmental Health risk assessment of total suspended particulate exposure to an employee of PT Semen Padang. *Proceed. Int. Conf. Public Health*, 65: 15-20.

Hamiresa, G., Yuwono, A.S. and Anwar, S. 2006. The emission factor of dust-fall and TSP from Andisol soil for ambient air quality change assessment. *J. Earth Sci.*, 11(21): 1-15

Hasan, H., Mohamad, A. and Salleh, N.H.M. 2017. This study applied the Markov chain model to the daily average wind speed data recorded at the meteorological stations in northern Peninsular Malaysia. *J. Appl. Phys. Sci.*, 3(2): 52-57.

He, G., Zhang, L. and Lu, Y. 2009. Environmental impact assessment and environmental audit in large-scale public infrastructure construction: the case of the Qinghai-Tibet railway. *Environ. Manag.*, 44(3): 579-589.

Huang, H. 2020. Energy performance of a high-rise residential building retrofitted to passive building standard: A case study. *Appl. Thermal Eng.*, 181: 115902.

Irianto, R.Y. and Kusumayati, A. 2020. Health risk assessment on humans exposed to nitrogen dioxide in adults around steel industry. *Indian J. Public Health Res. Develop.*, 11(3): 16.

Istiqomah, N.A. and Marleni, N.N.N. 2020. Particulate air pollution in Indonesia: quality index, characteristic, and source identification. *IOP Conf. Series Earth Environ. Sci.*, 1651: 12084.

Isworo, S. 2019. Monitoring of surface water quality in train development activities plan between Makasar and Parepare, South Sulawesi Indonesia. *Asian J. Biol.*, 11: 1-17.

Johnsen, L.G. 2017. Gas chromatography-mass spectrometry data processing made easy. *J. Chromatogr. A*, 1503: 57-64.

Khan, J. 2018. Road traffic air and noise pollution exposure assessment—A review of tools and techniques. *Sci. Tot. Environ.*, 634: 661-676.

Kusminingrum, N. 2008. Potensi tanaman dalam menyerap CO<sub>2</sub> dan CO untuk mengurangi dampak pemanasan global. *Jurnal Peremukiman*, 3(2): 96-105.

Laksono, B.A. and Damayanti, A. 2015. Analysis of the sufficiency of Angsana trees (*Pterocarpus indicus*) in absorbing carbon monoxide (CO) due to motor vehicle activity on the Ahmad Yani Street Surabaya. *Journal of Applied and Natural Sciences*, 7(2).

- Licina, D., Tian, Y. and Nazaroff, W.W. 2017. Inhalation intake fraction of particulate matter from localized indoor emissions. *Build. Environ.*, 123: 14-22.
- Maryanti, M., Khadijah, H., Uzair, A.M. and Ghazali, M.M.M. 2017. The urban green space provision using the standards approach: issues and challenges of its implementation in Malaysia. *WIT Transactions on Ecology and the Environment*, 210: 369-379.
- Maryati, S. 2012. GIS database template for environmental management of mining in Indonesia. *J. Geogr. Inform. Sys.*, 4(1): 62-70
- Putra, F.M. and Sitanggang, I.S. 2020. Classification model of air quality in Jakarta using decision tree algorithm based on air pollutant standard index. *IOP Conf. Series Earth Environ. Sci.*, 528(1): 012053
- Ramadhani, I.S. 2018. Ambient air monitoring of nitrogen dioxide at Kalimati, Tirtomartani, Kalasan, Sleman, Yogyakarta. *MATEC Web Conf. EDP Sci.*, 20: 05.
- Sahu, C. and Sahu, S.K. 2019. Ambient air quality and air pollution index of Sambalpur: a major town in Eastern India. *Int. J. Environ. Sci. Technol.*, 16(12): 8217-8228.
- Saremi, P. 2020. The role of the transportation system in the development of the tourism industry in developing countries. *Indian J. Sci. Res.*, 11(1): 61-76.
- Siagian, E.S. 2017. Public-private partnerships in Indonesia: a comprehensive legal framework of significance to action and analysis. *Asia Paci. J. Public Admin.*, 39(1): 72-78.
- Stucki, D. and Stahl, W. 2020. Carbon monoxide—beyond toxicity? *Toxicol. Lett.* 333: 251-260
- Susanto, A. and Mulyono, N.B. 2018. Risk assessment method for identification of environmental aspects and impacts at ore processing industry in Indonesia. *J. Ecol. Eng.*, 19(2): 61.
- Ussiri, D.A.N. and Lal, R. 2017. *Carbon Sequestration for Climate Change Mitigation and Adaptation*. Springer, NY. pp 1-25
- Wu, S., Liang, F., Hu, D., Li, H., Yang, W. and Zhu, Q. 2019. Determining the critical micelle concentration of surfactants by a simple and fast titration method. *Anal. Chem.*, 92(6): 4259-4265.
- Zakaria, R. and Aly, S.H. 2020. Air dispersion modeling of gas turbine power plant emissions in Makassar by using AERMOD. *IOP Conf. Series Earth Environ. Sci.*, 611: 12153.



# Pork Lard Derived Biodiesel Production: Characterization, Engine Performance and Emission Analysis

Rohan Jeffrey Robert\* and C. R. Girish†\*

\*Department of Chemical Engineering, Manipal Institute of Technology, MAHE, Manipal-576104, India

†Corresponding author: C. R. Girish; girishcrt@gmail.com

Nat. Env. & Poll. Tech.  
Website: [www.neptjournal.com](http://www.neptjournal.com)

Received: 28-08-2021

Revised: 08-11-2021

Accepted: 13-11-2021

## Key Words:

High cholesterol fat  
Oxidation  
Esterification  
Blending  
Engine performance  
Exhaust emission

## ABSTRACT

The present work introduces a new methodology in the production of biodiesel from pork-lard waste having high cholesterol content and discusses its improved performance and emissions in a diesel engine. The traditional method of transesterification does not work with cholesterol due to the absence of triglycerides, therefore, the new improved method oxidizes cholesterol to fatty acids and then converts it to biodiesel ester. The procedure includes an acid reagent to break cholesterol and a renewable basic catalyst from seashells, for catalyzing the production. The acid-base system maintains the overall pH while yielding 95.6% conversion at the optimized conditions. The morphology of the produced catalyst was analyzed through FESEM and confirmed through XRD and EDX analyses. The physicochemical and ASTM properties were determined and the calorific value of the 20% biodiesel blend was found to be comparable with that of diesel. From the engine performance analysis, the thermal efficiency of the engine was observed to be higher and the exhaust emissions showed a maximum of 75% reduction in CO and 42.2% reduction in CO<sub>2</sub> emissions, proving it to be an environment-friendly fuel. Additionally, a 32.7% reduction in smoke opacity was also observed, thus decreasing the concentration of particulate matter in the atmosphere.

## INTRODUCTION

The rate of urbanization and industrialization is growing more rapidly than ever, and so is energy consumption. Due to the same, the dependency on fossil fuels has increased and is seen to be exhausting over these years (Judith et al. 2015). Although a good source of energy, fossil fuel consumption results in extensive environmental problems such as global warming and greenhouse effects (Asri et al. 2018). This increased dependency and associated environmental concerns have raised global energy security issues and the urge for alternate fuels (Shahid & Jamal 2020). A few of the most promising and environmentally benign energy resources are solar, geothermal, wind, hydroelectric, and biomass energy (Cynamon & Bouwer 2015, Shahid & Jamal 2020).

Among these a potential option to replace or supplement the conventional petro-diesel is biodiesel. Unlike the latter, biodiesel does not contain any aromatic or sulfur compounds thus reducing the amount of CO, SO<sub>2</sub>, and Hydrocarbon particulates (Karmakar et al. 2010). Additionally, it is a renewable source of energy, and it is relatively less toxic (Atadashi et al. 2011, Mofijur et al. 2016). Since the carbon emissions are equal to or lesser than the amount in the atmosphere, they can be considered carbon neutral (Pua et al. 2012). With these under consideration, biodiesel would be an ideal replacement

or a possible supplement to conventional high-speed diesel (Sharma & Singh 2009, Rakopoulos et al. 2008).

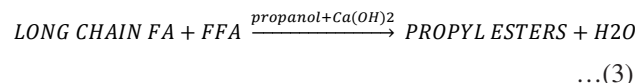
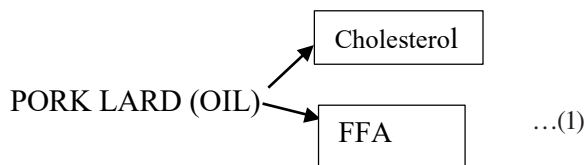
Biodiesel is usually produced from biomasses such as vegetable oils, edible/non-edible oils, and animal wastes (Mureed et al. 2018, Verma & Sharma 2016). Biodiesel production has become a topic of growing interest over the past few years, however, the consumption of edible or value-adding biomass as a source for these productions has questioned food security globally (Awolu & Layokun 2013, Živković et al. 2017, Choudhury 2014). Hence, non-edibles such as animal wastes from slaughter houses, for example, pork lard (Borugadda & Goud 2014, Baskar & Aiswarya 2016, Robert & Girish 2020, Živković et al. 2017) poultry waste (Adewale et al. 2015, Verma & Sharma 2016), beef tallow (Adewale et al. 2015, Andersen & Weinbach 2010, Verma & Sharma 2016), fish waste (Hong et al. 2013, Kara et al. 2018), etc. are considered.

Different methods of biodiesel production include transesterification and/or esterification, thermal cracking, pyrolysis, and micro-emulsions (Borugadda & Goud 2014). Transesterification among these is the most followed method. However, biodiesel can be produced through direct esterification as well (Zaher & Soliman 2015). Moreover, the nature and composition of the feed decide the method to be followed.

Transesterification is usually adapted when triglycerides are present in appreciable amounts. Triglycerides are branched ester compounds; transesterification converts one ester to a different ester (biodiesel) (Atadashi et al. 2013). If the feed oil under consideration contains more FFAs (free fatty acids), the production of biodiesel usually gets hindered by soap formation, if a basic catalyst is used (Atadashi et al. 2011, Shahzadi et al. 2018). The loss in yield is complemented by the complexity in biodiesel purification (Nakatani et al. 2009). An ideal method to overcome this drawback would be to employ an acidic catalyst. This would prevent soap formation.

Certain oils extracted from fats contain cholesterol. Regardless, the methods mentioned above do not account for converting cholesterol to biodiesel. The current work tries to develop a method to convert cholesterol along with the fatty acids into biodiesel esters. The method includes a single-stage reaction in two steps where an acidic catalyst would convert/oxidize cholesterol to fatty acids coupled with the conversion of fatty acids to biodiesel through an esterification reaction.

Nitric acid was carefully chosen as the oxidizing agent. The proposed conversion would follow the reaction shown in Eq. (2).



Esterification in step 2 was carried out using isopropanol in the presence of a calcium hydroxide ( $\text{Ca(OH)}_2$ ) catalyst as shown in Eq. (3). Since the first step involves a strong acid, the resultant would be highly acidic. Therefore,  $\text{Ca(OH)}_2$  in the second would help maintain the overall pH as well while serving as a catalyst.

Biodiesel usually has a higher viscosity than conventional diesel (Monirul et al. 2017). Higher viscosities would lead to issues such as the clogging of fuel injection elements (Venkatesan & Nallusamy 2020). This could be overcome by blending biodiesel with conventional diesel (Babu et al. 2018). Recent developments in biodiesel have shown its potential by subjecting these blends to different combustion and emission analyses.

The biodiesel produced from pine oil and soap nut oil was blended in different proportions and it was studied that Brake thermal efficiency (BTE) improved while smoke, hydrocarbons, and carbon monoxide emissions decreased (Monirul et al. 2017). *Pongamia pinnata* biodiesel–diesel blends when used as fuel in engines up to 40% blending showed higher BSFC values and emissions of CO,  $\text{CO}_2$ , HC,  $\text{NO}_x$  in exhaust gas improved (Sureshkumar et al. 2008). A similar study on *Pongamia pinnata* biodiesel blend with Butanol and Diethyl ether (DEE) as additives was conducted by Yadav et al. It was found that the BSFC could be decreased with addition of butanol and DEE in biodiesel–diesel blends (Yadav et al. 2018). Imdadul et al. (2017) from the experiments on biodiesel blends of candle nut oil of 10%, 20%, and 30% composition drew a conclusion that engine performance parameters such as BSFC increased to a value 1.5% and BTE decreased to 1.4% respectively. The emission parameters such as hydrocarbons and CO decreased reasonably and  $\text{NO}_x$  increased to 2.4% with respect to diesel (Imdadul et al. 2017). The potential of *Glauca* seed as feed stock for biodiesel blends was explored by Vijayaragavan et al. (2019), and blending was prepared with diesel and ethanol. It was reported that with biodiesel–diesel blends BTE and BSFC increased. But with ternary blending comprising of biodiesel–diesel–ethanol, the BSFC value decreased when compared to biodiesel–diesel blends (Vijayaragavan et al. 2019). The research conducted on canola oil biodiesel and its blends found that even with a 5% biodiesel blend showed that CO emission decreased to 14%. Thus the process proved to be environment friendly and reducing pollution (Roy et al. 2013).

Another study conducted by Alagu et al. used biodiesel–diesel blends with low concentrations of anti-oxidants additives such as butylated-hydroxytoluene (BHT) and butylated-hydroxyanisole (BHA). The experiments found that the BTE can be improved when additives are used in small proportions and it was effective in the blend (Alagu & Nagappan 2018). The efficacy of pentanol as an additive in cashew nut shell biodiesel blends were analysed by Devarajan et al. (2017) and reported that significant increase in BTE and reductions in CO, HC,  $\text{NO}_x$ , and smoke emissions. But BSFC values were compromised (Devarajan et al. 2017). Bragadewaran et al. (2018) also conducted experiments using additive Methyl tertiary butyl ether in *Calophyllum inophyllum* biodiesel blends to improve the engine performance. It was noticed that HC, CO and  $\text{NO}_x$  decreased by 63.9%, 6.4% and 3.37% respectively. Therefore, the results proved that the addition of MTBE improved the fuel combustion and reduced HC, CO, and  $\text{NO}_x$  emissions (Bragadeshwaran et al. 2018). Waste cooking oil was utilized to produce biodiesel and blends of 10% and 15% were prepared with diesel. It was studied that the composition of CO,  $\text{CO}_2$  and HC emis-



sions in exit gas reduced to appreciable levels. However, the  $\text{NO}_x$  emissions were reported higher when compared with diesel emission (Babu et al. 2018). Mahua oil and its various blends were prepared and the performance and emissions were investigated by Godignur et al. The study indicated that CO and HC emissions reduced as biodiesel in the blend increased (Godiganur et al. 2009). A study on orange oil biodiesel blends in engine at different compression ratios (CR) 17, 17.5 and 18:1 were conducted to check the engine performance. From the experimental findings, improved BTE and BSFC values were observed along with reduced CO and HC emissions (Karthickeyan et al. 2017). Thus, it can be concluded that limited literature is available on the study of engine performance and emission characteristics by using biodiesel obtained especially from animal waste as the feedstock. By doing this, it addresses two issues such as waste disposal management as well as finding a potential supplement to the existing fuel needs.

Thus, the present work attempts to produce biodiesel from pork lard waste which is a high cholesterol-containing fat using calcium hydroxide ( $\text{Ca}(\text{OH})_2$ ) as the catalyst, produced from sea shells. The work was carried out by oxidizing the cholesterol to fatty acid, and the resultant fatty acid was then esterified to propyl esters. The produced biodiesel was blended with commercial diesel in different proportions to check the calorific value. Based on the preliminary results obtained, the biodiesel blend having the better calorific value was used as fuel and the engine performance and emission characteristics were investigated.

In the previous work, ethyl biodiesel was produced while carrying out a direct esterification reaction (Robert & Girish 2020). The current study takes into account the chemistry that was concluded in the first research and worked towards a better fuel while using a prepared basic catalyst from a renewable source. While the first study was focused on developing a method to convert cholesterol-containing fats to biodiesel, the current work supplements the previous study by developing a better fuel with improved production yield. This study also tests the performance and emissions of the newly developed fuel in an engine, and compares the values with conventional diesel, hence proving the potential of the environmentally benign fuel. While most of the research focuses on using methyl or ethyl alcohol, the current study aims to show that isopropyl alcohol can also be used to produce biodiesel from waste animal fats. Additionally, the study also aims to show that  $\text{Ca}(\text{OH})_2$  can also be used as a basic catalyst for esterification instead of conventional KOH or NaOH. Furthermore, this research focuses on developing a fuel that would contribute lesser towards the emissions while producing a better energy output.

## MATERIALS AND METHODS

### Materials

The feedstock, pork lard fat was directly obtained from the local market in Hebri, Udupi, India. The semi-soft white solid fat was taken from the loin and the intestinal area. The solid fat was dry and heated in an open pan and the molten fat or liquid fat is collected and is used for the reaction as described elsewhere [18]. The molten pork lard rich in cholesterol was pale yellow, with a foul smell, and has a density of 0.790 g/cc. The catalyst, Seashells used for the synthesis of the catalyst was collected from the coastal area of Malpe, Udupi, India. Other reagents used in the experiments are Isopropyl alcohol (99%, Finar chemicals) and Nitric acid (Fisher chemicals) (assay 70%).

### Catalyst Preparation

The seashells collected from the seashore were washed thoroughly with distilled water to remove any sand or salt present in the shells. After the thorough wash, the seashells were dried in a hot air oven at 90°C.

The shells were subjected to calcination at 900°C for 2.5 h. Before subjecting it to calcination inside the muffle furnace, the shells were crushed using a ball mill to increase the surface area for calcination. Calcination reaction converts the calcium carbonate [ $\text{Ca}(\text{CO}_3)$ ] to calcium oxide (CaO). The obtained CaO was then mixed with an excess of water to convert CaO to calcium hydroxide ( $\text{Ca}(\text{OH})_2$ ). The slurry obtained was heated in the oven at 90°C overnight to remove moisture. The calcium hydroxide obtained was directly used in the esterification process.

### Characterization of Sea Shell Catalyst

The surface morphology of the catalyst prepared from seashells was studied using Scanning Electron Microscopy (SEM), Zeiss Company, Germany. The detection of calcium and carbon ions was carried out by Energy Dispersive X-ray (EDX) analysis.

The formation of calcium hydroxide in the catalyst was confirmed by the powder XRD technique (Rigaku X-ray diffractometer) with a high-intensity  $\text{Cu K}\alpha$  radiation ( $\lambda = 1.54 \text{ \AA}$ ) at 40 kV and 20 mA. The measurement was conducted at a  $2\theta$  angle between 10° to 80° at a scanning rate of  $2^\circ \text{ min}^{-1}$  or with  $0.0130^\circ$  increasing step size.

### Esterification

Before the esterification process, the feed which is initially a regular animal fat was heated in an open pan till the entire

caul fat melted. The remains of the fat were filtered out from the melted fat and this was used for the process.

The experimental setup consists of a 3-necked flask fitted with a reflux distillation column. One end of the three-neck is fitted with a thermometer and the other end was sealed using a glass cork. The experimental setup is shown in Fig. 1.

A given amount of pork caul fat (10 g) was taken in the 3-necked flask and was heated up to 60°C, and 1g of nitric acid was added to the fat. The reaction was allowed to carry out at 60°C for 15 min for the complete conversion of fat to long-chain fatty acids. The oxidized fat was then subjected to an esterification process with 6 g of isopropyl alcohol and 0.1 g of Ca(OH)<sub>2</sub> as a catalyst.

The required amount of the catalyst was added to the oxidized fat taken in the flask. The alcohol was separately heated to 60°C and this was added to the fat-catalyst mixture once the catalyst had completely diffused into the fat. The reaction time was found to be 6 h for complete conversion to fatty acid propyl esters.

### Purification

The propyl ester thus formed was impure with the presence of undesired products such as soap, water, and other possible side products or even excess catalyst. The reaction mixture was transferred to a decanter for gravity separation for over 6 h. This was followed by wet washing of biodiesel using warm distilled water (Atadashi et al. 2011). Washing was continued until the bottom layer produced a transparent layer. Any cloudiness in the bottom layer shows the pres-

ence of impurities in the biodiesel. The sample was allowed for gravity separation overnight as shown in Fig. 2, flask heated, and then immediately stored in airtight containers for further analysis.

### Characterization of Biodiesel

The physiochemical properties of the pork lard biodiesel (propyl ester) were calculated according to standard testing procedures prescribed under ASTM (American Standard for Testing and Materials) and IS (Indian Standard). Density (IS 1448-P16), Viscosity (IS1448), Flashpoint (IS1448-P21), Water by distillation (IS1448[P:40]:2014, and Copper corrosion (IS1448 P-15) were measured following the IS 1448 standard procedures. ASTM standards were used for evaluating properties such as Acid number (ASTM D664), the elements (ASTM D7111-2016), and the Calorific value (ASTM D4809), and later all the values were compared with the standard values. Calorific value was found using Bomb Calorimeter (Rajdhani Scientific Instruments Co., New Delhi).

The feed oil composition, oxidation of cholesterol to long-chain fatty acids, and the conversion to fatty acid propyl esters were examined and confirmed by gas chromatography (Robert & Girish 2020). The gas chromatograph-mass spectroscopy instrument (Agilent GC model 7890A and MS model 5975C MSD) equipped with a column DB 5 MS having dimensions (30 mL x 0.25 mm ID x 0.25 um film thickness) was employed for the analysis. The mass spectrometer was operated in the electron impact ionization mode

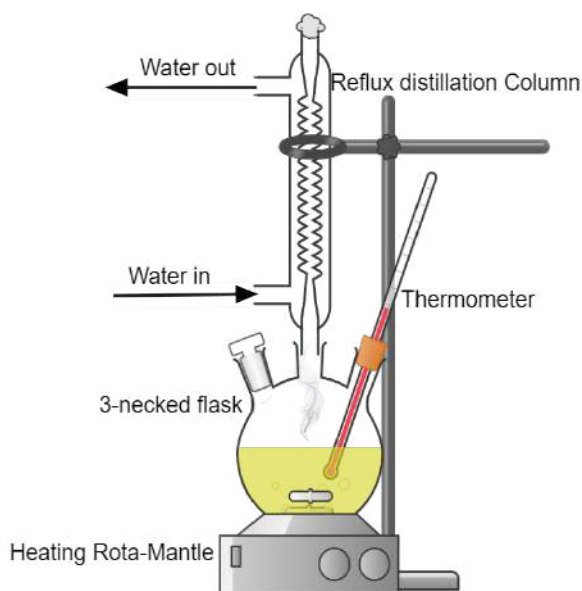


Fig. 1: Experimental setup for esterification.

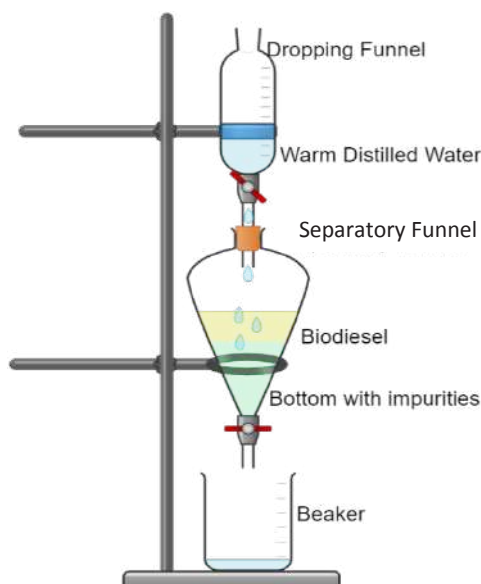


Fig. 2: Experimental setup for biodiesel purification.

at 70 eV in the scan range of 30–700 m/z. Helium was used as the carrier gas flowing at a rate of 1 mL/min. The sample was diluted with hexane and 1 $\mu$ L of the sample is injected into the instrument at an inlet temperature of 260°C. The column initial temperature was at 40°C and was later raised to 290°C at 6°C/min with a total run time of 47 min. The temperature of the transfer line and ion source was kept at a value of 300°C and 230°C respectively. Peaks obtained from the analysis were identified by comparing with standards of mass spectra from the NIST libraries 2011. The yield of biodiesel obtained after the reaction was calculated as in Eq. (4) (Nabora et al. 2019):

$$\% \text{ yield} = \frac{\text{weight of biodiesel obtained}}{\text{weight of feed oil taken}} \times 100 \quad \dots(4)$$

### Blending of Biodiesel, Engine Performance, and Emission Analysis

Various blends were prepared by adding the required amount of biodiesel to commercial diesel. The experiments were done by preparing different blends such as B20, B50, and B80. For example, B20 blending was prepared by adding 20 g of biodiesel to 80 g of diesel in a 3-necked flask and subjected to stirring for 1 hour at 60°C. Then the calorific values of all the blends were measured using the standard method (ASTM D4809). Then depending on the preliminary studies obtained from the calorific values, the B20 blend was selected for measuring engine performance and emission characteristics. Under engine performance, parameters such as brake-specific fuel consumption (BSFC) and brake thermal efficiency (BTE) were calculated. The emission characteristics such as carbon monoxide (% vol), hydrocarbon (in ppm), carbon dioxide (% vol), NO<sub>x</sub> (in ppm), and smoke (%) were measured. Moreover, the blends with a higher ratio of biodiesel will significantly increase BSFC and decrease BP and BTE (Nirmala et al. 2020), and have lower calorific values and higher densities which is not ideal for fuel (Raheman et al. 2013). The readings obtained from the engine performance and emission characteristics for the B20 blend were compared with high-speed commercial diesel (B0). These properties are measured to analyze the fuel performance when running a diesel engine in real-time.

The engine used in this experimental setup was the Kirloskar TV1 vertical model IC diesel engine having the power of 3.5kW @1500 rpm equipped with a single-cylinder, four strokes, constant speed, and water cooled. It has other features such as a cylinder bore of 87.50 mm, a stroke length of 110.00 mm, connecting rod length of 234.00 mm, a dynamometer arm length of 185.0 mm, and the CR ranging from 12:1 to 18:1 was used to test the fuel. The samples were subjected to the fuel line to test the performance and emission characteristics of B0 and B20 blends. Engine loads

were varied from 0-12Kg to perform the test on the fuel and its blend. The fuels were loaded into the engine's fuel line without any modifications and the engine was run at CR of 17.5 and 18 configurations. The engine was run for 3-5 min at each load to attain stability and then the readings such as engine speed, emission parameters, and fuel consumed were noted down. The exhaust gas analyzer (AVL DiGas 444) was used to measure the emission parameters such as HC, CO, CO<sub>2</sub>, NO<sub>x</sub>, and oxygen and the smoke meter (AVL 437C) was used for measuring the opacity of polluted air in diesel exhaust gases i.e. smoke of the fuels.

### CALCULATIONS

The parameters BSFC and BTE were calculated using the formulae

$$\text{Engine power (kW)} = 2\pi NT \times 10^{-3} \quad \dots(5)$$

$N$  is engine speed (revolutions per second)

$$T = (\text{load in Kg} * 9.81 * r) \quad \dots(6)$$

$T$  is engine torque (N m),  $r$  is dynamometer arm length

$$\text{Fuel mass flow rate} \left(\frac{g}{h}\right) = 3600 \times \text{fuel vol flow rate} \left(\frac{ml}{s}\right) \\ \times \text{fuel density} \left(\frac{g}{ml}\right) \quad \dots(7)$$

$$\text{BSFC} = \frac{\text{Fuel mass flow rate}}{\text{Engine power}} \quad \dots(8)$$

$$\text{BTE} = \frac{3600 \times C_p}{\text{BSFC} \left(\frac{g}{kWh}\right)} \quad \dots(9)$$

$C$  is the calorific value of the fuel (MJ/Kg)

## RESULTS AND DISCUSSION

### Characterization of Sea Shell Catalyst

The scanning electron microscopic image of the calcium hydroxide catalyst is shown in the figure. The pictures were taken at 1 $\mu$ m (40.0KX). Fig. 3A shows the images of calcium carbonate as observed similarly by (Tshizanga & Funmilayo 2017). Fig 3B shows the produced calcium hydroxide catalyst. The comparison between the two images shows the change in morphology between the raw material and prepared catalyst.

From EDX analysis, it was found that calcium is present as the main component of the catalyst. The higher percentage of oxygen shows the presence of calcium hydroxide, calcium oxide, and some traces of unconverted calcium carbonate which is shown in Fig. 4.



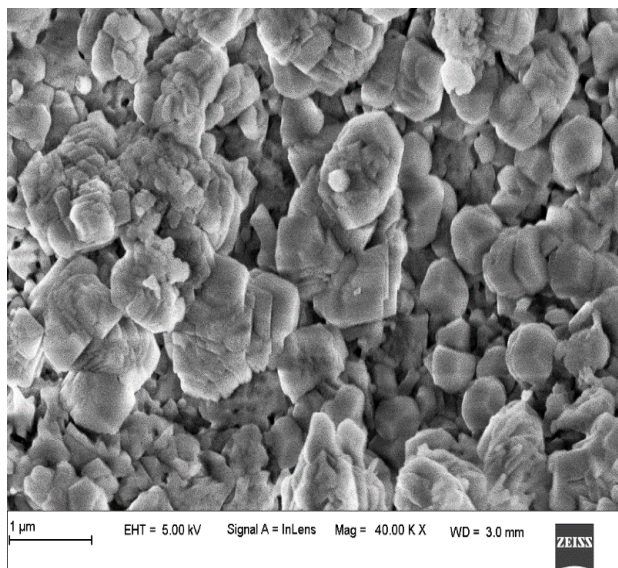


Fig. 3A: SEM image of seashell before calcination

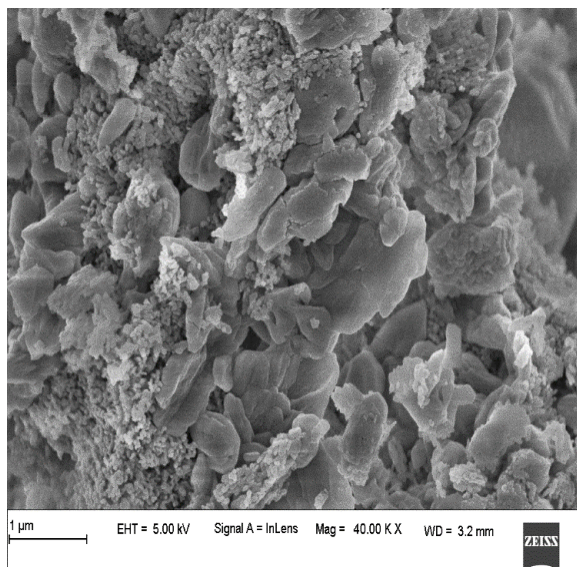


Fig. 3B: SEM image of the seashell catalyst

Fig. 5 shows the XRD patterns of the calcium hydroxide catalyst prepared from seashells. It can be seen that the peaks obtained from the XRD patterns are matching with those reported from the ICSD standard diffraction file. The distinct peaks were observed for the catalyst between  $2\theta=10-80^\circ$ . The intensities of the major peaks for calcium hydroxide (ICSD Reference No:01-081-2041) namely [001], [100], [101], [102], [110], and [111] corresponds to the position at peaks  $18.05^\circ$ ,  $28.70^\circ$ ,  $34.11^\circ$ ,  $47.13^\circ$ ,  $50.84^\circ$  and  $54.39^\circ$  respectively with hexagonal structure. This confirmed the presence of calcium hydroxide in the prepared catalyst and similar kinds of results were reported in the work (Chingakham et al. 2019, Margaretha et al. 2012). The component

calcium carbonate (ICSD Reference No:01-072-1907) was found at  $39.37^\circ$ ,  $43.12^\circ$  and  $48.15^\circ$  with trigonal configuration. Other minor components quartz low silica oxide (ICSD Reference No: 01-070-2538) at  $59.70^\circ$  with hexagonal structure and calcium oxide (ICSD Reference No:01-075-0264) at  $32.38^\circ$  with the cubic structure were observed.

#### Effect of Reaction Parameters

The yield of biodiesel produced depends upon the parameters such as the amount of catalyst, alcohol to oil ratio, the temperature of the reaction, and the time taken to complete the reaction. To produce a maximum yield, the reaction has to be optimized while consuming fewer reagents to keep

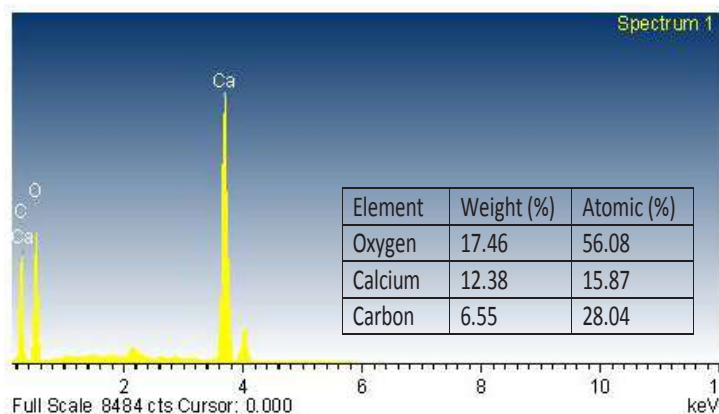


Fig. 4: EDX analysis of the sea shell catalyst.



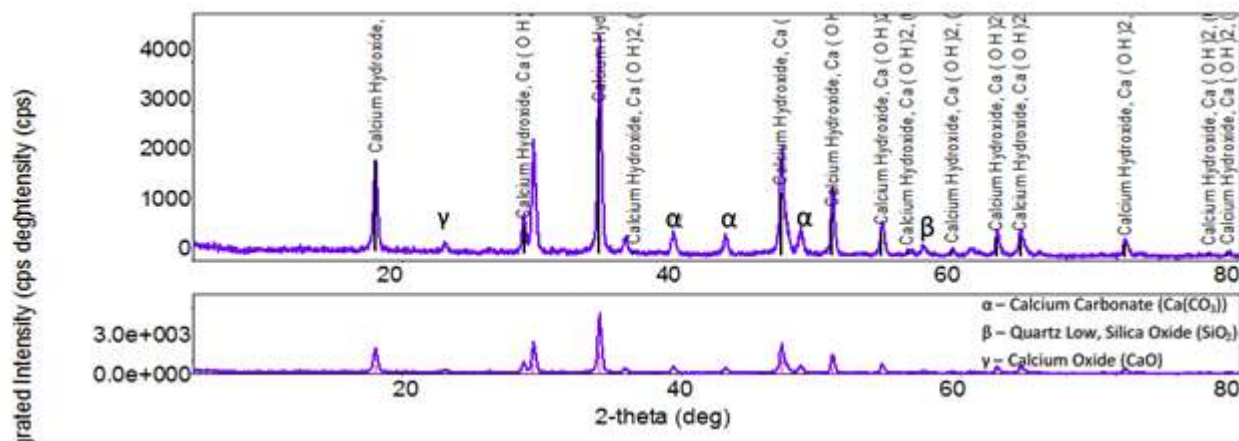


Fig. 5: XRD analysis of calcium hydroxide catalyst.

the cost and energy of production as low as possible. The range of the parameters for esterification has been selected from the preliminary experiments. It has to be considered that all the reagents for the reaction have been measured in terms of mass rather than volume. Since the experiments were carried out over a long period of time due to external weather conditions, the volume of the reagents could vary. Hence, the mass has been taken as the base of measurement, since it would be more reliable.

To study the significance of each reaction parameter, experiments were carried out by varying one parameter while keeping the other parameters constant (Fadhil et al. 2017).

### Effect of Propyl Alcohol

The influence of propyl alcohol on biodiesel yield was observed by varying the amount of alcohol to oil ratio in the range of 3:10 to 8:10. The temperature was maintained at 68-70°C for 6 h and 0.1 g of  $\text{Ca}(\text{OH})_2$  catalyst was used. It was observed that as the amount of alcohol increased the yield also increased up to 95% at an alcohol to oil ratio of 6:10. This is because the increase in alcohol continuously converts fat to propyl esters (Saravanan et al. 2019). It was found that increasing the amount of alcohol beyond 6g shows a small decrease in yield as the propyl esters are being formed as shown in Fig. 6.

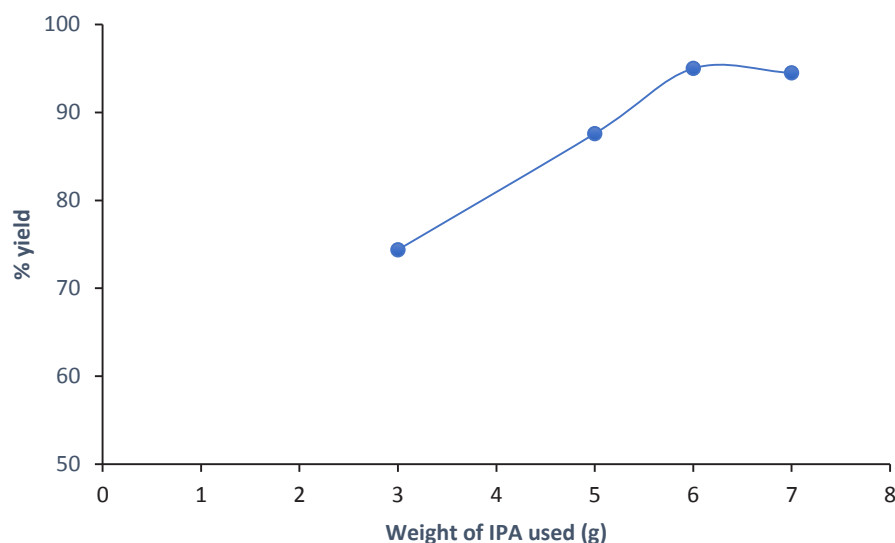
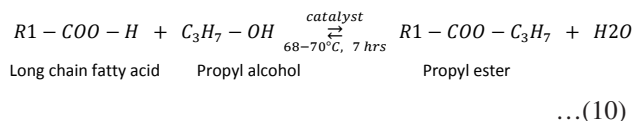


Fig. 6: Effect of propyl alcohol on esterification.



This small decrease in yield may be because of the shift in reaction to attain an equilibrium (Maneerung et al. 2016). Another possible explanation for this decrease in yield is a potential interaction between excess isopropyl alcohol and the catalyst which would decrease the amount of catalyst available for the reaction (Asri et al. 2018).

### Effect of Catalyst Loading

The optimum dosage of catalyst determines the maximum extent of biodiesel conversion. The effect of catalyst loading was observed by varying the amount of  $\text{Ca}(\text{OH})_2$  used from 0.1 to 0.5 g with respect to 10 g of oil under esterification at 68-70°C for 6 h. A maximum yield of 92% was observed at 0.1 g of catalyst as shown in Fig. 7. For every increase after 1 g, the yield decreased significantly to an extent where no yield was observed as thick viscous mass and emulsions were found. The decrease in yield could be due to poor diffusion of reagents (Viola et al. 2012). This poor diffusion is due to the increased viscosity of the mixture in the presence of an excess catalyst (Ezebor et al. 2014). Hence, there is a significant mass transfer resistance that affects the reactant system. Similar findings were observed by the authors on the effect of catalyst loading (Ashok et al. 2018). Since the reaction deals with fatty acids and not triglycerides, the formation of soap can be ruled out (Zhang & Jiang 2008).

### Effect of Temperature

The effect of temperature on esterification was carried out with 10g of oil, 6g of IPA, and 0.1 g of  $\text{Ca}(\text{OH})_2$  for 6 hours. The temperature was varied between 30°C and 80°C and their corresponding yields were observed in the experiments. With an increase in temperature up to 65-70°C, there was a marginal increase in yield. It was observed that 65-70°C was optimum and the maximum yield of 95.6% was reported. It was also observed that beyond 70°C the yield decreased noticeably. The readings are reported in Fig. 8.

The initial increase in yield is because of the accelerated diffusion of the catalyst into the reactant system (Ning & Niu 2017). This is because the mass transfer rate is directly proportional to temperature (Stamenković et al. 2008). Further heating of the reaction system beyond 70°C causes the vaporization of IPA in the reaction system as its volatile even under room temperature. This causes a lowering of IPA concentration in the reaction system which leads to poorer conversion and hence a low yield was obtained. A similar trend of results was reported in the work (Maneerung et al. 2016, Ning & Niu 2017, Ashok et al. 2018).

### Effect of Reaction Time

The effect of reaction time on biodiesel yield was investigated by varying the reaction time between 4hr to 10 h and by taking 10 g of oil, 6 g of IPA, and 0.1 g of  $\text{Ca}(\text{OH})_2$  catalyst. As the reaction time increased, the yield increased to give a maximum of 95.6% at 6 hours. Beyond 6 hrs, there was a

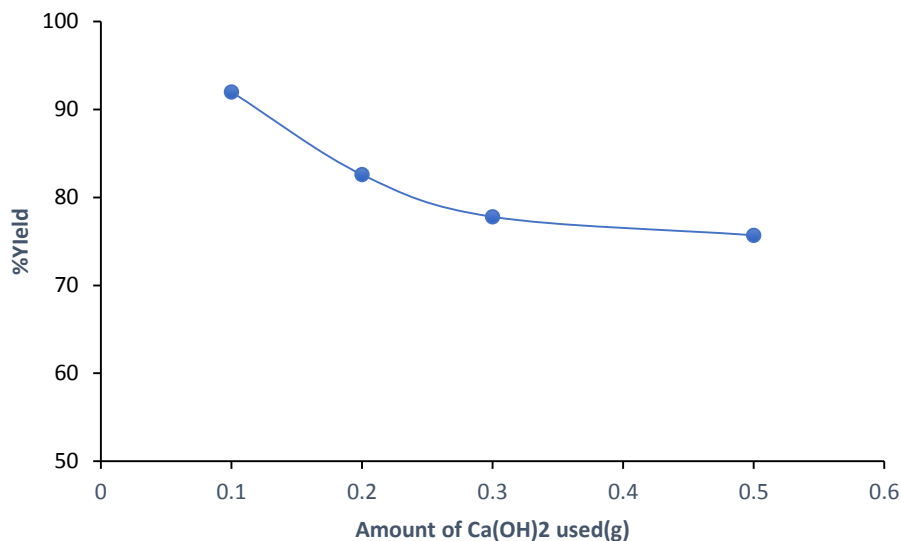


Fig. 7: Influence of catalyst loading on esterification.

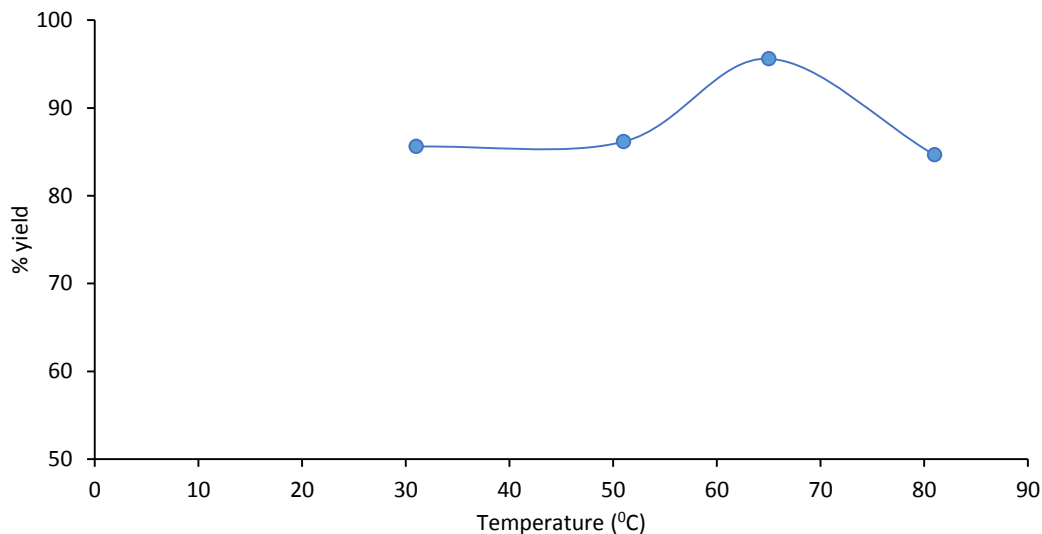


Fig. 8: Effect of temperature on transesterification.

small decrease in yield and thereafter it gave constant yield. The effect of reaction temperature on yield is represented in Fig. 9.

The small decrease in yield may be due to the equilibrium of the system. This may cause the reaction to shift towards the reactant side (Nabora et al. 2019) and in turn, decrease the number of propyl esters to maintain equilibrium. The yield values remained consistent beyond 6 hrs showing that the system has reached equilibrium and all possible conversions had taken place (Asri et al. 2018). Similar results were discussed in the work (Niju et al. 2015).

### Characterization of Biodiesel

#### Gas chromatography analysis of biodiesel (propyl esters):

GC results provide peaks that help to identify different compounds present along the x-axis, the retention time. This qualitative analysis provides a technique to test the purity of the produced biodiesel and most importantly, a method to track the reaction conversion at each step of the production methodology (Gupta et al. 2018). The presence of cholesterol in the feed and the oxidation of cholesterol to fatty acids are reported as well with relevant GC-MS support. The GC profile for the fat has been presented in table 1. Similarly,

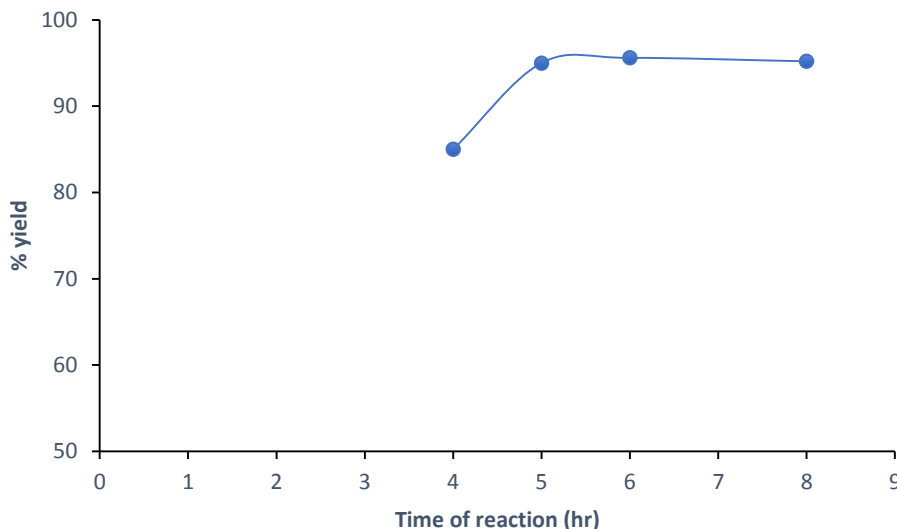


Fig. 9: Influence of reaction time on esterification.

Table 1: Feed oil composition obtained using a gas chromatograph.

Sl.No.	Feed oil composition	Molecular formula	Molecular weight	Content [%]	Retention time, min
1	Hydroperoxide, 1-methylhexyl	C <sub>7</sub> H <sub>16</sub> O <sub>2</sub>	132.2	5.704	4.166
2	2-Heptenal, (E)-	C <sub>7</sub> H <sub>12</sub> O	112.16	4.510	7.618
3	Nonanal	C <sub>9</sub> H <sub>18</sub> O	142.2	2.250	11.408
4	2-Decenal, (E)-	C <sub>10</sub> H <sub>18</sub> O	154.24	6.686	15.304
5	2,4-Decadienal	C <sub>10</sub> H <sub>16</sub> O	152.23	8.366	16.629
6	Heptadecane, 2,6,10,14-tetramethyl-	C <sub>21</sub> H <sub>44</sub>	296.57	1.394	20.581
7	E-14-Hexadecenal	C <sub>16</sub> H <sub>30</sub> O	238.40	1.565	24.102
8	3-Trifluoroacetoxydodecane	C <sub>14</sub> H <sub>25</sub> F <sub>3</sub> O <sub>2</sub>	282.34	2.122	31.856
9	Butanamide	C <sub>4</sub> H <sub>9</sub> NO	87.12	2.302	32.460
10	Hexadecanoic acid, 2-hydroxy-1-(hydroxymethyl)ethyl ester	C <sub>19</sub> H <sub>38</sub> O <sub>4</sub>	330.50	5.577	34.227
11	Unknown			1.973	36.608
12	E,E-1,9,17-Docosatriene	C <sub>22</sub> H <sub>40</sub>	304.6	7.498	36.690
13	RT Cholesterol	C <sub>27</sub> H <sub>46</sub> O	386.65	50.053	44.521

the peaks from the ester GC profile were analyzed and the presence of Isopropyl Palmitate, i-Propyl 9-octadecenoate, and Isopropyl stearate in major proportions were confirmed in Fig. 10. This finding was in accordance with the expected chemical reaction presented in Eq. (10). The conversion of cholesterol to fatty acids and further conversion to corresponding propyl esters are reported in Tables 2 and 3 respectively. The average molecular weight of the biodiesel was estimated to be 316.54 g.mol<sup>-1</sup>.

#### Determination of physicochemical properties of biodiesel:

The different properties of the produced biodiesel were determined as per standard procedures and are shown in Table 4. The properties such as density, viscosity, water content, acid number, flash point, presence of sodium, potassium, and calorific value were evaluated.

Flashpoint is very significant from the safety aspects when storage and transportation of fuel are under considera-

Table 2: The composition of nitric acid-treated feed oil using gas chromatography

Sl.No.	Feed oil composition	Molecular formula	Molecular weight	Content [%]	Retention time, min
1	Pyridine	C <sub>5</sub> H <sub>5</sub> N	79.10	6.03	4.268
2	n-Hexadecanoic acid	C <sub>16</sub> H <sub>32</sub> O <sub>2</sub>	256.4	17.28	19.898
3	2-octyl-Cyclohexane	C <sub>14</sub> H <sub>28</sub>	196.3	3.39	21.575
4	9-Octadecenoic acid, (E)-	C <sub>18</sub> H <sub>34</sub> O <sub>2</sub>	282.4	46.65	21.63
5	Octadecanoic acid	C <sub>18</sub> H <sub>36</sub> O <sub>2</sub>	284.4	16.58	21.77
6	Allyl octadecyl ester	C <sub>23</sub> H <sub>42</sub>	382.5	5.93	22.34
7	9-Octadecenal, (Z)-	C <sub>18</sub> H <sub>34</sub> O	266.4	4.15	23.89

Table 3: Fatty acid propyl ester composition from GC-MS analysis

Sl.No.	Fatty acid propyl ester composition	Molecular formula	Molecular Weight [g.mol <sup>-1</sup> ]	Fatty acid ester [%]	Retention Time, min
1	Isopropyl Palmitate	C <sub>19</sub> H <sub>38</sub> O <sub>2</sub>	298.5	27.638	21.086
2	i-Propyl 9-Octadecenoate	C <sub>21</sub> H <sub>40</sub> O <sub>2</sub>	324.5	51.338	22.692
3	Isopropyl stearate	C <sub>21</sub> H <sub>42</sub> O <sub>2</sub>	326.6	21.024	22.923



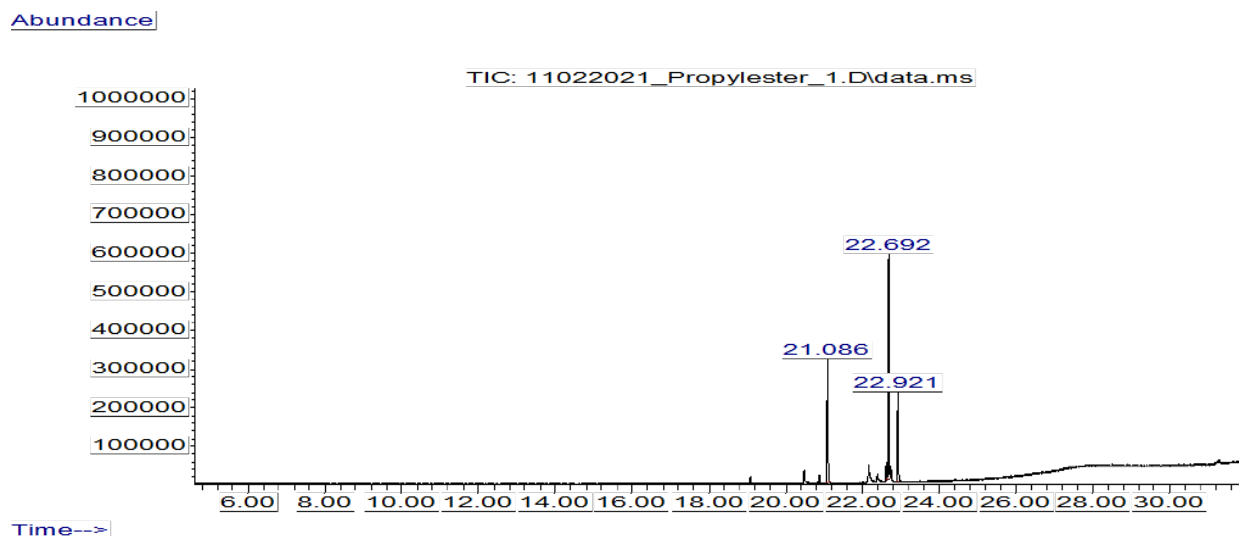


Fig. 10: GC-MS profile of propyl esters.

tion. The higher flashpoint for a fuel shows that the fuel has a larger storage capacity and less risk of fire accidents (Chavan et al. 2017, Sánchez-Arreola et al. 2019). The acid value shows the corrosiveness of the fuel because the engine and storage tanks having fuels with high acid values corrode fast (Al-Muhtaseb et al. 2018). The increase in viscosity affects fuel injection into the engine chamber and this affects the quality of combustion (Mazaheri et al. 2018, Sánchez-Arreola et al. 2019). The moisture content is to be maintained as low as possible to enhance the combustion (Chavan et al. 2017). All the physicochemical properties evaluated were within the range specified by the Standard procedures and have satisfied ASTM standards.

**Determination of calorific value of biodiesel and its blends:** Calorific value is a measure of the fuel's ability to generate energy on combustion. Therefore, for a given amount of fuel, the power output will be high for fuel with a high calorific value (Kakati et al. 2017). The calorific value of fuel affects the BSFC and BTE of the diesel engine (Jena et al. 2010).

From the experiments, it could be seen that the calorific value of B100 was  $35.7 \text{ MJ.kg}^{-1}$  when compared to diesel which was  $43.6 \text{ MJ.kg}^{-1}$  Fig. 11. The calorific value was in accordance with the standard EN 14213 range which is  $35 \text{ MJ.kg}^{-1}$  (Shankar et al. 2017). As the ratio of biodiesel in the blend increases, the calorific value

Table 4: Physico-chemical properties of biodiesel.

Sl.No.	Property	Units	Method	Result	Std Range
1	Density at 15.0°C	$\text{g.mL}^{-1}$	IS 1448-P16	0.863	0.86 - 0.88
2	Kinematic viscosity at -40°C	cSt	IS 1448	11.93	8to12
3	Flash point	°C	IS 1448 - P21	52	35to65
4	Calorific Value	$\text{MJ/Kg}$	ASTM D4809	35.7	>35
5	Water by distillation	%	IS 1448 [P:40]:2014	1.1	1.1
6	Copper corrosion (3h at 50°C)		IS 1448 P-15	1a	Not worse than class 1.
7	Acid number (Inflection end -point)	$\text{mg KOH.g}^{-1}$	ASTM D664 (Method A)-2017a	9.3	5 to 20
8	Elements by ICP		ASTM D7111-2016		1
	Sodium	$\text{mg.kg}^{-1}$		<1	
	Potassium	$\text{mg.kg}^{-1}$		<1	

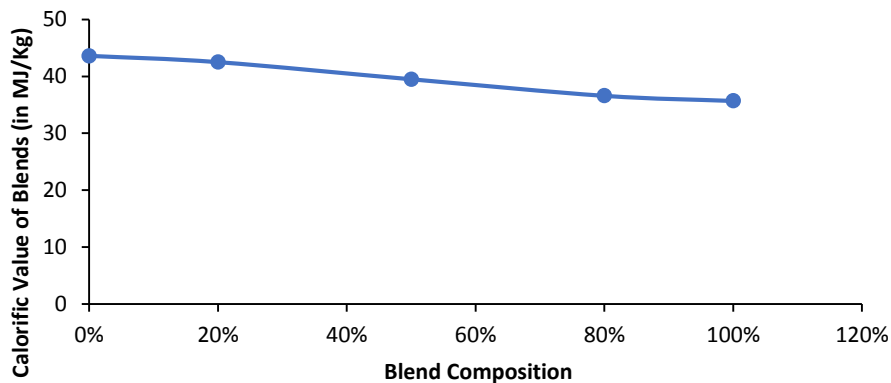


Fig. 11: Calorific values of biodiesel blends.

decreases. Similar conclusions were drawn by researchers (Mofijur et al. 2015). Although the calorific value decreased with blend ratio, the B20 blend had a closer and comparable value when compared to diesel. Hence B20 was selected for engine performance and emission analyses. The decrease in calorific value is because of the increase in oxygen content (Patel & Sankhavara 2020) and frictional losses due to the increased density of the fuel mixture (Dash et al. 2010.).

### Engine Performance Analysis

Brake-specific fuel consumption (BSFC) and brake thermal efficiency (BTE) are the parameters used to quantify the significance of the fuel performance in the engine.

**BSFC:** An ideal engine should produce high brake power while consuming less fuel (Zaher & Soliman 2015). Generally, as the load on the engine increases, the BSFC value decreases. This is because BSFC is the ratio of total fuel consumption to brake power and as the load increases brake power increases more generously than the total fuel consumed and thus bringing down the overall ratio of BSFC (Nirmala et al. 2020, Sureshkumar et al. 2008). From the results, it could be seen from Fig. 12A, that at a CR of 17.5, BSFC for all loads was higher than or nearly equal to that of commercial diesel B0. A similar trend of results was reported by the authors in previous works (Sureshkumar et al. 2008, Teoh et al. 2019). It could be observed that at a load of 12 kg, the readings for B20 and B0 were almost coinciding with an increase of just  $16\text{g.KWh}^{-1}$ . Although the BSFC at CR17.5 were high for B20, the difference between the readings was not more than an average of 3.7%.

However, at CR 18 the B20 blend produced better BSFC when compared to B0 as shown in Fig. 12B. There was an average decrease of 5.1% BSFC over the range of loads. A similar trend of results with lower BSFC readings was

reported by the authors (Asri et al. 2018). Lower BSFC describes the fuel to be more efficient during burning with improved combustion characteristics (Rosha et al. 2019). At CRs biodiesel blends perform better than commercial diesel as combustion characteristics increases due to improved mixing of the fuel and air (Rosha et al. 2019).

Another possible reason for the lower BSFC may be the synergistic effect of biodiesel with diesel. It was justified that, the oxygen present in the biodiesel must have helped the overall blend achieve better combustion (Raheman et al. 2013). On the other hand, few researchers explained that the BSFC increases as a result of leaner combustion due to the presence of increased oxygen content in the blend. When the combustion becomes extra lean, more fuel may be required to achieve a given power output (Kadir et al. 2020). The present work produced biodiesel which consists of esters in the range C16-C20 when compared to other works, the amount of oxygen does not increase enormously when the blend ratio increases. Therefore, it can be concluded that the increase in oxygen in B20 blend is ideal enough to improve the combustion characteristics at higher CR and also not contribute to extra lean combustion.

**BTE:** It is the ratio of total brake power to the chemical energy from the fuel (Mishra et al. 2020). It evaluates the potential of a given fuel in transforming its chemical energy into useful work (Sivaramakrishnan 2018). It was observed that BTEs were at an average of 1.1% less for B20 when compared to B0. The small difference in BTE is due to the lower calorific value and higher density of the B20 blend. However, as the load increases, the BTE of B20 was coinciding with B0 and at the highest load of 12 kg, the value was higher for B20 (BTE(B20)- 26.79%, BTE(B0)- 26.62%) (Fig. 13A). This is because of the reason that at higher loads, BTE increases because of increased brake power (Sundar & Udayakumar 2020).

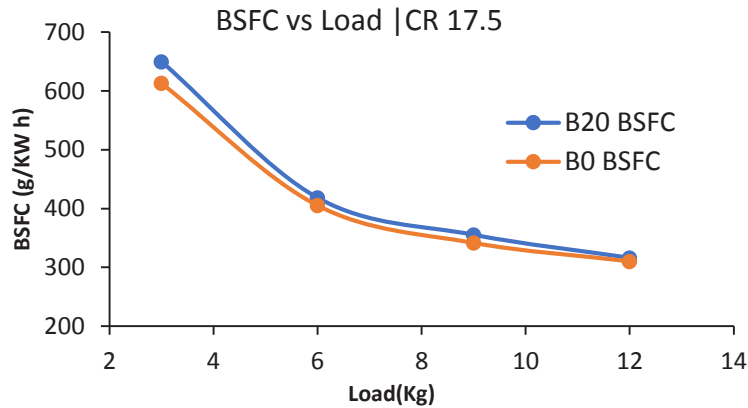


Fig. 12A: BSFC of B20 and B0 for varying Loads at CR 17.5.

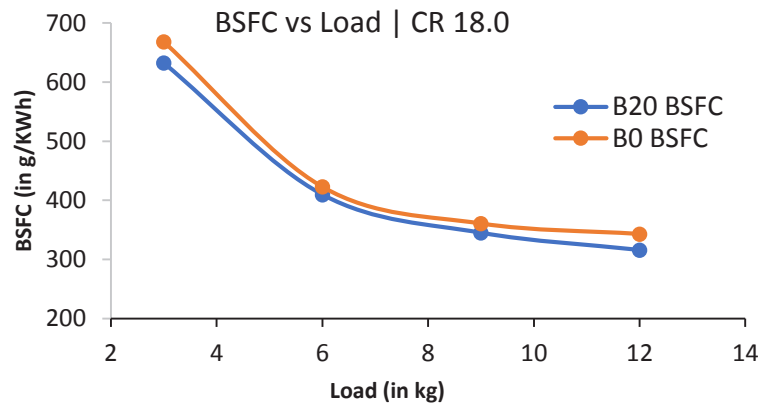


Fig. 12B: BSFC of B20 and B0 for varying Loads at CR 18.

For CR of 18, BTE was observed to be higher for B20 than commercial diesel B0 for all the loads. There was an average increase of 8.2% on all loads and as discussed with respect to CR of 17.5, at a maximum load of 12 Kg highest increase in BTE was observed (BTE(B20)- 26.80%, BTE(B0)- 24.06 %) as shown in Fig. 13B. This increase in thermal efficiency at higher CR is because of the improved combustion due to the increase in cylinder temperature and expansion work (Dash et al. 2020).

### Exhaust Emission and Combustion Analysis

The exhaust gas from the engine during the B20 and B0 run was analyzed for its emission characteristics ranging from the composition of the gaseous mixture and smoke opacity. The significance of these analyses is aimed to prove that the current fuel under study contributes lesser towards the emission of greenhouse gases and air pollution. Researchers have shown that even low blends of biodiesel can bring down the emission to a significant level (Mofijur et al. 2016).

Anderson & Weinbach (2010) had shown that although there was a slight increase in fuel consumption for the biodiesel blend, there could be a potential decrease in CO<sub>2</sub> emissions and it was an appreciable finding. Moreover, the B20 blend had comparable calorific value with commercial diesel it was subjected to emission analyses as well.

**CO and CO<sub>2</sub> emissions:** Fig. 14A and Fig. 14B show the combined CO and CO<sub>2</sub> percentage emissions over varying loads at CR 17.5 and 18 respectively. CO emission corresponds to incomplete combustion i.e., partial-oxidation of the fuel. Over the ranges of load for both CRs, the CO emission for the blend B20 was very much less than that of pure diesel B0. At CR 18, the analyzer recorded an average of 75% reduction in CO emission when compared to CR 17.5, which was 46%. The reduced CO emission is because the increased biodiesel ester composition enriches the fuel with more oxygen. Since these extra oxygen molecules promote further oxidation, there will be an improvement in combustion characteristics with the increase in blend ratio (Tüccar et al. 2014).

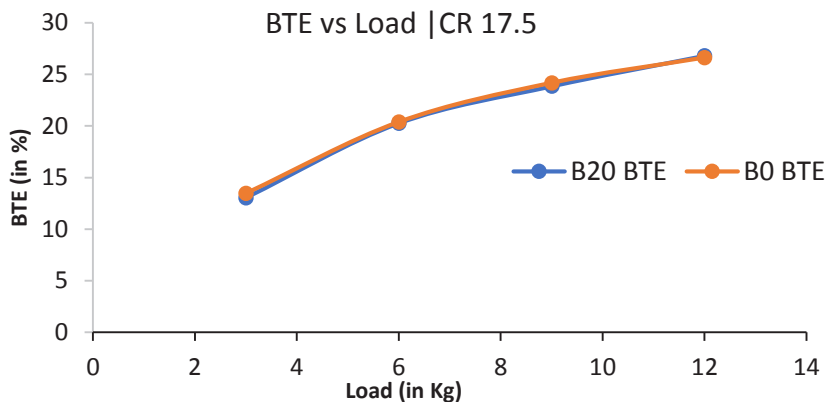


Fig. 13A: Variation of BTE with increasing loads at CR 17.5.

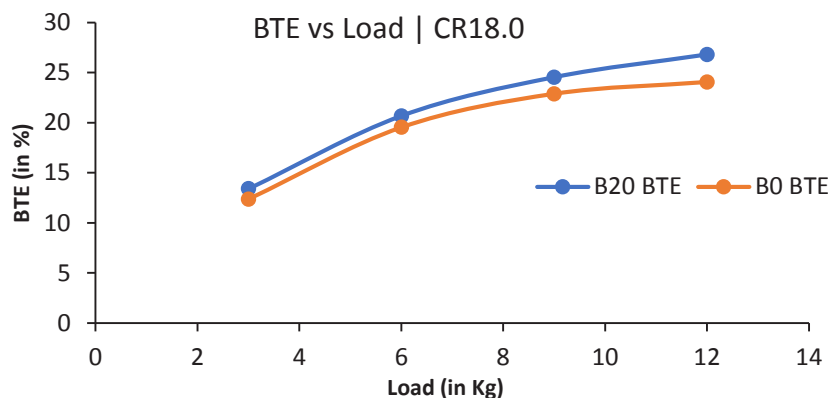


Fig. 13B: Variation of BTE with increasing loads at CR 18.

Furthermore, in comparison of these emissions over CRs, it could be concluded that at a higher CR of 18.0, both CO and CO<sub>2</sub> emissions were appreciably lesser than the emissions at a CR of 17.5. At higher CRs as discussed earlier, the pressure, as well as the temperature in the cylinder, is relatively high.

Hence, combustion characteristics are enhanced due to this elevation in temperature (Kaisan et al. 2017). With respect to CO<sub>2</sub> emissions, at CR 17.5 an average reduction of 42.2% was observed whereas, at CR18, it was recorded as 41.2%. From the above results obtained from CR 17.5 and CR 18, it could be proved that blending has decreased the overall CO<sub>2</sub> and CO emissions. The reduced CO<sub>2</sub> emissions are because of the decrease in carbon atoms present in the fuel blend compared to diesel (Babu et al. 2018).

**NO<sub>x</sub>:** NO<sub>x</sub> corresponds to different oxides of Nitrogen. It was reported by the researcher that most biodiesel and its blends produce NO<sub>x</sub> emissions which are more than that produced by commercial diesel (Nirmala et al. 2020). Biodiesel contains more oxygen and this sums up to a better and improved combustion. Hence, more NO<sub>x</sub> emissions are

recorded due to this increased combustion (Imdadul et al. 2017). Similar observations were recorded in the present study as given in Fig. 15.

At higher CRs, as concluded earlier with respect to CO emissions, there is an increase in temperature and therefore, combustion advances, and more NO<sub>x</sub> gases are released (Rahman et al. 2014). Similar findings were observed in the present work as well. As a general trend for all CRs, with an increase in load, NO<sub>x</sub> emissions increase due to increased fuel consumption at higher loads (Nguyen et al. 2020).

Although NO<sub>x</sub> emissions are recorded to be higher for B20 at both CRs, the magnitude of the increase may not be accounted is considering the emissions are in ppm levels. For CR 17.5 and 18.0, the average increase in NO<sub>x</sub> emissions is 0.25% and 3.35% respectively signifying that NO<sub>x</sub> emissions for B20 and B0 are comparable.

**HCs:** The emission of lesser hydrocarbon (HC) corresponds to better and cleaner combustion (Imdadul et al. 2017, Godiganur et al. 2009). HC at all loads and CRs are lower for the B20 blend than for B0, and the reason for this decrease



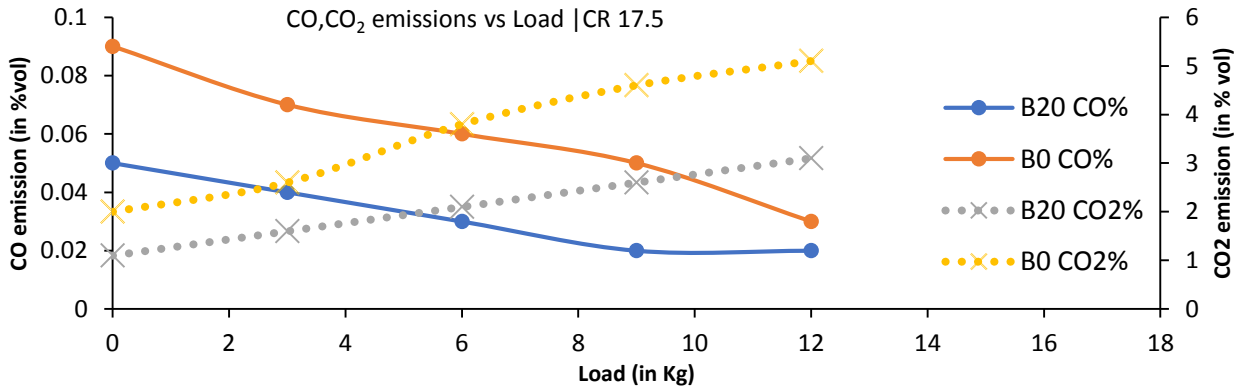


Fig. 14A: CO and CO<sub>2</sub> emissions with increasing load at CR17.5.

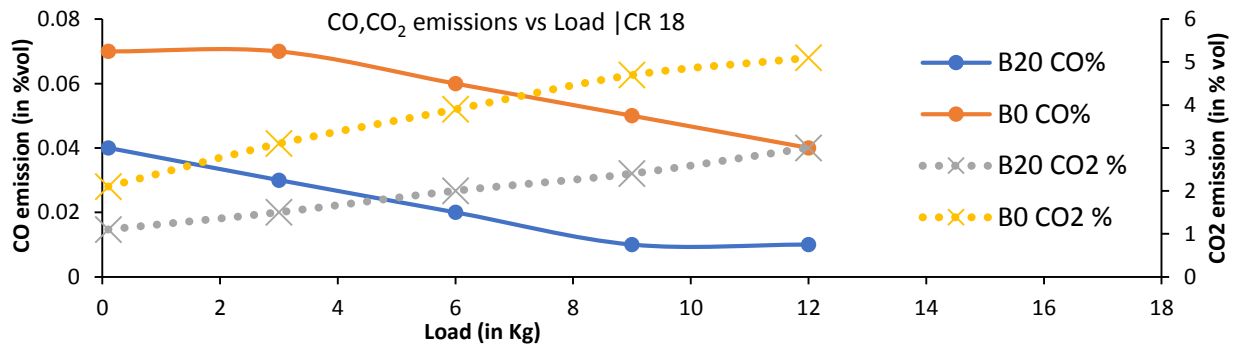


Fig. 14B: CO and CO<sub>2</sub> emissions with increasing load at CR 18.

attributes to the complete or enhanced combustion of the fuel mixture (Rahman et al. 2013). With the increasing amount of biodiesel in the blend, the concentration of oxygen increases.

es. Therefore, enhanced combustion is observed due to the better oxidation of hydrocarbons (Sivaramakrishnan 2018). As load increases, for all CRs, the HC emission increases

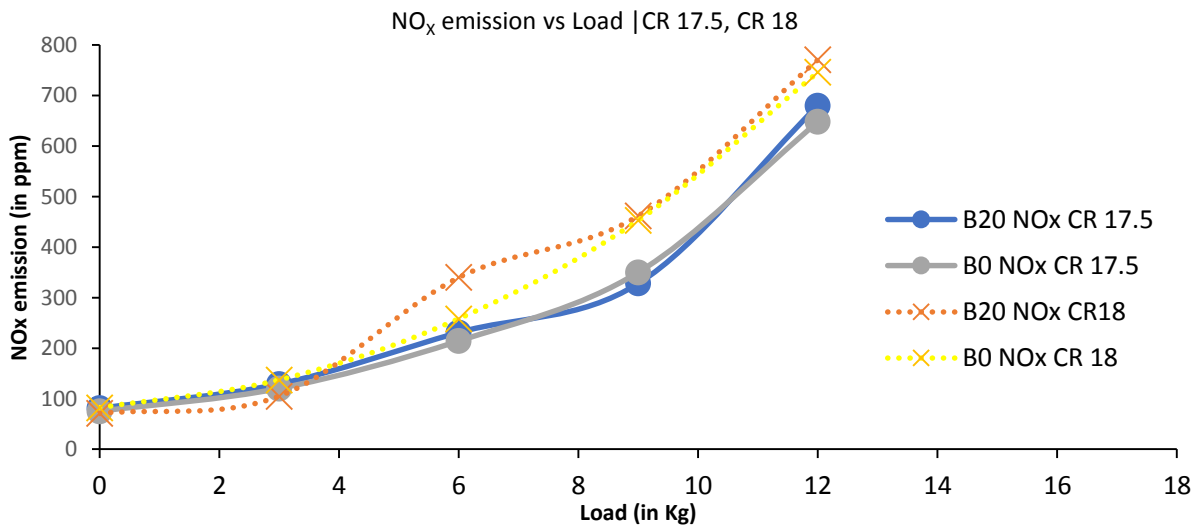


Fig. 15: NO<sub>x</sub> emissions with varying loads at CR 17.5 and CR18.

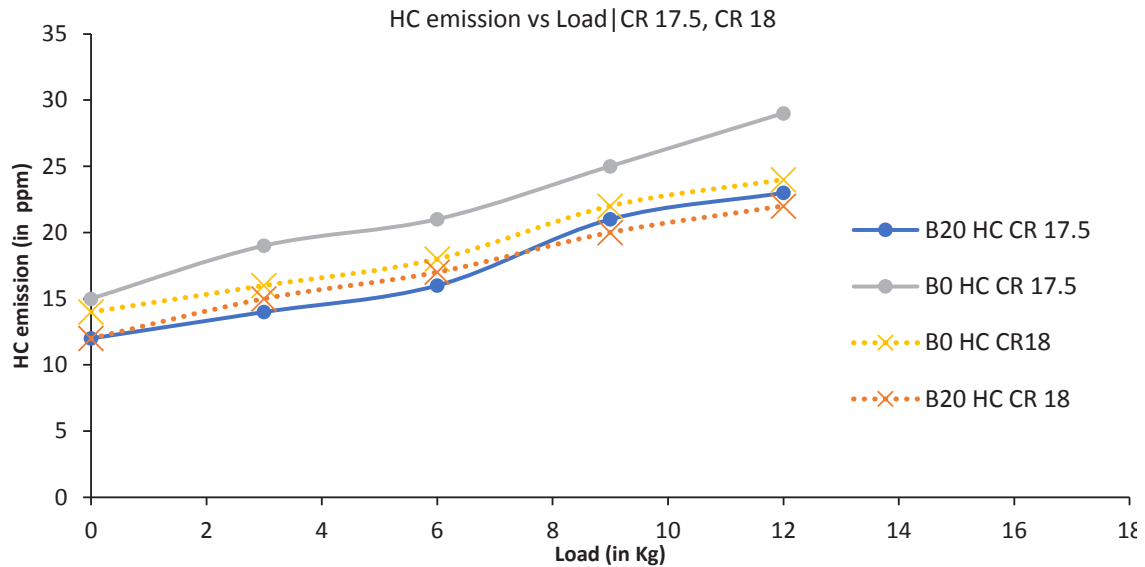


Fig. 16: Hydrocarbon emission with increasing load at CR 17.5 and CR 18.

significantly. To maintain the engine speed at higher loads, more fuel is consumed. Hence more combustion takes place resulting in the release of more hydrocarbons irrespective of fuel blend. From the data reported in Fig. 16, it could be concluded that at CR 17.5 and CR 18, there were an average decrease of 21% and 9% HC emissions respectively. It is also very important to observe that at CR 18, the HC emissions were lower than that at CR 17.5. The reason behind this observation is common to those reported earlier under other emission parameters as elevated temperature and pressure contribute towards better combustion.

**Smoke Opacity:** The lack of air or oxygen in the combustion chamber causes smoke during combustion. In addition to this, an increased C/H ratio in fuel and accumulation of fuel can also cause increased smoke in the chamber (Jeevanantham et al. 2019). The variation in Smoke Opacity with increasing loads is presented in Fig 17. It could be observed that with an increase in load, the smoke opacity also increases. It was also observed that the smoke opacity for B20 was lesser compared to B0 for all CRs. An average decrease of 19.3% and 32.7% in smoke opacity was found between B0 and B20 at CR 17.5 and CR 18 respectively. This decrease

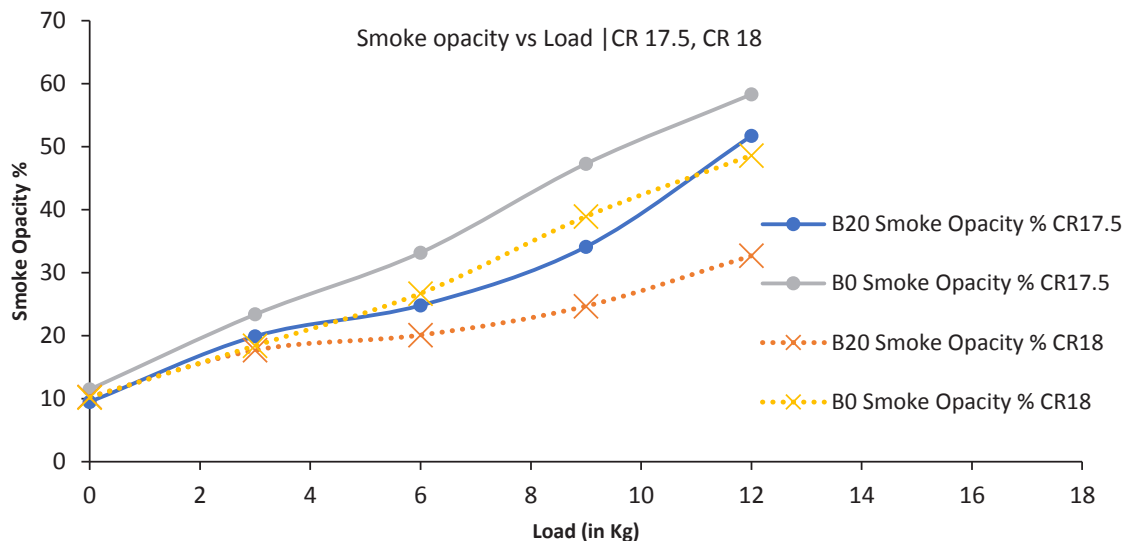


Fig. 17: Smoke opacity with varying loads at CR 17.5 and CR 18.

between B0 and B20 is because of the oxygenated fuel mixture as discussed earlier as well as in the work (Kakati & Gogoi 2016). The enrichment of oxygen in fuel facilitates combustion and the presence of more oxygen oxidizes further soot in the combustion chamber (Can 2020, Rosha et al. 2019). As far as CRs are concerned, smoke opacity decreased with increased CR from 17.5 to 18.

## CONCLUSION

Waste pork fat from the slaughterhouse was used as the feedstock for producing biodiesel. Due to the presence of high cholesterol content, the traditional method of producing biodiesel could not be carried out because of the absence of triglycerides. Hence, an economical way of producing biodiesel using seashells as a potential renewable catalyst was explored. The presence of calcium hydroxide in the produced catalyst was confirmed through XRD and FESEM-EDX analysis. The idea behind  $\text{Ca}(\text{OH})_2$  as the catalyst proves the chemistry that any basic compound with available  $\text{OH}^-$  ions can act as the catalyst. This significantly means that any potential source with the ability to produce a basic compound can be used as the catalyst. The influence of operating parameters such as alcohol to oil ratio, temperature, amount of catalyst, and reaction time on the biodiesel yield was investigated. From the esterification reaction, the maximum yield of 95.6% was obtained and the optimum conditions were found to be alcohol to oil ratio of 6:10, 0.1 g  $\text{Ca}(\text{OH})_2$  catalyst, temperature 65-70°C, and reaction time of 6 h. The presence of propyl esters in the produced biodiesel after esterification was confirmed through the peaks obtained from GC-MS analysis. Since the biodiesel produced had promising and satisfactory parameters in accordance with ASTM standards, further investigations were required to check the potential of biodiesel blending. Hence the produced B20 blend showed a similar calorific value to that of commercial diesel (B0). The promising B20 blend was further subjected to engine tests to analyze its performance and emission characteristics.

During the investigation, different operating conditions such as variable loads and CR of the engine were tested with the B20 blend as the fuel and compared with B0. The experimental findings portray the B20 blend as a promising fuel and the results are reported as follows.

The BSFC at CR 18 was lower by 5% for the B20 blend when compared to B0. However, at CR 17.5 the BSFC rating was higher for the B20 blend. BSFC of the engine decreases with increased compression, as higher CRs favor efficient combustion.

- The Brake Thermal efficiency (BTE) of the engine, was recorded higher at CR18. Nonetheless, at CR17.5, the

BTE values were almost the same for B20 and B0. At full load conditions, maximum efficiency was observed.

- A gas analyzer recorded the emissions from the engine exhaust and significant improvements in the emissions were projected. This is a result of the advanced combustion of the better-oxygenated fuel.
- At both, the CRs, CO, and  $\text{CO}_2$  emissions were very much lower for B20 than for B0. The average reductions in  $\text{CO}_2$  emissions were 41.2% and 42.2% at CR 17.5 and CR18 respectively. Similarly, the average decrement in CO emissions was found to be 46% and 75% at CR17.5 and CR18 respectively.
- The hydrocarbon emissions also followed the above trend producing emissions which are 21% and 9% lesser for B20 at CR 17.5 and CR18 respectively. The  $\text{NO}_x$  emissions were higher at both the CRs and the increase was only 0.25% and 3.35% at CR 17.5 and CR18 respectively. The smoke emissions were also recorded at appreciable low levels at B20 loading compared with B0. An average reduction of 19.3% and 32.7% in smoke opacity was obtained at CR 17.5 and CR 18 respectively.

With the above findings, it could be easily concluded that B20 served as a better fuel. At both the engine configurations, especially at CR 18, B20 was found to be more efficient while consuming lesser fuel. This projects the potential scope of supplementing the future energy requirements. Complementing this, B20 also addresses an important concern regarding greenhouse gases, global warming, and air pollution since the fuel stands out remarkably as the emission levels are appreciably low. By commercializing the pork lard biodiesel, problems related to waste disposal from slaughterhouses can be resolved. Also, the biodiesel produced is less toxic and non-hazardous, thus the approach can be considered an environmentally benign process.

## ACKNOWLEDGEMENT

The authors would like to thank the Department of Chemical Engineering at Manipal Institute of Technology, India for providing the logistics as well the operational needs during the research.

## REFERENCES

- Adewale, P., Dumont, M.J. and Ngadi, M. 2015. Recent trends of biodiesel production from animal fat wastes and associated production techniques. *Renew. Sustain. Energy Rev.*, 45: 574-588. <https://doi.org/10.1016/j.rser.2015.02.039>
- Alagu, K. and Nagappan, B. 2018. The impact of antioxidant additives on the performance and emission characteristics of the CI engine was fuelled with a B20 blend of rice bran biodiesel. *Environ. Sci. Pollut. Res. Int.*, 25(18): 17634-17644.

- Al-Muhtaseb, A.H., Jamil, F., Al-Haj, L., Zar Myint, M.T., Mahmoud, E., Ahmad, M.N.M., Hasan, A. O. and Rafiq, S. 2018. Biodiesel production over a catalyst prepared from biomass-derived waste date pits. *Biotechnol. Rep.*, 20: 284. <https://doi.org/10.1016/j.btre.2018.e00284>
- Andersen, O. and Weinbach, J.E. 2010. Residual animal fat and fish for biodiesel production. Potentials in Norway. *Biomass Bioenergy*, 34(8): 1183-1188. <https://doi.org/10.1016/j.biombioe.2010.03.010>
- Ashok, A., Kennedy, L.J., Vijaya, J.J. and Aruldoss, U. 2018. Optimization of biodiesel production from waste cooking oil by magnesium oxide nanocatalyst synthesized using coprecipitation method. *Clean Technol. Environ. Policy*, 20(6): 1219-1231. <https://doi.org/10.1007/s10098-018-1547-x>
- Asri, N.P., Soe'eb, S., Poedjojono, B. and Suprpto, R. 2018. Alumina supported zinc oxide catalyst for the production of biodiesel from kemambi oil and optimization to achieve the highest yields of biodiesel. *Euro-Mediterr. J. Environ. Integr.*, 3(1): 1-7. <https://doi.org/10.1007/s41207-017-0043-8>
- Atadashi, I.M., Aroua, M.K., Abdul Aziz, A.R. and Sulaiman, N.M.N. 2013. The effects of catalysts in biodiesel production: A review. *J. Ind. Eng. Chem.*, 19(1): 14-26. <https://doi.org/10.1016/j.jiec.2012.07.009>
- Atadashi, I.M., Aroua, M.K., Aziz, A.R.A. and Sulaiman, N.M.N. 2011. Refining technologies for the purification of crude biodiesel. *Appl. Energy*, 88(12): 4239-4251. <https://doi.org/10.1016/j.apenergy.2011.05.029>
- Awolu, O.O. and Layokun, S.K. 2013. Optimization of two-step transesterification production of biodiesel from neem (*Azadirachta indica*) oil. *Int. J. Energy Environ. Eng.* 4(1): 1-9. <https://doi.org/10.1186/2251-6832-4-39>
- Babu, V., Atanu, B., Paul, K. and Chaudhari, A.J. 2018. Influence of waste cooking oil methyl ester biodiesel blends on the performance and emissions of a diesel engine. *Waste Biomass Valoriz.*, 9(2): 283-292. <https://doi.org/10.1007/s12649-016-9749-0>
- Baskar, G. and Aiswarya, R. 2016. Trends in catalytic production of biodiesel from various feedstocks. *Renew. Sustain. Energy Rev.*, 57: 496-504. <https://doi.org/10.1016/j.rser.2015.12.101>
- Borugadda, V.B. and Goud, V.V. 2014. Thermal, oxidative and low-temperature properties of methyl esters prepared from oils of different fatty acids composition: A comparative study. *Thermochim. Acta*, 577: 33-40. <https://doi.org/10.1016/j.tca.2013.12.008>
- Bragadeshwaran, A., Kasianantham, N., Ballusamy, S. and Tarun, K. R. 2018. Experimental study of methyl tert-butyl ether as an oxygenated additive in diesel and Calophyllum inophyllum methyl ester blended fuel in CI engine. *Environ. Sci. Pollut. Res. Int.*, 25(33): 33573-33590.
- Can, Ö. 2020. Combustion characteristics, performance, and exhaust emissions of a diesel engine fueled with a waste cooking oil biodiesel mixture. *Energy Conv. Manag.*, 87: 676-686. <https://doi.org/10.1016/j.enconman.2014.07.066>
- Chavan, S.B., Yadav, M., Singh, R., Singh, V. and Kumbhar, R.R. 2017. Production of biodiesel from three indigenous feedstock : Optimization of process parameters and assessment of various fuel properties. *Environ. Prog. Sustain. Energy*, 36(3): 126. <https://doi.org/10.1002/ep>
- Chingakhm, C., David, A. and Sajith, V. 2019. Fe<sub>3</sub>O<sub>4</sub> nanoparticles impregnated eggshell as a novel catalyst for enhanced biodiesel production. *Chinese J. Chem. Eng.*, 27(11): 2835-2843. <https://doi.org/10.1016/j.cjche.2019.02.022>
- Choudhury, H.A. 2014. Single-step ultrasonic synthesis of biodiesel from crude jatropha curcas oil. *AICHE J.*, 60(5): 1572-1581. <https://doi.org/10.1002/aic>
- Cynamon, D. and Bouwer, E.J. 2015. Prospects for biodiesel production from algae-based wastewater treatment in Brazil : A review. *Renew. Sustain. Energy Rev.*, 52: 1834-1846. <https://doi.org/10.1016/j.rser.2015.08.030>
- Dash, S.K., Chavan, S.B., Kumar, A., Ahamed, M.S. and Lingfa, P. 2020. *Jatropha Biodiesel Blends as Renewable Diesel Fuel Additives*. Springer, Singapore. <https://doi.org/10.1007/978-981-15-1607-8>
- Devarajan, Y., Munuswamy, D.B. and Nagappan, B.K. 2017. Emissions analysis on a diesel engine fuelled with cashew nut shell biodiesel and pentanol blends. *Environ. Sci. Pollut. Res.*, 24(14): 13136-13141. <https://doi.org/10.1007/s11356-017-8915-7>
- Ezebor, F., Khairuddean, M., Abdullah, A.Z. and Boey, P.L. 2014. Oil palm trunk and sugarcane bagasse derived heterogeneous acid catalysts for the production of fatty acid methyl esters. *Energy*, 70: 493-503. <https://doi.org/10.1016/j.energy.2014.04.024>
- Fadhil, A.B., Al-tikrity, E.T.B. and Albadree, M.A. 2017. Biodiesel production from mixed non-edible oils, castor seed oil, and waste fish oil. *Fuel*, 210: 721-728. <https://doi.org/10.1016/j.fuel.2017.09.009>
- Godiganur, S., Murthy, C.H.S. and Prathap, R. 2009. 6BTA 5 . 9 G2-1 Cummins engine performance and emission tests using methyl ester mahua (*Madhuca indica*) oil/diesel blends. *Renewable Energy*, 34(10): 2172-2177. <https://doi.org/10.1016/j.renene.2008.12.035>
- Gupta, J., Agarwal, M. and Dalai, A.K. 2018. Marble slurry derived hydroxyapatite as heterogeneous catalyst for biodiesel production from soybean oil. *Canad. J. Chem. Eng.*, 96(9): 1873-1880. <https://doi.org/10.1002/cjce.23167>
- Hong, I.K., Park, J.W. and Lee, S.B. 2013. Optimization of fish-oil-based biodiesel synthesis. *J. Ind. En. Chem.*, 19(3): 764-768. <https://doi.org/10.1016/j.jiec.2012.10.011>
- Imdadul, H.K., Zulkifli, N.W.M., Masjuki, H.H. and Kalam, M.A. 2017. Experimental assessment of non-edible candlenut biodiesel and its blend characteristics as diesel engine fuel. *Environ. Sci. Pollut. Res. Int.*, 24(3): 2350-2363. <https://doi.org/10.1007/s11356-016-7847-y>
- Jeevanantham, A.K., Nanthagopal, K., Ashok, B., Al-Muhtaseb, A.H., Thi-yagarajan, S., Geo, V.E., Chyuan, H. and Samuel, K.J. 2019. Impact of the addition of two ether additives with high-speed diesel: Calophyllum inophyllum biodiesel blends on NO<sub>x</sub> reduction in CI engine. *Energy*, 185: 39-54. <https://doi.org/10.1016/j.energy.2019.07.013>
- Jena, P.C., Raheman, H., Kumar, G.V.P. and Machavaram, R. 2010. Biodiesel production from a mixture of mahua and Simarouba oils with high free fatty acids. *Biomass Bioenergy*, 34(8): 1108-1116. <https://doi.org/10.1016/j.biombioe.2010.02.019>
- Judith, J., Amelia, L., Espitia, A. and Sodre, R. 2015. Potential vegetable sources for biodiesel production : Cashew, coconut, and cotton. *Mater. Renew. Sustain. Energy*, 4(1): 1-7. <https://doi.org/10.1007/s40243-014-0041-6>
- Kadir, M., Zeki, Y. and Mustafa, Y. 2020. The performance, emissions, and combustion characteristics of an unmodified diesel engine running on the ternary blends of pentanol/safflower oil biodiesel/diesel fuel. *J. Thermal Anal. Calorim.*, 56: 789. <https://doi.org/10.1007/s10973-020-09376-6>
- Kaisan, M.U., Anafi, F.O., Nuszowski, J., Kulla, D.M. and Umaru, S. 2017. Exhaust emissions of biodiesel binary and multi-blends from cotton, jatropha, and neem oil from stationary multi cylinder CI engine. *Transport. Res. Part D*, 53: 403-414. <https://doi.org/10.1016/j.trd.2017.04.040>
- Kakati, J. and Gogoi, T.K. 2016. Biodiesel production from Kutkura (*Meyna spinosa* Roxb . Ex .) fruit seed oil : Its characterization and engine performance evaluation with 10 % and 20 % blends. *Energy Conv. Manag.*, 121: 152-161. <https://doi.org/10.1016/j.enconman.2016.05.019>
- Kakati, J., Gogoi, T.K. and Pakshirajan, K. 2017. Production of biodiesel from Amari Amoor Wallichii King tree seeds using optimum process parameters and its characterization. *Energy Conv. Manag.*, 135: 281-290. <https://doi.org/10.1016/j.enconman.2016.12.087>
- Kara, K., Ouanji, F., Lotfi, E.M., Mahi, M., Kacimi, M. and Ziyad, M. 2018. Biodiesel production from waste fish oil with high free fatty acid content from Moroccan fish-processing industries. *Egypt. J. Petrol.*, 27(2): 249-255. <https://doi.org/10.1016/j.ejpe.2017.07.010>
- Karmakar, A., Karmakar, S. and Mukherjee, S. 2010. Bioresource technology properties of various plants and animals feedstocks for biodiesel production. *Bioresour. Technol.*, 101(19): 7201-7210. <https://doi.org/10.1016/j.biortech.2010.04.079>



- Karthickeyan, V., Balamurugan, P., Rohith, G. and Senthil, R. 2017. Developing of ANN model for prediction of performance and emission characteristics of VCR engine with orange oil biodiesel blends. *J. Brazil. Soc. Mech. Sci. Eng.*, 39(7): 2877-2888. <https://doi.org/10.1007/s40430-017-0768-y>
- Maneerung, T., Kawi, S., Dai, Y. and Wang, C. 2016. Sustainable biodiesel production via transesterification of waste cooking oil by using CaO catalysts prepared from chicken manure. *Energy Conv. Manag.*, 123: 487-497. <https://doi.org/10.1016/j.enconman.2016.06.071>
- Margaretha, Y.Y., Prastyo, H.S., Ayucitra, A. and Ismadji, S. 2012. Calcium oxide from pomacea sp. shell as a catalyst for biodiesel production. *Int. J. Energy Environ. Eng.*, 3(1): 1-9. <https://doi.org/10.1186/2251-6832-3-33>
- Mazaheri, H., Chyuan, H., Masjuki, H.H., Amini, Z., Harrison, M.D., Wang, C., Kusumo, F. and Alwi, A. 2018. Rice bran oil-based biodiesel production using calcium oxide catalyst derived from *Chicoreus brunneus* shell. *Energy*, 144: 10-19. <https://doi.org/10.1016/j.energy.2017.11.073>
- Mishra, S., Chauhan, A. and Mishra, K.B. 2020. Role of binary and ternary blends of WCO biodiesel on emission reduction in a diesel engine. *Fuel*, 262: 116604. <https://doi.org/10.1016/j.fuel.2019.116604>
- Mofijur, M., Masjuki, H.H., Kalam, M.A., Rasul, M.G., Atabani, A.E., and Hazrat, M.A. 2015. Effect of biodiesel-diesel blending on physico-chemical properties of biodiesel produced from moringa oleifera. *Procedia Eng.*, 105: 665-669. <https://doi.org/10.1016/j.proeng.2015.05.046>
- Mofijur, M., Rasul, M.G., Hyde, J., Azad, A.K., Mamat, R. and Bhuiya, M.M.K. 2016. Role of biofuel and their binary (diesel-biodiesel) and ternary (ethanol-biodiesel-diesel) blends on internal combustion engines emission reduction. *Renew. Sustain. Energy Rev.*, 53: 265-278. <https://doi.org/10.1016/j.rser.2015.08.046>
- Monirul, I.M., Kalam, M.A., Masjuki, H.H., Zulki, N.W.M., Shahir, S.A., Mosarof, M.H. and Ruhul, A.M. 2017. Influence of poly (methyl acrylate) additive on cold flow properties of coconut biodiesel blends and exhaust gas emissions. *Renew. Energy*, 101: 702-712. <https://doi.org/10.1016/j.renene.2016.09.020>
- Mureed, K., Kanwal, S., Hussain, A., Noureen, S., Hussain, S., Ahmad, S., Ahmad, M. and Waqas, R. 2018. Biodiesel production from algae grown on food industry wastewater. *Environ. Monitor. Assess.*, 190(5): 3-13. <https://doi.org/10.1007/s10661-018-6641-3>
- Nabora, C.S., Kingodu, C.K. and Kivevele, T.T. 2019. Tamarindus Indica fruit shell ash: A low cost and effective catalyst for biodiesel production from Parinari curatellifolia seeds oil. *SN Appl. Sci.*, 1(3): 1-9. <https://doi.org/10.1007/s42452-019-0256-3>
- Nakatani, N., Takamori, H., Takeda, K. and Sakugawa, H. 2009. Transesterification of soybean oil using combusted oyster shell waste as a catalyst. *Bioresour. Technol.*, 100(3): 1510-1513. <https://doi.org/10.1016/j.biortech.2008.09.007>
- Nguyen, T., Pham, M. and Le, T. 2020. Spray, combustion, performance, and emission characteristics of a common rail diesel engine fueled by fish-oil biodiesel blends. *Fuel*, 269: 117108. <https://doi.org/10.1016/j.fuel.2020.117108>
- Niju, S., Mohamed, K., Sheriffa, M. and Anantharaman, N. 2015. Preparation of biodiesel from waste frying oil using a green and renewable solid catalyst derived from the eggshell. *Environ. Process Sustain. Energy*, 34(1): 248-254. <https://doi.org/10.1002/ep>
- Ning, Y. and Niu, S. 2017. Preparation and catalytic performance in the esterification of a bamboo-based heterogeneous acid catalyst with microwave assistance. *Energy Conv. Manag.*, 153: 446-454. <https://doi.org/10.1016/j.enconman.2017.10.025>
- Nirmala, N., Dawn, S.S. and Harindra, C. 2020. Analysis of performance and emission characteristics of Waste cooking oil and *Chlorella variabilis* MK039712. 1 biodiesel blends in a single cylinder, four strokes diesel engine. *Renew. Energy*, 147: 284-292. <https://doi.org/10.1016/j.renene.2019.08.133>
- Patel, R.L. and Sankhavara, C.D. 2020. Biodiesel production from Karanja oil and its use in diesel engine : A review. *Renew. Sustain. Energy Rev.*, 71: 464-474. <https://doi.org/10.1016/j.rser.2016.12.075>
- Pua, F., Fang, Z., Zakaria, S., Guo, F. and Chia, C. 2012. Correction: Direct production of biodiesel from high-acid value *Jatropha* oil with solid acid catalyst derived from ligninPua, F., Fang, Z., Zakaria, S., Guo, F. and Chia, C. (2012). Correction: Direct production of biodiesel from high-acid value *Jatropha* o. *Biotechnology for Biofuels*, 5(1), 66.
- Raheman, H., Jena, P. C. and Jadav, S. S. 2013. Performance of a diesel engine with blends of biodiesel ( from a mixture of oils ) and high-speed diesel. 1-9.
- Rahman, S.M.A., Masjuki, H.H., Kalam, M.A., Abedin, M.J. and Sanjid, A. 2014. Assessing idling effects on a compression ignition engine fueled with *Jatropha* and Palm biodiesel blends. *Renew. Energy*, 68(10): 644-650. <https://doi.org/10.1016/j.renene.2014.02.050>
- Rahman, S.M.A., Masjuki, H.H., Kalam, M.A., Abedin, M.J., Sanjid, A. and Sajjad, H. 2013. Production of palm and Calophyllum inophyllum-based biodiesel and investigation of blend performance and exhaust emission in an unmodified diesel engine at high idling conditions. *Energy Conv. Manag.*, 76: 362-367. <https://doi.org/10.1016/j.enconman.2013.07.061>
- Rakopoulos, D.C., Rakopoulos, C.D., Kakaras, E.C. and Giakoumis, E.G. 2008. Effects of ethanol-diesel fuel blends on the performance and exhaust emissions of heavy-duty DI diesel engine. *Energy Conv. Manag.*, 49(11): 3155-3162. <https://doi.org/10.1016/j.enconman.2008.05.023>
- Robert, R.J. and Girish, C.R. 2020. Production of biodiesel from pork lard waste and characterization of its properties. *J. Eng. Sci. Technol.*, 15(6): 3876-3890.
- Rosha, P., Kumar, S., Kumar, S., Cho, H., Singh, B. and Dhir, A. 2019. Effect of compression ratio on combustion, performance, and emission characteristics of compression ignition engine fueled with palm ( B20 ) biodiesel blend. *Energy*, 178: 676-684. <https://doi.org/10.1016/j.energy.2019.04.185>
- Roy, M.M., Wang, W. and Bujold, J. 2013. Biodiesel production and comparison of emissions of a DI diesel engine fueled by biodiesel – diesel and canola oil – diesel blends at high idling operations. *Appl. Energy*, 106: 198-208. <https://doi.org/10.1016/j.apenergy.2013.01.057>
- Sánchez-Arreola, E., Bach, H. and Hernández, L.R. 2019. Bioresource technology reports biodiesel production from cascabela ovata seed oil. *Bioresour. Technol. Rep.*, 7: 100220. <https://doi.org/10.1016/j.biteb.2019.100220>
- Saravanan, S., Sivanandi, P., Pandian, S. and Choksi, H. 2019. Conversion of a low-value industrial waste into biodiesel using a catalyst derived from brewery waste : An activation and deactivation kinetic study. *Waste Manag.*, 100: 318-326. <https://doi.org/10.1016/j.wasman.2019.09.030>
- Shahid, E.M. and Jamal, Y. 2020. Production of biodiesel : A technical review. *Renew. Sustain. Energy Rev.*, 15(9): 4732-4745. <https://doi.org/10.1016/j.rser.2011.07.079>
- Shahzadi, I., Sadaf, S., Iqbal, J., Ullah, I. and Bhatti, H.N. 2018. Evaluation of mustard oil for the synthesis of biodiesel: Pretreatment and optimization study. *Environ. Prog. Sustain. Energy*, 37(5): 1829-1835. <https://doi.org/10.1002/ep.12833>
- Shankar, A.A., Pentapati, P.R. and Prasad, R.K. 2017. Biodiesel synthesis from cottonseed oil using homogeneous alkali catalyst and using heterogeneous multiwalled carbon nanotubes : Characterization and blending studies. *Egypt. J. Petrol.*, 26(1): 125-133. <https://doi.org/10.1016/j.ejpe.2016.04.001>
- Sharma, Y.C. and Singh, B. 2009. Development of biodiesel: Current scenario. *Renew. Sustain. Energy Rev.*, 13(6-7): 1646-1651. <https://doi.org/10.1016/j.rser.2008.08.009>
- Sivaramkrishnan, K. 2018. Investigation on performance and emission characteristics of a variable compression multifuel engine fuelled with Karanja biodiesel–diesel blend. *Egypt. J. Petrol.*, 27(2): 177-186. <https://doi.org/10.1016/j.ejpe.2017.03.001>

- Stamenkovi , O.S., Todorovi , Z.B., Lazi , M.L., Veljkovi , V.B. and Skala, D.U. 2008. Kinetics of sunflower oil methanolysis at low temperatures. *Bioresour. Technol.*, 99(5): 1131-1140. <https://doi.org/10.1016/j.biortech.2007.02.028>
- Sundar, K. and Udayakumar, R. 2020. Comparative evaluation of the performance of rice bran and cottonseed biodiesel blends in VCR diesel engine. *Energy Rep.*, 6: 795-801. <https://doi.org/10.1016/j.egyr.2019.12.005>
- Sureshkumar, K., Velraj, R. and Ganesan, R. 2008. Performance and exhaust emission characteristics of a CI engine fueled with *Pongamia pinnata* methyl ester ( PPME ) and its blends with diesel. *Renew. Energy*, 33: 2294-2302. <https://doi.org/10.1016/j.renene.2008.01.011>
- Teoh, Y.H., How, H.G., Masjuki, H.H., Nguyen, H., Kalam, M.A. and Alabdulkarem, A. 2019. Investigation of particulate emissions and combustion characteristics of a common-rail diesel engine fueled with *Moringa oleifera* biodiesel- diesel blends. *Renew. Energy*, 136: 521-534. <https://doi.org/10.1016/j.renene.2018.12.110>
- Tshizanga, N. and Funmilayo, E. 2017. Optimization of biodiesel production from waste vegetable oil and eggshell ash. *South Afr. J. Chem. Eng.*, 23: 145-156. <https://doi.org/10.1016/j.sajce.2017.05.003>
- Tüccar, G., Tosun, E., Özgür, T. and Aydın, K. 2014. Diesel engine emissions and performance from blends of citrus *sinensis* biodiesel and diesel fuel. *Fuel*, 132: 7-11. <https://doi.org/10.1016/j.fuel.2014.04.065>
- Venkatesan, V. and Nallusamy, N. 2020. Pine oil-soapnut oil methyl ester blends : A hybrid biofuel approach to eliminate the use of diesel in a twin-cylinder off-road tractor diesel engine. *Fuel*, 262: 116500. <https://doi.org/10.1016/j.fuel.2019.116500>
- Verma, P. and Sharma, M.P. 2016. Review of process parameters for biodiesel production from different feedstocks. *Renew. Sustain. Energy Rev.*, 62: 1063-1071. <https://doi.org/10.1016/j.rser.2016.04.054>
- Vijayaragavan, M.R., Subramaniam, G. and Ramachandran, L. 2019. An experimental study on the performance combustion and emission characteristics of diesel : *Simarouba glauca* biodiesel blended fuel for diesel engine with ethanol as an additive. *Environ. Process Sustain. Energy*, 38(5): 1-9. <https://doi.org/10.1002/ep.13206>
- Viola, E., Blasi, A., Valerio, V., Guidi, I., Zimbardi, F., Braccio, G. and Giordano, G. 2012. Biodiesel from fried vegetable oils via transesterification by heterogeneous catalysis. *Catal. Today*, 179(1): 185-190. <https://doi.org/10.1016/j.cattod.2011.08.050>
- Yadav, A.K., Dewangan, A. and Mallick, A. 2018. Effect of n-butanol and diethyl ether on performance and emission characteristics of a diesel engine fueled with diesel: *Pongamia* biodiesel blend. 144(6): 1-6. [https://doi.org/10.1061/\(ASCE\)EY.1943-7897.0000570](https://doi.org/10.1061/(ASCE)EY.1943-7897.0000570)
- Zaher, F.A. and Soliman, H.M. 2015. Biodiesel production by direct esterification of fatty acids with propyl and butyl alcohols. *Egypt. J. Petrol.*, 24(4): 439-443. <https://doi.org/10.1016/j.ejpe.2015.10.007>
- Zhang, J. and Jiang, L. 2008. Acid-catalyzed esterification of *Zanthoxylum bungeanum* seed oil with high free fatty acids for biodiesel production. *Bioresour. Technol.*, 99(18): 8995-8998. <https://doi.org/10.1016/j.biortech.2008.05.004>
- Živković, S.B., Veljković, M.V., Banković-Ilić, I.B., Krstić, I.M., Konstantinović, S.S., Ilić, S.B., Avramović, J.M., Stamenković, O.S. and Veljković, V.B. 2017. Technological, technical, economic, environmental, social, human health risk, toxicological, and policy considerations of biodiesel production and use. *Renew. Sustain. Energy Rev.*, 79: 222-247. <https://doi.org/10.1016/j.rser.2017.05.048>



# Sustainable Utilization of Textile Dyeing Sludge and Coal Fly Ash by Brick Production Through Traditional Kilns

G. C. Saha\*, M. A. Hasanath\*, M. N. Uddin\*† and M. Hasan\*

\*Department of Civil Engineering, Dhaka University of Engineering & Technology, Gazipur, Bangladesh

†Corresponding author: M. N. Uddin

Nat. Env. & Poll. Tech.  
Website: [www.neptjournal.com](http://www.neptjournal.com)

Received: 18-08-2021

Revised: 11-10-2021

Accepted: 24-10-2021

## Key Words:

Dyeing sludge

Coal fly ash

Brick production

Compressive strength

Leachability

## ABSTRACT

The fundamental purpose of this study was to evaluate the technical feasibility of incorporating fly ash (FA) and dyeing sludge (DS) in the production of brick. An attempt was taken to replace 10% to 100% clay by DS and FA in brick-making by volume. A brick firing kiln was used to burn the uniform-shaped bricks after replacing clay with DS and FA. Size and shape, hardness, soundness, water absorption, efflorescence, dry density, loss of ignition, firing shrinkage, specific gravity, compressive strength, and leaching tests were carried out to study the properties of these bricks. The compressive strength of the brick ranged from 6.25 MPa to 0.33 MPa and indicates a decreasing pattern in strength with the increase in the volume of DS and FA. Only 18.8% water absorption capacity was found in control bricks without DS and FA, while a maximum absorption of 40.19% was found for a particular combination of DS and FA. Similarly, dry density decreased with the increase in the volume of DS and FA. Besides, efflorescence in bricks was found within the allowable limits for certain combinations of DS and FA, which exceeded the allowable limits for other combinations. The presence of heavy metals (Ni, Zn, Cr, Cu, and Pb) in the extraction solution was insignificant. Based on the results of this study, we recommend that up to 10% clay can be substituted with DS and FA without substantially affecting the quality of bricks.

## INTRODUCTION

The textile sector plays an invaluable role in facilitating job creation, tax collection, and economic growth in many developing countries like Bangladesh. Considering the significant presence of textile industries in Bangladesh and many other countries, it is important to address the adverse environmental effects that these industries. Textile operation includes the refining or conversion, by various methods, of raw resources into finished products that involve the use of a high volume of water and the generation of wastewater that requires treatment before disposal. In Bangladesh, approximately 1500 textile industries produce about 2.82 million cubic meters of effluent daily (Concern 2014). The accelerated growth of the textile industry over the past decades and the discharge of untreated or poorly treated effluent into the environment has become a serious environmental concern. The volume of wastewater from textile industries is projected to cross 349 million m<sup>3</sup> by 2021, if traditional dyeing activities remain in use, from an estimated amount of 217 million m<sup>3</sup> in 2016 (Hossain et al. 2018). Earlier research reported that the concentrations of contaminants in textile effluent exceed the national discharge standards (Ahsan et al. 2019).

Apart from effluent from textile industries, the management of sludge generated during the treatment of textile

wastewater is also becoming a major concern. Many textile industries are finding it difficult to manage the sludge generated at their effluent treatment plants (ETPs) (Gomes et al. 2012). Textile sludge typically contains high amounts of metal ions and phosphorus, potassium, and nitrogen from chemical agents used in different phases of textile dyeing/processing [in particular aluminum (Al) and iron (Fe) from coagulants, flocculants depending upon the treating process] (Ghaly et al. 2014). Conventional treatment of textile effluent has the potential to contribute approximately 1.14 kg of sludge per cubic meter of effluent treated (Concern 2014). Uncontrolled disposal of textile sludge at landfills or waste dumping sites can, therefore, cause contamination of water and soil (Ashraf et al. 2014).

Diverse approaches for sludge treatment exist in developing nations to minimize sludge mass and decrease possible health risks associated with sludge disposal and treatment. Popular processing and disposal approaches in developing countries include incineration, composting, and landfilling (Guha et al. 2015). Landfilling of textile sludge could significantly contribute to the pollution of air, water, and soil (Iqbal et al. 2014). Incineration of solid sludge necessitates the use of an appropriate furnace, fuel, and specialized/trained personnel; possible air pollution from incineration is a major concern. Landfilling and composting are often not the

preferred sludge management methods due to the presence of heavy metals and volatile organic compounds in sludge (Patel & Pandey 2009). Consequently, appropriate treatment and processing of such sludge are needed for sustainable management (Liew et al. 2004). Research works have been carried out for the treatment/processing of various industrial sludge, including sludge from the paper factory (Goel & Kalamdhad 2017), tannery industries (Juel et al. 2017), water treatment (Ponkarthikeyan et al. 2016), etc. Several studies have been undertaken for processing or stabilizing toxic sludge as a substitute for soil in fired clay bricks and tiles. Balasubramanian et al. (2006) reported that specimens of sludge-cement did not reach the requirements for structural use; however, quality as well as other characteristics of certain products e.g., paving tiles and blocks, were acceptable for non-structural uses. Jahagirdar et al. (2013) proposed that sludge could be used in various building products at a maximum of 15%; the durability was, nonetheless, decreased to near 3.5 MPa. On a lab scale, most of the studies showed favorable outcomes for bricks in a controlled environment, however, limited experiments were conducted to manufacture bricks in the kiln (Juel et al. 2017).

Coal is the world's most important and plentiful fossil fuel. The fly ash (FA), produced throughout the coal combustion process in the thermal electricity generation, is one of the byproducts which contributes to significant environmental pollution. It has been estimated that the global generation of fly ash is around 0.60 billion tons each year. Its consumption has not matched the growing amount of fly ash generated worldwide. In comparison with their production, the consumption of FA is far less. The most significant and widespread application of fly ash in Bangladesh is the partial substitution in Portland cement, clay, and the production of construction materials. Numerous studies into the utilization of FA as a substitute raw resource in the production of new materials are being undertaken around the World (Behera et al. 2014). Many scholars have researched the application of FA in bricks made from clay (Balasubramanian et al. 2021, 2006). FA is suitable for 10% lighter brick manufacturing in comparison with clay bricks (Moyo et al. 2019). FA often possesses pozzolanic properties, which further improve durability and decrease absorption of water (Yao et al. 2014). Leiva et al. (2016) reported that FA bricks improved their strength properties at 1000 °C, and claimed that FA bricks have superior heat resistance to traditional clay bricks.

Brick is the most prominent and common building material being used worldwide. A variety of bricks are being used as a building material, e.g., sundried or unburnt clay brick, FA brick, burnt clay brick, sand-lime or calcium silicate brick, and concrete brick. Clay-fired bricks are mostly utilized as

a traditional building material in most developing countries. Because burnt clay bricks are stronger than sun-dried clay bricks. Using topsoil of agricultural lands is the traditional method of obtaining the clay needed for the manufacture of bricks (Biswas et al. 2018). Environment-friendly alternatives to clay for brick making might be a solution to maintain soil fertility and topsoil. With the exception of financial growth and the conservation of agricultural fertile land, the replacement of clay with textile dyeing sludge (DS) and FA often achieves the sustainable goal of safe disposal of waste materials (Moyo et al. 2019).

To the best of our knowledge, textile dyeing sludge (DS) and coal fly ash (FA) are not experimented with together in brick making. In the current study, we focused on the use of DS and FA together in brick manufacturing. The prime focuses of this study were (i) sustainable utilization of DS and FA in brick making with the partial replacement of clay, (ii) burning the DS-FA clay bricks in a traditional kiln, and (iii) investigating its influence on several mechanical and durability properties, and (iv) to examine the leaching of heavy metals from the developed bricks.

## MATERIALS AND METHODS

### Materials Collection

Textile dyeing sludge (DS) and Coal fly ash (FA) have been used as partial replacements for clay for making bricks, and the properties of these bricks have been evaluated to assess the potential use of DS and FA in bricks. DS was collected from the biological effluent treatment plant of Epyllion Fabrics Limited, Gazipur, Bangladesh which has a capacity of dyeing 30000 kg of textile/day. On the other hand, FA was collected from the coal used in a Barapukuria Thermal Power Plant (BTPP), Dinajpur, Bangladesh; clay was collected from the local area of Gazipur, which is used to manufacture bricks in brickfields.

### Materials Characterization

Collected DS was dewatered using sunlight for three days, and pulverized followed by oven-drying at 110°C for 24 hours to analyze physical and chemical properties. DS, FA, and clay were diluted by distilled water at a ratio of 1:5 and mixed completely using a mechanical shaker to test physio-chemical parameters. The blend was then filtered by Whatman filter paper and tested for pH and EC using a digital multimeter (Multi 3430). Chloride and sulfate concentrations of the diluted samples were determined by the Mohr method and a Spectrophotometer (HACH DR-2800), respectively. Besides, the physical properties of the samples were determined according to ASTM D854-00 and ASTM D



2216. Atterberg limits of the mixed materials were computed following ASTM D 4318. Also, the chemical composition of DS, FA, and clay was quantified using X-Ray Fluorescence (XRF) analysis (Shimadzu XRF-1800). Additionally, the concentration of heavy metals in DS was determined using atomic absorption spectrophotometer (AAS). An acid extraction procedure (aqua regia) was employed to digest the solution to quantify the concentrations of heavy metals (Santoro et al. 2017).

### Experimental Design and Brick Making

Ten different combinations of clay, DS, and FA have been used to fabricate bricks with three replications of each presented in Fig. 1. Brick, which is made of clay only, has been considered as a control or reference brick. The volume of clay was replaced by DS and FA up to 100% gradually, as

presented in Table 1. A wooden mold of 254×127×76 mm was used to cast and shape the brick. Water was added depending on the nature of the raw material and their plasticity and it was 1920, 1950, 2050, 2130 2240, 2350, 2450, 2660, 2800, 2920, and 3000 ml in C-0, C-1, C-2, C-3, C-4, C-5, C-6, C-7, C-8, C-9, and C-10, respectively. After the formation of brick, they were sun-dried for 6 days to remove the free water and burnt in the conventional brick kiln for 15 days at 2100°F (approximately).

### Field and Laboratory Tests of Brick

Field tests have been carried out according to ASTM C134-95, ASTM C88, and the fingernail scratch method. The compressive strength and water absorption capacity of fabricated brick were determined according to ASTM C67M-21. After curing, their frog marks were filled and

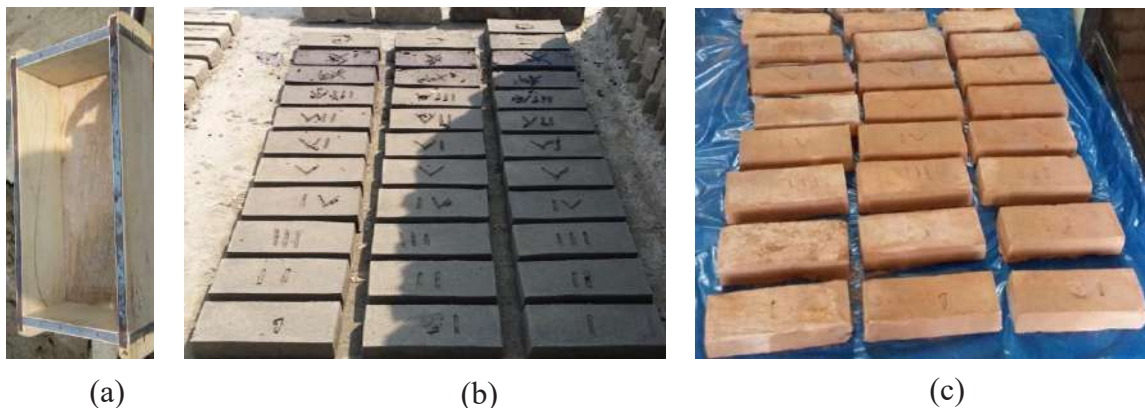


Fig. 1: Brick making, (a) wooden mold, (b) sun-dried bricks, (c) burnt bricks.

Table 1: Combination of materials for brick fabrication.

Combination ID	No. of replications	Volumetric percentage of material		
		Clay	Dyeing sludge (DS)	Fly ash (FA)
C-0	3	100	0	0
C-1	3	90	5	5
C-2	3	80	10	10
C-3	3	70	15	15
C-4	3	60	20	20
C-5	3	50	25	25
C-6	3	40	30	30
C-7	3	30	35	35
C-8	3	20	40	40
C-9	3	10	45	45
C-10	3	0	50	50

flushed by 1:4 thin cement sand mortar. Then the bricks were cut into two equal pieces along their lengths before tests for compressive strength (Fig. 2). On the other hand, efflorescence and specific gravity (for brick chips or coarse aggregate) were determined following ASTM C67M-20 and ASTM 127-15 methods. Some other physical properties of the fabricated bricks, i.e., loss of ignition (LOI), dry density, firing shrinkage, and thermal conductivity, were determined according to ASTM D7348-13, ASTM C20-00, ASTM C210-95, and ASTM C177-19 methods, respectively. The heavy metal leaching test of brick was tested for all combinations where the European standard method stated at prEN 1744-3:2000 was followed. Leachate was collected on the 1<sup>st</sup>, 4<sup>th</sup>, 7<sup>th</sup>, 15<sup>th</sup>, and 30<sup>th</sup> days after curing in distilled water.

## RESULTS AND DISCUSSION

Replacing the clay with more than 70% by DS and FA made the brick too soft at the time of burning, the combination from C-8 to C-10 was found unburnable whereas bricks of other combinations (C-0 to C-7) could be burnt. That is

why the results of C-0 to C-7 have been taken, analyzed, and presented in this study.

### Characteristics of Materials

The pH of DS, FA, and clay was found to be 6.45, 6.8, and 7.11, respectively, indicating that the pH of all raw materials is in the neutral range. From a previous study, it has been found that pH DS and FA are 6.9 and 6.2, respectively (Gebrati et al. 2019). The EC values of DS, FA, and clay are 4.06, 0.25, and 0.72  $\text{mS}\cdot\text{cm}^{-1}$ , respectively. The specific gravity of DS, FA, and clay was found to be 1.36, 2.30, and 2.84, respectively. The specific gravity of the DS and FA is less than clay; therefore, the addition of these materials can reduce the subsequent unit weight of the material.

The porosity of DS, FA, and clay was found to be 60%, 48%, and 37%, respectively (Table 2). The porosity of DS and FA has been found comparatively higher than clay, which indicates the liquid limit of DS and FA would be higher than clay. Sulfate concentration in DS and FA was 14.40  $\text{mg}\cdot\text{kg}^{-1}$  and 4.80  $\text{mg}\cdot\text{kg}^{-1}$ , respectively, whereas it was found below the detection limit in the clay. On the other hand, the existence

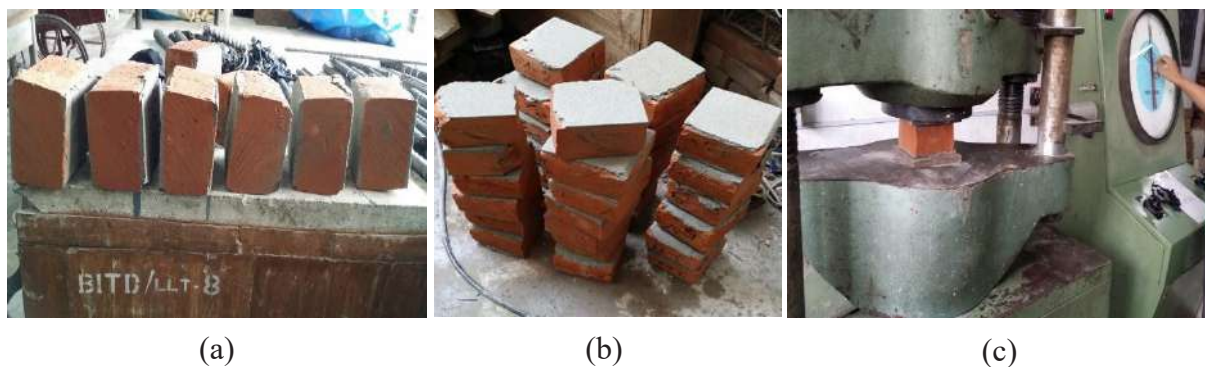


Fig. 2: Testing properties of brick, (a) prepared bricks for a compression test, (b) mortar layered brick, (c) crushing strength test using UTM.

Table 2: Characteristics of raw materials.

Parameter	Unit	Raw materials		
		Dyeing sludge	Fly ash	Clay
pH		6.45	6.80	7.11
EC	$\text{mS}\cdot\text{cm}^{-1}$	4.06	0.32	0.72
Specific gravity		1.36	2.30	2.84
Moisture content	%	89.00	00.03	15.71
Porosity	%	60	48	37
Void ratio		1.50	0.92	0.58
Dry density	$\text{kg}\cdot\text{m}^{-3}$	850.50	1554	2072
Chloride	$\text{mg}\cdot\text{kg}^{-1}$	182	12	9
Sulphate	$\text{mg}\cdot\text{kg}^{-1}$	14.4	4.8	Nil

of chloride and sulfate indicates the presence of salt that can give rise to efflorescence (Sing et al. 2018).

The major chemical components of brick clay are silica, alumina, iron oxide, magnesia, lime, and alkalis (Šveda et al. 2017). In this study, it has been observed that silica content in clay and FA were 65.40% and 64.19%, respectively, which presents good quality sample characteristics (Punmia et al. 2004). However, the silica content in DS was very low (29.26%) compared to the other two samples (Fig. 3). Besides, alumina determines the plasticity in the soil, where 20 to 30% alumina is suitable for brick. Higher than this range can make the brick too hard or brittle (Punmia et al. 2004). The alumina content in clay, FA, and DS has been found at 12.08%, 22.69%, and 0.70%, respectively. It indicates the unsuitability of DS for brick manufacturing because of the low amount of alumina. The effect of moisture on the plasticity of the pulverized materials has been evaluated by the Atterberg limits test. In the current study, PI decreased with the increase in the volume of DS and FA (Fig. 4). The highest PI was found to be 17.2% in the control combination,

whereas the lowest was 9.38% in the combination of 30% clay, 35% in DS, and 35% in FA. In general, a plasticity index (PI) greater than 23 is suitable for good-quality bricks.

Heavy metal content i.e., nickel, zinc, chromium, copper, and lead in dry DS was determined after extraction through acid digestion (aqua regia) by AAS. The concentration of Zn, Cu, Cr, Pb, and Ni were found at 177, 314, 1.0, 2.4, and 10.4 mg.kg<sup>-1</sup>, respectively (Table 3).

The existence of unwanted heavy metals in brick might be an issue of concern if it comes out with water or leach. It may be a good technique to handle sludge containing heavy metals by brick-making at a low cost if it does not leach metals (Kadir et al. 2018).

**Field Investigations of Brick**

The relative size of a brick (average of 3 combinations) made utilizing FA and DS was almost similar up to combination C-3 compared to the control bricks (Table 4). From visual observation, no porous surface was found in the bricks of

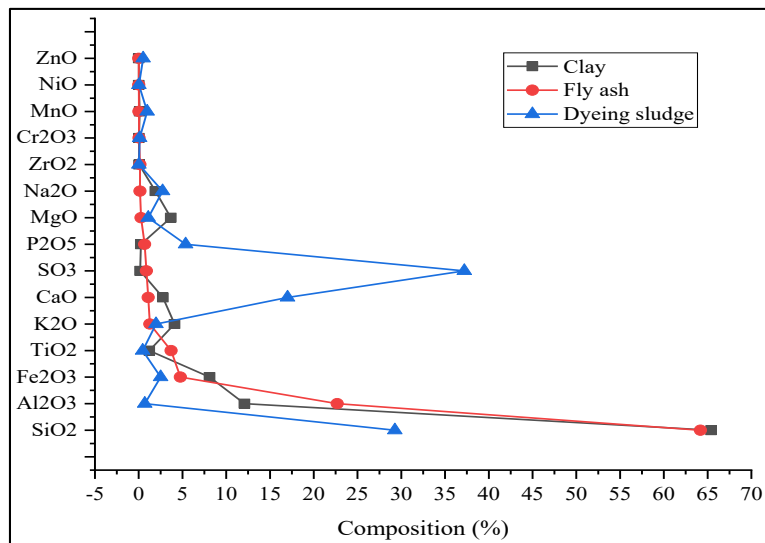


Fig. 3: Chemical compositions dyeing sludge, fly ash, and clay.

Table 3: Heavy metal concentration in textile dyeing sludge.

Heavy metal	Unit	Concentration
Zn	mg.kg <sup>-1</sup>	177
Cu	mg.kg <sup>-1</sup>	314
Cr	mg.kg <sup>-1</sup>	1.00
Pb	mg.kg <sup>-1</sup>	2.40
Ni	mg.kg <sup>-1</sup>	10.40

Table 4: Results from field investigation of fabricated brick.

Combination	Dimension of brick [mm]	Soundness	Hardness	Structure
C-0	241.10 × 113.17 × 69.78	Metallic	Hard	Non-Porous
C-1	241.50 × 114.76 × 70.11	Metallic	Hard	Non-Porous
C-2	243.28 × 114.60 × 70.12	Metallic	Hard	Non-Porous
C-3	246.22 × 116.67 × 70.77	Metallic	Hard	Non-Porous
C-4	246.43 × 117.10 × 71.26	Metallic	Hard	Non-Porous
C-5	246.50 × 117.59 × 71.67	Metallic	Hard	Non-Porous
C-6	247.10 × 118.17 × 72.60	Non-Metallic	Not Hard	Porous
C-7	247.41 × 118.29 × 72.42	Non-Metallic	Not Hard	Porous

combination C-1 to C-5. However, fabricated bricks of combination C-6 and C-7 showed a negligible amount of pore space on their surfaces. The porosity of brick affects not only its strength but also density, thermal conductivity (Fig. 5f), specific gravity, and water absorption capacity (Šveda et al. 2017).

Brick specimens of combination C-0 to C-5 are sufficiently hard when it was tested by the fingernail scratching method, whereas C-6 and C-7 have been found comparatively less when scratch marks were visualized during fingernail scratching.

### Laboratory Test Results of Brick

It is observed that the water absorption capacity of bricks increased with an increase in the volume of DS and FA (Fig. 5a). It is 18.8% in control, whereas it increased up to 40.2% in the C-7 combination. The recommended water absorption for good brick ranges from 15% to 20%. From a previous study, 14% and 27% water absorption capacity was calculated when mixed by 6% and 30% textile DS, respectively (Baskar et al. 2006).

In this study, it was found that the specific gravity (from brick chips) ranges from 2.40 to 1.99 for combinations of C-0 to C-7, respectively (Fig. 5b). The decreasing pattern of specific gravity of brick chips is in agreement with the previous result during material characterization (Table 2).

The weight loss of the bricks during burning is mostly due to the organic and the inorganic compounds because organic compounds in the compact specimen can gasify and/or oxidize to CO<sub>2</sub> and H<sub>2</sub>O while the CaCO<sub>3</sub> decomposes at high temperature (Wang et al. 2011). For a standard clay brick, the maximum weight loss on ignition (LOI) criterion is 15% (Juel et al. 2017), whereas the brick up to C-5 combination reaches the standard in the current study (Fig. 5c).

From the experimental results, it is also observed that dry density ranges from 1.43 g.cc<sup>-1</sup> to 0.95 g.cc<sup>-1</sup> for combinations C-0 to C-7. Also, the dry density decreased with the increase of the volume of DS and FA (Fig. 5d). A proportional relationship between the dry density and waste materials (FA and DS) has been observed, with the obvious reason being textile DS and FA. The dry density was 1.45 g.cc<sup>-1</sup> for bricks made with 35% of sludge with clay in this study, whereas a dry density of 1.80 g.cc<sup>-1</sup> was reported in a previous study (Jahagirdar et al. 2013).

Compressive strength is the most significant characteristic for determining a construction material's engineering application. It was observed that compressive strength declined from 6.25 MPa for combination C-1 to 0.33 MPa for combination C-7. The compressive strength of the control combination was found to be 6.64 MPa (Fig. 6).

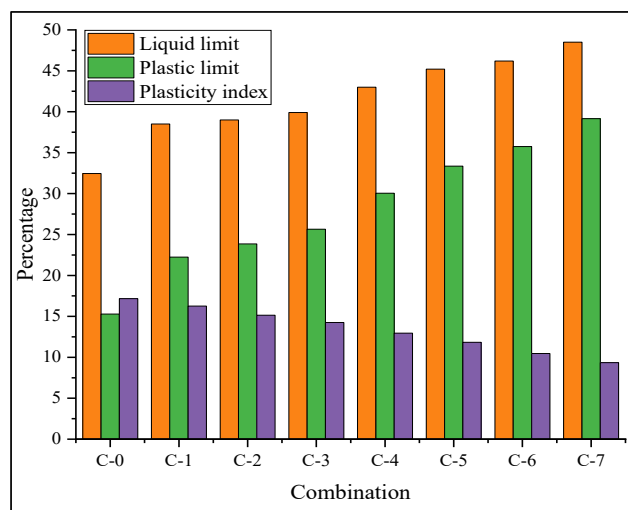


Fig. 4: Atterberg limits of the combinations of clay, DS and FA.



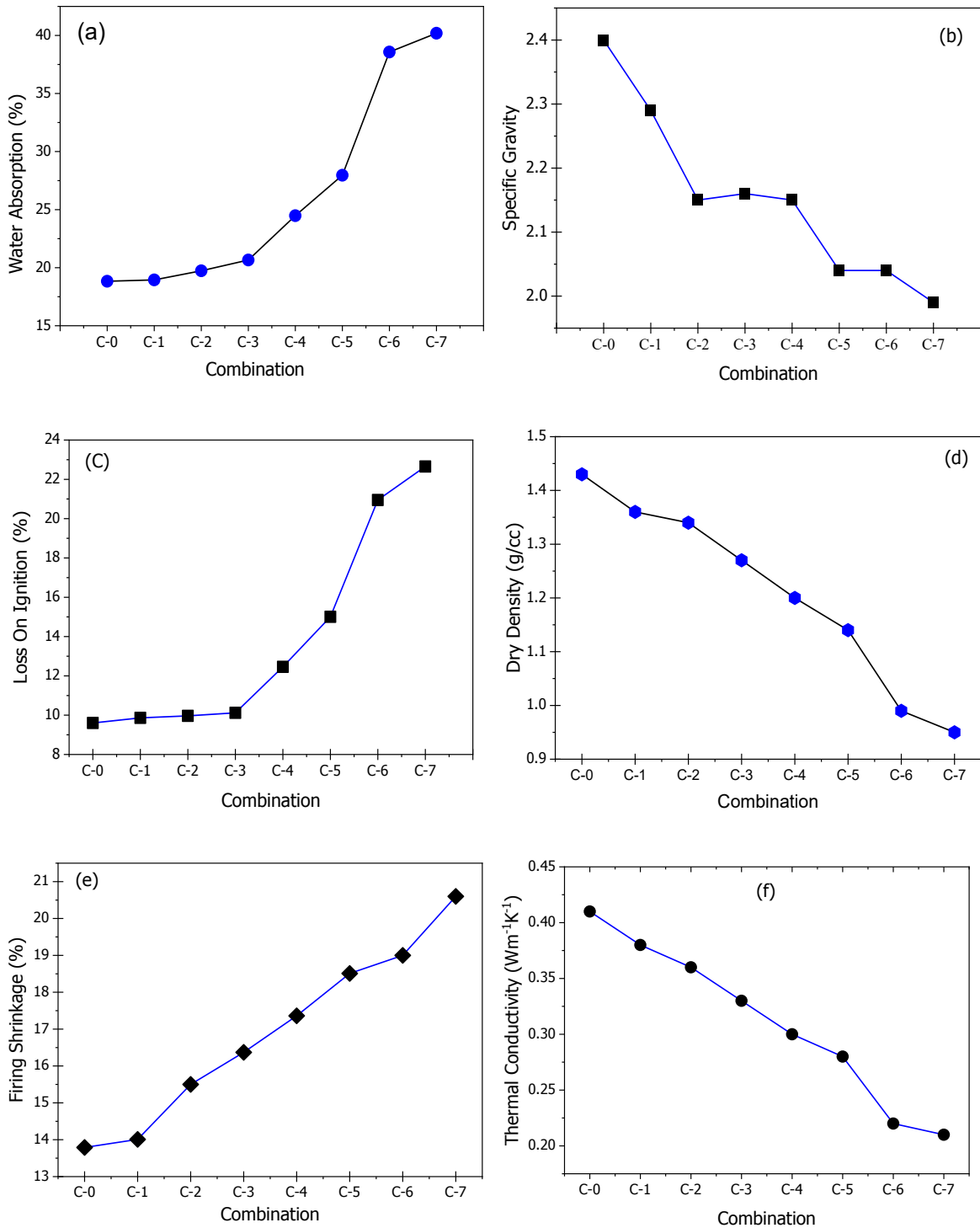


Fig. 5: Laboratory investigations of manufactured brick; (a) water absorption capacity, (b) specific gravity of brick chips, (c) loss on ignition, (d) dry density of brick, (e) shrinkage due to firing, (f) thermal conductivity of brick.

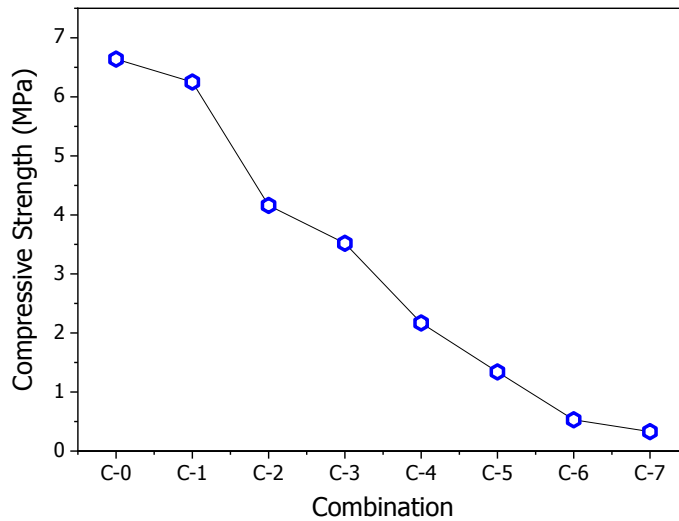


Fig. 6: Compressive strength of brick made by clay, dyeing sludge, and fly ash.

Besides, it was observed that the strength of the brick specimens declined with the increasing volume of DS and FA in brick. The probable reason for this decreasing strength pattern is that the adhesiveness of the mixture decreased and the internal pore size of the brick increased with the increase of DS and FA gradually. Compressive strength is 6.50 MPa when 10% clay was replaced by waste materials, and this is in agreement with a previous study that 10% replacement of clay by textile dyeing sludge can bring 3.65 to 6.5 MPa compressive strength (Jahagirdar et al. 2013).

Table 5 presents the efflorescence that occurs due to the presence of trapped or dissolved salts in water. It normally finds its way out of the material through the tiny pores after

being dissolved in water. In the current study, efflorescence increased with the increase of DS and FA; hence it was contaminated by salts. Outcomes of efflorescence are humid wall leading to multiple damages namely unhygienic conditions, corrosion, insect attack of woodwork, destruction of brickwork, damage to interior decoration decorations, cracking of plaster, etc.

Toxicity Characteristics Leaching Procedure (TCLP) test results of the dyeing sludge are given in Table 6. The leaching test was carried out only for the C-7 combination due to the maximum amount of DS and FA in this combination. An insignificant concentration of Cr and Cu was detected at the combination of 30% clay, 35% dyeing sludge, and 35% fly ash (C-7).

Table 5: Efflorescence status of brick.

Combination	Efflorescence			
	Nil (No deposition area by salt)	Slight ( $\leq 10\%$ covering area by salt)	Moderate ( $\leq 50\%$ covering area by salt)	High ( $\geq 50\%$ covering area by salt)
C-0		√		
C-1		√		
C-2		√		
C-3		√		
C-4			√	
C-5			√	
C-6				√
C-7				√

Table 6: Concentrations of heavy metals from leaching test.


Comb.	Heavy metals [mg.L <sup>-1</sup> ]	1 day	4 days	7 days	15 days	30 days	Concentration limits (USEPA 1996)
C-7	Zn	ND	ND	ND	ND	ND	1200
	Pb	ND	ND	ND	ND	ND	500
	Ni	ND	ND	ND	ND	ND	8
	Cr	ND	0.00030	0.00090	0.00110	0.00140	20
	Cu	.00009	0.00009	0.00010	0.00010	0.00010	800

## CONCLUSION

Based on experimental findings, we have come to the following conclusions: the highest compressive strength of brick has been obtained in control brick (6.64 MPa), while a range of 6.25 MPa and 0.33 MPa have been measured from combination C-1 to C-7. Water absorption, loss of ignition, firing shrinkage, and efflorescence increased with the consequent increase in the volume of DS and FA. This is due to the presence of degradable substances in raw materials. However, it appears that up to a combination of C-3 bricks can be used as a non-load bearing structure like partition wall, parapet wall, etc. Besides, the maximum thermal conductivity of the bricks was estimated to be  $0.41 \text{ Wm}^{-1}.\text{K}^{-1}$  in the control specimen and the minimum was  $0.21 \text{ Wm}^{-1}.\text{K}^{-1}$  in combination with C-7. A linear relationship between thermal conductivity and the volume of waste materials was observed. However, the addition of DS and FA improved the thermal insulation capacity of the bricks. Therefore, a leaching test was carried out to check the presence of heavy metals extracted from the bricks made with DS and FA. Metal leachate was found insignificant and according to the acceptable sludge regulated limit set by USEPA.

## ORCID

M. A. Hasanath  : <https://orcid.org/0000-0002-7500-591X>

M.N. Uddin  : <https://orcid.org/0000-0002-8452-3479>

## REFERENCES

- Ahsan, M.A., Satter, F., Siddique, M.A.B., Akbor, M.A., Ahmed, S., Shajahan, M. and Khan, R. 2019. Chemical and physicochemical characterization of effluents from the tanning and textile industries in Bangladesh with a multivariate statistical approach. *Environ. Monit. Assess.*, 191(9): 1-24.
- Ashraf, M.A., Maah, M.J. and Yusoff, I. 2014. Soil contamination, risk assessment, and remediation. *Environ. Risk Assess. Soil Contam.*, 1: 3-56.
- Balasubramanian, T., Karthik, P.M.S., Sureshkumar, S., Bharath, M. and Arun, M. 2021. Effectiveness of industrial waste materials used as ingredients in fly ash brick manufacturing. *Mater. Today*, 11: 14-23
- Balasubramanian, J., Sabumon, P.C., Lazar, J.U. and Ilangoan, R. 2006. Reuse of textile effluent treatment plant sludge in building materials. *Waste Manag.*, 26(1): 22-28.
- Baskar, R., Begum, M.S. and Sundaram, S. 2006. Characterization and reuse of textile effluent treatment plant waste sludge in clay bricks. *J. Univ. Chem. Technol. Metall.*, 41(4): 473-478.
- Behera, M., Bhattacharyya, S.K., Minocha, A.K., Deoliya, R. and Maiti, S. 2014. Recycled aggregate from C&D waste & its use in concrete: A breakthrough towards sustainability in the construction sector: A review. *Construct. Build. Mater.*, 68: 501-516.
- Biswas, D., Gurley, E.S., Rutherford, S. and Luby, S.P. 2018. The drivers and impacts of selling soil for brick making in Bangladesh. *Environ. Manag.*, 62(4): 792-802. <https://doi.org/10.1007/s00267-018-1072-z>
- Concern, W. 2014. Bangladesh Waste Database 2014. Waste Concern, Dhaka.
- Gebrati, L., El Achaby, M., Chatoui, H., Laqbaqbi, M., El Kharraz, J. and Aziz, F. 2019. Inhibiting effect of textile wastewater on the activity of sludge from the biological treatment process of the activated sludge plant. *Saud. J. Biol. Sci.*, 26(7): 1753-1757. <https://doi.org/10.1016/j.sjbs.2018.06.003>
- Ghaly, A.E., Ananthashankar, R., Alhattab, M. and Ramakrishnan, V.V. 2014. Production, characterization, and treatment of textile effluents: A critical review. *J. Chem. Eng. Process. Technol.*, 5(1): 1-18.
- Goel, G. and Kalamdhad, A.S. 2017. An investigation on the use of paper mill sludge in brick manufacturing. *Construction and Building Materials*, 148, 334-343.
- Gomes, L., Silva, F., Barbosa, S. and Kummrow, F. 2012. Ecotoxicity of sludges generated by textile industries: A review. *Ecotoxicol. Environ. Contam.*, 7(1): 89-96.
- Guha, A.K., Rahman, O., Das, S. and Hossain, S. 2015. Characterization and composting of textile sludge. *Resour. Environ.*, 5(2): 53-58.
- Hossain, L., Sarker, S.K. and Khan, M.S. 2018. Evaluation of present and future wastewater impacts of textile dyeing industries in Bangladesh. *Environ. Develop.*, 26: 23-33.
- Iqbal, S.A., Mahmud, I. and Quader, A. 2014. Textile sludge management by incineration technique. *Proceed. Eng.*, 90: 686-691.
- Jahagirdar, S.S., Shrihari, S. and Manu, B. 2013. Utilization of textile mill sludge in burnt clay bricks. *Int. J. Environ. Protect.*, 3(5): 6-13.
- Juel, M.A.I., Mizan, A. and Ahmed, T. 2017. Sustainable use of tannery sludge in brick manufacturing in Bangladesh. *Waste Manag.*, 60: 259-269. <https://doi.org/10.1016/j.wasman.2016.12.041>
- Kadir, A.A., Hassan, M.I.H., Salim, N.S.A., Sarani, N.A., Ahmad, S. and Rahmat, N.A.I. 2018. Stabilization of heavy metals in fired clay brick incorporated with wastewater treatment plant sludge: Leaching analysis. In: *Journal of Physics: Conference Series*, 995(1): 012071.
- Leiva, C., Arenas, C., Alonso-Fariñas, B., Vilches, L.F., Peceño, B., Rodriguez-Galán, M. and Baena, F. 2016. Characteristics of fired bricks with co-combustion fly ashes. *J. Build. Eng.*, 5: 114-118.
- Liew, A.G., Idris, A., Wong, C.H.K., Samad, A.A., Noor, M.J.M.M. and Baki, A.M. 2004. Incorporation of sewage sludge in clay brick and its characterization. *Waste Manag. Res.*, 22(4): 226-233.
- Moyo, V., Mguni, N.G., Hlabangana, N. and Danha, G. 2019. Use of coal fly ash to manufacture a corrosion-resistant brick. *Proced. Manuf.*, 35: 500-512.

- Patel, H. and Pandey, S. 2009. Exploring the reuse potential of chemical sludge from textile wastewater treatment plants in India: A hazardous waste. *Am. J. Environ. Sci.*, 5(1): 106.
- Ponkarthikeyan, P., Ganesh, R. and Sheerin, F.A. 2016. Experimental study on bricks using water treatment sludge. *Int. J. Res. Appl. Sci. Technol.*, 4(11): 485-493.
- Punmia, D.B.C., Jain, A.K. and Jain, A.K. 2004. Brick: In Basic of Civil Engineering. Laxmi Publications (P) Ltd., Chennai, India, pp. 33.
- Santoro, A., Held, A., Linsinger, T.P.J., Perez, A. and Ricci, M. 2017. Comparison of total and aqua regia extractability of heavy metals in sewage sludge: The case study of certified reference material. *TrAC: Trends in Anal. Chem.*, 89: 34-40. <https://doi.org/10.1016/j.trac.2017.01.010>
- Sing, P.A., Sangal, A., Saini, R. and Sharma, N. 2018. Efflorescence in brickwork. *Int. Res. J. Eng. Technol.*, 5(2): 1683-1688.
- Šveda, M., Janík, B., Pavlík, V., Štefunková, Z., Pavlendová, G., Šín, P. and Sokolá, R. 2017. Pore size distribution effects on the thermal conductivity of the fired clay Dody from lightweight bricks. *J. Build. Phys.*, 41(1): 78-94. <https://doi.org/10.1177/1744259116672437>
- USEPA. (1996) Hazardous waste characteristics scoping study. US Environmental Protection Agency, Office of Solid Waste, Washington DC.
- Wang, Q., Li, Y. and Wang, Y. 2011. Optimizing the weight loss on ignition methodology to quantify organic and carbonate carbon of sediments from diverse sources. *Environ. Monit. Assess.*, 174(1-4): 241-257. <https://doi.org/10.1007/s10661-010-1454-z>
- Yao, Z., Ji, X., Sarker, P., Tang, J., Ge, L., Xia, M. and Xi, Y. 2014. A comprehensive review on the applications of coal fly ash. *Earth Sci. Rev.*, 141(2015): 108-111. <https://doi.org/10.1016/j.earscirev.2014.11.016>





# Evaluation of Source Emissions Dispersion Potential Near a Coastal Village of Maharashtra, India

P. P. Nandusekar\*, U. S. Mukkannawar\*\*, R. G. Jaybhaye\*\*\*, U. D. Kulkarni\*\*\*\* and P. N. Kamble\*†

\*Department Environmental Sciences, Savitribai Phule Pune University, Pune, India

\*\*Indian Institute of Tropical Meteorology (Ministry of Earth Sciences, Govt. of India), Pune, India

\*\*\*Department of Geography, Savitribai Phule Pune University, Pune, India

\*\*\*\*M. J. College, Jalgaon, Maharashtra, India

†Correspondence author: P. N. Kamble: [kpramod09@gmail.com](mailto:kpramod09@gmail.com), [pnkamble@unipune.ac.in](mailto:pnkamble@unipune.ac.in)

Nat. Env. & Poll. Tech.  
Website: [www.neptjournal.com](http://www.neptjournal.com)

Received: 05-02-2022  
Revised: 15-03-2022  
Accepted: 23-03-2022

## Key Words:

AERMOD  
Meteorology  
Emission inventory  
Coke oven  
Pellet plant

## ABSTRACT

Industrial emissions are a serious environmental problem worldwide due to particulates and toxic gases. This study aims to generate an activity-specific emission inventory and estimate emissions dispersion extent in the vicinity of the coastal industrial village by simulating the existing coke oven and pellet plant emissions using the steady-state plume model. Continuous air quality monitoring results were compared with the predicted consequential emissions for the year 2018-19. The maximum ground-level concentrations of particulate and gases within the modeling simulation domain were observed at 9005 m away from the center. They were predicted to be  $116.39 \mu\text{g.m}^{-3}$ ,  $79.14 \mu\text{g.m}^{-3}$ ,  $52.97 \mu\text{g.m}^{-3}$ , and  $211.86 \mu\text{g.m}^{-3}$ . Data analysis showed that air mass transport from the project to the receptor sites resulted in ambient air concentrations higher than those observed in the other sites. Overall predicted results obtained from AERMOD Cloud simulations were shown to have less bias than the measured results. They recommended considering it as appropriate for the prediction of annual average concentration.

## INTRODUCTION

Environmental sustainability plays a critical role in the overall sustainable development of a nation. In this scenario, air pollution has become a severe problem for all countries across the globe. This growing problem concerns and needs urgent attention. Air pollution is caused by industrial activity, processes, and operation and is associated with vehicular movement caused due to fossil fuel burning (vehicular emissions). In addition, Air pollution has increased at an alarming speed due to industrial development proliferating. Air pollution's impact on health, property, agriculture, and the atmosphere is a significant concern worldwide. Unwanted and excess material, toxic gaseous dust, aerosol soot particles, and harmful hazardous substances are a substantial concern with the population increasing leads to air pollution. According to a study conducted by the World Health Organization (WHO) in 2006, it was found that 25% of deaths in developed countries occur due to air pollution (Tyagi 2015).

The iron and steel sector is the core of the Indian economy. As per the Ministry of Steel, domestic steel production surged from 109.85 Million Tons Per Annum (MTPA) in 2014-15 to 142.24 MTPA in 2018-19, accounting for a 6.8% compounded annual growth rate (CAGR) during these five

years (Ministry of Steel 2014). The sector is exceptionally resource-intensive and polluting. The steel industry is part of the European Union's emissions trade scheme (ETS) for exploring new ways to reduce emissions (Thomas 2021). Since the advent of industry, the steel industry has been a significant emissions source globally, mainly from its furnaces and cupolas (Kim & Worrell 2002, Amodio 2012, Vallero 2014). Used production routes, product mix, production energy efficiency, fuel mix, fuel mix carbon intensity, and electricity carbon intensity account for the steel industry emissions (Arvola et al. 2011). Ferroalloy industries contribute to the economic process and environmental imbalance to express pollution (Reddy et al. 2017). Various air pollution control methods like bag filters, bag Houses, electrostatic precipitators, gas cleaning plants, scrubbers, etc., are applied to control air pollution in integrated steel plants and their effect. Many researchers have contributed to achieving a clean and sustainable environment by reducing exhaust emissions (Li et al. 2019, Smirnova et al. 2020).

Recent studies have shown that a series of models can conduct an air quality assessment pertaining to the study's objective; e.g. plume rise model, dispersion model, photochemical model, meteorological modeling, particle models,

deposition models, odor modeling statistical models are present in the present scenario (CPCB 1998, CPCB 2010a, Gulia et al. 2015, Invernizzi 2020). Modeling the behavior of pollutants in the atmosphere using coupled mathematical equations helps understand the existing air environment. The assimilative capacity for the atmosphere of the study area was studied through pollution dispersion potential by process emission estimation and administered through an air dispersion model (Chaulya 2019).

Meteorological elements such as wind speeds, relative humidity, wind direction, temperature, and others influence the dispersion and transportation of released pollutants from point and non-point sources. Given the same, it is vital to do ambient air monitoring for the different pollutant entities in the vicinity of the plant. The prime steel pockets in India are trying to mitigate the air pollution problem through mathematical modeling and have achieved remarkable results (Govender & Sivakumar 2020). The air pollution emission modeling is a numeric tool for describing the causal relationship between emissions, meteorology, atmospheric concentration, and deposition. The pollutant concentration is mainly affected by ground deposits, diffusion, transportation, and chemical transformation factors (Nuterma & Baklanov 2007). Forecasting is critical in evaluating the overall air quality in any region of the world. The results are vital, mainly related to health concerns regarding growing air pollution in developing countries (Sharma & Parvez 2003, Gogikar 2019). Air pollution dispersion study in an integrated steel plant helps understand the concentration and direction to consider action planning further. Present research estimates emissions dispersion pattern from coke oven and pellet plant operations in Dolvi area of Maharashtra. The

investigation accounts for the site-specific meteorological and topographical characteristics. This study aimed to determine the diurnal and spatial variability of pollutant emissions that affect air quality levels.

## MATERIALS AND METHODS

### Study Area

The site is a prime steel unit situated in Dolvi village at  $73^{\circ}00'00''$ - $73^{\circ}05'00''$  E longitude and  $18^{\circ}40'00''$  to  $18^{\circ}45'00''$  N latitude with an average altitude of 1.7 m above MSL. The area is covered in the Survey of India Topo-sheet No. 47 F/2 [1:50000 scale]. The study area proposed in the present study is an integral part of one of the leading steel units in the country. The Dolvi plant caters to several industries: automotive, projects and construction, machinery, oil and gas, consumer durable, etc. The study domain of a 10 km radius is depicted in Fig. 1.

It covers requisite infrastructure, i.e., standalone jetty, rail, and road connectivity. Domain call out shows the current study's identified point source (stacks) and continuous ambient air quality monitoring stations (CAAQMS). The study area is plain with slightly undulating terrain. Most of the area is gently sloping from East to West and is present in the valley surrounded by small hills of greater than 35% slope gradient. It is located in a valley surrounded by hills having the steepest slope of  $57.4^{\circ}$ . The study area lies on the bank of River Amba, and there is a sub-creek passing through (Fig. 2). There are six Reserved Forests within a 10 km radius with no major industries in the vicinity.

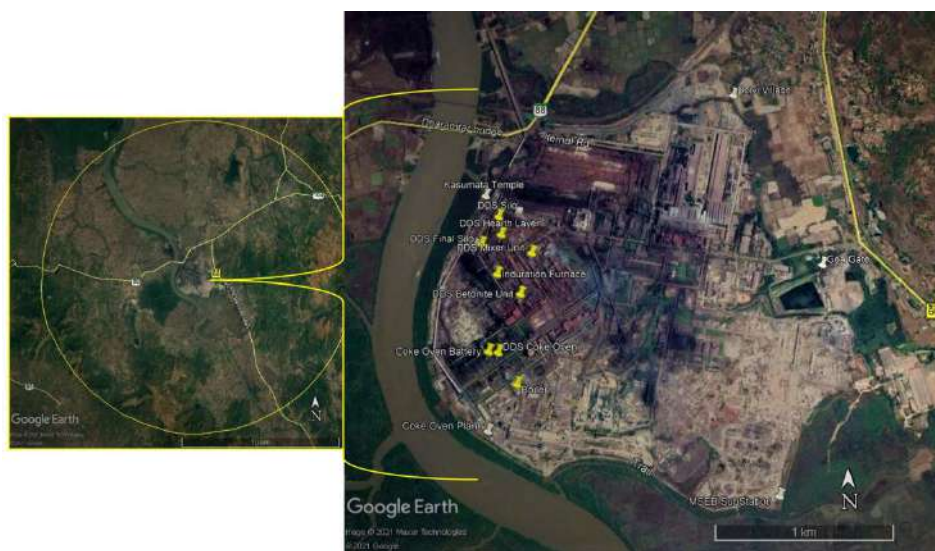


Fig. 1: Study Area (10 km) & insight stacks with CAAQMS.

### Meteorological Background of the Study Area

Meteorological conditions have a considerable impact on pollution concentrations in the environment. Wind speed and direction data determine the extent of pollutant transport, dispersion, and dilution from an emission source to a receptor. The local wind rose pattern leads to an optimum network design of air quality monitoring stations (Mukkanawar et al. 2014). The chemical reactions in the atmosphere are influenced by air temperature and solar radiation, while precipitation permits pollutant concentrations to fluctuate. Variations in meteorological factors have an impact on the concentrations and dispersion of pollutants in the atmosphere. The mean rainfall in winters was substantially higher than in other seasons, according to long-term meteorological data shown in Table 1. Several cross-sectional studies and

reports on continuous ambient air quality monitoring have identified significant winter pollutants (Joshi & Mahadev 2011, Sancini et al. 2014, NEERI Technical Report 2019, 2021). Furthermore, due to geographical characteristics and lower wind speeds, air pollution levels tend to be trapped.

The study area follows a typical west coast climate, characterized by abundant and regular seasonal rainfall, humid weather in summer, and high humidity throughout the year. The Indian Meteorological Department climatological data from 1951-1980 at Alibaug shows that January is the coldest month ( $\sim 17^{\circ}\text{C}$ ) and April-May is the hottest month ( $\sim 40^{\circ}\text{C}$ ), accounting to be oppressive summer. We also explored a global weather service provider, Meteoblue, to study the regional weather pattern. They operate a series of weather models and integrate open data from various sources into

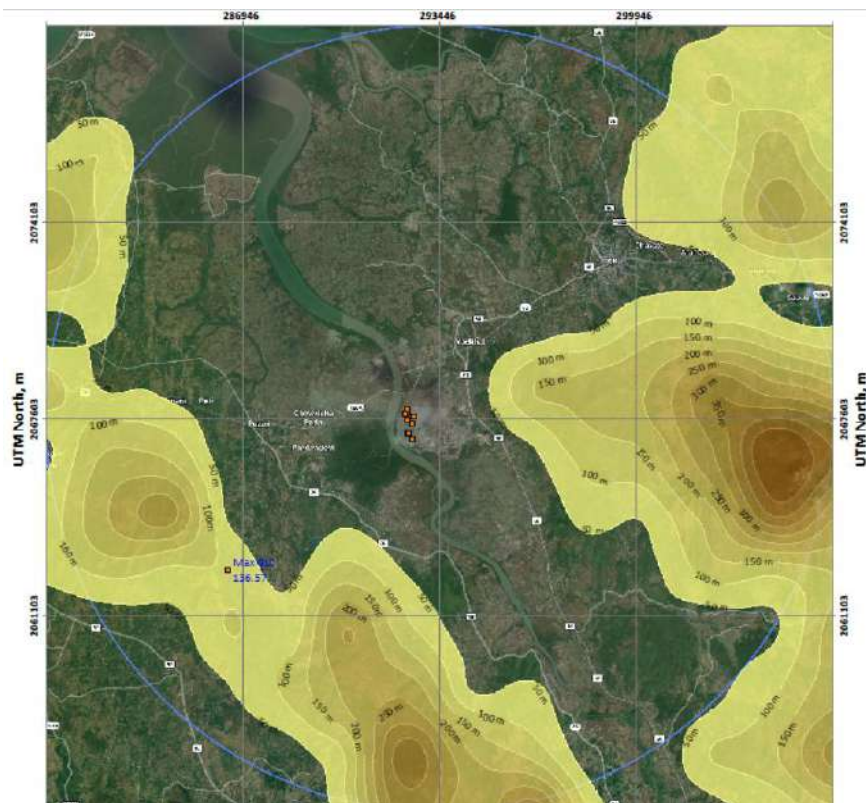


Fig. 2: Topographic contour levels of the study area.

Table 1: Dispersion coefficient  $s_y$  and  $s_z$  for stability class 'C'.

Dispersion co-eff.	Distance from source						
	400 m	700 m	1000 m	2000 m	4000 m	7000 m	10000 m
$s_y$	44 m	74 m	105 m	200 m	370 m	610m	840 m
$s_z$	26 m	43 m	61 m	115 m	220 m	360 m	510 m

(Source: Baines & Turner 1969)



the weather database to give valued data. Climate diagrams were based on 30 years of hourly weather model simulations that illustrate typical climate patterns.

Fig. 3 presents 30 km resolution simulated information in graphical format. Here, the minimum annual temperature varies between 17°C to 26°C and the maximum temperature between 27°C to 38°C. Conventionally the wind direction at IMD station at Alibaug is the North-West. At the onset of the monsoon, the winds move the course at 90° south and start blowing from South-West. From June to September, the sky remains moderately covered with clouds heavily.

The summer and cold seasons are the driest part of the year when relative humidity levels vary from 64-90%. The relative humidity is higher in the Southwest monsoon and retreating monsoon season, generally 81-90%. With the onset of the monsoon, the weather becomes slightly more relaxed and continues to be so throughout the monsoon period. The region experiences rainfall for about 75.6 days a year. The analysis of long-term rainfall data indicates July – is a higher rainy month with >300 mm rainfall, followed by August (~250 mm) and June (~200 mm). Average annual rainfall over the district averages 2200-3000 mm on the plains and >5000 mm in the hilly areas. Uran (2197 mm) and Mahad (3360 mm) are comparatively the least rainy northwest regions.

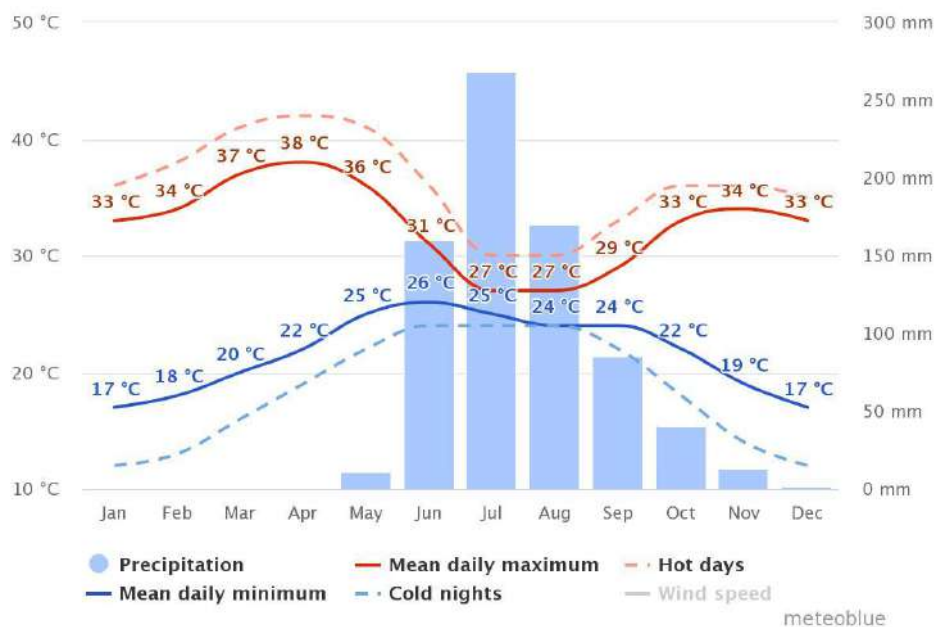
### Data Collection and Analysis

The project is part of an integrated steel plant located on the

west coast of Maharashtra. The 615.14 ha premises accommodate a series of processing units, i.e. Sponge iron plant, oxygen plant, Sinter plant, Blast furnace, Hot strip mill, Billet caster Bar mill, Coke oven Plant, Pellet plant, etc. We have considered a dedicated coke oven plant and pellet plant, where foremost processing occurs. We have identified potential conventional and non-conventional sources of pollutant emissions and estimated the load. Historical patterns and information about the monitoring station are essential considerations when interpreting air quality data. The unit has five continuous air quality monitoring stations in the region that record ambient pollutant levels at a pre-defined daily interval.

Regional weather data collected from the IMD Alibaug office and onsite weather station helped in site-specific details. The weather in the region is slightly unstable, as stated in IMD data, and the Pasquill atmospheric stability criteria for a wind velocity of one centimeter per second is class C. According to the guidelines on air quality models (PROBES/70/1997-1998), the model employs rural dispersion and regulatory defaults. The current study used meteorological data from one season (October–December) to determine the dispersion of pollution concentrations. The data on the mixing heights were obtained from the atlas of the meteorological monograph of the Indian meteorological department (Attri et al. 2008).

AERMOD's excellent efficiency for dispersion modeling of air pollutants up to a 50-km diameter of the pollutant



(Source: <https://www.meteoblue.com/en/weather/historyclimate/climatemodelled/18.690N73.040E>)

Fig. 3: Typical regional weather phenomenon.



source has been established in several studies throughout the world (Hanna et al. 2001, Cimorelli et al. 2005, Mohan et al. 2011, Gulia et al. 2015, Peter & Nagendra 2021). AERMOD (version 21112) is a steady-state Gaussian Plume Model used worldwide in a single wind field to transport emitted species, and it relates to surface upper air and meteorological observation. It also combines geophysical data (Gulia et al. 2015). AERMOD Cloud<sup>®</sup> application incorporates popular U.S. EPA air dispersion models AERMOD and ISCST3 into one integrated graphical interface to plot resultant isopleths. The model takes care of the rural dispersion and regulatory defaults options as per guidelines on air quality models (PROBES/70/1997-1998). AERMOD Cloud<sup>®</sup> algorithm has three separate components: dispersion model – AER-MIC, terrain preprocessor – AERMAP, and meteorological preprocessor – AERMET. Standalone integral processors enable smooth data flow across the modules and model. The application is used mainly to comply with the regulatory requirements (Cimorelli et al. 2005, Nagendra et al. 2012).

The primary pollutants of concern are PM<sub>10</sub>, PM<sub>2.5</sub>, Sulphur Dioxide (SO<sub>2</sub>), and Nitrogen Oxide (NO<sub>x</sub>). The total emissions from different sources depend upon source configuration, type and amount of fuel used emission factors, combustion/burning process rate, and the performance of control devices. The emission factors are obtained from the secondary sources classified by the end-use, fuel type, and furnace/boiler used in the industries and power plants. An emissions factor describes the link between the number of pollutants emitted into the atmosphere and the number of raw materials processed or fuel used in any polluting process. It is a relationship between the types and amounts of pollutants emitted and production capacity, the amount of fuel consumed, or the number of vehicle miles driven.

The EPA's emissions factor and process information for more than 200 air pollution source categories has been compiled in the AP-42 database since 1972. The present study refers to the fifth edition of AP-42 and updates in Volume I, Stationary Point and Area Sources (EPA 1995), and Emission Factor Documentation for AP-42 Section 12.2 Coke Production final report (EPA 2008). Stack height calculations referred from Emission Regulations – Part IV, CPCB '86, and the pollution control board consented criteria were implied. The widespread method based on the data available was to use emissions in terms of pollutant mass emitted per second.

### Pollutant Dispersion

A three-decade-old air quality dispersion model assisted in predicting local or regional air pollution levels in various circumstances, including weather, topographic features, and divergent sources (Venkatram 1979, Weil et al. 1992,

US-EPA 1998, Stein et al. 2007, Irwin 2014). When it is technically impossible to measure specific spots or areas due to contaminants from many sources, dispersion models are considered an alternate option (US-EPA 2009, Li et al. 2019).

Ground-level concentrations directly downwind at a distance of x meter from the source are given by following the Gaussian Plume source dispersion equation,

$$C_{(x,y,z)} = \frac{Q}{2\pi\bar{u}_x\sigma_y\sigma_z} \exp\left\{-\frac{y^2}{2\sigma_y^2}\right\} \exp\left\{-\frac{z^2}{2\sigma_z^2}\right\} \quad \dots(1)$$

Where,  $C_{(x,y,z)}$  = Concentration at ground level at a distance x meter from the bottom of chimney the downwind direction, µg/s; X = Downwind distance along plume mean center from source (200m to10000m); Q = Emission rate, µg/s; H = (h + Δh), effective height, m; Δh = Plumb rise, m; H = Height of the chimney, m;  $\sigma_y$  = standard deviations plume concentration (dispersion co-efficient) in horizontal direction, m;  $\sigma_z$  = standard deviations plume concentration (dispersion co-efficient) in Vertical direction, m

The value of the dispersion coefficient is determined by distance x, wind speed, and atmospheric stability conditions. The regional meteorological station determines a stability class. The wind direction fluctuation approach (Slade 1965) estimates hourly stability as suggested by the CPCB (PROBES/70/1997-1998). The determined Dispersion coefficients are given in Table 1.

### Emission Estimation

An emission inventory summarizes the pollutant emission potential in the immediate region of the proposed project activity under present conditions (Jang et al. 2020). Because they do not account for atmospheric reactions or unequal impacts of air pollutants on a mass basis, emission inventories have limitations (Wang et al. 2020). The plant has two major emission areas: the coke oven plant and the pellet plant having coke oven batteries, boiler, and dusting units attached to sub-units and silos.

Stack parameters considered are; height, diameter, temperature, velocity, volumetric flow rate, and emission rates. Table 2 and Table 3 illustrate stack details and emission estimated. A total of eight stacks were presently attached to their respective equipment through which the emissions are likely to come out.

### Model Input Parameters

AERMOD Cloud has been used for evaluating the emission scenarios for the proposed project. The inputs to the model are defined in five functional pathways, as represented in the following sections. Each of these operational parameters

includes several options that may be user-defined or set as default; the details of some of these essential elements used in the model run have given below.

#### A. Control pathway inputs

- Default option with Rural Setting
- Background concentration
- Averaging period of 24 hrs. as per NAAQS pollutant type

#### B. Source pathway inputs

- Includes definition of source, its locations
- Stack source parameters include emissions (g/s)

#### C. Receptors pathway inputs

- Cartesian grid starting at the SE corner of the ward with 2000m increment over X & Y coordinates, thus forming a receptor output grid radius of 13km

#### D. Meteorology pathways inputs

- One hourly data for the study period was used as an input in the meteorology processor to generate model ready one hourly input surface & profile meteorology files.

- Roughness length of 1m of measurement height, displacement height of 0.2m, Albedo of 0.2 at 10m height above ground
- The minimum wind speed ( $0.5 \text{ m.s}^{-1}$  lower than  $1 \text{ m.s}^{-1}$  considered as calm by IMD), predominant wind direction – SW, mixed layer height (900-750 m) denoting slightly unstable, and minimum heat flux  $20 \text{ W.M}^{-2}.\text{s}^{-1}$ )
- The Bowen ratio=Sensible Heat flux/Latent Heat Flux as a function of the month to allow smaller Bowen Ratios during the Indian monsoon season when the ground is wet and latent heat fluxes become significant (from 2 in non-monsoon to 0.5 in monsoon)
- The potential temperature gradient above the mixed layer ( $0.008 \text{ degrees/m}$ )

#### E. Output Pathway

Model run executed for the pollutant at stipulated average period and compared with NAAQS standards criteria. The contour for 1st highest reading is shown for each pollutant based on the uncontrolled and controlled scenario. Model outputs pollutant spatial distribution isopleths were plotted

Table 2: Stack details.

Sr. No.	Stack Attached to	Gas Quantity [ $\text{kg.h}^{-1}$ ]	Height [m]	Diameter [m]	Temperature [ $^{\circ}\text{C}$ ]	Velocity [ $\text{m.sec}^{-1}$ ]	Pollution Control Device
1	Coke Oven (Battery A & B)	3375	145	4.50	200	12.0	Natural Draft
2	Ground De-dusting system	162000	31	2.50	100	20.0	Bag Filters
3	Boiler	3475	40	2.00	150	12.0	-
4	Dedusting 1 & 2 (Mixer Unit)	NA	30.5	1.15	50	15.8	Bag Filters
5	Dedusting 3 (Betonite Unit)	NA	30.5	0.89	50	17.2	Bag Filters
6	Main ESP (Induration Furnace)	42100	100	6.25	110	20.0	ESP
7	Dedusting 7 (Hearth Layer)	NA	30.5	1.35	50	15.3	Bag Filters
8	Dedusting 8 (Final Product Silo)	NA	30.5	2.00	50	15.8	Bag Filters
9	Dedusting 9 (Final Product Silo)	NA	30.5	0.69	50	15.8	Bag Filters

Table 3: Stack emission estimates (g/sec).

Sr. No.	Stack Attached to	PM <sub>10</sub>	PM <sub>2.5</sub>	SO <sub>2</sub>	NO <sub>x</sub>
1	Coke Oven (Battery A & B)	36.2	24.6	18.1	72.5
2	Ground De-dusting system	2.9	2.0	-	-
3	Boiler	27.1	18.4	13.6	54.4
4	Dedusting 1 & 2 (Mixer Unit)	1.3	0.9	-	-
5	Dedusting 3 (Betonite Unit)	1.0	0.7	-	-
6	Main ESP (Induration Furnace)	19.9	13.5	9.9	39.9
7	Dedusting 7 (Hearth Layer)	1.6	1.1	-	-
8	Dedusting 8 (Final Product Silo)	2.3	1.6	-	-
9	Dedusting 9 (Final Product Silo)	0.8	0.5	-	-

across the impact zone. These isopleths were superimposed on the road-satellite hybrid tile map of the proposed region.

## RESULTS AND DISCUSSION

### Ambient Air Quality

The ambient air quality (AAQ) in a research region reveals the overall state of the environment. AAQ is a critical requirement for a healthy environment, and its depletion has a variety of long-term health consequences. Only if there are proportionate amounts of natural gases like oxygen and nitrogen and harmful gases like SO<sub>2</sub>, NO<sub>x</sub>, CO, CO<sub>2</sub>, Hydrocarbons, and others, introduced from diverse polluting sources can AAQ be regarded as exemplary. During the 2018-19 year, the study area's ambient air quality was measured using a network of five dedicated continuous ambient air quality stations located around the campus (Fig. 1). Ambient levels of PM<sub>10</sub>, PM<sub>2.5</sub>, SO<sub>2</sub>, and NO<sub>x</sub> were studied at 24 hourly average. During the study period, the missing information period varies between 0.3% and 33.3%. The maximum variation was mainly due to onsite construction activity disrupting power and communications supply, at times due to routine maintenance. The daily mean concentrations of particulates varied between 17.4-25.1 μg.m<sup>-3</sup> and 43.7-49.1 μg.m<sup>-3</sup> for PM<sub>2.5</sub> and PM<sub>10</sub>, respectively. At the same time, the daily mean gaseous concentrations varied between 5.9-9.9 μg.m<sup>-3</sup> and 7.3-31.8 μg.m<sup>-3</sup> for SO<sub>2</sub> and NO<sub>x</sub>, respectively. The observed levels were compared with the permissible National Ambient Air Quality Standard (NAAQS) stipulated by Central Pollution Control Board, New Delhi (CPCB 2009). A comparative account of observed concentration with the prescribed standards is given in Table 4. The average concentrations were found within the prescribed NAAQS.

### Meteorology

The plant has dedicated standalone weather stations installed within premises for uninterrupted meteorological data gather-

ing. The local representative wind data play an essential role in processing the meteorological information. And the same as defined in the AERMOD-AERMET metrological pathway.

Fig. 4 exhibits an annual and seasonal wind rose to integrate the prevailing wind directions for the modeling period. The wind rose was analyzed based on the wind direction, wind speed, and wind blowing frequency (Zelenko & Lisac 1994). Western winds were found dominant in the study area. Annual average winds blow from the southeast direction, i.e. 53% predominantly 132° directions. The study area shows minor variation in the predominant wind direction and does not vary much during the three seasons. Though, the wind flow intensity differs considerably. Post-monsoon winds blow from eastern areas. The annual average wind speed was 1.41 m.s<sup>-1</sup>, and the seasonal average was 1.84 m.s<sup>-1</sup>, 1.86 m.s<sup>-1</sup>, and 0.84 m.s<sup>-1</sup>, respectively, during pre-monsoon, monsoon, and post-monsoon, respectively. The calm winds' annual frequency was 11.07%.

The site-specific hourly meteorological data is processed with an AERMET meteorological processor. It generates two different model-ready databases, namely surface (\*.sfc) and upper (\*.pfl) meteorological profile formats (Cimorelli et al. 2004, Kumar et al. 2021). The AERMAP processor assigns a surface property to the receptor and source locations. Discrete grids assess dispersed pollutants' impact on the receptors and sensitive points (USEPA 2018). The domain of the study area had complex rural terrain, having process buildings, a river, hill range, etc., in the surrounding area. Air pollution dispersion contour maps are generated as isopleths, i.e. modeling study outputs, using both characteristic terrain data and emissions of the identified source. The modeling steps are illustrated (Fig. 5).

### Dispersion of Air Pollutants

The dispersion maps of the estimated particle and gaseous ground level concentrations were constructed based on the

Table 4: Summary of AAQ monitoring results (2018-19).

Station Code	AAQM Station	PM <sub>2.5</sub> [μg.m <sup>-3</sup> ]	PM <sub>10</sub> [μg.m <sup>-3</sup> ]	SO <sub>2</sub> [μg.m <sup>-3</sup> ]	NO <sub>x</sub> [μg.m <sup>-3</sup> ]
Permissible NAAQS (CPCB)	Residential, Industrial, rural area & other area	60	100	80	80
	Sensitive	60	100	80	80
Locations		Mean(±SD)	Mean(±SD)	Mean(±SD)	Mean(±SD)
AQ1	Kasumata Temple	17.7 (±8.0)	49.1 (±21.3)	7.3 (±2.3)	31.8 (±14.5)
AQ2	Coke Oven Plant	23.3 (±10.2)	43.7 (±18.2)	5.9 (±4.1)	8.8 (±2.1)
AQ3	MSEB Substation	19.5 (±13.0)	43.7 (±24.1)	7.3 (±2.0)	21.7 (±9.3)
AQ4	Goa Gate	25.1 (±9.9)	46.7 (±19.5)	9.9 (±2.4)	15.7 (±6.7)
AQ5	Dolvi Village	17.4 (±9.3)	47.7 (±22.5)	7.3 (±10.0)	7.3 (±2.5)

AERMOD analysis results for the highest averages of daily (24 h) concentrations obtained from Cartesian grid receptors. A POST FILE section in the model output pathway gives reporting choices. During the analysis, it uses hourly meteorological data when it calculates daily as 24 h mean. Continuing the maximum daily concentrations by year are

reported. A similar algorithm is also used for the annual output, assuming full years and taking a yearly average. The ground-level concentration (GLC) estimates and incremental concentrations with respect to identified sources were mapped within the assigned domain. The daily limits for ambient air pollutant concentrations were compared with

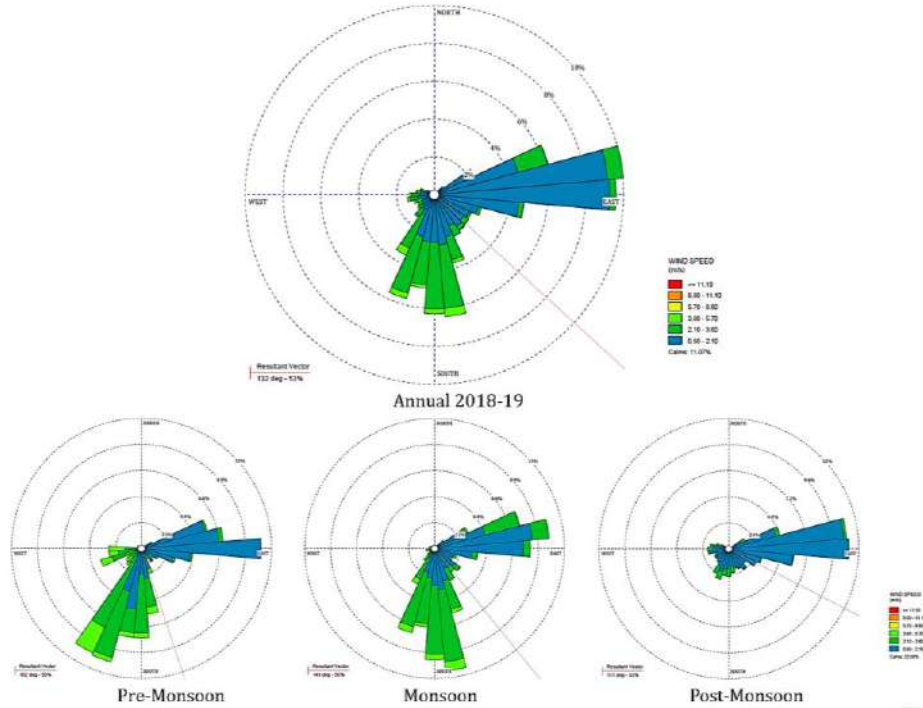


Fig. 4: Wind-rose 2018-19.

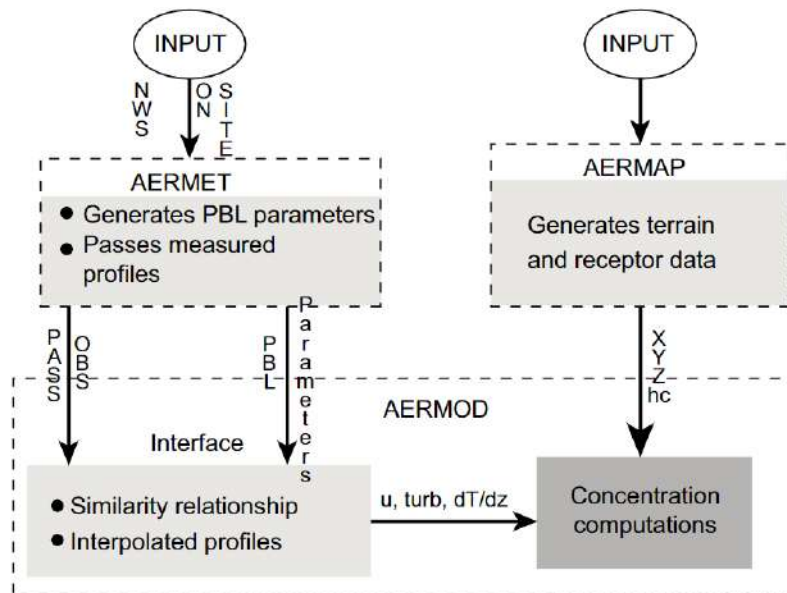


Fig. 5: AREMOD process flow (Cimorelli et al. 2004).



the stipulated NAAQS standards to assess the influence of specified activity.

According to the AERMOD modeling result, It is noticeable that the wind direction was observed from the West for the specific day and time when the maximum daily concentration was predicted.

October 24, 2018, was a highly polluted day at an elevation of 131.9m at a distance of 9,055m to the West of the reference point. The emission source's hourly modeled concentrations of identified pollutants illustrate the maximum daily peaks (Fig. 6-9). The maximum GLC of pollutants  $PM_{10}$ ,  $PM_{2.5}$ ,  $SO_2$ , and  $NO_x$  is predicted to be  $116.39 \mu\text{g}\cdot\text{m}^{-3}$ ,  $79.14 \mu\text{g}\cdot\text{m}^{-3}$ ,  $52.97 \mu\text{g}\cdot\text{m}^{-3}$ , and  $211.86 \mu\text{g}\cdot\text{m}^{-3}$ , respectively. Particulate matter and oxides of nitrogen have been found to exceed the prescribed limits of  $100 \mu\text{g}\cdot\text{m}^{-3}$ ,  $60 \mu\text{g}\cdot\text{m}^{-3}$ , and  $80 \mu\text{g}\cdot\text{m}^{-3}$ , respectively (CPCB 2009). The maximum daily concentration of  $SO_2$  from the activity conforms to the official limits. Target unit of an iron and steel industry operates through closed environments, the preparation of raw materials, accumulation of fines in Pellet plant, manufacturing of coke in coke ovens for feeding of burden to blast furnace, conversion of hot metal to steel, and shaping of steel, granulation of slag, recovery of chemicals in by-product plant, etc. All the processes mentioned above impact the surrounding environment (NEERI Technical Report 2019, 2021). Similar observations were reported in iron and steel industry-associated book chapters by Vallero (2014) along with Kumar and Kumar (2016). A concomitant effort is being made in the steel sector to explore the possibilities of using newer technologies to conserve the surrounding environment.

Along with a series of sectors, the Central Pollution Control Board (CPCB), in collaboration with the Ministry of Environment Forest and Climate Change, decreed several rules and regulations for industrial units that run on various fossil fuels and emit harmful emissions gases. The manufacturing activity regulations articulate, that the most regulated process exhaust emissions should pass through an unobstructed, vertical stack. The stack should be of sufficient height to ensure appropriate upward dispersion of the exhaust. It will minimize the ground level concentration of air pollutants where individuals may be exposed (Tadmor 1971, CPCB 1998, Bhanarkar et al. 2002). Also, the upward dispersion will not affect the wind blowing over adjacent buildings or buildings in the closest proximity. This may result in eddies in the downwind building cavity and wake areas, resulting in a significant increase of pollutant GLC and pulling the contaminated air back into the building through air intakes, windows, and doors (Lee & Stern 1973, Schnelle et al. 2015). The nine stacks of the present study

have variable heights ranging from 30.5 m to 145 m based on the emission intensity and prescribed limits. The isopleth resultant justifies the phenomenon with a higher process stack accounting for a distant ground-level concentration. This simulation defends the released emissions continually from the stack, resulting in spread out toward further downwind locations, showing the meteorological parameters' significant influence.

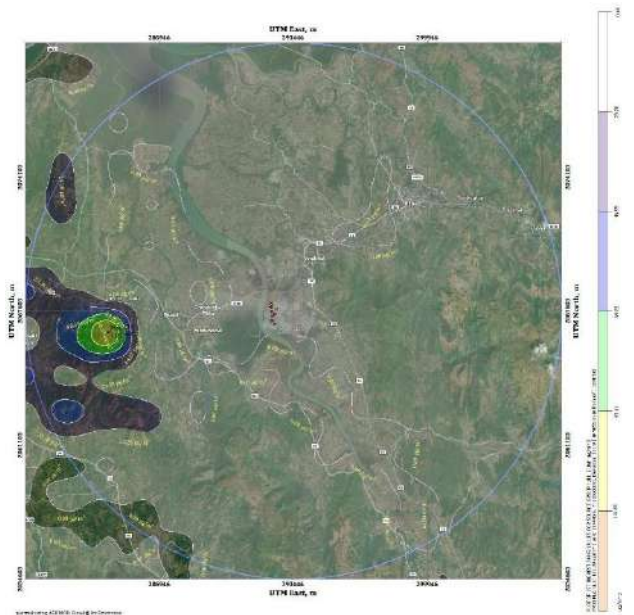


Fig. 6: AERMOD  $PM_{10}$  dispersion isopleth.

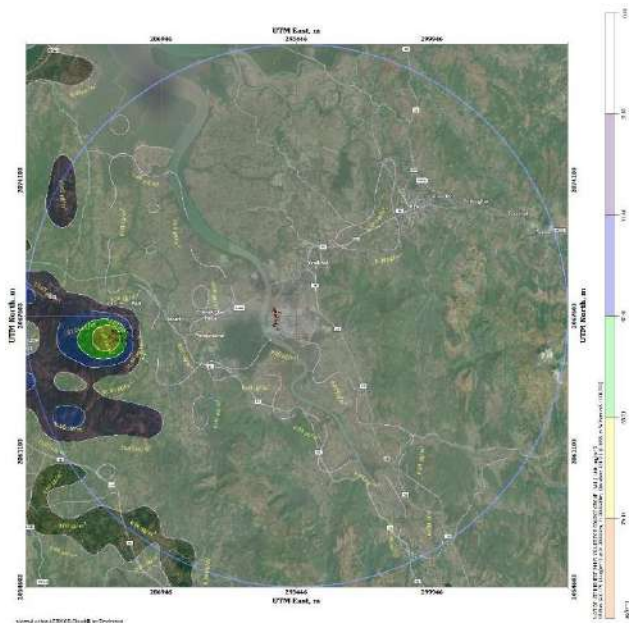


Fig. 7: AERMOD  $PM_{2.5}$  dispersion isopleth.

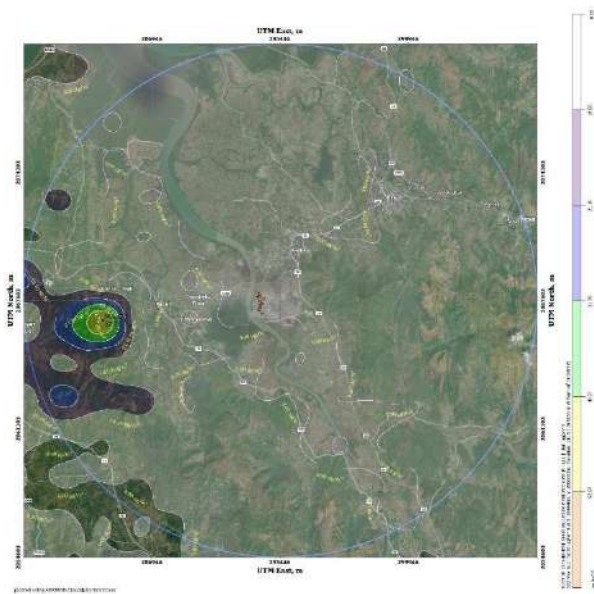


Fig. 8: AERMOD SO<sub>2</sub> dispersion isopleth.

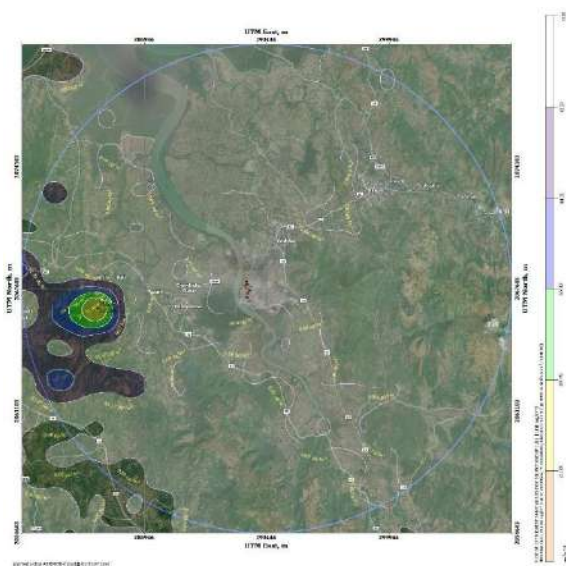


Fig. 9: AERMOD NO<sub>x</sub> dispersion isopleth.

## CONCLUSION

Understanding an atmospheric pollutant dispersion pattern is essential for meeting the stipulated emission reduction goals and minimizing adverse health impacts. Therefore, the emissions inventory and dispersion modeling studies have proven to be instrumental in limiting the environmental effects and responding to related concerns of urban local bodies and societies. The current research was the first to use an independent air quality modeling approach to exam-

ine pollutant dispersion discharged into the atmosphere by a coke and pellet mill near a seaside village. The American Meteorological Society/ Environmental Protection Agency Regulatory Model (AERMOD) was used to estimate the causative influence on the surrounding communities. The decade weather data illustrates the prevailing direction is southwestern winds. The source, including all active stacks with requisite air pollution control, devices attached to the coke oven plant, and pellet plant were considered to study dispersion extent. Considering the source effect shows a noticeable determination that the village area was in the background (upwind) of the source. Predicted isopleths were resultant of point source emissions only, and no other area or fugitive sources showed distant GLC during the study. There is always a risk of double-counting or omission of estimating emissions in processes peculiar sectors. It is evident that the emission factor assumes various fuel combustion practices. These were used to produce heat in the charging, sintering, purification, refining, etc. Coke ovens are heated by the mixture of blast furnace and coke oven gas, which is also transferred to the plant's on-site pellet production processes. The present study put a stage for continual improvement in emission estimation with periodically available contemporary emissions factors. Also, the technological advancements will reduce the efforts and monetary implications for the same.

## ACKNOWLEDGEMENT

The authors express sincere thanks to Prof. Suresh Gosavi, Head, Department of Environmental Sciences, Savitribai Phule Pune University (SPPU), and also thankful to Dr. Anand Rai, General Manager and Head, Department of Environment, and Mr. Gajraj Singh Rathore, President of JSW steel plant Geetapurm Dolvi, Tal. Pen and District Raigad, Maharashtra (India) for providing necessary equipment facilities to carry out the present research work and giving their constant support and encouragement to complete this research work and Amba River Coke Ltd. (ARCL) management for their continued support during the study. Appreciations also go to the Indian Institute of Tropical Meteorology, Indian Meteorological Department, Pollution Control Board, Faculty of Environment Science SPPU, and AERMOD Cloud model development team for providing valuable inputs for smooth operations during the study. We extend a special thanks to members of the ARCL for their general assistance.

## REFERENCES

- Amodio, M. 2012. How a steel plant affects the air quality of a nearby urban area: a study on metals and PAH concentrations. *Aerosol Air Qual. Res.*, 13(2): 497-508.



- Arvola, J., Harkonen, J., Mottonen, M., Haapasalo, H. and Tervonen, P. 2011. Combining steel and chemical production to reduce CO<sub>2</sub> emissions. *Low Carbon Econ.*, 2: 115-122.
- Attri, S., Singh, S., Mukhopadhyay, B. and Bhatnagar, A. 2008. Atlas of Hourly Mixing Height and Assimilative Capacity of Atmosphere in India. India Meteorological Department. <http://www.worldcat.org/title/atlas-of-hourly-mixing-height-and-assimilative-capacity-of-atmosphere-in-india/oclc/639036996>
- Baines, W. and Turner, J. 1969. Turbulent buoyant convection from a source in a confined region. *J. Fluid. Mech.*, 37: 51-80.
- Bhanarkar, A., Gajghate, D. and Hasan, M. 2002. Assessment of air pollution from small-scale industry. *Environ. Monit. Assess.*, 80(2): 125-133.
- Central Pollution Control Board (CPCB). 1998. Assessment of Impact on Air Environment: Guidelines for Conducting Air Quality Modelling, Privesh Newsletter. The Central Pollution Control Board, New Delhi, India.
- Central Pollution Control Board (CPCB). 2010. Air Quality Monitoring, Emission Inventory and Source Apportionment Study for Indian Cities, National Summary Report. The Central Pollution Control Board, New Delhi, India
- Central Pollution Control Board (CPCB). 2009. Archived Technical Reports. The Central Pollution Control Board, New Delhi, India
- Chaulya, S.K. 2019. Air quality modeling for prediction of dust concentrations in iron ore mines of Saranda region, Jharkhand, India. *Atmos. Pollut. Res.*, 10(3): 675-688.
- Cimorelli, A., Perry, S., Venkatram, A., Weil, J., Paine, R., Robert, W., Lee, R., Peters, W., Brode, R. and Paumier, J. 2004. AERMOD: Description of Model Formulation (EPA-454/R-03-004). USEPA, Washington, DC, USA.
- Cimorelli, A., Perry, S., Venkatram, A., Weil, J., Paine, R., Wilson, R., Lee, R., Peters, W. and Brode, R. 2005. AERMOD: A dispersion model for industrial source applications. Part I: General model formulation and boundary layer characterization. *J. Appl. Meteorol.*, 44: 682-693.
- EPA. 1995. AP-42: Compilation of Air Emission Factors, U.S. Environmental Protection Agency, Research Triangle Park, NC.
- EPA. 2008. Emission Factor Documentation for AP-42 Section 12.2. Coke Production – Final Report, U.S. Environmental Protection Agency, Research Triangle Park, NC.
- Gogikar, P. 2019. Seasonal prediction of particulate matter over the steel city of India using neural network models. *Model. Earth Syst. Environ.*, 5: 227-243.
- Govender, P., and Sivakumar, V. 2020. Application of k-means and hierarchical clustering techniques for analysis of air pollution: A review (1980–2019). *Atmos. Pollut. Res.*, 11(1): 40-56.
- Gulia, S., Nagendra, S., Khare, S. and Khanna, I. 2015. Urban air quality management: A review. *Atmos. Pollut. Res.*, 6(2): 286-304.
- Hanna, S., Egan, B., Purdum, J. and Wagler, J. 2001. Evaluation of the ADMS, AERMOD, and ISC3 dispersion models with the OPTEX, Duke Forest, Kincaid, Indianapolis, and Lovett field datasets. *Int. J. Environ. Pollut.*, 16(1-6): 301-314.
- Invernizzi, M.B. 2020. An odor impact assessment by considering short-term ambient concentrations: A multi-model and two-site comparison. *Environ. Int.*, 144: 105990.
- Irwin, J.S. 2014. A suggested method for dispersion model evaluation. *J. Air Waste Manag. Assoc.*, 64(3): 255-264. DOI: 10.1080/10962247.2013.83314
- Jang, Y., Lee, Y., Kim, J., Kim, Y. and Woo, J. 2020. Improvement of China point source for improving bottom-up emission inventory. *Asia-Pacific J. Atmos. Sci.*, 56: 107-118. <https://doi.org/10.1007/s13143-019-00115-y>
- Joshi, P. and Mahadev, S. 2011. Distribution of air pollutants in ambient air of district Haridwar (Uttarakhand), India: A case study after the establishment of State Industrial Development Corporation. *Int. J. Environ. Sci.*, 2(1): 237-258.
- Kim, Y. and Worrell, E. 2002. International comparison of CO<sub>2</sub> emission trends in the iron and steel industry. *Energy Policy*, 30(10): 827-838.
- Kumar, A., Dikshit, A. and Patil, R. 2021. Use of simulated and observed meteorology for air quality modeling and source ranking for an industrial region. *Sustainability*, 13(8): 4276. <https://doi.org/10.3390/su13084276>
- Kumar, D. and Kumar, D. 2016. Management of Coking Coal Resources, Elsevier, The Netherlands. <https://doi.org/10.1016/B978-0-12-803160-5.00001-0>.
- Lee, W. and Stern, A. 1973. The stack height requirements are implicit in the federal standards of performance for new stationary sources. *J. Air Pollut. Control Assoc.*, 23(6): 05-513.
- Li, Y., Huang, G., Cui, L. and Liu, J. 2019. Mathematical modeling for identifying cost-effective policy of municipal solid waste management under uncertainty. *J. Environ. Inform.*, 34: 55-67.
- Ministry of Steel. 2014. Investment Facilitation & Make In India, <https://steel.gov.in/make-india>
- Mohan, M., Bhati, S., Sreenivas, A. and Marrapu, P. 2011. Performance evaluation of AERMOD and ADMS-urban for total suspended particulate matter concentrations in megacity Delhi. *Aerosol Air. Qual. Res.*, 11(7): 883-894.
- Mukkannawar, U., Ojha, A., Shenvi, V. and Kumar, R. 2014. Network design and evaluation through PM10 & PM2.5 mass loading. *Int. J. Curr. Microbiol. App.*, 3(11): 675-682.
- Nagendra, S., Khare, M., Gulia, S., Vijay, P., Chithra, V., Bell, M. and Namdeo, A. 2012. Application of ADMS and AERMOD Models to Study the Dispersion of Vehicular Pollutants in Urban Areas of India and the United Kingdom. Proceedings of 20<sup>th</sup> WIT International Conference on Air Pollution, May 16-18, 2012, Coruna, Spain, WIT Press, England, pp. 3-12.
- National Ambient Air Quality Standards, 2009. Ministry of Environment, Forests and Climate Change (MoEF&CC), Government of India, New Delhi, India
- NEERI Technical Report. 2019. Carrying Capacity Study of the Dolvi Area – Baseline Environmental Report Winter Season JSW Steel Ltd., Dolvi Works.
- NEERI Technical Report. 2021. Carrying Capacity Study of the Dolvi Area – Air Environment, JSW Steel Ltd., Dolvi Works.
- Nuterman, R. and Baklanov, A. 2007. Overview and application of obstacle resolved models for airflow and pollution transport. *Sci. Rep.*, 11: 03-07.
- Peter, A. and Nagendra, S. 2021. Dynamics of PM 2.5 pollution in the vicinity of the old municipal solid waste dumpsite. *Environ. Monit. Assess.*, 193(5): 1-16.
- Reddy, K., Murali K.KVSG., Reddy, S. and Asadi, S. 2017. An analytical approach for environmental pollution control through solid waste management: A model study. *Int. J. Civ. Eng.*, 8(11): 579-590.
- Sancini, G., Farina, F., Battaglia, C., Cifola, I., Mangano, E., Mantecca, P., Camatini, M. and Palestini, P. 2014. Health risk assessment for air pollutants: alterations in lung and cardiac gene expression in mice exposed to Milano winter fine particulate matter (PM2.5). *PLoS One*, 9(10): 109685.
- Schnelle, K., Ternes, M. and Dunn, R. 2015. Air Pollution Control Technology Handbook. Second Edition. CRC Press, Boca raton, Florida. <https://doi.org/10.1201/b19286>
- Sharma, R. and Parvez, S. 2003. Spatial and seasonal variability of ambient concentrations of particulate matter around an integrated steel plant: A case study. *J. Sci. Ind. Res.*, 62: 838-845.
- Slade, D.H. 1965. DispersIon Estimated from Pollutant Release of a Jew seconds to eight hours il/ DI/ratioll Technical Note, 2, ARC-I, US, ESSA, 23.
- Smirnova, M., Nikitin, V., Pestov, D. and Zhu, Z. 2020. Mathematical modeling of air pollution in city tunnels and evaluating mitigation strategies. *Transp. Res. Interdiscip. Perspect.*, 416: 100086. <https://doi.org/10.1016/j.trip.2019.100086>.

- Stein, A., Isakov, V., Godowitch, J. and Draxler, R. 2007. A hybrid modeling approach to resolve pollutant concentrations in an urban area. *Atmos. Environ.*, 41: 9410-9426.
- Tadmor, J. 1971. Consideration of deposition of pollutants in the design of a stack height. *Atmos. Environ.*, 5(7): 473-482.
- Thomas, A. 2021. Heart of steel: How trade unions lobby the European Union over emissions trading. *Env. Polit.*, <https://doi.org/10.1080/09644016.2021.1871812>
- Tyagi, R.K. 2015. Improved intake manifold design for IC engine emission control. *Int. J. Eng. Sci. Technol.*, 10(9): 1188-1202.
- US-EPA. 1998. Revised draft user's guide for the AMS/EPA regulatory model-AERMOD. Office of Air Quality Planning and Standards. Emissions. USEPA Monitoring and Analysis Division. Research Triangle Park, North Carolina.
- US-EPA, 2009. AERMOD Implementation Guide. US Environmental Protection Agency. Office of Air Quality Planning and Standards. Emissions Monitoring and Analysis Division. Research Triangle Park, North Carolina
- US-EPA, 2018. YEAR IN REVIEW. [https://www.epa.gov/sites/default/files/2019-01/documents/epa\\_2018\\_yearinreview\\_0128-4.pdf](https://www.epa.gov/sites/default/files/2019-01/documents/epa_2018_yearinreview_0128-4.pdf)
- Vallero, D. 2014. *Fundamentals of Air Pollution*. Fifth Edition, Academic Press, Cambridge, MA. <https://doi.org/10.1016/B978-0-12-401733-7.12001-8>.
- Venkatram, A. 1979. The expected deviation of observed concentrations from predicted ensemble means. *Atmos. Environ.*, 13(11): 1547-1549.
- Wang, Y., Niu, B., Ni, J., Xue, W., Zhu, Z., Li, X. and Zou, G. 2020. New insights into concentrations, sources, and transformations of NH<sub>3</sub>, NO<sub>x</sub>, SO<sub>2</sub> and PM at a commercial manure-belt layer house. *Environ. Pollut.*, 262: 114355.
- Weil, J., Sykes, R. and Venkatram, A. 1992. Evaluating air-quality models: Review and outlook. *J Appl. Meteorol.*, 31: 1121-1145.
- Zelenko, B. and Lisac, I. 1994. On the statistical wind rose analysis. *Theor. Appl. Climatol.*, 48: 209-214. <https://doi.org/10.1007/BF00867051>



# Modeling of Leachate Generation from Landfill Sites

Yeshi Choden†, Kinley Pelzang, Abeshik Dev Raj Basnet and Krishna Bdr Dahal

Department of Civil Engineering, College of Science and Technology, Royal University of Bhutan, Phuentsholing, Bhutan

†Corresponding author: Yeshi Choden; yeshichoden.cst@rub.edu.bt

Nat. Env. & Poll. Tech.  
Website: [www.neptjournal.com](http://www.neptjournal.com)

Received: 27-05-2021  
Revised: 10-08-2021  
Accepted: 27-08-2021

### Key Words:

Leachate  
Landfill  
Leachate generation  
Precipitation  
Fusion method

### ABSTRACT

With rapid urbanization and industrialization, Bhutan is developing at a fast pace due to which solid waste generation is increasing day by day and hence its management has become a great issue. One of the management issues that are faced in the management of landfills is the generation of toxic soup from landfills known as leachate which is one of the causes of water and soil pollution. The landfills in Bhutan lack a proper leachate management system and those that have leachate collection tanks are very uneconomical due to unreliable methods being used to determine the leachate generated amount. Leachate generation from municipal solid waste (MSW) landfills by various methods such as Standard, Rational, and Mass balance methods was determined, analyzed the results and ultimately developed a reliable method for determining the amount of leachate generated by a landfill known as "Fusion method". The quantified leachate volume from the study area was 4565.98 m<sup>3</sup> with the annual precipitation amount being 15156.09 m<sup>3</sup> with the developed (fusion) method. Validation of the model was performed on data from Deir Al Balah landfill, Gaza strip, Palestine. The validated amount of leachate generation is about 123,833.08 m<sup>3</sup> by the fusion method, while the actual amount of leachate generated was about 114,351 m<sup>3</sup> from which the percentage difference between the fusion method and the actual amount of leachate generated was found to be only 8.29%, compared to other methods with % error ranged from 10-55 %.

### INTRODUCTION

Bhutan is a small developing country with a total area of 38,394 km<sup>2</sup>. The country is developing rapidly with exponential population growth and economic progress. The population of the country was estimated to be 771,608 in the year 2020, out of which 45.8% lived in the rural area and 54.2% lived in urban areas (National Statistics Bureau 2018). The National Environment Commission's (NEC) report has pointed out that, with rapid socio-economic growth, increased population, and urbanization, the country is seeing an increase in the volume of solid waste generated. Hence its management is becoming a great issue with many problems evolving (National Environment Commission 2016). One such problem is the generation of toxic soup from landfills known as leachate which is formed when waste is subjected to biological and physiochemical transformation. These are highly toxic and can pollute the land, groundwater, and waterways. Bhutan has about 25 open dumpsite landfills and almost all of them lack a leachate treatment/management system which was mentioned in the BSE report 2016 by the NEC of Bhutan (National Environment Commission 2016).

Leachate is highly polluted and complex wastewater containing high amounts of dissolved and suspended

matter generated from percolated water through the waste in landfills. Leachate treatment is very important as it could threaten the surrounding ecosystem when discharged and mixed with groundwater. The increase in municipal solid waste in the country has led to a major issue. (Raghab et al. 2013) explained the formation processes of the leachate generation. Then the anaerobic treatment of leachate was performed using coagulation and flocculation processes. They utilize natural low-cost materials to enhance the chemical treatment process. The result of the study concluded that the treatment was obtained using alum and accelerator (perlite and bentonite). The leachate generation mainly depends on the precipitation and the moisture contained by the waste. The water balance method has been used to determine the rate of leachate generation and found that the estimated amount by the water balance method is coming close to the actual leachate rate, although using closed landfills was reported as a limitation of the study (Baziene et al. 2013). Also, the moisture content of the waste plays a big role in the production of the leachate. It is the moisture content of the waste which results in the production of leachate generated by the waste itself and the amount of precipitated rainfall entered into the waste. Even though, the leachate generation by waste itself depends on a number of



factors, moisture content by the waste is one of the major factors which contribute to leachate generation (Hashisho & El-Fadel 2014).

Bhutan does not have a proper waste or leachate treatment system. Since the wastes are dumped from different sources and unseparated, leachate generated will consist of different constituents such as highly toxic chemicals and heavy metals (World Bank 2000). Also, Landfill leachate has been one of the most prominent threats to living beings, especially aquatic animals. Studies have been carried out and studied about the social and environmental risk associated with landfill leachate, its deterioration effects on ecosystems and thus proper quantification of leachate generated from a dumpsite if significant to prevent its pollution effect on ground and water (Ololade et al. 2019).

Various methods are implemented for quantifying the amount of leachate generated by a landfill such as the standard method, rational method, and many other conventional methods. But some conventional methods either overestimate or underestimate the amount of leachate which leads to the design of uneconomical tanks for the leachate collection system. Estimation of leachate generation from MSW landfills in Selangor was performed using the formula  $V = 0.15 \times R \times A$  for the calculation of leachate generation. The area (A) of the landfill was calculated using Google Earth and multiplied by annual rainfall (R). Since only two factors are considered, the estimated leachate generated was mostly assumption based. For the calculation of leachate generation, they have selected the closed landfill but most of the landfills are always active. Mainly because of closed landfills the leachate generated by the waste itself was neglected (Ibrahim et al. 2017). Other scenarios could be, the generation of leachate being more and as a result, the tank will overflow during peak season. (Komilis & Athiniotou 2014) have developed a model called as monthly water budget model for the estimation of leachate generation. For the validation of the model, they have used actual leachate generated at the field as they have a record of two years. The main drawback of the model was the negligence of runoff.

This study emphasizes studying various conventional methods and eventually developing a more reliable method and then calculating the leachate generated by a landfill using all of the methods. According to the literature reviews, it was observed that there are a number of parameters that affect the quantification of leachate generation, and all of the above methods that have been reviewed lacked one or more parameters in their method which affects the reliability of the result for calculation of leachate generation. For instance, even if all the parameters are considered for calculation, the complexity increases. Moreover, to obtain some parameters

there is a requirement of expensive and complex equipment. Thus, this research aims to develop a model that quantifies the leachate generation considering more onsite parameters and presents less percentage error compared to other methods.

## STUDY AREA

Phuentsholing Thromde is located in the south-western foothills of the country with an area of 15.6 sq. km housing a projected population of more than 30,000 including the floating population. The Thromde produces a total amount of 7200 tons of waste annually all being dumped in the only landfill located at Pekarshing (Fig. 1) which is seven km away from the town. Currently, 15-20 tons of waste are dumped at the landfill per day. The waste composition of the landfill is 5% textile, 7% yard, 8% organic material, 6% paper, 12% plastic, 13% Inert Material, 40% Glass, and 9% Metals (Choden et al. 2021).

Through an experimental study, the following data were obtained:

- Field density 14%
- The moisture content of the soil was 12.11%
- The density of the soil was 201.132 Kg.m<sup>-3</sup>
- The total area of the landfill is 3030.49 m<sup>-2</sup>

With a total of 7.2 km<sup>2</sup> designated area, only 1.2 km<sup>2</sup> area has been used as a landfilling site. The landfill is divided into two parts i.e., an old inactive landfill and a new operational landfill as seen in Fig. 1. The design capacity of the landfill is 24 metric tons per day (Mt.d<sup>-1</sup>) with a design period of 10 years. The landfill is an open dumpsite system. The annual precipitation for the year 2020 is 15,156.09 m<sup>3</sup> for the landfill area.

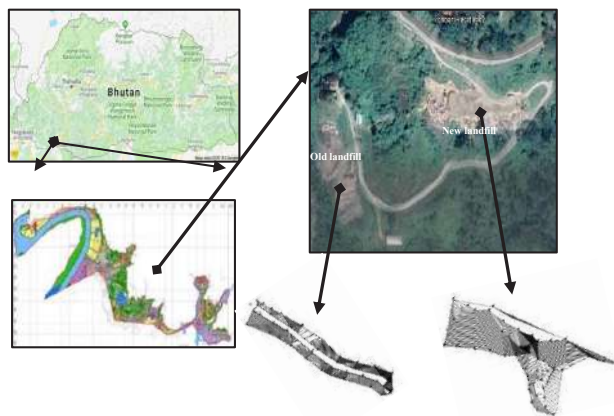


Fig. 1: Pekarshing landfill.

**MATERIALS AND METHODS**

The methodology emphasizes studying various conventional three methods, eventually developing a more reliable method and then calculating the leachate generated by a landfill using all of the methods. All the conventional methods were carefully studied and a new method (fusion) was developed. The calculation for leachate generation by Pekarshing landfill was done. A model was developed for the quantification process and then the result of the model was compared with conventional results.

**Standard Method**

A standard method is a simple mathematical model to estimate the amount of leachate generated from municipal solid waste (MSW). It is one of the most used methods or models to estimate the leachate generated in municipal landfills even these days. Many countries in the world adopted this method as it is simple and also has been used for a long time. This method does not consider many parameters. Instead, coefficient 0.15 is taken to consider all the losses in the landfill. The total quantity of leachate is a fraction of the total precipitation (about > 75%) in the active phase and <10% in the closed phase. Peak rate (volume per unit time) is a function of the peak precipitation and height of waste. If the peak precipitation occurs when the waste height/thickness is small, the peak leachate rate is directly proportional to the peak precipitation rate. Whereas if the peak precipitation occurs when the thickness is full of height, the effect is delayed and the peak leachate rate is less than the peak precipitation rate. The relation for the estimation of leachate using this method is shown in equation 1 (Ibrahim et al. 2017).

$$V = 0.15 \times R \times A \quad \dots(1)$$

Where;

V is the volume of leachate discharge in a year (m<sup>3</sup>. year<sup>-1</sup>).

R is annual rainfall (m).

A is the surface area of the landfill (m<sup>2</sup>).

**Rational Method**

The rational method requires certain parameters to be considered to calculate the amount of leachate generated. The parameters are rainfall precipitation, area of the landfill, and leachate generation coefficient. In the case of coefficient, it is considered based on the nature of the landfill, i.e. if it is a currently used landfill or an old landfill that was disbanded. For an old landfill, the coefficient considered is 0.3 and for a currently operational landfill, the coefficient considered is 0.5. Therefore, the amount of leachate generated is calculated by equation 2 (JICA 2009).

$$Q = I_j \times C \times A \quad \dots(2)$$

Where;

Q is the amount of leachate generated.

I<sub>j</sub> is rainfall mm/month.

C is the coefficient of leachate generated.

A is the area of the landfill.

**Mass Balance Method**

This is one of the conventional methods to calculate leachate generation. It takes into consideration the leachate generated by waste itself. In most of the methods, the leachate generated by waste itself is neglected which leads to incorrect estimation. Unlike the other two conventional methods, it considers more parameters like the amount of waste produced, infiltration, and precipitation (Yang et al. 2015).

Equation 3 is used for the calculation of mass balance:

$$L = PI + W_s \quad \dots(3)$$

where;

PI is the leachate generated from the precipitation infiltrated and it can be calculated from

$$PI = \sum_c^n \frac{P \times (I_c/100) \times t_c}{\rho \times h}$$

P represents precipitation in mm per month,

I<sub>c</sub> represents the ratio of infiltration,

t<sub>c</sub> is the time period of the top cover,

ρ is the density of the waste in tons per m<sup>3</sup> and,

h is the uniform height of the waste in m.

PI is the leachate generated by precipitation infiltrated in liter per ton.

Phuntsholing thromde produces waste of 450 to 600 tons of waste per month and the uniform height of the waste is considered 3.5 m. The density of the waste on the landfill was found to be 0.202 tons per m<sup>3</sup> and the soil cover c was done every month. The ratio of infiltration in the year 2020 was found to be 35%.

W<sub>s</sub> is the leachate generated by waste itself or the water squeezed from the waste. Now to calculate the W<sub>s</sub> we have:

$$W_s = IDM \times \left( \frac{IMCDM}{100} - \frac{FCCDM}{100} \right) \times 1000$$

Where;

- W<sub>s</sub> is the leachate produced by waste itself in liter per ton,

- IDM is the initial dry mass which is calculated from

$$IDM = \left( 1 - \frac{IMC}{100} \right),$$

- IMC is the moisture content of the waste,

- IMCDM is the initial moisture content of the dry mass calculated as

$$IMCDM = \frac{IMC}{1 - \left(\frac{IMC}{100}\right)}$$

- $F_{cc}$  is the field capacity of the waste in % and,  $F_{cc}DM$  is

$$\text{the field capacity of the dry mass i.e., } F_{cc}DM = \frac{F_{cc}}{1 - \left(\frac{F_{cc}}{100}\right)}$$

Since both the PI and  $W_S$  have the same unit i.e., liter per ton, from which we can observe that the factors directly depend on the waste generation and not on the area of the waste covered which is one of the drawbacks of this method. The mass balance method considers more input parameters compared to the other two conventional methods.

**Fusion Method**

Compared to other conventional methods, this method takes into account, the number of parameters for the calculation of leachate generation. In the standard method and rational method, a certain percentage (15% for standard method, 30-50% for rational method) of precipitation is considered for the leachate generation and in the case of the mass balance method, important parameters such as area of contribution and precipitation are not considered for calculation of the leachate generation.

In this fusion method, all the above problems stated are resolved. It considers all the parameters such as runoff, evaporation, precipitation, leachate generated by waste itself, and area of contribution.

To develop the mathematical model, the water budget equation is used, which states that the continuity equation for water in various phases for a given area is written as:

$$\text{Mass inflow} - \text{Mass outflow} = \text{Change in storage} \\ V_i - V_o = \Delta S \quad \dots(i)$$

Considering the precipitation as the only source of water entering the landfill and other sources like groundwater and spring water are not considered because the location of the landfill should not be near any water source.

$$V_i = P \text{ (precipitation)}$$

It is known that in a given watershed the losses of water are given by runoff (R), evaporation (E), leachate that enters the landfill and comes out (L), and the transpiration (T). Consider the losses due to the transpiration as negligible.

$$V_o = R + E + L$$

Substitute the  $V_i$  and  $V_o$  in equation i;

$$P - R - L - E = \Delta S \quad \dots(ii)$$

Now to understand the change in the storage capacity, field capacity is needed, which is the maximum holding capacity of the waste. When there is no water in the waste, it is known as wilting point. The drainable water between the field capacity and saturation point is the liquid that comes as the leachate which is all shown in Fig. 2.

It can be written as;

$\Delta S$  as field capacity – leachate generated by waste itself.

$\Delta S = (F_{cc} \times I) - W_S$ ; where I is the infiltration which can find out by  $I = P - R - E$

Substituting the  $\Delta S$  in equation ii;

$$P - R - L - E = (F_{cc} \times I) - W_S$$

Making L the subject we get,

$$L = P - R - E - (F_{cc} \times I) - W_S \quad \dots(iii)$$

The above equation iii is known as the fusion formula and it is the formula that is being proposed for the calculation of the leachate generation. Since numbers of parameters are considered in this method, less percentage error could be expected.

Table 1 shows the calculation for leachate generation by various methods and Table 2 shows the calculation for leachate generation using the fusion method at the Pekarshing landfill. The total area of landfill is 3030.49 m<sup>3</sup> and waste generation is 600 tons per month. Leachate generated is 4565.98 m<sup>3</sup> which is 30.13% of precipitation, i.e., 15156.09 m<sup>3</sup> calculated in Table 3.

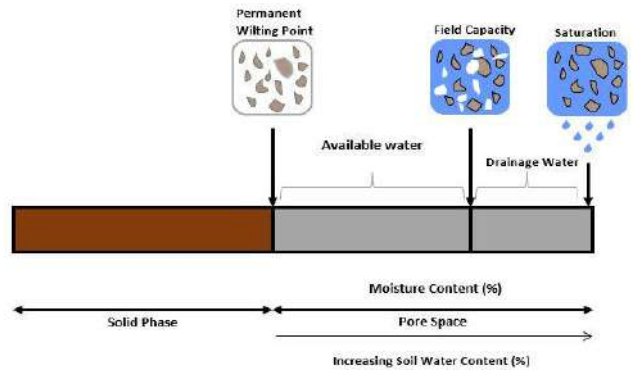


Fig. 2: Field capacity of soil.

Table 1: Leachate amount by various methods.

Method	Estimated Leachate generation in Pekarshing landfill in 2020 [m <sup>3</sup> ]
Standard Method	2273.41
Rational Method	6095.41
Mass Balance method	2346.35
Fusion Method	4565.98

Table 2: Estimation of Leachate generation by fusion method in Pekarshing landfill.

Sl.No.	Month Parameters	Jan	Feb	Mar	Apr	May	Jun	Jul	Aug	Sep	Oct	Nov	Dec
1	Rainfall (R)	0	40.8	113.2	207.3	533.1	1549.4	973.2	650.4	826.2	107.6	0	0
2	Area (A <sub>1</sub> )	356.32	356.32	356.32	356.32	356.32	356.32	356.32	356.32	356.32	356.32	356.32	356.32
3	Area (A <sub>2</sub> )	1191.89	1191.89	1191.89	1191.89	1191.89	1191.89	1191.89	1191.89	1191.89	1191.89	1191.89	1191.89
4	Area (A <sub>3</sub> )	204.68	204.68	204.68	204.68	204.68	204.68	204.68	204.68	204.68	204.68	204.68	204.68
5	Area (A <sub>4</sub> )	1277.6	1277.6	1277.6	1277.6	1277.6	1277.6	1277.6	1277.6	1277.6	1277.6	1277.6	1277.6
6	Evaporation	0	12.4	22.6	32.8	71.5	67.5	60.3	0	40.8	52.2	0	0
7	Runoff Coefficient (C <sub>1</sub> )	0.3	0.3	0.3	0.3	0.3	0.3	0.3	0.3	0.3	0.3	0.3	0.3
8	Runoff Coefficient (C <sub>2</sub> )	0.6	0.6	0.6	0.6	0.6	0.6	0.6	0.6	0.6	0.6	0.6	0.6
9	Runoff Coefficient (C <sub>3</sub> )	0.3	0.3	0.3	0.3	0.3	0.3	0.3	0.3	0.3	0.3	0.3	0.3
10	Runoff Coefficient (C <sub>4</sub> )	0.7	0.7	0.7	0.7	0.7	0.7	0.7	0.7	0.7	0.7	0.7	0.7
11	Field capacity	0.14	0.14	0.14	0.14	0.14	0.14	0.14	0.14	0.14	0.14	0.14	0.14
12	Water hold by waste in mm (A <sub>1</sub> )	0.00	2.26	7.93	15.72	42.23	142.39	86.93	63.74	75.26	3.24	0.00	0.00
13	Water hold by waste in mm (A <sub>2</sub> )	0.00	0.55	3.18	7.02	19.84	77.32	46.06	36.42	40.56	-1.28	0.00	0.00
14	Water hold by waste in mm (A <sub>3</sub> )	0.00	2.26	7.93	15.72	42.23	142.39	86.93	63.74	75.26	3.24	0.00	0.00
15	Water hold by waste in mm (A <sub>4</sub> )	0.00	-0.02	1.59	4.11	12.38	55.62	32.43	27.32	28.99	-2.79	0.00	0.00
16	Actual leachate generation area 1	0.00	4.95	17.36	34.42	92.44	311.67	190.28	139.51	164.72	7.08	0.00	0.00
17	Actual leachate generation area 2	0.00	4.02	23.25	51.37	145.29	566.08	337.21	266.67	296.93	-9.39	0.00	0.00
18	Actual leachate generation area 3	0.00	2.84	9.97	19.77	53.10	179.03	109.30	80.14	94.62	4.07	0.00	0.00
19	Actual leachate generation area 4	0.00	-0.18	12.48	32.29	97.16	436.55	254.53	214.39	227.50	-21.89	0.00	0.00
20	Field capacity	14	14	14	14	14	14	14	14	14	14	14	14
21	Initial moisture content	12.11	12.11	12.11	12.11	12.11	12.11	12.11	12.11	12.11	12.11	12.11	12.11
22	IMCDM	13.78	13.78	13.78	13.78	13.78	13.78	13.78	13.78	13.78	13.78	13.78	13.78
23	FFCDM	16.28	16.28	16.28	16.28	16.28	16.28	16.28	16.28	16.28	16.28	16.28	16.28
24	IDM	0.86	0.86	0.86	0.86	0.86	0.86	0.86	0.86	0.86	0.86	0.86	0.86
25	Precipitation [m <sup>3</sup> ]	0.00	123.64	343.05	628.22	1615.55	4695.44	2949.27	1971.03	2503.79	326.08	0.00	0.00
26	Ws (leachate generated from waste) (Lr <sup>-1</sup> )	21.56	21.56	21.56	21.56	21.56	21.56	21.56	21.56	21.56	21.56	21.56	21.56
27	Total amount of waste generated per month [ton]	450	450	450	450	450	450	450	450	450	450	450	450
28	Leachate from waste [m <sup>3</sup> ]	9.70	9.70	9.70	9.70	9.70	9.70	9.70	9.70	9.70	9.70	9.70	9.70
29	Total leachate amount (monthly)[m <sup>3</sup> ]	9.70	21.34	72.76	147.55	397.69	1503.03	901.03	710.41	793.48	-10.42	9.70	9.70

## Modeling Using Python Programming

A software is developed using python which directly displays the result of maximum precipitation of the month, total annual precipitation, and the graph showing monthly precipitation vs monthly leachate generation for a year. It has advantages such as:

1. To ease the calculation due to complex input parameters
2. To reduce human error during calculation
3. To cover up the time constraint
4. To make it user-friendly

To develop this software, python programming was used as the software language because it is user-friendly and it contains a wide range of library functions that ease programming. To develop this model, Qt designer is used to enhance programming, and two different types of library functions were also used namely, PyQt5 and matplotlib. Qt

Designer is software that is used for making GUI (Graphical User interference) for a developed program. The software that was developed is termed YAKK and it is 58.2 Mb in size. It can be installed in any Windows OS and doesn't need any additional software like Python or PyCharm etc.

Fig. 3 shows the dashboard of software from which a user can choose the method, they want to use for the calculation of leachate generated by a landfill. Upon choosing a method, the next dialogue box will be displayed, where the user needs to input the required parameters. For example, if a user selects a standard method or mass balance method, Fig. 4 and Fig. 5 dialogue box is displayed respectively.

Now the user needs to input the required parameters and then click 'OK' for calculating the amount of leachate generated and the result will be displayed which the user can save for future reference. The displayed result will be as Fig. 6.

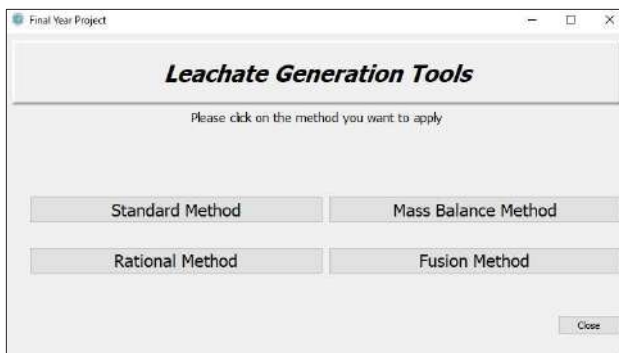


Fig. 3: Main dashboard.



Fig. 4: Standard method dialogue box.

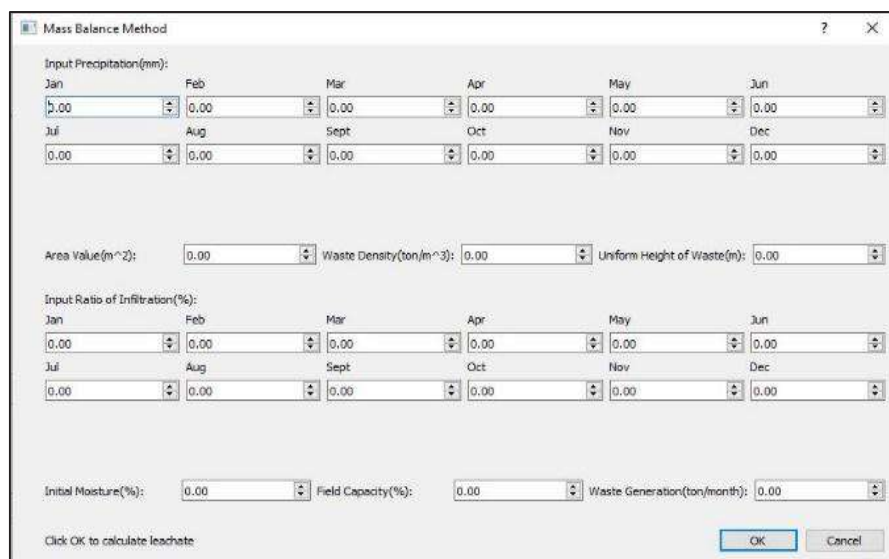


Fig. 5: Mass balance method dialogue box.



Table 3: Estimation of Leachate generation by fusion method in Deir Al Balah landfill.

Year	P [mm]	A [m <sup>2</sup> ]	R [mm]	E [mm]	L [m <sup>3</sup> ]	(IMC) [%]	IM - CDM	FC [%]	FF - CDM	IDM	Year	Total amount of waste generated per year [ton]	Leachate generation from waste itself [m <sup>3</sup> ]	Water hold by waste	Total amount of leachate generated in [m <sup>3</sup> ]	Cumulative leachate generation
1997	315	35000	54	221	1400.00	20	25.0	16	19.05	0.80	47.62	77000	3666.67	224.00	4842.67	4842.67
1998	217	35000	37	152	980.00	20	25.0	16	19.05	0.80	47.62	88000	4190.48	156.80	5013.68	9856.34
1999	132	35000	22	92	630.00	20	25.0	16	19.05	0.80	47.62	88000	4190.48	100.80	4719.68	14576.02
2000	255	35000	43	179	1155.00	20	25.0	16	19.05	0.80	47.62	95000	4523.81	184.80	5494.01	20070.03
2001	550	35000	94	385	2485.00	20	25.0	16	19.05	0.80	47.62	90700	4319.05	397.60	6406.45	26476.48
2002	391	60000	66	274	3060.00	20	25.0	16	19.05	0.80	47.62	88000	4190.48	489.60	6760.88	33237.35
2003	373	60000	63	261	2940.00	20	25.0	16	19.05	0.80	47.62	84000	4000.00	470.40	6469.60	39706.95
2004	317	60000	54	222	2460.00	20	25.0	16	19.05	0.80	47.62	82000	3904.76	393.60	5971.16	45678.11
2005	346	60000	59	242	2700.00	20	25.0	16	19.05	0.80	47.62	91000	4333.33	432.00	6601.33	52279.45
2006	245	60000	42	172	1860.00	20	25.0	16	19.05	0.80	47.62	105000	5000.00	297.60	6562.40	58841.85
2007	410	60000	70	287	3180.00	20	25.0	16	19.05	0.80	47.62	99000	4714.29	508.80	7385.49	66227.33
2008	373	60000	63	261	2940.00	20	25.0	16	19.05	0.80	47.62	98372	4684.38	470.40	7153.98	73381.31
2009	373	60000	63	261	2940.00	20	25.0	16	19.05	0.80	47.62	101103	4814.43	470.40	7284.03	80665.34
2010	332	60000	56	232	2640.00	20	25.0	16	19.05	0.80	47.62	116234	5534.95	422.40	7752.55	88417.90
2011	386	60000	66	270	3000.00	20	25.0	16	19.05	0.80	47.62	133030	6334.76	480.00	8854.76	97272.66
2012	353	60000	60	247	2760.00	20	25.0	16	19.05	0.80	47.62	133118	6338.95	441.60	8657.35	105930.01
2013	415	60000	70	290	3300.00	20	25.0	16	19.05	0.80	47.62	143273	6822.52	528.00	9594.52	115524.53
2014	376	60000	64	263	2940.00	20	25.0	16	19.05	0.80	47.62	122618	5838.95	470.40	8308.55	123833.09

\*P: precipitation A: area, R: Runoff, E: evaporation, L: leachate, MC: moisture content, FC: field capacity, WHC: water holding capacity

## Validation of the Model

It is always recommended to validate a model before relying on its accuracy and finding the percentage error. For validation of the Fusion model, the actual amount of leachate generated by a landfill is required along with the necessary parameters but in developing countries like Bhutan, historical data of leachate generated are not found. Moreover, data such as the chemical composition of the leachate and actual leachate generation by landfill are significant. It is necessary for quantifying leachate production and forecasting leachate generation. For this reason, the leachate generation data couldn't be obtained from any landfill in Bhutan as no records are kept by the concerned authority.

So, for the validation of the formula, the data from the Deir Al Balah landfill, Gaza strip, Palestine was used. They have recorded the data for leachate generated by the landfill for 18 years from 1997 to 2014 (Abunama et al. 2017). Their study has a record of required data for the model like field capacity, moisture content of the landfill, evaporation, and runoff data which are necessary parameters in the fusion method.

Using the standard method and rational method the leachate generation at the Deir Al Balah landfill was estimated to be about 51103.5 m<sup>3</sup> and 166407.5 m<sup>3</sup> respectively which gives the percentage error as 53.31% and 45.52% respectively. From the mass balance method, the leachate generation was about 102300.07 m<sup>3</sup> giving an error of 10.54%. By application of the fusion method, the leachate generation at the Deir Al Balah landfill was calculated to be about 123,833.08

m<sup>3</sup> while the actual amount of leachate generated was about 114,351 m<sup>3</sup> as in Table 3. So, the percentage difference between the fusion method and the measured amount was found to be 8.29%.

The results and differences could be more clearly noticed in the following Fig. 7 and 8 graphs are given below. It can be seen that the fusion method has the lowest percentage error i.e. 8.29% followed by the mass balance method with 10.54%, the rational method with 45.52%, and lastly the standard method with 55.31%.

## CONCLUSION

The leachate generated in the Pekarshing landfill is 4565.98 m<sup>3</sup> from the dumped waste area of 3030.49 m<sup>2</sup> with rainfall of 5001.2 mm in the year 2020. From the annual precipitation of 15156.09 m<sup>3</sup>, the leachate generation was 30.12 % of the total precipitation amount. About 7.2% of the total precipitation was lost in evaporation, 47.5% of the total precipitation was lost as surface runoff, and 15.18% of the total precipitation was water content in the waste itself. The amount of leachate generated in the Pekarshing landfill by the standard method is 2273.41 m<sup>3</sup> and by the rational method is 6029.46 m<sup>3</sup>. Fig. 9 shows the comparison of precipitation with quantified leachate amount by various methods.

The following are the main source for the production of leachate generation:

- Higher precipitation leads to higher leachate generation as we can see in Fig. 6.

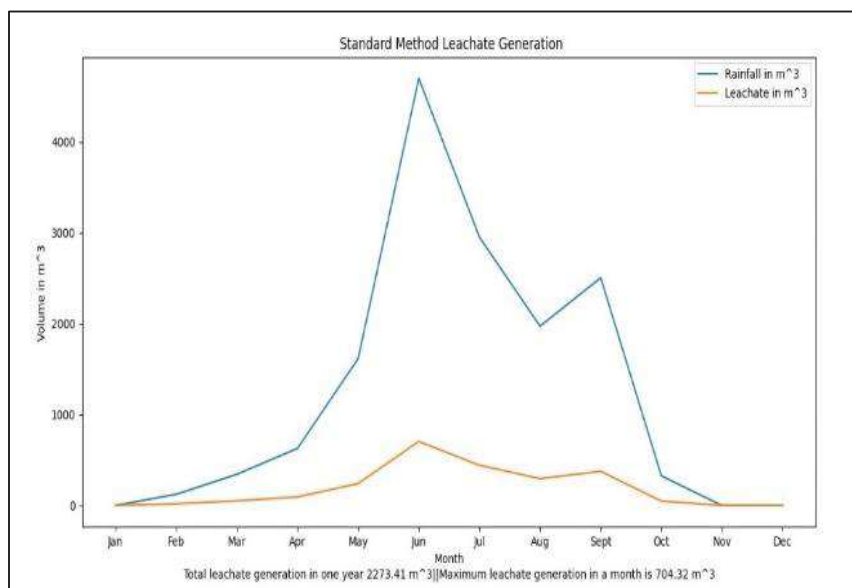


Fig. 6: Final result.

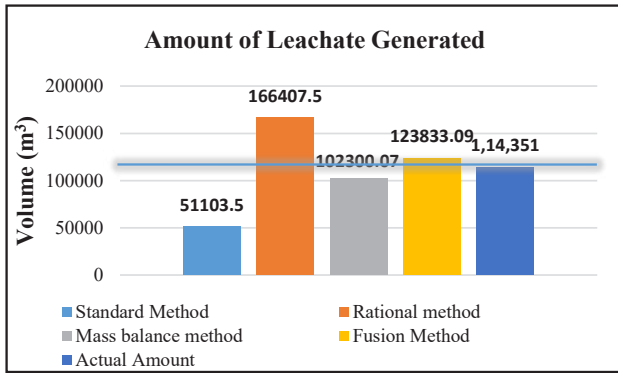


Fig. 7: Estimation of leachate generated by Deir Al Balah landfill by various methods.

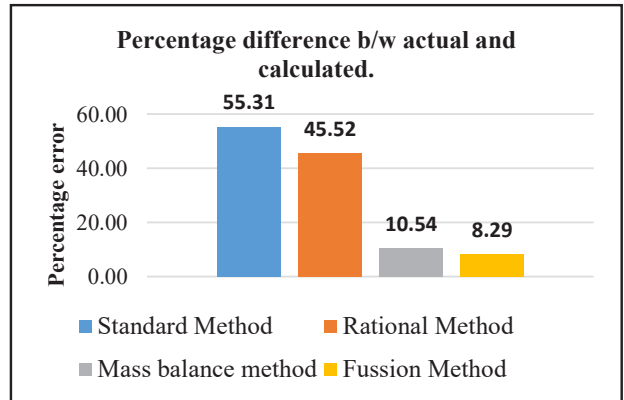


Fig. 8: Difference in percentage error with actual leachate amount.

- When the moisture content of the waste is high it causes higher leachate production.
- Larger the landfill area higher the leachate generation.
- Directly proportional to waste generation and type of waste.
- The field capacity of the waste.

The estimation of leachate generation over time is a complex method mainly because of the factors that influence the leachate generation change over time. With a model developed for the calculation of leachate generation, it will help users to do the calculation faster and easier. The chances of human error are decreased and since the developed formula has less percentage error, we could use it to get a more economic design of leachate management system.

Some of the conclusions drawn from the result of the study are:

1. The generation of leachate depends upon a number of parameters.
2. Precipitation is the main factor contributing to leachate production.
3. Increase in waste generation will result in higher leachate production.
4. It was observed that the fusion method has less percentage error compared to other conventional methods.
5. The composition of the waste affects leachate generation because it affects the field capacity and moisture content of the waste.
6. Fusion methods consider more parameters which makes them more flexible and can be used for other types of landfills.
7. Leachate production could be seen in absence of precipitation too, mainly because of waste compaction and water held by the waste.

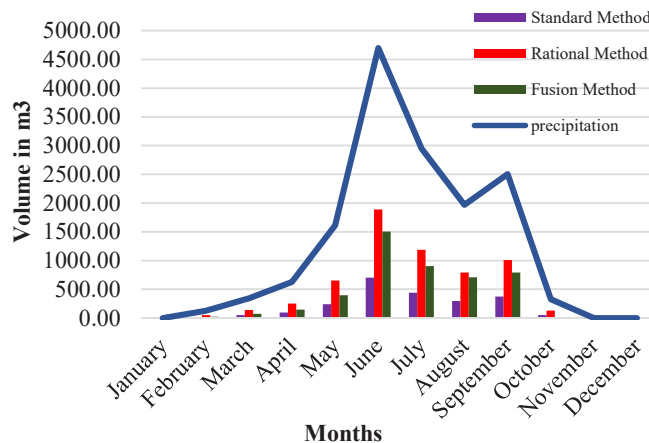


Fig. 9: Comparison of precipitation with quantified leachate amount by various methods.

8. Leachate generation over time increases as the waste generation increases.
9. The landfill system which does not have a leachate management system could pose a great threat to the environment and the people living around it.

## REFERENCES

- Abunama, T., Othman, F., Alslaibi, T. and Abualqumboz, M. 2017. Quantifying the generated and percolated leachate through a landfill's lining system in Gaza strip, Palestine. *Pol. J. Environ. Stud.*, 26(6): 2455-2461. <https://doi.org/10.15244/pjoes/73803>
- Baziene, K., Vasarevicius, S., Baltrenas, P. and snf Baltreinaite, E. 2013. Influence of total precipitation and air temperature on the composition of municipal landfill leachate. *Environ. Eng. Manag. J.*, 12(1), 175-182. <https://doi.org/10.30638/eemj.2013.020>
- Choden, Y., Tenzin, T., Karchung, Norbu, K., Wangmo, S. and Zangmo, P. 2021. Estimation of energy content in municipal solid waste of Bhutan and its potential as alternate powers source. *Environ. Conserv. J.*, 22(1): 27-33. <https://doi.org/https://doi.org/10.36953/ECJ.2021.221205>
- Hashisho, J. and El-Fadel, M. 2014. Determinants of optimal aerobic bio-reactor landfilling for the treatment of the organic fraction of municipal waste. *Critic. Rev. Environ. Sci. Technol.*, 44(16): 1865-1891. <https://doi.org/https://doi.org/10.1080/10643389.2013.803798>
- Ibrahim, T.N.T., Mahmood, N.Z. and Othman, F. 2017. Estimation of leachate generation from MSW landfills in Selangor, Malaysia. *Asian J. Microbiol. Biotechnol. Environ. Sci.*, 19(1): 44-49.
- JICA. 2009. The study on solid waste management plan final report. Available from [https://openjicareport.jica.go.jp/pdf/11549052\\_01.pdf](https://openjicareport.jica.go.jp/pdf/11549052_01.pdf)
- Komilis, D and Athiniotou, A. 2014. A water budget model for operating landfills: An application in Greece. *Waste Manag. Res. J. Sustain. Circular Econ.*, 32(8): 717-725. <https://doi.org/https://doi.org/10.1177%2F0734242X14545505>
- National Environment Commission. 2016. Bhutan State of the environment report 2016. Available from [www.nec.gov.bt](http://www.nec.gov.bt)
- National Statistics Bureau. 2018. Population and Housing Census of Bhutan. Available from [www.nsb.gov.bt](http://www.nsb.gov.bt)
- Ololade, O.O., Mavimbela, S., Oke, S.A. and Makhadi, R. 2019. Impact of leachate from a northern landfill site in Bloemfontein on water and soil quality: Implications for water and food security. *Sustainability (Switzerland)*, 11(15): 237. <https://doi.org/10.3390/su11154238>
- Safaa, M., Raghav, A., Ahmed M., Abd, E.M. and Hala, A.H. 2013. Treatment of leachate from municipal solid waste landfill. *HBRC*, 9(2): 187-192. <https://doi.org/https://doi.org/10.1016/j.hbrcj.2013.05.007>
- World Bank. 2000. What a waste. Available from <https://datatopics.worldbank.org/what-a-waste/>
- Yang, N., Damgaard, A., Kjeldsen, P., Shao, L.M. and He, P.J. 2015. Quantification of regional leachate variance from municipal solid waste landfills in China. *Waste Manag.*, 46: 362-372. <https://doi.org/10.1016/j.wasman.2015.09.016>





# Use of Agricultural Waste-Based Biosorbents for the Removal of Heavy Metals from Aqueous Solution: A Review

K. Harshala\*† and N. D. Wagh\*\*

\*School of Applied Sciences, Amity University, Mumbai-410206, India

\*\*Department of Environment Science, School of Applied Sciences, Amity University, Mumbai-410206, India

†Corresponding author: K. Harshala; harshala26@rediffmail.com

Nat. Env. & Poll. Tech.

Website: [www.neptjournal.com](http://www.neptjournal.com)

Received: 05-06-2021

Revised: 10-10-2021

Accepted: 22-10-2021

## Key Words:

Agricultural waste  
Crop residue  
Biosorption  
Kinetics  
Regeneration

## ABSTRACT

Agriculture is the immemorial benefaction of man for the existence and welfare of the human race. Being an agricultural country, it is the prime source of livelihood in India. This review focused on the present scenario of Indian Agriculture with respect to crop production, factors affecting productivity, and agricultural waste-related issues in India. Agrowaste can be helpful to farmers but economic costs are less than the cost of collection, transportation, and processing for profitable use. In this consequence, the review has presented considerable information on the alternative use of agrowaste to control water pollution. The review focused the light on the replacement of conventional chemicals with agro-based waste to develop fully green and sustainable biosorbents. It also highlighted the potential of biosorbents and biosorption technology in terms of their adsorption capacities, cost-effectiveness, binding mechanisms, and interfering factors such as pH, temperature, initial concentration, dose, and pre-treatments. Biosorption isotherms and sorption kinetics models were used for the characterization of agrowaste and developed biosorbent, and recovery of sorbent was also reviewed. The review concluded that further research is required to investigate novel biosorbents that may be a good option for bioremediation for the removal of a large range of toxic heavy metals. The utilization of plant waste as biosorbent will also open a new window of agricultural waste management.

## INTRODUCTION

### Agricultural Sector in India

Agriculture is the backbone of the Indian economy; it will continue to be so for a long time. It supports about 17 percent of the world's population from 2.3 percent of the world's land area and 4.2 percent of the world's water resources (Pandey 2009). India has adopted modern methods of cultivation and contrived significant progress. Agricultural Science and engineering have altered its image from a "begging bowl" to a "breadbasket" by adapting effective infrastructure and sustainable use of natural resources. Over the last five decades, Indian agriculture has evolved into a mature and modern business. India is the world's second-largest producer of rice, wheat, spices, spice products, and vegetables and fruits (APEDA 2018-19).

### Agricultural Waste-Related Issues in India

United Nations defines agricultural waste as waste produced as a result of various agricultural operations (UN, Glossary of Environment Statistics, 1997). Agricultural waste is a non-commodity product of agricultural product production and processing that may contain material that is beneficial

to individuals but whose economic value is less than the cost of collection, transport, and processing for profitable use. Agricultural waste can take the form of liquid, slurry, or solids, depending on the system and type of agricultural activity (Obi et al. 2016). Unsustainable agricultural development leads to huge adverse effects on the rural and global environment (Nguyen 2017, Pappu et al. 2006).

**Crop residue waste:** According to the Indian Ministry of New and Renewable Energy (MNRE), the annual generation of crop residues in India is an average of 500 million tons. After the utilization of these crop residues as fodder or fuel still, there is a leftover of 140 Mt of which 92 Mt is burned each year (Ministry of Agriculture, India 2014) The 'rice-wheat cropping system' (RWCS) is the best planting system in South Asia (Hobbs & Morris 1996) which is followed by many Indian states. Rice and wheat contribute about 70% of the crop residues. Based on Jain et al. (2013) and the Intergovernmental Panel on Climate Change (IPCC), more than 25% of crop residues have been burnt on the farm. It was also reported that across all states the fraction of burnt crop residue ranged from 8–80% for paddy waste (Jain et al. 2013) Among various crop residue, major contributors were 43% of rice, wheat 21%, sugarcane 19%, and oilseed 5%

(Sahai et al. 2010). During the post-harvest period, 80% of the crop is burned.

**Emission of greenhouse and other gases:** Burning crop residues is a major source of GHGs, as well as other chemically relevant trace gases, aerosols, and other hydrocarbons. Burning rice straw emits Carbon (C) as CO<sub>2</sub> (70%), CO (7%), and CH<sub>4</sub> (0.66%) whereas 2.09% of Nitrogen (N) is emitted as N<sub>2</sub>O (Ministry of Agriculture, India 2014). Apart from that, large amounts of particulates containing a mixture of organic and inorganic species such as Polycyclic Aromatic Hydrocarbons (PAHs), Polychlorinated Dibenzop-dioxins (PCDDs), and Polychlorinated Dibenzofurans (PCDFs) are emitted (PCDFs). Greenhouse gases contribute to global warming and climate change (Gadde et al. 2009). A huge annual welfare loss (Rs. 76 million) in terms of health damage is caused by air pollutants created by agricultural residue open burning (Kumar et al. 2015, Lohan et al. 2017). Furthermore, one of the significant repercussions of stubble burning is the loss of soil flora and fauna, including microbes (Kaur & Rani 2016).

## APPLICATION OF AGRICULTURAL WASTE FOR POLLUTION CONTROL

Using agricultural waste products to reduce pollution is a long-term strategy that can also provide additional revenue for producers (Manique et al. 2012). Agricultural waste with carboxyl, hydroxyl, and other active groups can be used as a biomass-based adsorbent to accomplish the “treatment waste by waste” effect (Dai et al. 2018). It was suitable for recovering ecological pollutants due to its loose surface, porosity, exceptional mechanical strength, and chemical stability. Several research papers showed how different forms of agricultural wastes can be used to adsorb metal ions from aqueous solutions (Hossain et al. 2012a, 2012b).

### Removal of Inorganic Contaminants

Removal of inorganic contaminants could be carried out using waste biosorbents through modern and traditional treatment methods. The studies carried out by various workers for the application of agrowaste for the removal of inorganic contaminants are given in Table 1.

### Removal of Organic Contaminants

The studies carried out by various workers for the application of agrowaste for the removal of organic contaminants are given in Table 2.

### Getting Rid of Harmful Gases

The rapid increase of greenhouse gases like carbon dioxide (CO<sub>2</sub>) and nitrous oxide (N<sub>2</sub>O) is one of the reasons for global

warming and climate change (Dai et al. 2018). Hydrogen sulfide (H<sub>2</sub>S) and carbon dioxide (CO<sub>2</sub>) are common pollutants in the production/processing of oil and gas, wastewater treatment plants, combustion of fossil fuel, and landfill gases, which can cause corrosion and harmful gaseous emissions (Bamdad et al. 2018).

Application of biochar developed by carbonization of leaf waste at 400°C removed 84.2% H<sub>2</sub>S successfully from raw biogas in a continuous adsorption tower for 25 min (Sahota et al. 2017). Sugarcane bagasse (SB) and Hickory wood (HW), which were used to make biochar at a higher temperature, had the maximum physisorption of CO<sub>2</sub> (73.55 mg.g<sup>-1</sup> at 25°C) (Creamer et al. 2014) The CO<sub>2</sub> adsorption efficiency on charcoal rice straw was found to be around 80 mg.g<sup>-1</sup> at 20 °C in a study (Huang et al. 2015). The highest performance conditions were obtained by treating soybean straw with CO<sub>2</sub> and NH<sub>3</sub> at high temperatures, with the absorptivity of 49.87 mg.g<sup>-1</sup> (Zhang et al. 2016). The surface chemistry, porous structure, and morphology of activated carbon were studied, and the absorptivity was found to be 78.10 mg.g<sup>-1</sup> (Shahkarami et al. 2015)

## ADSORPTION

Adsorption is a surface phenomenon, in which the transfer of molecules from the bulk solution to the solid surface is done, depending on the concentration gradient (Qiu et al. 2009). This process is parameter-dependent such as molecular weight, shape, or polarity of the adsorbing material, which holds the molecule strongly and makes separation easier. The adsorption rate is equal to the square root of contact time with the adsorbent (Mathew et al. 2016).

### Types of Adsorption Processes

The process of adsorption can be achieved by batch, semi-batch, and continuous processes. In batch, processes contact time of adsorbing material and adsorbent play's an important role (Mishra & Tripathi 2008). Adsorbate and adsorbent are attracted to one other by attractive forces such as weak Van der Waals forces or strong chemical bonds. At low temperatures, weak van Der Waals forces are active in physisorption (Fraissard 1997). While chemical forces or chemical bonds are active in chemisorption, its efficacy is determined by the adsorbent's surface area (Apple & Ma 2002).

### Factors Affecting the Adsorption Process

Biosorption depends on many factors that are related to environmental conditions that can affect the process. Factors that interfere with the biosorption process are:

**Temperature:** Biosorption efficiency remains uninfluenced within the range 20-35°C °C, at high temperatures, e.g.,

Table 1: Application of agrowaste for removal of heavy metals, nitrogen and phosphorus.

Sr. No.	Removal of pollutant	Argowaste as adsorbent	Adsorption capacity (mg.g <sup>-1</sup> ) or %	References
1.	Heavy metal Lead (II)	Wheat bran	69-87 mg.g <sup>-1</sup>	Bulut & Baysal 2006
		Coir fibers	263 mg.g <sup>-1</sup>	Kadirvelu & Namasivayam 2000
		Pumpkin waste	14.286 mg.g <sup>-1</sup>	Okoye et al. 2010
		Tea leaves	96%	Ahluwalia & Goyal 2005
		heartwood powder of Areca catechu		Goyal 2005
		Acid-modified rice straw	97%	Chakravarty et al. 2010
		Rice straw		
		Plum stone	18.98 mg.g <sup>-1</sup>	Guo et al. 2015
	Nickel (II)	Banana peels	42.55 mg.g <sup>-1</sup>	Amer et al. 2017
			80.65 mg.g <sup>-1</sup>	Parlayıcı & Pehlivan 2017
			>90%	Ibisi & Asoluka 2018
	Copper (II)	Tobacco stem	97.32 mg.g <sup>-1</sup>	Rao et al. 2014
		Cocoa shell	97.59 mg.g <sup>-1</sup>	Kalaivani et al. 2014
		Peel orange fruit	96%	Ajmal et al. 2000
		pomegranate peel	52 mg.g <sup>-1</sup>	Bhatnagar & Minocha 2009
	Zinc (II)	Mango peel	46.09 mg.g <sup>-1</sup>	Iqbal et al. 2009
		Sorghum bicolor	15.151 mg.g <sup>-1</sup>	Salman et al. 2020
		Sugar beet pulp	28.5 mg.g <sup>-1</sup>	Aksu & Isoglu 2005
		Watermelon shell	9.54 mg.g <sup>-1</sup>	
		Potato peel	84.74 mg.g <sup>-1</sup>	Mohammed & Ibrahim 2016
	Cadmium (II)			Guechi & Hamdaoui 2015
		Sorghum bicolour	17.241 mg.g <sup>-1</sup>	Salman et al. 2020
		Banana peels	>90%	Ibisi & Asoluka 2018
		Sawdust	94.02%	Naiya et al. 2008a
	Zinc (II)	Neem bark	86.24%	Naiya et al. 2008b
Chromium (VI), (III)	Sawdust	87.23%	Naiya et al. 2008a	
	Neem bark	84.75%	Naiya et al. 2008b	
	Modified groundnut shell	131 mg.g <sup>-1</sup>	Owalude & Tella 2016	
	mango kernel	7.8 mg.g <sup>-1</sup>	Rai et al. 2016	
	Date palm leaves	98%	Fawzy et al. 2015	
Arsenic (III), (V)	Broad bean shoots	95%	Fawzy et al. 2015	
	Banana peels	96%	Ali et al. 2016	
	Java plum seeds	97%	Shakoor et al. 2018	
	Rice polish	41.18 and 49 µg/ g, respectively	Hasan et al. 2009	
Nitrogen	Chir pine leaves		Shafique et al. 2012	
	Walnut shell	3.27 mg.g <sup>-1</sup>	Saqib et al. 2013	
	Rice husk	88%	Amin et al. 2006	
		89% and 87% respectively		
Ammoniacal nitrogen	Banana peels	-	Akpor et al. 2013	
	Sugarcane bagasse ash	60%	Mor et al. 2019	
Phosphate	Rice husk	89%	Mor et al. 2016	
	Banana peels	-	Akpor et al. 2013	

50°C, biosorption activity and kinetic energy of the adsorbate increases which may destruct the physical structure of the biosorbent. Adsorption reactions are generally exothermic and the degree of adsorption increases with falling temperature (White et al. 1997, Abdi et al. 2015). There could be a modification in the equilibrium capacity of the adsorbent for a particular adsorbate due to a change in temperature. There is better adsorption acquired at higher temperatures (Park et al. 2010, Malkoc & Nuhoglu 2005, Goyal et al. 2003).

**pH:** pH affects the movement of the functional groups in the adsorbent, the solution chemistry of the metals, and the competition between metallic ions (Joo & Hassan 2010). It has been shown that the affinity of cations in the functional groups present on the cellular surface is strongly dependent on the solution pH (Alfarra et al. 2014). The biosorption capacity reduces with low pH values and increases with pH until it reaches optimum pH. Metal ions precipitated due to the high concentration of hydroxyl anions in the solution

Table 2: Application of agrowaste for removal of organic contaminants.

Sr. No.	Removal of pollutant	Argowaste as adsorbent	Adsorption capacity (mg.g <sup>-1</sup> ) or %	References
1.	Dyes Methylene Blue Dye	Lemon leaf powder	19.19 mg.g <sup>-1</sup>	Sarath Babu & Yamini 2020
		Cauliflower leaves		
	Azodyes (Congo red, Crystal violet, Methyl orange) Synolon black HWF-FS	Rice husk composite	149.22 mg.g <sup>-1</sup>	Ansari et al. 2016
		Linseed oil cake	77-81%	Rafique & Zulfiqar 2014
		Fruit shell of Bengal gram		
Acid blue 25	<i>Cucumis sativus</i>	6.89 mg.g <sup>-1</sup>	Safa 2015	
	Crystal violet		29.41 mg.g <sup>-1</sup>	Krishna et al. 2016
2.	Drugs Fluoroquinolone		40.82 mg.g <sup>-1</sup>	Smitha et al. 2012
		Rice husk	63.50 mg.g <sup>-1</sup>	Ashrafi et al. 2015
3.	Pesticides 2,4-dichlorophenoxyacetic acid	Bagasse fly ash	7.14 mg.g <sup>-1</sup>	Deokar et al. 2016
4.	Aromatic compounds phenol	<i>Acacia tortilis</i> pod shell	95%	Malakootian et al. 2018
		Rice husk ash	95%	Mandal et al. 2019
5.	Oil substances	Banana peels	5-7 mg.g <sup>-1</sup>	Alaa El-Din et al. 2017

when the pH was greater than 5.5. As a result, the trials were not carried out at pH levels higher than 5.5 (Witek-Krowiak et al. 2010)

**Pre-treatment:** Because of the nature of biosorbent application, physical treatments such as drying, boiling, autoclaving, and mechanical disruption will cause changes in binding properties. Chemical treatments, such as alkali treatment, improve biosorption capacity, which is especially visible in some fungal systems with higher metal affinities (Abdi & Kazemi 2015).

**Acidity:** Biosorption is comparable to the ion-exchange process, in which biomass is used as a natural ion-exchange medium with weakly acidic and basic groups (Ahalya et al. 2003). Metal biosorption has been shown to be strongly pH-dependent in almost every system studied. At low pH, cations and protons compete for binding sites, which explains why metal absorption of Cu, Cd, Ni, Co, and Zn is normally reduced (Obi et al 2016).

**Biomass concentration:** The concentration of biomass in solution influences the specified metal uptake (Modak & Natarajan 1995). The adsorption of metal by biomass is shown to be greater at low cell densities at a given equilibrium concentration (Gourdon et al. 1990). Because an increase in biosorbent concentration actively encourages interference between binding sites, the specific metal absorption increases at lower biomass concentrations (Zouboulis et al. 1997). Metal ions cannot get to the exact location of the binding

site because of the high biomass concentration (Malkoc & Nuhoglu 2005).

**Initial metal ion concentration:** The initial metal ion concentration provides an important driving force for controlling all-metal mass transfer resistance between the fluid and adsorbed phases (Kutahyali et al. 2010). When the initial metal ion concentration is high, all-metal ions in the solution engage with binding sites, accelerating adsorption by roughly 99% until saturation is reached.

**Agitation speed:** Increasing the agitation speed accelerates the biosorption of adsorptive metal by lowering the mass transfer resistance, however, it may harm the biosorbent's physical structure (Park et al. 2010)

**Contact time:** Physical adsorption of metal at the cell surface is claimed to be fast and occurs in a short period. The active sites on the adsorbent become occupied as the contact time increases and gradually diminishes with time until it reaches equilibrium (Mishra & Tripathi 2008, Witek-Krowiak et al. 2010).

**Biosorbent size:** Decrease biosorbent size is favorable for batch process due to the higher surface area of the biosorbent, but due to its low mechanical strength and clogging of the column, it is not advantageous for column process (Park et al. 2010, Abdi et al. 2015).

**Other pollutant concentration:** Various metals and coexisting metals present in wastewater compete with a target

pollutant for binding sites and can form any complex with it. This can be reduced by the biosorptive removal of the target metal ions (Park et al. 2010)

**MECHANISM OF HEAVY METAL CAPTURE**

Weak forces, chemical reactions, and ionic strength interact in biosorption, resulting in stronger binding. (Achak et al. 2009) These interactions can occur inside or outside of the pores, as well as on the surface of agricultural wastes (Silva et al. 2013). The actual mechanism of biosorption is still a mystery. Although several mechanisms for heavy metal ion binding to sorbent surfaces have been suggested (Salman et al. 2015) Adsorption mechanisms such as chemisorption, ion exchange, surface adsorption, complexation reactions, electrostatic interactions, diffusion via pores, and others are predicated by ionic interactions that occur during adsorption. Fig. 1 shows the many pathways involved in the biosorption of heavy metals

It is possible that different mechanisms can operate concurrently to varying degrees. The study of mechanisms involved in the uptake of Cr (III) and Cr (VI) by *Cupressus lusitanica* bark revealed that the principal mechanisms for Cr (III) biosorption is found to be Ion exchange and electrostatic interaction (Netzahuatl-Munoz et al. 2012). In the adsorption of Cu (II), Zn (II), and Pb (II) ions using orange peels, the process was governed by ion-exchange predominantly (Feng & Guo 2012). The study of removal of Pb (II) from aqueous solution using *Triticum aestivum* followed adsorption as well as ion-exchange mechanism (Farooq et al. 2007). Similar results were found using potato peel for Pb (II), Zn (II), and Cd (II) adsorption (Taha et al. 2011).

The dominant mechanisms involved in the biosorption of Cr (III) and Cu (II) onto soybean meal waste are ion exchange, precipitation, and chelation by hydroxyl and carboxyl groups. (Witek-Krowiak et al. 2016). The study stated that in the removal of Pb (II) from an aqueous solution, the prime responsible groups were the carboxyl and hydroxyl groups that existed on the surface of sorghum biomass (Salman et al. 2014). The study of Ni (II) sorption onto *Caesalpinia bonducella* seed powder described that the functional groups hydroxyl, amine, carboxyl, and carbonyl were responsible for the adsorption mechanism. (Gutha et al. 2011) While the involvement of carboxyl and hydroxyl groups in the uptake of the metal ions by grafted polymerization-modified orange peel was also explored (Feng et al. 2011) Adsorption of low concentrations of lead, zinc, and cobalt (less than 100 mg.L<sup>-1</sup>) from an aqueous solution utilizing a mangosteen shell explained the involvement of amino and carboxyl groups (Zein et al. 2010) Various other studies affirmed the effective interaction of carboxyl and hydroxyl groups towards heavy metal ions (Vieira et al. 2012, Araújo et al. 2010, Martín-Lara et al. 2013). As biosorption process may be influenced by conditions such as the chemical state of binding sites, the number of binding sites, their availability, and attraction between the sites and metal ions (Volesky 1994)

**ADSORPTION ISOTHERMS**

Adsorption isotherm represents the equilibrium relationship between the concentration of sorbate in the solution and the adsorbate concentration in the adsorbent at a constant temperature (Vijayaraghavan & Yun 2008). It is a plot of the amount of sorbate per unit weight of adsorbent  $q_e$  versus the equilibrium solute concentration in the solution  $C_e$ . Adsorp-

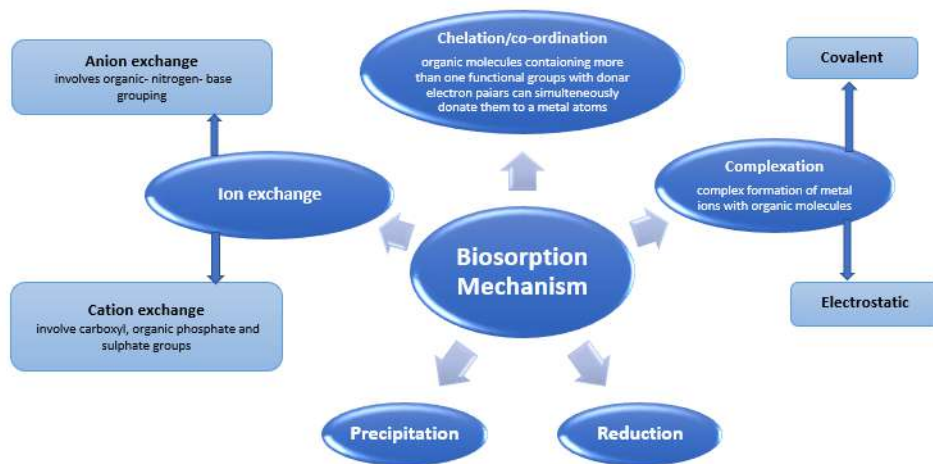


Fig.1: Mechanism of biosorbents.



tion isotherm is used to calculate the capacity of a biosorbent to attract the adsorbate. Some typical isotherm shapes are represented as arithmetic graphs in Fig. 2 (Abbas et al. 2014)

From the above curves, it will be noticed that the adsorption is a specific property that depends on the type of the adsorbate-adsorbent system (Vijayaraghavan & Yun 2008). Various isotherm equations exist to analyze the equilibrium behavior of an adsorption system, but the well-known adsorption isotherm models used for single solute systems are Langmuir (1918) and Freundlich's (1906) isotherms. Both adsorption isotherm models appear to be more appropriate for explaining the relationship between  $q$  (quantity adsorbed at equilibrium,  $\text{mg.g}^{-1}$ ) and  $C$  (concentration of adsorbates remained in the bulky solution at the equilibrium,  $\text{mg.L}^{-1}$ ). Description and nomenclature of different adsorption equilibrium models are given in Table 3.

Literature shows that most of the studied biosorption systems followed the Langmuir equilibrium model which indicated that monolayer adsorption was the possible mechanism of metal ions retention on the biomass surface (Khairia & Al-Qahtani 2016, Fawzy et al. 2015, Rai et al. 2016, Salman et al. 2020) Freundlich isotherm model elucidated the adsorption on heterogeneous surfaces with interactivity occurring between the adsorbed molecules and is not restricted to a monolayer formation (Febrianto et al. 2009) Some studies revealed that the metal ion adsorption follows the Freundlich model more as compared to others (Guiza 2017, Sadeek et al. 2015, Pino et al. 2006, Naiya et al. 2008b, Giwa et al. 2013)

## ADSORPTION KINETICS

Adsorption kinetics is the measurement of the adsorption uptake over time at constant pressure or concentration and is applied to measure the adsorbate diffusion in the pores. Numerous studies have been evaluated using the pseudo-first-order kinetic model and pseudo-second-order kinetic model.

## Pseudo-First-Order Model

Pseudo-first-order is derived from the fact that the rate of reaction is proportional to the number of free accessible binding sites present on the biosorbent material (Ho et al. 2000)

The linear form of the Lagergren pseudo-first-order rate statement is:

$$\ln(q_e - q_t) = \ln q_e - k_1 t$$

Where,  $q_e$  and  $q_t$  are the amounts of metal ion absorbed ( $\text{mg.g}^{-1}$ ) on adsorbent at equilibrium at time  $t$  respectively.  $k_1$  is the rate constant of pseudo-first-order adsorption ( $\text{min}^{-1}$ ). Taking  $\ln(q_e - q_t)$  on the y-axis and ' $t$ ' on the x-axis, a linear plot is generated having the slope ' $-k_1$ ' and intercept ' $\ln q_e$ '. From value of intercept ' $q_e$ ' can be calculated and compared to the experimental value. The precision between the calculated and experimental ' $q_e$ ' values gives an idea about the possible order of the biosorption process.

## Pseudo-Second-Order Model

The pseudo-second-order model is derived from the fact that the rate of biosorption is proportional to the square of several active binding sites on the surface of the biosorbent.

The linear form of pseudo-second-order model expression is:

$$\frac{t}{q_t} = \frac{1}{k_2 q_e^2} + \frac{t}{q_e}$$

Where,  $k_2$  ( $\text{g.mg}^{-1}.\text{min}^{-1}$ ) is the rate constant of the pseudo-second-order kinetic equation,  $q_e$  and  $q_t$  is the amount of metal ion absorbed ( $\text{mg.g}^{-1}$ ) on adsorbent at equilibrium at time  $t$  respectively. A plot between  $(t/q_t)^{-1}$  and  $(t)$  should generate a straight-line having slope of  $(1/q_e^{-1})$  and intercept  $(1/k_2 q_e^{-2})$ . The calculated  $q_e$  value compared with that of the experimental value. Another important factor that determines the applicability of a specific model to the experimental ki-

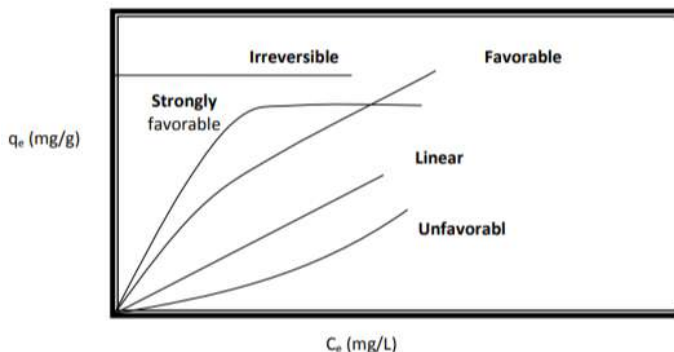


Fig. 2: Types of adsorption equilibrium isotherm relations (Abbas et al. 2014).

Table 3: Adsorption equilibrium models: description and nomenclature.

Isotherm Model	Model equation	nomenclature	Reference
Langmuir	$q_e = \frac{q_m K_L C_e}{1 + K_L C_e}$	$q_e$ (mg/g) = adsorption capacity at equilibrium; $C_e$ (mg.L <sup>-1</sup> ) = metal concentration at equilibrium; $q_m$ (mg.g <sup>-1</sup> ) = monolayer adsorption capacity of adsorbent; $K_L$ = Langmuir constant representing energy constant in relation to the heat of adsorption.	Langmuir 1918
Freundlich	$q_e = K_F C_e^{1/n}$	$q_e$ (mg.g <sup>-1</sup> ) = adsorption capacity at equilibrium; $C_e$ (mg.L <sup>-1</sup> ) = metal concentration at equilibrium; $K_F$ (L.g <sup>-1</sup> ) and $n$ are indicative of the extent of adsorption and the degree of non-linearity, respectively	Freundlich 1906
Redlich-Peterson	$q_e = \frac{K_{RP} C_e}{1 + \alpha_{RP} C_e^\beta}$	$K_{RP}$ = Redlich-Peterson constant (L.g <sup>-1</sup> ); $\alpha_{RP}$ = constant having unit (L.mg <sup>-1</sup> ); $C_e$ (mg.L <sup>-1</sup> ) = metal concentration at equilibrium; $\beta$ = exponent that lies between 0–1	Redlich and Peterson 1959
Koble -Corrigan	$q_e = \frac{A_{KC} C_e^p}{1 + B_{KC} C_e^p}$	$A_{KC}$ , $B_{KC}$ , and $p$ are the Koble -Corrigan parameters. This model is valid when $p > 1$	Koble and Corrigan 1952
Sips	$q_e = \frac{K_s C_e^{\beta_s}}{1 + \alpha_s C_e^{\beta_s}}$	$K_s$ (l.g <sup>-1</sup> ) and $\alpha_s$ (l.mg <sup>-1</sup> ) are the Sips isotherm constants and $\beta$ is the exponent which lies between 1 and 0.	Sips 1948
Tempkin	$q_e = 1/n(K_T C_e)$ $B_1 = \frac{RT}{K_T}$	$B_1$ (kJ.mol <sup>-1</sup> ) = heat of adsorption; $K_T$ (L.mol.kJ.g <sup>-1</sup> ) = adsorption potential; $q_e$ (mg.g <sup>-1</sup> ) = adsorption capacity at equilibrium; $C_e$ (mg.L <sup>-1</sup> ) = metal concentration at equilibrium	Tempkin and Pyzhev 1940
Dubinin– Radushkevich	$q_e = q_m e^{-B_{DR} \epsilon^2}$	$q_e$ (mg.g <sup>-1</sup> ) = adsorption capacity at equilibrium; $q_m$ (mg.g <sup>-1</sup> ) = Dubinin– Radushkevich monolayer capacity; $B_{DR}$ = constant related to sorption energy; $\epsilon$ = Polanyi potential	Dubinin and Radushkevich 1947
Flory-Huggins	$\frac{\theta}{C_o} = K_{FH} (1 - \theta)^n$	$\theta$ = degree of surface coverage; $K_{FH}$ and $n$ are the indications of its equilibrium constant and model exponent.	Horsfall and Aye-baemi, 2005
Hill	$q_e = \frac{q_m C_e^n}{K_D + C_e^n}$	-	Hill 1910
Unilan	$q_e = \frac{q_m}{S} \ln \left[ \frac{1 + d \exp(S) C_e}{1 + d \exp(-S) C_e} \right]$	$S$ and $d$ = temperature-dependent model constants.	Ismadji and Bhatia 2000
Khan	$q_e = \frac{q_m b_k C_e}{(1 + b_k C_e)^{a_k}}$	$b_k$ and $a_k$ = model constant and model exponent	Khan et al. 1997
Radke-Prausnitz	$q_e = \frac{\alpha_R r_R C_e^{\beta_R}}{\alpha_R + r_R C_e^{\beta_R - 1}}$	$\beta_R$ is the model exponent, and $\alpha_R$ and $r_R$ are model constants.	Vijayaraghavan et al. 2006
Toth	$q_e = \frac{q_m C_e}{(b_T + C_e^n)^{1/n}}$	$q_e$ (mg.g <sup>-1</sup> ) = adsorption capacity at equilibrium; $C_e$ (mg.L <sup>-1</sup> ) = metal concentration at equilibrium; $b_T$ (mg.g <sup>-1</sup> ) = Toth maximum adsorption capacity; $q_m$ = the Toth constant; $n$ = the Toth model exponent	Toth 1971

netic data is the coefficient of determination  $R^2$ . Its value of close to 1 ( $R^2 > 0.98$ ) shows the fitness of experimental data to the kinetic model. The ideal pseudo-second-order model indicates that there is a binding between one divalent metal and two monovalent binding sites (Salman et al. 2014). From the literature review, it is worth noting that numerous other studies have recorded the best fit of the pseudo-second-order model to biosorption kinetic data. (Salman et al. 2020, Sadeek et al. 2015, Saman et al. 2019, Santos et al. 2010, Chakravarty et al. 2010).

## RECOVERY AND RESTORATION

Reuse of bio sorbent could be achieved by using restoration and regeneration for a low amount of pollutants (Khatoun & Rai 2016, Carolin et al. 2017). It is preferable that the desorbing medium should not be damaging to the biosorbent, but should help to recover, the loaded metals onto the surface of the biomass after biosorption (Gupta et al. 2015). The study of adsorbent reclamation can be utilized for the prevention of secondary pollution resulted due to waste adsorbents (Anirudhan & Sreekumari 2011). Literature reveals that Acids (such as HCl,  $H_2SO_4$ , and  $HNO_3$ ) were mostly used in the case of recovery of heavy metal(s) from bio adsorbents (Lata et al. 2014).

The results derived from the study for the percentage recovery of Ni (II) and Cu (II) ions using the *Delonix regia* pods revealed that at different desorbing medium concentrations, the percentages recovery of metal ions was different. The studies also affirmed that a comparatively less concentration of acid is required to recover more than 50 % of the metal ions from the biomass (Babalola et al. 2020). An investigation was carried out to determine the reusability potential and stability of the pre-treated watermelon (*Citrullus lanatus*) rind showed 98.1% recovery of  $Pb^{2+}$  ions (Lakshmi pathya & Saradab 2015).

The study of Sorghum root biomass for removal of Cu(II) and Cr(VI) ions from an aqueous medium was carried out using HCl and  $HNO_3$  as eluting agents. The formula used to calculate the desorption efficiency of biomass was,

$$\text{desorption efficiency} = \frac{\text{amount of metal ions desorbed}}{\text{amount of metal ions adsorbed}} \times 100$$

Using HCl as eluting agent desorption efficiency of Cu(II) and Cr(VI) ions from sorghum root biomass was shown to be 93 and 96%, whereas using  $HNO_3$  desorption efficiency was 84 and 89% respectively (Choudhary et al. 2014).

In the study of the use of NaOH,  $HNO_3$ , and EDTA as eluting agents for desorption of Cr(III) ions from sorghum stalk biomass, EDTA showed high desorbing efficiency in comparison with NaOH and  $HNO_3$  for Cr(III) ions due to the

nature of metal-sorghum bonding. Desorption percentages for Cr(III) ions using 0.05 M EDTA and 0.1 M EDTA were shown to be 75% and 71%, respectively at 55°C (Bernardo et al. 2009)

## CONCLUSION

Being the second-largest economy with year-round crop cultivation, India generates abundant agricultural waste including crop residue. Agricultural waste when not effectively used increases the burden of rural agricultural production and also cause pollution in the rural environment. Multiple-use of agro wastes can productively minimize air pollution by the burning of crops.

The utilization of agrowaste in environmental remediation furnishes an economical substitute for extracting toxic heavy metal ions from real wastewater and supports in recovering environmental damages. As a biosorbent shows an affinity for certain metals, a composite biosorbent containing more than one biosorbent can be tested for the removal of multiple metal ions from contaminated water.

From the literature review, it becomes clear that an appropriate modification method for the preparation of biosorbent can improve the adsorptive capacity of agricultural waste. Good removal efficiencies proved that; biomass-based adsorbent is an absolute solution to cope with heavy metal contamination.

Agricultural wastes-based biosorbent with uneven structures that contain high binding sites with metal craving functional groups like hydroxyl, carboxyl amine, and other active groups, that effectively remove pollutants.

The process of biosorption is influenced by pH, dose, temperature, concentration particle size, and other factors. The majority of the studies emphasized studying the biosorption process concerning kinetic, equilibrium, and thermodynamics, which proclaimed that Langmuir and pseudo-second-order models are dominant isotherm and kinetic models, respectively.

The study of regeneration of biosorbent unveiled that a single regenerating agent effective for one adsorbent was not necessarily efficacious for another adsorbent. Further exploration is desired to invent the best possible eluent that can be relevantly used for many adsorbents.

The development of effective green conversion and technology will be an indicator of the development of biological adsorption. Using agricultural waste as a biomass adsorbent can not only eliminate the damage to the current practice of agricultural waste but also are of significant economic benefits.

## REFERENCES

- Abbas, S.H., Ibrahim, M., Ismail, I.M., Tarek, M., Mostafa, T.M., Abbas, H. and Sulaymon, A.H. 2014. Biosorption of heavy metals: A review. *J. Chem. Sci. Technol.*, 3(4): 74-102.
- Abdi, O. and Kazemi M. 2015. A review study of biosorption of heavy metals and comparison between different biosorbents. *J. Mater. Environ. Sci.*, 6(5): 1386-1399.
- Achak, M., Hafidi, A., Ouazzani, N., Sayadi, S. and Mandi, L. 2009. Low-cost biosorbent "banana peel" for the removal of phenolic compounds from olive mill wastewater: Kinetic and equilibrium studies. *J. Hazard. Mater.*, 166(1): 117-125. doi: 10.1016/j.jhazmat.2008.11.036.
- Agricultural and Processed Food Products Export Development Authority (APEDA), Department of Commerce and Industry, Union Budget 2018-19, Ministry of Agriculture and Farmers Welfare, Crisil.
- Ahalya, N., Ramachandra, T.V. and Kanamadi, R.D. 2003. Biosorption of heavy metals. *Res. J. Chem. Environ.*, 7: 71-79, 2003.
- Ahluwalia, S.S. and Goyal, D. 2005. Removal of heavy metals by waste tea leaves from aqueous solution. *Eng. Life Sci.*, 5(2): 158-162. DOI: 10.1002/elsc.200420066.
- Ajmal, M., Rao, R.A.K., Ahmad, R. and Ahmad, J. 2000. Adsorption studies on *Citrus reticulata* (fruit peel of orange): Removal and recovery of Ni (II) from electroplating wastewater. *J. Hazard. Mater.*, 79(1-2): 117-131. doi:10.1016/S0304-3894(00)00234-x.
- Akpor, O.B., Nwonuma, C.O., Edewor-Kuponiya, T.I. and Amira, O.J. 2013. The role of ripe *Musa sapientum* (plantain) peels in the removal of phosphorus and nitrogen from an aqueous solution. *J. Biol. Agric. Healthcare*, 3(13): 2013.
- Aksu, Z. and Isoglu, I.A. 2005. Removal of copper (II) ions from aqueous solution by biosorption onto agricultural waste sugar beet pulp. *Process Biochem.*, 40(9): 3031-3044. doi: 10.1016/j.procbio.2005.02.004.
- Alaa El-Din, G., Amer, A.A., Malsh, G. and Hussein M. 2017. Study on the use of banana peels for oil spill removal. *Alex. Eng. J.*, 57(3): 2061-2068. <http://doi.org/10.1016/j.aej.2017.05.020>.
- Alfarra, R.S., Ali, N.E. and Yusoff, M.M. 2014. Removal of heavy metals by natural adsorbent: Review. *Int. J. Biosci.*, 4(7): 130-139.
- Ali, A., Saeed, K. and Mabood, F. 2016. Removal of chromium (VI) from aqueous medium using chemically modified banana peels as efficient low-cost adsorbent. *Alex. Eng. J.*, 55(3): 2933-2942. <http://dx.doi.org/10.1016/j.aej.2016.05.011>.
- Amer, H., El-Gendy, A. and El-Haggag, S. 2017. Removal of lead (II) from aqueous solutions using rice straw. *Water Sci. Technol.*, 76(5): 1011-1021.
- Amin, M.N., Kaneco, S., Kitagawa, T., Begum, A., Katsumata, H., Suzuki T. and Ohta, K. 2006. Removal of arsenic in aqueous solutions by adsorption onto waste rice husk. *Industrial & Engineering Chemistry Research*, 45(24): 8105-8110. doi:10.1021/ie060344j.
- Anirudhan, T.S. and Sreekumari, S.S. 2011. Adsorptive removal of heavy metal ions from industrial effluents using activated carbon derived from waste coconut buttons. *J. Environ. Sci.*, 23(12): 1989-1998. doi:10.1016/S1001-0742(10)60515-3.
- Ansari, S.A., Khan F. and Ahmad, A. 2016. Cauliflower leave, an agricultural waste biomass adsorbent, and its application for the removal of mb dye from aqueous solution. *Equilib. Kinetics Thermody. Stud.*, 54: 111. doi: 10.1155/2016/8252354.
- Apple, C. and Ma, L. 2002. Heavy metals in the environment concentration, pH, and surface charge effects Cd and Pb sorption in three tropical soils. *J. Environ. Qual.*, 21: 581-589.
- Araújo, C.S.T., Alves, V.N., Rezende, H.C., Almeida, I.L.S., de Assunção, R.M.N., Tarley, C.R.T. and Coelho, N.M.M. 2010. Characterization and use of Moringa oleifera seeds as biosorbent for removing metal ions from aqueous effluents. *Water Sci. Technol.*, 62(9): 2198-2203. doi:10.2166/wst.2010.419
- Ashrafi, S.D., Kamani, H., Jaafari, J. and Mahvi A.H. 2015. Experimental design and response surface modeling for optimization of fluoroquinolone removal from aqueous solution by NaOH-modified rice husk. *Desalination and Water Treatment*. doi:10.1080/19443994.2015.1080188.
- Babalola, B.M., Babalola, A.O., Akintayo, C.O., Lawal, O.S., Abimbade, S.F., Oseghe, E.O., Akinola, L.S. and Ayanda, O.S. 2020. Adsorption and desorption studies of *Delonix regia* pods and leaves: removal and recovery of Ni (II) and Cu (II) ions from aqueous solution. *Drink. Water. Eng. Sci.*, 16: 15-27. <https://doi.org/10.5194/dwes-13-15-2020>
- Bamdad, H., Hawboldt, K. and MacQuarrie, S. 2018. A review on common adsorbents for acid gas removal: Focus on biochar. *Renew. Sustain Energy*, 81: 261. <http://doi.org/10.1016/j.rser.2017.05.261>
- Bernardo, G.R.R., Rene, R.M. J. and Catalina, M.. 2009. Chromium (III) uptake by agrowaste biosorbents: Chemical characterization, sorption-desorption studies, and mechanism. *J. Hazard. Mater.*, 170(2-3): 845-854. doi: 10.1016/j.jhazmat.2009.05.046
- Bhatnagar, A. and Minocha, A.K. 2009. Biosorption optimization of nickel removal from water using *Punica granatum* peel waste. *Coll. Surf B Biointerfaces*, 76(2): 544-548. <https://doi.org/10.1016/j.col-surf.2009.12.016>
- Bulut, Y. and Baysal, Z. 2006. Removal of Pb (II) from wastewater using a wheat brand. *J. Environ. Manag.*, 78(2): 107-113.
- Carolin, C.F., Kumar, P.S., Saravanan, A., Joshiba, G.J. and Naushad, M. 2017. Efficient techniques for the removal of toxic heavy metals from the aquatic environment: A review. *J. Environ. Chem. Eng.*, 5(3): 2782-2799. <http://dx.doi.org/doi:10.1016/j.jece.2017.05.029>
- Chakravarty, P., Sarma, N.S. and Sarma, H.P. 2010. Biosorption of cadmium (II) from aqueous solution using heartwood powder of *Areca catechu*. *Chem. Eng. J.*, 162(3): 949-955.
- Choudhary, S., Goyal, V. and Singh, S. 2014. Removal of copper (II) and chromium (VI) from aqueous solution using sorghum roots (*S. bicolor*): a kinetic and thermodynamic study. *Clean Technol. Environ. Policy*, 17(4): 1039-1051. doi:10.1007/s10098-014-0860-2.
- Creamer, A.E., Gao, B. and Zhang, M. 2014. Carbon dioxide capture using biochar produced from sugarcane bagasse and hickory wood. *Chem. Eng. J.*, 249: 174-179. doi: 10.1016/j.cej.2014.03.105
- Dai, Y., Sun, Q., Wang, W., Lu, L., Liu, M., Li, J., Yang, S., Sun, Y., Zhang, K., Xu, J., Zheng, W., Hu, Z., Yang, Y., Gao, Y., Chen, Y., Zhang, X., Gao, F. and Zhang, Y. 2018. Utilizations of agricultural waste as adsorbent for the removal of contaminants: A review. *Chemosphere*, 211: 235-253. DOI: 10.1016/j.chemosphere.2018.06.179
- Deokar, S.K., Mandavgane, S.A. and Kulkarni, B.D. 2016. Adsorptive removal of 2,4-dichlorophenoxyacetic acid from aqueous solution using bagasse fly ash as an adsorbent in batch and packed-bed techniques. *Clean Technol. Environ. Policy*, 18(6): 1971-1983. doi:10.1007/s10098-016-1124-0
- Dubinin, M.M. and Radushkevich, L.V. 1947. The equation of the characteristic curve of activated charcoal. *Proceed. Acad. Sci. Phys. Chem. Section*, 55: 331.
- Farooq, U., Khan, M.A. and Athar, M. 2007. *Triticum aestivum*: A novel biosorbent for lead (II) ions. *Agrochimica*, 51(6): 309-318.
- Fawzy, M., Nasr, M., Abdel-Gaber, A. and Fadly, S. 2015. Biosorption of Cr (VI) from aqueous solution using agricultural wastes, with an artificial intelligence approach. *Sep. Sci. Technol.*, 51(3): 416-426. <http://dx.doi.org/10.1080/01496395.2015.1115068>
- Febrianto, J., Kosasih, A.N., Sunarso, J., Ju, Y.H., Indraswati, N. and Ismadji, S. 2009. Equilibrium and kinetic studies in adsorption of heavy metals using biosorbent: A summary of recent studies. *J. Hazard. Mater.*, 162(2-3): 616-645. doi: 10.1016/j.jhazmat.2008.06.042
- Feng, N. and Guo, X. 2012. Characterization of adsorptive capacity and mechanisms on adsorption of copper, lead, and zinc by modified orange peel. *Transact. Nonferr. Metals Soc. China*, 22(5): 1224-1231. doi:10.1016/S1003-6326(11)61309-5



- Feng, N., Guo, X., Liang, S., Zhu, Y. and Liu, J. 2011. Biosorption of heavy metals from aqueous solutions by chemically modified orange peel. *J. Hazard. Mater.*, 8: 114. DOI:10.1016/j.jhazmat.2010.08.114
- Fraissard, J.P. 1997. *Physical Adsorption: Experiment, Theory, and Applications*. Vol. 491. Springer Science & Business Media, Berlin, Germany.
- Freundlich, H.M.F. 1906. Over the adsorption in solution. *J. Phys. Chem.*, 57: 385-471.
- Gadde, B., Bonnet, S., Menke, C. and Garivait, S. 2009. Air pollutant emissions from rice straw open field burning in India, Thailand, and the Philippines. *Environ. Pollut.*, 157(5): 1554-1558. doi: 10.1016/j.envpol.2009.01.004.
- Giwa, A.A., Bello, I.A., Oladipo, M.A. and Adeoye, D.O. 2013. Removal of cadmium from wastewater by adsorption using the husk of melon (*Citrullus lanatus*) seed. *Int. J. Basic Appl. Sci.*, 2(1): 110-123.
- Gourdon, P., Bhande, S., Rus, E. and Sofer, S.S. 1990. Comparison of cadmium biosorption by gram-positive and gram-negative bacteria from activated sludge. *Biotechnol. Lett.*, 12: 839-842.
- Goyal, N., Jain, S.C. and Banerjee, U.C. 2003. Comparative studies on the microbial adsorption of heavy metals. *Adv. Environ. Res.*, 7: 311-319.
- Guechi, E.K. and Hamdaoui, O. 2015. Evaluation of potato peel as a novel adsorbent for the removal of Cu (II) from aqueous solutions: equilibrium, kinetic, and thermodynamic studies. *Desalin. Water Treat.*, 57(23): 10677-10688.
- Guiza, S. 2017. Biosorption of heavy metal from aqueous solution using cellulose waste orange peel. *Ecol. Eng.*, 99: 134-140. doi: 10.1016/j.ecolog.2016.11.043
- Guo, L., Liang, L.Y., Wang, Y.J. and Liu, M.D. 2015. Biosorption of Pb<sup>2+</sup> from aqueous solution by rice straw modified with citric acid. *Environ. Prog. Sustain.* 35(2): 359-367.
- Gupta, V.K., Nayak, A. and Agarwal, S. 2015. Bioadsorbents for remediation of heavy metals: Current status and their prospects. *Environ. Eng. Res.*, 20(1): 1-18. DOI: <https://doi.org/10.4491/eeer.2015.018>
- Gutha, Y., Munagapati, V.S., Alla, S.R. and Abburi, K. 2011. Biosorptive removal of Ni (ii) from aqueous solution by *Caesalpinia bonducella* seed powder. *Sep. Sci. Technol.*, 46(14): 2291-2297. doi:10.1080/01496395.2011.590390
- Hasan, S.H., Ranjan, D. and Talat, M. 2009. Rice polish for the removal of arsenic from aqueous solution: optimization of process variables. *Ind. Eng. Chem. Res.*, 48(9): 4194-4201. doi:10.1021/ie801822d
- Hill, A.V. 1910. The possible effect of aggregation of molecules of hemoglobin on its dissociation curve. *J. Physiol.*, 40(4), iv-vii.
- Ho, Y.S., Ng, J.C.Y. and McKay, G. 2000. Kinetics of pollutant sorption by biosorbents: Review. *Sep. Purif. Methods*, 29(2): 189-232.
- Hobbs, P. and Morris, M. 1996. Meeting South Asia's Future Food Requirements from Rice-Wheat Cropping Systems: Priority Issues Facing Researchers in the Post-Green Revolution Era. NRG Paper 96-01, CIMMYT, Mexico, pp. 1-56.
- Horsfall, M. and Ayebeami, I. 2005. Equilibrium sorption study of Al<sup>3+</sup>, Co<sup>2+</sup> and Ag<sup>+</sup> in aqueous solutions by fluted pumpkin (*Telfairia Occidentalis* HOOK) Waste Biomass. *Spiff Acta. Chim. Slov.*, 52: 174-181.
- Hossain, M.A., Ngo, H.H., Guo, W.S. and Setiadi T. 2012. Adsorption and desorption of copper (II) ions onto garden grass. *Bioresour. Technol.*, 121: 386-395. doi: 10.1016/j.biortech.2012.06.119.
- Hossain, M.A., Ngo, H.H., Guo, W.S. and Nguyen, T.V. 2012. Palm oil fruit shells as biosorbent for copper removal from water and wastewater: Experiments and sorption models. *Bioresour. Technol.*, 113: 97-101. doi: 10.1016/j.biortech.2011.11.111.
- Huang, Y.F., Chiueh, P.T., Shih, C.H., Lo, S.L., Sun L., Zhong Y. and Qiu, C. 2015. Microwave pyrolysis of rice straw to produce biochar as an adsorbent for CO<sub>2</sub> capture. *Energy*, 84: 75-82. doi: 10.1016/j.energy.2015.02.026.
- Ibisi, N.E. and Asoluka, C.A. 2018. Use of agro-waste (Musa paradisiaca peels) as a sustainable biosorbent for toxic metal ions removal from contaminated water. *Chem. Int.*, 4(1): 52-59.
- Iqbal, M., Saeed, A. and Kalim, I. 2009. Characterization of adsorptive capacity and investigation of the mechanism of Cu<sup>2+</sup>, Ni<sup>2+</sup> and Zn<sup>2+</sup> adsorption on mango peel waste from constituted metal solution and genuine electroplating effluent. *Sep. Sci. Technol.*, 44(15): 3770-3791.
- Ismadji, S. and Bhatia, S.K. 2000. Adsorption of flavor esters on granular activated carbon. *Canad. J. Chem. Eng.*, 78(5): 892-901. doi:10.1002/cjce.5450780506.
- Jain, N., Bhatia, A. and Pathak, H. 2013. Emission of air pollutants from crop residue burning in India. doi: 10.4209/aaqr.2013.01.0031
- Joo, J. and Hassan, S.H.A. 2010. Comparative study of biosorption of Zn (II) by *Pseudomonas aeruginosa* and *Bacillus cereus*. *Int. Biodeter. Biodegrad.*, 64(8): 734-741. doi: 10.1016/j.ibiod.2010.08.007.
- Kadirvelu, K. and Namasivayam, C. 2000. Agricultural by-product as metal adsorbent: sorption of lead (II) from aqueous solution onto coir pith carbon. *Environ. Technol.*, 22(10): 1091-1097.
- Kalaivani, S.S., Vidhyadevi, T., Murugesan, A., Baskaralingam, P., Anuradha, C.D., Ravikumar, L. and Sivanesan, S. 2014. Equilibrium and kinetic studies on the adsorption of Ni (II) ion from an aqueous solution using the cocoa shell. *Desal. Water Treat.*, 54: 1629-1641.
- Kaur, A. and Rani J. 2016. An approach to detect stubble burned areas in Punjab by digitally analyzing satellite images. *J. Res.*, 2(6): 2395-3411
- Khairia, M. and Al-Qahtani, M. 2015. Water purification uses different waste fruit cortexes for the removal of heavy metals. *J. Taibah Univ. Sci.*, 10(5): 700-708. Doi: 10: 1016/j.jtusc.2015.09.001
- Khan, A.R., Attaullah, R. and Al-Haddad, A. 1997. Equilibrium adsorption studies of some aromatic pollutants from dilute aqueous solutions on activated carbon at different temperatures. *J. Coll. Interface Sci.*, 194(1): 154-165. doi:10.1006/jcis.1997.5041
- Khatoun, H. and Rai, J.N. 2016. Agricultural waste materials as biosorbents for the removal of heavy metals and synthetic dyes: A review. *Oct. Jour. Env. Res.*, 4(3): 208-229.
- Koble, R.A. and Corrigan, T.E. 1952. Adsorption isotherms for pure hydrocarbons. *Ind. Eng. Chem.*, 44(2): 383-387. doi:10.1021/ie50506a049.
- Krishna, L.S., Yuzir, A., Yuvaraja, G. and Ashok Kumar, V. 2016. Removal of Acid Blue25 from aqueous solutions using Bengal gram fruit shell (BGFS) biomass. *Int. J. Phytoremed.*, 19(5): 431-438. doi:10.1080/15226514.2016.1244161.
- Kumar, P., Kumar, S. and Joshi, L. 2015. Socioeconomic and environmental implications of agricultural residue burning: S case study of Punjab, India. *Environ. Sci.*, 2015: 144.
- Kutahyali, C., Sert, S., Cetinkaya, B., Inan, S. and Eral, M. 2010. Factors affecting lanthanum and cerium biosorption on *Pinus brutia* leaf powder. *Sep. Sci. Technol.*, 45: 1456-1462.
- Lakshmi pathya, R. and Saradab, N.C. 2015. Metal ion-free watermelon (*Citrullus lanatus*) rind as adsorbent for the removal of lead and copper ions from an aqueous solution. *Desal. Water Treat.*, 57(33): 1-11. DOI: 10.1080/19443994.2015.1072064.
- Langmuir, I. 1918. The adsorption of gases on plane surfaces of glass, mica, and platinum. *J. Am. Chem. Soc.*, 40(9): 1361-1403. doi:10.1021/ja02242a004.
- Lata, S., Singh, P.K. and Samadder, S.R. 2014. Regeneration of adsorbents and recovery of heavy metals: a review. *Int. J. Environ. Sci.*, 12(4): 741. DOI 10.1007/s13762-014-0714-9.
- Lohan, S.K., Jat, H.S., Yadav, A.K., Sindhu, H.S., Jat, M.L., Choudhary, M., Peter, J.K. and Sharma, P.C. 2017. Burning issues of paddy residue management in northwest states of India. *Renew. Sustain. Energy Rev.*, 81: 693-706. <http://dx.doi.org/10.1016/j.rser.2017.08.057>.
- Malakootian, M., Hossein, K., Mahvi, A.H., Mansoorian, H.J. and Khanjani, N. 2018. Agrowaste-based eco-friendly bio-adsorbent for the removal of phenol: adsorption and kinetic study by *Acacia tortilis* pod shell. *Chiang Mai J. Sci.*, 45(1): 355-368. <http://epg.science.cmu.ac.th/ejournal>.
- Malkoc, E. and Nuhoglu, Y. 2005. Investigations of nickel (II) removal from aqueous solutions using tea factory waste. *J. Hazard. Mater.*, 127(1-3): 120-128. doi: 10.1016/j.jhazmat.2005.06.030.



- Mandal, A., Mukhopadhyay, P. and Das, S.K. 2019. The study of adsorption efficiency of rice husk ash for removal of phenol from wastewater with low initial phenol concentration. *SN Appl. Sci.*, 129: 1992 <https://doi.org/10.1007/s42452-019-0203-3>.
- Manique, M.C., Faccini, C.S., Onorevoli, B., Benvenuti, E.V. and Caramão E.B. 2012. Rice husk ash is an adsorbent for purifying biodiesel from waste frying oil. *Fuel*, 92(1): 56-61. <http://doi.org/http://dx.doi.org/10.1016/j.fuel.2011.07.024>.
- Martín-Lara, M.A., Blázquez, G., Ronda, A., Pérez, A. and Calero, M. 2013. Development and characterization of biosorbents to remove heavy metals from aqueous solutions by chemical treatment of olive stone. *Ind. Eng. Chem. Res.*, 2(31): 10809-10819. doi:10.1021/ie401246c.
- Mathew, B.B., Jaishankar, M., Biju, V.G. and Nideghatta, K. 2016. Role of Bioadsorbents in Reducing Toxic Metals. *Beeregowda*<http://dx.doi.org/10.1155/2016/4369604>
- Mishra, A. and Tripathi B.D. 2008. Utilization of fly ash in adsorption of heavy metals from wastewater. *Toxicol. Environ. Chem.*, 90(6): 1091-1097. doi:10.1080/0272240801936786.
- Modak, J.M. and Natarajan, K.A. 1995. Biosorption of metals using non-living biomass-a review. *Miner. Metall. Proc.*, 12: 189-199.
- Mohammed, T.J. and Ibrahim, R.I., 2016. Remediation of Cu (II) from well water of Iraq by using cortex of fruits and agricultural waste. *Chem. Eng.*, 41(2): 345-355.
- Mor, S., Chhoden, K. and Khaiwal, R. 2016. Application of agro-waste rice husk ash for the removal of phosphate from the wastewater. *J. Clean. Prod.*, 129: 673-680. DOI: 10.1016/j.jclepro.2016.03.088.
- Mor, S., Negi, P. and Ravindra, K. 2019. Potential of agro-waste sugarcane bagasse ash for the removal of ammoniacal nitrogen from landfill leachate. *Environ. Sci. Pollut. Res.*, 7: 52. doi:10.1007/s11356-019-05563-7.
- Naiya, T.K., Bhattacharya, A.K. and Das, S.K. 2008b. Adsorption of Pb (II) by sawdust and neem bark from aqueous solutions. *Environ. Prog.*, 27(3): 313-328. doi:10.1002/ep.10280.
- Naiya, T.K., Chowdhury, P., Bhattacharya, A.K. and Das, S.K. 2008a. Sawdust and neem bark as low-cost natural biosorbent for adsorptive removal of Zn (II) and Cd (II) ions from aqueous solutions doi: 10.1016/j.cej.2008.08.002.
- Netzahuatl-Muñoz, A.R., Guillén-Jiménez, F., de, M., Chávez-Gómez, B., Villegas-Garrido, T.L. and Cristiani-Urbina, E. 2011. Kinetic study of the effect of ph on hexavalent and trivalent chromium removal from aqueous solution by *Cupressus lusitanica* Bark. *Water Air Soil Pollut.*, 223(2): 625-641. doi:10.1007/s11270-011-0888-4.
- Nguyen, T.H. 2017. An overview of agricultural pollution in Vietnam: The crop sector 2017. World Bank, Washington DC.
- Obi, F.O., Ugwuishiwu, B.O. and Nwakaire, J.N.2016. Agricultural waste concept, generation, utilization, and management. *Nig. J. Technol.*, 35(4): 34 <http://dx.doi.org/10.4314/njt.v35i4.34>.
- Okoye, A.I., Ejikeme, P.M. and Onukwuli, O.D.2010. Lead removal from wastewater using fluted pumpkin seed shell activated carbon: adsorption modeling and kinetics. *Int. J. Environ. Sci. Technol.*, 7(4): 793-800.
- Owalude, S.O. and Tella, A.C. 2016. Removal of hexavalent chromium from aqueous solutions by adsorption on modified groundnut hull. *Beni-Suef Univ. J. Basic Appl. Sci.*, 5(4): 377-388. <http://dx.doi.org/10.1016/j.bjbas.2016.11.005>.
- Pandey, M.M. 2009. Indian agriculture: An introduction Submitted to Fourth Session of the Technical Committee of APCAE 10-12 February 2009, Chiang Rai, Thailand.
- Pappu, A., Saxena, M. and Asolekar, S. R. 2006. Solid wastes generation in India and their recycling potential in building materials. *Buil. Environ.*, 42(6): 2311-2320. doi: 10.1016/j.buldev.2006.04.015.
- Park, D., Yun, Y.S. and Moon Park, J.2010. The past, present, and future trends of biosorption. *Biotechnol. Bioprocess. Eng.*, 15: 86-102.
- Parlayıcı, . and Pehlivan, E., 2017. Removal of metals by Fe3O4 loaded activated carbon prepared from plum stone (*Prunus nigra*): Kinetics and modeling study. *Powder Technol.*, 317: 23-30.
- Pino, G.H., de Mesquita L.M.S., Torem M.L. and Pinto G.A.S. 2006. Bi-adsorption of Heavy Metals by Powder of Green Coconut Shell. *Sep. Sci. Technol.*, 41(14): 3141-3153. doi:10.1080/01496390600851640.
- Qiu, H., Lv, L., Pan, B., Zhang, Q., Zhang, W. and Zhang, Q. 2009. Critical review in adsorption kinetic models. *J. Zhejiang Univ. Sci. A*, 10(5): 716-724. doi:10.1631/jzus. a0820524.
- Rafique, U. and Zulfiqar, S. 2014. Synthesis and technological application of agro-waste composites for treatment of textile wastewater. *Int. J. Agric. Innov. Res.*, 3(3): 2319-1473.
- Rai, M.K., Shahi, G., Meena, V., Meena, R., Chakraborty, S., Singh, R.S. and Rai B.N. 2016. Removal of hexavalent chromium Cr (VI) using activated carbon prepared from mango kernel activated with H<sub>3</sub>PO<sub>4</sub>. *Resour. Efficient Technol.*, 2(1): 63-70. <http://dx.doi.org/10.1016/j.refit.2016.11.011>.
- Rao, C.N., Subbarayudu, K., Vijaya, Y. and Subbaiah, M.V. 2014. Adsorption of Ni (II) from aqueous solution by activated carbons derived from tobacco stem. *Desalin. Water Treat.* 54(12): 3392-3399.
- Redlich, O. and Peterson, D.L. 1959. A useful adsorption isotherm. *J. Phys. Chem.*, 63(6): 1024-1024. doi:10.1021/j150576a.5
- Sadek, S.A., Negm, N.A., Hefni, H.H.H. and Wahab, M.M.A. 2015. Metal adsorption by agricultural biosorbents: Adsorption isotherm, kinetic and biosorbents chemical structures. *International J. Biol. Macromol.*, 81: 400-409. doi: 10.1016/j.ijbiomac.2015.08.031
- Safa, Y. 2015. Utilization of mustard and linseed oil cakes: novel biosorbents for removal of acid dyes. *Desal. Water Treat.*, 57(13): 5914-5925. doi:10.1080/19443994.2015.1007087
- Sahai, S.C., Sharma, C., Singh, S.K. and Gupta, P.K. 2010. Assessment of trace gases, carbon, and nitrogen emissions from field burning of agricultural residues in India. *Nutr. Cycl. Agroecosys.*, 89: 143-157. DOI 10.1007/s10705-010-9384-2.
- Sahota, S., Vijay, V.K., Subbarao, P.M.V., Chandra, R., Ghosh, P., Shah, G., Vijay, V., Vaibhav Koutu, V. and Thakur, I.S. 2017. Characterization of leaf waste-based biochar for cost-effective hydrogen sulfide removal from biogas. *Bioresour. Technol.*, 250: 635-641. doi.org/10.1016/j.biortech.2017.11.093.
- Salman, M., Athar M. and Farooq U. 2015. Biosorption of heavy metals from aqueous solutions using indigenous and modified lignocellulosic materials. *Reviews in Environmental Science and Bio/Technology*, 14(2), 211-228. doi:10.1007/s11517-015-9362-x
- Salman, M., Athar, M., Farooq, U., Rauf, S. and Habiba, U. 2014. A new approach to modification of an agro-based raw material for Pb (II) adsorption. *Korean J. Chem. Eng.*, 31(3): 467-474. doi:10.1007/s11814-013-0264-8
- Salman, M., Rehman, R., Farooq, U., Tahir, A. and Mitu, L. 2020. Biosorptive removal of cadmium (ii) and copper (ii) using microwave-assisted thiourea-modified sorghum bicolor agrowaste. *J. Chem.*, 43: 1643. <https://doi.org/10.1155/2020/8269643>.
- Saman, N., Kong, H., Mohtar, S.S., Johari, K., Mansor, A.F., Hassan, O., Ali N. and Mat, H. 2019. A comparative study on dynamic Hg (II) and MeHg (II) removal by functionalized agrowaste adsorbent: breakthrough analysis and adsorber design. *Korean J. Chem. Eng.*, 36(7): 1069-1081. DOI: 10.1007/s11814-019-0285-z
- Santos, V.C.G.D., Tarley, C.R.T., Caetano, J. and Dragunski, D.C. 2010. Assessment of chemically modified sugarcane bagasse for lead adsorption from aqueous medium *Water Sci. Technol.*, 62: 201.
- Saqib, A.N.S., Waseem, A., Khan, A.F., Mahmood, Q., Khan, A., Habib, A. and Khan, A.R. 2013. Arsenic bioremediation by low-cost materials derived from Blue Pine (*Pinus walllichiana*) and Walnut (*Juglans regia*). *Ecol. Eng.*, 51: 88-94. doi: 10.1016/j.ecoleng.2012.12.063
- Sarath Babu, B. and Yamini, G. 2020. Removal of methylene blue dye by using lemon leaf powder as an adsorbent. *Water Resour. Manag.*, 11(2): 341-359. [https://doi.org/10.1007/978-981-15-0706-9\\_10](https://doi.org/10.1007/978-981-15-0706-9_10)

- Shafique, U., Ijaz, A., Salman, M., Zaman, W., Jamil, N., Rehman, R. and Javaid A. 2012. Removal of arsenic from water using pine leaves. *J. Taiwan Instit. Chem. Eng.*, 43(2): 256–263. doi: 10.1016/j.jtice.2011.10.006
- Shahkarami, S., Dalai, A.K., Soltan, J., Hu, Y. and Wan, D. 2015. Selective CO<sub>2</sub> capture by activated carbons: Evaluation of the effects of precursors and pyrolysis process. *Energy Fuels*, 29(11): 7433-7440. doi: 10.1021/acs.energy.fuels.5b00470.
- Shakoor, M.B., Niazia, N.K., Bibia, I., Shahidd, M., Saqiba, Z.A., Nawaze, M.F., Shaheen, S.M., Wangh, H., Tsangj, D.C.W., Bundschuh, J., Okl, Y.S. and Rinklebe J. 2018. Exploring the arsenic removal potential of various biosorbents from water. *Compare. Stud. Environ. Int.*, 123: 567-579. <https://doi.org/10.1016/j.envint.2018.12.049>.
- Silva, C.R., Gomes, T.F., Andrade, G.C.R.M., Monteiro, S.H., Dias, A.C.R., Zagatto, E.A.G. and Tornisielo, V.L. 2013. Banana peel as an adsorbent for removing atrazine and ametryne from waters. *J. Agric. Food Chem.*, 61(10): 2358-2363. doi:10.1021/jf304742h.
- Sips, R. 1948. combined form of Langmuir and Freundlich equations. *J. Chem. Phys.*, 10
- Smitha, T., Santhi, T., Prasad, A.L. and Manonmani, S. 2012. Cucumis sativus is used as an adsorbent for the removal of dyes from an aqueous solution. *Arab. J. Chem.*, 10(1): 244-251. <http://dx.doi.org/10.1016/j.arabjc.2012.07.030>
- Taha, G., Arifien, A.E. and Elnahas, S. 2011. The removal efficiency of potato peels as a new biosorbent material for uptake of Pb(II) Cd(II) and Zn(II) from their aqueous solutions. *J. Solid Waste Technol. Manag.*, 37(2): 128-140. <https://doi.org/10.5276/JSWTM.2011.128>.
- Tempkin, M. and Pyzhev, V. 1940 Kinetics of ammonia synthesis on promoted iron catalysts. *Acta Physicochim.*, 12: 217-222.
- Toth, J. 1971. State equation of the solid-gas interface layer. *Acta Chim. Acad. Sci. Hungar.*, 69(3): 311-328.
- United Nations, Glossary of Environment Statistics, Studies in Methods, Series F, 67, Department for Economic and Social Information and Policy Analysis, Statistics Division, New York, USA, 1997.
- Vieira, M.G.A., Almeida Neto, A.F., de Silva, M.G.C., Nóbrega, C.C. and Melo Filho, A.A. 2012. Characterization and use of natural and calcined rice husks for biosorption of heavy metal ions from aqueous effluents. *Brazil. J. Chem. Eng.*, 29(3): 619-634. doi:10.1590/s0104-66322012000300019.
- Vijayaraghavan, K. and Yun, Y.S. 2008. Bacterial biosorbents and biosorption. *Biotechnol. Adv.*, 26(3): 266-291. doi: 10.1016/j.biotechadv.2008.02.002.
- Vijayaraghavan, K., Padmesh, T., Palanivelu, K. and Velan, M. 2006. Biosorption of nickel (II) ions onto *Sargassum wightii*: Application of two-parameter and three-parameter isotherm models. *J. Hazard. Mater.*, 133(1-3): 304-308. doi: 10.1016/j.jhazmat.2005.10.016.
- Volesky, B. 1994. Advances in biosorption of metals: Selection of biomass types. *FEMS Microbiol. Rev.*, 14(4): 291-302. doi:10.1111/j.1574-6976.1994.tb00102.x
- White, C., Sayer, J.A. and Gadd, G.M. 1997. Microbial solubilization and immobilization of toxic metals: key biogeochemical processes for treatment of contamination. *FEMS Microbiol. Rev.*, 20: 503-516.
- Witek-Krowiak, A. and Reddy H.K. 2013. Removal of micro elemental Cr (III) and Cu (II) by using soybean meal waste – Unusual isotherms and insights of binding mechanism. *Bioresour. Technol.*, 127: 350-357. doi: 10.1016/j.biortech.2012.09.072
- Witek-Krowiak, A., Szafran, R.G. and Modelski, S. 2010. Biosorption of heavy metals from aqueous solutions onto peanut shells as a low-cost biosorbent. *Desalination*, 7: 042. doi: 10.1016/j.desal.2010.07.042
- Zein, R., Suhaili, R., Earnestly, F., Indravati, M. and Munaf, E. 2010. Removal of Pb (II), Cd (II), and Co (II) from aqueous solution using *Garcinia mangostona* L. fruit shell. *J. Hazard. Mater.*, 4: 76. DOI: 10.1016/j.jhamat.2010.04.076.
- Zhang, X., Wu, J., Yang, H., Shao, J., Wang, X., Chen, Y. and Chen, H. 2016. Preparation of nitrogen-doped microporous modified biochar by high-temperature CO<sub>2</sub>-NH<sub>3</sub> treatment for CO<sub>2</sub> adsorption: Effects of temperature. *RSC Adv.*, 6(100): 98157-98166. doi:10.1039/c6ra23748g
- Zouboulis, A.L., Matis, K.A. and Hancock, I.C. 1997. Biosorption of metals from dilute aqueous solutions. *Sep. Purif. Meth.*, 26: 255-295.



# Spatial Differentiation and Dynamic Evolution of Agricultural Carbon Emissions in Fujian Province of China

Kai Su<sup>\*(\*\*)</sup> †, Hongyun Chen<sup>\*\*</sup> and Cuili Gan<sup>\*\*</sup>

\*Academy of Agricultural Planning and Engineering, Ministry of Agriculture and Rural Affairs, Beijing 100125, China

\*\*Anxi College of Tea Science, Fujian Agriculture and Forestry University, Fuzhou 350002, China

†Corresponding author: Kai Su; fjsk1311@163.com

Nat. Env. & Poll. Tech.  
Website: [www.neptjournal.com](http://www.neptjournal.com)

Received: 17-08-2021

Revised: 24-09-2021

Accepted: 26-10-2021

## Key Words:

Agricultural carbon emissions  
Correlation effects  
Spatial-temporal differentiation  
Spatial autocorrelation

## ABSTRACT

The previous literatures have insufficient content on spatial dependence and heterogeneity of agricultural carbon emissions (ACEs), which is inconsistent with the actual situation, weakening the practical significance of research conclusions. To fill this knowledge gap, this study attempts to explore the spatial evolution pattern of ACEs at the city-scale in the Fujian Province of China from spatio-temporal latitudes and adopts the exploratory spatial data analysis method (ESDA) to analyze the spatial correlation effects of ACEs. The findings revealed that ACEs in Fujian show a downtrend as a whole. From the perspective of carbon sources of ACEs, agricultural materials and livestock breeding caused the largest emissions, accounting for 73.82% of the total ACEs, while rice growth led to the smallest carbon emissions, accounting for 26.18% of the total ACEs. We also found that there is obvious non-equilibrium in the spatial distribution of ACEs and their intensity, showing a strong spatial correlation; and although a relatively obvious clustering area has been formed, the spatial autocorrelation of most regions is not significant. Accordingly, we suggest that exploring the “carbon compensation mechanism”, is conducive to stimulating the low-carbon agricultural production behavior with positive externalities, to reduce agricultural carbon emissions.

## INTRODUCTION

As a semi-artificial-semi-natural composite ecosystem, however, the agricultural ecosystem is one of the important sources of carbon emissions from human activities. Data displayed that 10-14% of global greenhouse gas emissions are directly emitted by agricultural production (Paustian et al. 2016). Existing research results exhibited that China's greenhouse gas (GHG) emissions from agricultural sources account for about 17% of the country's total GHG emissions, among which CH<sub>4</sub> and NO<sub>2</sub> from the agricultural sector account for 50% and 92% of the total emissions, respectively (Rebolledo-Leiva et al. 2017). At present, China is advancing the process of agricultural modernization, which will likely emit more carbon emissions during its realization; meanwhile, in the context of climate change, agricultural production activities have become very sensitive and fragile, which is the most vulnerable to climate change. Therefore, study on agricultural carbon emissions (ACEs) has gradually become one of the hotspots in the research field of climate change and carbon emissions.

In view of the important contribution of ACEs to global GHG emissions, scholars have done a lot of research work on agricultural low-carbon development and put forward many

enlightening viewpoints and conclusions around ACEs. For example, Adewale et al. (2019) found that only by clarifying the factors behind the difference in total carbon emissions can the agricultural sector effectively reduce GHG emissions. Balsalobre-Lorente et al. (2019) investigated EKC (Environment Kuznets Curve) hypothesis for BRICS, and the empirical results verified an inverted U-shaped relationship between ACEs and economic growth. On the other hand, Chinese scholars have conducted a large number of empirical discussions on the aspects of ACEs measurement and agricultural carbon emissions intensity (Huang et al. 2019, Pang et al. 2020), influencing factor decomposition and regional differences (Wang et al. 2020, Xiong et al. 2020), agricultural carbon footprint (Li et al. 2021), agricultural ecological compensation from a low-carbon perspective (Chen & Jiang 2018a, 2018b), ACEs performance (Wang et al. 2019) and carbon productivity (Xu et al. 2019). However, most of the above studies regarded the study area as independent homogeneous units, and seldom consider the spatial dependence and heterogeneity of ACEs, which is inconsistent with the actual situation, weakening the practical significance of the research conclusions. Furthermore, scholars often choose an adjacency weight matrix to represent spatial attributes when constructing spatial econometric models, which not only ignore the possible interaction

of spatial non-adjacent units but also can not reflect the effect difference caused by geographical distance.

There is a large gap between the endowment of agricultural natural resources and the level of agricultural economic development, it is necessary to conduct more empirical analysis in different regions of China to better reveal the regional differences in agricultural carbon emissions. Since “the Belt and Road” (B&R) initiative was put forward, the areas along the route have gradually become the target of research areas related to carbon emissions (Fan et al. 2019, Muhammad et al. 2020). However, studies focusing on ACEs and their carbon effects in the core area of “B&R” have not yet been found. Fujian Province has been designated as the “core area of the 21st-Century Maritime Silk Road”, and as “a demonstration area of China’s ecological civilization”, its agricultural production must be combined with its regional advantages to achieve low-carbon agricultural development. The greenhouse effect caused by carbon emissions has led to a decline in the capacity of agro-ecosystem services in Fujian Province (Su et al. 2020). Based on this, it is necessary to explore agricultural carbon emissions and their spatial evolution in the core area, to provide a reference basis for the sustainable development of the agricultural sector.

Accordingly, to fill this knowledge gap, this study tried to expand the existing research from the following two aspects based on previous studies. Firstly, by discussing the spatial-temporal distribution characteristics of ACEs, this study was conducive to a more comprehensive grasp of the law of ACEs. Secondly, ESDA was used to capture the spatial dependence effect caused by the interaction between regions, and to discuss the spatial correlation and agglomeration of regional carbon emissions. This study attempted to combine the characteristics of spatial-temporal distribution with spatial dependence, which is helpful to understand the inherent logical relationship of ACEs. This is rarely mentioned in previous studies on the spatial-temporal distribution of ACEs. Therefore, based on the calculated data of ACEs in Fujian Province of China from 2005 to 2019, this study applied the ESDA method to capture the correlation effect between ACEs in cities to accurately grasp the evolution law of ACEs. The results of this study can not only provide a reference basis for measures to reduce regional agricultural carbon emissions, but also provide research ideas for related research in other regions/countries.

## MATERIALS AND METHODS

### Study Area Overview

Fujian Province is located on the southeast coast of the

Chinese mainland (between 115°50′ ~ 120 °40′ E and 23°18′ - 28°22′ N), with a total land area of 121,400 square kilometers. Its geographical features are that 90% of the land area is mountainous and hilly while the rest is arable land (Su et al. 2020). It belongs to the subtropical marine monsoon climate; the annual temperature and the annual precipitation are 17°C to 21°C and 1,351 to 2,645 millimeters, respectively.

Additionally, Fujian was also one of the earliest provinces in China to carry out the policy of reform and opening-up, which has a GDP of 4.24 trillion CNY in 2019, an increase of 7.6% (FPBS, 2020). And, the resident population of Fujian Province was 39.73 million, and the per capita GDP was 107139 CNY, an increase of 6.7% over the previous year. Moreover, its sown areas of farm crops reached  $164.8 \times 10^4$  hectares, of which  $82.2 \times 10^4$  hectares were grain crops (FPBS 2020). As the “core area of the 21st-Century Maritime Silk Road”, and a demonstration area of China’s ecological civilization, its agricultural production must be combined with its regional advantages to achieve low-carbon agricultural development.

### Calculation of Agricultural Carbon Emissions (ACEs)

The calculation of ACEs in this study mainly considers the carbon emissions generated in the process of agricultural production, which are specifically calculated from the following three aspects. That is carbon emissions caused by the input of agricultural materials, CH<sub>4</sub> emissions from paddy fields, CH<sub>4</sub> and N<sub>2</sub>O emissions produced by the manure management system, and enteric fermentation in the process of livestock breeding. The calculation equation of ACEs is as follows.

$$ACEs = E_a + E_b + E_c + E_d + E_e + E_f + E_g + E_h + E_j + E_k \dots(1)$$

where, ACEs are agricultural carbon emissions ( $\times 10^4$  t);  $E_a$ ,  $E_b$ ,  $E_c$ ,  $E_d$ ,  $E_e$ , and  $E_f$  denote carbon emissions caused by the use of chemical fertilizers, pesticides, agricultural film, agricultural machinery, agricultural diesel, and agricultural irrigation, respectively;  $E_g$  represents CH<sub>4</sub> emissions from paddy fields;  $E_h$  represents CH<sub>4</sub> emissions produced by enteric fermentation in the process of livestock breeding;  $E_j$  and  $E_k$  denote CH<sub>4</sub> and N<sub>2</sub>O emissions produced by the manure management system in the process of livestock breeding, respectively.

$$E_a = (Q_{a1} \times A_1 + Q_{a2} \times A_2 + Q_{a3} \times A_3 + Q_{a4} \times A_4) \times 10^{-7} \dots(2)$$

$$E_b = Q_b \times B \times 10^{-7} \dots(3)$$

$$E_c = Q_c \times C \times 10^{-7} \dots(4)$$

$$E_d = [(S_d \times D) + (W_d \times F)] \times 10^{-7} \quad \dots(5)$$

$$E_e = Q_e \times G \times 10^{-7} \quad \dots(6)$$

$$E_f = S_f \times H \times 10^{-7} \quad \dots(7)$$

$$E_g = \sum (EF_i \times AD_i) \times 10^{-7} \quad \dots(8)$$

$$E_h = \sum (EF_{CH_4, enteric, i} \times AP_i) \times 10^{-7} \quad \dots(9)$$

$$E_j = \sum (EF_{CH_4, manure, i} \times AP_i) \times 10^{-7} \quad \dots(10)$$

$$E_k = \sum (EF_{N_2O, manure, i} \times AP_i) \times 10^{-7} \quad \dots(11)$$

The meanings of the symbols in the above equations and the carbon emissions coefficient values of each carbon source are shown in Table 1.

For ease of analysis, we convert CH<sub>4</sub> and N<sub>2</sub>O into CO<sub>2e</sub>, and calculate equations as follows:

$$E_{convert} = \frac{[(E_h + E_j) \times 28 + E_k \times 265]}{44/12} \quad \dots(12)$$

where  $E_{convert}$  represents the total amount of CH<sub>4</sub> and N<sub>2</sub>O converted into carbon equivalent ( $\times 10^4$ t). 28 and 265 denote the global warming potentials (GWP) values of CH<sub>4</sub> and N<sub>2</sub>O for a 100-year time horizon, respectively (Pachauri et al. 2014).

Table 1: Carbon emissions coefficient of ACEs sources.

Symbols	Carbon sources	Symbols	Coefficient	Data sources
$Q_{a1}$	Nitrogenous Fertilizer (kg)	$A_1$	1.74000 kg/kg	(Lu et al. 2008)
$Q_{a2}$	Phosphate Fertilizer (kg)	$A_2$	0.16509 kg/kg	(West & Marland 2002)
$Q_{a3}$	Potash Fertilizer (kg)	$A_3$	0.12028 kg/kg	(West & Marland 2002)
$Q_{a4}$	Compound Fertilizer (kg)	$A_4$	0.38097 kg/kg	(Tian et al. 2015)
$Q_b$	Pesticide (kg)	$B$	4.93410 kg/kg	(West & Marland 2002)
$Q_c$	Agricultural film (kg)	$C$	5.18000 kg/kg	(Tian et al. 2015)
$S_d$	Farmland tillage (hm <sup>2</sup> )	$D$	16.47 kg/hm <sup>2</sup>	(Wang et al. 2016)
$W_e$	Farm machinery (kw)	$F$	0.18 kg/kw	
$Q_e$	Agricultural diesel	$G$	0.5927 kg/kg	(West & Marland 2002)
$S_f$	Agricultural irrigation	$H$	266.48 kg/hm <sup>2</sup>	
$EF_i$	Single-cropping rice (hm <sup>2</sup> )	$AD_i$	215.5 kg/hm <sup>2</sup>	(NCSC n.d.)
	Double-cropping early rice (hm <sup>2</sup> )		211.4 kg/hm <sup>2</sup>	
	Double-cropping late rice (hm <sup>2</sup> )		224.5 kg/hm <sup>2</sup>	
$EF_{CH_4, enteric, i}$	Cow (head/a)	$AP_i$	76.1 kg/head/a	(NCSC n.d.)
	Sheep (head/a)		8.8 kg/head/a	
	Pig (head/a)		1 kg/head/a	
$EF_{CH_4, manure, i}$	Cow (head/a)	$AP_i$	5.73 kg/head/a	(NCSC n.d.)
	Sheep (head/a)		0.27 kg/head/a	
	Pig (head/a)		5.08 kg/head/a	
	Poultry (head/a)		0.02 kg/head/a	
	Rabbit (head/a)		0.08 kg/head/a	
$EF_{N_2O, manure, i}$	Cow (head/a)	$AP_i$	1.261 kg/head/a	(NCSC n.d.)
	Sheep (head/a)		0.113 kg/head/a	
	Pig (head/a)		0.175 kg/head/a	
	Poultry (head/a)		0.007 kg/head/a	
	Rabbit (head/a)		0.007 kg/head/a	



## Calculation of Agricultural Carbon Emissions Intensity (ACEI)

ACEI discussed in this study mainly refers to carbon emissions produced by economic benefit per unit of the agricultural sector, based on the total agricultural economic output value (*AGDP*) and agricultural carbon emissions of each city, ACEI can be expressed as:

$$ACEI = ACE / AGDP \quad \dots(13)$$

## Exploratory Spatial Data Analysis (ESDA)

The commonly used spatial correlation indexes include Global Moran's *I* and Local Moran's *I*. Global Moran's *I* is used to measure the spatial correlation of variable attribute values between neighboring regions in the whole region. But Global Moran's *I* measure the spatial correlation characteristics of variable attribute values as a whole, but it cannot measure the specific types of spatial correlation of variable attribute values in different provinces. This requires the use of Local Moran's *I*. For details of the expression of Global Moran's *I* and Local Moran's *I*, please see reference (Su & Lee 2021).

## Data Acquisition and Processing

The data of chemical fertilizers, pesticides, agricultural film, the total power of agricultural machinery, crop area and livestock number, etc., used in this study were all from the Statistical Yearbook of Fujian Province (2006-2020) and the statistical yearbooks of 9 prefecture-level cities (2006-2020).

In addition, to eliminate the impact of price fluctuations, the actual agricultural GDP was recalculated based on the constant price in 2005, and then the agricultural carbon emissions intensity was calculated.

## RESULTS AND DISCUSSION

### Temporal Evolution Characteristics of ACEs and ACEI

According to equations (1-12), agricultural carbon emissions caused by each carbon source in Fujian Province from 2005 to 2019 were as shown in Fig. 1.

As can be seen from Fig. 1, ACEs in Fujian Province displayed an overall downward trend from 2005 to 2019. It dropped from  $549.3 \times 10^4 \text{t}$  in 2005 to  $393.9 \times 10^4 \text{t}$  in 2019, a decrease of 28.28%, with an average annual decline of 1.89%. The change in agricultural carbon emissions in Fujian Province can be roughly divided into three stages. 2005-2007 was the first stage, ACEs continue to reduce, and the rate of decline continues to decline. Then, 2007-2013 is the second stage, ACEs are relatively stable. It is worth noting that since 2013, ACEs in Fujian Province have dropped sharply, and in these six years, the total carbon emissions have dropped from  $507.0 \times 10^4 \text{t}$  (2014) to  $393.9 \times 10^4 \text{t}$  (2019), with an average annual growth rate of -3.72%. The negative growth rate of carbon emissions may be due to the decline of carbon emissions caused by the reduction of livestock-breeding scale and adjustment of

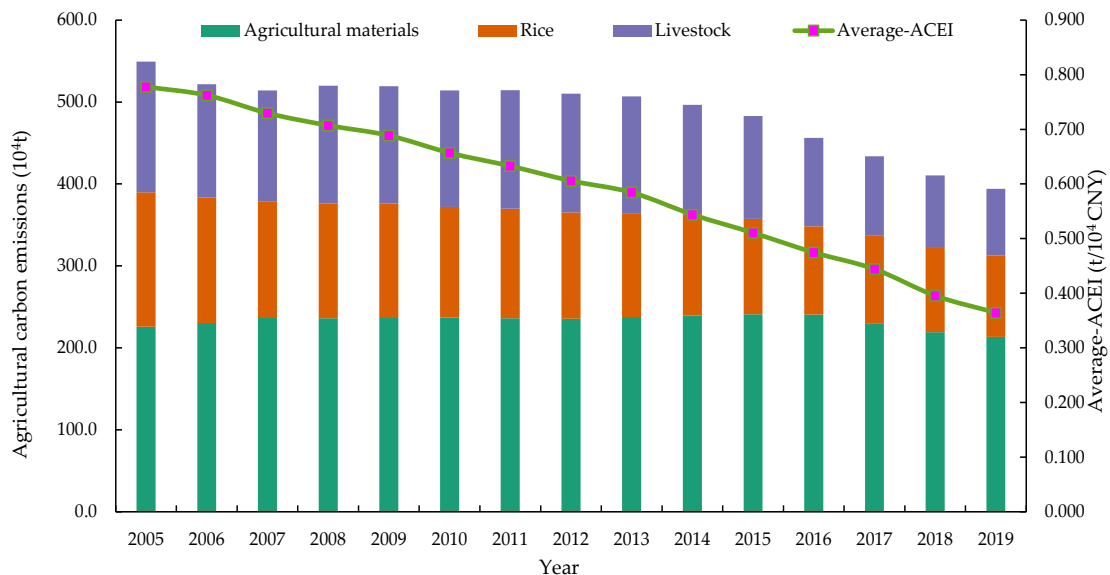


Fig. 1: Total ACEs and ACEI in Fujian Province during 2005-2019.

breeding structure; on the other hand, due to the decline of agricultural income, the agricultural labor force has been transferred to non-agricultural industries, resulting in a decline in agricultural production activities. In general, the fluctuation trend of ACEs in Fujian Province in the whole sample range in the past 15 years showed the evolution characteristics of three stages, i.e., “fluctuation decline - maintaining stability - rapid decline”. This demonstrated that Fujian Province has a certain degree of control over carbon emissions in the process of agricultural development, and the meaning of the development of ecological agriculture has been strengthened. Additionally, the average agricultural carbon emissions intensity (ACEI) in Fujian Province has generally shown a downward trend since 2005, from 0.778 t/10<sup>4</sup> CNY in 2005 to 0.364 t/10<sup>4</sup> CNY in 2019, with an average annual decline of 4.24%. The entire sample has fluctuated and the amplitude is also quite different. The largest drop in 2018 reached 10.97%, followed by the largest drop of 7.87% in 2019, and the third one was the drop of 7.03% in 2016. The smallest drop was in 2006, it was only 1.98%. It can be seen that the various characteristics of ACEI are consistent with the variation trend of ACEs.

From the perspective of specific carbon source classification, carbon emissions caused by rice growth, livestock-breeding, and agricultural materials decreased from 164.1×10<sup>4</sup>t, 159.3×10<sup>4</sup>t, and 225.9×10<sup>4</sup>t in 2005 to 99.6×10<sup>4</sup>t, 81.0×10<sup>4</sup>t, and 213.3×10<sup>4</sup>t in 2019, with a decrease of 39.28%, 49.14%, and 5.58%, respectively. Among them, the proportion of carbon emissions brought by carbon emissions from agricultural materials has been maintained at about 42.4% and is showing an upward trend year by year. This is directly related to the extensive use of agricultural materials (chemical fertilizers, pesticides, agricultural film, agricultural diesel, etc.). Moreover, the carbon emissions caused by rice paddy account for 23.3% and exhibited a downward trend year by year. This may be directly related to the abandonment of a large amount of agricultural land in Fujian Province and the decline of rice planting area year by year. It can be seen that ACEs caused by agricultural materials and livestock-breeding account for about 65.8% of total emissions, which is the most important factor for ACEs in Fujian Province.

The above analysis is only from the perspective of total carbon emissions in Fujian Province. Due to the different agricultural resource endowments and economic development of each region, the characteristics of carbon emissions are different. Therefore, it is necessary to analyze the structural differences between ACEs in different cities (Table 2).

It can be seen from Table 2 that Zhangzhou City had the largest total ACEs, reaching 77.86×10<sup>4</sup>t, which was 12.71

times that of Xiamen City(6.13×10<sup>4</sup>t); followed by Nanping (64.52×10<sup>4</sup>t), Longyan(54.96×10<sup>4</sup>t), Sanming (54.22×10<sup>4</sup>t), Fuzhou (45.34×10<sup>4</sup>t), Quanzhou (43.36×10<sup>4</sup>t), Ningde (33.81×10<sup>4</sup>t), and Putian (18.38×10<sup>4</sup>t) from highest to lowest; the last one is Xiamen, which has the least ACEs in 2019. The results of the above agricultural carbon emissions structure displayed that the main sources of ACEs in 9 cities of Fujian Province are agricultural materials and livestock breeding, accounting for an average of about 65.8%, while the proportion of carbon emissions caused by rice growth is the smallest, only 23.3%. It is worth noting that Zhangzhou City, Nanping City, and Longyan City have the largest carbon emissions of agricultural materials, rice growth, and livestock breeding, reaching 59.59×10<sup>4</sup>t, 24.68×10<sup>4</sup>t, and 18.33×10<sup>4</sup>t in 2019, respectively.

### Spatial Differentiation Characteristics of ACEs and ACEI

To further reveal the spatial evolution characteristics of ACEs and ACEI in each city in Fujian Province, this study used ArcGIS10.8 to classify ACEs and ACEI to get their spatial distribution Figs (Fig. 2 and Fig. 3) based on the classification principle of the natural breaks method.

According to Fig. 2, the changing pattern of ACEs in the coastal areas (Ningde, Fuzhou, Putian, Quanzhou, Xiamen, and Zhangzhou) of Fujian Province is relatively stable compared with the inland areas (Nanping, Sanming, and Longyan). Among them, the ACEs of Zhangzhou have always been a high emission area. The reason is that Zhangzhou is a big agricultural city, which is the main grain-producing area in Fujian Province. This makes more input in agricultural materials lead to increased carbon emissions. In addition, it is worth pointing out that Xiamen is a special economic zone of China, which has always been a low-emission area of ACEs in Fujian Province. This is because Xiamen's agricultural development model mainly uses agricultural landscape resources and agricultural production conditions to develop a leisure agricultural development model that integrates sightseeing, leisure, and tourism. As a result, its ACEs have been at a low level.

Since carbon emissions intensity considers the impact of total resources on the distribution, it can more accurately reflect the extent of regional ACEs. From the perspective of ACEI (Fig. 3), the spatial distribution of ACEs intensity in different cities of Fujian Province is uneven, and there are obvious differences. ACEI of Nanping City, Ningde City, and Longyan City have been in high-intensity areas. The degree of agricultural modernization in these cities still lags, the development model of agriculture is still “high input and high output”, the development model of the agricultural industry

Table 2: Total and components of ACEs for 9 cities in Fujian Province, 2005-2019. ( $\times 10^4$ t).

City	Year	Rice	Livestock	Agricultural materials	Total
Fuzhou	2005	18.51	19.07	29.90	67.48
	2019	6.46	9.93	28.95	45.34
Xiamen	2005	1.27	6.35	4.38	12.00
	2019	0.31	1.56	4.26	6.13
Ningde	2005	16.69	6.10	15.23	38.03
	2019	9.67	4.31	19.83	33.81
Putian	2005	7.52	10.30	11.22	29.04
	2019	2.98	2.20	13.20	18.38
Quanzhou	2005	17.41	21.17	27.14	65.71
	2019	9.37	10.38	23.61	43.36
Zhangzhou	2005	18.36	26.21	66.63	111.20
	2019	7.79	10.48	59.59	77.86
Sanming	2005	26.98	18.48	22.25	67.71
	2019	19.73	9.66	24.83	54.22
Longyan	2005	24.86	30.17	19.17	74.19
	2019	18.64	18.33	17.99	54.96
Nanping	2005	32.48	21.46	28.55	82.48
	2019	24.68	14.16	25.69	64.52

is relatively single, and the total agricultural output mainly depends on agricultural materials input. As a result, the ACEI of these cities is at a high level.

### Spatial Correlation Analysis of ACEs and ACEI

This study used ArcGIS10.8 to conduct spatial autocorrelation analysis on ACEs data of 9 cities in Fujian Province of China from 2005 to 2019. The variation curves of Moran's  $I$  index and  $P$ -value for each year were shown in Fig. 4.

As can be seen from Fig. 4, the Moran's  $I$  index from 2005 to 2019 is positive and all passed the significance test at the level of 5%, indicating that the spatial distribution of ACEs and ACEI at the city-scale in Fujian Province is not completely random, but has significant spatial dependence characteristics. From the Moran's  $I$  index, it showed a downward trend as a whole, which indicates that the spatial correlation between ACEs and ACEI is weakening.

The global Moran's  $I$  index can only explain the overall spatial dependence of ACEs for each city in Fujian Province, however, it cannot represent the specific structure and spatial correlation of spatial dependence of ACEI. Hence, to better grasp the local spatial pattern of ACEI, the LISA clustering map of 2005 and 2019 was drawn by using ArcGIS

10.8, according to the spatial and temporal distribution characteristics of different cities (Fig. 5).

As shown in Fig. 5, at a significant level of 5%, the local spatial dependence of agricultural carbon emissions for each city in Fujian Province is relatively obvious. From the LISA agglomeration map in 2005, it can be seen that ACEI in Fujian Province has formed high-high agglomeration areas (Sanming) and low-low agglomeration areas (Putian). According to the LISA agglomeration map in 2019, the high-low agglomeration area expanded (Quanzhou and Ningde). It can be seen that although a certain agglomeration area has been formed, the spatial autocorrelation in most areas is not significant, and the agglomeration effect is very limited. In particular, the diffusion effect and demonstration effect of the low-low agglomeration region have not yet played a significant role, and the area of the high-low agglomeration area has expanded.

### CONCLUSION

Considering the deficiency of past literature studies on spatial heterogeneity of factors affecting agricultural carbon emissions (ACEs), this study first constructed a system for measuring ACEs, and calculated ACEs and agricultural carbon emissions intensity (ACEI) at the city-scale of 'The Belt

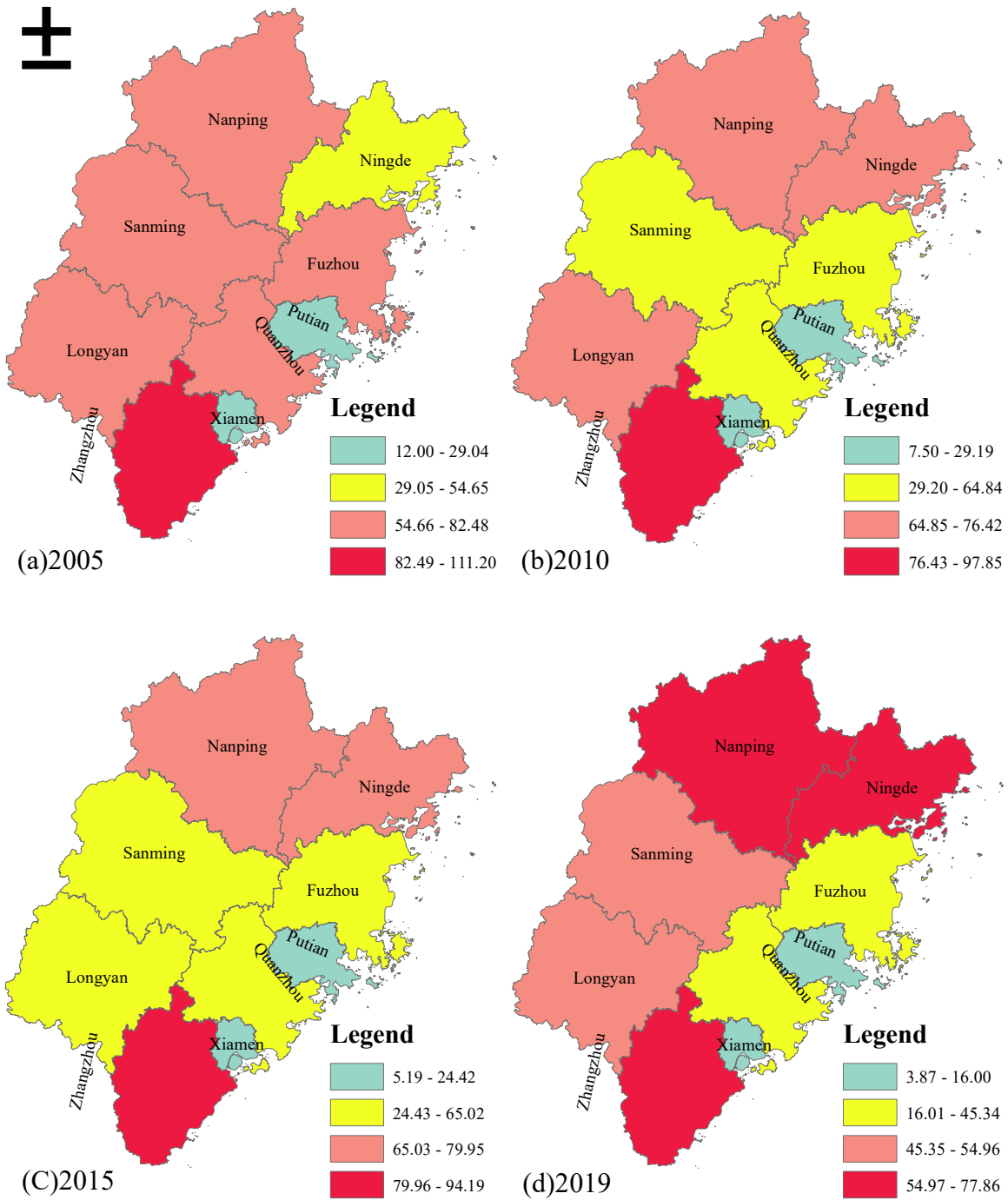


Fig. 2: Spatial distribution of ACEs in Fujian Province during 2005-2019 ( $10^4t$ ).

and Road' Core Area (Fujian Province) in China from 2005 to 2019. Then, the evolution characteristics of agricultural carbon emissions, intensity, and structure in Fujian Province were discussed from spatio-temporal latitudes. Finally,

ESDA was applied to analyze the spatial correlation of ACEI and to explore the spatial agglomeration area of ACEI. Accordingly, the main conclusions and corresponding optimization measures of this study are summarized as follows.

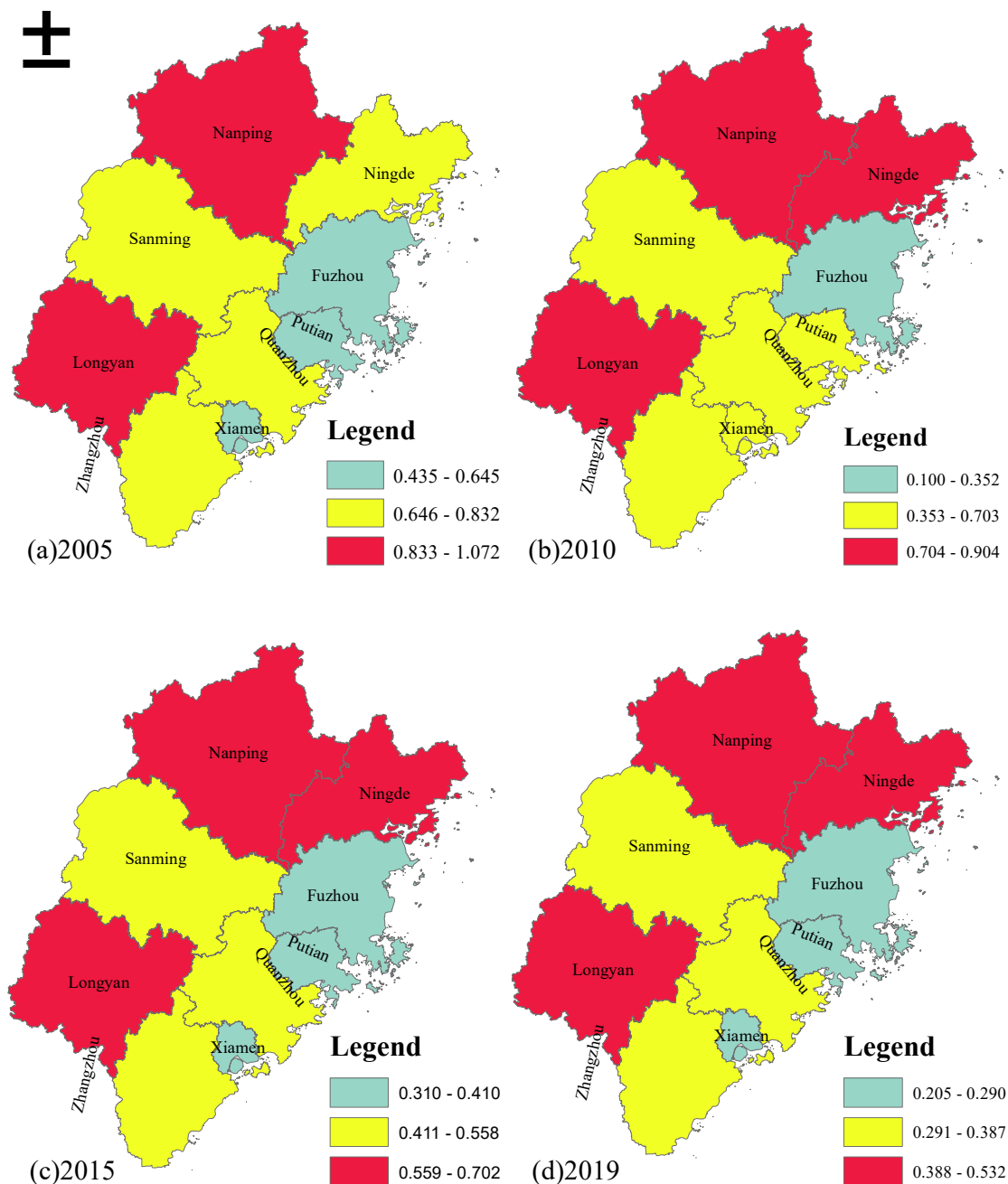


Fig. 3: Spatial distribution of ACEI at the city-scale in Fujian Province from 2005-2019 ( $10^4$ ).

(1) In this study, more sources of carbon emissions, especially methane and  $N_2O$ , were considered when constructing the measurement system of ACEs. This makes our result reveals a relatively more accurate estimation of ACEs for this study area compared with those from the other studies (e.g. Zhang & Zhang 2020). ACEs in Fujian Province demonstrated a downward trend as a whole during 2005-2019.

Results exhibited that ACEs in Fujian Province decreased from  $549.3 \times 10^4$  t in 2005 to  $393.9 \times 10^4$  t in 2019, with an average annual decline of 1.89%. In terms of carbon sources of ACEs, agricultural materials cause the largest emissions, with an average annual emission of  $233.0 \times 10^4$  t, accounting for 47.59% of the total ACEs, while rice growth leads to the smallest carbon emissions, with an average annual emission



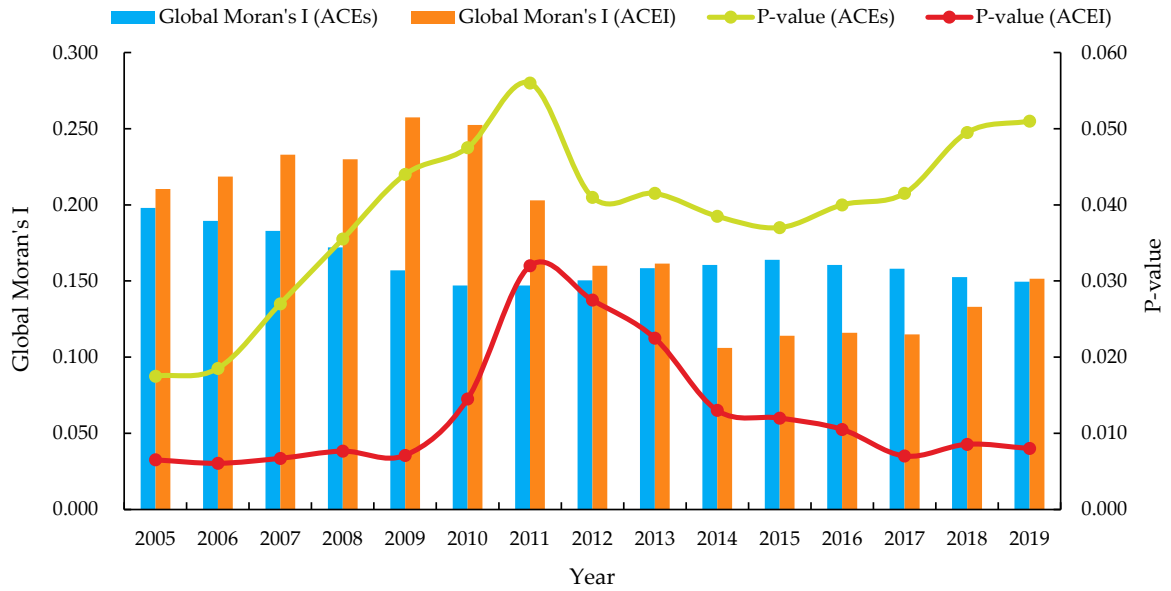


Fig. 4: Global Moran's *I* index of ACEs and ACEI for each city in Fujian Province from 2005-2019.

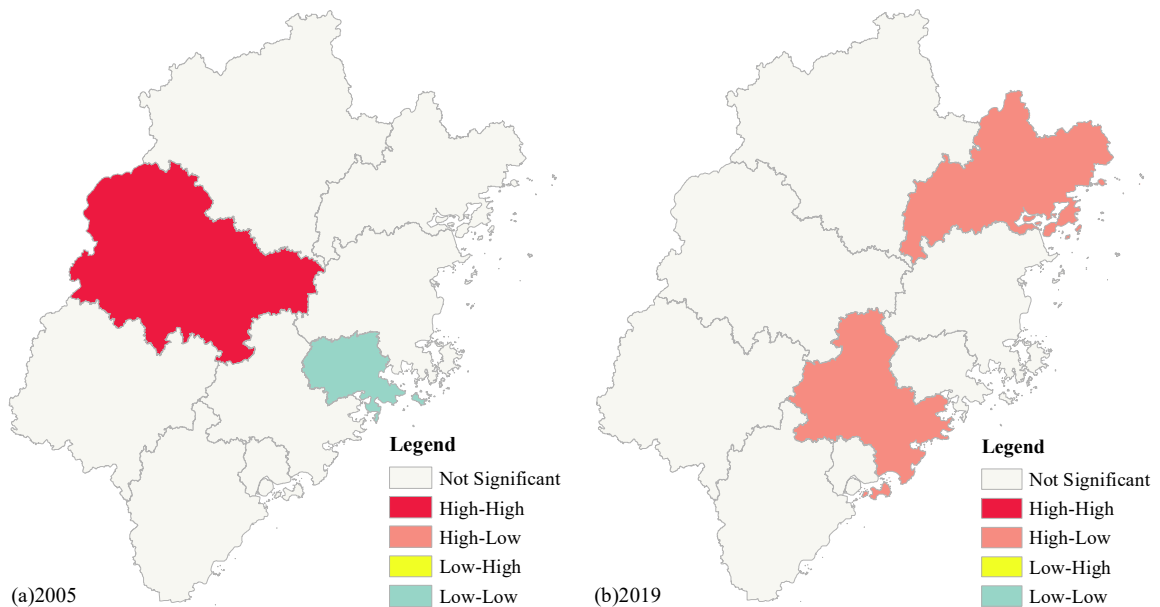


Fig. 5: LISA clustering map of ACEI in Fujian Province.

of  $128.2 \times 10^4$  t, accounting for 26.18% of the total ACEs. In addition, ACEI displayed a downward trend as a whole, with a decline rate of 63.56%, and an average annual decrease of 4.24%. There are fluctuations and differences in ACEs of Fujian Province from 2005 to 2019. Therefore, we suggest that the government should formulate differentiated policies

on agricultural carbon reduction. This is because each city's agricultural natural resource endowment and technological level are different, so the evolution of its ACEs has its characteristics, and there are differences in the sources of carbon emissions. Only in this way can we improve the effectiveness of agricultural carbon reduction.

(2) The spatial distribution of ACEs and ACEI in Fujian Province is different. Except for Xiamen and Putian, ACEs of other cities all exceeded  $50 \times 10^4 \text{t}$ , accounting for 95.05% of the province's total emissions. Among them, the top three regions in terms of carbon emissions are Zhangzhou City, Nanping City, and Longyan City. These areas are the main rice-growing areas in Fujian Province, with a large input of agricultural materials and relatively developed animal husbandry, which make a greater contribution to the total carbon emissions. So, the government should further guide consumers/farmers to choose agricultural products with green and low-carbon scientifically and reasonably to form a low-carbon consumption pattern of agricultural products. Moreover, the results showed that methane emission from paddy fields is also the main source of ACEs. Thus, in addition to formulating differential policies, the government should also choose reasonable management measures to cultivate new agricultural varieties. For instance, Some scholars have found a kind of low methane and high starch rice (SUSIBA2) (Su et al. 2015), which opened up a new idea for the breeding of new varieties in the later stage.

(3) There exists an obvious spatial correlation of ACEs for each city in Fujian Province. From 2005 to 2019, the Moran's *I* index values were positive and passed the significance test, indicating that ACEs and ACEI in Fujian Province showed obvious spatial dependence. According to LISA's clustering map and significance map, although a relatively obvious clustering area has been formed, the spatial autocorrelation of most regions is not significant. Therefore, it is necessary to further strengthen regional cooperation and jointly control the key carbon sources. Meanwhile, we believe that the government and scholars should further explore the seamless integration of ecological compensation mechanism and carbon trading system, namely, "carbon compensation mechanism". Previous studies have shown that ecological compensation plays an important role in the green and low-carbon development of the agricultural sector (Cui et al. 2021, Xiong et al. 2019). Through this compensation mechanism, low-carbon agricultural production behavior with positive externalities can be stimulated, and carbon emissions can be reduced. For example, the behavior of using environmentally friendly technologies (such as organic application, ecological control of diseases and insect pests) and livestock and poultry farming manure treatment (biogas treatment), etc.

## ACKNOWLEDGMENTS

The authors gratefully acknowledge the financial support from the Independent R & D project of the Academy of Agricultural Planning and Engineering of China (Grant

No. SC202101), the Natural Science Foundation of Fujian Province, China (Grant No. 2021J01650).

## REFERENCES

- Adevale, C., Reganold, J.P., Higgins, S., Evans, R.D. and Carpenter-Boggs, L. 2019. Agricultural carbon footprint is farm specific: A case study of two organic farms. *J. Clean. Prod.*, 229: 795-805.
- Balsalobre-Lorente, D., Driha, O.M., Bekun, F.V. and Osundina, O.A. 2019. Do agricultural activities induce carbon emissions? The BRICS experience. *Environ. Sci. Pollut. Res.*, 26: 25218-25234.
- Chen, R. and Jiang, Z. 2018a. Transverse space ecological compensation of low-carbon agriculture in China. *China Popul. Environ.*, 28: 87-97.
- Chen, R. and Jiang, Z. 2018b. Study on ecological compensation standard for farmers' low carbon agricultural production. *J. Arid L. Resour. Environ.*, 32: 63-70.
- Cui, Y., Khan, S.U., Deng, Y., Zhao, M. and Hou, M. 2021. Environmental improvement value of agricultural carbon reduction and its spatiotemporal dynamic evolution: Evidence from China. *Sci. Total Environ.*, 754: 142170.
- Fan, J.L., Dai, Y.B., Wan, S.L., Zhang, M., Cao, Z., Wang, Y. and Zhang, X. 2019. Determinants of carbon emissions in 'Belt and Road initiative' countries: A production technology perspective. *Appl. Energy*, 239: 268-279.
- Fujian Provincial Bureau of Statistics (FPBS). 2020. *Fujian Statistical Yearbook 2020*. China Statistics Press, Beijing.
- García-Marco, S., Abalos, D., Espejo, R., Vallejo, A. and Mariscal-Sancho, I. 2016. No-tillage and liming reduce greenhouse gas emissions from poorly drained agricultural soils in Mediterranean regions. *Sci. Total Environ.*, 566-567: 512-520.
- Huang, X., Xu, X., Wang, Q., Zhang, L., Gao, X. and Chen, L. 2019. Assessment of agricultural carbon emissions and their spatiotemporal changes in China, 1997–2016. *Int. J. Environ. Res. Public Health*, 16: 3105.
- Li, M., Liu, S., Sun, Y. and Liu, Y. 2021. Agriculture and animal husbandry increased the carbon footprint on the Qinghai-Tibet Plateau during the past three decades. *J. Clean. Prod.*, 278: 123963.
- Lu, F., Wang, X., Han, B., Ouyang, Z., Duan, X. and Zheng, H. 2008. Assessment of the availability of nitrogen fertilization in improving carbon sequestration potential of China's cropland soil. *Chin. J. Appl. Ecol.*, 19: 2239-2250.
- Muhammad, S., Long, X., Salman, M. and Dauda, L. 2020. Effect of urbanization and international trade on CO<sub>2</sub> emissions across 65 belt and road initiative countries. *Energy*, 196: 117102.
- NCSC n.d. Guidelines for Preparing Provincial Greenhouse Gas Inventories.
- Pachauri, R.K., Allen, M.R., Barros, V.R., Broome, J., Cramer, W., Christ, R., Church, J.A., Clarke, L., Dahe, Q. and Dasgupta, P. 2014. *Climate Change 2014: Synthesis Report. Contribution of Working Groups I, II, and III to the Fifth Assessment Report of the Intergovernmental Panel on Climate Change*. IPCC. [https://epic.awi.de/id/eprint/37530/1/IPCC\\_AR5\\_SYR\\_Final.pdf](https://epic.awi.de/id/eprint/37530/1/IPCC_AR5_SYR_Final.pdf).
- Pang, J., Li, H., Lu, C., Lu, C. and Chen, X. 2020. Regional differences and dynamic evolution of carbon emission intensity of agriculture production in china. *Int. J. Environ. Res. Public Health*, 17: 1-14.
- Paustian, K., Lehmann, J., Ogle, S., Reay, D., Robertson, G.P. and Smith, P. 2016. Climate-smart soils. *Nature*, 532: 49-57.
- Rebolledo-Leiva, R., Angulo-Meza, L., Iriarte, A. and González-Araya, M.C. 2017. Joint carbon footprint assessment and data envelopment analysis for the reduction of greenhouse gas emissions in agriculture production. *Sci. Total Environ.*, 593-594: 36-46.
- Su, J., Hu, C., Yan, X., Jin, Y., Chen, Z., Guan, Q., Wang, Y., Zhong, D., Jansson, C., Wang, F., Schnürer, A. and Sun, C. 2015. Expression of barley SUSIBA2 transcription factor yields high-starch low-methane rice. *Nature*, 523: 602-606.

- Su, K. and Lee, C. 2021. Spatial dependence pattern of energy-related carbon emissions and spatial heterogeneity of influencing factors in China: Based on ESDA-GTWR Model. *Nat. Environ. Pollut. Technol.*, 20: 29-38.
- Su, K., Wei, D.Z. and Lin, W.X. 2020. Evaluation of ecosystem services value and its implications for policy-making in China – A case study of Fujian province. *Ecol. Indic.*, 108: 105752.
- Tian, Z., Ma, X. and Liu, R. 2015. Interannual variations of the carbon footprint and carbon eco-efficiency in agro-ecosystem of Beijing, China. *J. Agric. Resour. Environ.*, 32: 603-612.
- Wang, C., Zhan, J., Bai, Y., Chu, X. and Zhang, F. 2019. Measuring carbon emission performance of industrial sectors in the Beijing–Tianjin–Hebei region, China: A stochastic frontier approach. *Sci. Total Environ.*, 685: 786-794.
- Wang, G., Liao, M. and Jiang, J. 2020. Research on agricultural carbon emissions and regional carbon emissions reduction strategies in China. *Sustain.*, 12: 2627.
- Wang, L., Zhao, J. and Chen, S. 2016. Analysis of ecosystem carbon sources/sinks and carbon footprint in farmland ecosystem of Shandong Province. *J. China Agric. Univ.*, 21: 133-141.
- West, T. and Marland, G. 2002. A synthesis of carbon sequestration, carbon emissions, and net carbon flux in agriculture: comparing tillage practices in the United States. *Agric. Ecosyst. Environ.*, 91: 217-232.
- Xiong, C., Chen, S. and Yang, D. 2019. Selecting counties to participate in agricultural carbon compensation in China. *Polish J. Environ. Stud.*, 28: 1443-1449.
- Xiong, C., Chen, S.S. and Xu, L. 2020. Driving factors analysis of agricultural carbon emissions based on extended STIRPAT model of Jiangsu Province, China. *Growth Change*, 51: 1401-1416.
- Xu, X., Huang, X., Huang, J., Gao, X. and Chen, L. 2019. Spatial-temporal characteristics of agriculture green total factor productivity in China, 1998–2016: Based on more sophisticated calculations of carbon emissions. *Int. J. Environ. Res. Public Health*, 16: 3932.
- Zhang, Y. and Zhang, L. 2020. Research on agricultural carbon emission and agricultural economic growth in “The Belt and Road” core area. *J. Northeast Agric. Sci.*, 45: 106-110.





# Dynamic Changes and Precision Governance of Soil Erosion in Chengde City Using the GIS Techniques and RUSLE Model

Xiaoping Yan\*, Leixiang Wu\*\*, Jun Xie\*†, Yongqian Wang\*\*\*, Chencheng Wang\*\*\* and Bing Ling\*\*

\*College of Water Conservancy and Hydropower Engineering, Sichuan Agricultural University, Ya'an 625014, Sichuan, PR China

\*\*Institute of Water Ecology and Environment, China Institute of Water Resources and Hydropower Research, Beijing 100089, PR China

\*\*\*College of Resources and Environment, Chengdu University of Information Technology, Chengdu 610225, Sichuan, PR China

†Corresponding author: Jun Xie; yan1227108150@163.com

Nat. Env. & Poll. Tech.  
Website: [www.neptjournal.com](http://www.neptjournal.com)

Received: 26-08-2021

Revised: 10-11-2021

Accepted: 15-11-2021

## Key Words:

Soil erosion  
Precision governance  
RUSLE  
GIS  
Chengde city

## ABSTRACT

Soil erosion is one of the major environmental problems facing the world. The multi-scale characteristics of soil erosion and the complexity of its influencing factors put forward higher requirements for soil erosion prevention and control. Based on GIS technology and the RUSLE model, this paper quantitatively studies the temporal and spatial variation characteristics of soil erosion intensity in Chengde City(CC) from 2003 to 2018 and analyzes the temporal and spatial characteristics of R, K, LS, C, P factors according to the model calculation results, and analyzes the formation mechanism of key units of soil erosion in CC. The results show that: The area of tolerable erosion in CC in 2018 was 35152.19 km<sup>2</sup> (accounting for 90.22% of the total area), which was at the level of tolerable erosion on the whole. The average soil erosion modulus of CC in 2003, 2006, 2009, 2012, 2015, and 2018 were 41.38, 45.06, 46.58, 83.66, 27.67, and 73.34 t.km<sup>-2</sup>.y<sup>-1</sup>, reaching the maximum value of 83.66 t.km<sup>-2</sup>.y<sup>-1</sup> in 2012, showing a rising trend and then declining trend in the research period. Soil erosion deteriorated in some areas of CC and regional differences increased, which caused serious environmental problems. Fitting results showed that the R factor was one of the important factors for the increase of regional differences and average erosion modulus. According to the characteristics of the problem, a precise governance model of soil erosion prevention based on the intensity and causes of soil erosion was put forward, and a "landing" scheme of soil erosion prevention and control measures was put forward. Furthermore, the control of soil and water loss in key areas should be strengthened in the future.

## INTRODUCTION

Soil erosion refers to the process of soil denudation by external forces such as water power and wind power, as well as the transport of denudated soil by wind and runoff, which eventually leads to a series of eco-environmental problems (Wang & Zhao 2020). Worldwide, prevention and control of soil erosion and other forms of land degradation caused the attention of policymakers, land managers, and politicians, and this is reflected in many global initiatives, including but not limited to the Global Land Assessment of Degradation (GLASOD), the United Nations Convention to Combat Desertification (UNCCD), and the United Nations Environment Programme (UNEP) report (Ustin et al. 2009). Water and soil conservation planning requires scientific and reasonable soil erosion assessment to clarify the intensity, area, and spatial distribution of regional soil erosion to carry out soil and water conservation activities in a targeted manner (Lin et al. 2020). In addition, after the implementation of regional

soil erosion assessment, how to promote the "landing" of soil erosion assessment results and prevention measures is also an important link in soil and water conservation activities. "Landing" means that the assessment results can be "landed" on specific plots or small-scale ranges to provide decision-makers with specific soil erosion prevention and control areas (Gu et al. 2020).

At present, a variety of quantitative soil erosion assessment models have been developed all over the world, which can be mainly divided into three types: conceptual, physical process-based, and empirical statistics-based (Kwanele & Njoya 2019). Among the three models, an empirical statistical model is the simplest model with low computational requirements and easy application, so it has been widely used around the world (Antonello et al. 2015). The Universal Soil Loss Equation (USLE) was proposed in the mid-1960s. Renard et al. (1997) modified USLE and obtained the RUSLE model. Liu et al. (2002), based on



the USLE model, fully considered the characteristics and geographical characteristics of slope erosion in China and proposed the Chinese Soil Loss Equation (CSLE). RUSLE model is considered to be the most commonly used empirical model for soil erosion assessment (Biddoccu et al. 2020), as a computer-based model, the rapid development of computer technology, remote sensing technology, and geographic information system greatly promoted the development and application of RUSLE (Xiao et al. 2015). It provides a clear idea for understanding the causes of soil erosion. China's ecological governance mode means that China's governance policies are usually implemented on a large scale (Wen & Zhen 2020). In the early stage of governance, large-scale governance measures can achieve rapid and obvious governance effects, but they also have certain drawbacks. For example, Chengde City(CC) has implemented large-scale environmental protection projects such as the Conversion of Cropland to Forest Project(CCFP) for many years, and its forest area has increased significantly, and the overall situation of soil erosion has improved significantly. However, from May to July 2019, sediment deposition and water quality index exceeded the standard in the Pianqiaozi section of the mainstream of Luanhe River in the territory of CC for three consecutive months, and local soil and water loss broke out. The pattern and process of geographical phenomena change with the change of measurement scale, which means that the laws observed at one scale may not be directly applied at another scale. Therefore, the effectiveness of prevention measures is closely related to regional characteristics, and policies should be adjusted according to specific geographical conditions (Wen & Théau 2020). In addition, in the existing soil erosion assessment studies based on remote sensing data, the evaluation results are usually presented in the spatial form of soil erosion modulus, soil erosion amount,

or erosion intensity distribution map, and the presentation form is mostly “speckled” with great spatial variability, so the “landing” of erosion evaluation cannot be well realized (Gu et al. 2020), more reasonable “landing” options still need to be explored.

In this paper, high-precision RS data and the RUSLE model were used to quantitatively study the spatial-temporal variation characteristics of soil erosion in Chengde City(CC) and accurately identified the regional coordinates with large soil erosion modulus and the influencing factors of soil erosion. In view of the above scale and “landing” problems, a town-scale soil erosion control planning model was proposed, and a “landing” scheme was proposed.

## MATERIALS AND METHODS

### Study Area

Chengde City (CC) is located in the northeast of Hebei Province, with Inner Mongolia grassland in the north and Beijing and Tianjin in the south, and Liaoning Province to the east. The city ranges from 115°54'-119°15' E and 40°12'-42°37' N. The total area of CC is 39519 km<sup>2</sup>, it is a temperate continental monsoon climate with an annual rainfall of 402.3-882.6 mm and an annual average rainfall of 530.13 mm. The main river in CC is the Luanhe River, which is one of the main water systems in the Haihe River Basin. It not only supports the economic and social development in the region but also serves as the water conservation area and ecological protection area of Beijing and Tianjin. Fig. 1 gives the details on Pianqiaozi town and the study area.

### Data Source

(1) Daily precipitation data of Chengde, Fengning, and other

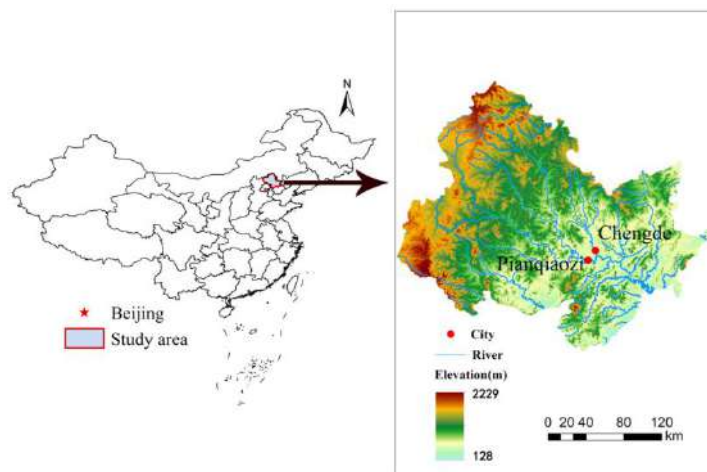


Fig. 1: Study area.

rainfall stations from 2003 to 2018. (2) The soil type map of CC extracted from the national soil data types includes the data on the physical and chemical properties of all soil types. (3) 30 m resolution GDEM data. (4) 30 m resolution Landsat5 TM/Landsat8 OLI data (5) 500 m resolution MODIS level 3 land cover types data set. 500 m MOD12Q1 data and 1000 m soil physical and chemical data were resampled to 30 m to keep consistent with the spatial scale of TM data for subsequent processing.

**RUSLE MODEL**

In this study, based on the Revised Universal Soil Loss Equation (RUSLE), combined with GIS technology and RS data source, the numerical values of five factors (R, K, LS, C, P) affecting soil erosion in CC were calculated by ArcGIS10.2 software and the spatial distribution maps were drawn. The expression equation of the RUSLE model is as follows:

$$A = R \times K \times LS \times C \times P \quad \dots(1)$$

Where *A* is the soil loss (t.km<sup>-2</sup>.y<sup>-1</sup>). *R* is the rainfall erosivity factor (MJ.mm.hm<sup>-2</sup>.h<sup>-1</sup>.y<sup>-1</sup>). *K* is the soil erodibility factor [t.ha.h.(ha.MJ.m)<sup>-1</sup>]. *LS* is the slope length and steepness factor (dimensionless). *C* is the vegetation cover and management factor (dimensionless). *P* is the conservation practice factor (dimensionless).

(1) Rainfall erosivity factor R

Rainfall is the direct driving force of soil erosion, as raindrops splash and separate soil particles, and runoff formed by rainfall will further scour and denude the soil and carry the soil, thus forming soil erosion. Richardson et al. (1983) first proposed the daily rainfall erosivity model. Zhang et al. (2002) modified Richardson’s daily rainfall erosivity model by using the daily rainfall data of 71 representative weather stations in China. This revised Richardson daily rainfall erosivity model was used in this study to calculate rainfall erosivity R, with the formula as follows:

$$R = \alpha \sum_{j=1}^n P_{dj}^\beta \quad \dots(2)$$

Table 1: Data source table.

Data	Format	Source	Spatial resolution	Time span
MODIS land use/cover data	Raster	https://lpdaac.usgs.gov/	500 m	2003-2018
GDEM	Raster	http://www.gscloud.cn/	30 m	N/A
Soil data	Raster	http://vdb3.soil.csdb.cn/	1000 m	N/A
Rainfall data	Text	Hydrological stations in CC	N/A	2003-2018
Landsat5 TM/ Landsat8 OLI data	Raster	http://www.usgs.gov/	30 m	2003-2018

Note: N/A means not applicable.

$$\alpha = 2.239 \times \beta^{-7.3967} \quad \dots(3)$$

$$\beta = 0.6243 + \frac{27.346}{P_{d12}} \quad \dots(4)$$

Where  $P_{dj}^\beta$  is the actual rainfall on the day when the daily rainfall is greater than 12 mm.  $\alpha$ ,  $\beta$  are the model parameters, which needs to be calculated according to the regional precipitation characteristics.  $P_{d12}$  is the average rainfall with daily rainfall greater than 12 mm.

(2) Soil erodibility factor K

K is a necessary parameter in the soil loss model. Soil erodibility refers to the ease with which soil can be dispersed and transported under the action of erosive forces such as raindrop impact and runoff scour. Soil physical properties, including soil structure, texture, organic matter, and soil infiltration ratio, determine soil erodibility and soil erosion resistance. However, soil structure and soil infiltration ratio are often difficult to obtain. Therefore, this study adopted the calculation method of K value developed by Williams et al. (1990) based on the EPIC model, which mainly considered soil organic carbon and particle size composition data. Formula:

$$K = \left\{ 0.2 + 0.3 \exp\left[0.0256SAN\left(1 - \frac{SIL}{100}\right)\right] \right\} \times \left( \frac{SIL}{CAL + SIL} \right)^{0.3} \times \left[ 1 - \frac{0.25C}{C + \exp(3.72 - 2.95C)} \right] \times \left[ 1 - \frac{0.7SN1}{SN1 + \exp(-5.51 + 22.9SN1)} \right] \quad \dots(5)$$

Where,  $SN1 = 1 - \frac{SAN}{100}$ , *SAN* (0.05-2.0 mm) is gravel content (%). *SIL* (0.002-0.05 mm) is silt content (%). *Cal* (<0.002 mm) is the clay content (%). *C* is the organic carbon content (%). The unit of K value calculated by the formula is the American system. In this paper, the K value is converted to an international system for analysis.

(3) Slope length and steepness factor LS

Slope length and steepness factor LS include slope length

factor  $L$  and steepness factor  $S$ . Slope length factor  $L$  affects the velocity of surface runoff, and steepness factor  $S$  affects the scale and intensity of material flow and energy conversion. For gentle slope and steep slope, the formula proposed by Liu et al. (2002) was adopted respectively for calculation, and the formula is as follows:

$$S = \begin{cases} 10.8 \times \sin \theta + 0.036 & \theta < 5^\circ \\ 16.8 \times \sin \theta - 0.5 & 5^\circ < \theta < 10^\circ \\ 21.9 \times \sin \theta - 0.96 & \theta \geq 10^\circ \end{cases} \dots(6)$$

Where  $S$  is the steepness factor, and the unit is radian;  $\theta$  is the slope, and the unit is the angle. The slope length factor  $L$  was extracted by using the modified formula proposed by Wischmeier et al. (1960). Formula:

$$L = (\lambda \div 22.13) \dots(7)$$

$$m = \begin{cases} 0.2 & \theta \leq 1^\circ \\ 0.3 & 1^\circ < \theta \leq 3^\circ \\ 0.4 & 3^\circ < \theta \leq 5^\circ \\ 0.5 & \theta > 5^\circ \end{cases} \dots(8)$$

Where,  $\lambda$  is the slope length, and  $m$  is the slope length index.

(4) Vegetation coverage and management factor  $C$

$C$  refers to the ratio of soil loss on the land with specific vegetation cover or field management to the soil loss on the bare fallow land with clear tillage or no vegetation cover under the same soil, slope, and rainfall conditions. The higher the value of  $C$ , the greater the amount of soil erosion caused by this kind of land use. In this study, the most widely used Normalized Difference Vegetation Index (NDVI) was used to estimate vegetation coverage. Vegetation coverage  $f$  (Equation 10) was calculated based on NDVI data, and then the  $C$  factor value was calculated based on the model established by Cai et al. (2000). Formula:

$$NDVI = (NIR - R) / (NIR + R) \dots(9)$$

$$f = (NDVI - NDVI_{min}) / (NDVI_{max} - NDVI_{min}) \dots(10)$$

$$C = \begin{cases} 1 & f = 0 \\ 0.6508 - 0.3461 \times \lg f & 0 < f < 78.3\% \\ 0 & f \geq 78.3\% \end{cases} \dots(11)$$

Where  $NIR$  is the near-infrared band,  $R$  is the red band,  $f$

is the vegetation coverage, and  $C$  is the vegetation coverage and management factor.

(5) Conservation practice factor  $P$

$P$  is a quantitative index reflecting the influence degree of soil and water conservation measures on soil and water loss. By referring to previous research results on  $P$  value, this paper assigned the value of 1 to the land use types that can be considered as having not taken any measures, such as forest, shrub lands, grassland, and unused land. Land use types that in principle will not produce soil erosion, such as water bodies, and urban and construction land, were assigned as 0, while other land use types were assigned according to the empirical  $P$  value formula proposed by Lufafa et al. (2003). Formula:

$$P = 0.2 + 0.03S \dots(12)$$

Where  $P$  is the factor of conservation practice, and  $S$  is the percentage slope.

**RESULTS AND DISCUSSION**

**Spatial and Temporal Characteristics of Soil Erosion in CC**

From the perspective of space, the overall soil erosion in CC was good, at a tolerable erosion level, and soil erosion mainly occurs in local areas. To accurately identify the area where soil erosion occurs, the areas with a soil erosion modulus of 0 are defined as the area where no erosion occurs. At the regional scale, researchers are usually more concerned about the characteristics of soil erosion areas. The ArcGIS 10.2 software was used to make statistics on the erosion area data of CC. In 2018, it was found that the area of tolerable and below erosion was 35152.19 km<sup>2</sup>, accounting for about 90.02% of the total area of CC. And its area proportion was the largest, it showed a trend of decreasing first and then increasing. The area of light erosion was 3736.77 km<sup>2</sup>, accounting for 9.57%, and the area of moderate erosion was 138.87 km<sup>2</sup>, accounting for 0.36%. The area of severe erosion was 20.37 km<sup>2</sup>, accounting for about 0.05% (Fig. 2, 3, and Table 3). During the study period, the area of very severe erosion occurred for the first time in 2018, with an area of about 0.71 km<sup>2</sup>, indicating that local soil erosion had worsened. In 2018, the areas with large soil erosion modulus in CC were mainly distributed in Wulingshan Forest Park, Yingshouyingzi Mining Area of Xinglong County, and Luanping County. In addition, soil erosion modulus along the Luanhe River was also high, which was related to the local

Table 2: P factor value table.

Land use type	Forest	Shrub lands	Grassland	Unused land	Waterbody	Urban and Construction land	Other
P	1	1	1	1	0	0	0.2+0.003S

agricultural planting along the river area and the high slope of the hillside along the river. The light and above erosion areas in CC were mainly concentrated in the Wuling Mountain Forest Park in the northeast of Xinglong County, Kuancheng County, Weichang County, and Fengning County (Fig. 2). In the study of soil erosion, light and above erosion areas are generally considered as soil erosion areas, so the above areas are the key areas for soil erosion control.

In terms of time, the average soil erosion modulus in CC increased at first and then decreased, and its value reached the maximum value of  $83.66 \text{ t}\cdot\text{km}^{-2}\cdot\text{a}^{-1}$  in 2012 (Table 4). The area of light and above soil erosion area in CC increased firstly and then decreased, reaching the maximum value of  $6386.93 \text{ km}^2$  (accounting for 16.45%) in 2012 and then decreased gradually (Table 3 and Fig. 3), which was consistent with the changing trend of average soil erosion modulus, indicating that the overall soil erosion situation in CC gradually improved in recent years. According to the statistics of the variation range of soil erosion modulus in each year, the maximum soil erosion modulus in CC showed a trend of decreasing first and then increasing and reaching the maximum value of  $12202.2 \text{ t}\cdot\text{km}^{-2}\cdot\text{y}^{-1}$  in 2018 (Table 4). The standard deviation is the arithmetical square root of the

statistical variance of a data set, which can reflect the degree of dispersion of a data set. The standard deviation of soil erosion modulus in CC from 2003 to 2018 was calculated, and it was found that the standard deviation in the study area first decreased and then increased, and the value reached the maximum value of 232.38 in 2018 (Table 4), which was significantly larger than that in other years. These two sets of data indicated that in recent years, the dispersion of soil erosion modulus in the study area has increased and the difference in soil erosion status between regions has become larger. Compared with the data for 2012 and 2018 in Table 3, it was found that the light erosion area and moderate erosion area of CC in 2018 were smaller than that of 2012, but the severe erosion area was larger than in 2012, and the very severe soil erosion area appeared for the first time. By the same token, comparing the data of 2003 and 2018, it was found that the areas of light and above erosion in 2018 are larger than that in 2003. The reason was that the condition of some tolerable-erosion areas deteriorated and developed into higher-grade soil erosion areas. To sum up, after the implementation of large-scale soil and water conservation measures in CC, the soil erosion situation had gradually improved in recent years, but due to the scale characteristics

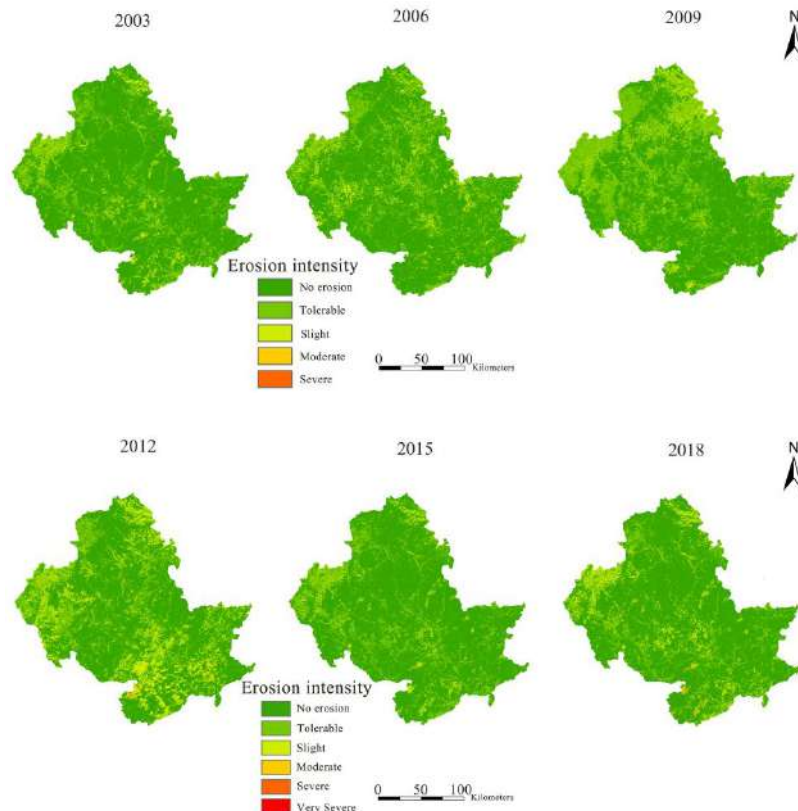


Fig. 2: Interannual variation of soil erosion in CC from 2003 to 2018.

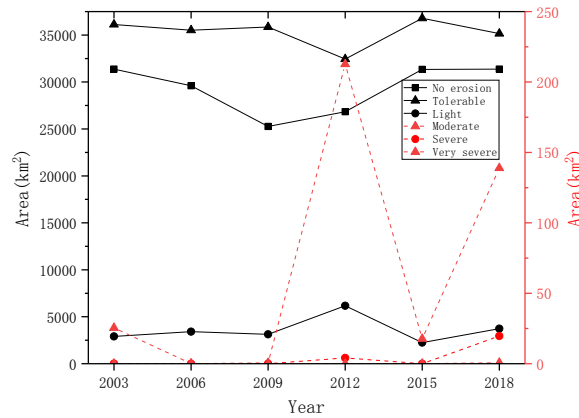


Fig. 3: Interannual variation of soil erosion intensity area in CC from 2003 to 2018.

of geographical phenomena, the causes of soil and water loss in some areas did not match with large-scale environmental protection measures. As a result, the difference in soil erosion between local areas was gradually increasing, and the local condition was deteriorating.

**Analysis of Erosion Factors of the RUSLE Model**

**Analysis of R factor**

The R factor was calculated by the formula (2) and the

R-value was counted by ArcGIS 10.2. The annual average R-value from 2003 to 2018 was 1778.22 MJ-mm-hm<sup>-2</sup>.h<sup>-1</sup>.y<sup>-1</sup> (Table 5). According to the research results of Liu et al. (2013), the average annual rainfall erosivity in CC ranges from 500 to 2000 MJ.mm.hm<sup>-2</sup>.h<sup>-1</sup>.y<sup>-1</sup>, indicating that the calculated results of the R factor are reliable. The data of R factor, average soil erosion modulus, and standard deviation were input into SPSS Statistics software for processing. The statistical results showed that R had a strong correlation with standard deviation, and the coefficient of determination R<sup>2</sup>

Table 3: Proportion (%) of different erosion intensities in CC (dimension of soil erosion modulus is t.km<sup>-2</sup>.y<sup>-1</sup>).

Erosion intensity	No erosion [0]	Tolerable [0-200]	Light (200-2500]	Moderate (2500-5000]	Severe (5000-8000]	Very Severe (8000-15000]
	Proportion	Proportion	Proportion	Proportion	Proportion	Proportion
2003	80.33	92.50	7.44	0.07	0	0
2006	76.03	91.22	8.78	0	0	0
2009	64.82	91.99	8.02	0	0	0
2012	69.11	83.55	15.89	0.55	0.01	0
2015	80.26	94.20	5.75	0.05	0	0
2018	80.33	90.02	9.57	0.36	0.05	0

Table 4: Characteristics of soil erosion modulus in CC from 2003 to 2018.

Year	Minimum modulus of erosion (t.km <sup>-2</sup> .y <sup>-1</sup> )	Maximum modulus of erosion (t.km <sup>-2</sup> .y <sup>-1</sup> )	Average modulus of erosion (t.km <sup>-2</sup> .y <sup>-1</sup> )	Standard deviation Dimensionless)
2003	0	6207.87	41.38	131.55
2006	0	3170.07	45.06	119.32
2009	0	3775.75	46.58	92.63
2012	0	8520.08	83.66	215.40
2015	0	2168.74	27.67	86.40
2018	0	12002.2	73.34	232.38



Table 6: Classification and distribution area of soil erodibility K (t.ha.h.(MJ.mm.ha)<sup>-1</sup>) value in CC.

Soil types	K ranges	Area (km <sup>2</sup> )	Proportion (%)
High-difficult erosion soil	<0.1	0	0.00
Difficult erosion soil	0.1-0.2	7498.95	19.00
Relative-difficult erosion soil	0. 2-0. 25	5534.92	14.02
Relative-easy erosion soil	0. 25-0.3	17877.10	45.29
Easy erosion soil	0.03-0.4	6738.73	17.07
High-easy erosion soil	>0.4	1823.84	4.62

is 0.9362 (Fig.4a). There is a strong correlation between the R factor and dispersion degree of soil erosion modulus in the study area. The greater the R, the greater the difference between regions of soil erosion and the more significant problem of local erosion. The correlation between R and average soil erosion modulus is relatively strong, and the coefficient of determination R<sup>2</sup> is 0.6854 (Fig. 4b). R factor was not the main factor for increasing soil erosion modulus from 2003 to 2009. R factor was the important reason for increasing soil erosion

modulus from 2009 to 2018. The areas with high R-values in 2018 were mainly Xinglong County and Kuancheng County in the south of CC (Fig. 5a), with the annual average values of 3902.65 MJ.mm.hm<sup>-2</sup>.h<sup>-1</sup>.y<sup>-1</sup> and 2841.18 MJ.mm.hm<sup>-2</sup>.h<sup>-1</sup>.y<sup>-1</sup> (Table 5). Respectively, all of them were significantly higher than the average value of 1778.22 MJ.mm.hm<sup>-2</sup>.h<sup>-1</sup>.y<sup>-1</sup> in the study area. The soil erosion in these areas was greatly affected by rainfall erosivity factor R, so soil erosion control should pay attention to the influence of the R factor.

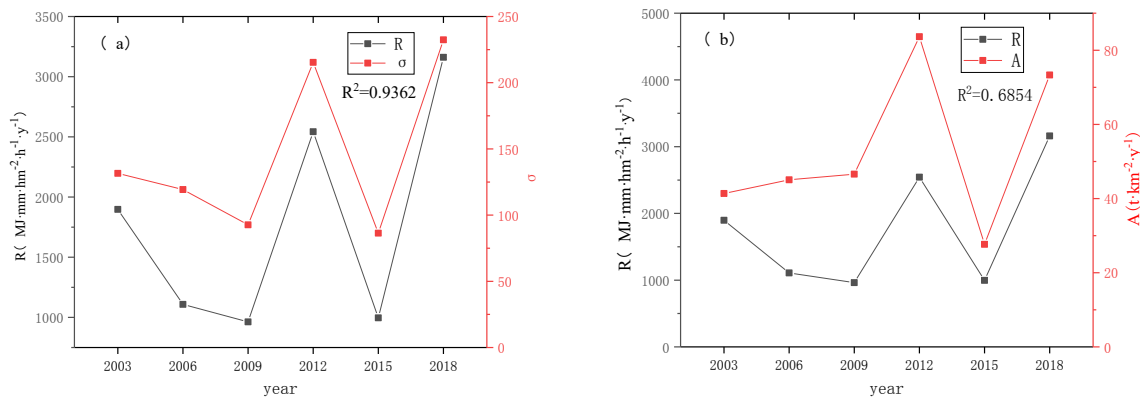


Fig. 4: Relationship map of R with standard deviation(σ) and average soil erosion modulus(A).

Table 5: Statistical table of annual average R (MJ.mm.hm<sup>-2</sup>.h<sup>-1</sup>.y<sup>-1</sup>) value of each meteorological station in CC.

Year	Chengde station	Chengde county	Fengning	Kuancheng	Longhua	Luanping	Pingquan	Weichang	Xinglong	Study area
2003	1252.18	2438.44	405.48	2408.69	911.46	1291.86	1945.8	2038.6	4385.56	1897.56
2006	1757.29	1024.61	1943.23	559.23	667.91	879.22	877.49	1031.7	1233.38	1108.23
2009	527.77	912.19	338.8	1530.81	466.88	887.73	696.25	784.81	2522.18	963.05
2012	1655.05	2248.54	641.28	5834.3	1319.43	1653.46	2209.72	1660.27	5666.67	2543.19
2015	1273.48	819.14	984.56	1382.83	675.25	390.15	943.07	1429.1	1069.18	996.31
2018	1540.74	2905.46	940.48	5331.21	2041.46	3107.11	1182.69	2860.61	8538.94	3160.97
Muti-year average	1334.42	1724.73	875.64	2841.18	1013.73	1368.26	1309.17	1634.18	3902.65	1778.22

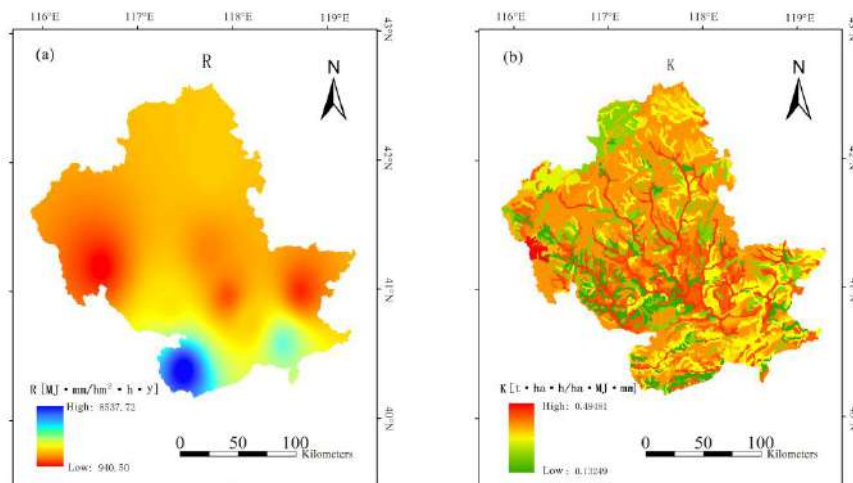


Fig. 5: Distribution of R and K in CC. R factor(a) spatial distribution of data from the data in 2018.

### Analysis of K factor

The distribution map of soil erodibility in CC was obtained by model calculation, as shown in Figure 5b. Moreover, soil erodibility in CC was classified according to other soil erodibility studies, as shown in Table 6. From Table 6, the main soil type in CC is easy erosion soil (Including relative-easy erosion soil, easy erosion soil, and high-easy erosion soil), accounting for 66.98% of the area of CC, and the area of relative-easy erosion soil is 17877.1 km<sup>2</sup>, accounting for the largest proportion, up to 45.29%, which is consistent with the research results of Men et al. (2004). According to the spatial distribution map of K value (Fig. 5b), the soil erodibility in the study area is high. The soil erodibility is high along the Luanhe River and near the urban built-up areas, and the soil erodibility is also high in Fengning County in the west of CC. The areas with a high K value are prone to soil erosion caused by the K factor, and the influence of the K value should be taken into account in the development of soil and water conservation measures.

### Precision Governance Mode of Soil Erosion

At present, the quantitative evaluation results of soil erosion are usually presented in the form of soil erosion modulus distribution maps and soil erosion intensity distribution maps, most of which are “speckled”, and cannot determine the exact location of severely eroded areas. It cannot achieve the “landing” of soil erosion assessment and treatment well, and its spatial orientation of soil and water conservation planning is not clear (Fig. 2). As a result, it is necessary to explore a more appropriate presentation mode on this basis (Gu et

al. 2020). China is delimiting key areas of soil and water loss (Li et al. 2018), and key areas need to be scientifically delimited on a scale. In previous practice, the planning and management of water conservation with small watersheds as the unit has achieved remarkable results (Chen et al. 2019). Therefore, this paper proposed a town-level administrative unit scale soil erosion control model based on soil erosion intensity and causes. It is suitable for areas with prominent local soil erosion problems and few measured data, and the town-level scale is similar to the small watershed scale.

Due to the large area of CC and the sparse population of the ethnic autonomous county within the territory, there are few measured data, so it is not consistent with the actual situation to evaluate and control soil erosion by field exploration and field investigation. Based on the calculation results of the RUSLE model, the precise governance model analyzed the regional sediment source, erosion sediment-producing environment, and sediment transport process, listed the moderate and above soil erosion areas as key treatment units, and identified the precise longitude and latitude of key units. It analyzed the cause combination of key units by combining the spatio-temporal characteristics of R, K, LS, C, and P factors. The planning results and landing schemes of soil erosion prevention and control based on this model were detailed in Fig. 6 and Table 7. This paper takes the problem section (Pianqiaozi section) as the outflow point and the watershed gathered at the outflow point as the key research area to elaborate in detail. Decision-makers can develop specific small-scale soil erosion control measures based on Fig. 6, Table 7 and local conditions to effectively solve local water and soil erosion problems.

## DISCUSSION AND CONCLUSION

After the implementation of large-scale ecological control projects in CC (such as CCFP), the area of no erosion increased to 31367.66 km<sup>2</sup> in 2018 and the average soil erosion modulus decreased from 83.66 t.km<sup>-2</sup>.y<sup>-1</sup> in 2012 to 73.34 t.km<sup>-2</sup>.y<sup>-1</sup> in 2018. The overall soil erosion improved in CC. This situation exists widely in most parts of China, such as the Loess Plateau, Shenzhen City, and so on (Zhang & Li 2018, Zhu et al. 2021). However, due to the multi-scale characteristics of soil erosion and the complexity of its influencing factors, large-scale control policies often leave some local problems at the same time. As shown by the phenomenon of sediment deposition and water quality index exceeding the standard in Pianqiaozi, the outbreak of local soil and water loss will also cause serious environmental problems. This kind of situation also exists widely in Shenzhen City, the Loess Plateau, and other areas (Zhang & Li 2018, Jin et al. 2021). Large-scale control measures are not suitable for local soil erosion, which will cost a lot of manpower and material resources, and the control effect may not meet expectations. Therefore, China is delineating the key areas of soil and water loss (Li et al. 2018) and replacing large-scale control with the way of controlling the key areas.

The integration of RS, GIS, and soil erosion models to make a series of maps of soil erosion changes can find the fragile areas of soil erosion from the point of view of spatio-temporal change, which is helpful to analyze the change process of regional soil erosion from emergence, development to extinction. However, most of the pictures made by this method are “speckled”, which cannot determine the exact location of the serious erosion area and cannot quickly and accurately realize the “landing” of soil erosion assessment.

Therefore, a precise governance model of soil erosion was proposed. It covers the calculation, assessment, identification, and cause analysis of the whole process of soil erosion prevention, which can quickly identify local soil erosion problems and put forward targeted prevention and control measures. However, the adaptability of the accurate soil erosion control model proposed in this paper to the overall areas with poor soil erosion needs to be strengthened, the key control units in the areas with poor soil erosion will be many and large, and the task of small-scale control is heavy. The study has theoretical and practical significance for soil erosion control in CC, can provide some reference for relevant research, and can also provide a supplementary treatment idea for large-scale governance mode in China.

In 2018, the area of tolerable and below erosion in CC was 35152.19 km<sup>2</sup>, accounting for 90.22% of the total area. CC was generally at the level of tolerable erosion, but soil erosion in local areas showed a worsening trend. The average soil erosion modulus of CC in 2003, 2006, 2009, 2012, 2015, and 2018 were 41.38, 45.06, 46.58, 83.66, 27.67, and 73.34 t.km<sup>-2</sup>.y<sup>-1</sup>, reaching the maximum value of 83.66 t.km<sup>-2</sup>.y<sup>-1</sup> in 2012, showing a rising trend and then declining trend in the research period. After large-scale water and soil conservation measures were implemented in CC, the overall soil erosion situation gradually improved. However, due to the scale problem, the prevention and control measures did not consider the regional characteristics, so the local soil erosion problem aggravated and the regional differences gradually increased, which eventually led to the sediment deposition and water quality exceeding the standard in the Pianqiaozi section. Local erosion can still cause serious environmental problems with the continuous improvement of overall soil erosion. Fitting results showed that the R

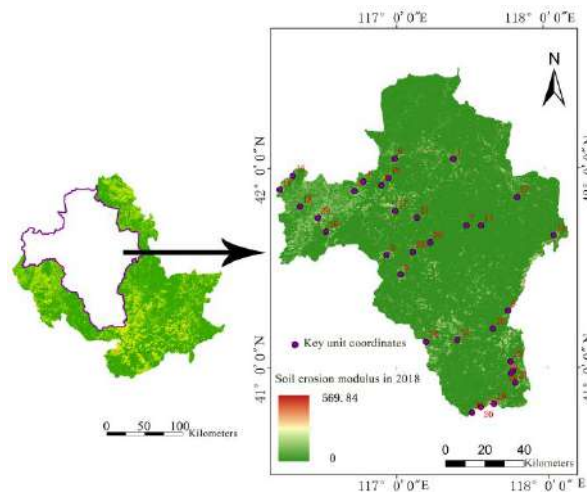


Fig. 6: Accurate location of high-value points of soil erosion modulus.

Table 7: Distribution table of key locations of soil erosion at the town scale.

Main Influencing Factors	Number	Longitude (E)	Latitude (N)	Town
R, K, LS, C, P	1	117°23'01"	42°2'59"	Yangebai town
	2	116°53'55"	41°55'07"	Xilongtou town
	3	116°56'08"	41°34'01"	Guojiatun town
	4	116°46'40"	41°56'13"	Laowopu town
	5	116°43'07"	41°53'22"	Waimengou town
	6	117°1'45"	41°28'15"	Xiguanying town
LS, R	7	117°28'15"	41°43'00"	Bugugou town
	8	117°44'39"	41°17'16"	Longhua town
	9	116°59'23"	42°3'06"	Laowopu town
	10	116°56'43"	41°57'13"	Xilongtou town
	11	117°34'04"	41°42'58"	Shanwan town
LS, C, P	12	117°11'52"	41°8'00"	Fengshan town
	13	118°3'10"	41°39'45"	Tangshanying town
K, LS, C, P	14	116°12'56"	41°53'38"	Caiyuan town
	15	116°18'13"	41°57'48"	Caiyuan town
	16	116°31'43"	41°41'05"	Sichakou town
	17	116°59'34"	41°47'22"	Nanshanzui town
C, LS	18	116°21'04"	41°48'38"	Wanshengshui town
R, LS, C	19	117°38'43"	40°49'11"	Fuyingzi town
	20	117°33'29"	40°48'14"	Fuyingzi town
	21	117°29'58"	40°46'34"	Changshanyu town
	22	117°24'14"	41°8'34"	Xigoumanzu town
	23	117°45'33"	41°1'57"	Xidimanzu town
K, LS, R	24	117°46'26"	40°59'07"	Xidimanzu town
	25	117°45'37"	40°58'21"	Xidimanzu town
	26	117°38'28"	41°11'50"	Longhua town
	27	117°48'39"	41°51'20"	Siheyon town
P, LS	28	117°6'34"	41°35'01"	Guojiatun town
	29	116°28'25"	41°45'10"	Sichakou town
	30	117°13'30"	41°37'55"	Jianfang town
	31	117°8'17"	41°45'20"	Jianfang town
	32	117°47'11"	40°55'33"	Pianqiaozi town

factor was one of the important factors for the increase of regional differences and average erosion modulus. According to the characteristics of the problem, a precise governance model of soil erosion prevention and control based on the intensity and causes of soil erosion was put forward to make up for the deficiencies of the top-down large-scale management mode in China, and a "landing" scheme of soil erosion prevention and control measures was put forward.

## ACKNOWLEDGEMENT

This work was supported by the National Natural Science Foundation of China (Grant no. 51879279).

## REFERENCES

Antonello, A., Maria, A. and Filomena, C. 2015. Remote sensing and GIS to assess soil erosion with RUSLE3D and USPED at river basin scale in southern Italy. *Catena*, 131: 174-185.

- Biddoccu, M., Guzmán, G., Capello, G., Thielke, T. and Gómez, J.A. 2020. Evaluation of soil erosion risk and identification of soil cover and management factor (C) for RUSLE in European vineyards with different soil management. *Int. Soil Water Conserv. Res.*, 8(4): 337-353.
- Cai, C.F., Ding, S.W., Shi, Z.H., Huang, L. and Zhang, G.Y. 2000. Study of applying USLE and geographical information system IDRISI to predict soil erosion in a small watershed. *J. Soil Water Conserv.*, 14(02): 19-24.
- Chen, Z.C., Ma, L.J., Guo, F.Y., Ma, X.L. and Chu, Y. 2019. Study on the influence of land use patterns on the comprehensive harnessing effects of soil and water erosion. *Nature Environ. Pollut. Technol.*, 18(3): 919-930
- Gu, Z.J., Xie, Y., Li, A., Liu, G. and Shi, Y.D. 2020. Evaluation of soil erosion in Northeast China by CSLE model. *J. Agric. Eng.*, 36(11): 49-56.
- Jin, F.M., Yang, W.C., Fu J.X. and Li, Z. 2021. Effects of vegetation and climate on the changes of soil erosion in the Loess Plateau of China. *Sci. Tot. Environ.*, 773:145514.
- Kwanele, P. and Njoya, S.N. 2019. The assessment of water-borne erosion at catchment level using GIS-based RUSLE and remote sensing: A review. *Int. Soil Water Conserv. Res.*, 7(1): 27-46.
- Li, Z.X., Zou, H.T., Zhao, H. and Qi, J.W. 2018. Delineation method of key control area of soil and water loss at the county scale. *Sci. Soil Water Conserv. in China*, 16(06): 56-63.
- Liu, B.T., Tao, H.P., Song, C.F., Guo, B., Shi, Z., Zhang, C., Kong, B. and He, B. 2013. Spatiotemporal variation trend of rainfall erosivity in China from 1960 to 2009. *Geogr. Res.*, 32(02): 245-256.
- Liu, B.Y., Zhang, K. and Xie, Y. 2002. An Empirical Soil Loss Equation: Proceedings 12th International Soil Conservation Organization Conference. Tsinghua University Press, Beijing, China, pp:1-8.
- Lin, J.K., Guan, Q.Y., Tian, J., Wang Q.Z., Tan, Z., Li, Z.J. and Wang, N. 2020. Assessing temporal trends of soil erosion and sediment redistribution in the Hexi Corridor region using the integrated RUSLE-TLSD model. *Catena*, 195: 104756.
- Lufafa, A., Tenywa, M.M., Isabirye, M., Majaliwa, M.J.G. and Woome, P.L. 2003. Prediction of soil erosion in a Lake Victoria basin catchment using a GIS-based Universal Soil Loss model. *Agric. Sys.*, 76(3): 883-894.
- Men, M.X., Zhao, T.K., Peng Z.P. and Yu, Z.R. 2004. Soil erodibility of Hebei Province Based on soil particle size distribution model. *Agric. Sci. China*, (11): 1647-1653.
- Renard, K.G., Foster, G.R., Weesies, G.A., Mccool, D.K. and Yoder, D.C. 1997. Predicting Soil Erosion By Water: A Guide to Conservation Planning with the Revised Universal Soil Loss Equation (RUSLE). Agricultural Handbook 703, United States Department of Agriculture, Washington DC, USA, pp. 1-407.
- Richardson, C.W., Foster, G.R. and Wright, D.A. 1983. Estimation of erosion index from daily rainfall amount. *Trans. ASAE*, 26(1): 0153-0156.
- Ustin, S.L., Palaciosorueta, A., Whiting, M.L., Whiting, M.L. and Li, L. 2009. Recent Advances in Remote Sensing and Geoinformation Processing for Land Degradation Assessment. CRC Press, Leiden, Netherlands, pp:1-16.
- Wang, H. and Zhao, H. 2020. Dynamic changes of soil erosion in the Taohe River basin using the RUSLE model and Google Earth Engine. *Water* 12(5): 1293.
- Wang, Z.J. and Yuan, S. 2020. Assessment of soil erosion in the Qinba mountains of the southern Shaanxi Province in China using the RUSLE model. *Sustainability*, 12(5): 1733.
- Wen, X. and Théau, J. 2020. Assessment of ecosystem services in restoration programs in China: A systematic review. *Ambio*, 49(2): 111.
- Wen, X. and Zhen, L. 2020. Soil erosion control practices in the Chinese Loess plateau: A systematic review. *Environ. Develop.*, 34: 100493.
- Williams, J.R., Jones, C.A. and Dyke, P.T. 1990. The EPIC Model Documentation. USDA-ARS, Washington DC, pp. 3-122.
- Wischmeier, W.H. and Smith, D. D. 1960. A universal soil-loss equation to guide conservation farm planning. *Trans. Congr. Soil Sci.*, 1: 418-425.
- Xiao, L.L., Yang, X.H., Chen, S.X. and Cai, H.Y. 2015. An assessment of erosivity distribution and its influence on the effectiveness of land use conversion for reducing soil erosion in Jiangxi, China. *Catena*, 125:50-60.
- Zhang, Y. and Li, T. 2018. Study on soil erosion in Shenzhen based on GIS and RUSLE model. *J. Appl. Basic Eng. Sci.*, 26(06): 1189-1202.
- Zhang, W., Xie, Y. and Liu, B.Y. 2002. Study on the method of calculating rainfall erosivity by daily rainfall. *Geogr. Sci.*, (06): 705-711.
- Zhu, X.Y., Zhang, R.Z. and Sun, X.W. 2021. Spatiotemporal dynamics of soil erosion in the ecotone between the Loess Plateau and Western Qinling Mountains based on RUSLE modeling, GIS, and remote sensing. *Arab. J. Geosci.*, 14(1): 33.







# Biodegradation of Natural Rubber by Fungi and Bacteria

Abhinav Joseph\*, Pawan Gupta\*\*†, Gahin De\*\*\*, Manohar Lal\*\*\*\*, Mukesh Kumar Meena\*\*\*\*\*,  
Laliteswar Pratap Singh\*\*\*\*\* and Jyotsna Rattan\*\*\*\*\*

\*School of Chemical Engineering and Physical Sciences, Lovely Professional University, Phagwara, India

\*\*Ganpat University, Shree S. K. Patel College of Pharmaceutical Education and Research, Gujarat, India

\*\*\*School of Bioengineering and Biosciences, Lovely Professional University, Phagwara, India

\*\*\*\*Department of Chemistry, Zakir Husain Delhi College, University of Delhi, Delhi, India

\*\*\*\*\*Department of Pharmaceutical Sciences, Mohanlal Sukhadia University, Udaipur, Rajasthan, India

\*\*\*\*\*Narayan Institute of Pharmacy, Gopal Narayan Singh University, Jamuhar Sasaram (Rohtas), Bihar, India

† Corresponding author: Pawan Gupta; pkg02@ganpatuniversity, pawanpharma79@hotmail.com

## Nat. Env. & Poll. Tech.

Website: [www.neptjournal.com](http://www.neptjournal.com)

Received: 09-09-2021

Revised: 29-10-2021

Accepted: 18-11-2021

### Key Words:

Natural rubber

Vulcanization

Fungi

Bacteria

Rubber degrading enzymes

## ABSTRACT

Environmental pollution is currently one of the major problems that are threatening biodiversity, ecosystems, and human health around the world. Natural rubber, which is one of the most significant polymers due to its variety of uses, has now become a serious environmental concern. Rubber waste management poses one of the greatest problems because it is extremely resilient and persists in the environment despite several mitigation efforts. Biodegradation is an eco-friendly alternative to conventional disposal methods and has gained tremendous interest in recent years. Several studies on rubber biodegradation utilizing fungi and bacteria have been reported. However, except for a few studies on technical applications, the majority of research on these microbes has focused on the fundamentals of rubber biodegradation. The challenge with biodegradation as a potential solution for rubber waste management is that we have limited mechanistic insight into rubber biodegradation, and the complicated composition of rubber products inhibits cell growth and activity of microbes. Thus it becomes important to fully comprehend the mechanism of rubber biodegradation and continue the search for new microbial strains so that the acquired knowledge can be utilized to develop a biodegradation process suitable for scale-up. In this short review, rubber degradation using fungi and bacteria is highlighted.

## INTRODUCTION

Rubber, due to its exceptional qualities like flexibility, longevity, and a wide range of uses, has become one of the most essential commodities in today's world. As per the Malaysian Rubber Council, world production of rubber increased by 3.3% to 7.0 million tonnes in the first quarter of 2021, compared to 6.8 million tonnes in the same period of 2020. Similarly, world consumption of rubber grew by 14.8% to 7.4 million tonnes in the first quarter of 2021, compared to 6.5 million tonnes in the same period of 2020 (Malaysian Rubber Council 2021). With the increase in consumption, wastage of rubber in the form of used rubber products especially scrap tires has increased. Rubber waste management is an extremely challenging task for Municipal Corporation. The biggest challenge comes in the form of recycling. Rubber is highly durable and inherently non-biodegradable, leaving them stagnant in landfills for hundreds of years, occupying valuable space. Many cities have scrap tire stockpiles, which cause public health, environmental, and aesthetic issues (Yehia 2004).

Many plants, primarily from the Euphorbiaceae, Compositae, Moraceae, Eucommiaceae, Celastraceae and Apocynaceae families, produce rubber by enzymatic activities. Chemically NR is a polyisoprene polymer. There are mainly two types of polyisoprenoids based on isomerism, the cis isomer natural rubber (NR) [poly(*cis*-1,4-isoprene)] and the trans isomer gutta-percha (GP) [poly(*trans*-1,4-isoprene)] (Fig. 1).

Natural Rubber can be obtained from plants such as *Hevea brasiliensis* (rubber tree), *Parthenium argentatum* (guayule), *Taraxacum kok-saghyz* (Russian dandelion), *Dyera costulata* (jelutong). Gutta-percha on the other hand can be obtained from *Palaquium gutta* (gutta-percha), *Manikara zapota* (chico), *Eucommia ulmoides* (Tochu), *Euonymus europaeus* (spindle tree), *Mimusops balata* (balata) (Yikmis & Steinbüchel 2012). For commercial uses, NR is produced from the latex of *Hevea brasiliensis*, a South American plant endemic to the Amazon Valley. The first scientific or commercial interest in rubber was demonstrated by Frenchman Charles Marie de Condamine, who submitted a report to the

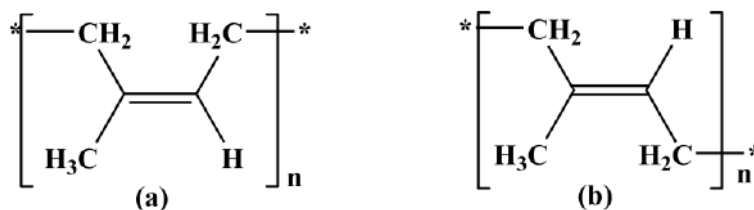


Fig. 1: Chemical structures of (a) Natural rubber (NR) [poly(cis-1,4-isoprene)] (b) Gutta-percha (GP) rubber [poly(trans-1,4-isoprene)].

Paris Academy of Sciences in 1745 after visiting Ecuador and observing the local use of *Hevea* latex. Priestly, an English scientist, named the raw material, 'Rubber' in 1770 after noticing that it can remove pencil markings. In 1839, Goodyear discovered vulcanization, ushering in a golden age of the rubber industry (Hurley 1981). The discovery of synthetic polyisoprene by German scientist Fritz Hofmann in 1909 paved the way for large-scale production of synthetic poly (cis-1,4-isoprene) with a molecular structure similar to NR (Yikmis & Steinbüchel 2012).

The latex (colloid liquid in the aqueous phase) of these plants is converted to rubber by coagulation (chemically and electrically) and drying. Rubber at this stage is a soft, sticky, thermoplastic material with low tensile strength and elasticity. These properties have a straightforward molecular structural basis. A variety of polymeric chains of varying lengths make up the material. Most notably no crosslinking is present. As a result, while being known for millennia, rubber in this form did not find any significant application until the discovery of vulcanization (Kumar & Nijasure 1997). During vulcanization (Fig. 2) rubber is heated in the presence of sulfur, resulting in the three-dimensional cross-linking of chain rubber molecules (polyisoprene) bonded to each other

by sulfur atoms. Other compounds such as hydrogen sulfide, sulfur monochloride, benzoyl chloride, etc. can also be applied for vulcanization. This process improves the elasticity, tensile strength, resilience, and water-absorbing capacity of rubber. Moreover, vulcanized rubber is resistant to oxidation, abrasion, wear, and tear. It also has a wide useful range of temperatures.

As discussed earlier, the major problem with rubber products is their disposal after use. One way to counter this problem is recycling. However, unlike polythene, it cannot be simply melted and reshaped again into the product due to cross-linking (formed during vulcanization) (Nayanashree & Thippeswamy 2013). The rubber wastes such as tires are conventionally buried in landfills or are held in stockpiles. However, it does nothing to help with the disposal issues that come with rubber waste as it is not biodegradable in landfills and remains immobile in stockpiles leading to several environmental problems. Rubber waste especially tires can also be thermally degraded at around 800°C to produce Tar Pyrolysis Oil (TPO), which has diesel-like properties. This process, in addition to being complex, costly, and labor-intensive, has the potential to pollute the air and water due to poor process management. Tyre abrasion has been identified as one of the primary sources of microplastics which subsequently enter the food chain and cause biological contamination. Left-over tire crumbs can be utilized to generate asphalt for roads, playground rubber flooring, sports or bicycle tracks, or to alter the structural qualities of concrete. However, in all of these mitigation methods, the rubber remains in the environment and is degraded very slowly (Basik et al. 2021). In recent times, microbial bioremediation of wastes has gained tremendous interest. Bioremediation using bacteria and fungi has found its way into many diverse applications such as treatment of antibiotics present in water (Singh et al. 2017), textile azo dye decolorization and detoxification (Karnwal 2019), oil cleaning from water bodies (Rahul et al. 2018), removal of pesticide (Sidhu et al. 2019), herbicides (Digvijaya et al. 2017, Mukherjee et al. 2018), explosive materials (Gorontzy et al. 1994), toxic heavy metals (Gehlot & Singh 2018, Karnwal 2018, Kaur et al. 2018 & Mishra et al. 2016) from soil and water, etc. Biodegradation is an eco-friendly

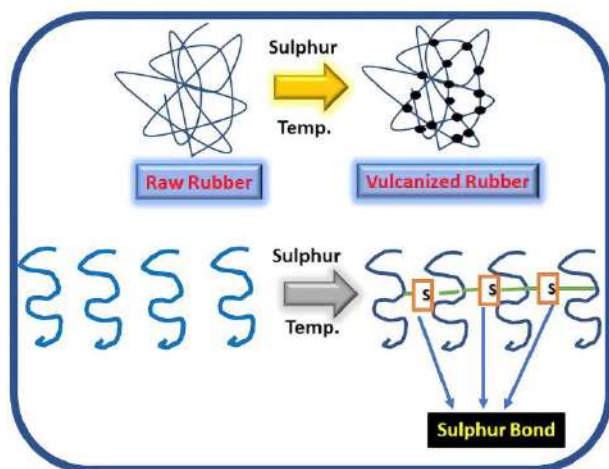


Fig. 2: Mechanism of vulcanization.

alternative to traditional disposal methods in which microorganisms break down complex organic compounds in waste products into simpler compounds and eventually into the water and either carbon dioxide (aerobic) or methane (anaerobic). While microorganisms can break down the majority of natural substances, they frequently lack the enzymes required to degrade most manmade compounds, including synthetic rubbers. Compounds with a molecular structure that microorganisms have not been exposed to (for example, synthetic rubbers and polymers) are typically resistant to biodegradation. They ultimately endanger the ecosystems by contaminating and accumulating in the environment.

During microbial degradation, rubber polymers are mineralized and redistributed through the Elemental cycles (Enoki et al. 2003, Cui et al. 2005). The biodegradation process progresses through four stages: bio-deterioration, bio-fragmentation, assimilation, and mineralization. The chemical and physical properties of the polymer are altered during the first stage, while enzymatic cleavage permits the polymer to be broken down during the second. The assimilation is the uptake of molecules by microbes; and finally, the mineralization phase, which is characterized by the emission of CO<sub>2</sub> and H<sub>2</sub>O in aerobic settings and CO<sub>2</sub>, CH<sub>4</sub>, and H<sub>2</sub>O in anaerobic conditions (Pathak & Navneet 2017).

Microbial rubber degradation has been the subject of a number of studies in recent years. Both fungi and bacteria have been shown to degrade rubber, however, the process is slow (Onyeagoro et al. 2012). NR is primarily composed of hydrocarbons, with minor amounts of lipids, sugar, resins, proteins, and minerals. The growth of microorganisms is aided by these organic contaminants. Microbial processes have advantages over chemical and physical processes as they are non-toxic and do not produce any hazardous substance. However, several challenges remain, the most significant of which being microorganism sensitivity to numerous chemicals, including rubber additives, which are used to improve tire durability and operation across a wide temperature range (Yikmis & Steinbüchel 2012). This brief review outlines the microbial degradation of rubber by fungi and bacteria.

## DEGRADATION OF NATURAL RUBBER BY FUNGI

De Vries was the first to explore the biodegradation of rubber by fungi. The biodegradation of rubber was studied using several *Penicillium* and *Aspergillus* strains in a 10% (w/v) aq. NaCl liquid medium with natural rubber as the substrate. After a 19-month to 5-year incubation period, there was a 6% rise in biomass and a 15.5–30.9 percent drop in the weight of the rubber material (Shah 2020). Schade reported the growth of fungi *Monascus purpureus* and *Monascus rubber* on purified natural rubber substrate (Schade 1937).

After a decade Kalinenko (1938) identified fungal strains from *Aspergillus* and *Penicillium* as rubber degraders (Kalinenko 1938). In soil burial tests conducted on NR vulcanized sheets of specific composition, Kwiatkowska et al. (1980) discovered considerable weight losses after 91 days, equivalent to 40% of the initial weight. They identified *Fusarium solani* fungal strain on the rubber's surface and held it responsible for the observed weight loss by degradation (Kwiatkowska et al. 1980). Borel et al. (1982) found that *Fusarium solani* degrades rubber faster than other fungi utilized in his studies, such as *Paecilomyces lilacinus*, *Phoma eupyrena*, and *Cladosporium cladosporioides* (Borel et al. 1982). A fungal strain, *Penicillium variable* was isolated by Williams from a damaged NR sample following soil burial. Using solution viscosity measurements, Williams discovered a 15% decrease in the molecular weight of polyisoprene after 70 days due to breakdown by the *Penicillium variable* (Williams 1982). Atagana et al. (1999) in their study on fungal degradation of waste from the rubber processing industry, demonstrate that *Mucor* species have the potential to metabolize the aqueous fraction obtained during coagulation of latex thereby lowering BOD in a reasonable manner (Atagana et al. 1999). Stevenson et al. (2008) proposed a multistage tire rubber recycling process that included using the fungus *Recinicium bicolor* in the first stage of detoxification to remove pollutants that inhibit microbial growth (Stevenson et al. 2008). Nayanashree et al. isolated two fungal strains of *Aspergillus niger* and *Penicillium* from rubber pieces that had previously been dumped in the soil. Both these strains were found to be effective in rubber degradation with *Aspergillus niger* showing 28.3% degradation, while *Penicillium* sp. showing a 25.9% degradation in two months (Nayanashree & Thippeswamy 2013). Mohamed et al. studied the ability of *Penicillium chrysogenum* and *Aspergillus niger* to metabolize and degrade rubber latex obtained from *Calotropis procera* by analyzing the rise in fungal protein content, reduction in molecular weight and intrinsic viscosity of latex and growth of these stains on rubber surface (Mohamed et al. 2017). Singh et al. (2017) in their study found that fungal species *Aspergillus niger* and *Phlebia radiate* can degrade NR, with *Aspergillus niger* having the highest degrading potential, accounting for 27.27% on the scale of NR weight loss (Singh et al. 2017). In his study on the biodegradation of unvulcanized natural rubber by microorganisms, Bosco et al. (2018) discovered that filamentous fungus (*Alternaria alternata*) isolated from an NR surface and yeast (*Rhodotorula mucilaginosa*) isolated from NR liquid culture were both effective in promoting NR biodegradation (Bosco et al. 2018). Recently genome sequencing of a fungal species *Rigidoporus microporus*

was carried out by Oghenekaro et al. (2020) This fungus is known to cause white root rot disease in the rubber tree and can grow on latex. In the genome sequencing, however, no homologs of bacterial proteins involved in latex degradation were found thus indicating that not all latex-tolerant strains have rubber-degrading genes (Oghenekaro et al. 2020, Basik et al. 2021). The role of fungus in rubber deterioration is mostly descriptive, indicating solely its potential to degrade NR. Table 1 summarizes the list of fungi mentioned in this review.

## DEGRADATION OF NATURAL RUBBER BY BACTERIA

Many studies have been carried out in recent years to identify and characterize the efficient rubber-degrading bacteria, as well as to understand the metabolic basis for natural rubber breakdown. Until recently, many bacterial strains have been discovered that can consume rubber as their only source of carbon and energy (Shah et al. 2013). These bacteria can be categorized into two groups based on their differing methods of rubber degradation. The Members of the first group (Group B) produce translucent halos when grown on solid media containing latex particles, indicating the excretion of a polyisoprene-cleaving enzyme (Fig. 3a), while members of the second group (Group A) do not form translucent halos or develop on latex plates, instead require direct contact with the rubber and grow adhesively on its surface in liquid cultures using it as the source of carbon and energy (Fig. 3b) (Linos et al. 2000).

The most effective Group B members include *Streptomyces*, and *Micromonospora*, whereas CNM (*Corynebacterium*, *Nocardia*, *Mycobacterium*) are the most potent rubber degraders from Group A (Shah 2020). The first publication on microbial degradation of NR was done by Akio et al. where they used *Nocardia* sp. strain 835A to degrade NR vulcan-

izates (Tsuchii et al. 1985). The majority of known NR degraders are Gram-positive bacteria, which have been widely reported, whereas, only a few Gram-negative NR-degrading bacteria have been discovered and described in the scientific literature. *Xanthomonas* sp. strain 35Y (Tsuchii & Takeda 1990) (now reclassified as *Steroidobacter cummioxidans* strain 35Y (Sharma et al. 2018)) is the first Gram-negative bacteria known to degrade rubber. Table 2 summarizes the list of NR degrading bacteria reported in the literature until now.

Research has confirmed that there are three enzymes responsible for the degradation of natural rubber; Latex clearing protein (Lcp) which was first identified and characterized in *Streptomyces* sp. strain K30 (Rose et al. 2005) and Rubber oxygenase (RoxA and RoxB) first found in *Xanthomonas* sp.

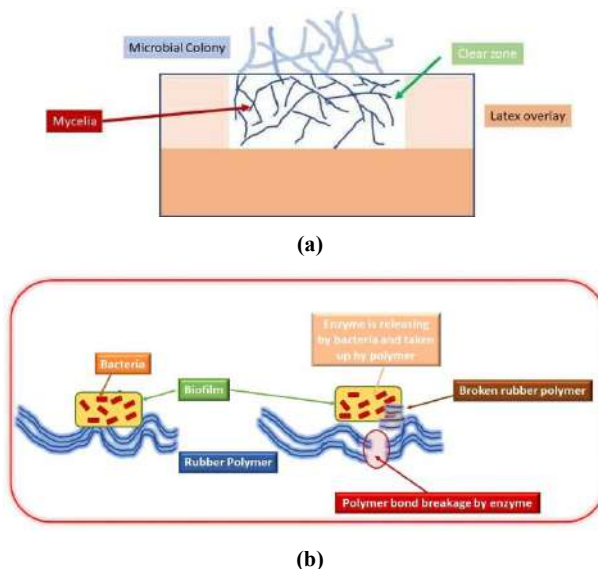


Fig. 3: NR degradation strategy of (a) Group B bacteria and (b) Group A bacteria. (Adapted from Basik et al. 2021).

Table 1: List of NR degrading fungal strains mentioned in this review.

Fungal Strain	References
<i>Monascus rubber</i> , <i>Monascus purpureus</i>	(Schade 1937)
<i>Fusarium solani</i>	(Kwiatkowska 1980)
<i>Paecilomyces lilacinus</i> , <i>Phoma eupyrena</i> , <i>Cladosporium cladosporioides</i>	(Borel et al. 1982)
<i>Penicillium variable</i>	(Williams 1982)
<i>Mucor</i> species	(Atagana et al. 1999)
<i>Recinicium bicolor</i>	(Stevenson et al. 2008)
<i>Aspergillus niger</i>	(Nayanashree & Thippeswamy 2013, Singh et al. 2017)
<i>Penicillium chrysogenum</i>	(Mohamed et al. 2017)
<i>Phlebia radiata</i>	(Singh et al. 2017)
<i>Alternaria alternata</i> , <i>Rhodotorula mucilaginosa</i>	(Bosco et al. 2018)



Table 2: List of NR degrading bacteria reported in the literature.

Bacteria	Group	Enzyme Involved	References
<b>Gram-positive</b>			
<i>Streptomyces sp.</i> strain K30	B	Lcp	Birke et al. 2015, Rose & Steinbüchel 2005, Röther et al. 2016, Yikmis et al. 2008
<i>Streptomyces sp.</i> strain CFMR 7	B	Lcp	Nanthini et al. 2017, Nanthini & Sudesh 2017
<i>Streptomyces griseus</i> 1D	B	Lcp	Bode et al. 2001, Jendrossek et al. 1997
<i>Streptomyces coelicolor</i> 1A	B	Lcp	Jendrossek et al. 1997, Bode et al. 2000
<i>Micromonospora aurantiaca</i> W2b	B	Unknown	Linos et al. 2000
<i>Rhodococcus rhodochrous</i> RPK1	A	Lcp	Watcharakul et al. 2016
<i>Gordonia westfalica</i> Kb2	A	Lcp	Berekaa et al. 2000
<i>Gordonia polyisoprenivorans</i> VH2	A	Lcp	Hiessl et al. 2012, Oetermann et al. 2018
<i>Gordonia polyisoprenivorans</i> Kd2	A	Lcp	Berekaa et al. 2000, Linos et al. 1999
<i>Nocardia nova</i> SH22a	A	Lcp	Luo et al. 2014
<i>Nocardia farcinica</i> E3	A	Lcp	Ibrahim et al. 2006
<i>Nocardia farcinica</i> NVL3	A	Lcp	Linh et al. 2017
<i>Paenibacillus lautus</i>	A	Unknown	Hapuarachchi et al. 2016
<i>Achromobacter sp.</i>	A	Unknown	Berekaa et al. 2005
<i>Mycobacterium fortuitum</i> NF4	A	Unknown	Linos et al. 2000
<b>Gram-negative</b>			
<i>Steroidobacter cummioxidans</i> strain 35Y	B	RoxA, RoxB	Sharma et al. 2018
<i>Rhizobacter gummiphilus</i> NS21	B	RoxA, RoxB	Imai et al. 2013
<i>Pseudomonas aeruginosa</i> AL98	A	Unknown	Linos et al. 2000
<i>Pseudomonas citronellolis</i>	A	Unknown	Bode et al. 2000
<i>Acinetobacter calcoaceticus</i>	A	Unknown	Bode et al. 2001

strain 35Y (Jendrossek & Reinhardt 2003). To date, almost all gram-positive rubber-degrading bacteria have been found to release the Lcp protein, whereas gram-negative bacteria have been shown to carry the RoxA and RoxB genes (Shah et al. 2020).

## RUBBER DEGRADING ENZYMES AND MECHANISM

Rubber is a high molecular weight polymer that cannot be absorbed directly by cells; instead, it must first be broken down extracellularly into low molecular components that may then be transported over the cell membrane and used for metabolism. Previous research works on rubber degradation has therefore largely focused on extracellular enzyme attack on the polyisoprene molecule (Birke et al. 2017). For this, both Gram-positive and Gram-negative bacteria use two unrelated types of enzymes i.e., Latex clearing protein (Lcp) and Rubber oxygenase (RoxA and RoxB). Lcp is a mono-heme cytochrome-b protein while Rubber oxygenase Rox A and Rox B are both Diheme cytochrome-c dioxygenase

proteins (Shah 2020). Several studies have been reported on RoxAs and Lcps (Birke et al. 2015, Iicu et al. 2017, Schmitt et al. 2010, Seidel et al. 2013 & Yikmis et al. 2012) whereas RoxB has been discovered only recently (Birke et al. 2017). The amino-acid sequences of RoxAs and RoxBs have no notable similarities to those of Lcps. Regardless, all three enzymes attack the polyisoprene molecule's cis double bond oxidatively, resulting in cleavage products with aldehyde and keto end groups, as well as some isoprene units in between. Rubber is broken down by Lcp into a variety of compounds, ranging from C20 tetra-isoprenoids to higher oligo-isoprenoids. RoxA, on the other hand, only makes one polyisoprene cleavage product, ODTD, a C15 oligoisoprenoid. The active sites of Lcp and RoxA are distinct, as evidenced by their diverse products. The active site of Lcp is thought to be more surface accessible and should be closer to the substrate-binding site, whereas the active site of RoxA is buried deep within the enzyme structure and has no direct open access to the protein surface. An exo-type cleavage mechanism is proposed for RoxA to explain the regular spacing between

two adjacent cleavage sites, however, an endo-type cleavage mechanism is proposed for Lcp to explain the wide range of cleavage products (Birke & Jendrossek 2014, Jendrossek & Reinhardt 2003). Although RoxB and RoxA share the same fundamental amino acid sequence and other features, the cleavage products for RoxB were discovered to be identical to those observed for Lcp. RoxB is related to Lcp and, unlike RoxA, cleaves polyisoprene in an endo-type manner, as indicated by the detection of a variety of oligo-isoprenoids of varying lengths (Birke et al. 2017). Table 3 summarizes the characteristics of NR degrading enzymes.

The Lcp, RoxA, and RoxB enzymes are responsible for the extracellular cleavage of polyisoprene. These degraded isoprene derivatives are transported into the bacterial cell which is responsible for rubber degradation. In the intracellular space of the bacteria, there are a variety of enzymes that are found to be important for rubber metabolism. These enzymes are Acyl CoA Synthase, Acyl CoA Dehydrogenase, Dienoyl CoA Reductase, Enoyl CoA Isomerase, Enoyl CoA Reductase, 3-Hydroxyacyl CoA Dehydrogenase, Acyl CoA Acetyltransferase,

$\alpha$ -Methylacyl Racemase, Acyl CoA Dehydrogenase, Acyl CoA Hydratase, 3-Hydroxyacyl CoA dehydrogenase, and Acyl CoA Acetyltransferase. As a result of degradation by these enzymes, further degradation is done by the beta-oxidation process. During these processes, the degradation product of the rubber finally is converted into the propionyl-CoA and acetyl-CoA which are easily taken up by the bacteria for their metabolic processes like glycolysis and TCA cycle (Methylcitrate cycle and Methylmalonil pathway). The time required for the degradation depends on the amount of propionyl-CoA and acetyl-CoA formed and taken by bacteria during the number of cycles for degradation. Fig. 4 explains the role of different enzymes in the rubber degradation by different bacterial enzymes.

## FUTURE PERSPECTIVES

Although NR biodegradation is a more environmentally acceptable alternative to traditional disposal methods, it is a slow and low-yielding process. This is because living microbes catalyze solid and impure substrates, resulting in slow

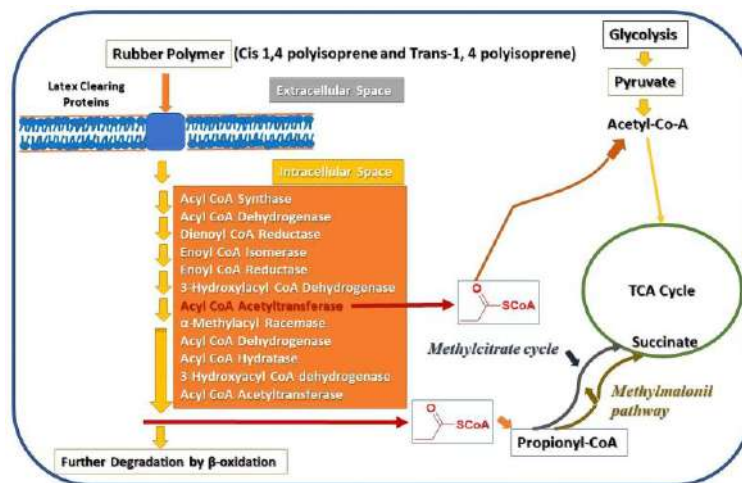


Fig. 4: Proposed metabolic pathway of poly(cis-1,4-isoprene) in *Gordonia polyisoprenivorans* VH2 (Adapted from Andler 2020).

Table 3: Characteristics of NR degrading enzymes (Shah et al. 2020, Basik et al. 1989, Birke et al. 2017, Birke & Jendrossek 2014)

	RoxA	RoxB	Lcp
Identified and Characterized from	<i>Xanthomonas sp.</i> strain 35Y	<i>Xanthomonas sp.</i> strain 35Y	<i>Streptomyces sp.</i> strain K30
Bacteria	Gram-negative	Gram-negative	Gram-positive
Co-factor	Diheme cytochrome-c dioxygenase protein	Diheme cytochrome-c dioxygenase protein	Mono-heme cytochrome-b protein
Molecular Mass	~73 kDa	~70 kDa	~40 kDa
Mechanism of Cleavage	Exo	Endo	Endo
Rubber Degradation Product	12-oxo-4,8-dimethyltrideca-4,8-diene-1-al (ODTD) a C15 oligo-isoprenoid	Mixture of C20, C25, C30 and higher oligo-isoprenoids	Mixture of C20, C25, C30 and higher oligo-isoprenoids

reactions (long incubation periods), and they are sensitive to chemical substances such as rubber additives in most cases. A cost-effective strategy for treating massive amounts of rubber waste has been proposed using enzymes with a high-efficiency expression system and a low-cost recovery methodology. It is critical to screen all of the enzymes involved in total rubber degradation to achieve this (Andler 2020).

For an effective rubber waste recycling approach, Stevenson et al. proposed a multistage process involving detoxification, desulfurization-devulcanization, and total or partial biodegradation. The detoxification process involves the use of certain fungal and bacterial species to remove toxic additives from the rubber. This is followed by desulfurization-devulcanization which involves removing the sulfur cross-links in the vulcanized rubber by the sulfur utilizing microorganisms. Detoxification boosts the biodegradability of rubber while also lowering the environmental risks connected with its disposal. It has also been shown to help in the growth of desulfurizing bacteria for devulcanization (Stevenson et al. 2008). Table 4 lists some fungi and bacteria which can be utilized for Detoxification and Devulcanization in multistage NR degradation.

Another approach toward sustainable NR degradation would be to combine green chemistry with biological processes. Catalytic agents for the oxidation of specific rubber additives obtained from the vulcanization process, in particular, can be exceedingly effective and time-saving when compared to biological procedures. However, in doing so green chemistry principles, such as the use of cleaner solvents, the reduction of by-products, and the reduction of energy requirements, should be considered (Andler 2020).

The resistance of synthetic rubber towards microbial biodegradation is mostly because they have not been available

Table 4: Some useful microbes screened for the detoxification and devulcanization (Stevenson et al. 2008)

Fungi	Bacteria
Detoxification	
<i>Pleurotus. sajor-caju</i>	<i>Rhodococcus</i> sp.
<i>Trametes versicolor</i>	<i>Corynebacteria</i>
<i>Recinicium bicolor</i>	<i>Pseudomonas</i>
	<i>Escherichia coli</i>
Desulfurization-Devulcanization	
	<i>Thiobacillus. ferrooxidans</i>
	<i>Thiobacillus. thioparus</i>
	<i>Thiobacillus. thiooxidans.</i>
	<i>Rhodococcus</i>
	<i>Sulfolobus acidocaldarius</i>

for long enough in natural evolution for microorganisms to create degradative enzymes to use the compound. To degrade novel synthetic compounds, microorganisms will need to acquire new genes and genetic functions that encode catabolic enzymes. Gene transfers between microorganisms can result in the emergence of a specific degradative pathway. In response to synthetic compounds, microbes have occasionally shown response by producing degrading enzymes, however, there may be no optimal control on the pathway. Thus, to sum up, microbes need a long period to acclimatize to synthetic material, and to achieve effective biodegradation of synthetic rubber, this natural process of biodegradation should be accelerated. Recently a novel material ENSO RESTORE™ RL a rubber additive was proposed to attract the specific naturally occurring microbes and rapidly acclimatize them to synthetic material. This additive has a unique property that it is inert to rubber resin and does not contribute directly to rubber degradation thus preserving the rubber’s shelf life. The test results showed the effectiveness of ENSO RESTORE™ RL to acclimatize the flora within the test inoculum such that synthetic rubber can be used as the only carbon source and effectively biodegraded. Unexpectedly, this material was shown to work for synthetic rubber but not for natural rubber. It was found that the anaerobic environment such as those found in landfills only promotes the biotic degradation process through extra-cellular and intra-cellular enzymes and not the abiotic oxidation through free oxygen which is the first step in the natural rubber degradation. Furthermore, most of the earlier studies on NR materials involved isolated microbes and enhanced environmental conditions which do not correspond to the natural habitat involving multiple different species (2013).

By using the microbial consortia and imitating the microbial activity naturally present in tire dump soil, Bosco et al. (2018) investigated the biodegradation of rubber. This naturally chosen microbial biomass was found to be capable of utilizing NR as the only source of carbon and breaking down NR efficiently, as evidenced by a 15.6 percent dry weight loss. The predominant bio degraders in this investigation were found to be aerobic biomass, primarily filamentous fungi (Bosco & Mollea 2021)

**CONCLUSION**

Natural rubber (NR) is one of society’s most significant polymers. It is a valuable raw material that is utilized to produce over 40,000 distinct products. Medical equipment, surgical gloves, plane, and automobile tires, pacifiers, apparel, and toys are just a few of the products made from it. Today, synthetic polyisoprene with a purity of 98 to 99% may be produced with physical qualities that are identical

to natural rubber. However, they lack the stress stability, processability, and other characteristics of natural rubber (Rose et al. 2005). The major problem associated with the rubber products is their disposal after use, as there is currently a lack of knowledge on the fate of rubber materials in nature. The rate at which rubber decomposes is determined by the type of rubber, its composition, and the surrounding environment. Rubber can be reused, recycled, or disposed of using conventional methods, however, the end product is still rubber mostly microparticles that disintegrate slowly in the environment (Basik et al. 2021). Scientists have been exploring several ways to efficiently break down rubber and rubber-generated wastes since the discovery of distinct rubber-degrading microbes and their genes responsible for the enzymes that digest different types of rubber. Microbial degradation is eco-friendly, which is why it is preferred over chemical and physical degradation. Fungi have been tested for their ability to degrade NR since 1928. However, later publications on rubber-degrading fungi were essentially descriptive, merely stating that it could degrade NR. Many bacterial strains that can use rubber as their sole source of carbon and energy have been discovered to date. However, with the exception of a few studies on technical applications, most research on these bacteria has concentrated on the fundamentals of rubber biodegradation. Despite our growing knowledge of enzyme activity, we still have a limited understanding of enzyme action on rubber substrates and the bacteria, molecular, and environmental factors that influence it. As a result, it's critical to keep looking for new strains and completely comprehending the mechanism of rubber biodegradation to apply the wealth of knowledge gathered to build NR biodegradation processes and systems that can be scaled up.

## REFERENCES

- Andler, R. 2020. Bacterial and enzymatic degradation of poly (cis-1, 4-isoprene) rubber: Novel biotechnological applications. *Biotechnol. Adv.*, 54(1): 107606.
- Atagana, H.I., Ejechi, B.O. and Ayilumo, A.M. 1999. Fungi are associated with the degradation of wastes from the rubber processing industry. *Environ. Monit. Assess.*, 55(3): 401-408.
- Basik, A.A., Sanglier, J.J., Yeo, C.T. and Sudesh, K. 2021. Microbial degradation of rubber: Actinobacteria. *Polymers*, 13(12): 1989.
- Berekaa, M.M., Barakaat, A., El-Sayed, S.M. and El-Aassar, S.A. 2005. Degradation of natural rubber by *Achromobacter* sp. NRB and evaluation of culture conditions. *Pol. J. Microbiol.*, 54(1): 55.
- Berekaa, M.M., Linos, A., Reichelt, R., Keller, U. and Steinbüchel, A. 2000. Effect of pretreatment of rubber material on its biodegradability by various rubber degrading bacteria. *FEMS Microbiol. Lett.*, 184(2): 199-206.
- Birke, J. and Jendrossek, D. 2014. Rubber oxygenase and latex clearing protein cleave rubber to different products and use different cleavage mechanisms. *Appl. Environ. Microbiol.*, 80(16): 5012-5020.
- Birke, J., Röther, W. and Jendrossek, D. 2015. Latex clearing protein (Lcp) of *Streptomyces* sp. strain K30 is ab-type cytochrome and differs from rubber oxygenase A (RoxA) in its biophysical properties. *Appl. Environ. Microbiol.*, 81(11): 3793-9.
- Birke, J., Röther, W. and Jendrossek, D. 2017. RoxB is a novel type of rubber oxygenase that combines properties of rubber oxygenase RoxA and latex clearing protein (Lcp). *Appl. Environ. Microbiol.*, 83(14): e00717-e00721.
- Bode, H.B., Kerkhoff, K. and Jendrossek, D. 2001. Bacterial degradation of natural and synthetic rubber. *Biomacromolecules*, 2(1): 295-303.
- Bode, H.B., Zeeck, A., Plüchhahn, K. and Jendrossek, D. 2000. Physiological and chemical investigations into microbial degradation of synthetic poly (cis-1, 4-isoprene). *Appl. Environ. Microbiol.*, 66(9): 3680-3685.
- Borel, M.A., Kergomard, R. and Renard, M.F. 1982. Degradation of natural rubber by *Fungi imperfecti*. *Agr. Biol. Chem.*, 46(4): 877-881.
- Bosco, F. and Mollea, C. 2021. Biodegradation of natural rubber: a microcosm study. *Water Air Soil Pollut.*, 232(6): 1-15.
- Bosco, F., Antonoli, D., Casale, A., Gianotti, V., Mollea, C., Laus, M. and Malucelli, G. 2018. Biodegradation of unvulcanized natural rubber by microorganisms isolated from soil and rubber surface: A preliminary study. *Bioremediat. J.*, 22(1-2): 43-52.
- Clark, T. 2013. Advancements in rubber disposal: Biodegradation and the Environment. In *Proceedings of the International Latex Conference*.
- Cui, Q., Wang, L., Huang, Y., Liu, Z. and Goodfellow, M. 2005. *Nocardia jiangxiensis* sp. nov. and *Nocardia miyunensis* sp. nov., isolated from acidic soils. *Int. J. Syst. Evol. Microbiol.*, 55: 1921-1925.
- Digvijaya, S., Parishamita, G., Kumar, A. and Kourb, R.T. 2017. Isolation and identification of Imazethapyr (Herbicide) degrading soil microorganism from Punjab Region (India). *J. Pharm. Sci. Res.*, 9(12): 2356-2360.
- Enoki, M., Doi, Y. and Iwata, T. 2003. Oxidative degradation of cis- and trans-1, 4-polyisoprenes, and vulcanized natural rubber with enzyme-mediator systems. *Biomacromolecules*, 4(2): 314-320.
- Gehlot, P., and Singh, J. (eds.). 2018. *Fungi and their role in sustainable development: Current perspectives*. Springer, Singapore.
- Gorontzy, T., Drzyzga, O., Kahl, M.W., Bruns-Nagel, D., Breitung, J., Loew, E.V. and Blotvogel, K.H. 1994. Microbial degradation of explosives and related compounds. *Crit. Rev. Microbiol.*, 20(4): 265-284.
- Hapuarachchi, S.N.S., Kariyapper, S.R., Gunawardana, M.B.D.M.D., Egodage, S. and Ariyadasa, T.U. 2016. Biodegradation of natural rubber latex by a novel bacterial species isolated from soil. In *Moratuwa Engineering Research Conference (MERCCon)*, 5-6 April 2016, Morutawa, Sri Lanka, IEEE, Cambridge, MA, pp. 293-296.
- Hiessl, S., Schuldes, J., Thürmer, A., Halbsguth, T., Bröker, D., Angelov, A., Liebl, W., Daniel, R. and Steinbüchel, A. 2012. Involvement of two latex-clearing proteins during rubber degradation and insights into the subsequent degradation pathway revealed by the genome sequence of *Gordonia polyisoprenivorans* strain VH2. *Appl. Environ. Microbiol.*, 78(8): 2874-2887.
- Hurley, P.E. 1981. History of natural rubber. *J. Macromol. Sci. A.*, 15(7): 1279-1287.
- Ibrahim, E.M., Arenskötter, M., Luftmann, H. and Steinbüchel, A. 2006. Identification of poly (cis-1, 4-isoprene) degradation intermediates during growth of moderately thermophilic actinomycetes on rubber and cloning of a functional lcp homologue from *Nocardia farcinica* strain E1. *Appl. Environ. Microbiol.*, 72(5): 3375-3382.
- Ilcu, L., Röther, W., Birke, J., Brausemann, A., Einsle, O. and Jendrossek, D. 2017. Structural and functional analysis of latex clearing protein (Lcp) provides insight into the enzymatic cleavage of rubber. *Sci. Rep.*, 7(1): 1-1.
- Imai, S., Yoshida, R., Endo, Y., Fukunaga, Y., Yamazoe, A., Kasai, D., Masai, E. and Fukuda, M. 2013. *Rhizobacter gummiphilus* sp. nov., a rubber-degrading bacterium isolated from the soil of a botanical garden in Japan. *J. Gen. Appl. Microbiol.*, 59(3): 199-205.
- Jendrossek, D. and Reinhardt, S. 2003. Sequence analysis of a gene product synthesized by *Xanthomonas* sp. during growth on natural rubber latex. *FEMS Microbiol. Lett.*, 224(1): 61-65.



- Jendrossek, D., Tomasi, G. and Kroppenstedt, R.M. 1997. Bacterial degradation of natural rubber: a privilege of actinomycetes. *FEMS Microbiol. Lett.* 150(2): 179-88.
- Kalinenko, V.O. 1938. The role of Actinomycetes and bacteria in decomposing rubber. *Mikrobiologiya*, 17: 119-128.
- Karnwal, A. 2018. Use of bio-chemical surfactant producing endophytic bacteria isolated from rice root for heavy metal bioremediation. *Perantanika J. Trop. Agric. Sci.*, 41(2): 699- 714.
- Karnwal, A. 2019. Textile azo dye decolorization and detoxification using bacteria isolated from textile effluents. *BioTechnologia*, 100(4): 373-385.
- Kaur, P., Singh, S., Kumar, V., Singh, N. and Singh, J. 2018. Effect of rhizobacteria on arsenic uptake by macrophyte *Eichhornia crassipes* (Mart.) Solms. *Int. J. Phytoremed.*, 20(2): 114-120.
- Kumar, C.S.S.R. and Nijasure, A.M. 1997. Vulcanization of rubber. *Resonance*, 4: 55-59.
- Kwiatkowska, D., Zyska, B.J. and Zankowicz, L.P. 1980. Microbiological deterioration of natural rubber sheet by soil microorganisms. *Biodegradation*, 4: 135-141.
- Linh, D.V., Huong, N.L., Tabata, M., Imai, S., Iijima, S., Kasai, D., Anh, T.K. and Fukuda, M. 2017. Characterization and functional expression of a rubber degradation gene of a *Nocardia* degrader from a rubber-processing factory. *J. Biosci. Bioeng.*, 123(4): 412-418.
- Linosa, A., Berekaa, M.M., Reichelt, R., Keller, U., Schmitt, J., Flemming, H.C., Kroppenstedt, R.M. and Steinbüchel, A. 2000. Biodegradation of cis-1, 4-polyisoprene rubbers by distinct actinomycetes: microbial strategies and detailed surface analysis. *Appl. Environ. Microbiol.*, 66(4): 1639-1645.
- Linosa, A., Reichelt, R., Keller, U. and Steinbüchel, A. 2000. A gram-negative bacterium, identified as *Pseudomonas aeruginosa* AL98, is a potent degrader of natural rubber and synthetic cis-1, 4-polyisoprene. *FEMS Microbiol. Lett.*, 182(1): 155-161.
- Linosa, A., Steinbüchel, A., Spröer, C. and Kroppenstedt, R.M. 1999. *Gordonia polyisoprenivorans* sp. nov., a rubber-degrading actinomycete isolated from an automobile tyre. *Int. J. Syst. Evol. Microbiol.*, 49(4): 1785-1791.
- Luo, Q., Hiessl, S., Poehlein, A., Daniel, R. and Steinbüchel, A. 2014. Insights into the microbial degradation of rubber and gutta-percha by analysis of the complete genome of *Nocardia nova* SH22a. *Appl. Environ. Microbiol.*, 80(13): 3895-3907.
- Malaysian Rubber Council. 2021. Industry Overview of World Rubber Production, Consumption and Trade. Available at: [https://www.myrubbercouncil.com/industry/world\\_production.php](https://www.myrubbercouncil.com/industry/world_production.php) (Accessed: 2021).
- Mishra, V., Gupta, A., Kaur, P., Singh, S., Singh, N., Gehlot, P. and Singh, J. 2016. Synergistic effects of Arbuscular mycorrhizal fungi and plant growth-promoting rhizobacteria in bioremediation of iron contaminated soils. *Int. J. Phytoremed.*, 18(7): 697-703.
- Mohamed N.H., Ismail M.A., Abdel-Mageed W.M. and Shoreit, A.A.M. 2017. Biodegradation of natural rubber latex of *Calotropis procera* by two endophytic fungal species. *J. Bioremediat. Biodegrad.*, 8(1): 380.
- Mukherjee, D., Singh, S., Kumar, M., Kumar, V., Datta, S. and Dhanjal, D.S. 2018. Fungal Biotechnology: Role and Aspects. In Gehlot, P. and Singh, J. (ed.), *Fungi and their Role in Sustainable Development: Current Perspectives*, Springer, Singapore, pp. 91-103.
- Nanthini, J. and Sudesh, K. 2017. Biodegradation of natural rubber and natural rubber products by *Streptomyces* sp. strain CFMR 7. *J. Polym. Environ.*, 25(3): 606-616.
- Nanthini, J., Ong, S.Y. and Sudesh, K. 2017. Identification of three homologous latex-clearing protein (lcp) genes from the genome of *Streptomyces* sp. strain CFMR 7. *Gene*, 628: 146-155.
- Nayanashree, G. and Thippeswamy, B. 2013. Natural rubber degradation by *Aspergillus niger* and *Penicillium* sp. *Int. J. Recent Sci. Res.*, 4(9): 1337-1341.
- Oetermann, S., Vivod, R., Hiessl, S., Hogeback, J., Holtkamp, M., Karst, U. and Steinbüchel, A. 2018. Histidine at position 195 is essential for association of Heme-b in Lcp1 VH2. *Earth Syst. Environ.*, 2(1): 5-14.
- Oghenekaro, A.O., Kovalchuk, A., Raffaello, T., Camarero, S., Gressler, M., Henriessat, B., Lee, J., Liu, M., Martínez, A.T., Miettinen, O. and Mihalcheva, S. 2020. Genome sequencing of *Rigidoporus microporus* provides insights on genes important for wood decay, latex tolerance, and interspecific fungal interactions. *Sci. Rep.*, 10(1): 1-5.
- Onyeagoro, G.N., Ohaeri, E.G. and Timothy U.J. 2012. Studies on microbial degradation of natural rubber using dilute solution viscosity measurement and weight loss techniques. *Int. J. Basic Appl. Sci.*, 1(2): 449-460.
- Pathak, V.M. and Navneet, M. 2017. Review on the current status of polymer degradation: A microbial approach. *Bioresour. Bioprocess.*, 4: 15.
- Rahul, D., Risha, K., Bhattacharjee R. and Kumar G. 2018. Isolation of biosurfactant-producing bacteria for oil cleaning from water bodies. *Pollut. Res.*, 37: 166-170.
- Rose, K. and Steinbüchel, A. 2005. Biodegradation of natural rubber and related compounds: recent insights into a hardly understood the catabolic capability of microorganisms. *Appl. Environ. Microbiol.*, 71(6): 2803-2812.
- Rose, K., Tenberge, K.B. and Steinbüchel, A. 2005. Identification and characterization of genes from *Streptomyces* sp. strain K30 responsible for clear zone formation on natural rubber latex and poly (cis-1, 4-isoprene) rubber degradation. *Biomacromolecules*. 6(1): 180-8.
- Röther, W., Austen, S., Birke J. and Jendrossek, D. 2016. Molecular insights in the cleavage of rubber by the latex-clearing protein (Lcp) of *Streptomyces* sp. strain K30. *Appl. Environ. Microbiol.* AEM-02176.
- Schade, A.L. 1937 Observations on a *Monascus* isolated from rubber. *Mycologia*, 29(3): 295-302.
- Schmitt, G., Seiffert, G., Kroneck, P.M., Braaz, R. and Jendrossek, D. 2010. Spectroscopic properties of rubber oxygenase RoxA from *Xanthomonas* sp., a new type of dihaem dioxygenase. *Microbiology*, 156(8): 2537-48.
- Seidel, J., Schmitt, G., Hoffmann, M., Jendrossek, D. and Einsle, O. 2013. Structure of the processive rubber oxygenase RoxA from *Xanthomonas* sp. *Proc. Natl. Acad. Sci.*, 110(34): 13833-13838.
- Shah, A.A., Hasan, F., Shah Z., Kanwal N. and Zeb, S. 2013. Biodegradation of natural and synthetic rubbers: A review. *Int. Biodeterior. Biodegrad.*, 83: 145-157.
- Shah, M.P. (ed.) 2020. *Microbial Bioremediation and Biodegradation*. Springer Nature, Singapore.
- Sharma, V., Siedenburg, G., Birke, J., Mobeen, F., Jendrossek, D. and Prakash, T. 2018. Metabolic and taxonomic insights into the gram-negative natural rubber degrading bacterium *Steroidobacter cummioxidans* sp. nov., strain 35Y. *PloS One*, 13(5): e0197448.
- Sidhu, G.K., Singh, S., Kumar, V., Dhanjal, D.S., Datta, S. and Singh, J. 2019. Toxicity, monitoring and biodegradation of organophosphate pesticides: a review. *Crit. Rev. Environ. Sci. Technol.*, 49(13): 1135-1187.
- Singh, S., Farooq, D. and Thakur, R. 2017. Screening of Natural Rubber Degradation by Fungi: *Aspergillus* and *Phlebia* Sp. and Bacteria *Pseudomonas* and *Streptomyces* sp. *Res. J. Pharm. Technol.*, 10(11): 3939-44.
- Singh, S.K., Khajuria, R. and Kaur, L. 2017. Biodegradation of ciprofloxacin by white-rot fungus *Pleurotus ostreatus*. *Biotech*, 7(1): 69.
- Stevenson, K., Stallwood, B. and Hart, A.G. 2008. Tire rubber recycling and bioremediation: A review. *Bioremediat. J.*, 12(1): 1-11.
- Tsuchii, A. and Takeda, K. 1990. A rubber-degrading enzyme from a bacterial culture. *Appl. Environ. Microbiol.*, 56(1): 269-274.
- Tsuchii, A., Suzuki, T. and Takeda, K. 1985. Microbial degradation of natural rubber vulcanizates. *Appl. Environ. Microbiol.*, 50(4): 965-970.
- Watcharakul, S., Röther W., Birke J., Umsakul K., Hodgson B. and Jendrossek D. 2016. Biochemical and spectroscopic characterization of purified Latex Clearing Protein (Lcp) from newly isolated rubber degrading *Rhodococcus rhodochrous* strain RPK1 reveals novel properties of Lcp. *BMC Microbiol.*, 16(1): 1-3.



- Williams, G.R. 1982. The breakdown of rubber polymers by microorganisms. *Int. Biodetn. Bull.*, 18(2): 31-36.
- Yehia, A.A. 2004. Recycling of rubber waste. *Polym. Plast. Technol. Eng.*, 43(6): 1735-1754.
- Yikmis, M. and Steinbüchel, A. 2012. Historical and recent achievements in the field of microbial degradation of natural and synthetic rubber. *Appl. Environ. Microbiol.*, 78(13): 4543-51.
- Yikmis, M. and Steinbüchel, A. 2012. Importance of the latex-clearing protein (Lcp) for poly (cis-1, 4-isoprene) rubber cleavage in *Streptomyces* sp. K30. *Microbiol. Open*, 1(1): 13-24.
- Yikmis, M., Arenskötter, M., Rose, K., Lange, N., Wernsmann, H., Wiefel, L. and Steinbüchel, A. 2008. Secretion and transcriptional regulation of the latex-clearing protein, Lcp, by the rubber-degrading bacterium *Streptomyces* sp. strain K30. *Appl. Environ. Microbiol.* 74(17): 5373-5382.



# Effects of Submerged Macrophyte Decomposition on Water Quality

Fangbo Zhang\*, Zhiqin Li\*\*, Lei Tang\*, Jingting Wang\*, Chao Shen\*\*\*, Xiaojia He\*\*\*\*, Ran Li\*, Jingjie Feng\*† and Naiwen Li\*\*\*\*\*

\*State Key Laboratory of Hydraulics and Mountain River Engineering, Sichuan University, Chengdu 610065, China

\*\*School of Civil Engineering, Architecture and Environment, Xihua University, Chengdu 610039, China

\*\*\*Chengdu Engineering Corporation Limited, Power China, Chengdu 610041, China

\*\*\*\*College of Water Resource and Hydropower, Sichuan University, Chengdu 610065, China

†Corresponding author: Jingjie Feng; fengjingjie@scu.edu.cn

## Nat. Env. & Poll. Tech.

Website: [www.neptjournal.com](http://www.neptjournal.com)

Received: 20-07-2021

Revised: 25-09-2021

Accepted: 04-10-2021

## Key Words:

Submerged macrophytes

Decomposition

Nutrient release

Aquatic ecological restoration

## ABSTRACT

Submerged macrophytes play an important role in aquatic ecosystems and are widely used in aquatic ecological restoration. However, when submerged macrophytes fade, litter, or even decompose, they may cause adverse effects on water quality. In this article, indoor experiments were carried out to study the quantitative influence of submerged plant decomposition on water quality. Six submerged macrophytes commonly used in aquatic ecological restoration in Sichuan Province, including *Elodea canadensis* Michx., *Potamogeton wrightii* Morong, *Potamogeton crispus* L., *Vallisneria spirulosa*, *Ceratophyllum demersum* L., and *Potamogeton pectinatus* L., were selected to measure the change processes of nutrients during macrophyte decomposition at 10°C, 20°C and 30°C. The results showed that the decomposition of submerged plants released nutrients into the water body, causing water pollution. At 10°C, the total phosphorus (TP) concentration of water bodies containing submerged plant litter increased by 1.97 to 5.97 times on the 50th day compared to the 5th day, while the TP concentration of the blank control group without hydrophytes decreased from 0.39 mg.L<sup>-1</sup> to 0.22 mg.L<sup>-1</sup> due to self-purification. The ammonia nitrogen (NH<sub>3</sub>-N) concentration increased by 3.82-9.58 times on the 50th day compared with the 5th day, while the value in the blank control group decreased from 1.42 mg.L<sup>-1</sup> to 0.78 mg.L<sup>-1</sup>. This result indicated that the water body had a certain self-purification ability, but the decomposition of aquatic macrophytes had a negative impact on this progress. Increasing temperatures could accelerate plant decay processes. Initially, the concentrations of NH<sub>3</sub>-N and TP were high with high temperatures. After 45 days of reaction, the NH<sub>3</sub>-N and TP concentration in the water bodies appeared to be 30°C < 20°C < 10°C, indicating that decomposition was further advanced when the temperature was higher. This study provides a theoretical basis for water ecological management and water quality protection.

## INTRODUCTION

Submerged macrophytes, which are important parts of shallow lake ecosystems, play a crucial role in material circulation and abiotic and biotic processes in shallow lakes and are effective measures used to repair water pollution (Gao et al. 2017, Wang et al. 2018). However, a large amount of organic matter and nutrients can be released into the water column when submerged plants decay, a process in which plant tissues are broken down and discharged, causing the dissolved oxygen in the water to decrease, even forming black and odorous water (Zhang et al. 2018, Chen & Wang 2019). Therefore, it is necessary to study the decomposition of aquatic plants to provide scientific guidance for the removal of withered plants in aquatic ecological restoration and the long-term maintenance of water quality.

The decomposition process of aquatic macrophytes is related not only to the nature of the plants but also to

changes in the external environment (Zhou et al. 2018). Factors affecting the decomposition of aquatic macrophytes include plant species, dissolved oxygen, pH, temperature, microorganism species, and nutrient conditions (Liu et al. 2017, Yang et al. 2020). Corstanje et al. (2006) studied the effect of nutrient availability on the decay of aquatic plants, and the results showed that nutrient enrichment increased the decay rate of *Typha latifolia*, while the decomposition of *Cladium jamaicense* was not significant, which indicated that different plant species have different sensitivities to nutrient conditions. Li et al. (2014) simulated the decay process of *Hydrilla verticillata* Royle in Lake Taihu in spring at four biomass levels and found that there was no significant correlation between the decay rate and the initial biomass; however, different carbon: nitrogen (C:N) ratios and carbon forms could affect the concentrations of total nitrogen (TN) and total phosphorus (TP) in the decay process. Passerini et al. (Passerini et al. 2016) studied the de-

composition process of *Eichhornia azurea*, *Eleocharis* sp., and *Salvinia auriculata* and found that oxygen and temperature had a significant effect on decomposition. Compared with anoxic conditions, decomposition was accelerated by 1.25 times under conditions of oxygen availability, while a temperature increase of 10°C accelerated decomposition by 1.35 times. Zhang et al. (2017) conducted experiments to examine the effects of nitrogen enrichment and temperature in the decomposition processes of *Deyeuxia angustifolia* and *Carex lasiocarpa* and found that nitrogen enrichment slowed decomposition at 5°C and 15°C but had neutral or positive effects at 25°C, which suggested that increased temperatures were conducive to the decay process. Grasset et al. (2017) carried out an in situ decomposition experiment and selected three aquatic plants that were decomposed with different nutrient contents in seven wetlands along a nutrient gradient. The results showed that the plant mass loss for competitive and ruderal species was higher, and a higher nutrient content accelerated the decay rate. Yu et al. (2019) studied the decay process of *Zizania latifolia* and found that a large amount of nutrients was released into the overlying water during the experiment, and the nutrient content increased with increasing plant biomass. Due to the limitation of in situ experimental controllability, which is vulnerable to water temperature, water quality, plant biomass, and other experimental conditions, the results are not consistent. Meanwhile, related studies did not use raw water in laboratory experiments, though there are differences between the test results and natural conditions. In addition,

the local dominant plants were selected in previous experiments, which limited the application of the test results in other regions. Furthermore, local dominant plants were used in most experiments, which limited the popularization and application of the achievements in other regions.

Therefore, this paper selected submerged macrophytes commonly used in aquatic ecological restoration in Sichuan Province and conducted experiments with natural raw water to study the impact of aquatic plant decomposition on the C, N, and P of the overlying water under controlled temperature conditions to guide the design, management, and maintenance of submerged macrophytes in local aquatic ecological restoration.

## MATERIALS AND METHODS

Experiments were conducted at the State Key Laboratory of Hydraulics and Mountain River Engineering (SKLH) at the Sichuan University of China. Submerged plants were placed in water columns at specific temperatures for the decomposition experiments. Meanwhile, an experiment was carried out in a water column without submerged macrophytes and used as a blank control group to determine the changes in various water quality indicators in the overlying water.

### Experimental Materials

**Macrophytes:** Six submerged macrophytes, including *Elodea canadensis* Michx., *Potamogeton wrightii* Morong, *Potamogeton crispus* L., *Vallisneria spinulosa*, *Ceratophyllum*



Fig. 1: Submerged macrophytes selected for experiments.

*demersum* L., and *Potamogeton pectinatus* L. were selected as research objects (Fig. 1).

The initial fresh weight was 25 g, and the distribution density of submerged macrophytes in the water column was  $6.25 \text{ g}\cdot\text{L}^{-1}$ . Using nylon bags to conduct decomposition experiments of the submerged macrophytes, large mesh litter bags were considered likely to cause plant decomposition, and litter bags that were 200 mesh in size were selected; the weighed plants into them and immersed in the water column.

**Sampled water:** To ensure the consistency of pollutant characteristics between the experimental water and the natural river water, the Jinjiang River in Chengdu was sampled as the reaction water. The location of the sampling site is shown in Fig. 2.

**Sediment:** In the experiments, the surface sediment of the same reach of the Jinjiang River was collected synchronously with sampled water, and the freshly collected sediment was treated with an 18-mesh screen to remove plant residues and debris. A 10-cm-thick layer of treated sediment was placed at the bottom of the water column as the reaction basis.

## Experimental Device

A plexiglass cylinder with a height of 50 cm and a diameter of 11 cm was selected as the experimental container, where the water column was 4 L, and the thickness of the bottom sediment was 10 cm. Submerged macrophytes were placed in the cylinder to monitor the changes in water quality indicators during the decay process. The experimental device is shown in Fig. 3. To control the experimental temperature conditions, experiments were conducted under conditions of constant temperature and humidity at the laboratory of Sewth-Z-285.

## Setup of Scenarios

Water temperature conditions of  $10^{\circ}\text{C}$ ,  $20^{\circ}\text{C}$ , and  $30^{\circ}\text{C}$  were set. The experimental scenarios are shown in Table 1.

## Methods for Monitoring and Measurement

To comprehensively reflect the changes in water quality during the submerged plant decay process, the water quality detection indexes during the experiments were selected as follows: pH, DO (dissolved oxygen), water temperature,

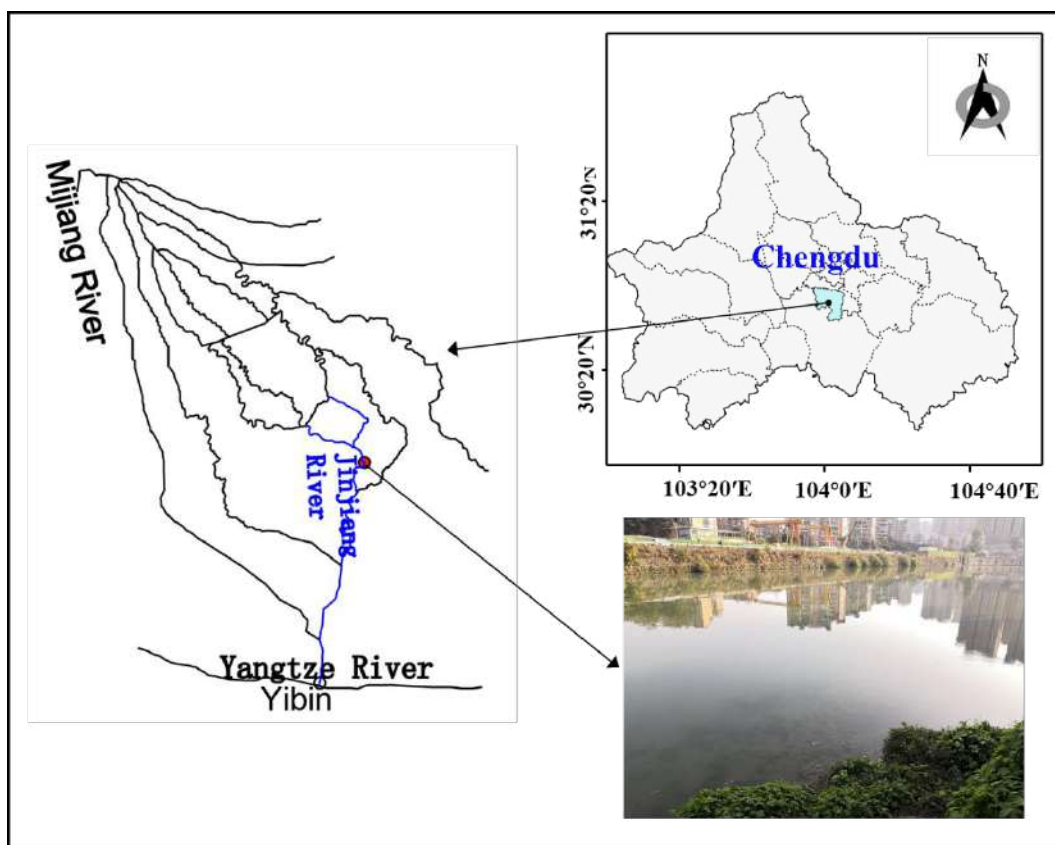


Fig. 2: Location of the sampling site.



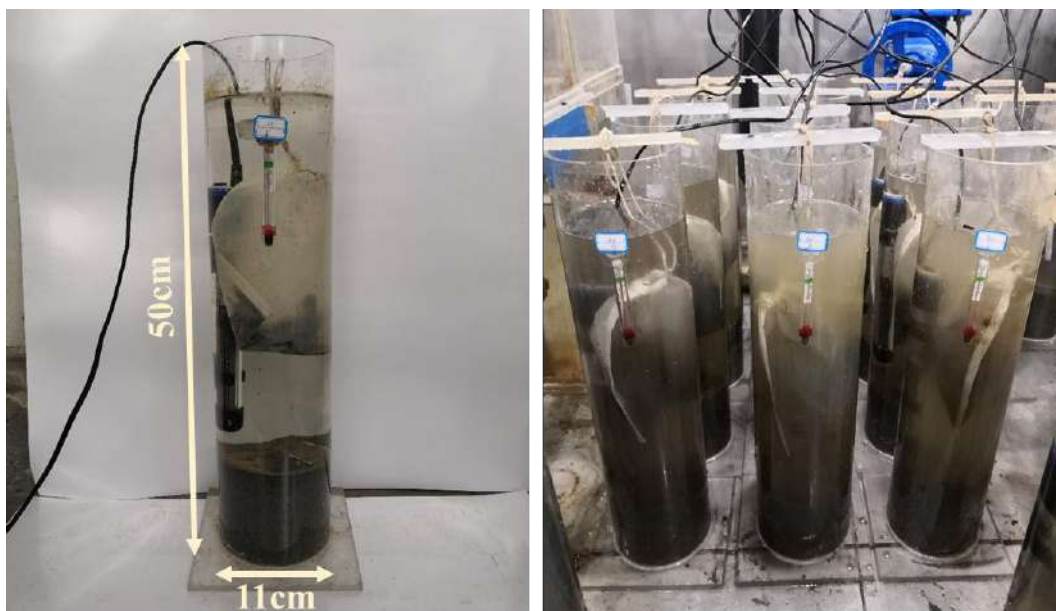


Fig. 3: Experimental device used to study the decomposition of submerged macrophytes.

Table 1: Scenarios of decomposition experiments.

Selected submerged macrophyte	Water temperature [°C]	Name of scenario
<i>Elodea canadensis</i> Michx.	10	10-1
	20	20-1
	30	30-1
<i>Potamogeton wrightii</i> Morong	10	10-2
	20	20-2
	30	30-2
<i>Potamogeton crispus</i> L.	10	10-3
	20	20-3
	30	30-3
<i>Vallisneria spirulosa</i>	10	10-4
	20	20-4
	30	30-4
<i>Ceratophyllum demersum</i> L.	10	10-5
	20	20-5
	30	30-5
<i>Potamogeton pectinatus</i> L.	10	10-6
	20	20-6
	30	30-6
Blank	10	10-0
	30	30-0

Cond (conductivity), SD (Secchi depth; transparency), TOC (total organic carbon), COD (chemical oxygen demand), TP (total phosphorus),  $\text{NH}_3\text{-N}$  (ammonia nitrogen),  $\text{NO}_2\text{-N}$  (nitrite nitrogen), and  $\text{NO}_3\text{-N}$  (nitrate-nitrogen). During the decay process, the wet-weight biomass of submerged plants was measured simultaneously. The measurement methods of each index are shown in Table 2.

## RESULTS AND DISCUSSION

### Biomass of Submerged Macrophytes and Apparent Properties of Water Bodies

As shown in Fig. 4, the biomasses of six submerged plants during the decay process were compared. Different plants had different changes under the same temperature conditions, and the biomass changes of the same plant were also different under different temperatures. At 10°C, the wet-weight biomass of most submerged macrophytes increased after the decay process, which may have been due to the transportation and shelving of experimental plants, in which a great amount of the initial moisture content of plants was lost. After the aquatic plants were placed in the litter bags and decomposed in the water column, the water absorption of the plant residue increased, which led to an increase in the moisture content of the residue in the litter bag. Among all submerged plants, the wet-weight biomass of *Potamogeton pectinatus* L. increased the most, which might have been



Table 2: Determination methods of the decay experiment index.

Monitoring index	Determination method	National standard
pH	Glass electrode method	GB 6920-86
DO	Electrochemical probe method	HJ 506-2009
Water temperature	Thermometer or reversing thermometer method	GB 13195-91
Conductivity	Conductivity metre method	GB/T 6908-2008
SD	Diaphanometer and disc method	SL 87-1994
TOC	Combustion oxidation nondispersive infrared absorption method	HJ 501-2009
COD	Dichromate method	HJ 828-2017
TP	Ammonium molybdate spectrophotometric method	GB 11893-89
NH <sub>3</sub> -N	Nessler's reagent spectrophotometry	HJ 535-2009
NO <sub>2</sub> <sup>-</sup> -N	Diazo-couple spectrophotometry	GB/T 5750.5-2006
NO <sub>3</sub> <sup>-</sup> -N	Thymol spectrophotometry	GB/T 5750.5-2006

due to the strong water absorption and relatively difficult decomposition process. At 20°C and 30°C, after a period of decomposition, the biomass of *Elodea canadensis* Michx. and *Potamogeton crispus* L. both decreased, which may have been related to the temperature difference. Under aerobic conditions, decomposition was independent of temperature variation, and the effect was always antagonistic; however, in anaerobic decomposition, the increase in temperature advanced decomposition (Paccagnella et al. 2020).

As shown in Fig. 5, at the initial state of the experiments, the transparency of most water bodies was poor. In the control

group without submerged plants, the transparency of the water column was greatly improved. Compared with the transparency of water columns under different temperatures, the transparency of water bodies containing submerged plants was already very low at the initial state, which may have been due to the transparency being measured after the experimental water body was stable, in which the soluble organic compounds leached faster, causing the water transparency to decrease (Tamire et al. 2017). The transparency changed slightly except for the groups containing *Potamogeton pectinatus* L., which might have been because *Elodea canadensis*

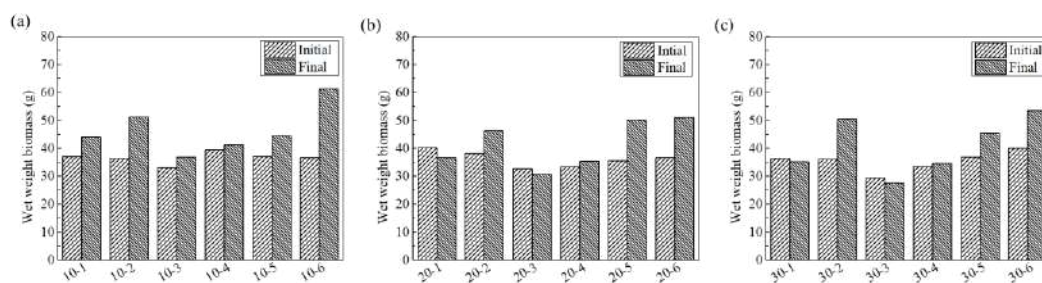


Fig. 4: Comparison of the initial and final states of wet-weight biomass of submerged macrophytes.

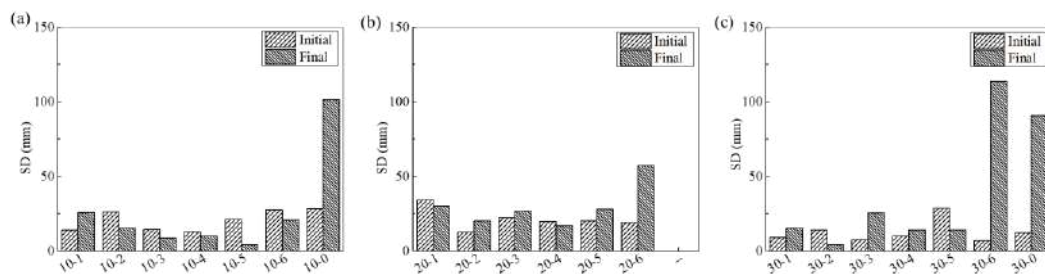


Fig. 5: Comparison of the initial and final states of transparency of the water column.

Michx., *Potamogeton wrightii* Morong, *Potamogeton crispus* L., *Vallisneria spinulosa* and *Ceratophyllum demersum* L. experienced a rapid leaching stage, in which the organic matter was broken and released into the water body; in contrast, *Potamogeton pectinatus* L. was hard to decompose, and its shape was well preserved, so the transparency of the water body was less affected.

### Basic Physicochemical Properties of Water Bodies

As shown in Fig. 6, all of the water bodies were weakly alkaline. At different temperatures, the pH of the water bodies containing submerged plants was 7.2-7.9 in the initial state. After the reaction period, it increased slightly to 7.8-8.5. In general, the pH in all water bodies increased slightly after the reaction, which might have been due to hydrogen ions produced by nitrification reacting with carbonic acid, which caused the pH value to rise, leading to the pH of the final state being slightly higher than that the initial state. Because nitrifying bacteria can remain active in a pH range of 6.5-8.5 (Tyson et al. 2004), the pH of all water bodies was conducive to the progress of nitrification.

Conductivity is a measure of the ability of a substance or solution to conduct electrical current through water, and this value can reflect the concentration of dissolved inorganic salts and be used as a basis for the determination of water quality (Gupta et al. 2013). As shown in Fig. 7, the conductivity of the water bodies containing submerged plants was between 456-584  $\mu\text{S}$  in the initial state and increased to 615-

953  $\mu\text{S}$  in the final state. Under the same water temperature conditions, there was no significant difference in the conductivity of each group of water bodies containing submerged plants, but there was an obvious difference under different water temperature conditions, indicating that the conductivity may be more susceptible to the influence of temperature than to the difference in plant species. The higher the temperature was, the faster the conductivity increased, and the maximum increase in conductivity was observed at 30°C.

DO is an important indicator in water bodies and can directly reflect their state. As shown in Fig. 8, at 10°C, the DO value of the water bodies containing submerged plants was severely anoxic, with a DO value of 0.40-4.21 mg/L, and the DO value of all water bodies was very low in the final state. At 30°C, the DO concentration of the water bodies containing *Elodea canadensis* Michx., *Potamogeton crispus* L., *Vallisneria spinulosa*, and *Potamogeton pectinatus* L. was lower, which indicated that the increase in temperature promoted decomposition. In the final state, the DO concentration of water bodies was lowest at 10°C. The DO concentration of water bodies at 20°C and 30°C was slightly higher than that at 10°C, which might have been due to the slower decay of submerged plants at 10°C, causing the decay process at 10°C to lag behind that at 20°C and 30°C. It can be seen from the DO concentration of various water bodies under different temperatures that water bodies containing submerged plants had already experienced serious oxygen consumption in the initial state, and the low dissolved oxygen concentration of

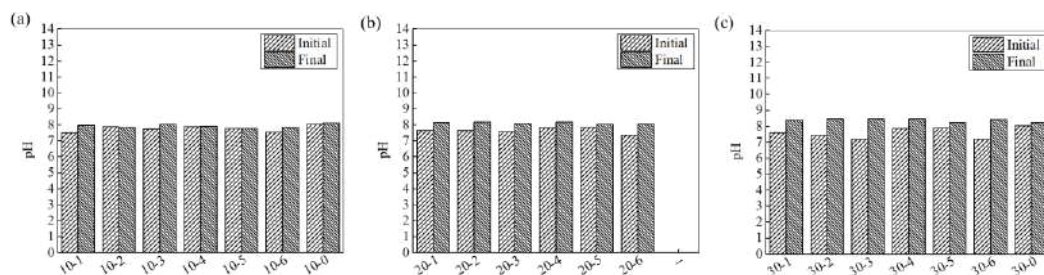


Fig. 6: Comparison of the initial and final states of the pH values of the water bodies.

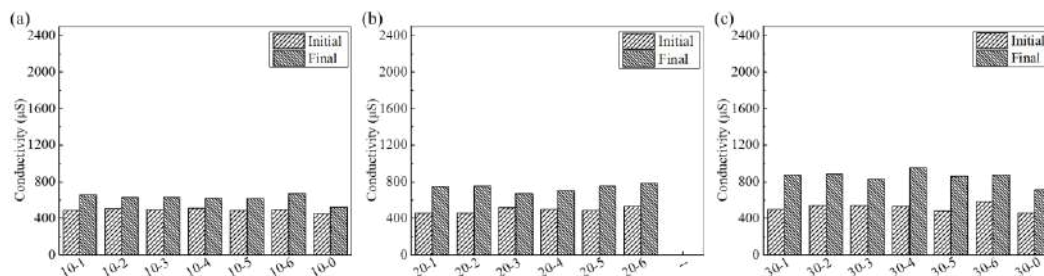


Fig. 7: Comparison of the initial and final states of conductivity of water bodies.

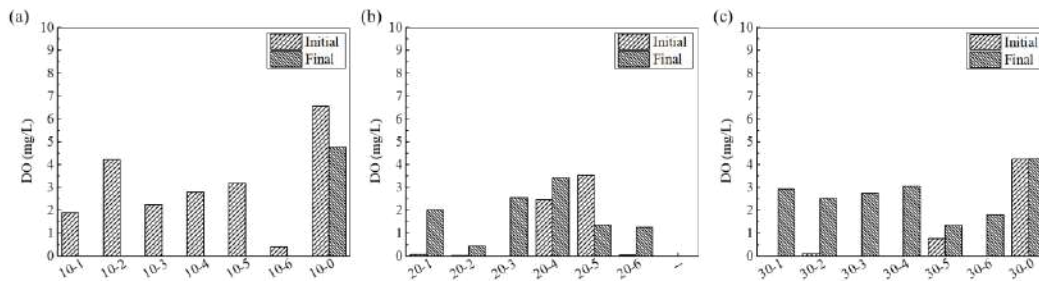


Fig. 8: Comparison of the initial and final states of the DO concentration of water bodies.

the water body caused by oxygen consumption might have induced the black and odorous water.

### Contents of C, N and P in Water Bodies

As shown in Fig. 9, compared with the control group, the COD concentration of water bodies containing submerged plants did not increase significantly at 10°C, which might have been due to the slow decay process and the mild release of organic matter under this water temperature. At 20°C and 30°C, the COD concentration of the water bodies containing submerged plants increased after decomposition. In the initial stage, a large amount of soluble substances in the plant residues dissolved quickly, which led to an increase in organic matter and other reducing substances in the water body. As the decay process continued, the dissolved oxygen in the water body was consumed and decreased to a low degree,

which might have inhibited the decomposition of organic matter; additionally, the increase in the DO concentration in the later period would increase the degradation of organic matter (Wu et al. 2017). Thus, the overall COD concentration showed a trend of first increasing and then slowly decreasing.

Fig. 10 shows the total organic carbon (TOC) concentrations of all groups in the initial and final states. In the initial state, the TOC concentration of water bodies under different temperatures was as follows: 10°C > 20°C > 30°C. In the final state, the TOC concentrations of water bodies under different temperatures had only small differences. In the early period of decomposition, the dissolution of soluble organic carbon in the plant residues led to a rapid increase in the TOC concentration, and then, due to the degradation of microorganisms, it gradually decreased. After some time, sparingly soluble substances appeared in the decomposition process,

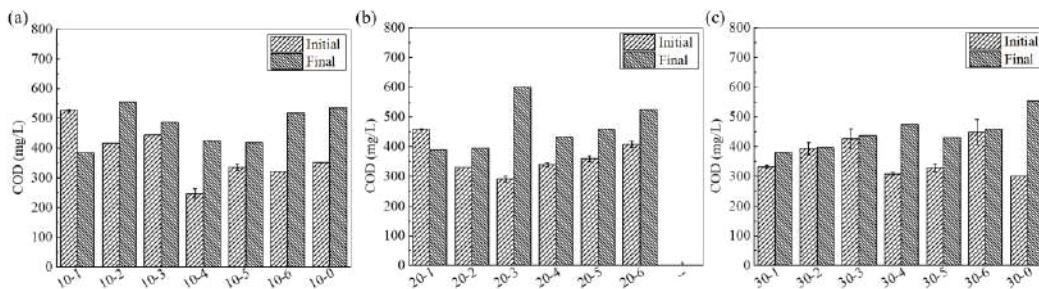


Fig. 9: Comparison of the initial and final states of the COD concentration of water bodies.

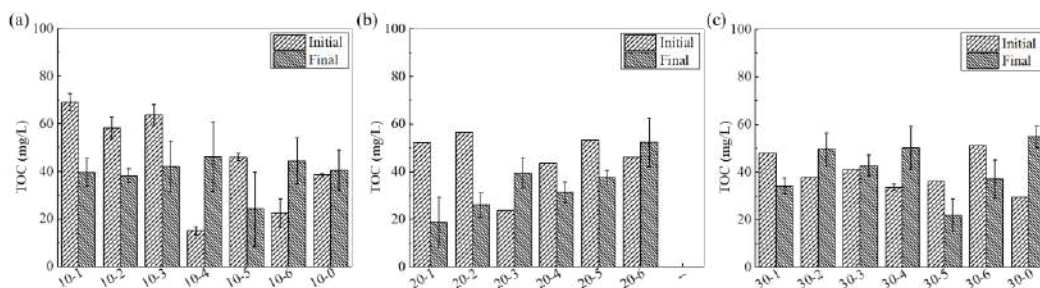


Fig. 10: Comparison of the initial and final states of the TOC concentration of water bodies.



and the TOC concentration in the water bodies tended to be stable. Since the initial state of the experiments measured in this article had already experienced the reaction for 5 days, the TOC concentration in water bodies had reached a high concentration, and the increased temperature accelerated the degradation of organic matter. Thus, the experiments had already reached the next stage in the 20°C and 30°C conditions, so the TOC concentrations of all water bodies appeared higher in the initial state at 10°C. Because the decay process had progressed to a stable stage in the final state, there was no significant difference in the TOC concentration of all groups at different temperatures.

Fig. 11 shows that the  $\text{NH}_3\text{-N}$  concentration in water bodies in the final state was significantly higher than that in the initial state, and the  $\text{NH}_3\text{-N}$  concentration in water bodies under different temperatures showed different changes. In the initial state of decomposition, the concentration of all groups

showed a trend of having a higher temperature and a higher initial concentration, that is, 30°C > 20°C > 10°C. However, after 45 days of reaction, the  $\text{NH}_3\text{-N}$  concentration in all water bodies was as follows: 30°C < 20°C < 10°C. In the initial stage of the decay process, the leaching and mineralization of organic nitrogen led to a rapid increase in the  $\text{NH}_3\text{-N}$  concentration in the water bodies, which was subsequently affected by nitrification and gradually decreased (Huang et al. 2017). In the initial state, the  $\text{NH}_3\text{-N}$  concentration in the water bodies was higher when the temperature was higher, which was caused by the increased water temperature promoting nutrient release. After the reaction proceeded for some time, the  $\text{NH}_3\text{-N}$  concentration of the water bodies under low temperature was greater than that under higher temperature, which might have been because the low temperature caused a slower decay rate, delaying the release of  $\text{NH}_3\text{-N}$  caused by aquatic plant decomposition.

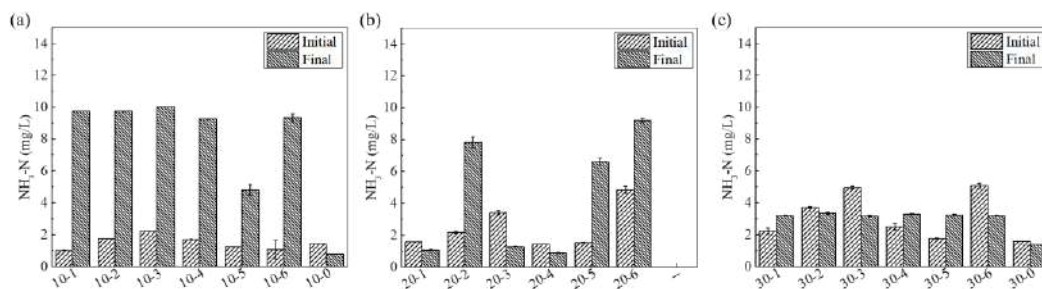


Fig. 11: Comparison of the initial and final states of the  $\text{NH}_3\text{-N}$  concentration of water bodies.

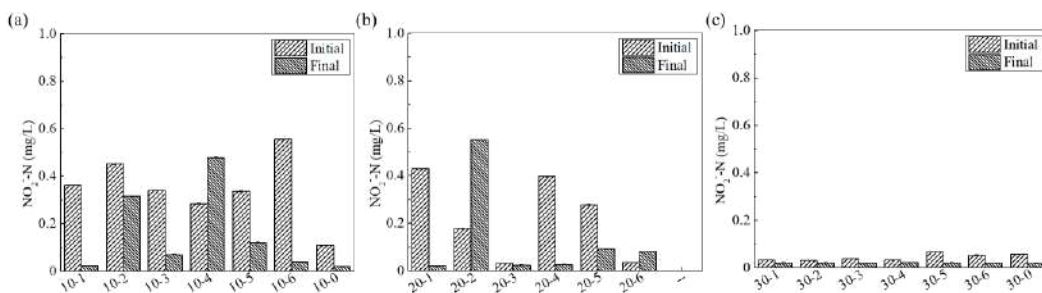


Fig. 12: Comparison of the initial and final states of the  $\text{NO}_2\text{-N}$  concentration of water bodies.

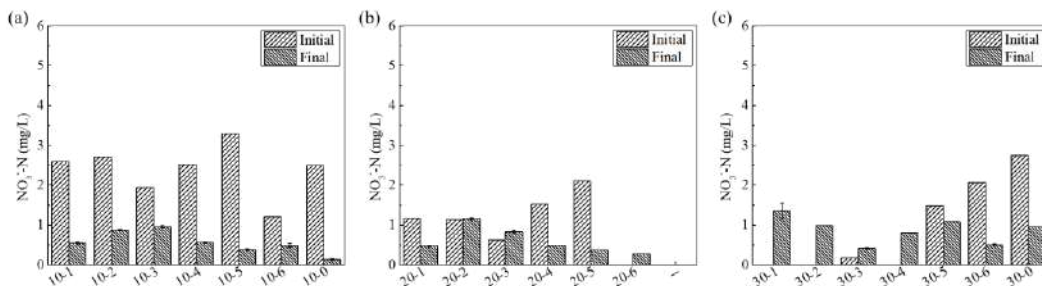


Fig. 13: Comparison of the initial and final states of the  $\text{NO}_3\text{-N}$  concentration of water bodies.

The  $\text{NO}_2^-$ -N concentration of water bodies under different temperatures showed a trend in which the final state had a lower concentration than the initial state (Fig. 12). At  $10^\circ\text{C}$ , the  $\text{NO}_2^-$ -N concentration in water bodies was 0.11-0.56 mg/L in the initial state, except when it increased in the water bodies containing *Vallisneria spinulosa*; however, in the other groups, the value decreased to 0.02-0.32 mg/L after 45 days of reaction. At  $20^\circ\text{C}$ , the  $\text{NO}_2^-$ -N concentration in the water bodies was 0.03-0.43 mg/L in the initial state, except when it increased in the water bodies containing *Potamogeton wrightii* Morong; however, in the other groups, the value decreased to 0.02-0.09 mg/L in the final state. At  $30^\circ\text{C}$ , the  $\text{NO}_2^-$ -N concentration of water bodies was 0.03-0.07 mg/L in the initial state and decreased to approximately 0.02 mg/L in the final state.

The variation in the  $\text{NO}_3^-$ -N concentration in water bodies under different temperatures was different (Fig. 13). At  $10^\circ\text{C}$ , the  $\text{NO}_3^-$ -N concentration of the water bodies was 1.20-3.29  $\text{mg}\cdot\text{L}^{-1}$ , and it significantly decreased to 0.13-0.95  $\text{mg}\cdot\text{L}^{-1}$  in the final state. At  $20^\circ\text{C}$ , the  $\text{NO}_3^-$ -N concentration of the water bodies containing submerged plants was lower than that at  $10^\circ\text{C}$  in the initial state. Except for the increase in  $\text{NO}_3^-$ -N concentration in the water bodies with *Ceratophyllum demersum* L. and *Potamogeton pectinatus* L., the values in the water bodies with the other species all decreased. At  $30^\circ\text{C}$ , the  $\text{NO}_3^-$ -N concentrations of the water bodies containing *Elodea canadensis* Michx., *Potamogeton wrightii* Morong, and *Vallisneria spinulosa* were all low, and the  $\text{NO}_3^-$ -N concentrations of the water bodies containing these three types of submerged plants and *Potamogeton crispus* L. increased in the final state.

The  $\text{NO}_2^-$ -N and  $\text{NO}_3^-$ -N concentrations in water bodies both declined, which might have been due to the nitrogen element in the water body and the sediment transformation from nitrogen to  $\text{N}_2\text{O}$ ,  $\text{N}_2$ , and other gases that escaped under the combination of ammonification, nitrification, and denitrification, resulting in the contents of  $\text{NO}_2^-$ -N and  $\text{NO}_3^-$ -N being lower in the final state than in the initial state.

The variation in the nitrate concentration was significantly related to temperature, and denitrification was inhibited under low temperatures; additionally, an increase in temperature was conducive to the progress of denitrification (Song et al. 2013). Thus, the nitrate concentration of water bodies was lower when the temperature was higher in the final state.

Fig. 14: Comparison of the initial and final states of the TP concentration of water bodies shows the comparison of the TP concentration in the initial and final states. At  $10^\circ\text{C}$ , the TP concentration in water bodies in the initial state was 0.34-0.53  $\text{mg}\cdot\text{L}^{-1}$ , except when the value decreased in the control group; in the remaining groups, the TP concentration increased to 0.90-3.14  $\text{mg}\cdot\text{L}^{-1}$  in the final state. At  $20^\circ\text{C}$ , the TP concentration in the water bodies containing submerged plants was 0.38-1.23  $\text{mg}\cdot\text{L}^{-1}$  in the initial state and increased to 0.77-2.14  $\text{mg}\cdot\text{L}^{-1}$  in the final state. At  $30^\circ\text{C}$ , the TP concentration of the control group and that in the water bodies containing *Potamogeton crispus* and *Potamogeton wrightii* Morong decreased in the final state. In the early period of decomposition, the amount of P released from the plant residues to the water bodies increased rapidly, reaching a maximum after approximately 15 days, and then sedimentation occurred with an increase in time, resulting in a gradual decrease in the P concentration (Wang et al. 2018). The TP concentration of the control group in the final state was lower than that in the initial state, which might have been due to the sedimentation and transformation of TP in the absence of nutrient inputs, resulting in a decrease in the TP concentration. The TP concentration in the water bodies containing submerged plants increased in the final state, which might have been caused by the decomposition of submerged plants releasing P nutrients into the water bodies, increasing the TP concentration.

### Uncertainty of Results

During the experiment, high-frequency continuous monitoring of the water quality change process was not conducted, and precise quantitative monitoring and descriptions of the

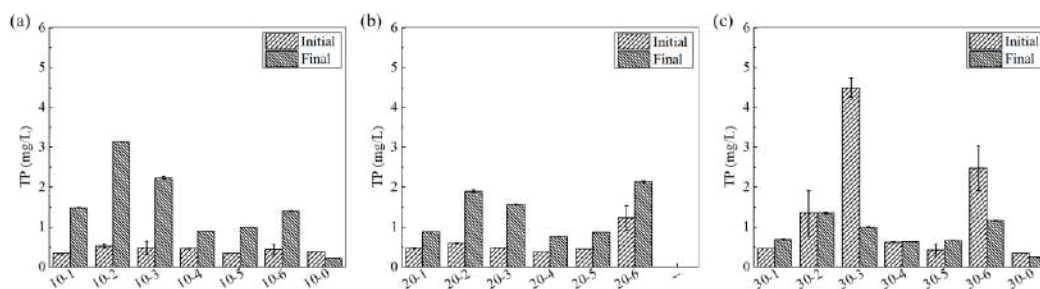


Fig. 14: Comparison of the initial and final states of the TP concentration of water bodies.



variations in some black and odorous indexes in the reaction process were not yet available.

This article measured the changes in water quality indicators during decomposition but did not consider the changes in various indicators in plant tissues and sediments. In the future, we will systematically study the cyclic transformation of substances in complex water-plant-sediment systems and add special monitoring and research on odor-causing factors to further analyze the impact of the plant decay process on the environment.

## CONCLUSION

In this article, six submerged plants commonly used in aquatic ecological restoration in Sichuan Province, including *Elodea canadensis* Michx., *Potamogeton wrightii* Morong, *Potamogeton crispus* L., *Vallisneria spirulosa*, *Ceratophyllum demersum* L., and *Potamogeton pectinatus* L., were selected to conduct decomposition experiments under different temperature conditions.

The results showed that (1) the decomposition of submerged plants could release nutrients into water bodies. The TP concentration of the water bodies containing submerged plants at 10°C increased by 1.97-5.97 times on the 50th day compared with the 5th day, while the control group decreased from 0.39 mg.L<sup>-1</sup> to 0.22 mg.L<sup>-1</sup>. The NH<sub>3</sub>-N concentration of the water bodies containing submerged plants increased by 3.82-9.58 times on the 50th day compared with the 5th day, while the control group decreased from 1.42 mg.L<sup>-1</sup> to 0.78 mg.L<sup>-1</sup>, which showed that the water body had a self-purification ability, but the decomposition of aquatic plants changed the self-purification ability of the water body, causing pollution. (2) The increase in temperature accelerated the decay processes of aquatic plants. In the final stage, the decay process was promoted by increasing the temperature. When the temperature was higher, the decomposition of aquatic plants progressed to a later stage, and the water quality was worse under lower temperatures.

## ACKNOWLEDGEMENTS

This work was supported by the Sichuan Science and Technology Program (Grant No. 2019YFS0505, 2018JY0598).

## REFERENCES

- Chen, S. and Wang, D. 2019. Responses of decomposition rate and nutrient release of floating-leaved and submerged aquatic macrophytes to vertical locations in an urban lake (Nanhu Lake, China). *Chem. Ecol.*, 35(5): 431-444.
- Corstanje, R., Reddy, K.R. and Portier, K.M. 2006. *Typha latifolia* and *Cladium jamaicense* litter decay in response to exogenous nutrient enrichment. *Aquat Bot.*, 84(1): 70-78.
- Gao, H., Qian, X., Wu, H., Li, H., Pan, H. and Han, C. 2017. Combined effects of submerged macrophytes and aquatic animals on the restoration of a eutrophic water body: A case study of Gonghu Bay, Lake Taihu. *Ecol. Eng.*, 102: 15-23.
- Grasset, C., Levrey, L.H., Delolme, C., Arthaud, F. and Bornette, G. 2017. The interaction between wetland nutrient content and plant quality controls aquatic plant decomposition. *Wetl. Ecol. Manag.*, 25(2): 211-219.
- Gupta, N., Yadav, K.K., Kumar, V. and Singh, D. 2013. Assessment of physicochemical properties of Yamuna River in Agra City. *Int. J. Chem. Research.*, 5(1): 528-531.
- Huang, J., Zhou, W., Gu, J., Wu, S., Gao, M. and Lei, M.. 2017. Decomposition of emergent aquatic plant (Cattail) litter under different conditions and the influence on water quality. *Water Air Soil Poll.*, 65:111-121
- Li, C., Wang, B., Ye, C. and Ba, Y. 2014. The release of nitrogen and phosphorus during the decomposition process of submerged macrophytes (*Hydrilla verticillata* Royle) with different biomass levels. *Ecol. Eng.*, 70: 268-274.
- Liu, G., Sun, J., Tian, K., Xiao, D. and Yuan, X. 2017. Long-term responses of leaf litter decomposition to temperature, litter quality, and litter mixing in plateau wetlands. *Freshwater Biol.*, 62(1): 178-190.
- Paccagnella, Y.C., Bianchini, I. and Da Cunha-Santino, M.B. 2020. Decomposition dynamics of two aquatic macrophytes: response of litter interaction with temperature and dissolved oxygen availability. *Braz. J. Bot.*, 6: 1-13.
- Passerini, M.D., Cunha-Santino, M.D. and Bianchini, I. 2016. Oxygen availability and temperature as driving forces for decomposition of aquatic macrophytes. *Aquat Bot.*, 130: 1-10.
- Song, N., Yan, Z., Cai, H. and Jiang, H. 2013. Effect of temperature on submerged macrophyte litter decomposition within sediments from a large shallow and subtropical freshwater lake. *Hydrobiologia*, 714(1): 131-144.
- Tamire, G., Mengistou, S. and Degefe, G. 2017. Decomposition rates and nutrient Leaching efficacy of the Dominant Macrophytes in Lake Ziway, Ethiopia. *Int. J. Aqua. Sci.*, 8(2): 96-106.
- Tyson, R.V., Simonne, E.H., White, J.M. and Lamb, E.M. 2004. Reconciling Water Quality Parameters Impacting Nitrification in Aquaponics: The pH levels. *Proceedings of the Florida State Horticultural Society*, 6-8 June 2004, Florida, USA, Florida State Horticultural Society, Goldenrod, USA, pp. 79-83.
- Wang, L., Liu, Q., Hu, C., Liang, R., Qiu, J. and Wang, Y. 2018. Phosphorus is released during the decomposition of the submerged macrophyte *Potamogeton crispus*. *Limnology*, 19 (3): 355-366.
- Wu, X., Qi, C., Xu, X., Zhou, Y., Wang, M. and Wang, G. 2017. Simulation of cyanobacteria decay's impacts on nutrients in the water. *Acta Sci Circumst.*, 37: 2846-2853.
- Yang, Y., Wang, J., Wang, Y. and He, Z. 2020. The biomass decay rate and influencing factors of four submerged aquatic vegetation in Everglades wetland. *Int J Phytoremediat.*, 22 (9): 963-971.
- Yu, C., Shi, C., Tang, J., Ji, Q., Wang, X., Xu, X. and Wang, G. 2019. Release of taste and odor compounds during *Zizania latifolia* decay: A microcosm system study. *Environ Pollut.*, 254: 112954.
- Zhang, L., Zhang, S., Lv, X., Qiu, Z., Zhang, Z. and Yan, L. 2018. Dissolved organic matter released in overlying water and bacterial community shifts in biofilm during the decomposition of *Myriophyllum verticillatum*. *Sci. Total Environ.*, 633: 929-937.
- Zhang, X., Sun, X. and Mao, R. 2017. Effects of litter evenness, nitrogen enrichment, and temperature on short-term litter decomposition in freshwater marshes of Northeast China. *Wetlands*, 37(1): 145-152.
- Zhou, X., Feng, D., Wen, C. and Liu, D. 2018. Decomposition dynamic of two aquatic macrophytes *Trapa bispinosa* Roxb. and *Nelumbo nucifera* detritus. *Environ. Sci. Pollut. Res.*, 25(16): 16177-16191.



# Assessment of Drinking Water Accessibility and Quality in the Indo-Bhutan Himalayan Foothill Region of Assam, India

S. Saha\*†, A. K. Bhagabati\* and R. Thakur\*\*

\*Department of Geography, Gauhati University, Guwahati, Assam

\*\*North Eastern Regional Institute of Water and Land Management, Tezpur, Assam

†Corresponding author: S. Saha; [sourav.saha626@gmail.com](mailto:sourav.saha626@gmail.com)

## Nat. Env. & Poll. Tech.

Website: [www.neptjournal.com](http://www.neptjournal.com)

Received: 07-07-2021

Revised: 12-10-2021

Accepted: 22-10-2021

### Key Words:

Himalayan foothill  
Drinking water  
Water Accessibility  
Water quality index

## ABSTRACT

Despite fairly heavy rainfall, the Bhutan Himalayan foothill region of Assam has been facing serious water scarcity problems mainly due to the subsurface structure and soil condition. The local people of the region with their community efforts and traditional knowledge have developed a water management system locally known as Dong-bandh. This traditional canal water system provides the most reliable source of water to the people residing in the area. Besides the canals, they also collect water from the streams, natural springs, and wells. The quality of water is getting deteriorated over time under the influence of the growing population and their activities in the upstream areas. The present study is an attempt to investigate the status of water accessibility in the area and the quality of the drinking water used by the people. For this study, data and information have collected through field investigation, GPS survey, focus group discussion, and interviews with some key informants. A total of 14 drinking water samples were collected randomly from 14 foothill villages (both from the ground and surface) and tested to determine various physiochemical characteristics. The results were compared with the WHO and BIS/ICMR water quality standards. Finally, the status of water quality was analyzed in terms of the Water Quality Index (WQI). The WQI values were found to lie between 21.75 to 502.38.

## INTRODUCTION

Easy availability and accessibility of safe drinking water are not only the pre-requisite for preventing diseases but also for improving the economic condition and quality of life (Khound & Bhattacharyya 2018, Nabila et al. 2014, Rawal et al. 2018, Rickert et al. 2016). United Nations (Sustainable Development Goal 6.1) make a target to achieve universal and equitable access to safe and affordable drinking water facilities by 2030. But still, billions of people across the world have been suffering from a lack of safe and adequate drinking water supply (Mandour 2012). According to an estimate, there were 2.2 billion people throughout the world without safely managed drinking water in 2017, out of which 144 million people used surface water (UNICEF & WHO 2019). The condition is more acute in highly populated countries like India where more than 163 million people still do not have clean and safe drinking water. The people in the Himalayan region have been primarily using surface water and natural spring for their drinking purposes (Sharma et al. 2005). However, the water quality is deteriorating currently due to the rapid population growth, deforestation, and expansion of agriculture, industries, and other anthropogenic activities (Effendi 2016, Mir et al. 2019, Sabha et al. 2019, Seth et al. 2016). Therefore, the assessment of water quality

has become a matter of concern in recent times for ensuring a safe drinking water supply and reduction of water-borne diseases (Ameen 2019).

Like other people of the Himalayan states in India, the local communities in the Bhutan Himalayan foothill region of Assam also mainly depend on surface water for their survival. The indigenous communities of this region have invented a traditional canal water management system, locally called the *dong-bandh* system. They have diverted the river/stream water by putting small check dams and canalizing into their villages through earthen canals, called *dong*. These century-old traditional donges have been used as the principal source of drinking water in the entire Bhutan Himalayan foothill region of the State (Saha et al. 2020). In the recent past, few community wells have been constructed by the government in some villages. But the construction of a dug well or tube well is very difficult due to rocky underground sub-surface and very low level of groundwater. Construction of dug well is also very costly; therefore, the individual households cannot effort such costs. Very recently, the government has also installed a deep tube well and water tank locally called 'pani tanki' in the villages of this area. But the number of deep tube wells is not sufficient. Only one deep tube well was installed in some villages against every 50-120

households. However, this initiative of the government has reduced the drinking water supply problems of this area to some extent. However, many of the government-supported wells and tube wells have become defunct. Therefore, many villages along the Himalayan foothill zone still depend on man-made canals, natural springs, small streams, and rivers. Although few research works on the water management system of this region were done, the issues of drinking water accessibility and quality were not addressed in any one of these works. Therefore, the present study has been carried out to know the status of drinking water accessibility and quality in this foothill region.

## BACKGROUND OF THE STUDY AREA

This study has been carried out in the Bhutan Himalayan foothill region of the Baksa district in Assam, India. The study area lies along the Indo-Bhutan border extending from 26°42'11" N to 26°49'57" N latitude and from

91°4'39" E to 91°44'20" E longitude (Fig. 1). The area encompasses a geographical area of 513.25 sq. km. with a population of 204381 as per the 2011 Census. The area is located between the Shiwalik Himalayan range on the north and the floodplain zone of the mighty Brahmaputra river on the south; Barnadi Wildlife Sanctuary on the east and Manas National Park on the west. The average elevation of the area varies between 350m and 70m. The region is crisscrossed by several perennial and ephemeral streams and is covered with dense forests. It receives heavy rain during the monsoon season (June- September). The average annual rainfall of the area is 2971.6 mm and the average monthly rainfall during monsoon ranges between 568.15 mm and 274.16 mm. The people of this area, however, face major water scarcity difficulties, particularly during the winter and pre-monsoon season, due to heavy deposition of coarse sediments due to the sharp fall in gradient and the sub-surface flow of channel water due to high porosity of sediments (Saha et al. 2021).

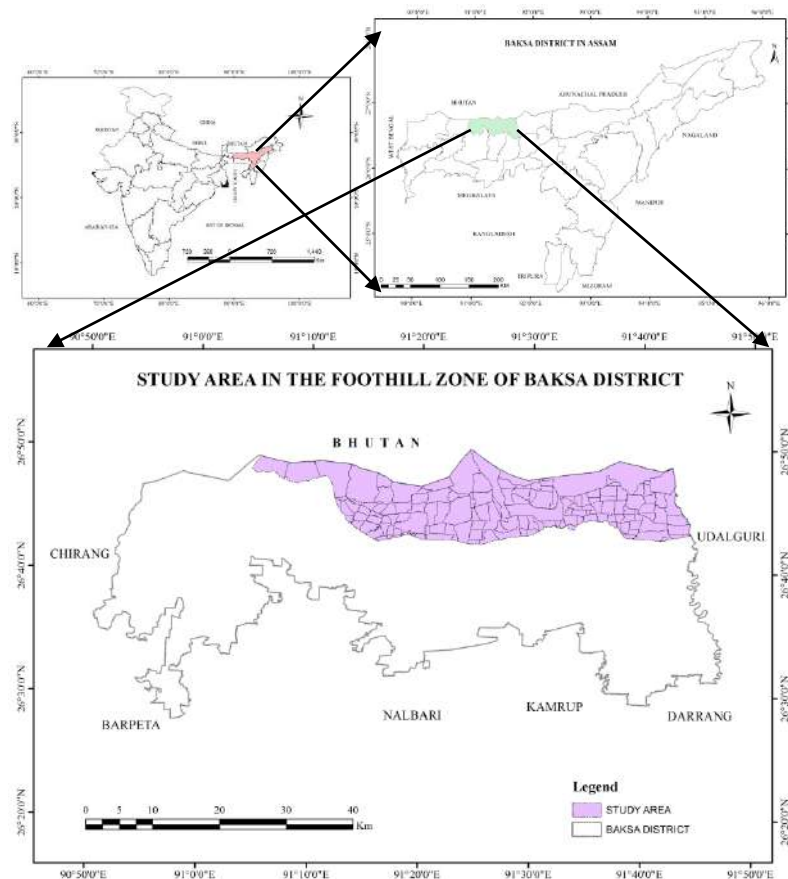


Fig. 1: Location of the study area.

**MATERIALS AND METHODS**

The study has been carried out in two different stages. First, personal field observation has been performed throughout the area in different seasons. After getting a general idea about the area, a total of 17 villages were selected randomly. One drinking water source from each village has been selected for collecting different information such as location, household dependency, management system, seasonal variation of water availability, and nature of water collection. PRA, focus group discussion (FGD), and interviews with the key informants and stakeholders were conducted to understand the status of drinking water availability and accessibility in the area.

In the second stage, we try to investigate the quality of drinking water. To study the status of water quality, 14 water samples (S1-S14) from both ground, as well as surface water, were collected from 14 randomly selected villages. The samples were collected during the pre-monsoon season. The water samples were collected in 1L high-density polyethylene bottles. Before collecting the sample, the bottles were rinsed thrice with the sample water (APHA AWWA and WEF 1992). Surface water samples were collected from the center of the canals at 1/3<sup>rd</sup> depth from the surface water level where the velocity was sufficiently high (Khound & Bhat-tacharyya 2018). Two sets of samples were collected from each sample location. Untreated raw water was collected first and the second was acidified with nitric acid. Then the bottles were labeled with sample numbers and place names. The

geographical coordinates of each sample site were recorded with GPS (GARMIN-GPSMAP 64s) (Table 1). Finally, the collected water samples were transported to the Northern Eastern Regional Institute of Water and Land Management (NERIWALM) in Tezpur, Assam (India) for analysis.

**Measurement of Parameters**

Selected parameters were measured for all the samples. The pH, electric conductivity, total dissolved solids (TDS), salinity, dissolved oxygen (DO), and turbidity were measured by using a water analyzer. The instrument was calibrated with standard solutions as per the Systronic Water Analyser 371 manual. The concentrations of sulfate and phosphate were determined by using a UV-Visible spectrophotometer. The amount of calcium, magnesium, chloride (Cl<sup>-</sup>), total alkalinity, and total hardness were estimated by using titration. All the measurement was carried out in triplicate to minimize the errors. The concentration of iron, lead, cadmium, chromium, and arsenic was measured directly by using Atomic Absorption Spectrophotometer (AAS). All the measured parameters were analyzed and compared with standard limits of the Bureau of Indian Standards (BIS), Indian Council of Indian Medical Research (ICMR) and the World Health Organization (WHO) for drinking water quality. Finally, the water quality index (WQI) has been calculated by adopting the ‘weighted arithmetic index method’ (Brown et al. 1970).

$$WQI = \sum Q_n W_n / \sum W_n$$

Table 1: Water sample collection sites.

Location	Village name	Coordinate		Elevation(M)	Types
		Latitude	Longitude		
S1	Dihira	26° 44' 17.49'' N	91° 21' 26.64'' E	86	Surface
S2	Chaulkara	26° 45' 38.27'' N	91° 24' 6.38'' E	124	Ground
S3	Uttarkuchi	26° 46' 47.50'' N	91° 25' 32.28'' E	123	Ground
S4	No.1 Paharpur	26° 47' 42.96'' N	91° 26' 55.98'' E	149	Surface
S5	Jharbasti	26° 46' 18.54'' N	91° 26' 46.31'' E	124	Surface
S6	Moithabari	26° 43' 37.96'' N	91° 26' 21.26'' E	106	Ground
S7	Hatiduba	26° 45' 51.06'' N	91° 30' 26.62'' E	94	Ground
S8	Ganeshguri	26° 46' 32.20'' N	91° 33' 00.74'' E	165	Surface
S9	Unthaibari	26° 47' 44.28'' N	91° 35' 29.90'' E	180	Surface
S10	Manjurgaon	26° 48' 13.15'' N	91° 37' 30.02'' E	153	Surface
S11	No. 1 Dongargaon	26° 48' 4.78'' N	91° 37' 19.84'' E	156	Ground
S12	Guwabari	26° 47' 3.10'' N	91° 40' 40.73'' E	140	Surface
S13	Deuchunga	26° 46' 22.35'' N	91° 42' 49.37'' E	124	Ground
S14	No. 2 Dogargaon	26° 46' 17.77'' N	91° 41' 53.62'' E	125	Surface

Source: Field survey, 2020

Where  $Q_n$  refers to the quality rating scale of the  $n^{\text{th}}$  water quality parameter;  $W_n$  refers to the unit weight of the  $n^{\text{th}}$  water quality parameter.

For computing WQI, we first calculate the Q value by using the following formula-

$$Q_n = 100 \left\{ \frac{(V_n - V_i)}{(V_s - V_i)} \right\}$$

Where,  $V_n$  = the amount of  $n^{\text{th}}$  parameter present,  $V_i$  = ideal value of the parameter i.e.  $V_i=0$ , except  $P^H$  ( $v_i=7$ ) and DO ( $V_i=14.6 \text{ mg.L}^{-1}$ );  $V_s$  = recommended standard value

for  $n^{\text{th}}$  parameter

Unit weight ( $W_n$ ) is calculated by the following equation-

$$W_n = K / V_s$$

Where  $k$  = proportionality constant and it is calculated by the following equation-

$$K = \left[ \frac{1}{\sum 1/V_s} \right]$$

The status of water quality based on the water quality index (WQI) value and their possible uses are shown in Table 5.

Table 2: Selected drinking water sources and their supplies in sample villages.

Village	Location	Elevation [m]	Selected drinking water sources	Dependent households
Daragaon	26°46'54.93" N 91°23'1.79" E	171	Locally managed spring fed pipe line	60
Dihira	26°44'18.5" N 91°21'27" E	87	Community well	35
Bhangrikuchi Dimapur	26°46'47.60" N 91°23'41.04" E	154	Dong (traditional canal)	80
Ganeshguri	26°47'3.34" N 91°24'27.94" E	149	Chaulkara <i>dong</i> (traditional canal)	50
Chaulkara village	26°45'38.27" N 91°24'6.83" E	124	<i>Pani tanki</i> (Deep tube well)	65
Uttarkuchi village	26°46'47.50" N 91°25'32.28" E	106	<i>Pani tanki</i> (Deep tube well)	70
Dakhinkuchi	26°45'24.90" N 91°26'23.32" E	106	<i>Pani tanki</i> (Deep tube well)	120
Bhabanipur village	26°44'32.01" N 91°25'21.32" E	68	Community well	85
Jharbasti	26°46'18.54" N 91°26'46.31" E	124	<i>Pani tanki</i> (Deep tube well)	170
Jalah basti	26°46'34.13" N 91°27'9.38" E	111	Natural Spring	40
Moithabari village	26°43'52.64" N 91°26'17.27" E	96	<i>Pani tanki</i> (Deep tube well)	100
Hatiduba village	26°45'51.06" N 91°30'26.62" E	94	<i>Pani tanki</i> (Deep tube well)	70
Angarkata N.C	26°44'35.60" N 91°30'1.39" E	99	Community well	40
Unthaibari	26°47'44.28" N 91°35'29.90" E	180	Unthaibari <i>dong</i> (traditional canal)	65
No.1 Dongargaon	26°48'4.78" N 91°37'19.84" E	156	Natural Spring	240
No.2 Dongargaon	26°46'17.17" N 91°41'53.62" E	124	Garo <i>dong</i> (traditional canal)	250
Deuchunga	26°46'22.35" N 91°42'49.37" E	126	<i>Pani tanki</i> (Deep tube well)	180

Source: Field survey, 2020



## RESULTS AND DISCUSSION

### Drinking-Water Accessibility

Scarcity of drinking water is the most serious problem in the entire foothill region of the district and the problems become more acute during the winter and pre-monsoon season. Around 80-90% of villagers of this foothill region do not have a drinking water source on their premises. Only a small section of the villagers residing in the southern belt of this region have access to drinking water at their premises. The majority of the population of this entire zone collects their drinking water from the different locally invented sources, such as dong (canals), nijora (natural springs), ponds, small streams, and rivers (Table 2). Very recently, the government of Bodoland Territorial Council (B.T.C) has constructed a deep tube well and water tank, locally called ‘pani tanki’ in the villages of this area.

The existing drinking water source of this region forms a unique spatial pattern (Fig. 2). If we observe very carefully, we can classify the drinking water sources into five parallel belts. Natural spring, locally called Nijhora is the primary source of drinking water in the villages of the extreme northern belts of the foothill zone. Besides the natural springs, the villagers also collect their drinking water from nearby *dongs* (canals), streams, and rivers. Just south of this belt many villagers depend on traditional *dongs* for their drinking water. There is no community well or deep tube well in this zone. Few deep tube wells were installed by the government a few years back but most of these are now defunct. As the

groundwater level is very low, a deep tube well could not work during the winter season. Thus, according to WHO’s standard classification, the sources of drinking water in these two zones can be classified as the ‘untreated surface water’ category.

The villagers in the next zone were using locally managed traditional *dong* water for drinking purposes till recently. Very recently, the government installed a good number of deep tube wells and water tanks for drinking water supply. The installation of these deep tube wells and water tanks dramatically change the life of the villagers. Now the people of these belts are getting basic and limited water services. In every village, we found around 3-4 deep tube wells and water tanks. Around 50-120 households depend on one deep tube well. Every deep tube well has a pump machine for the withdrawal and storing of water. All the maintenance works are performed by the stakeholders. The local *Gaon Unmyan Samiti* (village development committee) makes a drinking water management committee under it and gives the responsibility of regulating and maintenance and fees collections. To fetch the drinking water, the villagers need to spend around 20-40 min for every round trip. It is noteworthy to mention that the responsibility of drinking water collection mainly relies on women and children. It has been estimated that the women of this area spend around 5-6 h per week on the collection of drinking water. Dug well and community well are the main source of drinking water in the villages in the fourth zone. As the construction of a well is very difficult and expensive, therefore, a well in every household

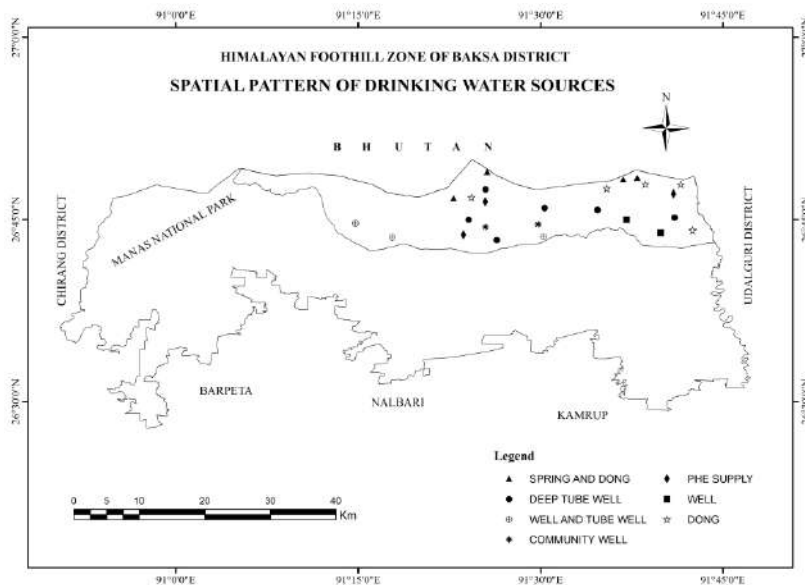


Fig. 2: Spatial pattern of drinking water sources in the foothill zone of Baksa.

premises is very rare. Community well is the primary source of drinking water. Like community deep tube well, around 50-60 households have to depend on one well. They need to walk around 200-500 m for collecting drinking water (Fig. 3). The majority of these wells are unprotected. Dug well and shallow tube wells are found in some villages in most southern belts of this region where the groundwater level is comparatively higher than in the northern part.

It is noteworthy here that the government has recently taken various projects to improve the drinking water supply in this entire foothill region. Public Health Engineering (PHE) water supply projects (pipe supply) have been taken in some villages such as Nikashi, Uttarkuchi, Subankhata, Chandranagar, and Guwabari, where the safely managed drinking water supply is available now. But the water supply is not available in the entire villages, some parts of these villages are receiving water supply from these PHE drinking water supply projects. Although the households under these water projects revive water supply through the pipeline in their home premises, the supply is only for specific time periods in a day. The drinking water supply project of the Utrakuchi and Subankhata area is now almost defunct.

### Seasonal Pattern of Drinking Water Accessibility

Focus group discussions (FGDs) with the local communities show that the drinking water accessibility of this region has been largely influenced by seasonal variation. A seasonal calendar- a widely used PRA tool- was applied to understand the seasonal variation in the reliability of drinking water. The participants reported that during the dry season

(December-April) scarcity of drinking water becomes more acute because many of the traditional drinking water sources such as *dong* (canal), and natural springs become dry. Water availability in Community Well as well as in deep tubes is also reduced significantly due to the fall of the groundwater table. The villagers, particularly the women and children need to spend more time in water fetching. Fig. 4 represents the drinking water-related issues that the local communities of four selected villages are facing through out the year.

It is seen that the drinking water source of Bhagrakuchi village is affected due to floods. During the rainy season, a large number of sediments and other eroded materials are mixed with *dong* water which makes the water undrinkable. The water fetching women and children of No.1 Dongargaon village reported that it becomes very difficult to access the natural spring during the rainy season due to flood water.

### Status of Water Quality Parameters

Different parameters of selected water samples were tested to understand the general characteristics of drinking water in the Bhutan Himalayan foothill zone of Assam. The abstract results of the water sample test are presented in Table 3. pH indicates the acidity or alkalinity nature of water which plays a significant role in the quality of water. The pH value of natural water generally falls within the range of 6-8. The average  $P^H$  value of the water samples was found to be 7.98. Although the average  $P^H$  value is within the permissible limit of BIS' ICMR and WHO standards, the  $P^H$  value in one sample site i.e. 8.83 was found beyond the permissible limit. Generally, pure water is not a good conductor of

Table 3: Descriptive statistics of the physiochemical parameters of sample water.

Parameter	Mean value	Median value	Standard deviation (SD)	BIS'ICMR Standard (2012)	WHO standard (1984)
pH	7.98 (7.12-8.83)	7.94	0.495	6.5- 8.5	6.5- 8.5
EC	283.64 (178-481)	264	81.94	300	300
TDS	177.37 (77.44-307.84)	168.96	58.33	500	1000
DO	4.72 (3.4-6.5)	4.6	0.960	5	-
Turbidity	19.96 (0.18-185)	1.25	49.64	5	5
Total hardness	187.4 (144-269.2)	176	36.49	200	500
Total Alkalinity	76.81 (42-238)	57	53.62	200	-
Chloride	2.85 (0.99-4.99)	2.74	1.08	250	250
Fluoride	0.06 (0.023-0.22)	0.05	0.04	1	1.5
Sulphate	11.45 (5.76-32.68)	10.22	6.73	150	400
Calcium	21.20 (8.83-36.84)	20.85	7.36	75	100
Magnesium	21.74 (13.73-34.67)	20.27	5.58	30	150

Note: The figure within parenthesis indicates the range of the value.

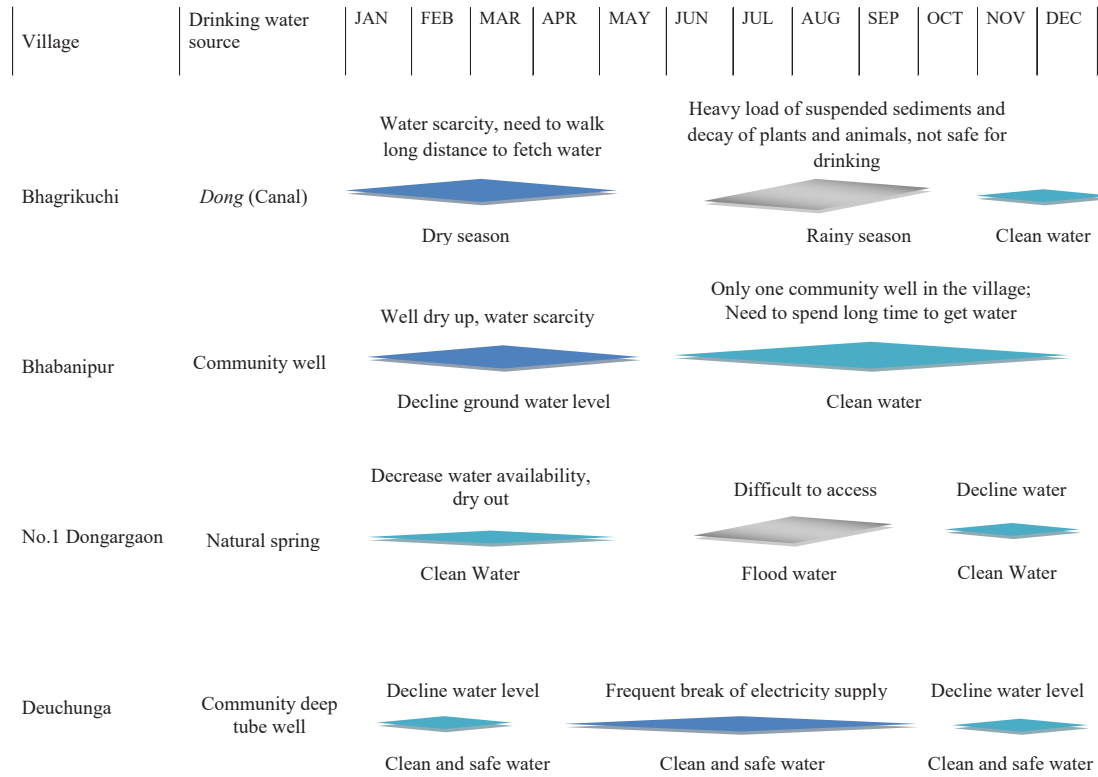
electricity but the presence of dissolved solids enhances the electric conductivity (Meride & Ayenew 2016). Electric conductivity (EC) measures the capacity of electric current transmission of water. It is also an indirect measurement of dissolved salts in a water sample. The electric conductivity (EC) value of water samples ranges between 178-481 $\mu$ S.  $P^H$  in most of the sites was found within the desirable limit of BIS and WHO standards except for three sites i.e. SI-4, SI-8, and SI-10. Measurement of TDS indicates the amount of total dissolved solids particles present in the water. TDS values of the sample water were found within the desirable limits of ICMR and WHO with a maximum record of 307.84  $mg.L^{-1}$ . The amount dissolves oxygen present in water is called DO which is one of the major indicators of water quality. Good quality water must have more than 4 $mg^{\prime}L$  dissolved oxygen (Lkr et al. 2020). The amount of dissolved oxygen (DO) across the foothill region was recorded within the range of 3.4-6.5  $mg.L^{-1}$ . Turbidity is the measurement of water clarity. A higher level of turbidity adversely affects the aquatic life both plants and animals (Pant et al. 2017). There is a very significant variation of water turbidity values among the sample sites ranging from 0.18 NTU to 185 NTU. Although the turbidity values in the case of the majority of the sample sites are within the desirable limit i.e. 5 of BIS and WHO, few sample sites have excessive value. Turbidity in the water sample of the Paharpur-Lebra canal (sample site-4) was found extremely high (185 NTU) which is very harmful to aquatic plants and animals. Water hardness refers to the

measure of divalent metal cation, mainly calcium and magnesium (Diggs & Parker 2009). The dissolve metallic ions from sedimentary rocks, surface runoff from the surrounding area, etc. are the major natural sources of water harness. The observed hardness values of the collected water sample of the area were range from 144 to 269.2  $mg.L^{-1}$ .

Total alkalinity is the acid-neutralizing capacity of the water. The mean value of total alkalinity (76.81  $mg.L^{-1}$ ) was found within the desirable limit of BIS i.e. 200. The maximum concentration (238  $mg.L^{-1}$ ) was recorded at sample site-9 which exceeds the BIS standard limit. The concentration of chloride in all the water samples was found (between 0.99 and 4.99  $mg.L^{-1}$ ) within the BIS and WHO desirable limits. The mean concentration of fluoride was 0.06  $mg^{\prime}l$  with the values ranging from 0.023 to 0.22  $mg.L^{-1}$ . Several minerals such as barite, gypsum, etc. are natural contributors to sulfate in water. A higher concentration of sulfate in drinking water causes different diseases such as diarrhea, dehydration, etc. The concentration of sulfate in the water sample varies between 5.76 and 32.68  $mg.L^{-1}$ . Sulfate concentration values in all the sample sites under investigation were recorded within the desirable limits of BIS and WHO. Both calcium and magnesium dissolves are common minerals found in water that makes the water hard. These minerals are also essential nutrients for human health. The concentration of calcium was recorded within the range of 8.83 to 36.84  $mg.L^{-1}$ . The mean magnesium value in the water sample was observed at 21.74  $mg.L^{-1}$ . All the observed values of calcium and magnesium



Fig. 3: Scenario of drinking water sources in the Himalayan foothill zone of Baksa district, Assam, India.



Source: Based on focus group discussion, 2020

Fig. 4: Seasonality of drinking water status in the foothill region of the Baksa district.

for all the sample sites were found within the permissible limit of the World Health Organization (WHO).

Table 4 shows the concentration level of some selected heavy metals in the water sample sites. It is seen that the concentration of arsenic which is very hazardous to human health is below the detection level (BDL). Similarly, the concentration of cadmium (Cd) and lead (P) is also below the detection level. The following data reveals that the drinking water of this area is almost free from hazardous heavy metal contamination. But the mean concentration level of chromium (0.15ppm) and iron (1.03ppm) exceeds the BIS and WHO standard limits.

The water quality index is one of the most effective methods of water quality analysis which describe the overall quality of water in a single term (Akter et al. 2016, Tyagi et al. 2013). The method of water quality index was first formulated by Horton (1965) and Brown et al. (1970) and subsequently different modified WQI methods were developed by several scientists (Saeedi et al. 2009). The water quality index (WQI) has now been widely used throughout the world as an effective tool for evaluating the quality of ground and surface water (Ameen 2019, Bora & Goswami 2017, Samantray et al. 2009, Şener et al. 2017). ‘Weighted Arithmetic Index’ method was applied in the present study.

Table 4: Descriptive statistics of selected heavy metal concentration in sample water.

Parameter	Mean value	Median value	Standard deviation(SD)	BIS'ICMR Standard (2012)	WHO standard (1984)
Arsenic (As)	BDL	-	-	0.01	0.05
Chromium (Cr)	0.15	0.15	0.01	0.05	0.05
Cadmium (Cd)	BDL	-	-	0.003	0.003
Iron (Fe)	1.03	0.65	0.93	0.30	0.30
Lead (Pb)	BDL	-	-	0.01	0.01

Note: Concentration level is measured in ppm (parts per million)

Table 5: Range of water quality index, status, and possible uses (Brown et al. 1972).

Range of WQI	Water quality status (WQS)	Probable utility
<25	Excellent	Suitable for drinking, irrigation, and industrial uses
26-50	Good	Suitable for drinking, irrigation, and industrial purposes
51-75	Poor	Not suitable for drinking, only irrigation, and industrial use
76-100	Very poor	Irrigation purpose only
>100	Unsuitable for drinking and fish cultivation	Proper treatment is essential before any kind of use

The procedure for calculation of WQI applying weighted arithmetic index (WAI) starts with the estimation of 'unit weight' assigned for every physiochemical parameter considered for the study. By assigning the 'unit weight', the different dimensions and units of the selected parameters are converted into a common. Table 6 shows the drinking water quality standard (as per the BIS'ICMR) and the assigned 'unit weight' of every selected parameter for determining the water quality index (WQI).

The maximum 'unit weight' value is assigned to fluoride (0.627), DO (0.125), and turbidity (0.125) which indicates the importance of these parameters in the assessment of water quality. These parameters also play a very significant role in the computation of the water quality index (WQI). The measured values of all the twelve physiochemical parameters for all the sample sites and their corresponding WQI values are presented in Tables 7, 8, 9, 10, and 11. It is seen that the pH, DO, turbidity and fluoride are the most significant water parameters in determining the WQI score.

The overall water quality index value and water quality status of all the sample sites are presented in Table 12. The observed WQI values among 14 sample sites range from 21.75 to 502.38. It is seen that the WQI value in the majority of the sample sites falls under the category of good quality water status ( $25 < \text{WQI} < 50$ ). The lowest WQI value i.e. 21.75 was found at Uttarkuchi village (S3), whereas the higher WQI value i.e. 502.38 was recorded at the village No.1 Paharpur (S4). The WQI values of the groundwater sample sites S2, S3, S6, and S7 are recorded as less than 30 except the sample site S11 which is a natural spring. WQI value of S11 is 34.26. The average WQI values of the surface water samples are found to be slightly higher than the groundwater sample. The sample sites S4 and S5 recorded unsuitable water quality status. The village Dihira (S1) recorded very poor quality water status with a WQI value of 87.63. The pollution level in the sample site S4 is extremely high. Electric conductivity (EC), turbidity, DO, total hardness, and magnesium level were recorded

Table 6: Relative weight of water parameters used for determination of water quality index.

Parameter	BIS' ICMR standard (2012) ( $V_s$ )	Unit Weight ( $W_n$ )
pH	6.5-8.5	0.077
Electric conductivity	300	0.002
TDS	500	0.001
DO	5	0.125
Turbidity	5	0.125
Total hardness	200	0.003
Total alkalinity	200	0.003
Chloride	250	0.002
Fluoride	1	0.627
Calcium	75	0.008
Sulphate	150	0.004
Magnesium	30	0.02
$\sum W_n = 0.997 (\cong 1.00)$		



Table 7: Determination of WQI for sample sites 1, 2 and 3.

Parameter	Site -1			Site-2			Site-3		
	Vn	Qn	QnWn	Vn	Qn	QnWn	Vn	Qn	QnWn
pH	8.03	85.83	6.61	7.75	62.50	4.81	7.82	68.33	5.26
Ec	212.00	70.67	0.14	330.00	110.00	0.22	291.00	97.00	0.19
TDS	77.44	15.48	0.02	211.20	42.24	0.04	186.24	37.25	0.04
DO	6.50	83.33	10.42	5.80	91.67	11.46	5.40	95.83	11.98
Turbidity	26.00	520.00	65.00	2.10	42.00	5.25	0.18	3.60	0.45
Total hardness	144.00	72.00	0.22	196.00	98.00	0.29	170.00	85.00	0.26
Total alkalinity	56.00	28.00	0.08	58.00	29.00	0.09	58.00	29.00	0.09
Chloride	1.50	0.60	0.00	4.00	1.60	0.00	5.00	2.00	0.00
Fluoride	0.05	5.26	3.30	0.03	3.32	2.08	0.03	3.01	1.89
Calcium	26.49	35.32	0.28	47.93	63.91	0.51	41.63	55.51	0.44
Sulphate	11.52	7.68	0.03	6.40	4.26	0.02	7.24	4.83	0.02
Magnesium	18.92	63.06	1.26	18.54	61.80	1.24	16.06	53.53	1.07
$\sum QnWn$ 87.36 WQI=87.63			$\sum QnWn$ 26.01 WQI=26.08			$\sum QnWn$ 21.69 WQI=21.75			

Table 8: Determination of WQI for sample sites 4, 5 and 6.

Parameter	Site-4			Site-5			Site-6		
	Vn	Qn	QnWn	Vn	Qn	QnWn	Vn	Qn	QnWn
pH	8.53	127.50	9.82	8.25	104.17	8.02	7.12	20.83	1.60
Ec	481.00	160.33	0.32	242.00	80.67	0.16	213.00	71.00	0.14
TDS	307.84	61.57	0.06	154.88	30.98	0.03	136.32	27.26	0.03
DO	6.10	88.54	11.07	5.20	97.92	12.24	4.70	103.13	12.89
Turbidity	185.00	3700.00	462.50	50.00	1000.00	125.00	4.10	82.00	10.25
Total hardness	234.00	117.00	0.35	180.00	90.00	0.27	160.00	80.00	0.24
Total alkalinity	108.00	54.00	0.16	50.00	25.00	0.08	46.00	23.00	0.07
Chloride	3.50	1.40	0.00	2.00	0.80	0.00	3.50	1.40	0.00
Fluoride	0.22	22.00	13.79	0.05	4.74	2.97	0.02	2.31	1.45
Calcium	36.58	48.77	0.39	30.27	40.36	0.32	29.85	39.80	0.32
Sulphate	32.68	21.79	0.09	13.56	9.04	0.04	6.82	4.54	0.02
Magnesium	34.67	115.57	2.31	25.37	84.57	1.69	20.77	69.23	1.38
$\sum QnWn$ 500.87 WQI=502.38			$\sum QnWn$ 150.82 WQI=151.27			$\sum QnWn$ 28.40 WQI=28.49			

beyond the BIS standard limits at this site. Turbidity level at S4 was found to be 185 NTU which is higher than the permissible limit of BIS and WHO i.e. 5 NTU. A large number of waste materials from the recently developed coal mining and limestone quarrying sites in the Bhutan territory are mixing with the Lebra river water, which is

the primary source of water pollution in this area. Besides, large-scale deforestation in the upper catchment area is also badly affecting the quality of water. The growing pollution level in the Lebra river has become a serious threat to the life and livelihoods of the villagers in Lebra-Santipur and No.1 Paharpur village. Water has become unfit

Table 9: Determination of WQI for sample sites 7, 8 and 9.

Parameter	Site -7			Site-8			Site-9		
	Vn	Qn	QnWn	Vn	Qn	QnWn	Vn	Qn	QnWn
p <sup>H</sup>	7.44	36.67	2.82	8.83	152.50	11.74	7.85	70.83	5.45
Ec	178.00	59.33	0.12	351.00	117.00	0.23	311.00	1.04	0.00
TDS	113.92	22.78	0.02	224.64	44.93	0.04	199.04	39.81	0.04
DO	4.60	104.17	13.02	3.40	116.67	14.58	3.40	116.67	14.58
Turbidity	0.26	5.20	0.65	1.30	26.00	3.25	1.20	24.00	3.00
Total hardness	158.00	79.00	0.24	172.00	86.00	0.26	200.00	100.00	0.30
Total alkalinity	42.00	21.00	0.06	140.00	70.00	0.21	238.00	119.00	0.36
Chloride	4.00	1.60	0.00	2.50	1.00	0.00	2.00	0.80	0.00
Fluoride	0.07	6.65	4.17	0.07	7.22	4.53	0.03	3.19	2.00
Calcium	29.85	39.80	0.32	23.54	31.39	0.25	47.51	63.35	0.51
Sulphate	9.63	6.42	0.03	15.18	10.12	0.04	10.82	7.21	0.03
Magnesium	24.11	80.37	1.61	13.73	45.77	0.92	19.77	65.90	1.32
$\sum QnWn = 23.06$ WQI=23.13			$\sum QnWn = 36.06$ WQI=36.17			$\sum QnWn = 27.59$ WQI=27.67			

Table 10: Determination of WQI for sample sites 10, 11 and 12.

Parameter	Site -10			Site-11			Site-12		
	Vn	Qn	QnWn	Vn	Qn	QnWn	Vn	Qn	QnWn
p <sup>H</sup>	8.32	110.00	8.47	7.36	30.00	2.31	8.30	108.33	8.34
Ec	213.00	71.00	0.14	286.00	95.33	0.19	241.00	80.33	0.16
TDS	136.32	27.26	0.03	183.04	36.61	0.04	154.24	30.85	0.03
DO	4.00	110.42	13.80	4.60	104.17	13.02	4.10	109.38	13.67
Turbidity	2.20	44.00	5.50	0.40	92.00	11.50	1.20	24.00	3.00
Total hardness	150.80	75.40	0.23	236.00	118.00	0.35	166.80	83.40	0.25
Total alkalinity	65.40	32.70	0.10	47.40	23.70	0.07	62.00	31.00	0.09
Chloride	3.00	1.20	0.00	3.00	1.20	0.00	2.50	1.00	0.00
Fluoride	0.06	5.63	3.53	0.07	6.76	4.24	0.05	5.44	3.41
Calcium	32.80	43.73	0.35	47.93	66.57	0.53	37.02	49.36	0.39
Sulphate	5.76	3.84	0.02	8.22	5.48	0.02	12.02	8.01	0.03
Magnesium	16.74	55.80	1.12	28.27	94.23	1.88	18.08	60.27	1.21
$\sum QnWn = 33.28$ WQI=33.38			$\sum QnWn = 34.16$ WQI=34.26			$\sum QnWn = 30.59$ WQI=30.68			

for drinking, therefore they need to walk a long distance for fetching water. Cultivation of fish in their household ponds is destroyed and ponds have become abundant (Fig. 5). Irrigation fields are also adversely affected due to high levels of pollution and siltation.

## CONCLUSION

The present study gives an account of the status of water accessibility and the quality of the existing drinking water sources. The physiochemical analysis of water quality reveals that the majority of the values are within the drinking water

Table 11: Determination of WQI for sample sites 13, and 14.

Parameter	Site -13			Site-14		
	Vn	Qn	QnWn	Vn	Qn	QnWn
pH	7.67	55.83	4.30	8.50	125.00	9.63
Ec	380.00	126.67	0.25	242.00	80.67	0.16
TDS	243.20	48.64	0.05	154.85	30.97	0.03
DO	4.22	108.13	13.52	4.10	109.38	13.67
Turbidity	0.50	10.00	1.25	0.47	9.40	1.18
Total hardness	269.20	134.60	0.40	186.80	93.40	0.28
Total alkalinity	50.60	25.30	0.08	54.00	27.00	0.08
Chloride	3.00	1.20	0.00	1.00	0.40	0.00
Fluoride	0.04	3.71	2.33	0.05	5.03	3.15
Calcium	64.13	85.51	0.68	35.32	47.09	0.38
Sulphate	8.50	5.67	0.02	12.09	8.06	0.03
Magnesium	25.36	84.53	1.69	23.97	79.90	1.60
$\sum QnWn = 24.57$ WQI=24.64			$\sum QnWn = 30.19$ WQI=30.28			

Table 12: Water quality index value and water quality status.

Sampling site	Village	Water quality index (WQI)	Water quality status (WQS)
S1	Dihira	87.63	Very poor
S2*	Chaulkara	26.08	Good
S3*	Uttarkuchi	21.75	Excellent
S4	No.1 Paharpur	502.38	Unsuitable
S5	Jharbasti	151.27	Unsuitable
S6*	Moithabari	28.49	Good
S7*	Hatiduba	23.13	Excellent
S8	Ganeshguri	36.17	Good
S9	Unthaibari	27.67	Good
S10	Manjurgaon	33.38	Good
S11*	Manjurgaon	34.26	Good
S12	Guwahati	30.68	Good
S13*	Deuchunga	24.64	Excellent
S14	No.2 Dogargaon	30.28	Good

Note: Sample site with \* sign indicates the groundwater source

standard limits of WHO and BIS. From the calculated water quality index (WQI) values of all the sample sites, it can be concluded that the quality of water is good in all the sites except No.1 Paharpur (site 4) and Jharbasti village (site 5). Deforestation, open cast coal and limestone mining in the hilly region of Bhutan territory are mainly responsible for

the degradation of water quality of this region. As the local communities of this entire foothill region have been using the surface water (through the *dong-bandh* irrigation system) for drinking as well as irrigation purposes, therefore government intervention is very essential to overcome these issues.



Fig. 5: Coal mining waste mixed with the water of Lebra-Santipur and No.1 Paharpur village.

## ACKNOWLEDGMENT

The authors gratefully acknowledge the support from the ICSSR Short-Term Doctoral Fellowship Grant (RFD' Short-Term' 19-20' GEN' GEOG' 39). The authors also acknowledge the NERIWALM, Tezpur for the support in laboratory tests.

## REFERENCES

- Akter, T., Johura, F.T., Akter, F., Chowdhury, T.R., Mistry, S.K., Dey, D., Barua, M.K., Islam, M.A. and Rahman, M. 2016. Water quality index for measuring drinking water quality in rural Bangladesh: A cross-sectional study. *J. Health, Popul. Nutri.*, 35(1): 1-12.
- Ameen, H.A. 2019. Springwater quality assessment using water quality index in villages of Barwari Bala, Duhok, Kurdistan Region, Iraq. *Appl. Water Sci.*, 9(8): 1-12.
- American Public Health Association, American Water Works Association, and Water Environment Federation (APHA, AWWA, and WEF). 1992. *Standard Methods for Examination of Water and Wastewater*, 18<sup>th</sup> edn, American Public Health Association, American Water Works Association, and Water Environment Federation, Washington, DC, USA.
- Bora, M. and Goswami, D.C. 2017. Water quality assessment in terms of water quality index (WQI): A case study of the Kolong River, Assam, India. *Appl. Water Sci.*, 7(6): 3125-3135.
- Brown, R.M., McClelland, N.I., Deininger, R.A. and Tozer, R.G. 1970. A water quality index-do we dare. *Water Sew. Works*, 117(10): 1051.
- Brown, R.M., McClelland, N.I., Deininger, R.A. and O'Connor, M.F. 1972. A water quality index-crashing the psychological barrier. In Thomas, W.A. (ed.), *Indicators of Environmental Quality*, Springer, Boston, MA, pp. 173-182.
- Diggs, H.E. and Parker, J.M. 2009. Aquatic Facilities. In Hessler, R. and Noel, M. (eds.), *Planning and Designing Research Animal Facilities*, Academic Press, CA, pp. 323-331.
- Effendi, H. 2016. River water quality preliminary rapid assessment using pollution index. *Procedia Environ. Sci.*, 33: 562-567.
- Khound, N.J. and Bhattacharyya, K.G. 2018. Assessment of water quality in and around Jia-Bharali river basin, North Brahmaputra Plain, India, using multivariate statistical technique. *Appl. Water Sci.*, 8(8): 1-21.
- Lkr, A., Singh, M.R. and Puro, N. 2020. Assessment of water quality status of Doyang river, Nagaland, India, using water quality index. *Appl. Water Sci.*, 10(1): 1-13.
- Mandour, R.A. 2012. Human health impacts of drinking water (surface and ground) pollution Dakahlyia Governorate, Egypt. *Appl. Water Sci.*, 2(3): 157-163.
- Meride, Y. and Ayenew, B. 2016. Drinking water quality assessment and its effects on residents' health in Wondo genet campus, Ethiopia. *Environ. Syst. Res.*, 5(1): 1-7.
- Mir, S.A., Qadri, H., Beigh, B.A., Dar, Z.A. and Bashir, I. 2019. Assessment of nutrient status and water quality index of Rambhara stream, Kashmir Himalaya, India. *J. Pharma. Phytochem.*, 8(3): 172-180.
- Nabila, B., Ahmed, B. and Kacem, M. 2014. An assessment of the physico-chemical parameters of Oran sebkha basin. *Appl. Water Sci.*, 4(4): 351-356.
- Pant, B., Lohani, V., Trakroo, D.M. and Tewari, H. 2017. Study of water quality by physicochemical analysis of a Himalayan lake of Uttarakhand, India. *Ecol. Environ. Conserv.*, 23(2):1128-1134.
- Rawal, I., Joshi, H. and Chaudhary, B.L. 2018. Water quality assessment using physicochemical and bacteriological parameters of Fateh Sagar Lake, Udaipur, India. *Water Resour.*, 45(3): 427-435.
- Rickert, B., Chorus, I. and Schmolli, O. 2016. *Protecting Surface Water For Health: Identifying, Assessing and Managing Drinking-Water Quality Risks in Surface-Water Catchments*. World Health Organization.
- Sabha, I., Bhat, S.U., Hamid, A. and Rather, J.A. 2019. Monitoring stream water quality of Dagwan stream, an important tributary of Dal Lake, Kashmir Himalaya. *Arab. J. Geosci.*, 12(8): 1-17.
- Saeedi, M., Abessi, O., Sharifi, F. and Maraji, H. 2009. Development of groundwater quality index. *Environ. Monit. Assess.*, 163(1-4): 327-335.
- Samantray, P., Mishra, B.K., Panda, C.R. and Rout, S.P. 2009. Assessment of water quality index in Mahanadi and Atharabanki Rivers and Taldanda Canal in Paradip area, India. *J. Hum. Ecolo.*, 26(3): 153-161.
- Saha, S., Deka, N. and Bhagabati, A.K. 2020. Participatory water resource management in the Bhutan Himalayan foothill environment of Baksa district, Assam. *Int. J. Rural Manag.*, 16(1): 62-80.
- Saha, S., Deka, N. and Bhagabati, A.K. 2021. Traditional Water Management System and Agricultural Sustainability in a Himalayan Foothill Village of Assam, India. In Haldar, A.R., Alam, A. and Satpati, L. (eds.), *Habitat, Ecology and Ecosystems*, Springer, Cham, pp. 279-292.
- Şener, Ş., Şener, E. and Davraz, A. 2017. Evaluation of water quality using the water quality index (WQI) method and GIS in Aksu River (SW-Turkey). *Sci. Total Environ.*, 584: 131-144.
- Seth, R., Mohan, M., Singh, P., Singh, R., Dobhal, R., Singh, K.P. and Gupta, S. 2016. Water quality evaluation of Himalayan rivers of Kumaun region, Uttarakhand, India. *Appl. Water Sci.*, 6(2): 137-147.
- Sharma, S., Bajracharya, R.M., Sitaula, B.K. and Merz, J. 2005. Water quality in the Central Himalayas. *Curr. Sci.*, 61: 774-786.
- Tyagi, S., Sharma, B., Singh, P. and Dobhal, R. 2013. Water quality assessment in terms of water quality index. *Am. J. Water Resour.*, 1(3): 34-38.
- United Nations Children's Fund (UNICEF) and World Health Organization (WHO). 2019. *Progress on Household Drinking Water, Sanitation and Hygiene 2000-2017: Special focus on inequalities*. New York.







# The Influence of Floodplain Vegetation Patches on Hydrodynamic Characteristics: A Case Study in the Old Course of Fuhe River

Da Li\*, Zhonghua Yang\*†, Junjie Zheng\*, Fangping Liu\*\* and Gang Ge\*\*\*

\*State Key Laboratory of Water Resources and Hydropower Engineering Science, Wuhan University, Wuhan 430072, China

\*\*Jiangxi Irrigation Experiment Central Station, Nanchang 330031, China

\*\*\*School of Life Science, Nanchang University, Nanchang 330031, China

†Corresponding author: Zhonghua Yang; yzh@whu.edu.cn

Nat. Env. & Poll. Tech.  
Website: [www.neptjournal.com](http://www.neptjournal.com)

Received: 17-09-2021  
Revised: 10-11-2021  
Accepted: 20-11-2021

## Key Words:

Fuhe river  
Floodplain  
Vegetation patches  
Hydrodynamic characteristics  
Equivalent Manning coefficient

## ABSTRACT

As an important part of the river ecosystem, vegetation has a significant influence on hydrodynamic characteristics, water quality, river morphology, and ecological habitat. Combining vegetation survey with the verified numerical model, this study aims to analyze the impact of floodplain vegetation patches on hydrodynamic characteristics in the old course of Fuhe River under various combinations of incoming flow discharges, and flood diversion discharges, and changes in the land use type. The equivalent Manning coefficient was adopted to quantify the additional resistance induced by plants in the vegetation module of the numerical model. According to simulating results, vegetation patches would cause the water level to rise and velocity to decrease, which mainly affects the upstream of the old course of Fuhe River. And with the increase in incoming discharge, water level difference and velocity difference have an upward trend. It is also found that the resistance of *Zizania latifolia* to river flow is strongest followed by sugarcane, crops, and weeds because of the differences in vegetation characteristics. Furthermore, compared with existing vegetation conditions, converting farmland to *Zizania latifolia* and expanding farmland induce a moderate rise in water level upstream while the decreasing velocity happens in the area where land use type is changed. And there are areas where velocity increases located opposite to the velocity decreasing area because of the adjustment of cross-section velocity distribution caused by plants.

## INTRODUCTION

In nature, aquatic plants are abundant in rivers and also have a significant influence on the river ecosystems by altering flow fields, stabilizing river beds, sheltering aquatic animals, and enhancing water quality. With the popularization of the concept of ecological rivers and river restoration, aquatic vegetation is introduced in the design of ecological rivers and restoration engineering projects. Therefore, more and more attention is paid to the vegetation impact on natural river ecosystems, which is helpful for better river management and protection.

Aquatic plants directly impact flow dynamics. First of all, compared with non-vegetated rivers, the existence of aquatic plants would induce additional flow resistance, which causes the flow velocity to slow down and the water level to rise. To quantify the obstruction of vegetation, the vegetation drag coefficient,  $C_D$  is introduced as an important parameter that is related to the vegetation characteristics and the flow conditions. In the previous studies, several predicting formulas

$C_D$  were proposed, which were systematically reviewed and summarized by Liu et al. (2020) and D'ippolito et al. (2021). And the profile of velocity distribution in vegetated channels is also affected by vegetation. Generally, the velocity in the emergent vegetation layer almost distributes uniformly while the velocity distribution profile is variable along the water depth in the submerged canopy layer. Therefore, to describe the key parameter in the submerged vegetation layer, different velocity models were proposed, such as the two-layer velocity model (Yang & Choi 2010) and the three-layer velocity model (Nepf 2012). Besides, bed shear stress (Etminan et al. 2018, Yang et al. 2015), Reynolds shear stress (Choi & Kang 2004, Dijkstra & Uittenbogaard 2010), the development of shear layer caused by vegetation (Ghisalberti & Nepf 2006), and other turbulent characteristics (Zhao et al. 2019) were focused on.

Heavily affected by the flow field, sediment transport in vegetated channels is also changed. In terms of sediment transport in vegetated rivers, previous research mainly concentrated on the initiated sediment motion (Cheng et al.

2020), bed-load transport rate (Yang & Nepf 2018), the distribution profile of suspended sediment concentration (SSC) (Huai et al. 2019, Li et al. 2020), the sediment erosion and deposition (Follett & Nepf 2018, Västilä & Järvelä 2018). Compared with non-vegetated channels, the critical flow velocity and the turbulent kinetic energy are supposed to be better indicators for predicting the initiated sediment motion and the bed-load transport rate, respectively (Tinoco & Coco 2016). In terms of the SSC distribution profile, recent studies mainly depend on three theories: the diffusion theory, the gravitational theory, and the random displacement model. As for the sediment erosion and deposition in vegetated channels, flume experiments found that sediment particles are usually scoured from the leading area of the vegetation region but deposited in the latter length of the vegetation area or behind the patch.

To simulate the interaction between the flow dynamics and vegetation, a lot of numerical models were proposed in the previous studies. In these numerical models, the widely adopted numerical methods are Boussinesq wave equations (Augustin et al. 2009, Huang et al. 2011), Navier-Stokes equations, and 2D shallow water equations (Bai et al. 2016, Wu & Marsooli 2012).

This study firstly introduces the vegetation module, which adopts the equivalent Manning coefficient to quantify vegetation resistance, into the hydrodynamic model. And based on the field vegetation investigation results, this paper aims to investigate how the vegetation patches on floodplains influence the flow dynamics in the old course of the Fuhe River by considering the combined effect of flood diversion and the changes in vegetation types, which is helpful to better river management and flood prevention.

## MATERIALS AND METHODS

### Hydrodynamic Module

This paper adopts the well-balanced two-dimensional shallow water equation which considers vegetation factors, wind stress, and Coriolis force. Its conservative form is described as:

$$\frac{\partial \mathbf{U}}{\partial t} + \frac{\partial \mathbf{F}}{\partial x} + \frac{\partial \mathbf{G}}{\partial y} = \mathbf{S}_b + \mathbf{S}_t + \mathbf{S}_f + \mathbf{S}_v \quad \dots(1)$$

where  $\mathbf{U}$  is the vector of conserved variables;  $\mathbf{F}$  and  $\mathbf{G}$  are the vectors of fluxes along the  $x$  and  $y$  directions respectively;  $t$  represents time;  $x$  and  $y$  denote the Cartesian coordinates;  $\mathbf{S}_b$  is the vector of slope source term;  $\mathbf{S}_t$  is the vector of turbulence resistance source term;  $\mathbf{S}_f$  is the vector of source term of river bed friction, and  $\mathbf{S}_v$  is the vector of source term of additional resistance induced by vegetation. The vectors

mentioned above are defined as:

$$\mathbf{U} = \begin{bmatrix} \eta \\ q_x \\ q_y \end{bmatrix}, \mathbf{F} = \begin{bmatrix} q_x \\ q_x^2/h + \frac{1}{2}g(\eta^2 - 2\eta z_b) \\ q_y \end{bmatrix}, \mathbf{G} = \begin{bmatrix} q_y \\ q_x \\ q_y^2/h + \frac{1}{2}g(\eta^2 - 2\eta z_b) \end{bmatrix}$$

$$\mathbf{S}_b = \begin{bmatrix} 0 \\ -g\eta \frac{\partial z_b}{\partial x} \\ -g\eta \frac{\partial z_b}{\partial y} \end{bmatrix}, \mathbf{S}_f = \begin{bmatrix} 0 \\ -\frac{gn_b^2}{h^{1/3}}u\sqrt{u^2+v^2} \\ -\frac{gn_b^2}{h^{1/3}}v\sqrt{u^2+v^2} \end{bmatrix}, \mathbf{S}_v = \begin{bmatrix} 0 \\ -\frac{F_{vx}}{\rho} \\ -\frac{F_{vy}}{\rho} \end{bmatrix} \quad \dots(2)$$

where  $g$  is the acceleration of gravity;  $h$  denotes water depth;  $z_b$  is river bed elevation;  $\eta$  denotes water level and  $\eta = h + z_b$ ;  $u$  and  $v$  are velocity components in  $x$  and  $y$  directions, respectively;  $q_x = hu$  and  $q_y = hv$  represent the discharges per width in  $x$  and  $y$  directions; and  $n$  is Manning coefficient of the river bed.

In the shallow water equation, the depth-averaged turbulent shear stress is determined according to the Boussinesq assumption and it is written as:

$$\mathbf{S}_t = \begin{bmatrix} 0 \\ \frac{\partial(hT_{xx})}{\partial x} + \frac{\partial(hT_{yx})}{\partial y} \\ \frac{\partial(hT_{xy})}{\partial x} + \frac{\partial(hT_{yy})}{\partial y} \end{bmatrix}, \begin{cases} T_{xx} = 2\nu_t \frac{\partial u}{\partial x} \\ T_{xy} = T_{yx} = \nu_t \left( \frac{\partial u}{\partial y} + \frac{\partial v}{\partial x} \right) \\ T_{yy} = 2\nu_t \frac{\partial v}{\partial y} \end{cases} \quad \dots(3)$$

where  $\nu_t$  is eddy viscosity which can be quantified by the following equations:

$$\nu_t = 0.5hu^*, u^* = \left[ c_f(u^2 + v^2) \right]^{1/2}, c_f = gn_b^2/h^{1/3} \quad \dots(4)$$

### Vegetation Module

Vegetation usually grows on the floodplain, inducing additional flow resistance. At present, plants can be divided into rigid and flexible vegetation according to rigidity. Rigid vegetation is usually treated as cylindrical piles while flexible vegetation cannot be treated as the same since it could be deflected by river flow. Thus, the mean deflected height is used as the characteristic height of flexible vegetation. To quantify the additional vegetation resistance, vegetation drag

force and equivalent Manning coefficient were proposed, respectively.

In terms of vegetation drag force, it is commonly described based on the drag coefficient (Whittaker et al. 2015):

$$\mathbf{F}_v = \frac{1}{2} \rho \lambda C_D C_a^{\psi/2} h |\mathbf{U}_c| \mathbf{U}_c \quad \dots(5)$$

where  $\rho$  is water density;  $\lambda$  denotes the projected area of vegetation per unit volume of water in the direction of water flow;  $\mathbf{U}_c$  is the mean velocity in the vegetation layer (Stone & Shen 2002);  $C_a$  is Cauchy number of flexible;  $\psi$  is the parameter representing the flexibility of vegetation, which ranges from -1 to 0. For rigid vegetation, the value of  $\psi$  is 0.  $C_D$  is related to flow velocity, vegetation characteristics, and fluid viscosity. Schlichting and Gersten (2017) proposed a method (Eq. (6)) to determine the drag coefficient based on the Reynolds number.

$$C_D = \begin{cases} 3.07e^{-0.168} & \text{Re} = uD/\nu < 800 \\ 1.0 & 800 \leq \text{Re} < 8000 \\ 1.2 & 8000 \leq \text{Re} < 10^5 \end{cases} \quad \dots(6)$$

Where Re is Reynolds number and D is the vegetation diameter. And due to differences in morphological characteristics of various types of vegetation, different empirical formulas to quantify the value  $C_D$  have been proposed (Etiman et al. 2017, Sonnenwald et al. 2019). However, in the shallow water mathematical model, the drag coefficient is often taken as a constant ranging from 0.8 to 1.5.

For the area in rivers covered with vegetation patches, the equivalent Manning coefficient is used to determine the combined resistance of river bed resistance and the additional resistance induced by vegetation. The combination of the source terms of resistance  $\mathbf{S}_f$  and  $\mathbf{S}_v$  in Eq. (1) could be written as:

$$\mathbf{S}_f + \mathbf{S}_v = \begin{bmatrix} 0 \\ -\frac{g(n_v^2 + n_b^2)}{h^{1/3}} u \sqrt{u^2 + v^2} \\ -\frac{g(n_v^2 + n_b^2)}{h^{1/3}} v \sqrt{u^2 + v^2} \end{bmatrix} = \begin{bmatrix} 0 \\ -\frac{gn^{-2}}{h^{1/3}} u \sqrt{u^2 + v^2} \\ -\frac{gn^{-2}}{h^{1/3}} v \sqrt{u^2 + v^2} \end{bmatrix} \quad \dots(7)$$

Where  $n_v$  denotes the Manning coefficient quantifying the vegetation resistance and  $n_b$  is the Manning coefficient of river bed resistance.  $\bar{n} = \sqrt{n_v^2 + n_b^2}$  is equivalent Manning coefficient in vegetation area. Based on the principle of equivalence, the equation to determine the equivalent

Manning coefficient is proposed (Huai et al. 2012), which could be described as:

$$\bar{n} = \sqrt{(1-c)n_b^2 + \frac{2C_D \alpha_v \xi^2 c \min(h, h_v) h^{1/3}}{g \pi D}} \quad \dots(8)$$

Where  $c$  is vegetation density and  $c = c_v \min(h, h_v)/h$ ;  $c_v$  is the ratio of vegetation volume to water volume in the vegetation layer;  $\alpha_v$  indicates shape factor whose value is usually 1.0 for cylindrical vegetation;  $\xi$  is a constant called velocity correction factor which is nearly 1.0;  $h_v$  is vegetation height.

In the vegetation module of a mathematical model, an equivalent Manning coefficient is adopted to represent the combined resistance of the vegetation patch. The equivalent Manning coefficient of each vegetation patch needs to be determined according to the water depth and vegetation characteristics (density, diameter and height) of each vegetation patch.

**Numerical Scheme**

Eq. (1) is spatially discretized by applying the cell-centered finite volume method based on the Godunov scheme, which can be described as:

$$\mathbf{U}_{i,j}^{m+1} = \mathbf{U}_{i,j}^m - \frac{\Delta t}{\Delta x_{i,j}} \left[ \mathbf{F}_{i+\frac{1}{2},j} - \mathbf{F}_{i-\frac{1}{2},j} \right] - \frac{\Delta t}{\Delta y_{i,j}} \left[ \mathbf{G}_{i,j+\frac{1}{2}} - \mathbf{G}_{i,j-\frac{1}{2}} \right] + \Delta t \mathbf{S}_{i,j} \quad \dots(9)$$

Where  $m$  denotes time level;  $i$  and  $j$  represent cell indexes;  $\Delta t$  is time step;  $\Delta x$  and  $\Delta y$  are space steps in  $x$  and  $y$  directions, respectively;  $\mathbf{F}_{i+\frac{1}{2},j}$ ,  $\mathbf{F}_{i-\frac{1}{2},j}$ ,  $\mathbf{G}_{i,j+\frac{1}{2}}$  and  $\mathbf{G}_{i,j-\frac{1}{2}}$  are the vectors of fluxes in the east, west, north, and south interfaces respectively.

The cell boundary fluxes are calculated using the approximate Riemann solver of the HLLC format, which considers the influence of the medium wave (Toro et al. 1994). This study adopts the two-stage explicit Runge-Kutta scheme (Hou et al. 2013) to achieve a second-order temporal accuracy and update the conserved flow variables at a new time level. Besides, to obtain the second-order accuracy in space, the MUSCL scheme was chosen to linearly reconstruct the conserved flow variables in each cell. The numerical computation in this study was performed by our program which has proved the capability of the finite-volume Godunov-type scheme (Bai et al. 2016, Zhu et al. 2018).

## Study Area and Field Investigation

As a tributary of Fuhe River, the old course of Fuhe River is located in Jiangxi Province, China, as shown in Fig. 1. The old course of Fuhe River starts from the flood diversion sluice of Jianjiang River and flows to Gangqian dam, with a total length of 18km approximately. The width of the river channel ranges from 100 to 800 meters. As a section of the West Main Canal of Ganfu Plain, the old course of Fuhe River is an important part of non-engineering measures of Fuhe River for flood control by holding the discharged water from the mainstream of Fuhe River. During the non-flood season, the incoming water is completely introduced by Jiaoshi Barrage Dam and flows into the old course of Fuhe River through West Main Canal. The entire river, especially the upper reaches, has a good ecosystem and is less affected by human activities.

The vegetation distribution in the old course of the Fuhe River was investigated in 2017, including vegetation species, location, density, height, and other characteristics. The main vegetation species and land use types are shown in Fig. 2. According to the field survey results, *Eichhornia crassipes* and *Zizania latifolia* are the absolute dominant species, accounting for approximately 51.80% and 54.27%

of the survey plots, respectively. The biomass of the two dominant plants reaches the maximum level in September and then decreases from September to November. Based on the rigidity and submergence of vegetation, the distribution of vegetation species and land use types are simplified as shown in Fig. 3 to quantify the resistance coefficient of each zone easily. The study area is divided into 75 sub-areas in total. The vegetation species, water blocking structures, and basic parameters of each sub-area are listed in Table 1.

## VALIDATION

A set of flume experiment data and a set of measured data from the old course of Fuhe River were adopted to verify the numerical model. The flume experiment conducted by Pasche and Rouvé (1985) is about overbank flow on floodplains covered with vegetation. The experiment was conducted in a tilting flume with a bottom slope of 0.0005 and a bottom Manning coefficient of 0.01. The flume is 25.5 m long and 1 m wide with a trapezoidal cross-section. Two vegetation densities were considered, 0.013 (Run M-1) and 0.025 (Run M-2), with the corresponding flow discharge of  $0.0345 \text{ m}^3 \cdot \text{s}^{-1}$  and  $0.0365 \text{ m}^3 \cdot \text{s}^{-1}$ , respectively. The hydrological data measured in the old course of Fuhe River includes the in-

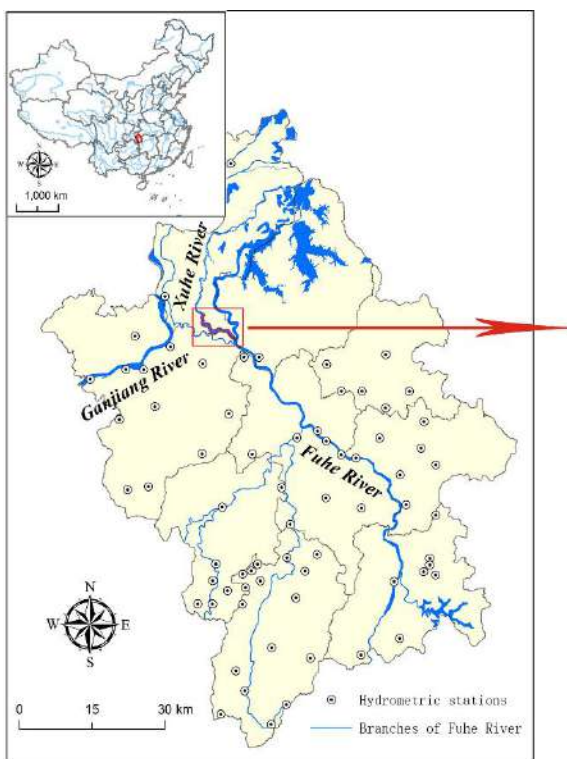


Fig. 1: Location of the old course of Fuhe River.



Table 1: Details of each sub-area.

Species	Area Number	Height [m]	Diameter [m]	Density
Weeds	1-3	0.12	0.0025	0.0108
	19	0.14	0.0021	0.0082
Sugarcane	4	2.20	0.0420	0.0130
Crops	5-13	0.21	0.0024	0.0100
Zizania latifolia	15	1.70	0.0087	0.0118
	16	1.74	0.0085	0.0121
	20	2.20	0.0150	0.0176
	22, 23, 25, 26, 30	1.75	0.0085	0.0120
<i>Eichhornia crassipes</i>	14, 17, 18, 21, 24, 27-29, 31-34	-	-	-
Fishing net	35-50	-	-	-
Ponds	51-75	-	-	-

coming discharge of 70 m<sup>3</sup>/s, the mean water level at the exit cross-section of 26.54m, and the flow velocity distribution of three cross-sections (CS-1, CS-2, and CS-3).

The comparison results between the measured and the calculated velocity profiles by the numerical model in this study are shown in Fig. 4. It is found the simulated velocity is in good agreement with the measured velocity, and the numerical model could basically reflect the adjustment effect of vegetation on the floodplain, proving the model has

good simulation capabilities. Besides, the simulation result calibrated the Manning coefficient of the main channel of the old course of Fuhe River to 0.021.

**APPLICATIONS**

To analyze the influence of vegetation on the hydrodynamics of the old course of Fuhe River, this study considered different vegetation development conditions and different combinations of coming discharge from upstream and the

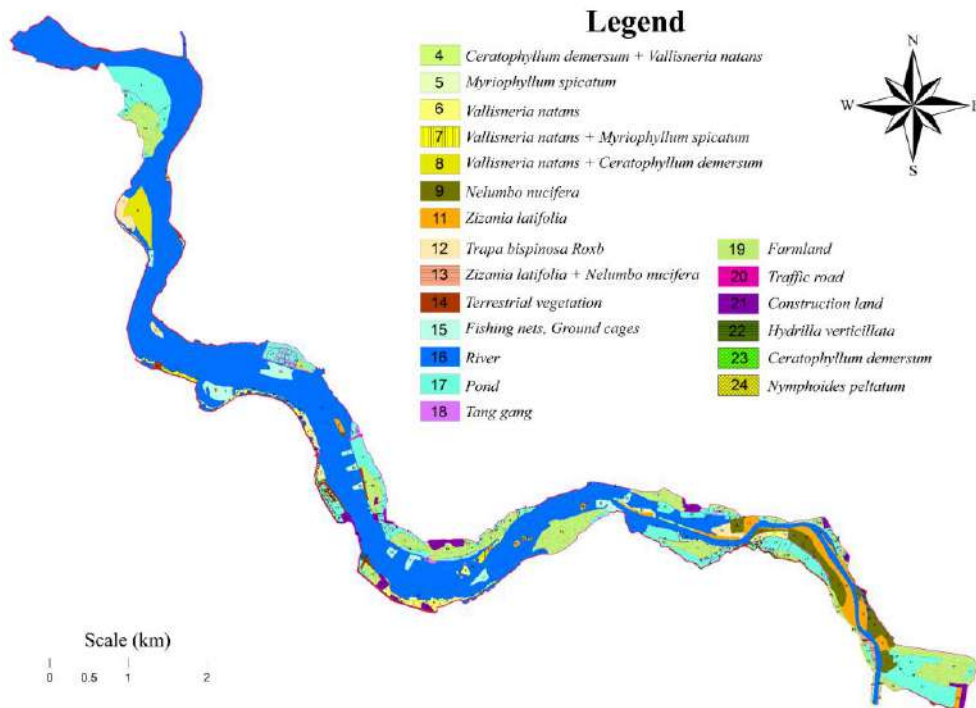


Fig. 2: Vegetation distribution map and land use type of the old course of Fuhe River.



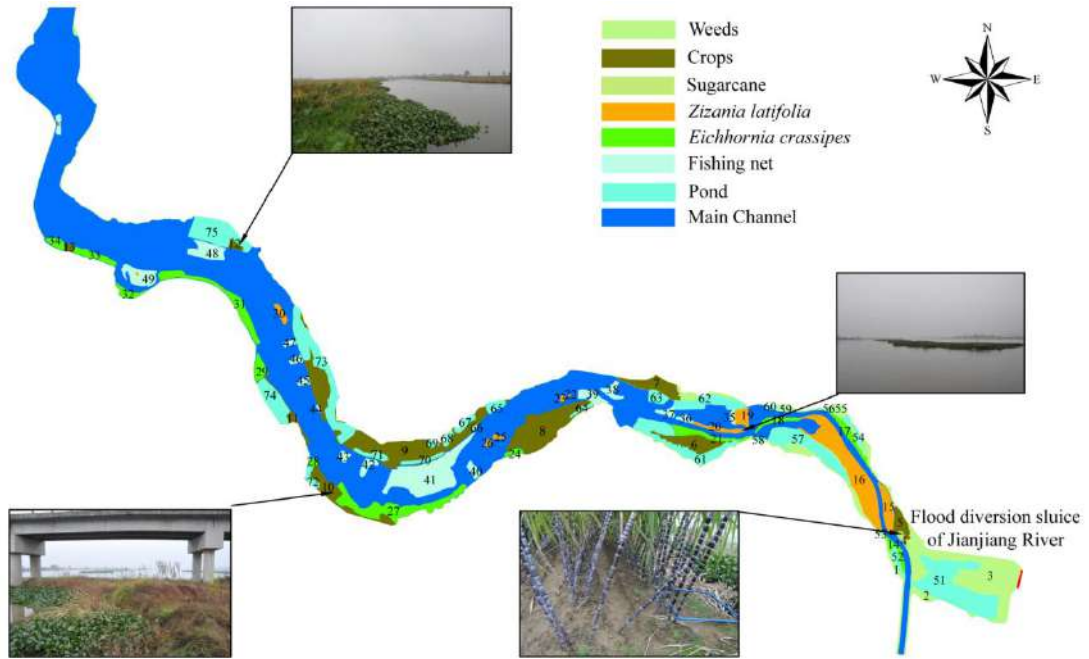


Fig. 3: The simplified map of vegetation distribution and land use types.

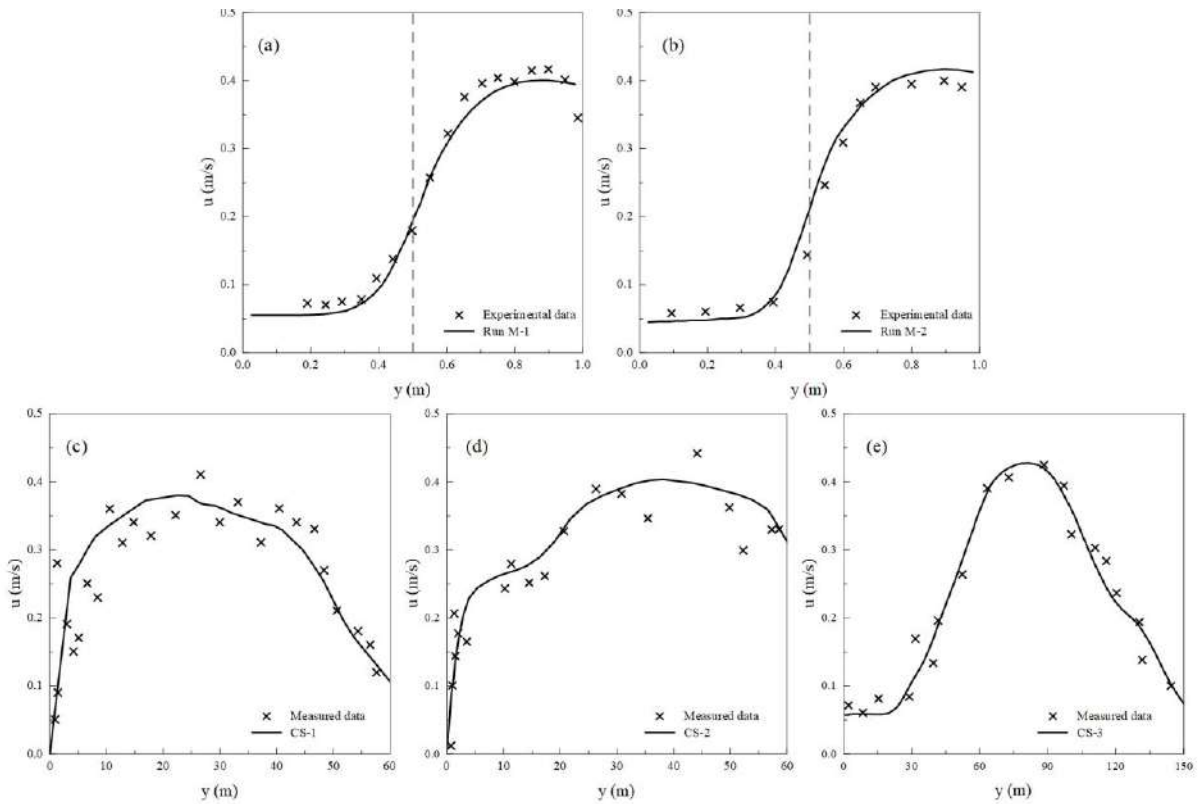


Fig. 4: Comparison results of the simulated and measured velocity.

floodwater discharged from the flood diversion gate. The running conditions simulated by the numerical model are listed in Table 2. The results and analysis would be presented in the following sub-section.

**Influence of Vegetation on Hydrodynamics without Flood Diversion**

Run A and B listed in Table 2 are the cases without considering the floodwater discharged from the Jianjiang River flood diversion sluice. Based on the vegetation module, the Manning coefficient distribution diagrams of Run A-1 and Run B-1 are shown in Fig. 5. The water depth in the area of *Zizania latifolia* increases with the increase of flow discharge and the resistance of *Zizania latifolia* in the non-submerged state to the water flow has an increasing trend with the value of Manning coefficient ranging from 0.13 to 0.14. According to Fig. 5, the Manning coefficient of the area near the

mainstream is greater than that of the central area of *Zizania latifolia* since the water depth is greater in the area near the mainstream, reflecting the roughness of non-submerged vegetation zone increases with water depth rising.

Comparison results in water level and velocity of Run A and Run B are illustrated in Fig. 6 to demonstrate the water-blocking effect of vegetation. The water level of Run A-1 and Run B-1 rises compared to Run A-2 and Run B-2, indicating the strong water-blocking effect of *Zizania latifolia*. However, affected by the downstream outlet boundary, the increment of water level is gradually weakened from upstream to downstream. And the largest water level increment exists near the flood diversion gate. The largest water level rises by about 0.09 m in Run A, which is less than the largest rising water level of 0.12 m in Run B. Besides, the mean rising water level of Run B is greater than that of Run A because of the larger incoming discharge. The existence

Table 2: Details of each simulated condition.

Run	$Q[m^3.s^{-1}]$		Water Level at Exist Cross-section [m]	Vegetation Condition
	West Main Canal	Jianjiang River flood diversion sluice		
A-1	70	0	21.54	Existing vegetation
A-2				No vegetation
B-1	110	0	21.80	Existing vegetation
B-2				No vegetation
C-1	110	200	27.50	Existing vegetation
C-2				No vegetation
C-3				Convert farmland to <i>Zizania latifolia</i>
C-4				Expand farmland
D-1	110	400	28.00	Existing vegetation
D-2				No vegetation
D-3				Convert farmland to <i>Zizania latifolia</i>
D-4				Expand farmland

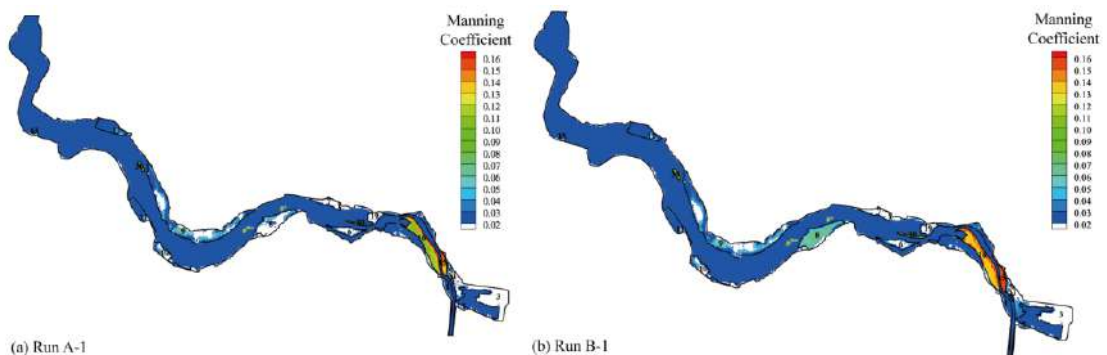


Fig. 5: Manning coefficient diagrams of Run A-1 and Run B-1.

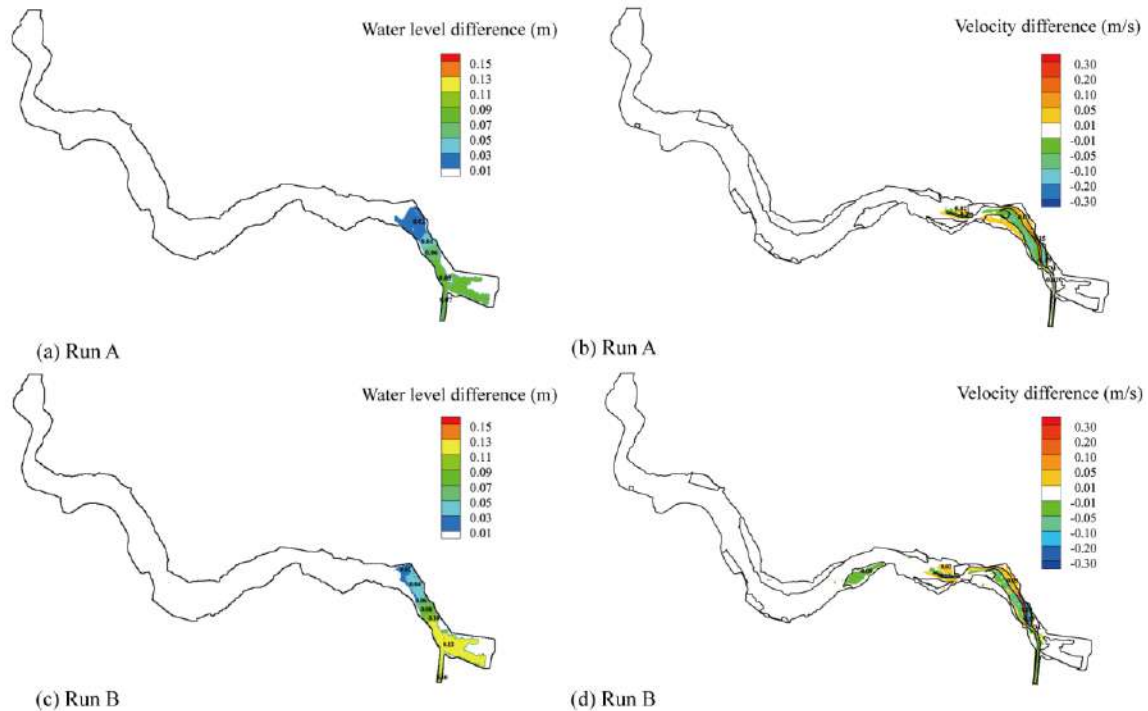


Fig. 6: (a) Water level difference between Run A-1 and A-2; (b) Velocity difference between Run A-1 and A-2; (c) Water level difference between Run B-1 and B-2; (d) Velocity difference between Run B-1 and B-2.

of vegetation causes the velocity in the vegetation area decreases obviously with the largest velocity reduction of  $0.2 \text{ m}\cdot\text{s}^{-1}$  and the velocity in the mainstream increases. And the mean velocity of the whole cross-section decreases because of the rising water level. Similarly, the difference in velocity increases when the incoming discharge gets larger.

### Influence of Vegetation on Hydrodynamics Considering Flood Diversion

Considering the floodwater discharged from the flood diversion gate of Jianjiang River, this study analyzed the influence of existing vegetation on the hydrodynamics of the old course of Fuhe River. According to the flood control plan of the Fuhe River basin, the typical flood diversion discharges are  $200 \text{ m}^3\cdot\text{s}^{-1}$  (Run C) and  $400 \text{ m}^3\cdot\text{s}^{-1}$  (Run D) respectively.

The Manning coefficient distribution diagrams of Run C-1 and Run D-1 considering the existing vegetation were shown in Fig. 7. It can be seen the roughness of the *Zizania latifolia* area is the largest, followed by the areas of sugarcane, crops, and grass. By studying the roughness induced by *Zizania latifolia*, there are differences in the distribution of roughness in the *Zizania latifolia* area, which is related to the regional topographical fluctuations. Changes in topographical conditions affect the submergence ratio of vegeta-

tion, inducing different water-blocking effects. Besides, the Manning coefficient value of vegetation area in Run C-1 is significantly larger than that in Run D-1 by comparing Fig. 7 (a) and (b). Actually, it is related to the relative ratio of water depth to vegetation height. Originally, the water depth is close to vegetation height in Run C-1. However, with the flood diversion discharge increasing to  $400 \text{ m}^3\cdot\text{s}^{-1}$ , the water depth generally spreads over the top of the plant, and the average resistance of vegetation along the water depth shows a downward trend.

Changes in water level difference and velocity difference under the simulated conditions considering flood diversion are similar to that without considering flood diversion. The water-blocking effect of vegetation patches causes water levels rising and the major area of rising water level is mainly near the flood diversion gate of the Jianjiang River. The largest rising water levels under the diversion discharge of  $200 \text{ m}^3\cdot\text{s}^{-1}$  and  $400 \text{ m}^3\cdot\text{s}^{-1}$  are 0.17 m and 0.18 m. According to the analysis above, the Manning coefficient decreases since the plants are overwhelmed by water with the discharge increasing to  $400 \text{ m}^3\cdot\text{s}^{-1}$ . However, the mean rising water level under the condition of high flood diversion is larger than that with lower flood diversion. In terms of velocity difference, *Zizania latifolia* located in the upper reaches of the old course

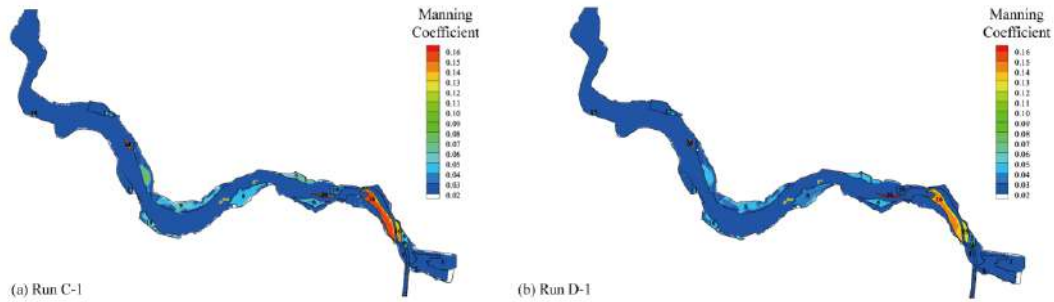


Fig. 7: Manning coefficient diagrams of Run C-1 and Run D-1.

of the Fuhe River has a greater obstruction to river flow. In contrast, other vegetation with low height on floodplains generally appear to be completely submerged under the condition of high flood diversion, and their water-blocking effect is weakened, which is reflected in the smaller decline in the velocity of vegetation area.

To analyze the vegetation influence on velocity distribution, 4 monitoring cross-sections were selected and their locations were presented in Fig. 8 (b) and (d). Changes in velocity distribution are illustrated in Fig. 9. With diversion discharge rising, the velocity of each cross-section generally increases. Besides, it clearly shows a changing trend which is

the velocity in the main channel increases while the velocity on the floodplain decreases because of the obstruction of plants on the floodplain.

Considering the ratio of the discharge in the main channel ( $Q_m$ ) to the discharge on floodplains ( $Q_f$ ), diversion ratios ( $Q_m/Q_f$ ) of each cross-section under different flood diversion and vegetation conditions were given in Table 3. The diversion ratio decreases with the increase of flood diversion discharge under the same vegetation condition. As affected by the vegetation, the diversion ratio increases, which means more discharge flows into the main channel, causing the adjustment of velocity distribution.

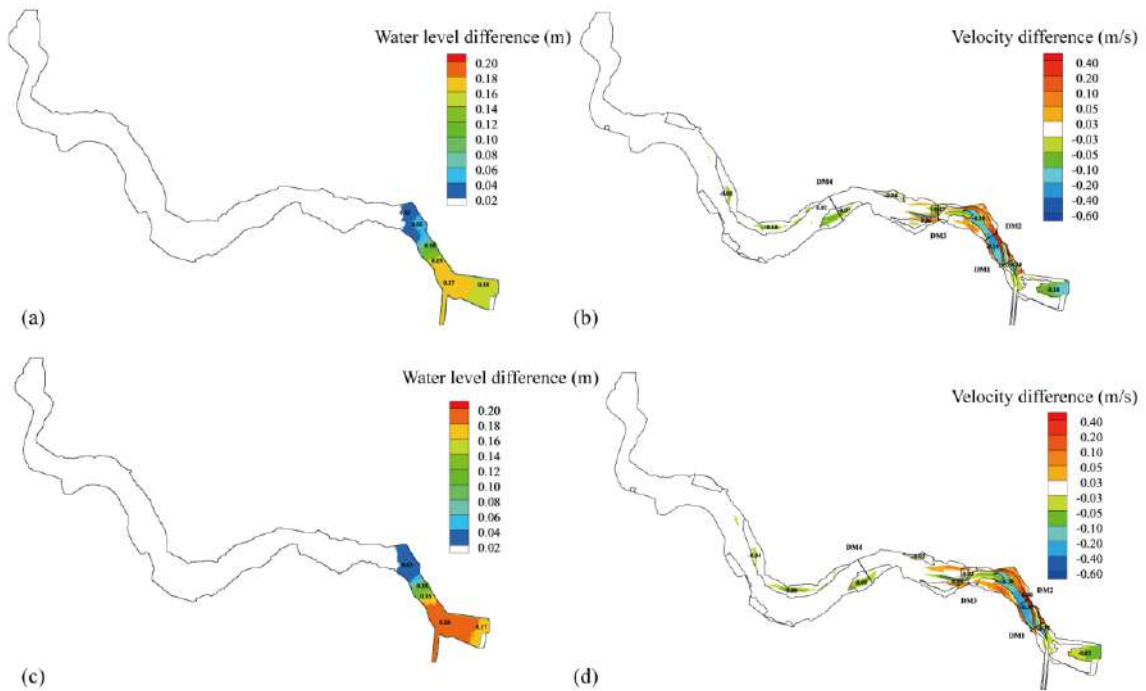


Fig 8: (a) Water level difference between Run C-1 and C-2; (b) Velocity difference between Run C-1 and C-2; (c) Water level difference between Run D-1 and D-2; (d) Velocity difference between Run D-1 and D-2.

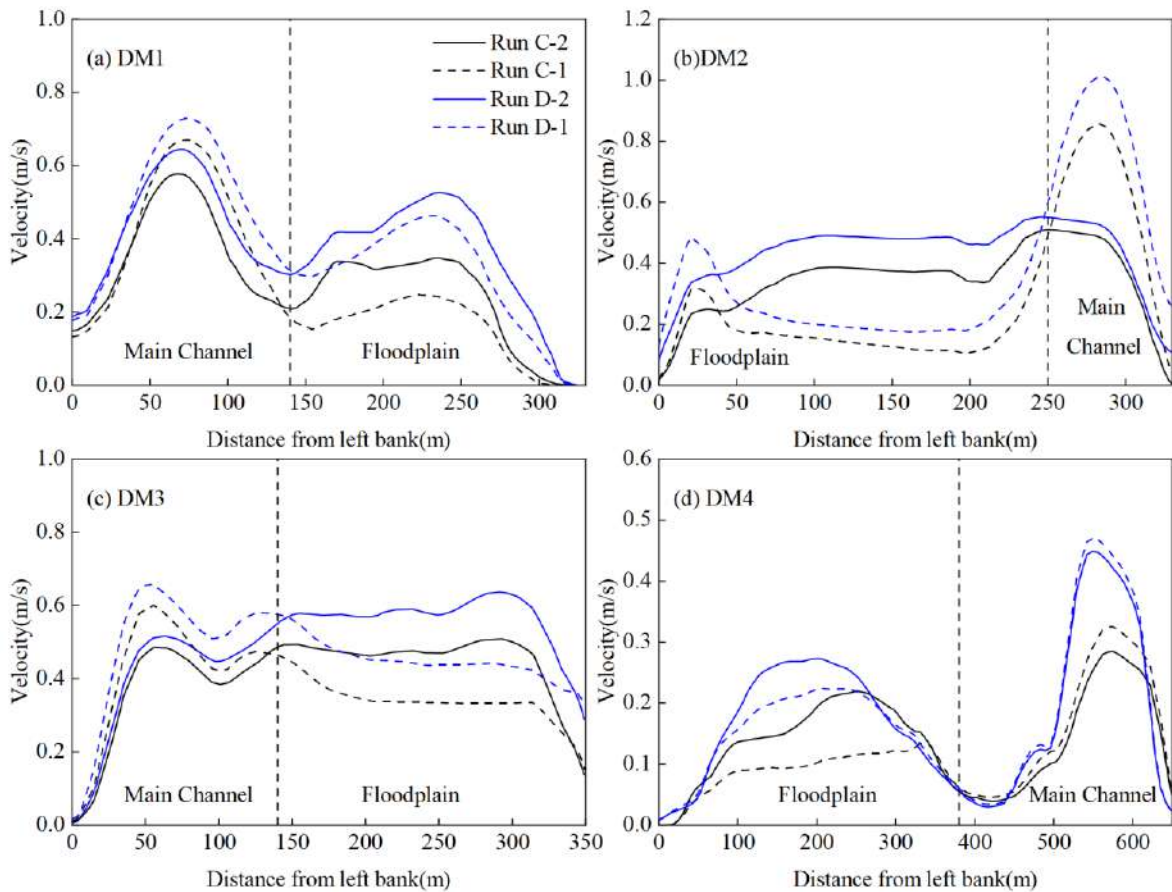


Fig. 9: Velocity distribution of 4 monitoring cross-sections.

### Influence of Vegetation on Hydrodynamics Considering Different Vegetation Development Conditions

Social development is accompanied by the contradiction between environmental protection and human survival. On the one hand, to weaken the impact of human activities on the old course of the Fuhe River, the farmland is considered to be converted into the area for growing *Zizania latifolia* which is helpful to promote water quality and ecological environment. On the other hand, with the increase in population, more farmland is needed for growing crops. Hence, to study the influence of changes in land use type on the hydrodynamics in the old course of the Fuhe River, this study considered these two kinds of land use type change illustrated in Fig. 10.

Under the flood diversion discharges of  $200\text{m}^3\cdot\text{s}^{-1}$  and  $400\text{m}^3\cdot\text{s}^{-1}$ , the Manning coefficient diagram of each condition was shown in Fig. 11. By comparing Fig. 11 (a) and (b), it could be seen that the Manning coefficient in the areas converted from farmland to growing *Zizania latifolia* has a

significant increase with the flood diversion discharge rising. It is because the topography of these areas is relatively high and *Zizania latifolia* is not completely submerged when the flood diversion discharge increases to  $400\text{m}^3\cdot\text{s}^{-1}$ . Therefore, with water depth increasing, the emergent *Zizania latifolia* has stronger resistance to water flow. In terms of expanding farmland in the old course of Fuhe River, the Manning coefficient of each farmland area decreases with the flood diversion discharge increasing from  $200\text{m}^3\cdot\text{s}^{-1}$  to  $400\text{m}^3\cdot\text{s}^{-1}$ .

Table 3: Diversion ratio of each cross-section under different conditions.

Run	Diversion ratio			
	DM1	DM2	DM3	DM4
C-1	3.70	3.03	2.83	3.92
C-2	3.43	1.67	2.52	3.03
D-1	2.25	2.27	1.43	2.49
D-2	1.08	1.22	1.38	2.14



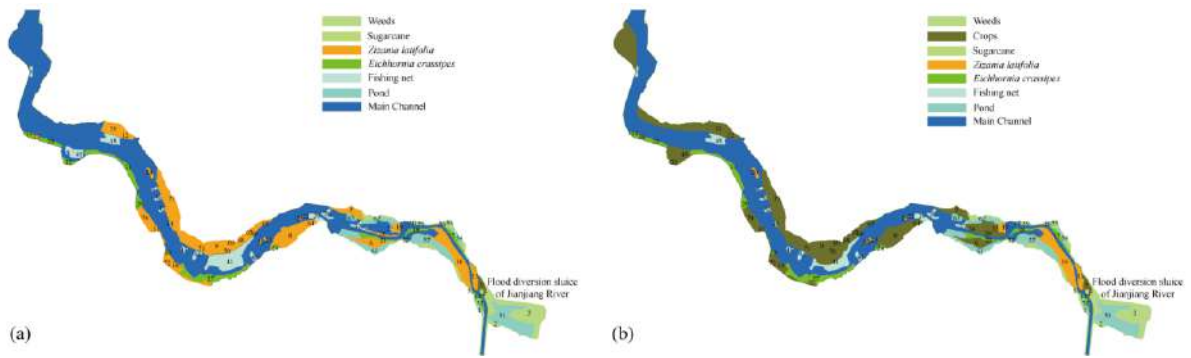


Fig. 10: (a) Convert farmland to *Zizania latifolia*; (b) Expand farmland.

By comparing Run C-3 with Run C-1 and Run D-3 with Run D-1, it was found changes in land use type would cause water levels rising and the significantly affected area is the upstream area of the old course of Fuhe River. Compared with the existing vegetation condition, the largest water level difference is about 0.035m under the flood diversion discharge of  $400\text{m}^3\cdot\text{s}^{-1}$ . As for velocity, the affected area is mainly the region where land use type is changed. The decreasing velocity in crop areas indicates that the water-blocking effect of *Zizania latifolia* is stronger than that

of crops. Besides, the decrease in velocity of the river bank where farmland is located causes the floodplain velocity on the opposite bank to increase. In terms of expanding farmland, water level and velocity differences are similar to the changing trend illustrated in Fig. 12.

**CONCLUSION**

This study adopted an equivalent Manning coefficient to establish the mathematical model of the vegetation module.

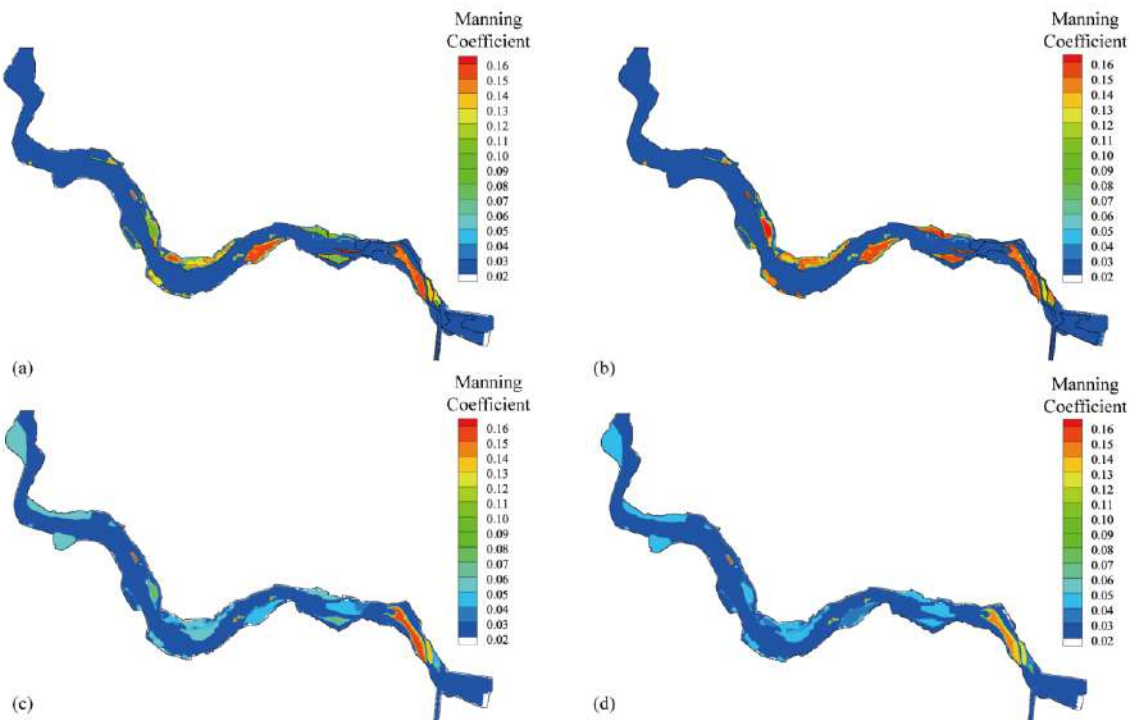


Fig. 11: Manning coefficient diagrams for (a) Run C-3; (b) Run D-3; (c) Run C-4; (d) Run D-4.

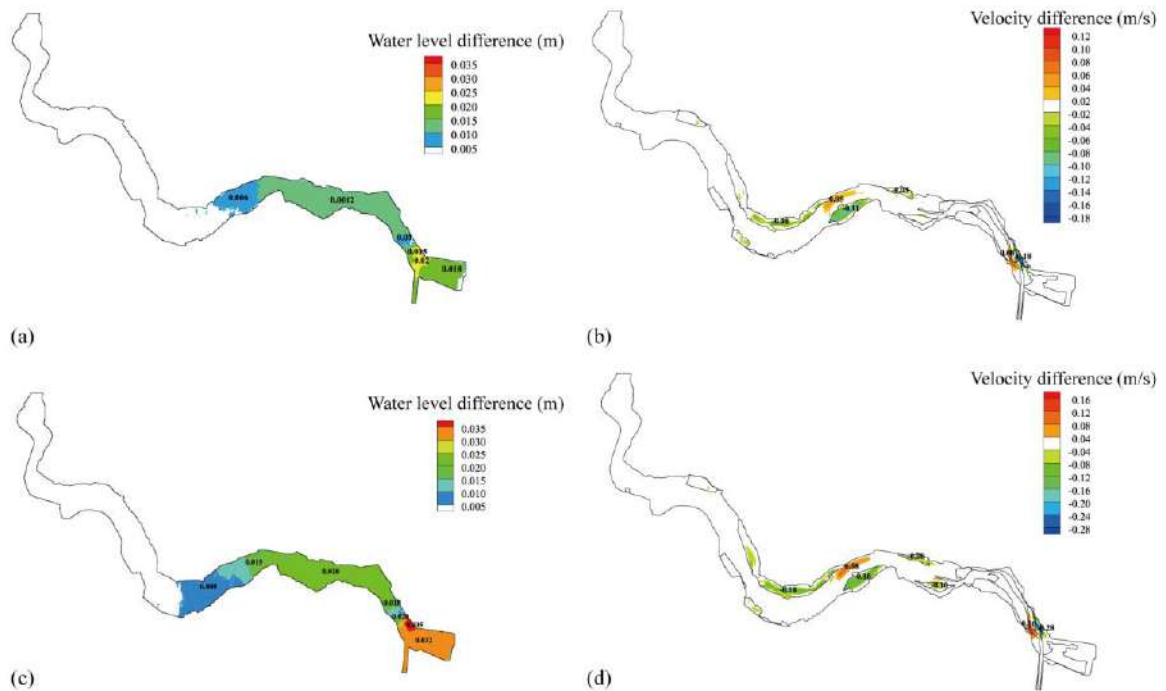


Fig. 12: (a) Water level difference between Run C-3 and C-1; (b) Velocity difference between Run C-3 and C-1; (c) Water level difference between Run D-3 and D-1; (d) Velocity difference between Run D-3 and D-1.

Combined with the hydrodynamic module and field investigation, the influence of vegetation patches on the hydrodynamics in the old course of the Fuhe River was studied by considering various combinations of incoming discharge, flood diversion discharge, and changes in land use type, which could be summarized as below.

- (1) The differences in vegetation characteristics (height, diameter, and density) lead to different resistance effects to water flow. Under the same running condition, *Zizania latifolia* has the strongest water-blocking effect followed by sugarcane, crops, and weeds.
- (2) The resistance effect of vegetation patches on floodplains causes the local flow velocity to decrease and the water level to rise, which would lead to the adjustment of cross-section velocity. The magnitude of water level difference and velocity difference is related to vegetation resistance and cross-section width.
- (3) With the increase in incoming discharge and flood diversion discharge, water level difference and velocity difference induced by vegetation increase.
- (4) Converting farmland to *Zizania latifolia* and expanding farmland have similar water-blocking effects. And velocity decreasing in the farmland area on the one side of the river bank would lead to an increase in velocity on the other side of the river bank.

## ACKNOWLEDGEMENT

This work was supported by the National Natural Science Foundation of China (Grant No. 51879199) and Major Technology Innovation of Hubei Province (No. 2019ACA154).

## REFERENCES

- Augustin, L.N., Irish, J.L. and Lynett, P. 2009. Laboratory and numerical studies of wave damping by emergent and near-emergent wetland vegetation. *Coast. Eng.*, 56(3): 332-340.
- Bai, F., Yang, Z., Huai, W. and Zheng, C. 2016. A depth-averaged two-dimensional shallow water model to simulate flow-rigid vegetation interactions. *Procedia Eng.*, 154: 482-489.
- Cheng, N.S., Wei, M. and Lu, Y. 2020. Critical flow velocity for incipient sediment motion in open channel flow with rigid emergent vegetation. *J. Eng. Mech.*, 146(11): 04020123.
- Choi, S.U. and Kang, H. 2004. Reynolds stress modeling of vegetated open-channel flows. *J. Hydraul. Res.*, 42(1): 3-11.
- D'ippolito, A., Calomino, F., Alfonsi, G. and Lauria, A. 2021. Flow resistance in the open channel due to vegetation at reach scale: A review. *Water*, 13(2): 116.
- Dijkstra, J.T. and Uittenbogaard, R.E. 2010. Modeling the interaction between flow and highly flexible aquatic vegetation. *Water Resour. Res.*, 46: w12547.
- Etminan, V., Ghisalberti, M. and Lowe, R. J. 2018. Predicting bed shear stresses in vegetated channels. *Water Resour. Res.*, 54(11): 9187-9206.
- Etminan, V., Lowe, R.J. and Ghisalberti, M. 2017. A new model for predicting the drag exerted by vegetation canopies. *Water Resour. Res.*, 53(4): 3179-3196.
- Follett, E. and Nepf, H. 2018. Particle retention in a submerged meadow and its variation near the leading edge. *Estuaries and Coasts*, 41(3): 724-733.

- Ghisalberti, M. and Nepf, H. 2006. The structure of the shear layer flows over rigid and flexible canopies. *Environ. Fluid Mech.*, 6(3): 277-301.
- Hou, J., Liang, Q., Simons, F. and Hinkelmann, R. 2013. A stable 2D unstructured shallow flow model for simulations of wetting and drying over rough terrains. *Comput. Fluids*, 82: 132-147.
- Huai, W., Yang, L., Wang, W. J., Guo, Y., Wang, T. and Cheng, Y. 2019. Predicting the vertical low suspended sediment concentration in vegetated flow using a random displacement model. *J. Hydrol.*, 578: 124101.
- Huai, W.X., Yang, S.C., Yang, Z.H. and Li, D. 2012. Numerical study of the behavior of the vegetated channel flow. *J. Shenzhen Univ. Sci. Eng.*, 29: 56-60 (in Chinese).
- Huang, Z., Yao, Y., Sim, S.Y. and Yao, Y. 2011. Interaction of solitary waves with emergent, rigid vegetation. *Ocean Eng.*, 38(10): 1080-1088.
- Li, D., Yang, Z., Zhu, Z., Guo, M., Gao, W. and Sun, Z. 2020. Estimating the distribution of suspended sediment concentration in submerged vegetation flow based on gravitational theory. *J. Hydrol.*, 587: 124921.
- Liu, M.Y., Huai, W.X., Yang, Z.H. and Zeng, Y.H. 2020. A genetic programming-based model for a drag coefficient of emergent vegetation in open channel flows. *Adv. Water Resour.*, 140: 103582.
- Nepf, H.M. 2012. Flow and transport in regions with aquatic vegetation. *Annu. Rev. Fluid Mech.*, 44: 123-142.
- Pasche, E. and Rouvé, G. 1985. Overbank flow with vegetatively roughened flood plains. *J. Hydraul. Eng.*, 111(9): 1262-1278.
- Schlichting, H. and Gersten, K. 2017. *Boundary-Layer Theory*. Springer Berlin Heidelberg, Berlin, Heidelberg.
- Sonnenwald, F., Stovin, V. and Guymier, I. 2019. Estimating drag coefficient for arrays of rigid cylinders representing emergent vegetation. *J. Hydraul. Res.*, 57(4): 591-597.
- Stone, B.M. and Shen, H.T. 2002. Hydraulic resistance of flow in channels with cylindrical roughness. *J. Hydraul. Eng.*, 128(5): 500-506.
- Tinoco, R.O. and Coco, G. 2016. A laboratory study on sediment resuspension within arrays of rigid cylinders. *Adv. Water Resour.*, 92: 1-9.
- Toro, E.F., Spruce, M. and Speares, W. 1994. Restoration of the contact surface in the HLL-Riemann solver. *Shock Waves*, 4(1): 25-34.
- Västilä, K. and Järvelä, J. 2018. Characterizing natural riparian vegetation for modeling of flow and suspended sediment transport. *J. Soils Sed.*, 18(10): 3114-3130.
- Whittaker, P., Wilson, C.A.M.E. and Aberle, J. 2015. An improved Cauchy number approach for predicting the drag and reconfiguration of flexible vegetation. *Adv. Water Resour.*, 83: 28-35.
- Wu, W. and Marsooli, R. 2012. A depth-averaged 2D shallow water model for breaking and non-breaking long waves affected by rigid vegetation. *J. Hydraul. Res.*, 50(6): 558-575.
- Yang, J.Q., Kerger, F. and Nepf, H.M. 2015. Estimation of the bed shear stress in vegetated and bare channels with smooth beds. *Water Resour. Res.*, 51(5): 3647-3663.
- Yang, J.Q. and Nepf, H.M. 2018. A turbulence-based bed-load transport model for bare and vegetated channels. *Geophys. Res. Lett.*, 45(19): 10428-10436.
- Yang, W. and Choi, S. U. 2010. A two-layer approach for depth-limited open-channel flows with submerged vegetation. *J. Hydraul. Res.*, 48(4): 466-475.
- Zhao, H., Yan, J., Yuan, S., Liu, J. and Zheng, J. 2019. Effects of submerged vegetation density on turbulent flow characteristics in an open channel. *Water*, 11(10): 2154.
- Zhu, Z., Yang, Z., Bai, F. and An, R. 2018. A new well-balanced reconstruction technique for the numerical simulation of shallow water flows with wet/dry fronts and complex topography. *Water*, 10(11): 1661.





# Studies on the Isolation of Lipids from Mangrove Isolated Cyanobacterial Species

P. Devesh, B. Aishwarya and R. Gyana Prasuna†

Department of Microbiology and Food Science & Technology, GITAM School of Science, Gandhi Nagar, Rushikonda, Visakhapatnam-530045, Andhra Pradesh, India

†Corresponding author: R. Gyana Prasuna; gravi@gitam.edu

Nat. Env. & Poll. Tech.  
Website: [www.neptjournal.com](http://www.neptjournal.com)

Received: 04-09-2021

Revised: 15-11-2021

Accepted: 19-11-2021

## Key Words:

Mangroves  
Cyanobacteria  
Phytoplankton  
Lipids

## ABSTRACT

Cyanobacteria are an important source of food and a primary producer of the aquatic food chains. Cyanobacteria are universally photosynthetic, with a higher plant type of photosynthesis, a large number of those also have the pivotal character of nitrogen fixation. Phytoplankton is made up of mostly cyanobacteria and microalgae. The microalgae store food in the form of lipids and serve as the source of energy as well as lipids for the fish. The lipid content of the fish depends on the diet that they take, and some of the lipids like the omega 3 and omega 6 fatty acids are derived from specific microalgae, like the marine protists and dinoflagellates including *Thraustochytrium*, *Schizochytrium*, and *Phaeodactylum*. Cyanobacteria being nutritionally more independent with nitrogen and carbon fixing ability, are more economical to grow in bulk. Hence the present work was aimed to screen the high lipid-containing cyanobacteria for use as fish feed. Five different cyanobacterial isolates, originally obtained from the mangroves were used as the sample cyanobacteria. The mangroves are a unique and at the same time stressful ecosystem. The significance of choosing cyanobacteria from this area is to allow for the isolation of cyanobacteria with unique characteristics. It is known that microorganisms from harsh or unique environments have even more potential for developing special survival strategies and for the production of more secondary metabolites. These cyanobacteria from stress environments can grow in conditions where other cyanobacteria or microalgae do not survive well. The isolation of lipids was performed by different extraction methods and separation using different solvent compositions was performed. The standard growth and biochemical studies of the cyanobacteria were conducted, followed by the assessment of their lipid content and variability. Out of the five isolates, a higher number of lipids were observed in AS1-(1) and AS2-(2). Lipids were isolated in chloroform-methanol and three variations of TLC were used to separate the lipids. The three are the single mobile phase, two mobile phase systems, and 2D development solvent system. The separation of the lipids gave the best results with the two mobile phase system, in which two different mobile solvent mixtures were used sequentially. The isolates AS1-(1) and AS2-(2) exhibited higher lipids, hence they could be a potentially suitable candidate as a fish feed.

## INTRODUCTION

### Cyanobacteria

Cyanobacteria (blue-green algae) are a group of bacteria showing higher plant-like photosynthesis. Cyanobacteria appeared approximately 2.5-3 billion years old and thus are the oldest oxygenic phototrophs on Earth. Even the development of an oxygen-rich atmosphere on Earth is attributed to cyanobacterial photosynthesis (Kumar et al. 2019, Garcia-Pichel 2009).

The cyanobacteria show oxygenic photosynthesis. However, they differ from the higher plants in having only one type of Chlorophyll, the Chlorophyll *a*, and lacking the chlorophyll *b*. Combinations of Chlorophyll *a*, together with other pigments like phycobilins, and carotenoids, result in the most commonly observed blue-green color of the cyanobacteria. The ability to change the pigment composition, by

altering the proportion of various pigments is another unique character. This allows harvesting light as per the light quality available allowing it to grow even in the polar regions, open ocean, and desert regions. In addition, the cyanobacterial nitrogen fixation can be a significant source of biologically available nitrogen in these ecosystems. Cyanobacteria are also one of the primary colonizers of many new ecosystems

Cyanobacteria is a large, heterogeneous group resembling the eukaryotic algae in many ways, including morphological characteristics and ecological niches. In fact, they were considered a type of algae before being regrouped in the kingdom Monera with the other prokaryotes, including the bacteria (Garcia-Pichel 2009).

Cyanobacteria are structurally simple with only one or two types of vegetative cells. Some of the species form the spores with thick walls called the akinetes, which might allow the cyanobacteria to tide over the stressful conditions.



Despite such simple and unspecialized structural evolution, the cyanobacteria show morphologically diverse forms. They show a very wide occurrence, in both the aquatic and terrestrial habitats (Sompong et al. 2005). They have widespread occurrence due to their physiological diversity, the filamentous species also occur either freely or in groups forming trichomes. Species such as certain *Nostoc* forms synthesize extracellular mucilage embedding the filaments in them and forming large structures like bunches and balls. The filamentous forms include nonheterocystous, and heterocystous genera. Heterocysts are specialized cells harboring enzymes for nitrogen fixation, a process by which atmospheric nitrogen ( $N_2$ ) is converted to a biologically useful form ( $NH_3$ ). All heterocystous and some non-heterocystous coccoid/filamentous cyanobacteria also fix nitrogen. By nitrogen fixation, the cyanobacteria can occupy the most varied ecosystems, including those devoid of reduced nitrogen compounds (Prasanna et al. 2009)

Most cyanobacteria do not grow in the absence of light (they are obligate phototrophs); however, some can grow in the dark if there is a sufficient supply of glucose to act as a carbon and energy source, this could be required for the symbiotic associations with plants where they are harbored away from light or when buried below the soil layers.

In addition to being photosynthetic, many species of cyanobacteria can also “fix” atmospheric nitrogen—that is, they can transform the gaseous nitrogen of the air into compounds that can be used by living cells. Particularly efficient nitrogen fixers are found among the filamentous species that have specialized cells called heterocysts (Garlapati et al. 2020). The heterocysts are thick-walled cells that have special structural features to make them impermeable to oxygen; they provide the anaerobic (oxygen-free) environment necessary for the operation of the nitrogen-fixing enzymes. In Southeast Asia, nitrogen-fixing cyanobacteria often grow abundantly in rice paddies, thereby eliminating the need to apply nitrogen fertilizers (Chittora et al. 2020)

Cyanobacteria reproduce asexually, either utilizing binary or multiple fission in unicellular and colonial forms or by fragmentation and spore formation in filamentous species. Under favorable conditions, cyanobacteria can reproduce at explosive rates, forming dense concentrations called blooms. Cyanobacteria blooms can color a body of water. For example, many ponds take on an opaque shade of green as a result of overgrowths of cyanobacteria, and blooms of phycoerythrin rich species cause the occasional red color of the Red Sea. Cyanobacteria blooms are especially common in waters that have been polluted by nitrogen or phosphorous wastes; in such cases, the overgrowths of cyanobacteria can consume so much of the water’s dissolved oxygen that fish

and other aquatic organisms perish (Ariosa et al. 2003). Two species, which fall under this category, are *Anabaena* and *Microcystis* (Watson et al. 2015, Kumar et al. 2019).

Cyanobacteria are one of the most successful organisms having survived so many ecological and environmental changes, in their atmosphere. There has been very little change in their structure. The physiological adaptations to global change have played a significant role in the success of cyanobacteria. As a group, they can tolerate desiccation, very cold and very hot temperatures, hypersalinity, variable visible light conditions, and high ultraviolet light conditions (Garcia Pichel 2009, Yamamoto 2009).

Cyanobacteria account for a larger proportion of the phytoplankton. Though the cyanobacteria have a simple structural variability, they are limited to only three cell types. They still show a wide variety of morphological, genetic, and ecological diversity in their occurrence in nature (Nayak et al. 2007). The cyanobacteria also present a very wide secondary metabolite production, with applications in the food, feed, pharmaceutical, and nutraceutical industries (Berg & Smalla 2009, Kumar et al. 2019, Carpine & Sieber 2021).

In addition to the large variability of production, the stability of the products of cyanobacterial origin has attracted scientists towards them (Carpine & Sieber 2021). The metabolites are stable over a wide range of pH and temperature and are generally easily soluble in water. There are over 200 genera of cyanobacteria, however, the production of secondary metabolites is more commonly reported from the cyanobacteria belonging to the order Oscillatoriales (49%), Nostocales (26%), Chroococcales (16%), Pleurocapsales (6%), and Stigonematales (4%) (Gerwick et al. 2008).

Foods containing the required amounts of essential nutritional compounds, such as carbohydrates, proteins, fats, vitamins, and minerals, are termed functional foods. They are designed to also contain certain bioactive compounds, exhibiting additional benefits for human health. Such bioactive compounds are generally derived from various plant or microbial sources (Liu et al. 2021).

One of the microorganisms used as a source of bioactive compounds cyanobacteria, has been exploited as a potential food supplement since ancient times. *Spirulina maxima* and some other cyanobacteria have been used as food for more than 600 years (Afnovandra et al. 2021, Alagawany et al. 2021).

The population of the world is on an ever-increasing wave from six billion in 1999 to seven billion in 2011, which may easily reach nine billion by 2050. The population puts pressure on the agricultural resources. Not only the population has to be provided with food, but also it has to be balanced

to overcome the nutritional deficiency. The fish is worldwide recognized as a delicacy with local flavors of each place. In addition, it is a very healthy alternative to providing nutrient-rich food. Fish also occupy a very special place, being one of the richest and in many cases the only way of obtaining omega 6 fatty acids, which helps to provide the crucial balance to the omega 3 fatty acids (Castej6 & Se6or6ns 2020, Jovanovic et al. 2021).

The food needs require that we check into alternative resources for food as well as active principles such as prebiotics, probiotics, or essential fatty acids (Afnovandra et al. 2021, Alagawany et al. 2021).

Despite a large number of plants and other sources being used as a source of active principles of health care or to provide nutrient benefits, cyanobacteria are still underutilized. *Spirulina* are probably the only cyanobacteria that have been utilized to a larger extent (Alagawany et al. 2021).

### Cyanobacteria as A Source of Lipids and Protein For Fish Feed

#### Use of Lipids in Fish Feed

- Lipids play important physiological roles in providing energy, essential fatty acids, and fat-soluble nutrients for the normal growth and development of fish.
- Fish oil, because of its high content of essential fatty acids, is used as the main lipid source in marine fish feeds.

Cyanobacteria are considered to have given rise to the higher eukaryotic chloroplasts through endosymbiosis. This appears true as the cyanobacterial lipids are similar to those in the inner envelope membranes and thylakoid membranes of the chloroplasts of higher plants. On the other hand, they show differences from those of many other bacteria, which generally show phospholipids as a major component of glycerol lipids. The cyanobacteria exhibit monogalactosyldiacylglycerol, digalactosyldiacylglycerol, and sulfoquinovosyldiacylglycerol, and a phospholipid, phosphatidylglycerol, as major glycerolipids (Oliveira et al. 2018, Uma et al. 2020). They also contain glycolipids. In the absence of reliable morphological and structural characteristics to differentiate between the different cyanobacterial genera, one taxonomic classification is also based on the type of fatty acids in the cyanobacteria. The lipids are also most sought after for commercial uses as the source of essential fatty acids for fish and animals and more vigorously in the recent past as the source of biofuel (Uma et al. 2020).

The ability to act as an important source of lipids and oils is due to the fast growth of many of the cyanobacteria. As also the significant quantities produced by many. The lipids

of cyanobacteria are generally esters of glycerol and long fatty acids. They may be either saturated or unsaturated. In the natural environment, cyanobacteria serve as one of the natural sources of essential fatty acids for animals (Semanti et al. 2021). These are also the same as required in the human diet. These essential fatty acids include the C18 linoleic (18:2 $\omega$ 6) and  $\gamma$ -linolenic (18:3 $\omega$ 3) acids and their C20 derivatives, eicosapentaenoic acids (20:5 $\omega$ 3) and arachidonic acid (20:4 $\omega$ 6). Certain filamentous cyanobacteria show a higher production of the polyunsaturated fatty acids accounting for 25 to 60 % of the total fatty acids. (4-6). Marine microalgae have been studied more with respect to the accumulation of lipids. Some cyanobacteria also show accumulation of lipids as reserve material.

## MATERIALS AND METHODS

### Isolation and Purification of Test Strains

A total of six heterocystous filamentous cyanobacteria were used in this study. All these strains were isolated from rice fields of Visakhapatnam and mangroves of Kakinada, India. The strains were subjected to purification by plating, sub culturing in sterile nitrogen source-free BG-11 agar medium (Rippka et al. 1979).

Cultures were inoculated in 500 and 1000 mL Erlenmeyer flasks containing 40% of the volume as BG-11 nitrogen source free medium and incubated at 28 $\pm$ 2 $^{\circ}$ C, in continuous light intensity from the cool white light source.

### Culture Conditions

The cyanobacteria were maintained on the standard BG 11 broth or agar medium. The medium composition is as under. Citric acid monohydrate (C<sub>6</sub>H<sub>8</sub>O<sub>7</sub>) - 6 g.L<sup>-1</sup>, Ferric ammonium citrate (C<sub>6</sub>H<sub>8</sub>FeNO<sub>7</sub>) - 6 g.L<sup>-1</sup>, dipotassium hydrogen orthophosphate (K<sub>2</sub>HPO<sub>4</sub>) - 40 g.L<sup>-1</sup>, magnesium sulfate heptahydrate (MgSO<sub>4</sub>) - 75 g.L<sup>-1</sup>, calcium chloride dihydrogen (CaCl<sub>2</sub>) - 36 g.L<sup>-1</sup>, sodium carbonate (Na<sub>2</sub>CO<sub>3</sub>) - 20 g.L<sup>-1</sup>, ethelene diamine tetra acetic acid (EDTA) - 1 g.L<sup>-1</sup> (0.1g.100 mL<sup>-1</sup>), trace metal solution. After proper mixing of solution, the medium was sterilized in an autoclave at a temperature of 121 $^{\circ}$ C, maintaining 15lb/inch<sup>2</sup> pressure for 15 min. Stock - 2 (ferric ammonium citrate) and stock - 3 (dipotassium hydrogen phosphate solutions) were sterilized separately and added to the medium after cooling as per Stanier et al. (1971).

### Inoculation

**Soil dilutions:** 1 g of soil sample was taken and serially diluted until 10<sup>-9</sup> dilutions. 10<sup>-6</sup> and 10<sup>-7</sup> dilution tubes of each culture were used to inoculate in 5 mL of BG11 broth

medium. An observation for growth was made after 10 to 15 days.

**Direct soil suspension:** For another set, 1g of soil sample was taken and added to 20 mL of saline or BG11 medium in 100 mL conical flasks. Put on a shaker for about 2 h for a complete suspension of the soil sample. Left to settle overnight and then inoculated the supernatant on solid BG 11 medium.

**Direct slide inoculation:** The soil sample was suspended in a minimum amount of water, and allowed to settle. The supernatant was later observed under the microscope. Capillary tubes were used to pick up visible cyanobacterial filaments, on observation and the tubes were put directly into 10 mL of BG11 broth medium in test tubes. The inoculated test tubes were incubated for growth.

**Culture maintenance:** The test cyanobacteria inoculated both on agar and broth medium were subcultured periodically. The colonies on Petri plates were used for restreaking and plating onto agar media to maintain the cultures. Re-streaking was performed monthly.

**Growth:** To assess the growth of various test organisms, a growth curve was made by repeated growth measurement over a period of 10-12 days. For this, the 20 mL culture tubes were used with the 5 mL of BG 11 broth. A homogenized thick suspension of the cyanobacterial samples was prepared by centrifuging actively growing culture suspension followed by homogenization. Homogenization was performed using a mechanical glass homogenizer in laminar airflow to maintain sterile conditions. An equal quantity of the thick suspension was added as inoculum in each of the tubes to a final O.D. to 0.08 -0.09 at 663 nm.

These inoculated culture tubes were transferred to culture racks. Care was taken to ensure all the tubes were equidistant from the light source. Every alternate day 3 test tubes with the suspension were utilized individually for doing growth and biochemical analysis. Growth measurement of samples was carried out at a 2-day interval for 16 days. Absorbance was measured in UV-Visible Spectrophotometer at 670 nm (Plate 13).

**Lipid estimation:** Equal quantity of cultures of the six cyanobacteria cultures AS2(2), AS1(2), AS1(1), AS5(1), AS4(2), and AS3(1) was taken. The cultures were homogenized in mortar and pestle. From this homogenized culture again, equal quantities of each culture were taken in three replicates each.

An equal amount of the homogenized culture was taken in centrifuge tubes and centrifuged at 5000 rpm for 5 min at 16 degrees temperature in high-speed centrifugation. The pellet was extracted in chloroform and methanol (2:1) repeatedly for complete extraction. The extracted solution

was transferred to the preweighed Petri dish and kept the plates in a hot air oven for 1 hour at 45 degrees temperature, for evaporation of the supernatant and collection of lipids. After complete evaporation, the Petri dishes were removed from the hot air oven and the weight of the dish was recorded. The lipids were redissolved in 1 mL of extract solvent and collected and stored in Eppendorf tubes.

### Preparation of Tlc Plates

TLC plates were poured using silica slurry and allowed to dry. After drying the TLC plates were kept in the hot air oven for 3 hours at 80 degrees temperature for activation.

### Lipid separation Using TLC

The separation of isolated cyanobacterial lipids was carried out in 3 ways as follows:

1. Single mobile phase
2. Dual mobile phases
3. 2D direction system

#### Single Mobile Phase

Chloroform, methanol, acetic acid, and water (80 mL: 9 mL: 12 mL: 2 mL) were used in the mobile phase.

#### Procedure

**Single mobile solvent system:** The lipid samples were loaded about 2cm from the bottom end of the TLC plate. For the single mobile solvent system, after a run covering 70% of plates, the plates were dried and developed with iodine crystals in a glass chamber, Followed later with the UV observation.

**Two mobile phase solvent systems:** In this method, the TLC was first run in the mobile phase of chloroform, methanol, and water (60 mL: 30 mL: 5 mL) till the 50% run was over. Whereafter the second mobile phase made of hexane, diethyl ether, and acetic acid was used (80 mL: 20 mL: 1.5 mL).

**2D development system:** The lipid extract from a single organism was taken in the TLC plate and treated with two solvent systems, after the completion of the run in one direction with one solvent system, the run was completed in the second direction after turning the TLC plate by 90 degrees. The first run of TLC plates was run in this solvent after rotating by 90 degrees, so that the run line of lipids in the first direction is towards the bottom, till the solvent front reached about 90% of the TLC plate. After drying the TLC plate, The chromatogram was developed with iodine crystals in a glass chamber.

Protein estimation for the different cultures (AS3-(1), AS2(4), AS1-(2), AS2-(2), AS5-(1), AS1(1)) was done using

Folin's method. 1mg of algal biomass + 1 mL of 1N NaOH was taken in a test tube and placed in a boiling water bath for 10min. The blank/sample tubes were added with reagent A ( 1 mL of freshly prepared Na-K tartrate solution containing 0.5% of  $\text{CuSO}_4$  and 2%  $\text{Na}_2\text{CO}_3$ ) and incubated for 10min. After incubation 0.5 mL of reagent B (Folin reagent) was added and incubated again for another 15min. Finally, the supernatant absorbance was recorded at 650nm. BSA solution standard curve was used to estimate the protein content (Lowry et al. 1951)

### Carbohydrates

Carbohydrates in the six test cultures were estimated by the anthrone method. 1mg of algal sample and 1.25 mL of double distilled water were added to a test tube, to this suspension freshly prepared Anthrone reagent (4 mL) was added and mixed thoroughly in the same way blank/ standard/sample tubes were prepared and these tubes were placed in boiling water bath for 10 min. The absorbance of the supernatant was observed at 620 nm against blank. The carbohydrate content was analyzed with a standard glucose curve (Spiro 1966)

## RESULTS AND DISCUSSION

### Growth Observation

The growth curve of all the six isolates was plotted (Fig. 1). It was observed that all the isolates showed an increase in growth as the time passed however in general an increase in

growth was obtained from the fourth day after inoculation. The highest growth was obtained in AS-2(2). Followed by AS-2(4) and AS 1(1).

### Protein

The protein content of the isolates was also quantified as a standard growth parameter. The protein values were taken after a growth of 15 days for all the cultures (Fig. 2). An equal quantity of the biomass was taken for protein assay. The highest amount of protein was obtained with AS3(1) with 38 micrograms per milligram protein, followed by As-2(2) with less than 37  $\mu\text{g}/\text{mcg}$  per mg. The minimum quantity was observed in AS-5(1) at 28  $\mu\text{g}/\text{mcg}$  per mg.

### Estimation of Carbohydrates

**Carbohydrate analysis:** Carbohydrate content was highest in AS1 (1) followed by AS-2(4) and AS-2(2). The graphs and results show that carbohydrate content was low in AS-5[1] and the highest carbohydrate content was seen in AS-2[4] followed by AS-3[1] (Fig. 3).

### Lipids

**RF value of lipids in single mobile phase:** The five cyanobacterial isolates each showed separation of two lipid spots. With almost similar Rf, in the common range of 0.45 to 0.48 and 0.52 to 0.54.

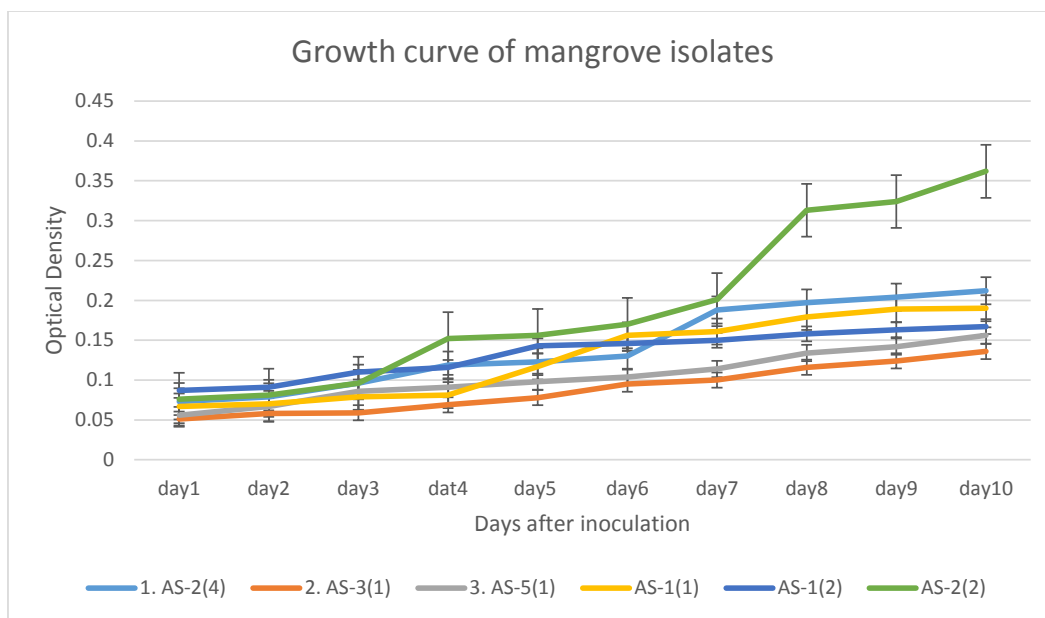


Fig. 1: Growth curve of the six cyanobacteria (Mangrove isolates), the growth was recorded every day for up to 10 days. Growth was measured as optical density at 663 nm.

**RF value of lipids in two mobile phases:** In two mobile phase systems AS1-(1) showed the largest number of the lipid spots with 9 separate spots developing with iodine followed by AS2-(2) (Plates 1-3 and 7-9)). AS4-(2)(Plate 10), and AS5-(1) (Plates, 12) both showed the development

of seven lipid spots the least number were observed in AS3-(1) (plate-11). AS1-(2) showed the development of only six spots (plates 4-6). This result clearly indicates the much better separation of lipids spots of the cyanobacteria with the two solvent systems.

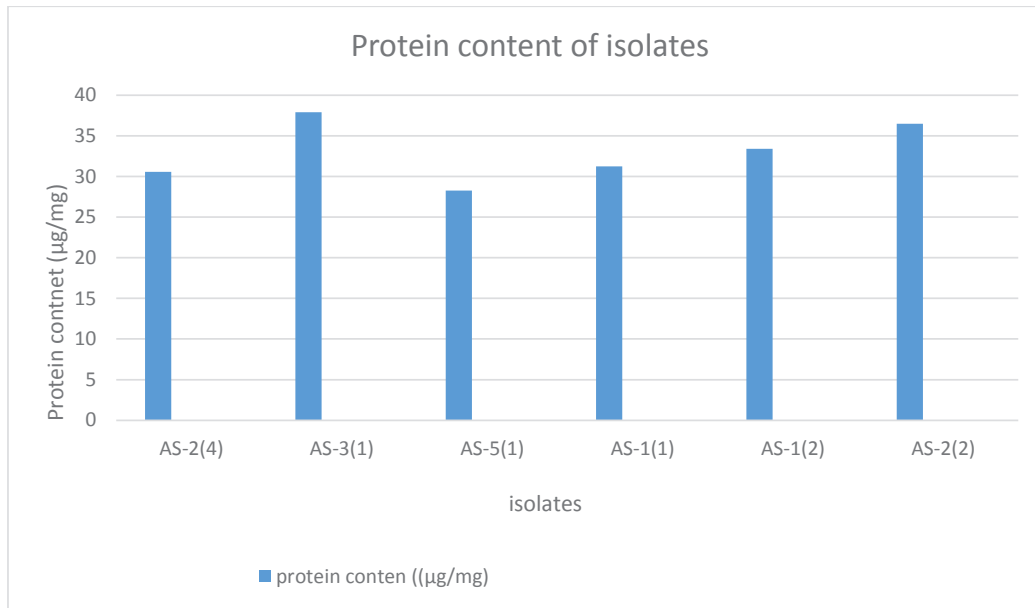


Fig. 2: Protein content of test cyanobacterial isolates (AS-2(4), AS-3(1), AS-5(1), AS-1(1), AS-1(2), and AS-2(2)) was tested for 15 DOI cultures of equal biomass (as a Chl *a* measure).

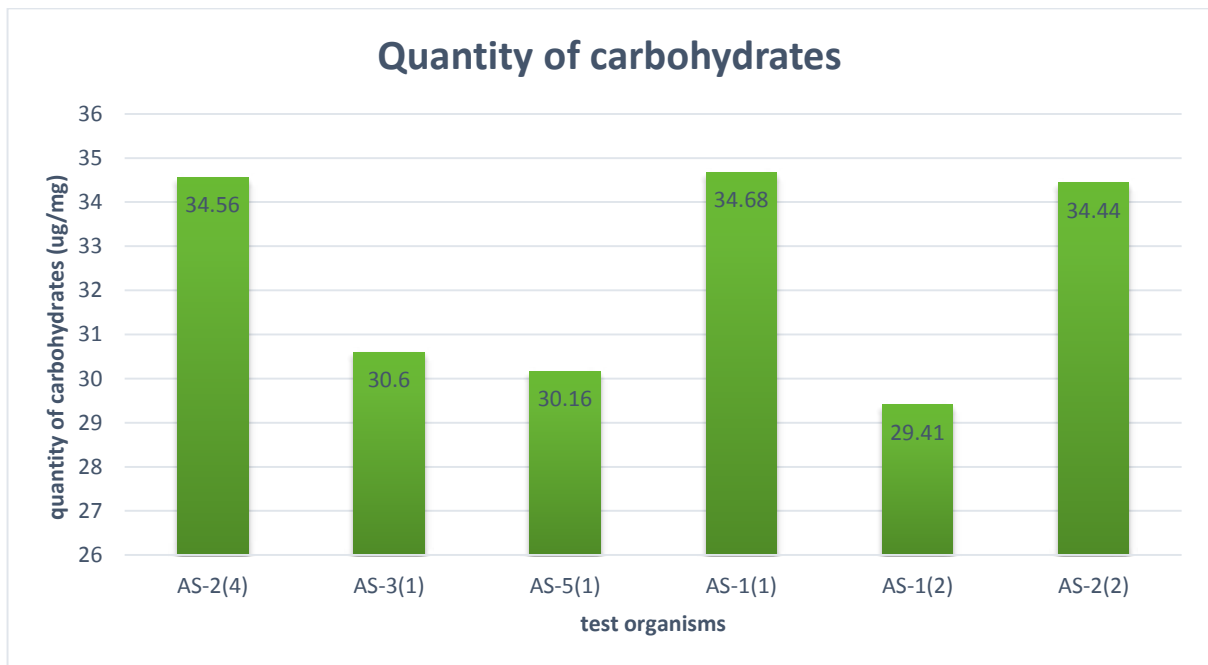


Fig 3. Quantification of carbohydrates in cyanobacterial isolates by anthrone method. Equal biomass (as a measure of OD at 663nm) of all five isolates was used to test for total carbohydrate.



**RF value of lipids in the 2D development system**

1. AS1-(1)

**Step-1**

chloroform : methanol: water



**Plate 1:** Lipid separation using Two mobile phases; Step 1, of 2D separation of isolate AS1-(1)

**Step-2**

Hexane: Diethyl ether: Acetic acid



**Plate 2:** Lipid separation using Two mobile phases; Step 2, lipids after separation of isolate AS1-(1)

**Step-3**

Treating with iodine

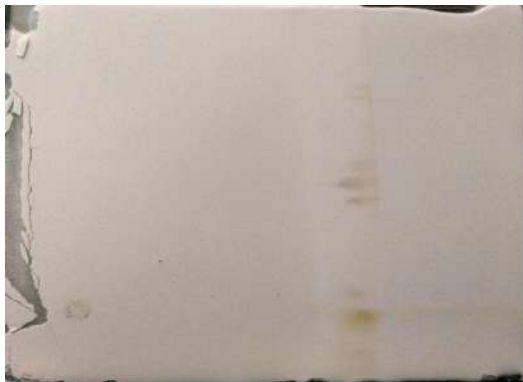


**Plate 3:** Lipid separation using Two mobile phases; Step 3, lipids stained with Iodine vapors of isolate AS1-(1)

2. AS1-(2)

**Step-1**

chloroform: methanol: water

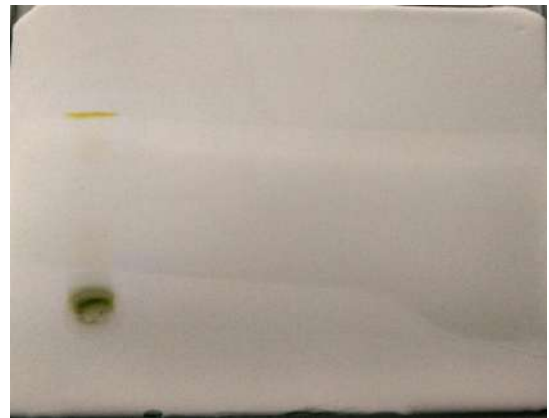


**Plate 4:** lipid separation using Two mobile phases; Step 1, of 2D separation of isolate AS1-(2)

**Step-2**

Hexane: Diethyl ether: Acetic acid



**Plate 5:** Lipid separation using Two mobile phases; Step 2, lipids after separation of isolate AS1-(2)

**Step-3**

Treating with iodine



**Plate 6:** Lipid separation using Two mobile phases; Step 3, lipids stained with Iodine vapors of isolate AS1-(2)

## 3. AS2-(2)

**Step-1**

chloroform : methanol : water



**Plate 7:** Lipid separation using Two mobile phases; Step 1, of 2D separation of isolate AS2-(2)

## 4. AS4-(2)



**Plate 10:** Lipid separation using Two mobile phases AS4-(2)

**Step-2**

Hexane : Diethyl ether : Acetic acid

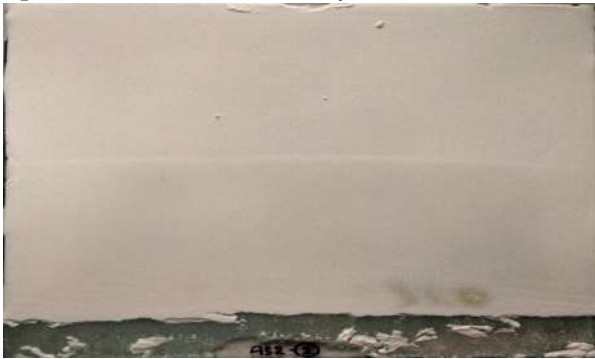


**Plate 8:** Lipid separation using Two mobile phases; Step 2, of 2D separation of isolate AS2-(2)

## 5. AS3-(1)



**Plate 11:** Lipid separation using Two mobile phases AS3-(1)

**Step-3** Treating with iodine

**Plate 9:** Lipid separation using Two mobile phases; Step 3, of 2D separation of isolate AS2-(2)

## 6. AS5-(1)



**Plate 12:** Lipid separation using Two mobile phases AS5-(1)



**Plate 13:** Cultures growing under the light.

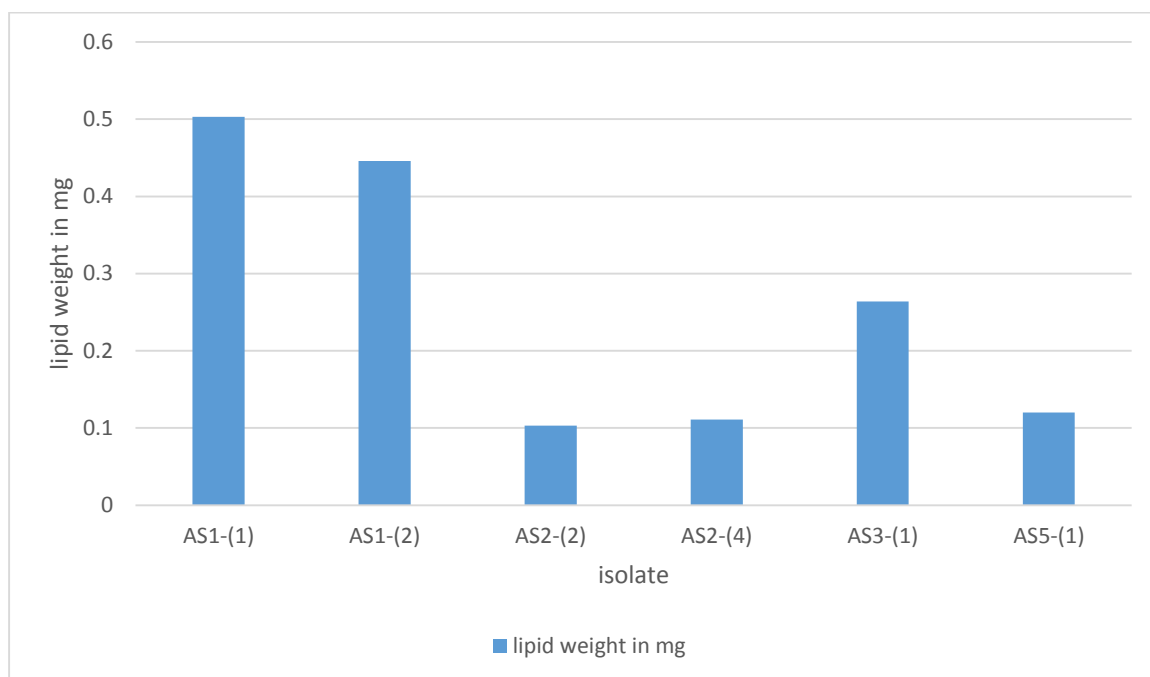


**Fig. 4:** Lipid weight (Lipid isolated from the same amount of culture).

The third type of lipid separation used was the 2D system, however, we were unable to find good development of spots, which may have been likely due to the need for standardization of the solvent system.

The lipid weight of the lipid isolated from the same amount of culture is shown in Fig. 4. Just as observed with

the number of lipid spots developed in the two solvent systems, the lipid quantity was highest in AS1-1, however, AS1-(2) which showed production of 0.446 mg of the lipid exhibited only six spots.

It is well known that lipid production differs quantitatively and qualitatively depending on the need in different

cyanobacteria. It would be interesting to find out if the higher number of lipids produced would improve the lipid levels of a fish diet or the high quantity.

**Conclusion:** Our work points out that mangrove cyanobacteria can be used as a source of good protein and lipid content for fish or other aquatic animals.

The lipid content of cyanobacteria could prove a very important source for introducing lipids into fish.

## ACKNOWLEDGMENT

RGP thanks the Ministry of Earth Sciences for the Major Research project with no. 27/04/2017; MoES/36/OOIS/Extra/57/2016. BA thanks the MOEs grant for the JRF grant. The authors thank GITAM GSS for providing the facilities to work.

## REFERENCES

- Afnovandra, B., Zulkarnain, P., Arif Juliar, C., Abdi Dharma, K., Zakaria, I.J., Syafrizayanti, A.B. and Putra, M.Y. 2021. Omega-3 fatty acids of microalgae as a food supplement: A review of exogenous factors for production enhancement. *Algal Research*, 60.
- Alagawany, M., Taha, A.E., Ahmed Noreldin, K.A., El-Tarabily, M. and Abd El-Hack, E. 2021. Nutritional applications of species of *Spirulina* and *Chlorella* in farmed fish: A review, *Aquaculture*, 542.
- Ariosa, Y., Carrasco, D., Qucsedda, A. and Valentine E.F. 2003. Incorporation of different sources and light response curves of nitrogenase and photosynthesis by cyanobacterial blooms from rice fields. *Microbial Ecol.*, 51: 394-403
- Berg, G. and Smalla, K. 2009. Plant species and soil type cooperatively shape the structure and function of microbial communities in the rhizosphere. *FEMS Microbiol. Ecol.*, 68: 1-13.
- Carpine, R. and Sieber, S. 2021. Antibacterial and antiviral metabolites from cyanobacteria: Their application and their impact on human health. *Curr. Res Biotechnol.*, 3: 65-81.
- Castej6, N. and Se6or6ns, F.J. 2020. Enzymatic modification to produce health-promoting lipids from fish oil, algae and other new omega-3 sources: A review, *New Biotechnology*, 57: 45-54.
- Chittora, D., Mukesh, M., Tansukh, B., Prashant, S. and Sharma, K. 2020. Cyanobacteria as a source of biofertilizers for sustainable agriculture. *Biochem. Biophys. Rep.*, 22: 1-8.
- Garcia-Pichel, F. 2009. Cyanobacteria. In Schmidt, T. (ed), *Encyclopedia of Microbiology*, Third Edition, Elsevier Publications, The Netherlands, pp. 107-124
- Garlapati, D., Thangavel, M., Susaimanickam, A., Tharifkhan, S.A., Devanesan, A.A. and Arivalagan, P. 2020. Applications of microalgal and cyanobacterial biomass on a way to safe, cleaner, and sustainable environment. *J. Clean. Prod.*, 11: 253.
- Gerwick, W.H., Coates, R.C., Engene, N., Gerwick, L., Grindberg, R.V., Jones, A.C. and Sorrels, C.M., 2008. Giant marine cyanobacteria produce exciting potential pharmaceuticals. *Microbe-American Society for Microbiology*, 3(6): 277.
- Hushchyna, K. and Nguyen-Quang, T., 2020. A New Index Contributing to an Early Warning System for Cyanobacterial Bloom Occurrence in Atlantic Canada Lakes. *Nat. Env. & Poll. Tech.*, 19(5): 1887-1897.
- Jovanovic, S., Dietrich, D., Becker, J., Kohlstedt, M. and Wittmann, C. 2021. Microbial production of polyunsaturated fatty acids-high-value ingredients for aquafeed, superfoods, and pharmaceuticals. *Curr. Opinion Biotechnol.*, 69: 199-211.
- Kumar, D.S., Tyagi, M.B. and Kumar, A. 2019. Applications in Biotechnology in Cyanobacteria. In Mishra, A.K., Tiwari, D.N. and Rai, A.N. (eds), *Cyanobacteria: From Basic Science to Applications*, Elsevier, The Netherlands, pp. 327-346.
- Li, R., Wilhelm, S.W., Carmichael, W.W. and Watanabe, M.M. 2008. Polyphasic characterization of water bloom-forming *Rapidiopsis* species (cyanobacteria) from central China. *Harmful Algae*, 7: 146-153.
- Liu, D., Liberton, M., Hendry, J.L., Aminian-Dehkordi, J., Maranas, C.D. and Himadri, B.P. 2021. Engineering biology approaches for food and nutrient production by cyanobacteria. *Curr. Opinion Biotechnol.*, 67: 1-6.
- Lowry, O., Rosebrough, N., Farr, A.L. and Randall, R. 1951. Protein measurement with the Folin phenol reagent. *J. Bio. Chem.*, 193(1): 265-275.
- Mahajan, G.B. and Balachandra, L. 2017 Sources of antibiotics: Hot springs. *Biochem. Pharmacol.*, 134: 35-41.
- Nayak, S., Prasanna, R., Prasanna, B.M and Sahoo, D.B. 2007. Analyzing diversity among Indian isolates of *Anabaena* (Nostocales, Cyanophyta) using morphological physiological and biochemical characters. *World J. Microbiol. Biotechnol.*, 23: 1575-1584.
- Oliveira, D.T., Vasconcelos, C.T., Feitosa, A.M.T., Aboim, J.B., Oliveira, A.B, Luciana P.X., Santos, A.S., Goncalves, E.C., Filho, G.N.D.R. and Nascimento, L.A.S.D. 2018. Lipid profile analysis of three new Amazonian cyanobacteria as potential sources of biodiesel. *Fuel*, 234: 785-788.
- Prasanna, R., Jaiswal, P., Nayak, S., Sood, A. and Kaushik, B.D. 2009. Cyanobacterial diversity in the rhizosphere of rice and its ecological significance. *Indian J. Microbiol.*, 49: 89-97.
- Rippka, R., Deruelles, J., Waterbury, J.B., Herdman, M., and Roger, Y.S. 1979. Generic assignments, strain histories, and properties of pure cultures of Cyanobacteria. *J. General Microbiol.*, 111: 1-61.
- Semanti, P.R.S., Robin, R.P. and Purvaja, R.R. 2021. Fatty acid signatures of sediment microbial community in the chronically polluted mangrove ecosystem, *Marine Pollut. Bull.*, 17: 172.
- Sompong, U., Hawkins, P.R., Besley, C. and Peerapornpisal, Y. 2005. The distribution of cyanobacteria across physical and chemical gradients in hot springs in northern Thailand. *FEMS Microbiol. Ecol.*, 52(3): 365-376.
- Spiro, R.G. 1966 Analysis of sugars found in glycoproteins. *Methods Enzymol.*, 8: 3-26.
- Stanier, R., Kunisawa, R., Mandel, M. and Cohen-Bazire, G. 1971. Purification and properties of unicellular blue-green algae (order Chroococcales). *Bacteriol Rev.*, 35:171-205.
- Uma, V.S., Gnanasekaran, D., Lakshmanan, U. and Dharmar, P. 2020. Survey and isolation of marine cyanobacteria from the eastern coast of India as a biodiesel feedstock. *Biocatal. Agric. Biotechnol.*, 24: 1-8.
- Varshney, P., Mikulic, P., Vonshak, A., Beardall, J. and Wangikar, P.P. 2015. Extremophilic micro-algae and their potential contribution to biotechnology. *Bioresour. Technol.*, 184: 363-372.
- Ward, O.P. and Singh, A. 2005. Omega-3/6 fatty acids: Alternative sources of production. *Process Biochem.*, 40(12): 3627-3652.
- Watson, S.B., Brian, A.W., Scott, N.H., Hans, W., Paerl, B.W. and Brooks, W. 2015. Harmful Algal Blooms, In John, W., Sheath, J. and Patrick, K. (eds.), *In Aquatic Ecology Freshwater Algae of North America*, Second Edition, Elsevier, The Netherlands, pp. 873-920.
- Yamamoto, Y. 2009. Effect of temperature on recruitment of cyanobacteria from the sediment and bloom formation in a shallow pond. *Plank. Benthos*, 4(3): 95-103.



# An Investigation of a Hybrid Plasma Gasification System for Various Waste Plastics Thermochemical Degradation in the Fuel Extraction Process

Akhilesh Kumar Dewangan<sup>†</sup>, Isham Panigrahi and R. K. Paramguru

School of Mechanical Engineering, KIIT Deemed to be University, Bhubaneswar, Odisha, India

<sup>†</sup>Corresponding author: Akhilesh Kumar Dewangan; akhilesh.dewangan@kiit.ac.in

Nat. Env. & Poll. Tech.  
Website: [www.neptjournal.com](http://www.neptjournal.com)

Received: 27-08-2021

Revised: 10-11-2021

Accepted: 14-11-2021

## Key Words:

Hybrid plasma gasification  
Energy recovery  
Degradation  
Pyrolysis  
Alternative fuel

## ABSTRACT

Organic junk contamination is one of the serious environmental concerns throughout today's world. Heavy usage of throwaway plastics devastates nature by obstructing rainwater drainage. From constant exposure to sunlight and warmth, plastics release hazardous gasses into the atmosphere. To reflect the vastly increased amount of various waste plastics, a scaled hybrid plasma gasification reactor is being introduced, which uses an advanced pyrolysis process to break down the plastic waste. The design is simple, transportable, easy to handle, and required very little repair work on long-period usage. Thermochemical investigations are carried out at temperatures ranging from 400 to 600 degrees Celsius, with heating rates ranging from 15 to 22 degrees Celsius per minute, yielding 76-88 percent pyrolysis oil, 10-23 percent syngas, and 4-15 percent chars as besides. It occurs when the molecular architecture of polymers is separated, resulting in the creation of Synthesis gas, which is then condensed into synthesis petroleum fuel. The highest yielding of oil utilizes gas and solid char is determined at 550°C, 600°C, and 450°C respectively, according to the computed pyrolysis kinetic parameter on oil recovery from various waste plastics. The mono-graphic analysis is also used to classify different waste residual char. The model reduces the volume of waste plastic by 89.2%, lowering the detrimental impacts on all living things while simultaneously producing a synthesis of petroleum fuel as a by-product that may be utilized as a replacement or addition to traditional fuel.

## INTRODUCTION

Households and hospitals generate a large amount of plastic waste from single-use items. It's no secret that single-use plastic has a harmful effect on the environment. Plastic trash degradation takes between 8 and 1200 years. As a result, it forms a layer over the land surface that acts as a shield to rainfall sinking into the land. Furthermore, it produces hazardous gases into the surroundings as a result of constant solar radiation and heat, which causes health problems for living creatures so it is also partially accountable for environmental warming (Dutta & Paul 2019). In India, around 2,73,84,000 kg of plastic waste is generated every day (Manuja et al. 2020). Today, plastic waste management has become a major concern in developed countries (Gupta et al. 2015). It has been reported that by 2022, India's annual plastic consumption will increase from 15 million tonnes to 24 million tonnes annually. As a result of synthetic polymers made from petroleum as raw material (Salandra 2018), India's plastic manufacturing industries have grown over the past seven degenerations. Polyethylene Terephthalate, Polyethylene, High-Density Polyethylene, Acrylonitrile butadiene styrene, Low-Density Polyethylene, Polyvinyl Chloride, Polypropylene, Polystyrene, polyamide, and

polybutylene terephthalate are some of the most important synthetic plastic polymer products. These products generate 52% of the plastic waste that ends up in rivers and on land. As a result, India's single-use plastic waste management is a major concern. For hospital waste, however, there are no international standards for the classification of the waste. World Health Organization (WHO) estimates that 20 percent of plastic hospital wastes are potentially unsafe materials that may contain a transferrable, poisonous, or irradiated element (Fang et al 2020). From the perceptive of ecological preservation and preventing infection, it has innumerable implications to improve the appropriate and safe treatment and disposal of medical waste plastics.

The thermolysis process also knowns as gasification or pyrolysis, is one of the most important chemical recycling technologies for waste plastic. In this process splitting frequency involve a temperature at which plastic molecules vibrates is directly proportional to the temperature of the molecules and a high temperature and restriction of oxygen cause material breakdown, which might result in syngas, liquids, or wax as the ultimate product, depending on the conditions of pyrolysis (Rahimi & García 2017). For the recycling of plastic waste, experts have devised and tested a variety of methods. Mechanical recycling techniques are



ideal, but plastic trash must be homogeneous and uncontaminated during the recycling process for it to be successful (Punčochář et al. 2012).

Thermolysis or gasification is an alternative to burning treatment that has been extensively investigated (Pinto et al. 2002, Sekiguchi & Orimo 2004), with several patents already in place. Even now, thermal plasma technology is a well-known technology, and its research is ongoing. Metallurgical processing, synthesizing, and coating processes are all well-known applications for this technique (Sekiguchi and Orimo 2004). In the plasma process, an electron breaks the molecules as travel through a high electrical field, which causes dissociation, ionization, and, excitation of the originating material. This creates exciting molecular species, ionic and active radical forms that trigger the chemical plasma reaction (Tendero et al. 2006, Fridman et al. 2008).

Considering safety concerns, the most important use of thermal plasma waste treatment is the obliteration of hazardous materials (Pun ochá et al. 2012, Samal 2017), instead of conventional recycling or mechanical recycling techniques. Compared to the standard pyrolysis process, thermal plasma pyrolysis provides many advantages. As a result of a high amount of energy for the thermolysis process, it produces a high temperature. As a result of the rapid heating of the material, certain significant reactions occur that do not emerge in the traditional pyrolysis approach (Heberlein & Murphy 2008). As a result of the higher temperature, it generates more syngas (a volatile substance including CO, H<sub>2</sub>, CH<sub>4</sub>, C<sub>2</sub>H<sub>2</sub>, and other hydrocarbons) with a lower tar content, which may be utilized immediately to drive gas turbine power plants or

stored for use in other applications. Organic carbon solids waste may be transformed into valuable gaseous fuel by using the thermal plasma method, as demonstrated in previous bench-scale studies (Mumbach et al. 2019).

The research investigation focused on a hybrid plasma gasification reactor system for waste plastic as organic material. The main areas that have been presented for studies are gathered detailed details on the characteristics of waste plastic materials in the pyrolysis process. On hybrid plasma, pyrolysis to evaluate the pyrolysis oil recovery rate and kinematics parameters with varied temperature variances in different waste plastic. On conduct comparative investigations of residual weight analysis using a variety of temperature ranges from the pyrolysis process. And investigate waste char slag from various organic carbon solids waste during hybrid plasma pyrolysis.

## MATERIALS AND METHODS

### Setup and Procedure

Experimental setup equipped with a hybrid heating technology on the combination of the bottom electric heater with advanced cylindrical plasma heater for batch gasification reactor. The reactor has a volumetric capacity of eight kg per hour of organic waste materials. Fig. 1 shows the schematic diagram of a hybrid plasma gasification reactor. The hybrid plasma gasification reactor vertical type, heating furnace height of 0.80 m, and diameter of 0.25 m. A screw feeder-powered motor feeds small bits of organic waste from top feeding storage raw material storage, and then into the

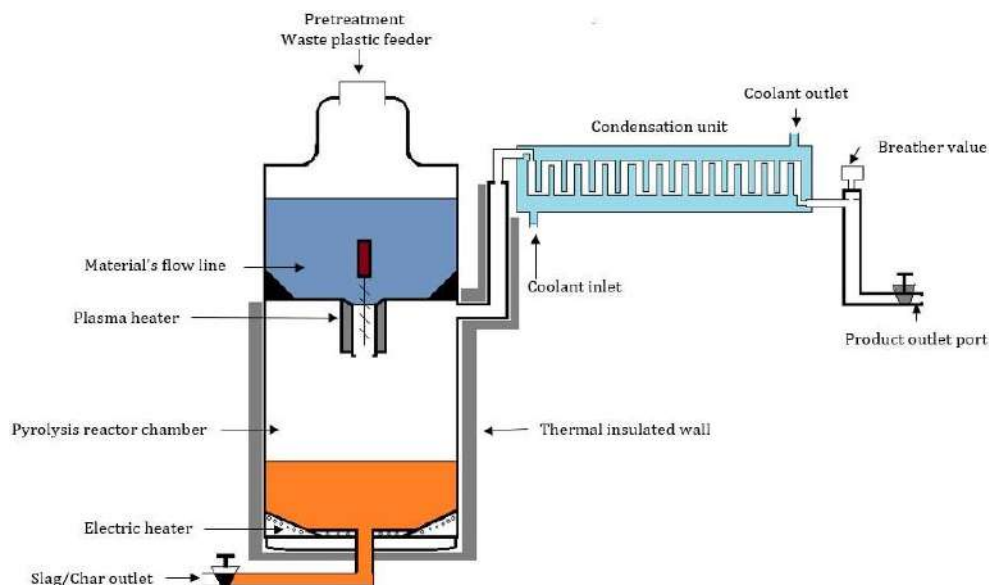


Fig. 1: Schematic diagram of hybrid plasma gasification reactor.

plasma gasification unit. An optional inert (nitrogen) gas port for supply to the reactor chamber with a control pressure valve for the removal of oxygen for the pyrolysis method. The inner part of the plasma heater is revealed in Fig. 2. The plasma heater's surface is composed of stainless steel and has two layers. To prevent heat loss, both sides of the plasma heater are coated with refractory clay. Fig. 2 shows a graphite electrode set at an equal distance between stainless steel half-circular rings anodes fixed within the plasma heater in such a way that voltage from the power source can generate high temperature at the feeder point without damaging the heater pipe in the reactor. A molten liquid sterling motor and a sterling motion unit are employed at the bottom of the furnace, coupled with an 800 W modified electric heater attached at the bottom of the reactor, due to the high viscosity of the liquid state.

Waste from the reactor chamber is collected via a waste slag/char outflow. The pressure sensor is used to determine the stability of the reactor, while the temperature sensor is a K-type thermocouple. For the condensation process, pressurized syn-gases are fed into the condenser. The condensation of synthesis gas takes place in a liquid heat exchanger. Fig. 1 depicts the coolant inlets and outflow port. Subsequently, it is stored in the final collector container through the product outlet valve. The temperature profile up to 600°C was used to investigate the temperature distribution in the reactor chamber during pyrolysis without raw material and a thermal plasma system. Fig. 3 shows a temperature distribution profile. The temperature was measured in an empty reactor chamber at a 15°C time interval. Fig. 4 shows the placement of the thermocouple and it's used for the measurement of temperature during the experiment.

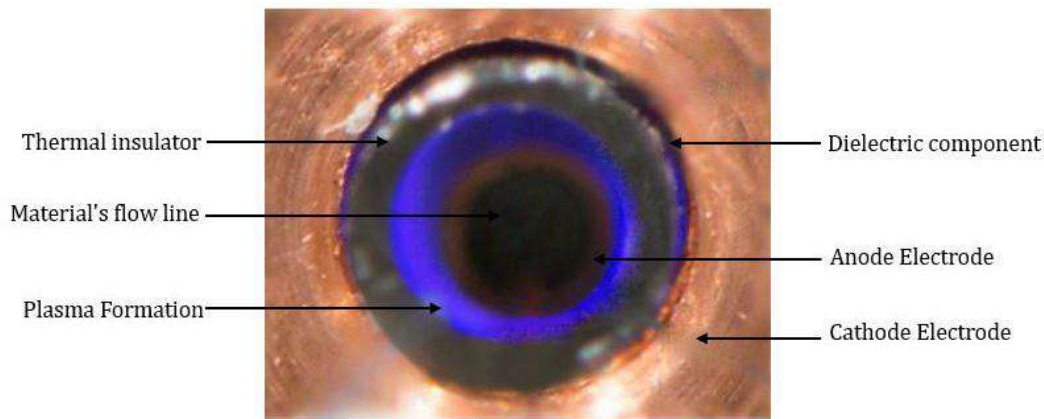


Fig. 2: Inside view of plasma heater.

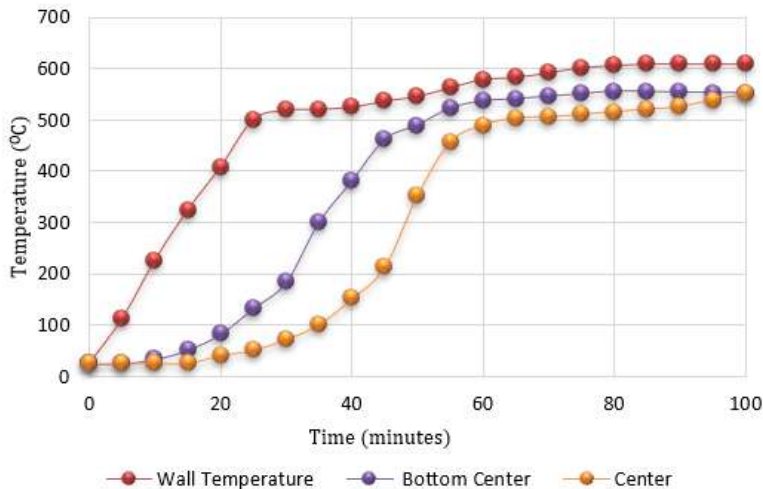


Fig. 3: Empty chamber temperature distribution profile.

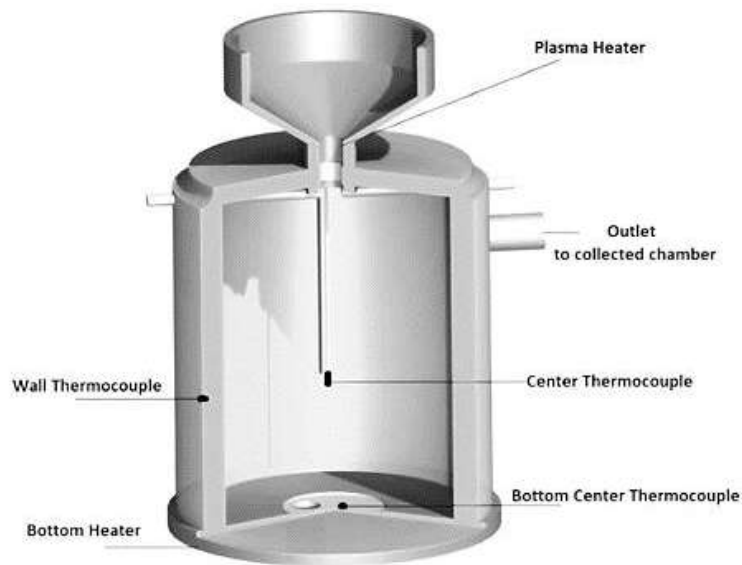


Fig. 4: Placement of thermocouple in the pyrolysis chamber.

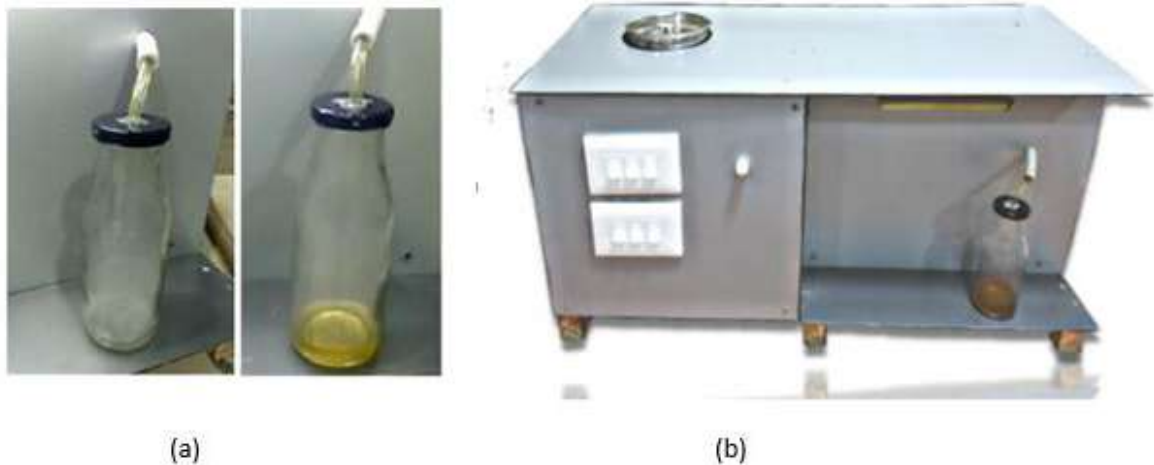


Fig. 5: (a) Pyrolysis oil collector unit (b) View of reactor setup.

Fig. 5 depicts the entire bench-scale 8 kg hybrid plasma gasification reactor setup with filtered syngas and a pyrolysis oil collector. Completely operational electric operated apparatus featuring 650°C thermally brake temperatures, single phase 230 V AC electrical heater, and a plasma heater system. A cylinder container with a tapering bottom half shell makes up a plasma heater. It is made up of four squared graphite electrodes that serve as the cathode in an electrical system with a high current DC source transformer.

### Materials

The organic garbage (waste plastic) was obtained from the

Kalinga Institute of Medical Science (KIMS) and the municipal corporation of Bhubaneswar, Odisha. Selected, it's been divided into seven separate sterilized and dried waste plastic grads. For the aim of the experiment, each waste sample plastic was obtained in an identical mass ratio. Various forms of plastic were gathered for pyrolysis/gasification are shown in Fig. 6. Table 1 shows several types of waste plastic, as well as their generic kind and plastic-type indication. Individual types of plastic trash may be seen in the experiment. Following classification, the items are chopped into small pieces ranging from 10 to 40 millimeters in length using a cutter machine.

Table 1: List of collected waste plastic Materials (Punčochář et al. 2012, Deng et al. 2008, Lin et al. 2010, Klemeš et al. 2020, Qin et al. 2018).







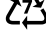
S No.	Mark	Code	Type of plastics	Waste plastic materials
1	PET		Polyethylene Terephthalate	Saline bottles, juice containers, Mineral water bottles, soft drink bottles, vacutainers, photographic film
2	HDPE		High-density polyethylene	one-off dustbin pouch, milk pouch, Packaging sheets, or pouch
3	PVC		Polyvinyl Chloride	Tube for blood and Urine, Sample collector bottle
4	LDPE		Low-density polyethylene	Sample collector small bag, Disposable gloves, trash bag
5	PP		Polypropylene	Disposable masks-shoe-covers & caps, cytotoxic drugs packaged, dustpans worn one, Syringes body and plunger
6	PS		Polystyrene	ET Tube, Suction's tube & bags, Plastic cover for light handles,
7	PE, PA, ABS, PBT		Polyethylene, polyamide, acrylonitrile butadiene styrene, polybutylene terephthalate	Plastic Bag Warmer Patients ID Bands, Gloves, Intravenous tubes, and sets,



Fig. 6: Various forms of gathered waste plastic for gasification.

## RESULTS AND DISCUSSION

### Oil Recovery Rate with Calculated Pyrolysis Kinetic Parameter

According to an oil recovery investigation, increasing reactor temperatures reduces oil recovery time. As a consequence

of the shorter time that volatiles spends in the reaction chamber, carbon bonding separation with high molecular heaviness composition occurs, increasing the concentration of the pyrolysis oil generated. The kinetic parameters were derived using the Arrhenius plot technique during every oil recovery process. Fig. 7 shows the oil recovery rate from

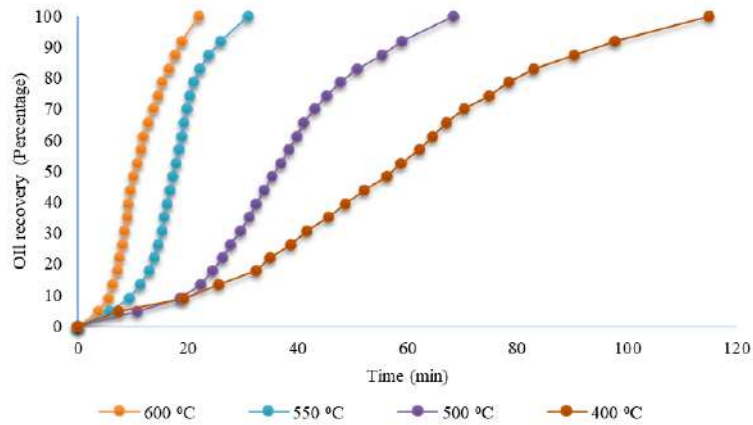


Fig. 7: Oil recovery rate for PET at a heating rate of nearly 18°C/minutes.

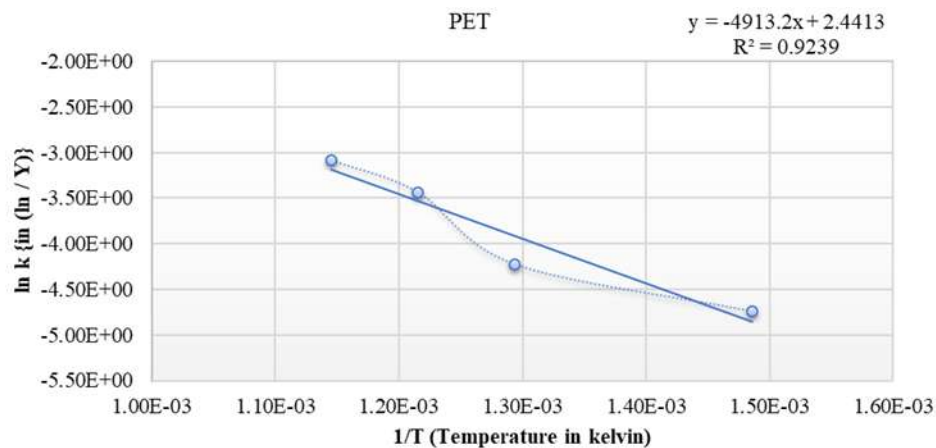


Fig. 8: Graphical calculation of activation energy for PET.

PET it takes 22, 31, 69, and 114.8 min at 600, 550, 500, and 400°C respectively. Fig. 8 shows a graphical calculation of activation energy based on kinetic parameters for PET.

Fig. 9 shows the oil recovery rate from HDPE takes 26, 31, 69.8, and 115.5 min at 600, 550, 500, and 400°C respectively. However, the pattern of oil recovery percentage increase with time for PET and HDPE. Fig. 10 shows a graphical calculation of activation energy based on kinetic parameters for HDPE.

Fig. 11 shows the oil recovery rate from PVC takes 38, 43, 84, and 132 min at 600, 550, 500, and 400°C respectively. The pattern of oil recovery increment from PVC concerning time is similar up to 70% of oil recovery as PET, HDPE, and LDPE showed, but in this case, the oil recovery rate decreases after 70% oil recovery. Fig. 12 shows a graphical calculation of activation energy based on kinetic parameters for LDPE.

Fig. 13 shows the oil recovery rate from LDPE takes 23, 34, 72, and 117 min at 600, 550, 500, and 400°C respectively. However, the pattern of oil recovery percentage increase with time for PET and HDPE. Fig. 14 shows a graphical computation of activation energy based on kinetic parameters for LDPE.

Fig. 15 shows the oil recovery rate from PP takes 24, 33, 64, and 113 min at 600, 550, 500, and 400°C respectively. The pattern of oil recovery from PP is similar to 80% oil recovery like that of PET, HDPE, and LDPE, and beyond that, the trend does not match. Fig. 16 shows a graphical calculation of activation energy based on kinetic parameters for PP.

Fig. 17 shows the oil recovery rate from PS takes 19, 27, 44, and 92 min at 600, 550, 500, and 400°C respectively. The pattern of oil recovery is similar to a nearly straight line till 80% oil recovery but the oil recovery rate decreases



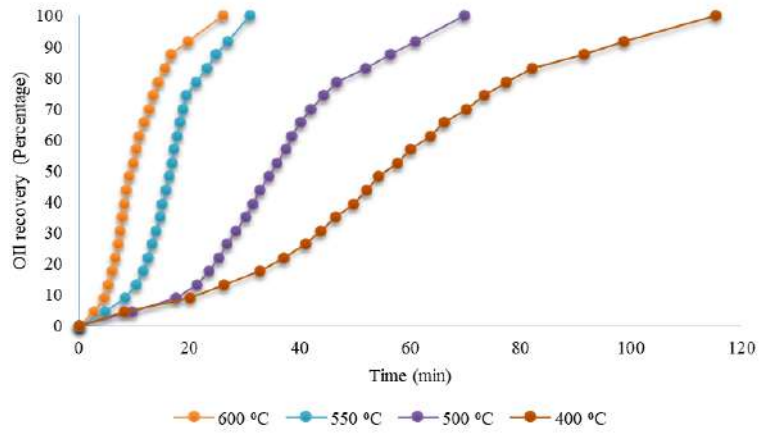


Fig. 9: Oil recovery rate for HDPE at a heating rate of nearly 18°C/minutes.

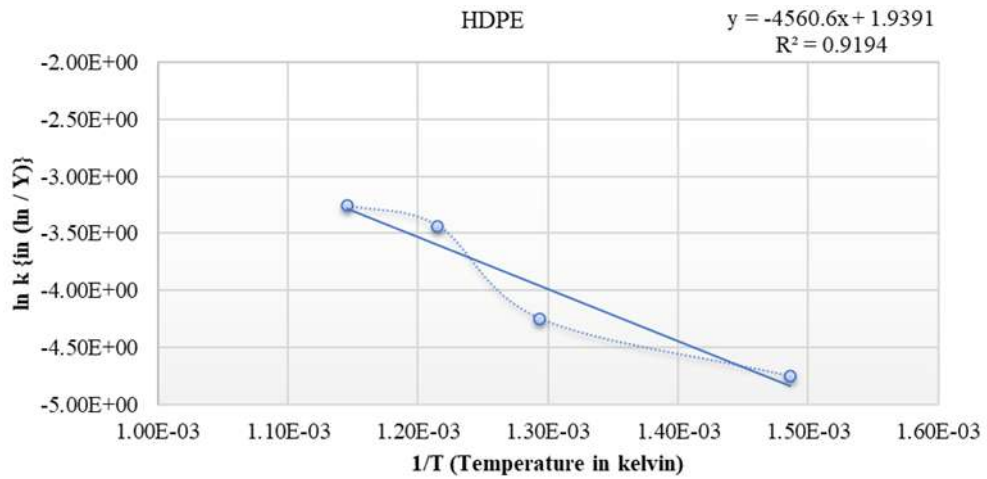


Fig. 10: Graphical calculation of activation energy for HDPE.

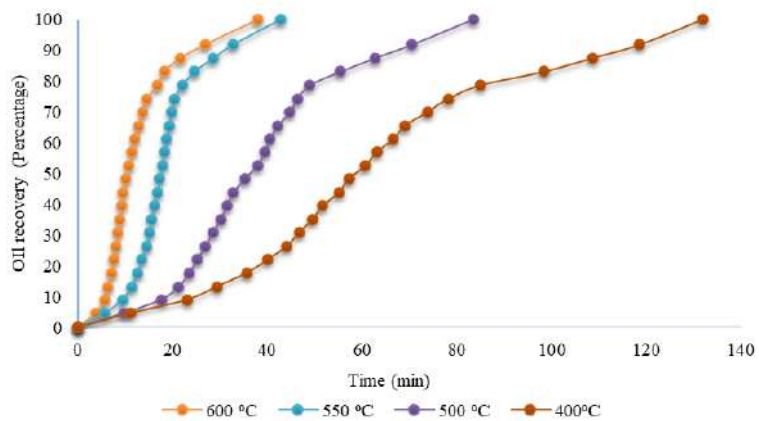


Fig. 11: Oil recovery rate for PVC at a heating rate of nearly 18°C/minutes.

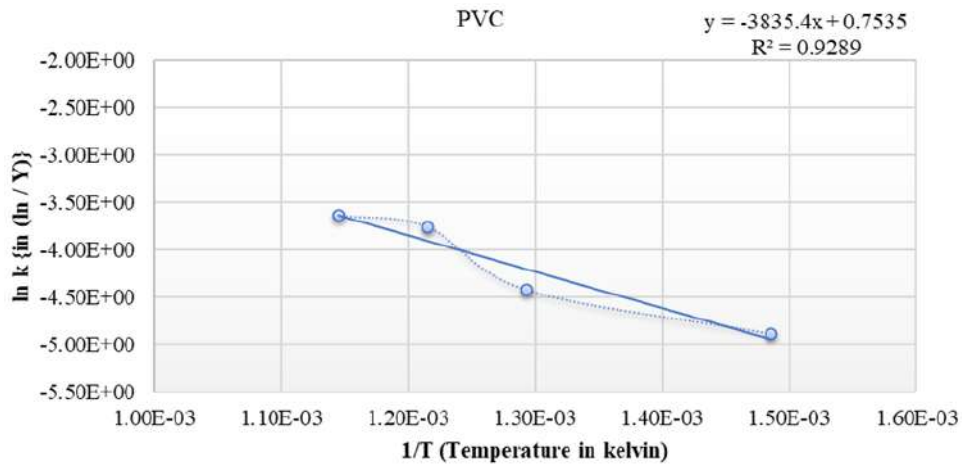


Fig. 12: Graphical calculation of activation energy for PVC.

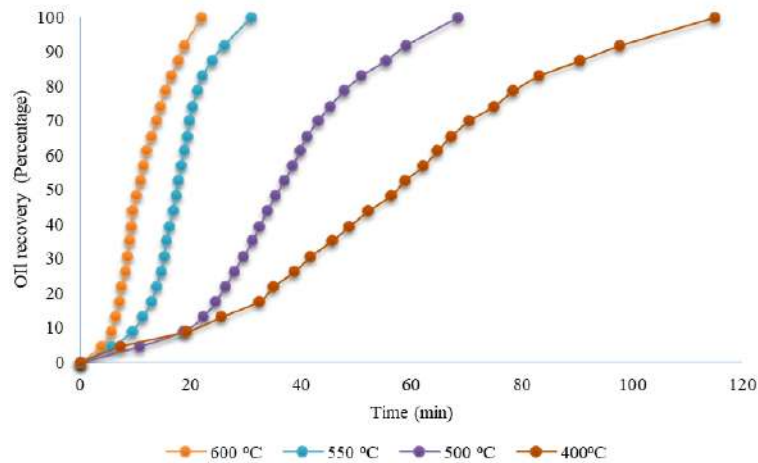


Fig. 13: Oil recovery rate for LDPE at a heating rate of nearly 18°C/minutes.

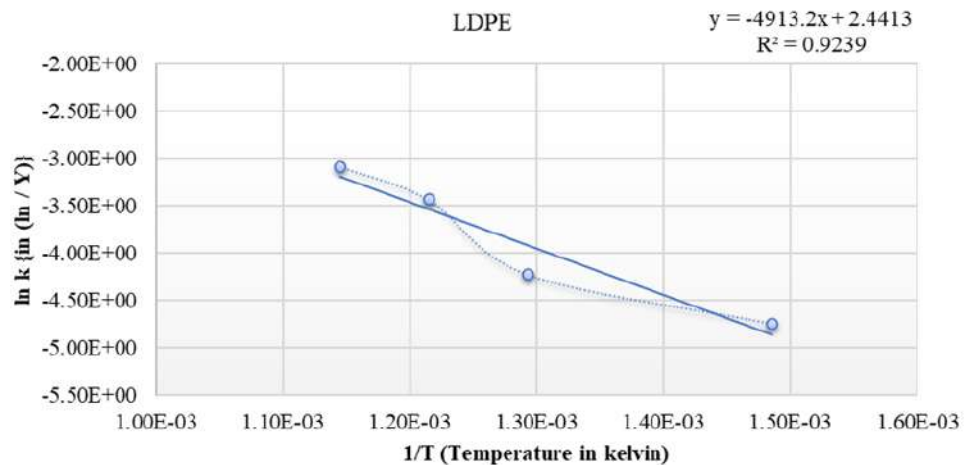


Fig. 14: Graphical calculation of activation energy for LDPE.

afterward. Fig. 18 shows a graphical calculation of activation energy based on kinetic parameters for PS.

Fig. 19 shows the oil recovery rate from a mixture of various plastics, where the mixture is prepared by taking the equal weight of each kind of plastic. It takes 28, 37, 82, and 135 min at 600, 550, 500, and 400°C respectively. The pattern of oil recovery is similar to a nearly straight line till 80% oil recovery but the oil recovery rate decreases afterward. Fig. 20 shows a graphical calculation of activation energy for mixed plastics based on kinetic parameters.

The oil recovery pattern is comparable to all prior tests, although the results for 550°C and 600°C are virtually identical to earlier trials. In all cases, oil production began when the temperature of the reactor core reached 380°C, with

sluggish oil recapturing in the first stage and increasing when the temperature of the reactor was above 450°C. Oil recovery was extremely quick at high operating temperatures. At lower temperatures, polypropylene and polyethylene terephthalate break down, followed by hydrogen abstraction and random scission. In the early stages, degradation is caused by polystyrene end chain scission followed by scission, resulting in increased gas production such as hydrogen and methane. Increases in process temperature cause deterioration, which is followed by scission formation of larger quantities of extended chain hydrocarbon, resulting in higher liquid yield in all cases.

The Arrhenius plot is generated and shown in the above figures. Each plot in the figures shows S-shape curves which

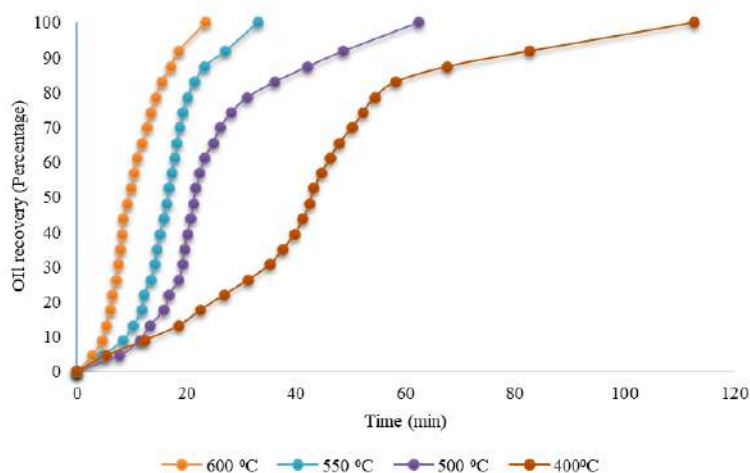


Fig. 15: Oil recovery rate for PP at a heating rate of nearly 18°C/minutes.

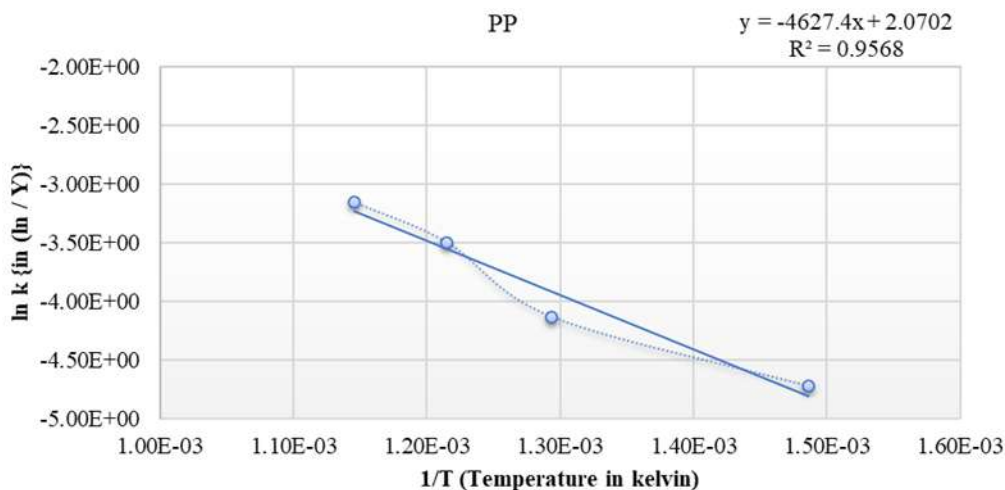


Fig. 16: Graphical calculation of activation energy for PP.

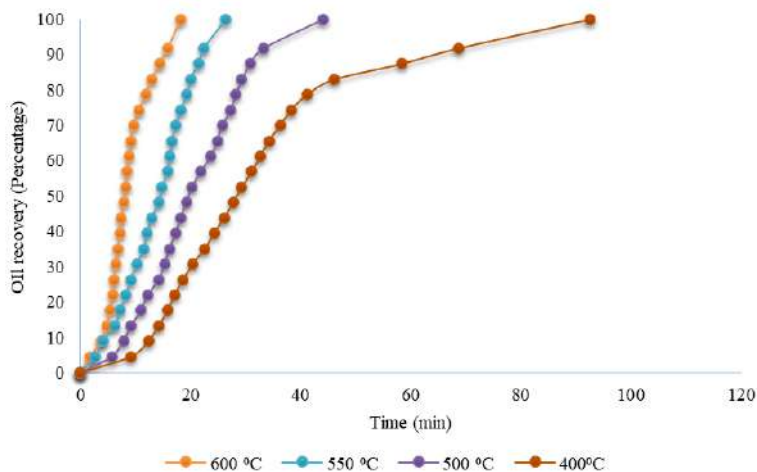


Fig. 17: Oil recovery rate for PS at a heating rate of nearly 18°C/minutes.

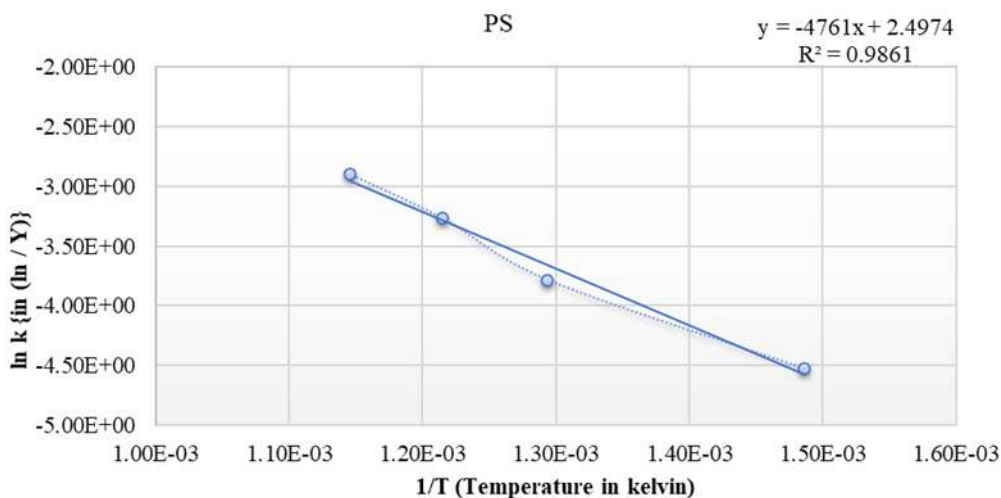


Fig. 18: Graphical calculation of activation energy for PS.

means that the kinetics of the reaction follows the nucleation and grain growth model and Johnson and Mehl (Sarkar & Ray 1990) equation:  $\ln[-\ln(1-\alpha)] = n \ln(k') + n$ . The calculated value of activation energy for polyethylene terephthalate (PET) is 40.84 kJ.mole<sup>-1</sup> and exponential factor 11.488/second; similarly, high-density polyethylene (HDPE) is 37.91 kJ.mole<sup>-1</sup>, exponential factor 6.896/second; Low-density polyethylene (LDPE) is 40.84 kJ.mole<sup>-1</sup>, exponential factor 11.487/second; Polyvinyl chloride (PVC) is 31.88 kJ.mole<sup>-1</sup>, exponential factor 2.124/second; Polypropylene (PP) is 38.47 kJ.mole<sup>-1</sup> exponential factor 7.926/second; Polystyrene (PS) 39.58 kJ.mole<sup>-1</sup> exponential factor 12.150/second; and Mixed 39.51 kJ.mole<sup>-1</sup> exponential factor 7.784/second.

Wu et al. (1993) recorded lower values of 233-326 kJ.mol<sup>-1</sup> for HDPE, 194-206 kJ.mol<sup>-1</sup> for LDPE, 184-265 kJ.mol<sup>-1</sup> for PP, and 172 kJ.mol<sup>-1</sup> for PS. Again, Sorum et

al. (2001) identified commercial-grade activation energy as 445.1 kJ.mol<sup>-1</sup> for HDPE, 340.8 kJ.mol<sup>-1</sup> for LDPE, 336.7 kJ.mol<sup>-1</sup> for PP, and 311.5 kJ.mol<sup>-1</sup> for PS respectively. Similarly, Diaz-Silvarrey and Phan (2016) found activation energy waste as HDPE 375.59 kJ.mol<sup>-1</sup>, LDPE 267.61 kJ.mol<sup>-1</sup>, PP 261.22 kJ.mol<sup>-1</sup>, PS 192.61 kJ.mol<sup>-1</sup>, and PET 197.61 kJ.mol<sup>-1</sup> respectively.”

The activation energy (40.89 kJ.mol<sup>-1</sup>) is far smaller compared to that above. This demonstrates the benefit of the plasma reaction which reduces energy activation (Sabat 2014, Rajput et al. 2016). The semi-batch pyrolysis thermal reactor is more impactful in the terms of disposal of waste plastic.

### Residual Weight Analysis

The weight fractions of all plastic samples vary with temperature in this investigation. It has been determined that LDPE

and PET have distinct weight fraction curve patterns. Fig. 21 also illustrates a distinct pattern of the curve after 52°C and 500°C at a rate of 18°C for PS and PP, respectively. This indicated the normal thermal degradation process during pyrolysis (Mumbach et al. 2019).

**Characteristics**

**Pyrolysis oil**

During the investigation, we obtained the product as pyrolysis oil from various waste plastic elements. Fig. 22 depicts the collection of pyrolysis oil in containers and waste plastic samples with oil extraction. Fig. 23 depicts the collection of a waste plastic sample with oil extraction.

In terms of pyrolysis oil’s characteristics, we tested all collected samples for density at 28 °C using the ISO-1183

method, kinematic viscosity at 23°C using the ISO-3104 method, flash point using the ISO 2719 standard method, fire point using the ISO 2592 method, calorific value using a bomb calorimeter, pour point using the ISO 3016 testing method, and ash content using the ISO 3451 testing method. Table 2 shows lists all of the physical characteristics of waste plastic pyrolysis oil with petroleum diesel and petrol. Table 2, showing the comparison of (Renewable diesel and petrol) parameter properties of all plastic pyrolysis oil, indicated that it can be a substitute as a furnace oil for the power plant or as an industrial diesel. Mixed pyrolysis oil can be blended with diesel/ petrol and used for automobile cars.

**Waste Char**

After the examination, we got char as a waste of the plastic pyrolysis of the different plastic waste materials. Under the

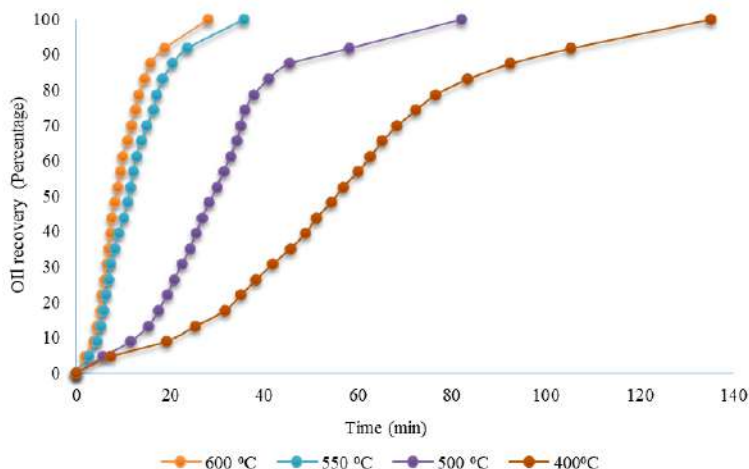


Fig. 19: Oil recovery rate for mixed plastics at a heating rate of nearly 18 °C/minutes.

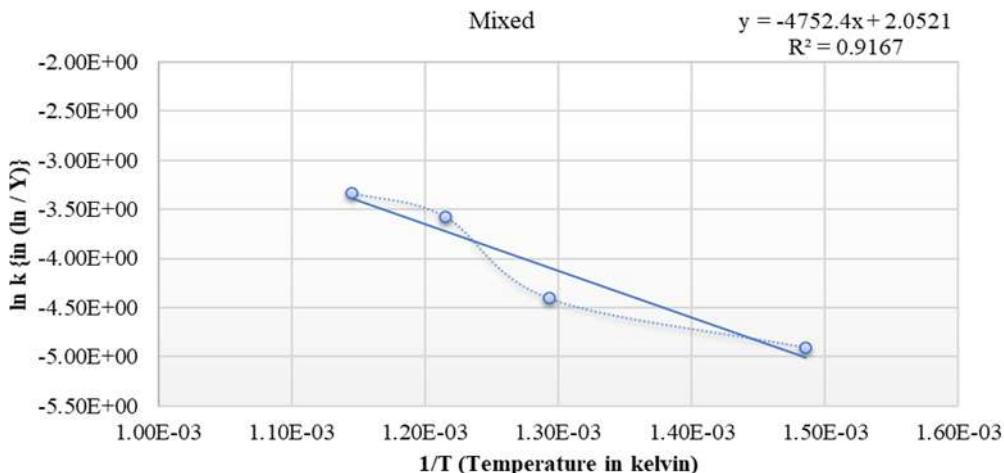


Fig. 20: Graphical calculation of activation energy for mixed plastics.



micrographic observation of the individual plastic material of char, SEM images of plastic char are shown in Fig. 24 (a), (b), (c), (d), (e), and (f)

Polyethylene Terephthalate (a) char is being seen with a 15X magnification at 1200  $\mu\text{m}$  and 150X magnification at 600  $\mu\text{m}$  respectively. We observed that some carbon black sub-

stance was present in char. It indicates the presence of printed paint and marks on PET-type plastic waste material that has not completely decomposed during thermal pyrolysis.

Low-density polyethylene (b) char is being seen with a 15X magnification at 1200  $\mu\text{m}$  and 150X magnification at 600  $\mu\text{m}$  respectively. We observed the absence of carbon

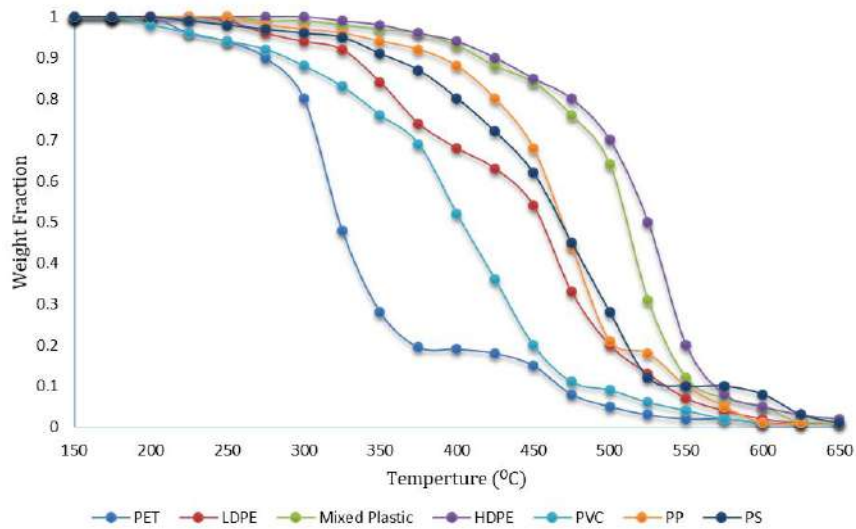


Fig. 21: Comparative residual weight analysis with the temperature at a rate of 18 °C for specific and mixed plastic waste.



Fig. 22: Oil extraction by thermal plasma pyrolysis of Hospital plastic waste materials.

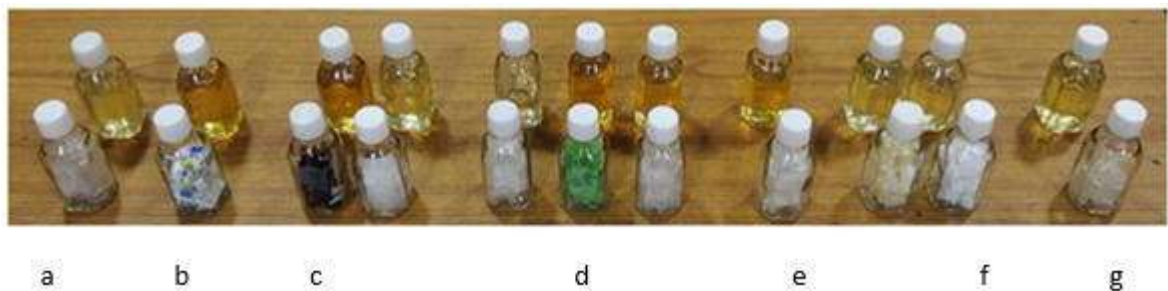


Fig. 23: Waste plastic sample with oil extraction by thermal plasma pyrolysis (a)PET, (b)LDPE, (c)HDPE, (d)PP, (e)PS, (F)PVC, (g) ABS, PA, PBT.

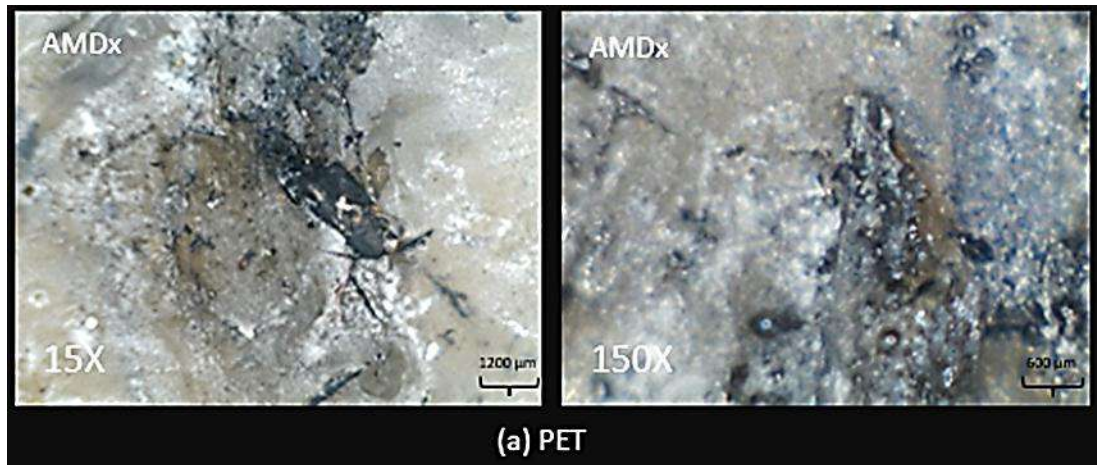


Fig. 24: (a) Microscopic view of Polyethylene Terephthalate waste char.

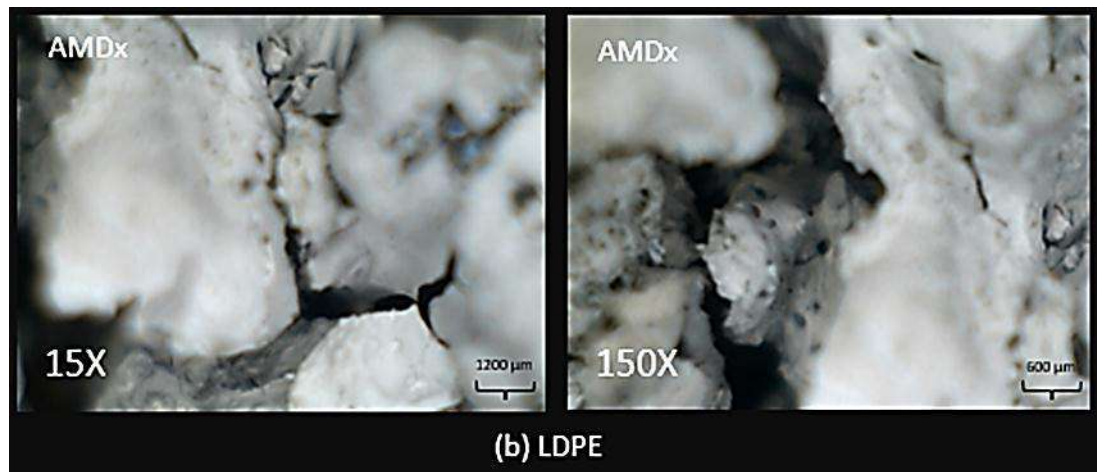


Fig. 24: (b) Microscopic view of Low-density polyethylene waste char.

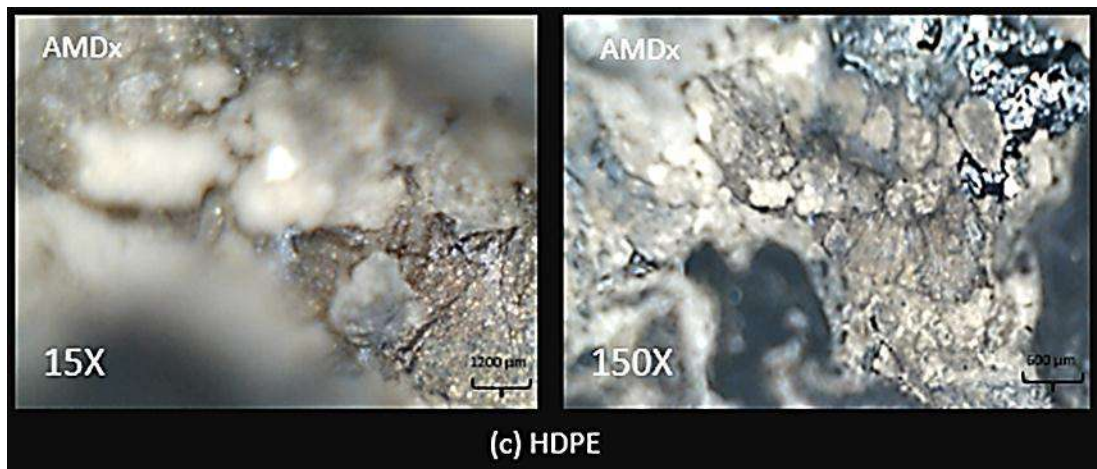


Fig. 24: (c) Microscopic view of High-density polyethylene waste char.



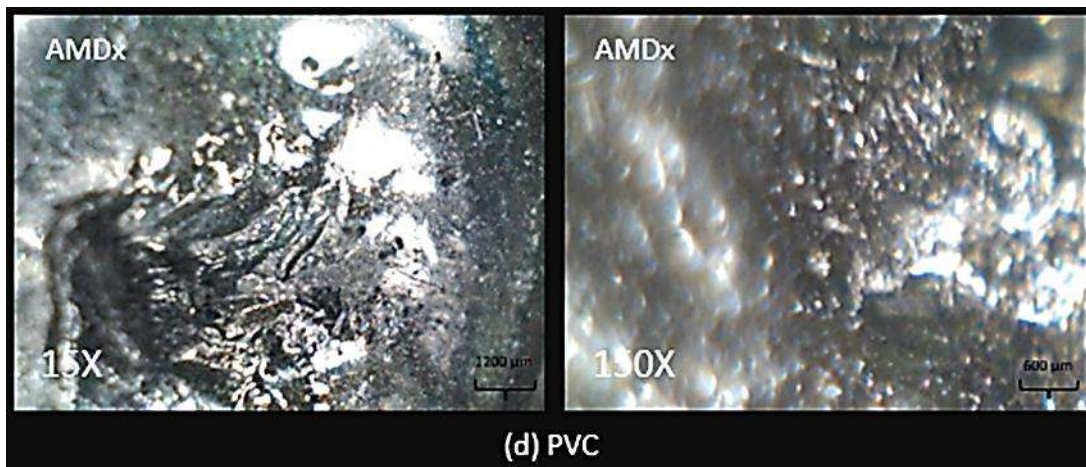


Fig. 24: (d) Microscopic view of polyvinyl chloride waste char.

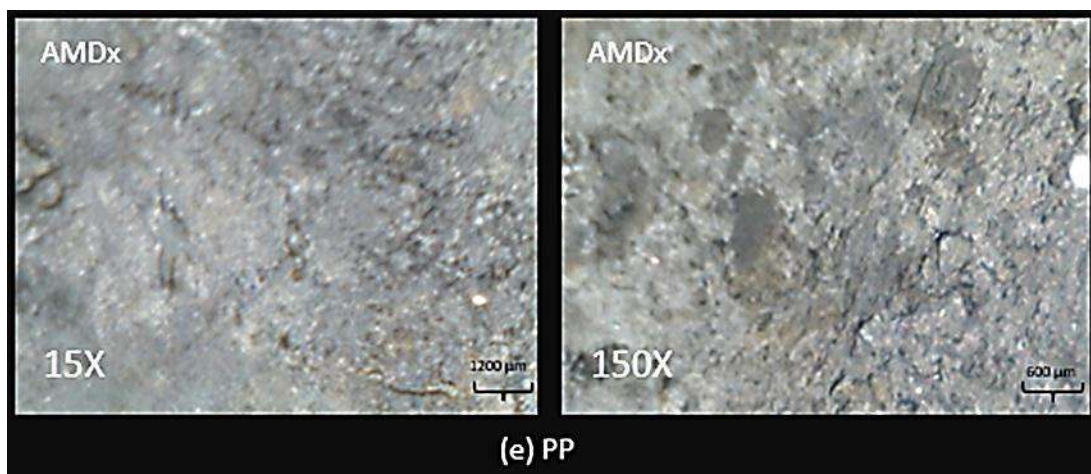


Fig. 24: (e) Microscopic view of polypropylene waste char.

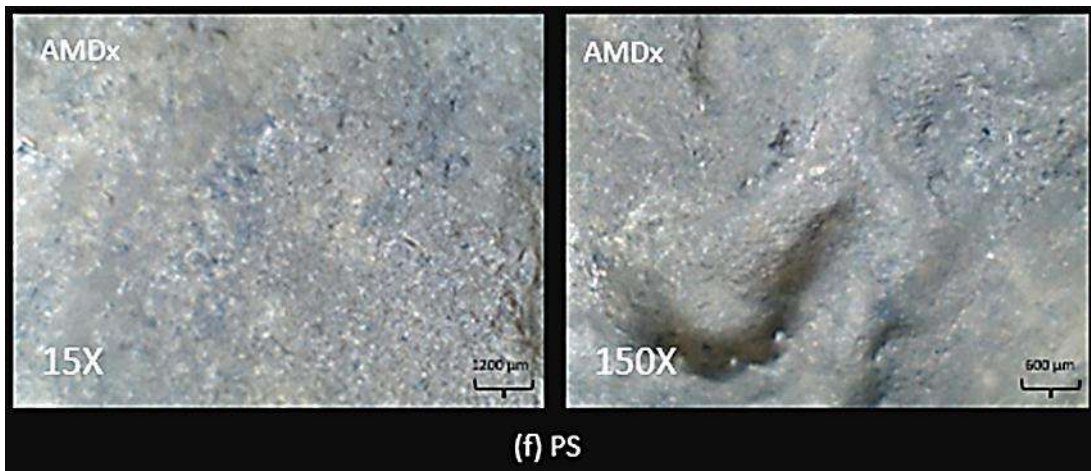


Fig. 24: (f) Microscopic view of polystyrene waste char.

Table 2: The physical characteristics of various plastic pyrolysis oils.

Physical properties	Pyrolysis Oil from different types of plastic waste							Petroleum	
	PET	HDPE	LDPE	PVC	PP	PS	Mixed	Diesel	Petrol
Density @ 26°C [g.cm <sup>-3</sup> ]	0.88	0.87	0.76	0.82	0.84	0.83	0.91	0.84-0.86	0.82-0.86
Kinematic viscosity [mm <sup>2</sup> .s <sup>-1</sup> ]	3.92	4.86	4.97	5.82	4.16	2.85	6.02	3.04-4.83	1.12-3.27
Flash point [C°]	28.2	47.8	40.0	39.0	30	27.1	32	52-94	42-108
Calorific value [MJ.kg <sup>-1</sup> ]	27.8	41.5	39.8	21.6	40.8	43.0	40.01	35.7-42.7	34.2-46.48
Pour point (C°)	-18	-5	-9	4	-9	-67	5	0.0 - 55	0.0-50
Ash content [wt %]	0.002	0.04	0.02	0.04	0.002	0.006	0.01	-	-

black substance present in char. It indicates the material has completely decomposed during the pyrolysis process.

High-density polyethylene (c) char is being seen with a 15X magnification at 1200 µm and 150X magnification at 600 µm respectively. We observed about 3.68% - 3.97% carbon black substance with ash and large bonding molecular particles present in char. It is quite low. It means that HDPE materials decomposed during the pyrolysis process.

Polyvinyl Chloride (d) char is being seen with a 15X magnification at 1200 µm and 150X magnification at 600 µm respectively. We observed about 28.86% - 30.28% carbon black substance with ash and compact bonding molecular particles present in char. It indicates the presence of additive added into PVC that is commonly composed of the inorganic residual compound for the improvement of properties of PVC.

Polypropylene (e) char is being seen with a 15X magnification at 1200 µm and 150X magnification at 600 µm respectively. We observed a random uniform structure of molecular bonding present in char. It indicates that the material degraded during the pyrolysis operation.

Polystyrene (f) char is being seen with a 15X magnification at 1200 µm and 150X magnification at 600 µm respectively. We observed that char has a consistent structure of molecular bonding. It indicates that the material was degraded during the pyrolysis operation.

## CONCLUSION

Hybrid plasma pyrolysis is most effective in the terms of activation energy i.e., nearly about 40.89 kJ.mol<sup>-1</sup> generating yielding of 76-88% pyrolysis oil, 10-23% syngas, and 4-15% chars as a product. The calorific value of pyrolysis oil is about 39-41 MJ per kg, indicating that it has the highest potential energy value as an alternative for petroleum-based diesel and petrol. The current investigations show that there are a plethora of options for developing hybrid plasma gasification technologies that apply to organic waste plastic materials disposal treatment with material and energy recapture.

## REFERENCES

- Deng, N., Zhang, Y. F. and Wang, Y. 2008. Thermogravimetric analysis and kinetic study on pyrolysis of representative medical waste composition. *Waste Management*, 28(9), 1572-1580.
- Diaz-Silvarrey, L. and Phan, A. 2016. 'Kinetic study of municipal plastic waste', *International Journal of Hydrogen Energy* 41(37), 16352-16364.
- Dutta, M. and Paul, G. 2019. Gallic acid protects rat liver mitochondria ex vivo from bisphenol A induced oxidative stress mediated damages. *Toxicology reports*, 6, 578-589.
- Fang, S., Jiang, L., Li, P., Bai, J. and Chang, C. 2020. Study on pyrolysis products characteristics of medical waste and fractional condensation of the pyrolysis oil. *Energy*, 195, 116969.
- Fridman, G., Friedman, G., Gutsol, A., Shekhter, A. B., Vasilets, V. N. and Fridman, A. 2008. *Applied plasma medicine. Plasma processes and polymers*, 5(6), 503-533.
- Gupta, N., Yadav, K. K. and Kumar, V. 2015. A review on current status of municipal solid waste management in India. *Journal of environmental sciences*, 37, 206-217.
- Heberlein, J. and Murphy, A. B. 2008. Thermal plasma waste treatment. *Journal of Physics D: Applied Physics*, 41(5), 053001.
- Klemeš, J. J., Van Fan, Y., Tan, R. R. and Jiang, P. 2020. Minimising the present and future plastic waste, energy and environmental footprints related to COVID-19. *Renewable and Sustainable Energy Reviews*, 127, 109883.
- Lin, H. T., Huang, M. S., Luo, J. W., Lin, L. H., Lee, C. M. and Ou, K. L. 2010. Hydrocarbon fuels produced by catalytic pyrolysis of hospital plastic wastes in a fluidizing cracking process. *Fuel Processing Technology*, 91(11), 1355-1363.
- Manuja, S., Pandey, S. and Bhatia, A. 2020. Assessing Management of Plastic Straws Attached with used Beverage Cartons-A Case Study of 3 Metropolitan Cities of India. (IJERT) Vol. 9 (6):601-606p.
- Mumbach, G. D., Alves, J. L. F., Da Silva, J. C. G., De Sena, R. F., Marangoni, C., Machado, R. A. F. and Bolzan, A. 2019. Thermal investigation of plastic solid waste pyrolysis via the deconvolution technique using the asymmetric double sigmoidal function: Determination of the kinetic triplet, thermodynamic parameters, thermal lifetime and pyrolytic oil composition for clean energy recovery. *Energy Conversion and Management*, 200, 112031.
- Pinto, F., Franco, C., André, R. N., Miranda, M., Gulyurtlu, I. and Cabrita, I. 2002. Co-gasification study of biomass mixed with plastic wastes. *Fuel*, 81(3), 291-297.
- Pun ochá, M., Ruj, B. and Chatterj, P. K. 2012. Development of process for disposal of plastic waste using plasma pyrolysis technology and option for energy recovery. *Procedia Engineering*, 42, 420-430.
- Qin, L., Han, J., Zhao, B., Wang, Y., Chen, W. and Xing, F. 2018. Thermal degradation of medical plastic waste by in-situ FTIR, TG-MS and TG-GC/MS coupled analyses. *Journal of Analytical and Applied Pyrolysis*, 136, 132-145.

- Rahimi, A. and García, J. M. 2017. Chemical recycling of waste plastics for new materials production. *Nature Reviews Chemistry*, 1(6), 1-11.
- Rajput, P., Bhoi, B., Paramguru, R. K. and Mishra, B. K. 2016. Effect of plasma state and alloying addition on reduction of Fe<sub>2</sub>O<sub>3</sub> by a low-temperature hydrogen plasma. *High Temperature Material Processes: An International Quarterly of High-Technology Plasma Processes*, 20(4).
- Sabat, K.C. 2014. Reduction of oxide minerals by hydrogen plasma: an overview. *Plasma Chemistry and Plasma Processing* 34.1 and 1-23.
- Salandra, R. 2018. Knowledge dissemination in clinical trials: exploring influences of institutional support and type of innovation on selective reporting. *Research Policy*, 47(7), 1215-1228.
- Samal, S. 2017. Thermal plasma technology: The prospective future in material processing. *Journal of cleaner production*, 142, 3131-3150.
- Sarkar, S. B. and Ray, H. S. 1990. Analysis of kinetic data by Johnson-Mehl equation. *Journal of thermal analysis*, 36(1), 231-242.
- Sekiguchi, H. and Orimo, T. 2004. Gasification of polyethylene using steam plasma generated by microwave discharge. *Thin Solid Films*, 457(1), 44-47.
- Sorum, L., Gronli, M. and Hustad, J. 2001. Pyrolysis characteristics and kinetics of municipal solid wastes, *Fuel* 80, 1217-1227.
- Tendero, C., Tixier, C., Tristant, P., Desmaison, J. and Leprince, P. 2006. Atmospheric pressure plasmas: A review, *Spectrochimica Acta Part B: Atomic Spectroscopy* 61(1), 2-30.
- Wu, C., Chang, C., Hor, J., Shih, S., Chen, L. and Chang, F. 1993. On the thermal treatment of plastic mixtures of MSW: Pyrolysis kinetics, *Waste Management* 13(3), 221-235.





# Assessing the Capacities of Different Remote Sensors in Estimating Forest Stock Volume Based on High Precision Sample Plot Positioning and Random Forest Method

Yang Hu\* and Zhongqiu Sun\*\*†

\*School of Ecology and Environment, Ningxia University, Yinchuan 750021, China

\*Breeding Base for State Key Laboratory of Land Degradation and Ecological Restoration in Northwest China, Ningxia University, Yinchuan 750021, China

\*Key Laboratory for Restoration and Reconstruction of Degraded Ecosystem in Northwest China of Ministry of Education, Ningxia University, Yinchuan 750021, China

\*\*Academy of Inventory and Planning, National Forestry and Grassland Administration, Beijing 100714, China

†Corresponding author: Zhongqiu Sun; qiuqiu8708@163.com

Nat. Env. & Poll. Tech.  
Website: [www.neptjournal.com](http://www.neptjournal.com)

Received: 20-07-2021

Revised: 25-09-2021

Accepted: 04-10-2021

## Key Words:

Forest stock volume  
Sentinel-1  
Sentinel-2  
Landsat-8  
PALSAR2/PALSAR  
Random forest

## ABSTRACT

Forest stock volume (FSV) is an important forest resource indicator. Satellite images from various sensors have been used to estimate FSV. However, there is still a lack of comparative studies on the estimation of FSV with remote sensing data obtained by different sensors. In addition, there is a lack of high-precision ground sample positioning methods, which can improve the matching of ground data and remote sensing data to a certain extent, and improve the estimation accuracy. In this research, a new ground sample plot positioning method was proposed, which could achieve sub-meter positioning accuracy in forest areas, greatly improving the matching accuracy of ground sample plot data and remote sensing data. Based on this high-precision positioning method and the random forest algorithm, we compared and quantified the ability of different sensors to estimate the FSV. The results by random forest modeling showed that the images from a single sensor, Sentinel-2, performed best in the test dataset ( $R^2 = 0.57$ ,  $RMSE = 70.12 \text{ m}^3 \text{ ha}^{-1}$ ). For the data from two sensors, the best performance was achieved by the combined Sentinel-2 and PALSAR2/PALSAR data, which had an  $R^2$  of 0.62 with  $RMSE$  of  $65.51 \text{ m}^3 \text{ ha}^{-1}$  in the validation data. The images from the three sensors, Sentinel-2, Landsat-8, and PALSAR2/PALSAR, achieved a modeling accuracy of  $R^2$  (0.62) and  $RMSE$  ( $65.40 \text{ m}^3 \text{ ha}^{-1}$ ). The results clearly showed the capacity of the different sensor data to estimate FSV based on the high precision sample plot positioning method, and it will help forest researchers investigate and estimate the FSV in the future.

## INTRODUCTION

As an important part of terrestrial ecosystems, forests play vital roles in both economic development and ecosystem protection. Forests are an important renewable natural resource that is crucial to the strategic timber security of a country (Xia et al. 2019). At the same time, forest ecosystems are the largest carbon pools in terrestrial ecosystems (Sun et al. 2020). Due to the close relationship between forests and carbon (Mitchard 2018), any change in forests directly impacts carbon sequestration (Zhang et al. 2020). Also, forest ecosystems play an irreplaceable role in ecosystems that includes absorbing carbon dioxide from the air, providing animal habitat, maintaining the carbon balance, and mitigating global climate. The management and monitoring of forests mainly require focusing on the information about wood resources, which can be assessed through the volume of trees, which is

commonly known as the forest stock volume (FSV). Forest resource inventories are primarily conducted to estimate the existing FSV in forests, which has practical relevance for ecological environmental monitoring and sustainable forest management. Therefore, accurately assessing FSV at the regional and national scales is of great significance.

Currently, some studies have been performed based on a single sensor data or the combination of various sensor data for FSV estimation. For instance, Chrysafis et al. (2017) performed FSV estimation research using Sentinel-2 and Landsat-8 data in Greece. By modeling with the random forest (RF) algorithm, they obtained the best FSV prediction result with Sentinel-2 data ( $R^2 = 0.63$ ,  $RMSE = 63.11 \text{ m}^3 \text{ ha}^{-1}$ ). Muaya et al. (2019) estimated the FSV of a small-scale forest plantation in Tanzania with Sentinel-1(SAR), Sentinel-2, and ALOS PALSAR2 data with multiple linear regression

algorithms. They found that the Sentinel-2 data (RMSEr = 42.03%, pseudo- $R^2 = 0.63$ ) performed better than the combined Sentinel-1 and Sentinel-2 data (RMSEr = 46.98%, pseudo- $R^2 = 0.52$ ), and Sentinel-1 performed worst (RMSEr = 59.48%, pseudo- $R^2 = 0.18$ ). These studies showed that different data combinations had different forest parameter estimation results. Further research is needed to evaluate the feasibility and limitations of multi-sensor integrated datasets to estimate forest parameters (such as FSV). On the other hand, the complex collinearity among independent variables is an urgent problem during the process of model construction that cannot be avoided in traditional linear regression models, for example, some parametric methods. However, RF, which is a non-linear algorithm, could solve complex collinearity problems. Compared to the multiple regression algorithm, the resistance to collinearity and robustness to outliers of the RF algorithm make it uniquely feasible for predicting forest parameters using remote sensing variables (Breiman 2001).

In addition to remote sensing data and modeling algorithms, the importance of ground truth from sample plot data should not be ignored. However, the positioning accuracy of traditional handheld GPS units in forest areas is very low, and the error can even exceed 30 m (Stefanoni et al. 2018). Given the large position deviation in forests, it is necessary to find a positioning method to solve this problem. Huang et al. (2013) found that the accurate plot location recorded by DGPS (1-meter accuracy) reduced the geolocation error and thus achieved high prediction accuracy in the estimation of forest AGB (Huang et al. 2013).

This study has two objectives: (1) to test and determine a new forest sample plot positioning method that can achieve sub-meter accuracy in deep mountain forests and (2) to assess the performance of different sensor datasets (Sentinel-1, Sentinel-2, Landsat-8, and PALSAR2/PALSAR) in estimating FSV based on ground sample plots using the new positioning method. This paper will propose a new forest sample plot positioning method, clarify the performance of the yearly Sentinel-1, Sentinel-2, Landsat-8, and PALSAR2/PALSAR data in estimating the FSV in Southern China, especially Hunan Province, and even promote the estimation of FSV throughout the whole country.

## MATERIALS AND METHODS

### High-Precision Positioning Experimental Design

Three GNSS receivers produced by the Hi-Target Navigation Technology Corporation (H32 Almighty GNSS RTK System) were used in this experiment. A GNSS receiver was set up in a wide urban area, which ensured that the GNSS receiver could receive satellite signals well and use the continuously

operating reference stations (CORS) service to achieve accurate positioning. The other two GNSS receivers were set up in the dense forest, in which the canopy density reached 0.7 or more. All three GNSS receivers worked together for 30 min at each designed distance (Fig. 1).

### Measurement Accuracy Evaluation Method on Positioning

The CORS service was used in all GNSS receivers to obtain the coordinates  $R (X_r, Y_r)$  as true positioning values. All GNSS receivers could also obtain the coordinates  $E (X_e, Y_e)$  after the post-decomposition calculation. Then, equation (1) was used to calculate the  $D_{error}$ , which represented the positioning accuracy.

$$D_{error} = \sqrt{(X_r - X_e)^2 + (Y_r - Y_e)^2} \quad \dots(1)$$

### Sample Plot Data Collection

A total of 459 sample plots were investigated from October 1, 2017, to April 1, 2018, in Hunan province (Table 1, Fig. 2). The newly designed sample plot positioning method was used to position the individual tree and sample plot centers. The Vertex Laser VL5 was used to measure the tree heights. A DBH tape was used to measure the diameter at the breast height of the trees. All trees in the sample plots with DBHs greater than 5 cm were measured. The shape of the sample plot was a circle with a diameter of 30 m. The FSV of the sample plot was calculated (Hu et al. 2020) and extended to the hectare scale. To accurately match the remote sensing pixels, the sample plots were resampled to a cell size of 25 m  $\times$  25 m. To normally distribute the FSV data, the data were processed with a normal transformation function ( $f(FSV) = FSV^\lambda$ ,  $\lambda = 0.4$ ) (Pan et al. 2019).

### Landsat-8 Surface Reflectance Tier 1 Data

Landsat-8 Surface Reflectance Tier 1 data were available on the Google Earth Engine (GEE) platform. To match the date of our sample plot data and fully cover the research area, the date filter was set from May 1, 2017, to October 31, 2017, and May 1, 2018, to October 31, 2018. Clouds and cloud shadows were masked by the "pixel-qa" band. A "median" function was applied to extract the median value of all overlapping images, and seven characteristic spectral bands (e.g., B2, B3, B4, B5, B6, B7, B10) were finally calculated. All calculated bands were resampled to a 25 m resolution.

### Sentinel-2 Level-1C Data

Sentinel-2 Level-1C product was used to extract the spectral characteristics, and the date filter was set from May 1, 2017, to October 31, 2017, and May 1, 2018, to Oct 31, 2018. Three

Table 1: Summary of normally transformed sample plots.

Forest types	Main species	Number of plots	FSV (m <sup>3</sup> ha <sup>-1</sup> )				
			Min	Max	Mean	Median	Std
Broadleaf forest	<i>Quercus</i> , <i>Cinnamomum camphora</i> , <i>Phoebe zhenan</i> , <i>Alniphyllum fortunei</i> , <i>Liquidambar formosana</i> , <i>Schima superba</i> , Gum trees, etc.	169	1.15	11.30	5.95	6.14	2.11
Needleleaf forest	<i>Cunninghamia lanceolata</i> , <i>Pinus massoniana</i> , <i>Cupressus funebris</i> , <i>Metasequoia glyptostroboides</i> , <i>Cryptomeria</i> , etc.	231	1.52	12.72	6.38	6.46	2.20
Mixed forest	<i>Cunninghamia lanceolata</i> , <i>Pinus massoniana</i> , <i>Cupressus funebris</i> , <i>Quercus</i> , <i>Cinnamomum camphora</i> , <i>Phoebe zhenan</i> , <i>Alniphyllum fortunei</i> , etc.	59	1.78	11.43	6.77	7.04	2.33

available bands were first used to mask the clouds in the images. The QA60 band is a cloud mask band that is used to mask opaque clouds with a threshold setting of less than 1. Then, the B1 band was used to mask cirrus clouds with a threshold setting of less than 1500. The B2 band was used to mask cirrus clouds with a threshold setting of greater than 2500. After that, the “median” function was used to extract

pixel values. Eleven bands were calculated (i.e., B2, B3, B4, B5, B6, B7, B8, B8A, B10, B11, B12), and all bands were resampled to a 25 m resolution.

**Global PALSAR2/PALSAR Data**

The global 25 m PALSAR2/PALSAR mosaic data are available from January 1, 2007, to January 1, 2018, on the GEE

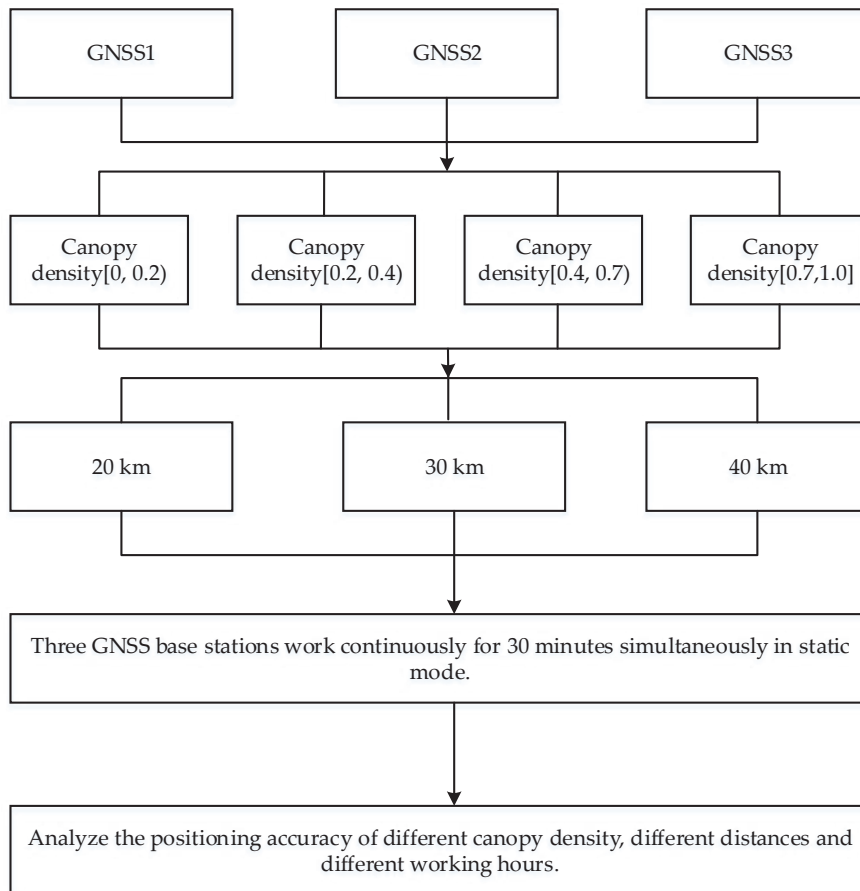


Fig. 1: Flowchart of the GNSS positioning experiment.

platform. The 2017 yearly mosaic data was used to match our sample plot data. The HH and HV bands were selected and processed in windows of different sizes (1 × 1 pixel, 3 × 3 pixels, 5 × 5 pixels, 7 × 7 pixels, 9 × 9 pixels, 11 × 11 pixels, 13 × 13 pixels). Then, equation (2) was used to convert the DN values to gamma naught values in decibel units (dB) (Qin et al. 2017).

$$\gamma^0 = 10 \log_{10} DN^2 - 83.0 \text{ dB} \quad \dots(2)$$

**Sentinel-1 SAR Data**

The Sentinel-1 SAR ground range detected (GRD) dataset has data that starts on October 3, 2014, on the GEE platform; the further data processing was conducted based on the research of Hird et al. (2017), including (1) masking the edges of the images using the angle; (2) filtering out windy days using climate forecasts; (3) performing angle correction; and (4) filtering with different windows (1 × 1 pixel, 3 × 3 pixels, 5 × 5 pixels, 7 × 7 pixels, 9 × 9 pixels, 11 × 11 pixels, 13 × 13 pixels).

**RF Regression Algorithm**

The RF regression algorithm is a popular regression algo-

rithm in this field of study. It uses the bootstrap method to generate multiple datasets to build multiple decision trees (regression trees). The average of the predicted values of the multiple decision trees is used as the final output of the RF regression model. The RF regression model can be mathematically summarized as follows: given a data sample  $X$  and a prediction set  $Y$ , a forest-dependent on the random variable  $\theta$  is planted on this basis to form a tree predictor  $h(X, \theta_k)$ , which outputs the result as a numerical value. The RF predictor is obtained by averaging these trees  $\{h(X, \theta_k)\}$  with respect to  $k$  ( $k$  represents the number of sub-training datasets). The RF regression function is as follows:  $Y = E_{\theta}h(X, \theta_k)$ . The out-of-bag (OOB) data was used to calculate the prediction error (PE) of each regression tree (Equation (3)).

$$PE = E_{\theta} E_{X,Y} (Y - h(X, \theta_k))^2 \quad \dots(3)$$

The principle of the RF regression is as follows (Fig. 3):

In the model development (number = 321, ratio = 0.7) and model test (number = 138, ratio = 0.3), the performance of each RF model was evaluated by the coefficient of determination ( $R^2$ ) and root mean square error (RMSE) (Wang et al. 2019).

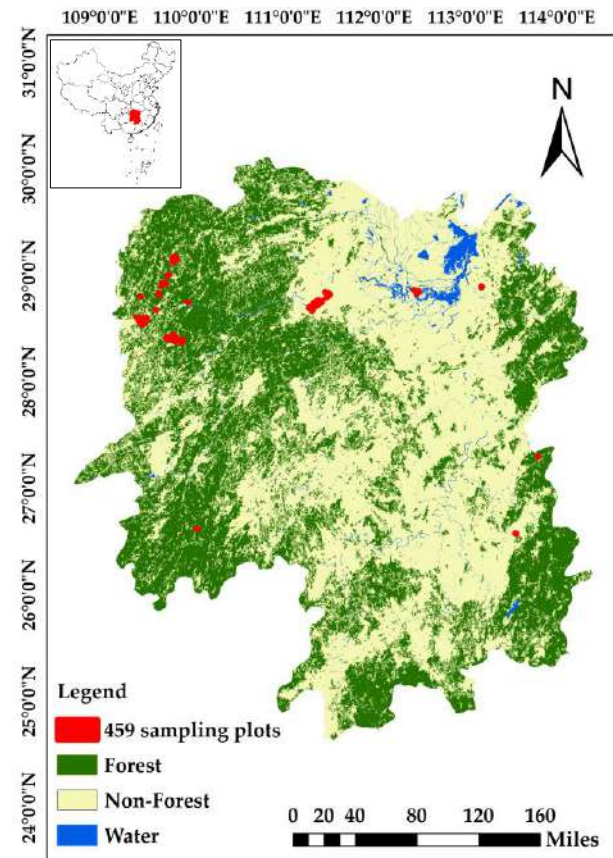


Fig. 2: Sample plots spatial distribution in Hunan, China.

$$R^2 = \frac{\sum_{i=1}^m (f_i - \bar{y})^2}{\sum_{i=1}^m (y_i - \bar{y})^2} \quad \dots(4)$$

$$RMSE = \sqrt{\frac{1}{m} \sum_{i=1}^m (y_i - f_i)^2} \quad \dots(5)$$

Where  $f_i$  is the modeling predictor;  $y_i$  is the measured value of the sample plot;  $\bar{y}$  is the mean measured value of the sample plot; and  $m$  is the number of training and test data points.

**Variable Selection**

Variable selection is necessary when modeling with a large number of independent variables. It simplified the models, shortens the training times, breaks the curse of dimensionality, and enhances the generalization by reducing over-fitting. In this study, the “VSURF” package in R 3.5.3 was used to select variables for different data combinations (Genuer et al. 2015).

**RESULTS**

**The Newly Designed Differential Positioning Accuracies**

Through the static relative positioning test under different distances, different times, and different stand environments, it can be concluded that distance, time, and forest stand environment all have different effects on the positioning accuracy



(Fig. 4). Under the forest stand conditions of the first canopy density level, the GNSS receiver can reach a positioning accuracy of 0.50 m within a static range of 30 km for 10 minutes. However, under the second canopy density forest stand condition, the static duration of more than 25 min at a distance of 30 km is required to achieve a positioning accuracy of 0.50 m. Under the third canopy density forest stand conditions, at least 20 minutes of the static state is required at a distance of 30 km.

**Selection of Variables for Image Classification**

For the Sentinel-1 and PALSAR2/PALSAR variables, only 2 variables (HH, VV) were included in each window size, and the variable selection step was not conducted. The preprocessing step was performed first to decide which window size had a stronger relationship with the FSV. However, considering the weak performance of the Sentinel-1 data, we only selected the PALSAR2/PALSAR variables of 11×11 window size to estimate the FSV.

The “VSURF” package was used for the Sentinel-2 and Landsat-8 variables. For the Sentinel-2 variables, 5 out of 11 variables were selected: blue band (B2), green band

(B3), red band (B4), red edge 1 band (B5), and SWIR 1 band (B11). In Landsat-8 variables, 6 out of 9 variables were selected: ultra-blue band (B1), green band (B3), red band (B4), near-infrared band (B5), shortwave infrared-2 band (B7), and brightness temperature band (B11). The variable combinations for all cases are summarized in Table 2.

**FSV Estimation with the RF Regression Model**

For the training data, Fig. 5 shows the performance of different data combinations in the training phase. The best performance was the data combination with Sentinel-2, Landsat-8, and PALSAR2/PALSAR, with the highest  $R^2 = 0.94$  and the lowest RMSE = 32.19 m<sup>3</sup>.ha<sup>-1</sup>. The worst performance was the PALSAR2/PALSAR (except Sentinel-1), with the lowest  $R^2 = 0.86$  and the largest RMSE = 47.75 m<sup>3</sup>.ha<sup>-1</sup>.

For the test data, Fig. 6 shows the performance of different data combinations in the test phase. The best performance was also the combined Sentinel-2, Landsat-8, and PALSAR2/PALSAR data, which had the highest  $R^2(0.62)$  and the lowest RMSE (65.40 m<sup>3</sup>.ha<sup>-1</sup>). The worst performance was the PALSAR2/PALSAR (except Sentinel-1), which had the lowest  $R^2 = 0.25$  and the largest RMSE = 81.87 m<sup>3</sup>.ha<sup>-1</sup>.

Table 2: The selected variables for RF modeling.

Sensor(s)	Variable selection												
P11	H11	V11											
S2	S2_B2	S2_B3	S2_B4	S2_B5	S2_B11								
L8	L8_B1	L8_B3	L8_B4	L8_B5	L8_B7	L8_B11							
S2+P11	S2_B2	S2_B3	S2_B4	S2_B5	S2_B11	H11	V11						
L8+P11	L8_B1	L8_B3	L8_B4	L8_B5	L8_B7	L8_B11	H11	V11					
S2+L8	S2_B2	S2_B3	S2_B4	S2_B5	S2_B11	L8_B1	L8_B3	L8_B4	L8_B5	L8_B7	L8_B11		
S2+L8+P11	S2_B2	S2_B3	S2_B4	S2_B5	S2_B11	L8_B1	L8_B3	L8_B4	L8_B5	L8_B7	L8_B11	H11	V11

Note: S2 stands for Sentinel-2, L8 stands for Landsat-8, P11 stands for PALSAR2/PALSAR in an 11×11 window size, and H11 stands for HH in an 11×11 window size, and V11 stands for HH in an 11×11 window size.

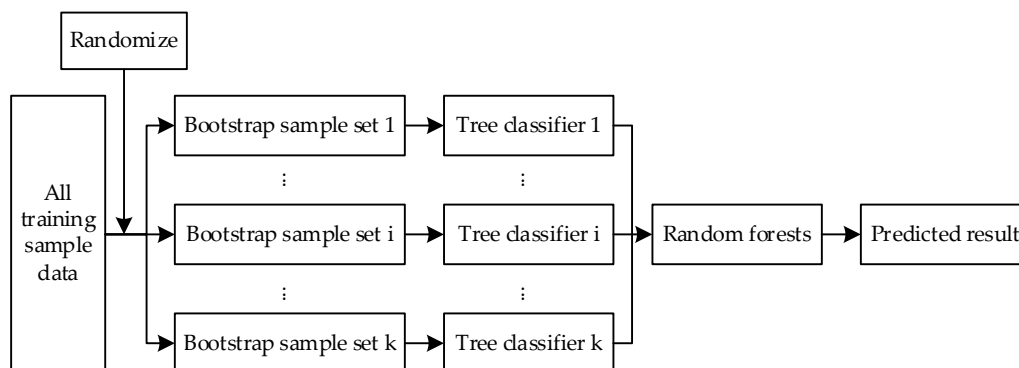


Fig. 3: Flowchart of the RF principle.



**DISCUSSION**

**The Potential Of Multi-Sensor Image Data to Improve FSV Estimation**

For the Sentinel-1 SAR data, the performance of FSV estimation was very poor. A similar study also found that the Sentinel-1 SAR data did not perform well in estimating FSV, with an  $R^2$  of only 0.18 (Mauya et al. 2019). The main reason for the poor performance may be the saturation problem (Huang et al. 2018). Since the SAR-C band is easily affected by speckle noise in complex forests, some studies have only used Sentinel-1 SAR on grass fields (Crabbe et al. 2019).

When considering the L-band PALSAR2/PALSAR dataset, it performed slightly better than the SAR-C band

dataset because the PALSAR2/PALSAR L-band dataset had a higher saturation than the Sentinel-1 SAR-C band dataset in estimating FSV. However, it still did not perform well. Some studies also showed that the ALOS PALSAR data did not perform well in forest biomass estimation (Zhao et al. 2016). Saturation is a major cause of poor performance. Some studies have also found that saturation problems could occur in some forest areas using ALOS PALSAR data to estimate FSV (Antropov et al. 2013). In our sample plot data, the sample values ranged from  $1.42 \text{ m}^3 \cdot \text{ha}^{-1}$  to  $577.49 \text{ m}^3 \cdot \text{ha}^{-1}$ , and many sample values were under  $100 \text{ m}^3 \cdot \text{ha}^{-1}$ , which may be the main reason for our poor modeling result.

For the single dataset, Sentinel-2 performed best both in the training phase and test phase, which showed that the

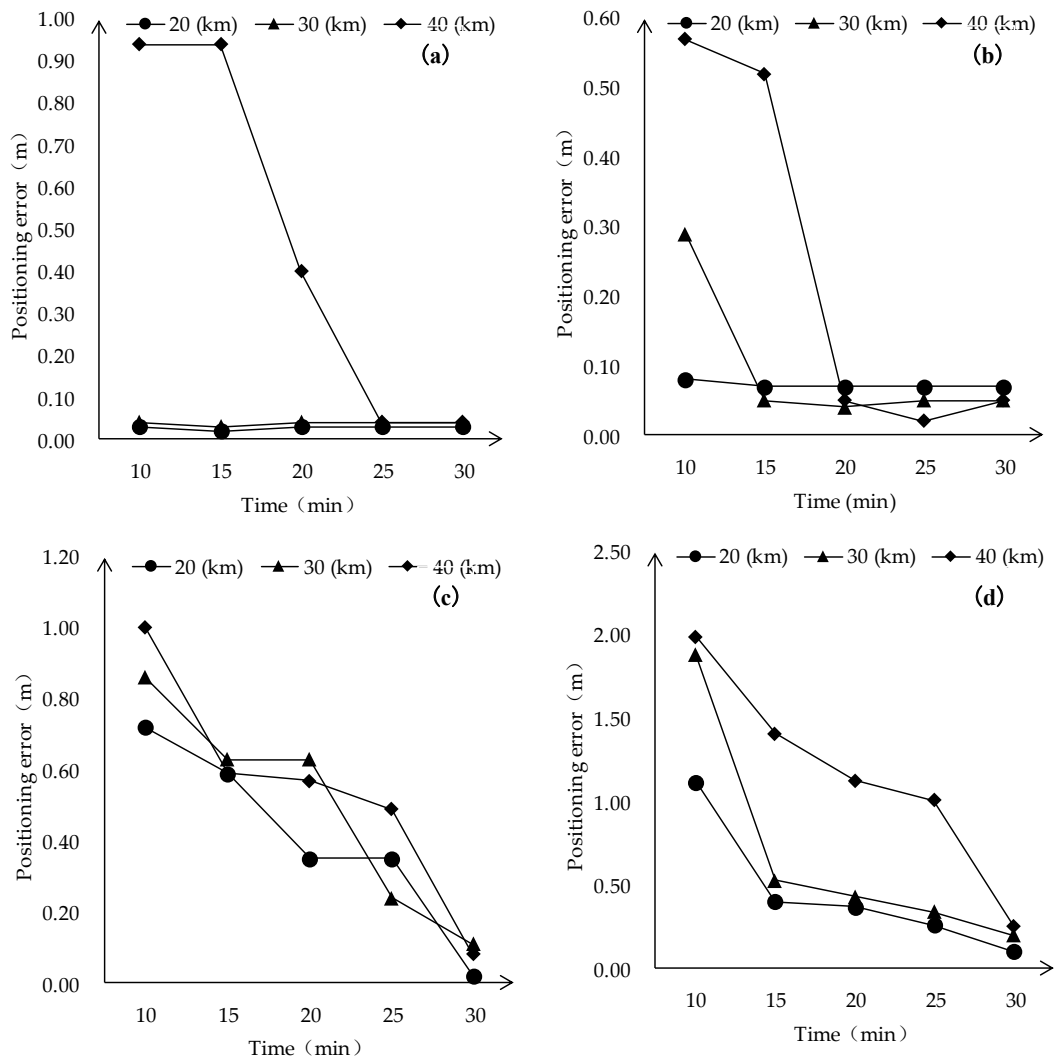


Fig. 4: Static relative positioning error at different distances, different times, and different forest environments: (a) non-forest area, (b) the first canopy density level forest area, (c) the second canopy density level forest area, and (d) the third canopy density level forest area.

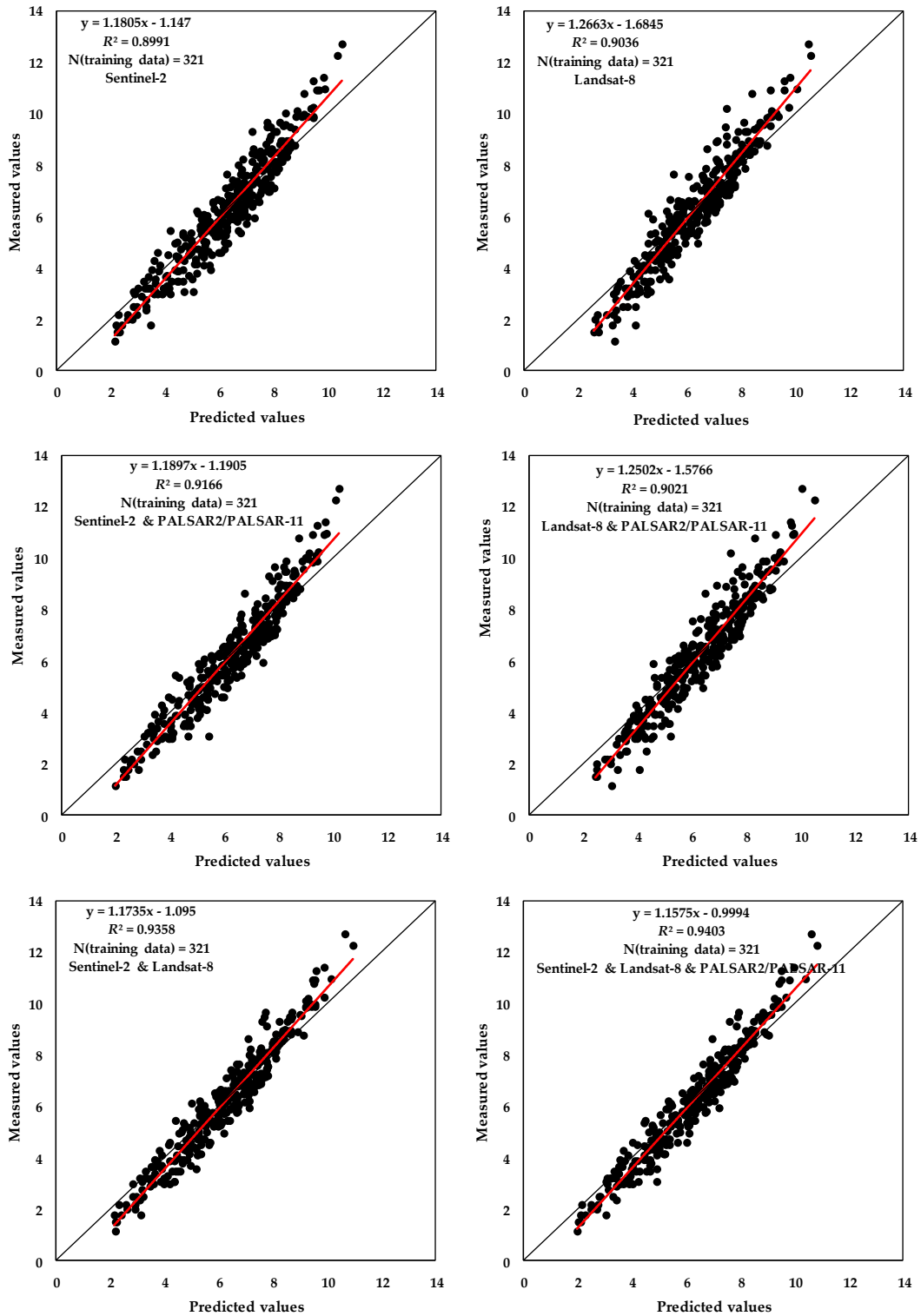


Fig. 5: The performance of the different sensors in the training phase.

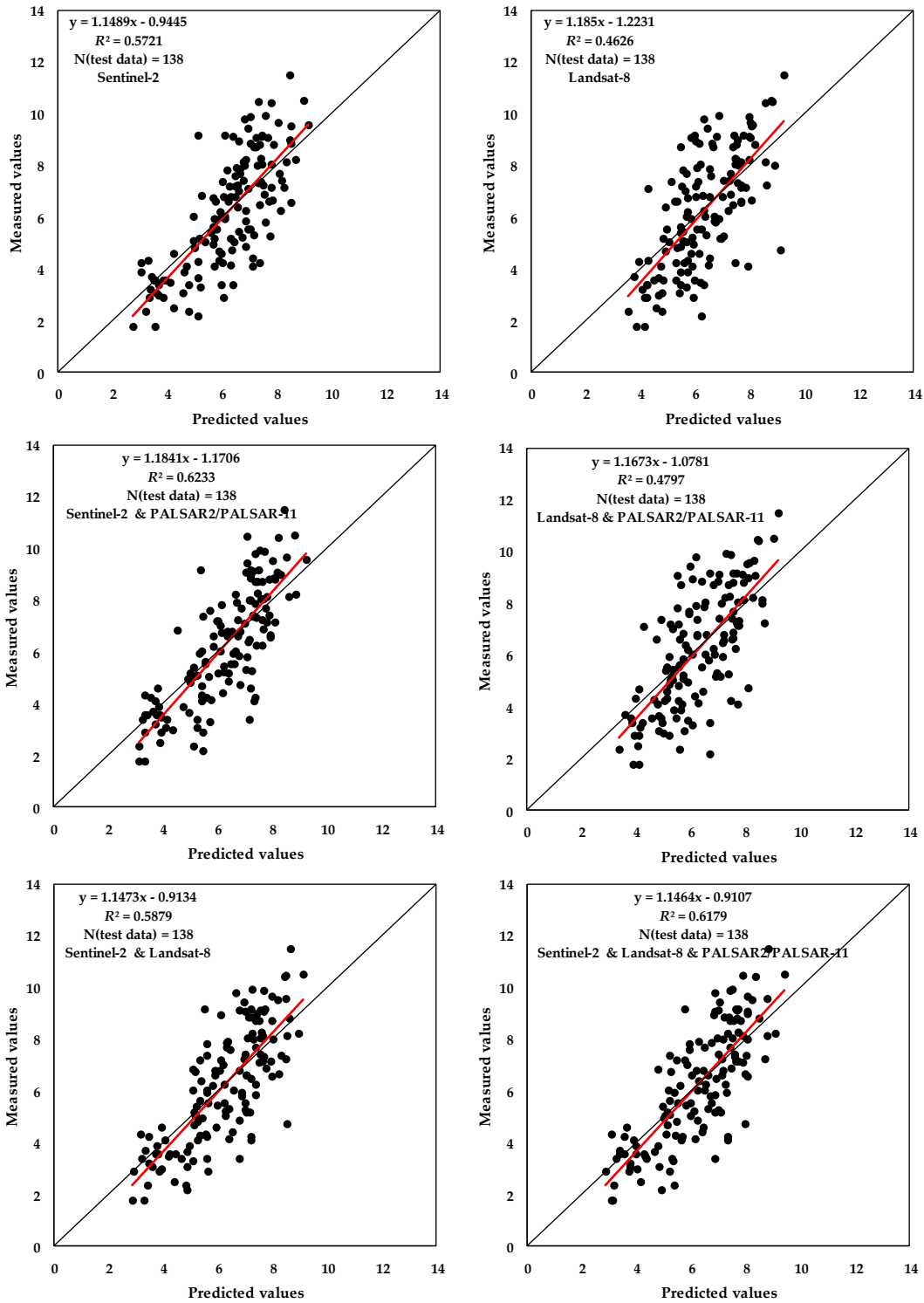


Fig. 6: The performance of different sensors in the test phase.

Sentinel-2 dataset was more appropriate than the Landsat-8 dataset, with B5 (red edge 1) possibly having a positive effect on the FSV estimation. Some studies have proven that the red edge information was related to FSV and biomass estimation (Vaglio et al. 2014). For the data combination, although the combined Sentinel-2, Landsat-8, and PALSAR2/PALSAR data performed best, the Sentinel-2 and PALSAR2/PALSAR datasets performed only slightly worse than the three data combinations. The combined Landsat-8 and PALSAR2/PALSAR data not only had the worst performance among the data combinations but also performed worse than the Sentinel-2 data. This showed that it was unnecessary to use Landsat-8 data when Sentinel-2 data was being used to estimate FSV. Additionally, adding PALSAR2/PALSAR may only create a small level of positive feedback for FSV estimation.

Although the fusion of the three data sources improved the prediction performance under the RF regression model, the test accuracy was still not high. This was caused by the saturation of the data. In forestland with a small FSV, sparse trees and bare ground directly impact the spectral and microwave signals, which affects the accuracy of modeling. Spectral unmixing may be a way to improve the modeling accuracy (Lu et al. 2005). In forestland with a high FSV, optical image and microwave signal saturation were the main reasons leading to the decline in the prediction model's performance. To date, there has been no effective way to solve the saturation problem caused by the data itself (Lu et al. 2016). However, some studies have found that the LiDAR data performed quite well in the forest research field based on its unique ability to penetrate the canopy (Hu et al. 2019).

### Potential of Machine Learning Methods and High-Quality In-Situ Data to Improve FSV Estimation

To achieve such modeling results in a large mountain area in Southern China with a large range of sample values, two points should be considered to achieve the ambitious goals of the study. The first point is the optimized RF algorithm. The best parameters (mtry, ntree) were calculated first to build the regression trees, which may have improved the accuracy of the regression model prediction. With some studies using default values (mtry is  $\sqrt{n}$  or  $\frac{n}{3}$ , n is the number of modeling variables; ntree is 500 or 1000) for RF modeling, we calculated the two parameters using the MSE as a criterion, which would reduce the modeling time and improve modeling accuracy. Although the RF algorithm has been widely used and demonstrated to work quite well in comparison with other machine learning methods, deep

learning methods should not be ignored. Some studies have used different deep learning methods to estimate forest parameters (Zhang et al. 2019). Based on this, additional research should also be conducted in the future.

The second point is the advanced sample positioning technology used in this research. Three GNSS receivers formed a triangulation model and one GNSS receiver was set in the urban area using the CORS service, which allowed it to obtain accurate coordinates as control points to correct the coordinates of the other two GNSS receivers, the positioning accuracy reached the sub-meter level. Compared with the traditional sample positioning method, this new positioning method would help match sample plots with the pixels of remote sensing images more accurately (Hu et al. 2019).

### Likely Sources of Uncertainty in FSV Estimations

In this study, we acknowledge that the Sentinel-2 TOA data was not the best choice for FSV estimation. Although we extracted cloudless images, some factors, such as aerosols, will still have a certain effect on the reflectivity of the ground objects. However, processing the Sentinel-2 TOA data to BOA data at provincial or even national scales is unrealistic. The large volume of data would take a researcher several months or even years to complete on a local computer. Many studies have been conducted and demonstrated that it was acceptable to use TOA data to estimate forest parameters (Lin et al. 2015) and those for wetlands (Hird et al. 2017). However, we still recommend using Sentinel-2 BOA data to carry out research when BOA data are available in the future.

The sample plot data was another source of uncertainty in the FSV estimations. The uncertainty of sample data collection came from the measurement of the trees, the sample plot size, and the tree volume formula (Gao et al. 2018). The measurements of the trees mainly included tree height and DBH, which are directly related to the tree volume and therefore directly related to the FSV of the sample plot. The sample plots used in this study were circle plots with a diameter of 30 m, which was different from the resampling pixel size of remote sensing data. Although the FSV was calculated based on the size of the area and the center position of the plot, since pixels and sample plots were not directly matched, some errors will inevitably occur. This problem could be solved quite well by setting up large-area sample plots and using the pixel coordinates to directly extract the tree volumes in the plots. For the tree volume formula, not all tree species have corresponding calculation equations. Tree volume calculation through tree species classification will also have a certain impact on the original volume value. In addition, if the sample plot data are sufficient and follow

a normal distribution, the prediction accuracy of the model may be further improved (Mohd et al. 2018).

## CONCLUSION

In this study, a new positioning method was proposed to obtain the center coordinates of sample plots and achieved an accuracy within 0.5 m. The sample plots were used to assess the capacity of the different sensor datasets to estimate FSV. Finally, the results showed that the Sentinel-1 SAR data and PALSAR2/PALSAR data was not suitable for estimating FSV in Southern China. However, the PALSAR2/PALSAR data could provide positive feedback when combined with other sensor data. Although the combined Sentinel-2, Landsat-8, and PALSAR2/PALSAR data performed best, the combination performed only slightly better than the combined Sentinel-2 and PALSAR2/PALSAR data. The third best performance was the Sentinel-2 data, which had a performance that was very close to that of the combined Sentinel-2 and PALSAR2/PALSAR data. Using Sentinel-2 data to estimate FSV is a good choice on a provincial scale. Combining Landsat-8 and PALSAR2/PALSAR data could not greatly improve the accuracy of the estimation. We will attempt to use LiDAR data and deep learning methods to estimate FSV in the future.

## ACKNOWLEDGEMENT

This work was funded by the Natural Science Foundation of Ningxia Province (Grant number 2021AAC03017), and the Ningxia Key Research and Development Project (2018BFG02015). The authors are grateful to the Chinese Academy of Inventory and Planning, and the National Forestry and Grassland Administration, for providing the in situ data used in this study.

## REFERENCES

- Antropov, O., Rauste, Y., Ahola, H. and Hame, T. 2013. Stand-level stem volume of boreal forests from spaceborne SAR imagery at L-Band. *IEEE J. Sel. Topics Appl. Earth Observ. Remote Sens.*, 6(1): 35-44.
- Breiman, L. 2001. Random forests. *Mach. Learn.*, 45: 5-32.
- Chrysafis, M., Siachalou, R. and Patias, M. 2017. Assessing the relationships between growing stock volume and Sentinel-2 imagery in a Mediterranean forest ecosystem. *Remote Sens. Lett.*, 8(6): 508-517.
- Crabbe, R.A., Lamb, D.W., Edwards, C., Andersson, K. and Schneider, D. 2019. A preliminary investigation of the potential of Sentinel-1 radar to estimate pasture biomass in a grazed, native pasture landscape. *Remote Sens.*, 11(7): 872.
- Gao, Y., Lu, D., Li, G., Wang, G., Chen, Q., Liu, L. and Li D. 2018. Comparative analysis of modeling algorithms for forest aboveground biomass estimation in a subtropical region. *Remote Sens.*, 10(4): 627.
- Genuer, R., Poggi, J. and Tuleau-Malot, C. 2015. VSURF: An R package for variable selection using random forests. *R J.*, 7(2): 19-33.
- Hird, J., H., Evan, D.L., Gregory, M.D. and Jahan, K. 2017. Google earth engine, open-access satellite data, and machine learning in support of large-area probabilistic wetland mapping. *Remote Sens.*, 9(12): 1315.
- Hu, Y., Wu, F. Sun, Z., Andrew, L., Gao X., Li, W. and Peng D. 2019. the laser vegetation detecting sensor: a full waveform, large-footprint, airborne laser altimeter for monitoring forest resources. *Sensors*, 19(7): 35-63.
- Hu, Y., Xu, X., Wu, F., Sun, Z., Hung, W., Meng, Q., Peng, D. and Xiao, X. 2020. Estimating forest stock volume in Hunan Province, China, by Integrating with situ plot data, Sentinel-2 images, and linear and machine learning regression models. *Remote Sens.*, 12(1): 186.
- Huang, W., Sun, G., Dubayah, R., Cook, B., Montesano, P. and Ni, W. 2013. Mapping biomass change after forest disturbance: Applying LiDAR footprint-derived models at key map scales. *Remote Sens. Environ.*, 134: 319-332.
- Huang, X., Ziniti, B., Torbick, N. and Ducey, M. 2018. Assessment of forest above-ground biomass estimation using multi-temporal C-band Sentinel-1 and Polarimetric L-band PALSAR-2 Data. *Remote Sens.*, 10(9): 1424.
- Lin, C., Popescu, S.C., Gavin, T., Khongor, T., Chang, C.I. and Prasad, V.K. 2015. Classification of tree species in overstorey canopy of the subtropical forest using quick bird images. *PLoS One*, 10(5): e125554.
- Lu, D., Batistella, M. and Moran E. 2005. Satellite estimation of aboveground biomass and impacts of forest stand structure. *Photogr. Eng. Remote Sens.*, 71(8): 967-974.
- Lu, D., Chen, Q., Wang, G., Liu, L., Li, G., and Emilio, M. 2016. A survey of remote sensing-based aboveground biomass estimation methods in forest ecosystems. *Int. J. Digital Earth*, 9(1): 63-105.
- Mauya, E.W., Koskinen, J., Tegel, K., Hmlinen, J. and Kyhk, N. 2019. Modeling and predicting the growing stock volume in small-scale plantation forests of Tanzania using multi-sensor image synergy. *Forests*, 10(3): 279.
- Mitchard, T.A. 2018. The tropical forest carbon cycle and climate change. *Nature*, 559(7715): 527-534.
- Mohd, N.A., Latif, Z.A. and Suratman, M.N. 2018. Modeling above-ground live trees biomass and carbon stock estimation of tropical lowland Dipterocarp forest: Integration of field-based and remotely sensed estimates. *Int. J. Remote Sens.*, 39(8): 2312-2340.
- Pan, P., Sun, Y., Ouyang, X., Zang, R. and Zhang, N. 2019. Factors affecting spatial variation in vegetation carbon density in *Pinus massoniana* lamb: Forest in subtropical China. *Forests*, 10(10): 88
- Qin, Y., Xiao, X., Dong, J., Zhou, Y. and Moore, B. 2017. Annual dynamics of forest areas in South America during 2007–2010 at 50-m spatial resolution. *Remote Sens. Environ.*, 201: 73-87.
- Stefanoni, H., Reyes-Palomeque, G., Castillo-Santiago, M., George-Chacón, S., Huechacona-Ruiz, A. and Tun-Dzul, F. 2018. Effects of sample plot size and GPS location errors on aboveground biomass estimates from LiDAR in tropical dry forests. *Remote Sens.*, 10(10): 1586.
- Sun, W. and Liu, X. 2020. Review on carbon storage estimation of forest ecosystem and applications in China. *Forest Ecosyst.*, 7(1): 1-14.
- Vaglio, L.G, Qi, C., Lindsell, J.A., Coomes, D.A., Frate, F.D., Guerriero, L., Pirotti, F. and Valentini, R. 2014. Above-ground biomass estimation in an African tropical forest with lidar and hyperspectral data[J]. *ISPRS J. Photogr. Remote Sens.*, 89: 49-58.
- Wang, J., Xiao, X., Bajgain, R., Starks, P. and Chang, Q. 2019. Estimating leaf area index and aboveground biomass of grazing pastures using Sentinel-1, Sentinel-2, and Landsat images[J]. *ISPRS J. Photogr. Remote Sens.*, 154: 189-201.
- Xia, H., Qin, Y., Feng, G., Meng, Q. and Liu, G. 2019. Forest phenology dynamics to climate change and topography in a geographic and



- climate transition zone: The Qinling mountains in Central China. *Forests*, 10(11): 1007.
- Yu, Z., Ji, Y., Cy, B., Rui, C., Bo, T. B. and Han, L. B. 2020. Contributions of national key forestry ecology projects to the forest vegetation carbon storage in China. *Forest Ecol. Manag.*, 462: 117981.
- Zhang, L., Shao, Z., Liu, J. and Cheng, Q. 2019. Deep learning-based retrieval of forest aboveground biomass from combined LiDAR and Landsat 8 Data. *Remote Sens.*, 11(12): 1459.
- Zhao, P., Lu, D., Wang, G., Liu, L., Li, D., Zhu, J. and Yu, S. 2016. Forest aboveground biomass estimation in Zhejiang Province using the integration of Landsat TM and ALOS PALSAR data. *Int. J. Appl. Earth Observ. Geoinform.*, 53: 1-15.





# Efficient Adsorptive Performance of Graphene Oxide by Nano Clay

Wenjie Yu, Biao Qian, Beifeng Lv, Haibo Kang<sup>†</sup>, Ping Jiang, Wei Wang and Na Li

School of Civil Engineering, Shaoxing University, Shaoxing 312000, China

<sup>†</sup>Corresponding author: Haibo Kang; 18020852079@usx.edu.cn

Nat. Env. & Poll. Tech.  
Website: [www.neptjournal.com](http://www.neptjournal.com)

Received: 30-07-2021

Revised: 26-09-2021

Accepted: 04-10-2021

## Key Words:

Adsorption  
Graphene oxide  
Nano clay

## ABSTRACT

Research regarding the use of Nano clay to remove toxic GO (Graphene oxide) from wastewater was limited. Through a variety of characterization techniques and methods, the adsorption performance and mechanism of Nano clay for GO were systematically studied. The related effects of solution pH, temperature, adsorbent dose, and GO concentration were studied in detail. The results show that the aggregation and deposition of GO on Nano clay depends on the pH value of the solution and the type and concentration of the electrolyte, and the isotherm data fits well with the Langmuir equation. Under the best conditions (pH=3.0), the maximum removal rate is 97.8% ( $C_0=60 \text{ mg}\cdot\text{L}^{-1}$ ), and the adsorption capacity is  $245.8 \text{ mg}\cdot\text{g}^{-1}$  ( $C_0=80 \text{ mg}\cdot\text{L}^{-1}$ ,  $T=303\text{K}$ , equilibrium time=24 h,  $m=10 \text{ mg}$ ). Specifically, the dissolution of Nano clay at a relatively low pH or a high pH value helps the aggregation of GO. The results of this study provide key information for predicting the fate of GO in the land-water transition zone where Nano clay exists.

## INTRODUCTION

With many advanced properties of the hydrophilic surface, easy modification, and good dispersion in water (Liu et al. 2019a, 2019b), graphene oxide (GO) has been used in various fields. In view of the increasing production of graphene-based nanomaterials and their incorporation in consumer products, they are likely to be discharged into the sewage treatment plant (Burkart et al. 2015) and further into the environment. When the wastewater is untreated or inadequately treated, the high concentration of GO in the wastewater will threaten the lives of animals and plants on the earth (Chen et al. 2019, Tabish et al. 2017). Although there is no known record of the precise concentration of GO in wastewater treatment plants, some authors have been modeling and testing to find possible concentrations. Chen et al. 2019, Tabish et al. 2017, Gottschalk et al. 2013). Currently, there are many different technologies used to remove GO from sewage. Due to its selectivity, low operating cost, affordability, simple operation, high efficiency, and reusable adsorbent, adsorption technology is considered to be one of the best methods to treat wastewater.

In recent years, many adsorbents have been studied for the removal of GO, such as layered double hydroxides (Wang et al. 2016), and  $\text{Al}_2\text{O}_3$  (Ren et al. 2014). Other low-cost adsorbents have also been studied. Clay minerals have been proposed as alternative adsorbents for GO. In addition, clay minerals are widely distributed and abundant in soil, which makes them a promising environmental adsorbent for industrial processes (Deng et al. 2017). Due to the widespread

existence and availability in soil and sediments, clay has been used as a flocculant and adsorbent for the treatment of suspended particles, pathogenic organisms, and toxic compounds in water (Rozhina et al. 2019). In the past thirty years, the use of clay and clay minerals for water treatment has been extensively studied (Hızal & Yılmazo lu, 2021). Examples of such applications include removing grease from water, building clay linings to intercept organic leachate in waste treatment sites, absorbing heavy metals and destroying endocrine chemicals, and recovering nitrogen from nitrogen-rich wastewater. Therefore, there is greater potential for adsorption of GO using natural clays.

The purpose of this study is to evaluate the potential use of Nano clay as a natural adsorbent for the removal of GO under the same experimental conditions. In the adsorption studies, all the parameters that affect the adsorption were studied, such as the amount of adsorbent, the pH value of the aqueous solution, and the initial concentration of GO.

## MATERIALS AND METHODS

### Materials

All chemicals (analytical grade) used in the experiment were purchased from Sinopharm Chemical Reagent Co., Ltd. (Shanghai, China). Nano clay was purchased from Hubei Gold Fine Montmorillonite Technology Co., Ltd. (Hubei, China). The content of montmorillonite is greater than 91.27%. The particle size of nano clay is in the range of 1-2 nm, the surface area is in the range of  $220\text{-}270 \text{ m}^2\cdot\text{g}^{-1}$  and

the density is in the range of 0.03-0.37 g.cm<sup>-3</sup>. The graphene oxide aqueous solution was purchased from Suzhou Tanfeng Graphene Technology Co., Ltd. (Jiangsu, China).

### Batch Experiments

Removal experiments were carried out in a series of vials with teflon-lined nuts fitted with batch technology. A certain amount of Nano clay (0.01 g) was added to the vial to achieve the required concentration of different ingredients. The required initial pH value (3-10) of the suspension in each vial was adjusted by adding negligible 0.1 mol.L<sup>-1</sup> NaOH or HCl. The vials containing these mixtures were placed on a horizontal shaker and shook at a constant speed of 220 rpm for 1 hour. Subsequently, the vial was taken out of the shaker and left to stand on a flat surface for 24 hours to allow the aggregates of Nano clay and GO to settle completely. Finally, the residual concentration of GO ( $C_e$  (mg.L<sup>-1</sup>)) in the supernatant was determined by a UV-vis spectrophotometer (UV-2550, PerkinElmer) at a wavelength of 221 nm (Wang et al. 2016). Formulas 1-3 were used to calculate the relevant parameters:

$$R\% = \frac{C_0 - C_e}{C_0} \times 100\% \quad \dots(1)$$

$$q_e = \frac{(C_0 - C_e) \times V}{m} \quad \dots(2)$$

$$K_d = \frac{Q_e}{C_e} \quad \dots(3)$$

Where,  $C_0$  (mg.L<sup>-1</sup>) and  $C_e$  (mg.L<sup>-1</sup>) represent the initial and equilibrium concentrations of GO, and  $Q_e$  represents the amount of adsorption.

### Characterization

Using CuK $\alpha$  radiation, the crystal structure of the absorbent was detected by an X-ray diffractometer (XRD, Empyrean). The functional groups were identified by Fourier Transform Infrared Spectroscopy (FT-IR, NEXUS), and the scanning range was 400-4000cm<sup>-1</sup>. Scanning electron microscope (SEM, JSM-6360LV), atomic force microscope (AFM, SPA400), and high-resolution transmission electron microscope (HRTEM, JEM-2100F) were used to study the morphology and element composition of the composite material. X-ray photoelectron spectroscopy (XPS) was performed by a Thermo ESCALAB 250 spectrometer, which applied a focused monochromatic Al K $\alpha$  X-ray source (hm=1486.6 eV).

## RESULTS AND DISCUSSION

### Structural and Morphological Characterization

**XRD analysis:** The assessment of the structures of nano-

clay materials is strongly supported by the XRD patterns. The crystalline structures of products were identified with XRD. 2 $\theta$  values were recorded in the XRD patterns of GO, Nano clay, and Nano clay/GO in the range from 5° to 90°, as shown in Fig. 1. As can be seen from the figure, GO and nano clay have obvious diffraction peaks. The adsorption of Nano clay on GO was evaluated by XRD. After Nano clay adsorbs GO, the diffraction peak structure changes. It can be seen from the figure that after Nano clay adsorbs GO, the characteristic peak of Nano clay still exists, but becomes weaker. A weak peak around the GO (001) one is detected in nano clay/GO, and a small variation in its position can be due to an expansion of the stacking of the GO layer. This shows that Nano clay/GO is a mixture of nano clay and GO. This is because the XRD test only scans the surface of the sample, while GO /nano clay is the sample obtained from the adsorption of GO by nano clay. The XRD results show that the XRD pattern is similar to that of nano

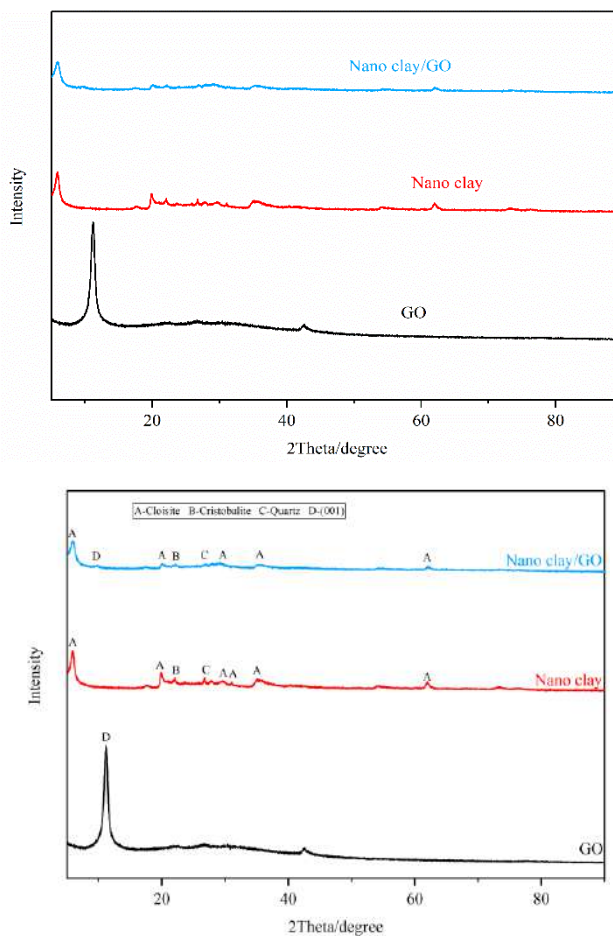


Fig. 1: XRD analysis of GO, Nano clay, and Nano clay/GO. (Adsorption conditions for Nano clay:pH=3,  $C_0=60$  mg.L<sup>-1</sup>,  $m=80$  mg,  $T=303$ K).

clay and cannot be observed to be similar to that of GO. Diffraction peaks indicate that there is a large amount of nano clay on the surface of the sample, and the GO portion in the GO/nano clay is blocked by the nano-clay. The change of structure is beneficial to improve the adsorption capacity of the adsorbent (Yan et al. 2010).

**SEM analysis:** To investigate the surface morphology and structure distribution before and after GO adsorption with SEM. The morphology and microstructure of the material were analyzed by a scanning electron microscope (SEM). The SEM micrographs of GO, Nano clay, and Nano clay/GO are shown in Fig. 2 (a, b, c). The lamellar structure of GO is visible in the SEM image (Fig. 2a). The porous structure of Nano clay is regarded as a layered structure, with irregular particle shapes, agglomerates of variable size, and sharp edges (Fig. b), which is consistent with earlier reports (Yi et al. 2015). On the other hand, when nano clay adsorbs GO, it can be seen that nano clay is covered with a film similar to GO (Fig. 2c) and GO is distributed on the porous network surface of Nano clay with less stacking, indicating that Nano clay has adsorbed GO.

**TEM analysis:** The structural evolution of the material preparation process was observed under transmissive electron microscopy, and the morphology and particle diameter of the product before and after adsorption can be further analyzed (Qi et al. 2015). TEM and XRD together are one of the main

tools used to determine the dispersion of clay nanoparticles, and the obtained TEM image correlates well with the XRD results (Bae et al. 2009). The structure evolution during the preparation of the material was observed under the transmission electron microscope. GO is a multi-layer folded gauze (Liu et al. 2015) (Fig. 3a). When Nano clay absorbs GO, a layer of black substance is obviously attached to the surface of GO in flake shape, and the wrinkles will be significantly reduced or even disappeared (Fig. 3b), which is consistent with XRD diffraction pattern results and SEM images.

**AFM analysis:** We use AFM images from different dimensions to characterize micro-morphology evolution in the material preparation process (Zhang et al. 2019). AFM was used to further illustrate the above results. Fig. 4 shows the representative 2D AFM images of GO and Nano clay/GO. The cross-sectional analysis and white lines of the AFM image are shown in Figs. 4b and d. From the evolution of the AFM micromorphology, the thickness of GO measured by AFM shows that all samples exhibit a single layer or double layer, which is consistent with previous research results (Liu et al. 2018). However, as the thickness of Nano clay/GO increases, Nano clay is buried in the GO sheet, indicating that Nano clay successfully adsorbs GO. Representative results of AFM images are consistent with previous XRD, FT-IR, SEM, and TEM analyses.

**XPS analysis:** XPS was also used to further investigate the

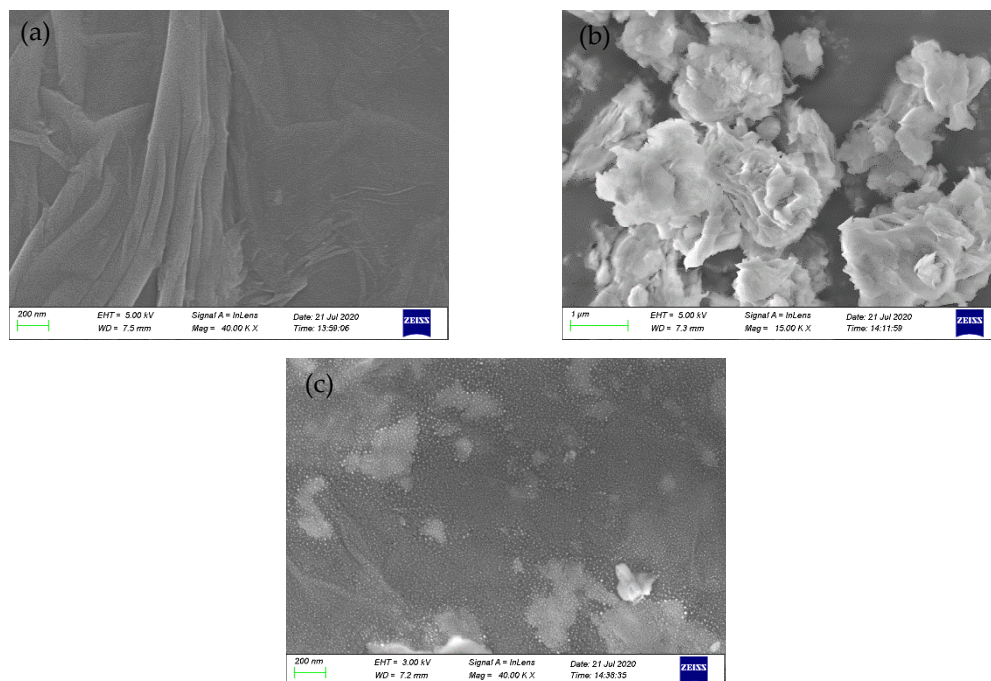


Fig. 2: SEM images of (a) GO, (b) Nano clay, and Nano clay/GO (c). (Adsorption conditions for Nano clay:pH=3,  $C_0=60 \text{ mg.L}^{-1}$ ,  $m=80 \text{ mg}$ ,  $T=303\text{K}$ ).



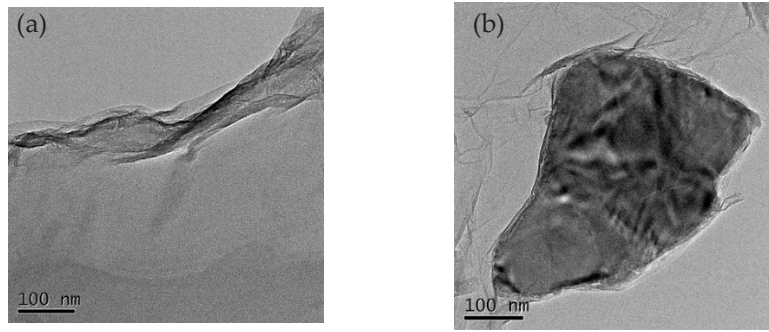


Fig. 3: TEM analysis of GO(a), and Nano clay/GO (b). (Adsorption conditions for Nano clay: pH=3,  $C_0=60 \text{ mg.L}^{-1}$ ,  $m=80 \text{ mg}$ ,  $T=303\text{K}$ ).

adsorption mechanism. XPS is a surface-sensitive technique for the analysis of the chemical environments of elements. The chemical environment changes of the element in a functional group due to adsorption can be identified through the shift of binding energy in the corresponding XPS spectrum (Ciftyurek et al. 2019). The XPS spectra of Nano clay adsorbing GO are related to the characteristic peaks of C 1s and O 1s in the original GO, respectively. As shown in Fig. 5, various

strong peaks can be observed, such as Al 2p, Mg 1s, N 1s, Cl 2p, Cl 1s, O 1s, and C 1s, indicating that the main elements on the surface of the sample are magnesium, aluminum, and oxygen. Compared with the C 1s before GO adsorption, the strength of C 1s after GO adsorption by Nano clay is significantly reduced. From the high-resolution C 1s spectra before GO adsorption, the C 1s spectra can be deconvoluted and integrated into four components, which are about 284.8 eV,

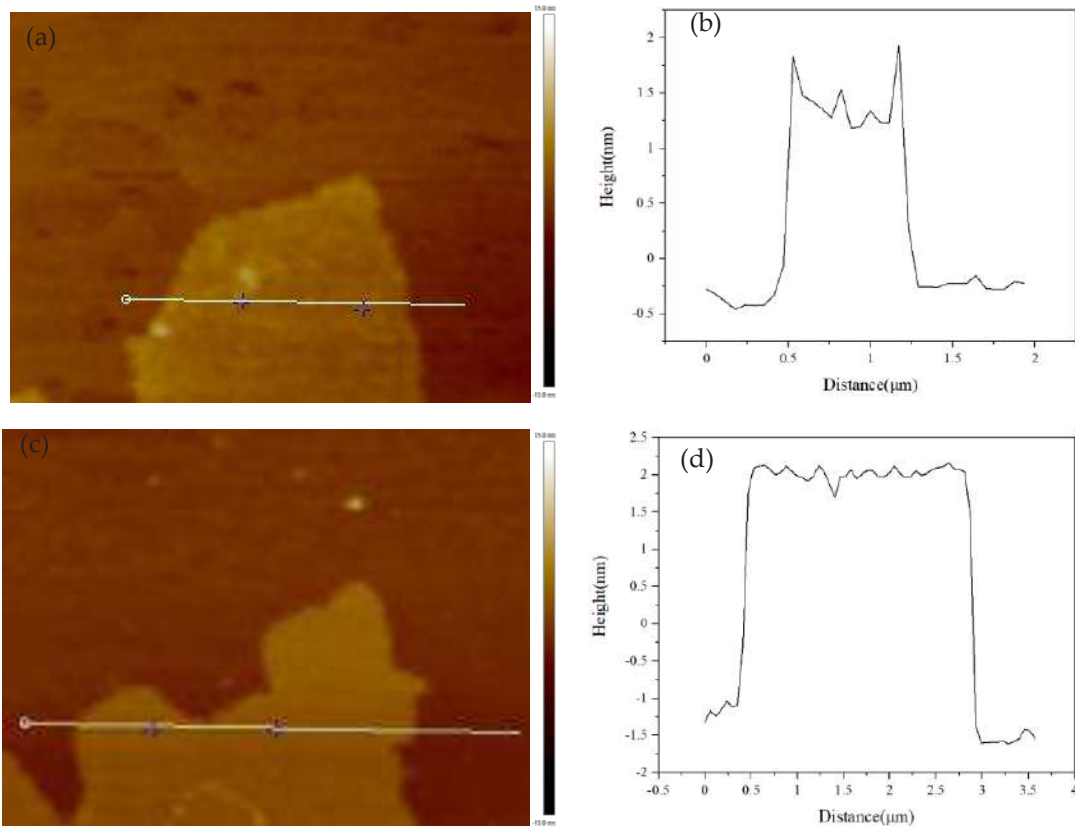


Fig. 4: AFM analysis of GO(a), corresponding height profiles(b), and Nano clay/GO (c), corresponding height profiles (d). (Adsorption conditions for Nano clay: pH=3,  $C_0=60 \text{ mg.L}^{-1}$ ,  $m=80 \text{ mg}$ ,  $T=303 \text{ K}$ ).

286.2 eV, 287.9 eV, and 289.0 eV, respectively (Wen et al. 2013) (Fig. 5 b). The first component with a binding energy of  $\sim 284.8$  eV is due to non-oxidized ring carbon, and the other three components are due to carbon in C-O ( $\sim 286.2$  eV), carbonyl carbon (C=O,  $\sim 287.9$  eV) and carboxylic acid Carbon (O-C=O,  $\sim 289.0$  eV). After GO is adsorbed by Nano clay, C=O disappears, indicating that the adsorption process of GO and Nano clay is carried out by C=O. According to the above analysis, Nano clay can effectively remove GO by adsorbing GO and attaching it to its surface.

### Adsorption Performance

**pH Effect:** The pH value of GO solution is an important

parameter for adsorption (E et al. 2020). Fig. 6 illustrates the change in the adsorption capacity of Nano clay on GO when the initial GO concentration is  $60 \text{ mg}\cdot\text{L}^{-1}$ . Visual fitting data shows that in the pH range of 3-10, the adsorption capacity first decreases and then increases, and performs best at pH=3. High surface area and adsorbent functional groups can improve the adsorption efficiency (Naser et al. 2016). As shown in Fig. 6, when  $\text{pH} < 5$ , the adsorption capacity, removal rate and distribution coefficient of Nano clay on GO first decrease with the increase of pH. However, when  $\text{pH} \geq 5$ , the above three indicators are reversed. The increase in pH may be related to the initial pH of GO. It is known that the surface charge of clay in the solution is negative

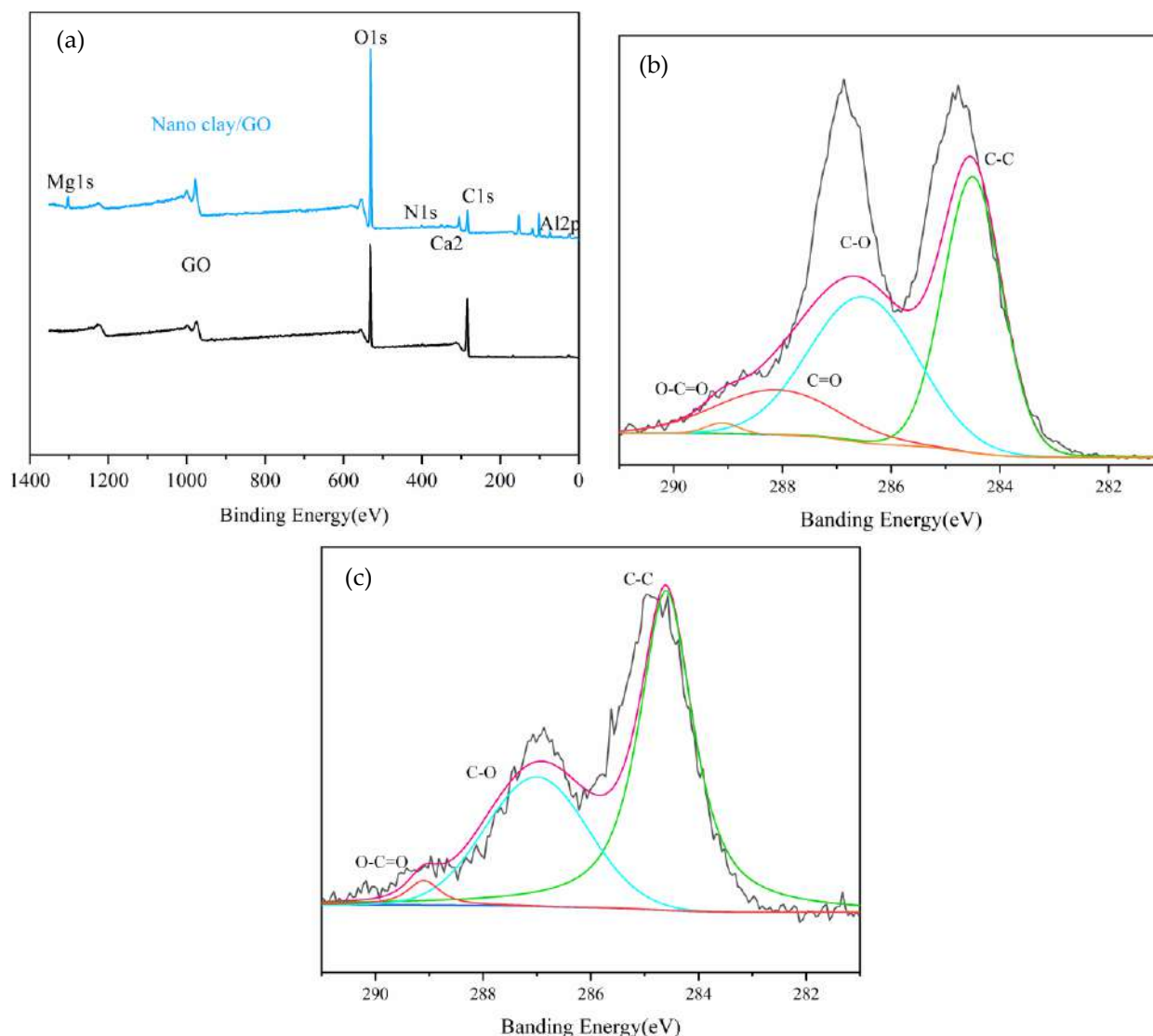


Fig. 5: XPS survey (a), C 1s spectra of GO (b) and C 1s spectra of Nano clay/GO (c) (Adsorption conditions for Nano clay:  $\text{pH}=3$ ,  $C_0=60 \text{ mg}\cdot\text{L}^{-1}$ ,  $m=80$  mg,  $T=303\text{K}$ ).

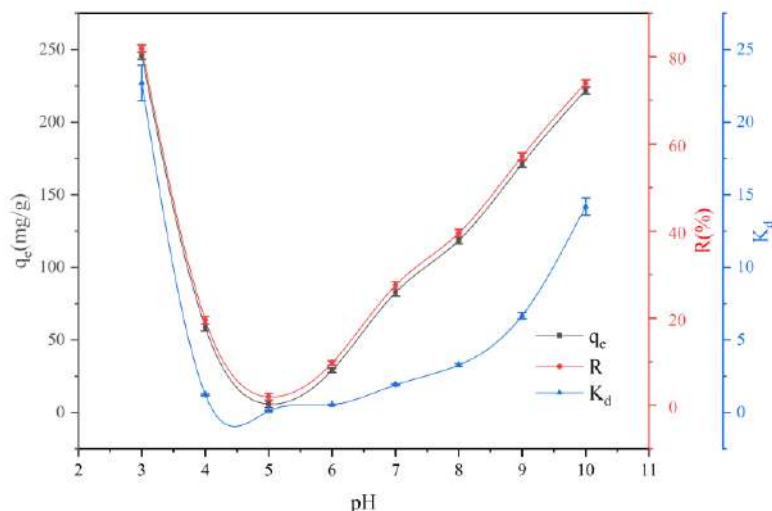


Fig. 6: Effect of pH on adsorption of GO by nano clay.

(Soleimani & Siahpoosh, 2015), GO is also negative, and the reaction between the two is electrostatic repulsion. Since the initial pH of GO solution is 4, when the pH of GO solution is set to 3, the addition of HCl brings the mutual attraction between  $H^+$  and nano clay (Zhang et al. 2019), which further enhances the repelling effect on GO. When the pH value decreases, the concentration of  $H^+$  decreases, and the repulsion of GO is weakened due to electrostatic action. GO is difficult to be separated from water by electrostatic action, which is manifested as the reduction of nano clay's adsorption capacity for GO. On the other hand, when pH is greater than 5, go deprotonation occurs due to carboxyl and hydroxyl groups, the surface charge is negative, and the degree of deprotonation increases with the increase of pH. The increased negative charge will intensify the electrostatic interaction between nano-clays and GO, and the adsorption capacity of nano-clays to GO increases under the impetus of electrostatic interaction (Ashour et al. 2017).

**Nano clay dosage:** The adsorption capacity, removal rate, and distribution coefficient of go with different adsorbents (10 mg, 15 mg, 20 mg, 25 mg, and 30 mg) are shown in Fig. 7. As a result, there will be an opportunity to expect less adsorbent consumption or higher adsorption efficiency. It can be seen that the removal rate decreases with increasing Nano clay dosage and tends to about 55%, and the distribution coefficient also decreases and tends to be 0. At the same time, as Nano clay dosage increases, the adsorption capacity gradually decreases from  $250 \text{ mg.g}^{-1}$  to  $50 \text{ mg.g}^{-1}$ . This is due to the aggregation of concentrated Nano clay particles, so the available active sites are reduced (Acisli et al. 2016). This indicates that the high adsorption capacity or high removal rate needs to be reasonably selected according to the

actual application. In this study, a 10 mg dose was used as an example for follow-up experiments.

**GO concentration:** The removal rate of Nano clay on GO was studied with different initial GO concentrations of  $20 \text{ mg.L}^{-1}$ ,  $40 \text{ mg.L}^{-1}$ ,  $60 \text{ mg.L}^{-1}$ , and  $80 \text{ mg.L}^{-1}$ , respectively. Fig. 8 shows that the removal capacity is affected by the initial GO concentration. With the increase of GO concentration, the adsorption capacity of Nano clay has been increasing. When the GO concentration is  $80 \text{ mg.L}^{-1}$ , the maximum adsorption capacity is  $300 \text{ mg.g}^{-1}$ . However, its removal rate and distribution coefficient show opposite trends, the removal rate is reduced from 89% to 72%. In addition, the distribution coefficient decreases with the increase of GO concentration, indicating that the environment with relatively high GO concentration is not conducive to the adsorption of GO by Nano clay.

#### Adsorption Isotherm and Thermodynamic Study

**Adsorption isotherm:** The change of adsorption isotherm is usually used to further analyze the migration mechanism, reflecting the interaction between the adsorbent and the adsorbate and the structural characteristics of the adsorbed layer. As depicted in Fig. 9, the relationship between  $C_e$  and  $q_e$  was described at  $T=303 \text{ K}$ ,  $313 \text{ K}$ , and  $323 \text{ K}$ . Two main trends in adsorption capacity can be seen in Fig. 9: (1) Under the same conditions, the equilibrium adsorption capacity of Nano clay decreases with the increase of working temperature; (2) Under the same conditions, the equilibrium adsorption capacity of Nano clay increases with the increase of the equilibrium GO concentration. Langmuir and Freundlich's models are commonly used to describe the equilibrium adsorption isotherms. The former is based on the assumption

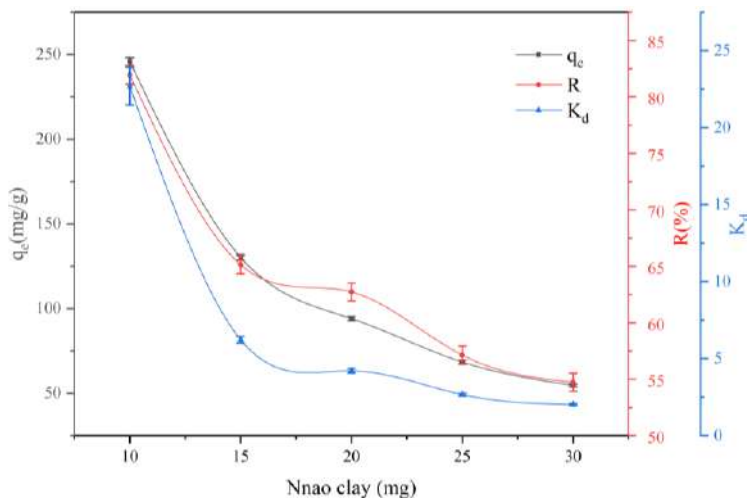


Fig. 7: Effects of nano clay mass on the adsorption of GO.

that a single layer is adsorbed on a surface with a limited number of adsorption sites and uniform adsorption energy, while the latter can be applied to non-ideal adsorption and multilayer adsorption on non-ideal surfaces. The adsorption data conforms to Langmuir (Dalvand & Mahvi 2020) and Freundlich (Wang et al. 2020) models, described as follows.

$$\frac{1}{q_e} = \frac{1}{q_m} + \frac{1}{K_L \times q_m} \times \frac{1}{C_e} \quad \dots(4)$$

$$\ln q_e = \ln K_F + \frac{1}{n} \ln C_e \quad \dots(5)$$

Where,  $C_e$  ( $\text{mg.L}^{-1}$ ) and  $q_e$  ( $\text{mg.g}^{-1}$ ) refer to the equilibrium concentration of GO in the supernatant and the amount

of GO adsorbed per unit of Nano clay weight at equilibrium, respectively.  $q_m$  ( $\text{mg.g}^{-1}$ ) represents the maximum adsorption capacity related to complete monolayer coverage, and  $K_L$  ( $\text{L}\cdot\text{mg}^{-1}$ ) is the Langmuir constant related to the energy and affinity of the adsorbent. The Freundlich constant  $K_F$  is related to the relative adsorption capacity ( $\text{mg.g}^{-1}$ ) of the adsorbent, and  $n$  is related to the high-energy heterogeneity. Several equations were used to analyze the balance of experimental data. The curves in Fig. 10 b-c respectively show the experimental data fitted by Langmuir and Freundlich models. From the result parameters, the correlation coefficient value ( $R^2$ ) of the Langmuir model (0.965-0.996) was higher than that of the Freundlich model (0.904-0.966),

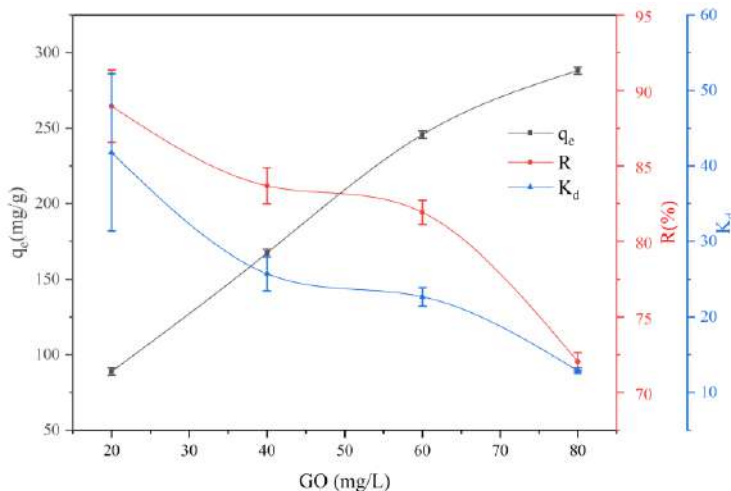


Fig. 8: Effects of GO content on the adsorption of GO by nano clay.

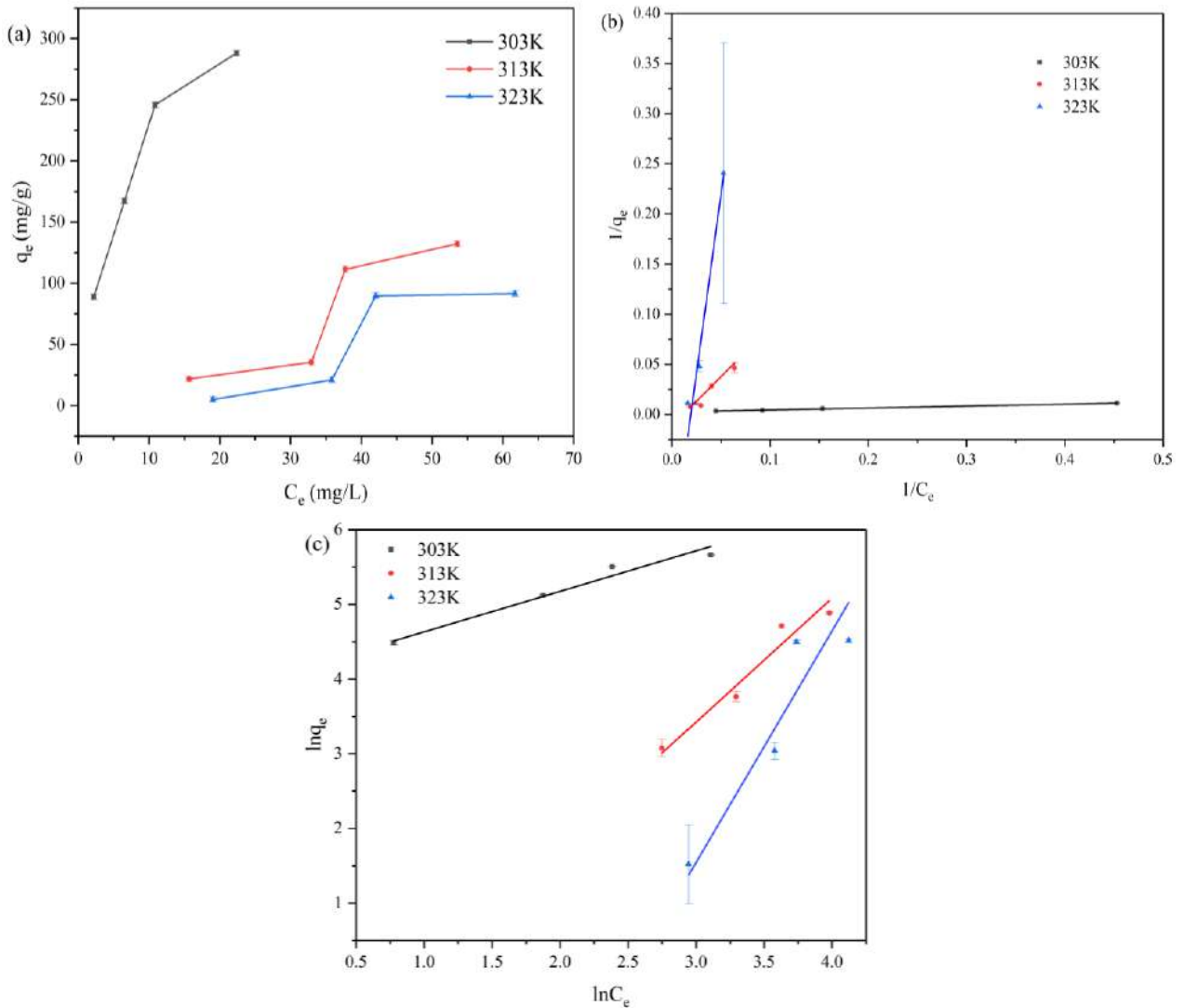


Fig. 9: (a) Adsorption isotherms of Nano clay on GO at  $T=303\text{K}$ ,  $313\text{K}$ , and  $323\text{K}$ ; (b) Equilibrium adsorption isotherms fitted by Langmuir model; (c) Freundlich model; Experimental conditions: Initial pH at 30, dosage =10 mg,  $T=303\text{K}$ .

indicating that the Langmuir model is more suitable for fitting the Nano clay adsorption process. Therefore, due to the Langmuir isotherm, the adsorption mechanism occurs in the single-layer adsorption mode (Sereshti et al. 2019). The corresponding correlation coefficients and other parameters are listed in Table 1, and the highest adsorption capacity is  $384.615\text{ mg}\cdot\text{g}^{-1}$ . It should be noted that when the temperature is 303 K, the value of  $n$  of Freund's constant is greater than 1. However, when the temperature is 313 K and 323 K, the value of  $n$  of Freund's constant is less than 1. This shows that Nano clay has a favorable adsorption effect on GO at a temperature of 303 K.

**Thermodynamic study:** To determine the possibility and

nature of the adsorption mechanism, thermodynamic research was carried out. The effect of temperature on adsorption was studied at 303 K, 313 K, and 323 K. The Van't Hoff thermodynamic model was applied to describe the adsorption mechanism of Nano clay (Hu et al. 2020). The adsorption thermodynamic parameters are calculated based on the value of the adsorption thermodynamic equilibrium constant ( $K_d$ ) obtained from various temperatures. The value of  $\ln K_d$  is then plotted against  $1/T$  to follow the linear form of the van't Hoff equation according to the equation.

The thermodynamic parameters of the adsorption process, namely the value of the standard Gibbs free energy ( $\Delta G^\theta$ ), standard enthalpy ( $\Delta H^\theta$ ) and standard entropy ( $\Delta S^\theta$ )



Table 1: Adsorption isotherm model parameters.

Model parameters	Langmuir				Freundlich		
	$q_m$ [mg.g <sup>-1</sup> ]	$K_L$ [L.mg <sup>-1</sup> ]	$R^2$	$1/n$	$K_F$ (mg <sup>1-n</sup> .L <sup>n</sup> .g <sup>-1</sup> )	$R^2$	
T/K	303	384.615	0.135	0.996	0.528	61.375	0.966
	313	86.207	0.130	0.968	1.564	0.300	0.909
	323	10.000	0.017	0.965	2.653	0.002	0.904

are calculated by the following formulas (Atkins & De Paula 2006):

$$\ln K_d = -\frac{\Delta H^\theta}{R} \times \frac{1}{T} + \frac{\Delta S^\theta}{R} \quad \dots(6)$$

$$\Delta G^\theta = \Delta H^\theta - T \times \Delta S^\theta \quad \dots(7)$$

Where, R is the molar gas constant (0.0083145 KJ.mol<sup>-1</sup>.K<sup>-1</sup>) and  $K_d$  is the distribution coefficient. In short,  $K_d$  has a linear relationship with  $1/T$  and is plotted in Fig. 10. The intercept and slope of the fitted curve can be obtained to calculate  $\Delta H^\theta$  and  $\Delta S^\theta$ , and then  $\Delta G^\theta$  can be further calculated. The thermodynamic parameters are summarized in Table 2. The negative value of  $\Delta H^\theta$  indicates that the adsorption of GO on Nano clay is exothermic, and the negative values and positive values of  $\Delta G^\theta$  indicate that the adsorption of GO on Nano clay is a spontaneous and non-spontaneous combination process, among them when the GO concentration is low, the process changes from spontaneous to non-spontaneous with increasing temperature. Higher working temperature makes  $\Delta G^\theta$  larger, indicating that high temperature inhibits

adsorption, which is consistent with the adsorption capacity results at different temperatures. According to the thermodynamic results, it is obvious that for Nano clay, as the temperature increases, the value of  $\Delta G^\theta$  becomes larger, which indicates that the adsorption process at low temperature is more favorable.  $\Delta S^\theta$  is all negative, indicating that the degree of freedom of the solid-liquid interface of GO on Nano clay increases during the adsorption process. Similar results have been reported in other studies of thermodynamics (Naghizadeh et al. 2017).

## CONCLUSION

The results of this study show that Nano clay has an adsorption effect on GO. The use of 10 mg of pH~3 adsorbent can produce a higher adsorption capacity (245.78 mg.g<sup>-1</sup>). The XRD and FT-IR show the changes in crystals and functional groups during adsorption and differentiation on the topography before and after adsorption can be observed with SEM, TEM, and AFM at different dimensions. XPS results show

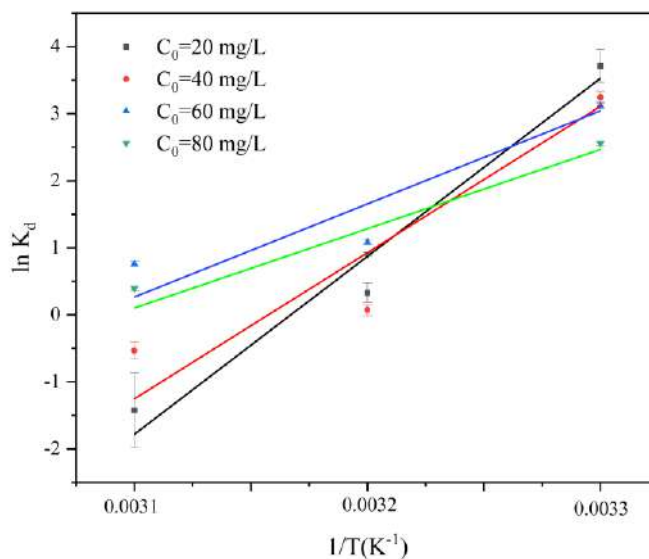


Fig. 10: The linear plot of  $\ln K_d$  versus  $1/T$  (K<sup>-1</sup>) for GO adsorption by Nano clay adsorbent.

Table 2: Values of thermodynamic parameters for the adsorption of Nano clay on GO.

Adsorbate	$C_0$	$\Delta H^0$	$\Delta S^0$	$\Delta G^0$ [kJ.mol <sup>-1</sup> ]		
	[mg.L <sup>-1</sup> ]	[kJ.mol <sup>-1</sup> ]	[KJ.mol <sup>-1</sup> .K <sup>-1</sup> ]	303 K	313 K	323 K
Nanoclay	20	-209.25	-0.66	-8.62	-1.99	4.63
	40	-157.02	-0.49	-7.11	-2.17	2.78
	60	-98.17	-0.30	-7.15	-4.15	-1.15
	80	-89.91	-0.28	-5.97	-3.19	-0.43

that the adsorption process of GO and Nano clay is carried out by C=O. The adsorption isotherm can be well fitted by the Langmuir model, which indicates single-layer adsorption. The equilibrium adsorption capacity of Nano clay decreases with the increase in working temperature. In addition, van't Hoff's thermodynamic model believes that the adsorption of Nano clay on GO is an exothermic adsorption process.

## ACKNOWLEDGMENTS

This research was funded by the National Natural Science Foundation of China (52179107).

## REFERENCES

- Acisli, O., Khataee, A., Karaca, S. and Sheydaei, M. 2016. Modification of nanosized natural montmorillonite for ultrasound-enhanced adsorption of Acid Red 17. *Ultrason. Sonochem.*, 31: 116-121.
- Ashour, R.M., Abdelhamid, H.N., Nasser, A.F., Abdel-Khalek, A.A., Ali, M.M., Uheida, A., Muhammed, M.Z. and Xiaodong, D. J. 2017. Rare-earth ions adsorption onto graphene oxide nanosheets. *Solvent Extr. Ion. Exch.*, 35(2): 91-103.
- Atkins, P. and De Paula, J. 2006. *Physical Chemistry* 8th edition. WH Freeman and company, New York.
- Bae, H.J., Park Hyun, J., Hong Seung, I., Byun Young, J., Darby Duncan, O., Kimmel Robert, M. and Whiteside, W.S. 2009. Effect of clay content, homogenization RPM, pH, and ultrasonication on mechanical and barrier properties of fish gelatin/montmorillonite nanocomposite films. *LWT - Food Sci. Technol.*, 42(6): 1179-1186.
- Burkart, C., Von Tumpling, W., Berendonk, T. and Jungmann D. 2015. Nanoparticles in wastewater treatment plants: A novel acute toxicity test for ciliates and its implementation in risk assessment. *Environ. Sci. Pollut. Res. Int.*, 22(10): 7485-7494.
- Chen, M., Sun, Y., Liang, J., Zeng, G., Li, Z., Tang, L., Zhu, Y., Jiang, D. and Song B. 2019. Understanding the influence of carbon nanomaterials on microbial communities. *Environ. Int.*, 126: 690-698.
- Ciftyurek, E., Smid, B., Li, Z., Matolin, V. and Schierbaum K. 2019. Spectroscopic understanding of SnO<sub>2</sub> and WO<sub>3</sub> metal oxide surfaces with advanced synchrotron-based; XPS-UPS and near ambient pressure (NAP) XPS surface sensitive techniques for gas sensor applications under operational conditions. *Sensors (Basel)*, 19(21): 64-78.
- Dalvand, A.R. and Mahvi, A.H. 2020. Kinetic and equilibrium studies on the adsorption of Direct Red 23 dye from aqueous solution using montmorillonite nanoclay. *Water Qual. Res. J.*, 55(2): 132-144.
- Deng, L., Yuan, P., Liu, D., Annabi-Bergaya, F., Zhou, J., Chen, F. and Liu, Z. 2017. Effects of the microstructure of clay minerals, montmorillonite, kaolinite, and halloysite, on their benzene adsorption behaviors. *Appl. Clay Sci.*, 143: 184-191.
- Tao, E., Dan, M., Yang, S. and Hao, X. 2020. Graphene oxide-montmorillonite/sodium alginate aerogel beads for selective adsorption of methylene blue in wastewater. *J. Alloys Com.*, 14: 832.
- Gottschalk, F., Sun, T. and Nowack, B. 2013. Environmental concentrations of engineered nanomaterials: Review of modeling and analytical studies. *Environ. Pollut.*, 181: 287-300.
- Hizal, J. and Yilmazo lu, M. 2021. Montmorillonite Clay Composite for Heavy Metal Removal from Water. In Inamuddin, A., Ahamed, M.I., Lichtfouse.W. and Asiri, A. A. (eds), *Green Adsorbents to Remove Metals, Dyes and Boron from Polluted Wate*, Springer, NY, pp. 93-112.
- Hu, G., Zhang, W., Chen, Y., Xu, C., Liu, R. and Han, Z. 2020. Removal of boron from water by GO/ZIF-67 hybrid material adsorption. *Environ. Sci. Pollut. Res. Int.*, 27(22): 28396-28407.
- Liu, L., Zhang, Y., He, Y., Xie, Y., Huang, L., Tan, S. and Cai, X. 2015. Preparation of montmorillonite-pillared graphene oxide with increased single- and co-adsorption towards lead ions and methylene blue. *RSC Adv.*, 5(6): 3965-3973.
- Liu, X., Xu, X., Sun, J., Duan, S., Sun, Y., Hayat, T. and Li, J. 2018. Interaction between Al<sub>2</sub>O<sub>3</sub> and different sizes of GO in an aqueous environment. *Environ. Pollut.*, 243: 1802-1809.
- Liu, X., Zhou, F., Chi, R., Feng, J., Ding, Y. and Liu, Q. 2019a. Preparation of modified montmorillonite and its application to rare earth adsorption. *Minerals*, 9(12): 44
- Liu, Z., Rios-Carvajal, T.P., Andersson, M., Ceccato, M., Stipp Susan, L.S. and Hassenkam, T. 2019b. Ion effects on molecular interaction between graphene oxide and organic molecules. *Environ. Sci. Nano*, 6(7): 2281-2291.
- Naghizadeh, A., Kamranifar, M., Yari, A.R. and Mohammadi, M.J. 2017. Equilibrium and kinetics study of reactive dyes removal from aqueous solutions by bentonite nanoparticles. *Desal. Water Treat.*, 97: 329-337.
- Naser, S., Najme, S., Irani, M., Gholamian, R. and Aliabadi, M. 2016. Removal of MTBE from aqueous solution using natural nanoclays of Iran. *Desal. Water Treat.*, 57(56): 27259-27268.
- Qi, T., Huang, C., Yan, S., Li, X.J. and Pan, S.Y. 2015. Synthesis, characterization, and adsorption properties of magnetite/reduced graphene oxide nanocomposites. *Talanta*, 144: 1116-1124.
- Ren, X., Li, J., Tan, X., Shi, W., Chen, C., Shao, D., Wen, T., Wang, L., Zhao, G., Sheng, G. and Wang, X. 2014. Impact of Al<sub>2</sub>O<sub>3</sub> on the aggregation and deposition of graphene oxide. *Environ. Sci. Technol.*, 48(10): 5493-5500.
- Rozhina, E., Batasheva, S., Danilushkina, A., Kryuchkova, M., Gomzikova, M., Cherednichenko, Y., Nigamatyanova, L., Akhatova, F. and Fakhullin R. 2019. Kaolin alleviates the toxicity of graphene oxide for mammalian cells. *Medchemcomm*, 10(8): 1457-1464.
- Sereshti, H., Zamiri, A.E., Esmaeili, B.M., Rashidi, N.H., Afzal, K.M. and Yilmaz, M. 2019. Removal of phosphate and nitrate ions aqueous using strontium magnetic graphene oxide nanocomposite: Isotherms, kinetics, and thermodynamics studies. *Environ. Prog. Sustain. Energy*, 39(2): 414.
- Soleimani, M. and Siahpoosh, Z.H. 2015. Ghezeljeh nanoclay as a new natural adsorbent for the removal of copper and mercury ions: Equi-

- librium, kinetics and thermodynamics studies. *Chin. J. Chem. Eng.*, 23(11): 1819-1833.
- Tabish, T.A., Pranjol, M.Z.I., Hayat, H., Rahat A.A.M., Abdullah, T.M., Whatmore, J.L. and Zhang S. 2017. In vitro toxic effects of reduced graphene oxide nanosheets on lung cancer cells. *Nanotechnology*, 28(50): 511.
- Wang, J., Zhang, J., Han, L., Wang, J., Zhu, L. and Zeng, H. 2021. Graphene-based materials for adsorptive removal of pollutants from water and underlying interaction mechanism. *Adv. Colloid. Interface Sci.*, 289.
- Wang, J., Wang, X., Tan, L., Chen, Y., Hayat, T., Hu, J., Alsaedi, A., Ahmad, B., Guo, W. and Wang, X. 2016. Performances and mechanisms of Mg/Al and Ca/Al layered double hydroxides for graphene oxide removal from aqueous solution. *Chem. Eng. J.*, 297: 106-115.
- Wang, Z., Gao, M., Li, X., Ning, J., Zhou, Z. and Li, G. 2020. Efficient adsorption of methylene blue from aqueous solution by graphene oxide modified persimmon tannins. *Mater. Sci. Eng. C. Mater. Biol. Appl.*, 23: 108.
- Wen, T., Wu, X., Tan, X., Wang, X. and Xu, A. 2013. One-pot synthesis of water-swellable Mg-Al layered double hydroxides and graphene oxide nanocomposites for efficient removal of As(V) from aqueous solutions. *ACS Appl. Mater. Interfaces*, 5(8): 3304-3311.
- Yan, L.G., Xu, Y.Y., Yu, H.Q., Xin, X.D., Wei, Q. and Du, B. 2010. Adsorption of phosphate from aqueous solution by hydroxy-aluminum, hydroxy-iron, and hydroxy-iron-aluminum pillared bentonites. *J. Hazard. Mater.*, 179(1-3): 244-250.
- Yi, F.Y., Zhu, W., Dang, S., Li, J.P., Wu, D., Li, Y.H. and Sun, Z.M. 2015. Polyoxometalates-based heterometallic organic-inorganic hybrid materials for rapid adsorption and selective separation of methylene blue from aqueous solutions. *Chem. Commun.*, 51(16): 3336-3339.
- Zhang, C., Luan, J., Yu, X. and Chen, W. 2019. Characterization and adsorption performance of graphene oxide - montmorillonite nanocomposite for the simultaneous removal of Pb(2+) and p-nitrophenol. *J. Hazard. Mater.*, 41: 378.
- Zou, Y., Wang, X., Ai, Y., Liu, Y., Li, J., Ji, Y. and Wang, X. 2016. Coagulation behavior of graphene oxide on nanocrystallined Mg/Al layered double hydroxides: Batch experimental and theoretical calculation study. *Environ. Sci. Technol.*, 50(7): 3658.





# Time Series Simulation and Forecasting of Air Quality Using In-situ and Satellite-Based Observations Over an Urban Region

A. Choudhary\*(\*\*\*)†, P. Kumar\*\*, S. K. Sahu\*\*\*, C. Pradhan\*\*\*, S. K. Singh\*\*\*\*, M. Gašparović\*\*\*\*\*,  
A. Shukla\*\*\*\*\* and A. K. Singh\*\*\*\*\*

\*†CoE Environment, Climate Change and Public Health, Utkal University, Bhubaneswar, Odisha, India

\*\*School of Environmental Sciences, Jawaharlal Nehru University, New Delhi, India

\*\*\*Department of Botany, Utkal University, Bhubaneswar, Odisha, India

\*\*\*\*K. Banerjee Centre of Atmospheric and Ocean Studies, IIDS Nehru Science Centre, University of Allahabad, India

\*\*\*\*\*Chair of Photogrammetry and Remote Sensing, Faculty of Geodesy, University of Zagreb, Zagreb, Croatia

\*\*\*\*\*Transport Planning and Environment Division, Central Road Research Institute, New Delhi, India

\*\*\*\*\*Department of Physics, Institute of Science, Banaras Hindu University, Varanasi, India

†Corresponding author: A. Choudhary; choudharyarti12@gmail.com

## Nat. Env. & Poll. Tech.

Website: [www.neptjournal.com](http://www.neptjournal.com)

Received: 27-10-2021

Revised: 10-12-2021

Accepted: 24-12-2021

### Key Words:

ARIMA

MODIS AOD

PM<sub>2.5</sub>

O<sub>3</sub>

NO<sub>2</sub>

simulation

Forecast

## ABSTRACT

Air quality is directly associated with the health of society. So, it becomes essential to forecast air pollution, which assumes an imperative part in air pollution warnings and control. A time-series simulation approach was adapted for the forecasting of monthly mean ambient air pollutants (PM<sub>2.5</sub>, O<sub>3</sub>, NO<sub>2</sub>) concentration and Aerosol Optical Depth (AOD) at an urban traffic site (Mathura Road, CSIR-CRRI) in New Delhi, India. Satellite-based aerosol loading (AOD<sub>550</sub>) retrieved from the Terra MODIS (Collection 6) enhanced Deep Blue (DB) algorithm was used for further analysis. The analysis considered the average monthly mean concentration of air pollutants and AOD between 2012-2017 and, simulates the concentrations of PM<sub>2.5</sub>, O<sub>3</sub>, NO<sub>2</sub>, and AOD for the same period and then forecasts air quality for the years 2020-2023. The forecasted results were validated with 24 months of in-situ and satellite data from 2018-to and 2019. In the year 2020, observed and simulated results are in lower agreement due to the shutdown of anthropogenic activities to combat pandemic situations. Otherwise, modeled and forecasted results are in good harmony with the in-situ and satellite observations. The results also signify that the time series Autoregressive Integrated Moving Average (ARIMA) modeling approach can be an effective and simple tool for air pollution simulation and future forecast. The results are evocative concerning the forecast of near future aerosol loading information and will also be profound to address the problems.

## INTRODUCTION

Indian cities are the epicenter of economic activity and are also on the front lines of some of the world's worst air quality (Choudhary & Gokhale 2016, 2019). Industrialization and unchecked population growth have resulted in increased resource consumption, further amplifying the problem of air pollution (Kumar et al. 2021, Pratap et al. 2020, Choudhary et al. 2020). Millions of casualties happened worldwide because of the worst air quality (Pandey et al. 2021). Air pollution remains one of the most important public health concerns across the globe for the last two decades, contributing to substantial premature mortality with a greater impact in developing nations (Balakrishnan et al. 2019). It is, therefore, important to provide time-to-time air quality forecasts at global, regional, and local scales to support public health authorities (Maji et al. 2021) and policy-makers and enable

them to take timely preventative action (Jia et al. 2020) in the short term, long term and event-specific scenarios (Vadrevu et al. 2020) to combat the atmospheric pollutions (Kumar et al. 2018).

In India, geographical boundaries are also favorable and supportive of deteriorating air quality. It is observed in the post-monsoon and winter seasons (October to November and December to February) (Kumar et al. 2020c, Prabhu et al. 2019). Despite this, some episodic events are also well known in India that lead to extremely poor air quality in a particular period of the year (Kumar et al. 2019, 2020a). For example, the rice-wheat crop buildup consumption (CRB) happens two times every year, in April–May wheat crop/Ravi crop and October–November rice crop/Kharif crop, respectively. These periods worsen air quality in many Indian cities (Sarkar et al. 2018). Post-monsoon (October–November)



period in India has other episodic events (such as Diwali and biomass burning), and adverse meteorology worsens the air quality. Diwali is associated with burning fire crackers in bulk (Singh et al. 2010) and massive crop residue burning increases the immense load on the local atmosphere. Faiz & Sturm (2000) have assessed that about 10% of respiratory ailments out of thousands of detailed cases are related to climatic contamination every year during these episodic events in Delhi. The Diwali episode lifts  $PM_{10}$  and total suspended particulate concentration two to three times in Hisar city, India (Ravindra et al. 2019). Likewise, Barman et al. (2008) additionally revealed that an episodic event Diwali increases pollutants  $PM_{10}$ ,  $SO_2$ , and  $NO_x$  concentrations 5.7, 6.6, and 2.7 times, respectively, in contrast to any regular day in Lucknow, India.

In the year 2020 to prevent the COVID-19 transmission, a worldwide lockdown was announced at a different time of the year, and the lockdown imprints were observed in the ambient atmosphere (Kumar et al. 2020b). In India, additionally, air contamination levels dropped altogether with the inconvenience of the 21-day lockdown. To understand the response to complete lockdown, many scientific reports were published to demonstrate the different aspects of air quality all about changes (Chen et al. 2020, Muhammad et al. 2020, Tobías et al. 2020, Xu et al. 2020). A significant decrease in  $PM_{2.5}$ ,  $NO_2$ , and CO concentration before and after lockdown (21-days) were reported by Srivastava et al. (2020) for two Indian cities. Kotnala et al. (2020) stated a 14-time reduction in  $NO_x$  concentration (342 to 24 ppb) in New Delhi during the lockdown.

Forecasting, in all aspects, is always very important to formulate the policies to control the situation and condition. Time series analysis is widely implied over the long-term data for comparative analysis and predicts current trends and future forecasts (Soni et al. 2015). The utilization of time series examination depends on the idea that there are some interior trends and patterns inside the data, for example, autocorrelation, patterns, or occasional variety. Several analyses applied the time-series approach to address the air quality by utilizing autoregressive, moving normal models and a mingle of both, known as an autoregressive integrated moving average (ARIMA) (Abish & Mohana 2013, Soni et al. 2014). ARIMA stays as the mainstream model these days due to its adaptability in addressing various sorts of time arrangements, autoregressive (AR), moving normal (MA), and autoregressive moving normal model (ARIMA), it can be defined as ARIMA (p, d, q). When the dataset is non-stationary, the difference will take part in stationary data (AbdRahman et al. 2013). The three stages viz. distinguish verification; assessment and analytic checking assure the precision of time series outcomes (Kumar et al. 2018).

ARIMA depends on the Box–Jenkins approach; it is broadly applied in air quality investigations (Box & Jenkins 1976). The insights concerning the ARIMA depicted else were (McBerthouex & Brown 2002). For time series examination, around 50–100 data points are required (Box & Jenkins 1976, Milionis & Davies 1994). Several researchers considering the impact of meteorological components and apply ARIMA models to anticipate submicron molecule fixations (Jian et al. 2012), day-by-day normal  $PM_{10}$  focuses (Liu 2009), and ozone fixation in metropolitan and provincial territories (Duen˜as et al. 2005).

The ARIMA model has widespread application due to its flexibility (Lai et al. 2019, Li et al. 2020, Singh et al. 2020). Therefore, this study's main objectives were as follows, 1) to forecast the future trend of pollutants ( $PM_{2.5}$ ,  $O_3$ , and  $NO_2$ ) and AOD, just after the pandemic episode by applying the ARIMA tool, and 2) to perform a comparative analysis of measured and simulated observations, 3) validation of forecasted results with 25% data (monthly mean of the year 2018–2019, 24 points). 4) Further study will also characterize the trends and variability of the year 2020, emphasizing the lockdown period.

## MATERIALS AND METHODS

### Data Source

A stationary stochastic ARIMA modeling approach was applied to forecast the monthly mean concentration of ambient air pollutants ( $PM_{2.5}$ ,  $O_3$ , and  $NO_2$ ) and AOD for the urban area of New Delhi, India. The part of data (from 2012–2017) of air pollutants ( $PM_{2.5}$ ,  $O_3$ , and  $NO_2$ ) have been obtained from the automated installed station at CSIR–Central Road Research Institute (CRRI), New Delhi and part of data obtained from CPCB (Central Pollution Control Board) India, for the CSIR–CRRI, New Delhi station for the year 2018–2020. The aerosol optical depth (AOD) at 550 nm was extracted daily for the period 2012 to 2020, from MODIS onboard the Terra satellite for the stations CSIR–CRRI (28.5517° N, 77.2750° E). MODIS measures spectral radiances from 0.55  $\mu m$  for land with a resolution of  $0.1^\circ \times 0.1^\circ$  (<https://earthobservatory.nasa.gov/global-maps>). The MODIS (Collection 6) enhanced Deep Blue (DB) AOD (Deep\_Blue\_Aerosol\_Optical\_Depth\_550\_Land\_Best\_Estimate) of level 2, was used in this study. The 24-h average time series data of ambient air pollutants ( $PM_{2.5}$ ,  $O_3$ , and  $NO_2$ ) were averaged into monthly data, similarly daily AOD data were also averaged into monthly AOD then applied the ARIMA for the further analysis.

### Quality Control Approach

For quality affirmation, the study used two strategies: (i)

outlier recognition and gap-filling procedures were applied to improve the nature of the dataset (Jesus et al. 2020), and (ii) a manual exclusion of zero, negative and invalid information, after reviewing of the dataset. This was applied for the AOD dataset since missing values were greater than those applied for the AOD dataset since missing values were greater than the 365 data points (around 11% of total data). The pollutants  $PM_{2.5}$ ,  $O_3$ , and  $NO_2$  have less than 1% missing values for the total assessment period since the gap-filling techniques are generally recommended when missing information rates are more prominent than 5% (Ottosen & Kumar 2019, Junger & De Leon 2015). Therefore, pollutants  $PM_{2.5}$ ,  $O_3$ , and  $NO_2$  were manually cleaned and used for the data analysis and interpretations.

### Time Series Approach: ARIMA

The ARIMA is a time series simulation method presented by Box & Jenkins in the 1970s and was applied for the current and near-future forecast of the aerosol load to the atmosphere (Kantz & Schreider 1997). Time-series data of the simulation object are considered a stochastic sequence, and this sequence is fitted with some numerical models. When the model is recognized, the future qualities can be anticipated over a wide time period (Kucharski et al. 2020). ARIMA can be defined as ARIMA (p, d, q), a model can be partitioned into three sorts, details are given else were (Kumar et al. 2015). The ARIMA model can discover the qualities and patterns of the time-series information and speculate the future behavior effectively (Kumar et al. 2018).

The time series ARIMA approach was applied to assess the air quality trend before and after the Pandemic episode and the near future air pollutants forecast. The section first portrays the 2012-2017 monthly variation of selected pollutants, section two is characterizing the pollutants' behavior of the year 2020 (Pandemic year), section three is demonstrating the ARIMA simulation and forecasted results, further comparative interpretation of measured, simulated results, and validation data, forecasted observations were described. Such figures are particularly useful in outlining proper approaches for air quality administration (Kumar et al. 2018). The monthly data for the year 2012-2017 (total of 72 data points, 75%

of data) was used for the simulation, and monthly data for the year 2018-2019 (25% of data) was used for the validation of the forecasted results (Kumar & Jain, 2009). The extraction and assessment of model boundaries are accomplished by utilizing the ARIMA by using the SPSS package. Different criteria were used to evaluate the model fits and goodness, explained else were (Gocheva-Ilieva et al. 2014).

## RESULTS AND DISCUSSION

### Year to Year Variation of Pollutants

Fig. 1 demonstrates the monthly variation of pollutants  $PM_{2.5}$ ,  $O_3$ ,  $NO_2$ , and AOD for the period 2012 to 2017. The cyclic and seasonality patterns are very distinct in the figure, particularly for the  $PM_{2.5}$  and AOD (Kumar et al. 2019, 2020a). Highest emission peaks observed for post-monsoon period (October-November, as per Fig. 1 post-monsoon months are: 10-11, 23-24, 35-36, 47-48, 59-60, 71-72). In the monsoon season, pollutants concentration drops to a minimum, the dropping peaks are also very apparent corresponding to the monsoon season (July-September, as per Fig. 1 monsoon months are: 7-9, 19-21, 31-33, 43-45, 55-57, 67-69). The  $O_3$  and  $NO_2$  also follow the cyclic seasonality trend, but the peaks get flattened with the proceeding years.

The descriptive statics of the data is depicted in Table 1. The higher skewness value (0.695 to 1.5) indicates that data are in non-symmetrical distribution. Likewise, the kurtosis ranges of 0.511 to 2.97 indicate leptokurtic distribution. The time series simulation approach, ARIMA was applied to the 2012-2017 (75% of data) data set for the future forecast. It was also observed from the data that  $PM_{2.5}$  concentrations are much higher (greater than double of NAAQS limit) as compared to NAAQS annual limit ( $40 \mu\text{g.m}^{-3}$ ) whereas the annual concentration of  $NO_2$  and  $O_3$  concentration is double the annual and 8-hourly NAAQS limit (19.48 ppb, 46.69 ppb), respectively.

### Pollutants Trend in 2020

To break the transmission of COVID-19 worldwide, the lockdown was forced at a different time in 2020. In India, the Government deployed a complete lockdown that

Table 1: Descriptive statistics of air pollutants.

Variables	Observations (N)	Minimum	Maximum	Mean	Skewness	Kurtosis
$PM_{2.5}$	67	16.76	295.20	111.58	0.82	1.21
$NO_2$	67	5.12	123.92	42.03	1.50	2.95
$O_3$	66	23.81	134.05	63.12	0.70	0.53
AOD <sub>550</sub>	71	0.42	1.56	0.82	0.87	0.51

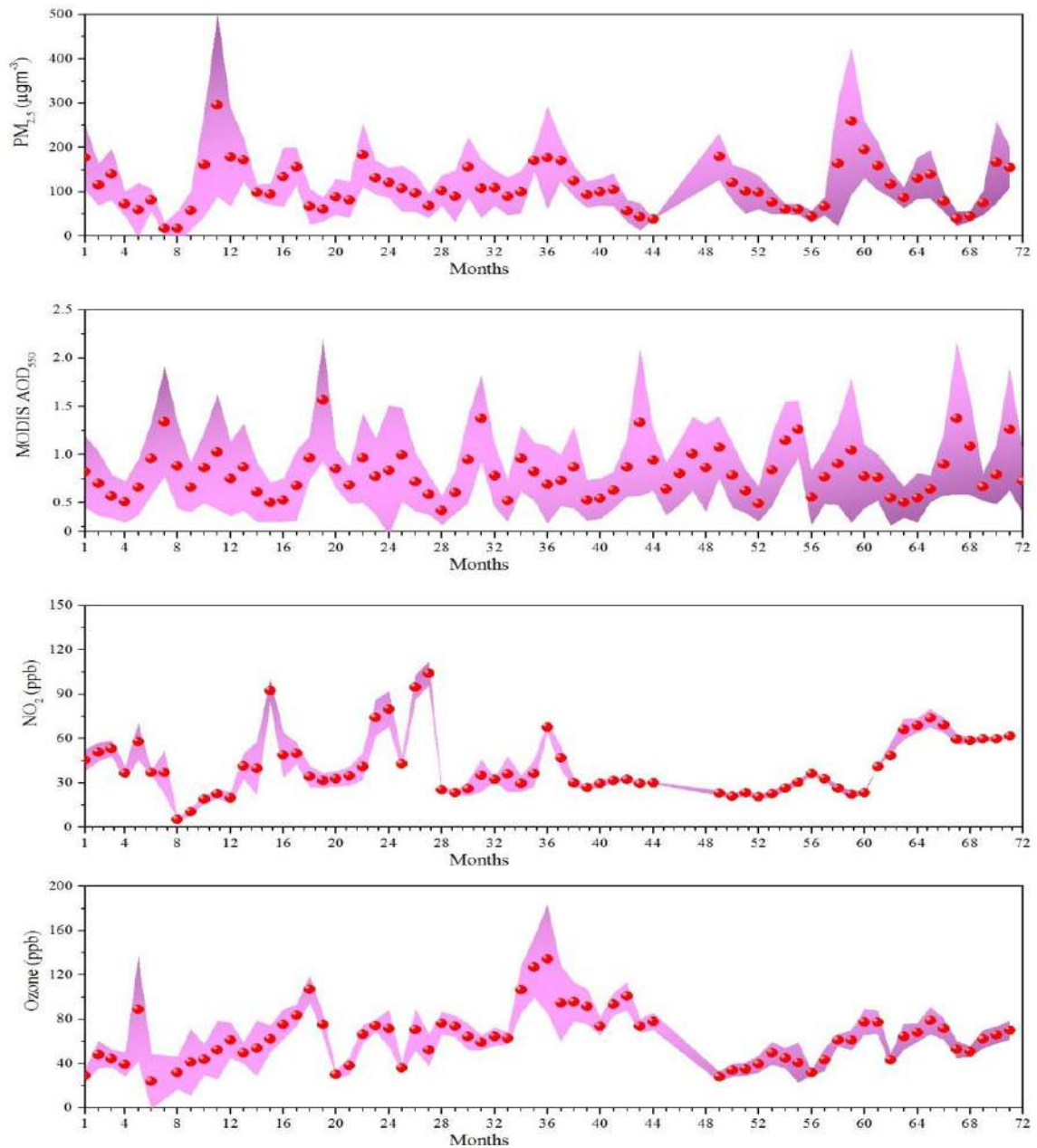


Fig. 1: The monthly variation of pollutants  $PM_{2.5}$ , AOD,  $NO_2$ , and  $O_3$  for 2012-2017.

stopped all the anthropogenic activities, which are the main source of air pollution in the atmosphere. Numerous published researches explained air quality with respect to lockdown (Kumar et al. 2020b). Indian government deployed complete lockdown for 21 days from 25<sup>th</sup> March, then slowly released the term and condition of lockdown until 31<sup>st</sup> May 2020. Therefore, very sharp drops in pollutants concentration were observed during 21 days of com-

plete lockdown. Fig. 2 depicted the trend of pollutants and AOD in the year 2020, the lockdown period is highlighted as yellow. After the lockdown period, due to the monsoon season wash-out, significant pollutant concentration drops were observed. The average concentration of the pollutants  $PM_{2.5}$ ,  $NO_2$ ,  $O_3$ , and AOD in the year 2020 was found as  $88.77 \pm 74 \mu g \cdot m^{-3}$ ;  $38.40 \pm 29.40$  ppb;  $18.40 \pm 9.12$  ppb and  $0.73 \pm 0.45$ , respectively. The maximum concentration is

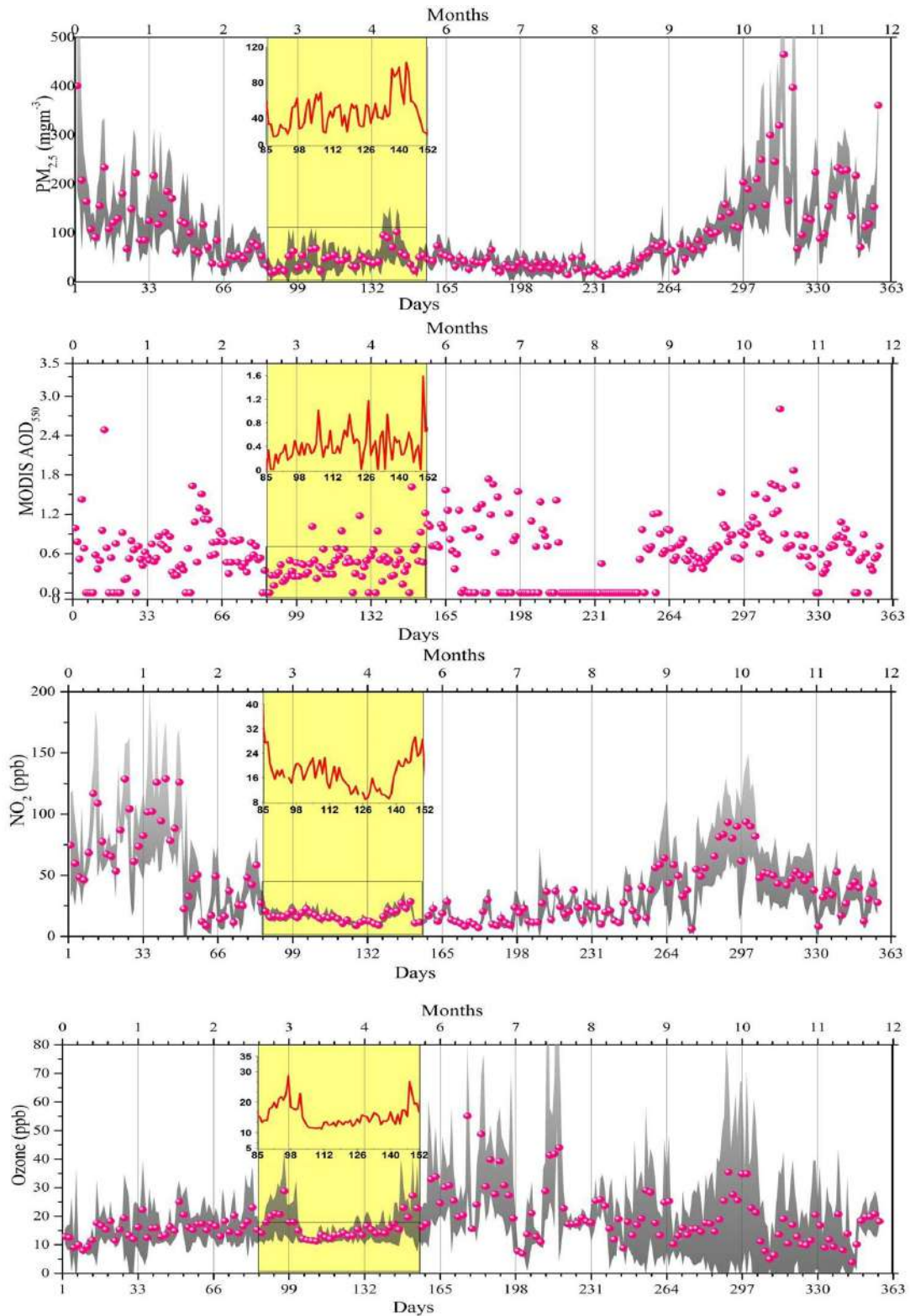


Fig. 2: Daily-based trend of PM<sub>2.5</sub>, MODIS AOD<sub>550</sub>, NO<sub>2</sub>, and O<sub>3</sub> during 2020, the lockdown period is highlighted as yellow.



reported as 473.92  $\mu\text{g}\cdot\text{m}^{-3}$ , 151.27ppb, 82.84 ppb; 2.80 for  $\text{PM}_{2.5}$ ,  $\text{NO}_2$ ,  $\text{O}_3$ , and AOD, respectively, and minimum concentration of  $\text{PM}_{2.5}$ ,  $\text{NO}_2$ ,  $\text{O}_3$ , and AOD is 12.05  $\mu\text{g}\cdot\text{m}^{-3}$ , 6.18 ppb, 3.90 ppb and 0.66, respectively. The lockdown duration average concentration was  $46.65\pm 23.42 \mu\text{g}\cdot\text{m}^{-3}$ ,  $16.58\pm 3.63$  ppb;  $15.69\pm 4.41$  ppb; and 0.46, respectively. The maximum lockdown concentration of  $\text{PM}_{2.5}$ ,  $\text{NO}_2$ ,  $\text{O}_3$ , and AOD was  $102.23 \mu\text{g}\cdot\text{m}^{-3}$ , 29.32 ppb, 28.72 ppb, and 1.62, respectively and minimum lockdown concentrations were reported as  $19.22 \mu\text{g}\cdot\text{m}^{-3}$ , 8.85 ppb, 11.22 ppb and 0.11, respectively.

The data are presented in Table 2 for a better relative overview. The pre-lockdown and lockdown pollutants concentration demonstrated that the concentration of the selected pollutant drops to half as compared to the past 9 years' concentration, except for AOD. In case AOD magnitude drops are around 25%.

### Time Series Simulation and Forecast

The ARIMA model was applied for simulation and forecasting pollutants concentration ( $\text{PM}_{2.5}$ ,  $\text{NO}_2$ , and  $\text{O}_3$ ) and MODIS AOD for CSIR-CRRI, Delhi-Mathura Road, urban area, New Delhi. The analysis considered the monthly average concentration of pollutants and AOD for 2012-2017 and simulated the monthly concentration of pollutants and AOD and forecast the pollutants and AOD for the period of forecast the pollutants AOD for 2020-2023. The large variations in  $\text{PM}_{2.5}$  values moderate variations in MODIS AOD; however, low variations were found in  $\text{NO}_2$  and  $\text{O}_3$  values (Fig. 3). The observed and simulated values of pollutants and AOD are lies within the upper control limit (UCL) and lower control limit

(LCL) boundary, indicating a satisfactory agreement between in-situ measurement and ARIMA-based simulations.

The measured and simulated observation trends for air pollutants ( $\text{PM}_{2.5}$ ,  $\text{NO}_2$ , and  $\text{O}_3$ ) and MODIS AOD<sub>550</sub> are found in good agreement, as depicted in Fig. 4. It is clearly shown that the monthly AOD values are found higher during pre-monsoon (May to June) and decreasing during monsoon (July to September) and again, increasing trends occur during post-monsoon (October to November) and winter (December to February) months, of almost every year. However, higher concentrations of  $\text{PM}_{2.5}$  were found during post-monsoon mainly due to biomass burning transported from the Punjab and Haryana states and during winter months due to transportation, biomass/wood burning, and fog.

Fig. 5 depicts the trends of the residuals ACF and PACF, demonstrating that all points are randomly distributed, and suggesting that model outcomes are satisfactory. Also, each pollutant's residual autocorrelations are small and are within the significance bounds limit.

The statistical significance of the model was evaluated by Normalized Bayesian Information Criterion (BIC), the R-square, Root Mean Square Error (RMSE), Mean Absolute Percentage Error (MAPE), Mean Absolute Error (MAE), and Ljung – Box Q statistic were used to test for the adequacy and statistical appropriateness of the model. The Ljung–Box Statistic of the model values for Normalized BIC lies between -4.393 to 7.062 for the 16 degrees of freedom (Table 3).

The stationary- $R^2$  also depicts the good fit between observed and simulated values. ARIMA performed better for  $\text{PM}_{2.5}$  (0.752) and  $\text{NO}_2$ , a lower value of  $R^2$  indicates moderate fit ( $R^2$ : 0.585) as compared to other pollutants.

Table 2: Overview of the pre-lockdown period, lockdown year, and lockdown period.

Variables		Pre-lockdown (2012-2017)	Lockdown year 2020	Lockdown period of 2020
AOD	Avg	0.60 $\pm$ 0.05	0.73 $\pm$ 0.45	0.46 $\pm$ .26
	Max	1.54	2.80	1.62
	Min	0.21	0.66	0.11
$\text{PM}_{2.5}$	Avg	111.58 $\pm$ 53.69	88.77 $\pm$ 74	46.65 $\pm$ 19.9
	Max	295.76	473.92	102.23
	Min	16.2	12.05	19.22
$\text{NO}_2$	Avg	13.93 $\pm$ 3.40	38.40 $\pm$ 29.40	16.58 $\pm$ 4.82
	Max	21.37	151.27	29.32
	Min	9.62	6.18	8.85
$\text{O}_3$	Avg	33.92 $\pm$ 16.81	18.40 $\pm$ 9.12	15.69 $\pm$ 3.70
	Max	76.45	82.84	28.72
	Min	12.14	3.90	11.22



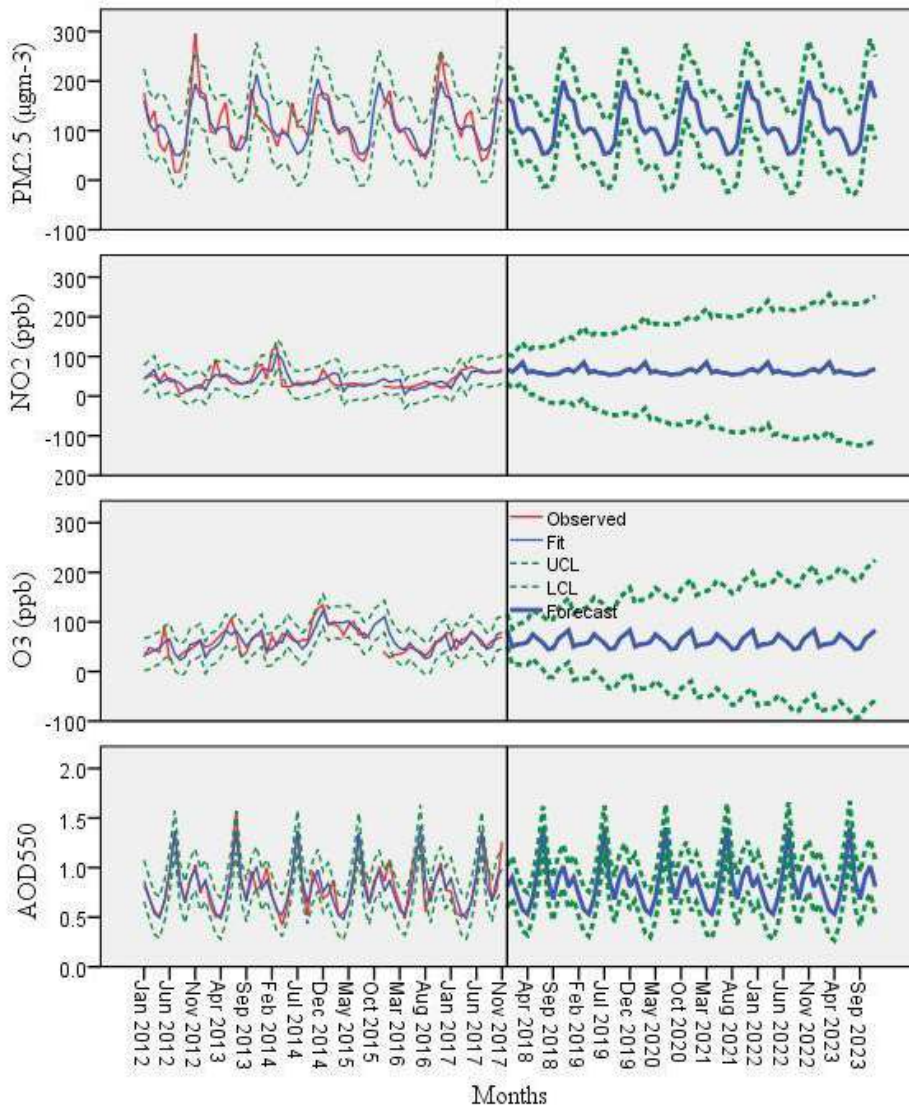


Fig. 3: Comparison of ARIMA model simulations and forecasting (blue line) with observed PM<sub>2.5</sub>, NO<sub>2</sub>, O<sub>3</sub>, and MODIS AOD<sub>550</sub> (red line).

The more or less similar values of the stationary-R<sup>2</sup> and the R<sup>2</sup> of all selected pollutants and AOD are indicating that the simulated model is reasonably good. Model fit statistics is given in Table 4.

The lower RMSE values (ranges of 0.105-32.084) between observed and simulated pollutants and AODs for a period of 2012-2017 are supportive of favorable results. The MAPE values are ranging 20-to 50, also indicating the

Table 3: Ljung Box statistics.

Normalized BIC	Statistic	DF	Sig.
7.062	52.938	16	0.000
5.869	54.806	16	0.000
5.703	34.432	16	0.005
-4.393	23.177	16	0.109

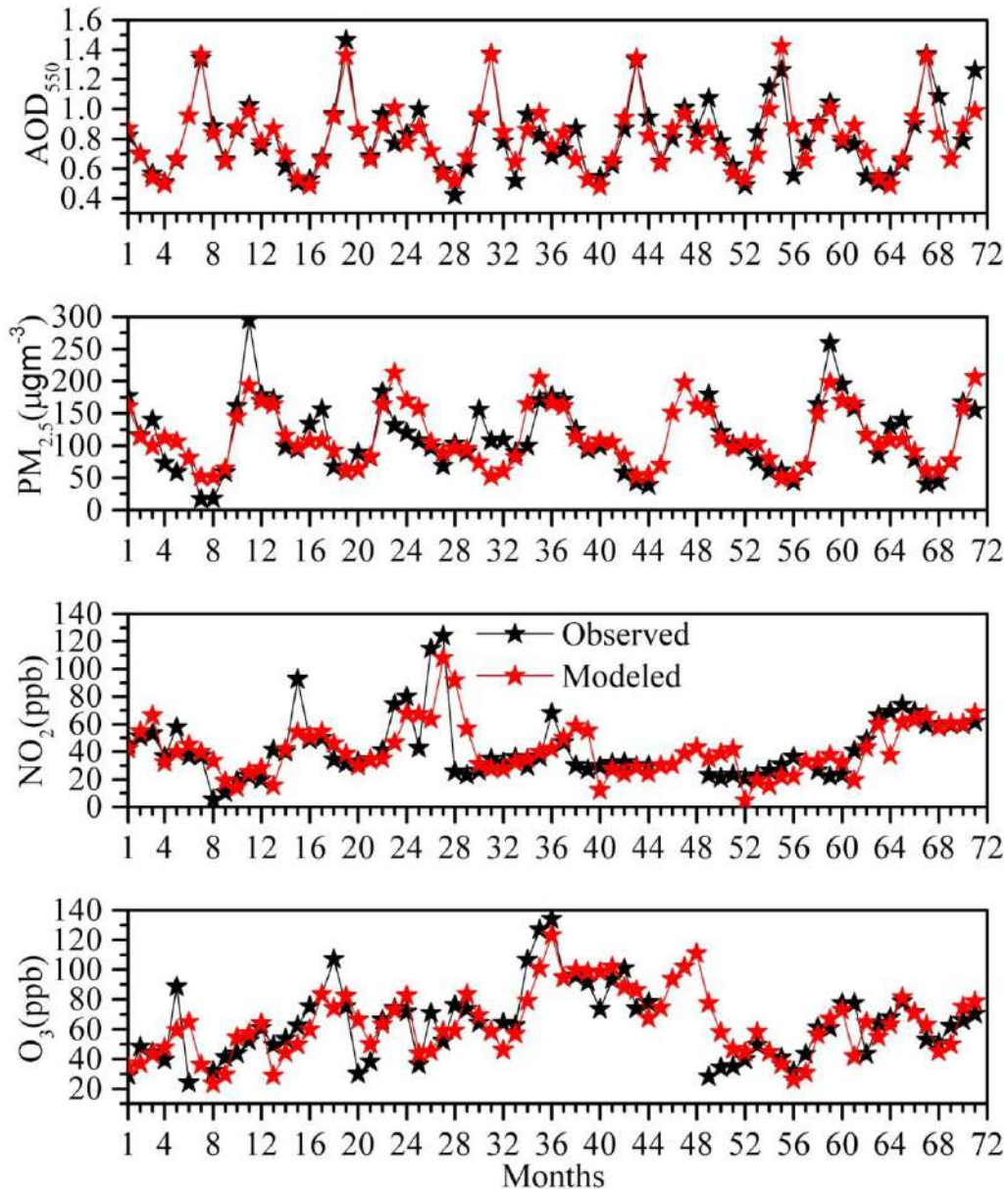


Fig. 4: Comparison of observed and simulated results of  $PM_{2.5}$ ,  $NO_2$ ,  $O_3$ , and MODIS  $AOD_{550}$ .

reasonability of the fitted model (Delurgio 1998). This indicates that the model has adequately captured the correlation in the time series.

The 24 months data for the year 2018-2019 were used for the validation of forecasted results. The obtained forecasts for the next 48 months (2020-2023) are also excellent compared to actual observations other than those used in the model, retaining the same trend. The forecasted results were (48 months in the year 2020-2023) validated with measured

observation (2018-2019, 24 data points) showing an agreeable association, as depicted in Fig. 6.

In Fig. 6, the year 2020 measure and simulated observations were also compared to know the difference between the pandemic year pollutants concentration and the regular data-based simulated value. The year 2020 has different trends of pollutants due to pandemic conditions. It is identified that there is a significant difference in magnitude of the pollutants, but the variable behavior remains the same

Table 4: Model Fit Statistics.

Variables	Stationary R-squared	R-squared	RMSE	MAPE	MAE	t-value	p-value
PM <sub>2.5</sub>	0.752	0.648	32.084	26.522	22.961	1.321	0.1025
NO <sub>2</sub>	0.585	0.383	17.672	41.479	12.253	4.813	0.0000
O <sub>3</sub>	0.700	0.537	16.246	23.850	12.065	4.709	0.0001
AOD <sub>550</sub>	0.744	0.824	0.105	9.236	0.073	1.290	0.1076

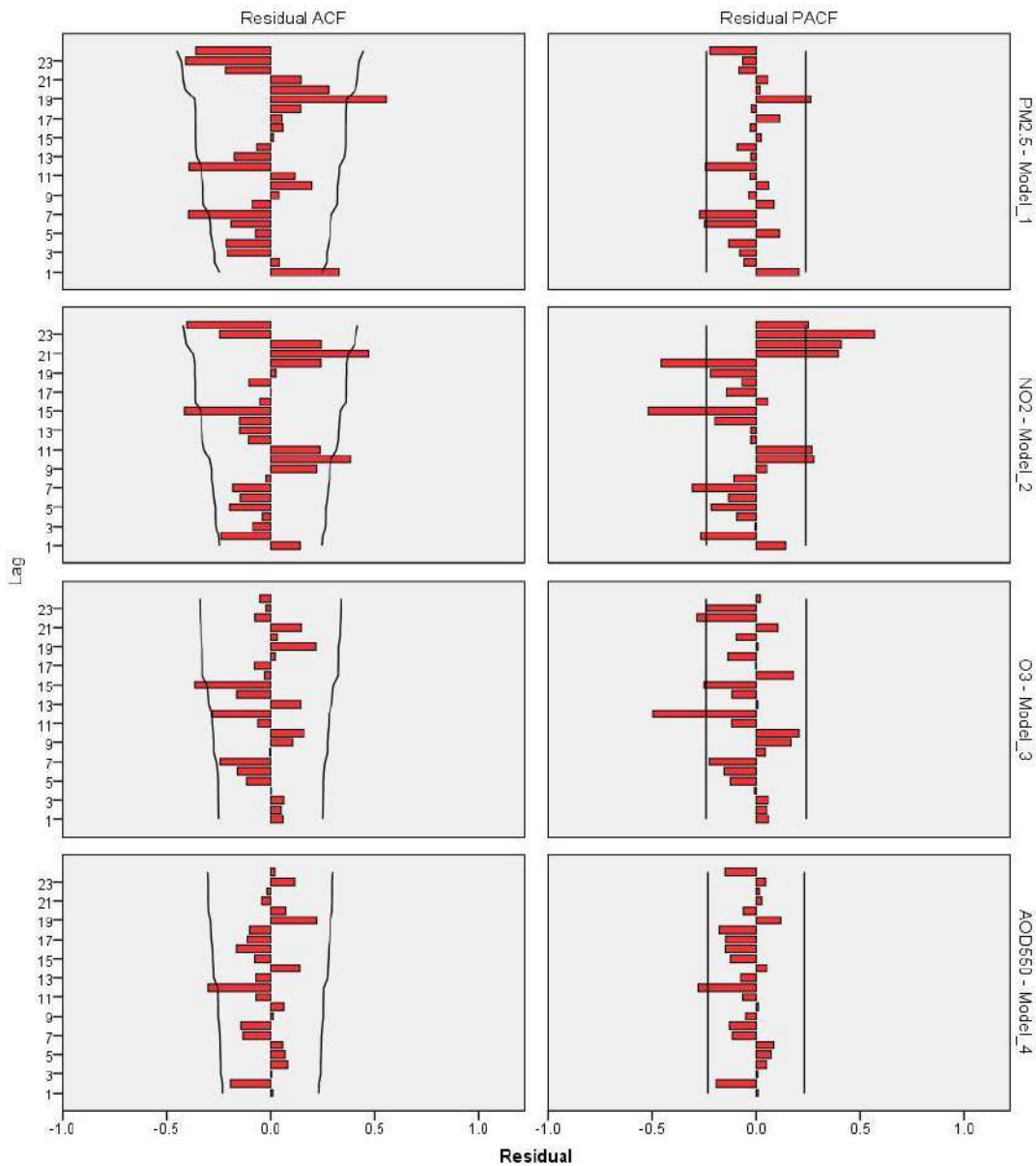


Fig. 5: Residuals of ACF and PACF for the selected models of PM<sub>2.5</sub>, NO<sub>2</sub>, O<sub>3</sub>, and MODIS AOD<sub>550</sub>.

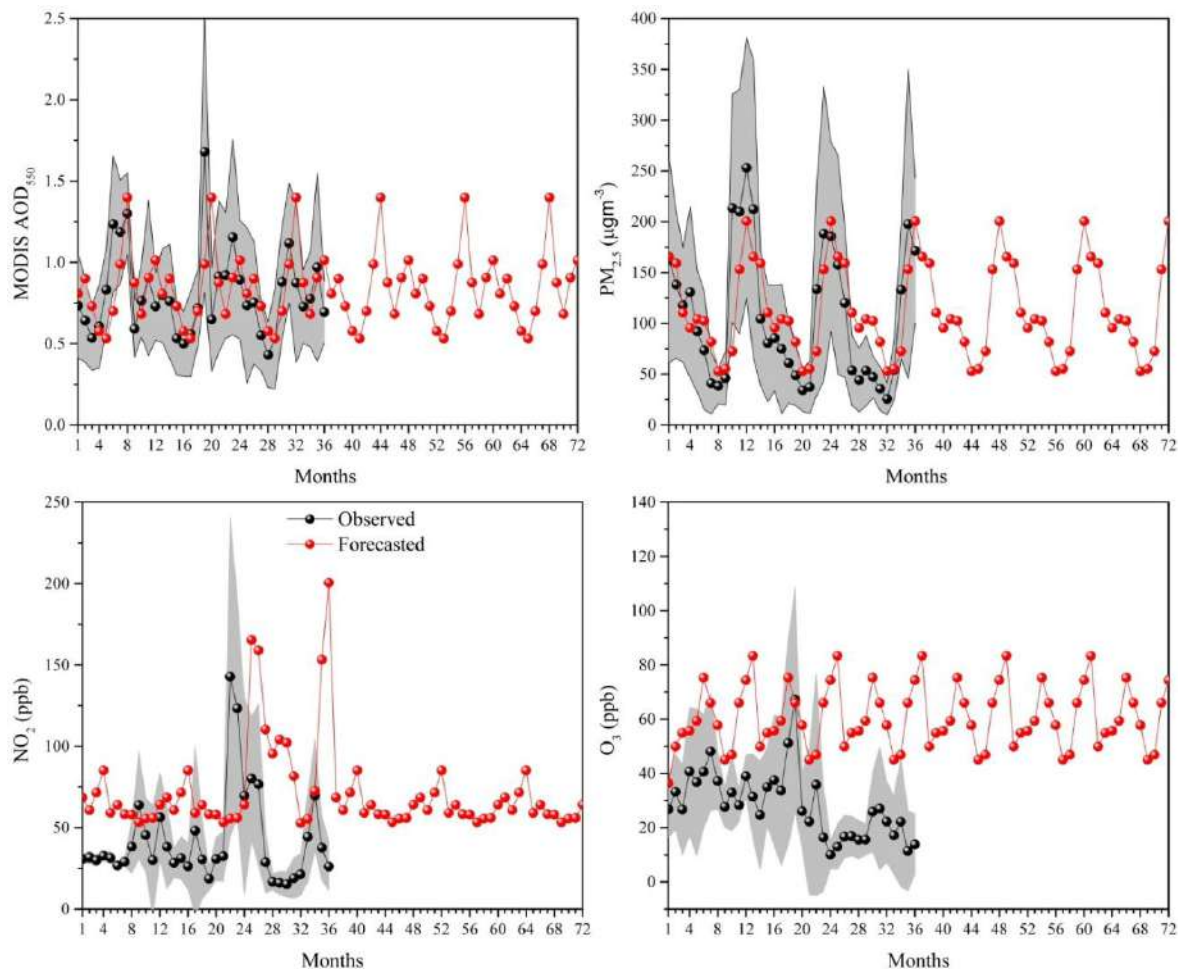


Fig. 6: Validation of modeled  $PM_{2.5}$ ,  $NO_2$ ,  $O_3$ , and MODIS  $AOD_{550}$  with observed  $PM_{2.5}$ ,  $NO_2$ ,  $O_3$ , and MODIS  $AOD_{550}$ .

in the case of  $PM_{2.5}$  and AOD whereas,  $O_3$  and  $NO_2$  have slightly different trends in contrast to a regular pattern. Based on the collective assessment of the model output, ARIMA simulation and forecasting results were found consistent. However, unpredictable meteorology and heterogeneity in the aerosol optical properties bring limitations in the model's output, for example, moderate to low performance of ozone concentrations might be due to these limitations (as observed in Fig. 6 for ozone concentration).

## CONCLUSION

The data statistics demonstrated the non-symmetrical data and leptokurtic distribution of pollutants  $PM_{2.5}$ ,  $O_3$ ,  $NO_2$ , and AOD from 2012 to 2017. The pre-lockdown and lockdown comparative analysis demonstrate that in the year 2020, except for AOD, pollutants concentration decreased to half in magnitude compared to the past nine years' concentration.

The simulated and forecasted result shows good agreement with the observed and validation data. Different model fit statistics, and the five accuracy measures criteria also demonstrated the harmony of results. In the context of air quality management, the ARIMA-based prediction demonstrates better suitability for the MODIS AOD,  $PM_{2.5}$ , and  $NO_2$  as compared to the  $O_3$  at an urban location in New Delhi. ARIMA approach, in combination with satellite data, can be a good option to forecast future aerosol load for areas where the ground data is a major limitation for the research.

## ACKNOWLEDGEMENT

Arti Choudhary acknowledges Rashtriya Uchchar Shiksha Abhiyan (RUSA) PDF scheme, order no. RUSA-1041-2016(PDF-XVIII) 25986/2020, for the financial support under the RUSA 2.0 project. The authors are also thankful to the MODIS team and NASA (<https://giovanni.gsfc.nasa>).



gov/giovanni/) and CPCB (Central Pollution Control Board) for providing satellite and pollutants data, respectively. One of the authors, Pradeep Kumar acknowledges to University Grant Commission (UGC), New Delhi for Dr. D.S. Kothari Postdoctoral fellowship awarded vide UGC sanction No.F.4-2/2006 (BSR)/ES/18-19/0041.

## REFERENCES

- AbdRahman, N.H., Lee, M.H., Latif, M.T. and Suhartono, S.J.J.T. 2013. Forecasting of air pollution index with artificial neural network. *J. Teknol.*, 63(2): 1141.
- Abish, B. and Mohanakumar, K. 2013. A stochastic model for predicting aerosol optical depth over the north Indian region. *Int. J. Remote Sens.*, 34: 1449-1458.
- Balakrishnan, K., Dey, S., Gupta, T., Dhaliwal, R.S., Brauer, M., Cohen, A.J. and Dandona, L. 2019. The impact of air pollution on deaths, disease burden, and life expectancy across the states of India: The global burden of disease study 2017. *Lancet Planet. Health*, 3(1): 26-39.
- Barman, S.C., Singh, R., Negi, M.P.S. and Bhargava, S.K. 2008. The ambient air quality of Lucknow City (India) during the use of fireworks during the Diwali Festival. *Environ. Monit. Assess.*, 137(1): 495-504.
- Box, G.E.P. and Jenkins, G.M. 1976. *Time Series Analysis, Forecasting, and Control* Revised. Holden Day, San Francisco.
- Chen, Q.X., Huang, C.L., Yuan, Y. and Tan, H.P. 2020. Influence of COVID-19 event on air quality and their association in Mainland China. *Aerosol Air Qual. Res.*, 20(7): 1541-1551.
- Choudhary, A. and Gokhale, S. 2016. Urban real-world driving traffic emissions during interruption and congestion. *Transp. Res. D Trans. Environ.*, 43, 59-70.
- Choudhary, A. and Gokhale, S. 2019. On-road measurements and modeling of vehicular emissions during traffic interruption and congestion events in an urban traffic corridor. *Atmos. Pollut. Res.*, 10(2), 480-492.
- Choudhary, A., Kumar, P., Gaur, M., Prabhu, V., Shukla, A. and Gokhale, S. 2020. Real-world driving dynamics characterization and identification of emission rate magnifying factors for auto-rickshaw. *Nat. Environ. Pollut. Technol.*, 19(1): 93-101.
- DeLurgio, S.A. 1998. *Forecasting Principles and Applications*. Irwin/McGraw-Hill, New York.
- Duen˜as C., Fern´andez M.C., Can˜ete S., Carretero J. and Liger E. 2005. A stochastic model to forecast ground-level ozone concentration in urban and rural areas. *Chemosphere*, 61(10): 1379-1389.
- Faiz, A. and Sturm, P.J. 2002. New directions: air pollution and road traffic in developing countries. *Develop. Environ. Sci.*, 1: 241-243.
- Gocheva-Ilieva, S.G., Ivanov, A.V., Voynikova, D.S. and Boyadzhiev, D.T. 2014. Time series analysis and forecasting for air pollution in a small urban area: a SARIMA and factor analysis approach. *Stoch. Environ. Res. Risk Assess.*, 28(4): 1045-1060.
- Jian, L., Zhao, Y., Zhu, Y.P., Zhang, M.B. and Bertolatti, D. 2012. An application of the ARIMA model to predict submicron particle concentrations from meteorological factors at a busy roadside in Hangzhou, China. *Sci. Total Environ.*, 426: 336-345.
- Jia, C., Fu, X., Bartelli, D. and Smith, L. 2020. Insignificant impact of the "Stay-At-Home" order on ambient air quality in the Memphis metropolitan area, USA. *Atmosphere*, 11(6), 630.
- Junger, W.L. and De Leon, A.P. 2015. Imputation of missing data in time series for air pollutants. *Atmos. Environ.*, 102: 96-104.
- Kantz, H. and Schreiber, T. 1997. *Nonlinear Time Series Analysis*. Cambridge University Press, Cambridge.
- Kucharski, A.J., Russell, T.W., Diamond, C., Liu Y., Edmunds J., Funk S., Eggo, R.M., Sun, F., Jit, M., Munday, J.D. and Davies, N. Early dynamics of transmission and control of COVID-19: A mathematical modeling study. *Lancet Infect. Dis.*, 11: 202.
- Kumar J., Kaur A. and Manchanda P. 2015. Forecasting the time series data using ARIMA with wavelet. *J. Comput. Math. Sci.*, 6(8): 430-438.
- Kotnala, G., Mandal, T.K., Sharma, S.K. and Kotnala, R.K. 2020. Emergence of blue sky over Delhi due to Coronavirus disease (COVID-19) lockdown implications. *Aerosol Sci. Eng.*, 5: 1-11.
- Kumar, M., Parmar, K.S., Kumar, D.B., Mhawish, A., Broday, D.M., Mall, R.K. and Banerjee, T. 2018. Long-term aerosol climatology over Indo-Gangetic Plain: Trend, prediction and potential source fields. *Atmos. Environ.*, 180, 37-50.
- Kumar, P., Choudhary, A., Singh, A.K., Prasad, R. and Shukla, A. 2019. Temporal Variation of Atmospheric Aerosols and Associated Optical and Metrological Parameters. *IEEE, Manhattan, New York*, pp. 1-3.
- Kumar, P., Choudhary, A., Singh, A.K., Prasad, R. and Shukla, A. 2020a. Aerosol parameters during winter and summer seasons and meteorological implications. *EDP Sci.*, 237: 11414.
- Kumar, P., Hama, S., Omidvarborna, H., Sharma, A., Sahani, J., Abhijith, K. V. and Tiwari, A. 2020b. Temporary reduction in fine particulate matter due to "anthropogenic emissions switch-off" during COVID-19 lockdown in Indian cities. *Sustain. Cities Soc.*, 62: 102382.
- Kumar, P., Kapur, S., Choudhary, A. and Singh, A.K. 2021. Spatiotemporal variability of optical properties of aerosols over the Indo-Gangetic Plain during 2011-2015. *Indian J. Phys.*, 5: 1-13.
- Kumar, P., Pratap, V., Kumar, A., Choudhary, A., Prasad, R., Shukla, A. and Singh, A.K. 2020c. Assessment of atmospheric aerosols over Varanasi: Physical, optical and chemical properties and meteorological implications. *J. Atmos. Sol. Terr. Phys.*, 209: 105424.
- Kumar, U. and Jain, V. K. 2009. ARIMA forecasting of ambient air pollutants (O<sub>3</sub>, NO, NO<sub>2</sub>, and CO). *Stoch. Environ. Res. Risk Assess.*, 24(5): 751-760.
- Lai, C.C., Shih, T.P., Ko, W.C., Tang H.J. and Hsueh, P.R. Severe acute respiratory syndrome coronavirus 2 (SARS-CoV-2) and coronavirus disease-2019 (COVID-19): The epidemic and the challenges. *Int. J. Antimicrob. Agents*, 20: 105924.
- Li Q., Guan X., Wu P., Wang X., Zhou L., Tong Y., Ren R., Leung K.S., Lau E.H., Wong J.Y. and Xing X. 2020. Early transmission dynamics in Wuhan, China, of novel coronavirus-infected pneumonia. *New Engl. J. Med.* 382: 1199-1207.
- Maji, K.J., Namdeo, A., Bell, M., Goodman, P., Nagendra, S.S., Barnes, J.H. and Alshetty, D. 2021. Unprecedented reduction in air pollution and corresponding short-term premature mortality associated with COVID-19 lockdown in Delhi, *Indian J. Air Waste Manag. Assoc.*, 14: 1-17.
- Milioni, A.E. and Davies, T.D. 1994. Regression and stochastic models for air pollution. I. Review, comments, and suggestions. *Atmos. Environ.*, 28: 2801-2810.
- Muhammad, S., Long, X. and Salman, M. 2020. COVID-19 pandemic and environmental pollution: A blessing in disguise? *Sci. Total Environ.*, 728: 138820.
- Ottosen, T. B. and Kumar, P. 2019. Outlier detection and gap filling methodologies for low-cost air quality measurements. *Environ. Sci. Process Impacts*, 21: 701-713.
- Pandey, A., Brauer, M., Cropper, M.L., Balakrishnan, K., Mathur, P., Dey, S. and Dandona, L. 2021. Health and economic impact of air pollution in the states of India: The global burden of disease study 2019. *Lancet Planet. Health*, 5(1): 25-38.
- Prabhu, V., Shridhar, V. and Choudhary, A. 2019. Investigation of the source, morphology, and trace elements associated with atmospheric PM<sub>10</sub> and human health risks due to inhalation of carcinogenic elements at Dehradun, an Indo-Himalayan city. *SN Appl. Sci.*, 1(5): 1-11.
- Pratap, V., Kumar, A., Tiwari, S., Kumar, P., Tripathi, A.K. and Singh, A.K. 2020. Chemical characteristics of particulate matter and their emission sources over Varanasi during the winter season. *J. Atmos. Chem.*, 77: 83-99.
- Ravindra, K., Singh, T. and Mor, S. 2019. Emissions of air pollutants from primary crop residue burning in India and their mitigation strategies for cleaner emissions. *J. Cleaner Prod.*, 208: 261-273.



- Sarkar, S., Singh, R.P. and Chauhan, A. 2018. Crop residue burning in northern India: An increasing threat to Greater India. *J. Geophys. Res. Atmos.*, 123(13): 6920-6934.
- Singh, D.P., Gadi, R., Mandal, T.K., Dixit, C.K., Singh, K., Saud, T. and Gupta, P.K. 2010. Study of temporal variation in ambient air quality during Diwali festival in India. *Environ. Monit. Assess.*, 169(1): 1-13.
- Singh, S., Parmar, K.S., Kumar, J. and Makkhan, S.J.S. 2020. Development of a new hybrid model of discrete wavelet decomposition and autoregressive integrated moving average (ARIMA) models in application to one month forecast the casualty's cases of COVID-19. *Chaos Solit. Fract.*, 135: 109866.
- Soni, K., Kapoor, S., Parmar, K. S. and Kaskaoutis, D. G. 2014. Statistical analysis of aerosols over the Gangetic-Himalayan region using ARIMA model based on long-term MODIS observations. *Atmos. Res.*, 149: 174-192.
- Srivastava, S., Kumar, A., Baudh, K., Gautam, A.S. and Kumar, S. 2020. The 21-day lockdown in India dramatically reduced air pollution indices in Lucknow and New Delhi, India. *Bull. Environ. Contam. Toxicol.*, 6: 1-9.
- Tobías, A., Carnerero, C., Reche, C., Massagué, J., Via, M., Minguillón, M.C. and Querol, X. 2020. Changes in air quality during the lockdown in Barcelona (Spain) one month into the SARS-CoV-2 epidemic. *Sci. Total Environ.*, 726: 138540.
- Vadrevu, K.P., Eaturu, A., Biswas, S., Lasko, K., Sahu, S., Garg, J.K. and Justice, C. 2020. Spatial and temporal variations of air pollution over 41 cities of India during the COVID-19 lockdown period. *Sci. Rep.*, 10(1): 1-15.
- Xu, K., Cui, K., Young, L.H., Wang, Y.F., Hsieh, Y.K., Wan, S. and Zhang, J. 2020. Air quality index, indicator air pollutants, and impact of COVID-19 event on the air quality near central China. *Aerosol Air Qual. Res.*, 20(6): 1204-1221.



# Biodegradation and Bioremediation of Petroleum Hydrocarbons in Marine Ecosystems by Microorganisms: A Review

Ramzi H. Amran\*(\*\*), Mamdoh T. Jamal\*, Arulazhagan Pugazhendi\*(\*\*\*), Mamdouh Al-Harbi\*, Mohammed Ghandourah\*\*\*\*, Ahmed Al-Otaibi \*\*\*\*\* and Md Fazlul Haque\*\*\*\*\*†

\*Department of Marine Biology, Faculty of Marine Sciences, King Abdulaziz University, Jeddah, KSA

\*\*Department of Marine Biology & Fisheries, Faculty of Marine Sciences & Environment, Hodeidah University, Al-Hodeidah, Yemen

\*\*\*Center of Excellence in Environmental Studies, King Abdulaziz University, Jeddah, KSA

\*\*\*\*Department of Marine Chemistry, Faculty of Marine Sciences, King Abdulaziz University, Jeddah, KSA

\*\*\*\*\*Department of Chemistry, Faculty of Science, University of Hail, Hail, KSA

\*\*\*\*\*Department of Zoology, Faculty of Biological Sciences, University of Rajshahi, Rajshahi, Bangladesh

†Corresponding author: Md Fazlul Haque; drfazlul@ru.ac.bd

Nat. Env. & Poll. Tech.  
Website: [www.neptjournal.com](http://www.neptjournal.com)

Received: 09-05-2021

Revised: 30-06-2021

Accepted: 15-07-2021

## Key Words:

Biodegradation  
Bioremediation  
Petroleum hydrocarbons  
Microorganisms  
Oil pollution

## ABSTRACT

Concern about increasing incidents of petroleum hydrocarbon spills and spillage into different marine environments is rising day by day due to enhanced human activities in marine water. The toxic compounds of spilled petroleum hydrocarbon in marine water lead to the immediate death of numerous marine organisms as well as initiate various vicious biogeochemical cycles in the marine environment resulting in prolonged toxic impacts on the marine environment. Recently, many sophisticated techniques, including physical methods, chemical methods, and biological methods, have been developed and adopted for the treatment of marine environments polluted with petroleum compounds. However, biological treatment is one of the most promising methods in this field by which microorganisms such as bacteria, fungi, and algae are used for biodegradation of pollutants such as the spilled petroleum hydrocarbon into neutralized or eco-friendly compounds. This review has been focused on different aspects of the pollution of the marine ecosystem by oil, mainly Petroleum hydrocarbons, the fate of spilled oil in marine environments and the role of microbial communities in it, as well as various techniques, especially the bioremediation and biodegradation of spilled oil including the factors affecting the capacity of techniques. Moreover, some future aspects of research in the field of biodegradation and bioremediation of spilled oil have been proposed.

## INTRODUCTION

Mineral oil is an important resource to produce the necessary energy for daily life. It is considered one of the most important materials to produce petroleum fuels such as kerosene and gasoline, and many other chemical compounds such as plastics, chemical reagents, solvents, and pharmaceuticals products. Moreover, more and more oil-related economic activities such as oil extraction, refining, transport, and marketing are being carried out because of the increasing global demand for oil for leading modern life. Importantly, half of the activities related to the transportation of the world's petroleum are achieved by seas and oceans (Varjani & Upasani 2016). As a result of this increased transportation of petroleum compounds by seas and oceans, there has been a significant risk of pollution of marine water by the incidence of oil spills from drilling oil wells, transmission pipelines, and transfer oil tankers around the world. Hence,

marine environments become one of the largest and most important reservoirs contaminated with petroleum hydrocarbons resulting in a severe form of pollution (Mahjoubi et al. 2018, Ławniczak et al. 2020). The pollution of marine environments with hydrocarbons is a global concern because of the potential consequences of this pollution on different environments, humans, and marine organisms (Ahmed & Fakhruddin 2018). Hence, rapid action is essential for the treatment of spilled hydrocarbons in a polluted environment. However, treatment of a polluted environment by chemical or physical methods is very expensive as well as difficult to use as compared to the biological methods in which biological agents, mainly microorganisms are used to clean and remove various chemicals from contaminated aquatic environments (Zheng et al. 2013, Ruhi 2017, Saha et al. 2017, Nasrin 2019, Rahman et al. 2019). However, biological methods such as the biodegradation of hydrocarbon pollutants take a longer period and have more complex mechanisms, depending on

the amount and nature of hydrocarbon contaminants and the availability of microorganisms (Xu 2018). Hence, microorganisms that degrade hydrocarbons play the main function in the biodegradation of contaminated environments, where these microorganisms flourish and adapt to these polluted environments (Adeleye 2018).

## FUEL OIL POLLUTION

Fuel oil is a natural combination of hydrocarbons that may be in a liquid, solid or gaseous state depending on both pressure and temperature. The extracted oil is not pure containing some impurities such as carbon dioxide, hydrogen sulfide, and some other complex components such as sulfur, nitrogen, oxygen, and other impurities (Hamidian et al. 2020). At the beginning of the twentieth century, great global economic changes were introduced. Consequently, these changes increased the encouragement of the industrial and technological revolution and relied on it as a pattern of prosperity. These changes led to a rise in the demand for the extraction, purification, processing, and transportation of petroleum products, which in turn caused the discharge of large quantities of petroleum waste, around 67 million tons waste per year (Nath & Cholakov 2009). Thus, pollution caused by releasing of fuel oil and their waste into the ecosystem become one of the main types of global pollution, and thus this problem has become the focus of attention to both developing and industrialized countries because of its deleterious effects on both living organisms as well as different environments (Luna et al. 2013). The pollution of the seas and oceans by fuel oil mainly results from the routine operations of oil extraction, refining, and washing operations as well as accidents during oil exploration, extraction, and transport operations. Moreover, natural drift from the seabed, sediment erosion, atmospheric sedimentation from incomplete oil combustion, runoff of rivers and oil-contaminated lands and waste, shipping and clearance, and illegal discharges also contribute to the pollution of marine water (Souza et al. 2014). The spilled fuel oil spreads into the water very quickly with a thickness of 1 mm. Fuel oil pollutants spread in the form of a thin coat on the marine water, which in turn interrupts the mechanisms of gas exchange between atmospheric oxygen and water surface, and thus the reduction of the amount of dissolved oxygen in the water resulting in a higher rate of mortality and morbidity of marine organisms. In addition, fuel oils imprinted into aquatic environments have toxic effects on humans and other terrestrial organisms depending on marine environments directly or indirectly (Hranova 2006). Petroleum hydrocarbons are non-homogenous compounds, so scrubbing these compounds from the marine environment is a difficult process. However, the natural biological process is one of the main ways to clean the environments that are

contaminated with hydrocarbons. This microbial degradation occurs naturally in different environments, where the potential microbial communities are available for decomposition and removal of oil pollutants naturally from the environment (Varjani 2017).

## THE FATE OF FUEL OIL IN THE MARINE ENVIRONMENT

Pollution of the marine environment by several hundred million gallons of crude oil products annually has been reported and its fate depends on many factors, whether physical, chemical, or biological (Saadoun 2015). These include biological processes, evaporation, hydrolysis, water emulsification, dispersion, sinking, sedimentation, and photolytic oxidation. Biological processes include microbial degradation, ingestion, and the assimilation of oil into the environment (Neff 2012). During these processes in the environment, the changes occur in the structure as well as in the physical and chemical characteristics of the original pollutants. However, the most vital weathering process is initiated in the water environment within 48 hours of oil spills, resulting in evaporation of the components of medium and light oil with a low boiling point into the atmosphere. The evaporation process may be liable for the loss of 33% to 66% of the amount of oil leaked into the aquatic environment (Yakimov 2004). For instance, one-third of the fuel oil spilled from the supertanker Amoco Cadiz evaporated in just three days. Many factors control the process of evaporation such as the common structure of the oil, wind velocity, surface area, air and water temperature, intensity of solar radiation, and abandoned metals (Fig. 1).

## RESPONSE OF MARINE MICROBIAL COMMUNITY TO FUEL OIL POLLUTION

Microbes that decompose hydrocarbons vigorously are usually found in the oceanic environment, where spilled hydrocarbons are used by these microbes as an energy source resulting in their enhanced growth and multiplication. Moreover, the number of hydrocarbons degrading microbes is also increased because of changes in some of the catalysts and other physiological factors in polluted marine ecosystems (Labud et al. 2007). Thus, the normal structure of the microbial community is affected by the overgrowth of hydrocarbon-degrading microbes in the marine ecosystem polluted with petroleum hydrocarbons (Xu 2018, Truskewycz 2019). For example, significant changes in the structure of the microbial community in the oil-polluted water of the Caspian Sea and the Persian Gulf were reported by Hassanshahian et al. (2010). Hence, the determination of the main microbial communities that are working on the degradation

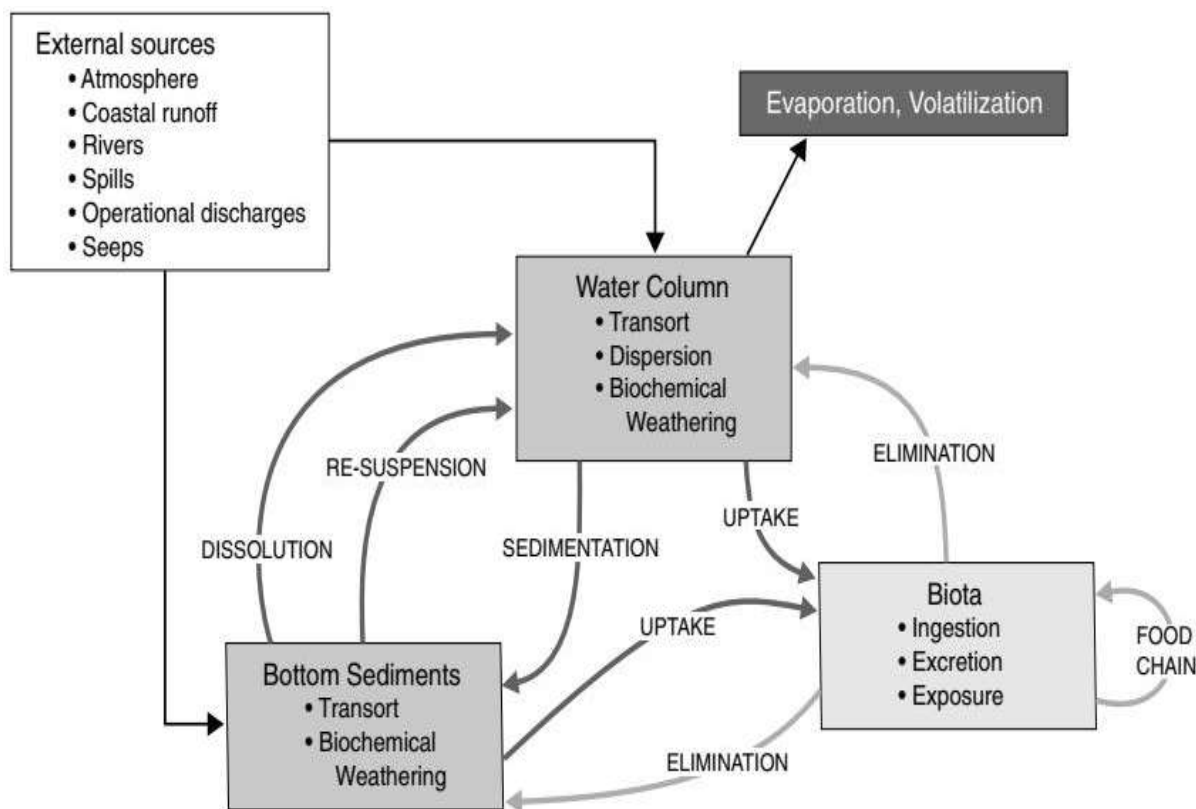


Fig. 1: A model for the fate of oil in the aquatic environments (Board et al. 2003).

of hydrocarbon pollutants is very important for understanding and developing treatment processes for contaminated sites.

The process of natural biodegradation is one of the efficient ways of removing hydrocarbon pollutants from different environments, especially non-volatile hydrocarbons from crude oil. Commonly, microbes such as bacteria, fungi, and yeast convert hydrocarbon compounds into simpler compounds, some of them are not soluble in water (Cappello 2012). It is hard to accomplish optimal biodegradation and bioremediation values for hydrocarbon pollutants in a short period, because of some non-biodegradable compounds which need more time to deteriorate, as well as many variables that impact the degree and range of biodegradation and bioremediation of contaminants (Cappello 2012, Varjani & Upasani 2017). Moreover, the quantity of some nutrients such as phosphorus and nitrogen is inadequate to support the growth of microorganisms in marine ecosystems naturally, however, supplementation of these substances to contaminated sites encourages the growth of hydrocarbons degrading microbes in marine ecosystems (Hassanshahian et al. 2010). However, some microbial communities finally can adapt to hydrocarbon contamination as they act to resist the toxic

effects of these pollutants, thereby increasing the number of microbial organisms that use hydrocarbon contaminants as food sources (Mahjoubi et al. 2018).

### OIL SPILL CLEANING BY BIODEGRADATION AND BIOREMEDIATION

Many methods namely physical, chemical and biological techniques are used to clean the areas contaminated with oil spills to protect the floras and faunas from further destruction and extinction. However, cleaning up the contaminated environments is often very difficult because of the influence of several factors. The physical or chemical method could be the first option that can be taken immediately after oil spills, even though both techniques have some drawbacks such as the requirement of many auxiliary materials, failure to complete elimination of the leaky oil, and further damage to the environment by the chemicals used for treatments (Kukkar 2020). Because of such disadvantages of physical and chemical methods, biodegradation and bioremediation have appeared as alternative approaches for removing oil from polluted environments.

## Biodegradation

Biodegradation of hydrocarbons is an important process in which microorganisms are applied to improve the natural cleaning procedures of hydrocarbon contaminants. However, the process of biodegradation of hydrocarbons is subject to many factors and a series of vital and often different interactions between microorganisms and other factors which mostly occurs on the surface of the contaminated water, and in the beaches, the sediments, and water column of the marine ecosystem. Ultimately, this method relies on the consumption of hydrocarbons by microorganisms to produce food, energy, and carbon dioxide. Biodegradation initiates instantly after the oil spill into the aquatic environment. Microbes naturally degrade oil in the water, and thus they grow and thrive in the contaminated environment due to the availability of food. This process continues with the presence of biodegradable hydrocarbons in the contaminated environment, culminating in the first month of the oil spill and decreasing over time to the depletion of nutrients from the environment. Nutrients (N, P, and K) play an important role in the thriving of potent microbial communities resulting in a faster rate of degradation of hydrocarbons along the polluted shoreline (Shewfelt et al. 2005). However, effective biodegradation of petroleum hydrocarbons by microorganisms is dependent on some physicochemical factors namely temperature, pH, dissolved oxygen in water, and nutrients that regulate the growth of the microorganisms as well as some biological factors such as an enzymatic activity that control the potency of biodegradation (Leahy & Colwell 1990, Varjani & Upasani 2017, Ahmed & Swargiary 2021). In addition to these, many other factors influence the biodegradation rates, for example, the chemical composition and the physical condition of the oil, the type, and quantity of spilled oil, the characteristics of the polluted ecosystem, etc. (Haritash & Kaushik 2009).

## Bioremediation

Bioremediation is one of the alternative techniques for the treatment of pollutants which is an inventive technique that relied on microorganisms to reduce toxic pollutants to harmless compounds such as H<sub>2</sub>O, CO<sub>2</sub>, CH<sub>4</sub>, and biomass without disturbing the ecosystem in the polluted environment (Ron & Rosenberg 2014). There are many types of microorganisms that have the potential for bioremediation of spilled hydrocarbon pollutants. These include yeast, fungi, algae, and bacteria (Naeem & Qazi 2019). The rate of bioremediation can be enhanced by the supplementation of some elements such as N to the oil-contaminated environments (Wang et al. 2011). Even if the marine environments polluted with spilled oil are cleaned, some compounds may last for decades on these beaches and environments, threatening the organisms living in these ecosystems (Owens et al. 2008).

Depending on the application process, the bioremediation process can be classified into two types, in situ bioremediation, and ex-situ bioremediation. In situ bioremediation techniques are the most desirable options, because of their low cost and avoiding drilling and transport of contaminants where treatment is done on-site. On contrary, ex-situ bioremediation which is the removal of the contaminant's physical material for treating contaminated environments is very costly as well as problematic due to the tough extraction of contaminants from underwater or soil (Farhadian et al. 2008). This technique is achieved by drilling and removal of contaminated soil and water, including composting, land farming, bioreactors (Vidali 2001), and biopiles (von Fahnstock & Wickramanayake 1998). Bioremediation processes can also be classified into two main approaches, i) Biostimulation and ii) Bioaugmentation (Varjani et al. 2013).

## Biostimulation

Biostimulation is defined as an environmental modification process to encourage the growth of existing microbes as well as to stimulate the biodegradation of pollutants to be treated in the modified environment. This process is applied in practice by adding nutrients or substances, for example, carbon, nitrogen, and phosphorus to the environment to be treated, as well as by ensuring appropriate environmental conditions such as moisture and oxygen content to promote microbial growth and natural biodiversity of microorganisms. Nitrogen, Phosphate, and molecular oxygen concentrations in seawater are important examples of abiotic factors. Therefore, Nitrogen and Phosphate are used to reduce the limit of these nutrients, which spurs the prosperity of degrading bacteria for petroleum hydrocarbons. Nitrogen and Phosphate based fertilizers such as nitrates, ammonium phosphate, urea, and phosphate, can be used in such cases because they have high solubility in water (Nikolopoulou & Kalogerakis 2009). Moreover, uric acid which is used as a source of nitrogen by several bacterial species, including *Alcanivorax* strains, can be a potent biological catalyst for the bioremediation of spilled oil (Ron & Rosenberg 2014).

## Bioaugmentation

Bioaugmentation is defined as the use of particular strains of microbial organisms, which could be either isolated or genetically modified to increase their capability for controlling pollution, for example cleaning spilled oil in contaminated marine ecosystems (Nzila et al. 2016). This process relies on the capability of microbes to metabolize pollutants and turn them into less toxic and less dangerous compounds. Biodegradation occurs naturally in contaminated environments by indigenous microorganisms which usually have limited capacity to degrade these compounds because of the



complex structure of compounds and unfavorable environmental conditions. Therefore, bioaugmentation is required in such conditions so that those complex compounds can be degraded completely by the specialized microbial organisms (Nzila et al. 2016).

Bioaugmentation also called the sowing of microorganisms in the contaminated sites, is used in marine ecosystems polluted with oil spills to promote the decomposition of spilled oil. This leads to the increase of microorganisms, where these microbes use hydrocarbons as the sole source of energy and carbon. These microbial organisms are called hydrocarbonoclastic microorganisms, mainly bacteria including many strains such as *Cycloclasticus*, *Thalassolituus*, *Alcanivorax*, *Oleispira*, and *Oleiphilus* (Nzila et al. 2018). *Cycloclasticus* strains prefer growth on aromatic hydrocarbons, for example, anthracene, phenanthrene, and naphthalene, while *Oleispira* sp. and *Oleiphilus* grow on aliphatic hydrocarbons, alkanolates, and alkanols (Nzila et al. 2018). Similarly, the strains of *Alcanivorax* sp. can grow on branched alkanes and n-alkanes only (Head et al. 2006).

### **Aerobic and Anaerobic Bioremediation**

The rate of bioremediation of hydrocarbon pollutants is less in the absence of oxygen (anaerobic) as compared with that in the presence of oxygen (aerobic). The bioremediation of hydrocarbons in the presence of oxygen is faster and easier because most species of bacteria, algae, and fungi have the potential to degrade in aerobic conditions (Haritash & Kaushik 2009). The addition of oxygen to contaminated environments increases the rate of biodegradation several times than the rates that occur naturally in these environments. In aerobic environments, microbes usually break down the hydrocarbon contaminants by forming alcohol by adding an unsaturated ring of polycyclic aromatic hydrocarbons or a hydroxyl group to the end of the alkanes. Hence, these compounds are easily soluble in water with oxygen. Moreover, aerobic microbes have a greater potential to degrade a broad range of hydrocarbons than anaerobic microbes resulting in effective bioremediation of hydrocarbon pollutants in aerobic conditions (Saxena et al. 2013). Despite the slow rates of anaerobic bioremediation, this is also important for the complete degradation of many hydrocarbons in the absence of oxygen, for example, deterioration of polycyclic aromatic hydrocarbons was reported within 90 days, while benzene degradation occurred in 120 weeks (Meckenstock 2016).

### **BIODEGRADATION AND BIOREMEDIATION OF FUEL OIL BY MICROORGANISMS**

There are many types of microorganisms such as bacteria,

algae, and fungi that decompose hydrocarbons in the environment, but bacteria and fungi are common and efficient members of them (Table 1) (Treu & Falandysz 2017, Kaur 2018). There are a few species of algae and protozoa with the ability to degrade hydrocarbons (Kachieng'a & Momba 2017). A particular group of hydrocarbons can be metabolized by an individual type of microorganisms while a consortium of microbes with wide enzymatic abilities can degrade down-mixed and compound hydrocarbons, for example, crude oil compounds in soil, freshwater, and marine waters (Varjani 2017).

### **Biodegradation by Bacteria**

Oil degradation passes through a series of different and sequential stages. Bacteria is the first group of microorganisms that are responsible for the first attack on oil spills to generate medium compounds that are later used by diverse types of other microorganisms (Hallbeck 2010). In marine environments, more than 200 species and 100 genera of microbes are known to degrade petroleum hydrocarbons; most of them are bacteria (Brakstad 2014). There are several potential strains of oil-degrading bacteria, such as *Oleiphilus*, *Cycloclasticus*, *Alcanivorax*, *Neptunomonas*, *Marinobacter*, etc. These bacteria act on the degradation of alkanes and aromatic hydrocarbons (Nzila et al. 2018). The other potential bacterial groups that degrade hydrocarbons in seawater and soil are *Acinetobacter*, *Achromobacter*, *Actinomycetes*, *Arthrobacter*, *Alcaligenes*, *Nocardia*, *Bacillus*, *Flavobacterium*, *Corynebacterium* sp, and *Pseudomonas* sp. (Villela et al. 2019). Similarly, there are some genera of bacteria such as *Rhodococcus*, *Corynebacterium*, *Mycobacterium*, *Pseudomonas* sp., *Brevibacterium*, *Arthrobacter* and *Nocardia* that degrade gaseous hydrocarbons, especially propane and/or butane (Giebel et al. 2011).

### **Biodegradation by Algae**

Phytoremediation is an important process in the treatment of petroleum hydrocarbon, which is a type of biological treatment by using micro-algae or macro-algae to clean the solid, liquid, or gaseous pollutants from contaminated soil, wastewater, and air (Naeem & Qazi 2020). However, the use of micro-algae in the bioremediation of petroleum hydrocarbons is still a major area of research. Some studies have shown that some algae including green algae, red algae, and brown algae have the potential to degrade some hydrocarbons into less harmful compounds to the environment, indicating their ability to handle crude oil pollution (Naeem & Qazi 2020). For example, the algae *Prototheca zopfii* and *Chlorella vulgaris* have the capacity for biodegradation of hydrocarbons resulting in a decrease in alkanes, iso-alkanes, and aromatic hydrocarbons in the contaminated environment (Walker et

al. 1975, Kalhor et al. 2017). In addition, the dry weight of *Chlorella vulgaris* increased with increased concentration of pollutants, indicating that crude oil has a positive effect on the Growth of types of algae (Kalhor et al. 2017).

### Biodegradation by Fungi

Fungi play a very significant role in the biodegradation of petroleum hydrocarbons in polluted aquatic environments (Table 1). In addition, the sediment contaminated with

Table 1: A list of microorganisms that degrade petroleum hydrocarbons in marine environment.

Genera	Species	References
Bacteria	<i>Aeromonas hydrophila</i>	(Sarwade & Gawai 2014)
	<i>Ochrobactrum anthropi</i>	(Bao 2012)
	<i>Acinetobacter lwoffii</i>	(Alkhatib et al. 2011)
	<i>Stenotrophomonas maltophilia</i>	(Juhasz et al. 2000)
	<i>Erythrobacter citreus</i>	(Udotong et al. 2008)
	<i>Pseudomonas aeruginosa</i>	(Thavasi et al. 2007)
	<i>Pseudomonas xanthomarina</i>	(Esmail & Obuekwe 2014)
	<i>Rhodococcus corynebacterioides</i>	(Gentili et al. 2006)
	<i>Neisseria elongata</i>	(Adoki & Orugbani 2007)
	<i>Vibrio fischeri</i>	(Bao 2012)
	<i>Bacillus megaterium</i>	(Das & Chandran 2011)
	<i>Enterobacter cloacae, Brevibacillus parabrevis B-1</i>	(Al-Jumaily & Al-Wahab 2012)
	<i>Bacillus pumilus</i>	(Maliji et al. 2013)
	<i>Chromobacterium violaceum</i>	(Yusoff 2008)
	<i>Bacillus cereus</i>	(Latha & Kalaivani 2012)
	<i>Klebsiella pneumoniae</i>	(Hii et al. 2009)
	<i>Achromobacter, Acinetobacter, Alcaligenes, Actinomycetes, Achromobacter, Acinetobacter, Alcaligenes, Actinomycetes, Archrobacter, Cycloclasticus, Coryneforms, Chromobacterium, Flavobacterium, Micrococcus, Microbacterium, Mycobacterium, Nocardia, Pseudomonas, Sarcina, Serratia, Streptomyces, Vibrio, Xanthomonas</i>	(Giebel et al. 2002)
	Fungus	<i>Aureobasidium, Candida</i>
<i>Rhodotorula</i>		
<i>Acronium, Aspergillus, Cladosporium, Mortierella, Saccharomyces, Trichoderma, Verticillium</i>		(Boguslawska-Wąs & Dąbrowski 2001)
<i>Fusarium solani</i>		(Al-Jawhari 2014)
<i>Aspergillus fumigatus</i>		(Chandran & Das 2012)
<i>Aspergillus niger</i>		(Okoro 2008)
<i>Aspergillus versicolor</i>		(Garapati & Mishra 2012)
<i>Cochliobolus lutanus</i>		(Al-Nasrawi 2012)
<i>Aspergillus saprophyticus</i>		(Ekundayo & Osunla 2013)
Yeast		<i>Aureobasidium, Pichia, Candida maltosa, Candida tropicalis, Candida apicola, Candida, Debaryomyces, Monilia, Rhodotorula, Torulopsis</i>
	<i>Exophiala xenobiotics</i>	(De Hoog et al. 2006)
	<i>Candida tropicalis</i>	(Beier et al. 2014)
	<i>Candida lipolytica</i>	(Das & Chandran 2011)
	<i>Candida maltose</i>	(Chrzanowski et al. 2006)
	<i>Candida tropicalis RETL-Cr1</i>	(Tuah et al. 2009)
	<i>Pichia ohmen YH-41</i>	(Shumin et al. 2012)
Algae	<i>Trichosporon asahii</i>	(Chandran & Das 2010)
	<i>Agmenellum, Amphora, Anabaena, Aphanocapsa, Chlorella, Chlamydomonas, Coccochlorise, Cylindrotheea, Dunaliella, Microcoleus, Nostoc, Oscillatoria, Petalonema, Porphyridium, Prototheca zopfii</i>	(Brakstad 2014)
		(Vigna et al. 2002)

spilled hydrocarbons is one of the preferred places where these fungi live to use carbon derived from the hydrocarbons (Hamad et al. 2021). However, research on the biodegradation of hydrocarbons by fungi has been focused mainly on the activity of enzymes produced by fungi in biodegradation processes. Several studies have shown that fungi have the potential to degrade total petroleum hydrocarbons with a wider range of other microbial organisms such as bacteria (Hamad et al. 2021).

## CONCLUSION

Bioremediation is a cost-effective and environment-friendly technology and is unique to the most promising ways to treat oil pollution in different ecosystems. It has been observed through several studies that the coasts contaminated with hydrocarbons can be recovered by biodegradation technology in 2-5 years. This paper presents the different aspects of biodegradation and bioremediation of petroleum hydrocarbon in the marine ecosystem. As oil spills increase in marine environments, there are many issues related to the process of biodegradation in marine ecosystems that need to be studied, such as the assessment of the risks involved after the bioremediation process and finding solutions. The risks of secondary products of metabolites of hydrocarbons should be determined in the environment and their treatment process should be explored. In addition, the effects of growing and developing microbes that degrade oil on local environments should be evaluated.

## REFERENCES

- Adeleye, A. 2018. Effect of microorganisms in the bioremediation of spent engine oil and petroleum-related environmental pollution. *J. Appl. Sci. Environ. Manag.*, 22: 157-167.
- Adoki, A. and Orugbani, T. 2007. Removal of crude petroleum hydrocarbons by heterotrophic bacteria in soils amended with nitrogenous fertilizer plant effluents. *Afr. J. Biotechnol.*, 6: 1529-1535.
- Ahmed, R.S. and Swargiary, M.D. 2021. Plastic and petroleum hydrocarbon degrading potentials of single and mixed bacterial cultures isolated from garbage areas of Darrang, Assam. *Nat. Env. Poll. Tech.*, 20(1): 275-280.
- Ahmed, F. and Fakhruddin, A. 2018. A review on environmental contamination of petroleum hydrocarbons and their biodegradation. *Int. J. Environ. J. Sci. Nat. Resour.*, 11: 1-7.
- Al-Jawhari, I.F.H. 2014. The ability of some soil fungi in biodegradation of petroleum hydrocarbon. *J. Appl. Environ. Microbiol.*, 2: 46-52.
- Al-Jumaily, E. and Al-Wahab, N. 2012. Nutritional requirement of Enterobacter cloacae for biodegradation of hydrocarbons. *Glob. J. Biol. Sci. Biotechnol.*, 1: 65-70.
- Al-Nasrawi, H. 2012. Biodegradation of crude oil by fungi isolated from the Gulf of Mexico. *J. Bioremed. Biodegr.*, 3: 1-6.
- Alkhatib, M.A.F., Alam, Z., Muyibi, S.A. and Husain, A. 2011. An isolated bacterial consortium for crude oil biodegradation. *Afr. J. Biotechnol.*, 10: 18763-18767.
- Bao, M. 2012. Biodegradation of crude oil using an efficient microbial consortium in a simulated marine environment. *Marine Pollut. Bull.*, 64: 1177-1185.
- Beier, A., Hahn, V., Bornscheuer, U.T. and Schauer, F. 2014. Metabolism of alkenes and ketones by *Candida maltosa* and related yeasts. *AMB Express*, 4: 75.
- Board, M., Board, O. S. and Council, N. R. 2003. Oil in the Sea III: inputs, fates, and effects. National Academies Press, Washington DC.
- Bogusławska-Wąs, E. and Dąbrowski, W. 2001. The seasonal variability of yeasts and yeast-like organisms in the water and bottom sediment of the Szczecin Lagoon. *Int. J. Hyg. Environ. Health*, 203: 451-458.
- Brakstad, O.G. 2014. Depletion and biodegradation of hydrocarbons in dispersions and emulsions of the Macondo 252 oil generated in an oil-on-seawater mesocosm flume basin. *Marine Pollut. Bull.*, 84: 125-134.
- Cappello, S. 2012. Effect of a bioemulsificant exopolysaccharide (eps 2003) on abundance and vitality of marine bacteria. *Water Air Soil Pollut.*, 223: 3903-3909.
- Chandran, P. and Das, N. 2010. Biosurfactant production and diesel oil degradation by yeast species *Trichosporon asahii* isolated from petroleum hydrocarbon contaminated soil. *Int. J. Eng. Sci. Technol.*, 2: 6942-6953.
- Chandran, P. and Das, N. 2012. Role of sophorolipid biosurfactant in degradation of diesel oil by *Candida tropicalis*. *Bioremediation Journal* 16: 19-30.
- Chrzanowski, Ł., Kaczorek, E. and Olszanowski, A. 2006. The Ability of *Candida maltosa* for hydrocarbon and emulsified hydrocarbon degradation. *Pol. J. Environ. Stud.*, 15: 241.
- Das, N. and Chandran, P. 2011. Microbial degradation of petroleum hydrocarbon contaminants: an overview. *Biotechnol. Res. Int.*, 6: 201.
- De Hoog, G., Zeng, J., Harrak, M. and Sutton, D. 2006. *Exophiala xenobiotica* sp. nov., an opportunistic black yeast inhabiting environments rich in hydrocarbons. *Antonie van Leeuwenhoek*, 90: 257-268.
- Ekundayo, F. and Osunla, C. 2013. Phytase activity of fungi from oil-polluted soils and their ability to degrade bonnylight crude oil. *Afr. J. Biotechnol.*, 12: 414.
- Esmail, A.S. and Obuekwe, C. 2014. Crude oil biodegradation activity in potable water. *Int. Biodeter. Biodegr.*, 93: 18-24.
- Farhadian, M., Vachelard, C., Duchez, D. and Larroche, C. 2008. In situ bioremediation of monoaromatic pollutants in groundwater: a review. *Bioresour. Technol.*, 99: 5296-5308.
- Garapati, V.K. and Mishra, S. 2012. Hydrocarbon degradation using fungal isolate: nutrients optimized by combined grey relational analysis. *Int. J. Eng. Res. Appl.*, 2: 390-399.
- Gentili, A. R., Cubitto, M. A., Ferrero, M. and Rodríguez, M. S. 2006. Bioremediation of crude oil polluted seawater by a hydrocarbon-degrading bacterial strain immobilized on chitin and chitosan flakes. *Int. Biodeter. Biodegr.*, 57: 222-228.
- Giebel, H.A. 2011. Distribution of Roseobacter RCA and SAR11 lineages in the North Sea and characteristics of an abundant RCA isolate. *ISME J.*, 5: 8-19.
- Hallbeck, L. 2010. Principal organic materials in a repository for spent nuclear fuel. SKB.
- Hamad, A. A., Moubasher, H. A., Moustafa, Y. M., and Mohamed, N. H. 2021. Petroleum hydrocarbon bioremediation using native fungal isolates and consortia. *The Scientific World Journal* 2021.
- Hamidian, R., Lashkarbolooki, M. and Amani, H. 2020. Evaluation of the surface activity of asphaltene and resin fractions of crude oil in the presence of different electrolytes through dynamic interfacial tension measurement. *J. Mol. Liq.*, 300: 112297.
- Haritash, A. and Kaushik, C. 2009. Biodegradation aspects of polycyclic aromatic hydrocarbons (PAHs): A review. *J. Hazard. Mater.*, 169: 1-15.
- Hassanshahian, M., Emtiazi, G., Kermanshahi, R.K. and Cappello, S. 2010. Comparison of oil-degrading microbial communities in sediments from the Persian Gulf and the Caspian Sea. *Soil Sed. Contam.*, 19: 277-291.
- Head, I.M., Jones, D.M. and Röling, W.F. 2006. Marine microorganisms make a meal of oil. *Nature Rev. Microbiol.*, 4: 173.
- Hii, Y.S., Law, A.T., Shazili, N., Abdul-Rashid, M. and Lee, C.W. 2009.

- Biodegradation of Tapis blended crude oil in marine sediment by a consortium of symbiotic bacteria. *Int. Biodeter. Biodegr.*, 63: 142-150.
- Hranova, R. 2006. Diffuse pollution of water resources: Principles and case studies in the southern African region. CRC Press, Boca Raton, Florida.
- Juhasz, A.L., Stanley, G. and Britz, M. 2000. Microbial degradation and detoxification of high molecular weight polycyclic aromatic hydrocarbons by *Stenotrophomonas maltophilia* strain VUN 10,003. *Lett. Appl. Microbiol.*, 30: 396-401.
- Kachieng'a, L. and Momba, M. 2017. Kinetics of petroleum oil biodegradation by a consortium of three protozoan isolates (*Aspidisca* sp., *Trachelophylum* sp., and *Peranema* sp.). *Biotechnol. Rep.*, 15: 125-131.
- Kalhor, A.X., Movafeghi, A., Mohammadi-Nassab, A.D., Abedi, E. and Bahrami, A. 2017. Potential of the green alga *Chlorella vulgaris* for biodegradation of crude oil hydrocarbons. *Marine Pollut. Bull.*, 123: 286-290.
- Kaur, A. 2018. Microbial degradation of hydrocarbons in the ecosystem. Springer, NY, pp. 343-351.
- Kukkar, D. 2020. Recent advances in carbon nanotube sponge-based sorption technologies for mitigation of marine oil spills. *J. Coll. Interf. Sci.*, 11: 16-23.
- Labud, V., Garcia, C. and Hernandez, T. 2007. Effect of hydrocarbon pollution on the microbial properties of sandy and clay soil. *Chemosphere*, 66: 1863-1871.
- Latha, R. and Kalaivani, R. 2012. Bacterial degradation of crude oil by gravimetric analysis. *Adv. Appl. Sci. Res.*, 3: 2789-2795.
- Ławniczak, Ł., Woźniak-Karczewska, M., Loibner, A.P., Heipieper, H. J. and Chrzanowski, Ł. 2020. Microbial degradation of hydrocarbons: Basic principles for bioremediation: A review. *Molecules*, 25: 856.
- Leahy, J.G. and Colwell, R.R. 1990. Microbial degradation of hydrocarbons in the environment. *Microbiol. Rev.*, 54: 305-315.
- Luna, J.M., Rufino, R.D., Sarubbo, L.A. and Campos-Takaki, G.M. 2013. Characterization, surface properties, and biological activity of a biosurfactant produced from industrial waste by *Candida sphaerica* UCP0995 for application in the petroleum industry. *Coll. Surf. B Biointerf.*, 102: 202-209.
- Mahjoubi, M., Cappello, S., Souissi, Y., Jaouani, A. and Cherif, A. 2018. Microbial Bioremediation of Petroleum Hydrocarbon-Contaminated Marine Environments. In Zoveidavianpoor, M. (ed), *Recent Insights in Petroleum Science and Engineering*, Intech Open, Rijeka, Croatia, pp. 325-350.
- Maliji, D., Olama, Z. and Holail, H. 2013. Environmental studies on the microbial degradation of oil hydrocarbons and its application in Lebanese oil-polluted coastal and marine ecosystems. *Int. J. Curr. Microbiol. Appl. Sci.*, 2: 1-18.
- Meckenstock, R.U. 2016. Anaerobic degradation of benzene and polycyclic aromatic hydrocarbons. *J. Mol. Microbiol. Biotechnol.*, 26: 92-118.
- Naeem, U. and Qazi, M.A. 2019. Leading edges in bioremediation technologies for removal of petroleum hydrocarbons. *Environ. Sci. Pollut. Res.*, 15: 1-13.
- Naeem, U. and Qazi, M.A. 2020. Leading edges in bioremediation technologies for removal of petroleum hydrocarbons. *Environ. Sci. Pollut. Res.*, 27: 27370-27382.
- Nasrin, T. 2019. Decolourization of azo dye by indigenous bacteria and its impact on seed germination. *Int. J. Biosci.*, 14: 197-210.
- Nath, B. and Cholakov, G.S. 2009. *Pollution Control Technologies-Volume II*. EOLSS Publications, Abu Dhabi.
- Neff, J.M. 2012. Composition and Fate of Petroleum and Spill-Treating. In Geraci, J. and Aubin, D. J. J. (eds), *Sea Mammals and Oil: Confronting the Risks*, Elsevier, The Netherlands, pp. 1-33.
- Nikolopoulou, M. and Kalogerakis, N. 2009. Biostimulation strategies for fresh and chronically polluted marine environments with petroleum hydrocarbons. *J. Chem. Technol. Biotechnol.*, 84: 802-807.
- Nzila, A., Razzak, S.A. and Zhu, J. 2016. Bioaugmentation: an emerging strategy of industrial wastewater treatment for reuse and discharge. *Int. J. Environ. Res. Public Health*, 13: 846.
- Nzila, A., Sankaran, S., Al-Momani, M. and Musa, M.M. 2018. Isolation and characterization of bacteria degrading polycyclic aromatic hydrocarbons: Phenanthrene and anthracene. *Arch. Environ. Protect.*, 44: 651.
- Okoro, C. 2008. Biodegradation of hydrocarbons in untreated produce water using pure fungal cultures. *Afr. J. Microbiol. Res.*, 2: 217-223.
- Owens, E.H., Taylor, E. and Humphrey, B. 2008. The persistence and character of stranded oil on coarse-sediment beaches. *Marine Pollut. Bull.*, 56: 14-26.
- Rahman, S.M.A., Saha, A.K., Ruhi, R.A., Haque, M.F. and Mohanta, M.K. 2019. Decolourization of textile azo dye direct red 81 by bacteria from textile industry effluent. *Int. J. Curr. Microbiol. Appl. Sci.*, 8: 1742-1754.
- Ron, E.Z. and Rosenberg, E. 2014. Enhanced bioremediation of oil spills in the sea. *Curr. Opin. Biotechnol.*, 27: 191-194.
- Ruhi, R.A. 2017. Decolourization of synthetic melanoidin by bacteria isolated from sugar mill effluent. *Rajshahi Univ. J. Zool.*, 36: 12-21.
- Saadoun, I. M. 2015. Impact Of Oil Spills On Marine Life. In Larramendy, M.L. and Soloneski, S. (eds), *Emerging Pollutants In The Environment-Current And Further Implications*, Intech Open, London, UK, pp. 75-104.
- Saha, A.K., Sultana, N., Mohanta, M.K., Mandal, A. and Haque, M.F. 2017. Identification and characterization of azo dye decolourizing bacterial strains, *Alcaligenes faecalis* E5. Cd and *A. faecalis* Fal. 3 isolated from textile effluents. *Am. Sci. Res. J. Eng. Technol. Sci.*, 31: 163-175.
- Sarwade, V. and Gawai, K. 2014. Biodegradation of phenol by alkaliphilic *Bacillus badius* D1. *J. Environ. Sci. Food Technol.*, 8: 28-35.
- Saxena, R., Gothawal, R., and Khan, M.N. 2013. The prospective in-silico approach in bioremediation of petroleum hydrocarbon: success so far. *Octa J. Environ. Res.*, 1: 45-63.
- Shewfelt, K., Lee, H. and Zytner, R.G. 2005. Optimization of nitrogen for bioventing of gasoline contaminated soil. *J. Environ. Eng. Sci.*, 4: 29-42.
- Shumin, Y., Zhaoyang, X. and Jinglia, T. 2012. Screening and identification of halotolerant yeast for hydrocarbon-degrading and its properties studies. *Afr. J. Microbiol. Res.*, 6: 1819-1828.
- Singer, M. and Finnerty, W. 1984. Microbial metabolism of straight-chain and branched alkanes. *FAO. Macmillan*, NY, USA.
- Souza, E.C., Vessoni-Penna, T.C. and de Souza Oliveira, R.P. 2014. Biosurfactant-enhanced hydrocarbon bioremediation: An overview. *Int. Biodeter. Biodegr.*, 89: 88-94.
- Thavasi, R., Jayalakshmi, S., Balasubramanian, T. and Banat, I.M. 2007. Effect of salinity, temperature, pH, and crude oil concentration on biodegradation of crude oil by *Pseudomonas aeruginosa*. *J. Biol. Environ. Sci.*, 1: 51-57.
- Treu, R. and Falandysz, J. 2017. Mycoremediation of hydrocarbons with basidiomycetes—a review. *J. Environ. Sci. Health Part B*, 52: 148-155.
- Truskewycz, A. 2019. Petroleum hydrocarbon contamination in terrestrial ecosystems—fate and microbial responses. *Molecules*, 24: 3400.
- Tuah, P., Rashid, N.A. and Salleh, M.M. 2009. Degradation pathway of phenol through ortho-cleavage by *Candida tropicalis* RETL-Cr1. *Borneo Sci.*, 24: 1-8.
- Udotong, I.R., Eduok, S.I., Essien, J.P. and Ita, B.N. 2008. The density of hydrocarbonoclastic bacteria and polycyclic aromatic hydrocarbon accumulation in the Iko River mangrove ecosystem, Nigeria. Report Sponsored and Published by the World Academy of Science, Engineering, and Technology, Paris, France, p. 34.
- Varjani, S.J. 2017. Microbial degradation of petroleum hydrocarbons. *Bioresour. Technol.*, 223: 277-286.
- Varjani, S.J. and Upasani, V. N. 2016. Carbon spectrum utilization by an indigenous strain of *Pseudomonas aeruginosa* NCIM 5514: Production, characterization and surface-active properties of biosurfactant. *Bioresour. Technol.*, 221: 510-516.
- Varjani, S.J. and Upasani, V.N. 2017. A new look at factors affecting microbial degradation of petroleum hydrocarbon pollutants. *Int. Biodeter. Biodegr.*, 120: 71-83.

- Varjani, S.J., Rana Dolly, P., Bateja, S. and Upasani Vivek, N. 2013. Original research article isolation and screening for hydrocarbon utilizing bacteria (HUB) from petroleum samples. *Int. J. Curr. Microbiol. App. Sci.*, 2: 48-60.
- Vidali, M. 2001. Bioremediation: An overview. *Pure Appl. Chem.*, 73: 1163-1172.
- Vigna, M., Alberghina, J., Del Mónaco, S. and Galvagno, M. 2002. *Prototheca zopfii* (Chlorophyta) is able to degrade "gas oil", recorded for the first time in contaminated waters in Argentina. *Darwiniana*, 40: 45-50.
- Villela, H. D., Peixoto, R. S., Soriano, A. U. and Carmo, F. L. 2019. Microbial bioremediation of oil-contaminated seawater: A survey of patent deposits and the characterization of the top genera applied. *Sci. Total Environ.*, 666: 743-758.
- von Fahnestock, F.M. and Wickramanayake, G. 1998. *Biopile Design, Operation, and Maintenance Handbook for Treating Hydrocarbon-Contaminated Soils*. U.S. Department of Energy Office of Scientific and Technical Information, US.
- Walker, J., Colwell, R., Vaituzis, Z. and Meyer, S. 1975. Petroleum-degrading achlorophyllous alga *Prototheca zopfii*. *Nature*, 254: 423.
- Wang, Q., Zhang, S., Li, Y. and Klassen, W. 2011. Potential approaches to improving biodegradation of hydrocarbons for bioremediation of crude oil pollution. *J. Environ. Protect.*, 2: 47.
- Xu, X. 2018. Petroleum hydrocarbon-degrading bacteria for the remediation of oil pollution under aerobic conditions: A prospective analysis. *Front. Microbiol.*, 9: 2885.
- Yakimov, M.M. 2004. The crude oil-induced structural shift of coastal bacterial communities of rod bay (Terra Nova Bay, Ross Sea, Antarctica) and characterization of cultured cold-adapted hydrocarbonoclastic bacteria. *FEMS Microbiol. Ecol.*, 49: 419-432.
- Yusoff, W.M.W. 2008. Development of three bacteria consortiums for the bioremediation of crude petroleum oil in contaminated water. *Online J. Biol. Sci.*, 8: 73-79.
- Zheng, C., Zhao, L., Zhou, X., Fu, Z. and Li, A. 2013. Treatment technologies for organic wastewater. *Water Treat.*, 11: 250-286.







# Palaeoclimatic Studies of the Late Quaternary Sediments from Chirakkara, Kollam District, Kerala, India

R. Megha\*, Divya Murali\*†, S. Amblikuttan\*, Rajesh Reghunath\* and K. Anoop Krishnan\*\*

\*Department of Geology, University of Kerala, Karyavattom Campus, University of Kerala, Trivandrum, India

\*\*National Centre for Earth Science Studies, Akkulam P.O., Trivandrum, India

†Corresponding author: Divya Murali; divyasooraj89@gmail.com

Nat. Env. & Poll. Tech.  
Website: [www.neptjournal.com](http://www.neptjournal.com)

Received: 22-08-2021

Revised: 16-10-2021

Accepted: 24-10-2021

## Key Words:

Palaeoclimatic studies  
Quaternary sediments  
Granulometric analysis  
Geochemical proxy

## ABSTRACT

The Quaternary period is considered one of the most eventful periods of all geologic periods. The present study intends to understand the paleo-environmental conditions that prevailed in the southern part of the Kerala State, India, during the Late Quaternary period. The present study aims to understand the climatic variability of the Holocene epoch in the Chirakkara region, the easternmost part of Polachira wetland, Kollam district, South Kerala, by using granulometric data and geochemical proxies. A core of 2.5 m in length has been collected from the study area, and both textural and TOC/TN analyses were carried out. The variation in grain size is attributed to the variations in the energy level of the transporting medium and turn to the climatic conditions, especially rainfall. The sediments encountered in the core are dominated by sand-sized particles indicating dynamic high energy conditions and high precipitation events. The ternary plot of the sediment samples also suggests violent environmental conditions during the deposition of the sediments. The predominance of low values of TOC/TN ratio found at both ends of the core indicates an autochthonous source for organic carbon, possibly due to the aggravated aquatic phytoplankton activity, and increased lake bioproduction, and/or decline in the delivery of organic matter from the terrestrial environment. High values of the TOC/TN ratio noted at the middle portion of the core at depths from 120 cm to 210 cm indicate the allochthonous source for the organic carbon. Among allochthonous sources, the C3-type plant is dominant, indicating a cool and wet climate. At the same time, the extremely high TOC/TN values at 170 cm core depth indicate a short period of hot and sunny climatic conditions. The analysis of the granulometric data and organic matter proxies suggest that the study area has experienced wet climatic conditions with occasional dry spells during the Late Quaternary Period.

## INTRODUCTION

Understanding the climatic variations of the recent past is highly essential for drawing comprehensive plans for protecting mother Earth. Paleoclimatic evidence preserved in geologic materials gives indirect indications of the past climatic conditions. Different proxies such as sedimentological, micropaleontological, and geochemical imprints are embedded in the Quaternary sediments (Chappell 1974, Fairbanks 1989, Charles et al. 1996, Naidu & Malmgren 1999, Thamban et al. 2001, Pandarinath et al. 2007). Various methods were suggested by many workers for the reconstruction of Quaternary paleoclimatic conditions (Bradley 1999, Mirecki et al. 1995, Slowey et al. 2002, Ishimura et al. 2012). Many studies relate the sea-level changes on the west coast of India to the climatic conditions of the Quaternary Period (Gupta 1972, Nair & Hashimi 1980, Kale & Rajaguru 1985, Baskaran et al. 1989, Somayajulu 1990, Shankar & Karbassi 1992, Hashimi et al. 1995, Pandarinath et al. 1998). The response of the river system along the west coast of India to the

climatic changes during the Late Quaternary Period has been studied by Mishra et al. (2003). Padmalal et al. (2012) conducted a study on India's fragile coast with special reference to Late Quaternary environmental dynamics. It is believed that the sea-level fluctuations after the Last Glacial Maximum of the Quaternary Period have resulted in the deposition of sediments along the Kerala coast during the later stage of the Quaternary (Thamban et al. 2001, Pandarinath et al. 2007, Shankar & Karbassi 1992, Hashimi et al. 1995). There were few attempts earlier to study the quaternary sediments found along the coastal belt of Kerala, where the focus was mainly on the sedimentological and textural parameters (Nair 1996, Samsuddin 1986, Rao et al. 2010, Padmalal et al. 2014, Vishnu Mohan 2015). The present study aims to reconstruct the Quaternary climatic conditions of the Kollam region, Kerala State, based on sedimentological and geochemical analysis.

## STUDY AREA

A core sample has been collected from the Chirakkara

region, the easternmost part of the Polachira wetland, Kollam district, South Kerala. Polachira is a wetland spread over an area of 600 hectares of sprawling land and at an altitude of 5 m above sea level, located in the Kollam District. Polachira wetland is a partially water-logged marshy basin. The wetland encircles the Paravur estuary of the Ithikkara River. It is a unique eco-geo system. As a result of the biodiversity and abundance of fish and mussels within the wetland, Polachira is a favorite destination for migratory birds too.

A core of 2.5 m in length has been collected from the study area at the latitude of  $8^{\circ}8'42''$  N and a longitude of  $76^{\circ}43'22.8''$  E (Fig. 1). The Study area receives an average of about 2555 mm of rainfall annually. The major source of rainfall is the southwest monsoon from June to September which contributes nearly 55% of the total rainfall of the year. The northeast monsoon season from October to December contributes about 24% and the remaining 21% is received from January to May as pre-monsoon showers. Out of the total 119 rainy days, 70 rainy days occur in the southwest monsoon season.

## MATERIALS AND METHODS

The recovered core has been subsampled at every 5 cm and preserved for further laboratory analyses. The textural

analysis of sediment samples was conducted by following standard methods such as sieving (Ingram 1971) and pipetting (Galehouse 1971). Total Nitrogen (TN) and Total Organic Carbon (TOC) in the core samples were measured using a CHN analyzer (Elementar Vario EL CUBE).

## RESULTS AND DISCUSSION

### Grain Size

The grain size depends on the type of environmental setting, transporting agent, length and time during transport, and depositional conditions. Hence, it acquires remarkable usefulness as an environmental proxy (McManus 1988, Stanley-Wood & Lines 1992). The variation in grain size can be attributed to the energy level, the velocity of water, and in turn the climatic conditions, especially rainfall (Pettijohn 1957). Clay size particles indicate lower energy levels and low-intensity rainfall patterns or a calm environment. During high precipitation events, the energy level of the transporting medium increases. As a result, the sediments being deposited will move to the coarser end, such as gravel, sand, etc. (Pettijohn 1957). The details of the downcore variation of the grain size parameters of the present study are summed up in Table 1.

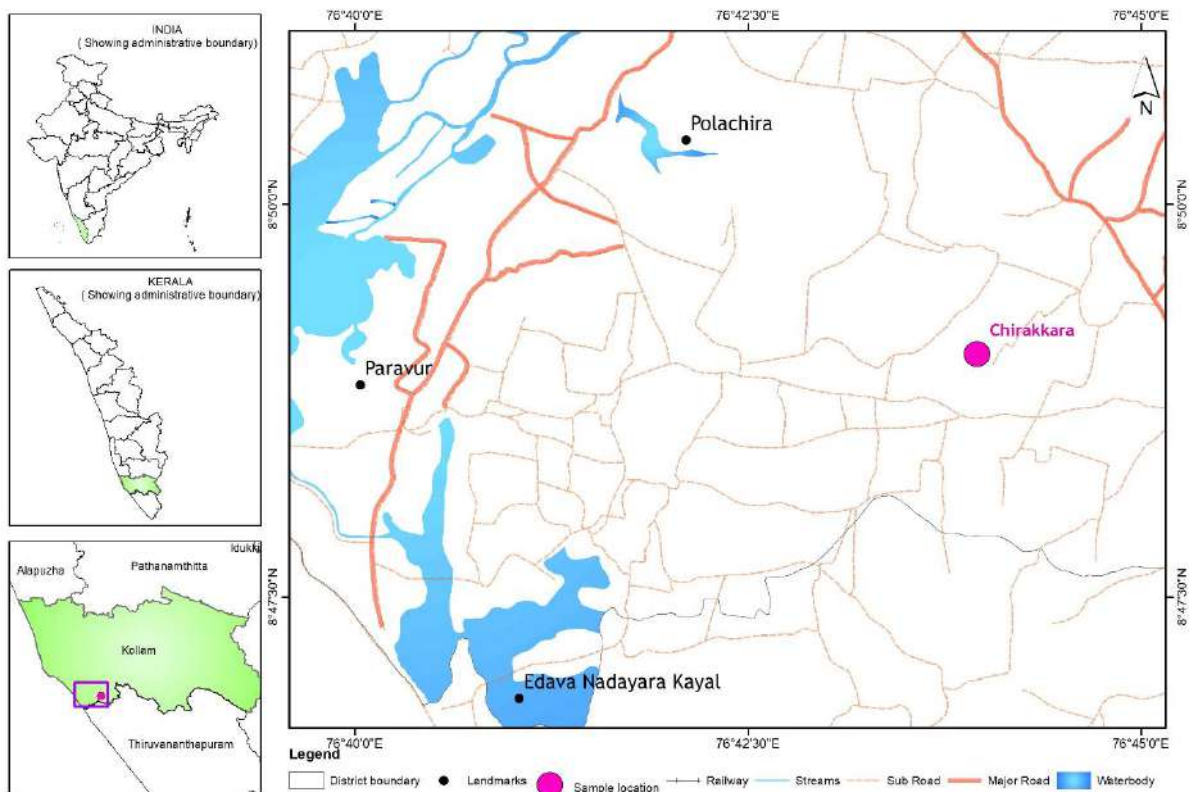


Fig. 1: Map of the study area.

In the present work, the sand content varies from 33.39 % to 91.42 %, and that of silt varies from 7.77% to 64.5%. All samples are characterized by a very low amount of clay particles, i.e., 0.45 % to 2.33 %. Both sand and silt content fluctuate drastically along the core length. The downcore variation of clay also shows an irregular variation (Fig. 2). The higher content of sand-sized particles indicates dynamic high energy conditions and high precipitation events.

The sediment classification scheme proposed by Picard (1971) also clearly reveals the dominance of sandy texture over the entire core length (Fig. 3). The upper portions of the core, up to a depth of 200cm are characterized by the alternative occurrence of sandy silt and silty sand sediments. The lower portions are dominated by sand-sized sediments. The sediment type sandy mud is present at a depth of 63 cm only.

The demarcation of diverse environments from granulometric studies can be done because particle distribution is tremendously reactive to the environment of deposition (Mason & Folk 1958, Friedman 1961, 1967, Griffiths 1962, Stapor & Tanner 1975, Nordstrom 1977, Goldberg 1980, Sly et al. 1982, Seralathan 1988, Padmalal 1992, Badarudeen

1997, Mohan 2000). The sediments that are laid down in different depositional environments, should have peculiar particle size distributions due to their differential erosion, transportation, and deposition (Lario et al. 2002). The hydrodynamic condition of deposition can be understood by using a ternary diagram proposed by Pejrup (1988) which mostly characterizes an aggregated fine fraction and a non-aggregated coarse fraction. The ternary diagram put forth by Pejrup (1988) has been applied in the core samples collected from Chirakkara to decipher the hydrodynamic dynamic condition of deposition that existed at that time. All samples fall in category IV of the ternary diagram (Fig. 4) indicating the dominance of violent environmental conditions during the deposition of the sediments.

### Total Nitrogen and Total Organic Carbon Percentage

Total organic carbon (TOC) and total nitrogen (TN) values of sediments can be used to unravel the palaeo-climatic conditions, since their ratios (TOC/TN) can differentiate marine and terrestrial sources of organic matter, the environment of deposition, etc. Total organic carbon and total nitrogen

Table 1: Down core variation of grain size parameters of the core samples.

Sample Number	Depth [cm]	Sand [%]	Clay [%]	Silt [%]	Sediment Type by Picard (1971)	Depositional environment after Pejrup (1988)
CK 1	53	42.34	2.33	55.33	Sandy silt	IV
CK 3	63	50.18	0.97	48.85	Sandy mud	IV
CK 5	73	74.82	0.48	24.7	Sand	IV
CK 6	78	80.61	0.55	18.84	Sand	IV
CK 7	83	78.04	0.45	21.51	Sand	IV
CK 9	90	62.52	1.92	35.56	Silty sand	IV
CK 11	100	68.17	0.57	31.26	Silty sand	IV
CK 13	110	62.67	0.73	36.6	Silty sand	IV
CK 15	120	54.76	0.84	44.4	Silty sand	IV
CK 17	130	36.05	1.30	62.65	Sandy silt	IV
CK 18	135	42.22	1.47	56.31	Sandy silt	IV
CK 19	140	45.55	1.40	53.05	Sandy silt	IV
CK 20	145	56.15	1.39	42.46	Silty sand	IV
CK 23	160	38.89	1.37	59.74	Sandy silt	IV
CK 25	170	33.39	2.11	64.5	Sandy silt	IV
CK 31	200	72.53	1.16	26.31	Silty sand	IV
CK 33	210	79.37	0.77	19.86	Sand	IV
CK 35	220	88.43	0.58	10.99	Sand	IV
CK 36	225	91.42	0.81	7.77	Sand	IV
CK 39	240	89.79	0.60	9.61	Sand	IV
CK 41	250	87.79	0.57	11.64	Sand	IV

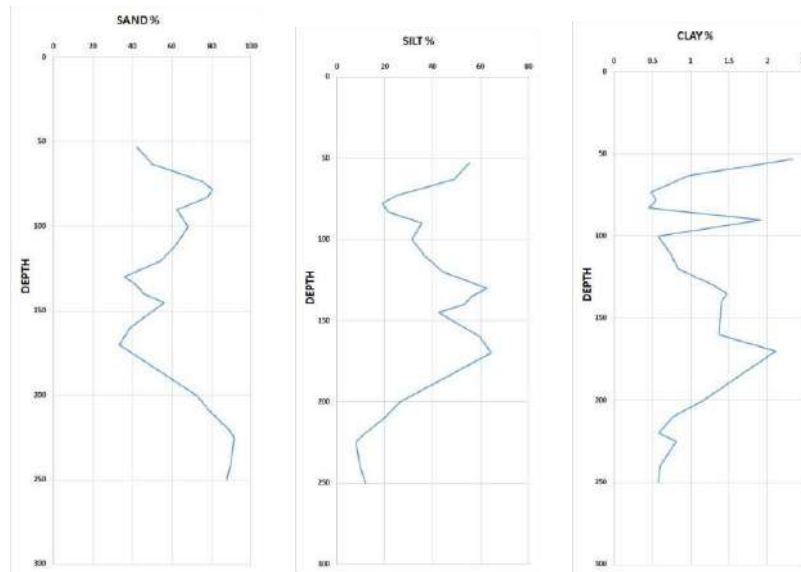


Fig. 2: Down core variation of sand, silt, and clay particles of the study area.

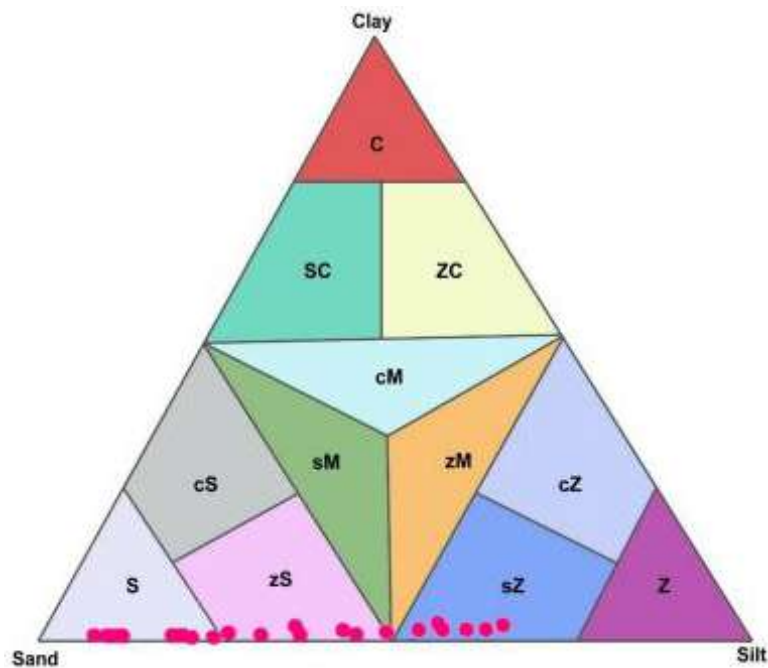


Fig. 3: Sediment type derived from Picard (1971).

content ratios have been used widely as biomarkers for the reconstruction of the depositional environments and to trace the environmental changes of the past (Dean 1999,1974, Avramidis et al. 2013, 2014, Badejo et al. 2014, Aasif Lone et al. 2018). Organic matter deposited in lakes has two principal sources: aquatic phytoplankton living in the lake (autochthonous) and terrestrial plants growing in the catch-

ment (allochthonous) (Meyers 1990). Aquatic phytoplankton contains relatively abundant proteins that are rich in organic nitrogen, and therefore the autochthonous organic matter is characterized by low TOC/TN ratios, between 4 and 10 (Meyers 1990). Terrestrial vascular plants are dominated by lignin and cellulose that are poor in nitrogen, and thus allochthonous organic matter has high TOC/TN ratios of 20



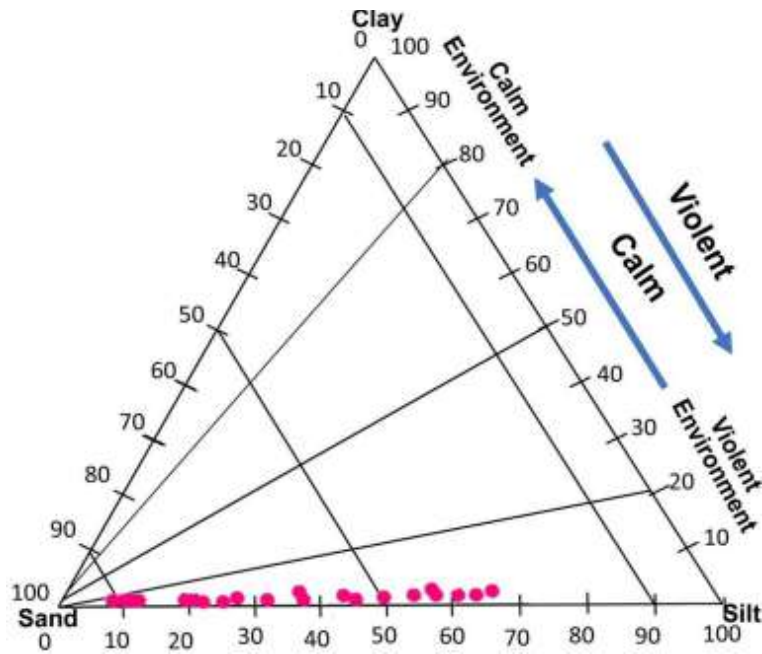


Fig. 4: Ternary plot of Pejrup (1988) showing the depositional environment.

and greater (Meyers 1990). Among the terrestrial plants' C3 vascular plants, which indicate cool & wet environments, has TOC/TN ratios around 12 and over (Tyson 1995), whereas, terrestrial C4 grasses, which indicate hot & sunny environment typically have TOC/TC ratios above 30 (Meyers 1994). In the present study, the TN values range from 0.05 to 0.40%, and that of the TOC ranges from 0.44 to 9.14%. The TOC/TN values range from 5.461 to 30.466% (Table 2).

The downcore variation pattern of both TOC and TN shows an irregular behavior, and that of TOC/TN shows a peak at the middle portion of the core (Fig 5). The upper and lower portion of the core is characterized by extremely low values of TOC/TN ratio, which indicates an autochthonous source for organic carbon, possibly due to aquatic phytoplankton activity and decline in the delivery of organic matter from the terrestrial environment and increased lake bioproduction. High values of the TOC/TN ratio present at the middle portion of the core depths, i.e., from 120 cm to 210 cm indicate the allochthonous source for the organic carbon. Among allochthonous source, the C3 type plant dominate which indicates a cool and wet climate, whereas, the extreme high TOC/TN values at 170 cm core depth indicate hot and sunny climatic conditions. The extreme high ratios at these depths also indicate intense fluvial activity which may be due to neo-tectonic activities or due to high precipitation events, as indicated by the granulometric analysis. On the west coast of India, the climate was arid around 11 kyrs BP (Hashimi & Nair 1986, Sarkar et al. 1990) and changed to

Table 2: Down core variation of TOC, TN, and TOC/TN.

Sample-Number	Core depth[cm]	TOC[%]	TN[%]	TOC/TN
CK 1	53	4.08	0.40	10.2
CK 3	63	1.57	0.20	7.85
CK 5	73	0.60	0.14	4.286
CK 6	78	0.69	0.12	5.75
CK 7	83	0.44	0.08	5.5
CK 9	90	0.49	0.05	9.8
CK 11	100	0.65	0.10	6.5
CK 13	110	0.52	0.08	6.5
CK 15	120	0.64	0.05	12.8
CK 17	130	2.37	0.16	14.812
CK 18	135	4.29	0.20	21.45
CK 19	140	1.98	0.16	12.375
CK 20	145	0.91	0.14	6.5
CK 23	160	2.78	0.24	11.583
CK 25	170	9.14	0.30	30.466
CK 31	200	6.61	0.26	25.423
CK 33	210	2.48	0.17	14.588
CK 35	220	0.80	0.13	6.154
CK 36	230	0.71	0.13	5.461
CK 39	240	1.0	0.13	7.692
CK 41	250	1.09	0.13	8.385

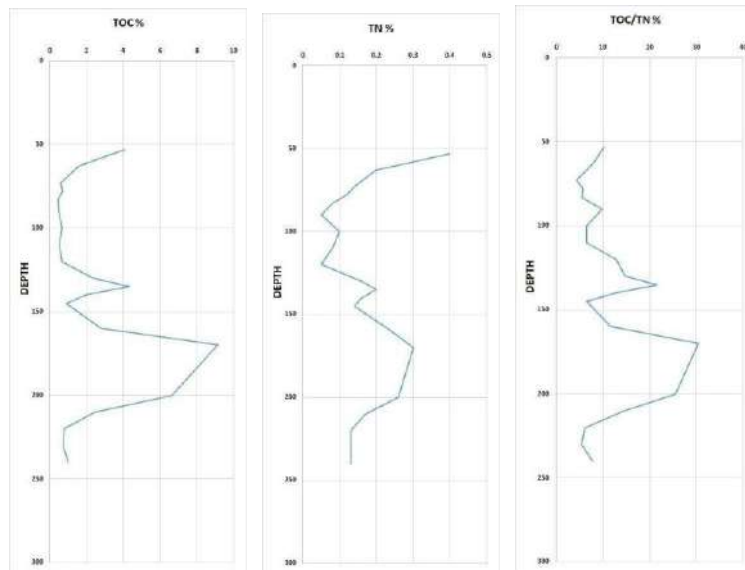


Fig. 5: Downcore variation of TOC, TN, and TOC/TN values.

warm and humid around 10 kyrs BP. Thereafter, the monsoon showers got intensified and remained so up to 7 kyrs BP (Nair & Hashimi 1980).

## CONCLUSION

The sediment analysis of the core sample recovered from the Polachira wetland at Kollam district, Kerala State, India, reveals that the study area had witnessed high precipitation conditions with occasional dry or hot and sunny climatic conditions in the recent past. The highly fluctuating as well as the higher content of sand-size particles indicates intermittent high energy conditions and high precipitation events. The ternary plot (Pejrup 1988) indicates violent environmental conditions during the deposition of these sediments. The upper and lower portions of the core are characterized by extremely low values of TOC/TN ratio, indicating an autochthonous source for organic carbon, possibly due to aquatic phytoplankton activity (Meyers 1990). It further indicates a state of limited delivery of organic matter from the terrestrial environment and increased lake bioproduction. High values of the TOC/TN ratio present at the middle portion of the core depths from 120 cm to 210 cm indicate the allochthonous source for the organic carbon. Among the allochthonous sources, the C3 type plant dominates indicating a cool and wet climate (Tyson 1995). The extremely high TOC/TN values noted at 170 cm core depth indicate hot and sunny climatic conditions. The granulometric analysis and the TOC/TN ratio values of the sediments suggest a state of overall cool and wet climatic conditions with occasional dry or hot and sunny environmental conditions during the later Quaternary period.

## ACKNOWLEDGEMENT

The authors thank the Department of Geology, the University of Kerala for the facilities provided. Central Laboratory for Instrumentation and Facilitation (CLIF), Karyavattom Campus, and the facilities at the National Centre for Earth Science Studies are thanked for providing laboratory facilities. The authors also thank the State Planning Board and the Government of Kerala for supporting the study in the form of project funds.

## REFERENCES

- Avramidis, P., Geraga, M., Lazarova, M. and Kontopoulos, N. 2013, Holocene record of environmental changes and palaeoclimatic implications in Alykes Lagoon, Zakynthos Island, western Greece, Mediterranean Sea. *Quaternary International*, 293: 184-195.
- Avramidis, P., Iliopoulos, G., Panagiotaras, D., Papoulis, D., Lambropoulou, P., Kontopoulos, N. and Christanis, K. 2014. Tracking Mid-to Late Holocene depositional environments by applying sedimentological, palaeontological and geochemical proxies, Amvrakikos coastal lagoon sediments, Western Greece, Mediterranean Sea. *Quaternary International*, 332: 19-36.
- Badarudeen, A. and Sajan, K. 1997. Sedimentology And Geochemistry of Some Selected Mangrove Ecosystems of Kerala, Southwest Coast of India (Doctoral dissertation, Cochin University of Science And Technology).
- Badejo, A.O., Choi, B.H., Cho, H.G., Yi, H.I. and Shin, K.H. 2014. Palaeoenvironmental reconstruction of the last 15,000 cal yr BP via Yellow Sea sediments using biomarkers and isotopic composition of organic matter. *Clim. Past Discuss.* 10: 1527-1565.
- Baskaran, M. and Chakrabarti, A. 1989. Biogenic faecal pellet mounds in Quaternary miliolites of Saurashtra, India. *Palaeogeography, Paleoclimatology, Paleoecology*, 73(3-4): 311-315.
- Bradley, R.S. 1999. *Paleoclimatology: Reconstructing Climates of the Quaternary*, Academic Press, San Diego.

- Chappell, J. 1974. Geology of coral terraces, Huon Peninsula, New Guinea: a study of Quaternary tectonic movements and sea-level changes. *Geological Society of America Bulletin*, 85: 553-570.
- Dean, W. E. 1974. Determination of carbonate and organic matter in calcareous sediments and sedimentary rocks by loss on ignition; comparison with other methods. *Journal of Sedimentary Research*, 44(1): 242-248.
- Dean, W. E. 1999. The carbon cycle and biogeochemical dynamics in lake sediments. *Journal of Paleolimnology*, 21(4): 375-393.
- Fairbanks, R. G. 1989. A 17,000 year glacio-eustatic sea level record: Influence of glacial melting rates on the Younger Dryas event and deep-ocean circulation. *Nature*, 342: 637-642.
- Friedman, G. M. 1967. Dynamic processes and statistical parameters compared for size frequency distribution of beach and river sands. *Journal of Sedimentary Research*, 37(2): 327-354.
- Galehouse, J. S. 1971. Sedimentation analysis. *Procedures in Sedimentary Petrology*, 69-94.
- Griffiths, D. H., King, R. F. and Rees, A. I. 1962. The relevance of magnetic measurements on some fine grained silts to the study of their depositional process. *Sedimentology*, 1(2): 134-144.
- Gupta, S. K. 1972. Chronology of the raised beaches and inland coral reefs of the Saurashtra coast. *The Journal of Geology*, 80(3): 357-361.
- Hashimi, N. H. and Nair, R. R. 1986. Climatic aridity over India 11,000 years ago: Evidence from feldspar distribution in shelf sediments. *Palaeogeography, Palaeoclimatology, Palaeoecology*, 53: 305-319.
- Hashimi, N.H., Nigam, R., Nair, R.R. and Rajagopalan, G. 1995. Holocene sea-level fluctuations on western Indian Continental margin: An update. *J. Geol. Soc. India*, 46: 157-162.
- Ingram, F. S. 1971. Sieve analysis. In: *Procedures in Sedimentary Petrology*, ed. R. E. Carver, pp. 49-68. Wiley/Interscience, New York.
- Ishimura, T., Tsunogai, U., Hasegawa, S., Nakagawa, F., Oi, T., Kitazato, H. and Toyofuku, T. 2012. Variation in stable carbon and oxygen isotopes of individual benthic foraminifera: tracers for quantifying the vital effect. *Biogeosciences Discussions*, 9(5).
- Kale, V.S. and Rajaguru, S.N. 1985. Neogene and Quaternary transgressional and regressional history of the west coast of India- An overview. *Bull. Deccan College Res. Inst.*, 44: 153-165.
- Lario, J., Spencer, C., Plater, A. J., Zazo, C., Goy, J. L. and Dabrio, C. J. 2002. Particle size characterisation of Holocene back-barrier sequences from North Atlantic coasts (SW Spain and SE England). *Geomorphology*, 42(1-2): 25-42.
- Lone, A. M., Shah, R. A., Achyuthan, H. and Fousiya, A. A. 2018. Geochemistry, spatial distribution and environmental risk assessment of the surface sediments: Anchar Lake, Kashmir Valley, India. *Environmental earth sciences*, 77(3): 1-20.
- Mason, C. C. and Folk, R. L. 1958. Differentiation of beach, dune, and aeolian flat environments by size analysis, Mustang Island, Texas. *Journal of Sedimentary Research*, 28(2): 211-226.
- Meyers, P.A. and Ishiwatari, R. 1993. Lacustrine organic geochemistry- An overview of indicators of OM sources and diagenesis in lake sediments. *Org. Geochem.*, 7: 867-900.
- Meyers, P.A. 1994. Preservation of elemental and isotopic source identification of sedimentary organic matter. *Chem. Geol.*, 114: 289-302.
- McManus, J. 1988. Grain size determination and interpretation. *Techniques in sedimentology*, 63-85.
- Mirecki, J. E., Wehmiller, J. F. and Skinner, A. F. 1995. Geochronology of Quaternary coastal plain deposits, southeastern Virginia, USA. *Journal of Coastal Research*, 1135-1144.
- Naidu, P. D. and Malmgren, B. A. 1999. Quaternary carbonate record from the equatorial Indian Ocean and its relationship with productivity changes. *Marine Geology*, 161(1): 49-62.
- Nair, K. K. 1996. Geomorphology and evolution of the coastal plain of Kerala. *Geological survey of India, Special Publication*, (40): 83-94.
- Nair, R. R. and Hashimi, N. H. 1980. Holocene climatic inference from the sediments of the western continental shelf. *Proceedings of Indian Academy of Sciences*, 89: 299-315.
- Nordstrom, K. F. 1977. The use of grain size statistics to distinguish between high-and moderate-energy beach environments. *Journal of Sedimentary Research*, 47(3): 1287-1294.
- Padmalal, D. 1992. Mineralogy and geochemistry of the sediments of Muvattupuzha river and central Vembanad estuary, Kerala, India. PhD thesis, Cochin University of Science and Technology, Kochi, pp. 122.
- Padmalal, D., Kumaran, K. P. N., Nair, K. M., Ruta B. Limaye, Vishnu Mohan, S., Baijural, B. and Anooja S. 2014. Consequences of sea level and climate changes on the morphodynamics of a tropical coastal lagoon during Holocene: An evolutionary model. *Quaternary International*, 333: 156-172.
- Pandarinath, K., Narayana, A. C. and Yadava, M. G. 1998. Radiocarbon dated sedimentation record up to 2 ka BP on the inner continental shelf off Mangalore, south-west coast of India. *Current Science*, 730-732.
- Pandarinath, K., Subramanya, K. R., Yadava, M. G. and Verma, S. P. 2007. Late Quaternary sedimentation records on the continental slope of SW coast of India - Implication for provenance, depositional and palaeomonsoonal conditions. *Journal of Geological Society of India*, 69: 1285-1292.
- Picard, M. D. 1971. Classification of fine-grained sedimentary rocks. *Journal of Sedimentary Research*, 41(1): 179-195.
- Pejrup, M. 1988. The triangular diagram used for classification of estuarine sediments: a new approach. Tide-influenced sedimentary environments and facies. Reidel, Dordrecht, pp. 289-300.
- Pettijohn, F. J. 1957. Paleocurrents of Lake Superior Precambrian quartzite. *Geological Society of America Bulletin*, 68(4): 469-480.
- Samsuddin, M. 1986. Textural differentiation of the foreshore and breaker zone sediments on the northern Kerala coast, India. *Sedimentary Geology*, 46: 135-145.
- Sarkar, A., Ramesh, R., Bhattacharyya, S. K. and Rajagopalan, G. 1990. Oxygen Isotope evidence for a stronger winter monsoon current during the last glaciation. *Nature*, 343: 549-551.
- Seralathan, P and Shajan, K. P. 1998. Studies on late quaternary sediments and sea level changes of the Central Kerala coast, India (Doctoral dissertation, Marine Geology and Geophysics, School of Marine Sciences).
- Shankar, R. and Karbassi, A. R. 1992. Sedimentological evidence for a palaeobeach off Mangalore, west coast of India. *Journal-Geological Society of India*, 40: 241-241.
- Slowey, N. C., Wilber, R. J., Haddad, G. A. and Henderson, G. M. 2002. Glacial-to-Holocene sedimentation on the western slope of Great Bahama Bank. *Marine Geology*, 185(1-2): 165-176.
- Sly, P. G., Thomas, R. L. and Pelletier, B. R. 1982. Comparison of sediment energy-texture relationships in marine and lacustrine environments. *Hydrobiologia*, 91(1): 71-84.
- Stanley-Wood, N. G. and Lines, R. W. (Eds.). 2007. *Particle Size Analysis*. Royal Society of Chemistry.
- Stapor, F. W. and Tanner, W. F. 1975. Hydrodynamic implications of beach, beach ridge and dune grain size studies. *Journal of Sedimentary Research*, 45(4): 926-931.
- Thamban, M., Rao, V. P., Schneider, R. R. and Grootes, P. M. 2001. Glacial to Holocene fluctuations in hydrography and productivity along the southwestern continental margin of India. *Palaeogeography, Palaeoclimatology, Palaeoecology*, 165: 113-127.
- Vishnu Mohan, Limaye, R. B., Padmalal, D., Ahmad, S. M. and Kumaran, K. P. N. 2017. Holocene climatic vicissitudes and sea level changes in the south western coast of India: Appraisal of stable isotopes and palynology. *Quaternary International*, 443: 164-176.





# Primary Sewage Sludge Treatment Using A Spiral Support System

C. P. Del Río-Galván\*†, R.C. Hernández-León\*\*, M.O. Franco-Hernández\*\* and J. Meléndez-Estrada\*\*\*

\*Instituto Politécnico Nacional, Unidad Profesional Interdisciplinaria de Ingeniería Campus Zacatecas, Calle circuito del gato #202, Col. Cd. Administrativa, Zacatecas, Zacatecas, Mexico

\*\*Instituto Politécnico Nacional, Unidad Profesional Interdisciplinaria de Biotecnología, Av. Acueducto S/N, Barrio la Laguna Ticomán, Gustavo A. Madero, Ciudad de Mexico, Mexico

\*\*\*Instituto Politécnico Nacional, Escuela Superior de Ingeniería y Arquitectura, Juan de Dios Bátiz s/n, U. P. Adolfo López Mateos. Gustavo A. Madero, Ciudad de Mexico, Mexico

†Corresponding author: C.P. Del Río-Galván; cdelrio@ipn.mx

Nat. Env. & Poll. Tech.  
Website: [www.neptjournal.com](http://www.neptjournal.com)

Received: 03-08-2021

Revised: 03-10-2021

Accepted: 06-10-2021

## Key Words:

Primary sewage sludge

Fecal coliforms

Stabilization

Conventional biodisc

Spiral support biodisc

## ABSTRACT

Sewage sludge (wastewater treatment solids) is an organic and nutrient resource that is generated during wastewater treatment and is utilized as biosolids in landfills, fertilizer, or compost it requires treatment to reduce the microbial load and the concentration of organic matter and pollutants such as metals. Aerobic digestion has been used for the stabilization of sewage sludge, and the use of biodiscs has been limited to primary sewage rather than sewage sludge. Therefore, this paper shows that the primary sewage sludge from a previously sonicated municipal sewage treatment plant can be stabilized using a spiral support biodisc, which is shown to be an effective mechanism with which to reduce the concentration of pathogenic microorganisms in residual sludge and also reduce the concentration of organic carbon, ammonia-nitrogen ( $\text{NH}_3\text{-N}$ ), and soluble phosphorus. The experimental results using the spiral support biodisc are better compared to those using the conventional biodisc.

## INTRODUCTION

Two of the main sources of municipal solid waste are organic waste that is produced in homes and the sludge from wastewater treatment (WWT) (Ahmadi-Pirlou et al. 2017). Sewage sludge is considered a by-product that is rich in nutrients like organic matter, phosphorous, and nitrogen (Chuang et al. 2020). Whenever possible the sludge should be returned to nature for environmental and economic reasons (Bartkowska 2014), for which the application of a previous stabilization treatment is generally required to make the sludge suitable for the required purpose. Such treatments yield a product with a lower microbial load which is more suitable for contact with and handling by humans. To determine the degree of stabilization that is achieved when using a given procedure, two stabilization criteria are preferably used: volatile solids content (VSC), reduction of indicator microorganisms, and reduction of pathogenic microorganisms (Mahamud et al. 1996).

The most common sludge stabilization methods are the biological processes of anaerobic digestion and aerobic digestion, but the latter is simpler and requires less capital, hence it has been commonly used in small- and medium-sized

wastewater treatment plants (WTPs). Notwithstanding, aerobic digestion requires large digestion tanks, due to the relatively long retention times that are in the range of 15 to 30 days (Song et al. 2010). One method of aerobic digestion that could be effective is the use of the rotating spiral support biodiscs (SSBs).

SSBs or rotating biological contactors (RBCs) consist of a tank that is open to the atmosphere and discs that are coupled by an equidistant axis, and the shafts are constantly rotated, alternately exposing the discs to atmospheric air and the organic matter in the liquid medium. This process facilitates the attachment and growth of microorganisms on the disc surface, thus forming a film of a few millimeters in thickness that covers the entire disc (Von Sperling, 2007). The microorganisms that form the biofilm are responsible for affecting the degradation of the pollutants that are contained in the liquid medium (Qiqi et al. 2012).

The biofilm that forms on the biodiscs carries out biochemical oxygen demand (BOD) removal, and the combined carbon oxidation, nitrification, and denitrification of effluents. As the discs rotate, the bacteria and fungi that constitute the biofilm are alternately exposed to ammoni-



um or nitrite from wastewater and to atmospheric oxygen (Qiqi et al. 2012).

Primary sewage sludge (which is mechanically treated and unstabilized), is not discarded at the original site from which the primary sewage was taken before treatment. This research aimed to stabilize primary sewage sludge using a system of rotating spiral support biodiscs (SSBs) at the laboratory scale.

## MATERIALS AND METHODS

### Sample Used

Residual sludge from the primary settler of a municipal wastewater treatment plant (WTP) that is located in Ecatepec, State of Mexico, Mexico was used.

Sludge with pH 6.7 that had previously been sonicated and adjusted to pH 5 with four different conditions of frequency and power was studied: 1) 80 kHz with 72 W of power; 2) 80 kHz with 48 W of power; 3) 45 kHz with 80 W of power; 4) 45 kHz and 56 W of power. The following were used as controls: a) non-sonicated mud without pH adjustment; b) non-sonicated mud with adjustment to pH 5 and c) sonicated mud at 45 kHz and 80 W of power without pH adjustment.

### Biodisc System

The system that was used in this study consists of a conventional biodisc (CB) and a spiral support biodisc (SSB), and both were located in parallel and operating simultaneously (Fig. 1). The CB and the SSB are made of polyesteramide (PEA) and they are joined longitudinally by a galvanized steel shaft with a length of 45 cm with two bearings and a



Fig. 1: Conventional biodisc system - CB (left) and spiral biodisc - SSB (right) used for stabilization of primary residual sludge.

maintained distance of 8 cm from the base with a capacity of 6.6 L (Fig. 2). The system is housed within a 33 cm long casing that holds the biodisc system at both ends.

For their operation, the CB and the SSB were operated in batch at the laboratory level with a 1 L volume of mud in each of the two systems and the rotation speed was adjusted to 1 rpm. After 15 days of biofilm formation using residual primary sludge, the treatment of this research lasted a total of 7 days.

As response variables to the primary sludge treatment by the CB and the SSB, the following were evaluated: total chemical oxygen demand (COD), total coliforms, fecal coliforms, and total organic carbon (TOC), ammonia-nitrogen ( $\text{NH}_3\text{-N}$ ), and soluble phosphorus.

### Physicochemical Analysis

Total COD was determined by using the closed reflux method (5220 C), total organic carbon (TOC), ammonia-nitrogen ( $\text{NH}_3\text{-N}$ ), soluble phosphorus, and total suspended solids (TSS) according to standardized methods (1995).

### Microbiological Analysis

Fecal coliforms and total coliforms were determined by using the most probable number (MPN/ml) technique that was modified from the Official Mexican Norm (NOM-004-SEMARNAT-2002) using sodium lauryl sulfate broth (LSB) for

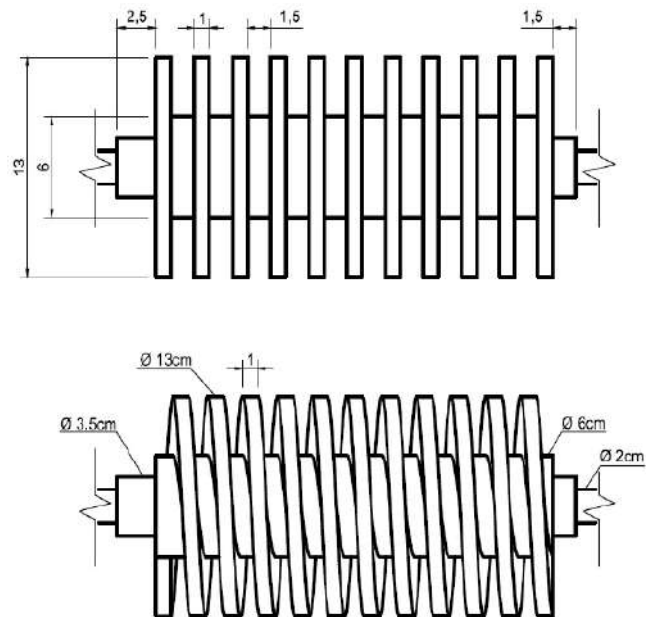


Fig. 2: Conventional biodisc system - CB (top) and spiral biodisc - SSB (bottom) (Reyes-Yañez et al. 2017).

total coliforms and bright green bile broth (BGBB) for fecal coliforms, incubating during 48 h for each test.

### Statistical Analysis

As a post hoc test to evaluate the difference between the means of the treatments with a significance level of 0.05, a one-way analysis of variance (ANOVA) and the Tukey test were performed on the obtained results.

## RESULTS AND DISCUSSION

### Total Coliforms

Both the sonication condition, the type of reactor used, and the interaction of these factors were statistically significant ( $P < 0.0001$ ) regarding the reduction of total coliforms. The treatments applied in the CB concerning the SSB that were statistically different were the control: 45 kHz with 80 W of power without pH adjustment, as well as the treatments with 80 kHz with 48 W of power and 45 kHz with 56 W of power. Greater removals of fecal coliforms were achieved in the sludge that was treated with the SSB, and the control without pH adjustment being sonicated at 45 kHz with 80 W

of power was outstanding (Fig. 3), since with this condition 99-100% of total coliforms were removed.

### Fecal Coliforms

Of the total fecal coliforms, 99-100% were eliminated in the SSB in 5 of the 7 conditions that were tested (Fig. 4): sonication condition, type of reactor, and interaction between these factors were statistically significant ( $P < 0.0001$ ).

pH 5 treatments without sonicating; 80 kHz with 72 W of power and 45 kHz with 56 W of power had statistically significant differences between them when applied in the CB concerning the SSB. Sonicated sludge treated in the SB removed approximately 60% more fecal coliforms. Tawfik et al. (2004) suggest that the adsorption of the biofilm to the rotating discs could be the mechanism by which the removal of *E. coli* occurs, although the participation of higher organisms or even sedimentation could contribute to the removal of pathogens in the rotary biodiscs.

In this research, higher levels of removal of fecal coliforms were expected in the sludge that was treated on the rotating discs. In previous research in the body of literature, Kulikowska et al. (2010) demonstrated that wastewater treat-

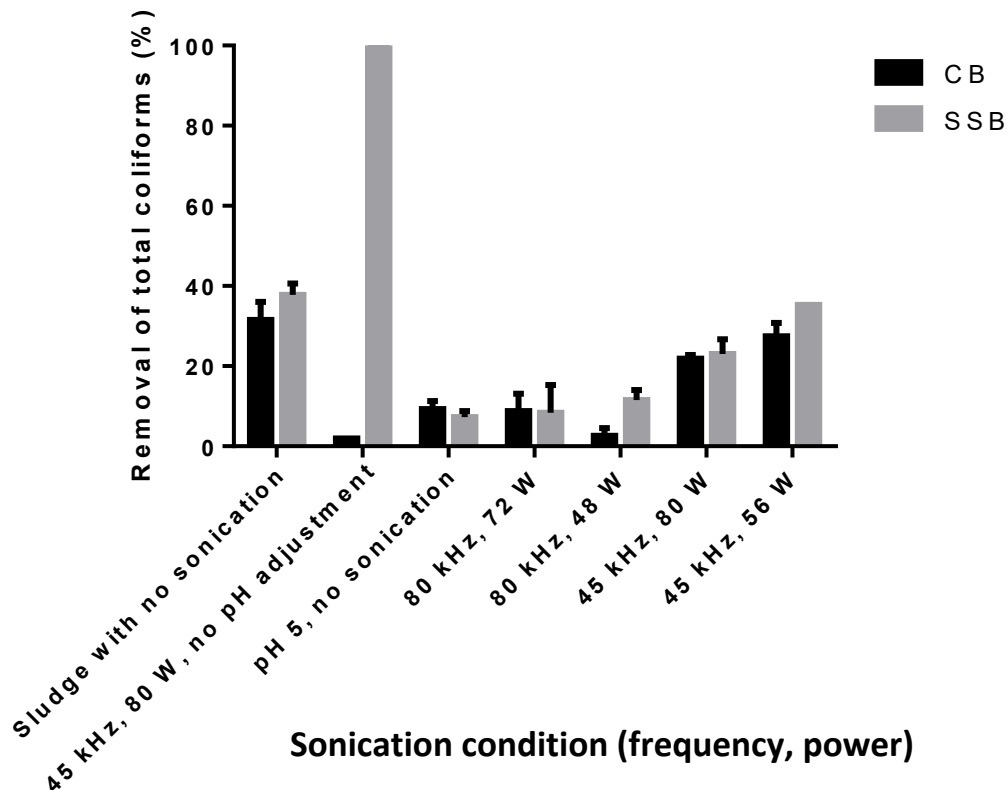


Fig. 3: Removal of total coliforms in the CB and the SSB in sludge pretreated with different sonication conditions.

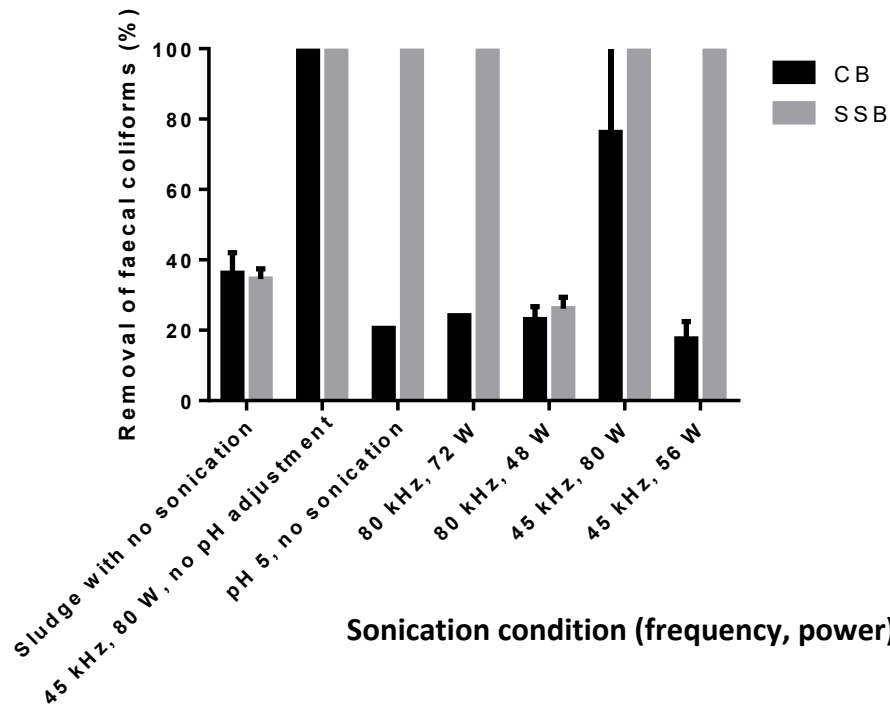


Fig. 4: Removal of faecal coliforms in CB and SSB in sludge pretreated under different sonication conditions.

ment using rotating discs can remove more than 99% of the faecal coliforms in the influent, while Hassard et al. (2014) affirm that rotating disc systems have a faecal coliform removal capacity greater than 90%. These previous results coincide with those obtained in this research with the treatments in the SSB, but not with those of the treatments in the CB, which could be explained by the greater surface area and therefore greater biofilm area of the SSB (Reyes-Yañez 2017).

Carbon and phosphorus were fully consumed in both the CB and the SSB after the 7 days of this experiment, regardless of the sonication conditions that were tested (Table 1). For the control (mud with no sonication and no pH adjustment), both carbon and phosphorus increased in concentration in both reactors. However, ammonia-nitrogen ( $\text{NH}_3\text{-N}$ ) had concentration decreases that were greater than 50% with all sonication conditions in the CB,

Table 1: Reduction of carbon, ammonia-nitrogen, and soluble phosphorus in the primary residual sludge after the sonication-aerobic reactor treatment.

Treatment	Freq. (kHz)	Power (W)	pH	CB Reactor			SSB Reactor		
				Reduction in C (%)	Reduction in $\text{NH}_3\text{-N}$ (%)	Reduction in P (%)	Reduction in C (%)	Reduction in $\text{NH}_3\text{-N}$ (%)	Reduction in P (%)
1	80	72	5	100±0	89.21± 0.56	100±0	100±0	93.58±0.33	100±0
2	80	48	5	100±0	92.26± 1.77	100±0	100±0	80.29± 1.56	20.08±11.33
3	45	80	5	100±0	53.72± 1.81	100±0	100±0	30.79± 8.99	100±0
4	45	56	5	100±0	62.5± 1.55	100±0	100±0	66.19± 4.41	100±0
5	45	80	6.7	100±0	74.14± 5.81	100±0	100±0	79.34±2.84	Increment 312.5±40.17
6	Control (Mud in its original condition)		6.7	Increment 531.25 ± 54.13	63.42±5.61	Increment 1040.1±461.59	Increment 493.75 ± 132.58	6.04±3.73	Increment
7	Sludge not sonicated		5	100±0	88.71±1.52	100±0	100±0	84.74±2.34	100±0

while in the SSB,  $\text{NH}_3\text{-N}$  had low levels of removal for the sonicated mud at 45 kHz and 80 W of power, as well as for the non-sonicated mud (Table 1). These results coincide with those of the research by Pynaert et al. (2003), who note that biodisc treatment systems tend to produce effluents that are rich in  $\text{NH}_3\text{-N}$  and poor in biodegradable organic carbon (BOC), finding the removal of  $89 \pm 5\%$  of the influent nitrogen, with  $\text{N}_2$  as the main final product in synthetic wastewater (SWW), when using a laboratory-scale rotating biological contactor (RBC; biological fixed-film treatment process).

Taking into account the final amount of fecal coliforms that were present in the sludge after applying the different sonication conditions and the subsequent treatment in the aerobic reactor, both in the CB and the SSB, the sludge was considered to be stabilized (Table 2), since it complied with the maximum permissible limits that have been established in the Official Mexican Norm (NOM-004-SEMARNAT-2002) and,

therefore, can be used as biosolids in categories of Class A, Class B, or Class C (Table 3), hence it can be asserted that the treatments in both reactors are effective in reducing the number of fecal coliforms. It is noteworthy that from the beginning of this experiment, there was no presence of *Salmonella* spp. or helminth eggs (ova) in the primary sludge, hence the treatment was evaluated by only considering the fecal coliforms.

When considering the results that were obtained from the treatment in the reactors (Table 2), all of the sludge that was treated in the CB and the SSB was considered to be Excellent biosolids or Good biosolids, in accordance with the provisions of NOM-004-SEMARNAT-2002 and they are applicable for forestry, agricultural, and soil improvement uses (Table 4). Additionally, Class A sludge can also be used in an urban setting with direct public contact. Therefore, adding biosolids to soil could contribute to increasing the quality of crops because of nitrogen and phosphorous concentration (Balaganesh et al. 2020).

Table 2: Fecal coliforms present in post-treatment treatments in CB and SSB.

Treatment	Conventional biodisc			Spiral support biodisc		
	Fecal coliforms (MPN.g <sup>-1</sup> )	Stabilized?	Class	Fecal coliforms (MPN.g <sup>-1</sup> )	Stabilized?	Class
Control (Mud with no sonication, in its original condition)	188 000	Yes	C	184 000	Yes	C
45 kHz, 80 W, no pH adjustment	0	Yes	A	0	Yes	A
pH 5, no sonication	30 000	Yes	C	0	Yes	A
80 kHz, 72 W, pH 5	36 000	Yes	C	0	Yes	A
80 kHz, 48 W, pH 5	72 700	Yes	C	46 300	Yes	C
45 kHz, 80 W, pH 5	10 000	Yes	C	0	Yes	A
45 kHz, 56 W, pH 5	60 700	Yes	C	0	Yes	A

Table 3: Maximum permissible limits for pathogens and parasites in sludge and biosolids established in the Mexican Norm NOM-004-SEMARNAT-2002.

Class	Fecal coliforms MPN.g <sup>-1</sup> on a dry basis	<i>Salmonella</i> spp. MPN.g <sup>-1</sup> on a dry basis	Helminth eggs /g on a dry basis
A	< 1 000	< 3	< 1
B	< 1 000	< 3	< 10
C	< 2 000 000	< 300	< 35

Table 4: Use of solids according to the type and class established in the Mexican Norm NOM-004-SEMARNAT-2002.

Type	Class	Exploitation
Excellent	A	Urban use WITH direct public contact during its application Those established for Class B and Class C
Excellent or Good	B	Urban use with NO direct public contact during its application Those established for Class C
Excellent or Good	C	Forestal use Soil improvement Agricultural use

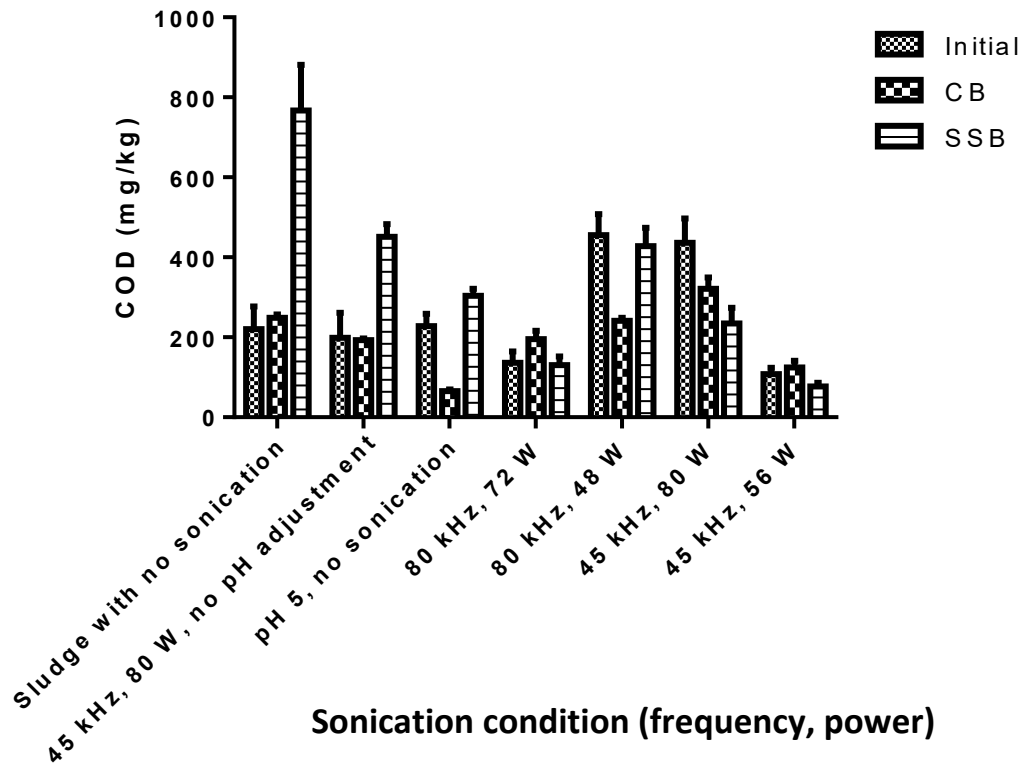


Fig. 5: Variation of COD in pretreated sludge with different sonication conditions in the CB and the SSB.

## COD

After sonicating the residual sludge under different conditions, and its subsequent treatment in the CB and the SSB, an increase in total chemical oxygen demand (COD) was observed in some cases, mainly in the SSB, while in the treatments in the CB a decrease in COD was observed (Fig. 5). The COD is an indirect parameter for measuring organic matter, hence the increase in this could represent the dispersion of aggregates that are present in the residual sludge or it could even be explained by the detachment of the biofilm from the discs or the spiral, with the biofilm remaining in the liquid phase and adding to the treatment process (Husham et al. 2012).

However, the decrease in COD could be due to the aerobic oxidation of organic matter that was carried out in the biodisc system, where many events occur simultaneously, including the transport of substrate and oxygen from the sludge to the biofilm microorganisms (Andreadakis et al. 1993).

Although the SSB treatments had greater levels of removal of fecal coliforms (Fig. 4), the opposite behavior was observed in the COD determinations (Fig. 5). These treatments are in contrast with what was reported by Reyes-Yañez et al.

(2017), who noted 82% removal of COD from wastewater treated for 180 h in their spiral reactor, against 74% removal of COD that was achieved by treatment in their disc reactor. In the present study, the differences that were found between the CB and the SSB could be due to the concentration of microorganisms, since the CB has a greater specific area and, therefore, a greater number of microorganisms. Another aspect could be the difference in the distribution of organic matter, nutrients, and aeration, which are facilitated by the movement which is generated by the spiral biodisc compared to the conventional biodisc (Reyes-Yañez et al. 2017).

It is noteworthy that after the treatment of the sludge in the CB and the SSB, the elimination of the characteristic bad odor (i.e., Hydrogen sulfide,  $H_2S$ ) of the mud was perceived, in addition to changes in the color of the mud, starting with dark brown and ending with light brown. This fact is explained by the concentration of organic matter that is present, with a darker color concerning the higher concentration of organic matter, as confirmed by Andreadakis et al. (1993) in their research when testing a biodisc at the laboratory level. Furthermore, the suspended solids (sediments) concentration (SSC) decreased by more than 95% in all of the conditions that were tested (Fig. 6). This result agrees with the result in



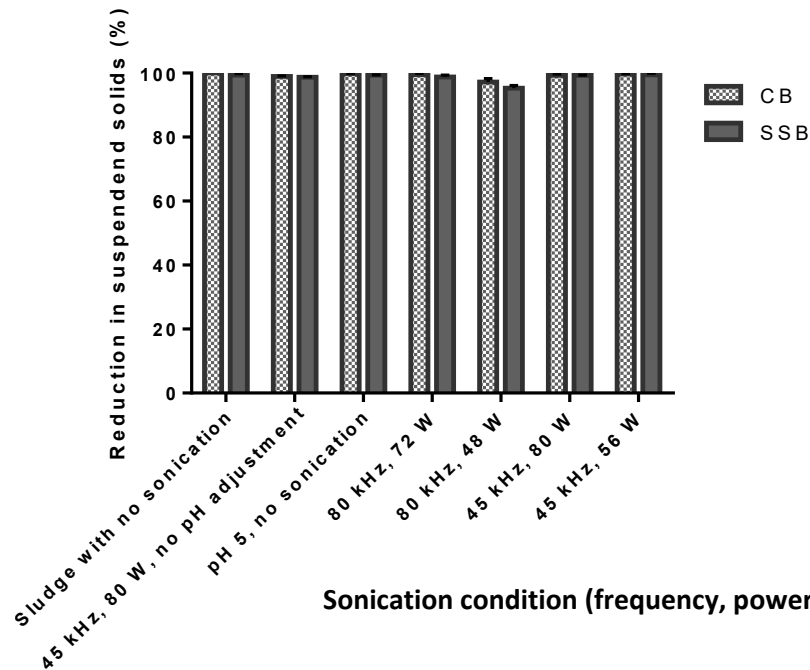


Fig. 6: Reduction of suspended solids in the mud after treatment with sonication and biodiscs - CB + SSB.

the research of Tawfik et al. (2004), where those authors note that most of the *E. coli* population was found in suspended solids, which would explain the decrease in fecal coliforms in the systems treated in both the CB and the SSB in the present study.

## CONCLUSION

After treating the primary sewage with the sequence of sonication-CB and sonication-SSB, in some cases, there was an increase in the concentration of organic matter that was measured as COD observed, while in some other cases, the concentration of organic matter decreased. In the primary sludge that was treated with the CB, the concentrations of total coliforms and fecal coliforms decreased, although the SSB eliminated fecal coliforms in most of the conditions that were tested. Notwithstanding, the sludge resulting from the treatment of both systems is considered to be made up of biosolids because they constitute a stabilized sludge following treatment, hence according to the Official Mexican Norm (NOM-004-SEMARNAT-2002) this can be used for urban, agricultural, soil improvement, and forestry uses. It is necessary to evaluate the treatment time of the sludge using the biodisc systems to determine the minimum time reached, in accordance with the parameters established in NOM-004-SEMARNAT-2002 regarding its proper use.

## ACKNOWLEDGEMENTS

The authors wish to thank the National Polytechnic Institute for the assignment of the paid leave of Professor Del Río Galván and the financing of the SIP20180132 and SIP20196618 projects.

## REFERENCES

- Ahmadi-Pirlou, M., Ebrahimi-Nik, M., Khojastehpour, M. and Ebrahimi, S.H. 2017. Mesophilic co-digestion of municipal solid waste and sewage sludge: Effect of mixing ratio, total solids, and alkaline pretreatment. *Int. Biodeterior. Biodegradation*, 125: 97-104. <https://doi.org/10.1016/j.ibiod.2017.09.004>
- Andreadakis, A.D., Hatzikonstantinou, G. and Christoulas, D. G. 1993. Carbon removal and nitrification by rotating biological contactors. *Environ. Technol.*, 14(5): 479-485. <https://doi:10.1080/09593339309385316>
- APHA. 1995. *Standard Methods for the Examination of Water and Wastewater*. 19th edn. Washington, D.C.
- Balaganes, P., Vasudevan, M., Suneethkumar, S.M., Shahir, S. and Natarajan, N. 2020. Evaluation of sugarcane and soil quality amended by sewage sludge-derived compost and chemical fertilizer. *Nat. Environ. Pollut. Technol.*, 19(4): 1737-1741. <https://doi:10.46488/NEPT.2020.v19i04.045>
- Bartkowska, I. 2014. Influence of the sewage sludge stabilization process on the value of its oxidation-reduction potential. *Environ. Technol.*, 35(17): 2160-2166. [doi:10.1080/09593330.2014.895052](https://doi:10.1080/09593330.2014.895052)
- Chuang, M., Hui-Jia, J., Bin, H., Nan, L., Ke, Z., Ji-hong, Z. and Hong-Zhong, Z. 2020. Changes in enzyme activity and bacterial succession during sewage sludge composting. *Nat. Environ. Pollut. Technol.*, 19(2): 695-701. <https://doi:10.46488/NEPT.2020.v19i02.024>

- Hassard, F., Biddle, J., Cartmell, E., Jefferson, B., Tyrrel, S. and Stephenson, T. 2015. Rotating biological contactors for wastewater treatment - A review. *SAF*, 94(C): 285-306. <https://doi.org/10.1016/j.psep.2014.07.003>
- Husham, T.I, Qiang, H., Al-Rekabi, W.S. and Qiqi, Y. 2012. Improvements in biofilm processes for wastewater treatment. *PJN*, 11(8): 610-636.
- Kulikowska, D., Jó wiak, T., Kowal, P. and Ciesielski, S. 2010. Municipal landfill leachate nitrification in RBC biofilm - Process efficiency and molecular analysis of microbial structure. *Bioresour. Technol.*, 101(10): 3400-3405. <https://doi.org/10.1016/j.biortech.2009.12.050>
- Mahamud, M., Gutiérrez, A. and Sastre, H. 1996. Biosolids generated in water treatment: (II). Treatment methods. *Water Eng.*, 3(II): 45-54. <https://doi.org/10.4995/ia.1996.2703>
- NOM-004-SEMARNAT-2002. Environmental Sludge Protection and Biosolids Specifications, and Maximum Permissible Limits of Pollutants for Their Use and Final Disposal. Government Norm, Mexico.
- Pynaert, K., Smets, B.F., Wyffels, S., Beheydt, D., Siciliano, S.D. and Verstraete, W. 2003. Characterization of an autotrophic nitrogen-removing biofilm from a highly loaded lab-scale rotating biological contactor. *Appl. Environ. Microbiol.*, 69(6): 3626-3635. <https://doi.org/10.1128/AEM.69.6.3626-3635.2003>
- Qiqi, Y., Qiang, H. and Husham, I.T. 2012. Review on moving bed biofilm processes. *PJN*, 11(9): 706-713. <https://doi.org/10.3923/pjn.2012.804.811>
- Reyes-Yañez, I.E., Meléndez-Estrada, J. and Cruz-Castro, O. 2017. Recent developments in the removal of organic matter using a spiral support system. *Int. J. Curr. Res.*, 9(2): 46583-46586
- Song, L.J., Zhu, N.W., Yuan, H.P., Hong, Y. and Ding, J. 2010. Enhancement of waste-activated sludge aerobic digestion by electrochemical pre-treatment. *Water Res.*, 44(15): 4371-4378. <https://doi.org/10.1016/j.watres.2010.05.052>
- Tawfik, A., Klapwijk, B., Van Buuren, J., El- Gohary, F. and Lettinga, G. 2004. Physico-chemical factors affecting the E. coli removal in a rotating biological contactor (RBC) treating UASB effluent. *Water Res.*, 38(5): 1081-1088. [https://doi.org/10.1016/S0043-1354\(03\)00345-2](https://doi.org/10.1016/S0043-1354(03)00345-2)
- Von Sperling, M. 2007. *Activated Sludge and Aerobic Biofilm Reactors*. Vol. 5. IWA Publishing, London.



# Isolation, Identification and Characterization of Novel Azo Dye Degrading Bacteria from the Industrial Effluents of Raipur City, Chhattisgarh

Deepali Rajwade\*, Sadhana Jaiswal\*\*, Vinit Singh Baghel\*\*\*† and Hemant Kumar\*\*\*\*

\*Department of Biotechnology, Govt. N.P.G. College of Science, Raipur, Chhattisgarh, India

\*\*Department of Microbiology, Govt. N.P.G. College of Science Raipur, Chhattisgarh, India

\*\*\*Department of Biotechnology, Guru Ghasidas University, Bilaspur, Chhattisgarh, India

\*\*\*\*Department of Biotechnology, Govt. V.Y.T. Post Graduate Autonomous College, Durg, Chhattisgarh, India

†Corresponding author: Vinit Singh Baghel; vsbaghel173@gmail.com

## Nat. Env. & Poll. Tech.

Website: [www.neptjournal.com](http://www.neptjournal.com)

Received: 26-08-2021

Revised: 10-11-2021

Accepted: 14-11-2021

### Key Words:

*Aneurinibacillus*

Azo-dye degradation

Bioremediation

Dye decolorization

Methyl orange

## ABSTRACT

Various chromophores are used to make our day-to-day life colorful. Dyes that are used at a large scale are made using these chromophores. The dyes, especially azo dyes are recalcitrant to the degradation due to the presence of aromatic rings in their structure. Several methods have been developed to reduce the harmful impacts of these dyes on the environment. However, none of the processes is safe and fully effective. In this study, we used bacteria as a bioremediation agent and optimized the various parameters for the bacteria to degrade the dye at its maximum ability. It was found that the isolated bacteria were *Aneurinibacillus* sp. and it completely decolorized methyl orange at a concentration of 20 mg.L<sup>-1</sup> after 4 days of incubation. The optimum pH for the functioning of bacteria was 5 and the activity decreased as the pH increased. It was also observed that the addition of glucose and yeast extract increased the dye degradation significantly.

## INTRODUCTION

Colors play an important role in our daily life. Dyes and dyestuffs are used to impart colors in the pharmaceutical, textile, printing, and food industries. Due to the presence of aromatic rings in their chemical structure, they are very stable and able to resist most degrading factors such as high temperatures, surfactants, and sunlight (Banat et al. 1996). Due to such high stability, they are tenacious. The most used dyes among all the dyes are azo dyes, which are characterized by nitrogen to nitrogen double bonds. Since the synthesis of azo dyes is cheaper and easy, they have a large spectrum of colors and have higher stability as compared to their natural counterparts they account for a large proportion of dyestuffs used in various industries (Chang & Kuo 2000). During and after the coloring process huge amounts of these dye effluents are discharged, which pollute local terrestrial habitats, rivers, and other aquatic bodies. These dyes released in the environment break down into their constituting chemicals such as amines, which have various harmful impacts such as mutagenic effects and chemical toxicity (Weisburger 2002, Xu et al. 2007). These dyes discharged in the water bodies get accumulated in them and hinder the sunlight penetration which in turn will affect various aquatic fauna and flora. A critical decrease in the photosynthetic ability of the aquatic

plants and dissolved oxygen level has been observed (Vandevivere et al. 1998). In addition to these, changes in the levels of various water quality parameters such as chemical oxygen demand, total organic carbon, and biochemical oxygen demands were also observed (Saratale et al. 2009).

Several physicochemical techniques such as membrane filtration, electrochemical techniques, ozonization, coagulation, and ion pair extractions have been used to treat these dye-containing effluents. However, there are various major roadblocks to these proposed methods such as they are expensive, complicated, time-consuming, not fully effective and when used produce a large amount of secondary pollution (Churchley 1994, Daneshvar et al. 2004, Forgacs et al. 2004, López-Grimau & Gutierrez 2006). Thus, the need for economical and safe elimination of these recalcitrant dyes was felt. The process of bioremediation using various bacterial isolates was then focused upon for better results and as hoped they yielded results that were cost-efficient and environment friendly at the same time (Ali et al. 2009, Senan & Abraham 2004). There have been many recent studies on the different bacterial isolates having the potential for dye degradation and have reported a large number of microorganisms having the potential for dye decolorization.

However, several attempts made by the researchers for the degradation of dyes have not yielded complete degradation or decolorization. In this context, the present study emphasizes the potential of a bacterial strain isolated from local industrial waste effluent of the dyeing industry for the degradation efficiency of  $C_{14}H_{14}N_3NaO_3S$  (methyl orange). It aims to optimize various cultural conditions (pH, dye concentration) and nutritional (carbon source) parameters for maximization of Methyl Orange dye decolorization which can be useful in providing an alternate method to accomplish dye degradation.

## MATERIALS AND METHODS

### Study Site

Three sites of the Raipur city in Chhattishgarh state of India i.e. Khans dry cleaner in Banzari road, Anshali cards printing in Phool chowk Lorapara, and M.I. industry polymers in Urla were chosen as the site for sample collection as they extensively use the dyes.

### Collection of Sample and Physicochemical Characterization

Samples in the form of liquid untreated effluent were collected in sterilized sealed plastic bottles from different sites and stored at 4°C in the refrigerator. The tests for the characterization of the sample were performed on the same day of collection. The samples were analyzed and characterized for various parameters such as pH, color, temperature, odor, chemical oxygen demand (COD), biochemical oxygen demand (BOD), dissolved oxygen (DO), total dissolved solids (TDS) and total suspended solids (TSS) using standard methods.

### Isolation and Screening of Dye Degrading Micro-organisms from Dye Effluents

The bacterial isolates present in the dye effluents were isolated by serial dilution pour plate technique on nutrient agar containing different dye concentrations of 30 mg.100mL<sup>-1</sup>, 40 mg.100mL<sup>-1</sup> and 50 mg.100mL<sup>-1</sup>. 0.1mL of serially diluted sample from three different concentrations (10<sup>-5</sup>, 10<sup>-6</sup> and 10<sup>-7</sup>) were spread over the solid medium. The plates were then put in an incubator for twenty-four hours and the temperature was maintained at 37 degrees Celsius. After the incubation period, the colonies showing a clear zone on agar plates were selected for further studies.

### Dye Degradation Study

Mineral salt media (MSM) consisting of 2.35 g sodium dihydrogen orthophosphate dehydrate, 0.07 g magnesium sulfate heptahydrate, 0.14 g of calcium chloride, 1 mg ferric

chloride and 1000 mL distilled water was used for the degradation test. Based on the screening process four isolates were selected for the methyl orange decolorization study. The dye decolorization experiment was carried out in 100 mL MSM with different concentrations of each dye, i.e. 10, 20, 30, 40 and 50 mg.L<sup>-1</sup>. Inoculum of the isolates, pre-incubated at 37°C for a day were taken out in the volume of 2mL and were inoculated in flasks containing MSM along with different dye concentrations. The flasks were then kept in the mechanical shaker and incubated at 37°C for 3 days. During the incubation period, the samples were withdrawn periodically and the absorbance was measured at the lambda max of methyl orange, i.e. 465 nm, before taking the absorbance the sample was centrifuged at ten thousand rpm for fifteen minutes. The MSM medium which was uninoculated and dye-free was used as blank. The tests were performed in a set of three and the results were compared with the blank.

$$\% \text{Decolourization} = \frac{\text{Initial OD} - \text{Final OD}}{\text{Initial OD}} \times 100$$

The dye degradation activity of the isolates was calculated and expressed in the terms of decolorization percentage. At lambda max, a decrease in the absorbance of the sample over time was monitored and the degradation efficiency was calculated from the following equation. The graph of time v/s OD was also plotted.

### Optimization of Factors

The micro-organism showing the highest decolorization efficiency was then taken and different parameters such as pH, presence, and absence of carbon source, and yeast extract were optimized. Since the previous study the maximum dye decolorization was observed in the sample containing dye at the concentration of 30 mg.mL<sup>-1</sup> so, this sample was then subjected to the different optimization experiments. pH values were optimized at 4, 7 and 9. To test the effect of the presence of glucose, 1% glucose was added to the media. Two flasks containing 50 mL of each sample without glucose were also prepared as blank. To test the effect of yeast extract on the decolorization activity, 0.05 g of yeast extract was added to 50 mL of MSM, and an uninoculated flask was used as a blank. And after the incubation period (24 h at 37°C) absorbance was taken at 530 nm.

### Bacterial Growth Curve and Generation Time

20 µL of isolate 1 showing the highest dye degradation potential was then inoculated in 200 mL autoclaved optimized media and then incubated in a shaking incubator at 37°C for one week. The medium was then taken out and optical density (OD) was measured at 620 nm every 30 minutes. Bacterial

generation time was calculated from the graph plotted between OD v/s Time in MS Excel 2013. The formula used for extraction of generation time was  $\text{LN}(2)/B$ . The value of B was obtained from the graph equation.

### Identification of Bacteria

Isolate 1 (ShivaniSI) showing the maximum potential for dye degradation was then subject to various biochemical tests for identification as per Bergy's manual. Apart from biochemical tests, the 16s rRNA analysis was also done by Chromous biotech lab, Bangalore, India. For the rest three isolates, only biochemical tests were performed.

## RESULTS AND DISCUSSION

### Collection of Samples

Fig 1. shows the samples collected from various places. The green bottle contains a sample from Anshali Shadi and Cards, pink from MI polymers, and dark blue from Khan's drycleaners Raipur. All the three places involved directly or indirectly in the processing and release of azo dyes. The samples from these places contain extreme concentrations of the azo dyes along with other coloring compounds and hence the effluents show bright colors.



Fig. 1: Samples collected from various places.

Table 1: Physicochemical investigations done on the samples collected from different locations.

S. No.	Site of sample collection	Nature of sample	Color	pH	Temperature	COD [mg.L <sup>-1</sup> ]	TSS [mg.L <sup>-1</sup> ]	TDS [mg.L <sup>-1</sup> ]
1	MI polymers, Urla, Raipur C.G.	Liquid	Light pink	8.2	28°C	1120	14200	28000
2	Khans dry cleaner Banzari road Raipur, C.G.	Liquid	Dark blue	10.7	26°C	2560	8000	19600
3	Anshali Shadi and cards Phool Chouk Raipur, C.G.	Liquid	Green	8.5	22°C	1040	11000	14000

### Physicochemical Characterization of Samples

Various physicochemical investigations done on the sample collected from above mentioned three locations are shown in Table 1. The samples were subjected to the pH estimation, and their temperature was checked. In addition to these to check the level of contamination of water chemical oxygen demand (COD), total suspended solids (TSS), and total dissolved solids (TDS) were analyzed. All the three samples gave high values for COD, TSS and TDS suggesting that the sources are highly polluted. Also, all the samples were alkaline, and the temperature varied between 22°C and 28°C.

### Isolation and Screening of Dye Degrading Microorganisms

Fig. 2 shows the isolation of the bacteria based on clear zone formation in the dye-loaded media. The bacteria were plated on the agar with dye in it. The colonies that were able to grow and degrade the dye by the production of extracellular enzymes, as seen in the third image from the top, were selected for further dye degradation experiment.

### Dye Decolorization Study

Decolorization percentage of methyl orange by Isolate 1 for different days is presented in Table 2. The isolate 1, showing the highest growth in the dye supplemented medium was further checked for its ability to degrade the higher concentrations of dye in its environment. The different aliquots of media were made and supplemented with different dye concentrations. The samples were taken out every 24 hours and checked for the degradation of dye by the bacterial inoculum. The isolates showed high degradation on the third day of inoculation in all the four concentrations.

Fig. 3 shows the degradation of methyl orange by the bacteria. The methyl orange gives a peak absorbance at 465 nm. The gradual decrease in the values of optical density at 465 nm indicates the degradation of methyl orange due to the action of the bacterial enzyme system and metabolic activities.



### Optimization of Different Factors

**Effect of pH:** The bacterial isolates on the first day of isolation were able to degrade only a small percent of the dye present in the sample this can be due to the sudden shock that they experienced when transferred from media to dye-containing media. However, after acclimatizing well in the media they showed good efficiency on the 2<sup>nd</sup> day at pH 5 suggesting the bacteria to be acidophilic. The effect of pH on the percent decolorization of dye is shown in Table 3.

**Effect of carbon source:** Bacteria like any other living being needs a carbon source for their proper functioning and supplementing the media with carbon sources like simple sugars can help in high energy generation in a short time. This easy energy can be used by bacteria to more efficiently metabolizing the compounds and give higher degradation efficiency as seen in Table 4. The efficiency on 3<sup>rd</sup> day increased to 94.17% just due to the addition of glucose.

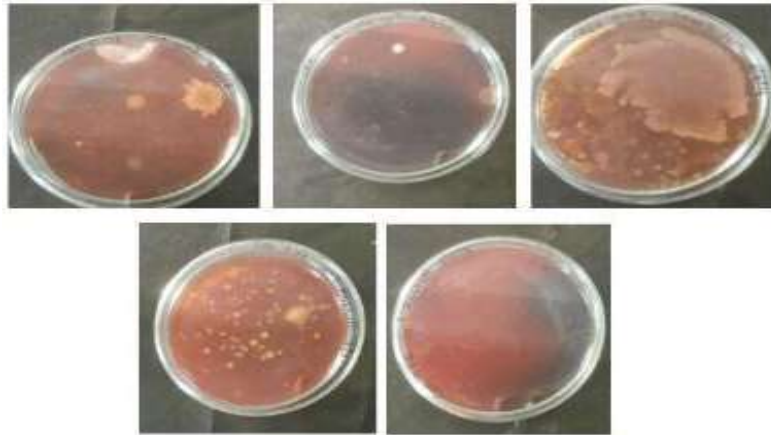


Fig. 2: Isolation of the bacteria based on clear zone formation in the dye-loaded media.

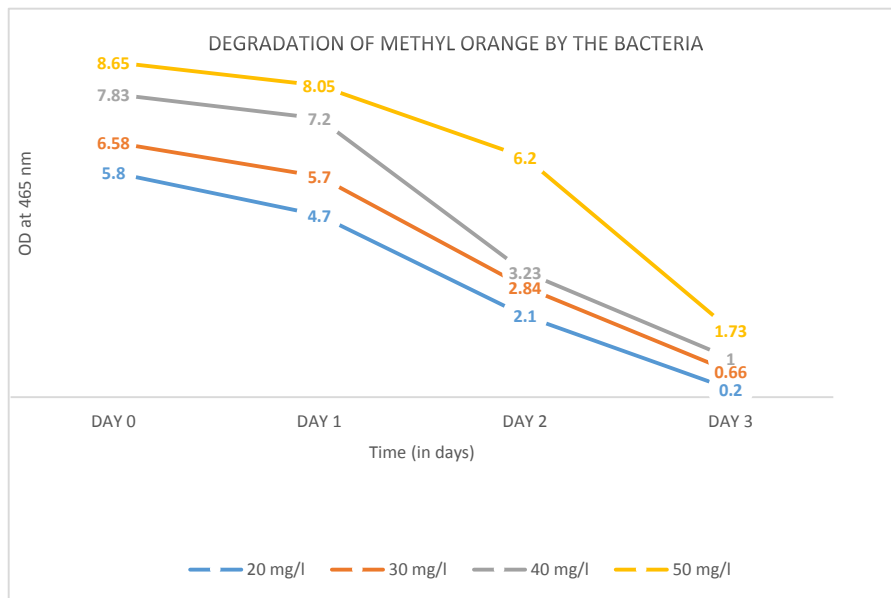


Fig. 3: Degradation of methyl orange by the bacteria.

### Effect of yeast extract and glucose addition to MSM:

The efficiency of the isolate was further checked by supplementing the media with yeast extract which functions as a nitrogen source. It was observed that the addition of yeast extract reduced the dye degradation time to nearly about 24 hours as compared to 3 days with only glucose and 5 days without yeast extract and glucose (Table 5).

### Bacterial Growth Curve and Generation Time

The generation time of the bacteria was calculated using the formula  $LN(2)/B$ . The calculated generation time for the bacteria was found to be 32 minutes.

The initial 60 minutes show the bacteria in the lag phase and getting ready to divide. A slight increase in the population number can be observed from 90 minutes to 120 minutes. After 120 minutes the bacteria enters the log phase which lasts for about 240 minutes. After the log phase due to the depletion of the nutrients and accumulation of the secondary metabolites the growth comes to a standstill phase known as the stationary phase. In this phase, the number of cells produced equals the number of cells death. This phase lasts for about 420 minutes post which the death phase sets in and cells eventually begin to die at a much higher rate than they are being generated due to the extreme depletion of the nutrients (Fig. 4).

### Identification of the Microorganisms

**Biochemical tests for the identification of bacteria:** The bacterial isolates were subjected to the biochemical tests and on their ability to produce some chemical or degrade the

other, they were classified into groups using Bergey's manual for systematic bacteriology. The isolate 1 that was selected for further studies showed positive gram staining, positive MR test and negative VP test, the bacterial strain produced catalase enzyme when  $H_2O_2$  was added. The strain however was unable to utilize the citrate added in the sample also it showed zero starch hydrolysis suggesting no production of amylase. The strain was positive for indole production, gelatin liquefaction, TSI agar test, nitrate reductase test and oxidase test (Table 6).

### Identification Through 16s rRNA Technique

#### Aligned sequence data of sample Shivani S1 (isolate 1) (A613mo)(1424bp)

```
GCCTATACATGCAAGTCGAGCGGACCAATGAA-
GAGCTTGCTCTTCGGCGGTTAGCGGCGGACG
GGTGAGTAACACGTAGGCAACCTGCCTGTACGACT-
GGGATAACTCCGGGAAACCGGAGCTAAT AC-
CGGATACTTCTTTCAGACCGCATGGTCTGAAA-
GGGAAAGACTTTTGGTACGTACAGATG-
GG CCTGCGGCGCATTAGCTAGTTGGTGGGG-
TAACGGCCTACCAAGGCGACGATGCGTAGCCGACCT
GAGAGGGTGATCGGCCACACTGGGACTGAGA-
CACGGCCCAGACTCCTACGGGAGGCAGCAGTA
GGGAATCTCCGCAATGGACGAAAGTCTGACG-
GAGCAACGCCGCGTGAACGATGAAGGTTTTTC
GGATCGTAAAGTTCTGTTGTTAGGGAAGAAC-
CGCCGGGATGACCTCCCGGTCTGACGGTACCTA
ACGAGAAAGCCCCGGCTAACTACGTGCCAG-
CAGCCGCGGTAATACGTAGGGGGCAAGCGTTGT
CCGGAATTATTGGGCGTAAAGCGCGCGCAGG-
CGGCTTCTTAAGTCAGGTGTGAAAGCCACGG
CTCAACCGTGAGGGCCACTTGAAACTGG-
GAAGCTTGAGTGCAGGAGAGGAGAGCGGAAT-
TCC ACGTGTAGCGGTGAAATGCGTAGAGATGTG-
GAGGAACACCCGTGGCGAAGGCGGCTCTCTGGC
CTGTAACTGACGCTGAGGCGCGAAAGCGTGG-
GGAGCGAACAGGATTAGATACCCTGGTAGTCC
ACGCCGTAAACGTTGAGTGCTAGGTGTTGGG-
GACTCCAATCCTCAGTGCCGAGCTAACGCAATAA
ACAAGCGGTGGAGCATGTGGTTTAATTCTGAAG-
```

Table 2: Decolorization percentage of methyl orange by Isolate 1.

Days	Dye concentration (in mg.L <sup>-1</sup> )			
	20	30	40	50
1 day	18.12%	12.56%	8.14%	7.06%
2 day	63.75%	56.73%	50.64%	21.80%
3 day	96.87%	89.90%	87.53%	80%

Table 3: Effect of pH on the percent decolorization of dye.

Days	pH 5	pH 7	pH 9
1 <sup>st</sup> day	4.23%	0.15%	4.14%
2 <sup>nd</sup> day	80.15%	78.11%	60.38%

Table 4: Comparative Percent decolorization (degradation) of sample on the addition of a carbon source.

Days	Without glucose	With glucose
1 <sup>st</sup> day	55.15%	89.32%
3 <sup>rd</sup> day	68.55%	94.17%

Table 5: Effect of yeast extract and glucose added in MSM in the percent degradation.

Sr. No.	Media	Time of Degradation
1	MSM + Yeast extract + Isolate 1.	After 24 hours
2	MSM +Glucose + Yeast extract + Isolate 1	After 24 hours
3	MSM + Glucose + Isolate 1	After 3 days
4	MSM + Isolate 1	After 5 Days

CAACGCGAAGAACCTTACCAGGGCTTGACAT  
 CCCGCTGACCCTCCTAGAGATAGGAGCTCTCT-  
 TCGGAGCAGCGGTGACAGGTGGTGCATGGTTG  
 TCGTCAGCTCGTGTCTGTGAGATGTTGGGTAA-  
 GTCCCGCAACGAGCGCAACCCTTGTCTTAGTT  
 GCCAGCATTTAGTTGGGCACTCTAGGGAGACTGC-  
 CGTCGACAAGACGGAGGAAGGTGGGGATG  
 ACGTCAAATCATCATGCCCTTATGTCCTGGGC-  
 TACACACGTGCTACAATGGATGGAACAACGG  
 GCAGCCAACTCGCGAGAGTGCGCGAATCCCT-  
 TAAAACCATTCTCAGTTCGGATTGCAGGCTG-  
 CA ACTCGCCTGCATGAAGCCGGAATCGCTAG-  
 TAATCGCGGATCAGCATGCCGCGGTGAATACGTT  
 CCGGGTCTTGTACACACCGCCCGTACACCAC-  
 GAGAGTTTGCAACACCCGAAGTCCGGTGAGGTA  
 ACCGCAAGGAGCCAGCCGCCGAAGTTGGCACTC-  
 CGCTGGGGAGTACGGCCGCAAGGCTGAAACT  
 CAAAGGAATTGACGGGGACCCGC

The aligned sequence of the bacterial strains showed a close and high similarity (99%) with the isolates of *Aneurinibacillus* strains (Table 7).

The phylogenetic tree was constructed on the basis of the aligned sequences to check for the evolutionary history of the bacterial strain. The phylogenetic trees also tell the close relative of the species. Our strain was more closely related to *Aneurinibacillus migulanus* strain RD 16s ribosomal RNA. It was also genetically related to other *Aneurinibacillus* strains although through a distant relative. Based on this observation our isolate was identified as *Aneurinibacillus* strain (Fig. 5).

## OBSERVATIONS AND DISCUSSION

Various physicochemical parameters shown in Table 1 were analyzed for proper management of effluent. The pH of effluents from all three sites fell under the alkaline category ranging from 8.2 to 10.7. PH is an important factor in the

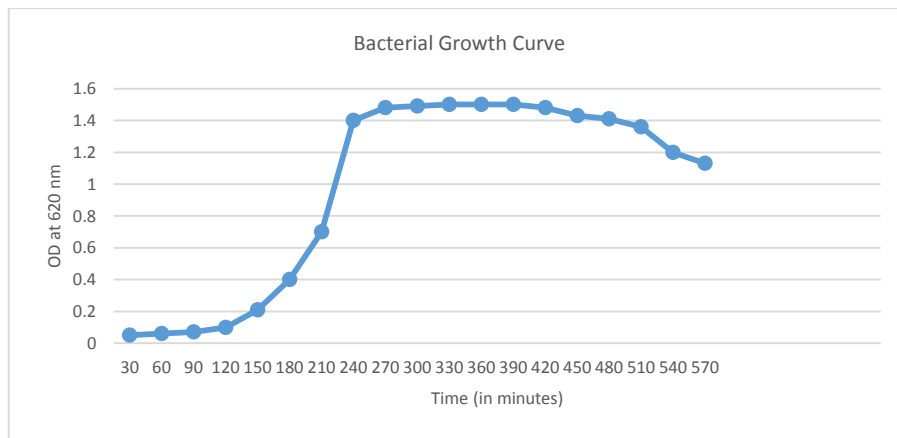


Fig. 4: Bacterial growth curve is taken at 620 nm after a week of incubation every 30 minutes.

Table 6: Results of the different biochemical tests done for the identification of the isolates.

S.No.	Name of test	Isolate No. 1 (A613mo)	Isolate No. 2 (K69mo)	Isolate No. 3 (K611tb)	Isolate No. 4 (K74tb)
1	Gram staining	+ ve	+ ve	+ve	+ve
2	MR-VP test	MR +ve, VP - ve	MR +ve, VP - ve	MR - ve, VP + ve	MR - ve, VP - ve
3	Catalase test	+ve	-ve	-ve	+ve
4	Citrate utilization	-ve	-ve	+ve	+ve
5	Indole production	+ve	+ve	+ve	+ve
6	Amylase production	-ve	+ve	+ve	+ve
7	Gelatin liquification	+ve	+ve	+ve	+ve
8	TSI agar test	+ve	+ve	+ve	+ve
9	Nitrate reductase	+ve	+ve	+ve	+ve
10	Oxidase test	+ve	+ve	+ve	+ve

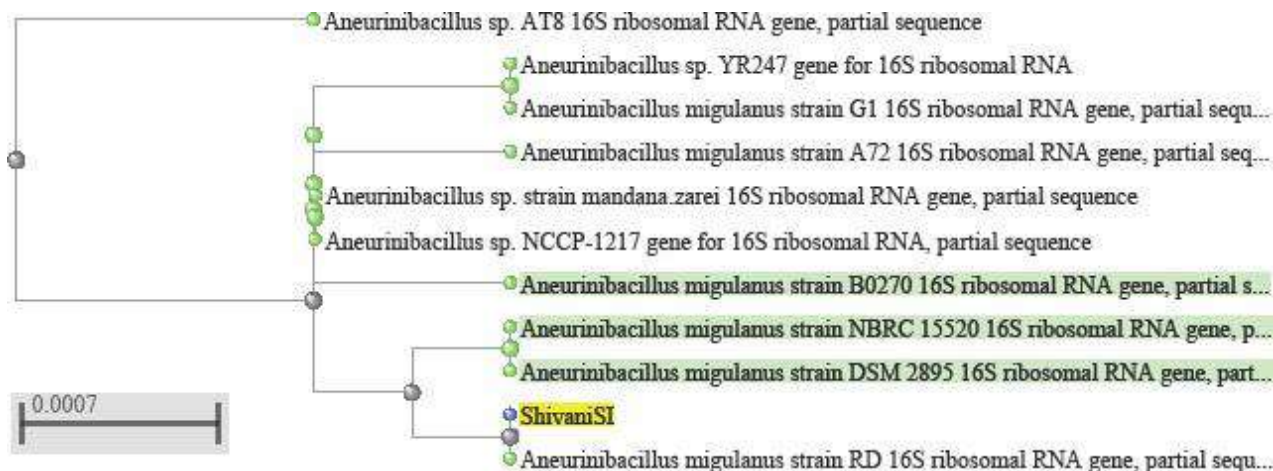


Fig. 5: Phylogenetic analysis based on the sequence alignment.

degradation of dye as it affects microbial growth & solubility of various chemicals and their reactions (Fernández-Calviño & Bååth 2010, Krishnan et al. 2017). The color of the effluent is the primary indicator of any water body being contaminated by the dye. The samples collected from the three study sites varied in the colors blue, pink, and Green (Fig. 1). The samples displayed high values of COD which indicates a huge amount of industrial pollutants in them (Lee & Nikraz 2015). This may be due to the various types of chemicals being used in different steps of the dyeing process. The highest TDS and TSS recorded were 28000 mg.L<sup>-1</sup> and 14200 mg.L<sup>-1</sup> respectively. High TDS and TSS values of the effluent affect the potability of the water body if untreated effluent is disposed of in it (Tariq et al. 2006).

Four different bacterial colonies were isolated from the effluents based on the production of clear zones observed (Fig. 2). Based on decolorization potential one isolate was chosen for further study. It was identified as *Aneurinibacillus* sp. through biochemical tests (Table 6) and 16s rRNA sequencing analysis (Table 7, Fig. 5). Its generation time was calculated using the standard growth curve by taking absorbance at 620nm (Fig. 4).

The maximum decolorization percentage (96.87%) of methyl orange was observed in a concentration of 20 mg.L<sup>-1</sup> after 3 days of incubation by *Aneurinibacillus* sp and almost complete decolorization was attained on the 4<sup>th</sup> day (Fig. 3). Table 2 indicates that an increase in the concentration of methyl orange decreases the dye degrading capacity of the bacteria. Decolorization of methyl orange dye by *Aneurinibacillus* strain decreased from acidic (80.15%) to neutral (78.11%) pH range (Table 3). To enhance dye decolorization efficiency additional carbon source in the form of glucose

was added to the sample. The addition of glucose to the sample led to 94.17% decolorization on the 3rd day (Table 4). It was observed that adding the yeast extract increased the decolorization potential, which is denoted by the complete decolorization of the sample after 24 hours while the addition of only glucose to the MSM required 3 days for complete decolorization. However, SM without any supplementation requires 5 days for complete decolorization (Table 5).

Previous studies done on various strains of *Aneurinibacillus* have explored its capacity in the biodegradation of various substances such as polylactic acid plastic, kraft

Table 7: Results of the sequence alignment for isolate No. 1.

S.No.	Organism's name	Accession No.	% match
1	<i>Aneurinibacillus migulanus</i> Strain RD	KX083693.1	99%
2	<i>Aneurinibacillus migulanus</i> Strain NBRC 15520	NR_113714	99%
3	<i>Aneurinibacillus migulanus</i> Strain DSM 2895	NR_112214.1	99%
4	<i>Aneurinibacillus</i> sp. YR274	LC110197.1	99%
5	<i>Aneurinibacillus migulanus</i> Strain B0270	NR_036799.2	99%
6	<i>Aneurinibacillus migulanus</i> Strain G1	JQ337949.1	99%
7	<i>Aneurinibacillus</i> sp. AT8	FJ821593.1	99%
8	<i>Aneurinibacillus migulanus</i> Strain A72	GU397386.1	99%
9	<i>Aneurinibacillus</i> sp. Strain mandana.zarei	KY270877.1	99%
10	<i>Aneurinibacillus</i> sp. NCCP-1217	LC065244.1	99%

lignin, collagen, polyethylene, and polypropylene (Chaisu et al. 2012, Murai et al. 2004, Raj et al. 2007, Skariyachan et al. 2018). But it is the first of its kind study done on evaluating the potential of *Aneurinibacillus* sp. in the biodegradation of Azo dyes. The possible mechanism by which the *Aneurinibacillus* sp. degrades the azo dye is by cleavage of the azo bond (-N=N-) with the help of H<sub>2</sub>O<sub>2</sub> produced during its metabolic activity. The azo dye degradation by the H<sub>2</sub>O<sub>2</sub> has already been established (Jaafarzadeh et al. 2018). However, further studies need to be done to understand the full mechanism of dye degradation by *Aneurinibacillus* sp.

## CONCLUSION

In this study bacterial strains having dye decolorizing capacity were isolated from colored effluents. The results indicate that this bacterium can be employed for the remediation of effluent from dye industries. Further studies are needed to elucidate the mechanism of dye degradation, the intermediates formed and the dye degradation potential of polluted waters in situ. Also, there is a possibility that the efficacy of reclamation of water bodies may enhance by the use of bacterial consortium.

## ACKNOWLEDGEMENT

The authors thank all the authors whose work has been cited in this work and whose work was used in designing the study

## REFERENCES

- Ali, N., Hameed, A. and Ahmed, S. 2009. Physicochemical characterization and Bioremediation perspective of textile effluent, dyes, and metals by indigenous bacteria. *J. Hazard. Mater.*, 164: 322-328. <https://doi.org/10.1016/j.jhazmat.2008.08.006>
- Banat, I.M., Nigam, P., Singh, D. and Marchant, R. 1996. Microbial decolorization of textile-dye-containing effluents: A review. *Bioresour. Technol.*, 58: 217-227.
- Chaisu, K., Charles, A.L., Guu, Y.K. and Chiu, C.H. 2012. Optimization of polylactic acid (PLA) plastic degradation by *Aneurinibacillus migulanus* using response surface methodology. *Int. Biol. Life Sci.*, 11: 22-27.
- Chang, J.S. and Kuo, T.S. 2000. Kinetics of bacterial decolorization of azo dye with *Escherichia coli* NO3. *Bioresour. Technol.*, 75: 107-111.
- Churchley, J.H. 1994. Removal of dye waste color from sewage effluent-the use of a full-scale ozone plant. *Water Sci. Technol.*, 30: 275.
- Daneshvar, N., Rabbani, M., Modirshahla, N. and Behnajady, M.A. 2004. Kinetic modeling of photocatalytic degradation of Acid Red 27 in UV/TiO<sub>2</sub> process. *J. Photochem. Photobiol. A Chem.*, 168: 39-45.
- Fernández-Calviño, D. and Bååth, E. 2010. Growth response of the bacterial community to pH in soils differing in pH. *FEMS Microbiol. Ecol.*, 73: 149-156.
- Forgacs, E., Cserhati, T. and Oros, G. 2004. Removal of synthetic dyes from wastewaters: a review. *Environ. Int.* 30, 953-971.
- Jaafarzadeh, N., Takdastan, A., Jorfi, S., Ghanbari, F., Ahmadi, M. and Barzegar, G. 2018. The performance study on ultrasonic/Fe<sub>3</sub>O<sub>4</sub>/H<sub>2</sub>O<sub>2</sub> for degradation of azo dye and real textile wastewater treatment. *J. Mol. Liq.*, 256: 462-470.
- Krishnan, J., Kishore, A.A., Suresh, A., Madhumeetha, B. and Prakash, D.G. 2017. Effect of pH, inoculum dose, and initial dye concentration on the removal of azo dye mixture under aerobic conditions. *Int. Biodeterior. Biodegrad.*, 119: 16-27.
- Lee, A.H. and Nikraz, H. 2015. BOD: COD ratio as an indicator for river pollution. *Int. Proc. Chem. Biol. Environ. Eng.*, 88: 89-94.
- López-Grimau, V. and Gutierrez, M.C. 2006. Decolourisation of simulated reactive dyebath effluents by electrochemical oxidation assisted by UV light. *Chemosphere*, 62: 106-112.
- Murai, A., Tsujimoto, Y., Matsui, H. and Watanabe, K. 2004. An *Aneurinibacillus* sp. strain AM-1 produces a proline-specific aminopeptidase useful for collagen degradation. *J. Appl. Microbiol.*, 96: 810-818.
- Raj, A., Chandra, R., Reddy, M.M.K., Purohit, H.J. and Kapley, A. 2007. Biodegradation of kraft lignin by a newly isolated bacterial strain, *Aneurinibacillus aneurinilyticus* from the sludge of a pulp paper mill. *World J. Microbiol. Biotechnol.*, 23: 793-799.
- Saratale, R.G., Saratale, G.D., Kalyani, D.C., Chang, J.S. and Govindwar, S.P. 2009. Enhanced decolorization and biodegradation of textile azo dye Scarlet R by using developed microbial consortium-GR. *Bioresour. Technol.*, 100: 2493-2500.
- Senan, R.C. and Abraham, T.E., 2004. Bioremediation of textile azo dyes by aerobic bacterial consortium aerobic degradation of selected azo dyes by bacterial consortium. *Biodegradation*, 15: 275-280.
- Skariyachan, S., Patil, A.A., Shankar, A., Manjunath, M., Bachappanavar, N. and Kiran, S. 2018. Enhanced polymer degradation of polyethylene and polypropylene by novel thermophilic consortia of *Brevibacillus* sps. and *Aneurinibacillus* sp. screened from waste management landfills and sewage treatment plants. *Polym. Degrad. Stab.*, 149: 52-68.
- Tariq, M., Ali, M. and Shah, Z. 2006. Characteristics of industrial effluents and their possible impacts on the quality of underground water. *Soil Env.*, 25: 64-69.
- Vandevivere, P.C., Bianchi, R. and Verstraete, W. 1998. Treatment and reuse of wastewater from the textile wet-processing industry: Review of emerging technologies. *J. Chem. Technol. Biotechnol. Int. Res. Process. Environ. Clean Technol.*, 72: 289-302.
- Weisburger, J.H. 2002. Comments on the history and importance of aromatic and heterocyclic amines in public health. *Mutat. Res. Mol. Mech. Mutagen*, 506: 9-20.
- Xu, W., Zhang, G., Li, X., Zou, S., Li, P., Hu, Z. and Li, J. 2007. Occurrence and elimination of antibiotics at four sewage treatment plants in the Pearl River Delta (PRD), South China. *Water Res.*, 41: 4526-4534.





# Marine Debris Management in the Parangtritis Beach Tourism Area, Yogyakarta During Covid-19 Pandemic

M. M. Sari\*†, I. W. K. Suryawan\*, B. S. Ramadan\*\*, I. Y. Septiariva\*\*\* and S. Notodarmojo\*\*\*\*

\*Faculty of Infrastructure Planning, Department of Environmental Engineering, Universitas Pertamina, Komplek Universitas Pertamina, DKI Jakarta, Jakarta Selatan, Indonesia

\*\*Department of Environmental Engineering, Faculty of Engineering, Universitas Diponegoro, Jl. Prof. H. Sudarto, SH Tembalang, Semarang, 50275, Indonesia

\*\*\* Study Program of Civil Engineering, Faculty of Engineering, Universitas Sebelas Maret, Jalan Ir Sutami 36A Surakarta, Jawa Tengah 57126, Indonesia

\*\*\*\*Department of Environmental Engineering, Faculty of Civil and Environmental Engineering, Institut Teknologi Bandung, Jl. Ganesha No. 10, Bandung 40132, Indonesia

†Corresponding author: M. M. Sari; mega.ms@universitaspertamina.ac.id

Nat. Env. & Poll. Tech.  
Website: [www.neptjournal.com](http://www.neptjournal.com)

Received: 15-10-2021

Revised: 13-12-2021

Accepted: 15-12-2021

## Key Words:

Plastics

Marine debris

COVID-19

Waste management

Masks

Parangtritis beach

## ABSTRACT

Parangtritis Beach, Yogyakarta, Indonesia, is one of the most visited tourist destinations for domestic and international tourists. These tourists are required to carry out health protocols by wearing masks during the COVID-19 pandemic. The high number of visits is linear with the generation of waste in tourist areas. Marine debris is defined as any solid material that settles, dumps, or is dumped, dumped, or disposed of in the marine and coastal environment. Efficient management of marine debris is a coordinated strategic approach to dealing with problems and inefficient law enforcement to improve the preservation of the marine environment. This study aimed to analyze the composition, characteristics, and management of marine debris in the Parangtritis Beach area during the COVID-19 pandemic. The amount of waste generated during the pandemic was recorded at 0.9 kg/m<sup>2</sup>.day. Sampling is carried out using the line transect method. The composition of waste consists of PET, PE, other plastics, biodegradable organics, and masks, each of which is 17.86%, 32.54%, 6.85%, 37.61% and 5.14%. Due to the COVID-19 pandemic, mask waste has become waste that has a new category, namely infectious. The characteristics of marine debris other than organic biodegradable tend to have a high calorific value so that it is possible to be processed by thermal processes. Thermal gravimetric analysis (TGA) shows that Polyethylene Terephthalate (PET), (Polyethylene) PE, and mask waste can be decomposed at a temperature of 260-550°C. Organic waste has been managed by processing Black Soldier Fly (BSF), while plastic waste can be processed into handicraft products. In contrast, the remaining plastic waste and masks are processed by a thermal process to allow waste to energy.

## INTRODUCTION

The Province of the Special Region of Yogyakarta is a tourist destination that provides various tourist attractions ranging from nature, culture, architecture, and historical heritage, and even Yogyakarta has many coastal beaches, with beauty, and uniqueness on each beach (Hudayanti et al. 2020, Wijayanti & Damanik 2019). The strategy and integrated economic development of the coastal area of Yogyakarta is an alternative form of the economic development model in responding to the challenges of carrying out economic development and regional development in an integrated and comprehensive manner through an integrated approach to developing the potential of the southern coast of Yogyakarta. One of the beaches that have the highest visits in Yogyakarta is Parangtritis Beach (Shidiq Darajat & Susilowati 2018).

This beach is legendary or is already very famous among tourists or visitors, and this beach is very crowded when the holidays arrive. To prepare for the arrival of hemp tourists, the manager provides several facilities for visitors to use when they come to Parangtritis Beach. Before the pandemic occurred, the volume of waste always increased along with the increasing number of tourism actors and tourists visiting the tourist area of Parangtritis Beach. The generation of waste that is increasing day by day and cannot be transported every day indicates that the less effective management system implemented by the management has resulted in the condition of the Parangtritis beach area becoming dirty and causing environmental disturbances. Garbage does not only come from tourists, but also from several small rivers that flow to Parangtritis Beach, and garbage is carried by the Opak River to the sea and swept away by waves towards the beach.

Some people in the Parangtritis Beach tourist area think that the facilities and infrastructure for waste management in the area are widely available. However, on the one hand, the community also believes that the available facilities and infrastructure do not yet have good quality. So that in fulfilling the function of the facilities or infrastructure is not optimal. One example that was observed was the Temporary Disposal Site (TPS) at the mouth of the Opak River. The existence of the TPS, in the absence of permanent buildings, causes garbage to overflow so that garbage can enter the river which will eventually pollute the river. Concern in the Parangtritis Beach tourist area may have been quite high, but public awareness has not been followed by a good perception of how to properly manage waste (Masjhoer 2017).

Environmental infrastructure facilities are closely related to environmental aesthetics in tourist attractions. Various environmental problems can occur due to the low availability of environmental instructors. One of the problems that are currently often encountered is marine debris management in the Parangtritis Beach area. Marine debris can cause several environmental impacts such as socio-economic issues for the community and the sustainability of marine organisms' ecosystems. It was noted that more than 800 species of marine and coastal organisms were affected by waste pollution due to ingestion and entanglement of marine debris (Secretariat of the Convention on Biological Diversity (SCBD) 2016). Marine debris can be a severe problem in coastal areas and small islands of Indonesia, marine organisms' habitats, and ecosystems (Purba et al. 2019). Based on the results of research from Jambeck et al. (2015), Indonesia is ranked 2nd as the largest producer of plastic waste in the world.

The movement of garbage in the sea knows no boundaries, so marine debris can also end up and accumulate in conservation areas. The marine conservation area is an area designated as a marine resource conservation area. Yogyakarta Coastal Area is an area that is rich in Conservation Areas. One of the closest to Parangtritis Beach is the Baros Mangrove Conservation Area, which has initially been clean and well-maintained, now it is dirty due to a lot of marine debris. This condition will be even more concerning with the COVID-19 pandemic. Conservationists have warned that the coronavirus pandemic could trigger a spike in marine debris. The large quantities of personal protective equipment such as masks and gloves were found to be new potential for environmental impacts in coastal areas in Indonesia. Recently, research in Indonesia has also found contamination of personal protective equipment in coastal areas such as Jakarta (Cordova et al. 2021) and Bali (Suryawan et al. 2021). This does not rule out the possibility of changes in pollution composition due to the COVID-19 pandemic at Parangtritis Beach, Yogyakarta. This study aims to analyze

the composition, characteristics, and management of marine debris in the Parangtritis Beach area during the COVID-19 pandemic.

## MATERIALS AND METHODS

### Marine Debris Generation and Composition

The time of collection of waste generation and composition of waste is carried out on Friday, March 12, 2021. Sampling is carried out using the line transect method. The requirement for the location to be used as a research site is to have a beach length of 100 m. Subsequently, the transects were divided into five transect installation areas with a distance of 20 m between transects. A total of 10 transects measuring 5×5 m were made with the transects positioned at the highest tide and lowest low tide. The 5×5m transects are further divided into sub-transects measuring 1×1 m. It is further divided into 25 sub-transects within the transect area, and then five sub-transects are randomly selected on each transect to be used as sampling areas. The five locations of the station research sub transect can be seen in Fig. 1. Parangtritis beach location coordinates are 8°1'18.5" S, 110°19'16.6" E.

The calculation of waste generation and composition refers to SNI 19-3964-1994 waste for each sub-transect. The composition of waste in the sampling area is divided into five types of waste: PET, PE, other plastics, biodegradable organics, and masks (Table 1). Waste from each source, whose weight and volume have been measured, is sorted

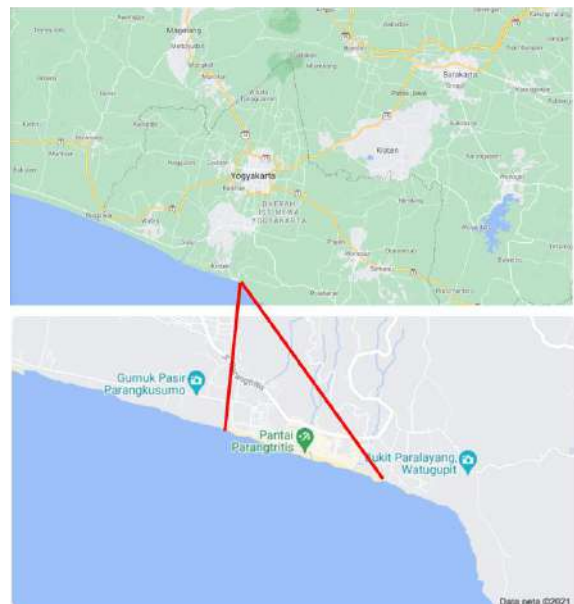


Fig. 1: Research location in Parangtritis beach, Yogyakarta (Google Map 2021).

based on five types of waste. Then each type of waste is measured by weight. Each collected waste is measured in weight (kg) so that later each waste will have a weight/weight (w/w) composition.

**Marine Debris Characteristics**

Characteristic tests were carried out in the form of chemical tests consisting of proximate analysis, namely water content, volatile content, fixed carbon, and ash content, as well as analysis of the calorific value of each raw material. A test of the characteristics of raw materials is carried out to determine the potential of each raw material.

**Waste Management Analysis**

Marine debris management was analyzed based on a literature review, both from existing conditions and from the literature review. In addition, from the results of characteristic testing, the most suitable processing for each component of marine debris. The management of mask waste is also adjusted to the applicable regulations in Indonesia.

**RESULTS AND DISCUSSION**

**The Amount of Marine Debris Before the Covid-19 Pandemic**

The volume of waste generated per day by residents and tourists is 1,547 liters per day at Parangtritis Beach. The volume of waste on holidays or national holidays is 7,364 liters per day. The waste management system in the Parangtritis Beach tourist area that has been carried out so far is considered not effective and efficient enough, it can be seen from the total waste generation has not been transported in one day to the final disposal. been implemented so far are

storage, collection, transportation of waste, and final disposal (Masjhoer 2017). At the beginning of 2021 during the New Year’s holiday, the amount of waste in the Parangtritis beach area reached 35 tons. This is because tourist objects that blend with nature or outdoors are in demand by tourists during the current Covid-19 pandemic. People who have been at home for a long time due to activity restrictions require refreshing. In addition, the difference in the categorization of waste after Covid is dominated by mask wastes from tourists.

**Marine Debris Generation and Composition**

Fig. 2 shows the generation for each transect location for sampling waste generation. The highest waste generation was found at location 5 with a value of 1.4 kg.m<sup>-2</sup>.day. L1 to L5 indicates the sampling location. Furthermore, the transect is divided into five transect installation areas with a distance between transects of 20 m. Then five sub-transects were randomly selected on each transect to be used as sampling areas. The average marine debris generation is 0.9 kg.m<sup>-2</sup>.day<sup>-1</sup>. The composition of the waste found along the coastline is primarily plastic, and only 32.54% (w/w) is included in biodegradable organic waste (Fig. 3). Another

Table 1: Examples of waste included in the composition of marine debris in Yogyakarta.

Component	Example
PET	Bottle Plastic
PE	Plastic Bags, Plastic Wrap, Plastic Packaging Waste, PE Rope
Other Plastic	Pipes, Windowsills, Toys, Automotive Components.
Biodegradable Organic Waste	Food, Leaf
Mask	N95 and Medical Masks

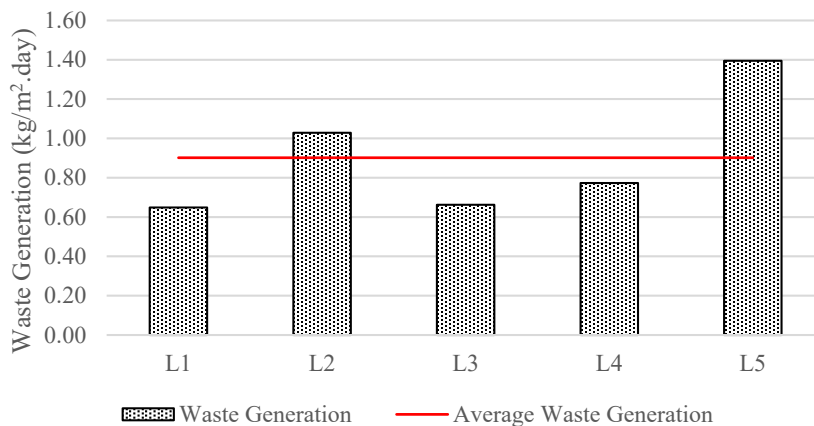


Fig. 2: The generation of marine debris during the COVID-19 pandemic at Parangtritis Beach, Yogyakarta.

finding regarding waste composition by counting pieces of waste at Parangkritis Beach is dominated by degradable waste such as wood, coconut shells, leaves, flower flakes (Mardiatno & Wiratama 2021). A new type of waste that will be a challenge during a pandemic is personal protective equipment, especially masks. It can be seen that the average mask waste is 5.14% (w/w).

To reduce and prevent the spread of COVID-19, one of the health protocols that must be carried out while traveling is the use of masks. Disposable masks can be one of the media for the spread of COVID-19; they must be appropriately managed. The Ministry of Environment & Forestry, Indonesia, issued Circular Letter Number SE.2/MENLHK/PSLB3/PLB.3/3/2020 concerning Management of Infectious Waste and Household Waste from Handling Corona Virus Disease (COVID-19), including guidelines for managing single masks wear. In general, disposable face masks used during the pandemic are made of non-renewable petroleum-based polymers that are not biodegradable, are harmful to the environment, and cause health problems (Dharmaraj et al. 2021). Medical mask waste and N95 masks are usually made of polypropylene (Jain et al. 2020). Mask in COVID-19 pandemic is categorized as infectious waste. If the Government has provided a special dropbox for masks in public spaces, the public can dispose of the disposable masks in the particular mask bins that have been provided. The lack of storage facilities can also cause tourists to throw masks carelessly. Fig. 3 shows the condition of mask waste that is thrown carelessly at the Parangkritis Beach location. After determining sample points and transects for Marine Debris Monitoring, we then proceed with waste identification as shown in Fig. 3. The process of identification and categorization of waste types by looking at the categories of types of waste generated during the pandemic, namely the process of sorting waste by type.

### Characteristics of Marine Debris

Proximate analysis is a test that includes testing water content, ash content, and volatile materials. Waste samples measured proximate and calorific values were free from water and sand contamination. The highest water content test results were found in biodegradable organic waste, namely 67.43%. Meanwhile, the lowest plastic waste is 0-2.34%. Plastic is a polymer that has unique and extraordinary properties. The nature of plastic tends not to absorb water. When plastic is degraded in a distilled water environment with seawater, sodium chloride (NaCl) in seawater will stick to the plastic surface (Safaat, 2020). PET, PE, masks, and other plastic wastes tend to have a higher calorific value than biodegradable organic waste. The calorific value for mask waste has a value of  $21.14 \text{ MJ.kg}^{-1}$ . Meanwhile, PET and PE plastic waste has a higher heating value -  $34.6 \text{ MJ.kg}^{-1}$  and  $35.06 \text{ MJ.kg}^{-1}$ , respectively. Overall, plastic from marine debris has considerable potential if it is dry, where the calorific value can reach  $44 \text{ MJ.kg}^{-1}$  (Pietrelli et al. 2017). During the COVID-19 pandemic, plastic waste (including surgical masks) produced during the pandemic had a high calorific value than other ordinary fuels (Dharmaraj et al. 2021). PE waste and masks are waste made of polypropylene material. So, the characteristics are the same where the water is absent. The absence of water tends to provide a high calorific value (Jain et al. 2020).

The density of waste data is needed to plan waste management systems, such as storage, transportation, and disposal. The density of waste from each type of waste shows varying results. According to Tchobanoglous & Vigil (1993), plastic waste usually has a density of  $64 \text{ kg.m}^{-3}$  (Tchobanoglous & Vigil, 1993). This is quite different from our findings in coastal areas where the density of plastic waste is more significant, namely between  $119.68\text{-}288.1 \text{ kg.m}^{-3}$ ; it is estimated that the plastic waste mixes with sand and seawater,

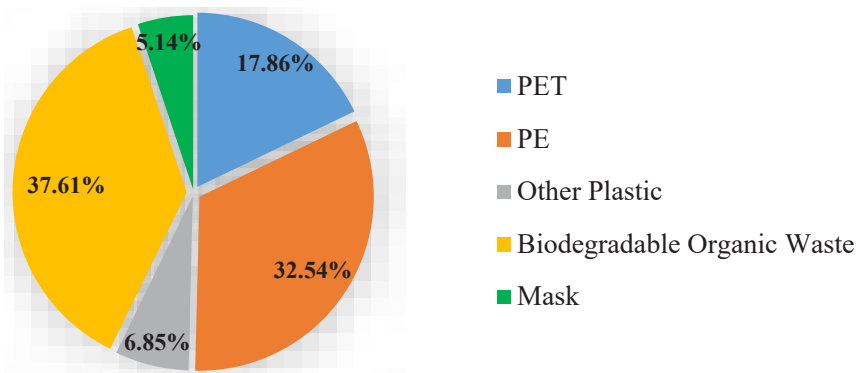


Fig. 3: The composition of marine debris during the COVID-19 pandemic at Parangkritis Beach, Yogyakarta.



the density increases. Sticky sand in plastic waste tends to be challenging to clean.

### Marine Debris Management

The urban waste management policy issued by the Ministry of Public Works and Public Housing in Indonesia is in accordance with SNI 3242:2008. Marine debris waste management operational engineering diagram can be seen in Fig. 5. Waste management is integral and integrated into a chain with a continuous sequence, namely: storage/container, collection, transfer, transportation, and disposal/processing.

Sorting and recycling activities are carried out as much as possible from the collection to the final disposal of the waste. As previously discussed, the waste management operational

system includes a waste processing and processing subsystem, which needs to be developed in stages by considering processing that relies on reuse, either directly, as raw materials or as an energy source. Removal of waste into the ground accompanied by backfilling is known as landfill. A sanitary landfill is a landfilling method whose application pays attention to environmental sanitation aspects.

### Thermal Gravimetric Analysis (TGA)

The decomposition temperature test was carried out by thermogravimetry (Fig. 6). The PET, PE, and mask waste undergo one-stage decomposition, namely in the temperature range of 260-550 °C. This temperature is quite good because it is not too high for the pyrolysis process. The ther-



Fig. 4: Existing condition of mask waste management at Prarangtritis Beach, Yogyakarta during the COVID-19 pandemic.



mal process in PE waste starts at a temperature of 371.51°C. Considerable polymer intermolecular bonds are broken due to increased temperature and are also assisted by radicals resulting from breaking intermolecular bonds (Wati et al. 2018). Sorum et al. state that the thermal degradation of PE occurs at 350-500°C, which is related to the degradation of the released hydrocarbons and becomes volatile (Sorum et al. 2001). In contrast to PE waste, the amount of PET waste residue tends to be higher at 12.95%. The thermal degradation process of PET follows ester link random scission, which results in the formation of oligomers (Lecomte & Ligat 2006). The initial degradation of PET may be due to some volatile impurities such as diethylene glycol (Dimitrov et al. 2013). Overall, the degradation process can cause the thermal degradation properties of plastic waste in coastal areas by seawater and UV radiation (Iñiguez et al. 2018). The mask waste appears to have a different graphic than PET and PE. Garbage masks change at a temperature

of 350-490°C. This value is similar to the study of Jung et al. (2021), which showed the primary degradation of the mask was at a temperature of around 330°C and ended up at 495 °C (Jung et al. 2021). Combustion of the mask with N<sub>2</sub> gas by pyrolysis allows the existence of inorganic compounds of Fe primarily and small amounts of Zn, Ti, Ca, and Mn (Jung et al. 2021).

### Marine Debris Management

In the results of interviews with 50 Parangtritis Beach tourists who are aware of and dispose of in their place only 16 visitors (32%), 22% or 46% throw garbage in careless places and ditches (Sujatmiko 2009). For this reason, the effort to solve the waste management problem that the Bantul Regency Government has carried out is to encourage community participation in solving environmental problems is to apply a waste bank. The solution offered to solve environmental problems in Gumuk Pasir (Parangtritis Beach) is creating

Table 2: Characteristics of marine debris for each component.

Component	Water Content	Volatile Matter	Fix Carbon	Ash Content	Caloric Value (MJ/kg)
PET	2.34%	95.20%	1.35%	1.11%	34.60
PE	0.00%	99.30%	0.66%	0.04%	35.06
Other Plastic	1.19%	94.20%	2.67%	1.94%	30.34
Biodegradable Organic Waste	67.43%	29.20%	1.89%	1.48%	9.17
Mask	0.00%	100.00%	0.00%	0.00%	21.13

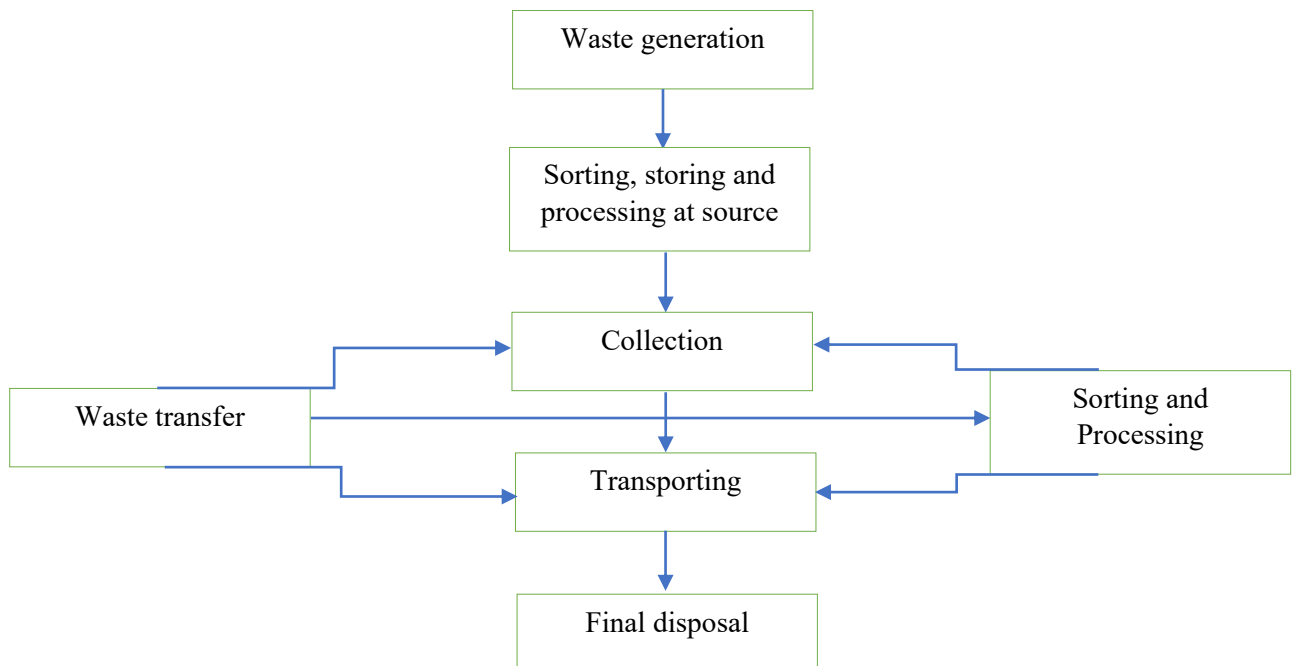


Fig. 5: Waste management operational engineering diagram.

the G-Fly Garbage Bank, which has a solopreneur concept by utilizing Black Soldier Fly larvae (Lisnawati et al. 2019). The utilization of BSF larvae was fed to marine fish as a substitute for traditional feed. The fish growth response was maximal when 25% or fewer BSF larvae were replaced with traditional feed (Cummins et al. 2017). Processing with futuristic BSF can support the basis of waste into biodiesel (Raksasat et al. 2021).

Plastic waste can be processed by recycling, and some types of inorganic waste that are not recycled are sent to waste collectors. Plastic waste can be focused on minimizing efforts. Continue and strengthen plastic restriction policies. According to Kuo & Huang marine debris, management can be done by strengthening plastic restriction policies, promoting marine environmental education, recycling fishing gear, and converting waste into energy (Kuo & Huang 2014). Currently, in Yogyakarta, there is still no policy on the use of single-use plastic. In Indonesia, several local governments have issued policies on using single-use plastic in Indonesia, such as Bali and Jakarta (Suryawan et al. 2021). Plastic waste recycling can be done through crafts such as flowerpots from used PET bottles, key chains, plastic bags, wallets, room decorations, and tablecloths. Waste that is not recycled will be sent to the garbage collector. Plastic waste with quality that cannot be recycled as handicraft products can be processed into refuse-derived fuel (RDF) fuel sources because it has a high calorific value than other waste materials. The mask waste is disposed of in the domestic trash after being crushed and wrapped in a tight plastic bag. In addition, if the Government has provided a dropbox for masks in public spaces, the public can dispose of the disposable masks in the mask bins that have been provided. The result of mask waste is recommended to be treated by thermal means to eliminate infectious properties. The processing that can be applied

is also the pyrolysis process, allowing the mask waste to energy.

## CONCLUSIONS

The average generation of marine debris based on the transect method is  $0.9 \text{ kg/m}^2 \cdot \text{day}$ . Meanwhile, the amount of waste is dominated by plastic types (PE, PET, and others), including masks. The amount of mask waste is 5.14%, which was not found before the pandemic condition. The characteristics of marine debris for PET, PE, other plastics, and masks have a high calorific value, making it possible to use a thermal process. The TGA thermal analysis process shows that PET, PE, and mask waste decomposes at a temperature of  $550^\circ\text{C}$ . Meanwhile, the existing biodegradable organic waste management is carried out using BSF, and plastic waste can be recycled into handicraft products. Meanwhile, plastic waste that cannot be recycled and mask waste must be treated with a thermal process.

## ACKNOWLEDGEMENT

This research was implemented and fully supported by the Japan Society for The Promotion of Science and Indonesia Directorate General of Research, Technology and Higher

Table 3: The density of marine debris for each component.

Component	Density [ $\text{kg}\cdot\text{m}^{-3}$ ]
PET	288.1
PE	267.84
Other Plastic	119.68
Biodegradable Organic Waste	317.6
Medical Mask	222.4

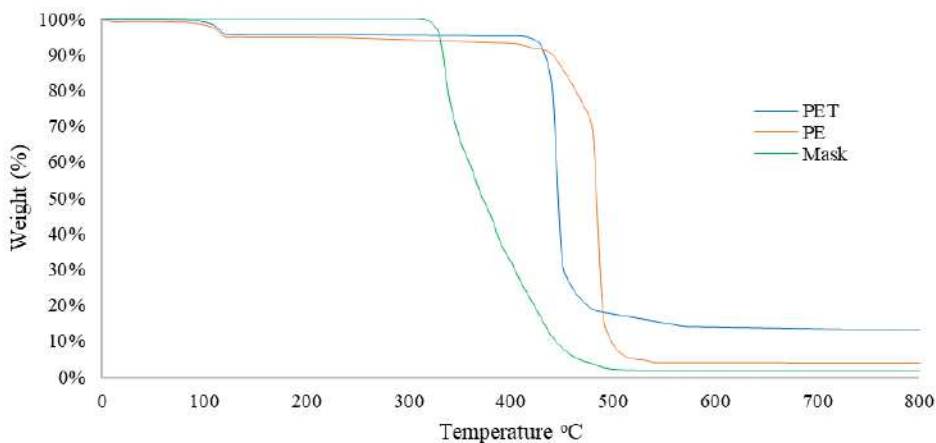


Fig. 6: Thermogravimetric analysis of marine debris for PET, PE, and mask.

Education (JSPS/DG-RSTHE), through a Bilateral Joint Research Projects 2019-2022 between Universitas Pertamina, Indonesia and Toyohashi University of Technology, Japan.

## REFERENCES

- Cordova, M.R., Nurhati, I.S., Riani, E., Nurhasanah, M. and Iswari, M.Y. 2021. Unprecedented plastic-made personal protective equipment (PPE) debris in river outlets in Jakarta Bay during COVID-19 pandemic. *Chemosphere*, 268: 129360. <https://doi.org/10.1016/j.chemosphere.2020.129360>
- Cummins, V.C., Rawles, S.D., Thompson, K.R., Velasquez, A., Kobayashi, Y., Hager, J. and Webster, C.D. 2017. Evaluation of black soldier fly (*Hermetia illucens*) larvae meal as a partial or total replacement of marine fish meal in practical diets for Pacific white shrimp (*Litopenaeus vannamei*). *Aquaculture*, 473: 337-344. <https://doi.org/10.1016/j.aquaculture.2017.02.022>
- Dharmaraj, S., Ashokkumar, V., Hariharan, S., Manibharathi, A., Show, P.L., Chong, C.T. and Ngamcharussrivichai, C. 2021. The COVID-19 pandemic face mask waste: A blooming threat to the marine environment. *Chemosphere*, 272: 129601. <https://doi.org/10.1016/j.chemosphere.2021.129601>
- Dimitrov, N., Kratofil Krehula, L., Pti ek Siro i, A. and Hrnjak-Murgi, Z. 2013. Analysis of recycled PET bottle products by pyrolysis-gas chromatography. *Polym. Degrad. Stability*, 98(5): 972-979. <https://doi.org/10.1016/j.polymdegradstab.2013.02.013>
- Google Map. 2021. Pantai Prangkritis. <https://www.google.com/maps/place/Kretek,+Kec.+Kretek,+Bantul,+Daerah+Istimewa+Yogyakarta/@-8.0250633,110.3280356,16z/data=!4m5!3m4!1s0x2e7b0069cad-bfcaf:0x4027a76e352fc80!8m2!3d-7.9921238!4d110.2972911?hl=id>
- Hidayanti, C., Setiadi, H. and Rizqihandari, N. 2020. The pattern of visiting restaurants in Glagah Beach, Kulon Progo Regency, Yogyakarta. *IOP Conf. Ser. Earth Environ. Sci.*, 561: 12009. <https://doi.org/10.1088/1755-1315/561/1/012009>
- Iñiguez, M.E., Conesa, J.A. and Fullana, A. 2018. Recyclability of four types of plastics exposed to UV irradiation in a marine environment. *Waste Manag.*, 79: 339-345. <https://doi.org/10.1016/j.wasman.2018.08.006>
- Jain, S., Yadav Lamba, B., Kumar, S. and Singh, D. 2020. Strategy for repurposing of disposed PPE kits by the production of biofuel: Pressing priority amidst COVID-19 pandemic. *Biofuels*, 30: 1-5. <https://doi.org/10.1080/17597269.2020.1797350>
- Jambeck, J., Geyer, R., Wilcox, C., Siegler, T.R., Perryman, M., Andrady, A., Narayan, R. and Law, K. L. 2015. The ocean. *Marine Pollut.*, 347(6223): 768.
- Jung, S., Lee, S., Dou, X. and Kwon, E.E. 2021. Valorization of disposable COVID-19 mask through the thermochemical process. *Chem. Eng. J.*, 405: 126658. <https://doi.org/10.1016/j.cej.2020.126658>
- Kuo, F.J. and Huang, H.W. 2014. Strategy for mitigation of marine debris: Analysis of sources and composition of marine debris in northern Taiwan. *Marine Pollut. Bull.*, 83(1): 70-78. <https://doi.org/10.1016/j.marpolbul.2014.04.019>
- Lecomte, H.A. and Liggat, J.J. 2006. Degradation mechanism of diethylene glycol units in a terephthalate polymer. *Polym. Degrad. Stab.*, 91(4): 681-689. <https://doi.org/10.1016/j.polymdegradstab.2005.05.028>
- Lisnawati, L., Agustina, A. and Dina Azzahra, S. 2019. G-Fly: Sociopreneur concept in waste treatment to improve the economy of the Gumuk Pasir community. *Sci. J. Stud. Reason. Res.*, 3(1): 64-75.
- Mardiarto, D. and Wiratama, H. 2021. Spatiotemporal analysis of marine debris existence in Parangtritis Coastal Area, Yogyakarta, Indonesia. *J Fish. Marine Res.*, 5(1): 14. <https://doi.org/10.21776/Ub.Jf-mr.2021.005.01.14>
- Masjhoer, J. M. 2017. Study of waste management in Parangtritis tourism area, Bantul Regency. *J. Tour.*, 6: 41-62
- Pietrelli, L., Poeta, G., Battisti, C. and Sighicelli, M. 2017. Characterization of plastic beach debris finalized to its removal: A proposal for a recycling scheme. *Environ. Sci. Pollut. Res.*, 24(19): 16536-16542. <https://doi.org/10.1007/s11356-017-9440-4>
- Raksasat, R., Kiatkittipong, K., Kiatkittipong, W., Wong, C.Y., Lam, M.K., Ho, Y.C., Oh, W.D., Suryawan, I.W.K. and Lim, J.W. 2021. Blended sewage sludge-palm kernel expeller to enhance the palatability of black soldier fly larvae for biodiesel production. *Processes*, 9(2): 1-13. <https://doi.org/10.3390/pr9020297>
- Safaat, M. 2020. Potential of metal oxides as photocatalysts for plastic degradation in seawater. *Oseana*, 45(1): 40-58. <https://doi.org/10.14203/oseana.2020.vol.45no.1.54>
- Secretariat of the Convention on Biological Diversity (SCBD) 2016. Marine debris: Understanding, Preventing and Mitigating the Significant Adverse Impacts On Marine and Coastal Biodiversity. SCBD.
- Shidiq Darajat, A. and Susilowati, M.H.D. 2018. Physical and facilities factors influencing tourist distribution in Bantul Regency, Special Region of Yogyakarta. *E3S Web Conf.*, 73: <https://doi.org/10.1051/e3sconf/20187303002>
- SNI 3242:2008 Concerning Waste Management in Settlement.
- Sørum, L., Grønli, M.G. and Hustad, J.E. 2001. Pyrolysis characteristics and kinetics of municipal solid wastes. *Fuel*, 80(9): 1217-1227. [https://doi.org/10.1016/S0016-2361\(00\)00218-0](https://doi.org/10.1016/S0016-2361(00)00218-0)
- Sujatmiko. 2009. Study of Groundwater Management in Parangtritis Tourism Area, Bantul Regency, Yogyakarta. Universitas Diponegoro.
- Suryawan, I. W. K., Rahman, A., Septiariva, I. Y., Suhardono, S. and Wijaya, I. M. W. 2021. Life Cycle Assessment of Solid Waste Generation During and Before Pandemic of Covid-19 in Bali Province. *Journal of Sustainability Science and Management*, 16(1): 11-21. <https://doi.org/10.46754/jssm.2021.01.002>
- Suryawan, I.W.K., Sarwono, A., Septiariva, I.Y. and Lee, C.H. 2021. Evaluating marine debris trends and the potential of incineration in the context of the COVID-19 pandemic in Southern Bali, Indonesia. *J. Fis. Marine Sci.*, 13(1): 111.
- Tchobanoglous, G. and Vigil, S.A. 1993. *Integrated solid waste Management Engineering Principles and Management*. McGraw-Hill, NY.
- Wati, R., Wardana, I., Winarto, W., Sukarni, S. and Puspitasari, P. 2018. Effect of Addition of MnFe2O4 Nanocatalyst on HDPE Plastic Waste Pyrolysis Process. *Journal of Mechanical Engineering*, 9(3): 221-225. <https://doi.org/10.21776/ub.jrm.2018.009.03.9>
- Wijayanti, A. and Damanik, J. 2019. Analysis of the tourist experience of management of a heritage tourism product: A case study of the Sultan Palace of Yogyakarta, Indonesia. *J.Heritage Tour.*, 14(2): 166-177. <https://doi.org/10.1080/1743873X.2018.1494182>



# Applications of Microbial Fuel Cell Technology and Strategies to Boost Bioreactor Performance

Quratulain Maqsood\*, Esha Ameen\*\*, Muhammada Mahnoor\*\*\*, Aleena Sumrin\*, Muhammad Waseem Akhtar\*\*\*, Riya Bhattacharya\*\*\*\* and Debajyoti Bose\*\*\*\*†

\*Centre for Applied Molecular Biology, University of the Punjab, Lahore, Pakistan

\*\*Department of Molecular Biology & Molecular Genetics, University of the Punjab, Lahore, Pakistan

\*\*\*Department of Rehabilitation Sciences, Akhtar Saeed Medical & Dental College Lahore, Pakistan

\*\*\*\* School of Biotechnology, Faculty of Applied Sciences & Biotechnology, Shoolini University of Biotechnology and Management Sciences, Solan, Himachal Pradesh, India

†Corresponding author: Debajyoti Bose: debajyoti1024@gmail.com

Nat. Env. & Poll. Tech.  
Website: [www.neptjournal.com](http://www.neptjournal.com)

Received: 21-09-2021

Revised: 02-12-2021

Accepted: 17-12-2021

## Key Words:

Microbial fuel cell  
Bioenergy  
Biosensors  
Electricity

## ABSTRACT

Renewable energy technologies are developing day by day. One of the novel renewable energy technologies is microbial fuel cells (MFC). MFCs are eco-friendly as it uses electroactive bacteria (exoelectrogens) to generate electricity by using organic and inorganic waste from the wastewater. Electricity generation and wastewater treatment are its primary applications. The construction of MFC consists of the electrodes which may be modified by using nanoparticles (gold and iron oxide) or pre-treatment methods (sonication and autoclave sterilization). This technology is further studied for the detection and reduction of toxic heavy metals in wastewater. The MFCs are also modified into microbial electrolysis cells to make biofuel such as hydrogen. The present review is based on the applications of the MFC, key challenges, and modification strategies.

## INTRODUCTION

These days the non-renewable energy resources are depleting rapidly which is causing environmental pollution. This problem can be solved by converting organic/inorganic waste energy into chemical energy or other forms of energy (Alipanahi et al. 2019). Several purification methods along with anaerobic fermentation are used to produce hydrogen and methane biofuels. Their sustainability depends upon the methods of renewable energy technologies (Bhowmick et al. 2019). The MFC has intrigued the researchers because it can generate bioenergy and treat wastewater simultaneously. It uses the metabolism of the microbes for energy generation and treatment of wastewater. It is also being used for bioremediation (Chandrasekhar et al. 2018).

MFCs are bioelectrochemical cells having an anode chamber (containing microorganisms and anolyte under anaerobic conditions) and a cathode chamber (containing an electron acceptor and a catalyst under aerobic/anaerobic conditions), connected by the PEM (proton exchange membrane) e.g., Nafion. The microorganisms at the anode chamber are called exoelectrogens which act as a biocatalyst.

The electrons are produced at the anode and transferred to the cathode through an electrical connection. The electrons react with protons and oxygen to release water (Cui et al. 2019). The exoelectrogen regulates the electrons in their outer membranes by themselves at the anode and transfers them to the cathode where they are reduced by the electron acceptors (oxygen). The most common use of MFC technology is electricity production. The electrons at the anode are produced by oxidation of organic matter which initiates a low redox potential and reduction at the electron acceptor of the cathode creates a high redox potential. The potential difference directs the electrons from the anode to the cathode to generate electricity (Das 2018).

The MFCs are constructed in different ways. Some use the pure culture (e.g., *G. sulfurreducens* and *Shewanella oneidensis*) and others use mixed culture (primary wastewater) for the electric current generation (Das & Ghangrekar 2020). The anode chamber is modified with nanoparticles or microbial genes to enhance the MFC performances. For instance, N-doped carbon nanoparticles are used which raises the power density to three times. On the other hand, *S. oneidensis* MR-1 with a flavin biosynthesis pathway of

*B. subtilis* raised the power output to 13 times (Delord et al. 2017). This technology operates on the biodegradation of the organic compounds of the wastewater. Hydrogen is produced by the modification of MFC into microbial electrolysis cells (MEC). The voltage is supplied by MFC to the MEC for hydrogen production. In this review article, applications of MFCs and improvement techniques are analyzed critically. The applications of the MFC include electricity production, bioremediation, treatment of wastewater, biosensors, and production of hydrogen (Do et al. 2020).

## THE MOLECULAR MACHINERY OF EXOELECTROGENS

The features that make the MFC technology prominent as the non-renewable technology are the use of molecular machinery of bacteria (biomolecules). These molecules transport the electrons between the anode and the cathode. For this purpose, the molecular machinery of *Geobacter* spp. and *Shewanella* spp. are widely studied. Extracellular electron transfer (EET) mechanisms have two types i.e. mediated electron transfer (MET) and direct electron transfer (DET) mechanisms are observed in these bacteria (ElMekawy et al. 2018). The most analyzed exoelectrogen in *G. sulfurreducens*. It creates a layer of biofilm with riboflavin secretion on the surface of the electrode and uses it as a substrate. With the help of the MET mechanism, the riboflavin reacts with c-type cytochromes (OM c-Cysts) in the outer membrane

to transport electrons to the surface of the electrode (Ezziat et al. 2019). *Shewanella oneidensis* also act as an exoelectrogen. It has nanowires-like structures extended from the periplasmic space and multiheme cytochromes in the outer membrane containing vesicles. This bacterium secretes riboflavin (RF) and flavin mononucleotide (FMN) which causes the reduction of many-electron acceptors. RF and FMN are the cofactors for OmcA and MtrC, respectively. The complexes of secretion and cofactor drive the transfer of electrons between electrodes (Flimban et al. 2019).

## MFCS FOR ELECTRICITY GENERATION

The MFC is mainly employed to produce electricity. The modification in the electrodes using metal catalysts can be done to increase the current density. In the first step, the exoelectrogens adapt to the anode surface to create a biofilm of 30  $\mu\text{m}$ -50  $\mu\text{m}$  thickness. The biofilm formation is further enhanced by the adhesins and components of extracellular matrix assembly and by cytochromes. The performance of MFC is amplified by using proper bacterial culture and substrate (Gajda et al. 2018a).

The electrons are transported between both electrode surfaces through an electrical connection where they bind with protons and an electron acceptor. Water produces with an oxygen electron acceptor at the cathode with a voltage of 0.805 V. The rate at which oxygen is reduced is increased by the platinum catalyst. For reducing oxygen, microorganisms

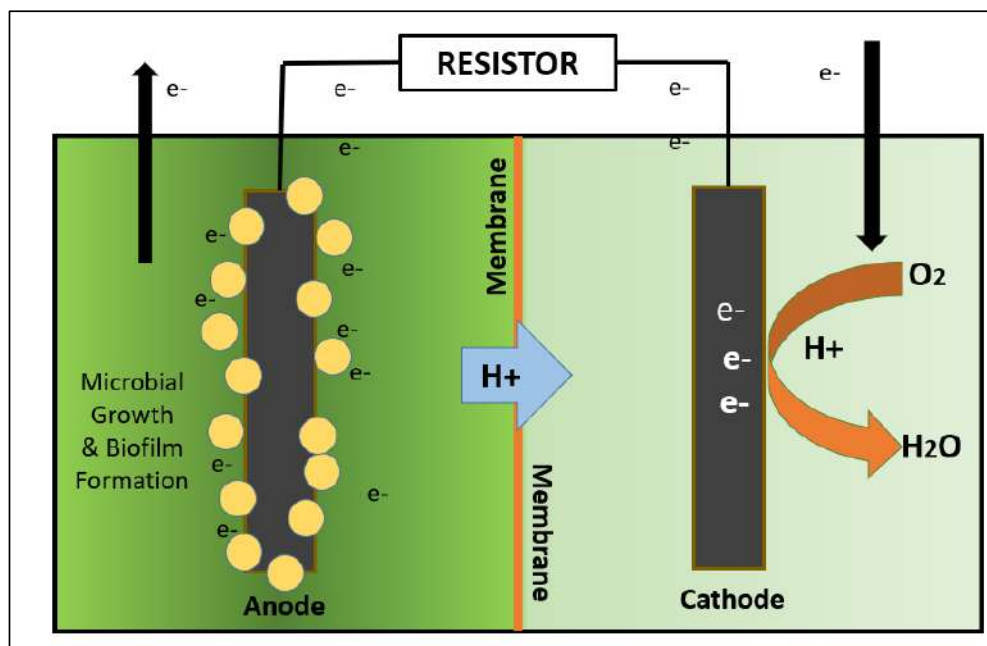


Fig. 1: In a double-chambered MFC, microbial growth takes place on the anode, as microbes consume organic matter, they donate electrons, which then travel the electrical circuit, and the reaction is completed at the cathode (Bose et al. 2018a).



can also be used and ferricyanide and potassium permanganate can act as electron acceptors (Gajda et al. 2018b). Fig. 1 shows some features of double-chambered MFC; for such systems, it is important to maintain the proper functioning via the selection of exoelectrogens, substrate, and electron acceptors. The community structure of microbes is affected by substrate type. For instance, *Geobacter* and *Shewanella* spp. only use acetate for electricity generation (Gajda et al. 2018).

Electrodes are modified with metal catalyst/nanoparticles/chemicals to raise the outputs. The cathode is also modified to alternate the expensive platinum catalyst with a cheaper one having the same properties. The research showed that these modifications lessen the internal resistance and start-up time of the system. The anode is modified with nitrogen-doped electrodes, heat-treated electrodes or gold nanoparticles, graphene, and carbon nanotubes to enhance the output performance, e.g. CNT-gold-titania nanocomposites ameliorate the MFC performance (Goswami & Mishra 2018).

The EET mechanism is boosted by using nitrogen-doped carbon nanoparticles coated on carbon cloth electrodes. *Shewanella oneidensis* MR-1 is inoculated in the two-chamber MFC. It increases the rate of electron transfer and power density by the absorption of flavins secreted by the organism. The studies show that the anode is sprinkled with the CNT powder which enhances the *G. sulfurreducens* biofilm

growth to decrease the internal resistance and the start-up time (Ivars-Barceló et al. 2018). The reduced start-up time promotes adherence of bacteria to the electrode. The carbon nanotube anode in the double-chambered MFC increases the power density up to 4 times as compared to the plain carbon cloth anode. It is suggested that ferric oxide shows a great affinity for c-type cytochromes in the outer membrane of *Shewanella*. The modification of electrodes with iron oxide increases bacterial growth and enhances the EET mechanism and metabolism of the biofilm (Jadhav et al. 2017).

## MFCs FOR WASTEWATER TREATMENT

In wastewater treatment, disposal of waste and recycling of polluted water with precautions are done. The industries and urban areas release polluted wastewater which can be treated the MFC technology in single-chambered MFCs as shown in Fig. 2. The wastewater has several compounds which are used as a substrate for bacterial growth. The chocolate industry or palm oil mill effluent (POME) releases wastewater which at as the biocatalysts for the oxidation of the substrate. This water is used as catholyte and electron acceptors. The following portion of this article deals with the efficiency of MFCs in the treatment of wastewater (Jatoi et al. 2021).

SPW is used to estimate the MFC efficiency for wastewater treatment. After operating MFC for 140 days, 98%

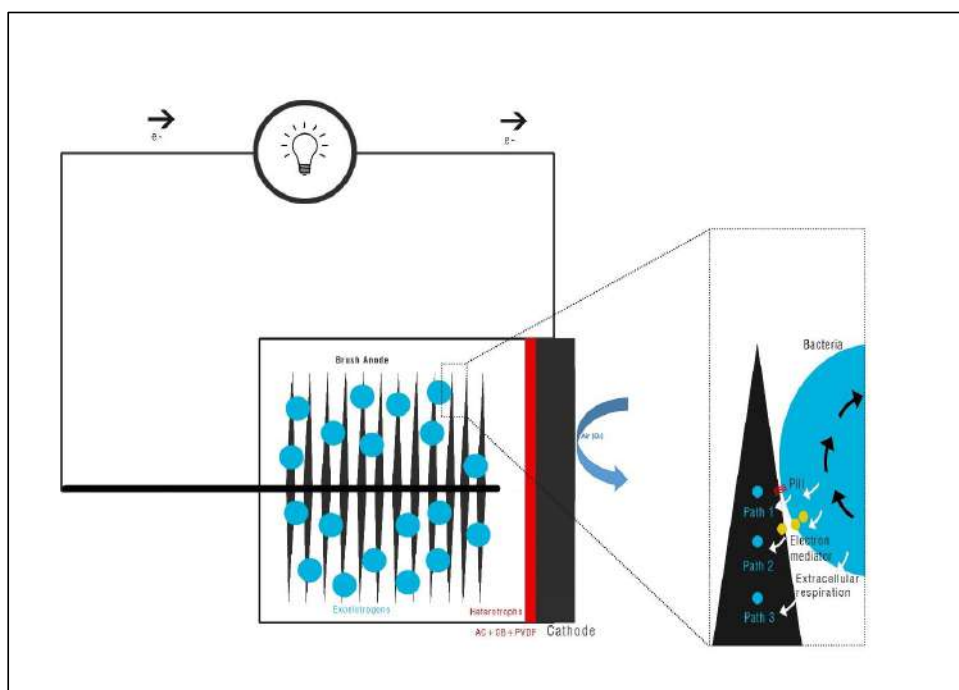


Fig. 2: Schematics of single chambered MFC, in such a system brush anodes, are used for microbial growth with air cathodes, having one side facing wastewater in the system and the other side exposed to the outside air (Bose et al. 2019b).

COD and 91% ammonia-nitrogen were removed. Likewise, a double-chambered MFC treated chocolate. It removed 75% COD, 65% BOD, and 68% total solid in batch mode. Lignocellulosic biomass cannot be removed by conventional techniques. Huang and Logan produced electricity in single-chambered MFC (sMFC) by using paper recycling wastewater (Jiang et al. 2018). After operating for 3 weeks, 76% COD and 96% cellulose were removed. This showed the degradation of lignocelluloses into smaller sugars by the bacterial community (Kaur et al. 2020).

The treatment of brewery wastewater was also performed by MFC. It had  $5000 \text{ mg.L}^{-1}$  COD and many sugars. These sugars donate electrons to MFC. For instance, the operation of air cathode sMFC at different concentrations of wastewater in a fed-batch removed COD differently. The low COD was removed from wastewater with less COD value. 58% and 98% COD were removed from  $84 \text{ mg.L}^{-1}$  and  $1600 \text{ mg.L}^{-1}$  concentration, respectively (Khan et al. 2017). Likewise, sMFC at  $600 \text{ mg.L}^{-1}$ - $660 \text{ mg.L}^{-1}$  COD concentrations removed 43- 46% COD after 2.13 hours of hydraulic resistance

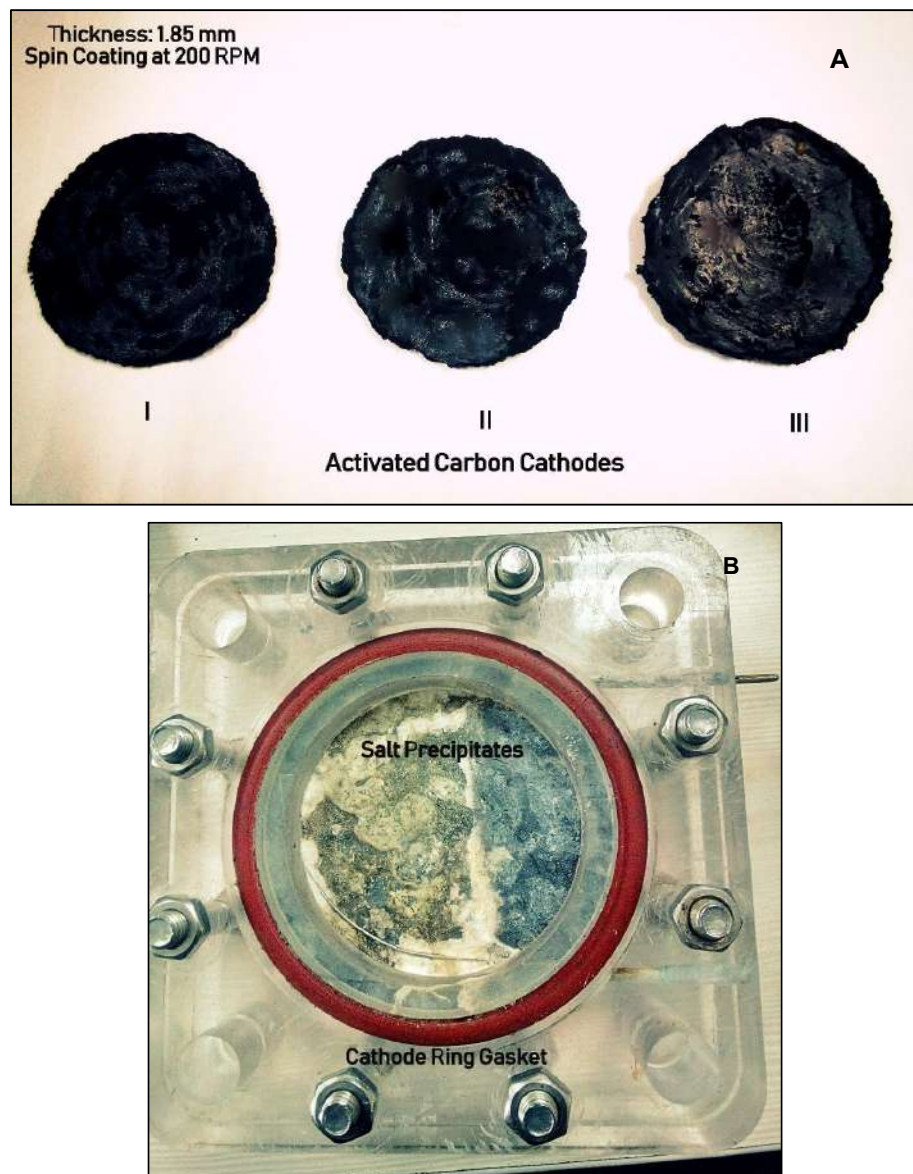


Fig. 3: (A) MFC Cathodes prepare from Activated carbon by a single-step phase inversion method (B) Fouling of MFC cathodes after fifteen full cycles (Adopted from Bose et al. 2018c).

in continuous mode. Ahn and Logan worked on air-cathode sMFC to check the effect of two different temperatures on MFC i.e. ambient temperature ( $23 \pm 3^\circ\text{C}$ ) and mesophilic temperature ( $30 \pm 1^\circ\text{C}$ ). It showed that the mesophilic temperature increased the percentage of COD removal and its removal rate. The efficiency of fed-batch MFC to remove COD is 2.5 times higher than the continuous mode (Khudzari et al. 2018).

The toxicity and COD value are very high in the wastewaters of mills. For instance,  $16000\text{ mg.L}^{-1}$  COD and ca.  $86\text{ mg.L}^{-1}$  cyanide were observed in cassava mill effluent. Palm oil industries release palm oil mill effluent (POME) which has a COD value of  $50000\text{ mg.L}^{-1}$  and a BOD value of  $25000\text{ mg.L}^{-1}$ . POME was treated by Cheng et al. in an up-flow membrane-less MFC (UML-MFC) coupling MFC and UASB (up-flow anaerobic sludge blanket) reactors. It removed 96% and 94%, of COD and nitrogen, respectively (Kodali et al. 2018).

The power density of MFC is raised by using wastewater with a high COD value. But, when the concentration of substrate is high, it causes electrode fouling, leading to restriction and accumulation of salts and precipitates as shown in Fig. 3. And the cathode has fewer protons available. Due to this fouling, wastewaters dilutions are used to regulate the performance of the MFCs. In addition, some pre-treatment methods can enhance the performance of the MFCs (Kumar et al. 2018a). For instance, the methanogens, using organic compounds of wastewater to generate methane, are killed by autoclaving. A 5% power density increase was suggested by autoclaving. On the other hand, sonication was used to treat raw wastewater. It increased the power density up to 16% and COD removal up to 5%. Furthermore, COD can be removed from wastewater by stirring technique. Although these pre-treatment techniques increase energy generation, they cannot be used for upscaling (Kumar et al. 2018b).

Domestic wastewater is highly biodegradable and can produce energy from degradation. Therefore, it is used as a substrate in MFC to construct public toilets and to produce electricity. This is an eco-friendly construction. For instance, an air-cathode sMFC (system for struvite extraction) was employed for the treatment of human urine and extraction of struvite (natural fertilizer), simultaneously (Kumar et al. 2019a). The anaerobic sludge was added to the anode. The substrate i.e. human urine had yeast extract and tryptone, 0.5%, and 1%, respectively. At the first level, the power gain was  $14.32\text{ W.m}^{-3}$  then in the third level decreased to  $11.76\text{ W.m}^{-3}$ . Further, the modification technique was used to increase electricity production and struvite purification. The sea salts were inoculated along with the substrate (urine) raised the power output, COD removal, and struvite extraction by

10%, 16-18%, and 21-94%, respectively. Now, human feces are also being used for electricity production. For instance, fermented human feces wastewater was inoculated in the two-chamber MFC. After operating MFC for 190 h, it generated  $70.8\text{ mW.m}^{-2}$  power density and reduced 78% COD (Kumar et al. 2019b).

In the first five months, the MFC operation removed 75% COD which lasted for a year. Its performance can be enhanced up to 94% COD removal by using 10 external resistors. A 90-L MFC was manufactured by Dong et al. It produced energy itself for 180 days of operation by treating brewery wastewater. It was observed that diluted wastewater showed ~87% whereas real wastewater showed 85% COD removal. By all mentioned scaling up processes, the performance of MFC technology can be improved by treating wastewater and increasing electricity production (Liu et al. 2020).

## MFCs FOR BIOREMEDIATION OF SPECIFIC CONTAMINATIONS

The electrons are generated by exoelectrogens in the anode of MFC, which are transferred to the cathode where reduction occurs at the electron acceptor. The rate of reduction is ameliorated by a catalyst. The electron acceptors used in MFC have features such as high redox potential, faster kinetics, inexpensive, and easily available. For instance, the commonly used electron acceptor of MFC is oxygen. But different toxic elements either organic or inorganic can be employed as the electron acceptor as shown in Fig. 4. Such systems are called sediment-Microbial fuel cells or s-MFCs. In cathode, they are reduced to less toxic forms. For instance, metal ions, perchlorate, nitrobenzene, azo dyes, and nitrates are being used as electron acceptors (Mathuriya & Pant 2019).

Many heavy metals are used as the electrodes of MFCs for their removal and reduction to non-toxic forms. When the heavy metal is used at the anode, its certain concentration is inoculated to the anolyte and the electron acceptor of the cathode is made up of heavy metal with high redox potential. Several mechanisms are being employed in the MFC for the removal of toxic heavy metals. One of the mechanisms is biosorption (microprecipitation, complexation, chelation, and ion exchange) which separate the toxic heavy metal in the MFCs (Mian et al. 2019). This process is carried out with the help of the biomolecules (polysaccharides, proteins, and lipids) containing certain functional groups (amine, sulfate, carboxylate, hydroxyl, and phosphate) present in the anolyte. In addition, sulfide was removed by the processes such as oxidation, volatilization, and electrode adsorption (Neethu et al. 2019). Cadmium (Cd) and zinc (Zn) was removed by an air-cathode sMFC with efficiencies of 90% and 97%,

respectively. Furthermore, vanadium (V) was used as the electron acceptor at the cathode in a dual-chamber MFC for its toxic removal. After operating for 10 days, the fuel cell removed ca. 70% V at ca. 970 mW.m<sup>-2</sup> power density.

The textile industries use several dyes used to color the fabric. Every year, these fabric dyes produce a huge amount of wastewater containing toxic elements, recalcitrant, and carcinogenic compounds. These are compounds are polluting the environment heavily; hence, this wastewater should be treated before release. It is an eco-friendly replacement for the production of electricity and wastewater treatment. The microorganisms in MFC are used for the reduction of the dye by decolorization technique. This decolorization is carried out in the anaerobic conditions at the anode. For instance, the congo red dye split into the intermediates (aromatic amines) by breaking the azo bond. Further degradation takes place at the cathode abiotically (Palanisamy et al. 2019).

After operating for a single day, the congo red dye was decolorized 98% with the help of bioelectrodes of sMFC. The electrons at the anode are produced by the microorganisms and protons by PEM. The electrons are transferred to the cathode where they react with protons to degrade the azo bond. The aromatic amines are formed as decolorized products of degradation. In the MFC, the bioremediation of pentachloroethene (PCE) and trichloroethene (TCE) is done by using *Geobacter lovleyi* (dechlorinating microorganisms) and graphite electrodes. The optimum conditions for the degradation were 50°C and pH 6 for 0.52 mg.L-h<sup>-1</sup> and 0.36 mg.L-h<sup>-1</sup>. Moreover, a soluble U(VI) was reduced to an insoluble form by *Geobacter* species by using c-type cytochromes of the outer membrane. Likewise, this same process also occurs in *S. oneidensis* using c-type cytochromes. The reduction of chromium to a less toxic form i.e. Cr (VI) to Cr (III) is done at anaerobic biocathodes in MFCs to pro-

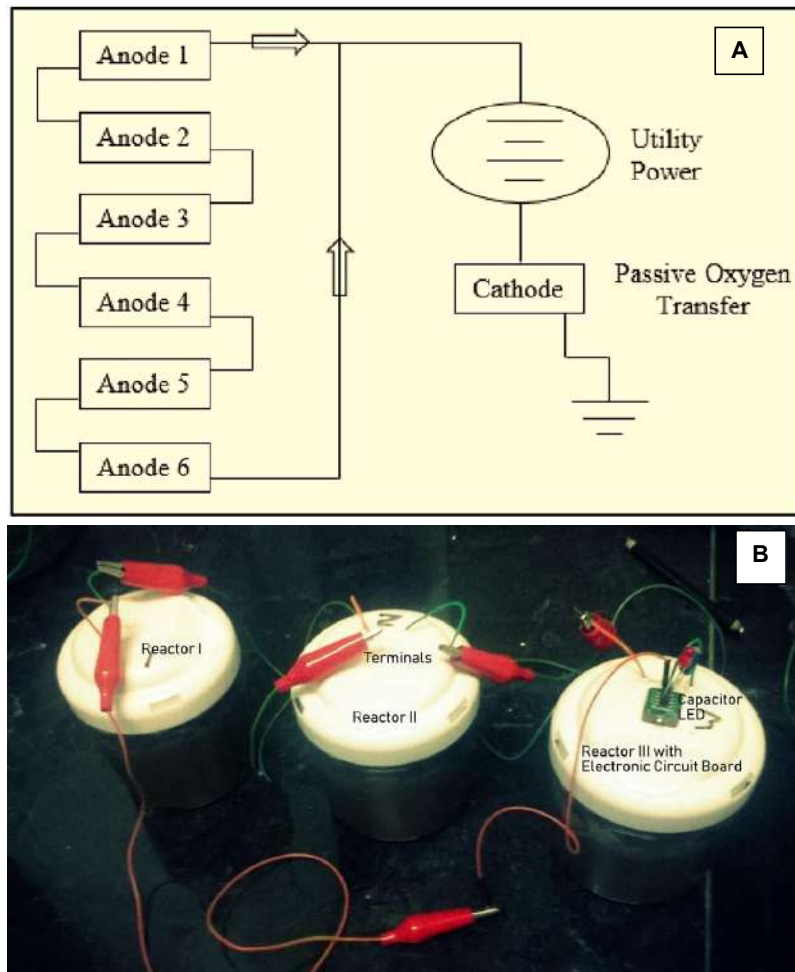


Fig. 4: (A) Schematic representation of s-MFC arrangement with multiple anodes and a single cathode (B) s-MFC reactors with contaminated soil sample connected to an electric circuit for power generation through bioremediation (Adopted from Bose et al. 2021d).



duce electricity (Qi et al. 2018).  $\text{Cr}(\text{OH})_3$  also precipitates during this process which raised the rate of reduction to  $19.7 \text{ mg}\cdot\text{L}^{-1}$ . The rate of reduction is increased in the aerobic condition at the cathode when *Shewanella oneidensis* MR-1 is a biocatalyst and lactate is a biomolecule. A recent 16S rRNA study suggested that a strain similar to *Klebsiella sp.* is able of removing 99.5% cyanide and ca. 88% COD from cyanide-containing wastewater (Rikame et al. 2018).

## MFCs AS BIOSENSORS

The MFC is now used as a biosensor for the detection of organic matter and toxic pollutants in the wastewaters. Usually, the transducers are used for the conversion of the energy of organic matter to the signals in the biosensors but MFC does not require transducers because MFC itself plays the role of a transducer. These biosensors use exoelectrogens which generate the signals in the anode (Bose et al. 2020e). The material of electrodes is used as transducers. The time span for the use of elements in the biosensor is enhanced by the biofilm formation of exoelectrogens (Sayed & Abm delkareem 2017).

The toxins are inoculated at the anode which changes the output voltage. The altered voltage is measured and considered as a detection signal. For instance, chromium is added to the anode which decreases the voltage because it causes growth inhibition of the exoelectrogens. Alternatively, acetate is added to the anode which increases the voltage because the growth of exoelectrogens is increased (Trapero et al. 2017). These sensors work on two mechanisms, i.e. flow-through and flow-by electrodes. The first mechanism circulates the water sample through the pores in the electrode, whereas the second mechanism moves the water sample parallel to the surface of the electrode. The MFC biosensor working in a flow-through mode enhances its sensitivity 40 folds by improving the ionic diffusion (Türk et al. 2018).

For the detection of toxicity, the MFC-based biosensors work in turn-off mode. The metabolism of the exoelectrogens is reduced because of the toxin concentration added to the anolyte which leads to the power output change. After detection, this toxicity is calculated by comparing the toxin concentration and electric signal output. Consequently, change in current (I) and inhibition ratio (IR) is measured. IR (inhibition ratio) is the amplitude of the output signal. The bioanodes are suggested to affect the toxic agent sensitivity in MFC biosensors. But both electrodes are modified to decrease the response time and amplify the capacity of detection. For instance, the potentiostat can be used to maintain the sensitivity of the MFC biosensor by optimizing the potential at the anode. The cathode working also influences the amplitude and the output signal precision.

## MICROBIAL ELECTROLYSIS CELLS FOR HYDROGEN PRODUCTION

A microbial electrolysis cell (MEC) is used for hydrogen gas production by using electricity. The MEC works on the same principle as MFC (Bose et al. 2020f). The electrons are produced at the anode by the exoelectrogens which react with protons and this reduction releases hydrogen gas. The voltage of 0.2 to 0.8 V is used for this reduction. MFC can generate such low voltage. The electrodes in MEC are made up of the same material as MFC (Wu et al. 2020). The platinum catalyst at the cathode can maintain the potential and catalyze hydrogen generation. All these reactions occur in an anaerobic environment which is favorable for methanogen growth.

The methane production contaminates the hydrogen gas and decreases the output. MEC produces more hydrogen than fermentation.  $0.05\text{--}1.05 \text{ mol}\cdot\text{H}_2\cdot\text{mol}\cdot\text{glycerol}^{-1}$  hydrogen is produced by fermentation and  $3.9 \text{ mol}\cdot\text{H}_2\cdot\text{mol}\cdot\text{glycerol}^{-1}$  by MEC. Sometimes, a single MFC generates an OCV of 0.5 V only because of the internal resistance, utilization of energy by bacteria, and high potential at the electrode. Hatzell et al. (2014) overcame this drawback by arranging a capacitor in a series configuration in the circuit which stops the voltage from reversing. This setup raises the hydrogen generation to 2.3 folds (Zhang et al. 2019).

The performance of MECs is limited by hydrogen utilization by methanogens (Regassa et al. 2021). To overcome this problem, the cathode is treated with oxygen or UV radiation which causes the inhibition of the methanogens. The cathode can be exposed to air which decreases 3.4% methane to 1%. The use of ultraviolet radiation confirmed 91% hydrogen concentration in the MEC. The antibiotics such as neomycin sulfate, 2-bromoethane sulfonate, 2-chloroethane sulfonate, and 8-aza-hypoxanthine also causes the inhibition of methanogens.

## OUTLOOK

MFCs are used as an eco-friendly technology for energy generation and wastewater treatment simultaneously. Organisms such as bacteria and algae have the potential for waste bioremediation (Arora et al. 2021). Different types of wastewaters can be used in MFC with bacteria, either as pure culture or mixed culture. Similar to how probiotics represent the larger domain of the bacteria along with the well-being of human beings (Iqbal et al. 2021), MFCs can utilize these microbes to reduce waste without increasing the carbon burden on the environment. The output performance of MFC is improved by reducing internal resistance, utilizing nanoparticles and genetically modified microorganisms, inoculating pre-treated



cultures, and lessening the start-up time. For instance, carbon paper anode coated with graphene nanocomposites reduces the start-up time and enhances the density of current up to 1800 mA.cm<sup>-2</sup>. This electricity is utilized to run electrical equipment. The MFC and anaerobic fermentation is used together to increase the removal efficiency of COD.

MFCs potentially reduce heavy metals. Heavy metals are used as anode and electron acceptors of the cathode. The biomolecules are used as anolytes and remove heavy metals up to 99.5%. The MFCs are also used as BOD/COD biosensors for the detection of toxicity in wastewater. The voltage change detects the presence of toxins. The sensitivity of an MFC biosensor is enhanced by using flow-through mode. MFC is altered to MEC to generate hydrogen. MECs' performance is limited by the hydrogen utilization by methanogens. The antibiotics and ultraviolet radiation treatment cause inhibition of those methanogens.

This technology is applied for many purposes, but still faces many challenges like maintaining the system for upscaling and providing inexpensive electrode elements. Another hurdle is choosing an electron acceptor for the cathode. Oxygen is mostly utilized as an electron acceptor but it can affect the metabolic activity of anaerobic bacteria. Platinum is widely employed for reducing oxygen, but it is a costly element. In addition, the reaction of platinum with the chemicals in the wastewater makes platinum poisonous, therefore, the platinum must be replaced with a better alternate for upscaling of MFCs.

## REFERENCES

- Arora, K., Kumar, P., Bose, D., Li, X. and Kulshrestha, S. 2021. Potential applications of algae in the biochemical and bioenergy sector. *Biotech.*, 11(6): 1-24.
- Alipanahi, R., Rahimnejad, M. and Najafpour, G. 2019. Improvement of sediment microbial fuel cell performances by design and application of power management systems. *International journal of hydrogen energy*, 44(31): 16965-16975.
- Bhowmick, G., Kibena-Pöldsepp, E., Matisen, L., Merisalu, M., Kook, M., Käärik, M. and Tammeveski, K. 2019. Multi-walled carbon nanotube and carbide-derived carbon supported metal phthalocyanines as cathode catalysts for microbial fuel cell applications. *Sustain. Energy Fuels*, 3(12): 3525-3537.
- Bose, D., Gopinath, M. and Vijay, P. 2018a. Sustainable power generation from wastewater sources using a microbial fuel cells. *Biofuels Bioprod. Bioref.*, 12(4): 559-576.
- Bose, D., Gopinath, M., Vijay, P., Sridharan, S., Rawat, R. and Bahuguna, R. 2019b. Bioelectricity generation and biofilm analysis from sewage sources using a microbial fuel cells. *Fuel*, 255: 115815.
- Bose, D., Dhawan, H., Kandpal, V., Vijay, P. and Gopinath, M. 2018c. Sustainable power generation from sewage and energy recovery from wastewater with variable resistance using a microbial fuel cells. *Enzyme Microb. Technol.*, 118: 92-101.
- Bose, D., Santra, M., Sanka, R.V.S.P. and Krishnakumar, B. 2021d. Bioremediation analysis of sediment microbial fuel cells for energy recovery from microbial activity in the soil. *Int. J. Energy Res.*, 45(4): 6436-6445.
- Bose, D., Mukherjee, A. and Mitra, G. 2020e. Energy recovery prospects of fuel cell technologies: sustainability and bioremediation. *Austr. J. Mech. Eng.*, 4: 1-13.
- Bose, D., Dey, A. and Banerjee, T. 2020f. Aspects of bioeconomy and microbial fuel cell technologies for sustainable development. *Sustain. Rec.*, 13(3): 107-118.
- Chandrasekhar, K., Kadier, A., Kumar, G., Nastro, R.A. and Jeevitha, V. 2018. *Challenges in Microbial Fuel Cell And Future Scope Microbial fuel cell* (pp. 483-499): Springer.
- Cui, Y., Lai, B. and Tang, X. 2019. Microbial fuel cell-based biosensors. *Biosensors*, 9(3): 92.
- Das, D. 2018. *Microbial Fuel Cell*. Springer, NY.
- Das, S. and Ghangrekar, M. 2020. Tungsten oxide as electrocatalyst for improved power generation and wastewater treatment in microbial fuel cells. *Environ. Technol.*, 41(19): 2546-2553.
- Delord, B., Neri, W., Bertaux, K., Derre, A., Ly, I., Mano, N. and Poulin, P. 2017. Carbon nanotube fiber mats for microbial fuel cell electrodes. *Bioresour. Technol.*, 243: 1227-1231.
- Do, M.H., Ngo, H.H., Guo, W., Chang, S.W., Nguyen, D.D., Liu, Y. and Kumar, M. 2020. Microbial fuel cell-based biosensor for online monitoring wastewater quality: A critical review. *Sci. Total Environ.*, 712: 135612.
- ElMekawy, A., Hegab, H., Pant, D. and Saint, C. 2018. Bio analytical applications of microbial fuel cell-based biosensors for onsite water quality monitoring. *J. Appl. Microbiol.*, 124(1): 302-313.
- Ezziat, L., Elabed, A., Ibsouda, S. and El Abed, S. 2019. Challenges of microbial fuel cell architecture on heavy metal recovery and removal from wastewater. *Front. Energy Res.*, 7: 10.
- Flimban, S.G., Ismail, I.M., Kim, T. and Oh, S.E. 2019. Overview of recent advancements in the microbial fuel cell from fundamentals to applications: Design, major elements, and scalability. *Energies*, 12(17): 3390.
- Gajda, I., Greenman, J. and Ieropoulos, I.A. 2018a. Recent advancements in real-world microbial fuel cell applications. *Curr. Opinion Electrochem.*, 11: 78-83.
- Gajda, I., Greenman, J., Santoro, C., Serov, A., Melhuish, C., Atanassov, P. and Ieropoulos, I. A. 2018b. Improved power and long-term performance of microbial fuel cell with Fe-NC catalyst in the air-breathing cathode. *Energy*, 144: 1073-1079.
- Gajda, I., Stinchcombe, A., Merino-Jimenez, I., Pasternak, G., Sanchez-Herranz, D., Greenman, J. and Ieropoulos, I.A. 2018. Miniaturized ceramic-based microbial fuel cell for efficient power generation from urine and stack development. *Front. Energy Res.*, 6: 84.
- Goswami, R. and Mishra, V. K. (2018). A review of design, operational conditions and applications of microbial fuel cells. *Biofuels*, 9(2): 203-220.
- Hatzell, K.B., Iwama, E., Ferris, A., Daffos, B., Urita, K., Tzedakis, T., Chauvet, F., Taberna, P.L., Gogotsi, Y. and Simon, P. 2014. Capacitive deionization concept based on suspension electrodes without ion exchange membranes. *Elect. Comm.*, 43: 18-21.
- Iqbal, Z., Ahmed, S., Tabassum, N., Bhattacharya, R. and Bose, D. 2021. Role of probiotics in prevention and treatment of enteric infections: A comprehensive review. *Biotech.*, 11(5): 1-26.
- Ivars-Barceló, F., Zuiliani, A., Fallah, M., Mashkour, M., Rahimnejad, M. and Luque, R. 2018. Novel applications of microbial fuel cells in sensors and biosensors. *Appl. Sci.*, 8(7): 1184.
- Jadhav, D.A., Deshpande, P.A. and Ghangrekar, M.M. 2017. Enhancing the performance of single-chambered microbial fuel cells using manganese/palladium and zirconium/palladium composite cathode catalysts. *Bioresour. Technol.*, 238: 568-574.
- Jafary, T., Daud, W. R. W., Ghasemi, M., Bakar, M. H. A., Sedighi, M., Kim, B. H. and Ismail, M. 2019. Clean hydrogen production in a full biological microbial electrolysis cell. *International journal of hydrogen energy*, 44(58): 30524-30531.
- Jatoi, A.S., Akhter, F., Mazari, S.A., Sabzoi, N., Aziz, S., Soomro, S.A. and Ahmed, S. 2021. Advanced microbial fuel cell for wastewater treatment: A review. *Environ. Sci. Pollut. Res.*, 28(5): 5005-5019.

- Jiang, Y., Yang, X., Liang, P., Liu, P. and Huang, X. 2018. Microbial fuel cell sensors for water quality early warning systems: Fundamentals, signal resolution, optimization, and future challenges. *Renew. Sustain. Energy Rev.*, 81: 292-305.
- Kaur, R., Marwaha, A., Chhabra, V.A., Kim, K.H. and Tripathi, S. 2020. Recent developments on functional nanomaterial-based electrodes for microbial fuel cells. *Renew. Sustain. Energy Rev.*, 119: 109551.
- Khan, M.D., Khan, N., Sultana, S., Joshi, R., Ahmed, S., Yu, E. and Khan, M. Z. 2017. Bioelectrochemical conversion of waste to energy using microbial fuel cell technology. *Process Biochemistry*, 57: 141-158.
- Khudzari, J. M., Kurian, J., Tartakovsky, B. and Raghavan, G. V. 2018. Bibliometric analysis of global research trends on microbial fuel cells using Scopus database. *Biochemical Engineering Journal*, 136: 51-60.
- Kodali, M., Herrera, S., Kabir, S., Serov, A., Santoro, C., Ieropoulos, I. and Atanassov, P. 2018. Enhancement of microbial fuel cell performance by introducing a nano-composite cathode catalyst. *Electrochim. Acta*, 265: 56-64.
- Kumar, A. G., Singh, A., Komber, H., Voit, B., Tiwari, B. R., Noori, M.T. and Banerjee, S. 2018. Novel sulfonated co-poly (ether imide) s containing trifluoromethyl, fluorenyl, and hydroxyl groups for enhanced proton exchange membrane properties: application in a microbial fuel cell. *ACS Appl. Mater. Interf.*, 10(17): 14803-14817.
- Kumar, R., Singh, L., Zularisam, A. and Hai, F. I. 2018. A microbial fuel cell is emerging as a versatile technology: a review of its possible applications, challenges, and strategies to improve the performance. *Int. J. Energy Research*, 42(2): 369-394.
- Kumar, S.S., Kumar, V., Kumar, R., Malyan, S. K. and Pugazhendhi, A. 2019. Microbial fuel cells as a sustainable platform technology for bioenergy, biosensing, environmental monitoring, and other low-power device applications. *Fuel*, 255: 115682.
- Kumar, S.S., Kumar, V., Malyan, S.K., Sharma, J., Mathimani, T., Maskarenj, M.S. and Pugazhendhi, A. 2019. Microbial fuel cells (MFCs) for bioelectrochemical treatment of different wastewater streams. *Fuel*, 254: 115526.
- Liu, D., Chang, Q., Gao, Y., Huang, W., Sun, Z., Yan, M. and Guo, C. 2020. High performance of microbial fuel cell afforded by metallic tungsten carbide decorated carbon cloth anode. *Electrochim. Acta*, 330: 135243.
- Mathuriya, A.S. and Pant, D. 2019. Assessment of expanded polystyrene as a separator in a microbial fuel cell. *Environ. Technol.*, 40(16): 2052-2061.
- Mian, M.M., Liu, G. and Fu, B. 2019. Conversion of sewage sludge into environmental catalyst and microbial fuel cell electrode material: A review. *Sci. Total Environ.*, 666: 525-539.
- Neethu, B., Bhowmick, G. and Ghangrekar, M. 2019. A novel proton exchange membrane developed from clay and activated carbon derived from coconut shell for application in the microbial fuel cells. *Biochem. Eng. J.*, 148: 170-177.
- Palanisamy, G., Jung, H.Y., Sadhasivam, T., Kurkuri, M.D., Kim, S.C. and Roh, S.H. 2019. A comprehensive review on microbial fuel cell technologies: Processes, utilization, and advanced developments in electrodes and membranes. *J. Clean. Prod.*, 221: 598-621.
- Qi, X., Ren, Y., Liang, P. and Wang, X. 2018. New insights in photosynthetic microbial fuel cells using anoxygenic phototrophic bacteria. *Bioresour. Technol.*, 258: 310-317.
- Regassa, H., Bose, D. and Mukherjee, A. 2021. Review of microorganisms and their enzymatic products for industrial bioprocesses. *Ind. Biotechnol.*, 17(4): 214-226.
- Rikame, S.S., Mungray, A.A. and Mungray, A.K. 2018. Modification of anode electrode in a microbial fuel cell for electrochemical recovery of energy and copper metal. *Electrochim. Acta*, 275: 8-17.
- Sayed, E.T. and Abdelkareem, M.A. 2017. Yeast as a biocatalyst in microbial fuel cells: Old yeasts-new questions. *InTech*, 11: 41-65.
- Trapero, J.R., Horcajada, L., Linares, J.J. and Lobato, J. 2017. Is microbial fuel cell technology ready? An economic answer towards industrial commercialization. *Appl. Energy*, 185: 698-707.
- Türk, K., Kruusenberg, I., Kibena-Pöldsepp, E., Bhowmick, G., Kook, M., Tammeveski, K. and Ghangrekar, M. 2018. Novel multi-walled carbon nanotube-based nitrogen impregnated Co and Fe cathode catalysts for improved microbial fuel cell performance. *Int. J. Hydro. Energy*, 43(51): 23027-23035.
- Wu, Q., Jiao, S., Ma, M. and Peng, S. 2020. Microbial fuel cell system: a promising technology for pollutant removal and environmental remediation. *Environ. Sci. Pollut. Res.*, 27(7): 6749-6764.
- Zhang, Y., Liu, M., Zhou, M., Yang, H., Liang, L. and Gu, T. 2019. Microbial fuel cell hybrid systems for wastewater treatment and bioenergy production: synergistic effects, mechanisms, and challenges. *Renew. Sustain. Energy Rev.*, 103: 13-29.





# Landslide Assessment Using Sentinel-1 SAR-C Interferometry Technique

Sudhir Kumar Chaturvedi†

Department of Aerospace Engineering, UPES, Dehradun-248007, India

†Corresponding author: Sudhir Kumar Chaturvedi, sudhir.chaturvedi@ddn.upes.ac.in

Nat. Env. & Poll. Tech.  
Website: [www.neptjournal.com](http://www.neptjournal.com)

Received: 03-08-2021

Revised: 23-09-2021

Accepted: 20-10-2021

## Key Words:

Landslide  
Risk assessment  
Human safety  
SAR-C  
Remote sensing

## ABSTRACT

Landslides might remain unknown or unnoticed for a long time in various remote areas due to the unavailability of optical images caused by cloud persistence, which creates difficulties for civil protection rescue operations, and disaster management as well. Rapid crisis response for humanitarian and reconstruction operations in the affected area after such dangerous landslides is necessary. Thus, a rapid detection map is necessary to detect the affected area with damage grade and level for further investigation and human safety protocols. To detect landslide incidents, the unprecedented availability of Sentinel-1 SAR-C band images provides new solutions and better safety reports. In this study, we performed an efficient evaluation of Sentinel-1 SAR C band images before and after landslide incidents. This study provides a comprehensive evaluation based on the advanced space-borne remote sensing technology aiming at SAR products for rapid damage detection and analysis with respect to the interferometric coherence and intensity correlation. We presented the results of a pilot study on the Rudraprayag Uttarakhand massive landslide incident, which includes the different types, sizes, slope expositions, and human safety aspects. Our study and outcomes represent an updated method, which provides a solution for critical terrain rescue operations and an upgraded geomatics map that provides subsidence data with historical data with topographical statistics. Finally, an outlook into the Sentinel-1 SAR-C analysis demonstrates probable solutions to certain constraints, enabling global applicability of the proposed damage assessment methods with the improved accuracy from 50 to 60 % for the obtained temporal resolution datasets.

## INTRODUCTION

Landslides are perhaps one of the most often occurring organic disasters around the world, constituting a severe hazard to human beings (human injury and loss of life) and infrastructure (destruction of construction/natural and ethnic heritage), and the organic atmosphere. Intense rain, earthquakes, and specified human pursuits are a number of the tripping facets of this landslide, which are shown in a variety of kinds and a broad selection of the volume of terrestrial materials (Tzouvaras et al. 2020). In an individual study, information from multiple detectors such as optical detectors, radar, UAVs, etc., was found efficiently to monitor the landslide. Recent studies show that interferometric SAR methods could satisfactorily be carried out in landslide observation, contributing to the understanding of its processes and dynamics, the mechanism of failure along with its mobility. In particular, two approaches of differential SAR interferometry (DInSAR) were employed for landslide investigation and observation as well as their outcome in comparison to earth tracking data demonstrated the viability of the technique in supplying information on the equilibrium of areas affected by slow-motion movements (Li et al. 2020). The more frequently used method of landslide distress tracking is Persistent Scattered Interferometry (PSI),

therefore various researchers have dealt with these specific situations. In other PSI scientific studies, information from various SAR assignments was united with each other as well as with present auxiliary data (geomorphological and geological, etc.) (Athos et al. 2020, Nguyen et al. 2020). The latest satellite SENTINAL-I assignment and available amount of data acquisition provided new inputs into the Landslide study, leading to a much more orderly watching of the aspects of uncertainty. Thus, research readings are completed introducing the principal elements of the interferometric dispensation of SENTINAL-I data, while in a respective Sentinel 1 information was manipulated as a way to upgrade inventory maps and also to monitor landslide activity. The recent study focuses on the claim of several processing methodologies: (a) interferogram generation, (b) assessment of the Digital Surface Model (DSM) earlier, and afterward the landslide function. Sentinel Application Platform (SNAP) was used in the current investigation, namely Sentinel-1 Toolbox (SITBX) created for the European Space Agency (ESA) by Array Systems Computing, German Space Centre (DLR), Brockmann Consult, and Ocean Data Lab.

In Fig. 1, a 3-dimensional topographic map depicts the landslide zone of Chandikadhar, Rudraprayag. As a result of enormous phase shifting of terrain geometry, the study

field, landslide description, and remote sensing survey of the landslide happened on October 21, 2019. The analysis area is Chandikadhar on the Kedarnath-Gaurikund Highway, Rudraprayag, Uttarakhand which is situated in north India (Fig. 1). The larger region is teeming with steep hillslopes and various inclinations that overpass stiff topographical angles in certain places (Vanama et al. 2020, Ahmed et al. 2020). The particle content is composed of three different geologic formations reflecting the elaborate geotectonic arrangement of the region. The study gives insight into the substantial successful software of the Advanced Differential Interferometric SAR (ADInSAR) procedure for landslide observation (Stankevich et al. 2020). For this reason, preprocessing along with post-processing suitability assessment methodologies were previously designed as essential components to verify the feasibility of the A-DInSAR ground deformation results for landslide observation. Specifically, preprocessing investigation is essential to value the structure of their A Differential Interferometry SAR technique for tracking previously mapped landslides as well as the finding of new subduction zones as a result of a previous discernibility chart (Meng et al. 2020). Meanwhile, post-processing analysis is vital to maintain consistency in assessing details such as landslide tracking. Differential Interferometry SAR techniques have advanced significantly, as evidenced by the development of SAR information assimilated by the ESA SENTINAL projects, which behave at advanced Spatial-Temporal settlement, and the growth of complex processing formulations (Table 1). So, the improvements from the DInSAR process necessitate a novel approach to assessing their probability

and constraints, which will be useful for local businesses such as environmental businesses and geological surveys in charge of large-scale landslide monitoring (Boni et al. 2020).

The procedure was developed and tested in the Rudraprayag area of Uttarakhand, in the Chandikadhar sector of the Kedarnath-Gaurikund Highway, using Sentinel-1 data from the ascending and descending modes from 2014 to 2020. The findings provide light on the complicated process' ability to detect monitor-able landslides, regions that require additional field data monitoring systems, and how to improve the representation of landslide movements by focusing on reliable measuring stations (Solari et al. 2019). The process may be used on almost any SAR platform, and it provides an instrument for connecting Sentinel 1 data for near real-time big landslide tracking that considers the benefits of A-DInSAR but also their limitations.

## MATERIALS AND METHODS

### Interferometric Coherence for Rapid Landslide

In the preceding section, the procedures involving Interferometric coherence and intensity correlation are explained. The difference in coherence or intensity significance values before and after the disaster to detect the shift, i.e., the damage caused by the disaster is analyzed. For instance, the coherence is first approximated using the pre-event InSAR pair ( $t_x$  and  $t_y$ ). This allows for the identification of artificially commanded sites and areas, which are distinguished by their considerably large coherence values in comparison to

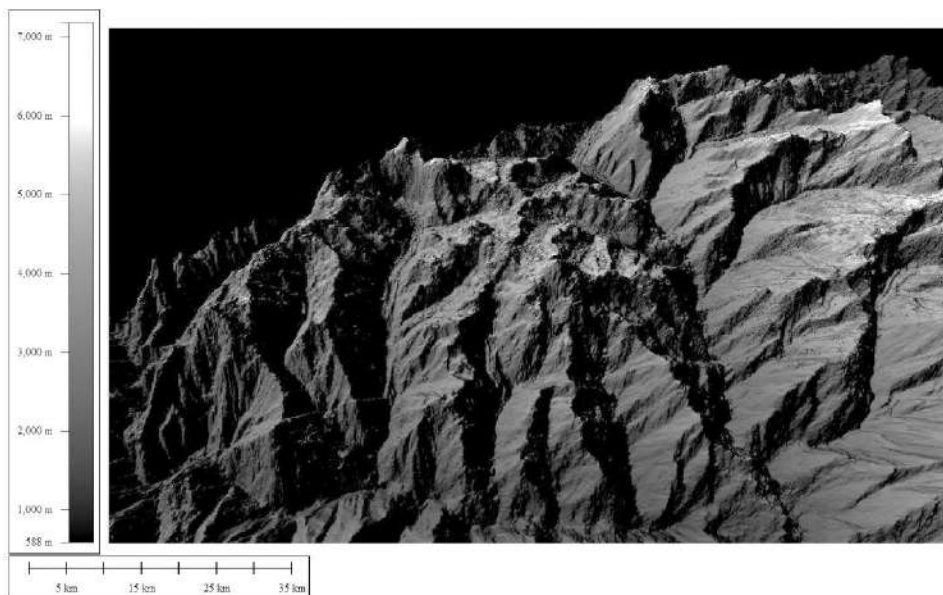


Fig. 1: Landslide zone 3-dimensional topographic map generated from Cartosat-1 DEM (30.401856° N, 78.930994° E).



Table 1: Advantages of the damage assessment approach.

Method (General)	Advantages	Achieved Accuracies
Interferometric coherence	Enables better differentiation of slightly damaged and undamaged areas.	45%–49%
SAR intensity correlation	More sensitive to larger changes (stronger damages) on the ground. Provides still useful information at spatial and temporal baselines, which are too large for useful coherence application.	41%–55%
Combination of coherence and intensity correlation (and SAR backscatter)	Strong increase of the damage assessment accuracy compared to the application of only interferometric coherence or intensity correlation, respectively.	52%–60%
Use of additional data (e.g., optical imagery and GIS data)	An additional increase in the damage assessment accuracy (compared to Section 3.3). Presentation of the damage level at meaningful distribution (e.g., city parcel boundaries, building blocks, etc.) enables the generation of damage maps more suited to the user.	77%–88%

stagnated areas. The coherence of the co-event InSAR sets  $t_y$  and  $t_z$  is computed in the second step. The phase-shifting concept is used to measure damage (Bakon et al. 2020, Luti et.al. 2020, Motagh et al. 2020)

The technique’s concept is that events that cause structural damage, such as earthquakes, hurricanes, flooding, and other natural disasters, dominate the de-correlation of their interferometric coherence. As a result, it is possible to specify the disaster related to the event by measuring the pre-disaster coherence as well as the co-disaster coherence. Hence, only areas controlled by urban structures could be assessed for damage (Nhu et al. 2020, Zhang et al. 2019)

$$ND = \frac{X_{pre} - X_{co}}{X_{pre} + X_{co}} \dots(1)$$

$X_{pre}$  represents the Pre-disaster SAR image set ( $t_x$  and  $t_y$  in Fig. 3) along with  $X_{co}$  symbolizing a pre and a post-disaster image set containing the event ( $t_y$  and  $t_z$  in Fig. 3). The normalized differences approach could be applied to both, the interferometry coherence  $ND_\gamma$  and also the intensity significance  $ND_\rho$ :

$$ND_\gamma = \frac{\gamma_{pre} - \gamma_{co}}{\gamma_{pre} + \gamma_{co}} \dots(2)$$

$$ND_\rho = \frac{\rho_{pre} - \rho_{co}}{\rho_{pre} + \rho_{co}} \dots(3)$$

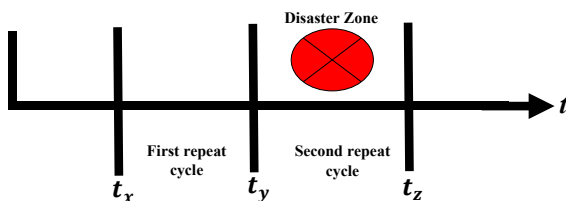


Fig. 2: The damage assessment interferometry Coherence method and SAR intensity correlation in which two image areas were acquired before the occasion which is  $t_x$  and  $t_y$  with respect to at least one SAR acquisition soon after the disaster at  $t_z$  condition.

The selection and conclusion of a practical threshold to distinguish between damaged and undamaged structures or to determine unique damage class ranges is critical for all change detection techniques (Intrieri et al. 2020). It is concentrated on the use of interferometric coherence for damage evaluation and introduced a coherence change index  $\tau$ , at which  $\gamma_{pre}$  is the coherence of this pre-disaster SAR image set ( $t_x$  and  $t_y$  in Fig. 3) and  $\gamma_{co}$  is your coherence calculated by a pre-plus a post-disaster image set for the event ( $t_y$  and  $t_z$  in Fig. 3):

$$\tau = \frac{\gamma_{pre}}{\gamma_{co}} \dots(4)$$

Every pixel in this field of interest has its coherence indicator calculated. In contrast to the first SAR imaging, one must consider that the coherence is calculated over a few spaces, resulting in a loss in spatial resolution. Damage assessment, on the other hand, is far more practicable at coarser models such as administrative boundaries or building codes than at that pixel worth. The minimum dimensions of this ground target to be studied throughout the damage evaluation process are predetermined by the spatial resolution of this SAR detector. It can range from single buildings to the availability of very high spatial resolution SAR data if data from SAR detectors with lower plasma resolution can be found (Table 2). (Wasowski & Pisano 2020, Hayati et al. 2019, Shang et al. 2020). Another process of disaster management systems was also discussed by Chaturvedi et al. (2016), Srivastava et al. (2017), Chaturvedi (2019), and Guven et al. (2018) in terms of modeling and simulations of its parameters in deep, intermediate, and shallower water regions. The noise reduction techniques in RADAR datasets have been developed by Sood et al. (2018).

### Datasets and Methodology

The methodology of interferogram for the calculation of ground displacement is a procedure that has just been ac-

Table 2: Synthetic Aperture Radar (SAR) missions relevant to this damage assessment study.

SAR Mission	Launch	Out of Service	Band *	Spatial Resolution (Azimuth and Ground Range) (m) **	Repeat Cycle (Days)
ERS-1	1991	2000	C	30	35
ERS-2	1995	2011	C	30	35
ENVISAT/ASAR	2002	2012	C	30	35
Radarsat-1	1995	2013	C	8-100	24
Radarsat-2	2007		C	2-160	24
Sentinel-1	2014		C	5-40	12 (6 ***)
J-ERS-1	1992	1998	L	18	46
ALOS/PALSAR	2006	2011	L	10-100	44
COSMO-SkyMed	2007		X	1-30	16 (4 ****)
TerraSAR-X	2007		X	1-40	11

tualized in the estimation of ground deformation in zones affected by a seismic tremor with massive consequences. Along these lines, this work, it was analyzed the particular technique in planning ground deformation after the event of a landslide. Specifically, the interferogram situation was done with the point of inspecting interferometric borders in territories exposed to distortion. In this manner, eight Sentinel-1 interferometric wide-area mode images were obtained and thus four sets were handled in this experiment. Correlation of interferometric DSM concerning assistance

variations after the landslide, two interferometric phase maps were made and, in this manner, looked at one another. Interferometric phase map precision has just been tried in a few examinations using information from various missions. In the particular work, 30 interferometric wide-area mode Sentinel-1 images, covering the territory of Chandikadhar, Rudraprayag, were acquired to deliver two interferometric phase-shifting maps, one preceding and another after the slide. It references that during the precise technique, it was viewed as the way that the ideal opposite benchmark for in-

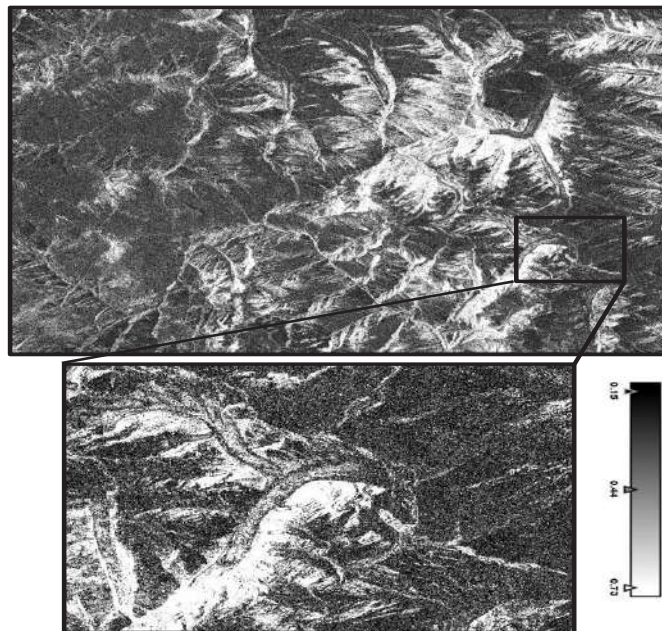


Fig. 3: Intensity interferogram VV SAR-C band landslide zone image analysis results from 12<sup>th</sup> October 2019 to 24<sup>th</sup> October 2019 (30.401856° N, 78.930994° E).

terferometric phase-shifting must be in the range somewhere in the range of 520m and 700m.

## RESULTS AND DISCUSSION

Interferogram phase regarding four interferometric sets, made by four Sentinel-1 interferometric wide-area mode images before the landslide and other four images after the case, were acquired and held utilizing the interferometric process. In the formed interferogram, a change of colors was introduced at the landslide territory, which didn't show up in a similar zone before the event of the landslide. . In a similar article, a large number of dynamic landslides were identified using a relating technique, demonstrating the utility of Sentinel-1 data for landslide investigation and observation. The outputs illustrate the color shift that occurs within the boundary lines that denote the landslide's bounds. It shows that the landslide's limitations were calculated using spatial data and that they have a startling level of precision as a result. Fig. 3 shows the intensity interferogram VV SAR-C band landslide zone image analysis from Chandikadhar, Rudraprayag area on October 12th, 2019. Moreover, to confirm the precision of the outcomes, another interferogram was produced utilizing information before the slide, in which no shading adjustment happened at the terrain structure of the slide. Specifically, outputs show the created interferogram of Sentinel-1 rising information, while comprising the originated interferogram of handling Sentinel-1 information. The subsequent meth-

odology, Correlation of interferometric DSM, was used to examine two interferometric DSM and was used to examine elevation changes after the slide. To build elevation models based on the correlation of the two interferometric DSMs, six segments were drawn diagonally to the center of the slide. For Counterbalancing, the rapid landslide phase interferogram procedure requires two Sentinel-1 Ground Range Detected (GRD) information, which has as of now preprocessed and registered. The benefit of the particular procedure is that no stage data is required, so no climatic segment is recollected for conclusive outcomes. Fig. 4 is the depiction of rapid landslide phase interferogram VV output from 12<sup>th</sup> October 2019 to 24<sup>th</sup> October 2019 (30.401856° N, 78.930994° E).

The handling was updated by setting the matrix azimuth and range dividing values in pixels, which correspond to similar boundaries. Certain parts of the slide, particularly in the uppermost reaches, appeared to move more in accordance with the principal body of the slide. The precise process necessitates some consistent focus to differentiate and measurements for the rest territory's progressions. The progressions in the impacted region of the slide were gigantic to the point where the calculation couldn't figure out how to discover any steady spot to measure the movement effectively.

## CONCLUSION

After a major disaster, quick emergency response is critical to support, humanitarian, and rescue efforts in the impacted

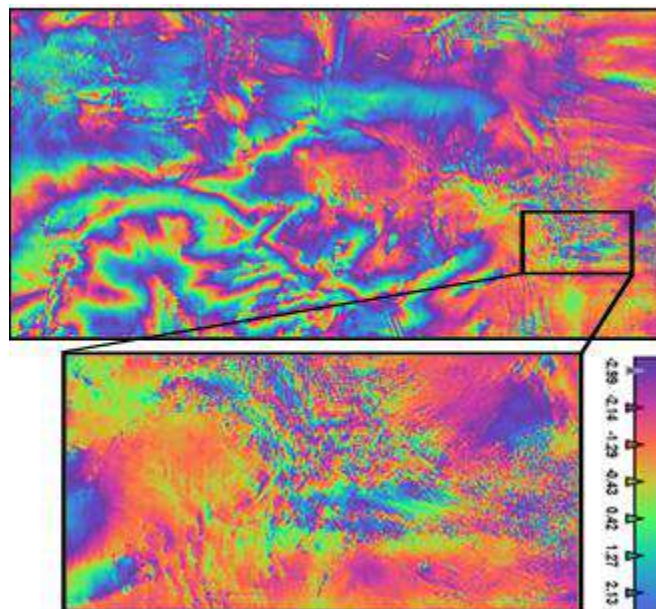


Fig. 4: Rapid landslide phase interferogram VV output from 12<sup>th</sup> October 2019 to 24<sup>th</sup> October 2019 (30.401856° N, 78.930994° E).



area. Quick disaster planning provides important information about the affected area, including the evaluation and type of disaster. Because of its quick response and ability to observe large areas at a low cost, satellite distant detection is crucial in disaster evaluation. As a result, SAR sensors are huge and provide useful imagery in a shorter period than optical sensors. A complete inspection of disaster assessment methods utilizing multi-temporal SAR methodology, for example, interferometric analysis and SAR detection were introduced. In opposed to this, both interferometric analyses, just as the SAR detection shows a decline of their qualities with expanding disaster level, as the period of the compound SAR backscatter fluctuations because of disaster at the ground. In this manner, the interferogram process is more capable to recognize lower disaster levels just as to even more likely separate between marginal disaster and massively affected structures. Unchanged regions have higher rationality estimation over a longer period at longer SAR frequencies, such as the L-band, as opposed to the shorter C or X-band, which also leads to better clarity in distinguishing between disaster and intact zones, and thus to better separation of both. This methodology can be divided into two categories: the first is the requirement for a rapid, relevant disaster evaluation methodology with high accuracy, and the second is the availability of any rate for two predicible SAR images acquired in a matter of seconds before the event at a similar image geometry as the post-calamity SAR assessments. The use of alternative datasets to pre and post-processed SAR images could be a potential answer for increasing the accuracy of disaster evaluation. For example, the accuracy of disaster evaluation strategies was increased from about 50% to 60% by combining radar and optical image datasets (because of just SAR assessments relationship and additionally coherence rate). As a result, a geodatabase comprising important GIS information and ongoing recalculation might be built up for any key territory of intrigue exposed to certain hazards. To evaluate the change location, i.e., disaster detection, a few strategies have been considered. Different investigations make use of more distinct alteration location approaches, such as the neural system-dependent system. The most important and advanced aspect of disaster assessment is identifying the disaster and determining its magnitude. As a result, space-based remote sensing applications are more precise and useful for any rapid detection of landslide-affected zones, resulting in improved safety and human rescue operations.

## ACKNOWLEDGEMENT

The authors would like to thank UPES Dehradun for facilitating the space to carry out the research work. Corresponding author thanks Mr. Saikat Banerjee and Sourav Basu

of CubicX India for the great support in terms of the data processing and analysis.

## REFERENCES

- Ahmed, B., Rahman, M.S., Sammonds, P., Islam, R. and Uddin, K. 2020. Application of geospatial technologies in developing a dynamic landslide early warning system in a humanitarian context: The Rohingya refugee crisis in Cox's Bazar, Bangladesh. *Geomat. Nat. Hazards Risk*, 11(1): 446-468.
- Athos, A., Lysandrou, V. and Hadjimitsis, G. 2020. Earth observation contribution to cultural heritage disaster risk management: A case study of Eastern Mediterranean open-air archaeological monuments and site. *Remote Sens.*, 12 (08): 60-67.
- Bakon, M., Czikhhardt, R., Papco, J., Barlak, J., Rovnak, M., Adamisin, P. and Perissin, D. 2020. remotIO: A Sentinel-1 multi-temporal InSAR infrastructure monitoring service with automatic updates and data mining capabilities. *Remote Sens.*, 12(11): 515-525.
- Boni, R., Bordoni, M., Vivaldi, V., Troisi, C., Tararbra, M., Lanteri, L., Zucca F. and Meisina C. 2020. Assessment of the Sentinel-1 based ground motion data feasibility for large scale landslide monitoring. *Landslides*, 17: 2287-2299.
- Chaturvedi, S.K., Guven, U. and Srivastava, P.K. 2016. Measurement of tsunami wave Eigenvalues in deep, intermediate, and shallower regions. *Curr. Sci.*, 110(12): 750-756.
- Chaturvedi, S.K. 2019. A case study of the tsunami detection system and ocean wave imaging mechanism using radar. *J. Ocean Eng. Sci.*, 04(03): 203-210.
- Guven, U., Chaturvedi, S.K. and Srivastava, P.K. 2018. Measurement and validation of tsunami Eigenvalues for the various water wave conditions. *J. Ocean Eng. Sci.*, 05(01): 41-54.
- Hayati N., Wolfgang N. and Sadarviana V. 2019. Ground deformation in the cilito landslides area was revealed by multi-temporal InSAR. *Geosciences*, 10(5): 11-19
- Intrieri, E., Frodella, W., Raspini, F., Bardi, F. and Tofani, V. 2020. Using satellite interferometry to infer landslide sliding surface depth and geometry. *Remote Sens.*, 12(9): 4-12.
- Li, M., Zhang, L., Ding, C., Li, W. and Luo, H. 2020. Retrieval of historical surface displacements of the Baige landslide from time-series SAR observations for retrospective analysis of the collapse event. *Remote Sens. Environ.*, 240: 55-60.
- Luti, T., Segoni, T.S., Catani, F., Munafò, M. and Casagly, N. 2020. Integration of remotely sensed soil sealing data in landslide susceptibility mapping. *Remote Sens.*, 12(9): 55-60.
- Meng, Q., Confuorto, P., Peng, Y., Raspini, F., Bianchini, S., Han, S., Liu, H. and Casagly, N. 2020. Regional recognition and classification of active loess landslides using two-dimensional deformation derived from Sentinel-1 interferometric radar data. *Remote Sens.*, 12(10): 54.
- Motagh, M., Roessner, S., Akbari, B., Behling, R., Vassileva, M.S., Haghighi, M.H. and Ulrich-Wetzell, H. 2020. Landslides Triggered by 2019 Extreme Rainfall and Flood Events in Iran: Results from Satellite Remote Sensing and Field Survey. In EGU General Assembly Conference Abstracts, p. 10715.
- Nguyen, V., Yariyan, P., Amir, M., Tran, A.D., Pham, T.D., Do, M.P., Ngo, P., Nhu, V., Long, N.Q. and Bui D. 2020. A new modeling approach for spatial prediction of flash floods with biogeography optimized CHAID tree ensemble and remote sensing data. *Remote Sens.*, 12(9): 61.
- Nhu, V., Mohammadi, A., Shahabi, H., Bin Ahmad, B., Al-Ansari, N., Shirzadi, A., Clague, J., Jaafari A., Chen, W. and Nguyen H. 2020. Landslide susceptibility mapping using machine learning algorithms and remote sensing data in a tropical environment. *Int. J. Environ. Res. Public Health*, 17(14): 101.

- Shang, J., Jiali, J., Liu, J., Poncos, V., Geng, X., Qian, B., Chen, Q. and Dong, T. 2020. Detection of crop seeding and harvest through analysis of time-series Sentinel-1 Interferometric SAR data. *Remote Sens.*, 12(10): 121.
- Srivastava, P.K., Guven, U. and Chaturvedi, S.K. 2017. A brief review on tsunami early warning detection using the BPR approach and post-analysis by SAR satellite dataset. *J. Ocean Eng. Sci.*, 02(02): 83-89
- Solari, L., Bianchini, S., Franceschini, R., Barra, A., Monserrat, O., Thuegaz, P., Bertolo, D., Crosetto, M. and Catani, F. 2019. Satellite interferometric data for landslide intensity evaluation in mountainous regions. *Int. J. Appl. Earth Observ. Geoinform.*, 6: 87
- Sood, A., Shah, A. and Katyal, A. 2018. MATLAB-based graphical user interface development of RADAR with the implementation of noise under various brands. *Lect. Notes Mech. Eng.*, 11: 69-76.
- Stankevich, S., Piestova, I., Kozlova, A., Titarenko, O. and Singh, S.K. 2020. Satellite Radar Interferometry Processing and Elevation Change Analysis for Geoenvironmental Hazard Assessment. In Srivastava, P.K., Singh, S.K., Mohanty, U.C. and Murty, T. (eds.), *Techniques for Disaster Risk Management and Mitigation*, John Wiley & Sons, New York, pp. 125-139
- Tzouvaras, M., Danezis, C. and Hadjimitsis, D.G. 2020. Small scale landslide detection using Sentinel-1 Interferometric SAR coherence. *Remote Sens.*, 12(10): 1560-1567
- Vanama, V.S.K., Mandal, D. and Rao, Y.S. 2020. GEE4FLOOD: rapid mapping of flood areas using temporal Sentinel-1 SAR images with Google Earth Engine cloud platform. *J. Appl. Remote Sens.*, 14(3): 414-425.
- Wasowski, J. and Pisano, L. 2020. Long-term InSAR, borehole inclinometer, and rainfall records provide insight into the mechanism and activity patterns of an extremely slow urbanized landslide. *Landslides*, 17(2): 445-457.
- Zhang, C., Liu, Y., Gao, P., Chen, W., Li, H., Hou, Y., Nuremanguli, T. and Ma, H. 2019. Landslide mapping with remote sensing: challenges and opportunities. *Int. J. Remote Sens.*, 41(4): 1555-1581.







# A Study on the Diversity of Pesticide-Resistant Bacterial Population from Different Agricultural Fields of Manjoor

T. R. Shanthi\*†, Mohammed Hatha\*\* and T. R. Satyakeerthy\*\*\*

\*Department of Environmental Science, Calicut University, Tenhipalam, Kerala, India

\*\*School of Marine Sciences, Cochin University of Science and Technology, Cochin, Kerala, India

\*\*\*IGNOU Regional Centre, Port Blair, Andaman Nicobar Islands-744101, India

†Corresponding author: T. R. Shanthi; shanthifa@yahoo.com

## Nat. Env. & Poll. Tech.

Website: [www.neptjournal.com](http://www.neptjournal.com)

Received: 10-09-2021

Revised: 22-10-2021

Accepted: 27-10-2021

### Key Words:

Pesticides

Heterotrophic bacteria

Pesticide-resistant bacteria

Diversity

## ABSTRACT

The regular usage of pesticides in agricultural fields results in the development of a pesticide-resistant microbial population. Vegetable cultivation is a common practice in the agricultural growing areas of Manjoor, Kerala. The present study was envisaged to understand the resistance of microorganisms to different types and doses of pesticides. The study revealed that heterotrophic bacteria are capable of resisting lower concentrations (0.01 and 0.001%) of the pesticides lindane and methyl parathion while a higher concentration of carbaryl (0.1%) could also be tolerated. In the soil sample where there was no prior addition of pesticides, the heterotrophic bacteria could only tolerate very low concentrations of pesticides. The results of mean pesticide-resistant bacterial load when compared to normal Total Heterotrophic Bacteria (THB) of soils indicate that pesticides exhibited an inhibitory effect on the heterotrophic bacteria of soils collected from different agricultural fields and the pesticide-resistant bacterial load was lower than normal THB.

## INTRODUCTION

Pesticides encompass a variety of different types of chemicals including herbicides, insecticides, fungicides, and rodenticides. These synthetic organic compounds intended to regulate the pests constitute an important aspect of modern agriculture, as they are necessary for economical pest management. Pesticides are broadly divided into many classes based on their chemical structure as the organochlorines, organophosphates, and carbamates of which the most important are organochlorine pesticides (OCPs).

Organochlorine pesticides are broad spectrum chlorinated hydrocarbons and representative compounds in this group include the chlorinated derivatives of diphenyl ethane (dichlorodiphenyltrichloroethane-DDT, its metabolites dichlorodiphenyldichloroethylene-DDE, dichlorodiphenyldichloroethane-DDD, and methoxychlor), hexachlorobenzene (HCB), the group of hexachlorocyclohexane ( $\alpha$ -HCH,  $\beta$ -HCH,  $\gamma$ -HCH and  $\delta$ -HCH), the group of cyclodiene (aldrin, dieldrin, endrin, chlordane, nonachlor, heptachlor, and heptachlor-epoxide), and chlorinated hydrocarbons (dodecachlorine, toxaphene, and chlordecone). Organochlorine pesticides are very stable compounds and it has been cited that the degradation of dichlorodiphenyltrichloroethane (DDT) in soil ranges from 4 to 30 years. They are liposoluble compounds and are capable of bioaccumulating

in the fatty parts of biological beings. Organophosphates are phosphoric acid esters or thiophosphoric acid esters which include pesticides like Malathion, dibrom, chlorpyrifos, temephos, diazinon, and terbufos. The organophosphate insecticides bind with the cholinesterase (ChE) enzyme at the neuromuscular junction and deactivate or inhibit the activity of the enzyme by irreversible phosphorylation. This results in elevated levels of acetylcholine (ACh), which acts on the muscarinic receptors situated at cholinergic junctions in skeletal nerve-muscular junctions, at nicotinic receptors in autonomic ganglia, and receptors in the central nervous system (CNS) (Kwong 2002). Carbamate pesticides are esters of carbamates and organic compounds derived from carbamic acid. This group of pesticides can be divided into benzimidazole-, *N*-methyl-, *N*-phenyl-, and thiocarbamates. Aldicarb, carbaryl, propoxur, oxamyl and terbucarb are carbamates. The carbamates are relatively unstable compounds that break down in the environment within weeks or months. These pesticides affect the nervous system by disrupting an enzyme that regulates acetylcholine, a neurotransmitter. The enzyme effects are usually reversible.

Many soil microorganisms have the ability to act upon pesticides and convert them into simpler non-toxic compounds. Most microbial degradation of pesticides occurs in the soil, which is the storehouse of multitudes of microbes both in quantity and quality, receives the chemicals in various

forms, and acts as a scavenger of harmful substances. The rate of biodegradation in soil depends on the availability of pesticide or metabolite to the microorganisms, physiological status of the microorganisms, survival and/or proliferation of pesticide degrading microorganisms at the contaminated site, and sustainable population of these microorganisms. Even though the physical and chemical forces also act in degrading the pesticides to some extent, microorganisms play a major role in the degradation of pesticides (Kumar et al. 2021).

The halogenated aliphatic compound, position, and the number of halogens are important in determining both rate and mechanism of biodegradation (Mulligan 2005) and since organochlorine pesticides possess halogen electron-withdrawing groups that generate electron deficiency in the molecule, they resist aerobic degradation (Rieger et al. 2002). However, these compounds can be attacked more readily under reductive conditions, which could be enhanced by the addition of auxiliary electron donors. For most pesticides, aerobic decomposition proceeds much faster than anaerobic decomposition; however, an exception to this is DDT, whose decomposition proceeds ten times faster under anaerobic conditions (Scott 2000).

Organophosphorus pesticides consist of ester or thiol derivatives of phosphoric, phosphonic, or phosphoramides acids. The main degradation pathway starts with the hydrolysis of the P-O alkyl or P-O aryl bonds (Ang et al. 2005) which diminishes as much as 100 times the toxicity of these compounds. Bacterial enzymes have been found to achieve such detoxifying reactions (Yañez-Ocampo et al. 2009). This reaction is performed by esterases or phosphotriesterases that have been described for a number of different genera of bacteria and fungi.

A number of bacterial genera have been identified as carbamate degraders (Parekh et al. 1995, Satish et al. 2017) and microorganisms in soil are known to degrade carbamate pesticides via hydrolysis or oxidation, of which microbial hydrolysis of carbofuran is well established (Chaudhry et al. 2002). The enzymatic hydrolysis of carboxyl esters by carboxyl esterases (CbEs) is based on the reversible acylation of a serine residue within the active center of the protein (Gupta 2006).

In vegetable growing areas, where immense pesticides of different pesticide groups are applied, a natural microbial population efficient to resist these pesticides might have evolved over time. But the effects of these pesticides on these pesticide degrading strains and the emergence of pesticide-resistant strains are not studied so far. In field or laboratory studies, pesticide impact on microbial biota is most often assessed by measuring the number of microorganisms (Cycon et al. 2009). Hence the present study was

conducted to understand the existence of a pesticide-resistant population and to compare the pesticide-resistant bacterial load associated with soils from six different agricultural fields of Manjoor, which is a predominant agricultural field in Kerala.

## MATERIALS AND METHODS

Soil samples are collected from six agricultural areas of Manjoor (S1 to S6). Six sites that practiced crop rotation after two or three life cycles of a crop were selected. The six sites were representing regions that produce different vegetables like Pea plant (station 1), Bitter gourd (station 2), Snake gourd (station 3), little gourd (station 4), and Cucumber (station 5). Station 6 is a pea plant growing area where pesticides are not added. A garden soil sample (station 7), from the nearby area, was also collected during the period which was used as a control.

For the estimation of the pesticide-resistant population, the pesticides used were lindane (an organochlorine pesticide manufactured by Jayakrishna Pesticides (P) Ltd, Salem), methyl parathion (an organo phosphorous pesticide manufactured by Agro Chemicals of India, Nashik), and carbaryl (a carbamate pesticide manufactured by S.S. Cropcare Ltd, Bhopal and marketed by Rhone-Poulenc Agrochemicals India Ltd).

### Quantification of Pesticide-Resistant Population

To estimate the pesticide-resistant population, 10 g of soil samples were homogenized with 90 mL sterile distilled water using a rotary shaker and serially diluted up to  $10^{-2}$ . Between each dilution, the samples were mixed thoroughly on a vortex mixer to release bacterial cells from soil particles. One hundred microliters of various dilutions of each sample were pipetted onto a surface dried mineral medium plate supplemented with various concentrations (0.1%, 0.01%, and 0.001%) of different pesticides. The sample was spread aseptically using a sterile L-rod and incubated in an inverted position at 37°C for 6-7 days. All the plating was done in duplicates. After incubation, the colony was enumerated using the conventional plate count method. The pesticide-resistant population was recorded as colony-forming units per gram of soil.

### Statistical Analysis

Results of the study were compiled and subjected to statistical analysis for drawing inferences. The techniques employed for the analysis of the data were Analysis of Variance (ANOVA) for comparison of treatment means and the  $\chi^2$  test for goodness of fit of proportions. For framing the ANOVA table for comparison of data on bacterial load, the figures

were converted to their corresponding logarithm values after adding 1 to all the observations wherever necessary.

**RESULTS**

The present study was carried out to determine the diversity of pesticide-resistant bacterial populations from different agricultural fields. The bacterial population’s resistance to organochlorine pesticide (lindane), organophosphorus pesticide (methyl parathion), and carbamate pesticide (carbaryl) was estimated.

**Quantification of Pesticide-Resistant Bacteria**

**Pesticide-resistant bacterial load in soils of pea plant:** The pesticide-resistant bacterial load of station 1 is represented in Table 1. The lindane resistant bacterial load in station1 ranged from  $4.8 \times 10^5$  to  $3.2 \times 10^6$  cfu.g<sup>-1</sup> and the mean lindane resistant bacterial load was  $1.21 \times 10^6$  cfu.g<sup>-1</sup>. The pesticide-resistant bacterial load was observed only when lindane impregnation was provided at a concentration of 0.01% and 0.001%. When the dosage was increased to a concentration of 0.1%, the bacterial growth was arrested. The methyl parathion-resistant bacterial load ranged from  $2.3 \times 10^6$  to  $9.8 \times 10^6$  cfu.g<sup>-1</sup> with a mean bacterial load of  $2.91 \times 10^6$  cfu.g<sup>-1</sup>. At a concentration of 0.1%, the bacterial load was absent. The carbaryl resistant bacterial load varied from  $3.8 \times 10^6$  to  $9.5 \times 10^7$  cfu.g<sup>-1</sup> and the mean carbaryl resistant bacterial load was  $1.8 \times 10^7$  cfu.g<sup>-1</sup>. A higher concentration of 0.1% of

carbaryl did not suppress the bacterial load in the samples collected from station 1.

**Pesticide-resistant bacterial load in bittergourd growing fields:** The results of the pesticide-resistant bacterial load of station 2 (Bittergourd growing fields of Manjoor) are represented in Table 2. In station 2 the bacterial load resistance to lindane varied from  $1.2 \times 10^5$  to  $9.6 \times 10^6$  cfu.g<sup>-1</sup> and the mean lindane resistant bacterial load was  $3.64 \times 10^6$  cfu.g<sup>-1</sup>. In station 2 the growth of heterotrophic bacteria was arrested at 0.1% of lindane concentration. The methyl parathion-resistant bacterial load in station 2 varied from  $2.6 \times 10^6$  to  $2.5 \times 10^7$  cfu.g<sup>-1</sup> and the mean bacterial load was  $1.11 \times 10^7$  cfu.g<sup>-1</sup>. The heterotrophic bacteria of station 2 could not tolerate a higher percentage of methyl parathion and hence no growth was noticed at a concentration of 0.1% pesticide. The carbaryl resistant bacterial load in station 2 ranged from  $0.4 \times 10^5$  to  $3.0 \times 10^7$  cfu.g<sup>-1</sup>. The mean pesticide-resistant load was  $8.45 \times 10^6$  cfu.g<sup>-1</sup>. The bacteria at station 2 could exhibit tolerance to carbaryl at all the three concentrations (0.001%, 0.01%, and 0.1%) studied.

**Pesticide-resistant bacterial load in snakegourd growing fields:** The results of the pesticide-resistant bacterial load of station 3 are represented in Table 3. The result indicates that in station 3 the heterotrophic bacteria could tolerate a pesticide concentration of 0.001% and 0.01% for lindane and methyl parathion, and for the pesticide carbaryl, it could tolerate all three concentrations (0.001%, 0.01%, and

Table 1: Load of bacteria from pea plant growing field capable of resisting various concentrations of Lindane, methyl parathion, and carbaryl pesticides.

Sampling months	Load of THB from station1 (Pea plant soil) tolerant to the pesticides								
	Lindane			Methyl parathion			Carbaryl		
	0.001%	0.01%	0.1%	0.001%	0.01%	0.1%	0.001%	0.01%	0.1%
January	$3.2 \times 10^6$	$5.4 \times 10^5$	-	$6.0 \times 10^6$	$2.3 \times 10^6$	-	$3.4 \times 10^7$	$1.2 \times 10^7$	$5.5 \times 10^6$
February	$4.8 \times 10^5$	$6.2 \times 10^5$	-	$9.3 \times 10^6$	$5.4 \times 10^6$	-	$9.3 \times 10^6$	$8.7 \times 10^6$	$6.3 \times 10^6$
March	$5.9 \times 10^5$	$2.4 \times 10^6$	-	$4.2 \times 10^6$	$6.7 \times 10^6$	-	$1.7 \times 10^7$	$9.5 \times 10^6$	$3.8 \times 10^6$
April	$1.0 \times 10^6$	$8.6 \times 10^5$	-	$9.8 \times 10^6$	$2.9 \times 10^6$	-	$2.0 \times 10^7$	$9.2 \times 10^7$	$4.0 \times 10^6$

Table 2: Load of bacteria from the Bittergourd growing field capable of resisting various concentrations of Lindane, methyl parathion, and carbaryl pesticides.

Sampling months	Load of THB from station 2 (Bittergourd soil) tolerant to the pesticides								
	Lindane			Methyl parathion			Carbaryl		
	0.001%	0.01%	0.1%	0.001%	0.01%	0.1%	0.001%	0.01%	0.1%
January	$5.2 \times 10^5$	$4.5 \times 10^6$	-	$2.5 \times 10^7$	$8.4 \times 10^6$	-	$2.7 \times 10^7$	$7.4 \times 10^6$	$3.6 \times 10^5$
February	$9.6 \times 10^6$	$6.0 \times 10^6$	-	$9.4 \times 10^6$	$2.6 \times 10^6$	-	$1.2 \times 10^7$	$5.6 \times 10^6$	$2.8 \times 10^5$
March	$6.7 \times 10^6$	$1.2 \times 10^5$	-	$7.1 \times 10^6$	$1.5 \times 10^7$	-	$3.0 \times 10^7$	$4.7 \times 10^6$	$1.3 \times 10^5$
April	$8.5 \times 10^5$	$8.4 \times 10^5$	-	$1.2 \times 10^7$	$9.4 \times 10^6$	-	$9.7 \times 10^6$	$6.2 \times 10^6$	$0.4 \times 10^5$

0.1%) studied. In station 3 the lindane resistant bacterial load exhibited a variation from  $1.0 \times 10^6$  to  $6.0 \times 10^6$  cfu.g<sup>-1</sup>. The mean lindane-resistant bacterial load was  $3.5 \times 10^6$  cfu.g<sup>-1</sup>. The methyl parathion-resistant bacterial load fluctuated from  $5.3 \times 10^6$  to  $3.4 \times 10^7$  cfu.g<sup>-1</sup>. The mean pesticide-resistant bacterial load was  $1.19 \times 10^7$  cfu.g<sup>-1</sup>. In station 3 the carbaryl resistant bacterial load encountered varied from  $8.4 \times 10^5$  to  $1.2 \times 10^7$  cfu.g<sup>-1</sup>.  $5.22 \times 10^6$  cfu.g<sup>-1</sup> was the mean carbaryl-resistant bacterial load.

**Pesticide-resistant bacterial load in littlegourd growing fields:** The results of the pesticide-resistant bacterial load are represented in Table 4. In station 4 (Littlegourd soil), the heterotrophic bacteria could not tolerate a higher concentration (0.1%) of all the three pesticides, and the tolerance

to lindane and methyl parathion at a concentration (0.01%) was expressed intermittently. In station 4, the lindane resistant bacterial load exhibited a variation from  $4.2 \times 10^5$  to  $2.8 \times 10^6$  cfu.g<sup>-1</sup>. The mean lindane-resistant bacterial load was  $1.01 \times 10^6$  cfu.g<sup>-1</sup>. The methyl parathion-resistant bacterial load showed a variation from  $8.7 \times 10^5$  to  $5.5 \times 10^6$  cfu.g<sup>-1</sup>. The mean methyl parathion-resistant bacterial load was  $3.04 \times 10^6$  cfu.g<sup>-1</sup>. The carbaryl-resistant bacterial load recorded a variation from  $7.4 \times 10^5$  to  $5.8 \times 10^6$  cfu.g<sup>-1</sup>. The mean carbaryl-resistant bacterial load was  $2.24 \times 10^7$  cfu.g<sup>-1</sup>.

**Pesticide-resistant bacterial load in cucumber growing fields:** The results of the pesticide-resistant bacterial load are represented in Table 5. The result indicates that in station 5

Table 3: Load of bacteria from the Snakegourd growing field capable of resisting various concentrations of Lindane, methyl parathion, and carbaryl pesticides.

Sampling months	Load of THB from station 3 (Snakegourd soil) tolerant to the pesticides								
	Lindane			Methyl parathion			Carbaryl		
	0.001%	0.01%	0.1%	0.001%	0.01%	0.1%	0.001%	0.01%	0.1%
January	$6.0 \times 10^6$	$5.4 \times 10^6$	-	$3.4 \times 10^7$	$7.5 \times 10^6$	-	$9.2 \times 10^6$	$6.3 \times 10^6$	$8.4 \times 10^5$
February	$2.3 \times 10^6$	$1.0 \times 10^6$	-	$1.6 \times 10^7$	$9.2 \times 10^6$	-	$1.2 \times 10^7$	$5.7 \times 10^6$	$2.0 \times 10^6$
March	$3.6 \times 10^6$	$3.2 \times 10^6$	-	$7.5 \times 10^6$	$5.3 \times 10^6$	-	$8.7 \times 10^6$	$2.9 \times 10^6$	$9.7 \times 10^5$
April	$2.9 \times 10^6$	$3.8 \times 10^6$	-	$8.9 \times 10^6$	$6.8 \times 10^6$	-	$9.3 \times 10^6$	$3.5 \times 10^6$	$1.3 \times 10^6$

Table 4: Load of bacteria from the Littlegourd growing field capable of resisting various concentrations of Lindane, methyl parathion, and carbaryl pesticides.

Sampling months	Load of THB from station 4 (Littlegourd soil) tolerant to the pesticides								
	Lindane			Methyl parathion			Carbaryl		
	0.001%	0.01%	0.1%	0.001%	0.01%	0.1%	0.001%	0.01%	0.1%
January	$4.2 \times 10^5$	-	-	$1.0 \times 10^6$	$8.7 \times 10^5$	-	$5.8 \times 10^6$	$7.4 \times 10^5$	$2.5 \times 10^5$
February	$7.5 \times 10^5$	$6.0 \times 10^5$	-	$4.8 \times 10^6$	-	-	$3.2 \times 10^6$	$9.6 \times 10^5$	$4.0 \times 10^5$
March	$2.8 \times 10^6$	-	-	$2.5 \times 10^6$	-	-	$2.5 \times 10^6$	$2.3 \times 10^6$	$1.7 \times 10^5$
April	$9.0 \times 10^5$	$6.2 \times 10^5$	-	$3.6 \times 10^6$	$5.5 \times 10^6$	-	$3.9 \times 10^6$	$3.0 \times 10^6$	$0.2 \times 10^5$

Table 5: Load of bacteria from the Cucumber growing field capable of resisting various concentrations of Lindane, methyl parathion, and carbaryl pesticides.

Sampling months	Load of THB from station 5 (Cucumber growing soils) tolerant to the pesticides								
	Lindane			Methyl parathion			Carbaryl		
	0.001%	0.01%	0.1%	0.001%	0.01%	0.1%	0.001%	0.01%	0.1%
January	$8.9 \times 10^5$	$1.8 \times 10^6$	-	$3.5 \times 10^6$	$1.4 \times 10^6$	-	$6.5 \times 10^6$	$2.0 \times 10^6$	$4.7 \times 10^5$
February	$1.4 \times 10^6$	$7.5 \times 10^5$	-	$2.8 \times 10^6$	$9.6 \times 10^5$	-	$4.0 \times 10^6$	$1.8 \times 10^6$	$2.9 \times 10^5$
March	$9.2 \times 10^6$	$6.7 \times 10^5$	-	$9.3 \times 10^5$	$7.8 \times 10^5$	-	$1.4 \times 10^6$	$3.2 \times 10^6$	$2.2 \times 10^5$
April	$0.5 \times 10^6$	$9.8 \times 10^5$	-	$2.4 \times 10^6$	$1.0 \times 10^6$	-	$3.1 \times 10^6$	$1.5 \times 10^6$	$0.5 \times 10^5$



(Cucumber growing soils) the heterotrophic bacteria could tolerate a pesticide concentration of 0.001% and 0.01% for lindane and methyl parathion, and for the pesticide carbaryl it could tolerate all the three concentrations (0.001%, 0.01%, and 0.1%) studied. In station 5, the lindane resistant bacterial load varied from  $6.7 \times 10^5$  to  $6.7 \times 10^5$  cfu.g<sup>-1</sup> and the mean lindane resistant bacterial load was  $2.02 \times 10^6$  cfu.g<sup>-1</sup>. Methyl parathion bacterial load varied from  $7.8 \times 10^5$  to  $3.5 \times 10^6$  cfu.g<sup>-1</sup> with a mean population of  $1.72 \times 10^6$  cfu.g<sup>-1</sup>. The pesticide-resistant bacterial load exhibited a variation from  $1.5 \times 10^6$  to  $6.5 \times 10^6$  cfu.g<sup>-1</sup> with a mean population of  $3.19 \times 10^6$  cfu.g<sup>-1</sup>.

#### Pesticide-Resistant Bacterial Load in Agricultural Field Soils of Pea Plant (Without Pesticide Addition)

The results of the pesticide-resistant bacterial load are represented in Table 6. The result indicates that in station 6 (soils of pea plant without pesticide addition), the heterotrophic bacteria could not tolerate a pesticide concentration of 0.01% and 0.1% for all the three pesticides, lindane methyl parathion, and carbaryl. The lindane resistant bacterial load varied from  $3.7 \times 10^5$  to  $1.4 \times 10^6$  cfu.g<sup>-1</sup> and the mean lindane resistant bacterial load was  $8.7 \times 10^5$  cfu.g<sup>-1</sup>. Methyl parathion bacterial load fluctuated from  $2.0 \times 10^6$  to  $5.8 \times 10^6$  cfu.g<sup>-1</sup> with a mean population of  $3.32 \times 10^6$  cfu.g<sup>-1</sup>. The pesticide-resistant bacterial load exhibited a variation from  $2.9 \times 10^6$  to  $5.3 \times 10^6$  cfu.g<sup>-1</sup> with a mean population of  $4.13 \times 10^6$  cfu.g<sup>-1</sup>.

#### Spatial Variation of Pesticide-Resistant Bacterial Load in Different Crops

Spatial variation of pesticide-resistant bacterial load in different crops is represented in Fig 1, 2, 3, and 4. There is a significant difference in bacterial resistance to lindane and methyl parathion pesticides in different crops ( $P < 0.05$ ) and between concentrations ( $P < 0.01$ ). Stations 2 (bitter gourd soils) and 3 (snake gourd soils) are having significantly higher lindane and methyl parathion-resistant bacterial loads compared to stations 1, 4, 5, and 6. Between stations 2 and 3, the difference in Total Heterotrophic Bacteria (THB) is not significant. 1% concentration is having significantly lower lindane and methyl parathion-resistant bacterial load compared to 0.01% and 0.1%. There is a significant difference in THB between crops ( $P > 0.05$ ) and no significant difference in concentrations ( $P > 0.05$ ) when the pesticide carbaryl was applied. Station 1 (pea plant soil) has a significantly higher carbaryl-resistant bacterial load compared to other stations.

#### Comparison of Pesticide-Resistant Bacterial Loads With Culturable Heterotrophic Bacterial Loads of Each Sampling Station

The results of the comparison of pesticide-resistant bacterial loads with culturable heterotrophic bacterial loads are represented in Fig. 5. The pesticide tolerant bacterial load was comparatively lower than the culturable bacterial loads of each sampling station.

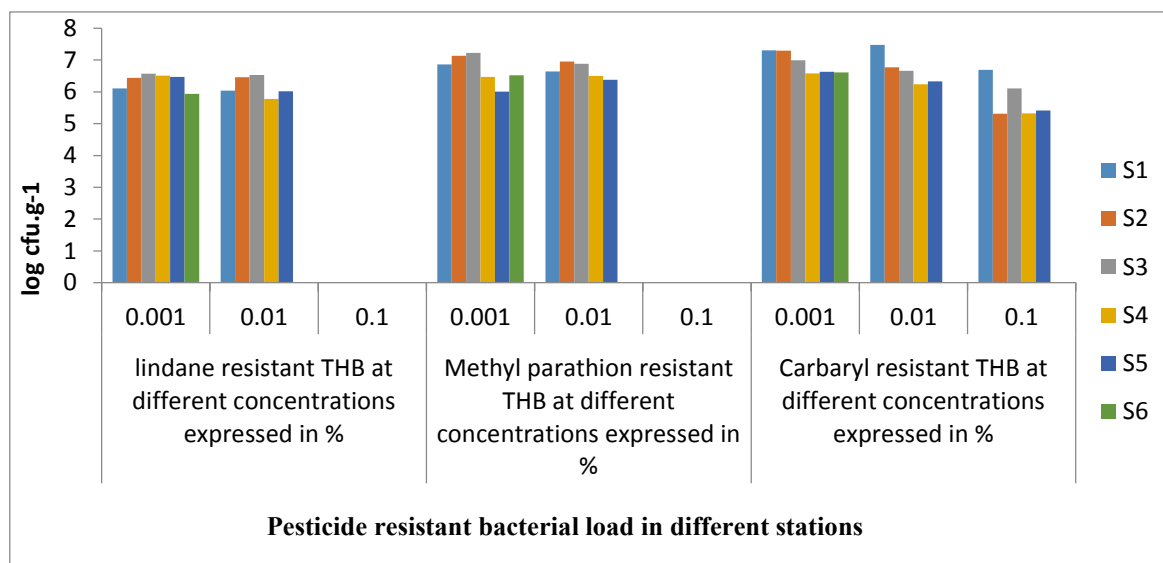


Fig 1: Spatial variation in a load of pesticide-resistant bacteria from different agricultural field soils of Manjor.

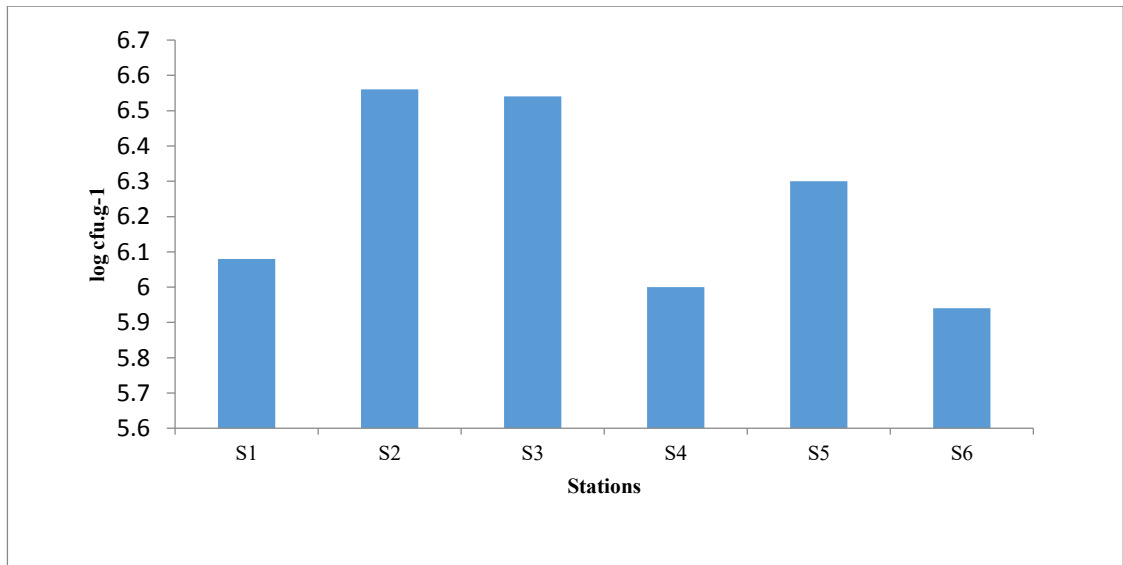


Fig. 2: Spatial variation of lindane resistant bacteria at different agricultural field soils of Manjoor.

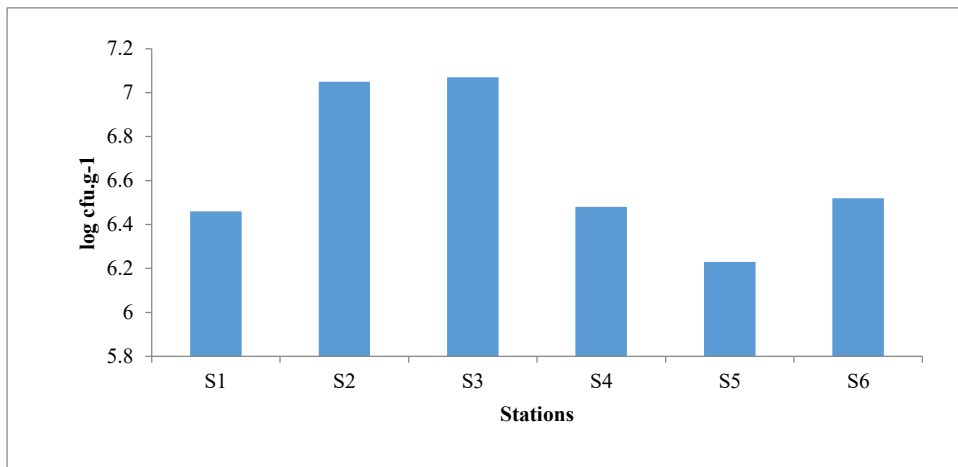


Fig 3: Spatial variation of methyl parathion-resistant bacteria at different agricultural field soils of Manjoor.

Table 6: Load of bacteria from the Pea plant growing field (without pesticides), capable of resisting various concentrations of Lindane, methyl parathion, and carbaryl pesticides.

Sampling months	Load of THB from station 6 (pea plant without pesticide addition) tolerant to the pesticides								
	Lindane			Methyl parathion			Carbaryl		
	0.001%	0.01%	0.1%	0.001%	0.01%	0.1%	0.001%	0.01%	0.1%
January	$3.7 \times 10^5$	-	-	$5.8 \times 10^6$	-	-	$2.9 \times 10^6$	-	-
February	$9.2 \times 10^5$	-	-	$2.4 \times 10^6$	-	-	$3.6 \times 10^6$	-	-
March	$1.4 \times 10^6$	-	-	$2.0 \times 10^6$	-	-	$4.7 \times 10^6$	-	-
April	$7.8 \times 10^5$	-	-	$3.1 \times 10^6$	-	-	$5.3 \times 10^6$	-	-

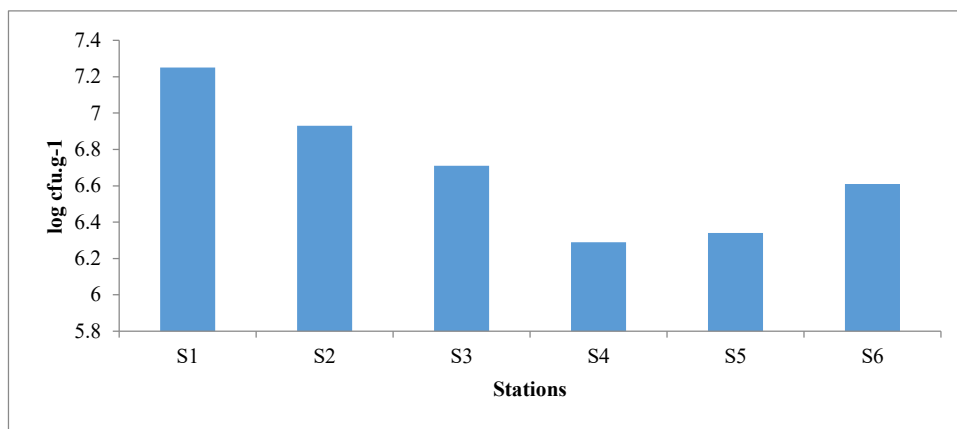


Fig. 4: Spatial variation of carbaryl resistant bacteria at different agricultural field soils of Manjoor.

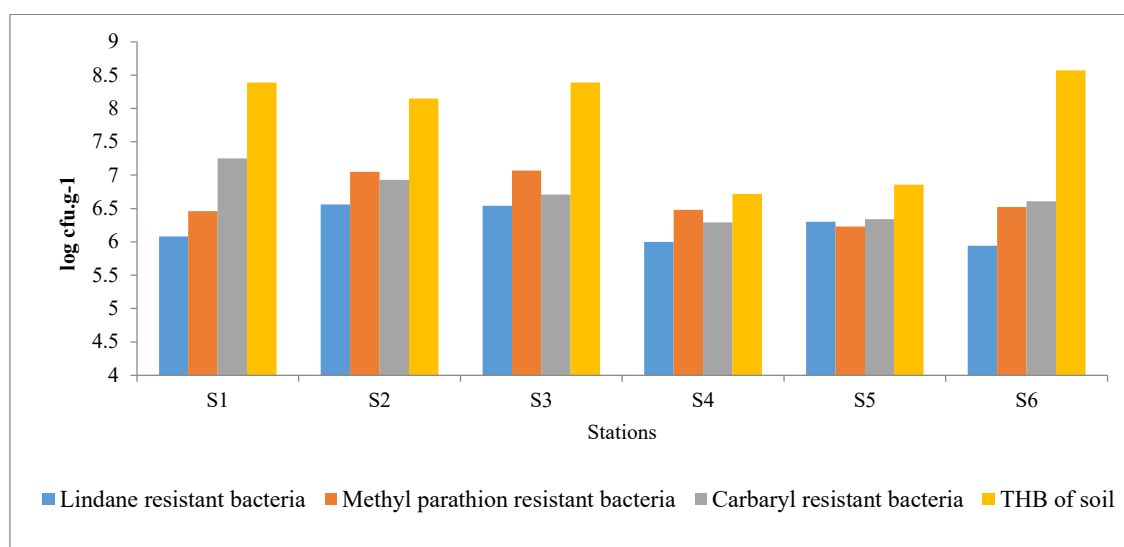


Fig. 5. Relative load of pesticide-resistant bacterial loads with that of total culturable heterotrophic bacterial loads of various agricultural field soils of Manjoor.

## DISCUSSION

The result of the heterotrophic bacteria capable of resisting pesticides indicated that pesticides used in Manjoor affected the total numbers of heterotrophic bacteria and the observed effects are strongly related to pesticide type and its dosage. The results indicate that at a small dosage the pesticides did not show any characteristic effect on the growth of the organisms while the higher dosage of 0.1% suppressed the growth of the organisms when lindane and methyl parathion were given as the sole carbon source. Similar results were observed when Singh (2001) conducted an in vitro study with endosulfan and nivar. When the dosage of pesticide was increased to 0.1% and 1% the growth of bacteria was arrested.

The results when compared to normal soils showed that pesticides exhibited an inhibitory effect on the heterotrophic bacteria of soils collected from different agricultural fields at various doses. Busse et al. (2001) also observed a decrease in the total number of heterotrophic bacteria after glyphosate application. In contrast, an increase in the total number of soil microorganisms in the field, as a response to pesticide application was observed in some studies (Monkiedje & Spiteller 2002, Amal et al. 2005). Hence the results obtained showed that pesticides depending on type and dosages might decrease or increase the microbial counts.

An organic substance of any kind cannot escape the onslaught of microbial degradation, insecticides and pes-

ticides are no exception. Pesticide residues are generally degraded and degradation products are assimilated by soil microorganisms (Rache & Coats 1988). This phenomenon of decrease or increase in the microbial counts could be expected as a result of the utilization of applied pesticides as a source of carbon, energy, and other nutrient elements by some soil microorganisms (Bhuyan et al. 1993) resulting in either proliferation or decrease in the number of organisms.

The load of the pesticide-resistant population in the soil samples incorporated with lindane was very low compared to pesticide-resistant populations of methyl parathion and carbaryl. The results indicate that the load of the pesticide-resistant population is dependent on the nature of pesticides and also is field-dependent. The result also indicated that they are able to utilize all the three pesticides at lower concentrations, although at varying degrees, and in our observations, 0.1% concentration of the pesticide suppressed the growth of heterotrophic bacteria in the soils of most of the cultivating fields.

When pesticides (lindane, methyl parathion, and carbaryl) were added to sample 6 (pea plant without pesticides), the heterotrophic bacteria could only tolerate very low concentrations of pesticides. The explanation for this could be that in soils where there have been no previous applications of the same pesticide or another pesticide with a similar chemical structure, heterotrophic bacteria will not be able to degrade or utilize the compound at an accelerated or enhanced rate (Arbeli & Fuentes 2007).

## CONCLUSION

The pesticide residues in the agricultural field soil can give the required selective pressure for the emergence of pesticide-resistant microorganisms. The load of the pesticide-resistant population in the soil samples incorporated with lindane was very low compared to pesticide-resistant populations of methyl parathion and carbaryl. The lindane and methyl parathion-resistant bacterial load were high in snake gourd and bitter gourd areas while the carbaryl resistant bacterial load was high in pea plant growing area.

Results of this study indicated that heterotrophic bacteria can withstand lower concentrations of the pesticides lindane and methylparathion (0.01% and 0.001%), while a higher concentration of carbaryl (0.1%) could only be tolerated. When the pesticides (lindane, methyl parathion, and carbaryl) were added to sample 6 (pea plant soil where there was no addition of pesticides), the heterotrophic bacteria could only tolerate very low concentrations of pesticides. The results of the mean pesticide-resistant bacterial load, when compared to normal THB of soils, indicate that pesticides exhibited an inhibitory effect on the heterotrophic bacteria of soils collected from different agricultural fields and the

pesticide-resistant bacterial load was lower than normal THB.

## REFERENCES

- Amal, C.D., Chakravarty, C., Sen, G., Sukul, P. and Mukherjee, D. 2005. A comparative study on the dissipation and microbial metabolism of organophosphate and carbamate insecticides in orchaqualf and fluvaquent soils of West Bengal. *Chemosphere*, 58: 579-584.
- Ang, E.L., Zhao, H.M. and Obbard, J.P. 2005. Recent advances in the bioremediation of persistent organic pollutants via biomolecular engineering. *Enzyme Microb. Technol.*, 37: 487-496.
- Arbeli, Z. and Fuentes, C.L. 2007. Accelerated biodegradation of pesticides: An overview of the phenomenon, its basis and possible solutions; and a discussion on the tropical dimension. *Crop Protect.*, 26: 1733-1746
- Bhuyan, S., Sreedharan, B., Adhya, T.K. and Sethunathan, N. 1993. Enhanced biodegradation of gamma – hexachlorocyclohexane ( $\gamma$ -HCH) in HCH (commercial) acclimatized flooded soil: factors affecting its developments and persistence. *Plastic Sci.*, 38: 49-55.
- Busse, M.D., Ratcliff, S.H., Shestak, C.J. and Powers, R.F. 2001. Glyphosate toxicity and the effects of long-term vegetation control on soil microbial communities. *Soil Biol. Biochem.*, 33: p. 1777-1789.
- Chaudhry, G.R., Mateen, A., Kaskar, B., Sardesai, M., Bloda, M., Bhatti, A.R. and Walia, S.K. 2002. Induction of carbofuran oxidation to 4-hydroxycarbofuran by *Pseudomonas* sp. *FEMS Microbiol. Lett.*, 214(2): 171-176.
- Cycon, M., Wójcik, M. and Piotrowska-Seget, Z. 2009. Biodegradation of the organophosphorus insecticide diazinon by *Serratia* sp. And *Pseudomonas* sp. and their use in bioremediation of contaminated soil. *Chemosphere*, 76: 494-501.
- Gupta, R.C. 2006. *Toxicology of Organophosphate and Carbamates Compounds*. Academic press, Cambridge, MA.
- Kumar, M., Yadav, A.N., Saxena, R., Paul, D., and Tomar, R.S. 2021. Biodiversity of pesticides degradation microbial communities and their environmental impact. *Biocatal. Agric. Biotechnol.*, 31: 101883
- Kwong, T.C. 2002. Organophosphate pesticides: biochemistry and clinical toxicology. *Therap. Drug Monitor.*, 24: 144-149.
- Monkiedje, A. and Spiteller, M. 2002. Effects of the phenyl amide fungicides, mefenoxam, and metalaxyl, on the biological properties of sandy loam and sandy clay soils. *Biol. Fertility Soil*, 35: 393-398.
- Mulligan, C.N. 2005. Environmental applications for biosurfactants. *Environ. Pollut.*, 133: 183-198.
- Parekh, N.R., Hartmann, A., Charnay, M.P. and Fournier, J.C. 1995. Diversity of carbofuran-degrading soil bacteria and detection of plasmid-encoded sequences homologous to the MCD gene. *FEMS Microbiol. Ecol.*, 17: 149-160.
- Rache, K.D. and Coats, J. 1988. Comparative biodegradation of organophosphorus insecticides in soil. Specificity of enhanced microbial biodegradation. *J. Agric. Food Chem.*, 36: 193-199.
- Rieger, P.A., Meier, H.M., Gerle, M., Vogt, U., Groth, T. and Knackmuss, H.J. 2002. Xenobiotics in the environment: present and future strategies to obviate the problem of biological persistence. *J. Biotechnol.*, 94: 101-123.
- Satish, G. P., Ashokrao, D.M. and Arun, S.K. 2017. Microbial degradation of pesticide: A review. *Afr. J. Microbiol. Res.*, 11(24): 992-1012. doi:10.5897/ajmr2016.8402
- Scott, H.D.. 2000. *Soil Physics: Agricultural and Environmental Applications*. 1st. edition. Iowa State University Press, Ames, Iowa, USA.
- Singh, R.P. 2001. Comparison of organochlorine pesticide levels in soil and groundwater of Agra, India. *Bull. Environ. Contam.Toxicol.*, 67: 126-132.
- Yañez-Ocampo, G., Penninckx, M., Jiménez-Tobon, G.A., Sánchez-Salinas, E. and OrtizHernández, M.L. 2009. Removal of two organophosphate pesticides employing bacteria consortium immobilized in either alginate or tezontle. *J. Hazard. Mater.*, 168: 1554-1561.



# Study on the Establishment of the Gastropod *Lymnaea stagnalis* (Linné, 1758) as a Bio-sentinel to Monitor the Water Quality of North Algerian Rivers: Case of the El-Malah River

I. Benali\*(\*\*)\*†, M. Bouderbala\* and N. Chèvre\*\*\*

\*Laboratory Network for Environmental Monitoring (LRSE), University of Oran I Ahmed Ben Bella, BP 1524 El M'naouer, 31000 Oran, Algeria

\*\*Faculty of Natural and Life Sciences, University of Science and Technology Mohamed Boudiaf USTO/MB, BP 1505 El Menaouar, 31036 Oran, Algeria

\*\*\*Faculty of Geosciences and Environment, University of Lausanne, 1015 Lausanne, Switzerland

†Corresponding author: I. Benali; [ibenali@yahoo.fr](mailto:ibenali@yahoo.fr)

Nat. Env. & Poll. Tech.  
Website: [www.neptjournal.com](http://www.neptjournal.com)

Received: 06-08-2021

Revised: 27-09-2021

Accepted: 24-10-2021

## Key Words:

Gastropods  
Sentinel species  
River El-Malah  
Biomarkers  
Condition indices  
Biometric parameters

## ABSTRACT

Biomonitoring is a key solution for assessing the effects and risks of pollutants to preserve the most vulnerable ecosystems, including aquatic ecosystems. This study aims in establishing the gastropod *Lymnaea stagnalis*, as a sentinel species to assess the water quality of the El-Malah river in the Algerian North-West. Three sites were chosen along the river: upstream (US), midstream (MS), and downstream (DS). The responsiveness of the aquatic snails has been compared using physiological and biological markers: condition index (CI), volumetric condition index (VCI), acetylcholinesterase (AChE), glutathione s-transferase (GST), and catalase (CAT). Additionally, the occurrence of changes in biometric parameters of the specimens has also been treated: shell height (SH), shell thickness (ST) total weight (TW), and the ratio ST/SH. Snails from the site MS reacted in front to the water deterioration with low biometric values (ST  $1.28 \pm 0.17$  cm; SH  $1.83 \pm 0.20$  cm; TW  $2.95 \pm 0.69$  cm), and condition indices values (CI  $31.19 \pm 3.58$ ; VCI  $2.09 \pm 0.53$  g.cm<sup>-3</sup>), thereby signaling smaller individuals compared to the population of site US. Whereas, no specimen was recorded in the site submitted to wastewaters discharge (DS). This indicates that the degradation of the water quality affected the growth and the viability of the snails. Furthermore, a significant induction in the GST activity ( $88.98 \pm 10.72$  nmol min<sup>-1</sup>mg<sup>-1</sup>), and a significant inhibition in the CAT activity ( $82.85 \pm 9.49$  μmol min<sup>-1</sup>mg<sup>-1</sup>) were recorded in the site MS, whereas no statistically significant variation was observed in AChE activity. *L. stagnalis* demonstrated biological and physiological variability between the studied contrasting sites of the El-Malah River. These results allow us to propose this species as a model in the ecotoxicology of western Algerian freshwaters.

## INTRODUCTION

Earth's freshwater surface accounts for only 3% of the total volume of terrestrial water. This surface supports life and other services that are vital to human well-being (Reddy et al. 2018), and are therefore important to survey and protect. In the North-Algerian fringe, rivers are vulnerable ecosystems because of the increase of anthropic pressure, i.e., water uses, mostly for irrigation, and industrial, agricultural, and domestic discharges. Thus, we need robust monitoring tools to survey the quality of these aquatic systems and protect their biodiversity.

Sentinel organisms can allow determine hot spots of pollution in rivers (Goncharov et al. 2020). But these organisms should have a wide geographical distribution and should be sensitive to environmental constraints. Currently,

no sentinel organisms are known for monitoring western Algeria freshwaters.

Worldwide, the most used sentinel species for aquatic systems are Mollusks. For salt and estuarine waters, some researchers used clams to evaluate the water quality in Spain (*Ruditapes philippinarum*) (Maranho et al. 2015), or India (*Meretrix casta*) (Avelyno et al. 2018). In recent studies, we successfully used the filtering mussel *Mytilus galloprovincialis*, as a bioindicator for evaluating the state of the Algerian coasts (Benali et al. 2017). Regarding freshwaters, zebra mussels *Dreissena polymorpha* have been proposed as possible reference bioindicator organisms (Châtel et al. 2015). However, bivalve-filtering organisms, which could be used as sentinel organisms, have not yet been identified in freshwater biotas from Northwestern Algeria. It would be therefore important to test and select an available sentinel species



that is endowed with specific reactivity to environmental stress.

Besides filtering organisms, gastropods are of particular interest for monitoring the pollution of aquatic areas. They can be found in all types of freshwater ecosystems (stagnant and current), where they constitute up to 50% of the benthic invertebrate biomass (Cummings et al. 2016). Indeed, gastropods have well-suited characteristics for ecotoxicology surveys: 1) they have limited migration patterns allowing for assessing site-specific impacts (Smitha & Mustak 2017); 2) they play a significant role as links in the food chain, as primary consumers (grazers and detritus feeders) (Côte et al. 2015); 3) as potential bio accumulators, they can give some indications on the behavior of persistent pollutants and their bioaccumulation potential. For all these reasons, it is interesting to test and evaluate gastropods as early warning sentinels of habitat deterioration in local freshwater biotopes.

A good candidate would be the gastropod *Lymnaea stagnalis* which is a fairly common species in ponds, lakes, and rivers across the northern continents of the world (Kemenes & Benjamin 2009), and the countries of northern Africa, such as Algeria. This snail has already been used to monitor the effects of organic and non-organic chemicals, and it was described as a model of choice for the study of human-induced ecotoxicological and evolutionary processes (Côte et al. 2015). Furthermore, this species was studied in the laboratory through bioassays tests using biological markers as pollution early-warning systems (Bouétard et al. 2013, Atli & Grosell 2016, Lance et al. 2016), but has not yet been used in biomonitoring studies conducted in the field. Through this study, we would like to demonstrate our interest in this species and establish it as a model for monitoring freshwater ecosystems in Algeria. Moreover, it is relevant and important to improve the knowledge of the sensitivity of biological responses of this organism, using ecotoxicological tools such as biomarkers, and to provide the first data on the health status of Algerian rivers through biomonitoring surveys.

Among other parameters, biomarkers are reliable and valuable indicators of toxic effects on bio-sentinel organisms (Valavanidis et al. 2006). They are considered the most promising tool in environmental health surveys. The primary goal of using biomarkers is to allow the early detection of pressure due to pollution (Nickolson & Lam 2005) at the biochemical, physiological, and behavioral levels before a dysfunction is visible at the community and ecosystem levels (Amiard et al. 1998). Physiological indices have also shown to be suitable indicators of chemical stress (Guerlet 2007). They serve to provide information on the physiological state and growth of organisms (Andral et al. 2004) and indicate physiological

disturbances between populations (Benali et al. 2017). By combining physiological and biochemical measurements (biomarkers), we can estimate the degree of chemical stress the organism was exposed to and therefore determine hot spots of pollution (Sharifinia et al. 2016). Furthermore, the quality of the habitat's water can be determined by the measurements of physico-chemical parameters. A relationship between the biotope's abiotic factors and the dynamics of gastropod populations (growth, survival) has already been demonstrated (Smitha & Mustak 2017).

Three biomarkers were chosen because of their biological involvement and their usual use in ecotoxicology surveys. 1) Catalase (CAT) is an intracellular antioxidant enzyme involved in defense systems against radicals: reactive oxygen species (ROS), produced by oxidizing ambient pollutants (Benali et al. 2015). CAT is essential for the degradation of hydrogen peroxide ( $H_2O_2$ ).  $H_2O_2$  is a precursor of the hydroxyl radical and is a species that is reactive with  $O_2$  causing DNA damage (Halliwell & Gutteridge 1999). 2) GST is an enzyme family involved in the metabolism of glutathione which belongs to non-enzymatic antioxidant systems (Valavanidis et al. 2006). GST is also known to be involved in the biotransformation mechanism of organic compounds in freshwater *Mollusks* (Lance et al. 2016). 3) Acetylcholinesterase (AChE) is a neurotoxicity biomarker. They participate in the functioning of the central and peripheral nervous systems. AChE is commonly used to detect the toxicity of organophosphate and carbamate pesticides (Tufi et al. 2016), but this enzyme is also sensitive to heavy metals (Mora et al. 1999) and hydrocarbons in *Mollusks* (Kopecka et al. 2006) and even plant oils (Lopez et al. 2015) and the temperature (Bocquené & Galgani 1998, Benali et al. 2015) can influence its activity.

The main goal of this study is to demonstrate the sensitivity and the usefulness of aquatic gastropod *Lymnaea stagnalis* as an ecological descriptor, of water quality in freshwater ecosystems from North-Western Algeria. This was done using morphometric parameters and measuring physiological and biochemical markers in individuals collected from different sites of the El-Malah river. We have also measured the water physico-chemical parameters of the study sites.

## MATERIALS AND METHODS

### Sampling Sites and Strategy

The El-Malah River has located 65 km from the city of Oran, which is the main city in western Algeria. This river is among the most important rivers in terms of flow and volume of water in western Algeria and is characterized by brackish water. Because of the urbanization, the river carries domestic

wastewater from several municipalities and as well from an industrial detergents fabricant. Moreover, an important agricultural area borders the river.

Three contrasting locations in El-Malah River were considered: upstream (US), midstream (MS), and downstream (DS) (Fig. 1). Into the river, we sampled *L. stagnalis* in two locations: US and MS, during the winter season, 2017. At the DS site, no specimen was noticed.

- The upstream side (US) (35°20'47.34''N, 0°59'06.62''W). This site seemed like a relatively preserved area regarding the clearness of the water and the biodiversity of species. Near this location, there is a freshwater source about 200m from the sampling point. In this study, the US is considered as a less impacted area in the river (reference site).
- The midstream side (MS) (35°21'03.83''N, 0°59'42.53''W). At this site, the water is muddy and the specimens are less developed morphologically than in the US. This place is characterized by a very important agricultural area with many cultures, and a part of the irrigation water is pumped directly from this site. We also noted the presence of metal and plastic wastes.
- The downstream side (DS) (35°24'57.76''N, 1°4'50.86''W). This side of the river is subject to a flow of waste-

waters from two neighboring localities (3830 m<sup>3</sup>.d<sup>-1</sup>), and an industry of detergent. As specified before, no specimen of the species *L. stagnalis* was observed in the river after the discharge of the sewage.

Samples of water were collected on the surface using polyethylene bottles, previously washed with distilled water. They were transported and frozen at -20°C in plastic bottles until physico-chemical analyses.

Twenty specimens of pond snail *L. stagnalis* (1.6±0.2 cm), were collected from each of the sampling areas. The specimens were immediately transported to the laboratory, where the morphometric measurements were done for the calculation of condition indices and the ratio. After a stabling period of 48 H, the whole soft tissue of the rest of the organisms was dissected and then stored at -80 °C for the biochemical measurements.

### Hydrological Parameters

Collected water samples in the three stations mentioned above were tested for different physico-chemical parameters. The water temperature was measured *in situ* and the other parameters: pH, electrical conductivity (EC), suspender matter, total phosphate, and orthophosphate were performed in the water company of Oran SEOR. The pH was measured with a

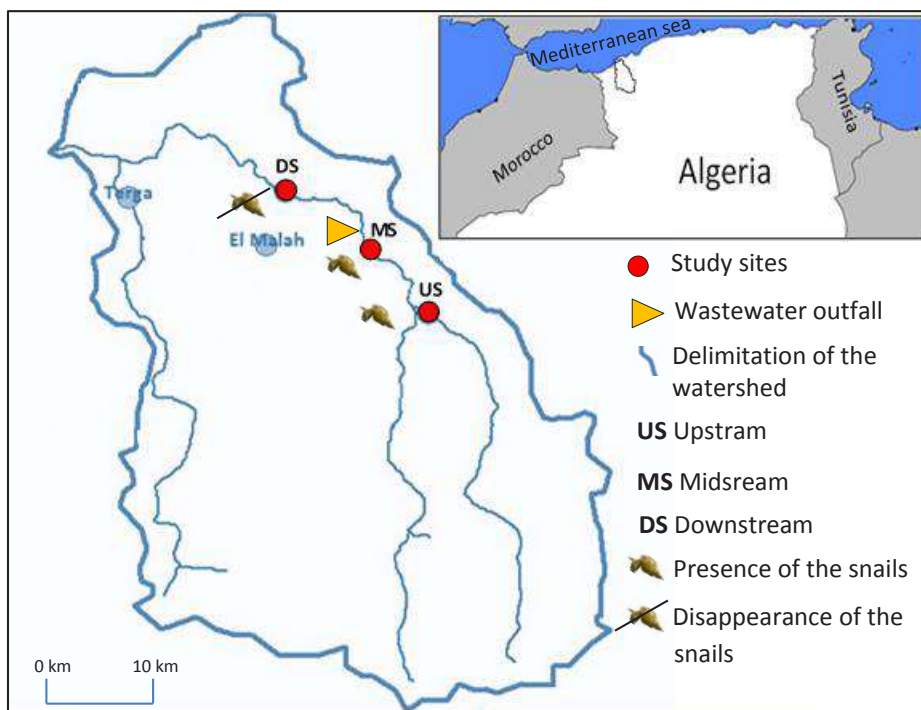


Fig. 1: Schematic locations of the study sites.

pH meter WTW *inoLab® Cond 7310* fitted with an electrode previously calibrated. The conductivity is measured with an electrical conductivity meter type WTW *inoLab® pH 7310* which directly measures the conductivity of the sample in ms/cm or  $\mu\text{s}/\text{cm}$ . Suspended matters were determined by filtering a volume of water on the cellulosic filter (0.45-micron meter). Total phosphate and orthophosphates were determined by colorimetric determination by a spectrophotometer (Rodier 2009). For the site DS, the physico-chemical data are those obtained in 2019 during the same season (winter).

## Biological Analyses

**Biometric Parameters and Physiological Condition Indices:** Morphometric parameters of fifteen specimens were considered in this study, including the shell high (SH), the thickness of the shell (ST) the total weight of the specimen (TW) (Fig. 2), and the ST/SH ratio (Zbikowska & Zbikowski 2005). We also calculated two condition indices to determine the physiological condition of the specimens: 1) CI: condition index, based on the wet chair. It is calculated using the ratio of (weight of soft tissues/total weight of specimens) multiplied by 100 (AFNOR 1985). 2) VCI: Volumic condition index, based on the shell volume. It is calculated according to the equation:  $3 \times \text{weight of soft tissue} / ((x(\text{ST}))^2 \times \text{SH})$  ( $\text{g} \cdot \text{cm}^{-3}$ ) (Guerlet 2007).

## Biochemical Markers

Three biomarkers were analyzed in the snails (AChE: acetylcholinesterase, CAT: catalase, and GST: glutathione S-transferase). Before the analyses, the whole soft tissues of five snails were dissected. For measuring AChE, the tissues were ground and homogenized in Tris-HCl buffer (0.1 M, pH 7.5) (1:4 w/v), while for the measures of CAT and GST, the tissues were ground in phosphate buffer (100 mM, pH 6.5) (1:5 w/v). The homogenates were centrifuged at 9000 g for 20 min at 4°C (Benali et al. 2017). Aliquots of the supernatant

(S9 fraction), containing the cytosol, endoplasmic reticulum, Golgi apparatus, and cytosolic proteins, were frozen at -80 °C until analysis.

The AChE activity was assayed by the method of Ellman et al. (1961). Acetylthiocholine is hydrolyzed by AChE to acetic acid and thiocholine. According to this method, the catalytic activity is measured by the increase of the yellow anion, 5-thio-2-nitrobenzoate (TNB), which absorbs at 412 nm; TNB is produced from thiocholine when it reacts with 5, 50-dithio-bis-2-nitro benzoic acid (DTNB). The enzyme kinetics reaction is measured for 20 min at 25°C using a spectrophotometer. For this method, 50  $\mu\text{L}$  of S9 was added to a reaction mixture containing 850  $\mu\text{L}$  Tris-HCl (0.1 M pH 7.5) and 50  $\mu\text{L}$  (1875 mM) DTNB. After preincubation, the reaction begins with the addition of 50  $\mu\text{L}$  of 8.25 mM acetylthiocholine. AChE activity was expressed in nmoles of thiocholine produced/min/mg protein.

The reaction mixture for the determination of GST activity consists of 20 mM of 1-chloro-2,4-dinitro-benzene (CDNB; Sigma) dissolved in 100 mM phosphate buffer at pH 6.5 with 100 mM of reduced glutathione and 10  $\mu\text{L}$  of the supernatant fraction S9. GST activity is determined at 340 nm at 25 °C for the 30s according to Habig et al. (1974). The results are calculated as nmol of substrate hydrolyzed  $\text{min}^{-1} \text{mg}^{-1}$  relative to the protein in the sample.

CAT activity was determined following the method described by Claiborne (1985), i.e., through the measurement of the rate of enzymatic decomposition of  $\text{H}_2\text{O}_2$  as a substrate at 240 nm for 30 s at 25 °C. In this application, 750  $\mu\text{L}$  of phosphate buffer (100 mM, pH 7.4) was added to 200  $\mu\text{L}$  of  $\text{H}_2\text{O}_2$  (500 mM) in a spectrophotometer tank. The enzymatic reaction starts by adding fraction S9. Enzyme activity was expressed in  $\mu\text{mole}$  of  $\text{H}_2\text{O}_2$  hydrolyzed/min/mg protein.

The quantity of proteins present in the S9 fraction was determined via the Coomassie blue method using bovine serum albumin (BSA) as the standard. The absorbance of samples was measured at 595 nm according to Bradford (1976).

## Statistical Analyses

Twenty specimens of *L. stagnalis* were collected per station for the calculation of physiological indices and biochemical measurements, which represent a total of 40 gastropods. Data are expressed as the mean  $\pm$  standard deviation. The data were tested for homogeneity of variance through a Levene test. Significant variations of biochemical markers and physiological indices recorded between the different study sites were tested with a one-way analysis of variance (ANOVA) at  $p < 0.05$ . Post-hoc comparisons were made using the significant honest difference (HSD) Duncan test ( $p < 0.05$ ,  $p < 0.001$ ), to discriminate between sites. Statistical analyses



Fig. 2: Schematic representation of the shell height measurement (SH), and the thickness of the shell (ST).

were performed using the STATISTICA software program (v. 6.1.478.0 Statsoft).

## RESULTS AND DISCUSSION

The general objective of the study was to evaluate if *L. stagnalis* could be sensitive to environmental disturbances and therefore used as sentinel species. This was done by studying their physiological and biochemical changes in different parts of the river, two sites presumed polluted (mid and downstream) in comparison with another site ostensibly less polluted (upstream). We first analyzed the physical appearance of the sampling sites.

### Physico-Chemical Parameters

The physico-chemical water quality of the El-Malah River has been determined in the three study sites: US, MS, and DS. The recorded analysis results shown in Table 1 have been compared to international standards of the World Health Organization (WHO 2006).

The results indicate that the values of the different parameters vary generally between the sites. Temperatures of the river water are higher in the site US (14°C), in comparison with the site MS (12°C), and the site DS (12°C), because of the naturally warm groundwater source that joins the river not far from the site US and warms this place. The pH of the water is higher in the site submitted to the flow of wastewaters (DS) (8.2), compared to US (7.21), and MS (6.98). The suspended matters (SM) are higher in the site MS (90 mg.L<sup>-1</sup>), and the site DS (30 mg.L<sup>-1</sup>), compared to the reference site (US), exceeding the threshold tolerable by WHO (30 mg.L<sup>-1</sup>). The elevation of suspended matters might be related to anthropic releases (wastewaters), and the clay nature of the floor. In the same line, we observe high concentrations of PO<sub>4</sub><sup>-3</sup> and total phosphates in the impacted sites MS (0.071 mg.L<sup>-1</sup> and 0.227 mg.L<sup>-1</sup>, respectively), and DS (1.73 mg/l and 2.95 mg/l, respectively), compared to the reference site

the US, with an exceedance of WHO permissible values in the site DS. These results indicate a longitudinal degradation of the water from the site US to the site DS, particularly linked to agriculture runoff containing fertilizer and wastewater outlets. Indeed, various authors described that the increase in the values of orthophosphates is a sign of urban influence (Peric et al. 2018), such as agriculture and wastewaters (Sharma et al. 2016, Sunantha & Vasudevan 2016). The electrical conductivity values (EC) are higher in all the studied sites: (8400 µs.cm<sup>-1</sup>); MS (8750 µs.cm<sup>-1</sup>); DS (5750 µs.cm<sup>-1</sup>). The high conductivity of El Malah river water is normal due to its brackish nature. However, the low value of the conductivity in the site DS could be linked to the significant inflows of wastewater which would dilute the water.

### Growth and Physiological Condition

The mean values of morphometric parameters (shell height, shell thickness, and total weight), and biometric ratio (ST/SH) for *L. stagnalis* are presented in Table 2. The general observation of the results shows significantly lower values ( $p < 0.05$ ) of all morphometric parameters (ST, SH, and TW) in the population collected midstream the river (MS) compared to the reference population collected upstream (US). Whereas no specimens were recorded in the site DS, which is subjected to a flow of wastewaters. The obtained results in the site MS suggest that the specimens sampled at the site exposed to human activity are smaller in size and therefore less developed than those from the reference site. This could indicate that degradation of river water quality affects snail growth. The shell morphological variability of *Lymnaea* has already been described as the result of an environmental influence (Zbikowska & Zbikowski, 2005), and a relationship was established between abiotic factors and the dynamics of gastropods (growth and survival) (Smitha & Mustak 2017). Moreover, the reduction of shell growth could be also related to the presence of pollutants such as trace metals, in particular, Zinc. Indeed, Soto et al. (2000)

**Table 1:** Quality physico-chemical parameters of water in the different sampling stations and comparison of values with the WHO standards

Sites/season	US site	MS site	DS site	WHO standards
Parameters	Winter 2017	Winter 2017	Winter 2019	
T [°C]	14	12	12	15-21
pH	7.21	6.98	8.2	6.5-8.5
Conductivity [µs.cm <sup>-1</sup> ]	8400*	8750*	5750*	1500
Suspender matter SM [mg.L <sup>-1</sup> ]	20	90*	32*	30
Total phosphate {mg.L <sup>-1</sup> }	0.048	0.071	1.73	0.5
Orthophosphate PO <sub>4</sub> <sup>3-</sup> [mg.L <sup>-1</sup> ]	0.150	0.227	2.95	1

\* Exceeding the WHO standards; - No threshold values.



summarized in their work that the reduced growth of flesh and shell of *Mollusks* (in their study case, mussels), was related to the bioavailability of Zinc in the environment. As described above, the midstream side of the river could be exposed to pesticides, containing Zinc, from agricultural lands near the sampling point. Alternatively, reduced shell growth could be related to other natural factors such as seasonal variations and food availability. In view of our results, we can suggest the use of the shell size of specimens as an indicator of habitat deterioration. The ratio (ST/SH) gave similar results for both populations indicating a similar shape of the shells. According to Zbikowska & Zbikowski (2005), this index indicates a slender shell shape when values are low and a large shell shape when values are high. Our results demonstrated that the water degradation of the river did not affect the morphological shape of specimens. Other studies on the subject could indicate if it might be a difference between populations of snails from other rivers. The disappearance of snails in the part of the river subjected to wastewater (DS) could indicate that pollution by domestic and/or industrial effluents has a strong impact on our species of snails.

Fig. 3A and 3B present the comparison of the results of physiological indices (CI and VCI) of the populations from the sites US and MS. The digital data of analyses are given in the Supporting Information. Here too, we have recorded

the same general trend. The lower values were found in the population MS compared to the reference population US, with significant differences for CI ( $p < 0.05$ ). Condition indices express the soft-tissue mass in relation to the total mass or measurements of the shell. Generally, we record high values of condition indices in the presence of organic matter of natural origin (algae, phytoplankton bloom) (Romeo et al. 2003) or anthropogenic origin (municipal waste) (Schiedek et al. 2006). In our case, the high values of CI and VCI at the site US can be related to the high biomass of algae *Cladophora sp.*, that adult snails are very fond of. Indeed, as it was mentioned above, the site US seemed relatively preserved and characterized by the biodiversity of species. However, the significant low values of the condition indices in the site MS might reflect the consequences of pollution, as this site is exposed to strong agricultural activity. Indeed, Guerlet (2007), described limitation of the growth has already been demonstrated, in the *L. stagnalis* exposed to high concentrations of herbicides (Diquat). In the same study, a negative correlation between ICV and the degree of contamination by heavy metals and HAPs in the Zebra mussels *Dreissena polymorpha* was demonstrated.

### Biochemical Markers

Fig. 4 compares the measured biomarker variations (GST,

Table 2: Means  $\pm$  standard deviation of biometric parameters, biometric ratios, and physiological indices of *L. stagnalis* from the upstream river site (US) and the downstream river site (DS).

	ST [cm] (Mean $\pm$ SD)	SH [cm] (Mean $\pm$ SD)	TW [g] (Mean $\pm$ SD)	ST/SH (Mean $\pm$ SD)
US site	0.62 $\pm$ 0.08	1.77 $\pm$ 0.22	1.07 $\pm$ 0.20	0.35 $\pm$ 0.05
MS site	0.54* $\pm$ 0.08	1.56* $\pm$ 0.14	0.78* $\pm$ 0.17	0.35 $\pm$ 0.04
DS site	-	-	-	-

SD: standard deviation; \* Significance set (bold\*) at  $p < 0.05$ ; – No specimens

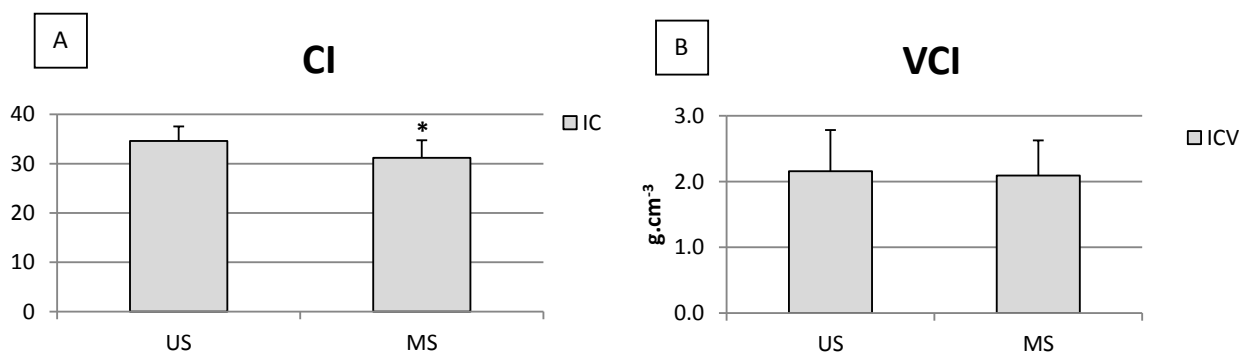


Fig. 3: Condition indices ( $n = 15$ , mean  $\pm$  SD); A) condition index (CI), B) volumic condition index (VCI) ( $g \cdot cm^{-3}$ ) of *L. stagnalis* collected from Upstream (US) and Midstream (MS) of the River. \* Indicates the difference between sites is significant at  $p < 0.05$ .



CAT, and AChE) between the populations of snails collected from the site US and the site MS. Fig. 4A is a comparison of GST activity between the studied sites and shows a highly significant difference ( $p < 0.05$ ), between the two populations of snails, with high values in the population of site MS. This induction of this enzymatic activity could be due to the presence of stressors such as pollutants of organic, biological or chemical nature. For example, a strong induction of GST activity has been demonstrated by exposing *L. stagnalis* to herbicides: glyphosate (Lance et al. 2016), diquat and aural (Guerlet 2007), copper sulfate contained in fungicides and molluscicides (Côte et al. 2015), and even during exposure to secondary metabolites of cyanobacteria (Lance et al. 2016). It has also been shown the role of GSTs in the detoxification of organic compounds such as organochlorines, in other mollusks, such as bivalves (Damiens et al. 2007). Moreover, in the presence of metal excess, gastropods may respond through mechanism adjustments, such as the bio-transformation system (detoxification) (Côte et al. 2015), to which GSTs enzymes belong.

Fig. 4B shows a significant variation ( $p < 0.05$ ) in CAT activity between the different sites, with the lowest value in the site MS, which is in contrast to the results of GST activity. As cited above, these enzymes participate in the

anti-oxidant defense systems against radicals. The decrease in CAT activity in the site MS might suggest that the enzymes have been submerged by the production of ROS upon exposure to oxidative stressors, such as pesticides, heavy metals, complex effluents, etc. (Guerlet 2007). Indeed, a collapse of the antioxidant defense mechanism, via the CAT activity, has already been demonstrated in several studies. Several authors have reported that long periods of exposure to contaminants, such as metals (Stoys et al. 2000, Duarte et al. 2011) or cyanobacteria toxins (Lance et al. 2006), can invade the antioxidant defense in the Mollusks. For instance, in the case of mussels, authors refer to a “biochemical adaptation” in the CAT responses (Lionetto et al. 2003), and their induction/inhibition depending on pollutant concentrations (Atli & Grosell 2016), the exposure time (Duarte et al. 2011), tissue or species (Atli & Grosell 2016).

No variation was statistically highlighted for the AChE activity between the studied sites (Fig. 4C). The values are substantially similar, to the last significant digit. Several hypotheses can be suggested to interpret our results. This could indicate that 1) there is no neurotoxic compound that may affect AChE activity in the presumed affected site DS; 2) pollutants are not present at a toxic dose; 3) snails have not been exposed to pollutants long enough for the toxic

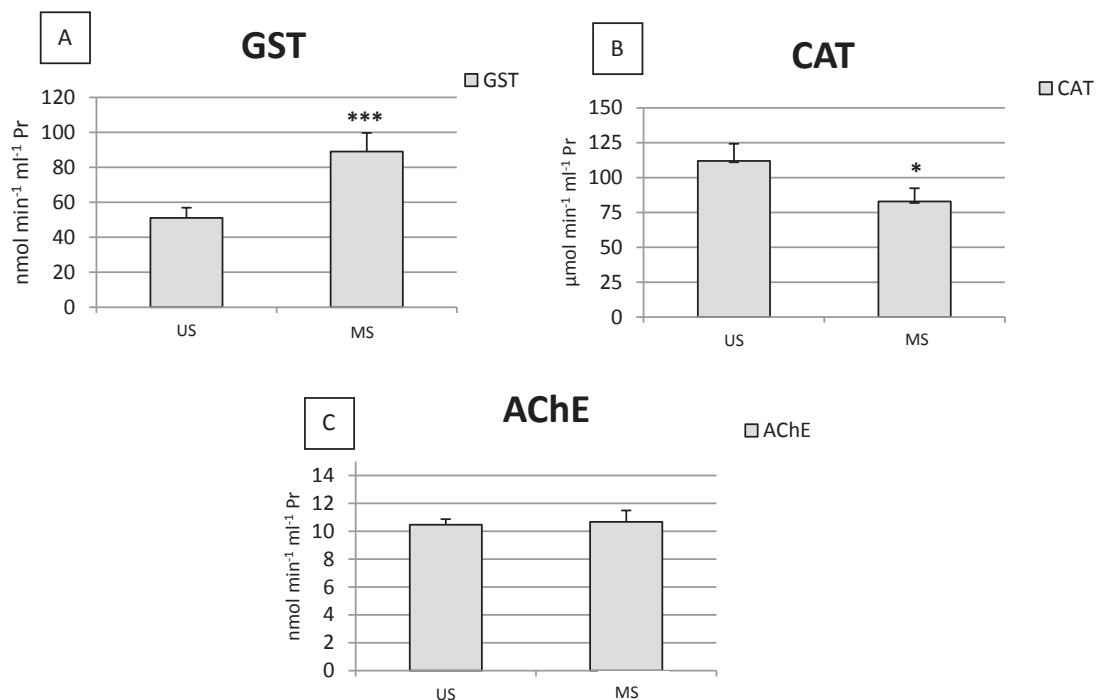


Fig. 4: Biomarker activity ( $n = 5$ , mean  $\pm$  SD) ; A) glutathion-s-transferase (GST), B) catalase (CAT) and C) acetylcholinesterase (AChE) in *L. Stagnalis* collected from Upstream (US) and Downstream (DS) of El-Malah River. \* Indicates the difference between sites is significant at  $p < 0.05$  and \*\*\* significant at  $p < 0.001$ .

effect to be expressed on cholinesterase activity; 4) both populations are prone to neurotoxic damage because of the presence of neurotoxic compounds. Comparing the level of AChE activity obtained for our species (09.86-11.87 nmol. min<sup>-1</sup>mg<sup>-1</sup>) with the literature, we can suggest that our last hypothesis might be the most plausible. Indeed, Gagnaire et al. (2008) have recorder values of 11.4-4.9 nmolmin<sup>-1</sup>mg<sup>-1</sup> in freshwater gastropods *Potamopyrgus antipodarum* exposed to an organophosphate and Schiedek et al. (2006) have reported low values of AChE activity, between 25-40 nmol min<sup>-1</sup> mg<sup>-1</sup>, in mussels at a site characterized by agricultural dominance. A decrease in the cholinesterase activity was extensively described (Tufi et al. 2016) depending on the time and dose of pollutants, such as insecticides (Lionetto et al. 2003, Gagnaire et al. 2008). However, the low values could be also related to the presence of heavy metals (Mora et al. 1999), hydrocarbons (Kopecka et al. 2004), and even the temperature can influence the enzyme activity (Bocquené & Galgani 1998, Benali et al. 2015).

## CONCLUSION

The presented pilot study aimed to propose the freshwater invertebrate *Lymnaea stagnalis*, as a model in ecotoxicology in west Algerian rivers. Our observations and results on the El Malah river revealed a longitudinal decrease in water quality, reflected by higher values of MS and nutrients (phosphates), and the presence of wastewater discharges. The physiological indicators measured on the *L. Stagnalis* individuals showed that the snail's growth was affected by river quality decrease and that a high level of pollution, led to the disappearance of the species. The antioxidant biomarkers showed significant variations in GST and CAT activities between populations, but no significant variability was observed for AChE activity.

This study allowed establishing a link between the absence of *Lymnaea stagnalis* and urban wastewater discharges and highlights the toxic effects of pollutants in the sites situated within the agricultural region. Considering the observed variability in the physiological and biochemical compartment of the snails *L. stagnalis* in the contrasted habitats, we suggest that freshwater species would be a suitable bioindicator of contaminant distribution within the river.

## ACKNOWLEDGMENTS

The authors are grateful to the Institute of Earth Surface Dynamics (IDYST), the University of Lausanne for its welcome.

## REFERENCES

- AFNOR 1985. Cupped oysters. Names and classification, NF V 45-056. pp. 5.
- Amiard, J.C. Gefard, A. and Amiard-Triquet, C. 1998. Metallothionein in the mussel *Mytilus edulis* as a biomarker of metal pollution: variability between sites, seasons, and organs. *J. Rech. Oceanogr.* 23: 25-30.
- Andral, B., Stanisiere, J.Y., Sauzade, D., Damier, E., Thebault, H., Galgani, F. and Boissery, P. 2004. Monitoring chemical contamination levels in the Mediterranean based on the use of mussel caging. *Mar. Pollut. Bull.*, 49: 704-712.
- Atli, G. and Grosell, M. 2016. Characterization and response of antioxidant systems in the tissues of the freshwater pond snail (*Lymnaea stagnalis*) during acute copper exposure. *Aqua. Toxicol.*, 176: 38-44.
- Avelyno, H.D., Shyama, S.K. and Praveen Kumar, M.K. 2018. The Backwater Clam (*Meretrix casta*) is a bioindicator species for monitoring the pollution of an estuarine environment by genotoxic agents Swizzle Furtado. *Mutat. Res. Gen. Tox. En.*, 825: 8-14.
- Benali, I., Boutiba, Z., Grandjean, D., De Alencastro, L.F., Rouane-Hacène, O. and Chèvre, N. 2017. Spatial distribution and biological effects of trace metals (Cu, Zn, Pb, Cd) and organic micropollutants (PCBs, PAHs) in mussels *Mytilus galloprovincialis* along the Algerian west coast. *Mar. Pollut. Bull.*, 115: 539-550.
- Benali, I., Boutiba, Z., Merabet, A. and Chèvre, N. 2015. Integrated use of biomarkers and condition indices in mussels (*Mytilus galloprovincialis*) for monitoring pollution and development of biomarker index to assess the potential toxicity of coastal sites. *Mar. Pollut. Bull.*, 95: 385-394.
- Bocquené, G. and Galgani, F. 1998. Biological effects of contaminants: Cholinesterases inhibition by organophosphate and carbamate compounds. *Proc. ICES Tech. Mar. Environ. Sci.*, 22: 1-13.
- Bouétard, A., Besnard, A.L., Vassaux, D., Lagadic, L. and Coutellec, M.A. 2013. Impact of the redox-cycling herbicide diquat on transcript expression and antioxidant enzymatic activities of the freshwater snail *Lymnaea stagnalis*. *Aqua. Toxicol.*, 126: 256-265.
- Bradford, M.M. 1976. A rapid and sensitive method for the quantitation of microgram quantities of protein utilizing the principle of protein-dye binding. *Anal. Biochem.*, 72: 248-254.
- Châtel, A., Faucet-Marquis, V., Gourlay-Francé, C., Pfohl-Leszkowicz, A. and Vincent-Hubert, F. 2015. Genotoxicity and activation of cellular defenses in transplanted zebra mussels *Dreissena poly morphis* along the Seine river. *Ecotoxicol. Environ. Safety*, 114: 241-249.
- Claiborne, A. 1985. Catalase Activity. In: Greenwald, R.A. (Ed), *Handbook of Methods for Oxygene Radical Research*. CRC Press, Boca Raton, FL, pp. 283-284.
- Côte, J., Bouétard, A., Pronost, Y., Besnard, A.L., Coke, M., Piquet, F., Caquet, T. and Coutellec, M.A. 2015. Genetic variation of *Lymnaea stagnalis* tolerance to copper: A test of selection hypotheses and its relevance for ecological risk assessment. *Environ. Pollut.*, 205: 209-217.
- Cummings, K.S., Jones, H.A. and Lopes-Lima, M. 2016. Rapid Bioassessment Methods for Freshwater Molluscs. 185-207. In T.H. Larsen (ed.), *Core standardized methods for rapid biological field assessment*. Conservation International, Arlington, VA, pp. 209.
- Damiens, G., Gnassia-Barelli, M., Loquès, F., Roméo, M. and Salbert, V. 2007. Integrated biomarker response index as a useful tool for environmental assessment evaluated using transplanted mussels. *Chemosphere*, 66: 574-583.
- Duarte, C.A., Giarratano, E., Amin, O.A. and Comoglio, L.I. 2011. Heavy metal concentrations and biomarkers of oxidative stress in native mussels (*Mytilus edulis chilensis*) from Beagle Channel Coast (Tierra del Fuego, Argentina). *Mar. Pollut. Bull.*, 62: 1895-1904.
- Ellman, G.L., Courtney, K.D., Andres, V. and Featherstone, R.M. 1961. A new and rapid colorimetric determination of acetylcholinesterase activity. *Biochem. Pharmacol.* 7: 88-95.
- Gagnaire, B., Geffard, O., Xuereb, B., Margoum, C. and Garric, J. 2008. Cholinesterase activities as potential biomarkers: Characterization in two freshwater snails, *Potamopyrgus antipodarum* (*Mollusca*, Hydrobiidae, Smith 1889) and *Valvata piscinalis* (*Mollusca*, Valvatidae, Müller 1774). *Chemosphere*, 71(3): 553-560.

- Goncharov, A.V., Baturina, N.S., Maryinsky, V.V., Kaus, A.K. and Chalov, S.R. 2020. Ecological assessment of the Selenga River basin, the main tributary of Lake Baikal, using aquatic macroinvertebrate communities as bioindicators. *J. Great Lakes Res.*, 46: 53-61.
- Guerlet, E. 2007. Use of cellular biomarkers in several species of invertebrates for the assessment of contamination in freshwater environments. *Ecol. Environ. Univ. Metz.* 13: 317.
- Habig, W.H., Pabst, M.J. and Jakoby, W.B. 1974. Glutathione S-transferases: The first enzymatic step in mercapturic acid formation. *J. Biol. Chem.*, 249: 7130-7139.
- Halliwell, B. and Gutteridge, J.M.C. 1999. The Chemistry of Free Radicals and Related "Reactive Species". In *Free Radicals in Biology and Medicine*, Third ed. Oxford University Press, Oxford, pp. 36-104.
- Kemenes, G. and Benjamin, P.R. 2009. *Lymnaea*. *Curr. Biol.*, 19(1): 9-11.
- Kopecka, J., Lehtonen, K.K., Barsiené, J., Broeg, K., Vuorinen, P.J., Gercken, J. Pempkowiak, J. 2006. Measurements of biomarker levels in flounder (*Platichthys flesus*) and blue mussel (*Mytilus Baltic*). *Mar. Pollut. Bull.*, 53: 406-421.
- Lance, E., Desprat, J., Holbech, B.F., Gérard, C., Bormans, M., Lawton, L.A., Edwards, C. and Wiegand, C. 2016. Accumulation and detoxication responses of the gastropod *Lymnaea stagnalis* to single and combined exposures to natural (cyanobacteria) and anthropogenic (the herbicide RoundUp®Flash) stressors. *Aquatic Toxicology* 177: 116-124.
- Lionetto, M.G., Caricato, R., Giordano, M.E., Pascariello, M.F., Marinosci, L. and Schettino, T. 2003. Integrated use of biomarkers (acetylcholinesterase and antioxidant enzymes activities) in *Mytilus galloprovincialis* and *Mullus barbatus* in an Italian coastal marine area. *Mar. Pollut. Bull.*, 46: 324-330.
- Lopez, M.D., Campoy, F.J., Pascual-Villalobos, M.J., Muñoz-Delgado, E. and Vidal, C.J. 2015. Acetylcholinesterase activity of electric eel is increased or decreased by selected monoterpenoids and phenylpropanoids in a concentration-dependent manner. *Chem. Biol. Interact.*, 229: 36-43.
- Maranho, L.A., Andre, C., Del Valls, T.A., Gagné, F. and Martín-Díaz, M.L. 2015. Adverse effects of wastewater discharge in reproduction, energy budget, neuroendocrine, and inflammation processes observed in marine clams *Ruditapes philippinarum*. *Estuar. Coast. Shelf Sci.*, 164: 324-334.
- Mora, P., Fournier, D. and Narbonne, J.F. 1999. Cholinesterases from the marine mussels *Mytilus galloprovincialis* LmK. and *Mytilus edulis* from the freshwater bivalve *Corbicula fluminea* Muller. *Comp. Biochem. Physiol. C*, 122: 353-361.
- Nickolson, S. and Lam, P.K.S. 2005. Pollution monitoring in Southeast Asia using biomarkers in the *Mytilidae* mussel *Perna viridis* (Mytilidae: Bivalvia). *Environ. Int.*, 31: 121-132.
- Peric, M.S., Kepčija, R.M., Miliša, M., Gottstein, S., Lajtner, J., Dragun, Z., Marijić, V.F., Krasnići, N. and Ivanković, D. Erk, M. 2018. Benthos-drift relationships as proxies for the detection of the most suitable bioindicator taxa in flowing waters - a pilot study within a Mediterranean karst river. *Ecotoxicol. Environ. Safety* 163: 125-135.
- Reddy, M.T., Sivaraj, N., Kamala, V., Pandravada, S.R., Sunil, N. and Dikshit, N. 2018. Classification, characterization, and comparison of aquatic ecosystems in the landscape of Adilabad District, Telangana, Deccan Region, India. *Open Access Lib. J.*, 5: 4459.
- Rodier J. (ed) 2009. *Water Analysis*. Dunod, pp. 1600.
- Romeo, M., Hoarau, P., Garelló, G., Gnassia-Barelli, M. and Girard, J.P. 2003. Mussel transplantation and biomarkers as useful tools for assessing water quality in the NW Mediterranean. *Environ. Pollut.*, 122: 369-378.
- Schiedek, D., Broeg, K., Barsiene, J., Lehtonen, K.K., Gercken, J., Pfeifer, S., Vuontisjärvi, H., Vuorinen, P.J., De donyte, V., Koehler, A., Balk, L. and Schneider, R. 2006. Biomarker responses as indication of contaminant effects in blue mussel (*Mytilus edulis*) and female eelpout (*Zoarces viviparus*) from the Southwestern Baltic sea. *Mar. Pollut. Bull.*, 53: 387-405.
- Sharifinia, M., Mahmoudifard, A., Imanpour Namin, J., Ramezanpour, Z. and Yap, C.K. 2016. Pollution evaluation in the Shahrood River: Do physico-chemical and macroinvertebrate-based indices indicate the same responses to anthropogenic activities? *Chemosphere*, 159: 584-594.
- Sharma, R.C., Singh, N. and Chauhan, A. 2016. The influence of physico-chemical parameters on phytoplankton distribution in a headwater stream of Garhwal Himalayas: A case study. *Egypt. J. Aqua. Res.*, 42: 11-21.
- Smitha, N. and Mustak, M.S., 2017. Gastropod diversity with physico-chemical characteristics of water and soil in selected areas of Dakshina Karnataka district of Karnataka, India. *Int. J. Fauna Biol. Stud.*, 4(1): 15-21.
- Soto, M., Ireland, M.P. and Marigomez, I. 2000. Changes in mussel biometry on exposure to metals: implications in the estimation of metal bioavailability in 'Mussel-Watch' programs. *The Science of the Total Environment* 247: 175-187.
- Stohs, S., Bagchi, D., Hassoun, E. and Bagchi, E. 2000. Oxidative mechanisms in the toxicity of chromium and cadmium ions. *J. Environ. Pathol. Toxicol. Oncol.*, 19: 201-213.
- Sunantha, G. and Vasudevan, N. 2016. Assessment of bacterial indicators and physico-chemical parameters in Tiruppur, Erode, and Chennai, Tamil Nadu (India). *Environ. Nanotechnology, Monitoring & Management*, 6: 219-260.
- Tufi, S., Wassenaar, P.N.H., Osorio, V., de Boer, J., Leonards, P.E.G. and Lamoree, M.H. 2016. Pesticide mixture toxicity in surface water extracts in snails (*Lymnaea stagnalis*) by an in vitro acetylcholinesterase inhibition assay and metabolomics. *Environ. Sci. Technol.*, 50(7): 3937-3944.
- Valavanidis, A., Vlachogianni, T., Dassenakis, M. and Scoullos, M. 2006. Molecular biomarkers of oxidative stress in aquatic organisms in relation to toxic environmental pollutants. *Ecotoxicol. Environ. Safe.* 64: 178-189.
- WHO, 2006. A proposal for Updating Lebanese Norm of Drinking Water (1999) based on WHO Guidelines. WHO, Washington DC.
- Žbikowska, E. and Žbikowski, J. 2005. Differences in shell shape of naturally infected *Lymnaea stagnalis* (L.) individuals as the effect of the activity of digenetic trematode larvae. *J. of Parasitology*, 91(5): 1046-1051.





# Financial Incentives for Promotion of Electric Vehicles in India- An Analysis Using the Environmental Policy Framework

Rajiv V. Shah

T. A. Pai Management Institute, Manipal Academy of Higher Education, Manipal-576104, Karnataka, India

†Corresponding author: Rajiv V. Shah; rajivshah13@gmail.com

Nat. Env. & Poll. Tech.  
Website: [www.neptjournal.com](http://www.neptjournal.com)

Received: 13-09-2021  
Revised: 30-10-2021  
Accepted: 15-11-2021

## Key Words:

Air pollution  
Financial incentives  
Electric vehicles  
Environmental policy  
EV policy  
JEL classification

## ABSTRACT

India has seen some of the most damaging social and environmental effects of air pollution in recent times. It has also committed at the COP 21 in Paris to help reduce global warming. Following this voluntary agreement, India plans to increase the share of electric vehicles to 30% of total vehicles sold by 2030 to reduce air pollution. This paper studies the major financial incentives and policy measures undertaken since 2015 as part of the EV policy and views it through the lens of the Environmental Policy Framework, which considers five major types of instruments: Regulations and Standards, Green Taxes, Incentives, and Subsidies, Carbon Credits and Voluntary Negotiations. Another instrument called 'Information Dissemination Measures' is added to this framework to help evaluate the current EV policy. We find that while there are good financial incentives, to begin with, charging infrastructure and research in battery technology needs to be increased in India. There is also an urgent need to improve communication and awareness about EVs and their role in the reduction of pollution to help overcome the hesitancy in adopting this new technology.

## INTRODUCTION

Global Warming has a direct connection with air pollution, especially with the emission of greenhouse gases. India has witnessed some of the most damaging environmental and social effects of air pollution in recent periods. It is estimated that about 1.2 million people in India died prematurely in 2019 from diseases directly related to air pollution (IEA 2021), making it the fifth leading cause of death in the country. Six of the ten most polluted cities in the world are situated in India (IEA 2021). In most cities, particulate matter concentration has constantly exceeded international and local standards, thus having an adverse effect on the quality of air inhaled by citizens. Close to half of India's population lives in areas having less than seven months of 'clean air days' as defined by the Central Pollution Control Board (CPCB) of India. The push for a better standard of living by increasing industrial activities has increased Carbon Dioxide emissions by over 55% in the last decade and is expected to go up by another 50% by 2040, thus making India one of the largest contributors to growth in carbon dioxide emissions worldwide (IEA 2021). It is in this context that India has committed to the Paris Agreement under the United Nations Framework Convention on Climate Change (UNFCCC 2015) (also called the Paris Agreement 2015 or COP 21) to reduce the emissions intensity of its GDP by 33-35% by 2030 from 2005 levels.

It has also committed to reducing global warming to below 1.5 degrees Celsius compared to pre-industrial levels. Currently, India is considered the only G-20 nation to be on track to achieve the renewable energy targets commensurate with a reduction of 2 degrees of global warming (Dubash et al. 2018).

About a third of the air pollution is caused due to transportation. Almost 40% of Nitrogen Oxides and 14% of Carbon dioxide emissions in India are due to transportation sector activities (Climate Transparency 2020). Efforts towards electrification of road transport and commissioning stringent emission norms can contribute significantly towards the reduction of sulfur dioxide, nitrogen oxides, and particulate matter emissions. This has a positive impact on the achievement of Sustainable Development Goals as agreed at the UN. The overall move towards electrification of vehicles can help in the achievement of SDG 7 (Affordable and sustainable energy), SDG 11 (Sustainable cities), and SDG 13 (Combat climate change and its impacts).

Technology is expected to play an important role in countering climate change and measures to mitigate the pollution. In its report, 'Air Pollution and Climate Policy Integration in India-Frameworks to deliver co-benefits, the International Energy Agency (2021) has suggested linkages between mitigative technology in certain sectors and environmental benefits as shown in Table 1.



Table 1: Mitigative technology and effect on emissions.

Sector	Technology interventions	Benefits: reduction in emission
Power	Use of renewable sources; air pollution control measure	Sulfur dioxide, nitrogen oxides, particulate matter, carbon dioxide
Transport	Electrification of road transport; vehicle emission norms	Sulfur dioxide, nitrogen oxides, particulate matter
Households	Use of LPG and PNG for cooking	Indoor air pollution and particulate matter
Industry	Energy efficiency; renewable sources of power; air pollution control measure	Sulfur dioxide, nitrogen oxides, particulate matter, carbon dioxide

(Source: IEA 2021)

India plans to increase the share of electric vehicles (EVs) to 30% of total vehicles sold, by 2030 in its effort to meet the EV 30@30 agreement. By 2040, 15% of four-wheelers and more than half of the two and three-wheelers in India are expected to be electric. The sale of electric vehicles in India has grown seven-fold from 22,000 units in 2015-16 to 155,400 units in 2019-20. Over 90% of these vehicles are electric two-wheelers (Society of Manufacturers of Electric Vehicles, n.d.). However, even with this growth, the sale of electric vehicles represents less than 1% of the total vehicles currently sold in India. This implies that unprecedented and imaginative measures will be required to meet the target of EV 30@30 policymakers. The initial push toward the adoption of EVs in India started with the National Electric Mobility Mission Plan launched in 2013 with the aim of having sales of 6 to 7 million electric and hybrid vehicles by 2020 (Dixit 2020). Thereafter, the government launched the Faster Adoption and Manufacturing of (Hybrid &) Electric Vehicles in India (FAME-India) Scheme in 2015 to give a clearer vision to the EV adoption plan.

This study analyses the incentives and measures undertaken as part of the overall policy to help increase the adoption of EVs in India. These measures are analyzed using the Environmental Policy Framework and its components to understand the balance of different types of policy instruments.

This introductory section is followed by the literature review and conceptual framework of environmental policy. Thereafter, the financial incentives and other measures are identified in the subsequent section. The findings are linked with the conceptual framework in the Analysis section. The conclusions and recommendations follow the analysis.

## PAST STUDIES

Toxic emissions from ICE vehicles are a major contributor to air pollution (Khurana et al. 2020). EVs can reduce air pollution, noise pollution, and greenhouse gas emissions from transportation activities, in addition to being energy efficient (Brady & O'Mahoney 2011, Figenbaum et al. 2013, Hawkins et al. 2013). EVs can contribute to the reduction

of oil demand, emission of carbon dioxide, and dependence on non-renewable sources of energy. They could facilitate a shift toward clean energy production, thus having a positive impact on the pollution levels in the country (Gomez Vilchez et al. 2013).

Despite the doubling of absolute carbon dioxide emissions, India is likely to meet its obligations made in Paris 2015 by the year 2030. On a per-capita basis, these emissions would be lower than current world averages. However, these forecasts assume that there will be a reduction from the current electricity demand estimates and a faster transition to energy from renewable sources (Dubash et al. 2018).

Tarei et al. (2021) identified five categories of factors that create barriers to the adoption of EVs: infrastructural issues, financial barriers, behavioral issues, technical factors, and external influences. An environmental policy aimed at encouraging the adoption of EVs can help overcome these barriers. Further, the sale of EVs increases not just with incentives, but also with a range of attractive cars to appeal to the social needs of customers (Figenbaum et al. 2013).

The components of each country's EV policy must be considered by looking at the characteristics of the economy and behavior patterns of the population (Rietmann & Lieven 2019a). An ideal policy mix would consist of tools to incentivize production and adoption of EVs on one hand and ban or disincentivize production and use of polluting vehicles on the other hand. It would be easier to target two-wheelers in the EV market due to their relatively low prices and to benefit the users of two-wheelers, who are more exposed and affected by air pollution (Shashidhar 2021, Vidhi & Shrivastava 2018).

Monetary incentives, regulatory measures, and infrastructure development have a positive correlation with the increase in the market share of EVs (Shekhar et al. 2019). Subsidies or tax benefits can provide the initial push to reduce air pollution (Wang & Fang 2018) and switch to EVs, followed by an increase in charging infrastructure (Rietmann & Lieven 2019b). An appropriate mix of policy tools is required for this change, which includes standards and norms in tandem

with incentives, or a 'carrot and stick' policy (Arimura 2008, Gomez Vilchez et al. 2013).

In addition to command-and-control tools and market-based incentives, there can be information-based instruments to help encourage eco-innovation. These information-based instruments could be voluntary in nature, such as the disclosure of emissions, potential environmental threats, etc. (Liao 2018). Leurent and Windisch (2011) found that in addition to command-and-control tools and market-based incentives there is another category called 'communication and diffusion instruments' that creates public awareness about EVs and encourages behavioral change. It consists of marketing and publicity activities and tries to understand and address the consumers' uncertainty about the use of EVs and related infrastructure.

Consumers' intention to adopt EVs is affected by attitude, usefulness, ease of use, and financial incentives among other factors. However, uncertainty or negative views of the consumer could impact the decision to buy an EV (Jaiswal et al. 2021). The purchase intention of an EV also depends on the buyer's attitude and impact on self-image. Advertising campaigns could appeal to the potential buyers' concern for the environment, and the possibility of being seen as high-status people and new technology adopters (Khurana et al. 2020). The Indian market is cost-sensitive, and ownership of cars represents a higher social status (Parmar et al. 2021).

Bakker & Trip (2013) forwarded six major suggestions for authorities to promote EVs: 1) Subsidies for consumers and EV businesses 2) Charging infrastructure to be set up at strategic locations- these public stations can also increase visibility and awareness, 3) Regulatory measures- these include free or discounted parking fees, permitting EVs on limited-access roads, toll discounts, mandating new housing projects to be EV ready, 4) Creating and spreading awareness through websites or apps with information about charging points, vehicles, etc., 5) Public transport through electric buses, and 6) Coordination between different forms of government, at the local, national and international level to ensure smooth and effective implementation of the EV strategy.

By encouraging newer technologies that reduce vehicle emissions, the quality of life is enhanced and so is the overall development of the region (Vidhi & Shrivastava 2018). While environmental subsidies can have a positive impact on an increase in environmental technology innovation and patents (Xiong & Shen 2020), this increase could be at the cost of the quality of patents and innovations (Han 2021). Among the strategies to reduce the cost of batteries which is one of the most expensive components of an EV, the top four strategies included incentives for cell manufacturing,

improving the availability of critical raw material and components to manufacture batteries, laying down standards and quality norms, and development of ancillary industries (Shekhar et al. 2019).

Greater coordination among stakeholders like city planners, municipal corporations, state, and central governments, electricity companies, and EV manufacturers is essential for the success of the EV policy (Bakker & Trip 2013, Shashidhar 2021). Dixit (2020) suggested three types of business models for the early adoption of EVs. The first is the PPP model, where the central government funds the electrification of state bus fleets, and the state government and private sector together collaborate to set up charging infrastructure. The second model is the pure government model, where the government decides to convert its entire fleet of vehicles to electric mode and sets up charging infrastructure using the services of public sector units. The third model is the manufacturer model where the EV seller sees a business opportunity in selling EVs and setting up charging infrastructure to attract users to the charging stations. Examples of all three models are seen in India in different contexts.

## CONCEPTUAL FRAMEWORK FOR DEVELOPMENT OF ENVIRONMENTAL POLICY

The conceptual framework for the development of an Environmental policy relies on two major categories of policy tools- Tax measures and non-tax measures. The tax measures include green taxes and incentives, while the non-tax measures include regulations, pollution permits, and voluntary negotiations. Alternatively, policy instruments have also been classified as command-and-control and incentive-based instruments. Literature suggests that an ideal environmental policy consists of some or all of these instruments, in varying proportions based on the need and characteristics of the economy (Arimura et al. 2008, Blackman & Harrington 2000, Braadbaart 1998, Gomez Vilchez et al. 2013, Kolstad 2000, Ligthart 1998, Wilson 1996).

The five types of instruments commonly used in the creation of environmental policy are outlined as under:

**Regulations and Norms:** These are alternatively called command-and-control measures and include bans and restrictions. If imposed in isolation, they could have a counter-productive effect and may induce polluters to misreport information and sidestep these regulations (Blackman & Harrington 2000, Ishikawa et al. 2012, Kolstad 2000). They also entail a systemic cost of reporting and conveying information (Joshi et al. 2001).

**Pollution Permits:** The most common permits are called carbon credits globally. They are a category of economic

instruments that allow businesses to buy and sell the right to pollute. Typically, if a business pollutes less than the norm, it earns credits to the extent of pollution saved. It can sell these credits to firms who have polluted more than the norms and by purchasing these credits, the polluting firms avoid being penalized. The major concern with this instrument is that it does not reduce pollution but simply shifts its location.

**Voluntary Negotiations:** An example of this could be the Paris 2015 agreement, where countries voluntarily decide to reduce pollution. This could be further picked up at the national level by companies wanting to project a more environment-friendly image and agreeing to accept pollution abatement technology.

**Green Taxes:** Taxes that try to internalize the cost of negative externalities due to pollution are called green taxes (Ligthart 1998). While these taxes are usually imposed on polluters, they can also be viewed as a measure to promote clean technology. For example, EVs can be promoted by levying a green tax on substitute goods, ie. Internal Combustion Engine (ICE) vehicles to make EVs appear more economical. Additionally, this instrument gives the government additional revenue to reduce pollution created by harmful activities.

**Incentives and Subsidies:** Sometimes called 'negative taxes', incentives, subsidies and tax deductions for reducing emissions, providing cheaper finance, etc. could indirectly help in pollution abatement (Ligthart 1998, Shah 2014)). These benefits could be specific to environment-friendly activities, or they could be generic, which could be used by all manufacturers.

In addition, there are information and communication-based instruments which help create awareness about polluting activities and environment-friendly measures, which in turn help to enhance or magnify the effect of the above five instruments (Leurent & Windisch 2011, Liao 2018, Shah & Guha 2021). This category of information-based instruments is being added as the sixth set of instruments to the existing five-point framework for this study, to understand the impact of the current policy for EVs in India.

## MEASURES TO PROMOTE THE PRODUCTION AND SALE OF EVS IN INDIA

The overall responsibility for planning and implementation of the FAME-India scheme lies with the Department of Heavy Industries. This scheme falls under the National Electric Mobility Mission Plan and aims at promoting the usage of economical and efficient electric and hybrid vehicles. The first phase of FAME ended in March 2019. Thereafter, the second phase, starting from April 2019 has been extended up to March 2022. The scheme targets the promotion of

electric buses, three-wheelers, four-wheeler passenger cars, and two-wheelers. The initial outlay for phase II is INR 100 billion, of which about 86% has been earmarked for demand creation through incentives. The breakup of fund allocation is as under:

The second phase aims to support 55,000 electric four-wheeler passenger cars and one million electric two-wheelers (GoI 2019). The demand incentives, which make up much of the budget outlay of the scheme are further broken up across different categories of EVs as given in Table 3.

The basis of the demand incentive calculation in Table 2 is the battery capacity measured in terms of kWh. Currently, the incentives are given at the flat rate of INR 20,000 per Kwh for buses, INR 15000 per Kwh for two-wheelers, and INR 10,000 for all other electric vehicles. There is a cap on the total incentive based on the cost of the vehicle (40% for buses and two-wheelers, 20% for others).

There are further incentives and subsidies granted by central and state governments to manufacturers and buyers of EVs in India. These, and the FAME incentives, can be broadly classified into two categories for ease of analysis- production level and purchase or consumer level. The first category deals with incentives to reduce the cost at the manufacturing level to enable production cost parity with

Table 2: Fund allocation for demand creation of EVs in India.

Sr no	Expenditure head	Fund allocation (%)
1	Demand incentives	85.96%
2	Charging Infrastructure	10%
3	Administrative expenses (Including publicity and Information, Education & Communication activities)	0.38%
4	Other Phase-I related expenses	3.66%
	Total	100%

Source: GoI, Gazette Notification for FAME-II: March 11, 2019.

Table 3: Demand incentive breakup of INR 85.96 billion across categories of EVs.

Category of EVs	INR [Billions]	Number of vehicles to be covered under the scheme
Buses	35.45	7090
4-wheelers (including strong hybrid)	5.51	55000
3-wheelers	25	500,000
2-wheelers	20	1,000,000
Total	85.96	

Source: GoI, Gazette Notification for FAME-II: March 11, 2019.

ICE vehicles. Purchase-related incentives help to smoothen out any variations that may remain after accounting for production-based incentives. It is possible to argue that some incentives in the former list could easily fit into the latter, or that some incentives are difficult to be strictly classified into any one category. This distinction is made only for ease of understanding. The break-up of production-based and purchase-related incentives are as under:

### **Production Level Incentives**

Demand incentives to manufacturers of EVs based on the FAME scheme as discussed above. The demand incentives based on Kwh of the EVs have increased substantially after 2019.

Manufacturers of components used in EVs can avail of full deduction of their infrastructure-related capital expenditure under section 35AD of the Income Tax Act 1961. While Income Tax Act allows for a deduction of mainly revenue expenditures, this section allows the EV firm to reduce its taxable profits further by subtracting their capital expenditures, thus paying little to zero taxes and improving cashflows.

From August 2019, the rate of GST (Goods and Services Tax) on EVs has been reduced to 5% from 12%. GST on chargers and charging stations has been reduced to 5% from 18%. The GST on the hiring of electric buses by local authorities has been completely exempted. Conversely, ICE vehicles attract GST @ 28%. Further, some states (eg. Andhra Pradesh) offer full State GST refunds to buyers on the purchase of EVs.

The Central Government has announced a Production-Linked Incentive (PLI) scheme in May 2021 to encourage the development of Advanced Chemistry Cells (ACC batteries) and has budgeted for INR 181 billion to be distributed as incentives to eligible manufacturers, thus helping reduce the costs of batteries which makes up almost half the cost of the EV (Shekhar et al. 2020). The scheme would be based on competitive bids and the minimum qualification criteria would depend on factors such as installed capacity, domestic value addition, and minimum investment amount. The commitment would entail setting up an ACC manufacturing facility with a capacity of at least 5GWh and ensuring at least 60% domestic value addition in the next five years (EY India 2021, Mohanty 2021).

### **Consumer Level Incentives**

In addition to the demand incentives at the Central level, various states also provide local incentives to make the purchase even more cost-effective. For example, the state of Gujarat offers incentives of INR 10,000 per kWh of battery capacity (maximum INR 20,000) for two-wheelers, INR 10,000

per kWh (up to INR 150,000) for four-wheelers, and a flat amount of INR 50,000 for three-wheelers. Similarly, states like Maharashtra and Delhi also offer substantial incentives to boost the central government measures. Many states in India have started offering incentives that include scrappage benefits in addition to direct subsidies.

According to section 80 EEB of the Income Tax Act 1961, from the year 2019, interest on a loan taken to purchase an electric vehicle is allowed as a deduction from taxable income up to an amount of INR 150,000. The loan must be taken from any financial institution and should be sanctioned between April 1, 2019, and March 31, 2023.

Registration charges for electric vehicles in India have been waived from August 2021 by the Ministry of Road Transport and Highways. EVs have also been exempted from paying road tax (Also called RTO tax) in many states. Road tax varies from state to state and in a state like Delhi, the rate can range from 4% to 15% depending on the type, value, and ownership of the vehicle.

EVs are exempted from payment of green tax on registration renewal (after 8-15 years). For ICE vehicles the current green tax on renewal of registration is in the range of INR 2000-3500 for a state like Maharashtra and up to 50% of road tax in Delhi.

## **ANALYSIS OF POLICY MEASURES**

The push for early adoption of EVs in India is a combination of multiple measures, the foremost being incentives, and subsidies. However, a major boost for this drive came when India agreed in Paris in 2015 to reduce pollution levels, specifically by deciding to have at least 30% of electric vehicles as part of the total vehicles sold by 2030. This gave the economy a vision and target that helped create policies to increase the adoption of EVs. In addition, there have been parallel moves to keep the taxes on polluting ICE vehicles high to act as a barrier for those looking at long-term investment in vehicles. The high taxes on fuels from non-renewable sources (like petrol, and diesel) have also forced consumers to consider cheaper alternatives.

The benefits outlined in the section above can be classified into the six categories of policy tools for environmental protection, as discussed earlier in the conceptual framework section. The GST and Income tax benefits, demand-based subsidies (central and state levels), PLI scheme, and waiver of road tax and registration charges can be collated under the 'Incentives and Subsidies' head. The higher GST on ICE vehicles and high taxes on fuels from non-renewable sources and the higher tax on ICE vehicle re-registration can be categorized as 'Green Taxes', albeit on substitute goods. The



stringent Bharat-VI pollution norms for ICE vehicles could be termed as 'Regulations and Standards'. The government's voluntary commitments regarding pollution reduction at the UNFCCC and the EV 30@30 decision are examples of voluntary negotiations and decisions. These could be followed up by voluntary decisions by major automakers in India to make a quick to gradual switch to EV production and setting up charging infrastructure. While there are no explicit carbon credit schemes in India (Chandra 2021), the awareness program is of extreme importance as it pertains to changing people's attitudes and behavior towards EVs. The budget outlay for Information, education, and communication is only 0.38% of the total funds allocated for demand incentives (Table 1). However, this activity will play a vital role in formalizing the transition to EVs in India.

When viewed through the Environment Protection Framework for policymaking, as discussed in the literature review section, the policy initiatives could be represented as in Fig. 1.

The figure highlights the focus on incentives and subsidies as a major instrument, which is necessitated by the high cost of EVs. India does not have an explicit carbon pricing scheme, though there are implicit mechanisms that penalize or reward carbon emissions. However, these schemes need to be developed further to make a meaningful impact (Chandra 2021). There is also an important role for awareness creation

(Leurent & Windisch 2011, Liao 2018) which can be a useful instrument to disseminate information about the benefits of EVs and can also be used to spread awareness of the other five instruments, thus helping increase their effects.

The government has also laid out norms for creating charging infrastructure for the EV firms, in line with the budget outlay for this purpose. Lack of charging infrastructure is one of the major barriers to the faster adoption of EVs (Rietmann & Lieven 2019a, Tarei et al. 2021), as there are not enough charging stations or battery-swapping facilities to create confidence in the minds of buyers. In addition, there is a need to create awareness about the benefits of EVs and the continuous availability, source cleanliness, and cost-economy of electricity for users. This may prove difficult for governments as they depend heavily on taxes generated from the production and sale of ICE vehicles and fuels from non-renewable sources. In the short run, such awareness campaigns carry the risk of derailing tax revenue budgets, though, in the long run, these measures could benefit the environment.

## CONCLUSIONS

This study shows that three types of policy instruments could play a vital role in helping make the transition to an electric fleet for the economy by 2030: 1) command-and-control measures, 2) economic or financial incentives and 3) information diffusion instruments. Human behavior is an impor-

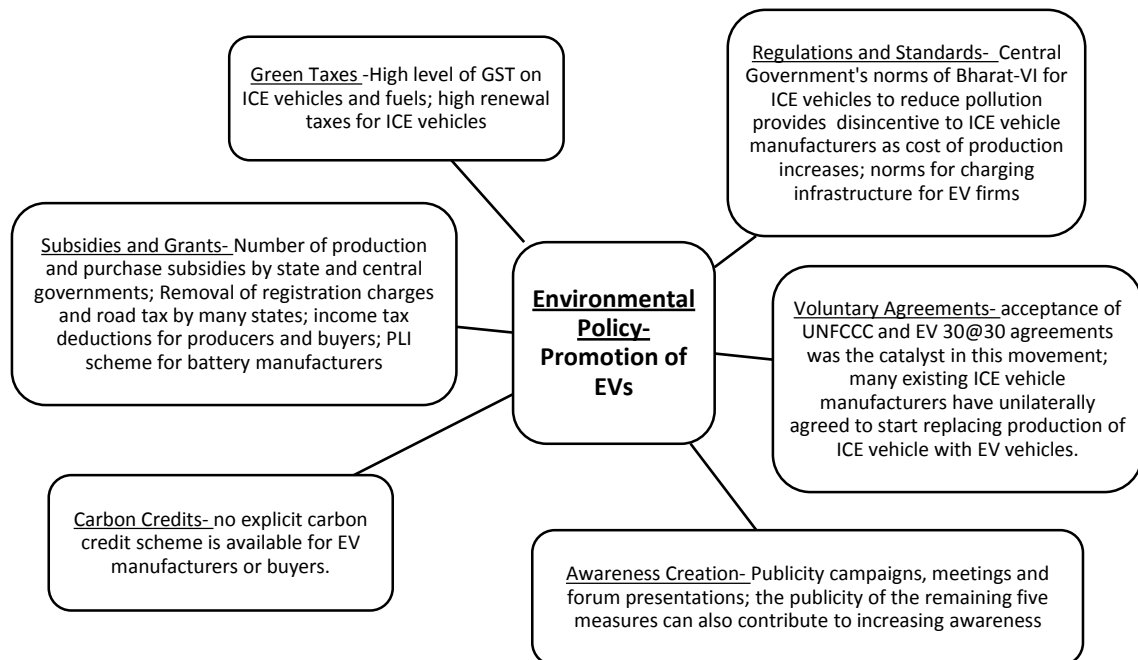


Fig. 1: EV policy initiatives linked to Environmental Policy Framework.



tant factor to be considered in policymaking and effective dissemination of information can help smoothen irrational behavior in relation to the proposed policy. For example, uncertainty about charging infrastructure could impact the buying behavior of consumers. This uncertainty could be countered with information about the number of charging stations, visibility of such stations and large vehicles being charged, and apps and websites giving updated information about charging infrastructure.

EV policy in India is being spearheaded by incentives and subsidies with good support from regulations, voluntary negotiations, and green taxes on polluting substitutes. Many of these incentives and benefits have been introduced in a meaningful and substantial manner only after 2019. Hence, the full impact of these measures on increase in sales of EVs is yet to be observed. However, to speed up the process, these measures need to be supported by awareness campaigns about the benefits of EVs and the pollution caused by ICE vehicles. In addition, information about the existing policy measures could help the consumer choose to move towards EVs as a preferred mode of transport and help the economy move towards reducing road pollution. Before this, the setting up of charging and battery-swapping stations, and research and development in battery technology need to be substantially improved for the awareness campaigns to have a substantial impact.

Post-FAME-II, there has been a substantial improvement in the intent and action of governments. However, there is an urgent need to focus on the creation of charging infrastructure, improve research in developing efficient batteries, and importantly, create awareness about EVs and policy measures to encourage the use of EVs.

## REFERENCES

- Arimura, T.H., Hibiki, A. and Katayama, H. 2008. Is a voluntary approach an effective environmental policy instrument: A case for environmental management systems. *J. Environ. Econ. Manag.*, 55(3): 281-295. <https://doi.org/10.1016/j.jeeem.2007.09.002>
- Bakker, S. and Trip, J.J. 2013. Policy options to support the adoption of electric vehicles in the urban environment. *Transport. Res. Part D Transport Environ.*, 25: 18-23. <https://doi.org/10.1016/j.trd.2013.07.005>
- Blackman, A. and Harrington, W. 2000. The use of economic incentives in developing countries: lessons from international experience with industrial air pollution. *J. Environ. Develop.*, 9(1): 5-44. <https://doi.org/10.1177/107049650000900102>
- Braadbaart, O. 1998. American bias in environmental economics: Industrial pollution abatement and incentives versus regulations. *Environ. Polit.*, 7(2): 134-152. <https://doi.org/10.1080/09644019808414396>
- Brady, J. and O'Mahoney, M. 2011. Travel to work in Dublin: The potential impacts of electric vehicles on climate change and urban air quality. *Transport. Res. Part D Transport Environ.*, 16: 188-193. <https://doi.org/10.1016/j.trd.2010.09.006>
- Chandra, T. 2021. Pricing Carbon: Trade-Offs and Opportunities for India. Observer Research Foundation, <https://www.orfonline.org/expert-speak/pricing-car>.
- Climate Transparency. 2020. Comparing G20 Climate Action and Responses to the Covid-19 Crisis: India.
- Dixit, A. 2020. India's EV policy. IAAE Energy Forum, Fourth Quarter 2020, pp. 34-37.
- Dubash, N.K., Khosla, R., Rao, N.D. and Bhardwaj, A. 2018. India's energy and emissions future: An interpretive analysis of model scenarios. *Environ. Res. Lett.*, 13(7): 74. <https://doi.org/10.1088/1748-9326/aacc74>
- EY India. 2021. How PLI scheme for battery manufacturing will boost India's EV market. Retrieved from [https://www.ey.com/en\\_in/tax/how-pli-scheme-for-battery-manufacturing-will-boost-india-ev-market](https://www.ey.com/en_in/tax/how-pli-scheme-for-battery-manufacturing-will-boost-india-ev-market)
- Figenbaum, E., Assum, T. and Kolbenstvedt, M. 2013. Electromobility in Norway: Experiences and opportunities. *Res. Transport. Econ.*, 50: 29-38. <https://doi.org/10.1016/j.retrec.2015.06.004>
- Gomez Vilchez, J.J., Jochem, P. and Fichtner, W. 2013. EV market development pathways - An application of system dynamics for policy simulation. *World Electr. Vehicle J.*, 6(4): 1030-1038. <https://doi.org/10.3390/wevj6041030>
- Government of India. The Gazette of India, dt.11/03/2019 §.
- Han, C. 2021. Impact of environmental subsidies on environmental technology innovation of polluting enterprises. *Nature Environ. Pollut. Technol.*, 20(3): 1277-1284. <https://doi.org/10.46488/NEPT.2021.v20i03.039>
- Hawkins, T.R., Singh, B., Majeau-Bettez, G. and Strømman, A.H. 2013. Comparative environmental life cycle assessment of conventional and electric vehicles. *J. Ind. Ecol.*, 17(1): 53-64. <https://doi.org/10.1111/j.1530-9290.2012.00532.x>
- IEA 2021. Air Quality and Climate Policy Integration in India. IEA, Paris. <https://doi.org/10.1787/c37f8d54-en>
- Ishikawa, J., Kiyono, K. and Yomogida, M. 2012. Is emission trading beneficial? Japan. *Econ. Rev.*, 63(2): 185-203. <https://doi.org/10.1111/j.1468-5876.2012.00570.x>
- Jaiswal, D., Kaushal, V., Kant, R. and Kumar Singh, P. 2021. Consumer adoption intention for electric vehicles: Insights and evidence from Indian sustainable transportation. *Technol. Forecast. Social Change*, 173: 121089. <https://doi.org/10.1016/j.techfore.2021.121089>
- Joshi, S., Krishnan, R. and Lave, L. 2001. Estimating the hidden costs of environmental regulation. *The Account. Rev.*, 76(2): 171-198.
- Khurana, A., Kumar, V.V.R. and Sidhpuria, M. 2020. A study on the adoption of electric vehicles in India: The mediating role of attitude. *Vision*, 24(1): 23-34. <https://doi.org/10.1177/0972262919875548>
- Kolstad, C.D. 2006. *Environmental Economics*. Oxford University Press, Oxford.
- Leurent, F. and Windisch, E. 2011. Triggering the development of electric mobility: A review of public policies. *Europ. Transport. Res. Rev.*, 3(4): 221-235. <https://doi.org/10.1007/s12544-011-0064-3>
- Liao, Z. 2018. Environmental policy instruments, environmental innovation, and the reputation of enterprises. *J. Clean. Prod.*, 171: 1111-1117. <https://doi.org/10.1016/j.jclepro.2017.10.126>
- Lighthart, J. 1998. The macroeconomic effects of environmental taxes-a closer look at the feasibility of "win-win" outcomes. Working Paper No. WP/98/75, IMF, Washington DC.
- Mohanty, A. 2021. COVID-19 has not affected the EV push in India. Retrieved September 1, 2021, from <https://www.vifindia.org/print/8412?via=Azure>
- Parmar, N., Misra, A., Ved, K. and Lad, O. 2021. Modeling the key barriers to the development of EV industry in India: using ISM and MICMAC analysis. *Int. Res. J. Eng. Technol.*, 8(4): 1030-1046.
- Rietmann, N. and Lieven, T. 2019a. How policy measures succeeded to promote electric mobility – Worldwide review and outlook. *J. Clean. Prod.*, 206: 66-75. <https://doi.org/10.1016/j.jclepro.2018.09.121>
- Rietmann, N. and Lieven, T. 2019b. A comparison of policy measures promoting electric vehicles in 20 countries. In Finger, M. and Audouin, M. (eds.), *The Governance of Smart Transportation Systems*, Springer International Publishing, NY, pp. 125-145. [https://doi.org/10.1007/978-3-319-96526-0\\_7](https://doi.org/10.1007/978-3-319-96526-0_7)

- Shah, R.V. 2014. Exploring the Need for Direct Tax Incentives for Plastic Waste Management in India. In Kreiser, L., Lee, S., Ueta, K., Milne, J.E. and Ashiabor, H. (eds.), *Environmental Taxation and Green Fiscal Reform: Theory and Impact*. Edward Elgar Publishing, Cheltenham, UK, Volume XIV, pp. 260-269. [https://doi.org/10.1163/\\_q3\\_SIM\\_00374](https://doi.org/10.1163/_q3_SIM_00374)
- Shah, R.V. and Guha, S. 2021. Private sector participation in solid waste management and regulatory strategy. *Econ. Polit. Weekly*, 56(32): 95-101.
- Shashidhar, K.J. 2021. Four policy issues to consider for electric vehicles in India. Retrieved January 9, 2021, from <https://www.orfonline.org/expert-speak/four-policy-issues-to-consider-for-electric-vehicles-in-india/>
- Shekhar, H., Sharma, S., Patel, U. and Sawant, V. 2019. Exploring Cost-Reduction Strategies for Electric Vehicle (EV) Batteries. Shakti Sustainable Energy Foundation, ICRIER, pp. 1-71. <https://doi.org/10.13140/RG.2.2.22198.65607>
- Society of Manufacturers of Electric Vehicles. n.d., EV Market Scenario India. Retrieved on October 28, 2021, from <https://www.smev.in/ev-sales>
- Tarei, P.K., Chand, P. and Gupta, H. 2021. Barriers to the adoption of electric vehicles: Evidence from India. *J. Clean. Prod.*, 291: 125847. <https://doi.org/https://doi.org/10.1016/j.jclepro.2021.125847>
- Vidhi, R. and Shrivastava, P. 2018. A review of electric vehicle lifecycle emissions and policy recommendations to increase EV penetration in India. *Energies*, 11(3): 1-15. <https://doi.org/10.3390/en11030483>
- Wang, J. and Fang, Y. 2018. Status, fiscal, and taxation policy adjustment of air pollution in China. *Nature Environ. Pollut. Technol.*, 17(3): 917-924.
- Wilson, D.C. 1996. Stick or carrot? The use of policy measures to move waste management up the hierarchy. *Waste Manag. Res.*, 14(4): 385-398.
- Xiong, H. and Shen, Y. 2020. Influence of government subsidies for green technology development on the performance of Chinese new-energy automobile enterprises. *Nature Environ. Pollut. Technol.*, 19(4): 1593-1598. <https://doi.org/10.46488/NEPT.2020.v19i04.026>



# Comparative Analysis of Compost Quality Produced from Fungal Consortia and Rice Straw by Varying C/N Ratio and its Effect on Germination of *Vigna radiata*

Pradeep Khyalia, Jyoti Dangi, Sheetal Barapatre, Geeta Dhania, J.S.Laura and Meenakshi Nandal†

Department of Environmental Sciences, Maharshi Dayanand University, Rohtak, Haryana, India

†Corresponding author: Meenakshi Nandal; nandalmeenakshi23@gmail.com

Nat. Env. & Poll. Tech.  
Website: [www.neptjournal.com](http://www.neptjournal.com)

Received: 14-09-2021

Revised: 14-11-2021

Accepted: 16-11-2021

## Key Words:

Organic waste  
Composting  
Inoculants  
Rice Straw  
Fungal consortia

## ABSTRACT

Composting is considered to be one of the best methods for handling organic waste. It is a natural process and takes months to give quality mature compost. Characteristics of initial wastes and process conditions are the compost maturity deciding factors. Some biological inoculants, e.g., bacteria and fungi, can reduce the compost time and improve its quality. This research is based on the hypothesis that using fungus consortia on rice straw will boost the activities of microbes and, as a result, the rate of composting. The hypothesis was tested by preparing compost using rice straw residue with and without the applications of fungal consortia. Fungal consortia of *Aspergillus flavus*, *Aspergillus fumigatus*, and *Aspergillus terreus* cellulose-degrading strains along with Pusa-1121 rice variety were used for the study. Different C/N ratios were achieved by varying rice straw, green leaves, poultry droppings, and fungal inoculant proportions. During various stages of composting, changes in total nitrogen, organic carbon, C/N ratios, and other parameters were calculated. The germination index of Mung beans (*Vigna radiata*) was used to measure the quality of the completed compost extract. Statistical analysis with the help of a two-tailed independent t-test at the confidence level of 95% was applied to determine the statistical difference between the treatments and control. It has been found that the Seed Germination index of treatment C/N 30 was 91.5% and that of C/N 26 was 79.1% which were significantly ( $p < 0.01$ ) different from the 54% GI of control.

## INTRODUCTION

Rice is an important crop farmed all over the world, second after maize, with an annual yield of roughly 800 million metric tonnes. India ranks second in the production of rice after China (Veena & Pandey 2011). More rice production will also lead to the generation of a large amount of rice straw. Although rice fulfills the world's food requirement, mishandling its straw waste will lead to different environmental problems. In India, Punjab, Himachal Pradesh, and Haryana burn 80 percent of rice straw, while Karnataka burns 50 percent and Uttar Pradesh burns 25 percent (Gupta et al. 2003). Many toxic chemicals are produced when the rice straw is burned, including carbon dioxide, carbon monoxide, methane, and nitrogen oxides (Gupta et al. 2004a, 2004b). According to a study, open-field rice straw burning contributes 0.05, 0.18, and 0.56 percent of Green House Gas emissions in India, Thailand, and the Philippines, respectively (Gadde et al. 2009). Another problem associated with Rice straw burning is the loss of nutrients in the soil. The solution to these issues rests in using rice straw as a source, as crop leftovers are good suppliers of plant nutrients and vital components for the agricultural ecosystem's stability (Ghosh et al. 2004). As a result, the use of organic matter as mineral fertilizers

is critical for long-term agricultural growth. Crop leftovers, animal shed wastes, rural and urban wastes, vegetable market wastes, and forest and industrialized wastes, all can be used as organic waste sources. India produces more than 3,000 million tonnes of organic waste annually (Gupta et al. 1998, Sharholy et al. 2008). Soil fertility and productivity get enhanced by recycling organic waste by composting in agriculture and using them as fertilizers (Tandon 1995, Chukwuka & Omotayo 2008, Ansari 2011).

When compared to other cereal straws, rice straw has a distinct chemical composition. On a dry weight basis, rice straw typically comprises lignin (10-15 percent), silica (75 percent), cellulose (40-50 percent), and hemicelluloses (9-12 percent) (Knauf & Moniruzzaman 2004). Consequently, rice straw waste is rich in silica and lignin, with a C/N ratio of roughly 80:1, making it difficult to decompose (Van Soest 2006, Kumar et al. 2008). Microorganisms are the bio-agents that degrade the waste matrix's cellulose and lignin components. These native microflorae are likely to produce higher enzymatic levels, which will speed up the composting process. However, only a few microbes efficiently use cellulose as a substrate (Kumar et al. 2010). A study by Cao et al. (2013) found that fungal consortia

of *Aspergillus fumigatus* degraded cellulose before other strains. Management of rice residue by directly incorporating straw into the soil has several drawbacks, including the immobilization of plant nutrients, notably nitrogen, and reducing subsequent crop germination (Nigam & Pandey 2009). As a result, farmers resort to in situ burning of crop wastes that are strewn around the field and impossible to collect (Jacobs et al. 1997, Reinhardt et al. 2001). However, governments are increasingly advising against burning crop leftovers since it could result in a significant economic loss. On the other hand, composting rice straw is emerging as a safe alternative option that results in the reusability of the nutrients contained within the residue (Banger et al. 1989, Gaiind et al. 2008, Sarkar & Chourasia 2017, Kumar & Singh 2021). Although a small amount of GHG is released during composting, the substrate with a low C/N ratio produces more  $\text{NH}_3$  and  $\text{CH}_4$  (Jiang et al. 2011). Carbon and nitrogen are essential for microbial breakdown. Therefore, the C/N ratio must be high at the start of the composting process for the process to get quickly (Ain et al. 2017). If the C/N ratio of paddy straw is too high, an exogenous nitrogen source must be added to lower the C/N ratio. As poultry droppings are high in nitrogen, mixing paddy straw with poultry droppings may be a suitable option for lowering the C/N ratio of paddy straw (Ashraf et al. 2007, Devi et al. 2010).

A study by Voběrková et al. (2017) revealed that the application of white-rot fungi and the fungal consortium had enhanced the degradation of organic waste which was indicated by a change in the C/N ratio, EC, pH, and higher Germination index. In the same manner, Wang & Ai (2016) reported the acceleration in the degradation process and formation of humic-like material, high composting efficiency, and degree of humification with the use of microbial activities on wheat bran. Heidarzadeh et al. (2019) found that the use of the fungal consortium of *Aspergillus* had reduced the C/N ratio and process time.

## MATERIALS AND METHODS

Rice straw was collected from the nearby village Madina, part of Rohtak district (Haryana), India. Pusa-1121 variety of rice was used in this study. Rice straw was cut into small pieces and delignified with 0.1% urea as the process makes it prone to degradation by cellulose enzymes. Rice straw was stacked in three bins for composting to achieve different C/N ratios by varying the ingredients (Rice Straw, Green leaves, Poultry droppings, and Fungal inoculant) proportions (Fig. 1 and Fig. 2). Composting was prepared by degrading rice straw using fungi (*Aspergillus sp.*) as inoculants, as shown in Table 1. *Aspergillus* species of fungal were provided by the laboratory at Maharshi Dayanand University, Rohtak.

### Analysis of Physico-Chemical Parameters of Compost

Compost bins were set up inverted to form heaps and for aeration, they were turned regularly. Compost samples were collected at an interval of 30 days, 60 days, and 90 days (Fig. 3). These samples were analyzed for the physico-chemical parameters through standard prescribed methods mentioned in Table 2.

### Seed Germination Index

Compost effectiveness was analyzed by subjecting the compost to the growth of seeds of Mung (*Vigna radiata*). First, seeds of *Vigna radiata* were dipped in 7% alcohol for about 3 min for disinfection purposes and then stirred intermittently for about 2 min in a suspension of 0.001  $\text{HgCl}_2$ . Next, the toxins of the seeds were removed by washing them properly with distilled water. After that, 10 mL of compost extract was put onto filter paper that had been spread on Petri plates. Following that, ten *Vigna radiata* seeds were sterilized and placed on filter paper. To prevent moisture loss, Petri plates were carefully taped and then incubated at room temperature for 72 h.



Fig. 1: Compost bins set up with different C/N ratios.



The percentage of seed germination, root elongation, and percentage of germination index (GI) was calculated as follows.

Calculation:

Seed germination (%) =

$$\frac{\text{No. of seeds germinated in compost extract}}{\text{No. of seed germinated in control}} \times 100$$



Fig. 2: Compost Piles of different C/N ratios.

Table 1: Treatments prepared for the compost:

Treatment	Initial C/N ratio	Rice Straw [g]	Green leaves [g]	Poultry dropping [g]	Fungal inoculant included
Treatment 1	26/1	500	1000	500	yes
Treatment 2	30/1	500	1000	500	yes
Treatment 3	Control	500	1000	500	No



30 Days Compost Sample



60 Days Compost Sample



90 Days Compost Sample

Fig. 3: Compost samples during processing.



Root elongation (%) =

$$\frac{\text{Mean root length in compost extract}}{\text{Mean root length in control}} \times 100$$

Germination Index =

$$\frac{\text{Seed germination(\%)} \times \text{Root elongation(\%)}}{100}$$

## RESULTS AND DISCUSSION

Rice straw was subjected to different physico-chemical parameters before processing for compost, as shown in Table 3. As a result, the moisture content of the straw was 11.7% and the C/N ratio calculated was 75.73:1. As the C/N ratio was high, poultry dropping was added to rice straw to decrease the ratio.

### Changes of Different Physico-Chemical Parameters of Compost from Control to Treatments

Compost samples were obtained at 30, 60, and 90 days, and physico-chemical analysis was performed. Fig. 4 depicts the changes in the parameters.

Due to the creation of ammonia, pH values typically range from weakly acidic to neutral or weakly alkaline, i.e., within the range 4.5-8.1. In general, the values are directly related to the activity of microorganisms involved in the composting process (Neklyudov et al. 2006). In all the sets, there was a trend of increasing pH with due course of composting. The ammonification process and biodegradation of short-chain fatty acids might be the reason for the rise in pH. Researchers recorded a similar increase in pH throughout the degradation period during composting of rice straw (Kaur & Katyal 2021). A significant ( $p < 0.05$ ) change was observed in pH value from control to treatments, as shown in Table 4. Moisture content showed a decreasing trend with composting time. Electrical conductivity increased in all the sets, as reported by other researchers (Barapatre et al. 2020). There was a significant difference ( $p < 0.05$ ) between EC of treatments C/N30 ( $2.55 \pm 0.06$ ) and C/N26 ( $2.02 \pm 0.09$ ) w.r.t control ( $1.84 \pm 0.04$ ). Electrical conductivity measures soluble salts in compost (Kumari et al. 2020) and regulates microbial activities (Shrivastava & Kumar 2015). The increase in EC could be due to an increase in phosphorous, calcium, sodium, potassium, and other ions concentration during composting (Bernal et al. 2009). The total organic carbon showed a trend of decreasing throughout the composting process. This might be due to the loss of carbon in the form of  $\text{CO}_2$ . The result complied with (Getahun et al. 2012). Total organic carbon of

90 days of compost showed a significant difference between control (19.19%) to first treatment (18.01%) and second treatment (18.02%). E4/E6 is the ratio of absorbance at 465 nm and 665 nm using a spectrophotometer. E4/E6 ratio is used for the humification index. With time, the ratio of E4/E6 has increased. It shows more production of humic and fulvic acid due to the degradation of organic material. Humic substances, the major component of soil organic matter in the compost, could increase shoot biomass via hormonal effects on root elongation and plant development (López-Bucio et al. 2003). Nitrogen, magnesium, Phosphorous, Calcium, Sodium, and potassium showed an increasing trend with the composting process. Treatments of all of these parameters were significantly ( $P < 0.05$ ) different from their control after 90 days of compost.

The C/N ratio is an essential metric for determining compost maturity and stability (Sharma & Garg 2018,

Table 2: Analytical techniques used for the evaluation of physico-chemical parameters of compost.

Parameters	Instrumental methods
pH	pH meter
Moisture content [%]	Gravimetric method
Electrical conductivity [ $\text{mS.cm}^{-1}$ ]	Conductivity meter
Total organic carbon [%]	Walkley and Black method (Walkley & Black 1934)
Total potassium [%]	Flame photometer
Total phosphorus [%]	Olsen method (Olsen et al.1954)
Total nitrogen [%]	Kjeldahl method (Katyal et al.1987, Bremner 1996)
E4/E6	Spectrophotometer
Total sodium [%]	Flame photometer
Total calcium [%]	EDTA method (Tucker & Kurtz-et 1961)
Total magnesium [%]	EDTA method (Tucker & Kurtz-et 1961)

Table 3: Physico-chemical Analysis of rice straw.

Parameters	Result
Electrical Conductivity [ $\text{mS.cm}^{-1}$ ]	5.37
Moisture content [%]	11.7
Total organic carbon [%]	46.2
Total Phosphorus [%]	0.25
Total Potassium [%]	1.26
Total Nitrogen [%]	0.61
C:N ratio	75.73:1

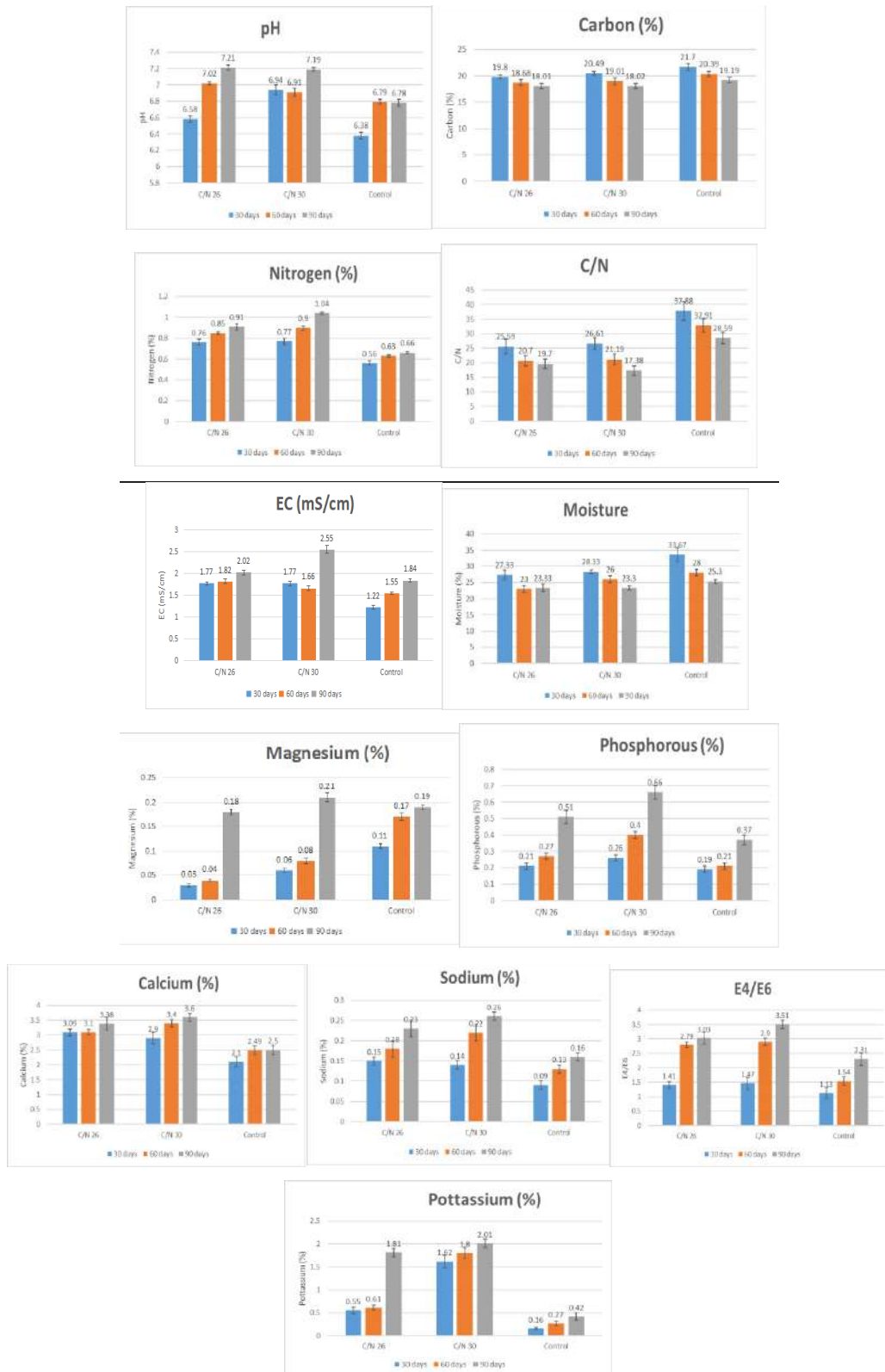


Fig. 4: Changes in the physico-chemical parameters during composting.

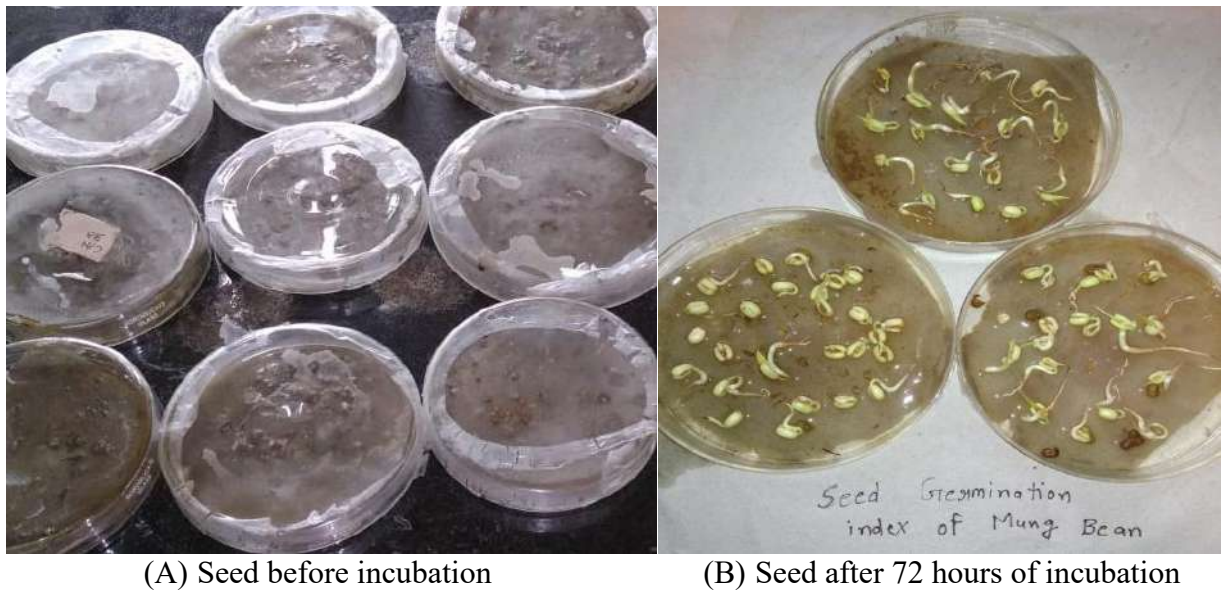


Fig. 5: (A-B).Seed germination of Mung (*Vigna radiata*).

Nozhevnikova et al. 2019). As carbon decreases and nitrogen increases, a decreasing trend was noted in all the treatments during composting, as also reported by (Chukwujindu & Dolin 2006). Initial ratio of C:N in C/N26 treatment was 25.59, which dropped to 19.07:1. C/N30 treatment had an initial C:N ratio of 26.61:1, which dropped to 17.38:1, while in the case of control, it dropped from 37.88:1 to 28.59:1. These results are in agreement with the finding of previous researchers (Barapatre et al. 2020). There was a significant ( $p < 0.05$ ) difference in the C:N ratio between treatments and control of 90 days of compost.

### Seed Germination Index of Mung Bean

Treatment two with an initial C/N ratio of 30 achieved a minimum C:N ratio of 17.38. The result showed that compost from treatment two had achieved maximum maturity and was suitable for applying in the agricultural field (Owis et al. 2016). A high C/N value in control, on the other hand, indicates that a significant amount of carbon has been left unused in compost (Dobermann & Fairhurst 2002). This is backed up by the fact that the Germination index (91.5%) of treatment two was the highest, followed by treatment one

Table 4: Changes in Physico-chemical parameters of Treatments from control.

Group	pH	Phosphorus [%]	Magnesium [%]	EC [ $\text{mS}\cdot\text{cm}^{-1}$ ]	Carbon [%]	C/N	Calcium [%]	E 4 / E6	Potassium [%]	Moisture (%)	Nitrogen (%)
Control	6.78	0.37	0.12	1.04	19.19	28.59	2.50	2.31	0.42	25.33	0.66
C/N 26	7.21*	0.51*	0.18*	2.02*	18.01*	19.7*	3.38*	3.03*	1.81*	23.33*	0.91*
C/N 30	7.19*	0.66*	0.21*	2.55*	18.02*	17.38*	3.60*	3.51*	2.01*	23.33*	1.04*

\* Significant at  $P < 0.05$ , Two-tailed independent t-test

Table 5: Seed germination index of Mung bean (*Vigna radiata*).

Treatments	Seed Germination [%]	Root Elongation [%]	Seed Germination Index [%]
Control	82.76	65.3	54
C/N 26	95.72**	82.72**	79.1**
C/N 30	98.96**	92.5**	91.5**

\* Significant at  $P < 0.01$ , two-tailed independent t-test

(79.1%) and control (54%) on the growth of Mung seeds. The same outcomes were reported by (Abdel-Hamid et al. 2004, Azim et al. 2014). Furthermore, the seed germination (%), root germination (%) and the seed germination index (%) of control were found statistically different ( $P < 0.05$ ) from treatment one and treatment two, as indicated in Fig. 5 and Table 5.

## CONCLUSION

Agricultural waste management is great concern throughout the world. The conversion of agricultural waste into compost will reduce pollution and when this compost is applied in the field will result in a high yield of crops and vegetables. Then the second aspect is reducing the time of composting without compromising the quality of compost. This study focused on both points. In this study, *Aspergillus Fumigatus*, *Aspergillus terreus*, and *Aspergillus flavus* consortia efficiently decomposed the rice straw, thus lowering decomposition time. This study concluded that compost matured in 90 days and contained a good level of nutrients. According to the study, supplementing rice straw with poultry droppings improves the organic matter content of the final compost. However, in all of the treatments, the final C/N ratio was below the permissible limit of compost maturity. Out of all the treatments, C/N 30 achieved the lowest C/N ratio, followed by C/N 26. Thus using an initial C/N ratio of 30 is recommended by this study. The Germination index of Mung bean verified the maturity of the compost prepared from the initial C/N ratio of 30 as this treatment showed the highest Germination index, which was significantly different from the Germination index of control.

## ABBREVIATIONS

EC: Electrical Conductivity

C/N: Carbon/Nitrogen

GHG: Green House Gas

GI: Germination Index

## REFERENCES

Abdel-Hamid, M.T., Horuchi, T. and Oba, S. 2004. Composting of rice straw with oilseed rape cake and poultry manure and its effects on faba bean (*Vicia faba* L.) growth and soil properties. *Bioresour. Technol.*, 93: 183-189

Ain, A.N., Hariz, A.M., Fariza, M.N. and Alyani, S.N. 2017. Physico-chemical and microbiological study during conventional composting using different rates of rice straw and cattle manure mixture. *J. Trop. Agric. Fd. Sci.*, 45(2): 145-154.

Ansari, A.A. 2011. Worm-powered environmental biotechnology in organic waste management. *Int. J. Soil Sci.*, 6: 25-30.

Ashraf, R., Shahid, F. and Ali, T.A. 2007. Association of fungi, bacteria, and actinomycetes with different composts. *Pak. J. Bot.*, 39(6): 2141-2151.

Azim, K., Ouyihya, K., Amellouk, A., Perissol, C., Thami Alami, I. and

Soudi, B. 2014. Dynamic composting optimization through C/N ratio variation as a startup parameter. *Build. Organic Bridges*, 3: 787-790

Banger, K.C., Shankar, S. Kapoor, K.K., Kukreja, K. and M.M. Mishra, 1989. Preparation of nitrogen and phosphorus enriched paddy straw compost and its effect on yield and nutrient uptake by wheat. *Biol. Fertil. Soils*, 8: 339-342.

Barapatre, S., Rastogi, M., Khosla, B. and Nandal, M. 2020. Synergistic effect of fungal consortia and C/N ratio variation on rice straw degradation. *Nature Environ. Pollut. Technol.*, 19(5 Suppl): 1831-1839.

Bernal, M.P., Albuquerque, J.A. and Moral, R. 2009. Composting of animal manures and chemical criteria for compost maturity assessment. A review. *Bioresour. Technol.*, 5453-5444: 22-100.

Bremner, J.M. 1996. Nitrogen-Total. In Sparks, D.L. (eds.), *Methods of Soil Analysis*. Part 3, SSSA Book Services, 5. SSSA, Madison, WI, pp. 1085-1121.

Cao, Y., Chang, Z., Wang, J., Ma, Y. and Fu, G. 2013. The fate of antagonistic microorganisms and antimicrobial substances during anaerobic digestion of pig and dairy manure. *Bioresour. Technol.* 136: 664-671.

Chukwujindu, J. and Dolin, P. 2006. Bisphosphonates and jaw osteonecrosis: updated experience with ibandronate. *Annals Of Oncol.*, 17: 289-289.

Chukwuka, K.S. and E.O. Omotayo, 2008. Effects of Tithonia green manure and water hyacinth compost application on nutrient-depleted soil in South-Western Nigeria. *Int. J. Soil Sci.*, 3: 69-74.

Devi, S., Sharma, C.R. and Singh, K. 2010. Microbiological biodiversity in poultry and paddy straw wastes in composting systems. *Brazo. J Microbiol.*, 3: 288-296.

Dobermann, A. and Fairhurst, T.H. 2002. Rice straw management. *BCI*, 16(1): 7-11.

Gadde, B., Bonnet, S., Menke, C. and Garivait, S. 2009. Air pollutant emissions from rice straw open field burning in India, Thailand, and the Philippines. *Environ. Pollut.*, 157(5): 1554-1558.

Gaind, S., Nain, L. and Patel, V.B. 2008. Quality evaluation of composted wheat straw, poultry droppings, and oilseed cakes. *Biodegradation*, 20(3): 307-317.

Getahun, T., Mengistie, E., Haddis, A., Wasie, F., Alemayehu, E., Dadi, D., Gerven, T.V. and Van der Bruggen, B. 2012. Municipal solid waste generation in growing urban areas in Africa: current practices and relation to socioeconomic factors in Jimma, Ethiopia. *Environ. Monit. Assess.*, 184 (10): 6337-6345.

Ghosh, P.K., Ramesh, P., Bandyopadhyay, K.K. Tripathi, K.M., Hati, A.K., Misra, A.K. and Acharya, C.L. 2004a. Comparative effectiveness of cattle manure, poultry manure, phosphocompost, and fertilizer-NPK on their cropping systems in vertisols of semi-arid tropics. *Crop yield and system performance. Bioresour. Technol.*, 95: 77-83.

Gupta, P.K., Sahai, S., Singh, N., Dixit, C. K., Singh, D. P. and Sharma, C. 2004b. Residue burning in rice-wheat cropping system: Causes and implications. *Curr. Sci. India*, 87(12): 1713-1715.

Gupta, R.K., Naresh, R.K., Hobbs, P.R., Jiaguo, Z. and Ladha, J.K. 2003. Sustainability of post-green revolution agriculture: the rice-wheat cropping systems of the Indo-Gangetic Plains and China. *Improv. Product. Sustain Rice-wheat Sys. Issues and Impacts*, 65: 1-25.

Gupta, S., K. Mohan, R. Prasad, S. Gupta and A. Kansal, 1998. Solid waste management in India: Option and opportunities. *Resour. Conserv. Recycl.*, 24: 137-154.

Heidarzadeh, M.H., Amani, H. and Javadian, B., 2019. Improving municipal solid waste compost process by cycle time reduction through inoculation of *Aspergillus niger*. *J. Environ. Health Sci. Eng.*, 6: 1-9.

Jacobs, J., Kreutzer, R. and Smith, D. 1997. Rice burning and asthma hospitalizations Butte County, California, 1983-1992. *Environ. Health Perspect.*, 105: 980-985.

Jiang, T., Schuchardt, F., Li, G., Guo, R. and Zhao, Y. 2011. Effect of C:N ratio, aeration rate, and moisture content on ammonia and greenhouse gas emission during the composting. *J. Environ. Sci.*, 23(10): 1754-1760.

Katyal, J.C., Singh, B., Vlek, P.L.G. and Buresh, R.J. 1987. Efficient nitro-



- gen use is affected by urea application and irrigation sequence. *Soil Sci. Soc. Am. J.*, 51(2): 366-370.
- Kaur, A., and Katyal, P. 2021. Microbial Interventions for Composting of Organic and Lignocellulose Waste. *Appl. Biochem. Microbiol.*, 57(1): 127-132.
- Knauf, M. and Moniruzzaman, M. 2004. Lignocellulosic biomass processing: A perspective. *Int Sugar J.*, 106(1263):147-150.
- Kumar, A., Gaiind, S. and Nain, L. 2008. Evaluation of thermophilic fungal consortium for paddy straw composting. *Biodegradation*, 19: 395-402.
- Kumar, M., Ou, Y.L. and Lin, J.G. 2010. Co-composting of green waste and food waste at a low C/N ratio. *Waste Manag.*, 30(4): 602-609.
- Kumar, P. and Singh, R.K. 2021. Selection of sustainable solutions for crop residue burning: an environmental issue in northwestern states of India. *Environ. Develop. Sustain.*, 23(3): 3696-3730.
- Kumari, N., Sharma, A., Devi, M., Zargar, A., Kumar, S., Thakur, U. and Giri, A. 2020. Compost from the food waste for organic production of cabbage, cauliflower, and radish under sub-tropical conditions. *Int. J. Recycl. Organic Waste Agric.*, 9(4): 367-383.
- López-Bucio, J., Cruz-Ramirez, A. and Herrera-Estrella, L. 2003. The role of nutrient availability in regulating root architecture. *Curr. Opin. Plant Biol.*, 6(3): 280-287.
- Neklyudov, A.D., Fedotov, G.N. and Ivankin, A.N. 2006. Aerobic processing of organic waste into composts. *Appl. Biochem. Microbiol.*, 42(4): 341-353.
- Nigam, P.S.N. and Pandey, A. 2009. *Biotechnology for Agro-Industrial Residues Utilisation: Utilization of Agro-Residues*. NY: Springer Science & Business Media.
- Nozhevnikova, A.N., Mironov, V.V., Botchkova, E.A., Litt, Y.V. and Russkova, Y.I. 2019. Composition of a microbial community at different stages of composting and the prospects for compost production from municipal organic waste. *Applied Biochemistry and Microbiology*, 55(3): 199-208.
- Olsen, S. R., Cole, C.V., Watanabe, F.S. and Dean, L.A. 1954. Estimation of available phosphorus in soil by extraction with  $\text{NaHCO}_3$ , USDA Cir.939.U.S.Washington.
- Owis, A.S., El-Etr, W.M., Badawi, F.S.F., El-soud, A.A. and Abdel-Wahab, A.F.M. 2016. Bioprocessing the crop residues with different amendments for producing high-quality compost. *Int. J. Chemtech. Res.*, 9: 43-54.
- Reinhardt, T.E., Ottmar, R.D. and Castilla, C. 2001. Smoke impacts from agricultural burning in a rural Brazilian town. *J. Air Waste Manage. Assoc.*, 51: 443-450.
- Sarkar, P. and Chourasia, R. 2017. Bioconversion of organic solid wastes into biofortified compost using a microbial consortium. *Int. J. Recycl. Org. Waste Agric.*, 4(6): 321-334.
- Sharholly, M., Ahmad, K., Mahmood, G. and Trivedi, R.C. 2008. Municipal solid waste management in Indian cities: A review. *Waste Manage.*, 28: 459-467.
- Sharma, K. and Garg, V.K. 2018. Comparative analysis of vermicompost quality produced from rice straw and paper waste employing earthworm *Eisenia fetida* (Sav.). *Bioresour. Technol.*, 250: 708-715.
- Shrivastava, P. and Kumar, R. 2015. Soil salinity: A serious environmental issue and plant growth-promoting bacteria as one of the tools for its alleviation. *Saudi journal of biological sciences*, 22(2): 123-131.
- Tandon, H.L.S. 1995. *Recycling of Crop, Animal, Human and Industrial Wastes in Agriculture. Fertilizer Development and Consultation Organization*, New Delhi, p. 148.
- Tucker, B.B. and Kurtz, L.T. 1961. Calcium and magnesium determinations by edta titrations. *Soil Sci. Soc. Am. J.*, 25: 27-29. <https://doi.org/10.2136/sssaj1961.03615995002500010016x>
- Van Soest, P.J. 2006. Rice straw, the role of silica, and treatments to improve quality. *Anim Feed Sci Technol.*, 130(3-4):137-171.
- Veena, S.S. and Pandey, M. 2011. Paddy straw as a substrate for the cultivation of Lingzhi or Reishi medicinal mushroom, *Ganoderma lucidum* (W. Curt.: Fr.) P. Karst. in India. *Int. J. Medicin. Mushrooms*, 13(4): 41.
- Vobrková, S., Vavrková, M. D., Burešová, A., Adamcová, D., Vršanská, M., Kynický, J. and Adam, V. 2017. Effect of inoculation with white-rot fungi and fungal consortium on the composting efficiency of municipal solid waste. *Waste Manag.*, 61: 157-164.
- Walkley, A. and Black, I. A. 1934. An examination of the Degtjareff method for determining soil organic matter and a proposed modification of the chromic acid titration method. *Soil Sci.*, 37: 29-37.
- Wang, Y. and Ai, P. 2016. Integrating particle physical geometry into composting degradation kinetics. *Bioresour. Technol.* 200: 514-520.





# Effects of Humic Acid Organic Fertilizer on Soil Environment in Black Soil for Paddy Field Under Water Saving Irrigation

Zheng Ennan, Yin hao Zhu, Jianyu Hu and Tianyu Xu<sup>†</sup>

School of Hydraulic and Electric Power, Heilongjiang University, Harbin 150080, China

<sup>†</sup>Corresponding author: Tianyu Xu; 1044459115@qq.com

Nat. Env. & Poll. Tech.  
Website: [www.neptjournal.com](http://www.neptjournal.com)

Received: 13-05-2022

Revised: 14-06-2022

Accepted: 15-07-2022

## Key Words:

Paddy field  
Black soil  
Humic acid  
Microorganisms  
Enzyme activities  
Soil fertility

## ABSTRACT

In the past decades, the application of organ fertilizer in agricultural soils has attracted wide attention. However, few studies have carefully explored the effects of humic acid organic fertilizer on soil microbial colonies, soil enzyme activities, and soil fertility. To provide a better growing environment for crops, we explore the best regulation mode of humic acid organic fertilizer in the farmland in the Songnen Plain Heilongjiang province. Through field experiment, we selected paddy as the test objective and applied humic acid organic fertilizer. Under the condition of water-saving irrigation, five fertilization levels were set up, which were NPK (local nitrogen level, 110 kg.hm<sup>-2</sup> pure nitrogen), NPKH1 (450 kg.hm<sup>-2</sup> humic acid organic fertilizer + 77 kg.hm<sup>-2</sup> nitrogen), NPKH2 (750 kg.hm<sup>-2</sup> humic acid organic fertilizer + 55 kg.hm<sup>-2</sup> nitrogen), NPKH3 (1050 kg.hm<sup>-2</sup> humic acid organic fertilizer + 33 kg.hm<sup>-2</sup> nitrogen) and PKH (1500 kg.hm<sup>-2</sup> humic acid organic fertilizer). The effects of different humic acid organic fertilizers on soil microbial colonies, soil enzyme activities, and soil fertility were discussed. The results showed that humic acid organic fertilizer could effectively change the structure of soil microbial colonies, soil enzyme activities, and soil fertility. Compared with NPK treatment, the bacteria, fungi, and actinomycete, urease, and catalase in PKH, NPKH3, NPKH2, and NPKH1 treatments increased, and significantly different under 0-10 cm layer conditions ( $P < 0.05$ ). With the increase of humic acid organic fertilizer application, soil organic matter and soil fertility from superior to inferior was PKH>NPKH3>NPKH2>NPKH1>NPK. Therefore, the application of humic acid organic fertilizer was an effective measure to improve soil fertility and increase the amount of soil colony structure and enzyme activities.

## INTRODUCTION

Heilongjiang, as an important province of output in China, plays the important role of “ballast stone” in ensuring national food security for the implementation of the strategy of grain storage on the land, and grain storage in technology. The protection of black soil for improving the grain production capacity, which is of great significance to further consolidate and enhance the advantages of agricultural green development and promote the construction of a strong agricultural province (Liang 2021). As an extremely precious agricultural resource, in the “fourteenth five-year plan” and the long-term goal of 2035 in China, the protection of black soil has been put forward, taking the effective protection of black soil as an important strategic task to promote the agricultural modernization in Heilongjiang province, China (Zhang 2021). In recent years, the application amount of organic fertilizer is insufficient, while the application amount of nitrogen fertilizer has increased greatly in Heilongjiang province (Chen et al. 2019). Therefore, it is necessary to reduce the input of nitrogen in farmland, scientifically reduce the application amount of chemical fertilizer, and reasonably

apply organic fertilizer, which is of great significance for improving soil fertility, the quality of agricultural products, and reducing agricultural non-point source pollution (Du et al. 2020).

In the process of agricultural planting, for the pursuit of high yield of crops, bringing the environmental problems of farmland ecological pollution because of increasing the amount of nitrogen fertilizer, therefore it is an inevitable demand for application of organic fertilizer in the sustainable development of agriculture in the future, also an important embodiment of agricultural green development, to adjust and solve the contradiction between the fertilizer of crop demand and soil fertilizer supply, and realize the balanced supply of nutrients, we can achieve the goal of reducing fertilizer and improving efficiency under the meeting the needs of crop growth conditions, and achieve the mutually beneficial goal of high crop yield and environmentally sustainable development. In the decades, due to a large amount of chemical fertilizer application, the fertilizer supply capacity and production capacity of black soil decreased significantly, so organic fertilizer instead of chemical fertilizer nitrogen is

one of the important measures to reduce fertilizer application, which not only improve soil fertility but also promote the growth of crops (Xu et al. 2018). Previous studies had shown that crop quality could be improved (Lu et al. 2015, Zhang et al. 2004), the crop photosynthesis and water and fertilizer utilization efficiency were increased (Huang et al. 2021, Zhang et al. 2019) by the application of organic fertilizer reasonably. It was also beneficial to the increase of plant height and stem diameter (He et al. 2019), reducing nitrogen leaching (Xie et al. 2021), and affecting the microbial community and enzyme activities in the root zone of crops (Liang et al. 2021), reducing greenhouse gas emissions from farmland effectively (Shu et al. 2021, Zhang et al. 2021), in the meantime, applying organic fertilizer in the soil would help to improve soil quality and maintain crop production. In addition, small-molecule organic matter in organic fertilizer had a positive effect on soil nutrient cycling and crop growth and development (Ma et al. 2021). Therefore, exploiting the environment-friendly fertilizer and reasonable fertilization measures is an important way to ensure crop growth, improve soil environmental effects and maintain sustainable agricultural development (Xu et al. 2020, Yu et al. 2020).

However, due to the influences of climate conditions, planting structure, and environmental effects of soil and water resources in Heilongjiang province, China, there are many uncertainties in soil environmental effects and organic fertilizer application in black soil areas. Therefore, how to further improve the quality of black soil and maintain crop productivity by increasing the application of organic fertilizer, is the main challenge of agriculture in Heilongjiang province. In our experiment, we have taken the paddy soil as an example, by the field experiment, under the water-saving irrigation condition, to study the impacts of humic acid organic fertilizer on the environmental effects of black soil, which is of great significance to seeking the technical mode of coordinated development of food production and agricultural sustainable utilization.

## MATERIALS AND METHODS

### Experimental Site

The experiment was performed at the National Key Irrigation Experimental Station located in Heping Town, Qing' an County, Suihua, Heilongjiang, China. The experimental site is located at 45°63' N and 125°44' E at an elevation of 450 m above sea level. This region consists of plain topography and has a semi-arid cold temperate continental monsoon climate, i.e., a typical cold region with a black glebe distribution area. The average annual temperature is 2.5°C, the average annual precipitation is 550 mm, and the average annual surface evaporation is 750 mm. The growth period of crops is 156-171d,

and there is a frost-free period of approximately 128 days.  $\text{yr}^{-1}$ . The soil at the study site is albic paddy soil, with a mean bulk density of 1.01  $\text{g}\cdot\text{cm}^{-3}$  and a porosity of 61.8 %. The basic physicochemical properties of the soil are as follows: the mass ratio of organic matter is 41.8  $\text{g}\cdot\text{kg}^{-1}$ , pH value is 6.45, the total nitrogen mass ratio is 15.06  $\text{g}\cdot\text{kg}^{-1}$ , the total phosphorus mass ratio is 15.23  $\text{g}\cdot\text{kg}^{-1}$ , total potassium mass ratio is 20.11  $\text{g}\cdot\text{kg}^{-1}$ , the mass ratio of alkaline hydrolysis nitrogen is 198.29  $\text{mg}\cdot\text{kg}^{-1}$ , the available phosphorus mass ratio is 36.22  $\text{mg}\cdot\text{kg}^{-1}$  and the exchangeable potassium mass ratio is 112.06  $\text{mg}\cdot\text{kg}^{-1}$  (Zheng et al. 2018).

### Experimental Design

The plants were maintained under water-saving conditions, that was, at the re-greening stage, a water layer (0~30 mm) was maintained, but the soil was allowed to dry during the yellow ripeness stage; the water layer was not applied after the irrigation period. The upper limit of irrigation was taken as the saturated water content. In the early and middle tillering stages, jointing stage, heading stage, and milk-ripe stage, the lower limit of irrigation was 85% of the saturated water content. The soil moisture content was measured using a moisture content analyzer (TPIME-PICO64/32) every day (once at 07:00 and 18:00). When the soil moisture content was lower than or close to the lower limit of irrigation, it was necessary to irrigate to the upper limit.

In this experiment, Five fertilization treatments were applied: 100% urea which was 110  $\text{kg}\cdot\text{ha}^{-1}$  (pure nitrogen) (NPK), 30% humic acid and 70% urea (NPKH1), 50% humic acid, and 50% urea (NPKH2), 70% humic acid and 30% urea (NPKH3), 100% humic acid which was 1500  $\text{kg}\cdot\text{ha}^{-1}$  (PKH). Urea and humic acid organic fertilizer were applied according to the proportion of base fertilizer: tillering fertilizer: and heading fertilizer (5:3:2). The amount of phosphorus and potassium fertilizers was the same for all treatments,  $\text{P}_2\text{O}_5$  (45  $\text{kg}\cdot\text{ha}^{-1}$ ) and  $\text{K}_2\text{O}$  (80  $\text{kg}\cdot\text{ha}^{-1}$ ) were used. Phosphorus was applied once as a basal application. Potassium fertilizer was applied twice: once as basal fertilizer and at the 8.5 leaf age (panicle primordium differentiation stage), at a 1:1 ratio (Zheng et al 2018).

The humic acid organic fertilizer was produced by Yunnan Kunming Grey Environmental Protection Engineering Co., Ltd, China. The organic matter  $\geq 61.4\%$ , the total nutrients (nitrogen, phosphorus, and potassium)  $\geq 18.23\%$ , of which  $\text{N} \geq 3.63\%$ ,  $\text{P}_2\text{O}_5 \geq 2.03\%$ ,  $\text{K}_2\text{O} \geq 12.57\%$ . The moisture was  $\leq 2.51\%$ , the pH value was 5.7, the worm egg mortality rate  $\geq 95\%$ , and the amount of fecal colibacillosis  $\leq 3\%$ . The fertilizer contained numerous elements necessary for plants. The contents of harmful elements including arsenic, mercury, plumbum, cadmium, and chromium were  $\leq 2.8\%$ , 0.01%,

7.6%, 0.1%, and 4.7%, respectively; these were much lower than the test standard.

### Plant Management

This study was performed with a randomized complete block design with three replications. The length and width of each plot were 10.0 m and 10.0 m, respectively (area = 100 m<sup>2</sup>). The rice was also planted around the cell as a protection row. A 40 cm deep plastic plate was embedded between the plots to prevent underground water-fertilizer exchange in each plot. The plant protection and pesticide application measures and field management conditions in each plot were consistent.

### Sampling and Measurements

The determination of soil enzymatic activities was based on the method of Huang et al. (2021). The activity of urease was determined by sodium phenol colorimetry, expressed as the quantity of mg of ammonia nitrogen released from 1 g of soil after 24 hours. The acid phosphatase activity was determined by the disodium phenyl phosphate colorimetric method, expressed as the quantity of mg of phenol released in 1 µg of soil after 24 hours. The soil catalase activity was determined by the permanganometric method, expressed as the quantity of mg of phenol released in 1 g of soil after 1 hour, all the treatments were repeated thrice. The soil microorganism was inoculated by the spread-plate method of Huang et al. (2021), The fungus was cultivated in Martin medium and its quantity was determined, the actinomycetes were cultivated in the modified Gao's No. 1 culture medium and its quantity was determined, the bacteria were cultivated in the beef extract-peptone medium and then their quantity was determined, the soil fertility was based on the method of Song (2019).

### Statistical Analysis

For statistical analysis, data processing was completed using Microsoft Excel 2010 followed by analysis with SPSS 19 software. The statistical results are reported as the mean value and were confirmed with an LSD (least significant difference) test.

## RESULTS

### Effects on Soil Microorganisms

The humic acid organic fertilizer had a significant impact on soil microorganisms (Fig. 1). Under the different soil layers, the bacteria, fungi, and actinomycetes from superior to inferior were 0-10 cm > 10-20 cm > 20-30 cm. However, the microorganism of each treatment was not significant under the 10-20 cm and 20-30 cm layers, but in the 0-10 cm soil layer, it was significant at a 5% probability level. In the 0-10 cm soil layer, the microorganism in NPKH4 and PKH treatments was higher than in NPK, NPKH1, and NPKH2 treatments ( $P < 0.05$ ), and the number of bacteria, fungi, and actinomycetes in NPKH4 and PKH treatments increased by 13.68%, 17.68%, 7.34% on average compared with NPK, NPKH1 and NPKH2 treatments ( $P < 0.05$ ), the increase of fungi was more than bacteria and actinomycetes.

### Effects on Soil Enzyme Activities

The humic acid organic fertilizer could affect the soil enzyme activities (Fig. 2), the urease and catalase activities in the 0-10 cm soil layer were significant at a 5% probability level, while acid phosphatase activity was not significant. In the 0-10 cm soil layer, the urease activity in NPK treatment decreased by 29.91% ( $P < 0.05$ ), 27.05% ( $P < 0.05$ ), 18.91% ( $P < 0.05$ ) and 18.84% ( $P < 0.05$ ) as compared with PKH,

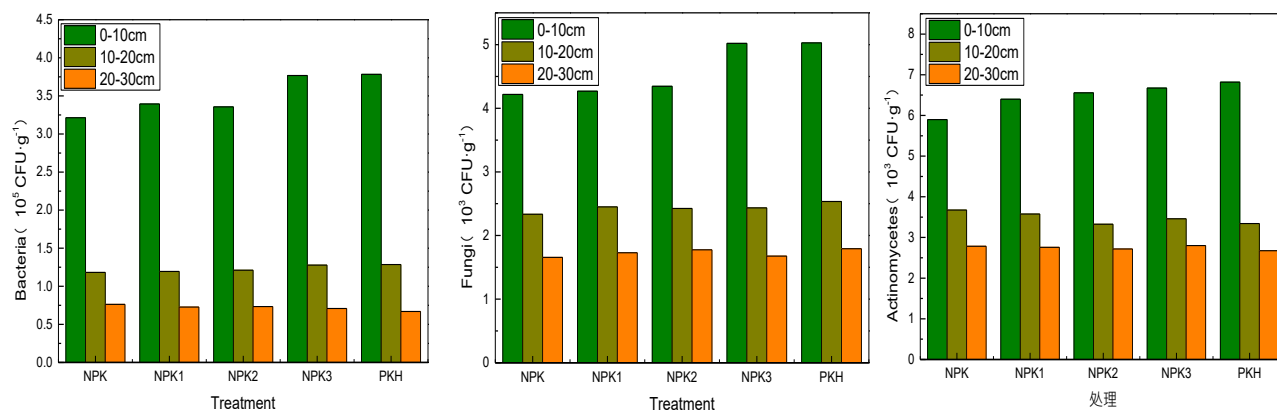


Fig.1: Change of soil microbial content in different soil layers under different fertilization treatments.

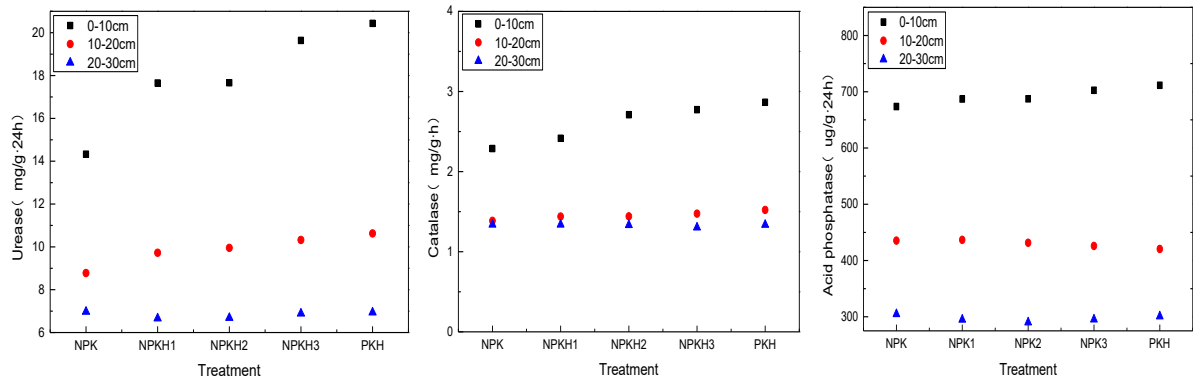


Fig. 2: Change of soil enzyme activities in different soil layers under different fertilization treatments.

NPKH3, NPKH2 and NPKH1; the catalase activity in NPK treatment decreased by 20.15% ( $P < 0.05$ ), 17.49% ( $P < 0.05$ ), 15.59% ( $P < 0.05$ ) and 5.31% ( $P > 0.05$ ) as compared with PKH, NPKH3, NPKH2 and NPKH1; the acid phosphatase activity in NPK treatment decreased by 5.31% ( $P > 0.05$ ), 4.11% ( $P > 0.05$ ), 1.98% ( $P > 0.05$ ) and 1.94% ( $P > 0.05$ ) as compared with PKH, NPKH3, NPKH2 and NPKH1. In the vertical direction of the soil, the soil enzyme activities decreased with the increase of soil depth, and there were no significant differences between the different treatments of 10-20 cm and 20-30 cm.

### Effects on Soil Organic Matter

The soil organic matter increased with the increase of humic acid amount (Table 1), from superior to inferior was  $PKH > NPKH3 > NPKH2 > NPKH1 > NPK$ . In the vertical direction of the soil, the soil organic matter in 0-10 cm soil was higher than 10-20 cm and 20-30 cm soil layers. Compared with NPK treatment, in 0-10 cm soil layer, the soil organic matter in PKH, NPKH3, NPKH2, and NPKH1 increased by 22.07% ( $P < 0.05$ ), 19.62% ( $P < 0.05$ ), 12.02% ( $P < 0.05$ ) and 6.42%. In the 10-20 cm soil layer, the soil organic matter in PKH and NPKH3 treatments was higher than in the others. However, in 20-30 cm soil layer, across all treatments, had no significant difference.

### Effects on N, P, K

The humic acid organic fertilizer increased soil total nitrogen, available phosphorus, and available potassium contents (Table 2). In 0-10 cm soil layer, the total nitrogen in PKH, NPKH3, NPKH2 and NPKH1 treatments increased by 30.10%, 25.10%, 23.43% and 9.47%, respectively than NPK; the available phosphorus increased by 38.30%, 36.49%, 29.67% and 8.54%, respectively; the available potassium increased by 20.32%, 19.30%, 12.59% and 6.17%, respectively. In 10-20 cm soil layer, total nitrogen in PKH, NPKH3, NPKH2 and NPKH1 treatments increased by 20.32%, 16.09%, 4.59% and 3.79%, respectively; the available phosphorus increased by 30.95%, 30.29%, 24.86, and 10.91%, respectively; the available potassium increased by 13.71%, 13.33%, 8.63% and 6.54%, respectively. In the 20-30 cm soil layer, the total nitrogen, available phosphorus, and available potassium increased by less than 10% as compared with the NPK treatment, and the increase was not significant.

### Principal Component Analysis of Each Index

Two principal components were obtained with basic characteristic values greater than 0.5. The contribution rate of the first principal component (urease, bacteria, fungi, soil organic matter, total nitrogen, and available potassium) to

Table 1: Contents of soil organic matter under different fertilization treatments ( $\text{g}\cdot\text{kg}^{-1}$ ).

Treatment	0-10cm	10-20cm	20-30cm
NPK	47.53c	44.99b	42.57a
NPK1	50.59bc	45.55b	42.61a
NPK2	53.25b	45.32b	42.74a
NPK3	56.86a	47.79a	42.78a
PKH	58.02a	48.54a	43.21a

Note: Different letters within columns have significant differences at  $P < 0.05$  according to the LSD test.

Table 2: Content of soil fertility elements under different fertilization treatments.

	Treatment	0-10cm	10-20cm	20-30cm
Total nitrogen (g.kg <sup>-1</sup> )	NPK	2.40b	2.17b	1.91a
	NPK1	2.62b	2.25b	1.99a
	NPK2	2.96a	2.27b	1.96a
	NPK3	3.01a	2.52a	2.07a
	PKH	3.12a	2.65a	2.10a
Available phosphorus (mg.kg <sup>-1</sup> )	NPK	47.65b	44.30c	41.37a
	NPK1	51.72b	49.14b	43.18a
	NPK2	61.79a	55.32ab	44.51a
	NPK3	65.04a	59.73a	45.01a
Available potassium (mg.kg <sup>-1</sup> )	PKH	65.90a	61.96a	45.49a
	NPK	153.15d	143.23c	132.40a
	NPK1	162.61c	152.60b	132.94a
	NPK2	172.44b	155.61ab	132.39a
	NPK3	182.71a	162.33a	132.11a
	PKH	184.27a	162.88a	134.17a

Note: Different letters within columns have significant differences at  $P < 0.05$  according to the LSD test.

the total variance was 90.08%, and the second principal component (catalase, acid phosphatase, and available phosphorus) was 6.47%. The cumulative contribution rate of the two principal components reached 96.55%, indicating that the two principal components could represent 96.55% of all soil environmental effects information. The order of the comprehensive evaluation scores of the two principal components, from superior to inferior was PKH>NPKH3>NPKH2>NPKH1>NPK (Fig.3), and the comprehensive score in PKH treatment was the highest.

## DISCUSSION

Soil microorganism is an important component of soil (Schutter & Fuhrmann 2001). The results showed that the bacteria, fungi, and actinomycetes in the 0-10cm soil layer increased significantly with the increase of humic acid organic fertilizer. Maybe the humic acid organic fertilizer improved the physical and chemical properties of soil, leading to the permeability and water retention of soil was improved, promoting the growth of crops and the metabolism of plant roots, stimulating the beneficial microbial activity of the soil, and speeding up the reproduction speed of soil microorganisms. The response of different microorganisms to humic acid organic fertilizer was also different. The increase of fungi was greater than that of bacteria and actinomycetes, the results from the humic acid organic fertilizer were acidic, and the fungi were dominant in an acidic environment, at the same

time, the fungi were strictly aerobic, the humic acid organic fertilizer could change the permeability of the soil, improve the gas exchange between the soil and the outside, therefore it provided a good living environment for the fungi. Through the application of humic acid organic fertilizer, the microorganisms increased, indicating that the humic acid organic fertilizer could improve the soil's environmental effects.

Urease, catalase, and acid phosphatase are closely related to plant nutrition (Zhang 2019). The results showed that the activities of urease and catalase in the 0-10cm soil layer increased with the increase of humic acid organic fertilizer, and acid phosphatase increased not significantly. The reasons may be that the soil aggregate structure was improved be-

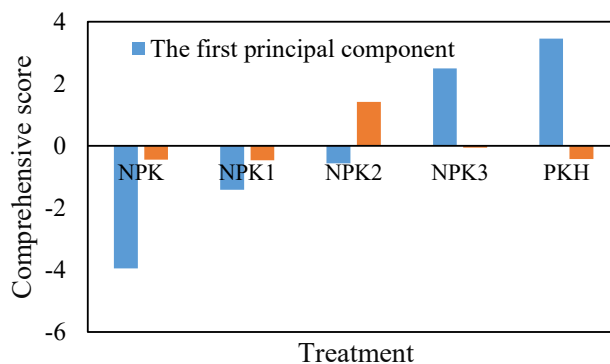


Fig.3: Score of principal components under different treatments.



cause of the humic acid organic fertilizer applied in the soil, which could combine well with the enzyme, therefore the enzyme activities were improved. Studies have shown that (Wang et al. 2012), the activities of soil protease and urease were positively correlated with soil aggregate structure, this also proved that the enzyme activities in urea treatment were lower than that in humic acid organic fertilizer treatments. In our experiment, the soil microorganisms increased significantly, it also could improve the enzyme activities. Fan and Hao (2019) showed that organic fertilizer had the greatest effects on urease, which was consistent with our conclusion. In our experiment, the activities of urease, catalase, and acid phosphatase in soil were measured. Combined with the previous conclusions, the results showed that the enzyme had a very sensitive response to soil fertilization, and the organic fertilizer could significantly improve the activities of soil enzymes. Therefore, in a sense, the application of organic fertilizer was a measure of adding enzyme.

As one of the components of soil, the soil organic matter plays an important role in the formation of soil, the protection of the soil environment, and the sustainable development of agriculture (Zhu 2012). In our experiment, we found, that the humic acid organic fertilizer could improve the soil organic matter, compared with the NPK treatment, the soil organic matter in the other treatments increased significantly, which was similar to the literature (Zeng et al. 2002, Wang et al. 2005). The Physical and chemical properties of soil could be improved because the soil organic matter increase, therefore the soil fertility also could be enhanced. while, the humic acid organic fertilizer also had significant effects on the total nitrogen, available phosphorus, and available potassium. The humic acid organic fertilizer contained a large number of water-stable groups with different particle sizes, which could reduce the leaching. And the humic acid organic fertilizer also contained a lot of available elements such as carbon, hydrogen, oxygen, nitrogen, phosphorus, and potassium, which was a good supplement to the soil elements. The application of organic fertilizer could improve soil organic matter and nutrient elements, the results of our study also confirmed the conclusion, that it was similar to the literature (Li et al. 2012, Ailinc et al. 2011, Gong & Lü 2014).

## CONCLUSION

The application of humic acid organic fertilizer in black soil had a positive impact on improving soil environmental effects. The number of soil microorganisms, enzyme activities, soil organic matter, total nitrogen, available phosphorus, and available potassium were all increased. According to the analysis of different soil layers, humic acid organic fertilizer had affected 0-10cm soil. In 0-10 cm soil, the soil

microorganisms increased significantly in NPKH3 and PKH treatments, while the soil enzyme activities were similar but inconsistent, showing that the acid phosphatase was no significant difference across all treatments, while the urease and catalase were obvious increased with the increase of humic acid organic fertilizer application. The contents of organic matter, total nitrogen, available phosphorus, and available potassium increased with the increase of humic acid organic fertilizer application and reached the maximum value in PKH treatment. The principal component analysis showed that humic acid organic fertilizer application had positive impacts on the improvement of soil environmental effects, and the PKH treatment was the best.

## ACKNOWLEDGEMENT

All authors thank the Basic Scientific Research Fund of Heilongjiang Provincial Universities: (2020-KYYWF-1042). We are grateful to the staff of the National Key Irrigation Experimental Station for their technical assistance.

## REFERENCES

- Ailinc, I.C., Jitreanu, G. and Bucur, D. 2011. Long-term effects of cropping system and mineral fertilization on production and soil fertility in the Moldavian Plain. *Cerc. Agron. Moldova*, 44(1): 23-34.
- Berlin, H., Meng, X.W., Xin, J.J., Yu, X.Z. and Guo, H.H. 2020. Effects of different tillage measures on soil microbes and enzymatic activity. *Nature Environ. Pollut. Technol.*, 19(04): 1443-1452.
- Chen, P., Nie, T.Z. and Chen, S.H. 2019. Recovery efficiency and loss of  $^{15}\text{N}$ -labelled urea in a rice-soil system under water-saving irrigation in the Songnen Plain of Northeast China. *Agric. Water Manag.*, 222: 139-153.
- Du, W.Y., Tang, S. and Wang, H. 2020. The status of the organic fertilizer industry and organic fertilizer resources in China. *Soil Fertilizer Sci. China*, (03): 210-219.
- Fan, J. and Hao, M.D. 2002. Kinetic characteristics of urease and alkaline phosphatase in dry land farming. *Agric. Res. Arid Areas*, 20(1): 35-37.
- Gong, D.Q. and Lü, J. 2014. Effects of soil texture on variations of paddy soil physical and chemical properties under continuous no-tillage. *Acta Ecol. Sin.*, 34(2): 239-246.
- He, H., Zhang, Y.T. and Wei, C.Z. 2019. Effects of different organic substitutions reducing fertilizer Patterson maize growth and soil fertility. *J. Soil Water Conserv.*, 33(05): 281-287.
- Huang, G.D., Song, Q.H. and Wang, X.H. 2021. Effects of fertilizers containing *Bacillus subtilis* on photosynthesis of soybean leaves and soil enzyme activities. *Soils Crops*, 10(01): 99-107.
- Li, Z., Jing, H.X. and Xie, C.S. 2012. Effects of green manure application on soil physical and chemical properties and chemical composition of flue-cured tobacco leaves. *Acta Agric. Boreali-Sin.*, 27(S1): 275-280.
- Liang, J. 2021. Speeding up the construction of a long-term mechanism of black land protection in Longjiang. *Heilongjiang Daily*, 03-09: 011.
- Liang, J.P., Xue, Z.Q. and Yang, Z.Y. 2021. Effects of microbial organic fertilizers on *Astragalus membranaceus* growth and rhizosphere microbial community. *Annals Microbiol.*, 71(1): 11-15.
- Lu, S.C., Wang, X.B. and Weng, F.J. 2015. Effect of different fertilization treatments on soil nitrate-nitrogen movement and the growth and quality of celery in the greenhouse. *Tianjin Agric. Sci.*, 21(11): 8-11.

- Ma, X.M., Li, H.X. and Xu, Y. 2021. Effects of organic fertilizers via quick artificial decomposition on crop growth. *Sci. Rep.*, 11(1): 45-56.
- Schutter, M.E. and Fuhrmann, J.J. 2001. Soil microbial community responses to fly ash amendment as revealed by analyses of whole soils and bacterial isolates. *Soil Biol. Biochem.*, 33(14): 1947-1958.
- Shu, X.X., Wang, Y.Q. and Wang, Y.L. 2021. Response of soil N<sub>2</sub>O emission and nitrogen utilization to the organic matter in the wheat and maize rotation system. *Sci. Rep.*, 11(1): 61-71
- Song, Y.Z. 2019. Effect of regulated deficit irrigation on growth and microenvironment of *Panax Notoginseng* under micro-sprinkler fertilization condition. *Kunming Univ. Sci. Technol.*, 5: 11-19
- Wang, B.R., Xu, M.G. and Wen, S.L. 2005. Effect of long time fertilizers application on soil characteristics and crop growth in red soil upland. *J. Soil Water Conserv.*, 19(1): 97-100.
- Wang, L.M., Li, W.H. and Fan, P. 2012. Variation in soil enzyme activities under long-term fertilization of tea garden in red-yellow soil area. *J. Tea Sci.*, 32(4): 347-352.
- Xie, S.W., Yang, F. and Feng, H.X. 2021. Organic fertilizer reduced carbon and nitrogen in runoff and buffered soil acidification in tea plantations: Evidence in nutrient contents and isotope fractionations. *Sci. Total Environ.*, 762: 143059
- Xu, D.B., Zhao, S.J. and Yuan, J.F. 2018. Chemical N fertilizer replaced with organic fertilizer affects the yield and quality of leaf vegetables and N leaching in soils. *Trans. Chinese Soc. Agric. Eng.*, 34(S1): 13-18.
- Yu, X.F., Yang, S.M. and Zou, B.L. 2020. Effects of combined application of rapeseed cake as organic manure and chemical fertilizer on yield, quality, and nutrient use efficiency of flue-cured tobacco. *Acta Pedolog. Sin.*, 57(06):1564-1574.
- Zeng, M. X., Wang, R.F. and Peng, S.Q. 2002. Summary of returning straw into the field of main agricultural areas in China. *Chinese J. Soil Sci.*, 33(5): 336-339.
- Zhang, D.J., Hu, X. and Ma, J H. 2021. Effects of tillage and fertility on soil nitrogen balance and greenhouse gas emissions of a wheat-maize rotation system in Central Henan Province, China. *Chinese J. Appl. Ecol.*, 11: 1-9.
- Zhang, Y.C., Shen, Y.R. and Yu, J. 2004. Effects of application of nitrogen fertilizers of different n forms on yields and quality of Chinese cabbage. *Jiangsu J. Agric. Sci.*, 20(3): 184-188.
- Zhang, Y.C. 2019. Effects of microbial organic fertilizer on quality of asparagus and soil nutrient availability. *Sichuan Normal Univ.*, 11: 44.
- Zhu, W.X. 2012. The impact of grassland, grazing on soil microbial biomass on the eastern Tibetan plateau. *Lanzhou Univ.*, 1: 5
- Zhang, Z.X., Feng, Z.J. and Qi, Z.J. 2019. Effects of compound microbial organic fertilizer with water-saving irrigation on photosynthetic and yield of rice. *Trans. Chinese Soc. Agric. Mach.*, 50(07): 313-321.
- Zheng, E N., Yang, H., Zhang, Z X. 2018. Influence of different nitrogen forms application on rice photosynthesis: fluorescence with water-saving irrigation in black soil region of Songnen Plain, Northeast China. *Paddy and water environment*. 16(04):795-804.
- Zhang, Q.W. 2021. Protect the black land and be the "ballast stone" of national food security. *Environ. Sci. Manag.*, 46(01): 1.





# Main Characteristics of Trails on Yarmouk Forest Reserve, A Quantitative Approach to Trails Assessment

Loay Alzriqat\*, Sana'a Odat\*\*† and Ismaiel Abuamoud\*\*

\*Department of Earth and Environmental Sciences, Faculty of Science, Yarmouk University, Irbid, Jordan

\*\*Department of Tourism Management, the University of Jordan, Amman, Jordan

†Corresponding author: Sana'a Odat; sanaa.owdat@yu.edu.jo

Nat. Env. & Poll. Tech.  
Website: [www.neptjournal.com](http://www.neptjournal.com)

Received: 08-05-2021

Revised: 10-08-2021

Accepted: 26-08-2021

## Key Words:

Ecotourism

Hiking trails

Yarmouk forest reserve

## ABSTRACT

The necessity to pay attention to the tourism sector and protect natural resources has sparked a growing interest in scientific studies on the international value of ecotourism. Furthermore, eco-friendly tourist attractions should be developed and expanded to achieve long-term tourism growth. To achieve this aim, however, it is important to recognize the adverse effects of visitor activity on the natural environment and the experience of tourism to direct management activities and, thus, to maintain the resources on which ecotourism ultimately depends. This study aimed to assess the environmental impact of the four trails in the Yarmouk Forest Reserve in the Irbid governorate in northern Jordan. Field trips were used to determine the trail's characteristics. The findings revealed a basic description of the reserve's four routes in terms of path width, trail surface type, kind of vegetation, landscapes, and tourist attractions.

## INTRODUCTION

Ecotourism is a rapidly growing industry that is well-known for its environmentally friendly approach to tourist-local destination engagement. Jordan is one of the few Middle Eastern countries having feasible or approved tourism options (Abuamoud et al. 2015). Jordan has established an integrated network of ecologically and culturally significant protected areas that covers 1.73 percent of the country's land area. In addition to their environmental protection efforts, these regions are frequently regarded as prominent tourist attractions, particularly for nature-based tourism. Jordanian protected area tourism, on the other hand, is still a relatively recent phenomenon (Jamaliah et al. 2019).

Hiking is generally defined as an activity involving, on foot, for sporting and cultural purposes, following paths that may or may not be marked. Hiking has long been associated with mountaineering and rambling groups across the country, however, there are significant regional differences. Hiking evolved from a sporting and cultural activity (mostly enjoyed by minorities and elitist groups) to a type of tourism and leisure, coinciding with the birth and consolidation of what has come to be known as alternative forms of tourism (Gómez-Martín 2019). Hiking in mountain regions and protected areas is usually the most significant recreational activity and can provide significant tourism income for the local population. In latest years, many rural locations have

made enormous attempts to facilitate hiking and thus benefit from the growing demand of visitors for nature destination experiences and events that promote their health and well-being (Nordbø & Prebensen 2015). Recreation trails are becoming acknowledged as drivers of financial and tourism growth. It also becomes evident that financial advantages can improve even if trails are designed and managed as a network of interconnected communities and attractions (Hungria et al 2013).

Tourism activity is a significant contributor of 18.7% of GDP to Jordan's national economy. Tourism ranked as one of Jordan's most important foreign exchange sources, in 2017, 7,659 USD billion was generated, and it is forecast to rise to 13,611 USD billion by 2028 (23.5% of GDP) and raise jobs to 332,000 in 2028 through a private sector partnership (WTTC 2018). Tourism, which includes restaurants, hotels, airlines, local communities, and ground transportation, provides a new type of business to the local community, producing new jobs and revenue (Abuamoud et al. 2019). According to the World Tourism Organization, tourism in the Middle East is anticipated to increase by 50% between 2010 and 2020 (UNWTO 2016).

## PAST STUDIES

Hiking, due to its low effect on natural environments, is one of these suitable forms of tourism within the reserve. It is

likely that natural disasters will both destroy the infrastructure and cause fatal injuries to tourists as hiking trails are laid down across natural landscapes (Luzhkova 2012). Recreational trails are recognized as economic drivers in tourism if they are established and maintained as a network of interconnected community links with a variety of complementary attractions and services. The number of economic benefits can also increase (Recreation Sites and Trails BC 2012). In 2018, 1.4 billion visitors from all over the world generated 1340 USD billion in income (UNWTO 2015). Most outdoor recreational activities can adversely impact the natural environment, and the growing popularity of outdoor recreation has inevitably led to broader and wider ecological effects on natural ecosystems (Lynn & Brown 2003). Nature-based tourism is considered to be one of the most popular forms of tourism and one of the few human activities permitted in many protected areas. Nature-based tourism including ecotourism has a variety of negative effects on wildlife in general, water, and soils (Ballantyne & Pickering 2012). Monitoring the condition of the trails, such as soil erosion, trail length, and informal trails is a task that requires constant monitoring to ensure the long-term conservation of the landscape and to restrict the area directly affected by trails (Ancin Murguzur et al. 2020). Many trail systems are designed and managed to maintain high traffic while reducing related impacts on the environment. Well-designed trails, for instance, avoid steep grades and (*fall line*) alignments parallel to landform grades that are difficult to drain and intercept natural water flows (Olive & Marion 2009). Trampling disruption can alter the look and composition of trailside vegetation by raising plant height and favoring trampling-resistant species. Loss of tree and shrub cover may increase exposure to sunlight, resulting in greater compositional changes when shade-intolerant plant species take over (Leung & Marion 2000). Trampling can cause more damage during the flowering and seeding seasons than during the non-productive seasons (Liddle 1997). Nevertheless, soil exposure on natural surface trails can lead to several impacts on the site, including soil compaction, muddiness, erosion, and widening of the trail (Cole 2004).

## STUDY AREA

Yarmouk Forest Reserve is located in the northernmost part of Jordan (Center Coordinates; East 754351/North 3618381). It is approximately 140 km north of Amman's capital city and 40 km north of Irbid city. The Royal Society Conservation of Nature (RSCN) established Yarmouk Natural Reserve on the 6th of January 2010 with the agreement of the Prime Minister, and it became part of the national reserves network, which is run and managed by the RSCN and is located in the northwestern part of Jordan on the border of Golan hill. The

Yarmouk Forest Reserve covers a total area of 20 km<sup>2</sup> (Fig. 1). From three different locations, the reserve is surrounded by tiny villages (RSCN 2015).

Yarmouk Forest Reserve is located within the Mediterranean biogeographical zone, which provides a warm climate in summer and a cold one in winter with an average rainfall of 400mm per year. Overlooking the River Yarmouk, which marks the border between Jordan and Syria, it protects a swathe of deciduous oak forest (85% of Jordan's surviving cover), along with two species of rare orchid, mammals including otters, hyenas, wolves, and the threatened mountain gazelle, reptiles, fish and birds. The Yarmouk Nature Reserve spreads over a small area (20Km<sup>2</sup>) of the hills beside Umm Qais. The total financial income for local communities living around Yarmouk Forest Reserve in 2019 has reached 225,504 JOD.

## MATERIALS AND METHODS

### Field Trips

At Yarmouk Reserve, a variety of procedures have been used to assess the current management scheme and practices, including visitor management, opening hours, illegal logging, soil erosion, topography, annual rainfall, and the percentage of vegetation cover (including trees and other plants) to the overall reserve area. To determine these characteristics, preliminary field research was conducted to assess the direct characteristics that can be assessed in the field, such as (the width of the trail between the outer (median) boundaries [m], the dominant type of surface, the presence of stairs along the trail, the number of information panels, the number of rest stops along the trail, food services throughout the trail, picturesque views, and the possibility of accommodation across the trail mountain

Other characteristics that can be assessed using Geographic Information System (GIS) software include trail length [m], kind of path, dominating ground cover type, several types of land cover, average trail slope [degree], and water flow parallel to or intersecting with the route segment. According to the methodologies for assessing the characteristics, we divided them into two groups: qualities directly tested in the field and attributes dissected using GIS software. From March to September 2019, the reserve management provided visitor statistics (4331 visitors). However, the year 2020, which is plagued by the Coronavirus (COVID-19), would result in significant losses in various sectors, particularly the tourism sector.

Trails have been divided into the: A) Easy trails: that is ideal for hikers and novices. Normally they are easy to follow, being along a Wadi, path, or lane. Grades are friendly



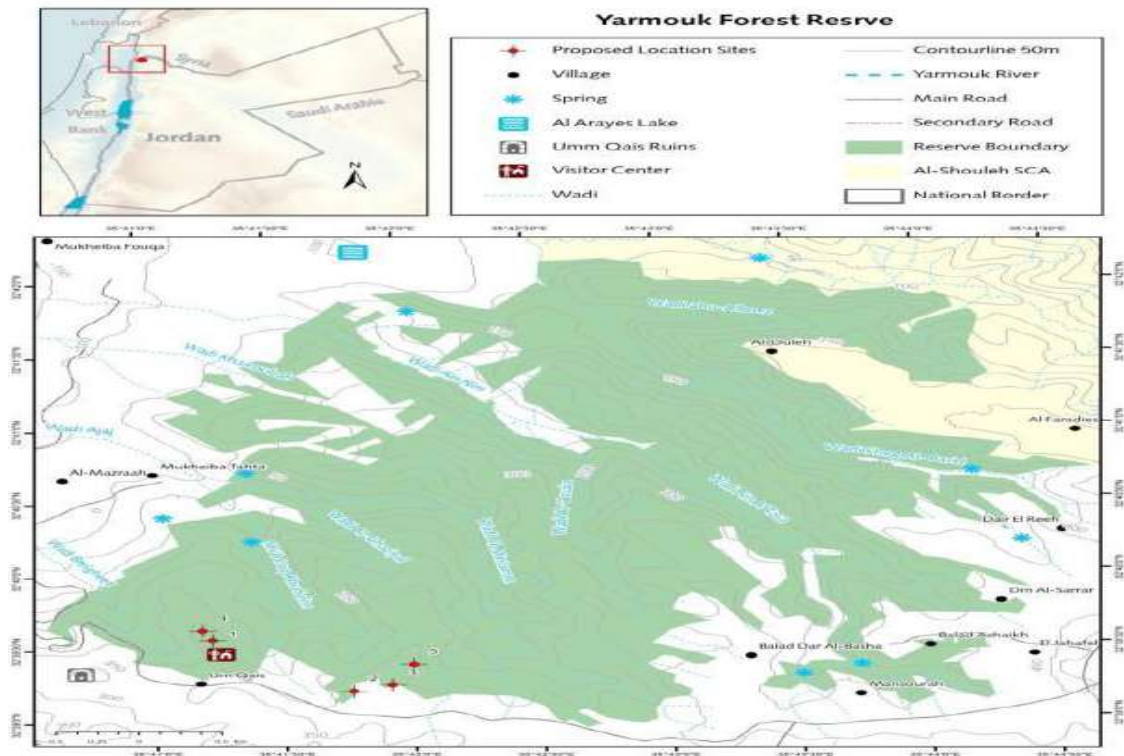


Fig. 1: Yarmouk forest reserve location.

and with be very few obstacles. B) Moderate trails: that is for intermediate or experienced hikers. The terrain is steeper and it is likely to meet more obstacles with no signs of the trail or specific directions that you can use. C) Advanced trails: that is also done for experienced hikers. The terrain can be steep and there are no direct paths, with the ability and self-reliance to navigate.

## Interviews

Interviews have been conducted with the reserve director manager and employee of the reserve to determine the natural features in the reserve, find out the number of tourists coming to the reserve, and know what the next projects in the reserve are. Interviews have been documented by voice record for each sample through the use of a smartphone, which has been taken and analyzed.

## RESULTS AND DISCUSSION

A total of 4 trail segments representing the basic space units in the Yarmouk Forest Reserve have been designated:

### Al-Hreith Educational Trail Condition in Yarmouk Forest Reserve

Field evaluation of the Al-Hreith educational trail segment

showed that the most common surface types were vegetation (60% of trail segment) and rocky (32% of trail segment) where there is slight erosion of the soil at the beginning of the trail due to the slope and rocky ground on which the soil is present, which enhances the process of erosion. The width of the Al-Hreith educational trail ranges from 1.7 m to 2.5 m in some areas. The edges of the trail were identified by small stones on the sides with the presence of few natural rock stairs. The trail is relatively short and educational, as there is no point for rest or places to supply the tourist with water or food; also, the trail contains information and warning panels (Figure 2). The trail starts with an exceptional perspective on the Oak timberland on one hand and the planted Pinewood on the other. During the walk, you will experience some annual plants and trees, for example, the Hawthorn *Rhamnus*, *Calicotome*, horse chestnut, and the *Chiliadenus*.

The trail gives proof of past human advancements, as you will discover water channels utilized in the Roman time, caves and sedimentary rocks, military trenches, and the point of cannon from the 1860s. Toward the end of the trail at an altitude 380 m above sea level where, you can see and appreciate a dazzling perspective on the lake of Tiberias, the Tur Mount, and the Golan Heights.



Fig. 2: Information panels on the Al-Hreith educational trail.

### Wadi Al-Muntamra Trail

Field evaluation of the Wadi Al-Muntamra trail segment showed that the most common surface types were gravels (65% of trail segment) and vegetation (30% of trail segment). The length of the Wadi Al-Muntamra trail reaches about 6 km, starting from Mansoura, by looking at the Golan Heights, and then disappears during the descent into the valley. The floor of the trail consists of gravel and stones when walking in the course of the valley, and the soil and plants when walking on the banks of the valley, where the width of the trail ranges between 0.7 to 1.8 m.

There are some caves and caverns of limestone extending along the valley, and some of them have been used as places for overnight cattle herds that spread in this region. The valley water is used to water the flocks of sheep and livestock. Like other trails, this trail is characterized by high plant diversity than the other trails with Oleander trees, Carob trees, and aquatic plants. At the end of the trail, the visitor sees a view of the Golan Heights, the Yarmouk River, and Lake Tiberias. To meet at the end of the Al-Shreif mountain trail in the village of Al-Mukhaiba Al-Tahta.

### Al-Shreif Mountain Trail Condition in Yarmouk Forest Reserve

Field evaluation of the Al-Shreif mountain trail segment showed that the most common surface types were rocky (75% of trail segment) and vegetation cover (20% of trail segment) where there is slight erosion along the trail because the base ground which enhances erosion. Stones were used to delineating the route's limits, which had been lost from much of the trail segment, either due to human actions or herds of

animals and sheep, which remained grazing in the area and scattered throughout most of the path's length.

The Al-Shreif mountain trail, which is around 5 km, has no rest spots or places to get water or food. In addition, the path lacks information and warning panels, particularly in the absence of the trail's features and limits, which necessitates the presence of a tourist guide with experience in the region. The width of the Al-Shreif mountain trail ranges from 1.5 m to more than 2 m in some areas. The trail starts from Umm Qais, all the way to the village of Al-Mukhaiba Al-Tahta passing through a semi-flat mountain range with slight elevations and slopes, and through rocky terrain that covers approximately 70% of the trail length.

The Al-Shreif mountain trail, upon reaching a panoramic site that rises 352 m above sea level, is characterized by a distinct view of the Lake of Tiberias, Safed, The Golan Heights, At-Tur Mount, the West Bank, and Al-sheikh Mountain in Syria and Lebanon (Figure 3), also the trail contains some caves, rock formations, and ancient Roman wells and water channels.

### Arqoub Romi Mountain Trail

The Arqoub Romi Mountain Trail is the longest trail in the Yarmouk Forest Reserve, with a length of about 12 km, and it is considered a moderately difficult trail, as most of the floor of this trail is rocky, as the ratio exceeds 75% of trail segment, vegetation (10% of trail segment), and gravels (13% of trail segment). The trail begins with views of the Great Rift Valley and the Golan Heights. After about 1.5 km, the trail splits into two sections: one for enjoying the best possible landscape view in the spring and summer, and



another for protecting us from the cold western air, which can be bothersome at times. The width of the Arqoub Romi mountain trail ranges from 1.6 m to 2.6 m, and there are no indications along the trail or locations to supply tourists with water and food save Ain Nene, which is located roughly 10 km from the trail's commencement.

Approximately after 8 km, the trail will lead to a panoramic site located 308 m above sea level, where visitors can find distinguished views of the Jordanian Himmah area and the presence of a Roman grave near the site in addition to some caves and rock formation. The Arqoub Romi mountain trail continues down toward Ain Nene, which rises 142 m above sea level, where water can be supplied there. And after about 200 m there is an abandoned military area consisting of several old buildings, where visitors are located on the area overlooking the Great Rift Valley that passes through the region and the Hejaz railway, which is used to come from Al Madinah Al Munawwarah to Bilad al-Sham to Turkey countries through the Ottoman period, before reaching the final station of Arqoub Romi mountain trail at Al-Arayes pond

## CONCLUSION

The Yarmouk Forest Reserve faces a variety of threats, including woodcutting, overgrazing, and wild plant collection (uprooting wild plants), and should draw on the experience of tourist-friendly countries in managing natural reserves and the activities that can be offered to attract more visitors, while also providing the highest level of wildlife protection. To avoid problems, outdoor recreation management in protected natural areas requires an understanding of visitor desires and

their use of the protected environment. In protected natural areas around the world, trails are an essential and expanding infrastructure that concentrates tourist mobility (Miller et al. 2017). Our study applied a quantitative approach to investigate the determinants of the visitor's path selection and how the path characteristics affect the number of visitors and the ability of the reserve management to preserve the environment.

Our study found that the Al-Shreif Mountain Trail, Wadi Al-Muntamra Trail, and the Arqoub Romi Mountain Trail need to be re-maintained in terms of reorganizing the boundaries of the trail, cleaning the sides of the trail of tree stumps and stiff branches, and cleaning the waste, especially the old car tires that are located in the Wadi Al-Muntamra (Fig. 3). It should also be highlighted that the region breeds guard dogs, who are commonly seen with herds of livestock and sheep, which could make the tourist journey dangerous.

The results of our study indicate that most of the surfaces of the trails in the reserve are rocky.

GIS was used to analyze all trails where they are used for hiking only. The dominant land cover types along trails were natural grasslands (predominant along 31% of segments) gravel (19% of segments), and rocky (46% of segments). The majority of the segments (45%) were located through four different land cover types and a water stream was absent along 75% of the trails. The results of GIS analyses are summarized in (Table 1).

An interview was conducted with the director of the reserve, Mohammed Malkawi, who spoke briefly about the reserve, saying: "The area of the reserve is about 20 square



Fig. 3: A and B) Tree stumps and stiff branches along with Arqoub Romi, and Muntamra trails; C) Old car tires along Al-Shreif, mountain trail

Table 1: The main characteristics that can be evaluated by GIS software.

Trail name	Trail length	Trail type (hiking, cycling, horse riding, etc.)	No. of land cover type	The dominant type of land cover	Average trail slope	Water stream
Al-Hreith Educational Trail	3556m	Hiking	2	Coniferous forests	8.65%	No stream
Wadi Al-Muntamra Trail	5713m	Hiking	4	Transitional forests – shrubs;	6.0%	stream following the trail
Al-Shreif Mountain Trail	3927m	Hiking	2	Natural grasslands	7.9%	No stream
Arqoub Romi Mountain Trail	6920m	Hiking	2	Natural grasslands	8.15%	No stream

km. It contains 43 types of mammals, 574 plant species, and 117 bird species. It is considered an important area for bird migration. On three continents Asia, Europe, and Africa, it is considered a resting station for birds, in addition to the fact that residential areas fall within its scope. The reserve is distinguished by its biological and environmental diversity, including the flat areas, the mountain, the valley, freshwater sources, and endangered animals. The reserve contains a pattern of deciduous oak woodlands (*Quercus ithaburensis*), which is Jordan's national tree, as well as the Jordanian national flower (black iris). The reserve's role in ecotourism has recently been active, and four tourism trails have been opened within the reserve at various lengths depending on the visitors' desires, including mountains, valleys, and an educational trail for school and university students. As for the problems and challenges facing the reserve in general and the management of the reserve in particular, Malkawi said: Among the most prominent problems that occur are tree cutting in the fall season, forest fires in the summer, and overgrazing, especially in the beginning of the spring season, as most of the region's residents depend on breeding Cattle. Regarding future projects, Malkawi explained the implementation of the ecolodge (environmental hostel) project, which has been approved, and one million Jordanian dinars have been customized for implementation to do it in two phases during the years 2019 and 2020 within the projects of the Irbid Governorate. It aims to advance the development and provide job opportunities for youth and the local community, to alleviate unemployment, specifically in the poorest regions. Quality requirements primarily ensure comparability and appreciation. Quality standards, which are primarily accommodation services, restaurants, transport companies, and visitor offices, can act as a marketing tool, a benchmark; and can be taken into account when establishing a strategy to better serve the requirements of visitors. Moreover, the increase of quality hiking tourism along Yarmouk reserve trails should contribute to the

development of a marketing strategy and a brand for hiking tourism.

Management was able to recognize the major consequences by soliciting the opinions and expectations of recent visitors to the Yarmouk forest reserve. The most major visible impacts were woodcutting, litter, and vegetation destruction, all of which have the potential to decrease ecotourism's natural experience offerings. Litter, erosion, deforestation, reserve infrastructure, and vegetation damage are among the most common management problems expressed by respondents. As a result, these management issues could be utilized to measure how visitors to the Yarmouk forest reserve affect the environment.

Finally, this research is one of the first to look at the effects of ecotourism and associated indicators in the Yarmouk Forest Reserve through the eyes of visitors. This effort lays the groundwork for a comprehensive visitor management structure in the Yarmouk Forests reserve. More broadly, the sociopolitical method used in this study leads to a better understanding of the ecotourist experience's consequences for ecotourism management in Jordan's natural ecosystems.

## REFERENCES

- Abuamoud, I., Alrousan, R.M. and Bader, M.A. 2015. Impacts of Ecotourism in Jordan: Wadi Rum. *Europ. J. Social Sci.*, 50(1): 119-129.
- Abuamoud, I., Ibrahim, A. and Hijawi, L. 2019. Estimating the economic impact of tourism in the North of Jordan through the IO approach. *Europ. Res. Stud. J.*, 22(1): 254-266.
- Ancin-Murguzur, F.J., Munoz, L., Monz, C. and Hausner, V.H. 2020. Drones as a tool to monitor human impacts and vegetation changes in parks and protected areas. *Rem. Sens. Ecol. Conserv.*, 6(1): 105-113.
- Ballantyne, M. and Pickering, C. 2012. Ecotourism is a threatening process for wild orchids. *J. Ecotour.*, 11(1): 34-47.
- Cole, D.N. 2004. Impacts of hiking and camping on soils and vegetation: A review. *Environ. Impacts Ecotour.*, 41: 60.
- Gómez-Martín, M.B. 2019. Hiking tourism in Spain: Origins, issues, and transformations. *Sustainability*, 11(13): 3619.
- Hungria, M., Nogueira, M.A. and Araujo, R.S. 2013. Co-inoculation of

- soybeans and common beans with rhizobia and azospirilla: strategies to improve sustainability. *Biol. Fert. Soils*, 49(7): 791-801.
- Jamaliah, M.M., Alazaizeh, M.M., Alzboun, N. and Alzghoul, Y.A. 2019. Protected area tourism in Jordan: An exploratory study. *Tour. Recreat. Res.*, 44(1): 41-53.
- Leung, Y.F. and Marion, J.L. 2000. Recreation Impacts and Management in the Wilderness: A State-of-Knowledge Review. In Cole, D.N., McCool, S.F., Parsons, D.J. and Brown, P.J. (eds.), *Wilderness Science in a Time of Change Conference, Volume 5*, USDA Forest Service Ogden, UT, pp. 23-48
- Liddle, M. 1997. *Recreation Ecology: The Ecological Impact of Outdoor Recreation and Ecotourism*. Chapman & Hall Ltd, London, UK.
- Luzhkova, N.M. 2012. Algorithm of hiking tourism development of protected areas of the federal level. *Reg. Resp. Environ. Glob. Changes North-Western Central Asia*, 2: 192-193.
- Lynn, N.A. and Brown, R.D. 2003. Effects of recreational use impacts on hiking experiences in natural areas. *Landsc. Urban Plan.*, 64(1-2): 77-87.
- Miller, A.B., Leung, Y.F. and Kays, R. 2017. Coupling visitor and wildlife monitoring in protected areas using camera traps. *J. Outdoor Recreat. Tour.*, 17: 44-53.
- Nordbø, I. and Prebensen, N.K. 2015. *Hiking as a Mental and Physical Experience*. Emerald Group Publishing Limited., Bingley, UK
- Olive, N.D. and Marion, J.L. 2009. The influence of use-related, environmental, and managerial factors on soil loss from recreational trails. *J. Environ. Manag.*, 90(3): 1483-1493.
- Recreation Sites and Trails BC. 2012. *Trails Strategy for British Columbia*. Retrieved February 8, 2016 from: <https://www.northcowichan.ca/assets/Departments/Parks-and-Recreation/PTMP/References.pdf>
- The Royal Society for the Conservation of Nature (RSCN). 2015. *Annual Report 2015*. Retrieved April 2015 from: [http://www.rscn.org.jo/sites/default/files/pdf\\_report/AnnualReport2015.pdf](http://www.rscn.org.jo/sites/default/files/pdf_report/AnnualReport2015.pdf)
- United Nations World Tourism Organization (UNWTO). 2015. Data (online). Retrieved 19 July 2015 from: <https://www.unwto.org/archive/global/publication/unwto-annual-report-2015>
- United Nations World Tourism Organization (UNWTO). 2016. *UNWTO Tourism Highlights: Key to Development, Prosperity And Well-Being of International tourism in 2016: Key Trends and Outlook*. Retrieved 2016 from: <https://www.e-unwto.org/doi/book/10.18111/9789284419029>
- WTTC. 2018. *Travel & Tourism Economic Impact*. Retrieved March 2018 from: <https://dossier-turismo.files.wordpress.com/2018/03/wttc-global-economic-impact-and-issues-2018-eng.pdf>







# Survival Study on Different Water Quality Prediction Methods Using Machine Learning

K. Kalaivanan and J. Vellingiri†

School of Information Technology and Engineering, Vellore Institute of Technology, Vellore-632014, Tamilnadu, India

†Corresponding author: J. Vellingiri; [vellingiri.j@vit.ac.in](mailto:vellingiri.j@vit.ac.in)

Nat. Env. & Poll. Tech.  
Website: [www.neptjournal.com](http://www.neptjournal.com)

Received: 04-09-2021

Revised: 24-10-2021

Accepted: 26-10-2021

## Key Words:

Water quality prediction

Machine learning

ANN

SVM

## ABSTRACT

Water quality analysis is an emergency approach in today's world because people cannot survive without it. As a result of urbanization, industrialization, agricultural practices, and human behavior, water quality analysis have numerous issues in today's world. Manually visiting the water collection station, collecting water samples, analyzing in the lab, feeding data into a database, and so on are all challenges in the water quality analysis processing. Artificial learning model technologies will be used to tackle these challenges. The variety of machine learning approaches to water quality analysis has resulted in a diversity of creation and implementation methods. The study examines artificial intelligence's advancement in water quality prediction from different angles ANN, FUZZY, SVM, and other AI models. The review investigated 40 articles between 2008 and 2020. Groundwater, ponds, lakes, and rivers all water resources were all included in the survey method. The findings of the survey will be used to guide the future study.

## INTRODUCTION

### Research Background

Water resources span around 70% of the earth's surface (Mishra & Dubey 2015). The water sources are split into two types such as surface water and groundwater. The rivers, lakes, reservoirs, and coastal regions are examples of surface water, whereas infiltration galleries and springs are examples of groundwater (Mustafa et al. 2017). River and groundwater are critical for environmental, social health, and economic growth (Pandhiani et al. 2020, Siebert et al.2010). Rivers provide 65 percent of the water used in agriculture, with the remainder used for drinking, industrial, and other human needs. Human influences such as sewage, urbanization, agricultural, and industrial waste have an impact on river water quality (Bhatti et al. 2019).

However, these problems are caused by changes in the chemical properties of the water and the inability to drink or irrigate (Sakai et al. 2018). The chemical composition of water is related to its physical, chemical, and biological features which are used to determine the condition of water (Bordalo et al. 2006). Some of the water quality variables used to quantify water quality includes Electrical Conductivity, Dissolved Oxygen, Total Dissolved Solid, Chemical Oxygen Demand, Turbidity, Temperature, and pH (Tchobanoglous et al. 1985, Nikoo et al. 2013). Contaminated water is the most dangerous to people's health in underdeveloped

countries, accounting for 80% of all health complications (Moore et al. 2003).

The National Sanitation Foundation of the United States proposed and adopted Water Quality Index in a global manner (Brown et al. 1970). The water quality index is another often-used indicator, which is required for massive data calculations, mathematical formulae, time, and effort. WQI categorizes WQ into excellent, poor, and worst according to standards established by regulatory agencies in the research field; results are scientific, yet they are presented in an easy-to-understand fashion (Fernández et al., 2004). Water quality analysis is fundamental in the River WQ analysis, monitoring, and control. Machine learning techniques for predicting water quality are currently based on training and testing techniques (Tung & Yaseen 2020). One of the several purposes of the model used to estimate water quality is to predict how it will change over time (Chen et al. 2018). Therefore, water quality forecasting is crucial for environmental monitoring, ecological sustainability, and human health (Fijani et al. 2019).

### Problem Statement

Because water is such an important natural resource for all living organisms, it's necessary to ensure that it's always safe to drink and use. Many environmental variables play a vital role in predicting water quality. The state of the water is changed due to the variation in the effects on the environment,

leading to industrial pollution, sewage, wastewater, human overuse, low levels of water, and over-utilization of land and sea resources (Dinka 2018). Water quality analysis was split into physical, chemical, and biological analysis methods. The water quality is predicted depending on turbidity level, moisture content, and water flows (Omer 2019).

Water quality analysis has become a difficult task due to global warming and the increase in population. The population growth leads to another concern water scarcity due to the lack of adequate infrastructure. Water consumption rises in tandem with population growth, affecting people all around the world. This reason leads to people consuming contaminated water which has been connected to the spread of water-borne diseases such as cholera, diarrhea, dysentery, and hepatitis. Twenty-seven waterborne diseases have been identified by the World Health Organization (WHO). Drinking water safety is acknowledged as a threat. This is an issue that worries both developed and developing countries across the world (Jury & Vaux 2007).

The traditional method of water quality forecasting is a manual approach, such as raw data collected at intervals and analyzed in the lab. This approach leads to a time-consuming process and a risky policy-making process related to water. The previous data collection approaches resulted in a dataset that was noisy and unbalanced. For the above reason, researchers spend a lot of time pre-processing and cleaning data (Pratt & Loizos 1992). Designing water-related data is challenging because of its nonlinearity, nonstationarity, and complexity (Chang et al. 2016). Because of the size of the data, traditional methods cannot meet current demand and require the use of artificial intelligence (AI) models and their development.

## METHOD

This survey paper focuses on a review of water quality prediction using AI. The initial step is to collect water quality papers from Springer, Elsevier, and IEEE and possible resources. The second strategy was to search for articles from 2008 to 2020 using terms such as water quality, river, lake, machine learning, and deep learning research. The contribution of this survey study is:

- To conduct a thorough literature study to determine the current machine learning approaches for water quality prediction.
- To draw attention to the flaws and limits of present approaches.
- To compare various sources of surface water with the Common AI Approach.
- To recommend future research directions.

## MACHINE LEARNING

Machine learning is the latest trending technology in water quality prediction. It is a technique that allows computers to learn automatically from previous results. Machine learning is a predictive analytics technique that makes predictions based on past data. Data and algorithms were incredibly important in machine learning (Kelleher 2019). In machine learning, most of the data is used in training, and less data is used in testing. It is an embrace of four of learning such as ANN, SVM, Fuzzy, and other AI models.

### Artificial Neural Network (ANN) Model

The ANN algorithm was introduced by McCulloch in the year of 1943 (McCulloch & Pitts 1943). It is a simple method used for nonlinear data and solves complex problems. The Artificial Neural Network type is analogous to a human brain. It has neurons that are interconnected in different layers of networks (Chen et al. 2020). ANN is composed of three layers such as entry, hidden, and exit. The user will be offered input in the extreme form of formats adopted by the input layer. There may be a hidden layer between the input and the output layer. It is capable of carrying out a wide range of tasks. The output layer provides a result based on the predicted response (Najah et al. 2014). Fig.1 represents ANN Architecture.

### Fuzzy Based Model

The Fuzzy based model was introduced by Zadeh (1965). Fuzzy Logic Systems (FLS) accepted incomplete, unclear, skewed input and produce the exact output. Fuzzylogic (FL) is a method similar to human thinking. The FL approach simulates human decision-making. Some logic blocks allow the device to recognize the number of inputs and outputs defined as true or false (Wang et al. 2003). The structure of Fuzzy Logic is depicted in Fig. 2.

### Support Vector Machine (SVM) Model

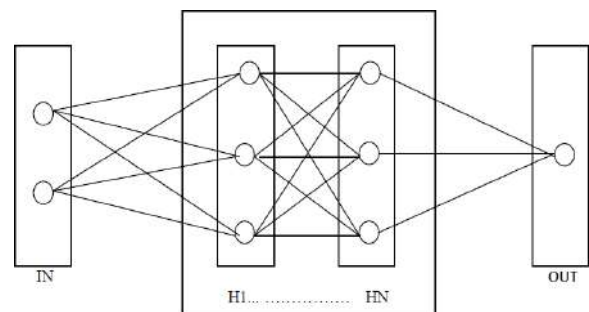


Fig. 1: ANN Architecture.

SVM is among the most effective classification and regression algorithms. The goal of the SVM algorithm is to make the simplest call purpose for bifurcate. A hyperplane is one of the best decision boundaries. It has two types such as linear and non-linear. Fig. 3 represents SVM Architecture.

**Others AI Models**

Some other models are also used to predict water quality such as hybrid and other models.

**KEY METHODS AND SYSTEMS FOR WATER QUALITY PREDICTION**

This part will cover water quality predictions such as inner relation analysis in water and pollution, various parameter predictions, anomaly detection methods in datasets, and dimension reduction in the feature selection process.

**Analysis of Inner Relationship in Water Quality Parameters**

Wu et al. (2019) introduced the adaptive frequency analysis method (ADP-FA) used to address data problems through the details of the intelligence frequency domain for internal relationships and personal discovery. The scalability characteristics were determined from the indicator, geography, and time domain. Prasad et al.(2020) developed different machine learning models that deal with binary and multi-class classi-

fication strategies used in water quality in lakes. They used the confusion matrix to test their work. The LSTM algorithm was found to provide the best level of accuracy and precision.

**Total Dissolved Solids (TDS) Prediction**

Niroobakhsh et al. (2012) compared two ANN models to predict TDS such as multi-layer perceptions (MLP) and the random forest (RF). The RF results can handle an enormous amount of information and can accurately forecast TDS levels. Tarke et al. (2016) An ANN model was used to predict the number of TDS within rivers. The backpropagation technique and the Levenberg-Marquardt optimization procedure are used to improve the ANN model’s performance.

**Dissolved Oxygen Prediction**

Ahmed & Shah (2017) designed an ANFIS-based model for estimating BOD levels in the river. ANFIS model predicted the BOD whose performance was assessed by Mean Squared Error (MSE), Mean Absolute Error (MSE), Correlation coefficient (R), and Nash model efficiency (E). As a result, the adaptive neuro-fuzzy inference approach can accurately predict biochemical oxygen demand. Chen et al. (2018) introduced a new model BPNN combined with the artificial bee colony (ABC) method for DO forecasting. According to the findings, enhanced ABC–BPNN beats regular BPNN in terms of accuracy and generalization in local searches.

**pH Prediction**

Rajae et al. (2018) tested ANN, WNN, MLR, and WMLR models for pH predicting. The WNN models used a wavelet transformation algorithm to predict pH levels in an advanced manner. This technique penetrates the mother wavelet while keeping its length constant. The WNN outperformed the others by eliminating the noise caused by the pH change.

**Salinity Prediction**

Melesse et al. (2020) used a hybrid machine learning model for salinity forecasting. M5-Prime, RF, and eight new hybrid algorithms were employed in this investigation. The water quality parameters such as pH, HCO, Cl, SO<sub>4</sub>, Na, Mg, Ca, and Total Dissolved Solid were chosen. The validation results MSP-based hybrid algorithms outperformed RF-based hybrid algorithms. Barzegar et al. (2017) applied ANN, ANFIS, WNN, and WANFIS models to predict saltiness. The dataset was preprocessed using a discrete wavelet to improve accuracy. As a result, the WANFIS and WNN models outperformed other models.

**Anomaly Detection Prediction**

Deng et al. (2015) introduced a new model hybrid Fuzzy

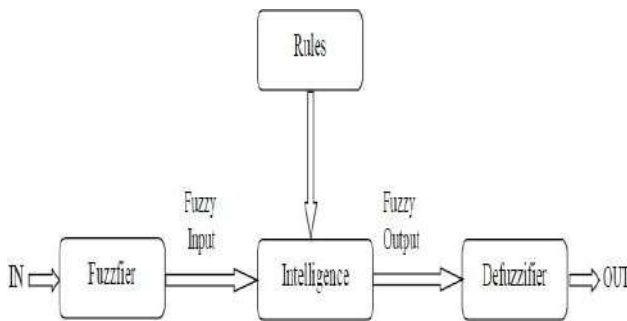


Fig. 2: Fuzzy Logic Structure.

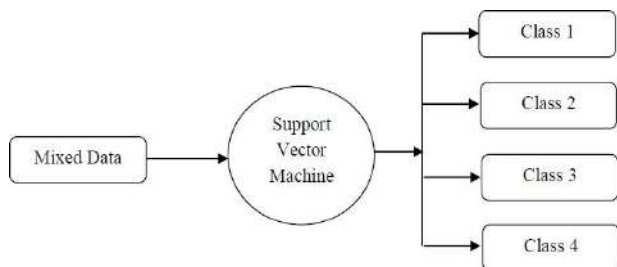


Fig. 3: Support Vector Model Architecture.

Time-series for reducing noise in the dataset. The Gaussian cloud algorithm and the heuristic GCT method were employed by FTS. The performance of results extensively compared ARIMA, RBFNN, NAR, SVM, ANN-GCT, and OSM models. The FTS surpassed other models. Muharemi et al. (2019) proposed a machine learning method for the detection of changes or anomalies found in water quality over time. The information was collected from a German public water firm. Logistic regression, linear discriminate analysis, SVM, ANN, DNN, RNN, and LSTM were introduced to improve the data quality. F-scoring, accuracy, and recall methods are used to evaluate efficiency. As a result, the LSTM performed better than the LR model.

### Dimension Reduction

Techniques for minimizing the number of parameters in a dataset are defined as dimensionality reduction. The dimension reduction technique increases machine learning performance at a high level. The ANN coupled discriminate analysis method was used by Voza & Vukovi (2018). This method was used to extract two parameters such as the water temperature and electrical conductivity. Singh et al. (2011) implemented the SVM method for dimension reduction purposes. This process is compared with kernel-based discriminate analysis (DA), kernel-based partial least square (KPLS), standard DA, and PLS methods. The findings of SVM modeling show promise in terms of managing huge amounts of WQ data for optimization, categorization, and prediction.

### COMPARISON OF DIFFERENT WATER QUALITY PREDICTION METHODS

In this review, machine learning approaches were used to simulate lake water quality, river water quality, and ground-water quality. This section discusses the present state of the water quality prediction technique comparative methodology in three categories of (1) ANFIS-FA with lake water (ii) ANFIS-WDT with river water (iii) ANFIS with groundwater is discussed in detail.

### Quality Risk Analysis For Sustainable Smart Water Supply Using Data Perception

Water source management is used to regulate the supply of drinking water. The control of the water source was essential to enhance the water quality for end-users. An Adaptive Frequency Analysis (Adp-FA) method was introduced for determining data for individual predictions. A practical solution for building a risk analysis method for the local water distribution system. The designed method was employed was used to test the spectrum analyzer, model accuracy, and processing time with ANN and RF techniques. A new

framework was introduced for the quality of the water examination with data processing mode. An Adp-FA method was employed for risk classification and prevention depending on water quality data acquired from the water distribution system. The developed technique can measure water quality indicators across many domains, including region and time.

The frequency property relationship between water quality indicators was examined for risk identification, forecast, and appraisal study. It observed a practical water source monitoring method using data obtained directly from industrial processes. It avoids issues such as the dependability of laboratory results and industrial applicability. It was beneficial to the exits water distribution system in the local infrastructural system. It established a link between readily available physical, chemical, and biological features. Pollution control decisions were made based on industrial and residential activities in water supply locations.

Cycle identification was used to find significant cycles for indicator changes in the temporal domain. The maximum value computation was used to monitor and estimate the amounts of the presence of various biological microorganisms. The training set adoption was used to do parameter adjustment. The created model was utilized to forecast the accurate bacteria indicators in tendency and values. The values were assigned different risk modes in accordance with applicable water source management regulations in different countries and locations. The decision support in water treatment plants was employed to forecast risky modes.

### Machine Learning Methods For Better Water Quality Prediction

Artificial intelligence (AI) was carried out to develop dynamic mathematical expressions. It can recognize complex and nonlinear correlations involving input and output data. The Johor River Basin has suffered significant deterioration as a result of development and human activities. Different methods like ANFIS, RBF-ANN, and MLP-ANN were introduced. The data collected from monitoring sites and experimental studies were polluted by the noise impulses with random and systematic error. It is difficult to build an accurate prediction when there is noisy data present. Based on previous data on water quality factors, a Neuro-Fuzzy Inference System (WDT-ANFIS) with an augmented wavelet de-noising technique was used. Ammoniacal nitrogen (AN), suspended solids (SS), and pH were among the water quality indicators measured. Three evaluation assessment process methods were introduced. The first evaluation was carried out using neural network connection weight partitioning, which determined the importance of each model parameter in the network. The second and third evaluation processes



established the beneficial input to create a single and combination of parameters correspondingly.

**Estimation Of Total Dissolved Solids (TDS) Using New Hybrid Machine Learning Models**

Groundwater (GW) is the main source of water for agricultural and residential purposes. GW quality was determined in an optimal manner. Decision-makers constructively handled groundwater sources when there was a clear understanding of the quantity and quality of GW. The ANFIS model was used to forecast hydrodynamic parameters and water quality indicators. The ANFIS model included an adaptive Takagaki-Sugeno fuzzy model. The ANFIS model has premises and subsequent parameters. The subsequent and premises parameters were regarded as choice parameters. As the objective function, RMSE was used. The fitness value calculation indicated the quality of the solutions. The optimization technique was used to modify the values of the agents. Because the training approach frequently produces a suboptimal answer when determining ANFIS parameters, the optimization algorithm was used to optimize and quantify the ANFIS parameters. In hybrid ANFIS and optimization methods, divides the first level data into training and test data. The second step involved training ANFIS based on training data.

**PERFORMANCE ANALYSIS OF WATER QUALITY PREDICTION TECHNIQUES**

To determine the different water quality prediction methods, a number of the data points are considered as input to conduct the testing. Different parameters were analyzed for improving the water quality prediction. For experimental consideration, water quality data is obtained from three separate water sources: lake water, river water, and groundwater. The dataset URL is given as <https://tnpcb.gov.in/water-quality.php>. The quantitative analysis is compared with different parameters such as,

- Prediction Time
- Prediction Accuracy and
- Error rate

**Analysis of Prediction Time**

Prediction time is calculated by counting the number of data points and the time required to estimate the water quality of one data point. The prediction time is determined as,

$$P_i = N * \text{Time consumed for predicting water quality of one data} \dots(1)$$

From (1), the prediction time (P<sub>i</sub>) is determined. ‘N’ represents the number of data points. The prediction time is expressed in milliseconds. Table 1 shows the prediction time as a function of the number of data points, which ranges from

25 to 250. The prediction accuracy comparison takes place on the existing Adp-FA method, WDT-ANFIS, and ANFIS model. The prediction time utilizing the Adp-FA method is comparatively reduced when compared to the WDT-ANFIS methodology and the ANFIS model, as shown in the table value. A graphical representation of the prediction time is shown in Fig. 4.

From Fig. 4, the prediction time depending on a different number of data points is described. The blue color line represents the prediction time of the Adaptive Frequency Analysis method. The red color and green color lines represent the prediction time of the WDT-ANFIS technique and the ANFIS model. From the above figure, it is clear that prediction time using the Adp-FA method is lesser when compared to the WDT-ANFIS technique and ANFIS model. This is because of introducing ANN and RF for improving the accuracy rate and minimizing the processing time. The modern data analysis methods were employed to tackle the water quality issues problems in management in smart water distribution systems for transferring knowledge across multiple indications, regions, and time domains. Consequently, the prediction time of the Adp-FA method is reduced by 16% when compared to the WDT-ANFIS technique and 40% when compared to the ANFIS model

**Analysis of Prediction Accuracy**

Prediction accuracy is defined as the ratio of the number of data points properly predicted to the total number of data points considered as input. As a result, the prediction accuracy is calculated as follows.

$$P_A = \left( \frac{\text{Number of patient data that are correctly predicted the water quality}}{\text{Number of data points}} \right) * 100 \dots(2)$$

Table 1: Tabulation of prediction time.

Number of data points	Prediction Time (ms)		
	Adp-FA method	WDT-ANFIS technique	ANFIS model
25	25	29	35
50	28	31	39
75	32	34	44
100	35	39	47
125	37	42	50
150	39	45	54
175	41	48	58
200	43	52	62
225	45	56	66
250	48	59	70

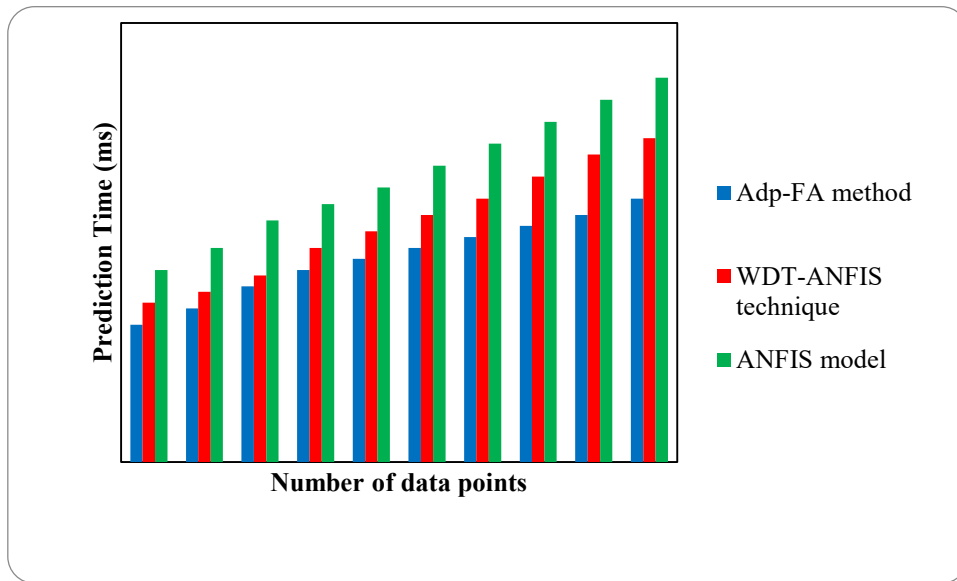


Fig. 4: Measurement of Prediction Time.

From (2), the prediction accuracy ( $P_A$ ) is determined. The prediction accuracy is expressed as a percentage (%). Table 2 shows the prediction accuracy as a function of the number of data points, which ranges from 25 to 250. The prediction accuracy comparison takes place on the existing Adp-FA method, WDT-ANFIS, and ANFIS model. According to the table values, the prediction accuracy of the WDT-ANFIS methodology is higher than that of the Adp-FA method and the ANFIS model. Fig. 5 depicts a graphical representation of prediction accuracy.

From Fig.5, the prediction accuracy based on different numbers of data points is described. The blue color line

Table 2: Tabulation of Prediction Accuracy.

Number of data points	Prediction Accuracy (%)		
	Adp-FA method	WDT-ANFIS technique	ANFIS model
25	67	72	64
50	69	74	76
75	71	77	73
100	75	80	75
125	72	78	77
150	70	75	79
175	74	79	82
200	77	82	85
225	80	85	88
250	83	88	89

represents the prediction accuracy of the Adaptive Frequency Analysis method. The red color and green color lines represent the prediction accuracy of the WDT-ANFIS technique and ANFIS model. It is clear from the statistics that the prediction accuracy using WDT-ANFIS technology is relatively high compared to the ANFIS model and the Adp-FA method. This is due to the application of a wavelet de-noising technique based on past water quality parameter data. Neural network connection load is estimated based on partitioning, which determines the importance of each input parameter in the network. The second and third evaluation processes were ascertained to construct the single and combination of parameters correspondingly. Consequently, the prediction accuracy of the WDT-ANFIS technique is increased by 7% when compared to the Adp-FA method and 11% when compared to the ANFIS model.

### Analysis of Error rate

The error rate is defined as the ratio of the number of data points that incorrectly predict the water quality of the total data points to be considered as input. Therefore, the error rate is assumed to be as follows.

$$E_R = \left( \frac{\text{Number of patient data that are incorrectly predicted water quality}}{\text{Number of data points}} \right) * 100 \dots(3)$$

From (3), the error rate ( $E_R$ ) is determined. The error rate is expressed as a percentage (%). Table 3 shows the error rate as a function of the number of data points, which ranges from 25 to 250. The Error rate comparison takes place on the

Table 3: Tabulation of error rate.

Number of data points	Error rate (%)		
	Adp-FA method	WDT-ANFIS technique	ANFIS model
25	21	25	15
50	24	28	17
75	27	31	19
100	22	26	18
125	20	22	16
150	18	20	14
175	22	24	17
200	26	28	20
225	30	33	23
250	33	37	26

Table 4: Merit and demerit.

Method	Merits	Demerits
ADP-FA	The approach is used to identify industrial contamination in waterways with ease.	The anticipated technique was difficult to implement in the absence of significant frequency effects.
WDT-ANFIS	Artificial neural weight vectors are employed in this approach to quickly identify input data.	Time consumption for water quality prediction was not reduced
ANFIS	This approach was used to predict dissolved solids in aquifers in a simple manner.	However, the accuracy of outputs was not improved by using multi-objective MFO.

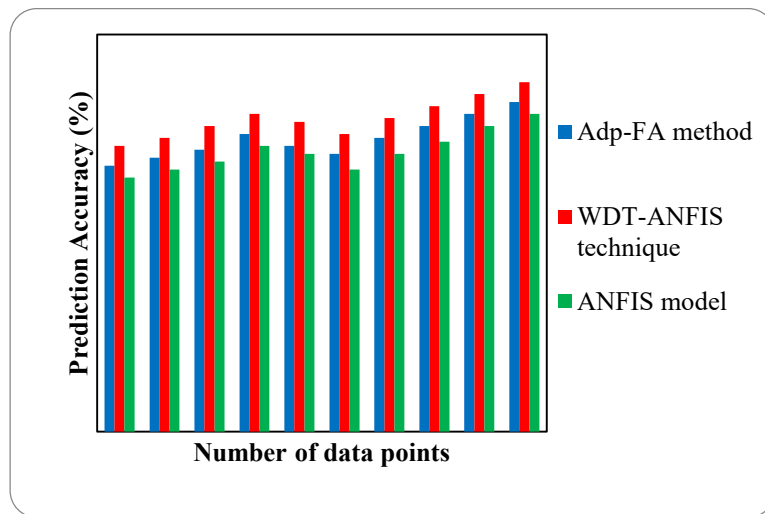


Fig.5: Measurement of prediction accuracy.

existing Adp-FA method, WDT-ANFIS, and ANFIS model. Fig. 6 depicts a graphical representation of the Error rate.

From above Fig. 6, the error rate based on the different numbers of data points is illustrated. The blue color line is also shown the error rate of the Adaptive Frequency Analysis method. The red color and green color lines are also shown

in the error rate of the WDT-ANFIS technique and ANFIS model. From the figure, it is clear that the error rate using the ANFIS model is comparatively lesser when compared to the WDT-ANFIS technique and Adp-FA method. This is due to the usage of the Takagaki-Sugeno fuzzy model with the assumption and subsequent parameters, which is flexible.

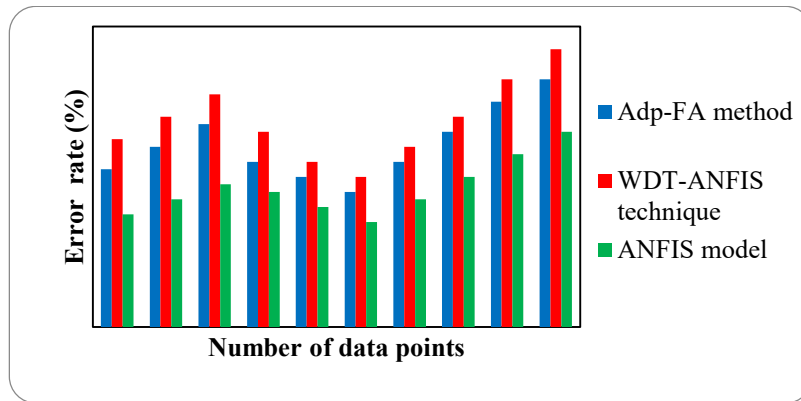


Fig. 6: Measurement of error rate.

The enhancement algorithm reached the optimal solution to determine the best ANFIS parameters. Consequently, the error rate of the ANFIS model is reduced by 32% when compared to the Adp-FA method and 49% when compared to the WDT-ANFIS technique.

## RESULTS AND LIMITATIONS OF THIS STUDY

The results section explains the comparative research of the aforesaid literature review approaches.

The comparison is based on the ANFIS model, which incorporates frequency analysis as well as the wavelet denoising approach. The assessment measures employed in this study are prediction accuracy, prediction time, and error rate. Table 4 shows the merit and demerit of the models.

## CONCLUSION AND FUTURE WORK

This paper presents a variety of survey techniques for water quality analysis using a machine learning approach. Many machine learning models are now being integrated with Big data and IoT to increase model performance. The performance in water quality prediction depends upon the accuracy and latency of detection, which is connected to the computing time of the model. According to the review, the time consumption of the machine learning models is not decreasing in estimating the quality of water.

Simultaneously, machine learning models lack certain information that allows them to handle real-time input.

The following list of research gaps and possibilities can be further explored in detail.

1. To introduce new hybrid ML models that can accurately forecast water quality.
2. To introduce new DL models for predicting water quality.

3. To improve optimization methods by adding new algorithms to forecast the water quality.

It is hoped that this work will contribute to the analysis of water quality in general and to an overview of the problem of predicting water quality as needed by people around the world.

## REFERENCES

- Ahmed, A.M. and Shah, S.M.A. 2017. Application of adaptive neuro-fuzzy inference system (ANFIS) to estimate the biochemical oxygen demand (BOD) of Surma River. *J. King Saud Univ. Eng. Sci.*, 29(3): 237-243.
- Barzegar, R., Adamowski, J. and Moghaddam, A.A. 2016. Application of wavelet-artificial intelligence hybrid models for water quality prediction: a case study in Aji-Chay River, Iran. *Stochastic Environ. Res. Risk Assess.*, 30(7): 1797-1819.
- Bhatti, N.B., Siyal, A.A., Qureshi, A.L. and Bhatti, I.A. 2019. Socio-economic impact assessment of small dams based on T-paired sample test using SPSS software. *Civil Eng. J.*, 5(1): 153-164.
- Bordalo, A.A., Teixeira, R. and Wiebe, W.J. 2006. A water quality index was applied to an international shared river basin: the case of the Douro River. *Environ. Manag.*, 38(6): 910-920.
- Brown, R.M., McClelland, N.I., Deininger, R.A. and Tozer, R.G. 1970. A water quality index-do we dare. *Water Sewage Works*, 117(10): 651.
- Chang, F.J., Chen, P.A., Chang, L.C. and Tsai, Y.H. 2016. Estimating spatio-temporal dynamics of stream total phosphate concentration by soft computing techniques. *Sci. Total Environ.*, 562: 228-236.
- Chen, S., Fang, G., Huang, X. and Zhang, Y. 2018. Water quality prediction model of a water diversion project based on the improved artificial bee colony-backpropagation neural network. *Water*, 10(6): 806.
- Chen, Y., Song, L., Liu, Y., Yang, L. and Li, D. 2020. A review of the artificial neural network models for water quality prediction. *Appl. Sci.*, 10(17): 5776.
- Deng, W., Wang, G. and Zhang, X. 2015. A novel hybrid water quality time series prediction method based on cloud model and fuzzy forecasting. *Chemometr. Intell. Lab. Syst.*, 149:39-49.
- Dinka, M.O. 2018. *Safe Drinking Water: Concepts, Benefits, Principles and Standards*. Water Challenges of an Urbanizing World, IntechOpen, London, pp.163-181.
- Fernández, N., Ramírez, A. and Solano, F. 2004. Physico-chemical water quality indices-a comparative review. *Bistua: Revista de la Facultad de Ciencias Básicas*, 2(1): 19-30.

- Fijani, E., Barzegar, R., Deo, R., Tziritis, E. and Skordas, K. 2019. Design and implementation of a hybrid model based on a two-layer decomposition method coupled with extreme learning machines to support real-time environmental monitoring of water quality parameters. *Sci. Total Environ.*, 648: 839-853.
- Jury, W.A. and Vaux, H.J. 2007. The emerging global water crisis: managing scarcity and conflict between water users. *Adv. Agro.*, 95: 1-76.
- Kelleher, J.D., 2019. *Deep Learning*. MIT Press, Cambridge, MA.
- McCulloch, W.S. and Pitts, W. 1943. A logical calculus of the ideas immanent in nervous activity. *Bull. Math. Biophys.*, 5(4): 115-133.
- Melesse, A.M., Khosravi, K., Tiefenbacher, J.P. and Heddam, S. 2020. River water salinity prediction using hybrid machine learning models. *Water*, 12(10): 2951.
- Mishra, R.K. and Dubey, S.C. 2015. Freshwater availability and its global challenge. *Int. J. Eng. Sci. Invent. Res. Develop.*, 2(6): 65-83.
- Mohammed, H., Hameed, I.A. and Seidu, R. 2018. Detection of water safety conditions in distribution systems based on artificial neural network and support vector machine. *Int. Conf. Adv. Intell. Syst. Inform.*, 61: 567-576.
- Moore, M., Gould, P. and Keary, B.S. 2003. Global urbanization and impact on health. *Int. J. Hyg. Environ. Health*, 206(5): 269-278.
- Muharemi, F., Logof tu, D. and Leon, F. 2019. Machine learning approaches for anomaly detection of water quality on a real-world data set. *J. Inform. Telecomm.*, 3(3): 294-307.
- Mustafa, A., Sulaiman, O. and Shahooth, S. 2017. Application of QUAL2K for water quality modeling and management in the lower reach of the Diyala river. *Iraqi J. Civ. Eng.*, 11: 66-80.
- Najah, A., El-Shafie, A., Karim, O.A. and El-Shafie, A.H. 2013. Application of artificial neural networks for water quality prediction. *Neural Comp. Appl.*, 22(1): 87-201.
- Nikoo, M.R., Karimi, A., Kerachian, R., Poorsepahy-Samian, H. and Daneshmand, F. 2013. Rules for optimal operation of reservoir-river-groundwater systems considering water quality targets: Application of M5P model. *Water Resour. Manag.*, 27(8): 2771-2784.
- Niroobakhsh, M., Musavi-Jahromi, S. H., Manshour, M., and Sedghi, H. 2012. Prediction of water quality parameter in Jajrood River basin: application of multi-layer perceptron (MLP) perceptron and radial basis function networks of artificial neural networks (ANNs). *African Journal of Agricultural Research*, 7(29): 4131-4139.
- Omer, N.H., 2019. Water quality parameters. *Water quality-science, assessments and policy*, p.18.
- Pandhiani, S.M., Sihag, P., Shabri, A.B., Singh, B. and Pham, Q.B. 2020. Time-series prediction of streamflows of Malaysian rivers using data-driven techniques. *J. Irrig. Drain. Eng.*, 146(7): 104020.
- Prasad, V.V.D., Venkataramana, L.Y., Kumar, P.S. and Prasannamedha, G. 2020. Water quality analysis in a lake using deep learning methodology: prediction and validation. *Int. J. Environ. Anal. Chem.*, 13: 45-56
- Pratt, B. and Loizos, P. 1992. *Choosing Research Methods: Data Collection for Development Workers (Vol. 7)*. Oxfam, Oxford, UK.
- Rajae, T., Ravansalar, M., Adamowski, J.F. and Deo, R.C. 2018. A new approach to predict daily pH in rivers based on the "à trous" redundant wavelet transform Algorithm. *Water, Air, & Soil Pollution*, 229(3):1-18
- Sakai, N., Mohamad, Z.F., Nasaruddin, A., Abd Kadir, S.N., Salleh, (ed.). 2018. Eco-Heart Index as a tool for community-based water quality monitoring and assessment *Ecological Indicators*, 91:38-46.
- Siebert, S., Burke, J., Faures, J. M., Frenken, K., (ed.). 2010. Groundwater use for irrigation—a global inventory. *Hydrology and earth system sciences*, 14(10):1863-1880.
- Singh, K.P., Basant, N. and Gupta, S. 2011. Support vector machines in water quality management. *Analytica chimica acta*, 703(2):152-162.
- Tarke, P.D., Sarda, P.R. and Sadgir, P.A. 2016. Performance of ANNs for prediction of TDS of Godavari river, India. *International Journal of Engineering Research*, 5(2):115-118.
- Tchobanoglous, G. and Schroeder, E.E. 1985. *Water quality: characteristics, modeling, modification*.
- Tung, T.M. and Yaseen, Z.M., 2020. A survey on river water quality modelling using artificial intelligence models: 2000-2020. *Journal of Hydrology*, 585:124670.
- Voza, D. and Vukovi , M. 2018. The assessment and prediction of temporal variations in surface water quality—a case study. *Environmental monitoring and assessment*, 190(7):1-16.
- Wang, K. 2003. *Intelligent condition monitoring and diagnosis systems: a computational intelligence approach (Vol. 93)*. IOS press.
- Wu, D., Wang, H., Mohammed, H. and Seidu, R. 2019. Quality risk analysis for sustainable smart water supply using data perception. *IEEE Transactions on Sustainable Computing*, 5(3): 377-388.
- Zadeh, L.A. 1996. Fuzzy sets. In *Fuzzy sets, fuzzy logic, and fuzzy systems: selected papers by Lotfi A Zade*, pp 394-432.
- Zhang, J., Zhu, X., Yue, Y. and Wong, P.W. 2017. August. A real-time anomaly detection algorithm/or water quality data using dual time-moving windows. In *2017 Seventh international conference on innovative computing technology*, pp. 36-41.







# Comprehensive Modeling of Seasonal Variation of Surface Ozone Over Southern Tropical City, Bengaluru, India

G. Dhanya\*†, T. S. Pranasha\*, Kamsali Nagaraja\*\*, D. M. Chate\*\*\* and G. Beig\*\*\*\*

\*Department of Physics, BMS College of Engineering, Bengaluru-560019, India

\*\*Department of Physics, Bangalore University, Bengaluru-560056, India

\*\*\*Centre for Development of Advanced Computing, Pune-411008, India

\*\*\*\*National Institute of Advanced Studies, Bengaluru-560012, India

†Corresponding author: G. Dhanya; gopidhanya85@gmail.com

Nat. Env. & Poll. Tech.  
Website: [www.neptjournal.com](http://www.neptjournal.com)

Received: 05-09-2021

Revised: 10-11-2021

Accepted: 21-11-2021

## Key Words:

Ozone

Tropospheric pollutant

Seasonal variation

Meteorological parameters

Statistical variations

## ABSTRACT

Surface ozone ( $O_3$ ) is an important pollutant. In this study we investigated the effects of precursor gases on the difference in ozone concentration utilizing various statistical methods like Multiple Linear Regression (MLR), Principal Component Regression (PCR), Artificial Neural Network (ANN), and Principal Component and Artificial Neural Network (PC-ANN) in conjunction with meteorological parameters for forecasting. The pollutants ozone ( $O_3$ ), carbon monoxide (CO), nitric oxide (NO), nitrogen dioxide ( $NO_2$ ), oxides of nitrogen ( $NO_x$ ), and the meteorological parameters temperature (temp), relative humidity (RH), solar radiation (SR), wind speed (WS) and wind direction (WD) observed during 2019 are taken as inputs for MLR, PCR, ANN, and PCANN. The mathematical models obtained from the numerical analysis showed that  $O_3$  concentration was significantly affected by the CO, NO,  $NO_2$ ,  $NO_x$ , temp, RH, SR, WS, and WD factors. PCR model's regression coefficient was lower than the MLR model, but the same for ANN and PCANN models was much better in all the seasons than the linear models such as MLR and PCR. The efficiency of all methods is inspected using several performance metrics.

## INTRODUCTION

Ozone ( $O_3$ ) is among the main air pollutants often related to global environmental degradation.  $O_3$  is a secondary contaminant arising from complex chemical effects in the atmosphere (Seinfeld & Pandis 2006). High concentrations of  $O_3$  are closely connected to meteorological backgrounds. They typically arise during hot days, when principal pollutants, oxides of nitrogen ( $NO_x$ ) and Non-Methane Hydrocarbons (NMHC) react photochemically, followed by intense solar radiation and higher temperatures (San José et al. 2005). Ozone destruction happens through various mechanisms, including the chemical reactions happening in the atmosphere and surface deposition. The photochemical loss of Ozone occurs by the photolysis of Ozone and its consequent reaction. The reaction with the water molecule produces OH and  $HO_2$  during midday through the generation of an  $O^1D$  molecule. Other ways in which Ozone is eliminated is by either dry or wet precipitation (Varotsos et al. 2000). Ozone has detrimental effects on both humans as well as plants. The analysis of Ozone variations is complicated due to the various precursors, and photochemical and meteorological processes in the air (Abdul-Wahab et al. 2002). Toh et al. (2013) have

shown that meteorological parameters significantly influence the effectiveness of the photochemical system linked to the creation and depletion of Ozone. Therefore, it is useful to establish a relation between these primary pollutants and meteorological variables that could be used to determine Ozone concentration (Elkamel et al. 2001).

Several models have been used to satisfy both these criteria: the influence of primary pollutants and meteorological parameters on Ozone and predicting the pollutant levels. Accordingly, these models are sorted into two groupings deterministic and the other as statistical. Deterministic models involve high resources and precision data (Azzi et al. 1995). Therefore, relying on statistical models is far more practical and economical than the deterministic models. Statistical models are simplistic, and they can be implemented in the real data that is available. The statistical models can classify output parameter relationships with input parameters deprived of cause and effect methodology.

Several statistical methods are proposed for analyzing and forecasting concentrations of Ozone. Graphical analysis, Multiple Linear Regression (MLR), Principal Component Analysis (PCA), and Artificial Neural Networks (ANN)

have been used to explain the variability of extensive data on air pollution (Abdul-Wahab et al. 2005, Sousa et al. 2007, Özbay et al. 2011). A commonly used technique for achieving a normalized input-output model for a given data set is the MLR process. It is used in biology, medicine, and environmental studies (Smith & Wachob 2006, Özbay et al. 2011).

The present study addresses the effect of precursor gases on the difference in O<sub>3</sub> concentration using MLR, PCR, ANN, and PCANN laterally with meteorological parameters. The primary objective is to link Ozone concentration to meteorological parameters and concentrations of prime pollutants, including the precursors.

## MATERIALS AND METHODS

### Study Area

The measurement site is located on the campus of B.M.S. College of Engineering, Basavangudi, a residential location in Bengaluru, India. Bengaluru (12.9410° N, 77.5655°E, 910 m above MSL) one of India's fastest-growing cities, is known as the 'Silicon Valley of India' due to information technology-based industries.

Surface O<sub>3</sub> concentration is measured continuously using a Serinus 10 O<sub>3</sub> analyzer based on the absorption of ultraviolet radiation with a specific wavelength, 254 nm. An Ecotech analyzer provides O<sub>3</sub> estimates in the range of 0-250 ppbv with a 0.5 ppb detection limit. The NO, NO<sub>2</sub>, and NO<sub>x</sub> concentrations are measured by a Serinus 40 NO<sub>x</sub> analyzer based on the chemiluminescence technique. The lower detectable value is 0.40 ppbv with a processing time of 40 s for the NO<sub>x</sub> analyzer. Wind speed, wind direction, ambient temperature, relative humidity, and rainfall are recorded using an Automatic Weather Station (AWS) which is also mounted in this location.

### Statistical Techniques

MLR, PCR, ANN, and PCANN were used to build four models. Statistical packages for Social Sciences 22.0 (SPSS 22.0) were used for MLR and PCR, while MATLAB R2019a was used for ANN and PCANN research.

**Multiple linear regression:** One of the most used methodologies for defining the linear relationship among the dependent variable and many other independent variables is Multiple Linear Regression (MLR). MLR uses a least square technique to suit the model, thus reducing the number of square differences amid experimental and predicted concentrations of O<sub>3</sub>.

The General MLR equation is given as follows:

$$Y = b_0 + \sum_{i=1}^p b_i x_i + \varepsilon$$

Where Y would be the dependent variable, b<sub>0</sub> is a constant, b<sub>i</sub> is independent variable coefficients, x<sub>i</sub> is independent variables, and ε is regression model error. Despite its effectiveness in several applications, MLR can experience tremendous difficulty once the independent variables are associated (Mcadams et al. 2000). Multicollinearity, or strong association in a regression equation between the independent variables, may make it hard to classify the utmost significant contributors to a physical method.

**Principal component regression (PCR):** PCR is Principal Component Analysis (PCA) and MLR collective method. Principal Components (PCs) produced by PCA are being utilized in MLR by employing an input variable, which reduces the multicollinearity and simplifies the model. The selected PCs with extreme PCA loadings assured that most of the original parameters were used in these models, making them suitable for usage in MLR as independent factors (Gvozdić et al. 2011).

**Principal component analysis (PCA):** PCA is a multivariate data technology that is applied in this analysis to minimize parameters and to include the most significant important parameter in variations of O<sub>3</sub>. PCA transforms these into a limited number of independent variables named principal components. PCs were extracted in such a way whereby its first principal component (PC1) represented the most considerable amount of overall variability in the collected data, while the remaining components (PC2, PC3) reported for the rest of the variations (Kovač-Andrić et al. 2009).

PCs are overall, expressed in terms

$$PC_i = l_{1i}X_1 + l_{2i}X_2 + \dots + l_{mi}X_m$$

PC<sub>i</sub> is the i<sup>th</sup> PC, and l<sub>mi</sub> is the observed loading X<sub>m</sub>.

In PCA, Bartlett's sphericity method is adopted to check whether variables are correlated with each other or not. Kaiser-Meyer-Olkin (KMO) verifies PCA's applicability to the set of data, and the value of KMO's > 0.5 suggests PCA's data suitability. The varimax rotation has been implemented, simplifying the model by making smaller and larger loads and ensuring that each component has a maximum association with just one printable factor and is minimally associated with some variables (Dominick et al. 2012).

**Artificial neural network (ANN):** ANN applications in atmospheric/environmental sciences started in the late 1990s

and were proven effective in model forecasting (Luna et al. 2014). The neuron is an essential building block for any ANN architecture. This network has three layers, namely input mode, hidden mode, and output mode. The input neurons encrypt information from an outside world, all the neurons in the previous layer receive signals from the hidden neurons, while the output neurons transmit back useful data to the outside world. The output value is obtained by applying a mapping function such as Sigmoid, Tangential, and linear hyperbolic. Maier & Dandy (2000) have explained in detail the application of ANN in environmental modeling.

**Principal component and artificial neural network (PC-ANN):** PCANN is a combination of PCA and ANN. PCs created from PCA are used instead of original variables as input variables. The accuracy of individual forecasts can be enhanced by combining predictions from various models (Zhang 2003). Even though such models are of rather complex architecture, they could be more useful in predicting the levels of Ozone.

### Performance Indicators

Various performance indicators were evaluated towards assessing the errors and accuracies of the models developed.

### Normalized Absolute Error (NAE)

NAE summates the expected and calculated value difference separated by a summation of the observed values (Elbayoumi et al. 2014).

$$NAE = \frac{\sum_{i=1}^n |P_i - O_i|}{\sum_{i=1}^n O_i}$$

### Root Mean Square Error (RMSE)

RMSE is the standard method of calculating a model's error when predicting quantitative data. It is formally defined as

$$RMSE = \sqrt{\frac{1}{n-1} \sum_{i=1}^n (P_i - O_i)^2}$$

### Index of Agreement (IA)

IA is a standardized model prediction error degree indicator, which ranges from 0 to 1. The formula is given by

$$IA = 1 - \left[ \frac{\sum_{i=1}^n (P_i - O_i)^2}{\sum_{i=1}^n (|P_i - \bar{O}| + |O_i - \bar{O}|)^2} \right]$$

IA equals 0 means that the expected and observed values do not match, while IA equals 1 means that the observed and predicted values are in perfect harmony.

### Mean Biased Error (MBE)

Mean biased error means that the prediction degree is either above or below the values. MBE level > 0 would be an indicator of over-prediction, while the level < 0 is an indicator of under-prediction.

$$MBE = \bar{P} - \bar{O}$$

where n indicates sample size,  $P_i$  has Predicted Ozone concentration;  $O_i$  is a concentration of detected Ozone;  $\bar{P}$  is expected concentration of Ozone;  $\bar{O}$  is average of the concentration of Ozone.

## RESULTS AND DISCUSSION

For the present study dataset of the year 2019 has been used for training and then these data were segregated into distinct seasons for model validation. The entire set of data was checked for normalization before being utilized in different models. In this study, four models for different seasons, winter, summer, monsoon, and post-monsoon, were used to estimate Ozone concentration using precursors and meteorological parameters.

### MLR

Regression-based methods were adopted to predict the impacts of identified variables on  $O_3$  differences (Abdul-Wahab et al. 2005). Stepwise multiple linear regression modeling was used in this study to determine the predictive equation designed for the concentration of Ozone as a result of the different parameters that are being measured. CO, NO,  $NO_2$ ,  $NO_x$ , Temperature (temp), Relative Humidity (RH), Solar Radiation (SR), Wind Speed (WS), and Wind Direction (WD) are the independent predictors while Ozone is the dependent or response variable that has been used in this study. The method automatically chooses the most important parameters and excludes those that are of the least significance.

As Variance Inflation Factor (VIF) fell under 5, multicollinearity problems were excluded. Autocorrelation has been assessed using the Durbin Watson test and the autocorrelation values are 1.78, 1.71, 0.92, and 1.13 for winter, summer, monsoon, and post-monsoon for the current data. The model description is presented in Table 1, which provides many correlations R,  $R^2$ , adjusted  $R^2$ , and best fit model solution. MLR model developed was evaluated by the coefficient of determination ( $R^2$ ) used to measure the capability of the designated parameters to elucidate the  $O_3$  concentration variations (Abdul-Wahab et al. 2005). The findings showed how MLR showed success with  $R^2$  at 0.933, 0.90, 0.95, and 0.90 during winter, summer, monsoon, and post-monsoon. For winter, the table's variables describe more than 93%

of the variance in Ozone concentration.  $\text{NO}_2$  appears to be the primary source of Ozone during summer. Among these meteorological parameters, temperature and solar radiation make significant contributions to high Ozone concentrations. The variation in  $\text{NO}_2$  and temperature explains the change in Ozone up to 95% for monsoon. However, post-monsoon, it accounts for 90% depending on the variable, as shown in the table.

For the MLR model using precursor gases and meteorological parameters,  $R^2$  calculated was found to range from 0.88 to 0.91. MLR model shows that the independent variables listed in the table explain more than 85 % of the variance in Ozone concentration during the different seasons. Fig. 1(a-d) shows a strong positive correlation between measured and modeled Ozone levels with a coefficient of 0.92, 0.89, 0.95, and 0.89 for winter summer, monsoon, and post-monsoon seasons. Fig. 2(a-d) shows the diurnal variation of observed and modeled Ozone for winter, summer, monsoon, and post-monsoon seasons. It indicates a strong agreement of diurnal variability between observed and predicted values

for the peak hours. It showed an overestimation for winter, summer, and monsoon during the morning and night hours while there was an underestimation during morning hours for the post-monsoon season.

### PCR

The main aim of PCR is to acquire a limited quantity of components that would elucidate much of the maximum variation in the predictor variables. The adequacy of data collected for PCA is evaluated by Bartlett's studies and Kaiser-Meyer-Olkin (KMO). Before using PCA for extraction, 10 linear variables,  $\text{O}_3$ , CO, NO,  $\text{NO}_2$ ,  $\text{NO}_x$ , temp, RH, SR, WS, and WD, were chosen. After PCA extractions, three variables were selected as the PCs built on eigenvalue greater than unity. PCs obtained in Table 2 obey varimax rotation as this maximizes the correlation of the parameters to only one factor and minimizes correlations between the parameters and the other factors (Dominick et al. 2012). The cumulative variances during winter, summer, monsoon, and post-monsoon were 96%, 95%, 93%, and 95%, respectively.

Table 1: Correlation of  $\text{O}_3$  concentration with models during the different seasons for MLR.

Season	Method	R	$R^2$	Adjusted $R^2$	Equation of Model
Winter	MLR	0.963	0.926	0.915	$\text{O}_3 = ((2.433 * \text{Temp}) - (1.029 * \text{WD}) + (0.051 * \text{SR}) + (241.964))$
Summer	MLR	0.950	0.903	0.889	$\text{O}_3 = ((-1.884 * \text{NO}_2) + (4.543 * \text{Temp}) + (0.029 * \text{SR}) - (48.529))$
Monsoon	MLR	0.977	0.954	0.950	$\text{O}_3 = ((-1.367 * \text{NO}_2) + (1.906 * \text{Temp}) - (8.838))$
Post Monsoon	MLR	0.950	0.902	0.888	$\text{O}_3 = ((-0.096 * \text{WD}) - (1.34 * \text{CO}) + (0.009 * \text{SR}) + (34.508))$

Table 2: Rotated Principal Components loadings during the different seasons.

	Winter			Summer			Monsoon			Post-Monsoon		
	PC1	PC2	PC3	PC1	PC2	PC3	PC1	PC2	PC3	PC1	PC2	PC3
NOx	0.991			0.974				0.992				0.971
NO2	0.965			0.892				0.903				0.942
CO	0.963			0.979				0.984				0.984
NO	0.962			0.926				0.925				0.927
Temperature		0.977			0.964		0.964				0.932	
RH		-0.983			-0.971		-0.957				-0.91	
WS			0.939		0.835		0.975				0.938	
WD	0.881					-0.802	-0.936					0.867
SR		0.621	0.594		0.589	0.701	0.897		0.403	0.835		
Ozone	-0.703		0.542		0.819		0.918			0.834		
Eigen value	5.263	2.635	1.744	4.019	3.903	1.619	5.535	3.841		4.405	4.103	1.034
% of Variance	52.626	26.35	17.437	40.188	39.032	16.191	55.346	38.405		44.054	41.034	10.341
Cumulative %	52.626	78.975	96.413	40.188	79.22	95.411	55.346	93.751		44.054	85.088	95.429



During winter, the first factor represented 52.6% of the total change and itemized six variables (NO, NO<sub>2</sub>, NO<sub>x</sub>, CO, WS, WD) as the crucial variables. While the second factor signified 26.3% of the total change and contained loadings of temperature and solar radiation, PCA then classified Ozone, SR, and WS onto the third factor, which characterized almost 17.4% of the total change. In summer, we observe on the first PC, NO, NO<sub>2</sub>, NO<sub>x</sub>, and CO have significant loadings with 52.6% of the variation of independent parameters. The second PC describes 39% of the discrepancy, and it is profoundly loaded on Ozone, temp, and WS. The third PC was heavily laden on wind direction and solar radiation which explains 16.2% changes.

The first PC stated 55.3% of the whole data variability for the monsoon results. They are heavily encumbered onto Ozone, temp, RH, WS, WD, and SR. The subsequent PC, which reported about 38.4% of the total changes, showed a distinction of only pollutants, namely CO, NO, NO<sub>2</sub> and NO<sub>x</sub>. The rest of the parameters were signified by the remaining main components, which successfully accounted for less of the total variation. The post-monsoon's first parameter included most of the carefully chosen meteorological variables with a collected variance of 44%. The second factor was constituted by many of the primary sources of pollutants with a difference of 41%, although WD exclusively characterized the third factor with approximately 10%. Thus, principal components obtained from PCA are implemented in the MLR model to find the best fit for variations in Ozone.

Table 3 shows the result of the PCR model. The analysis indicates that PCR during winter and post-monsoon showed optimum performance with R<sup>2</sup> values equivalent to 0.69 and 0.76, correspondingly. Therefore, more than 70% of the O<sub>3</sub> differences throughout winter and post-monsoon were described by the selected parameters. A significantly higher R<sup>2</sup> (0.90 and 0.93) was obtained during summer and monsoon, which indicated that these selected variables explained higher possibilities of O<sub>3</sub> variations. During these periods, R<sup>2</sup> values for the PCR analysis were crucially lower than R<sup>2</sup> values for the MLR analysis. The use of PCs as MLR inputs could not increase the models' efficiency to clarify the disparities in O<sub>3</sub>

concentrations through the different seasons. A scatter plot of modeled vs observed shows that the correlation between observed and modeled is moderately related for winter and post-monsoon, and shows a good correlation between the two for summer and monsoon (Fig. 1(a-d). Fig. 2 (a-d) shows the model offers strong consistency during peak Ozone hours in the summer, winter, and monsoon seasons, overestimating Ozone rates in the early morning and night hours. While for the post-monsoon season it over and underestimates the entire diurnal variation.

**ANN**

Models of artificial neural networks (ANN) can detect complex non-linear underlying interactions amid responses and forecasters and could be accomplished using many successful training methods. In this analysis, ANN was developed using MATLAB 2019a and used a feedforward backpropagation method. It has a layer of input, hidden, and output. There are 9 input parameters and one output parameter. The 9 input data that have been in the investigation are CO, NO, NO<sub>2</sub>, NO<sub>x</sub>, temp, RH, SR, WS, and WD. The entire data set is divided into 70% of training, 15% validation data set, and 15% the test data set. The number of neurons and the appropriate activation function are two of the major issues encountered when building the architecture of the hidden layer. Yang et al. (2005), have explained the number of neurons in the hidden layer can be evaluated using the following formula

$$n_h = 2n_i + 1$$

n<sub>h</sub> represents the number of neurons present in the hidden layer and n<sub>i</sub> represents the number of neurons present in the input layer. The ideal number of neurons in the hidden layer was 19 (n<sub>i</sub> = 9). The model with 19 neurons was explored, but the results were not promising. For better output, the model was optimized by using 5,10,15,19 neurons in the hidden layer while 10 neurons in the hidden layer only showed better results and so this is incorporated in the study.

For training, validation, and testing, datasets correlation coefficients were 0.99, 0.96, and 0.99, respectively for winter. The cumulative regression is 0.99. While for summer and

Table 3: Correlation of O<sub>3</sub> concentration with models during the different seasons for PCR.

	Method	R	R2	Adjusted R2	Equation of Model
Winter	PCR	0.810	0.670	0.630	O3= $(-0.282*PC2)+(0.057*PC3)+(49.478)$
Summer	PCR	0.950	0.902	0.887	O3= $(-8.13*PC1)+(2.877*PC2)+(0.036*PC3)-(41.728)$
Monsoon	PCR	0.966	0.934	0.928	O3= $(1.434*PC1)-((-0.372*PC2)-11.019)$
Post-monsoon	PCR	0.871	0.758	0.735	O3= $((0.529*PC1)-(0.078*PC2)+(4.445))$

monsoon it is 0.98, 0.99, and 0.99 for training, validation, and testing. The overall regression was 0.98. For post-monsoon, the training, validation, and testing were found to be 0.99, and the overall regression was 0.99. The complete regression using the ANN model showed closure to unity which is stronger than the other models. Fig. 1(a-d) shows the scatter plot of observed and predicted Ozone levels for different seasons. We observe that the correlation between observed and measured Ozone levels during winter, summer, monsoon, and post-monsoon is 0.99, 0.97, 0.97, and 0.99. ANN model is better when compared to the MLR and PCR models. Figure 2a-d displays the diurnal variation of Ozone observed and modeled by ANN. There was good agreement between the observed and modeled Ozone levels during peak hours for winter, monsoon, and post-monsoon seasons. While for summer season there is an overestimation during the night-time.

## PC-ANN

PC-ANN model was used, which was devoid of multicollinearity to make the ANN model efficient and straightforward. Model construction was initiated by applying PCA analysis to the data and then applying ANN on the generated three most explaining PCs. As a result, the input layer has 3 neurons, while the number of neurons in the hidden layer is 7 ( $2n_i + 1$ ). The model's performance was tested again by 5, 7, and 9 neurons in the hidden layer. The results displayed best with 7 neurons in the hidden layer. The dataset is divided into training (70%), validation (15%), and testing datasets (15%). The correlation coefficients of PC-ANN-based modeled datasets of training, validation, testing, and overall were 0.98, 0.99, 0.93, and 0.97 for the winter season. For summer and monsoon, the training, validation, testing, and overall were 0.99, 0.96, 0.99, and 0.99, respectively. During the

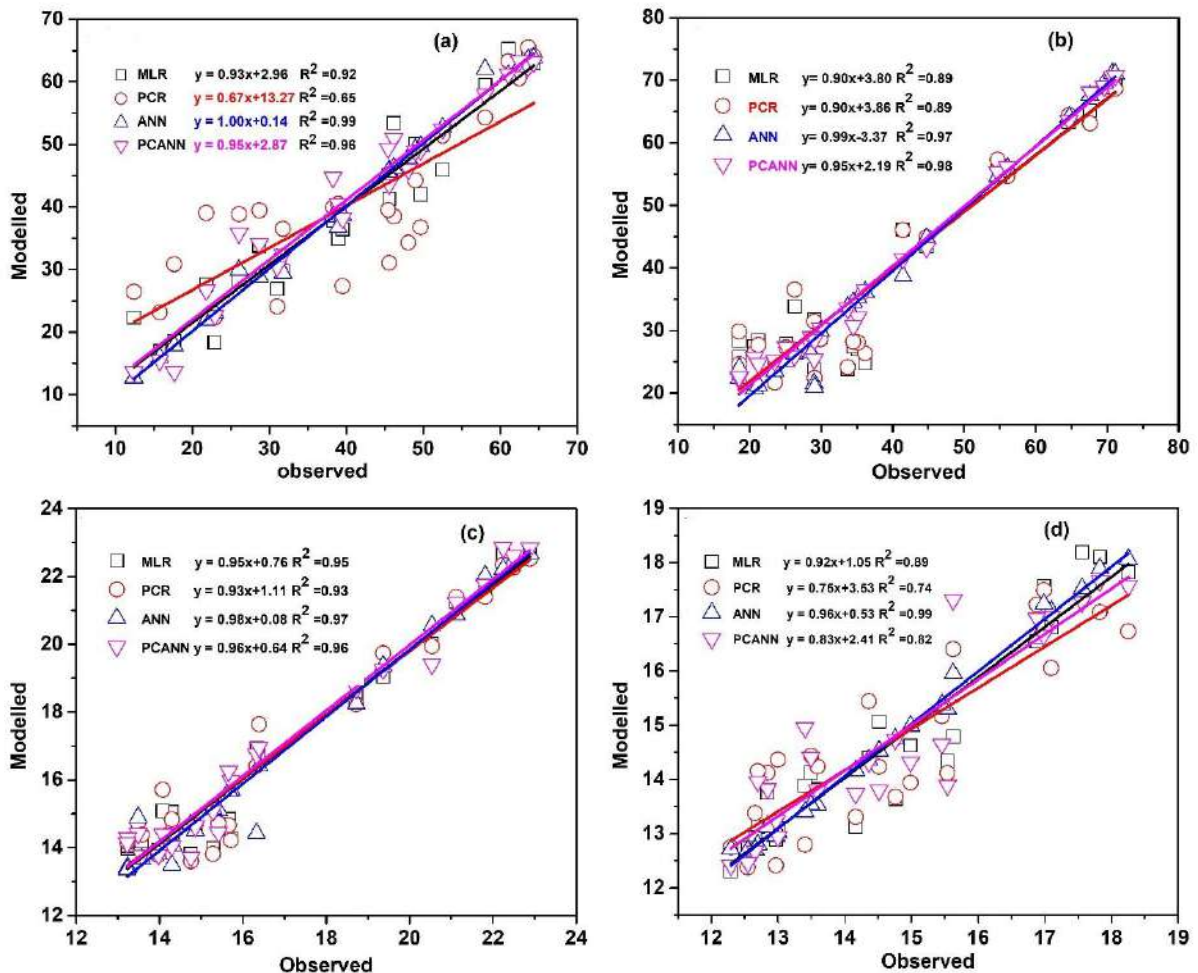


Fig. 1: Modelled vs Observed correlation graph for a winter, b summer, c monsoon, d post-monsoon seasons.

post-monsoon season, it was 0.89, 0.99, 0.94, and 0.90 for training, validation, testing, and overall results.

A scatter plot shows a strong correlation between modeled and observed Ozone levels for all the seasons and is shown in Fig. 1 (a-d). Fig. 2 (a-d) exhibits the diurnal variation of modeled and observed Ozone for PC-ANN analysis. There is a good agreement between the observed and the modeled values for peak hours' observations and overestimation was observed for all seasons during the early morning and late evening hours.

**Performance Indicators**

The performance of each of these models was measured using different error terms such as normalized absolute error, root mean square error, index of agreement, prediction accuracy,

and mean biased error. The value of NAE, RMSE, IA, PA, and MBE are shown in Table 4 for different seasons.

For the most accurate model, the NAE value must be near zero (Sharma et al. 2016). In the present data, the NAE is close to zero, indicating the accuracy of the models. The lower RMSE value shows that the model works well, though the higher RMSE value does not imply that the model is entirely incorrect as peak data take a high RMSE impact (Vlachogianni et al. 2011).

RMSE remained highest for MLR and PCR model and the smallest for the ANN and PC-ANN model. If IA in the model is nearer to one, it means that the forecasted values are adjacent to the observed values. It was nearest to 1, suggesting that the ANN-based method represents this model's best alignment with the observed set of data. The MBE

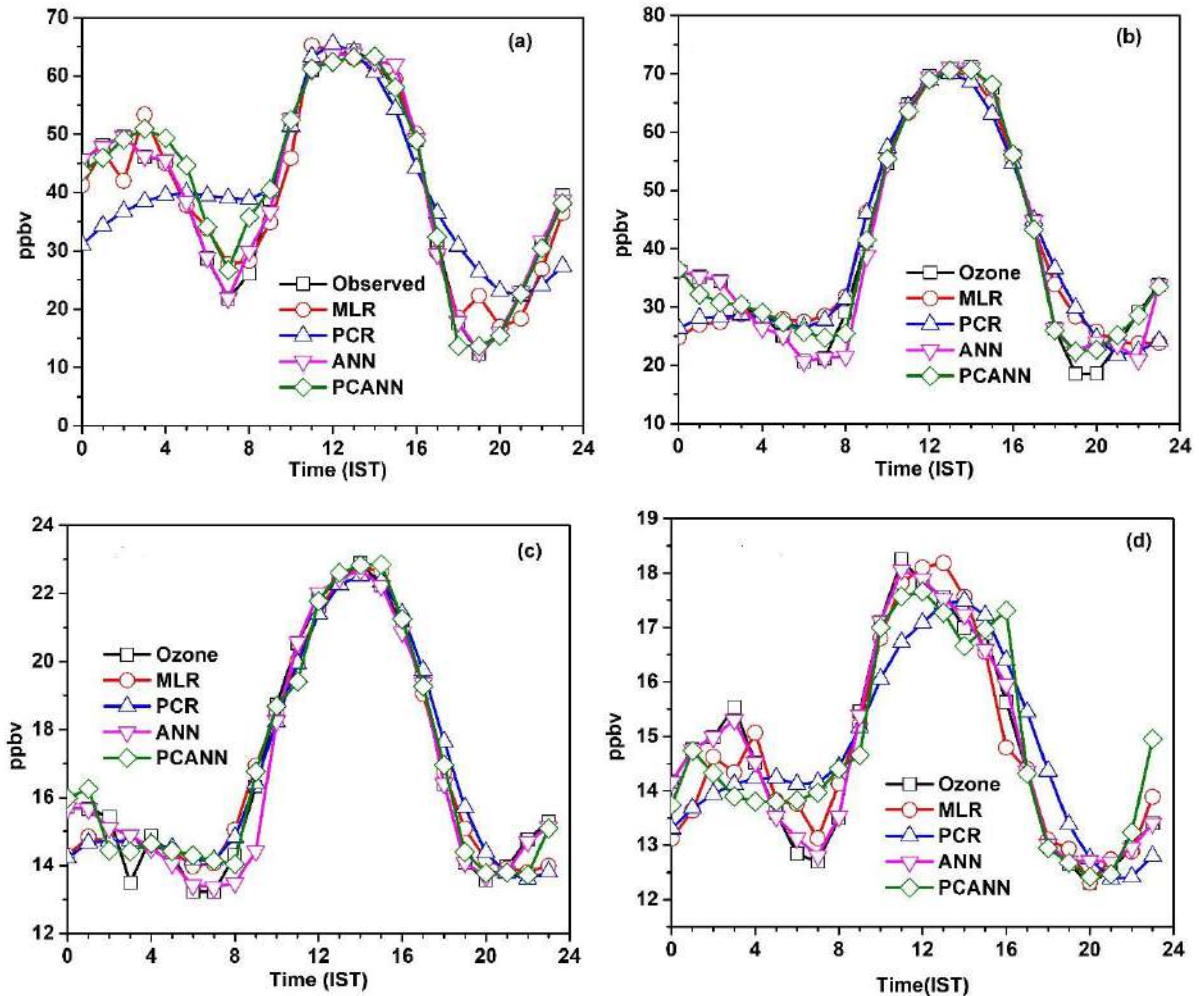


Fig. 2: Diurnal variation of experimental, MLR, PCR, ANN, and PCANN exhibited ozone level a winter b summer c monsoon d post-monsoon.

Table 4: Summary of Performance Indicators.

Winter PI	NAE	RMSE	IA	PA	MBE
MLR	0.115	0.697	0.905	0.77	-0.016
PCR	0.26	1.508	0.587	0.676	0.048
ANN	0.02	0.143	0.986	1.398	0.17
PC-ANN	0.074	0.462	0.883	1.527	1.09
Summer- PI	NAE	RMSE	IA	PA	MBE
MLR	0.152	0.891	0.924	1.667	0.012
PCR	0.154	0.91	0.919	1.062	-0.043
ANN	0.05	0.271	0.951	1.062	-0.492
PC-ANN	0.062	0.331	0.989	1.113	0.321
Monsoon- PI	NAE	RMSE	IA	PA	MBE
MLR	0.038	0.121	0.915	1.235	-0.017
PCR	0.045	0.145	0.925	1.461	0
ANN	0.019	0.062	0.976	1.795	-0.124
PC-ANN	0.028	0.091	0.919	0.109	0.082
Post-monsoon- PI	NAE	RMSE	IA	PA	MBE
MLR	0.032	0.098	0.971	1.102	-0.026
PCR	0.056	0.168	0.917	1.423	-0.008
ANN	0.008	0.023	0.997	0.946	0.032
PC-ANN	0.038	0.114	0.903	0.945	0.036

results show over and under prediction for the observed and predicted value. All these performance indicators suggest that ANN and PCANN models were the best compared to MLR and PCR-based models for predicting Ozone levels for all the seasons. Ozone concentrations predicted by these models vary. These variations are attributed to the complex set of reactions involving Ozone's precursor other than the ones used in the present study.

## CONCLUSION

Surface Ozone simulation was carried out with four statistical models. The first concept is built on MLR and the coefficients of regression for this model are 0.926, 0.903, 0.954, and 0.902 during winter, summer, monsoon, and post-monsoon. The second concept is the PCR model developed that uses factor analysis of principal components as the input parameter in multiple linear regression. The third model used was ANN which showed regression analysis results of training, validation, test, and overall unity. The fourth model is PCANN, and their regression coefficient is also close to unity. The reliability of all models is tested using various performance indicators. The governing equations developed from the regression techniques showed that O<sub>3</sub> concentration was significantly affected by parameters such as CO, NO,

NO<sub>2</sub>, NO<sub>x</sub>, temp, RH, SR, WS, and WD. The PCR model's regression coefficient was less than the MLR model, but the same for ANN and PCANN models was much better in all the seasons than the linear models such as MLR and PCR.

The present work is preliminary research on Bengaluru air pollution that might be used in various data analytical approaches to develop a forecasting model. An effective forecasting model of ambient air pollution is essential for demonstrating it to be a valuable tool for public health protection to build rigorous pollution control technologies and procedures.

## ACKNOWLEDGEMENTS

The Ministry of Earth Sciences (MoES) supports the Indian Institute of Tropical Meteorology (IITM), Pune. The authors sincerely express their thanks to Professor R. S. Nanjundiah, Director, IITM and MoES for the MAPAN air quality station at BMS College of Engineering, Bengaluru for the mutual benefit of academic research. The contents and conclusions in this research paper are of the authors and do not necessarily reflect the organizations' views. The authors from BMS College of Engineering sincerely express their thanks to the Principal, Professor B. V. Ravishankar.

## REFERENCES

- Abdul-Wahab, S.A. and Al-Alawi, S.M. 2002. Assessment and prediction of tropospheric ozone concentration levels using artificial neural networks. *Environ. Model Software*, 17(3): 219-228. doi: 10.1016/S1364-8152(01)00077-9.
- Abdul-Wahab, S.A., Bakheit, C.S. and Al-Alawi, S.M. 2005. Principal component and multiple regression analysis in modeling of ground-level ozone and factors affecting its concentrations. *Environ. Model. Software*, 20(10): 1263-1271. doi: 10.1016/j.envsoft.2004.09.001.
- Azzi, M., Johnson, G.M., Hyde, R. and Young, M. 1995. Prediction of NO<sub>2</sub> and O<sub>3</sub> concentrations for NO, plumes photochemically reacting in urban air. *Math. Comput. Model.* 21: 39-48.
- Dominick, D., Juahir, H., Latif, M.T., Zain, S.M. and Aris, A.Z. 2012. Spatial assessment of air quality patterns in Malaysia using multivariate analysis. *Atmos. Environ.*, 60: 172-181. doi: 10.1016/j.atmosenv.2012.06.021.
- Elbayoumi, M., Ramli, N.A., Md Yusof, N.F.F., Yahaya, A.S.B., Al Madhoun, W. and Ul-Saufie, A.Z. 2014. Multivariate methods for indoor PM10 and PM2.5 modeling in naturally ventilated school buildings. *Atmos. Environ.*, 94: 11-21. doi: 10.1016/j.atmosenv.2014.05.007.
- Elkamel, A., Abdul-Wahab, S., Bouhama, W. and Alper, E. 2001. Measurement and prediction of ozone levels around a heavily industrialized area: A neural network approach. *Adv. Environ. Res.*, 5(1): 47-59. doi: 10.1016/S1093-0191(00)00042-3.
- Gvozdić, V., Kovač-Andrić, E. and Brana, J. 2011. Influence of meteorological factors NO<sub>2</sub>, SO<sub>2</sub>, CO, and PM10 on the concentration of O<sub>3</sub> in the urban atmosphere of Eastern Croatia. *Environ. Model. Assess.*, 16(5): 491-501. doi: 10.1007/s10666-011-9256-4.
- Kovač-Andrić, E., Brana, J. and Gvozdić, V. 2009. Impact of meteorological factors on ozone concentrations modeled by time series analysis and multivariate statistical methods. *Eco. Inf.*, 4(2): 117-122. doi: 10.1016/j.ecoinf.2009.01.002.



- Luna, A.S., Paredes, M.L.L., De Oliveira, G.C.G. and Corrêa, S.M. 2014. Prediction of ozone concentration in tropospheric levels using artificial neural networks and support vector machine at Rio de Janeiro, Brazil. *Atmos. Environ.*, 98: 98-104. doi: 10.1016/j.atmosenv.2014.08.060.
- Maier, H.R., and Dandy, G.C. 2000. Neural networks for the prediction and forecasting of water resources variables: A review of modeling issues and applications. *Environ. Model. Software.*, 15(1): 101-124. doi: 10.1016/S1364-8152(99)00007-9.
- McAdams, H.T., Crawford, R.W. and Hadder, G.R. 2000. A vector approach to regression analysis and its application to heavy-duty diesel emissions. *SAE Tech. Papers*, 1: 19-61. <http://dx.doi.org/10.4271/2000-01-1961>
- Özbay, B., Keskin, G.A., Doğruparmak, Ş.Ç. and Ayberk, S. 2011. Multivariate methods for ground-level ozone modeling. *Atmos. Res.*, 102(1–2): 57-65. doi: 10.1016/j.atmosres.2011.06.005.
- San José, R., Stohl, A., Karatzas, K., Bohler, T., James, P. and Pérez, J.L. 2005. A modeling study of an extraordinary nighttime ozone episode over the Madrid domain. *Environ. Model. Software.*, 20(5): 587-593. doi: 10.1016/j.envsoft.2004.03.009.
- Seinfeld, J.H. and Pandis, S.N. 2006. *Atmospheric Chemistry and Physics: From Air Pollution to Climate Change*. 2nd edition. J. Wiley, Hoboken, N.J.
- Smith, C.M. and Wachob, D.G. 2006. Trends associated with residential development in riparian breeding bird habitat along the Snake River in Jackson Hole, WY, USA: Implications for conservation planning. *Bio. Cons.*, 128(4): 431-446. doi: 10.1016/j.biocon.2005.10.008.
- Sharma, S., Sharma, P., Khare, M. and Kwatra, S. 2016. The statistical behavior of ozone in an urban environment. *Sus. Environ. Res.*, 26(3): 142-148. doi: 10.1016/j.serj.2016.04.006.
- Sousa, S.I.V., Martins, F.G., Alvim-Ferraz, M.C.M. and Pereira, M.C. 2007. Multiple linear regression and artificial neural networks based on principal components to predict ozone concentrations. *Environ. Model. Software.*, 22(1): 97-103. doi: 10.1016/j.envsoft.2005.12.002.
- Toh, Y.Y., Lim, S.F. and Von Glasow, R. 2013. The influence of meteorological factors and biomass burning on surface ozone concentrations at Tanah Rata, Malaysia. *Atmos. Environ.*, 70: 435-446. doi: 10.1016/j.atmosenv.2013.01.018.
- Varotsos, C.A., Kondratyev, K.Y. and Cracknell, A.P. 2000. New evidence for ozone depletion over Athens, Greece. *Int. J. Rem. Sen.*, 21(15): 2951-2955. doi: 10.1080/01431160050121366.
- Vlachogianni, A., Kassomenos, P., Karppinen, A., Karakitsios, S. and Kukkonen J. 2011. Evaluation of a multiple regression model for the forecasting of the concentrations of NO<sub>x</sub> and PM<sub>10</sub> in Athens and Helsinki. *Sci. Total Environ.*, 409(8): 1559-1571. doi: 10.1016/j.scitotenv.2010.12.040.
- Yang, J., Rivard, H. and Zmeureanu, R. 2005. Online building energy prediction using adaptive artificial neural networks. *Energy Build.*, 37(12): 1250-1259. doi: 10.1016/j.enbuild.2005.02.005.
- Zhang, G.P. 2003. Time series forecasting using a hybrid ARIMA and neural network model. *Neurocomputing*, 50: 159-175. doi: 10.1016/S0925-2312(01)00702-0.







## Application of Geo-electrical Methods for Estimating Water Infiltration in Soils

Kaizar Hossain\*, Mohd Talha Anees\*\*†, Ahmad Farid Bin Abu Baker\*\*, Mohammad Muqtada Ali Khan\*\*\*, Amin E. Khalil\*\*\*\*, K. S. Ishola\*\*\*\*\*, Abdullah K. \*\*\*\*\*, Mohd Nawawi M. N. \*\*\*\*\*, and Mohd. Omar A. K. \*\*\*\*\*

\*Department of Environmental Science, Asutosh College, University of Calcutta, Shyamaprasad Mukherjee Road, Kolkata-700 026, West Bengal, India

\*\*Department of Geology, Faculty of Science, University of Malaya, Kuala Lumpur 50603, Malaysia

\*\*\*Faculty of Earth Science, Universiti Malaysia Kelantan, Jeli Campus, 17600 Jeli, Kelantan, Malaysia

\*\*\*\*Department of Geology, Faculty of Science, Helwan University, Helwan, Greater Cairo 11795, Egypt

\*\*\*\*\*Department of Geosciences, University of Lagos, Akoka, Lagos, Nigeria

\*\*\*\*\*Geophysics Section, School of Physics, Universiti Sains Malaysia, Minden 11800, Penang, Malaysia

\*\*\*\*\*School of Industrial Technology, Universiti Sains Malaysia, Minden 11800, Penang, Malaysia

†Corresponding author: Mohd Talha Anees; talhaanees\_alg@yahoo.in

Nat. Env. & Poll. Tech.  
Website: [www.neptjournal.com](http://www.neptjournal.com)

Received: 21-08-2021

Revised: 04-10-2021

Accepted: 26-10-2021

### Key Words:

Electrical resistivity tomography  
Hydraulic conductivity  
Infiltration rate  
Permeability  
Transient electromagnetic

### ABSTRACT

In this study, an alternative approach was applied for the characterization of the subsurface geological conditions to estimate the hydrological parameters in the absence of subsurface soil data. The study revealed that the hydrological parameters, estimated from the Transient Electromagnetic (TEM) and Electrical Resistivity Tomography (ERT), were significantly correlated with in situ data. Overall estimated infiltration rate (below 20 inches/h) predicted fine-grained soil was also associated with in situ data. A high correlation among the bulk electrical resistivity, porosity, and the resistivity of the pore fluid thereby confirmed the relevance of Archie's law used in this study. Furthermore, results showed that both TEM and ERT are vital tools for hydrological parameter estimation.

Soil water infiltration is a significant part of the hydrological cycle (Todd & Mays 1980). It depends on the distribution of subsurface soil texture and structure, which maintains soil moisture conditions. Infiltration in unconsolidated soils is proportional to grain size and distribution (Cui et al. 2017). While the infiltration in the clayey soil is slow because of the small grain size and high resistance to water movement. The spatial variability of soil structure is determined by soil profile observations and soil properties measurements such as bulk density and porosity. The tools available for the investigation of water movement in the soil are limited to a specific point measurement and are destructive, whereas the geophysical methods are usually non-invasive. They disturb neither the structure nor the water dynamics of the soil (Michot et al. 2003).

Infiltration rate can be measured using in-situ methods such as the double-ring method (Shaari et al. 2016, Fatehnia et al. 2016) and laboratory experiments (Morbidelli et al. 2015). However, it is difficult to carry out experiments in

high-relief areas due to slope steepness and logistic handling. Alternatively, geophysical methods are cost and time-effective methods for the proper assessment of subsurface soil parameters. As the soil's electrical conductivity varies due to the presence of pore water, saltwater, and temperature, electrical resistivity methods will be helpful to estimate subsurface hydrological factors such as hydraulic conductivity, porosity, and permeability (Anees et al. 2017).

In previous studies, electrical resistivity techniques have been used for different purposes such as groundwater developments (Kumar et al. 2016, Afshar et al. 2015), water distribution in landfills (Dumont et al. 2016), landslide investigation (Perrone et al. 2014), monitoring of seasonal water content variations (Chrétien et al. 2014, Brunet et al. 2010), porosity or hydraulic conductivity estimation (Chou et al. 2016, Niwas & Celik 2012, Ghose & Slob 2006) and infiltration estimation (Crosbie et al. 2014). Some of these studies used a variety of electrical resistivity techniques, such as electrical resistivity tomography (ERT), vertical electri-

cal sounding (VES), and time-domain-induced polarization (TDIP). Transient electromagnetic (TEM) is a geophysical method often used for subsurface hydrogeological mapping (Danielsen et al. 2003, Al-Garni & El-Kaliouby 2011). In the case of shallow depth investigations (up to a depth of 100 m), the instrumental setup of TEM is short and easy as compared to the other resistivity methods, which make it useful for a survey, especially in hilly terrain (Danielsen et al. 2003, Flores et al. 2013). TEM is the right technique for an accurate determination of the bulk resistivity of the subsurface geological units. In some situations, such as rough topography or limited space, laying down transmitter loops become difficult. In such cases, resistivity imaging techniques come to the rescue. Resistivity imaging is also given preference in those areas where the distribution of resistivity is multi-dimensional.

Electrical resistivity methods have been used to estimate the infiltration rate from empirical relationships (Noell et al. 2011, Chou et al. 2016). However, none of the studies have related the electrical resistivity and infiltration rate to flooding, which developed the motivation to conduct this study. The conventional methods to estimate the infiltration rate are based on the point or one-dimensional measurement. Whereas, in flood-related studies, two to three-dimensional measurements are required for accurate results. During flooding, the infiltration rate becomes slow as the large load of suspended particles quickly forms a clogging layer (Chen et al. 2013). Because of this, a shallow depth investigation should be enough to conduct infiltration rate measurement. Therefore, this study has two main purposes. The first is to estimate or identify soil-related parameters for empirical equations to estimate subsurface hydrological parameters. The second is the use of ERT and TEM to estimate the two-dimensional subsurface infiltration rate.

The main aim of this study was to characterize the spatial variability of soil structure in the hilly terrain of Kelantan State, Malaysia, using both TEM and ERT. The specific objectives were (i) to carry out in-situ subsurface resistivity distribution in terms of lateral and vertical variations in the resistivity values, (ii) to estimate soil parameters from empirical relationships in a data-sparse environment, and (iii) to develop multilayer regression models for the study area to know the accuracy of the estimated soil parameters and (iv) to validate the TEM and the ERT outputs with borehole and in situ data. The alternative approach of this study in the absence of soil parameter data will be helpful to estimate the multi-dimensional infiltration rate for flood vulnerability and risk analysis.

## MATERIALS AND METHODS

### Location and Details of the Study Area

The location of the study area is in Kelantan State, the

north-eastern part of Peninsular Malaysia. It lies between Latitudes 4°33'N and 6°14' N, longitudes 101°19'E and 102°39'E with an area of approximately 15000 km<sup>2</sup>. The elevation ranges from 0 to 2.2 km above mean sea level. The slope varies from 0 to 89 degrees. Sungai Kelantan is the main river, which divides approximately 107 km into Sungai Galas and Sungai Lebir (Fig. 1).

The climate is tropical, and humid with an average temperature range from 20 °C to 30 °C. The average annual rainfall is 3017 mm, and the average daily wind speed is 1.50 m.s<sup>-1</sup>. The regional geology of Kelantan consists of sedimentary and metasedimentary rocks in the central zone, while granite is situated on the eastern and western borders of the Boundary Range and Main Range respectively (Heng et al. 2006). According to the Department of Agriculture, Malaysia, there are 21 soil series in the catchment. But the area is dominated by three such as steep land (63.9%) followed by Durian-Munchong-Bungor (14.3%) and Rengam-Jerangau (5.4%). The eastern and western mountain ranges have a granitic soil cover that is composed of fine to coarse sand and clay. The minimum depth of soil cover is a meter on steep land, while the depths increase up to 18 m downstream. A fine sandy loam soil up to a few meters is found on the steep slope of the basin. At mid and downstream, a clay layer of an average depth of 4 m is situated. Also, there is a layer of fine to medium-grained sand in a few places. The depth of the clay layer decreases near the sea downstream while the depth of the fine to medium-grained sand layer increases.

### Data Acquisition

Electrical resistivities were measured through thirteen profiles of TEM and nine profiles of ERT surveys that covered upstream, midstream, and downstream of the study area. Survey locations were mostly on the river bank to know the infiltration rate, which is essential in floodplain hydrological modeling. TEM data were collected using a terra team Monex GeoScope instrument with a current of 5 A and 12 V batteries. The stacking time was set to 3 minutes with a 50 Hz noise filter to remove interference from the power lines. TEM profiles were in the form of loops. Each loop was 20 m × 10 m in dimension, which have eight 5 m × 5 m small loops to get high-resolution data (Fig. 2).

ERT data were collected through a 100 m profile at nine locations using the ABEM Terrameter system. The system had an automatic switch box and an array of 41 metal stake electrodes at 2.5 m electrode spacing. The Wenner-Schlumberger electrode spacing was used that allows measurements up to a depth of 40 m depth was used.

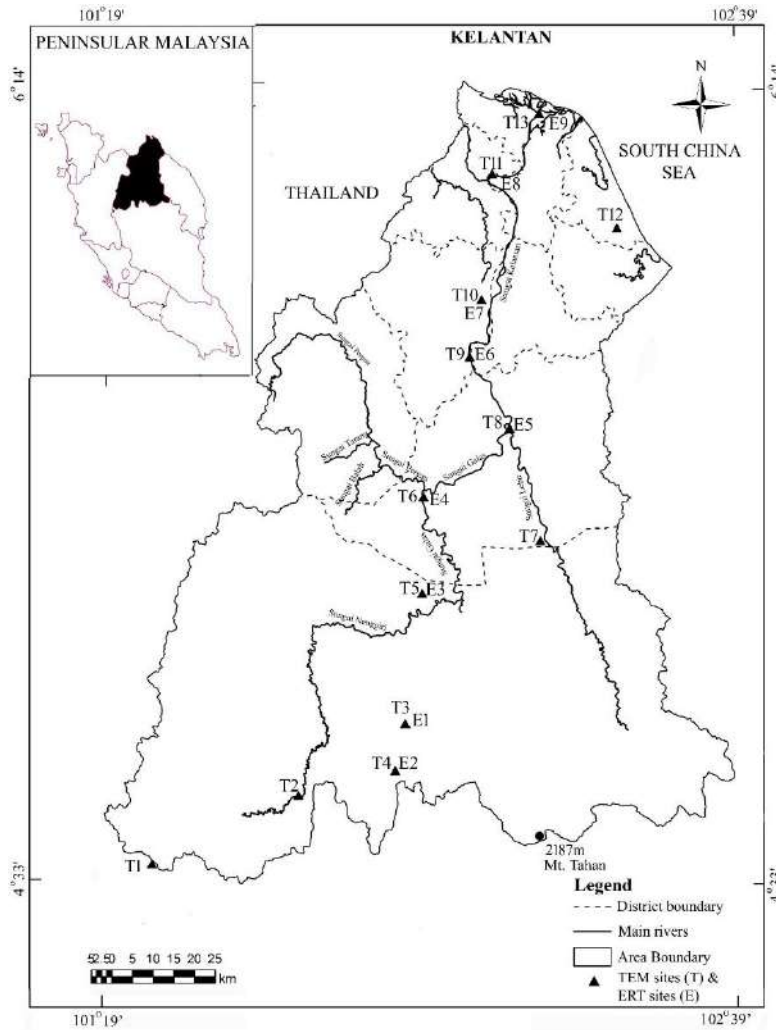


Fig. 1: Location of TEM and ERT sites in the study area.

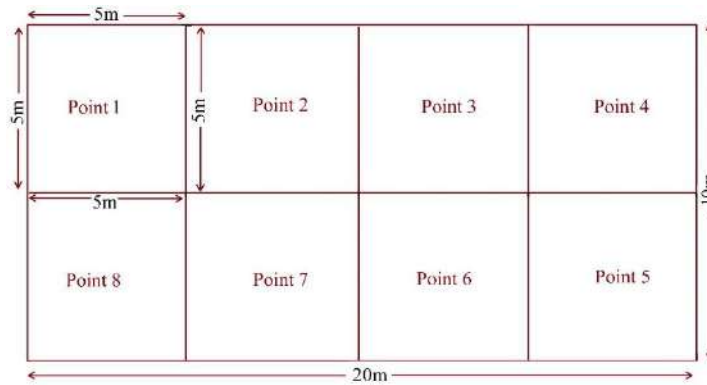


Fig. 2: TEM profiling with 5m-by-5m loop.

## In-situ Soil Sampling

In-situ soil samples with 20 cm depth were collected at thirteen locations. These samples were brought back to the laboratory, air-dried, and sieved through a 2 mm sieve. A hydrometer test was used to calculate the amount of sand, silt, and clay (Bouyoucos 1962). In addition, for results validation, the log data was collected from the Department of Mineral and Geoscience, Malaysia.

## Calculation of Porosity

For porosity calculation, the most widely used Archie's equation (Archie 1942) for electrical resistivity was selected, which is given as:

$$\rho = a\rho_w\phi^{-m} \quad \dots(1)$$

where  $\rho$  and  $\rho_w$  are bulk resistivity of rock or unconsolidated soil and resistivity of pore fluid in  $\Omega\text{m}$  respectively,  $\phi$  is the porosity of aquifer,  $a$  is the electrical tortuosity parameter, and  $m$  is the cementation factor. Eq. (1) is not valid for silt and clay because it only captures pore water conduction. It needs some modification for silt and clay. Therefore, the calculation of the cementation factor was by the equation (Choo et al. 2016):

$$m = m_{sand} \cdot (1 - VF_c) + m_{clay} \cdot VF_c \quad \dots(2)$$

where  $m_{sand}$  and  $m_{clay}$  are the cementation factors for pure sand and pure clay respectively.  $VF_c$  is the volume fraction of clay. The cementation factor was calculated for each site based on the clay percentage from Eq. (2). Pure sand and pure clay values were used at 1.55 and 2.11 respectively to modify the cementation factor (Choo et al. 2016). The cementation values vary from 1.58 (site number 11) to 1.74 (site number 3). As these cementation values were based on the 20 cm depth and it may not be the same as up to 20 m depth. Therefore, the average value of 1.66 was selected for the entire study area.

The electrical tortuosity parameter ( $a$ ), which is related to the path length of the current flow, is almost unity for unconsolidated sediments (Niwas & Celik 2012). Hence,  $a = 1$  was used for this study. Generally, pore fluid resistivity ( $\rho_w$ ) values are measured from laboratory experiments. Due to the lack of this data, the  $\rho_w$  values for different  $\rho$  were collected from previous studies. Based on Niwas and Celik (2012) and Choo et al. (2016) studies,  $\rho_w$  values for different bulk resistivity were identified, which are given in Table 1.

## Calculation of Permeability

Kozeny (1953) developed a relationship between porosity and intrinsic permeability, which is given as:

$$k = \frac{d^2}{180} \frac{\phi^3}{(1-\phi)^2} \quad \dots(3)$$

where  $k$  is intrinsic permeability, and  $d$  is grain size in a meter. Subsurface grain size data of different soil types were obtained from the literature. Based on the porosity values (from Eq. 1), the soil texture classification was identified through the United States Department of Agriculture (USDA) textural classification (Maidment 1993) and Geotechdata.info (2013). Medium particle diameter ( $d_{50}$ ) values were obtained from the United States Environmental Protection Agency (US EPA) Geotechnical Particle Size and Soil Classification Table (US EPA).

## Calculation of Hydraulic Conductivity and Infiltration Rate

The hydraulic conductivity was calculated from the equation used by Niwas and Celik (2012) whereas, for infiltration rate ( $I$ ), the Green-Ampt infiltration model using Darcy's law was selected, which is given as (Green and Ampt 1911):

$$I = \frac{dF}{dt} = K \left[ 1 + \frac{M\phi}{F} \right] \quad \dots(4)$$

where  $M$  is the water content in the soil layer and  $F$  is the total infiltrated volume between the surface of the soil and the wetting front, which can be calculated as:

$$F = M \times D \quad \dots(5)$$

where  $D$  is cumulative infiltration depth.  $\phi$  is the capillary pressure at the wetting front, which can be calculated by the equation (Morel-Seytoux et al. 1996):

$$\phi = \frac{0.046\beta + 2.07\beta^2 + 19.5\beta^3}{(1 + 4.7\beta + 16\beta^2)\alpha} \quad \dots(6)$$

where  $\alpha$  and  $\beta$  are van Genuchten-Mualem parameters (Van Genuchten 1980). The van Genuchten-Mualem parameters  $\alpha$  and  $\beta$  are needed to calculate the capillary pressure at the wetting front ( $\phi$ ), which were obtained from previous studies (Bohne et al. 1989, Chen et al. 2015).

Table 1: Pore water resistivity values for different ranges of bulk resistivity values for this study.

Bulk resistivity ( $\rho$ ) ( $\Omega\text{m}$ )	Pore water resistivity ( $\rho_w$ ) ( $\Omega\text{m}$ )
0.5-5	0.49
5-20	4.3
20-100	11.1
100-200	14.9
200-500	20.6
>500	77



## Regression Model and Validation

Linear regression was used to obtain the empirical relationships between bulk resistivity and pore water resistivity, bulk resistivity and porosity, and porosity and grain size. The borehole data was used to validate the TEM and ERT results. Infiltration rate (I) was validated using previous studies' results in the same study area (Shaari et al. 2016). They used the double ring method (up to 60 cm depth) to observe infiltration capacity at seven places in the Kota Bharu District, where sites numbers 13 and 11 of this study were located.

## Comparison of TEM and ERT Outputs

Direct comparison of the resistivity values from TEM and ERT is not possible because of their different mechanism for measuring the resistivity values. TEM produces eddy currents while the ERT produces direct currents (Firdaus 2018). However, a comparison of output patterns of TEM and ERT is possibly used in this study.

## RESULTS AND DISCUSSION

### Results of TEM and ERT Inversion Models

For this study, 20 m depth was selected due to the formation of clogging layers since the infiltration depth during flooding is low. For TEM, out of 13 places, the upper layer resistivity values of 11 locations ranged from 24  $\Omega\text{m}$  to 80  $\Omega\text{m}$ , which indicates that the upper layers were mostly fine soil, such as silt and clay with available water as the absorption water (Saarenketo 1998). Whereas, at the other two sites of TEM, identification of the upper layers were as clayey soil (160  $\Omega\text{m}$ ) and clayey sand (460  $\Omega\text{m}$ ) (Eluwole et al. 2018). For ERT, the upper layers of 6 locations were mostly a mixture of sand and clay. While at the rest of the three locations, silt and clay content were dominating. Overall, the average resistivity values of the upper layers ranged from 98  $\Omega\text{m}$  to 1421  $\Omega\text{m}$ , which indicates the presence of loamy soil (Eluwole et al. 2018). The overall results showed that the prediction of the output of both TEM and ERT was sand, silt, and clay content in the upper layer of soil.

### Porosity ( $\emptyset$ )

Results of the hydrometer analysis indicated that an average of 28% sand, 52% silt, and 20% clay were present at 20 cm depth, with approximately 6% of organic matter at all the locations. Based on these compositions, the study area is characterized by silty loam soil (Vaezi et al. 2016). The average porosities of the top layers (0 to 5m depth) were 0.24 (TEM) and 0.25 (ERT), which indicates the presence of silty sands (Das 2013). It shows closer prediction by both the techniques. Also, the variation in porosity

shows a mixture of clay and fine sand (Geotechdata.info 2013).

### Intrinsic Permeability (k) and Hydraulic Conductivity (K)

The results of soil texture classification, ranges of porosity, and medium particle diameter ( $d_{50}$ ) obtained from the literature are shown in Table 2.

The intrinsic permeability values ranged between  $10^{-10}$  to  $10^{-11}$   $\text{m}^2$ . It indicates that the soil in the study area is semi-permeable (Bear 1972), and it is dominant in silt and clay content at all the sites. As mentioned above, the study area is characterized by silty loam soil, which contains 70% silt and clay and 20% sand. It shows the distribution of small grain size and slow permeability in the silty loam soil (Shepherd 1989). TEM and ERT predicted accurate permeability values at all the sites except site number 13 in ERT. The top layer at site 13 is showing high resistivity values, which predict high porosity and hence high permeability ( $8.54 \times 10^{-11}$   $\text{m}^2$ ).

The hydraulic conductivity ( $K$ ) values ranged from  $10^{-4}$  to  $10^{-8}$   $\text{m}\cdot\text{s}^{-1}$ , which represents fine sand, silt, loess, and loam (Bear 1972, Freeze & Cherry 1979). The  $K$  values for TEM and ERT up to 5m depth were ranged from  $0.12 \times 10^{-5}$   $\text{m/s}$  to  $8.98 \times 10^{-5}$   $\text{m/s}$  and  $0.36 \times 10^{-5}$   $\text{m/s}$  to  $8.04 \times 10^{-5}$   $\text{m/s}$  respectively. The average  $K$  values up to 20 m depth for TEM and ERT were estimated as  $3.48 \times 10^{-5}$   $\text{m/s}$  and  $5.16 \times 10^{-5}$   $\text{m/s}$  respectively. These values showed the dominancy of silt and clay in subsurface soil, which makes it less permeable. These results conformed with the intrinsic permeability. Here also,  $K$  values at site 13 were high, which showed high sand content as compared to other sites.

### Infiltration Rate (I)

The infiltration rate values predicted by TEM and ERT varied from 10-4 to 10-6  $\text{m/s}$  in all the layers. If the conversion of these infiltration values is into inch per hour, then all the values lay under 20 inches/h except at site 13, which showed the presence of sandy loam to clay content in subsurface soil (Brouwer et al. 1988). The average infiltration rate predicted by the TEM showed clayey soil, while ERT predicted clay loam up to 20 m depth. At site 13, the infiltration rate was predicted by TEM showed clayey soil whereas, ERT showed a mixture of sand and clay loam. The higher infiltration rate predicted by the ERT at this site varied from 5m to 15m depth and 0 to 10 m distance. Other parts of this site were represented by the clay loam.

### Regression Models

The content of fines in soil has a proportional influence on its bulk resistivity. It means that soil with a relatively higher

Table 2: Identified soil texture classification based on porosity and identified medium grain size based on soil texture classification for this study. van Genuchten-Mualem parameters  $\alpha$  and  $\beta$  to calculate the capillary pressure at the wetting front ( $\phi$ ) for this study.

Texture classification	Porosity range		Medium grain size ( $d_{50}$ ) (mm)	$\alpha$	$\beta$
	Minimum	Maximum			
Sand	0.233	0.268	0.29	14.5	0.626
well graded sand	0.215	0.426	0.36	3.63	0.669
sandy gravel	0.21	0.32	0.22	3.63	0.669
Sandy loam	0.447		0.15	4.4	0.137
Sandy clay loam	0.398	0.400	0.14	5.9	0.324
Loamy sand	0.435	0.444	0.41	5.35	0.249
Loam	0.285	0.470	0.027	5.37	0.118
Silty sand	0.21	0.49	0.18	0.44	0.242
Silt loam	0.494	0.562	0.021	0.379	0.165
Silty or sandy clay	0.201	0.607	0.0067	0.095	0.153
silty/clayey fine sand	0.540	0.549	0.0147	1.5	0.588
Silt	0.515	0.526	0.0038	0.379	0.165
Silty clay	0.333	0.635	0.0024	0.479	0.152
Organic Silty clay	0.575	0.579	0.0024	0.479	0.152
Clayey sandy gravel	0.178	0.187	0.215	2.76	0.539
Clayey sand	0.15	0.37	0.14	2.205	0.588
Clay	0.472	0.475	0.0027	0.479	0.152

content of fines will have a higher bulk resistivity (Fig. 3b).

The Association of high values of porosity was with soils having a small amount of fines content. High porosity indicated the dominance of larger sand grains (Fig. 3c and 3d) (Li & Sherman 2015). Variations of porosity with grain size for both TEM and ERT are shown in Fig. 3 (e and f), where the porosity tends to decrease for soils with increasing grain size and then increases as the grain size decreases. The decline in the porosity values could result from an increment in the number of clay particles, which gradually filled the void spaces (Cameron & Buchan 2017) and separated the relatively bigger sand particles, thus, becoming the load-bearing unit of the soil.

### Validation of TEM and ERT Models

From the available well log data, two well logs (named BH 1 and BH 2) were found near the two sites and selected for comparison. The exact locations of BH 1 (6 m deep) were at site 13, whereas BH 2 (17 m deep) was sited 1.7 km from site number 11. The comparison of resistivity values from TEM and ERT with well-log data was based on the resistivity chart proposed by Palacky (1988).

In borehole BH1, the top layer of 1.2 m is made up of soft clay with some sand sediments. Below 1.2 m depth, sand

sediments increase in size with slightly clayey sediments to a depth of 4.2 m. Soft clay is again encountered at a depth between 4.2 m and 6.0 m, where the drilling terminated. At this site, from the TEM measurements, the bulk resistivity values were 30.7  $\Omega\text{m}$  (0 to 5 m depth), 30.7  $\Omega\text{m}$  (5 to 10 m depth), 23.8  $\Omega\text{m}$  (10 to 15 m depth), and 12.2  $\Omega\text{m}$  (15 to 20 m depth). The geological interpretation of these low resistivity values indicated the presence of clayey soil. At the same place and the same depth, the bulk resistivity values from ERT measurements were 82.9  $\Omega\text{m}$ , 38.3  $\Omega\text{m}$ , 56.8  $\Omega\text{m}$ , and 68.7  $\Omega\text{m}$  (Fig. 4).

In borehole log BH2, the first lithologic unit of this layer encountered at the depth of 1.8 m is clay sediment. This sediment (considered the second layer) extends to about 6 m in depth and is made of clay with some fine and medium-grained sand. The third layer (4.6 m deep) is of clay with some fine-grained sand, while the fourth layer (0.9 m deep) is of fine-grained sand with some clay. The fifth layer is encountered at depth of 1.3 m deep is of medium-grained sand with some clayey sediments. The last geological material encountered at depth of 2.2 m is clayey sediments. From the TEM survey, the bulk resistivity values for four layers were 23.5  $\Omega\text{m}$ , 23.6  $\Omega\text{m}$ , 41.9  $\Omega\text{m}$ , and 41.9  $\Omega\text{m}$  respectively, which indicated the clayey soil. Whereas from the ERT survey, the bulk resistivity values

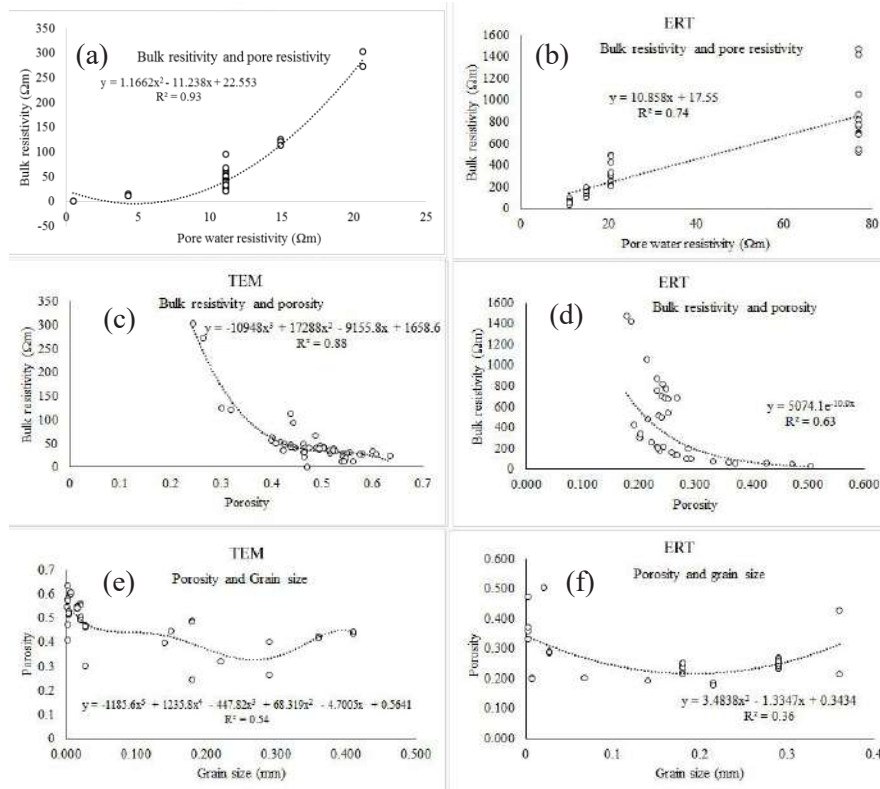


Fig. 3: Regression models (a) for bulk resistivity and pore water resistivity for TEM (b) for bulk resistivity and pore water resistivity for ERT (c) bulk resistivity and porosity for TEM (d) bulk resistivity and porosity for ERT (e) porosity and grain size for TEM (f) porosity and grain size for ERT.

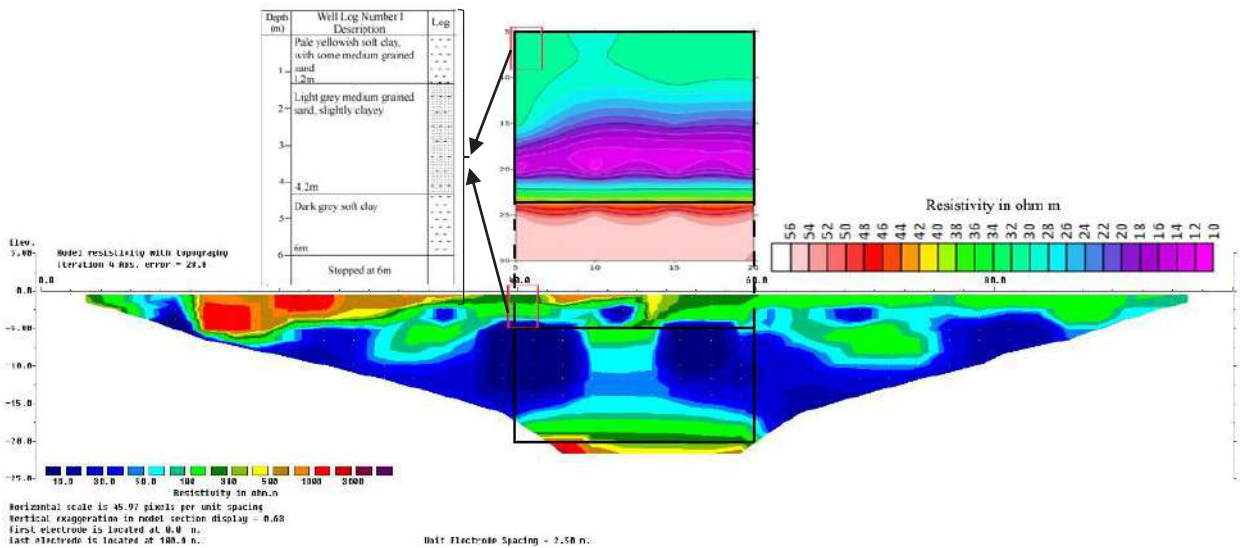


Fig. 4: Validation of TEM and ERT outputs with borehole data at site number 13.

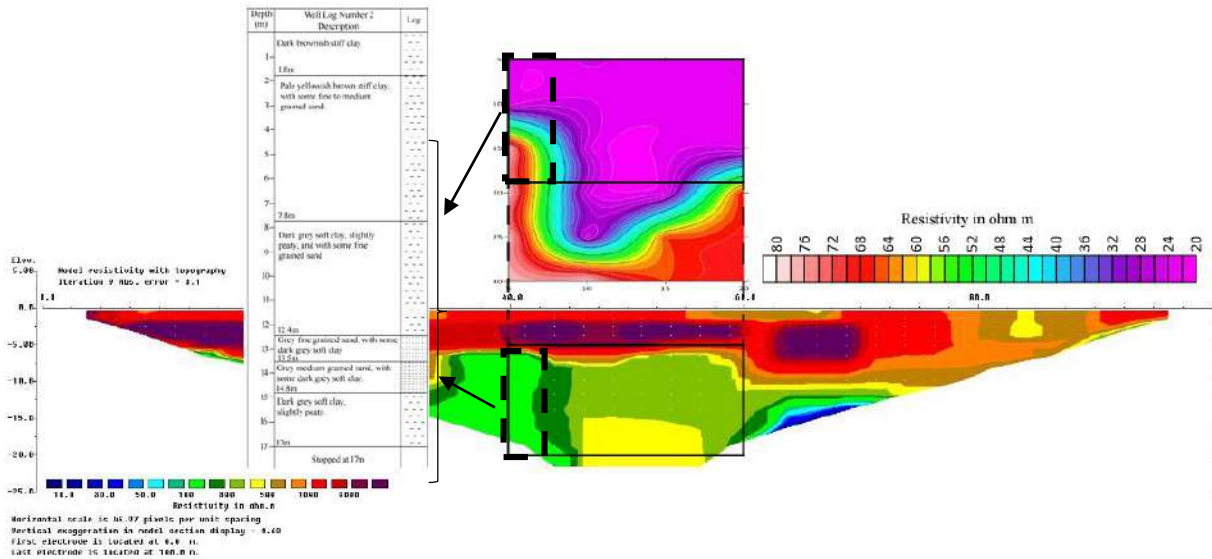


Fig. 5: Validation of TEM and ERT outputs with borehole data at site number 11.

were 1881.3  $\Omega\text{m}$ , 1503.9  $\Omega\text{m}$ , 1110.1  $\Omega\text{m}$ , and 1110.1  $\Omega\text{m}$  respectively.

These layers show the medium-grained sand at the top while fine-grained sand is below 5m depth. The borehole log data shows a mixture of fine and medium-grained sand with clay content in almost all layers (Fig. 5).

The observed infiltration capacity varies from 13.20  $\text{mm}\cdot\text{h}^{-1}$  to 206.3  $\text{mm}\cdot\text{h}^{-1}$ . For the upper layer, the estimated I at sites 11 and 13 for TEM were 15.09  $\text{mm}\cdot\text{h}^{-1}$  and 61.83  $\text{mm}\cdot\text{h}^{-1}$  respectively, while for ERT, the estimated I were 12.93  $\text{mm}\cdot\text{h}^{-1}$  and 253.95  $\text{mm}\cdot\text{h}^{-1}$  for sites 11 and 13 respectively. It was observed that the estimated I for TEM and ERT at both sites lies within the range of the observed infiltration capacity (Shaari et al. 2016). It should be noted here that sites number 11 and 13 are not exactly at the same place as the observed infiltration rate. Therefore, the range of the infiltration rate was considered for the validation. Hence, it can be concluded that both the techniques overall worked well in the estimation of the hydrological parameters. Also, because of the different types of currents used in TEM and ERT, the estimations were not exactly matched but have some range of the hydrological parameters.

## CONCLUSIONS

The results showed that, for TEM, the bulk resistivity was less than 80  $\Omega\text{m}$ , while for the ERT it was 1421  $\Omega\text{m}$ . This range was predicted by the mixture of sand, silt, and clay content in which silt and clay were dominating whereas the

average prediction was clayey soil for TEM and loamy soil for ERT. The porosity range by both the techniques showed closer estimation with in situ soil sample, which showed the presence of silty loam soil. The slow permeability and hydraulic conductivity range were observed by both the techniques, which also represented silty loam soil in the study area. The overall infiltration rate was less than 20 inches/h, which predicted the presence of fine-grained soil in the study area. The differences in the estimated infiltration rates at different depths reflect the differences in the recharge and precipitation.

The generated empirical equations serve as predictive tools from which bulk resistivity values could be obtained from the parameters such as pore water resistivity, porosity, and grain size measurements with good correlations obtained between these parameters. The relationships between bulk resistivity and pore water resistivity and bulk resistivity and porosity were found strong for both TEM and ERT based on the coefficient of determination. Also, validation results were in the range of the previous study, and the borehole data confirmed the presence of fine to medium-grained soil in the study area. The overall conclusion is that both geo-electrical methods worked well and have different capacities in the estimation of the hydrological parameter within the study area.

## ACKNOWLEDGEMENTS

We gratefully acknowledge the Malaysian Meteorological Department, Department of Irrigation and Drainage, Malaysia, School of Physics, School of Industrial Technology,



School of Civil Engineering of Universiti Sains Malaysia, and Department of Geoscience, Universiti Teknologi PETRONAS for providing the required research facilities, University fellowship, and data for this work. We would also like to acknowledge the University of Malaya for providing financial support through the grant GPF017B-2018 to carry out this work. Furthermore, we are also many thankful to Universiti Malaysia Kelantan for the financial support to publish this work.

## REFERENCES

- Afshar, A., Abedi, M., Norouzi, G.H. and Riahi, M.A. 2015. Geophysical investigation of underground water content zones using electrical resistivity tomography and ground-penetrating radar: A case study in Hesarak-Karaj, Iran. *Eng. Geol.*, 196: 183-193.
- Al-Garni, M.A. and El-Kalioubi, H.M. 2011. Delineation of saline groundwater and seawater intrusion zones using transient electromagnetic (TEM) method, Wadi Thuwal area, Saudi Arabia. *Arab. J. Geosci.*, 4(3-4): 655-668.
- Anees, M.T., Abdullah, K., Nawawi, M., Ab Rahman, N.N.N., Piah, A.R.M., Syakir, M., Omar, A.M. and Hossain, K. 2017. Applications of remote sensing, hydrology, and geophysics for flood analysis. *Indian J. Sci. Technol.*, 10(17): 450.
- Archie, G.E. 1942. The electrical resistivity log is an aid in determining some reservoir characteristics. *Trans. AIME*, 146(01): 54-62.
- Bear, J. 2013. *Dynamics of Fluids in Porous Media*. Courier Corporation.
- Bohne, K., Nitsche, C. and Leij, F. 1989. Requirements and use of indirect methods for estimating the hydraulic functions of unsaturated soils. Paper presented in the Proceedings of the International Workshop on Indirect Methods for Estimating the Hydraulic Properties of Unsaturated Soils, eds. MT van Genuchten, FJ Leij and L.J. Lund.
- Bouyoucos, G.J. 1962. Hydrometer method improved for making particle size analyses of soils. *Agro. J.*, 54(5): 464-465.
- Brouwer, C., Prins, K., Kay, M. and Heibloem, M. 1988. *Irrigation water management: Irrigation methods*. Training Manual, p. 9.
- Brunet, P., Clément, R. and Bouvier, C. 2010. Monitoring soil water content and deficit using Electrical Resistivity Tomography (ERT): A case study in the Cevennes area, France. *J. Hydrol.*, 380(1): 146-153.
- Cameron, K.C. and Buchan, G.D. 2017. Porosity: Pore Size Distribution. In Chesworth, W. (ed.), *Encyclopedia of Soil Science*, CRC Press, London, pp. 1782-1785.
- Chen, L., Xiang, L., Young, M.H., Yin, J., Yu, Z. and Genuchten, M.T. 2015. Optimal parameters for the Green-Ampt infiltration model under rainfall conditions. *J. Hydrol. Hydromech.*, 63(2): 93-101.
- Chen, W., Huang, C., Chang, M., Chang, P. and Lu, H. 2013. The impact of floods on infiltration rates in a disconnected stream. *Water Resour. Res.*, 49(12): 7887-7899.
- Choo, H., Song, J., Lee, W. and Lee, C. 2016. Effects of clay fraction and pore water conductivity on electrical conductivity of sand-kaolinite mixed soils. *J. Petrol. Sci. Eng.*, 147: 735-745.
- Chou, T. K., Chouteau, M. and Dubé, J. S. 2016. Estimation of saturated hydraulic conductivity during infiltration test with the aid of ERT and level-set method. *Vadose Zone Journal*, 15(7):1-19.
- Chrétien, M., Lataste, J., Fabre, R. and Denis, A. 2014. Electrical resistivity tomography to understand clay behavior during seasonal water content variations. *Eng. Geol.*, 169: 112-123.
- Crosbie, R.S., Taylor, A.R., Davis, A.C., Lamontagne, S. and Munday, T. 2014. Evaluation of infiltration from losing-disconnected rivers using a geophysical characterization of the riverbed and a simplified infiltration model. *J. Hydrol.*, 508: 102-113.
- Cui, Y.F., Zhou, X.J. and Guo, C.X. 2017. Experimental study on the moving characteristics of fine grains in wide grading unconsolidated soil under heavy rainfall. *J. Mount. Sci.*, 14(3): 417-431.
- Danielsen, J.E., Auker, E., Jørgensen, F., Søndergaard, V. and Sørensen, K.I. 2003. The application of the transient electromagnetic method in hydrogeophysical surveys. *J. Appl. Geophys.*, 53(4): 181-198.
- Das, B.M. 2013. *Advanced Soil Mechanics*. Fourth edition. CRC Press, London.
- Dumont, G., Pilawski, T., Dzaomuhlo-Lenieregue, P., Hiligsmann, S., Delvigne, F., Thonart, P., Robert, T., Nguyen, F. and Hermans, T. 2016. Gravimetric water distribution assessment from geoelectrical methods (ERT and EMI) in the municipal solid waste landfill. *Waste Manag.*, 55: 129-140.
- Eluwole, A.B., Olorunfemi, M.O. and Ademilua, O.L. 2018. Soil horizon mapping and textural classification using micro soil electrical resistivity measurements: A case study from Ado-Ekiti, southwestern Nigeria. *Arab. J. Geosci.*, 11(315): 1-11.
- Fatehnia, M., Paran, S., Kish, S. and Tawfiq, K. 2016. Automating double-ring infiltrometer with an Arduino microcontroller. *Geoderma*, 262: 133-139.
- Firdaus, M.A.R. 2018. *Site Suitability Mapping for Riverbank Filtration Using Spatial Analysis of Surface And Subsurface Characteristic*. Ph.D., School of Civil Engineering, Universiti Sains Malaysia, Pulau Penang, Malaysia.
- Flores, C., Romo, J.M. and Vega, M. 2013. On the estimation of the maximum depth of investigation of transient electromagnetic soundings: the case of the Vizcaino transect, Mexico. *Geof. Int.*, 52(2): 159-172.
- Freeze, A.R., and Cherry, J.A. 1979. *Groundwater*. Prentice-Hall International, INC., Englewood Cliffs, New Jersey.
- Ghose, R. and Slob, E. 2006. Quantitative integration of seismic and GPR reflections to derive unique estimates for water saturation and porosity in the subsoil. *Geophys. Res. Lett.*, 33(5): 1-4.
- Green, W.H. and Ampt, G. 1911. Studies on soil physics. *J. Agric. Sci.*, 4(1): 1-24.
- Heng, G.S., Hoe, T.G. and Hassan, W.F.W. 2006. Gold mineralization and zonation in the State of Kelantan. *Geol.Soc. Malaysia Bull.*, 52: 129-135.
- Kozeny, J. 1953. *Hydraulics*. Springer-Verlag, Wien.
- Kumar, D., Mondal, S., Nandan, M., Harini, P., Sekhar, B.S. and Sen, M.K. 2016. Two-dimensional electrical resistivity tomography (ERT) and time-domain-induced polarization (TDIP) study in hard rock for groundwater investigation: a case study at Choutuppal Telangana, India. *Arab. J. Geosci.*, 9(5): 355.
- Li, B. and Sherman, D.J. 2015. Aerodynamics and morphodynamics of sand fences: A review. *Aeol. Res.*, 17: 33-48.
- Maidment, D. R. 1993. *Handbook of Hydrology*. Volume 1. McGraw-Hill, New York.
- Morbideilli, R., Saltalippi, C., Flammini, A., Cifrodelli, M., Corradini, C. and Govindaraju, R.S. 2015. Infiltration on sloping surfaces: Laboratory experimental evidence and implications for infiltration modeling. *J. Hydrol.*, 523: 79-85.
- Morel-Seytoux, H.J., Meyer, P.D., Nachabe, M., Tourna, J., Genuchten, M.V. and Lenhard, R.J. 1996. Parameter equivalence for the Brooks-Corey and van Genuchten soil characteristics: Preserving the effective capillary drive. *Water Resour. Res.*, 32(5): 1251-1258. <https://doi.org/10.1029/96WR00069>
- Niwas, S. and Celik, M. 2012. Equation estimation of porosity and hydraulic conductivity of Ruhrtal aquifer in Germany using near-surface geophysics. *J. Appl. Geophys.*, 84: 77-85.
- Noell, U., Wießner, C., Ganz, C. and Westhoff, M. 2011. Direct observations of surface water-groundwater interaction using electrical resistivity tomography. In *Symposium H01 on Conceptual and Modelling Studies of Integrated Groundwater, Surface Water, and Ecological Systems, Held During the 25th General Assembly of the International Union of Geodesy and Geophysics, IUGG 93*, pp. 42-47.



- Palacky, G. 1988. Resistivity characteristics of geologic targets. *Soc. Explor. Geophys.*, 1: 53-129.
- Perrone, A., Lapenna, V. and Piscitelli, S. 2014. Electrical resistivity tomography technique for landslide investigation: a review. *Earth-Sci. Rev.*, 135: 65-82.
- Saarenketo, T. 1998. Electrical properties of water in clay and silty soils. *J. Appl. Geophys.*, 40(1-3): 73-88.
- Shaari, N.A., Ali, K.M.M. and Mukhtar, A. 2016. Estimation of infiltration rate in major soil types of Kota Bharu, Kelantan, Malaysia. *Bull. Geol. Soc. Malay.*, 62: 7-11.
- Shepherd, R.G. 1989. Correlations of permeability and grain size. *Groundwater*, 27(5): 633-638.
- Todd, D.K. and Mays, L. 1980. *Groundwater Hydrogeology*. John Wiley and Sons Inc., New York.
- Turesson, A. 2006. Water content and porosity are estimated from ground-penetrating radar and resistivity. *J. Appl. Geophys.*, 58(2): 99-111.
- Vaezi, A.R., Hasanzadeh, H. and Cerdà, A. 2016. Developing an erodibility triangle for soil textures in semi-arid regions, NW Iran. *Catena*, 142: 221-232.
- Van Genuchten, M.T. 1980. A closed-form equation for predicting the hydraulic conductivity of unsaturated soils. *Soil Sci. Soc. Am. J.*, 44(5): 892-898.



# Variation in the Alcohol Components of *Coffea arabica* L. Wastewater Distillate Fermented Under Different Conditions

E. Morales†, S. Chávez, L. García, A. C. Caetano, J. Veneros, M. Á. Barrena and M. Oliva

Instituto de Investigación para el Desarrollo Sustentable de Ceja de Selva (INDES-CES), Universidad Nacional Toribio Rodríguez de Mendoza (UNTRM), Chachapoyas 01001, Peru

†Corresponding author: E. Morales; eli.morales@untrm.edu.pe

Nat. Env. & Poll. Tech.  
Website: [www.neptjournal.com](http://www.neptjournal.com)

Received: 18-07-2021

Revised: 22-08-2021

Accepted: 03-10-2021

## Key Words:

*Coffea arabica*

Gas chromatography

Bio alcohols

Distillate

Ethanol

## ABSTRACT

Coffee is the second-most consumed beverage in the world, and its high demand is covered by countries such as Peru, where the waste generated in production causes environmental pollution. We sought to determine the concentration of alcohol components and other volatiles compounds present in the distillate, after fermenting wastewater from the first wash in the wet processing of *Coffea arabica* var. catimor under five conditions: C1 (pasteurized + 0.325 g sucrose + 8.000 g *S. cerevisiae*), C2 = (pasteurized + 8.000 g *S. cerevisiae*), C3 (0.325 g sucrose + 8.000 g *S. cerevisiae*), C4 = (8.000 g *S. cerevisiae*), and C5 = (natural state). The solid-phase microextraction technique was used to determine the composition of the distillates by gas chromatography (GC). 35 components were detected, 11 of them under all conditions. Ethanol was the most abundant element in all five fermentation conditions. Condition 1 shows the highest value at 97.29  $\mu\text{g}\cdot\text{mL}^{-1}$ , though all five concentrations can be considered high. This study shows that wastewater from the wet processing of coffee can have agro-industrial use as a value-added product. Postharvest Peruvian coffee is amenable to strategies aligned with the sustainable development goal of reducing food losses along production and supply chains.

## INTRODUCTION

Coffee is the second-most traded commodity in the world after oil (Giroto et al. 2018) and the second-most consumed beverage (Perrone et al. 2008). Peru is one of the main coffee-exporting countries, whose production is mainly driven by five regions, one being the Amazon region (Salas-López et al. 2020). Although coffee represents an important commercial asset at the international level (Acosta-Alba et al. 2020), its production has environmental impacts (Garde et al. 2017). The residues generated during fermentation in coffee processing plants are potential environmental problems and cause water pollution due to their high organic component and acidic nature (Woldesenbet & Chandravanshi 2016). When released directly into the environment, they are harmful to water bodies, flora, and aquatic fauna (Pérez-Sariñana et al. 2015).

The processing of coffee begins with the manual harvesting of ripe cherries (Rattan et al. 2015). Then the cherries can be processed by two methods, wet and dry (Gathuo et al. 1991). In the wet process, large volumes of high-strength wastewater are generated and they require treatment before disposal (Gathuo et al. 1991), in Peru there are no records of farms that perform the recycling process on these waters. The waste from this process contains large amounts of organic substrates that are suitable for bioconversion into value-added bioproducts (Zhang et al. 2019).

The coffee cherries are pulped and fermented between 12 and 18 h and then are usually dried (Davydenko et al. 2020, Sanz-Uribe et al. 2017). Waste from wet coffee processing, due to its high sugar content, can be used in the production of bioethanol (Zhang & Ordway 2003), which provides an alternative energy source from waste biomass and solves the problem of its elimination in the environment, as well as the problems it can cause to human health (Woldesenbet et al. 2016). However, the fermentation parameters are not precisely known. Besides the microorganisms present in the residue, it is also possible to use *Saccharomyces cerevisiae* inoculum (Einfalt et al. 2020). *S. cerevisiae* is capable of metabolizing C6 sugars (glucose, fructose, mannose, and galactose) (Kim et al. 2016). This can happen due to the presence of oxygen, which shows favorable conditions for yeast growth, and during anaerobiosis fermentation (utilization of sugar for energy production) occurs (Zhang & Ordway 2003). Approximately 95% of the industrial ethanol in the world is obtained through the fermentation of sugars, which must be separated as efficiently as possible from water-ethanol, but this is difficult due to its chemical affinities (Acosta & Zumalacárregui 2016).

Several microorganisms take part in the fermentation of coffee, and it is expected that these microorganisms participate in the fermentation of the must; however, these microorganisms could affect the quality of the distillates.

Pasteurization can be an alternative to eliminate these microorganisms and use only inoculum (Chagua & Malpartida 2020).

Between 2011 and 2015, up to 389,733 ha of coffee were replaced in Peru by the catimor variety, as it is resistant to coffee leaf rust (*Hemileia vastatrix*) (Díaz & Carmen 2017). Therefore, the waste is useful for the food, pharmaceutical, and cosmetic industries (Ferrell & Cockerill 2012), coffee wastewater contains reducing sugars that could become substrates for fermentation (De Bruyn et al. 2017).

The wet coffee process requires large amounts of water; some authors report a range between 1 and 10 m<sup>3</sup> of water per ton of coffee cherries and up to 15 m<sup>3</sup> of water per ton of clean beans (Hans-Dieter et al. 2009). Considering that Peru produced 228,000 tons of coffee in 2020 (Sanz-Uribe et al. 2017), 34,200,000 m<sup>3</sup> of wastewater was underutilized. Therefore, this work determined the abundance of alcohol components present in the distillate obtained after fermenting wastewater from the first washing in the wet processing of *C. arabica* under natural conditions, after pasteurization, and after being subjected to the activity of *S. cerevisiae* to determine their potential agro-industrial use as value-added products. In this way, coffee production is aligned with the sustainable development goals, namely, goal 12.3, which is to reduce per capita food waste by half and reduce food losses along with production and supply (Ferrell & Cockerill 2012).

## MATERIALS AND METHODS

### Obtaining Coffee Wastewater

*C. arabica* var. catimor was collected in May 2019 at the experimental station of the Universidad Nacional Toribio Rodríguez de Mendoza, district of Huambo, at coordinates 6° 20' 10" S, 77° 27' 58" W and an altitude of 1630 masl. The coffee wastewater was collected from the first wash of the wet process with 7 °Brix and transferred to the Agro-industrial Engineering laboratory in 5-liter containers.

### Execution of the Experiment for Fermentation, Distillation and net Yield

Five conditions were selected after the standardization procedure. For sucrose, pre-tests were carried out at 0.300 kg.L<sup>-1</sup>; 0.325 kg.L<sup>-1</sup>; 0.350 kg.L<sup>-1</sup>; 0.375 kg.L<sup>-1</sup> and 0.400 kg.L<sup>-1</sup>. And for *S. cerevisiae*, pre-tests were performed at 8 g.L<sup>-1</sup> and 9 g.L<sup>-1</sup>. A 2-liter fermenter was set up for each treatment. Then, according to treatment Table 1, determined the best condition was pasteurized, and sugar was added to a continuous stream (0.325 g; samples C1 and C3).

For the activation of *S. cerevisiae*, water was heated in an electric laboratory cooker until the temperature reached

80°C. Then the mixture was cooled to 40°C, at which time 8 g.L<sup>-1</sup> *S. cerevisiae* was added. Commercial brown sugar was also added. All treatments were fermented at room temperature (16-19°C) for 7 days, and the fermentation was stopped by refrigeration until further distillation (Wang et al. 2020). Then, 180 mL of each condition (C1, C2, C3, C4, and C5) was added to the distillation system. The distillation was cut off when the first 25 ml was obtained.

### Obtaining the Distillates

The distillates were made in a laboratory distiller with a capacity of 1 L. We kept the temperature of the balloon around 75°C without letting it exceed 80°C. The distillates were packed in amber glass flasks until further analysis.

### Volatile Compounds Analysis by SPME-GC-MS and net Yield Obtaining

The analyses of volatile compounds of the alcoholic distillates were performed using the solid-phase microextraction technique (SPME) and were analyzed by gas chromatography coupled to mass spectrometry (GC-MS), based on the method developed by Wang (2020) with some modifications. The distillate was transferred to a 20 mL vial with 1-butanol solution (1-butanol, 5 µL of 1.25 µg.µL<sup>-1</sup> water) as the internal standard. The amounts were chosen as representative of a high concentration of volatile substances. The vial was hermetically sealed and taken to a dry bath at 55°C for 15 min. After the equilibration period, the divinylbenzene/carboxen/polydimethylsiloxane fiber was exposed to the headspace of the vial for 30 min. After that time, the fiber was placed in the injection port at 250°C in split mode (1:1) and exposed for 6 min for the desorption of the compounds.

The presence and relative abundance of alcohol components present in the distillates were determined with a gas chromatograph (Agilent Technologies 7890B GC system) coupled to a mass detector (Agilent Technologies model 5977B MSD) equipped with a DB-5 MS IU capillary column (60 m length × 0.25 µm inner diameter × 1 µm film thickness). The total run time was 52 min. The oven program was as

Table 1: Characteristics of the different conditions of fermentation in *C. arabica* var. catimor wastewater distillate.

Fermentation condition	Pasteurized	Added sucrose [kg.L <sup>-1</sup> ]	<i>S. cerevisiae</i> (g.L <sup>-1</sup> )
C1	YES	0.325	8
C2	YES	NO	8
C3	NO	0.325	8
C4	NO	NO	8
C5	NO	NO	NO

follows: initial temperature of 40°C maintained for 2 min, rising by 3°C/min to 50°C and maintained for 1 min, rising to 110°C at a rate of 5°C/min and maintained for 1 min, rising to 200°C at 6°C/min, and rising to 250°C at 8°C/min, where it remained for approximately 11.5 min. The mass spectrometer recorded the total ionic current (70 eV) in a mass range of  $m/z$  30 to 550 (scan mode). The compounds were identified by comparison with the NIST library and the criteria for the identification of each compound required a mass spectrum matching score of  $\geq 70$ . For every sample, extraction, injection, detection, and identification were performed in quintuplicate on all samples. Of these, the execution in duplicate was without internal standard, and in triplicate with internal standard (with 1-butanol). A threshold of at least two detections was established to express the results of the presence and absence of each identified compound in the samples. Semi-quantitative concentrations of each compound were obtained and were multiplied by a constant for better visualization of the data. This is because the aliquots of the analyzed samples were quite small compared to the 20 mL vial used. These quantities were chosen to take into account that this sample constituted a distillate and, therefore, it was estimated that it contained a high concentration of volatile substances. However, it is important to note that this did not prevent the detection of the different compounds and the estimation of their relative concentration. Finally, after quantification of the compounds, the net yield for the condition was obtained for each mL of distillate. Only the values for the alcoholic components that were repeated in all conditions are shown.

## RESULTS

The GC analysis revealed the presence of 35 alcohol components in *C. arabica* var. catimor fermented under different conditions Table 2. We found 11 bioalcohol components under all conditions (ethanol; 1-propanol; 1-butanol, 2-methyl-; 1-butanol, 3-methyl-; hexanoic acid; 2-furan methanol, 5-ethenyltetrahydro- $\alpha,\alpha,5$ -trimethyl-, cis-; trans-linalool oxide (furanoid); linalool; phenylethyl alcohol; octanoic acid; benzaldehyde, 2,4-dimethyl-; and acetic acid, 2-phenylethyl ester). All are included in industrial use lists, and six of them have been cataloged for human consumption (Nguyen et al. 2021). Ethanol was the most abundant element. It was present in all five fermentation conditions, and condition 1 (unpasteurized + sucrose + 8 g *S. cerevisiae*) yielded the highest value, with 972.9  $\mu\text{g}\cdot\mu\text{L}^{-1}$  concentration. We also consider the ethanol values for the other conditions substantial (926.0  $\mu\text{g}\cdot\mu\text{L}^{-1}$  in C2 and 874.2  $\mu\text{g}\cdot\mu\text{L}^{-1}$  in C3). The 1-Dodecanol ranked second in conditions 1, 2, and 3, with values of 368.6, 362.4, and 271.8  $\mu\text{g}\cdot\mu\text{L}^{-1}$ , respectively, while in condition 4 its value decreased to 9.7  $\mu\text{g}\cdot\mu\text{L}^{-1}$ , and in condition 5 it disappeared.

The compound trans-Linalool oxide (furanoid) showed its highest concentration in condition 3.

## The Yield of Alcohol Produced in the Distillates

Fig. 1 compares the abundance of the main compound identified in the 5 conditions assayed, including ethanol. Of the 11 compounds identified in the distillates of the five conditions, ethanol was the most abundant, followed by 2-benzaldehyde, 2,4-dimethyl- in all cases. Conditions C1, C2, and C3 yielded distillates with higher ethanolic contents of 97.29, 92.6, and 87.42  $\mu\text{g}\cdot\text{mL}^{-1}$ , respectively. Conditions C4 and C5, without the addition of sucrose or yeast (fermented with native flora present in the collected wastewater), yielded distillates with lower ethanolic content (20.50 to 34.42  $\mu\text{g}\cdot\text{mL}^{-1}$ ). The content of the other compounds present was proportional in both groups Fig. 1.

## DISCUSSION

The 35 components in *C. arabica* var. catimor distillates found here correspond to quantitative GC measurements that have been performed frequently with a remarkable degree of reproducibility in agreement with Novotny (2003) and Lopes et al. (2020), and the search for the sustainable use of these components by adding value is an ideal transition to an economy of biological resources (Woldesenbet et al. 2016).

The alcohol components that were found in all the distillates of this study have important properties for industrial use (Brugnera et al. 2006). Their main use is agro-industrial because of the high amounts of ethanol (Xiao & Lu 2014). Other uses for its components are, for example, rocket fuel, the manufacture of plastics, agricultural pesticides, for medications to treat cancer patients (Nguyen et al. 2021), contact lenses, and textile cleaning (Wang et al. 2020). Some other potential uses are the manufacture of other chemical products, etching metals, solvent, and chemical laboratory analysis, fabric dyes, nylon production, and tanning of leathers (Sampaio et al. 2013). Another six components identified here have agro-industrial uses: 1-butanol, 2-methyl- (Kim et al. 2019); 1-butanol, 3-methyl- (Kim et al. 2019); linalool and benzaldehyde, 2,4-dimethyl- (Kim et al. 2019), especially in the production of alcoholic beverages, to improve the taste of their food products (Kim et al. 2016), as an aroma and essence of artificial fruits (Kim et al. 2016), and others.

Ethanol was the most abundant compound under all five conditions of this work. It is classified as one of the most important products of primary metabolism and one of the most produced in the world (Chin et al. 2011). It can reduce pollution from agricultural waste (Clarke & Bakker 2004). Work has been done to optimize these processes to achieve

Table 2: Semi-quantitative concentrations (mean  $\pm$  standard deviation) of alcohol components of the wastewater distillate of *Coffea arabica* L. fermented under five different conditions.

Name	CAS-Number	Retention Time	Conditions (mean $\times$ 10000) a				
			C1	C2	C3	C4	C5
Hydrazine **, ***	302-01-2	4.494	ND	ND	31.1 $\pm$ 2.4	ND	ND
Hydrazinecarboxamide ****	57-56-7	4.491	ND	38.3 $\pm$ 4.3	ND	ND	ND
Ethanol *, **, ***	64-17-5	5.349	972.9 $\pm$ 55.5	926.0 $\pm$ 27.4	874.2 $\pm$ 40.9	344.2 $\pm$ 14.2	299.0 $\pm$ 20.5
Acetic acid**	64-19-7	8.764	92.3 $\pm$ 9.7	114.3 $\pm$ 10.6	97.3 $\pm$ 7.0	42.5 $\pm$ 10.1	ND
Ethyl Acetate*,**	141-78-6	9.816	23.7 $\pm$ 1.7	19.8 $\pm$ 1.3	15.2 $\pm$ 0.7	ND	22.0 $\pm$ 3.4
1-Propanol, 2-methyl-*,**	78-83-1	10.415	19.1 $\pm$ 0.9	19.3 $\pm$ 1.6	17.7 $\pm$ 0.5	5.5 $\pm$ 2.0	6.2 $\pm$ 1.4
Acetoin*	513-86-0	13.9	ND	80.3 $\pm$ 15.1	72.6 $\pm$ 10.4	ND	ND
1-Butanol, 3-methyl-*,**	123-51-3	15.088	55.0 $\pm$ 2.7	49.4 $\pm$ 5.3	50.4 $\pm$ 3.1	31.2 $\pm$ 10.9	43.0 $\pm$ 6.7
1-Butanol, 2-methyl-*,**	137-32-6	15.285	ND	ND	ND	8.2 $\pm$ 3.0	11.6 $\pm$ 2.0
1-Cyclopentyl-2,2-dimethyl-1-propanol ***	337966-85-5	15.279	30.2 $\pm$ 4.0	ND	ND	ND	ND
Butanoic acid**	107-92-6	16.507	ND	ND	ND	6.4 $\pm$ 1.5	ND
Furfural**	98-01-1	19.544	ND	ND	ND	9.7 $\pm$ 3.2	9.0 $\pm$ 1.1
3-Furaldehyde	498-60-2	19.546	ND	ND	196.7 $\pm$ 7.9	ND	ND
Propanedioic acid, propyl	616-62-6	20.804	ND	14.1 $\pm$ 2.6	ND	ND	ND
Pentanoic acid*,**	109-52-4	20.805	14.2 $\pm$ 2.0	ND	10.4 $\pm$ 1.3	9.6 $\pm$ 3.5	9.6 $\pm$ 3.3
1-Hexanol	111-27-3	20.971	ND	ND	ND	ND	4.2 $\pm$ 0.6
CH3C(O)OCH(CH3)C(O)CH3**	4906-24-5	21.644	12.7 $\pm$ 1.3	ND	13.0 $\pm$ 1.4	ND	ND
1-Heptanol	543-49-7	22.366	ND	ND	ND	ND	4.0 $\pm$ 0.3
Hexanoic acid*,**	142-62-1	24.767	47.8 $\pm$ 7.1	47.6 $\pm$ 3.2	36.8 $\pm$ 3.8	17.0 $\pm$ 5.9	18.7 $\pm$ 5.5
Benzyl alcohol	100-51-6	27.678	ND	ND	9.3 $\pm$ 0.5	ND	ND
2-Furanmethanol, 5-ethenyltetrahydro-.alpha.,.alpha.,5-trimethyl-, cis-***	5989-33-3	29.025	89.5 $\pm$ 1.5	90.4 $\pm$ 1.7	96.4 $\pm$ 2.3	10.8 $\pm$ 2.0	13.0 $\pm$ 1.9
trans-Linalool oxide (furanoid)**	34995-77-2	29.513	65.0 $\pm$ 1.5	68.4 $\pm$ 2.3	69.1 $\pm$ 3.6	8.2 $\pm$ 1.8	9.5 $\pm$ 1.8
1,6-Octadien-3-ol, 3,7-dimethyl-, formate	115-99-1	29.648	ND	ND	26.2 $\pm$ 0.4	ND	ND
Linalool*,**	78-70-6	29.654	26.4 $\pm$ 1.5	25.1 $\pm$ 1.1	ND	ND	15.0 $\pm$ 0.4
Phenylethyl Alcohol**	60-12-8	30.384	48.5 $\pm$ 8.7	56.2 $\pm$ 4.7	57.3 $\pm$ 6.4	23.9 $\pm$ 5.3	ND
Octanoic acid**	124-07-2	31.168	42.2 $\pm$ 10.3	48.7 $\pm$ 7.8	27.4 $\pm$ 8.1	ND	ND
alpha.-Terpineol**	98-55-5	32.912	18.3 $\pm$ 2.1	ND	17.9 $\pm$ 0.6	ND	ND
Benzaldehyde, 2,4-dimethyl-*	15764-16-6	33.643	109.3 $\pm$ 14.7	104.7 $\pm$ 5.0	105.5 $\pm$ 9.3	17.9 $\pm$ 4.8	4.4 $\pm$ 0.7
Acetic acid, 2-phenylethyl ester**	103-45-7	34.268	18.5 $\pm$ 2.1	17.0 $\pm$ 1.0	13.1 $\pm$ 1.1	ND	18.7 $\pm$ 1.6
2-Buten-1-one, 1-(2,6,6-trimethyl-1,3-cyclohexadien-1-yl)-, (E)-*****	23726-93-4	37.562	14.9 $\pm$ 0.7	ND	9.0 $\pm$ 0.6	ND	ND
1-Dodecanol**	112-53-8	39.083	368.6 $\pm$ 35.7	362.4 $\pm$ 18.6	271.8 $\pm$ 15.7	ND	ND
2,4-Di-tert-butylphenol*****	96-76-4	39.843	82.3 $\pm$ 6.8	80.1 $\pm$ 6.9	71.0 $\pm$ 3.1	ND	ND

ND: Compound not determined, \*use in human consumption, \*\* industrial use, \*\*\* medicinal use, \*\*\*\* no use/unknown use. a Concentration relative ( $\mu\text{g. mL}^{-1}$ ) of the components was multiplied by 10000.



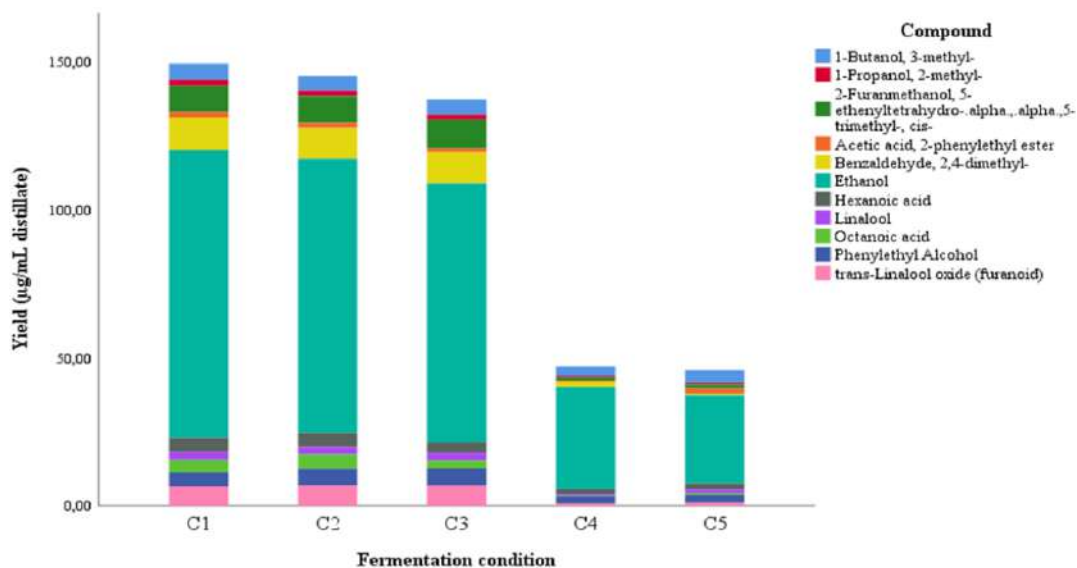


Fig. 1: The concentration of the 11 compounds present in the distillates obtained from fermented coffee wastewater under five conditions.

higher levels of sugar consumption and ethanol production due to effective exposure to the substrates (Ryan et al. 2004). Studies have shown when other residual coffee wastes, such as whole husks and ground coffee, have been used directly as substrates for the production of fermentative ethanol, final yields (g of ethanol/g of the substrate) of 0.008 and 0.007, respectively, have been achieved (Novotny 2003), 0.33 of coffee mucilage (Vidra & Németh 2018) and, this study reported 0.097 g.mL<sup>-1</sup> of wastewater. Despite the variation in its value between the different types of coffee waste, we think that the results reflect the presence of high ethanol values in this study.

The addition of sugar and *S. cerevisiae* to fermentation influences the ethanol yield (Roehr et al. 2001), as well as the concentration relative to the rest of the components that we measured. A lower amount of ethanol could be due to the consumption of sugar by other microorganisms that interfere with the fermentation process (Woldesenbet et al. 2016). In this sense, the initial concentration of sugars has positive effects on the fermentation, and the yield and productivity depend on the initial concentration of sugars (Phisalaphong et al. 2007). Here, the single application of 8,000 g of *S. cerevisiae* led to the greatest abundance of ethanol in the distillate (972.9 µg.µL<sup>-1</sup>). Coffee wastewater subjected to saccharification produced yields (based on sugar content) of ethanol of 15.3 g.L<sup>-1</sup> (Choi et al. 2012), 0.55 g.L<sup>-1</sup> (Bonilla-Hermosa & Schwan 2014), and 0.33 g ethanol/g sugar (Silva et al. 2010).

Thus, the present results support *S. cerevisiae* as the most common microorganism to produce ethanol due to its high consumption of sugars (Vučurović 2011). The results of the relative concentrations of the components are presented in Fig. 1.

The ethanol content and the presence of furfural compound in Condition 1 could have resulted from the application of *S. cerevisiae*. However, furfural is undesirable, because of the affectation of specific cell growth, and cell mass yield in ATP and ethanol, depending on its concentration in the fermentation medium (Palmqvist & Hahn-Hägerdal 2000). On the other hand, the presence of octanoic acid is associated with odors such as rancid and fatty, in this study, the lowest values of this compound (0.37-0.45 µg.mL<sup>-1</sup>) were evidenced for the C4 and C5 conditions. *S. cerevisiae* synthesizes a wide variety of alcohols during fermentation (Franca et al. 2008), and 1-propanol was found in all the assessed conditions.

Propanol, isobutane, and isoamyl alcohol are part of the so-called fusel oil and are formed by alcohols with more than two carbon atoms; they are formed by the fermentation of sugars. These compounds were also present in the distillates of this study. *S. cerevisiae* has a natural ability to adapt skillfully to inhibitory environments (Kim et al. 2020), and ethanol is the main byproduct of yeast fermentation, as its generation is notably associated with cell growth, viability, and metabolic activity (Mussatto et al. 2012).

In fermentation condition 1, the highest concentration of furfural was found, at 226.7 µg.µL<sup>-1</sup>. Other studies have detected butyric, propionic, and acetic acids, which represent a possibility for the use of other sources as substrates (de Melo Pereira et al. 2014).

Linalool can be produced by *S. cerevisiae* and *Pichia guilliermondii* in association with coffee (Ezeji et al. 2007). It was most abundant in condition C1, with a value of 26.4

$\mu\text{g}\cdot\mu\text{L}^{-1}$ . It has been identified as a fresh, citrus, and woody aroma in food products (Lee et al. 2009).

Acetic acid, was highest in condition C1, with a value of  $114.3 \mu\text{g}/\text{L}$ . 2-Buten-1-one, 1-(2,6,6-trimethyl-1,3-cyclohexadien-1-yl)-, (E)- was not detected under condition C4 or C5. 1-Dodecanol was most abundant under condition C1, with a value of  $368.6 \mu\text{g}/\mu\text{L}$ . Similarly, the compound 2,4-di-tert-butylphenol yielded the highest value of  $82.3 \mu\text{g}\cdot\mu\text{L}^{-1}$ , characteristic compounds of the distillates of coffee wastewater that are aromatic (Vázquez & Dacosta 2007). Acetic acid, present in conditions 1-4, is an unpleasant taste in coffee distillates and could damage the final quality of the distillates by giving them an onion flavor (Ezeji et al. 2007). However, we consider these values unimportant because they had less than  $92.3 \mu\text{g}\cdot\mu\text{L}^{-1}$ , and the condition C5 did not yield acetic acid.

## CONCLUSION

SPME and GC-MS allowed us to detect 35 alcohol components at different relative abundance values in five different distillates obtained from the wastewater fermentation of the first wash in the wet processing of *Coffea arabica* var. catimor. All distillates had ethanol as the most abundant alcohol, suggesting the potential agro-industrial use of Peruvian coffee as a postharvest value-added product.

## ACKNOWLEDGMENT

The authors acknowledge and appreciate the support of the Research Institute for Sustainable Development in Highland Forests (INDES-CES) of the National University Toribio Rodríguez de Mendoza de Amazonas (UNTRM). They also express thanks to the Engineer Exequiel Díaz Lozano, who contributed to the logistic.

## REFERENCES

Acosta-Alba, I., Boissy, J., Chia, E. and Andrieu, N. 2020. Integrating diversity of smallholder coffee cropping systems in environmental analysis. *Int. J. Life Cycle Assess.*, 25: 252-266.

Acosta, L. and Zumalacárregui, L. 2016. «Deshidratación de etanol empleando líquidos iónicos». *Univ. Ciencia y Tecnol.*, 20(80): 124-133.

Bonilla-Hermosa, V.A., Duarte, W.F and Schwan, R.F. 2014. Utilization of coffee by-products obtained from the semi-washed process for the production of value-added compounds. *Bioresour. Technol.*, 166: 142-150.

Brugnera, M.F., Santos, D.P. and Zanoni, M.V.B. 2006. Electrode modified with polyamino acid film for determination of hydrazine in the boiler water. *Ecl. Quim. São Paulo*, 31(4): 63-68.

De Bruyn, F., Zhang S.J., Pothakos, V., Torres, J., Lambot, C., Moroni, A.V., Callanan, M., Sybesma, W., Stefan Weckx, S. and De Vuyst, L. 2017. Exploring the impacts of postharvest processing on the microbiota and metabolite profiles during green coffee bean production. *Appl. Environ. Microbiol.*, 83(1): 1-16.

Chagua, R. and Malpartida, R.J. 2020. Time of pasteurization and its response to the chemical characteristics and antioxidant capacity of *Agave americana* L. *aguamiel. J. High Andean Res.*, 22(1): 45-57.

Chin, S.T., Eyres, G.T. and Marriott, P.J. 2011. Identification of potent odorants in wine and brewed coffee using gas chromatography-olfactometry and comprehensive two-dimensional gas chromatography. *J. Chromatogr. A*, 1218(42): 7487-7498.

Choi, I.S., Wi, S.G., Kim, S.B and Bae, H.J. 2012. Conversion of coffee residue waste into bioethanol using popping pretreatment. *Bioresour. Technol.*, 125: 132-37.

Clarke, R.J. and Bakker, J. 2004. *Wine flavor chemistry*. Blackwell Pub, Hoboken, NJ.

Davydenko, S., Meledina, T., Mittenberg, A., Shabelnikov, S., Vonsky, M. and Morozov, A. 2020. Proteomics answers which yeast genes are specific for baking, brewing, and ethanol production. *Bioengineering*, 7(4): 1-15.

Díaz, C. and Carmen, M. 2017. The baseline of the coffee sector in Peru. <https://www-undp-org.translate>.

Einfalt, D., Meissner, K., Kurz, L., Intani, K. and Müller, J. 2020. Fruit spirit production from coffee cherries-process analysis and sensory evaluation. *Bebidas*, 6(3): 57-68.

Ezeji, T., Qureshi, N. and Blaschek, H.P. 2007. Production of acetone-butanol-ethanol (ABE) in a continuous flow bioreactor using degermed corn and *Clostridium beijerinckii*. *Process Biochem.*, 42(1): 34-39.

Ferrell, J. and Cockerill, K. 2012. Closing coffee production loops with waste to ethanol in Matagalpa, Nicaragua. *Energy Sustain. Develop.*, 16(1): 44-50.

Franca, A.S., Gouvea, B.M., Torres, C., Oliveira, L.S. and Oliveira, E.S. 2008. Feasibility of ethanol production from coffee husks. *J. Biotechnol.*, 136: S269.

Garde, W.K., Buchberger, S.G., Wendell, D. and Kupferle, M.J. 2017. Application of Moringa Oleifera seed extract to treat coffee fermentation wastewater. *J. Hazard. Mater.*, 329: 102-109.

Gathuo, B., Rantala, P. and Maatta, R. 1991. Coffee industry wastes. *War. Sci. Tech* 24(1):53-60.

Giroto, F., Pivato, A., Cossu, R., Nkeng, G.E. and Lavagnolo, M.C. 2018. The broad spectrum of possibilities for spent coffee grounds valorization. *J. Mater. Cycles Waste Manag.*, 20(1): 695-701.

Hans-Dieter, B., Grosch, W. and Schieberle, P. 2009. *Food Chem.*, 4: 52.

Kim, D., Ximenes, E.A., Nichols, N.N., Cao, G., Frazer, S.E. and Ladisch, M.R. 2016. Maleic acid treatment of biologically detoxified corn stover liquor. *Bioresour. Technol.*, 216: 437-445.

Kim, S.J., Chen, J.T., Cheng, T., Gindulyte, J., He, S., He, Li, Q., Shoemaker, B.A., Thiessen, P.A., Yu, B., Zaslavsky, L., Zhang, J. and Bolton, E.E. 2019. PubChem in 2021: One data content and improved web interfaces. *Nucleic Acids Res.*, D13: 88-95.

Kim, E.J., Seo, D. and Choi, Y. 2020. Bio-alcohol production from spent coffee grounds and okara waste biomass by engineered *Bacillus subtilis*. *Biom. Conv. Bioref.*, 10(1): 167-73.

Lee, J.E., Seo, E.J., Kweon, D.H., Park, K.M. and Jin, Y.S. 2009. Fermentation of rice bran and defatted rice bran for butanol production using *Clostridium beijerinckii* NCIMB 8052. *J. Microbiol. Biotechnol.*, 19(5): 482-490.

Lopes, A.C.A., Andrade, R.P., de Oliveira, L.C.C., Santiago, W.D., de Resende, M.L.V. and Duarte, W.F. 2020. Production and characterization of a new distillate obtained from the fermentation of wet-processing coffee by-products. *J. Food Sci. Technol.*, 57(12): 4481-4491.

de Melo Pereira, G.V., Soccol, V.T., Pandey, A., Medeiros, A.B.P., Lara, J.M.R.A., Gollo, A.L. and Soccol, C.R. 2014. Isolation, selection, and evaluation of yeasts for use in the fermentation of coffee beans by the wet process. *Int. J. Food Microbiol.*, 188: 60-66.

Mussatto, S.I., Machado, E.M., Carneiro, L.M. and Teixeira, J.A. 2012. Sugars metabolism and ethanol production by different yeast strains from the coffee industry wastes hydrolysates. *Appl. Energy* 92: 763-768.

Nguyen, H.V.N., Chenoweth, J.A., Bebartha, B.S., Albertson, T.E. and Nowadly, C.D. 2021. The toxicity, pathophysiology, and treatment of acute hydrazine propellant exposure: A systematic review. *Military Med.*, 186(3-4): e319-26.

- Novotny, M. 2003. Gas chromatography. In Meyers, R.A. (ed), Elsevier, California, pp. 455-72.
- Palmqvist, E. and Hahn-Hägerdal, B. 2000. Fermentation of lignocellulosic hydrolysates. II: Inhibitors and mechanisms of inhibition. *Bioresour. Technol.*, 74(1): 25-33.
- Pérez-Sariñana, B.Y., León-Rodríguez, A.D., Saldaña-Trinidad, S. and Sebastian, P. J. 2015. Optimization of bioethanol production from coffee mucilage. *Bioresources*, 10(3): 4326-38.
- Perrone, D., Farah, A., Donangelo, C.M., de Paulis, T. and Martin, P.R. 2008. Comprehensive analysis of major and minor chlorogenic acids and lactones in economically relevant Brazilian coffee cultivars. *Food Chem.*, 106(2): 859-867.
- Phisalaphong, M., Budiraharjo, R., Bangrak, P., Mongkolkajit, J. and Limtong, S. 2007. Alginate-loofa as carrier matrix for ethanol production. *J. Biosci. Bioeng.*, 104(3): 214-217.
- Rattan, S., Parande, A.K., Nagaraju, V.D. and Ghiwari, G.K. 2015. A comprehensive review on the utilization of wastewater from coffee processing. *Environ. Sci. Poll. Res.*, 22(9): 6461-6472.
- Razmovski, R. and Vučurović, V. 2011. Ethanol production from sugar beet molasses by *S. cerevisiae* entrapped in an alginate-maize stem ground tissue matrix. *Enzyme Microb. Technol.*, 48(4-5): 378-385.
- Roehr, M., Kosárico, N., Vardar-Sukan, F., Pieper, H.J. and Senn, T. 2001. The biotechnology of ethanol: Classical and future applications. *Molecules*, 6(12): 1019-1020.
- Ryan, D., Shellie, R., Tranchida, P., Casilli, A., Mondello, L. and Marriott, P. 2004. Analysis of roasted coffee bean volatiles by using comprehensive two-dimensional gas chromatography-time-of-flight mass spectrometry. *J. Chromatogr. A*, 1054(1-2): 57-65.
- Salas-López, R., Gómez Fernández, D., Silva López, J.O., Rojas Briceño, N.B., Oliva, M., Terrones Murga, R.E., Trigos, D.I., Barboza Castillo, E. and Barrera Gurbillón, M.A. 2020. Land suitability for coffee (*coffea arabica*) growing in Amazonas, Peru: Integrated use of AHP, GIS and RS. *ISPRS. Int. J. Geo-Inform.*, 9(11): 673.
- Sampaio, A., Dragone, G., Vilanova, M., José, M., Oliveira, J.M., Teixeira, J.A. and Mussatto, S.I. 2013. Production, chemical characterization, and sensory profile of a novel spirit elaborated from the spent coffee ground. *LWT. Food Sci. Technol.*, 54(2): 557-563.
- Sanz-Urbe, J.R., Menon, S.N., Oliveros, C., Husson, J., Brando, C. and Rodriguez, A. 2017. Postharvest processing-revealing the green bean. In Folmer, B. (ed), *The Craft and Science of Coffee*. Elsevier Inc., The Netherlands, pp. 51-79
- Silva, J.P.A., Mussatto, S.I. and Roberto, I.C. 2010. The influence of initial xylose concentration, agitation, and aeration on ethanol production by *Pichia stipitis* from rice straw hemicellulosic hydrolysate. *Appl. Biochem. Biotechnol.*, 162(5): 1306-1315.
- Vázquez, H.J. and Dacosta, O. 2007. Alcoholic Fermentation: An option for renewable energy production from agricultural waste. *Eng. Res. Technol.*, 8(4): 249-259.
- Vidra, A. and Németh, A. 2018. Bio-produced acetic acid: A review. *Period. Polytech. Chem. Eng.*, 62(3): 245-256.
- Wang, Y., Jingwen Zhao, J., Xu, F., Wu, X., Hu, W., Chang, Y., Zhang, L., Chen, J. and Liu., C. 2020. GC-MS, GC-O, and OAV analyses of key aroma compounds in Jiaozhi Steamed Bread. *Grain Oil Sci. Technol.*, 3(1): 9-17.
- Woldesenbet, A.G., Woldeyes, B. and Chandravanshi, B.S. 2016. Bio-ethanol production from wet coffee processing waste in Ethiopia. *SpringerPlus* 5(1): 1-7.
- Xiao, Z. and Lu, J.R. 2014. Generation of acetoin and its derivatives in foods. *J. Agric. Food Chem.*, 62(28): 6487-697.
- Zhang, S.J., De Bruyn, F., Pothakos, F.V., Contreras, G.F., Cai, Z., Moccand, C., Weckx, S. and De Vuyst, L. 2019. Influence of various processing parameters on the microbial community dynamics, metabolomic profiles, and cup quality during wet coffee processing. *Front. Microbiol.*, 10(2621):1-24.
- Zhang, W. and Ordway, G.A. 2003. The  $\alpha$ 2C-adrenoceptor modulates GABA release in mouse striatum. *Molecular Brain Research*, 112(1-2): 24-32.





# Investigation on the Treatment of Slaughterhouse Wastewater in a Sequential Batch Reactor

Asad Ashraf and Izharul Haq Farooqi†

Department of Civil Engineering, Zakir Husain College of Engineering and Technology, Aligarh Muslim University, Aligarh-202 002, U.P., India

†Corresponding author: Izharul Haq Farooqi; asad.ashraf1981@gmail.com

Nat. Env. & Poll. Tech.  
Website: [www.neptjournal.com](http://www.neptjournal.com)

Received: 26-09-2021

Revised: 16-12-2021

Accepted: 24-12-2021

## Key Words:

UASB

Slaughterhouse wastewater

Sequencing batch reactor

Diffused air flotation

## ABSTRACT

In the present study, the treatment of slaughterhouse wastewater was carried out in a sequential batch reactor. A lab-scale column type reactor was fabricated with Perspex material having dimensions of 10 cm diameter, 100 cm height, and an effective volume of 7 liters provided with ports at different levels. The reactor performance was evaluated in terms of COD, BOD, TSS, TKN, and phosphorus removal. The reactor was operated for 432 days; the effectiveness of the reactor is the temperature of wastewater in the reactor. The removal efficiencies of COD and BOD were 84% and 80% in the reactor. The maximum TSS removal was around 87% and TKN's maximum removal efficiency was 61% in aerobic treatment. Phosphorus maximum removal efficiency was around 68%, in the meantime pH and alkalinity were also monitored, and no change in the pH was reported throughout the experiment. On the other hand, an aerobic SBR is also operated using wastewater after the DAF unit. In the same manner, the reactor was operated with initially diluted wastewater (05 times) and kept HRT 8 h. The reactor performance was studied in terms of COD, BOD, TSS, TKN, and phosphorus. The maximum removal efficiencies of COD and BOD were 80% and 81% respectively. The maximum removal efficiencies of TSS, TKN, and Phosphorus were 73%, 81%, and 69% respectively. It is concluded that the removal efficiency of COD was better in the anaerobic process as compared with the aerobic process in addition the generation of methane gas during the degradation of organic matter can be used for operating the aerobic unit by making some necessary arrangements. Besides this, it is also concluded that the removal efficiency of TKN was better in the aerobic process as compared with the anaerobic process. There was a buildup of VSS from 4500 mg.L<sup>-1</sup> to 6500 mg.L<sup>-1</sup> in the study.

## INTRODUCTION

Water shortage and contamination of available water reserves have engrossed global attention in recent years (Khan et al. 2015). The effluent coming from various industries such as slaughterhouses, food processing industries, chemical processing plants, and paper & pulp industries remain highly contaminated. The slaughterhouse wastewater is classified under the category of agricultural and food industries as industrial wastewater. On an average 15 liters of wastewater are generated in each mechanized slaughtering, amounting to about 630 million gallons of water annually in India itself (Central Pollution Control Board, Delhi, Ministry of Environment, Forest and Climate Change, Government of India, October 2017). Studies show that effluent generated from slaughterhouses contaminates both surface and groundwater bodies because of the slaughtering process, blood, fat, urine, and undigested food are produced and added to the nearby water streams (Alam et al. 2021). Slaughterhouse industries having high suspended solids, organic matter should not be discharged on the land or in sewers directly because of their

high concentration of COD, and BOD (Aziz et al. 2019, Mittal et al. 2006). Besides this, the addition of chemicals for the treatment of wastewater is not a good option because it increases the cost of the treatment, and disposal of sludge is uneconomical.

For the conventional treatment of slaughterhouse wastewater, methods based on anaerobic treatment processes are more advantageous over the other treatment system (Sindhu et al. 2012, Sunder et al. 2013) like the advanced oxidation process, electro-coagulation, and physicochemical process (Masse & Masse 2005, Del Nery et al. 2007, Khan et al. 2020). Advantages of the anaerobic process are high organic removal, less space required, less sludge generation, low energy requirement, working on high organic loading, less nutrients requirement, and methane gas production which can be used to operate the generators to be used for energy requirement in aerobic unit operations.

Few reactor configurations are used for the anaerobic treatment of industrial wastewater like upflow anaerobic sludge blanket reactor (UASB) (Rajakumar et al. 2012),



completely mixed anaerobic digester, fluidized and expanded bed reactors, and anaerobic filters, anaerobic sequencing batch reactor (ASBR) (Kundu et al. 2013). Among these, the anaerobic sequencing batch reactor had gained popularity as a better biological treatment option for the treatment of industrial wastewater. SBR systems can degrade the pollutants and can withstand higher organic loading (Masse & Masse 2000, Sombatsompop et al. 2011). Overall these SBR systems have some advantages over other conventional treatment technologies such as low energy consumption, and require less space with all the operations such as Fill, React/Aeration, Settle, and Draw taking place in a single tank (Khan et al. 2019, Bustillo-Lecompte et al. 2017, Chan et al. 2009).

The objective of this study was to assess the feasibility of a lab-scale anaerobic-aerobic SBR for the treatment of slaughterhouse wastewater and a comparative analysis with aerobic SBR treatment of slaughterhouse wastewater taken after Diffused Air Flotation (DAF) unit from a running slaughterhouse effluent treatment plant.

## MATERIALS AND METHODS

Two reactors were fabricated with Perspex material of similar dimensions and capacity, one anaerobic and the other aerobic as shown in Fig. 1. Considering the design and dimensions, an internal diameter of 10 cm and height of 100 cm, the working volume of the column type SBR was 7.065 L. A port at 10 cm below the top of the reactor

was made for the collection of effluent, while a port at the bottom of the reactor was made for the withdrawal of excess sludge generated. Both the reactors were seeded with respective sludge. Initially, the diluted wastewater was fed to the reactor and for acclimatization of micro-organisms, the HRT of 24 h was fixed, later on changing the dilution of wastewater as well as the HRT of the reactor. The anaerobic SBR consists of an anaerobic UASB in the bottom part and a port for effluent withdrawal at 0.75 m from the bottom. The aerobic SBR had an air supply port at the bottom and an effluent withdrawal port at 0.75 m from the bottom, and an excess sludge collection port at a height of 0.2 m from the bottom was provided in both the reactors.

The anaerobic sequential batch reactor (SBR) was seeded with two L of digested slaughterhouse UASB sludge. The aerobic sludge was fed in the reactor taken from the aeration tank of an activated sludge process treatment unit. The slaughterhouse wastewater was fed to the reactors having the following characteristics as given in Table 1.

## Operation Cycle

Initially, the raw wastewater was 10 times diluted in the reactor to avoid shock loading, keeping the HRT at 24 h for microorganisms to acclimatize. The dilutions of the raw sample were further varied as 5 times, 4 times, and so on in the end sample without dilution, varying the HRT of the reactor gradually. The dilutions were changed accordingly on the attainment of the steady-state conditions as shown in Table 2.

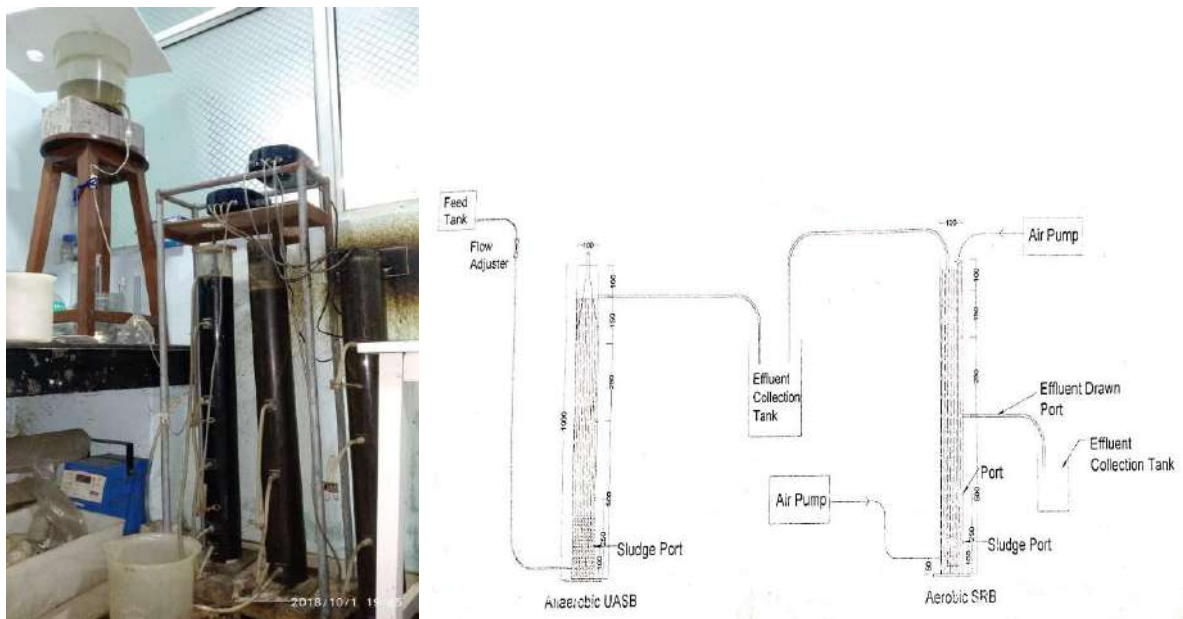


Fig. 1: Two reactors set up in parallel at lab scale and schematic diagram for the treatment of slaughterhouse wastewater.

Table 1: General characteristics of slaughterhouse wastewater.

S.No.	Wastewater Characteristics	Range
1	pH	6.8 to 8.5
2	Alkalinity (mg.L <sup>-1</sup> as CaCO <sub>3</sub> )	930 to 1350
3	Chemical Oxygen Demand (COD) (mg.L <sup>-1</sup> )	4700 to 6200
4	Biochemical Oxygen Demand (BOD) (mg.L <sup>-1</sup> )	2400 to 3200
5	Total Suspended Solids (TSS) (mg.L <sup>-1</sup> )	950 to 4200
6	Total Dissolved Solids (TDS) (mg.L <sup>-1</sup> )	5200 to 7200
7	Total Kjeldahl Nitrogen (TKN) (mg.L <sup>-1</sup> )	180 to 256
8	Phosphate (PO <sub>4</sub> ) (mg.L <sup>-1</sup> )	130 to 256

### Aerobic SBR While Using DAF Sample

The reactor was seeded with two L of digested sludge taken from the activated sludge process unit of a running treatment plant. The slaughterhouse wastewater fed to the reactor has the following characteristics as a DAF unit as shown in Table 3.

When the microorganisms were acclimating, the raw wastewater was diluted 05 times in the reactor to avoid shock loading, and the HRT was kept at 8 hours. When the microorganisms were acclimating, the dilution of the raw sample was changed 4 times, 3 times, 2 times, and without dilution, and the HRT was kept at 8 hours. When the micro-

organisms were acclimatizing, the dilution of the raw sample was changed 4 times, 3 times, 2 times, and without dilution, and HRT was kept as 8. The dilutions of the sample were changed when the steady-state conditions were reached as shown in Table 4.

### Experimental Setup and Operational Cycle

The reactors were operated with a cycle length of 24 h initially, after steady-state conditions were reached, then the dilution of the sample and cycle length of the reactors were changed to 18 h, 12 h, and 8 h. Anaerobic SBR reactor was fed continuously from the bottom and no air was supplied in the reactor. However, the aerobic SBR reactor was having

Table 2: COD values of influent feed to the anaerobic reactor.

S.No.	Dilution Factor	COD Influent in Reactor(mg.L <sup>-1</sup> )	Total Days
1	Ten Times	510	96 days
2	Five Times	1006	72 days
3	Four Times	1530	48 days
4	Three Times	2070	54 days
5	Two Times	3031	48 days
6	Without Dilution (Raw Wastewater)	6172	120 days

Table 3: Characteristics of slaughterhouse wastewater after the DAF unit.

S.No.	Wastewater Characteristics	Range
1	pH	7.20
2	Alkalinity (mg/l as CaCO <sub>3</sub> )	1130
3	Chemical Oxygen Demand (COD) ( mg.L <sup>-1</sup> )	4120
4	Biochemical Oxygen Demand (BOD) ( mg.L <sup>-1</sup> )	2390
5	Total Suspended Solids (TSS) ( mg.L <sup>-1</sup> )	2164
6	Total Dissolved Solids (TDS) ( mg.L <sup>-1</sup> )	4200
7	Total Kjeldahl Nitrogen (TKN) ( mg.L <sup>-1</sup> )	769
8	Phosphate (PO <sub>4</sub> ) (mg/l)	258

Table 4: COD values of Influent Feed to the Aerobic Reactor.

S.No.	Dilution Factor	COD Influent in Reactor (mg.L <sup>-1</sup> )	Total Days
1	Five Times	845	72 days
2	Four Times	1050	48 days
3	Three Times	1412	96 days
4	Two Times	2115	96 days
5	Without Dilution (Raw Wastewater)	4120	96 days

continuous oxygen supply to maintain the population of microorganisms, although aeration was turned off during adding of the effluent and its withdrawal.

The timing of the phase cycle for SBR was: Fill-05 min, React-23 hrs 10 min, Settle-40 min, Draw-05 min.

The analytical techniques used in this study were performed according to the method described in Standard Methods. pH, total dissolved solids, and dissolved oxygen were analyzed by using HACH HQ30d portable meter (USA) coupled with their respective probes. Analysis of alkalinity, TSS, BOD, and COD was analyzed by standard methods (APHA 2005). The analysis of Phosphate and total Kjeldahl nitrogen (TKN) was carried out by DR 5000 (HACH, USA) UV spectrophotometer.

## RESULTS AND DISCUSSION

Both the reactors were operated for varying hydraulic retention times (HRT) namely 24, and 18, 12, and 8 h respectively, and variable dilutions. The dilutions and HRT were changed when optimum removal was achieved in the last HRT and dilution. The maximum OLR applied was 6.172 kg COD.m<sup>-3</sup>.d<sup>-1</sup> for the anaerobic reactor and 1.311 kg COD.m<sup>-3</sup>.d<sup>-1</sup> for the aerobic SBR reactor.

The maximum removal efficiencies for the parameters COD, BOD, TSS, TKN, Phosphorus, pH, and alkalinity using anaerobic SBR treatment are tabulated as shown in Table 5.

However, the maximum removal efficiencies of COD, BOD, TSS, TKN, and Phosphorus achieved were 80%, 81%, 73%, 81%, and 69% respectively for slaughterhouse

Table 5: Maximum removal efficiencies attained in anaerobic SBR for the studied parameters.

S.No	Pollutants	Influent (mg.L <sup>-1</sup> )	Effluent (mg.L <sup>-1</sup> )	Removal Efficiency (%age)
1	pH	6.25	7.85	--
2	Alkalinity	1153	188	83%
3	COD	6250	1000	84%
4	BOD	2815	563	80%
5	TKN	1064	410	61%
6	TSS	4235	551	87%
7	Phosphorus	258	83	68%

Table 6: Maximum removal efficiencies attained in SBR for the studied parameters by aerobic SBR treatment after DAF unit.

S.No	Pollutants	Influent (mg/L)	Effluent (mg/L)	Removal Efficiency (% age)
1	pH	6.52	7.25	--
2	Alkalinity	953	160	83%
3	COD	4120	830	80%
4	BOD	2395	460	81%
5	TKN	769	204	73%
6	TSS	2164	410	81%
7	Phosphorus	258	78	69%

wastewater using aerobic SBR treatment after the DAF unit are shown below in Table 6.

The results of anaerobic-aerobic SBR using raw wastewater and employing a DAF unit were compared with Central Pollution Control Board (CPCB), INDIA effluent discharge standards as shown below in Table 7.

Graphs were plotted (Fig. 2 to Fig. 8) to show the variation of influent and effluent Chemical Oxygen Demand, Biochemical oxygen Demand, Total Kjeldahl Nitrogen, Total Suspended Solids, and Phosphorus removal efficiencies with time. In initial the wastewater was used for feeding to the reactor was keeping 10 times diluted and HRT was 24 h. The Influent parameters concentration of the wastewater sample when dilution keeping 10 times were 510 mg.L<sup>-1</sup>, 273 mg.L<sup>-1</sup>, 93 mg.L<sup>-1</sup>, 350 mg.L<sup>-1</sup>, and 20 mg.L<sup>-1</sup> respectively and the maximum removal efficiencies at this concentration

were 79%, 68%, 59%, 50%, and 42% respectively at steady-state condition.

The influent, effluent, and removal efficiency in terms of Chemical Oxygen Demand (COD) for the anaerobic-aerobic SBR with time is shown in Fig. 2 It is quite evident that, initially, when the concentration of wastewater was 10 times diluted (510 mg.L<sup>-1</sup>), and keeping HRT as 24 h, the removal of COD was 78%. When the steady-state condition was attained after 16 weeks, the dilution of the sample and HRT of the sample were gradually changed, until no dilution wastewater was fed to the reactor and the HRT was 8 h, and the highest COD removal efficiency was 84 percent after 72 weeks.

In the same manner, the BOD influent was 273 mg.L<sup>-1</sup> at 10 times dilution and 24 h HRT. After 16 weeks, the removal efficiency of the slaughterhouse wastewater after the anaerobic-aerobic process was 77%. Once the steady-state condition was reached, we gradually changed the dilution and HRT of the sample to 5 times and HRT to 18 h. After 28 weeks, the removal was 78% as shown in Fig. 3. Finally, after 72 weeks of feeding wastewater to the reactor without dilution and holding the HRT at 8 h, the maximum removal efficiency was obtained at 80%.

The influent and effluent Total Suspended Solids (TSS) concentration and removal efficiency for treated wastewater are shown in Fig. 4 In which the initial concentration of TSS was (350 mg.L<sup>-1</sup>) at 10 times dilution and the HRT

Table 7: Effluent discharge standards prescribed by the Central Pollution Control Board of India.

S.No.	Pollutants	CPCB Discharge Values (mg.L <sup>-1</sup> )
1	pH	6.50 to 8.50
2	COD	250
3	BOD	30
4	TKN	25
5	TSS	50
6	Phosphorus	1.0

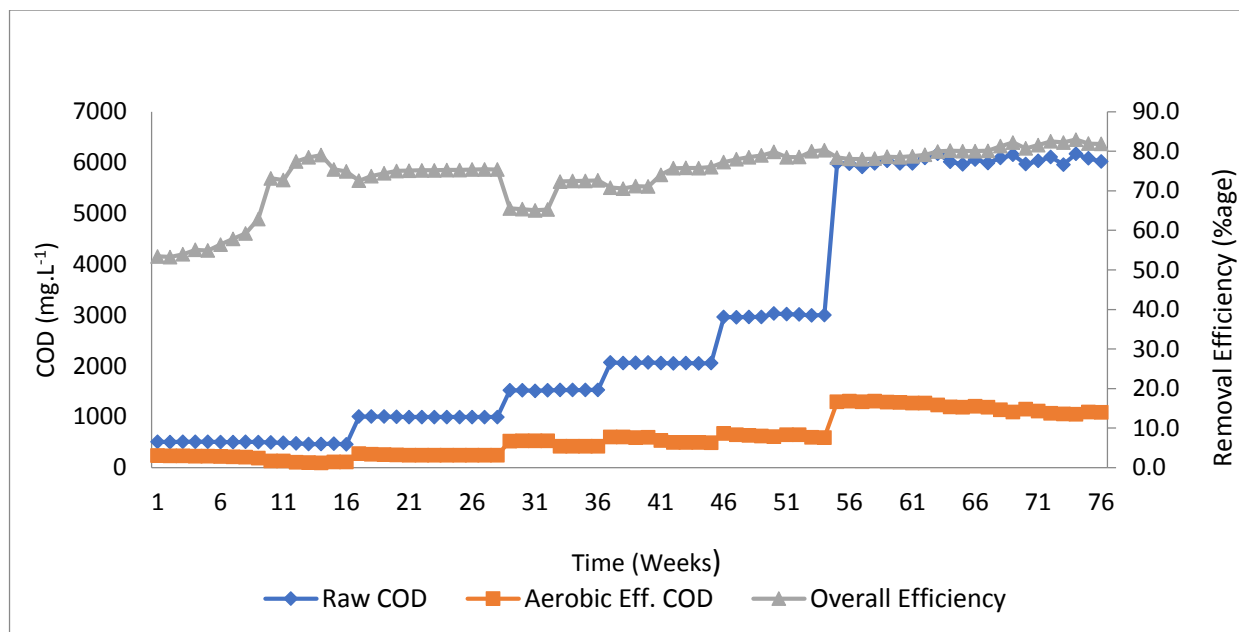


Fig. 2: Influent, effluent, and removal efficiency of COD with time.

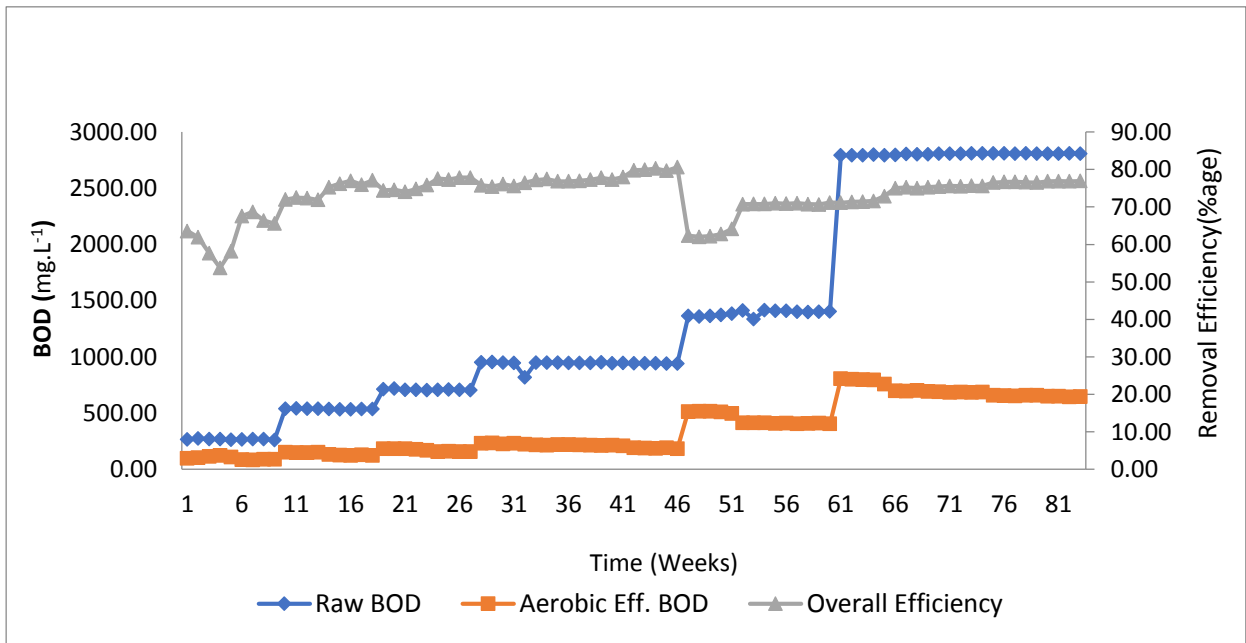


Fig. 3: Influent, effluent, and removal efficiency of BOD with time.

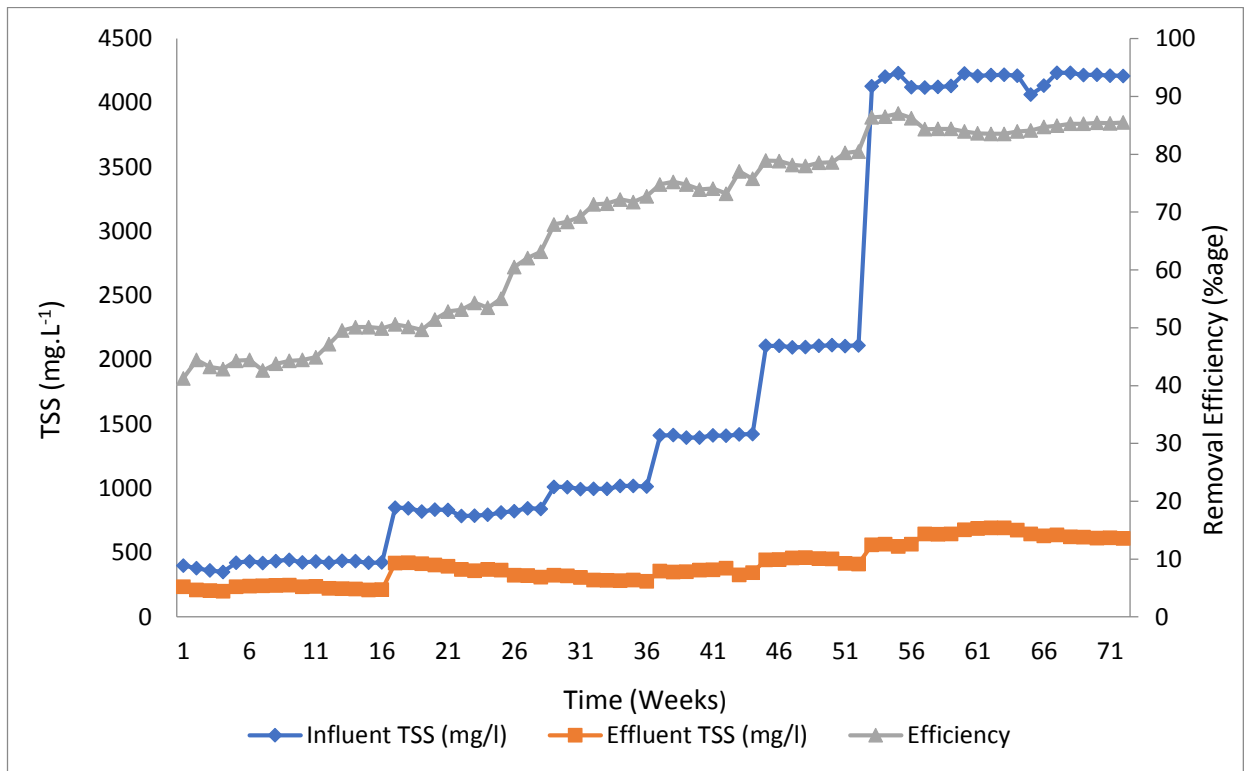


Fig. 4: Influent, effluent, and removal efficiency of TSS with time.



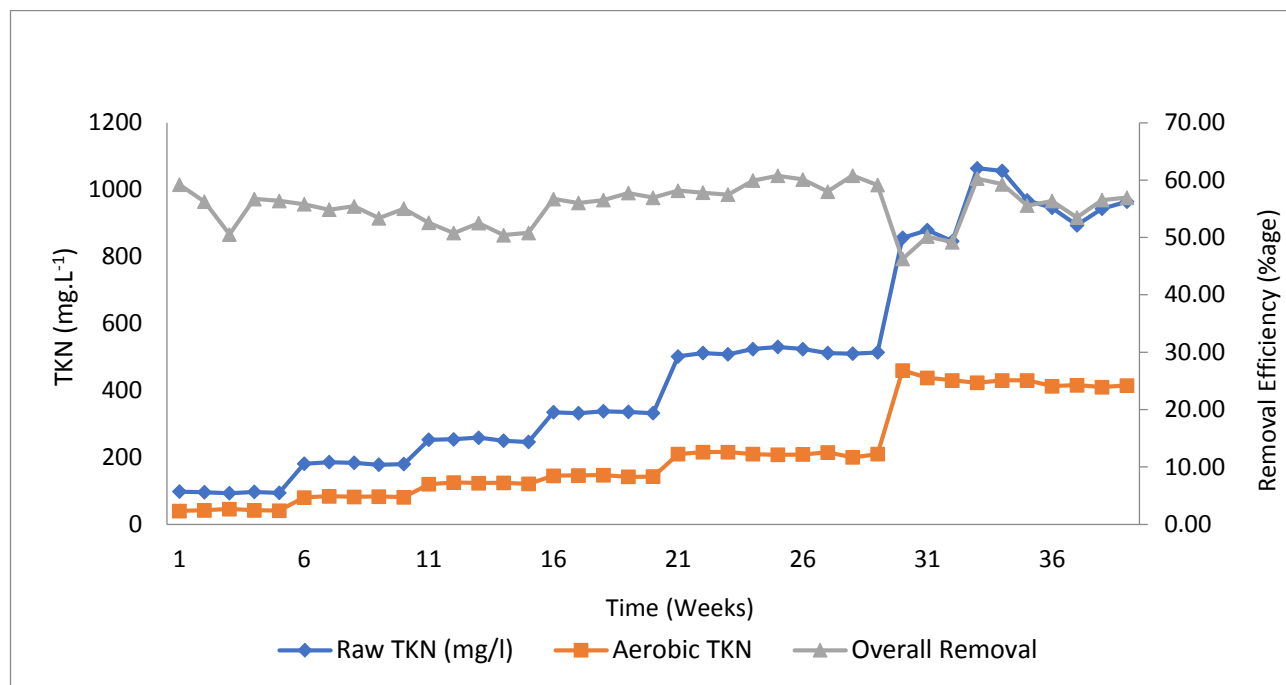


Fig. 5: Influent, effluent, and removal efficiency of TKN with time.

was 24 h. After 16 weeks, the removal efficiency of anaerobic-aerobic SBR was achieved at 50%, and the dilution of the sample and HRT of the reactor were gradually changed, with a dilution of the sample 5 times, 4 times, 3 times, 2 times, and without dilution being used, and the HRT being reduced to 18 hours, 12 h, and 8 h for the system. The removal efficiencies of the system for TSS was 63% after 28 weeks, at a dilution of 5 times. The concentration of the sample was ( $850 \text{ mg.L}^{-1}$ ). In the end, the maximum removal efficiency of the TSS was 87% when the concentration without dilution of sample was ( $4235 \text{ mg.L}^{-1}$ ) at HRT of 8 h after 72 weeks of reactor run.

The influent Total Kjeldahl Nitrogen (TKN) was ( $93 \text{ mg.L}^{-1}$ ) at dilution 10 times. The removal efficiency was 50% when the steady-state condition was reached. The dilution of the sample was gradually changed to 5 times, 4 times, 3 times, and 2 times, and the sample was used without dilution. In the end, the maximum removal efficiency of the TKN in the anaerobic-aerobic SBR system was 61%, keeping the HRT of the system was 8 h as shown in Fig. 5. The removal efficiency of TKN in the anaerobic SBR system was reported less as compared with the aerobic system. The removal efficiency of TKN did not increase throughout the process, and was in the range of 50% to 61% in the anaerobic-aerobic SBR system, as indicated in the graph.

The phosphorus present in the sample was due to the breakdown of the proteins, initially, the concentration was ( $20 \text{ mg.L}^{-1}$ ) at 10 times dilution, keeping HRT at 24 h. The removal efficiency of the phosphorus was only 38%, and the removal of phosphorus from the wastewater is very less. As the steady-state condition was reached, we gradually changed the HRT and dilution of the wastewater to 5 times, 4 times, 3 times, 2 times, without dilution, and HRT decreased to 18 h, 12 h, and 8 h. The maximum removal efficiency of phosphorus was 68% in the anaerobic-aerobic treatment system of SBR after 72 weeks, the removal efficiency and the influent and effluent phosphorus variation with time as shown in Fig. 6.

In an anaerobic-aerobic system the influent, pH was more or less unchanged throughout the experiment but at some points when the dilution of the sample changed then little bit changes were reported in the pH concentration, otherwise the pH remained unchanged as shown in Fig. 7. But the pH concentration of the treated effluent increased from 6.25 to 7.75.

Initially, the alkalinity of the wastewater was ( $1156 \text{ mg.L}^{-1}$ ) without dilution sample, and effluent alkalinity was obtained after treatment ( $188 \text{ mg.L}^{-1}$ ) the maximum removal of alkalinity is reported as 83% from the anaerobic-aerobic treatment system at HRT 8 h of the reactor the graph as shown in Fig. 8

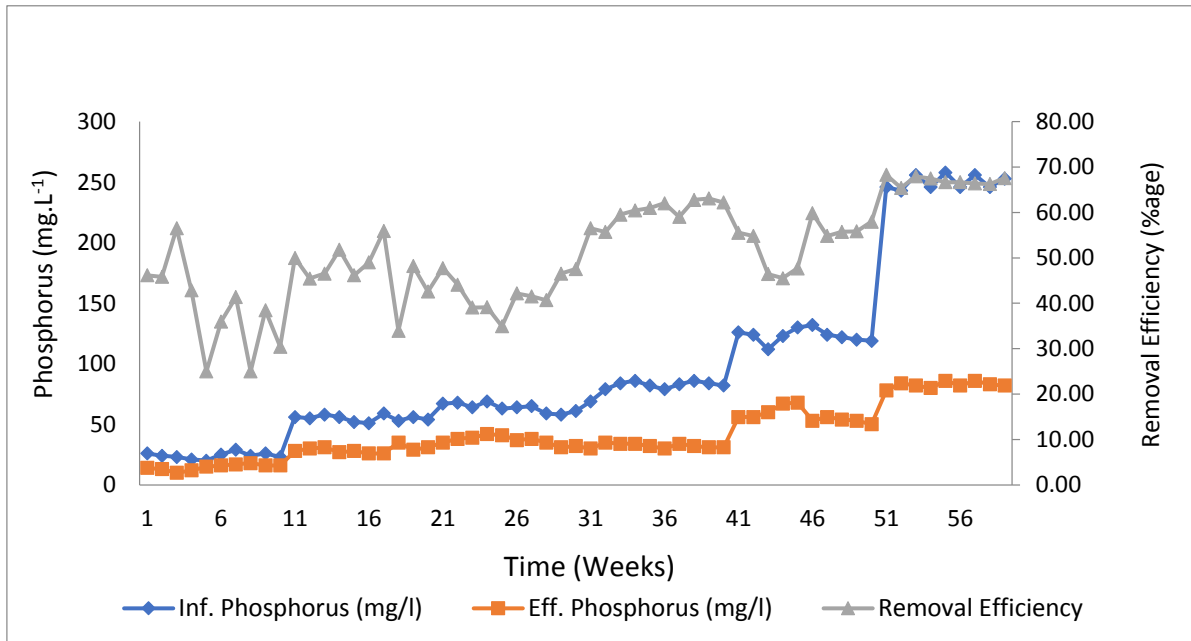


Fig. 6: Influent, effluent, and removal efficiency of phosphorus with time.

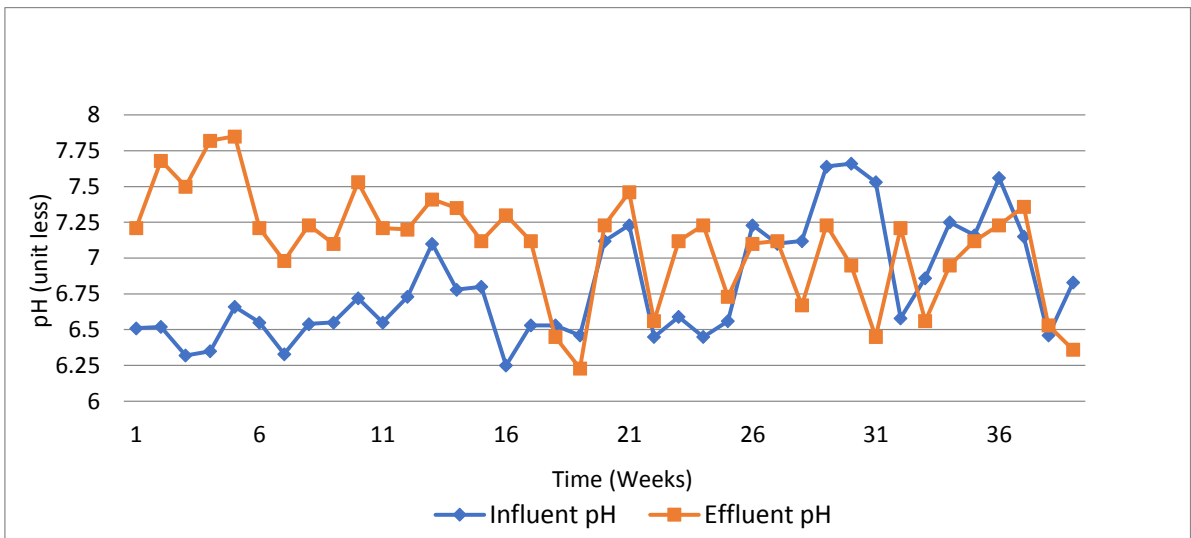


Fig. 7: Influent, effluent pH with time.

## CONCLUSION

This study used anaerobic and aerobic sequencing batch SBR reactors for slaughterhouse wastewater treatment, which proved to be easy to operate, less energy-consuming, requiring less space, and extremely efficient when compared to other conventional processes. In terms of addressing high organic loading and obtaining high removal efficiencies under steady-state conditions, an anaerobic-aerobic SBR

system was found to be a better solution for the treatment of slaughterhouse effluent. The maximum removal rates attained for Chemical oxygen demand, Biological oxygen demand, Total suspended solids, Total Kjeldahl nitrogen, and Phosphorus were 84%, 80%, 87%, 61%, and 68% respectively. It may also be concluded that the removal efficiency of COD/BOD in an anaerobic SBR system is better as compared with an aerobic SBR system using wastewater after the DAF unit. However, removal of TKN and Phosphorus from the waste-

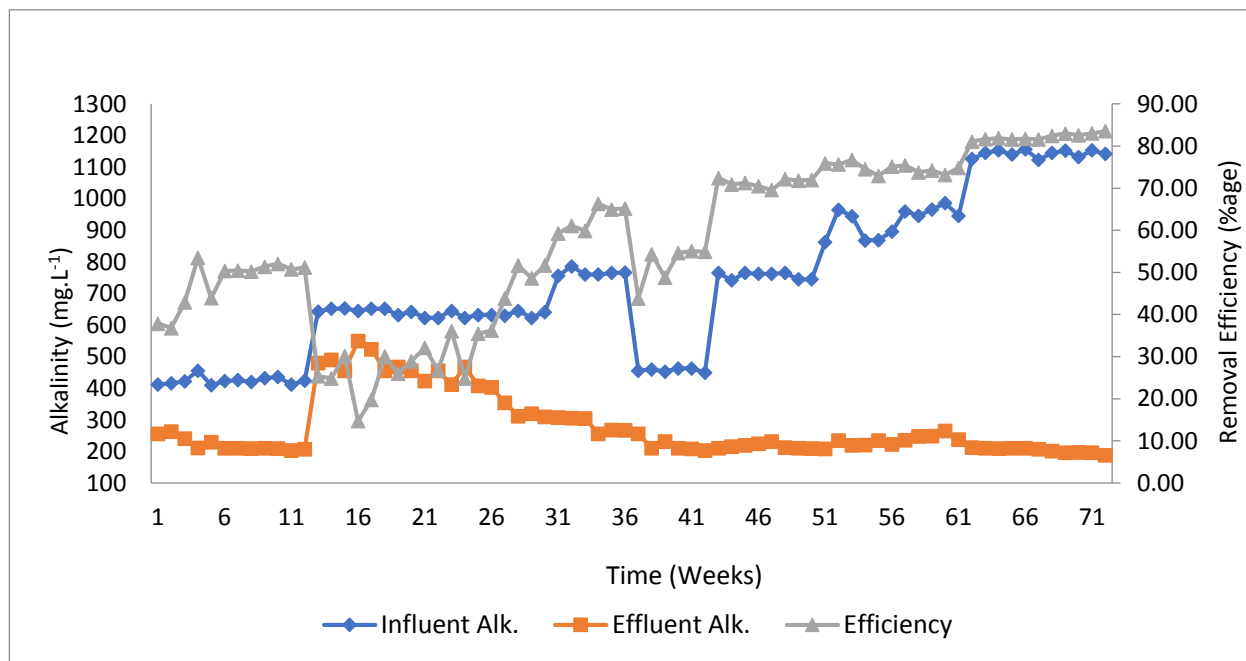


Fig. 8: Influent, effluent and removal efficiency of alkalinity with time.

water is better in aerobic SBR as compared with anaerobic SBR.

## ACKNOWLEDGEMENT

The authors are thankful to the Chairman of the Civil Engineering Department, A.M.U, Aligarh to provide the necessary facilities and laboratory equipment for my research work.

## REFERENCES

- Alam, R., Khan, S. U., Basheer, F. and Farooqi, I. H. 2021. Nutrients and organics removal from slaughterhouse wastewater using phytoremediation: A comparative study on different aquatic plant species. *IOP Conf. Series Mater. Sci. Eng.*, 1058: 012068.
- Aziz, A., Basheer, F., Sengar, A., Khan, S.U. and Farooqi, I.H. 2019. Biological wastewater treatment (anaerobic-aerobic) technologies for safe discharge of treated slaughterhouse and meat processing wastewater. *Sci. Total Environ.*, 66: 681-708.
- Bustillo-Lecompte, C.F. and Mehrvar, M. 2017. Treatment of actual slaughterhouse wastewater by combined anaerobic-aerobic processes for biogas generation and removal of organics and nutrients: An optimization study towards a cleaner production in the meat processing industry. *J. Clean. Prod.*, 141: 278-289.
- Chan, Y.J., Chong, M.F., Law, C.L. and Hassell, D.G. 2009. A review on the anaerobic-aerobic treatment of industrial and municipal wastewater. *Chem. Eng. J.*, 155(1-2): 1-18.
- Del Nery, V., De Nardi, I.R., Damianovic, M.H.R.Z., Pozzi, E., Amorim, A.K.B. and Zaiat, M. 2007. The long-term operating performance of a poultry slaughterhouse wastewater treatment plant. *Resour. Conserv. Recycl.*, 50(1): 102-114.
- Khan, N.A., Khan, S.U., Islam, D.T., Ahmed, S., Farooqi, I.H., Isa, M.H., Hussain, A., Changani, F. and Dhingra, A. 2019. Performance evaluation of column-SBR in paper and pulp wastewater treatment: Optimization and bio-kinetics. *Desalin. Water Treat.*, 156: 204-219.
- Khan, S.U., Asif, M., Alam, F., Khan, N.A. and Farooqi, I.H. 2020. Optimizing fluoride removal and energy consumption in a batch reactor using electrocoagulation: A smart treatment technology. In Ahmed, S., Abbas, S.M. and Zia, H. (eds), *Smart Cities: Opportunities and Challenges*, Springer, Singapore, pp. 767-778.
- Kundu, P., Debsarkar, A. and Mukherjee, S. 2013. Treatment of slaughterhouse wastewater in a sequencing batch reactor: performance evaluation and biodegradation kinetics. *BioMed. Res. Int.*, 2013: 1021-1036.
- Masse, O. and Masse, L. 2000. In anaerobic sequencing batch reactors. *Canad. Agric. Eng.*, 42(3): 131.
- Masse, L. and Masse, D.I. 2005. Effect of soluble organic, particulate organic, and hydraulic shock loads on anaerobic sequencing batch reactors treating slaughterhouse wastewater at 20 C. *Process Biochem.*, 40(3-4): 1225-1232.
- Mittal, G.S. 2006. Treatment of wastewater from abattoirs before land application: A review. *Bioresour. Technol.*, 97(9): 1119-1135.
- Rajakumar, R., Meenambal, T., Saravanan, P.M. and Ananthanarayanan, P. 2012. Treatment of poultry slaughterhouse wastewater in hybrid upflow anaerobic sludge blanket reactor packed with pleated polyvinyl chloride rings. *Bioresour. Technol.*, 103(1): 116-122.
- Sindhu, R. and Meera, V. 2012. Treatment of slaughterhouse effluent using upflow anaerobic packed bed reactor. *Int. Congress Inform. Environ. Energy Appl.*, 38: 1-7.
- Sombatsompop, K., Songpim, A., Reabroi, S. and Inkong-ngam, P. 2011. A comparative study of sequencing batch reactor and moving bed sequencing batch reactor for piggery wastewater treatment. *Maejo Int. J. Sci. Technol.*, 5(2): 191.
- Sunder, G.C. and Satyanarayan, S. 2013. Efficient treatment of slaughterhouse wastewater by anaerobic hybrid reactor packed with special floating media. *Int. J. Chem. Phys. Sci.*, 2: 73-81.





# Biomass Fired Thermal Power Generation Technology- A Route to Meet Growing Energy Demand and Sustainable Development

Amarnath Bose\*† and Devender Kumar Saini\*\*

\*Sustainability Cluster, School of Engineering (SOE), University of Petroleum and Energy Studies, Dehradun, India

\*\*Electrical Cluster, School of Engineering (SOE), University of Petroleum and Energy Studies, Dehradun, India

†Corresponding author: Amarnath Bose; bose.amarnath@gmail.com

## Nat. Env. & Poll. Tech.

Website: [www.neptjournal.com](http://www.neptjournal.com)

Received: 25-09-2021

Revised: 29-11-2021

Accepted: 02-12-2021

### Key Words:

Biomass

Thermochemical biomass technology

Biomass direct combustion

GHG emissions

Sustainable development

## ABSTRACT

Energy derived from biomass is a very promising energy alternative especially when we compare the same with fossil fuels (coal, liquid fossil fuels, etc.) as the plants can absorb the carbon dioxide during the photosynthesis process and therefore can reduce the greenhouse gas (GHG) emissions generated from fossil fuels. Further, the utilization of biomass in various biomass-based thermochemical conversion technologies could help to convert waste bio-resources into bio-energy. This review paper provides an overview of various types of available biomass resources along with their chemical composition and physical properties and their utilization for the generation of power (electricity) as an alternative to coal for power generation from a Thermal Power Plant or useful form of heat or fuels/chemicals for various other industrial processes. It includes the merits and demerits of biomass-fired thermal power plants with reference to efficiency, environmental emissions, and logistics, supply chain and storage for biomass. These review papers attempt to bring forward the effective methods which could be adopted for the efficient utilization of biomass for the purpose of power generation from biomass-based thermal power plants. Further, this could also help to substantially reduce green house gas emissions and carbon footprint and help to achieve sustainable development goals.

## INTRODUCTION

Biomass is a renewable energy source, derived from plants. It is one of the oldest energy sources and is been used by humankind for the generation of energy for centuries. It is still the major energy source (mainly for cooking and boiling water) in several countries and regions. Biomass is considered a CO<sub>2</sub>-neutral fuel, as it releases no net CO<sub>2</sub> emissions if carefully managed. The plants absorb the amount of CO<sub>2</sub> released from biomass combustion during photosynthesis. Moreover, biomass fuels have less Sulphur and usually have less nitrogen compared to coal. Therefore, biomass fuels have great potential and are more environmentally friendly due to reduced greenhouse gases emission(s) in comparison to existing fossil fuel-fired power plants. Due to this reason, the use of biomass as a fuel in the scope of clean environment technologies has gained great interest in recent years (Jack & Oko 2018, Kumar 2017).

Climate change which leads to global warming is the most notable problem in the present scenario (Change 2014). The conventional sources of energy are natural gas, coal, and nuclear energy of which electricity from coal is the major source. Globally, China is the major consumer of coal, with 2,866 mtce, which accounts for 53.0% of the world's share.

In the second place, India consumes 585 mtce, 0.4% less than last year (Ramirez Pons 2021). In India, about 60% of electricity is generated using coal (Mishra 2004, Reddy 2018) but the conversion efficiency is very low, and also during this conversion process, pollutants are released into the atmosphere which is hazardous to the environment (Goyal 2015). Since coal is in finite quantity so in the future it will come to extinction. By considering all these facts, an alternate source of energy could be a possible solution for sustainable development. Renewable energy is the solution to these problems. The increase in energy demand is directly proportional to the growth of the world population (Joshi & Beck 2018).

Due to increased concern over global warming and climate change (Walther et al. 2002), researchers are trying to discover alternative energy forms to replace conventional energy as a possible solution to counter the detrimental effects caused by fossil fuels. Biomass being carbon neutral has an advantage over other forms of renewable energy sources (Johnson 2009, Ragauskas et al. 2006). As per a report by Global Bioenergy Supply and Demand Projections (Tauro et al. 2018, Berndes 2002), biomass could make up to 60% of the overall renewable energy usage (Nakada et al. 2014). The world biomass demand by the year 2030 is expected to be 108 EJ (Nakada et al. 2014).



The world has vast amounts of biomass but much of them are unexplored. Various technologies are available to convert biomass into useful energy by thermochemical and biochemical processes. Among these technologies, the biomass-fired Steam Generator (Boiler) is the most common method and has shown the greatest potential for large-scale utilization of biomass energy, especially for power generation (Kumar 2017).

In India, public sector organization like National Thermal Power Corporation (NTPC) has demonstrated the co-firing of biomass (7% blending) along with coal in their Dadri plant in the state of Uttar Pradesh (MOP 2021).

In this review paper, a comparative analysis of various types of biomass fuels has been done along with the issues associated with the effective utilization of biomass in Thermo-chemical combustion technologies.

## COMPARATIVE ANALYSIS OF ELEMENTAL COMPOSITION AND PHYSICAL PROPERTIES OF BIOMASS

Biomass-based power generation technologies are highly dependent on the type of Biomass fuel. Biomass is generally analyzed as feedstock, which exhibits a variety of forms and properties that can impact power generation output.

Depending on the type of the bio-residue, the Biomass feedstock may largely vary in its physical characteristics like homogeneity and ash or moisture content, which ultimately affects the cost per unit of energy produced, transportation cost, treatment, and storage cost & efficiency of the power generation technology. The various types of feedstock include rural feedstock like forest residue and wood waste, agricultural residues, energy crops, and biogas from livestock

effluent while urban feedstock includes packing crates, pallets, wastewater, and sewage biogas, municipal solid waste, or food processing residues.

The feedstock is utilized to produce power through conversion technologies like thermochemical conversion processes, which include combustion, gasification, and pyrolysis, and biochemical processes like anaerobic digestion, etc.

### Resources of Biomass Feedstock

Biomass feedstock is generally heterogeneous to operate and it is composed of fibrous structure along with moisture and lignin, carbohydrates, sugars, and ash. Lignocellulose is present in plant biomass or woodstock. The biomass feedstock resources that are used as fuel for heat/gas/electricity generation are categorized as follows in Table 1.

### Elemental Composition of Various Types of Biomass

The Table 2 provides the detail of the elemental constituents of various types of Biomass residues based upon the proximate and ultimate analysis:

Table 2 provides us with detailed information on various types of biomass residual fuels which could be used in a steam generator of a Thermal Power Plant along with their percentage of carbon content which determines the calorific value and the percentage of ash & moisture content respectively.

Even though biomass fuels inherently have lower calorific value when compared with fossil fuels (coal, diesel, etc.), the “carbon neutral” concept puts biomass in a more advantageous position than fossil fuels. However, the high percentage content of moisture & physical characteristic of

Table 1: Biomass feedstock resources along with fuel analysis (M/s Sathyam Power Private Ltd.- 10 MW biomass-based power plant at Village Punjas, Tehsil Merta, Distt. Nagaur, Rajasthan, India).

S. No.	Constituents	Mustard	Jeera	Sindhi Saunf	Saunf	Cotton Stalk	Mehandi
1.	Moisture %	10.79	16	4.86	8.4	7.87	13.44
2.	Ash %	4.99	6.16	3.13	6.84	3.04	1.64
3.	Volatile matter %	65.76	77.2	81.4	78.57	82.27	78.72
4.	Fixed carbon (By difference)	18.46	0.65	10.61	6.19	6.82	6.16
5.	Carbon % by Mass	37.92	61.13	74.87	67.9	71.86	68.01
6.	Hydrogen % by Mass	6.87	5.5	5.49	5.5	5.48	5.5
7.	Oxygen % by Mass		10.85	10.25	10.64	10.28	10.26
8.	Nitrogen % by Mass	0.79	0.37	1.4	0.72	1.47	1.11
9.	Sulphur % by Mass	0.34	0.3	0.15	0.3	0.019	0.15
10.	Chlorine content % by Mass	0.16	0.14	0.07	0.16	0.007	0.014
11.	Oil content %	0.97					
12.	GCV	3760	2992	3200	3130	3925	3921

Table 2: Elemental compositions with physical properties for various types of biomass fuels (M/s Sathyam Power Private Ltd.- 10 MW biomass-based power plant at Village Punjas, Tehsil Merta, Distt. Nagaur, Rajasthan, India). Comparative analysis for elemental compositions with physical properties within biomass:

		Jeera Husk	Assaliya Husk	Sindhisva Husk	Saunf Husk
<b>A.</b>	<b>PROXIMATE ANALYSIS</b>				
1.	Gross Calorific Value (GCV) kcal.kg <sup>-1</sup>	3739.18	3973.09	4077.38	3651.06
2.	Net Calorific Value (NCV) kcal.kg <sup>-1</sup>	3617.7	3873.7	3971.7	3519.5
3.	Moisture (as received) [%]	5.28	4.32	4.61	5.72
4.	Total Ash [%]	5.62	4.96	3.89	6.98
5.	Volatile Matter [%]	79.25	83.82	79.49	80.22
6.	Fix Carbon [%]	9.85	6.89	12.01	6.31
7.	Chlorine content [%]	1.10	0.708	0.74	0.929
8.	Oil content [%]	0.482	0.628	0.082	0.766
9.	Ash Fusion temperature (°C)	1050	960	990	1055
10.	Calcium (Ca) [%]	0.549	1.82	0.6142	0.549
11.	Magnesium Oxide (MgO) [%]	0.285	0.281	0.465	0.2843
12.	Sodium (as Na <sub>2</sub> O) [%]	0.361	0.1315	0.542	0.409
13.	Potassium (as K <sub>2</sub> O) [%]	0.241	0.027	0.306	0.242
14.	Seed in the sample [%]	NIL	NIL	NIL	NIL
<b>B.</b>	<b>ULTIMATE ANALYSIS</b>				
15.	Carbon (as C) [%]	54.6	40.4	26.7	44.61
16.	Nitrogen (as N) [%]	2.8	0.87	3.61	2.17
17.	Sulphur (as S) [%]	1.7	1.3	0.71	0.55
18.	Hydrogen (as H) [%]	4.5	3.6	4.2	1.82
19.	Oxygen (as O) [%]	40.9	53.8	88.8	50.75

the ash which is produced in the steam generator should be a matter of concern & requires greater attention.

## GLOBAL SCENARIO OF BIOMASS-BASED THERMAL POWER GENERATION

Bioenergy grew by an evaluated 5 percent in 2019, dropping behind the normal annual development from 2011. In Sustainable Developments Scenarios (SDS), bioenergy production of electrical energy will rise by 6 percent annually by 2030 (Kang et al. 2020, IEA 2018).

Table 3 and Fig. 1 provide the global scenario of the utilization of biomass resources in various countries for the generation of power (electricity) and thermal energy (heat) produced from captive power plants wherein a gradual increase in its utilization is observed among most of the nations.

## INDIAN SCENARIO OF BIOMASS-BASED THERMAL POWER GENERATION

The percentage of biomass-independent power plants (IPP), Bagasse cogeneration, and non-Bagasse cogeneration power

plant are shown in Fig. 2 wherein the percentage share of bagasse-based biomass cogeneration is most prominent.

The biomass installed capacity in key Indian states is shown in Fig. 3 and Table 4. Karnataka, Uttar Pradesh, and Maharashtra are among the Indian states leading in biomass-based power plants indicating that the larger states have a greater potential for the effective utilization of their biomass residues both forest and agricultural by-products.

The State-wise installed capacity of biomass ipp/bagasse cogeneration/non-bagasse cogeneration in India is shown in Table 4.

## BIOMASS FUEL-FIRED THERMAL POWER PLANT

Among the many available technologies, the biomass-fired Steam Generator (Boiler) is the most common method and has shown the greatest potential for large-scale utilization of biomass energy, especially for power generation or the utilization of the heat produced during combustion of the biomass in a process like sugar manufacturing plant, etc. Fig.

Table 3: Technical features of biomass power and CHP plants around the world (IRENA 2015).

Country	Year	Efficiency	Capacity	
			Megawatt electric [MWe]	Megawatts thermal [MWt]
Austria	N/A		15	
Belgium	2010		24	
Denmark	2009		35	85
Finland	2002	29.9	14	28
Finland	2010	28.3	25	50
Finland	1996	23.2	17	48
Finland	1990		14	41
Germany	2002	16.5	9	
Germany	2004	19.4	20	65
Germany	2005	26.6	20	23
Germany	2009	19.0	8	30
Germany	2012		7	30
France	2010		30	
Hungary	2009		20	
Hungary	2010	31.5	50	
Ireland	2005	16.0	2.5	10
Ireland	2004	16.1	1.8	3.5
Netherlands	2002	29.9	25	
Portugal	1999	26.5	9	
Spain	2003	32.0	25	
Sweden	1982		65	129
Sweden	2009		83	200
United Kingdom	2000	32.0	38	
United Kingdom	2007	29.5	30	10
United Kingdom	2008	31.3	44	
United Kingdom	2009	36.0	14	
United Kingdom	2011		350	
United Kingdom	2012		50	
United Kingdom	2011		25	
United Kingdom	2011		40	
United Kingdom	2011		65	
United Kingdom	2012		100	
United Kingdom	2013		150	
United Kingdom	2012		295	
United Kingdom	2015		100	
Total			1905	

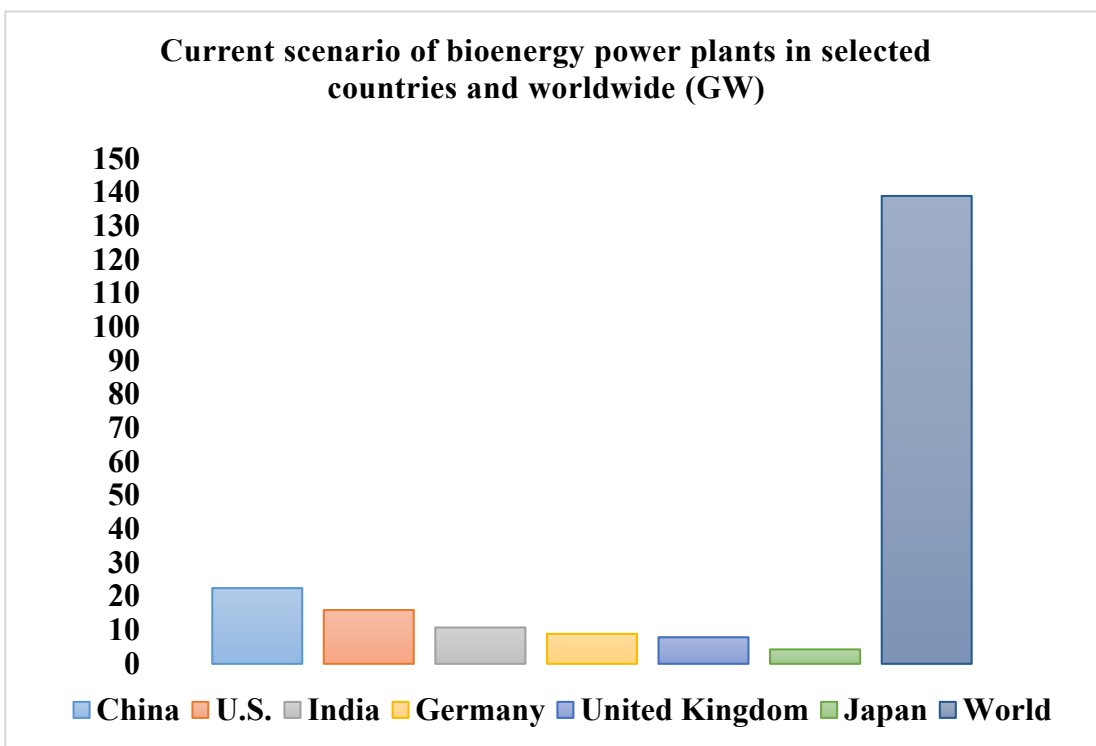


Fig. 1: Current scenario of bioenergy power plants in selected countries and worldwide (GW) (Paletto et al. 2019).

4 gives the detail of the process involved in Biomass-based Thermal Power

In the process shown in the figure above, the biomass feedstock enters the combustion chamber (furnace) of the steam generator (Boiler) along with air ( $O_2$ ) and water ( $H_2O$ ). During the combustion of the biomass feedstock, heat is produced which converts the water present inside the tubes of the boiler (water tube boiler) into steam. The steam is further routed to the steam turbine through the main steam pipeline, which makes the turbine rotor rotate. The generator, which is coupled with the steam turbine, produces electricity (Power) in this process. The hot flue gas exits the boiler into the atmosphere through the boiler chimney (De Jong & van Ommen 2014).

During the combustion process, the traditional Rankine cycle containing biomass getting burnt is utilized (oxidized) (Qiu et al. 2011, Drescher & Brüggemann 2007) to produce steam within a higher pressure boiler. The net power cycle efficiencies are approximately 23% to 25%. Steam turbine output is either completely condensed to generate power or partially or entirely utilized for several useful heating activities or in another process.

The energy conversion pathway shown in Fig. 4 is typical of a biomass-based Thermal Power Plant that was also taken

as a case study in M/s Sathyam Power Private Ltd.- a 10 MW biomass-based power plant at Village Punjas, Tehsil Merta, Distt. Nagaur, Rajasthan, India.

## BIOMASS THERMOCHEMICAL CONVERSION PROCESS- CHALLENGES

### Fuel Efficiency

Biomass fuel(s) characteristically have higher moisture content and low calorific value, which leads to a decrease in the temperature resulting in lower process efficiency. Moreover, the presence of alkali and chlorine in biomass fuel causes slagging on the heating surfaces of the equipment used for conversion (boiler for direct combustion, pyrolyzer for pyrolysis, or gasifier in case of biomass gasification process) which further leads to corrosion of the equipment surfaces.

However, the intangible benefits associated with biomass fuel should also be considered which ultimately increases the profitability of the plant operator:

Biomass is a renewable form of energy source which is replenishable.

The cost of biomass residual fuel is very low compared to fossil fuel.

Table 4: State-wise installed capacity of biomass (Garg &amp; Sharma 2020).

State/ Union Territories	Biomass Independent Power Production [In MW]	Bagasse Cogeneration [In MW]	Non-Bagasse Cogeneration [In MW]	Cumulative Installed Capacity (As of 31.12.2019)
1	2	3	4	5
Andhra Pradesh	171.2	206.9	105.57	483.67
Arunachal Pradesh	-	-	-	0
Assam	-	-	2	2
Bihar	12	100.5	12.2	124.7
Chhattisgarh	222.4	20	2.5	244.9
Goa	-	-	-	0
Gujarat	44.5	20.8	12	77.3
Haryana	19.4	102	89.26	210.66
Himachal Pradesh	-	-	9.2	9.2
Jammu & Kashmir	-	-	-	0
Jharkhand	-	-	4.3	4.3
Karnataka	137.3	1729.8	20.2	1887.3
Kerala	-	-	2.27	2.27
Madhya Pradesh	92.5	0	14.847	107.347
Maharashtra	217	2351	16.4	2584.4
Manipur	-	-	-	0
Meghalaya	-	-	13.8	13.8
Mizoram	-	-	-	0
Nagaland	-	-	-	0
Orissa	50.4	-	8.82	59.22
Punjab	138.5	161	173.95	473.45
Rajasthan	114.3	4.95	2	121.25
Sikkim	-	-	-	0
Tamil Nadu	218.7	750.4	43.55	1012.65
Telangana	60.1	98	2	160.1
Tripura	-	-	-	0
Uttar Pradesh	28	1929.5	159.76	2117.26
Uttarakhand	0.12	72.6	57.5	130.22
West Bengal	300	-	19.2	319.92
Total	1826.42	7547.45	772.047	10145.917

The environmental impacts especially associated with the environmental emissions are very low compared to conventional fossil fuel-based systems.

Thermochemical biomass-based technologies can very effectively utilize the agricultural & forest wastes by controlled combustion of the same which otherwise would be required to be burnt in the open in an uncontrolled manner leading to air pollution & deterioration of the environment.

### Environmental Impacts

With reference to the emission of CO<sub>2</sub> and other Green House Gases (GHGs) for biomass-based power generating systems, since CO<sub>2</sub> produced during its combustion is absorbed during photosynthesis which greatly reduces CO<sub>2</sub> emissions per unit of energy produced.

Moreover, the calorific value of agro-residue pellets is comparable to bituminous coal. Thus, technically, it can



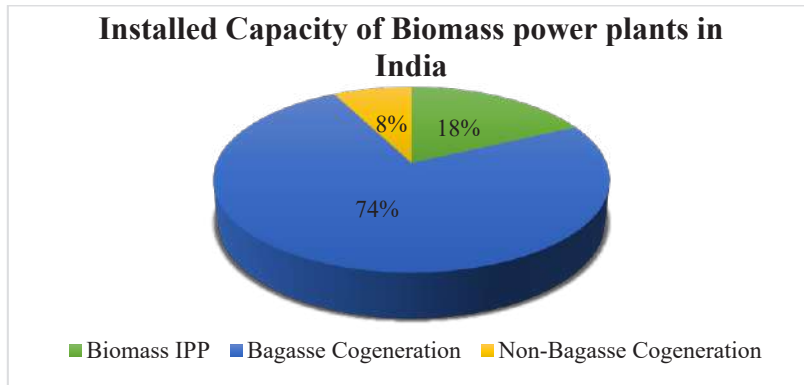


Fig. 2: Installed capacity of biomass power plants in India (Garg & Sharma 2020).

directly reduce the dependency on coal (fossil fuel) as an alternative to coal.

Additionally, systematic collection, segregation & rational distribution of biomass residue from the point of generation would also help to tackle the uncontrolled burning of agricultural residue in the open, which leads to the emission of

GHGs in large quantities into the atmosphere. This can also help to control air pollution to a greater extent.

**Supply Chain and Logistics of Biomass Fuel**

The handling and delivery of biomass fuel are different compared to fossil fuel (especially coal) as it is large in vol-

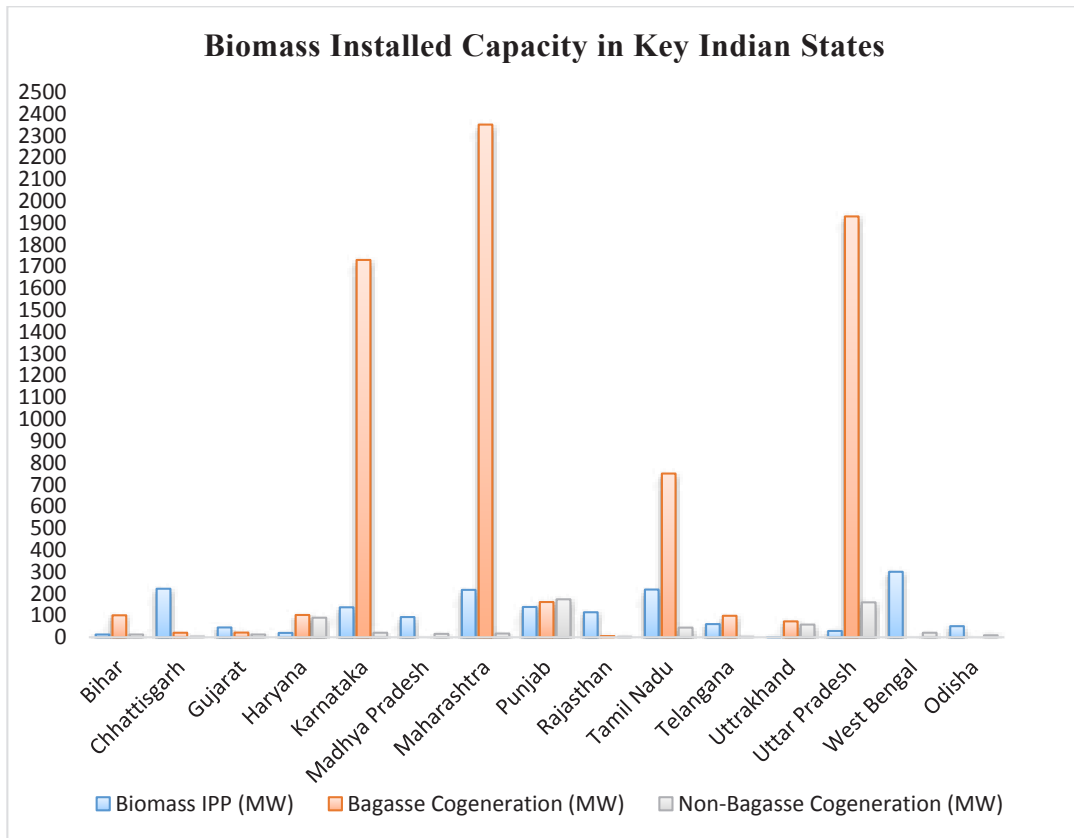


Fig. 3: Biomass installed capacity in the key Indian States (Garg & Sharma 2020).

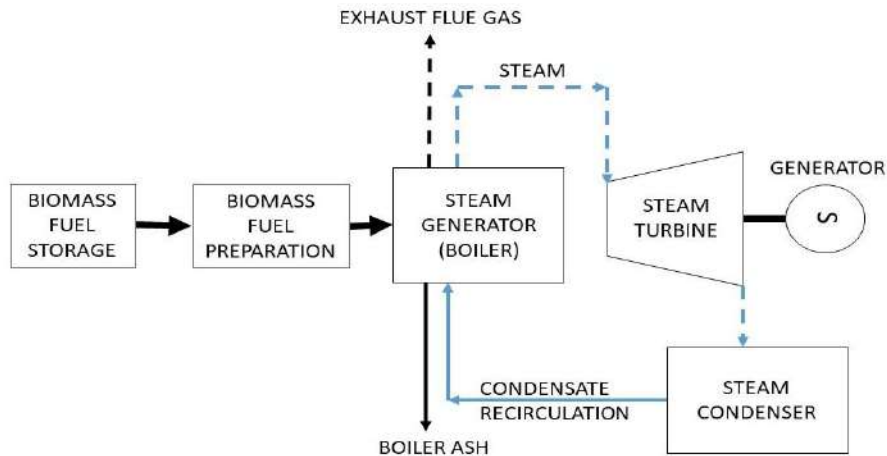


Fig. 4: Energy conversion pathway in a direct combustion biomass fired thermal power plant.

ume and its sources are scattered, so it is difficult to form a long-term stable acquisition of the fuel. The transportation, storage, and handling of the biomass pose some challenges as given below:

Due to its geographically scattered availability throughout the country, transporting the suitable biomass to the respective thermal power plants with the optimum mode of transportation is a challenge.

Dedicated fire preventive measures should be ensured, as it is highly inflammable more often due to the creation of methane gas because of the presence of microbes in the biomass residue.

The low density and high-volume nature of the biomass fuel require comparatively larger storage areas, which are required to be covered because of its hygroscopic nature.

The conveyer and storage facility should be covered adequately to restrict the spread of germs and dust into it. In addition, biomass fuel is required to be prevented from the ingress of water, which may lead to degradation of the quality of the fuel.

It is necessary to maximize the size of the storage. A bigger storage facility is also chosen because it encourages larger volumes to be bought at a sole time, resulting in a cheaper single price. In addition, it provides more suppleness in distribution preparation as well, and in the event of delayed delivery, acts as a replacement buffer.

Another critical aspect of dry biomass consideration is providing proper ventilation for avoiding condensation and mold protection, which can pose a significant health threat to spores when inhaled, as well as facilitating further drying and reducing the decay of biomass, which can result in the loss of energy content. To avoid high temperatures from be-

coming a fire threat, adequate ventilation is also necessary. The formation of carbon monoxide and other toxic gases is another threat that can be avoided by adequate ventilation.

## CONCLUSION

With growing advancements in the power industry, renewable energy gained rapid prominence in terms of the feasible solution against environmental problems like depletion of fossil fuels, high pollution, and contamination levels, global climate changes, effect on living beings, and also fulfilling the increasing demand of power (electricity), heat or alternative liquid fuels required by the growing population. Biomass is a high potential renewable resource that could be very effectively utilized for the sustainable production of energy.

Biomass energy is based on the idea that living organisms, such as plants and animals, consume  $\text{CO}_2$  from the atmosphere as they develop. As a result, when they are burnt, the amount of carbon released into the atmosphere is equal to the amount taken out earlier, a mechanism that could be termed carbon neutral. Thus, the agricultural/ forest residual waste which otherwise is burnt in an uncontrolled manner by the farmers could be efficiently utilized as biomass fuel. This approach would be cost-effective and provide sustainable waste management for the long-term renewable energy goals as well.

## REFERENCES

- Berndes, G. 2002. Bioenergy and water—the implications of large-scale bioenergy production for water use and supply. *Glob. Environ. Change*, 12(4): 253-271.
- Change, I.C. 2014. Mitigation of Climate Change. Contribution of Working Group III to the Fifth Assessment Report of the Intergovernmental Panel on Climate Change, 1454.

- De Jong, W. and van Ommen, J.R. 2014. Biomass as A Sustainable Energy Source for the Future: Fundamentals of Conversion Processes. John Wiley and Sons, New York.
- Drescher, U. and Brüggemann, D. 2007. Fluid selection for the Organic Rankine Cycle (ORC) in biomass power and heat plants. *Appl. Thermal Eng.*, 27(1): 223-228.
- Garg, J. and Sharma, S. 2020. Environmental Impact and Challenges Associated with Bio-Based Energy. In Pathak, P. and Srivastava, R. R. (eds), *Alternative Energy Resources*, Springer, Cham, pp. 273-292.
- Goyal, S.P. 2015. Press Information Bureau Government of India Ministry of Power Government India, Ministry Road Transport Highway, pp.1-3.
- IEA. 2018. World Energy Outlook 2018, IEA, Paris <https://www.iea.org/reports/world-energy-outlook-2018>
- IRENA. 2015, Biomass for Heat and Power Technology Brief. <https://www.irena.org/publications/2015/Jan/Biomass-for-Heat-and-Power>.
- Jack, T.A. and Oko, C.O.C. 2018. Exergy and exert economic analysis of a municipal waste-to-energy steam reheat power plant for Port Harcourt city. *Int. J. Ambient Energy*, 39(4): 352-359.
- Johnson, E. 2009. Goodbye to carbon-neutral: Getting biomass footprints right. *Environ. Impact Assess. Rev.*, 29(3): 165-168.
- Joshi, P. and Beck, K., 2018. Democracy and carbon dioxide emissions: assessing the interactions of political and economic freedom and the environmental Kuznets curve. *Energy Res. Social Sci.*, 39: 46-54.
- Kang, Y., Yang, Q., Bartocci, P., Wei, H., Liu, S.S., Wu, Z., Zhou, H., Yang, H., Fantozzi, F. and Chen, H. 2020. Bioenergy in China: Evaluation of domestic biomass resources and the associated greenhouse gas mitigation potentials. *Renew. Sustain. Energy Rev.*, 127:109842.
- Kumar, R. 2017. A critical review on energy, exergy, exergoeconomic and economic (4-E) analysis of thermal power plants. *Eng. Sci. Technol. Int. J.*, 20(1): 283-292.
- Ministry of Power (MOP). 2021. Revised policy for Biomass Utilization for Power Generation through co-firing in Coal-Based Power Plants. Government of India. File No- 11/86/2019- Th.II dated 8<sup>th</sup> October 2021. [https://powermin.gov.in/sites/default/files/Revised\\_Biomass\\_Policy\\_dtd\\_08102021.pdf](https://powermin.gov.in/sites/default/files/Revised_Biomass_Policy_dtd_08102021.pdf) last accessed on 29<sup>th</sup> November 2021.
- Mishra, U.C. 2004. Environmental impact of coal industry and thermal power plants in India. *J. Environ. Radioact.*, 72(1-2): 35-40.
- Nakada, S., Saygin, D. and Gielen, D. 2014. Global Bioenergy Supply And Demand Projections: A Working Paper For REmap 2030. International Renewable Energy Agency (IRENA), pp.1-88.
- Paletto, A., Bernardi, S., Pieratti, E., Teston, F. and Romagnoli, M. 2019. Assessment of the environmental impact of biomass power plants to increase the social acceptance of renewable energy technologies. *Helvion*, 5(7): p.e02070.
- Qiu, G., Liu, H. and Riffat, S. 2011. Expanders for micro-CHP systems with organic Rankine cycle. *Appl. Thermal Eng.*, 31(16): 3301-3307.
- Ragauskas, A.J., Williams, C.K., Davison, B.H., Britovsek, G., Cairney, J., Eckert, C.A., Frederick, W.J., Hallett, J.P., Leak, D.J., Liotta, C.L. and Mielenz, J.R. 2006. Biofuels Biomater. Sci., 311(5760): 484-489.
- Ramirez Pons, J. 2021. Evaluation of the coal plant closure policy. Application to the case of the Alcludia plant. Bachelor's Thesis, Universitat Politècnica de Catalunya.
- Reddy, B.S. 2018. Economic dynamics and technology diffusion in the Indian power sector. *Energy Policy*, 120:425-435.
- Tauro, R., García, C.A., Skutsch, M. and Masera, O. 2018. The potential for sustainable biomass pellets in Mexico: An analysis of energy potential, logistic costs, and market demand. *Renew. Sustain. Energy Rev.*, 82: 380-389.
- Walther, G.R., Post, E., Convey, P., Menzel, A., Parmesan, C., Beebee, T.J., Fromentin, J.M., Hoegh-Guldberg, O. and Bairlein, F. 2002. Ecological responses to recent climate change. *Nature*, 416(6879): 389-395.





# Applications of Marginal Abatement Cost Curve (MACC) for Reducing Greenhouse Gas Emissions: A Review of Methodologies

A. S. Nur Chairat\*, L. Abdullah\*†, M. N. Maslan\* and H. Batih\*\*

\*Faculty of Manufacturing Engineering, Universiti Teknikal Malaysia Melaka, Durian Tunggal 76100, Malaysia

\*\*Institut Teknologi PLN, Jakarta 11750, Indonesia

†Corresponding author: L. Abdullah; lokman@utem.edu.my

Nat. Env. & Poll. Tech.  
Website: [www.neptjournal.com](http://www.neptjournal.com)

Received: 23-07-2021

Revised: 04-10-2021

Accepted: 06-10-2021

## Key Words:

Marginal abatement cost curve  
Greenhouse gas emissions  
GHG analytic dimensions

## ABSTRACT

A wide range of Marginal Abatement Cost Curve (MACC) methods for reducing greenhouse gas (GHG) emissions has been introduced in various academic literature in the last decade to address various issues, to use different calculable logic, producing different results and implications. A detailed review has not been carried out on the application of MACC in terms of types of emissions, country/sector, and methodology used. This study is aimed at identifying, interpreting, and clarifying currently available literature on MACCs development from 2010-2020 by reviewing the previous applicability of three analytic dimensions including Greenhouse Gas (GHG) emission type, research objects, and modeling methodologies from top-down and bottom-up methods, providing researchers with information of past developments and future trends in this area. The result shows that CO<sub>2</sub> is one of the most studied GHG emissions in calculating marginal abatement costs and some countries/regions have not received much attention from researchers in assessing emission reductions. Finally, the MACC bottom-up methodology focuses on the application of the engineering model method and the distance function method is a favorite in the application of the top-down method. Furthermore, this study also highlights possible research opportunities, which may lead to more successful and impactful results in future MACC studies.

## INTRODUCTION

Over time, climate change has put a number of pressures on people's lives and in particular on the environment, leading to global warming (Grigoroudis et al. 2016, Gu & Wang 2018, Sununta et al. 2019). Governments around the world have made commitments to avoid serious climate change, by taking measures to reduce emissions of greenhouse gases (GHG) to stabilize the global average temperature rise to "well below" two degrees Celsius compared to temperature levels of the pre-industrial age (Talaui et al. 2020, UNFCCC 2015). To achieve this global target, an acceptable abatement plan must be developed to greatly reduce the total emission reduction costs. Estimating GHG abatement costs can help the government and firms make reasonable policy decisions. One tool for examining the relationship between environmental policy and technical change is the marginal abatement cost curve (MACC or MAC curve) (Ibrahim & Kennedy 2016, Kesicki 2013). Marginal abatement cost curves are a useful tool, which has been developed a lot over the last 20 years, for evaluating CO<sub>2</sub> mitigations options and comparing different abatement measures, and representing information on abatement costs of specific technology and potentials for a set of mitigation measures (Chen 2018, Ol-

iveira et al. 2015). Abatement cost is one of the fundamental criteria which provide policymakers with intuitive cognition of economic perspective (Teng et al. 2014). A MAC curve plots the shadow price corresponding to an emission constraint of increasing severity against the quantity abated and that cost curves are unique for each country and show the relationship between reduction in emissions and the marginal cost per unit of abatement (Juntueng et al. 2020, Zhang et al. 2017). A positive MAC value indicates that there is a cost to reducing emissions relative to the baseline, while a negative MAC value indicates a benefit in reducing GHG emissions relative to the baseline (Eory et al. 2013).

For global and country-specific scenarios, several studies have applied this tool for technology assessment and for comparing projects and opportunities for mitigation of GHG emissions (Lee & Wang 2019, Vogt-Schilb & Hallegatte 2011). Several applications of the MAC curve are found in the power sector, building, agriculture, shipping, residence, transport, and policy-making (Jones 2014, Luu et al. 2018). Its growing popularity is mainly due to its simplified representation of the complex relationship between emissions abatement efforts and the marginal cost of cutting one unit of CO<sub>2</sub> emissions (Sjostrand et al. 2019).



## CONCEPT OF MARGINAL ABATEMENT COST

The implication of estimating environmental costs per unit of product is to estimate the amount of MAC charged to each unit of product, meaning how much is the contribution (share) of one unit of product in reducing the amount of waste discharged into the environment (et al. 2016). Marginal cost is a decrease or increase in the total cost paid due to the addition or subtraction of one additional unit of product. The MAC is constructed to show the quantity of greenhouse gas (GHG) that can be abated with their comparable costs relative to a reference technology. Abatement cost calculation has been based on comparisons of different technology costs and emissions relative to BAU or baseline/reference model that is stated in the following general formula:

$$MAC = \frac{(Cost\ of\ GHG\ Mitigation\ Option - Cost\ of\ GHG\ BAU\ Model)}{(GHG\ Emission\ from\ BAU\ Model - GHG\ Emission\ from\ Mitigation\ Option)}$$

where,

$$Cost\ of\ GHG\ Mitigation\ Option = \sum_{i=1}^n (Capex_i + Opex_i) / (1 + funding\ cost)^{year\ of\ depreciation}$$

MAC uses the sum of capital expenditure (Capex) and operational expenditure (Opex) for each energy end-use were estimated based on the technology cost (González-Mahecha et al. 2019). Once the technical mitigation potential and marginal abatement cost have been quantified for each measure, the measures are then grouped and ranked based on their cost-effectiveness. The mitigation measures are ranked from left to right along the x-axis from the lowest to the highest MAC and the y-axis shows the cost per tonne of CO<sub>2</sub> equivalent (tCO<sub>2</sub>e) reduced (Selvakkumaran & Lim-meechokchai 2017). The key principle is that technologies should only be used when the abatement costs are lower than those of other mitigation strategies. The curves can be viewed as guidance for firms, entrepreneurs, and government officials contingent upon the degree of accumulation of the amount of GHGs abated by each measure represented. It also unmistakably shows which is the following, more costly technology that should be applied to obtain an extra abatement.

## CLASSIFICATION OF MACC METHOD

At the national, company, or level of society, the MACC can be developed using three methods: top-down/non-model-derived, bottom-up/model-derived, and hybrid (Tang et al. 2020). Each method has different advantages and disadvantages that may address the various concerns. For example, a high degree of technological detail becomes the major advantage of the bottom-up method, while it has a disadvantage which does not capture system-wide interactions, behavioral aspects are neglected, the baselines may be inconsistent and reduction potential double counted (Delarue et al. 2010,

Kesicki & Strachan 2011, Wächter 2013). The top-down approach for the sectorial level could be used to assess how markets address exogenous pressures, including an undertaken or pending policy action and its consequences for a system (Levihn et al. 2014), but are often required sophisticated financial modeling used to predict the emissions and costs of different policies so that they constitute a compromise and do not correspond to empirical relationships (Huang et al. 2016, Levihn et al. 2014). The hybrid method unites the strength characteristics of the top-down and bottom-up methods, however, due to high data requirements and the complexity of the quantification process, the hybrid approach has not been widely used (Jiang et al. 2020, Tanatvanit et al. 2004).

### Bottom-up Method

The bottom-up method estimates the MACC according to different policies and technology for mitigation (Bockel & Sutter 2012). This approach is focused on the choice of energy and technology, and cannot simulate the impact of energy price changes, factor prices, and other intermediate input costs; the production function model focuses on estimating the historical MAC, while it cannot simulate the policy change (Baker & Barron 2013, Tang et al. 2020). Fig. 1 displays an example graph of MACC, whereas top-down models often use piecewise-smooth functions and bottom-up models use a step function (Kiuila & Rutherford 2013). Many studies have investigated CO<sub>2</sub> emissions abatement strategies using the bottom-up approach with different applications and results, especially for countries and sectors level (Fan et al. 2017).

### Top-down Method

Contrary to the bottom-up approach, which emphasizes the comprehensive technology portfolio, the top-down approach concentrates on evaluating the cost of potential opportunities for a certain reduction objective, while disrupting production processes, responding to market behavior, obtaining hidden costs for producers and customers, and catching the price rebound effects (Huang et al. 2016). Table 1 shows the differences between the two methods. Furthermore, the top-down model can be divided into the microeconomic supply model and the Computable General Equilibrium (CGE) model which measures the impact of reductions in prices and general market behavior (Löffler & Hecking, 2016). The distance function is one of the micro-economic models that are widely used for constructing a production feasible set (or production frontier) subject to technical and economic conditions, to derive the shadow prices (or opportunity cost) of abating an additional unit of undesirable output in many

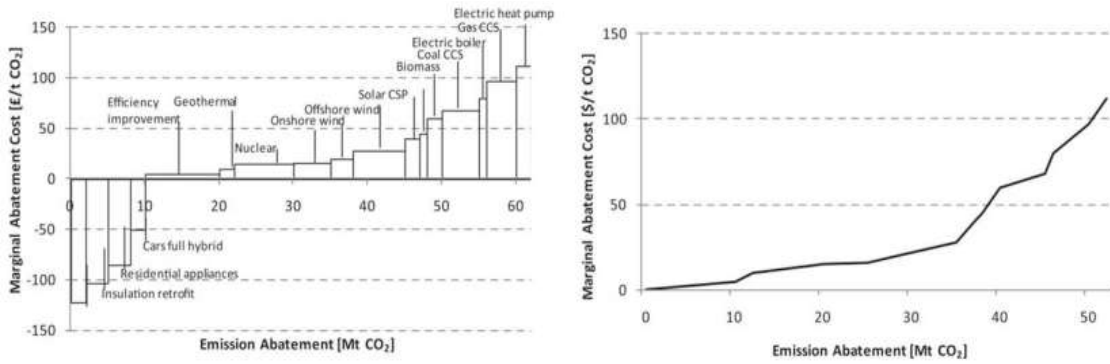


Fig. 1: Different MAC Curves using bottom-up method (left) and top-down method (right) (Kesicki & Ekins, 2012).

Table 1: Main differences in Bottom-up and Top-down methods.

Bottom-up Method	Top-down Method
Developed based on expert (scientific) judgment	Developed based on system modeling (MACC for energy system)
Presenting details of each mitigation option/technology	Modeling is considering energy supply and demand system
Not considering interactions between mitigation options, or supply & demand systems	Accommodating the development of mitigation options in the form of scenarios

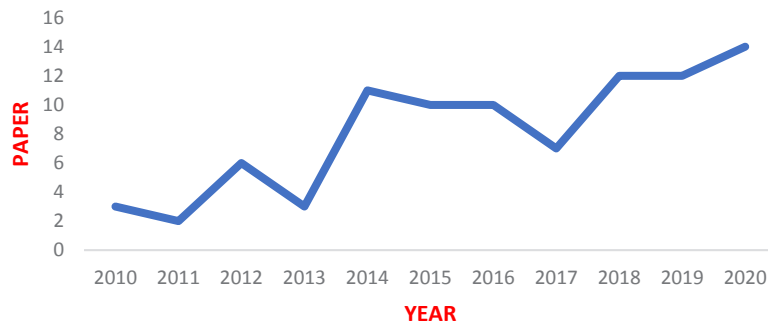


Fig. 2: Trends in MACC's research publications.

applications and locations (Chen 2015, Sala-Garrido et al. 2021).

eling methodologies which will be further elaborated as follow.

**MACC'S SCOPE OF APPLICATIONS**

MACC has since become increasingly widely used in particular regions, countries, industries, and/or pollutants (Eory et al. 2018). The timeframe, journal types, and keywords were identified for the literature collection framework. Literature published from 2010 to 2020 was the subject of attention. Fig. 2 shows the increasing number of MACC research publications in international journals. This study concentrates on central articles relevant to specific MACC using the top-down and bottom-up methods totaling 83 papers (Fig. 3) and explores the applicability of the first and second approaches through three analytic dimensions including GHG emission type, research objects, and mod-

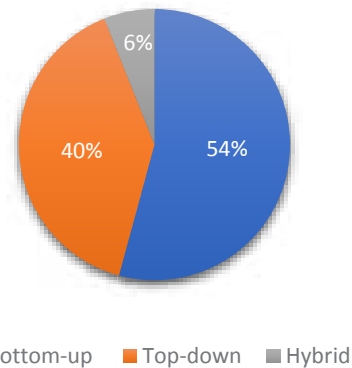


Fig. 3: MACC's research publications by methods.

**Applications on GHG Emissions**

Among the studies on the top-down and bottom-up methods, CO<sub>2</sub> is one of the most studied GHG emissions in calculating marginal abatement costs because it is the primary GHG that accounts for around three-quarters of emissions and is becoming an increasingly global focus. Many researchers quantified the CO<sub>2</sub> MAC in various sectors and used different modeling methodologies to develop MACCs. The MACC also enables a better understanding of the reduction potential for non-CO<sub>2</sub> sources and the incorporation in the economic modeling of non-CO<sub>2</sub> GHGs reductions, such as CH<sub>4</sub> or N<sub>2</sub>O (Verma et al. 2015). For non-CO<sub>2</sub> gas, a single optimized MACC technology-specific was developed by using boiler-level data as input for an integer linear program, minimizing system-wide cost control by ensuring an optimum distribution of NO<sub>x</sub> controls over the modeled detailed boiler specification (Vijay et al. 2010).

**Applications on Countries and Sectors**

Any research related to calculating the marginal cost of emission abatement always requires a research object in the form of a sector or country. The following figure shows

the total number of sectors and countries used as research objects in developing MACC from 2010 to 2020 (Fig. 4 and Fig. 5). The MAC calculation of a country or province is the most studied (20.5%), followed by the residence and building sector (14.5%), and power generation (13.3%). For example, the CO<sub>2</sub>, SO<sub>2</sub>, and NO<sub>x</sub> MACs are estimated from 2006–2014 through the shadow price framework for 105 Chinese urban areas (Ji & Zhou 2020). In European territory, the evaluation of planned development of the South/Central Stockholm District Heating network and potential mitigation options was analyzed by exploring the dynamic, path-dependent aspects (Levihn et al. 2014). Other researchers have also tried to evaluate and develop MACC in multi-sectors (12.1%) using top-down and bottom-up methods. MACC has also been applied to approximate global emission abatement, although the publication is running at a slow pace (3.6%).

In addition, other sectors, such as transportation, agriculture, oil, and infrastructure are starting to be researched on abating emissions to meet national emission reduction targets. The agricultural sector is the world’s second-largest emitter, after the energy sector (which includes emissions from power generation and transport). Scientists have also evaluated emission reductions in certain sectors that have

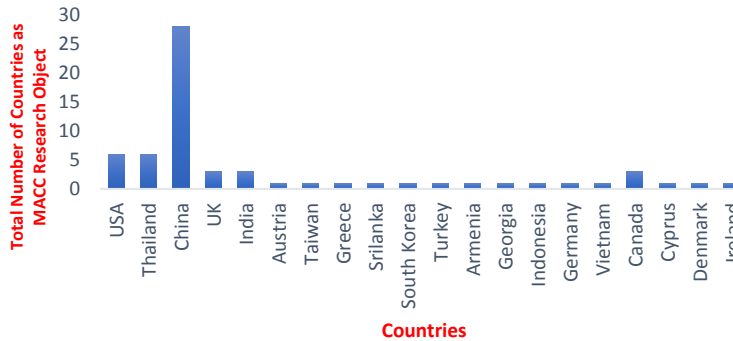


Fig. 4: MACC’s Research Publications by country.

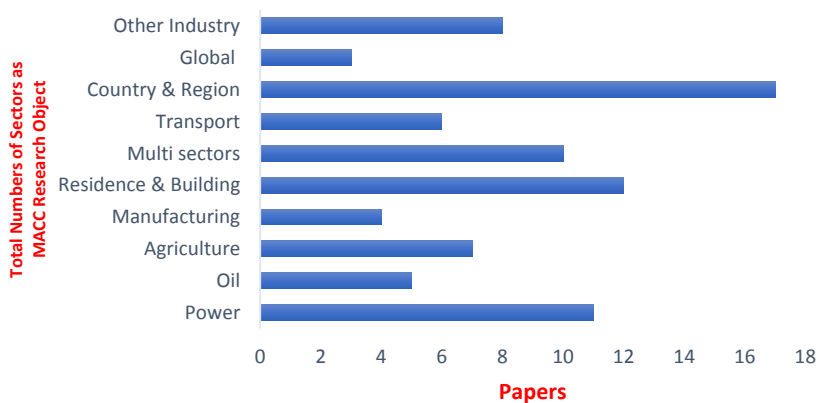


Fig. 5: MACC’s research publications by sector.

not been described in the previous points, such as maritime shipping or livestock (Schwartz et al. 2020).

**Applications with MACC Methodologies**

When scientists use top-up or bottom-up methods, the development of modeling scenarios should be further translated into a modeling methodology (Hasler et al. 2019, Mosnier et al. 2019). Assumptions and costs of the reduction measures are set up to generate marginal technologies costs and their potential to reduce GHG emissions (Marinoni & Grieken 2015). Ibrahim & Kennedy’s (2016) work is an example of bottom-up financial accounting methods. The technologies considered in their study are analyzed based on a Net Present Value (NPV) methodology that considers the prices of electricity, fuel, and energy in each city. There are still several research publications that include how the application of the NPV method for generating the MACC and this method is increasingly popular for private investors because of its simplicity in calculations and its capability to classify cost-effective measures.

The bottom-up engineering models approach has a riches of detailed energy system technical specifications and is better positioned to optimize the portfolio of options and minimize system cost. MARKAL studies that analyze MAC using typical bottom-up modeling are commonly used. In the transportation and residential sector, the MARKAL model was used to find the cost and potential abatement in the UK to overcome the shortcomings of existing approaches. Low Emission Analysis Platform (LEAP) is another energy model used to assess to evaluate the potential long-term potential and marginal costs of cogenerated electricity in the oil sands sector by means of a new combined market penetration model and bottom-up energy system modeling framework.

The CUECost model was implemented to create supply curves for pollution abatement using boiler-level data that explicitly accounts for technology cost and performance in the USA power sector (Vijay et al. 2010). The TIMES-GEECO model is an abbreviation of TIME’s model generator for “TIMES Gauteng Energy and Emission Cost Optimization”. For the Korean power sector, The Model for Energy Transi-

tion and Emission Reduction (METER), is used to derive the MACCs because it conveys very well the features of Korea’s energy system than any other model and is flexible enough to enable us to perform different analyses (Ahn & Jeon 2019). Mitigation measures in the Agriculture, Forestry and Other Land Use (AFOLU) sector used the AFOLU bottom-up (AFOLUB) model to estimate GHG emissions.

Top-down methods can be further divided into the distance function method and the CGE model (Wang et al. 2018). Numerous scholars prefer the distance function approach, which leads to several relevant studies. In particular, the measurement using the distance function can be constructed by using the parametric Stochastic Frontier Analysis (SFA) method or the non-parametric Data Envelopment Analysis (DEA) method. Parametric DDF was also used to propose a new method to estimate CO<sub>2</sub> mitigation costs for 46 firms in the USA (Wang et al. 2018). For the chemicals industry, a MACC is created for energy-saving measures in Germany, quantifying the uncertainties in the results and identifying key input parameters. An example of a Non-parametric DDF was implemented to determine what factors will affect a change in the marginal abatement cost on allocating the burden of the emissions reduction for 30 provinces in China. Although the top-down method with DDF has experienced growth in research publications over the last 5 years, several studies have also accommodated the creation of MACC with the CGE model.

**SUMMARY AND RESEARCH OPPORTUNITIES**

By consolidating the previous MACC research, several things have been the focus of previous MACC research (Table 2). First, among all GHG emissions, researchers only consider the CO<sub>2</sub> emissions (82.89%), which are the main emissions from the industry and becoming a global concern. Second, some countries/regions have not received much attention from researchers in assessing emission reductions and identifying specific technologies used. The final summary is the MACC bottom-up methodology focuses on the application of the engineering model method (46.05%) and the distance function method (34.21%) is a favorite in the application of the top-down method.

Table 2: Summary of emission, research object, and methodology in MACC researches.

	Emission Scope			Research Object		Methodology			
	CO <sub>2</sub>	Non-CO <sub>2</sub>	Mixed	Industry/Firm	Country/Region	Finance-Accounting	Engineering Model	Distance Function	CGE
Count	63	9	4	64	12	13	35	26	2
%	82.89	11.84	5.26	84.21	15.79	17.11	46.05	34.21	2.63

Based on summarizing part above, these are the following trends and possible research opportunities in MACC generation using the top-down and bottom-up methods:

- (i) Scientists have focused a lot on the residence, building, power, transport, or agriculture sector in building MACC (Taylor 2012). There are still other sectors that produce GHG emissions, but further research is needed, for example, the palm oil sector is one of the plantation commodities that is much needed by the global industrial sector.
- (ii) Current literature works are that the greater part of the research on the MACC of CO<sub>2</sub> only focused on regions and industries while few studies take a worldwide viewpoint. The MAC on GHG emissions from a global perspective needs and must be studied to obtain world environment sustainability (Akimoto et al. 2014, Hanaoka & Kainuma 2012).
- (iii) Even though China is the largest GHG emitter country, there is still a need for a more country-specific MACC analysis, especially for developing countries, such as India, Indonesia, or African countries (Gore & Annachatre 2017). Extension to developing countries would bring greater challenges to MAC research.
- (iv) Both top-down and bottom-up methods have been widely applied with a variety of modeling systems and have seen a drastic increase in MACC research publications. The above models can be improved in all areas, such as developing abatement option-specific information on the complexities that are associated with the implementation.
- (v) Low-cost mitigation solutions sound appealing, but there is reason to believe they are not the simplest to apply and policymakers are led to believe that the cheapest technology options are always the best options to realize, the reality proved to be different, however (Chappin et al. 2020). There is an opportunity to combine MACC with other decision support system tools e.g., Multi-Criteria Decision Analysis (MCDA) as a complementary tool alongside MAC curves.

## CONCLUSION

This paper provides a review of MACC applications from its methodologies point of view, in particular top-down and bottom-up methods. The focus of this study is on central international articles and the top-down and bottom-up MACC method with a total of 83 papers. This paper also looks at three analytical dimensions, including GHG emissions type, sectors and countries as research objects, and modeling methodologies, for the applicability of those

three approaches. MACCs are powerful instruments for understanding environmental policy and technological changes. When looking at the various ways that the MAC curve can impact different technologies, one can gain insights that can inform technology policy and emission policies. Furthermore, this study highlights the possible research opportunity, which may lead to more successful and interesting results for future MAC studies.

## ACKNOWLEDGEMENT

The authors would like to acknowledge the support of the Faculty of Manufacturing Engineering, Universiti Teknikal Malaysia Melaka and we express our sincere gratitude to the Research Center (LPPM) of Institut Teknologi PLN for its cooperation in providing the funds used.

## REFERENCES

- Ahn, Y. and Jeon, W. 2019. Power sector reform and CO<sub>2</sub> abatement costs in Korea. *Energy Policy*, 131: 202-214.
- Akimoto, K., Sano, F., Homma, T., Tokushige, K., Nagashima, M. and Tomoda, T. 2014. Assessment of the emission reduction target of halving CO<sub>2</sub> emissions by 2050: Macro-factors analysis and model analysis under newly developed socio-economic scenarios. *Energy Strat. Rev.*, 2(3-4): 246-256.
- Ariani, M., Setyanto, P. and Ardiansyah, M. 2016. Marginal abatement cost of greenhouse gas (GHG) emissions from the agricultural sector in Grobogan and East Tanjung Jabung regencies. *J. Environ. Sci.*, 14(1): 39-49.
- Baker, E. and Barron, R. 2013. *Technological Change and the Marginal Cost of Abatement*. Elsevier Inc, Amsterdam.
- Bockel, L. and Sutter, P. 2012. Using Marginal Abatement Cost Curves to Realize the Economic Appraisal of Climate Smart Agriculture Policy Options. Food And Agriculture Organization of the United Nations.
- Chappin, E.J.L., Soana, M., Arensman, C.E. and Swart, F. 2020. The Y factor for climate change abatement: A method to rank options beyond abatement costs. *Energy Policy*, 147: 605.
- Chen, C.C. 2015. Assessing the pollutant abatement cost of greenhouse gas emission regulation: A case study of Taiwan's freeway bus service industry. *Environ. Resour. Econ.*, 61(4): 477-495.
- Chen, J. 2018. Carbon efficiency and carbon abatement costs of coal-fired power enterprises : A case of Shanghai, China. *J. Clean Prod.*, 11: 64
- Delarue, E.D., Ellerman, A.D. and D'haeseleer, W.D. 2010. Robust MACCs? The topography of abatement by fuel switching in the European power sector. *Energy*, 35(3): 1465-1475.
- Eory, V., Pellerin, S., Carmona Garcia, G., Lehtonen, H., Licite, I., Mattila, H., Lund-Sørensen, T., Muldowney, J., Popluga, D., Strandmark, L. and Schulte, R. 2018. Marginal abatement cost curves for agricultural climate policy: State-of-the-art, lessons learned and future potential. *J. Clean Prod.*, 182: 705-716.
- Eory, V., Topp, C.F.E. and Moran, D. 2013. Multiple-pollutant cost-effectiveness of greenhouse gas mitigation measures in the UK agriculture. *Environ. Sci. Policy*, 27: 55-67.
- Fan, Y., Peng, B. and Bin, X.J.H. 2017. The effect of technology adoption on CO<sub>2</sub> abatement costs under uncertainty in China's passenger car sector. *J. Clean Prod.*, 154: 578-592.
- González-Mahecha, R.E., Lucena, A.F.P., Garaffa, R., Miranda, R.F.C., Chávez-Rodríguez, M., Cruz, T., Bezerra, P. and Rathmann, R. 2019. Energy & buildings greenhouse gas mitigation potential and abate-



- ment costs in the Brazilian residential sector. *Energy Build.*, 184: 19-33.
- Gore, M. and Annachatre, M. 2017. GHG abatement costs and potentials: An opportunity benefit for India through clean development mechanism (CDM). 2017 IEEE International Conference on Smart Grid and Smart Cities, pp. 78-83.
- Grigoroudis, E., Kanellos, F. D., Kouikoglou, V. S. and Phillis, Y. A. 2016. Optimal abatement policies and related behavioral aspects of climate change. *Environ. Develop.*, 19: 10-22.
- Gu, G. and Wang, Z. 2018. Research on global carbon abatement driven by R & D investment in the context of INDCs. *Energy*, 148: 662-675.
- Hanaoka, T. and Kainuma, M. 2012. Low-carbon transitions in world regions: Comparison of technological mitigation potential and costs in 2020 and 2030 through bottom-up analyses. *Sustain. Sci.*, 7(2): 117-137.
- Hasler, B., Hansen, L.B., Andersen, H.E. and Termansen, M. 2019. Cost-effective abatement of non-point source nitrogen emissions: The effects of uncertainty in retention. *J. Environ. Manag.*, 246: 909-919.
- Huang, S.K., Kuo, L. and Chou, K. 2016. The applicability of marginal abatement cost approach : A comprehensive review. *J. Clean Prod.*, 127: 59-71.
- Ibrahim, N. and Kennedy, C. 2016. A methodology for constructing marginal abatement cost curves for climate action in cities. *Energies*, 9(4): 227.
- Ji, D.J. and Zhou, P. 2020. Marginal abatement cost, air pollution, and economic growth: Evidence from Chinese cities. *Energy Econ.*, 86: 104658.
- Jiang, H.D., Dong, K.Y., Zhang, K. and Liang, Q.M. 2020. The hotspots, reference routes, and research trends of marginal abatement costs: A systematic review. *J. Clean Prod.*, 252(5): 119809.
- Jones, A. 2014. *The Mitigation of Greenhouse Gas Emissions in Sheep Farming Systems*. Bangor University, Wales.
- Juntueng, S., Towprayoon, S. and Chiarakorn, S. 2020. Assessment of energy-saving potential and CO<sub>2</sub> abatement cost curve in 2030 for the steel industry in Thailand. *Environ. Develop. Sustain.*, 12: 789.
- Kesicki, F. 2013. Marginal abatement cost curves: combining energy system modeling and decomposition analysis. *Environ. Model. Assess.*, 18(1): 27-37.
- Kesicki, F. and Ekins, P. 2012. Marginal abatement cost curves : A call for caution. *Clim. Policy*, 12(2): 219-236.
- Kesicki, F. and Strachan, N. 2011. Marginal abatement cost (MAC) curves : confronting theory and practice. *Environ. Sci. Policy*, 14(8): 1195-1204.
- Kiula, O. and Rutherford, T.F. 2013. Piecewise-smooth approximation of bottom-up abatement cost curves. *Energy Econ.*, 40: 734-742.
- Lee, C. and Wang, K. 2019. Nash marginal abatement cost estimation of air pollutant emissions using the stochastic semi-nonparametric frontier. *Europ. J. Operat. Res.*, 273(1): 390-400.
- Levihn, F., Nuur, C. and Laestadius, S. 2014. Marginal abatement cost curves and abatement strategies : Taking option interdependency and investments unrelated to climate change into account. *Energy*, 76: 336-344.
- Löffler, C. and Hecking, H. 2016. Greenhouse gas abatement cost curves of the residential heating market : A microeconomic approach. *Environ. Resour. Econ.*, 15: 25-36.
- Luu, Q.L., Nguyen, N.H., Halog, A. and Bui, H.V. 2018. GHG emission reduction in the energy sector and its abatement cost: A case study of five provinces in Mekong delta region Vietnam. *Int. J. Green Energy*, 15(12): 715-723.
- Marinoni, O. and Grieken, M. Van. 2015. ABATE : A new tool to produce marginal abatement cost curves. *Comput. Econ.*, 48: 367-377.
- Mosnier, C., Cara, D., Britz, W., Julliere, T., Jayet, P., Havlík, P., Frank, S. and Mosnier, A. 2019. Greenhouse gas abatement strategies and costs in French dairy production. *J. Clean. Prod.*, 236: 117589.
- Oliveira, R.D., Barioni, L.G., Zanett, T., Eory, V., Topp, C.F.E., Fernandes, F.A. and Moran, D. 2015. Developing a nationally appropriate mitigation measure for the greenhouse gas GHG abatement potential from livestock production in the Brazilian Cerrado. *Agric. Sys.*, 140: 48-55.
- Sala-Garrido, R., Mocholi-arce, M., Molinos-senante, M. and Maziotis, A. 2021. Marginal abatement cost of carbon dioxide emissions in the provision of urban drinking water. *Sustain. Prod. Consump.*, 25: 439-449.
- Schwartz, H., Gustafsson, M. and Spohr, J. 2020. Emission abatement in shipping - is it possible to reduce carbon dioxide emissions profitably ? *J. Clean. Prod.*, 254: 120069.
- Selvakumaran, S. and Limmeechokchai, B. 2017. Assessment of long-term low emission power generation in Sri Lanka and Thailand. *Sustain. Energy Technol. and Assess.*, 21: 121-141.
- Sjostrand, K., Lindhe, A., Soderqvist, T., Dahlqvist, P. and Rosen, L. 2019. Marginal abatement cost curves for water scarcity mitigation under uncertainty. *Water Resour. Manag.*, 33: 4335-4349.
- Sununta, N., Kongboon, R. and Sampattagul, S. 2019. GHG evaluation and mitigation planning for low carbon city case study: Dan Sai Municipality. *J. Clean. Prod.*, 228: 1345-1353.
- Talaei, A., Ahiduzzaman, M., Davis, M., Gemechu, E. and Kumar, A. 2020. Potential for energy efficiency improvement and greenhouse gas mitigation in Canada's iron and steel industry. *Energy Efficiency*, 13(6): 1213-1243.
- Tanatvanit, S., Limmeechokchai, B. and Shrestha, R. M. 2004. CO<sub>2</sub> mitigation and power generation implications of clean supply-side and demand-side technologies in Thailand. *Energy Policy*, 32: 83-90.
- Tang, B.J., Ji, C.J., Hu, Y.J., Tan, J.X. and Wang, X.Y. 2020. Optimal carbon allowance price in China's carbon emission trading system: Perspective from the multi-sectoral marginal abatement cost. *J. Clean. Prod.*, 253: 119945.
- Taylor, S. 2012. The ranking of negative-cost emissions reduction measures. *Energy Policy*, 48: 430-438.
- Teng, F., Wang, X., Pan, X. and Yang, X. 2014. Understanding marginal abatement cost curves in energy-intensive industries in China: Insights from a comparison of different models. *Energy Proced.*, 61: 318-322.
- UNFCCC. 2015. Paris Agreement: Conference of the Parties on Its Twenty-First Session. UNFCCC, Rio Di Janeiro, pp. 1-16.
- Verma, A., Olateju, B. and Kumar, A. 2015. Greenhouse gas abatement costs of hydrogen production from underground coal gasification. *Energy*, 85: 556-568.
- Vijay, S., DeCarolis, J.F. and Srivastava, R.K. 2010. A bottom-up method to develop pollution abatement cost curves for coal-fired utility boilers. *Energy Policy*, 38(5): 2255-2261.
- Vogt-Schilb, A. and Hallegatte, S. 2011. When Starting with the Most Expensive Option Makes Sense Use and Misuse of Marginal Abatement Cost Curves. No. 5803; Issue September.
- Wächter, P. 2013. The usefulness of marginal CO<sub>2</sub>-e abatement cost curves in Austria. *Energy Policy*, 61: 1116-1126.
- Wang, Y., Wang, Q., Hang, Y., Zhao, Z. and Ge, S. 2018. CO<sub>2</sub> emission abatement cost and its decomposition : A directional distance function approach. *J. Clean. Prod.*, 170: 205-215.
- Zhang, W., Stern, D., Liu, X., Cai, W. and Wang, C. 2017. An analysis of the costs of energy-saving and CO<sub>2</sub> mitigation in rural households in China. *J. Clean. Prod.*, 165: 734-745.





# Immobilization of Humic Acid on Bentonite and Its Application for Adsorption of Cs<sup>137</sup> and Am<sup>241</sup>

H. P. Suseno† and A. D. Warisaura

Department of Environmental Engineering, Institut Sains dan Teknologi AKPRIND, Yogyakarta, Indonesia

†Corresponding author: H. P. Suseno; hp\_suseno@akprind.ac.id

Nat. Env. & Poll. Tech.  
Website: [www.neptjournal.com](http://www.neptjournal.com)

Received: 30-07-2021  
Revised: 04-10-2021  
Accepted: 05-10-2021

## Key Words:

Adsorption  
Am<sup>241</sup>  
Cs<sup>137</sup>  
Humic acid  
Immobilization

## ABSTRACT

In the present work, immobilization of humic acid on bentonite and its application as an adsorbent of Cs<sup>137</sup> (Cesium) and Am<sup>241</sup> (Americium) is performed. The parameters studied are rate constant, adsorption capacity, and adsorption energy. This research started with the immobilization of humic acid on a bentonite surface followed by a stability test for immobilization of humic acid at various acidities. Adsorption of Cs<sup>137</sup> and Am<sup>241</sup> ions was conducted by first examining the optimum pH giving minimum complexed ions by the soluble fraction of humic acid and maximum adsorbed ions on the adsorbent. While adsorption energy and capacity were determined by the Langmuir isotherm adsorption model. The result shows that the amount of immobilization of humic acid on bentonite is 39.75 % (w/w) at optimum conditions. Immobilization of humic acid was stable up to pH 12.0. For both ions, optimum adsorption occurred at pH 5. At this optimum condition, the adsorption energies of 21.481 kJ.mol<sup>-1</sup> and 22.276 kJ.mol<sup>-1</sup> for Cs<sup>137</sup> and Am<sup>241</sup> are obtained, respectively. The result also shows that adsorption capacity and energy for Am<sup>241</sup> were higher than that for Cs<sup>137</sup> which indicates the affinity of Am<sup>241</sup> for both adsorbents was higher than that of Cs<sup>137</sup>.

## INTRODUCTION

Cesium (Cs<sup>137</sup>) and Americium (Am<sup>241</sup>) are the radioactive waste generated from plutonium-fueled power reactors or the result of nuclear weapon explosions. These radioactive can spread to the atmosphere as well as to the soil (Glikson 2017, Meszaros et al. 2016, Snow et al. 2019) and can be very harmful to human health. In the future, these radioactive emissions may increase since more nuclear power plant has been built around the world. Thus it is important to find out a sustainable method to encounter the Am<sup>241</sup> and Cs<sup>137</sup> pollution to the atmosphere and or to the soil. One method that can be utilized in controlling water pollution due to heavy metal and radioactive waste pollution is the adsorption method. The adsorption method was first introduced by Cihan et al. (2019). Mojiri et al. (2019) stated that adsorption is one method that can be used to treat waste. Adsorption is a method that is generally based on interactions between metals and functional groups that exist on the surface of the adsorbent that occurs through complex formation interactions and usually occur on solid surfaces that are rich in functional groups such as: -COOH, -OH, and NH (Yang et al. 2019, Kumar & Jiang 2016). The adsorbent that can be used for the purpose is humic acid which can be obtained from peat soil. According to Uda et al. (2017), Indonesia has peatlands of approximately 26.5 hectares, mostly in Kalimantan and Sumatra Island.

Humic acid is a very abundant and essential component in the natural environment and can bind to pollutants, both organic and inorganic pollutants (Ceci et al. 2019). Humic acid is a heterogeneous compound, consisting of many oxygen-containing groups (Boguta et al. 2019, Shi et al. 2018, Zhang et al. 2018). The various functional groups found in humic acid are the -COON, OH enolic, quinone, lactone, ether, and alcohol-OH groups (Zhang et al. 2018, Wu et al. 2019). The main functional groups found in humic acid are carboxylic groups, -OH phenolics and -OH alcoholic, in addition to other groups in minor quantities, such as carboxyl, phosphate, sulfate, amides, and sulfides which all can react with metal ions in solution. Spectroscopic studies show that the -COOH group is a group that plays a vital role in the formation of complexes between metal ions with humic and fulvic acid. Moreover, the interaction also involves OH groups, -C = O and -NH.

Humic acid immobilization has also been reported by Cruz-Zavala et al. (2018), which is by immobilizing humic acid in chitin, by combining humic acid molecules with chitin through electrostatic interactions due to different loads, so we get a combined adsorbent of humic and chitin acids and produce a decrease in humic acid solubility to highly alkaline acidity. To enrich the surface of an inorganic solid through immobilization with functional groups of organic compounds, the solid should have active sides such as

siloxane (-Si-O-Si-), silanol (-SiOH), and aluminol groups (-AlOH) which can be chemically bonded with immobilized organic compounds, besides the solids must also have a large surface area. Fig. 1 shows the reaction mechanism of humic acid-binding in the adsorption process according to Tunega et al. (2019) and Smilek et al. (2017). The reaction mechanism of humic acid-binding in the adsorption process of humic compounds is supporting solids can occur through the reaction between hydrophilic functional groups of humic acid (carboxylic groups) with -OH groups on the surface of the supporting solid

The humic acid molecular structure consists of a set of active groups/micelles that form polymers naturally with the basic structure of the aromatic ring. Because of the very complex structure of humic acid, its structure cannot be stated with certainty and can only be expressed in a hypothetical structure (El-Sayed et al. 2019). Humic and fulvic acids contain groups consisting of oxygen atoms (such as -OH, -COOH, and -C = O) with large concentrations per unit weight, so these compounds are hydrophilic (Ai et al. 2020). Some hypothetical structures of humic acid have been proposed by several researchers, such as Fuch, the German

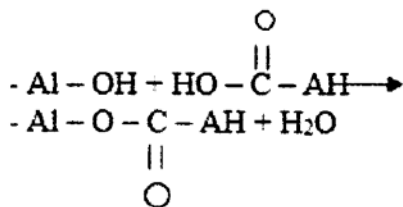


Fig. 1: Reaction mechanism of humic acid-binding in the adsorption process.

scientist, who proposed the structure of humic acid as shown in Fig. 2 (Klucakova & Veznikova 2017).

Another material that can be used as an adsorbent is bentonite. Based on the chemical nature of bentonite as ion exchange, bentonite can be used as an absorber in the treatment of liquid radioactive waste. Bentonite is a designation for commercial quality montmorillonite, with various compositions, but the formula is often stated as  $\text{Al}_2\text{O}_3 \cdot 4\text{SiO}_2 \cdot \text{H}_2\text{O} + \text{XH}_2\text{O}$ . The montmorillonite clay is a 2:1 clay type, a clay structure built by two tetrahedra sheets and one octahedral sheet. Two types of structures have been proposed for montmorillonite namely structures according to (1) Hofmann & Endell, and (2) Edelman & Favajee, as shown in Fig. 3 (Tournassat et al. 2018).

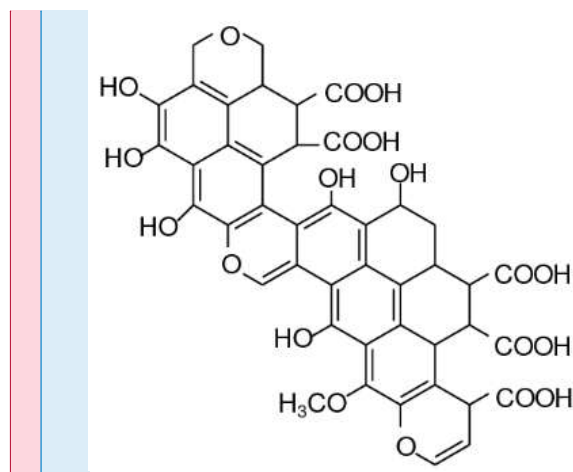


Fig. 2: Hypothetical structure of humic acid according to Fuch.

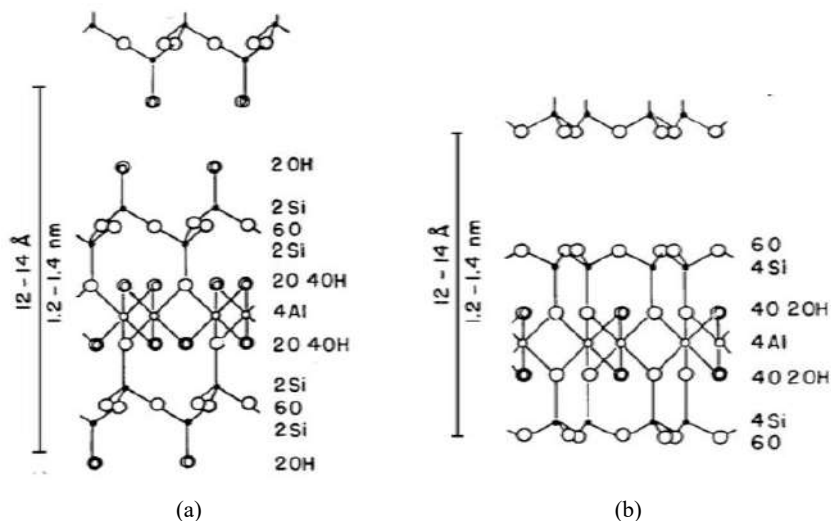


Fig. 3: The model of montmorillonite structure according to a) Edelman & Favajee, b) Hoffman & Endell.

The use of humic acid and bentonite as adsorbents for Cs<sup>137</sup> and Am<sup>241</sup> filtration is limited. Thus, the present work aims to investigate the potential use of humic acid from peat land and bentonite as Adsorption material of Cs<sup>137</sup> and Am<sup>241</sup>. The work investigates the immobilization of humic acid on bentonite and its characteristic in terms of rate constant, adsorption capacity, and adsorption.

## MATERIALS AND METHODS

**Immobilization of Humic Acid on Bentonite:** 60 mg of humic acid fills to three tubes in which the humic acid had been dissolved with 10 mL of 0.01 M NaOH and 100 mg of bentonite, with 0.001 M ion strength variation; 0.010 M and 0.100 M of NaNO<sub>3</sub>. Furthermore, a magnetic stirrer was performed to mix the solution for 1 h and allowed to stand overnight. It was then filtered and washed to produce neutral pH. The solid was dried at 66 °C in an oven until a constant weight was obtained. An ultraviolet spectrophotometer analyzed the filtrate at a wavelength of 466 nm.

**Identification and Clarification of Adsorbent Functional Groups:** To identify and clarify the changes in groups found on bentonite and humic acid, which are immobilized on bentonite with optimal ion strength, 1 mg of each sample was sampled to be dissolved and analyzed using an infrared spectrophotometer.

**Investigation of Adsorption of Cs<sup>137</sup> and Am<sup>241</sup> as the Function of Acidity:** Bentonite or AH-bentonite as much as

0.01 g and 10 mL of 100 ppm CsI<sup>37</sup> feed solution with pH of 1 were poured into vial continued with 60 min shaking and allowed to stand overnight. It would produce segregation of deposits and filtrates. The filtrates were analyzed by  $\beta$ -spectrometer. The following steps were conducted in terms of pH 3, 5, 7, and 9. The adsorption test procedure of Am<sup>241</sup> is similar to that of Cs<sup>137</sup>.

## RESULTS AND DISCUSSION

**Immobilization of Humic Acid on Bentonite:** Fig. 4 shows the immobilization reaction of humic acid on bentonite. The humic acid is a fraction of humic compounds that are insoluble in water solvents under acidic conditions (pH around 2), but it starts to dissolve if the pH of the solution

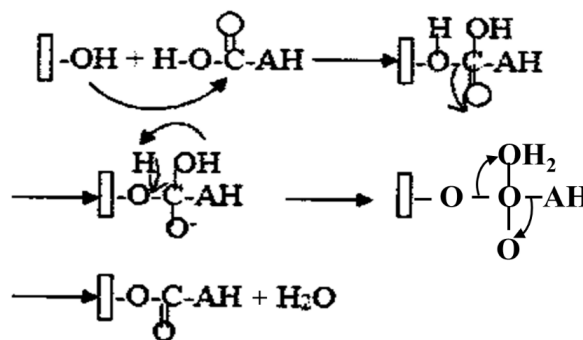


Fig. 4: Immobilization reaction of humic acid on bentonite.

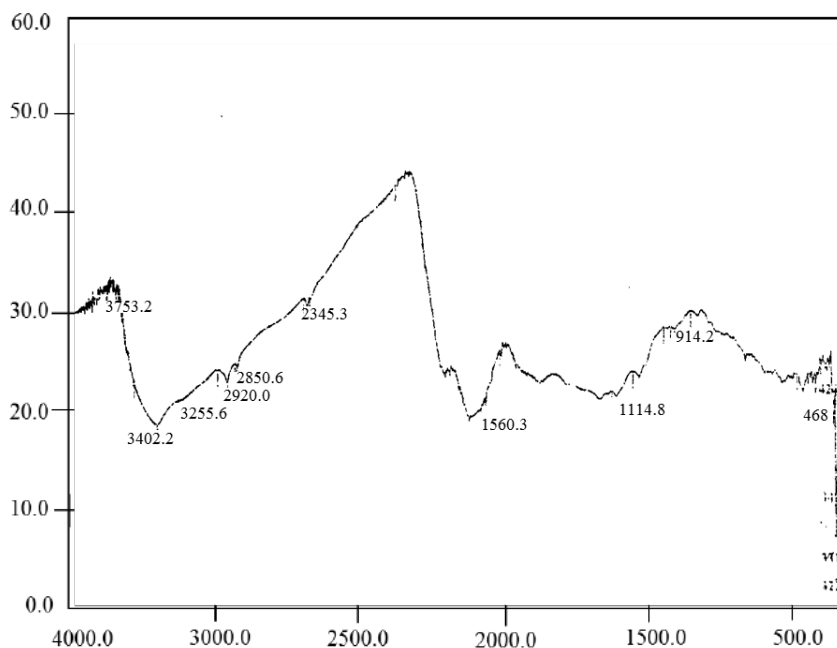


Fig. 5: Humic acid infrared spectra.



is above 2, and dissolves completely at pH above 6. At high pH, functional groups such as  $-\text{COON}^-$  and  $-\text{OH}$  phenolics from humic acid begin to be ionized, thus, weakening the intramolecular hydrogen bonds of humic acid, repelling inter-ionized groups and also as a result of hydration by water molecules. As a result of the dissolved fraction of humic acid, the interaction of humic acid with metal ions is not solely in the form of adsorption by insoluble fractions of humic acid, but also the interaction of complex formation between metal and dissolved humic acid fraction. Therefore, to study the adsorption of metals by humic acid at high pH, the treatment was applied to reduce the solubility of humic acid at high pH. To reduce the solubility of humic acid, the immobilization of humic acid on the surface of bentonite is carried out. The humic acid-binding reaction mechanism in the process of humic acid immobilization on bentonite occurs between functional groups of humic acid (carboxylic groups) with OH groups on bentonite through nucleophilic substitution reactions as follows. Therefore, bentonite solids that have silanol groups bind with humic acid through OH groups establishing nucleophilic substitution reactions to C atoms in the humic acid COOH groups.

**Spectra Characterization:** Fig. 5 presents infrared spectra of the humic acid. The spectra indicate widely absorbed

absorption at  $3402.2\text{ cm}^{-1}$  wave number shows the OH carboxylic stretching vibration, absorption at  $3255.6\text{ cm}^{-1}$  wave number is OH phenol vibration, absorption at  $2920.0\text{ cm}^{-1}$  wave number identifies the existence of aliphatic CH stretching vibrations, the absorption at  $2850.6\text{ cm}^{-1}$  wavenumber is the methylene group. The OH bending vibration of COOH and the C-O stretching vibration of COOH were identified by the absorption of  $1114.8\text{ cm}^{-1}$  wave number. The aromatic group of humic acid was identified by the absorption band at  $1560.3\text{ cm}^{-1}$  wave number indicates the presence of  $-\text{C}=\text{C}$  aromatic. The OH stretching vibration of  $-\text{COOH}$  is confirmed by the appearance of absorption bands at  $2345.3\text{ cm}^{-1}$  wave number. The absorption bands of the humic acid infrared spectrum following the infrared spectroscopic data of humic acid, which absorbs  $3300\text{ cm}^{-1}$  wavenumbers as a result of the  $-\text{OH}$  stretching vibration. The existence of C-H stretching vibrations at  $2900\text{ cm}^{-1}$  wavenumbers indicates the presence of C-H aliphatic, and weak absorption bands at wavenumbers around  $1500\text{ cm}^{-1}$  indicate the existence of aromatic  $\text{C}=\text{C}$  vibrations.

Meanwhile, Fig. 6 shows a spectrum of bentonite. The graph shows a wide absorption band of  $3431.1\text{ cm}^{-1}$  wave number; a sharp band at  $1637.5\text{ cm}^{-1}$ ; a wide band at  $1028.0\text{ cm}^{-1}$ ; and a sharp band at  $916.1\text{ cm}^{-1}$ . It is following the in-

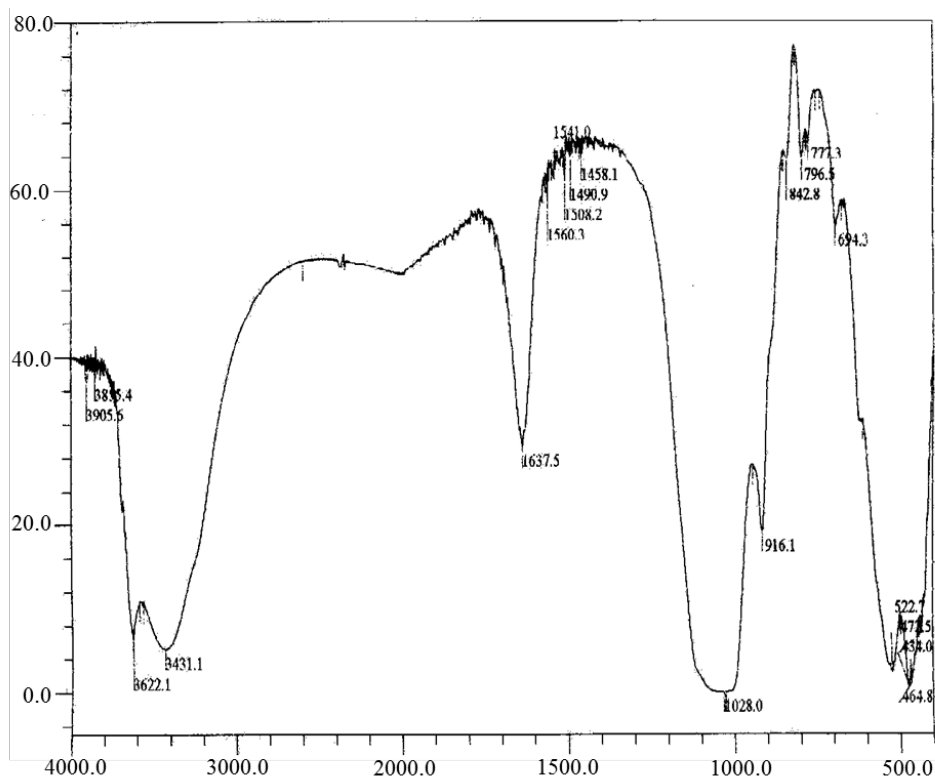


Fig. 6: Bentonite infrared spectra.

frared results of the reference montmorillonite which shows a wide band in the area of about 3420 cm<sup>-1</sup> for OH stretching vibrations and a wide band at 1050 cm<sup>-1</sup> for Si-O vibrations, bands for OH stretching vibrations, and bandwidth at 1050 cm<sup>-1</sup> for Si-O vibrations, sharp bands at wavenumbers 3622.1 cm<sup>-1</sup> for free stretching vibrations and sharp bands at 1637.5 cm<sup>-1</sup> are OH Stretching vibrations of water molecules and sharp bands at 910-920 cm<sup>-1</sup> wavenumber for Al-O vibrations.

Whereas, immobilized humic acid on bentonite spectra is shown in Fig. 7. The infrared spectra of the humic acid adsorbent immobilized on bentonite provide absorption peaks that are somewhat different from the infrared spectra of bentonite, namely the appearance of absorption at 2923.9 cm<sup>-1</sup> wavenumbers as CO aliphatic stretching vibrations and 2852.4 cm<sup>-1</sup> wavenumbers as methyl group vibrations. It clarifies the presence of humic acid in the adsorbent of

AH-bentonite. The absorption peak at 1035.7 cm<sup>-1</sup> wave number shows a decrease in the crystallinity of bentonite due to the immobilization occurrence of humic acid.

**Adsorption rate of Cs<sup>117</sup> and Am<sup>241</sup> on a single ion condition:** The adsorption equilibrium time needs to be determined to achieve maximum adsorption of adsorbate on the surface of the adsorbent. The shorter the reaction time, the higher the reaction rate. Increasing the interaction time will not increase the amount of metal adsorbed if the adsorption equilibrium has been reached. The value of the adsorption equilibrium constant (K) and the first-order reaction rate (k<sub>1</sub>) constant values obtained from calculations with the application of the kinetic model proposed by Chuanjiang et al. (2016) are presented in Table 1.

It can be seen from Table 1, that the value of the first-order reaction rate k<sub>1</sub> for CS<sup>137</sup> and Am<sup>241</sup> adsorption using HA-ben-

Table 1: The kinetics constants for Cs<sup>137</sup> and Am<sup>241</sup> adsorption (Chuanjiang et al. 2016).

Species	Adsorbent	Kinetics Parameter	
		K <sub>1</sub> [min <sup>-1</sup> ]	K [mol.L <sup>-1</sup> ]
CS <sup>137</sup>	AH-bentonite	1.2 x 10 <sup>-3</sup>	2881.8
	Pure bentonite	5.3 x 10 <sup>-4</sup>	1045.8
Am <sup>241</sup>	AH-bentonite	1.6 x 10 <sup>-3</sup>	5624.7
	Pure bentonite	9.8 x 10 <sup>-4</sup>	2724.4

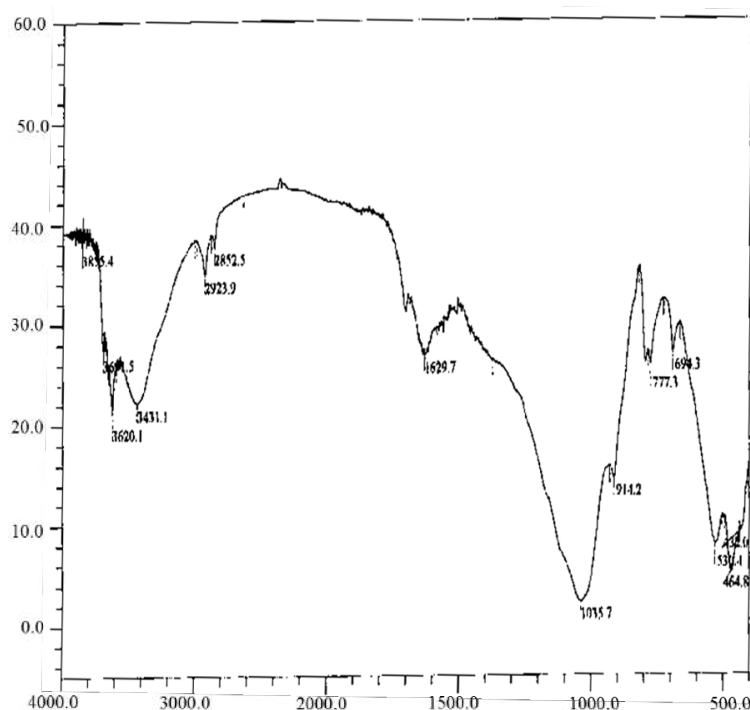


Fig 7: Infrared spectra of immobilized humic acid on bentonite.

tonite adsorbent is higher than pure bentonite adsorbents. It is due to the rich active site of HA-bentonite resulting from immobilized of humic acid on the surface, so HA-bentonite binds more efficiently to metal ions. The -COOH and -OH alcoholic and phenolic groups of humic acid that are immobilized on bentonite give new characteristics to the surface of the adsorbent. Those active groups have a significant role in binding metal ions, whereas, on bentonite, the binding of metal ions is dominantly determined by the presence of silanol (SiOH) groups on the surface of bentonite. The adsorption rate of Am<sup>241</sup> by the adsorbent of humic acid immobilized on bentonite increased higher compared with Cs<sup>137</sup>. It describes that Am<sup>241</sup> has a greater affinity compared with Cs<sup>137</sup> on HA-bentonite. It also can be seen that the adsorption rate of the Am<sup>241</sup> metal ion is higher than the adsorption rate of Cs<sup>137</sup> in both adsorbents. The electronegativity (the size of atoms in a molecule to attract electrons to itself) values of Am and Cs are 1.3 Å and 0.86 Å, respectively (Cotton 2014). The electronegativity value of Am is higher than Cs, so the bond between Am and the adsorbent surface-active site has a relatively higher covalent bond. The increased covalent bonds between Am and adsorbents make Am less dissolved and more Am adsorbed on the surface of the adsorbent. Cs with smaller electronegativity form relatively more polar bonds with active sites on the surface of the adsorbent. The effect caused by polarization by cation is the solubility in polar solvents such as water. Therefore, the bond between Cs and immobilized humic acid on bentonite is more polar. It makes Cs easier to dissolve in water, which resulted in more Cs in the solution.

Regarding K values, the adsorption capability of HA-bentonite towards Cs<sup>137</sup> and Am<sup>241</sup> is higher compared to bentonite. It is caused by the more prosperous active sites of HA-Bentonite as the result of humic acid immobilization on the bentonite surface. Humic acid, which is rich in the -COOH and -OH groups, both phenolic and alcoholic, will give new characteristics to surfaces that are bound to bentonite. These groups have a high affinity for binding metal ions, so it creates more active sites in binding metals, whereas, in bentonite groups, the silanol groups are responsible for the active sites. The adsorption capability of HA-bentonite adsorbent is higher than Am<sup>241</sup> compared with Cs<sup>137</sup> indicated by a higher K value. It occurs because Am<sup>241</sup> has a greater affinity than Cs<sup>137</sup> in interacting with the adsorbent. According to Vogel (1961), ions that have a higher charge will have more excellent adsorption capability than the smaller charges. Am<sup>3+</sup> has a total charge of +3, so the ability to adsorb is higher than Cs<sup>+</sup> ions whose total charge is only +1.

## CONCLUSION

The work on immobilization of Humic Acid on Bentonite

and Its Application for Adsorption of Cs<sup>137</sup> and Am<sup>241</sup> has been performed. It can be concluded that the more strength the ion concentration, the larger the immobilization of humic acid on bentonite was, and vice versa. The amount of immobilization of humic acid on bentonite is 39.75 % (w/w) at optimum conditions. Immobilization of humic acid was stable up to pH 12.0. For both ions, optimum adsorption occurred at pH 5. At this optimum condition, the adsorption energies of 21.481 kJ.mol<sup>-1</sup> and 22.276 kJ.mol<sup>-1</sup> for Cs<sup>137</sup> and Am<sup>241</sup> are obtained, respectively. The result also shows that adsorption capacity and energy for Am<sup>241</sup> were higher than that for Cs<sup>137</sup> which indicates the affinity of Am<sup>241</sup> for both adsorbents was higher than that of Cs<sup>137</sup>.

## ACKNOWLEDGEMENT

The authors thank the Ministry of Education, Culture, Research, and Technology of the Republic of Indonesia for the financial support for the publication of the work through the scheme of Program Kompetisi Kampus Merdeka (PKKM) 2021.

## REFERENCES

- Ai Y., Zhao C., Sun L., Wang X. and Liang L. 2020. Coagulation mechanisms of humic acid in metal ions solution under different pH conditions: A molecular dynamics simulation. *Sci. Total Environ.*, 702: 135072.
- Boguta, P., D'Orazio, V., Senesi, N., Sokolowska, Z. and Szewczuk-Karpisz, K. 2019. Insight into the interaction mechanism of iron ions with soil humic acids. The effect of the pH and chemical properties of humic acids. *J. Environ. Manag.*, 245: 367-374.
- Ceci, A., Pinzari, F., Russo F., Persiani, A.M. and Gadd G.M. 2019. Roles of saprotrophic fungi in biodegradation or transformation of organic and inorganic pollutants in co-contaminated sites. *Appl. Microbiol. Biotechnol.*, 103: 53-68.
- Chuanjiang, A., Yang, S., Huang, G., Zhao, S., Zhang, P. and Yao, Y. 2016. Removal of sulfonated humic acid from the aqueous phase by modified coal fly ash waste: Equilibrium and kinetic adsorption studies. *Fuel*, 165: 264-271.
- Cihan, A., Tokunaga, T.K. and Birkholzer, J.T. 2019. Adsorption and Capillary Condensation-Induced Imbibition in Nanoporous Media, *Langmuir*, 35 (29): 9611-9621.
- Cotton, F.A. 2014. *My Life in the Golden Age of Chemistry: More Fun Than Fun*. Elsevier, Amsterdam, The Netherlands
- Cruz-Zavala, A.S., Pat-Espadas, A.M., Rangel-Mendez, J.R., Chazarro-Ruiz, L.F., Ascacio-Valdes, J.A., Aguilar, C.N. and Cervantes, F.J. 2016. Immobilization of metal-humic acid complexes in anaerobic granular sludge for their application as solid-phase redox mediators in the biotransformation of iopromide in UASB reactors. *Bioresour. Technol.*, 207: 39-45.
- El-Sayed, M.E.A., Khalaf, M.M.R., Gibson, D. and Rice, J.A. 2019. Assessment of clay mineral selectivity for adsorption of aliphatic/aromatic humic acid fraction. *Chem. Geol.*, 511: 21-27.
- Glikson, A.Y. 2017. The Breach in the Earth's Radiation Shield. In Glikson, A.Y. (ed), *The Plutocene: Blueprints for a Post-Anthropocene Greenhouse Earth*, Springer, Cham, pp. 39-81.
- Klucakova, M. and Veznikova, K. 2017. Micro-organization of humic acids in aqueous solutions. *J. Mol. Struct.*, 1144: 33-40.

- Kumar, A.S.K. and Jiang, S.J. 2016. Chitosan-functionalized graphene oxide: A novel adsorbent for efficient adsorption of arsenic from aqueous solution. *J. Environ. Chem. Eng.*, 4(2): 1698-1713.
- Meszaros, R., Leelossy, A., Kovacs, T. and Lagzi, I. 2016. Predictability of the dispersion of Fukushima-derived radionuclides and their homogenization in the atmosphere. *Sci. Rep.*, 6(1): 43.
- Mojiri, A., Ohashi, A., Ozaki, N. and Kindaichi T. 2019. Pollutants removal from synthetic wastewater by the combined electrochemical, adsorption, and sequencing batch reactor (SBR). *Ecotoxicol. Environ. Safety*, 161: 137-144.
- Shi, W., Lü, C., He, J., En, H., Gao, M., Zhao, B. and Zhang, Y. 2018. Nature differences of humic acids fractions induced by extracted sequence as explanatory factors for binding characteristics of heavy metals. *Ecotoxicol. Environ. Safety*, 154: 59-68.
- Smilek, J., Sedlacek, P., Lastuvkova, M., Kalina, M. and Klucakova, M. 2017. Transport of organic compounds through porous systems containing humic acids. *Bull. Environ. Contam. Toxicol.*, 98: 373-377.
- Snow, M.S., Ward, J., Olson, J., Bucher, B., Delmore, J., Adamic, M. and Snyder, D. 2019. Carbon-14 content in surface soils near atmospheric and below ground nuclear detonations. *J. Environ. Radioact.*, 11: 208-209.
- Tournassat, C., Tinnacher, R.M., Grangeon, S. and Davis, J.A. 2018. Modeling uranium (VI) adsorption onto montmorillonite under varying carbonate concentrations: A surface complexation model accounting for the spillover effect on surface potential. *Geochim. Cosmochim. Acta*, 220: 291-308.
- Tunega, D., Gerzabek, M.H., Haberhauer, G., Lischka, H., Sole, R. and Aquino A.J. 2019. Adsorption process of polar and nonpolar compounds in a nanopore model of humic substances. *Eur. J. Soil Sci.*, 15: 1-11.
- Uda, S.K., Hein, L. and Surnarga, E. 2017. Towards sustainable management of Indonesian tropical peatlands. *Ecol. Manag.*, 25: 683-701.
- Vogel, J.L. 1961. Authoritarianism in the therapeutic relationship. *J. Consult. Psychol.*, 25(2): 102-108.
- Wu, J., Jiang, R., Lin, W. and Ouyang, G. 2019. Effect of salinity and humic acid on the aggregation and toxicity of polystyrene nano plastics with different functional groups and charges. *Environ. Pollut.*, 245: 836-843.
- Yang, X., Wan, Y., Zheng, Y., He, F., Yu, Z., Huang, J. and Gao, B. 2019. Surface functional groups of carbon-based adsorbents and their roles in the removal of heavy metals from aqueous solutions: A critical review. *Chem. Eng. J.*, 366: 608-621.
- Zhang, Z., Lü, C., He, J., Gao, M., Zhao, B., Zhou, B. and Zhang, Y. 2018. Nature differences of fulvic acid fractions induced by extracted sequence as explanatory factors for binding characteristics of Cu 2+. *Chemosphere*, 191: 458-466.
- Zhang, J., Yin, H., Chen, L., Liu, F. and Chen, H. 2018. The role of different functional groups in a novel adsorption-complexation-reduction multi-step kinetic model for hexavalent chromium retention by undissolved humic acid. *Environ. Pollut.*, 237: 740-746.







# Bio-medical Waste Remediation by Environmental Safe Gelatin Coated Blood Sample Paper and its Effective Utilization

P. Jayakumar\*, S. Padmanabhan\*\*†, R. Lilly\*\*\* and K. Suthendran\*\*\*\*

\*Sathyabama Institute of Science and Technology, Chennai, India

\*\*School of Mechanical and Construction, Vel Tech Rangarajan Dr. Sagunthala R & D Institute of Science and Technology, Chennai, India

\*\*\*Department of Naval Architecture and Offshore Engineering, Academy of Maritime Education and Training (AMET), Chennai, India

\*\*\*\*School of Computing, Kalasalingam Academy of Research and Education, Krishnankoil, Srivilliputhur, Tamil Nadu 626126, India

†Corresponding author: S. Padmanabhan; padmanabhan.ks@gmail.com

Nat. Env. & Poll. Tech.  
Website: [www.neptjournal.com](http://www.neptjournal.com)

Received: 28-02-2022

Revised: 28-03-2022

Accepted: 09-04-2022

## Key Words:

Bio-medical waste  
Environment issues  
Gelatin coating  
Blood sampling

## ABSTRACT

Sustainability in human development sets exact standards for the management of natural resources, including their extraction, use, and the introduction of waste products into a complex, inventive circuit as a consequence of exploitation. Because of the negative influence that medical waste has on the environment and people, it needs specific handling. Medical waste is increasing in amount all the time and has a wide range of consequences across a wide range of activity domains. This paper discusses various issues of the sustainable management of blood sample bio-medical waste and evaluates the properties of alternative samples which are made of gelatin-coated sample paper. A unique bar-coded paper-based blood sample method has prevented complications during blood tests and is much more environmentally friendly.

## INTRODUCTION

A healthy atmosphere is the most important element for living a healthy lifestyle. The waste that is created in various hospitals has a direct or indirect relationship with the human environment in one way or another. If the waste is not collected and disposed of in line with the standards, it has the potential to cause environmental damage. Calis & Arkan (2014) conducted a survey to determine if nursing students were aware of the harm caused by medical waste to the environment and human health.

Its characteristics and content are very diverse in biomedical waste, which covers a wide range of waste generated in a variety of settings such as hospitals, nursing homes, medical research facilities, clinics, and medical stores. Biological waste poses a threat to the health of the general public if it is not adequately controlled. Already, ten distinct forms of waste have been identified as being associated with health hazards. The number of hospitals and nursing homes is expanding in tandem with the increase in the human population, and as a result, the amount of trash being created is increasing as well (Mastorakis et al. 2011). The kind of specialty and

the grade of the hospitals have an impact on the quality and amount of waste generated daily, respectively. Furthermore, the location of the hospital will most likely influence the kind and amount of waste generated. A total of more than 30 tons of biological waste is generated daily by hospitals in major metropolitan areas. It is a source of serious worry because the majority of hospitals, particularly those administered by the government, are not adequately maintained (Mathur et al. 2012).

Because it cannot be made harmless before being buried in the ground or disposed of in water, medical waste has been labeled as a source of soil and water pollution. Growing demand for medical services throughout the globe, along with a rise in the usage of disposable medical goods, has contributed to the massive volume of medical waste created. Environmental pollution, unpleasant odor, and the growth and multiplication of insects, rodents, and worms are all consequences of poor medical waste management. It also increases the risk of disease transmission through the use of sharps that have been contaminated with blood, such as typhoid fever, cholera, and hepatitis A (Babanyara et al. 2013).

In the current context of this pandemic, waste management is crucial to the long-term development of mankind. The treatment and disposal of bio-clinical waste generate a large amount of hazardous biomedical waste. Medical waste creation and disposal is a major issue in developing nations with poor sanitation and large populations. Hospitals, clinics, and other medical facilities create hazardous waste and expose patients to potentially fatal infections. Trash management policies should outline how waste should be dealt with at each phase of the waste management process, from creation through treatment. To reduce the risk of health issues spreading, it is critical to raise public awareness via various communication and educational methods. Healthcare waste may include pathogens that might infect hospital patients, healthcare employees, and the general public (Biswapriya et al. 2021).

However, although the COVID-19 pandemic is supposed to have decreased air pollution and environmental-related noise, and has enhanced biodiversity and tourism sites, the effect of people staying at home and taking precautionary measures on waste management has been alarmingly negative. A waste problem seems to be developing as a result of the unusually high volume of waste generated by families and health-care institutions, which looks to be exacerbated by the hoarding of gloves, gowns, masks, and other protective apparel and equipment. Failure to appropriately manage waste created by health institutions and families may increase the spread of COVID-19 via secondary transmission (Atanu Kumar et al. 2021).

Medical waste can be infectious to both humans and the environment, posing a significant danger of contamination and cross-contamination. A medical waste treatment facility should be located close to the point of creation, according to references from the World Health Organization (WHO) and other standards. Every staff working in the hospital who is engaged in the segregation process must take personal accountability for their actions (Padmanabhan & Debabrata 2019). Hazardous materials may be transported less often if they are stored in an appropriate area and are properly prepared for disposal. When it comes to the transportation of biological waste, there is a considerable danger of unlawful or incorrect disposal by haulage workers, as well as the possibility of accidents. Furthermore, in certain metropolitan areas, the transportation of hazardous trash to treatment facilities is restricted (Diaz et al. 2005).

Alternative waste treatment technologies in the medical industry are being studied by Li et al. (2020), including their incineration, steam sterilization, microwave or ultraviolet heating systems as well as disposal in landfills; the results indicate that the established method is useful to help

prioritize waste treatment technology in the medical industry. The selection of the most sustainable waste treatment technology in the medical sector in today's economies takes place according to the decision-makers who simultaneously consider various criteria.

Insufficient training in effective waste management, poor waste management, and disposal methods, and a lack of financial and human resources are all prevalent issues with healthcare waste. The health of people and the environment are at risk if biological waste is not properly handled. In recent years. The blood collection uses biodegradable blood sample paper. Biodegradation of biological waste outperforms all other traditional disposal methods in terms of efficiency and cost. It's also more eco-friendly (Jha et al 2014). Due to its ability to do rapid and low-cost diagnostics and analyses in non-laboratory settings, paper-based devices have shown to be perfect for performing blood tests. These advancements make paper-based devices more practical for doing point-of-care blood testing in many settings. Because medical waste harms both the environment and humans, it requires special care. This study evaluates the features of an alternative sample composed of gelatin-coated sample paper and covers sustainable treatment of blood sample bio-medical waste. A new bar-coded paper-based blood collection procedure has reduced problems and is more eco-friendly.

## MATERIALS AND METHODS

A paper sheet is generated from a network structure formed by the interaction of cellulose and non-cellulose molecules. Hydrogen bonds are responsible for holding these materials together. By increasing the crossing between the cellulose fibers in a paper sheet, it is possible to increase the mechanical characteristics of these components in a paper sheet and create better mechanical properties overall. A variety of polymer compounds have been used to improve the interfiber bonding between the cellulose chains in the paper sheets that have been created. Increasing the breaking length and tear factor of paper sheets after they have been dipped in various polymer solutions has been shown (Battisti et al. 2017, Wang et al. 2020). When various polymeric materials are used to treat different types of paper sheets, the breaking length of the treated paper sheets may be increased. This can be attributed to an increase in inter-fiber bonding between the fiber and the polymer. Additionally, the polymeric substance includes functional groups that are capable of forming ionic or covalent interactions with the surface of the paper fiber. Most polymeric materials enhance the breaking length and tear factor of the treated paper sheets, which is generally a good thing (Kamel et al. 2004).

In part, because blood can serve as a window into one's health, it is the human biofluid that has received the greatest attention in scientific studies so far. An individual's general health may be determined by doing blood tests, which can be used to diagnose illnesses, assess the efficacy of treatment drugs, and collect information on a person's overall health. When subsequent treatment is required, it is becoming more important to do quick response blood tests (Linton et al. 2020). When it comes to performing blood tests in response to this need, paper-based devices have shown to be the most effective equipment because of their ability to do rapid and low-cost diagnostics and analyses in an environment other than the laboratory. Recent breakthroughs in paper-based blood testing are discussed, with a special focus on the specific procedures and assays that have been employed in each instance. Additional subjects explored in this work include how to enhance the signal intensity of these paper-based devices in the future, as well as how to use in situ synthesis of coating to improve the sensitivity, functionality, and operational simplicity of these devices (El-Sakhawy et al. 2018). Fig. 1 shows blood samples placed on a gelatin-coated paper.

For a broad variety of functional features, gelatin has been widely employed in the preparation of edible films and coatings. These characteristics include outstanding film-forming capabilities, a strong binding capacity with water, and emulsifying characteristics. Aside from that, it has a number of benefits such as cheap cost, high availability, biocompatibility, and biodegradability (Doppalapudi et al. 2014). As a result of their hydrophilic nature, gelatin-based films and coatings have a high water vapor transmission rate. When gelatin films come into touch with surfaces with high moisture content, their mechanical strength reduces as a result, limiting their use as packing materials. Nevertheless, it has also been reported that the crosslinking activity of the transglutaminase enzyme, which is believed to be a safe and

efficient cross-linking agent, may be used to increase the mechanical characteristics and permeability of gelatin film (Nada et al. 2000, Banerjee et al. 2015).

## GELATIN COATING

Gelatin seems to be inert and harmless when exposed to the human body. Biomedical device development will be aided by a thorough knowledge of nanoscale phenomena, which may be used to create antimicrobial surfaces, implants, and more. To better understand how gelatin is being used for biomedical purposes today, this study will concentrate on the most recent developments in that field's utilization and the most critical aspects that impact gelatin's biocompatibility, and the difficulties that lie ahead. Traditional disinfection techniques are not as successful as photocatalytic procedures thus, gelatin-coated surfaces with antibacterial qualities might be used in the healthcare business. Because gelatin-coated catheters are safe and have the potential for light disinfection for clinical usage, they are another interesting use of gelatin in biomedicine (Dupont 2002, Nur Hanani et al. 2014).

Figs. 3, 4, and 5 depict the effects of several gelatin-coating agents on the density, water absorption, air permeability, and bio blood sample paper sheets. Reduced air permeability, increased density, and higher water resistance are some of the functional features of this material. The permeability of the paper (also known as porosity) and the density of the paper are two more critical criteria to consider. Particle permeability of a paper web is a physical characteristic that describes the degree to which the web resists the passage of gas through it. The impact of varying concentrations of gelatin as a coating agent on the air permeability, water absorption, and density of coated bagasse paper sheets was investigated. The results clearly show that, when the proportion of gelatin-coating was increased, the air permeability of all samples reduced



Fig. 1: Blood samples on gelatin-coated paper with bar code.

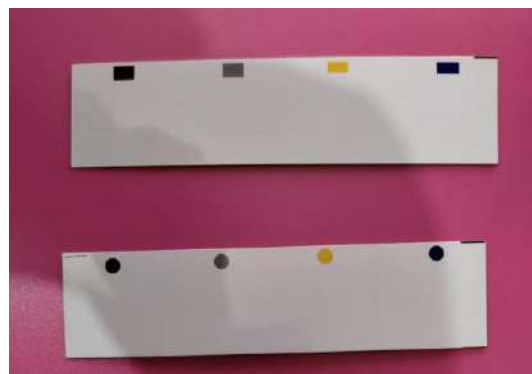


Fig. 2: Blood sample paper coated with gelatin with a color dot.

when compared to the control sheet. It has been shown that decreasing the number of spaces filled by gelatin enhances the resistance of the paper sheet to air movement. Only at 2 and 2.5 percent gelatin does water absorption demonstrate a significant increase in efficiency. The average apparent density of the blank sheet was  $8 \times 10^5 \text{ g.m}^{-3}$ , and the gelatin coating had a small effect on this parameter.

As seen in Fig. 5, when coated paper sheets were treated with a gelatin coating in contrast to the blank or with plain

biopolymer, a significant decrease in air permeability was observed, as compared to the blank or with plain biopolymer. When applied to gelatin sheets, coatings have the potential to promote cross-linking while simultaneously reducing the free volume of the polymeric matrix. As a consequence, the diffusion rate of air molecules through the sheet is decreased, and the sheet's air permeability is lowered. According to Figure 4, coating with gelatin individually resulted in the largest increase in water absorption. Comparing the air

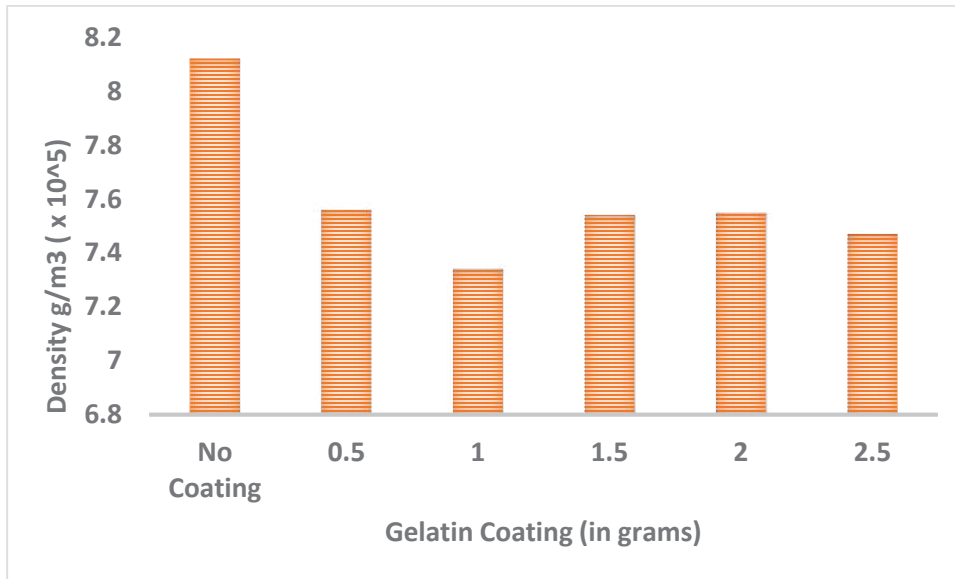


Fig. 3: Effect of gelatin coating on paper density.

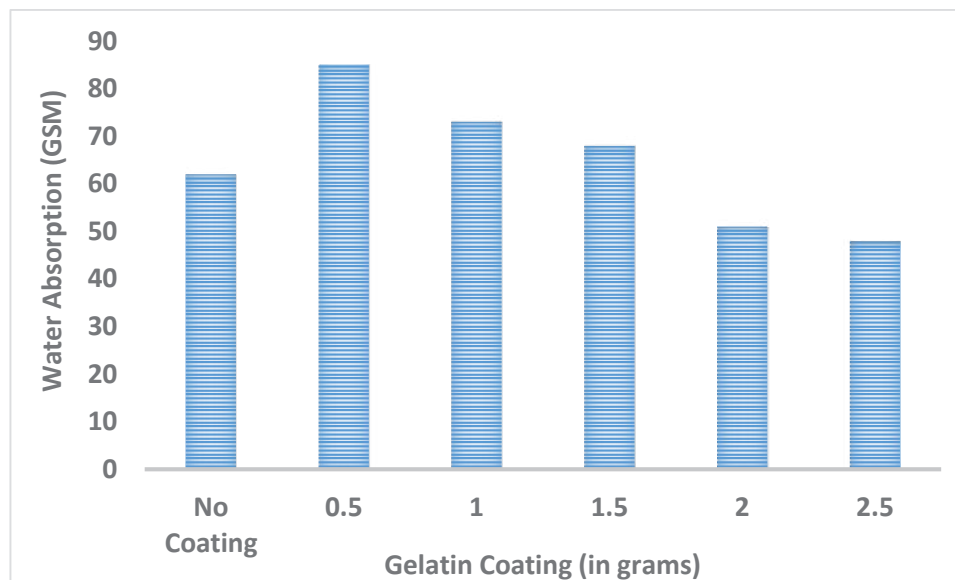


Fig. 4: Effect of gelatin coating on papers water absorption property.

permeability of the samples to the control sheet, the fraction of gelatin-coating was raised and the air permeability of all samples decreased. This is because the coating fills up the crevices between the paper sheets, hence increasing the resistance to the air passage. The application of gelatin to a substance increases the material's water absorption characteristics.

## RESULTS AND DISCUSSION

At various spots along with an 8-inch piece of glass, three drops of red blood cells are collected to determine the person's blood type. Separately mixed with the samples obtained and examined will be the three antigens (A, B, and Anti-D). If the antigen interacts with the blood cells, it causes agglutination; otherwise, it stays the same as before. This is the method through which blood types are categorized. Laboratory assistants are more likely than not to handle hundreds of samples of such blood types at a time, and they are more likely than not to put the plates in an upside-down posture while doing so. When deciding on the tests for the samples that have been inserted in this manner (Jayakumar et al. 2020), it will be erroneously determined. It has been decided to implement a new color-coding scheme to avoid similar errors. In other words, color coding comparable to the colors of the antigens is affixed to the side of the coated paper, as indicated in the accompanying image. Laboratory assistants may then inject the example antigens in the proper

locations during the test to accurately record the findings. According to the illustration in Fig. 4, a bar code is applied to the top of the blood sample paper, and we will go into further detail about this in a subsequent section.

A number of researchers used the sampling method using paper-based biological tests and were successful in their studies. To prevent the blood dot from escaping on the sides, the blood paper slide is constructed of gelatin-coated paper with a thickness of 0.28 mm and is glued on a piece of cardboard that has been perforated with a circular brim. The four colored marks on the board (Fig. 6), which correspond to the standard presented on the board, are used to mix the blood with different antigens and see the outcome. The gelatin-coated coating on the slide prevents the blood liquid from blotting on the surface. If the slide is cremated after use, there will be no dangerous chemicals released into the atmosphere as a result of burning, preventing contamination of the environment (Hao et al. 2021). Each slide card is labeled with a barcode that allows the patient's information to be identified. The findings demonstrate that the suggested color-coding system helps to decrease the number of mistakes that occur. During the study period, blood type tests were carried out using the suggested color-coding method, and the results showed that there were no technical problems. Using this procedure, there is a minor expense associated with driving color components into a microplate that may be utilized in a blood categorization test; nevertheless, there is no major damage to the plate.

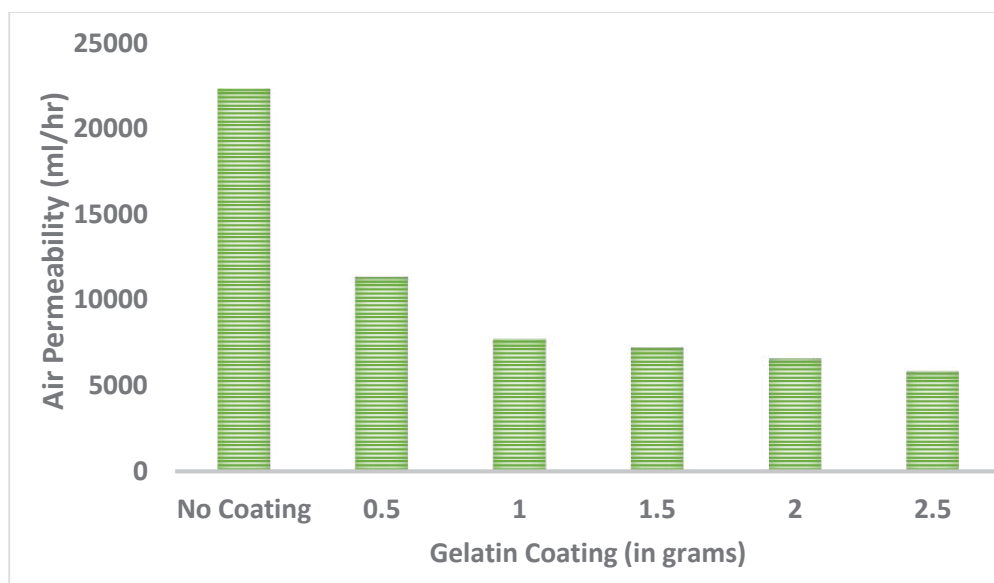


Fig. 5: Effect of gelatin coating on papers air permeability property.



### Effectiveness of Blood Sampling

It is possible to use gelatin, as a retention agent, to keep supporting materials attached to a paper sheet after they have stuck to the sheet. In terms of the retention agent, there are two possible mechanisms: coating the sheet surface with a gelatin suspension and wet end addition, which involves depositing gelatin onto individual fibers before sheet formation, resulting in an even distribution of gelatin loading throughout the sheet (Jha et al. 2014). If, for example, gelatin and hexadecanoic acid are mixed, the surface properties of the resulting mixture demonstrate a considerable increase in wetting and dispersion. It was discovered that the gelatin-coated paper had a larger dynamic elastic modulus than the other sheets. As a consequence of this, researchers are

attempting to develop a modern method of making advanced paper with a highly hydrophobic surface created by adding modified gelatin to cellulose fibers (Leila et al. 2017).

As a result, there was no obvious agglomeration problem between the coated particles, which shows that the gelatin particles may have been adequately coated on the blood sample paper during the blood sample papering process. In this particular instance, the irregular morphologies of the coated gelatin particles may be responsible for the uneven surface structure of the paper that was generated. Using blood sample paper (Figs. 7 & 8) for the creation of spots, researchers discovered a significant difference between the top and rear surfaces of both paper substrates (Tai et al. 2021). This was because the top and rear surfaces of both paper substrates

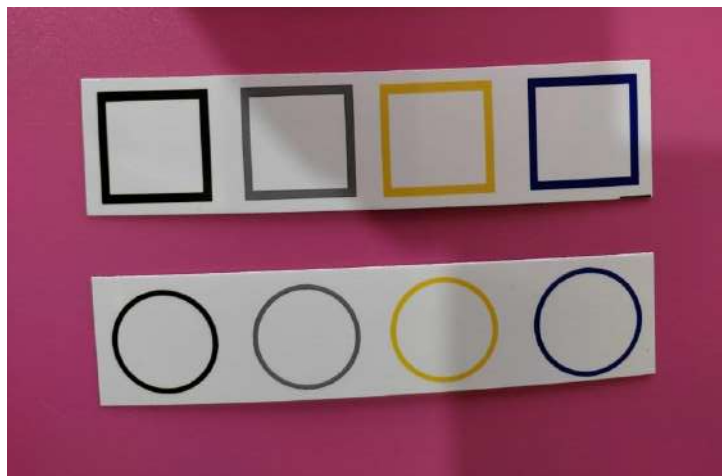


Fig. 6: Gelatin-coded blood sample paper with color code.

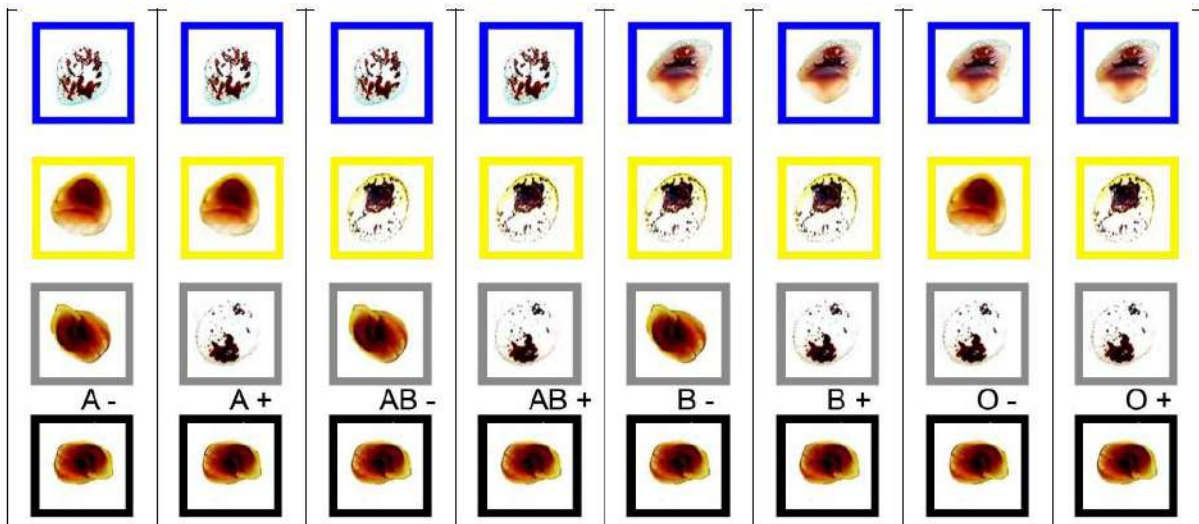


Fig. 7: Blood samples on gelatin-coated paper with bar code.

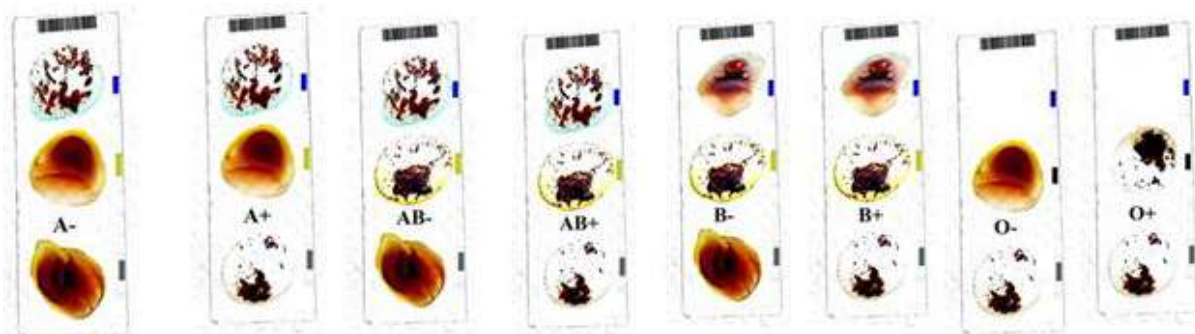


Fig. 8: Blood group identification on gelatin-coated paper.

were significantly different from one another. In the blood sample paper, it was proved that the applied bovine blood permeated the paper substrate in an even and uniform manner. The diameters of the spot on the top and back sides were both around the same size. As shown by the little difference between them, the color of the backside of the paper substrate inside the spot area was a shade or two darker than the color of the top surface. For example, when blood was deposited on gelatin-coated paper, the blood sample was completely blocked on the top side of the paper substrate and there was no prominent blood sample visible on the backside of the paper substrate, in contrast to the performance of commercially available polystyrene base paper (Gruner et al. 2015), which was demonstrated in Fig. 8.

That the one-sided gelatin-coated paper's surface could have caused this. In this way, the gelatin particles on top of the cellulose fibers contact directly with the blood sample, improving the experiment's efficiency. With the great ability of coated gelatin particles to adsorb blood and impede blood flow through the paper substrate, this may be helpful for spot detection of target compounds (Chauhan et al. 2013). A sub-punching approach may cause larger concentrations of blood samples between the edge and the center of the area. The uneven distribution of blood samples on the gelatin-coated paper results in a non-complete spot.

## CONCLUSION

Water, air, and soil quality have all been compromised as a result of biomedical waste. The volumes and proportions of various elements of wastes, as well as their management, treatment, and disposal procedures, varied in different healthcare settings, and treatment and disposal methods are insufficient in the majority of research conducted on this subject matter. Various studies have discovered risks linked with inadequate biomedical waste management as well as inadequacies in the present system in blood sampling. It is discussed in this article that there are different concerns with

the sustainable management of blood sample bio-medical waste, and it is evaluated the qualities of an alternative sample, which is made of gelatin-coated sample paper, in this study. A bar-coded paper-based blood sample technology has eliminated problems during blood testing and has made the process considerably more environmentally conscious. Biodegradable polymers, on the other hand, break down far more quickly than their conventional equivalents, which may take hundreds of years to degrade. When biodegradable materials decompose, carbon dioxide, water vapor, and organic matter are not detrimental to the environment. Because of this, they seem to be a better option in terms of sustainability. Humans have a moral imperative to safeguard the environment against pollution and other forms of environmental damage.

## REFERENCES

- Atanu Kumar, D., Nazrul Islam, M., Morsaline Billah, M. and Sarker, A. 2021. COVID-19 pandemic and healthcare solid waste management strategy: A mini-review. *Sci. Total Environ.*, 778: 146220.
- Babanyara, Y.Y., Ibrahim, D.B., Garba, T., Bogoro, A.G. and Abubakar, M.Y. 2013. Poor medical waste management (MWM) practices and its risks to human health and the environment: A literature review. *Int. J. Environ. Health Sci. Eng.*, 11(7): 1-8.
- Banerjee, A., Chatterjee, K. and Madras, G. 2015. Enzymatic degradation of polycaprolactone-gelatin blend. *Mater. Res. Express*, 2(4): 045303.
- Battisti, R., Fronza, N., Vargas Júnior, A., Silveira, S.M., Damas, M.S.P. and Quadri, M.G.N. 2017. Gelatin-coated paper with antimicrobial and antioxidant effect for beef packaging. *Food Pack. Shelf Life*, 11: 115-124.
- Biswapriya, J., Sanghamitra, P. and Nabnita, P. 2021. Impact of improper biomedical waste disposal on human health and environment during a Covid-19 pandemic. *Europe. J. Molecul. Clinic. Med.*, 8(3): 4137-4143.
- Calis, S. and Arkan, B. 2014. The views of the nursing students about the medical wastes and their effects on the environmental and human health. *Proced. Social Behavior. Sci.*, 116: 1472-1476.
- Chauhan, I., Chattopadhyay, S. and Mohanty, P. 2013. Fabrication of titania nanowires incorporated paper sheets and study of their optical properties. *Mater Express*, 3(4):343-349.
- Diaz, L.F., Savage, G.M. and Eggerth, L.L. 2005. Alternatives for the treatment and disposal of healthcare wastes in developing countries. *Waste Manag.*, 25(6): 626-637.
- Doppalapudi, S., Katiyar, S., Domb, A.J. and Khan, W. 2014. Biodegradable natural polymers. *Adv. Polym. Med.*, 16: 33-66.

- Dupont, A.L. 2002. Study of the degradation of gelatin in paper upon aging using aqueous size-exclusion chromatography. *J. Chromatogr. A*, 950(1-2): 113-124.
- El-Sakhawy, M., Nashy, E.S.H.A., El-Gendy, A. and Kamel, S. 2018. Thermal and natural aging of bagasse paper sheets coated with gelatin. *Nord. Pulp Paper Res. J.*, 33(2): 327-335.
- Gruner, N., Stambouli, O. and Ross, R.S. 2015. Dried blood spots - preparing and processing for use in immunoassays and molecular techniques. *J. Vis. Exp.*, 97: e52619.
- Hao, Y., Chiu, P.Y. and Chen, C.F. 2021. Paper-based analytical devices for point-of-care blood tests. *Biomicrofluidics*, 15: 041303.
- Jayakumar, P., Padmanabhan, S., Suthendran, K. and Sujith, M. 2020. Identification and analysis of blood group with a digital microscope using image processing. *IOP Conf. Series Mater. Sci. Eng.*, 923: 1-6.
- Jha, R.K., Jha, P.K., Chaudhury, K., Rana, S.V. and Guha, S.K. 2014. An emerging interface between life science and nanotechnology: Present status and prospects of reproductive healthcare aided by nano-biotechnology. *Nano Rev.*, 5: 22762.
- Kamel, S., El-Sakhawy, M. and Nada, A.M.A. 2004. Mechanical properties of the paper sheets treated with different polymers. *Thermochim. Acta*, 421(1-2): 81-85.
- Leila, S. and Frank, A.G. 2017. Paper-based point-of-care testing in disease diagnostics. *Bioanalysis*, 9(11): 841-843.
- Li, H., Li, J., Zhang, Z., Cao, X., Zhu, J. and Chen, W. 2020. Establishing an interval-valued fuzzy decision-making method for sustainable selection of healthcare waste treatment technologies in the emerging economies. *J. Mater. Cycles Waste Manag.*, 22: 501-514.
- Linton, N.M., Kobayashi, T., Yang, Y., Hayashi, K., Akhmetzhanov, A.R., Jung, S., Yuan, B., Kinoshita, R. and Nishiura, H. 2020. Incubation period and other epidemiological characteristics of 2019 novel coronavirus infections with right truncation: A statistical analysis of publicly available case data. *J. Clin. Med.*, 9: 538.
- Mastorakis, N.E., Bulucea, C.A., Oprea, T.A. and Dondon, P. 2011. The holistic approach of biomedical waste management system with regard to health and environmental risks. *Int. J. Energy Environ.*, 5: 309-318.
- Mathur, P., Patan, S. and Shobhawat, A.S. 2012. Need of biomedical waste management system in hospitals—An emerging issue—A review. *Curr. World Environ.*, 7(1): 117-124.
- Nada, A.A.M.A., Kamel, S. and El-Sakhawy, M. 2000. Physico-mechanical properties of paper treated with polymers. *Restaurator*, 21(4). doi:10.1515/rest.2000.238
- Nur Hanani, Z.A., Roos, Y.H. and Kerry, J.P. 2014. Use and application of gelatin as potential biodegradable packaging materials for food products. *Int. J. Biol. Macromol.*, 71: 94-102. doi:10.1016/j.ijbiomac.2014.04.027.
- Padmanabhan, K.K. and Debabrata, B. 2019. Health hazards of medical waste and its disposal. *Energy Toxic Org. Waste Heat Power Gener.*, 11: 99-118.
- Tai, W.C., Yu-Chi, C., Dean, C. and Lung-Ming, F. 2021. Lab-on-paper devices for diagnosis of human diseases using urine samples: A review. *Biosensors*. 11(8):260.
- Wang, X., Liu, Y., Liu, X., You, X. and Zhang, H. J. 2020. Degradable gelatin-based supramolecular coating for green paper sizing. *ACS Appl. Mater. Inter.*, 13 (1):1367-1376.



# Evaluation of Phenotypic Responses of Selected Rice (*Oryza sativa* L.) Cultivars to Hexavalent Chromium Stress in Soil

B. K. Das, P. K. Das and P. Dash†

Centre for Biotechnology, Siksha 'O' Anusandhan (Deemed to be University), Bhubaneswar-751003, Odisha, India

†Corresponding author: P. Dash; patitapabandash@soa.ac.in

Nat. Env. & Poll. Tech.  
Website: [www.neptjournal.com](http://www.neptjournal.com)

Received: 29-09-2021

Revised: 12-12-2021

Accepted: 22-12-2021

## Key Words:

Rice cultivars  
Hexavalent chromium stress  
Phenotypic responses  
Seedlings

## ABSTRACT

The current work is designed to search for suitable rice (*Oryza sativa* L.) cultivars capable of growing on Cr(VI), hexavalent chromium contaminated soils. The study of tolerance and phenotypical changes of three selected rice cultivars like Bina Dhan 11, Kalachampa, and Pratikshya, at the seedling stages, was done under soil Cr(VI) concentrations up to 300 mg.kg<sup>-1</sup> of soil. The 7-day seedlings of these rice cultivars growing on Cr(VI) treated soils were found to exhibit a significant reduction in shoot and root growth at  $p \leq 0.05$ . The experimental results support that 7-day seedlings of Bina Dhan 11 were found to be the best among the three cultivars under soil Cr(VI) stress conditions. The present work may help in selecting suitable rice cultivar for paddy cultivation on Cr(VI) contaminated crop lands present in mining and industrial belts. Further work on this aspect may be useful in increasing rice productivity, catering to the increase in demand for food.

## INTRODUCTION

Chromium (Cr), commonly used as a metal corrosion inhibitor is an important heavy metal with multiple oxidation states and has wide applicability in industrial sectors (Das et al. 2021a). It is the 17<sup>th</sup> most hazardous substance for the living biota (Hou et al. 2019). It is widely introduced to the environmental components with the release of industrial effluents, irrigation of contaminated water, and disposal of sludge and solid wastes. (Majhi & Samantaray 2020). The Cr(VI) is a hazardous soil chemical constituent and is treated as a highly toxic heavy metal by the USEPA (Das et al. 2017).

The natural sources of hexavalent chromium contamination of croplands can take place through volcanoes, eroded rocks, and soils (Wang et al. 2017). The human involved activities like tanning of leathers, electroplating, burning of fossil fuels, dyeing of textiles, welding, polishing, and mining are the major sources of release of chromium into the environment (Das et al. 2018). The high chromium concentration of 2000-5000 mg.L<sup>-1</sup> in the released effluents contributes to the pollution of major rivers supporting irrigation systems in India (Alka 2017). The release of 2000-3000 tons of chromium per annum from tanneries in India to surroundings shows the magnitude of chromium pollution (Ahmed et al. 2021). It is not only polluting the terrestrial ecosystem but also the aquatic ecosystems due to leaching and percolations (Das et al. 2021b).

The grains of cereals like rice (*Oryza sativa* L.) are a nutritious food to remove hidden hunger from the growing world population (Khush & Virk 2000). These grains contain enough polysaccharides, proteins, vitamins, fibers, minerals, and antioxidants (Swain et al. 2017). It is a food of demand across the globe, especially in Asia, as billions of people are consuming rice and its products in multiple forms. Despite its demand, the productivity of rice per unit hectare in India is low as it is only 2.23 tons (Jain 2019). The high solubility of Cr(VI) renders to be more toxic to the growing rice crops on cultivable lands in the vicinity of industrial and mining areas. It may show a loss in the yield of the crop during exposure to Cr(VI) (Dheeba et al. 2014).

Many rice varieties are released so far but are not free from constraints to grow on contaminated soils. The present study was designed to find out an improved rice cultivar tolerant to Cr(VI) toxicity, at early seedling stages. It may help in increasing the yield of grains per unit area of land under rice cultivation.

## MATERIALS AND METHODS

### Experimental Environment

The experimental study was done in two successive Kharif seasons from July to December in the years 2019 and 2020. It was done under greenhouse conditions at the Centre for Biotechnology, Ghatikia, Bhubaneswar. It was located at



85°46'31" E and 21°17'02" N in the subtropical belt of India. The mean temperature and humidity maintained inside the greenhouse during the experimental growth and monitoring were  $27 \pm 1^\circ\text{C}$  and  $82 \pm 2\%$ , respectively. The mild acidic clayey soil was used for seedling growth during the experiment with pH ranged in between 5.9 to 6.2.

### Selection of Cultivars

The certified seeds of ten *Oryza sativa* L. cultivars were collected randomly and used for preliminary screening. Three rice cultivars Pratikshya (ORS 201-5), Bina Dhan 11 (Ciherang Sub-1), and Kalachampa (FV-152), meeting the requisite criteria were selected for the present experimental study (Table 1).

### Experimental Design

The healthy and intact seeds of three selected rice cultivars were used in this experimental study. The selected seeds were surface sterilized with 0.1% mercuric chloride. 200 pre-germinated, sterilized seeds of each selected cultivar were sown in rows of trays containing soils moistened with distilled water. These trays were maintained at a temperature of  $27 \pm 1^\circ\text{C}$  in dark. After germination, the experiment was designed with a selection of 7-day-old seedlings of three cultivars based on a randomized block design with triplicate seedlings in each group. The selected cultivars were allowed to grow on pots having the capacity to carry 4 kg of homogenous soils. One triplicate group of seedlings was allowed to grow as a control on 3kg of homogenous soil without having any Cr(VI) contamination. The seven-day seedlings of each cultivar were allowed to grow on 3 kg of Cr(VI) contaminated homogenous clayey soil of variable concentrations ranging between  $30 \text{ mg.kg}^{-1}$  soil to  $300 \text{ mg.kg}^{-1}$  soil with a regular gap of  $30 \text{ mg.kg}^{-1}$  of soil. The 7-day old seedlings of each replication of all the treatment conditions and control were sampled and analyzed for various phenotypic parameters like thousand grains weight, seed germination efficiency, seedlings survival percentage under Cr(VI) contaminated soil conditions, and variation in growth of shoots and roots with the change in soil Cr(VI) concentrations under treatment conditions.

### Phenotypic Study of Selected Cultivars

The phenotypic parameters of the selected cultivars were

determined following the standard methodologies (Yoshida et al. 1976).

### Thousand Seeds Weight

Three rice cultivars having three replicates of each were constituted by taking 1000 randomly selected intact seeds. These randomly selected seed samples were used for the determination of 1000 grain weights.

### Seed Germination Efficiency

The three replicates of each of these three rice cultivars having 50 healthy seeds each were selected randomly for the determination of this parameter. The seed germination efficiency was determined based on the percent germination of seeds at  $27 \pm 1^\circ\text{C}$ .

$$\text{Germination per cent} = (\text{Gs} / \text{Ts}) \times 100$$

Where,

Gs = Number of seeds germinated to produce normal seedlings

Ts = Total number of seeds taken for germination

### Seedlings Survival Percentage

The three replicates of each of these three rice cultivars like Bina Dhan 11, Kalachampa, and Pratikshya having 30 healthy seedlings each were selected randomly for the determination of this parameter.

$$\text{Seedling survival percentage} = (\text{Ssn} / \text{Stn}) \times 100$$

Where,

Ssn = Number of normal seedlings survived after 7 days under Cr(VI) stress soil conditions.

Stn = Total number of normal seedlings taken for the study.

### Seedlings' Growth and Variations

The seedlings' growth in terms of shoot, root, and leaf length of three replicates of each of the selected rice cultivars like Bina Dhan-11, Kalachampa, and Pratikshya was recorded.

### Statistical Analysis

The statistical analysis was done using a statistical package for the social sciences (IBM SPSS statistics 21) analytical

Table 1: Characteristics of rice cultivars selected for the experiment.

Selected cultivars	Range of maturity (in days)	Cultivar type	Grains type	Range of cultivar productivity [ $\text{t.ha}^{-1}$ ]
Bina Dhan 11	95-105	Early group	Medium Slender	5. 83-6.12
Kalachampa	143 - 158	Late group	Medium bold	6.86-7.14
Pratikshya	138 - 152	Medium late group	Long slender	7.06-7.38



Table 2: Seed characteristics of selected rice cultivars.

Sl. No.	Cultivars	Thousand seeds weight [g]	Germination of seeds [%]
1	Bina Dhan 11	59.09	94
2	Kalachampa	61.45	88
3	Pratikshya	63.34	86

software. The analysis of variance (ANOVA) in respect of the mean response of cultivars to variation in Cr(VI) treatment concentrations was done under a split-plot design. The differences between treatment means were estimated using Tukey's HSD test at  $p \leq 0.05$ .

## RESULTS AND DISCUSSION

Rice is a major food crop in the Indian sub-continent and India is the second-largest rice-producing nation in the world after China. A person in India consumes approximately 68.2 kg of milled rice per year which confirms the importance of rice as a major staple food for the Indian population (Das et al. 2020). The yield of rice is highly affected due to contamination of agricultural soil with toxic industrial effluents rich in heavy metals like Cr(VI). The current work, therefore, strived to select the improved cultivars that could resist and grow well under high concentrations of soil Cr(VI) content.

### Seed Characteristics of Selected Rice Cultivars

The rice cultivar, Bina Dhan 11 records 94 per cent germination of seeds and it is maximum as compared to other cultivars like Kalachampa and Pratikshya (Fig. 1). The per cent germination of seeds in Kalachampa and Pratikshya are 88 and 86 per cent, respectively. In the present experiment, the per cent germination of seeds shows an inverse relationship with the weight of thousand seeds of the selected rice cultivars. It is supported by the findings of another study on *Pisum sativum* L. (Peksen et al. 2004). Based on a comparison of three selected cultivars, Bina Dhan 11 shows maximum seed germination (94 per cent) and simultaneously minimum thousand seeds weight (59.09 g). A thousand seeds weight is maximum in Pratikshya (63.34 g) and recorded minimal seeds germination as 86 per cent (Table 2).

### Seedlings Survival Percentage

The survival of seedlings on croplands is an important parameter to getting a better yield. It is required for farmers' acceptance and for meeting their socio-economic needs. The Bina Dhan- 11 is found to be a suitable rice cultivar as compared to Kalachampa and Pratikshya based on its survival percentage at the early seedling age of 7 days. It is observed that the survival of rice cultivar Pratikshya is intermediate

and is ranked in between the other two cultivars studied together (Fig. 1).

Cr at a very low concentration ( $0.06-1.0 \text{ mg.L}^{-1}$ ) is found to enhance growth and yield in *Oryza sativa* L. However,

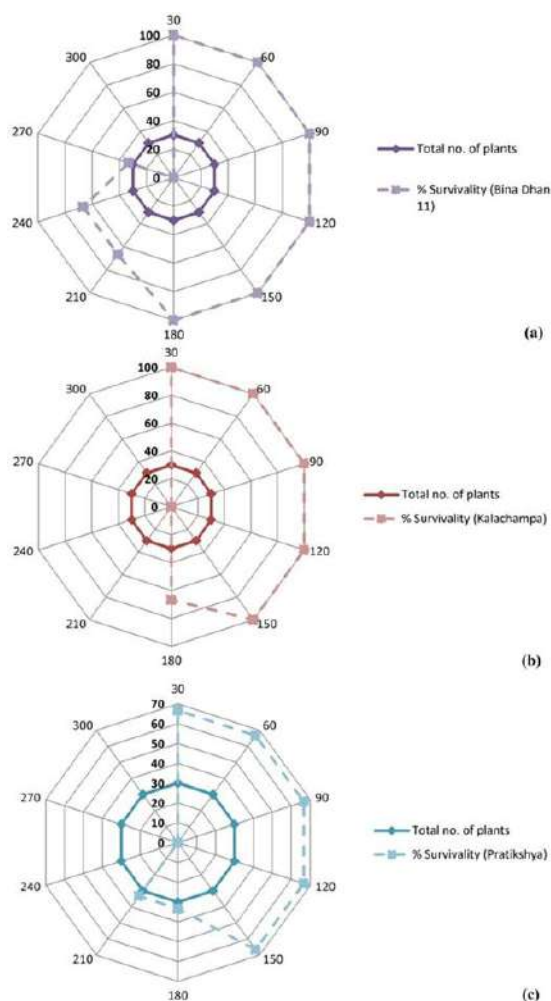


Fig. 1: Survival of seedlings of selected rice cultivars (a) Bina Dhan-11, (b) Kalachampa, and (c) Pratikshya under different soil Cr(VI) concentrations. (The values around the periphery of the graph show the different levels of soil Cr(VI) in  $\text{mg.kg}^{-1}$  and the values marked in bold denote the survival percentage of seedlings. The solid lines mark the number of 7-day-old seedlings subjected to treatment, and the dotted lines express the survival percentage at each concentration of soil Cr(VI)).

a higher concentration of toxic heavy metals hinders the survival of plants. It affects the germination process and negatively impacts the growth of rice crops (Javaid et al. 2020). This may be the possible reason behind the reduced survivability among the cultivars with an increase in soil Cr(VI) concentrations.

### Seedlings Growth and Variations

An increase in Cr(VI) load in the soil led to a gradual reduction in the shoot and root length of three rice cultivars during the 7-day treatment. The mean shoot growth of Bina Dhan 11 is  $2.10 \pm 0.01$  cms on soil contaminated with  $270 \text{ mg.kg}^{-1}$  soil is low as compared to its growth on  $0 \text{ mg.kg}^{-1}$  soil, treated as a control in the experiment. Similarly, the mean root growth of Bina Dhan 11 is  $13.47 \pm 0.20$  cms on soil contaminated with  $270 \text{ mg.kg}^{-1}$  soil is low as compared to its growth as a control. The mean shoot and root growth of rice cultivar Pratikshya are more as compared to the other two cultivars Bina Dhan 11 and Kalachampa on soil contaminated with  $210 \text{ mg.kg}^{-1}$  soil but this cultivar is unable to grow on soils contaminated with a higher concentration of Cr(VI) (Table 3). Plants treated with  $270 \text{ mg.kg}^{-1}$  soil Cr(VI) showed maximum reduction in the shoot (35.97% for Bina Dhan 11) and roots (16.07% for Bina Dhan 11) about controls (Table 4).

The Cr to be responsible for bringing about a reduction in the root and shoot of crop plants is supported by the findings of previous studies (Purohit et al. 2003, Sundaramoorthy et al. 2010). The reduction in morphological parameters of *Oryza sativa* L. due to Cr stress has received strong support from

the earlier studies (Gill et al. 2015, Shahid et al. 2017). The reduction in length of seedlings may be due to Cr stress-led constraint in nutrient uptake as well as alterations in the ultra-structural framework of mesophyll cells present in the rice leaves (Hussain et al. 2018). The decrease in chlorophyll content of leaves due to the loss of both chlorophyll a and b is observed under stress conditions (Das et al. 2008). The parameter like total sugar and starch content of seedlings are determining the tolerance of rice cultivars to stress conditions (Das et al. 2009).

The Cr has been reported to form insoluble complexes with soil nutrients, thus hindering their uptake in plants (Chigonum et al. 2019). The Cr has been playing a major role in disturbing the nutrient balance in plants. Excess of Cr has been reported to bring about a corresponding decrease in micro and macronutrients in *Oryza sativa* L. which may be attributed to the displacement of the nutrients from physiologically important binding sites and thus their reduced translocation into the crop (Shahzad et al. 2018).

### Correlation Studies

An increase in soil Cr(VI) concentrations resulted in a corresponding decrease in both the shoot and root length of the selected rice cultivars implying the existence of a negative correlation between the studied parameters (Fig. 2). Among the three selected rice cultivars the correlation between soil Cr(VI) and shoot length of Bina Dhan 11 ( $r = -0.795$ ) was much less as compared to Kalachampa ( $r = -0.926$ ), and Pratikshya ( $r = -0.913$ ). A similar trend was obtained between

Table 3: Effect of 7-day treatment of variation in soil Cr(VI) concentration on seedlings growth of selected rice cultivars.

Soil treatment code / Cr(VI) concentration in $\text{mg.kg}^{-1}$ soil	Shoot and root growth of 7-day seedlings of selected rice cultivars under soil Cr(VI) treatment conditions					
	Mean shoot growth $\pm$ S.E.M (cm)			Mean root growth $\pm$ S.E.M (cm)		
	Bina Dhan 11	Kalachampa	Pratikshya	Bina Dhan 11	Kalachampa	Pratikshya
T0 (control) / 0	$3.28 \pm 0.03$	$4.08 \pm 0.05$	$5.66 \pm 0.08$	$16.05 \pm 0.18$	$21.16 \pm 0.16$	$22.29 \pm 0.33$
T1 / 30	$3.18 \pm 0.01$	$3.90 \pm 0.02$	$5.50 \pm 0.06$	$15.52 \pm 0.18$	$18.82 \pm 0.16$	$22.24 \pm 0.23$
T2 / 60	$3.12 \pm 0.03$	$2.70 \pm 0.01$	$4.60 \pm 0.04$	$15.43 \pm 0.19$	$15.49 \pm 0.13$	$21.27 \pm 0.25$
T3 / 90	$3.12 \pm 0.01$	$2.50 \pm 0.01$	$4.23 \pm 0.11$	$15.03 \pm 0.02$	$14.74 \pm 0.16$	$19.38 \pm 0.22$
T4 / 120	$2.88 \pm 0.02$	$2.45 \pm 0.02$	$4.14 \pm 0.10$	$15.00 \pm 0.26$	$14.56 \pm 0.12$	$19.08 \pm 0.21$
T5 / 150	$2.68 \pm 0.02$	$2.18 \pm 0.06$	$3.81 \pm 0.03$	$14.64 \pm 0.23$	$14.19 \pm 0.09$	$18.70 \pm 0.17$
T6 / 180	$2.67 \pm 0.03$	$2.08 \pm 0.03$	$3.69 \pm 0.04$	$14.15 \pm 0.31$	$13.81 \pm 0.13$	$18.36 \pm 0.21$
T7 / 210	$2.48 \pm 0.02$	-	$3.53 \pm 0.04$	$14.09 \pm 0.15$	-	$18.07 \pm 0.20$
T8 / 240	$2.39 \pm 0.04$	-	-	$13.77 \pm 0.20$	-	-
T9 / 270	$2.10 \pm 0.01$	-	-	$13.47 \pm 0.20$	-	-
T10 / 300	-	-	-	-	-	-

Significant at  $p \leq 0.05$ ; '-' indicates the non-existence of cultivars at the specified concentration of soil Cr(VI).

Table 4: Mean percentage reduction in length of rice seedlings under variable soil Cr(VI) concentrations for 7 days.

Soil treatment code / Cr(VI) concentration in mg.kg <sup>-1</sup> soil	Mean Percentage reduction					
	Shoot growth			Root growth		
	Bina Dhan-11	Kalachampa	Pratikshya	Bina Dhan-11	Kalachampa	Pratikshya
T1 / 30	3.04	4.41	2.82	3.30	11.05	0.22
T2 / 60	6.09	33.82	18.72	3.86	26.79	4.57
T3 / 90	6.09	38.72	25.26	6.35	30.34	13.05
T4 / 120	12.10	39.95	26.85	6.54	31.19	14.40
T5 / 150	18.29	46.56	32.68	8.78	32.93	16.10
T6 / 180	18.59	49.01	34.80	11.83	34.73	17.63
T7 / 210	24.39	-	37.63	12.21	-	18.93
T8 / 240	27.13	-	-	14.20	-	-
T9 / 270	35.97	-	-	16.07	-	-
T10 / 300	-	-	-	-	-	-

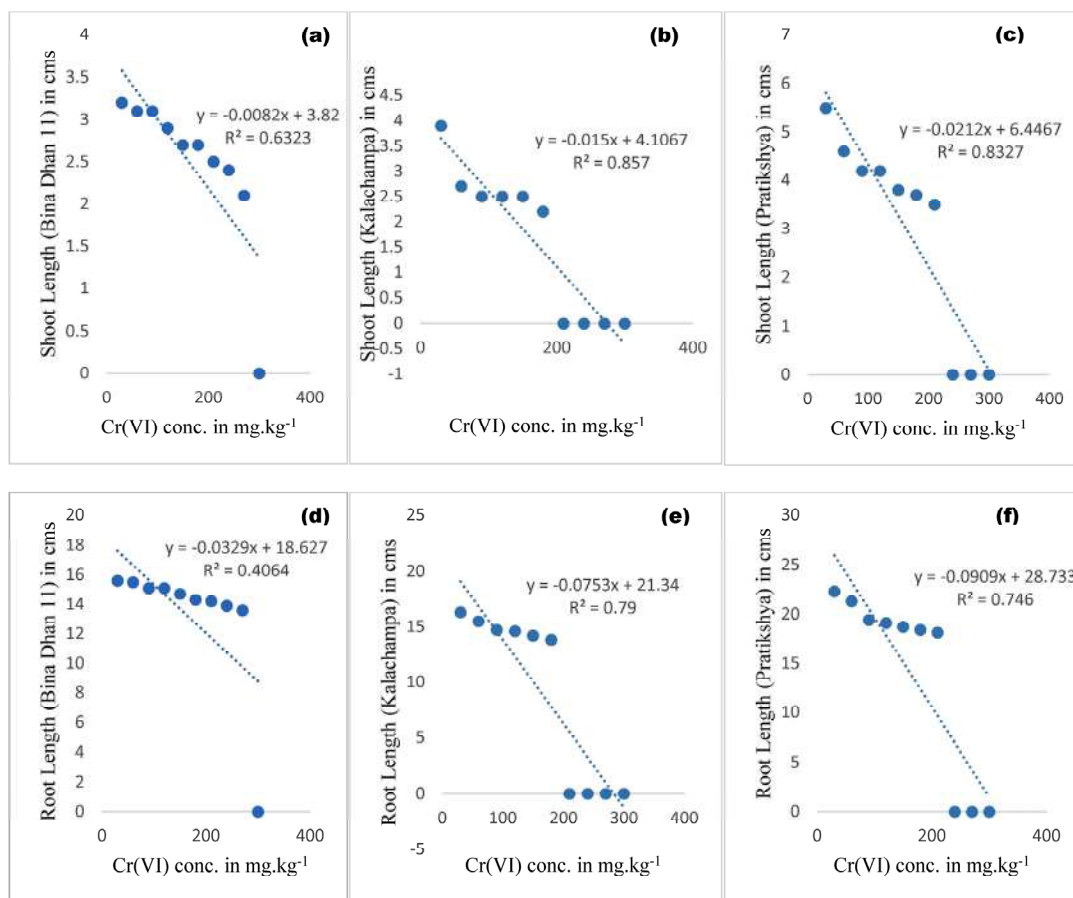


Fig. 2: Graph showing the correlation between varied soil Cr(VI) concentration and (a) shoot length of Bina Dhan 11 (b) shoot length of Kalachampa (c) shoot length of Pratikshya (d) root length of Bina Dhan 11 (e) root length of Kalachampa, and (f) root length of Pratikshya.

the reduction in mean root length and an increase in soil Cr(VI) concentrations. This confirms the better suitability of Bina Dhan 11 to Cr(VI) soil stress as compared to the other two cultivars.

### Cr(VI) Mediated Variations in Leaf Length

In the present study, the impact of Cr(VI) on the three selected rice cultivars was studied. It is observed that the size of the leaves varied negatively with a proportionate increase in Cr(VI) content in the soil. The leaf length gradually decreased with an increase in soil Cr(VI) content from 30 mg.kg<sup>-1</sup> soil to 270 mg.kg<sup>-1</sup> soil (Fig. 3). A leaf is a vital organ in plants and helps mostly in the process of photosynthesis. The total area of a leaf in a plant determines the efficiency of photosynthesis (Srivastava et al. 2021). It is observed that Cr(VI) shows a negative impact on leaf morphology in *O. sativa*. It is supported by the findings of another study on paddy (Sundaramoorthy et al. 2010). The Cr(VI) has also been found to impart toxic effects on other plants. The *Prosopis laevigata* when exposed to nutrient media enriched with a 3.4mM Cr(VI) concentration resulted in a reduced number of leaves (Buendía-González et al. 2010). In a similar study, *Lolium perenne* L. grown in nutrient media spiked with 0.5 mM of Cr(VI) resulted in the wilting of the leaves (Vernay et al. 2007). Chlorosis in the leaves of *Saccharum officinarum* was observed when exposed to a soil Cr(VI) concentration

of 40 mg.kg<sup>-1</sup>. On increasing the toxic metal concentration to 80 mg.kg<sup>-1</sup>, the leaves of the plant exhibited severe necrosis (Radha et al. 2000). Cr(VI) has been found to inhibit the biosynthesis of chlorophyll pigments in plants (Sharma et al. 2019), a possible reason behind reduced leaf area in the current study. An increase in Cr(VI) concentrations may lead to a reduction in the chlorophyll content which may be due to the inactivation of chlorophyll biosynthesis enzymes (Zlobin et al. 2015, Sharma et al. 2020).

Another probable reason for reduced leaf length can be attributed to either reduction in the number of leaf cells or a probable reduction in the size of the cells under Cr(VI) stress. Reduced cell size may also negatively affect the intracellular spaces thus leading to stunted growth of the leaves (Joshi et al. 1999).

### CONCLUSION

The current experimental approach is to find out a suitable rice cultivar capable of growing on Cr(VI) stress soil conditions. All the three rice cultivars Bina Dhan-11, Kalachampa, and Pratikshya have been able to survive on Cr(VI) stress soil conditions upto 180 mg.kg<sup>-1</sup>. The evaluation of selected phenotypic parameters reveals that Bina Dhan 11 is a suitable rice cultivar at the early seedling stage to grow on Cr(VI) stress soil conditions up to 270 mg.kg<sup>-1</sup> soil. Further work

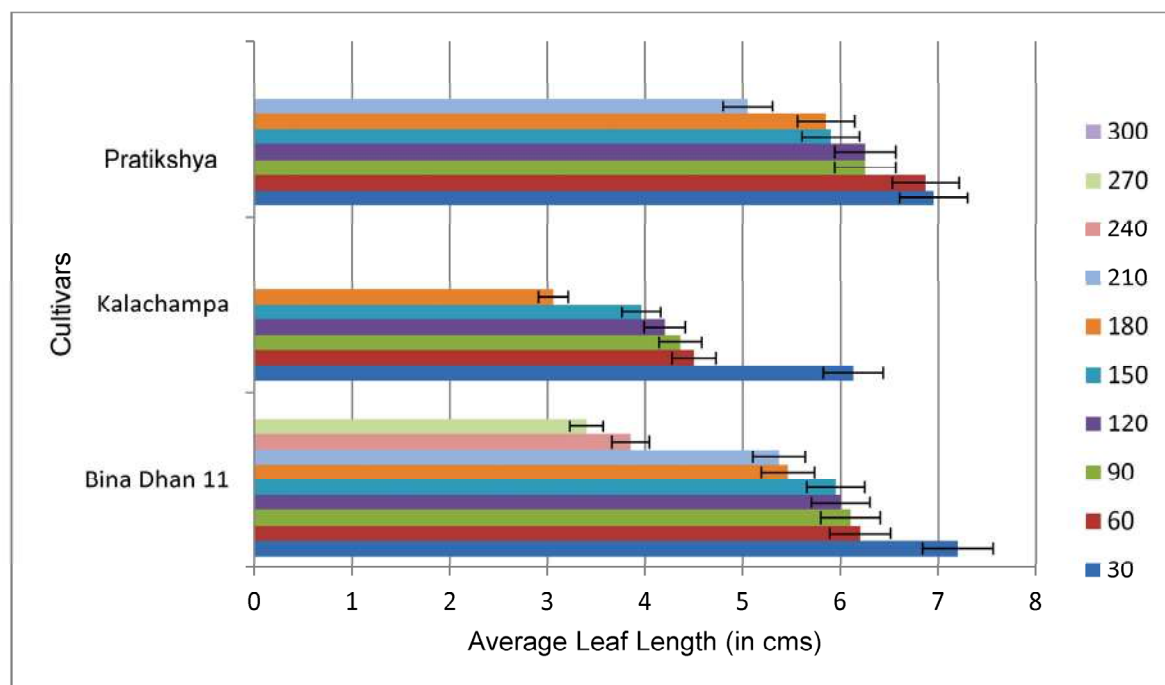


Fig. 3: Leaf length of rice cultivars under different concentrations (30-270 mg.kg<sup>-1</sup> soil) of Cr(VI).

on this aspect is useful in getting better paddy yield from Cr(VI) contaminated soil conditions.

## ACKNOWLEDGEMENT

The authors acknowledge the support provided by Siksha 'O' Anusandhan (Deemed to be University) during the course of this research.

## REFERENCES

- Ahmed, F., Fakhruddin, A.N.M., Fardous, Z., Chowdhury, M.A.Z., Rahman, M.M. and Kabir, M.M. 2021. Accumulation and translocation of chromium (Cr) and lead (Pb) in chilli plants (*Capsicum annum* L.) Grown on Artificially Contaminated Soil. *Nat. Environ. Pol. Tech.*, 20(1): 63-70.
- Alka, B. 2017. A review of hexavalent chrome. *Res. J. Chem.*, 7(7): 39-44.
- Buendía-González, L., Orozco-Villafuerte, J., Cruz-Sosa, F., Barrera-Díaz, C.E. and Vernon-Carter, E.J. 2010. *Prosopis laevigata* a potential chromium (VI) and cadmium (II) hyperaccumulator desert plant. *Bio. Res. Tech.*, 101(15): 5862-5867.
- Chigonon, W.J., Ikenna, O.C. and John, C.U. 2019. The dynamic impact of chromium on nutrient uptake from soil by fluted pumpkin (*Telfairia occidentalis*). *Am. J. Biosci. Bioeng.*, 7: 1-9.
- Das, B.K., Das, P.K., Das, B.P. and Dash, P. 2021a. Green technology to limit the effects of hexavalent chromium contaminated water bodies on public health and vegetation at industrial sites. *J. Appl. Bio. Biotech.*, 9(2): 28-35.
- Das, B.P., Dash, P. and Roy, A.T. 2009. Role of total sugar and starch content of rice seedlings at different ages in variable submergence tolerance. *ORYZA Int. J. Rice*, 46(4): 304-309.
- Das, B.P., Roy, A.T. and Dash, P., 2008. Effect of seedling age and submergence on chlorophyll content of rice cultivars. *ORYZA Int. J. Rice*, 45(2): 169-172.
- Das, P.K., Das, B.P. and Dash, P. 2018. Role of plant species as hyper-accumulators in the decontamination of hexavalent chromium contaminated soil. *Indian J. Environ. Prot.*, 38(12): 1016-1024.
- Das, P.K., Das, B.P. and Dash, P. 2020. Potentials of postharvest rice crop residues as a source of biofuel. In *Ref. Biom. Res. Sust. Energy Biop.*, 12: 275-301.
- Das, P.K., Das, B.P. and Dash, P. 2021b. Chromite mining pollution, environmental impact, toxicity, and phytoremediation: a review. *Environ. Chem. Lett.*, 19(2): 1369-1381.
- Das, P.K., Das, B.P. and Dash, P. 2017. Hexavalent chromium-induced toxicity and its remediation using macrophytes. *Poll. Res.*, 36: 92-98.
- Dheeba, B., Sampathkumar, P. and Kannan, K. 2014. Chromium accumulation potential of *Zea mays* grown under four different fertilizers. *Indian J. Exp. Bio.*, 52: 1206-1207.
- Gill, R.A., Ali, B., Islam, F., Farooq, M.A., Gill, M.B., Mwamba, T.M. and Zhou, W. 2015. Physiological and molecular analyses of black and yellow seeded *Brassica napus* regulated by 5-aminolivulinic acid under chromium stress. *Plant Phys. and Biochem.*, 94:130-143.
- Hou, S., Wu, B., Peng, D., Wang, Z., Wang, Y. and Xu, H. 2019. Remediation performance and mechanism of hexavalent chromium in alkaline soil using multi-layer loaded nano-zero-valent iron. *Environ. Poll.*, 252: 553-561.
- Hussain, A., Ali, S., Rizwan, M., Rehman, M.Z., Hameed, A., Hafeez, F., Alamri, S.A., Alyemeni, M.N. and Wijaya, L. 2018. Role of zinc-lysine on growth and chromium uptake in rice plants under Cr stress. *J. Plant Growth Regul.*, 37(4): 1413-1422.
- Jain, B.T. 2019. Effect of different production systems on flowering and maturity duration of basmati rice genotypes. *ORYZA Int. J. Rice*, 56(1): 11-17.
- Javadi, S., uz Zaman, Q., Sultan, K., Riaz, U., Aslam, A., Saba Sharif, N.E., Aslam, S., Jamil, A. and Ibraheem, S. 2020. 5. Heavy metals stress, mechanism, and remediation techniques in rice (*Oryza sativa* L.): A review. *Pure App. Bio.*, 9(1): 403-426.
- Joshi, U.N., Rathore, S.S. and Arora, S.K. 1999. Effect of chromium on growth and development of cowpea (*Vigna unguiculata* L.). *Indian J. Environ. Prot.* 19(1): 745-749.
- Khush, G.S. and Virk, P.S. 2000. Rice breeding: Achievements and future strategies. *Crop Improv.*, 27(2):115-144.
- Majhi, P. and Samantaray, S.M. 2020. Effect of hexavalent chromium on paddy crops (*Oryza sativa*). *J. of Pharmac. Phytochem.*, 9(2): 1301-1305.
- Peksen, E., Peksen, A., Bozoglu, H. and Gulumsar, A. 2004. Some seed traits and their relationships to seed germination and field emergence in pea (*Pisum sativum* L.). *J. of Agron.*, 3(4): 243-246.
- Purohit, S., Varghese, T.M. and Kumari, M. 2003. Effect of chromium on morphological features of tomato and brinjal. *Indian J. of Plant Physiol.*, 8(1): 17-22.
- Radha, J., Srivastava, S. and Madan, V.K. 2000. Influence of chromium on growth and cell division of sugarcane. *Indian J. of Plant Physiol.*, 5(3):228-231.
- Shahid, M., Shamshad, S., Rafiq, M., Khalid, S., Bibi, I., Niazi, N.K., Dumat, C. and Rashid, M.I. 2017. Chromium speciation, bioavailability, uptake, toxicity and detoxification in soil-plant system: A review. *Chemosphere*, 178:513-533.
- Shahzad, B., Tanveer, M., Rehman, A., Cheema, S.A., Fahad, S., Rehman, S. and Sharma, A. 2018. Nickel: Whether toxic or essential for plants and environment: A review. *Plant Physiol. Biochem.*, 132: 641-651.
- Sharma, A., Kapoor, D., Wang, J., Shahzad, B., Kumar, V., Bali, A.S., Jasrotia, S., Zheng, B., Yuan, H. and Yan, D. 2020. Chromium bioaccumulation and its impacts on plants: An overview. *Plants*, 9(1): 100.
- Sharma, A., Kumar, V., Shahzad, B., Ramakrishnan, M., Sidhu, G.P.S., Bali, A.S., Handa, N., Kapoor, D., Yadav, P., and Khanna, K. 2019. Photosynthetic response of plants under different abiotic stresses: A review. *J. Privant Growth Regul.*, 38: 1-23.
- Srivastava, D., Tiwari, M., Dutta, P., Singh, P., Chawda, K., Kumari, M. and Chakrabarty, D. 2021. Chromium stress in plants: Toxicity, tolerance, and phytoremediation. *Sustainability*, 13(9): 4629.
- Sundaramoorthy, P., Chidambaram, A., Ganesh, K.S., Unnikannan, P. and Baskaran, L. 2010. Chromium stress in paddy:(i) nutrient status of paddy under chromium stress:(ii) phytoremediation of chromium by aquatic and terrestrial weeds. *Compt. Rend. Biol.*, 333(8): 597-607.8
- Swain, R.K., Padhiary, A.K., Behera, S., Mishara, S.P., Jena, M., Swain, S.C. and Rout, S.K. 2017. Morpho physiological traits of some rice varieties in response to shallow water depth. *Int. J. Curr. Microbiol. App. Sci.* 6(11): 3950-3957.
- Vernay, P., Gauthier-Moussard, C. and Hitmi, A. 2007. Interaction of bio-accumulation of heavy metal chromium with water relation, mineral nutrition, and photosynthesis in developed leaves of *Lolium perenne* L. *Chemosphere*, 68(8): 1563-1575.
- Wang, Y., Su, H., Gu, Y., Song, X. and Zhao, J. 2017. Carcinogenicity of chromium and chemoprevention: A brief update. *Oncol. Targets Therapy*, 10: 4065-4079.
- Yoshida, S., Forno, D.A., Cock, J.H. and Gomez, K.A. 1976. Laboratory manual for physiological studies of rice. Third Edition, The International Rice Research Institute, Los Baños, Philippines, pp. 2-83.
- Zlobin, I.E., Kholodova, V.P., Rakhmankulova, Z.F. and Kuznetsov, V.V. 2015. *Brassica napus* responses to short-term excessive copper treatment with a decrease of photosynthetic pigments, differential expression of heavy metal homeostasis genes including activation of gene NRAMP4 involved in photosystem II stabilization. *Photosyn. Res.*, 125(1): 141-150.







# A Mini-Review on the Use of Constructed Wetland Systems for Water Treatment in Developing Countries

J. M Nyika† and M. O Dinka

The University of Johannesburg, Department of Civil Engineering Science, APK Campus 2006, Johannesburg, South Africa

†Corresponding author: J. M Nyika; joashmada2011@gmail.com

**Nat. Env. & Poll. Tech.**  
Website: [www.neptjournal.com](http://www.neptjournal.com)

Received: 15-09-2021  
Revised: 10-11-2021  
Accepted: 21-11-2021

## Key Words:

Constructed wetlands  
Contaminants  
Developing countries  
Pollutants  
Wastewater treatment

## ABSTRACT

The predominant scarcity of water globally has necessitated the invention of non-conventional resources to bridge the clean freshwater demand gap. Even in areas where there is access to water, inadequate quality and sanitation are pervasive problems, especially in developing countries. Resolving these intricate water-related problems, which emanate from population increase, the rise of urbanization and industrialization has not been realized using modern cost-, energy- and water-intensive technologies. In light of these challenges, wastewater treatment is a viable solution to supplement limited water resources. Of the available eco-technologies used in wastewater treatment for reuse, constructed wetlands (CWs) have proved to be the most effective. In this review, CWs are confirmed as reliable and low-cost green technologies with high effectiveness in wastewater treatment compared to conventional technologies. Therefore, their application among rural communities of developing countries is practical and highly advisable.

## INTRODUCTION

The world is currently sharing a recurrent problem of water scarcity where available natural water sources cannot meet the demand adequately (Suhad et al. 2018). According to Scheierling et al. (2011), more than 67 % of the globe will have a water shortage state in 2025 and 50 % will experience high water stress by 2030. The World Water Assessment Programme (WWAP) (2015) agreed with these projections claiming that they will result from increased water demand at all production levels and at least 40 % of the world will likely be water scarce by 2030. Other drivers of water scarcity include a high population growth rate, expansion of agricultural and industrial activities, climate change, and global warming. These drivers result in a sharp rise in wastewater generation trends. Wastewater contains pollutants such as biochemical and chemical oxygen demand, microbes, heavy metals, non-biodegradable organics, and particles that deteriorate water quality once it is released into freshwater resources making the resources unsustainable for aquatic life, irrigation, and potability (Suhad et al. 2018). Due to the soaring water scarcity situation, researchers are exploring the use of non-conventional sources to meet the ever-rising demand. Wastewater has been identified as a feasible alternative (Noori et al. 2014, Zhang et al. 2014, Almukhtar & Scholz 2015, Gorgoglione & Torretta 2018). The

reuse of wastewater, however must be taken up with caution considering its characteristic pollutants whose unregulated environmental release is risky to ecological health. This consideration necessitates wastewater treatment before reuse.

The use of constructed wetlands (CWs) serves as a promising and innovative solution for cost-effective and sustainable treatment of wastewater particularly in developing countries where conventional wastewater treatment infrastructure is limited due to financial constraints (Zhang et al. 2014). The countries in addition experience water scarcity owing to the rising population and economic growth. CWs are ecological technologies and engineered systems for wastewater treatment that incorporate physical, chemical, and biological processes to decontaminate water in natural wetland environs. Constructed wetlands have been successfully used to cleanse wastewater off suspended solids, heavy metals, nutrients, and organic compounds (Zhang et al. 2014, Gorgoglione & Torretta 2018, Suhad et al. 2018). The preference to use CWs is associated with their high removal efficacy, great potential to reuse nutrients and water, simplicity of operation, and cost efficiency (Almukhtar & Scholz 2015). Despite these successes, there have been limited studies focusing on the use of CWs in developing countries whose water status is dire due to the aforementioned drivers. This review study, therefore, focuses on the use of

ecological technology in wastewater treatment, the various types of CWs, and their effectiveness in cleansing wastewater with a particular focus on developing countries.

## CONSTRUCTED WETLANDS IN DEVELOPING COUNTRIES

The adoption of CWs in wastewater treatment for developing countries is on a rising trend due to its low energy requirements and ability to recycle large volumes fast according to Vymazal (2011). The technology has been used in developing countries to treat agricultural runoff (Yang et al. 2008), landfill leachate (Nahlik & Mitsch 2006), laboratory waste (Meutia 2001), and hospital wastewater (Shrestha et al. 2001), wastewater from sugar factories (Bojcevska & Tonderski 2007). In addition, CWs treat storm-water runoff (Sim et al. 2008, Avila et al. 2013), wastewater produced from oil processing (Ji et al. 2007), sludge effluent (Ahmed et al. 2008), lake and river water (Li et al. 2009, Tang et al. 2009). Domestic water (Zhai et al. 2011, Mburu et al. 2013), industrial wastewater (Chen et al. 2006, Maine et al. 2007), and agricultural wastewater (He et al. 2006, Zhang et al. 2014) have been treated using this ecological technique too.

Concerning the performance of CWs, their effectiveness in developing countries is favored by the warm subtropical and tropical climates of the regions, where these technologies are better performers compared to temperate regions (Kivaisi 2001, Zhang et al. 2014). In tropical regions unlike temperate regions, plant growth and microbial activity occur throughout the year, which are favorable prerequisites to CWs effectiveness (Kaseva 2004). Zhang et al. (2012) agreed with these sentiments claiming that tropical wetlands are exposed to direct sunlight and have higher temperatures year round, favor plant growth, and reduced microbial degradation time, which are important factors in wastewater treatment via CWs.

## TYPES OF CWS AND THEIR TREATMENT EFFICIENCY

Constructed wetlands are classified into three; subsurface flow (SSF), free water surface (FWS), and hybrid CWs (Zhang et al. 2014). SSF CWs are further classified into horizontal and vertical systems. The selection of a particular type of CW depends on the treatment goals, available area, cost, geographic location, and target pollutants for treatment (Horner et al. 2012).

### Free Water Surface Systems

The FWS systems are arranged with channels and tanks that are artificially or naturally waterproofed and where the water level remains constant above the medium surface and the

depth ranges between 0.3 and 0.6 m (Gorgoglione & Torretta 2018). Flow in the system originates from an inlet area to an outlet in a region with low flow velocity, low water depth, and plant bodies. Small channels that mimic the plug flow reactor help in standardizing flow. According to Vymazal (2011), FWS systems ensure wastewater encounters biologically active surfaces to enhance its hydraulic retention time and prevent hydraulic short-circuit formation. FWS systems remove suspended solids through sedimentation and filtration as well as organics via microbial degradation. Removal efficacy for pathogens, chemical and biological oxygen demand (COD, BOD), and total suspended solids (TSS) is above 70% while nitrogen removal efficacy ranges between 40 and 50 % (Kadlec & Wallace 2008). At slow rates, FWS systems can remove phosphorous from wastewater at an efficacy rate of 40 to 90% (Vymazal 2011). A summary of the applications of FWS systems in decontaminating wastewater pollutants and their specific effectiveness in named developing countries is shown in Table 1. The results show varied removal efficacies based on individual studies and the pollutant being removed.

### Subsurface Flow Systems

Subsurface flow (SSF) CWs are designed as horizontal (HSSF) or vertical (VSSF) where wastewater flows through a permeable medium (Vymazal 2011). In horizontal systems, wastewater flows towards the granular material horizontally and encounters anaerobic, anoxic, and aerobic conditions in the subsurface. The latter occurs near rhizomes and roots of plants that release oxygen to the substrate. Anoxic zones are rich with aerobic microbes, which transfer oxygen to the filter bed from the atmosphere. The redox conditions enable wastewater decontamination. Vertical CWs use a distribution system to feed wastewater to the entire surface and passes the media vertically (Zhang et al. 2014). The effluent introduction is discontinuous, unlike the horizontal systems where there is a continuous flow. Some of the studies demonstrating the effectiveness of SSF systems in developing countries, contaminants treated and plant species used are summarized in Table 2. Plant species in both vertical and horizontal systems enable purification by enhancing microbial activity at the rhizosphere and via oxygen release to the atmosphere from the root system to the surrounding environment (Gorgoglione & Torretta 2018).

From the comparisons of HSSF and VSSF, the former offers good conditions for denitrification though such systems have limited ability to denitrify ammonia. In VSSF systems,  $\text{NH}_3\text{-N}$  can be removed but denitrification barely occurs. The two systems have a moderate ability to remove total nitrogen (TN) while HSSF had better removal efficacy for total phosphorous (TP) compared to VSSF (Zhang et al.

Table 1: Application of FWS systems in decontaminating wastewater contaminants and their effectiveness in named developing countries.

Study Characteristics	Type of Wastewater	TSS	BOD	COD	NH <sub>4</sub> -N	NO <sub>3</sub> -N	TN	TP	Plant species	References
Petchaburi, Thailand Effluent level % removal Efficacy	Municipal waste- water	40.4 46.5	12.7 74.3	- -	51.8 75.4	- -	- -	2.2 44.9	<i>Typha angustifolia</i>	Klomjek & Nitisoravut 2005
Liaohu, China Effluent level % removal Efficacy	Oil-based wastewa- ter	- -	3.9 88	77 80	- -	- -	9.7 10.2	0.53 18.5	<i>Phragmites australis</i>	Ji et al. 2007
El Salvador Effluent level % removal Efficacy	Municipal waste- water	- -	20.1 80.8	72.8 65.2	0.54 94.75	- -	6.08 58.59	1.86 66.5	<i>T. angustifolia</i>	Katsenovich et al. 2009
Shanghai, China Effluent level % removal efficacy	Polluted river water	30 70	7.7 15.4	32 17.9	- -	- -	6.15 83.4	0.32 96	<i>P. australis</i>	Li et al. 2009
Nyanza, Kenya Effluent level % removal efficacy	Wastewater from sugar factories	11 76	- -	- -	2.9 36	- -	- -	4.1 29	<i>Echinochloa pyramidalis</i> <i>Cyperus papyrus</i>	Bojevska & Tonderski 2007
Putrajaya, Malaysia Effluent level % removal efficacy	Stormwater	- -	- -	- -	- -	0.96 70.7	- -	0.06 84.3	<i>Lepironia articulata</i> <i>Phragmites karka</i>	Sim et al. 2008
Peradeniya, Sri-Lanka Effluent level % removal efficacy	Municipal waste- water	45.8 71.9	19.2 68.2	- -	3.4 74.4	0.9 50	- -	1.36 19	<i>Scirpusgrossus</i> <i>T. angustifolia</i>	Jimadasa et al. 2006

\*All effluent levels are in mg.L<sup>-1</sup>

Table 2: Application of HSSF systems in decontaminating wastewater contaminants and their effectiveness in named developing countries.

Study Characteristics	Type of Wastewater	TSS	BOD	COD	NH <sub>4</sub> -N	NO <sub>3</sub> -N	TN	TP	Plant species	References
Taihu, Zhejiang, China Effluent Level % removal efficacy	Polluted lake water	- -	- -	4.23 39.6	1.16 32	0.37 65.3	2.29 52.1	0.052 65.7	<i>T. angustifolia</i>	Li et al. 2008
Shatian, China Effluent Level % removal efficacy	Municipal waste-water	7.92 86.78	7.68 86.4	33.9 76.72	- -	- -	9.11 44.93	0.56 81.7	<i>P. australis</i>	Saeed et al. 2012
Jiaonan, China Effluent level % removal efficacy	Municipal waste-water	30 57.1	11 66.7	125 60.9	- -	- -	63.8 11.1	2.98 -	- -	Song et al. 2009
Egypt Effluent level % removal efficacy	Greywater	8.9 82.2	29.1 70.3	58 65.9	- -	- -	4.6 36	1.7 32.4	<i>P. australis</i>	Abdel-Shafy et al. 2009
Juja, Kenya Effluent levels % removal efficacy	Blackwater	9 89	25 86.4	67 83.5	- -	- -	39.6 69.3	9.3 56.2		
Ocotian, Jalisco Effluent level % removal efficacy	Municipal waste-water	10.4 81.66	25.4 77.94	59.4 76.32	- -	- -	13.5 52.78	5 40.24	<i>Anthurium andreaeanum</i> <i>Strelitzia reginae</i>	Zurita et al. 2011
Dar es Salaam, Tanzania Effluent levels % removal efficacy	Municipal sludge	- -	- -	41.8 60.7	15.86 23.01	0.83 44.3	- -	- -	<i>P. mauritianus</i> <i>Typha latifolia</i>	Kaseva 2004
Mother Dairy Plant, India Effluent level % removal efficacy	Municipal waste-water	12 81	4 90	55 72	- -	- -	7.5 67	1.5 75	<i>P. australis</i>	Ahmed et al. 2008
Peradeniya, Sri Lanka Effluent levels % removal efficacies	Municipal waste-water	47.3 65.8	18.6 65.7	105.9 40.8	4.1 74.8	0.7 38.8	- -	8.03 61.2	<i>Hydrilla verticillata</i> <i>Scirpus grossus</i>	Tanaka et al. 2013
El Salvador Effluent levels % removal efficacies		32.13 84.15	62.8 22	147.13 56.2	- -	- -	12.04 39.3	2.61 -	<i>P. australis</i>	Katsenovich et al. 2009
Can Tho, Vietnam % removal efficacies		93	83	84	91	-	84	99	<i>P. vallatoria</i>	Trang et al. 2010

\*All effluent levels are in mg.L<sup>-1</sup>



Table 3: Application of HSSF systems in decontaminating wastewater contaminants and their effectiveness in named developing countries.

Study Characteristics	Type of Wastewater	TSS	BOD	COD	NH <sub>4</sub> -N	NO <sub>3</sub> -N	TN	TP	Plant species	References
Kampala, Uganda Effluent level % removal efficacy	Municipal wastewater	- -	- -	- -	7.1 75.43	0.09 60.87	16.1 72.48	2.6 83.23	<i>C. papyrus</i>	Kyambadde et al. 2004
Jalisco, Mexico Effluent level % removal efficacy		21.9 61.56	20.8 81.94	49.5 80.32	- -	- -	14.6 49.38	4.2 50.14	<i>Anthurium andreaeanum</i> <i>Strelitzia reginae</i>	Zurita et al. 2011
Wuhan, China Effluent level % removal efficacy		- -	- -	115.5 59.9	22.59 -	0.34 79.52	25.6 15	1.42 52	<i>Canna indica</i> <i>Typha orientalis</i>	Chang et al. 2012
Beijing, China Effluent level % removal efficacy		302.4 97	11.8 96	- -	30.7 90	- -	- -	5 88	<i>Salix babylonica</i>	Wu et al. 2011
Wuxi, China Effluent level % removal efficacy	Livestock wastewater	96 77.1	61.8 81.3	- -	32.9 61.7	- -	41.3 66.6	23.6 48.9	<i>P. communis</i> <i>P. typhia</i>	He et al. 2006
Taihu, China Effluent level % removal efficacy	Polluted lake water	- -	- -	4.25 40.4	0.89 45.9	0.5 62.9	2.37 51.6	0.05 51.6	<i>T. angustifolia</i>	Li et al. 2008
Tianjin, China Effluent level % removal efficacy	Polluted river water	- -	- -	68.9 35	1.7 71.3	- -	2.6 64.9	0.2 61.2	<i>T. latifolia</i>	Tang et al. 2009
Longdao, Beijing Effluent level % removal efficacy		10.9 92.6	6.9 90.5	38.3 73.5	18.5 10.5	- -	18.5 10.6	1.59 30.6	<i>P. australis</i> <i>Zizania aquatica</i>	Chen et al. 2008

\*All effluent levels are in mg.L<sup>-1</sup>

2014). A higher potential overall is evident in HSSF systems since their design incorporates substrate flooding and consistent redox potential in the bed, unlike VSSF which has intermittent feeding of wastewater resulting in oxygenation of the bed and subsequent desorption and release of some pollutants such as phosphorous (Vymazal 2011).

### Hybrid Systems

The subsurface and free water surface CWs cannot achieve the total removal of some pollutants such as TN. In a hybrid system, the various systems (surface and subsurface) are combined to optimize their advantages in a series of different types of CW systems (Vymazal 2011). Hybrid systems use VSSF to remove suspended solids and organics as well as offer nitrification environs while HSSF enables denitrification and further removal of TSS and organics. A summary of the application of hybrid CWs to treat wastewater and their effectiveness in some developing countries is summarized in Table 4. An analysis of the hybrid system results showed higher efficacy in wastewater treatment compared to the surface and subsurface systems though results differed based on the design characteristics of individual studies.

### DISCUSSION

The findings of this review confirm that CWs are promising technologies for the treatment of various types of wastewater including greywater, blackwater, laboratory, hospital, lake, and river water (Gorgoglione & Torretta 2018). HSSF systems have longer life cycles that lead to humic acid formation, which is effective for nitrogen and phosphorous removal through redox reactions. VSSF systems are good nitrifiers due to adequate oxygen supply, require simple hydraulics, and only require a small setup area. FWS CWs are green spaces for communities in addition to having a high capacity to remove water pollutants such as TSS, BOD, and COD while hybrid systems have a combination of these advantages. The effectiveness of these systems in wastewater pollutant removal depends on a number of factors apart from the individual type. These include temperature, vegetation type, hydrologic regime, and pollutant loading (Kadlec & Wallace 2008, Trang et al. 2010). At a low hydraulic loading rate and high hydraulic retention time, the movement of wastewater is slower, which allows for its prolonged interaction with microorganisms and rhizosphere and ultimately,

Table 4: Application of HSSF systems in decontaminating wastewater contaminants and their effectiveness in named developing countries.

Study Characteristics	Type of Wastewater	TSS	BOD	COD	NH <sub>4</sub> -N	NO <sub>3</sub> -N	TN	TP	Plant species	References
Chiang Mai, Thailand Effluent level % removal efficacy	UASB effluent	3 99	10 98	57 95	7 98	- -	77 79	0.3 99	<i>Scirpus grossus Linn</i>	Kantawanichkul et al. 2003
Santa Fe, Mexico Effluent Level % removal efficacy	Municipal waste- water	20 79	33 52	100 68	- -	- -	31 -	15 14	<i>T. latifolia</i> <i>P. australis</i>	Rivas et al. 2011
Kathmandu, Nepal Effluent level % removal efficacy	Greywater	2.6 97	5.2 97	29.1 93	0.5 96	- -	- -	2 35	<i>P. karka</i>	Shrestha et al. 2001
Jakarta, Indonesia Effluent level % removal efficacy	Laboratory waste- water	- -	- -	1.2 97.7	0.06 97.2	0.65 85.96	3.04 65.66	0.6 37.33	<i>Lemna sp.</i> <i>Typha sp.</i>	Meutia 2001
Bogota, Columbia Effluent level % removal efficacy	Municipal waste- water	10 96.9	28 92.26	- -	9 62.5	- -	15 63.4	3 40	<i>Typha sp.</i>	Arias & Brown 2009
Turkey Effluent level % removal efficacy		- -	- -	- -	3.2 91.2	0.3 88.8	4.6 91.3	- -	<i>P. australis</i> <i>Iris australis</i>	Tunesiper 2009
Kathmandu, Nepal Effluent level % removal efficacy	Hospital wastewater	2.8 92.3	3.3 97.	20.2 93.8	1.6 95.2	- -	- -	4.2 46.6	<i>P. karka</i>	Shrestha et al. 2001
Lugu, China Effluent level % removal efficacy	Municipal waste- water	3.2 96.6	- -	21 84.1	2.2 79.6	- -	- -	0.45 84.5	<i>Cyperus alternifolius</i>	Zhai et al. 2011

\*All effluent levels are in mg.L<sup>-1</sup> and UASB refers to up-flow anaerobic sludge bracket reactor.

better contaminant removal (Ranieri et al. 2013). Planted CWs are better performers unlike unplanted ones because their rhizosphere enhances the growth and activity of microbes by providing carbon from root exudates (Vymazal 2011). In tropical compared to temperate regions where plant growth occurs throughout the year and microbial activity is enhanced, CWs are more effective in contaminant removal. High temperatures of the tropics enhance biotic activity, which is a prerequisite for contaminant removal in CWs. Different macrophytes have varied abilities to take up nutrients and macrominorants and the selection of an appropriate species is an essential consideration in designing CW systems. Zhang et al. (2014) also noted that CW systems are cost sensitive and space intensive and hence the need to optimize essential factors using hybrid systems to reduce the costs and at the same time, obtain the best results for wastewater treatment. Compared to conventional wastewater treatment plants, CWs have low operation and maintenance costs but require ample and affordable land space (Gorgoglione & Torretta 2018).

## CONCLUSION

Constructed wetlands are promising ecological technologies whose emergence in developing countries is a viable, cost-effective, and suitable solution for wastewater treatment and use as an alternative water source to natural water sources that are scarce. They have been used in the treatment of greywater, blackwater, polluted river, and lake water among other types of wastewaters effectively. This review shows various CWs including VSSF, HSSF, FWS, and hybrid systems being useful in decontaminating pollutants such as TN, TP, COD, BOD, and TSS among others at different efficacy rates and based on the designs of the systems. Individual systems can be optimized by manipulation of design variables such as pollutant loading, vegetation species used, temperature, and hydrologic regimes of the CWs while availing enough space for such systems at reduced costs. Therefore, the use of CWs in developing countries is a promising step toward water security.

## REFERENCES

- Abdel-Shafy, H., El-Khateeb, M., Regelsberger, M., El-Sheikh, R. and Shehata, M. 2009. Integrated system for the treatment of blackwater and greywater via UASB and constructed wetland in Egypt. *Desal. Water Treat.*, 8(1-3): 272-278.
- Ahmed, S., Popov, V. and Trevedi, R. 2008. Constructed Wetland as Tertiary Treatment for Municipal Wastewater. Institution of Civil Engineers, WR2, pp. 77-84.
- Almuktar, S. and Scholz, M. 2015. Microbial contamination of Capsicum annuum irrigated with recycled domestic wastewater treated by vertical-flow wetlands. *Ecol. Eng.*, 82: 404-414.
- Arias, M. and Brown, M. 2009. Feasibility of using constructed wetlands for municipal wastewater treatment in Bogotá Savannah, Colombia *Ecol. Eng.*, 35: 1070-1078.
- Avila, C., Salas, J., Martín, I., Aragón, C. and García, J. 2013. Integrated treatment of combined sewer wastewater and stormwater in a hybrid constructed wetland system in southern Spain and its further reuse. *Ecol. Eng.*, 50: 13-20.
- Bojcevska, H. and Tonderski, K. 2007. Impact of loads, season, and plant species on the performance of a tropical constructed wetland polishing effluent from sugar factory stabilization ponds. *Ecol. Eng.*, 29: 66-76.
- Chang, J., Wu, S., Dai, Y., Liang, W. and Wu, Z. 2012. Treatment performance of integrated vertical-flow constructed wetland plots for domestic wastewater. *Ecol. Eng.*, 44: 152-159.
- Chen, T., Kao, C., Yeh, T., Chien, H. and Chao, A. 2006. Application of a constructed wetland for industrial wastewater treatment: A pilot-scale study. *Chemosphere*, 64: 497-502.
- Chen, Z., Chen, B., Zhou, J., Li, Z. and Zhou, Y. 2008. A vertical subsurface-flow constructed wetland in Beijing. *Commun. Nonlinear Sci. Numer. Simul.*, 13: 1986-1997.
- Gorgoglione, A. and Torretta, V. 2018. Sustainable management and successful application of constructed wetlands: A critical review. *Sustainability*, 10: 3390.
- He, L., Liu, H., Xi, B. and Zhu, Y. 2006. Effects of effluent recirculation in vertical flow constructed wetland on treatment efficiency of livestock wastewater. *Water Sci. Technol.*, 54(11-12): 137-146.
- Horner, J., Castle, J., Rodger, J. and Gulde, C. 2012. Design and performance of pilot-scale constructed wetland treatment systems for treating oil field-produced water from sub-Saharan Africa. *Water Air Soil Pollut.*, 223: 1945-1957.
- Ji, C., Sun, T. and Ni, J. 2007. Surface flow constructed wetland for heavy oil-produced water treatment. *Ecol. Eng.*, 98: 436-441.
- Jinadasa, K., Tanaka, N., Mowjood, M. and Werellagama, D. 2006. Free water surface constructed wetlands for domestic wastewater treatment: a tropical case study. *Chem. Ecol.*, 22(3):181-191.
- Kadlec, R. and Wallace, S. 2008. *Treatment Wetlands*. Second edition. CRC Press, Boca Raton, FL.
- Kantawanichkul, S., Somprasert, S., Aekasin, U. and Shutes, R. 2003. Treatment of agricultural wastewater in two experimental combined constructed wetland systems in a tropical climate. *Water Sci. Technol.*, 48(5): 199-205.
- Kaseva, M. 2004. Performance of a sub-surface flow constructed wetland in polishing pre-treated wastewater- a tropical case study. *Water Res.*, 38: 681-687.
- Katsenovich, Y., Hummel-Batista, A., Ravinet, A. and Miller, J. 2009. Performance evaluation of constructed wetlands in a tropical region. *Ecol. Eng.*, 35: 1529-1537.
- Kivaisi, A. 2001. The potential for constructed wetlands for wastewater treatment and reuse in developing countries: a review. *Ecol. Eng.*, 16: 545-560.
- Klomjek, P. and Nitisoravut, S. 2005. Constructed treatment wetland: a study of eight plant species under saline conditions. *Chemosphere*, 58: 585-593.
- Kyambadde, J., Kansime, F., Gumaelius, L. and Dalhammar, G. 2004. A comparative study of *Cyperus papyrus* and *Miscanthidium violaceum*-based constructed wetlands for wastewater treatment in a tropical climate. *Water Res.*, 38: 475-485.
- Li, L., Li, Y., Biswas, D., Nian, Y. and Jiang, G. 2008. Potential of constructed wetlands in treating the eutrophic water: evidence from Taihu Lake of China. *Bioresour. Technol.*, 99: 1656-1663.
- Li, X., Chen, M. and Anderson, B. 2009. Design and performance of a water quality treatment wetland in a public park in Shanghai, China. *Ecol. Eng.*, 35: 18-24.
- Maine, M., Suñe, N., Hadad, H. and Sánchez, G. 2007. Temporal and spatial variation of phosphate distribution in the sediment of free water surface constructed wetland. *Sci. Total Environ.*, 380: 75-83.
- Mburu, N., Tebitendwa, S., Rousseau, D., van Bruggen, J. and Lens, P. 2013. Performance evaluation of horizontal subsurface flow-constructed wetlands for the treatment of domestic wastewater in the tropics. *J. Environ. Eng.*, 139: 358-367.

- Meutia, A. 2001. Treatment of laboratory wastewater in a tropical constructed wetland comparing surface and subsurface flow. *Water Sci. Technol.*, 44(11-12): 499-506.
- Nahlik, A. and Mitsch, W. 2006. Tropical treatment wetlands dominated by free-floating macrophytes for water quality improvement in Costa Rica. *Ecol. Eng.*, 28: 246-257.
- Noori, M., Mahdye, M. and Norozi, R. 2014. Effects of municipal wastewater irrigation on physiological and phytochemical parameters of *Aegilops columnaris* Zhuk (Poaceae = Graminae). *IJRAFS*, 1: 1-9
- Ranieri, E., Gorgoglione, A. and Solimeno, A. 2013. A comparison between model and experimental hydraulic performances in a pilot-scale horizontal subsurface flow constructed wetland. *Ecol. Eng.*, 60: 45-49.
- Rivas, A., Barceló-Quintal, I. and Moeller, G. 2011. Pollutant removal in a multistage municipal wastewater treatment comprised of constructed wetlands and a maturation pond, in a temperate climate. *Water Sci. Technol.*, 64(4): 980-987.
- Saeed, T., Afrin, R., Mueyed, A. and Sun, G. 2012. Treatment of tannery wastewater in a pilot-scale hybrid constructed wetland system in Bangladesh. *Chemosphere*, 88: 1065-1073.
- Scheierling, S., Bartone, C., Mara, D. and Drechsel, P. 2011. Towards an agenda for improving wastewater use in agriculture. *Water Int.*, 36: 420-440.
- Shrestha, R., Haberl, R., Laber, J., Manandhar, R. and Mader, J. 2001. Application of constructed wetlands for wastewater treatment in Nepal. *Water Sci. Technol.*, 44(11-12): 381-386.
- Sim, C., Yusoff, M., Shutes, B., Ho, S., and Mansor, M. 2008. Nutrient removal in a pilot and full-scale constructed wetland, Putrajaya city, Malaysia. *J. Environ. Manage.*, 88: 307-317.
- Song, H., Li, X., Lu, X. and Inamori, Y. 2009. Investigation of microcystin removal from eutrophic surface water by the aquatic vegetable bed. *Ecol. Eng.*, 35: 1589-1598.
- Suhad, A., Almuktar, N., Abed, S. and Scholz, M. 2018. Wetlands for wastewater treatment and subsequent recycling of treated effluent: A review. *ESPR*, 25: 23595-23623.
- Tanaka, N., Jinadasa, K., Werellagama, D. and Mowjood, M. 2013. Constructed tropical wetlands with integrated submergent-emergent plants for sustainable water quality management. *J. Environ. Sci. Health A*, 41: 2221-2236.
- Tang, X., Huang, S. and Scholz, M. 2009. Nutrient removal in pilot-scale constructed wetlands treating eutrophic river water: assessment of plants, intermittent artificial aeration, and polyhedron hollow polypropylene balls. *Water Air and Soil Pollut.* 197: 61-73.
- Trang, N., Konnerup, D., Schierup, H., Chiem, N., Tuan, L. and Brix, H. 2010. Kinetics of pollutant removal from domestic wastewater in a tropical horizontal subsurface flow constructed wetland system: effect of hydraulic loading rate. *Ecol. Eng.*, 36: 527-535.
- Tuncsiper, B. 2009. Nitrogen removal in a combined vertical and horizontal subsurface-flow constructed wetland system. *Desalination*, 247: 466-475.
- Vymazal, J. 2011. Constructed wetlands for wastewater treatment: five decades of experience. *Environ. Sci. Technol.*, 45(1): 61-69.
- WWAP (World Water Assessment Programme) 2015. Facing the challenges. Case Studies and Indicators. UNESCO, Paris, France.
- Wu, S., Austin, D., Liu, L. and Dong, R. 2011. Performance of integrated household constructed wetland for domestic wastewater treatment in rural areas. *Ecol. Eng.*, 37: 948-954.
- Yang, Z., Zheng, S., Chen, J. and Sun, M. 2008a. Purification of nitrate-rich agricultural runoff by a hydroponic system. *Bioresour. Technol.*, 99: 8049-8053.
- Zhai, J., Xiao, H., Kujawa-Roeleveld, K., He, Q. and Kerstens, S. 2011. Experimental study of a novel hybrid constructed wetland for water reuse and its application in Southern China. *Water Sci. Technol.*, 64(11): 2177-2184.
- Zhang, D., Tan, S., Gersberg, R., Zhu, J., Sadreddini, S. and Li, Y. 2012. Nutrient removal in tropical subsurface flow constructed wetlands under batch and continuous flow conditions. *J. Environ. Manage.*, 96: 1-6.
- Zhang, D., Jinadasa, K., Gersberg, R., Liu, Y., Jern, W. and Tan, S. 2014. Application of constructed wetlands for wastewater treatment in developing countries: A review of recent developments (2000-2013). *J. Environ. Manage.*, 141: 116-131.
- Zurita, F., Belmont, M., De Anda, J. and White, J. 2011. Seeking a way to promote the use of constructed wetlands for domestic wastewater treatment in developing countries. *Water Sci. Technol.*, 63(4): 654-659.



# Study on Adsorption Properties and Mechanism of Graphene Oxide (GO) by Kaolin

Xingjiang Song\*, Lin Zhou\*\*, Haibo Kang\*\*\*†, Na Li\*\*, Wei Wang\*\* and Ping Jiang\*\*

\*Anhui and Huaihe River Water Resources Research Institute, Bengbu, China

\*\*School of Civil Engineering, Shaoxing University, Shaoxing, Zhejiang, P. R. China

†Correspondence author: Haibo Kang; 18020852079@usx.edu.cn

Nat. Env. & Poll. Tech.  
Website: [www.neptjournal.com](http://www.neptjournal.com)

Received: 30-07-2021

Revised: 04-10-2021

Accepted: 05-10-2021

## Key Words:

Graphene oxide

Kaolin

Adsorption properties

Adsorption mechanism

## ABSTRACT

Kaolin was used as an adsorbent to remove toxic graphene oxide (GO) from an aqueous solution. The adsorption properties and mechanism of GO by Kaolin were systematically studied by various characterization techniques and methods. The effects of pH, amount of adsorbent, and initial concentration of GO on the adsorption of GO by Kaolin were studied in detail. The results show that the interaction between GO and Kaolin is realized by the O-C=O bond, and the adsorption of GO by Kaolin is a chemical adsorption process. Under the optimized conditions (pH=3, T=303 K, equilibrium time = 6 h,  $C_0 = 60 \text{ mg}\cdot\text{L}^{-1}$ ), the removal rate of GO reached 97.1% (Kaolin=70 mg), and the adsorption capacity reached  $45.3 \text{ mg}\cdot\text{g}^{-1}$  (Kaolin=50 mg). According to the experimental results, Kaolin may be a promising material, which can effectively eliminate GO from an aqueous solution. The results of this study provide key information about the migration and potential fate of GO in the natural environment.

## INTRODUCTION

Since its discovery, graphene oxide (GO) has attracted worldwide attention due to its unique structure and remarkable physical and chemical properties. GO shows great potential in multidisciplinary fields, such as medical treatment, energy, environmental pollution control, etc. (Azadian et al. 2019, Baragao et al. 2020, Jing et al. 2019). Specifically, due to its high specific surface area and excellent structural convertibility, a series of GO-based nanomaterials have been used in wastewater treatment (Awad et al. 2018, İlayda et al. 2016, Xing et al. 2019). For example, GO was used as an adsorbent to remove sulfamethoxazole and ciprofloxacin from an aqueous solution successfully (Chen et al. 2015). Magnetic graphene/iron oxide composite was used for the removal of U(VI) from an aqueous solution by Zong et al. (2013). GO nanosheets treated with  $\text{Fe}_3\text{O}_4$  nanoparticles were used for simultaneous removal of Cu (II) and fulvic acid from an aqueous solution (Li et al. 2012). To effectively remove as (III) and (V), nano-sized zero valent iron reduced graphite oxide composites were prepared (Wang et al. 2014). GO/pyrrole composites can remove phenol and aniline from an aqueous solution (Hu et al. 2015).

Although GO and GO-based nanomaterials have been widely used as adsorbents for environmental pollution cleaning, GO is inevitably released into the environment

and ecosystem, including surface water and groundwater (Qi et al. 2014b). Accordingly, due to the toxicity of GO, more and more attention has been paid to the transport of GO and its negative impact on the environment. Many studies have shown that GO is toxic to organisms, including bacterial cells and human beings (Chowdhury et al. 2013). For example, Akhavan and Ghaderi (Akhavan & Ghaderi 2010) found that GO particles reduced the viability of staphylococcus aureus and Escherichia coli due to their sharp edges. In addition, GO can also produce cytotoxicity to human skin fibroblasts and HeLa cells (Liao et al. 2011). Besides, GO can cause high lung accumulation and long-term retention, which may lead to many lung diseases (Vallabani et al. 2011, Zhang et al. 2011). Once GO is released into the natural environment, it may threaten human health because of its nanostructure and toxicity. Therefore, it is necessary to remove GO from the natural aquatic environment, in which it is very important to understand its physical and chemical behavior.

In recent years, various types of natural clays and modified clays, such as Kaolin (Al-Degs et al. 2014), Tunisian montmorillonite (Wiem et al. 2018), sodium montmorillonite (Haouti et al. 2019), silica bentonite (Queiroga et al. 2019), polyamide vermiculite nanocomposites (Basaleh et al. 2019) and lithium feldspar clay sodium alginate composite materials (Pawar et al. 2018) have been used to remove ions, dyes, and heavy metals from the water environment.



Using natural clay as an alternative adsorbent to remove dyes from wastewater has the advantages of low cost, high adsorption performance, high porosity, good usability, good thermal stability, great ion-exchange potential, and non-toxicity (Bao et al. 2019, Puri & Sumana 2018). In this regard, Kaolin is one of the well-known rich and low-cost natural clays, which have crystalline structures all over the world (Yavuz & Saka 2013). Generally speaking, Kaolin is mainly composed of Kaolinite and some minerals such as quartz and mica (Vimonses et al. 2009). The surface of Kaolinite has a constant structural negative charge, which is due to the isomorphic substitution of  $\text{Si}^{+4}$  by  $\text{Al}^{+3}$  in the silicon layer. It is considered an active adsorption site for removing harmful substances from wastewater, which depends on the pH value of the solution (He et al. 2019, Mouni et al. 2017, Nandi et al. 2009). These characteristics cast kaolin high adsorption, kaolin adsorption of metal ions more research results, the adsorption capacity of Pb (II) is 118.5mg·g<sup>-1</sup>, (Nguyen et al. 2021), The highest adsorption rate can reach 85.1% (Hussain & Ali 2021).

There are few studies on the use of Kaolin as an adsorbent to remove GO in water environments at home and abroad (Mouni et al. 2017, Kryuchkova & Fakhruллин 2018). The adsorption behavior of GO by Kaolin was studied systematically. Specifically, Kaolin and GO before and after adsorption were characterized by SEM, TEM, XRD, FT-IR, and AFM for their microscopic morphology, lattice structure, and surface functional groups. The effects of pH value, the initial concentration of GO, and the amount of adsorbent on the adsorption performance were studied and evaluated in detail. Finally, XPS was used to study the difference between bond energy before and after adsorption, and the mechanism of interaction between Kaolin and GO was proposed. This work attempts to provide a new idea for the development of high-efficiency sorbents for capturing GO in the environment.

## MATERIALS AND METHODS

### Experimental Materials

Graphene aqueous solution (2 mg·mL<sup>-1</sup>) was used as the source of GO, and graphene aqueous solution was purchased from Suzhou Carbon Technology Co., Ltd. Kaolin (1250 mesh) was used as an adsorbent, which was purchased from Shanghai Beimo Industrial Co., Ltd. The chemical

constituents of Kaolin are shown in Table 1. 0.1 mol·L<sup>-1</sup> NaOH solution and 0.1 mol·L<sup>-1</sup> HCl solution were all analytically pure reagents.

### Feature Description

The crystal structure of the adsorbent was studied by X-ray diffraction (XRD). The functional groups were identified by Fourier transform infrared spectroscopy (FT-IR, NEXUS). The infrared scanning range was 400-4000 cm<sup>-1</sup>. Scanning electron microscopy (SEM, JSM-6360LV), Atomic force microscopy (AFM, SPA400), and High-resolution transmission electron microscopy (HRTEM, JEM-2100f) were used to study the morphology and structure of the materials before and after adsorption. X-ray photoelectron spectroscopy (XPS) analysis was performed by focusing a monochromatic Alka X-ray source (hm=1486.6eV) with Thermo ESCALAB250.

### Adsorption Experiment

First, an appropriate amount of GO solution was poured into a 50 mL container. Then, a certain amount of adsorbent was added in turn for the batch adsorption test. Afterward, the container was placed in an ultrasonic cleaner at a certain temperature for 30 min. Next, the container was put into a constant temperature shaker for 1 h under shaking to ensure the adsorption process. After the shaking is completed, it was left to stand for 12 h to make the reaction complete. Finally, 1 mL supernatant of the reaction solution was extracted and diluted to 25.0 mL. The residual GO concentration in the supernatant was analyzed at 210 nm wavelength by UV visible spectrophotometer (UV1800).

Different factors (Initial pH value of GO solution, concentration of GO solution, and amount of adsorbent) were optimized. First, when the temperature was 303 K and the GO concentration on the simulated aqueous solution was 60 mg·L<sup>-1</sup>, the initial pH of the GO solution (3.0-8.0) was changed and the amount of adsorbent was 50 mg. Second, when the temperature was 303 K, the initial pH of the GO solution was 3, and the initial GO concentration was 60 mg·L<sup>-1</sup>, the mass of the adsorbent (30-70 mg) was changed. Finally, when the temperature was 303 K, the initial pH of the GO solution was 3, and the amount of adsorbent was 70 mg, the experiment was carried out by changing the concentration of GO in an aqueous solution (20 mg·L<sup>-1</sup>-100 mg·L<sup>-1</sup>). Results of the optimized parameters of adsorption

Table 1: Chemical constituents of Kaolin.

SiO <sub>2</sub> (%)	Al <sub>2</sub> O <sub>3</sub> (%)	Fe <sub>2</sub> O <sub>3</sub> (%)	TiO <sub>2</sub> (%)	CaO (%)	MgO (%)	K <sub>2</sub> O (%)	Na <sub>2</sub> O (%)	MnO (%)
52±2	45±2	<0.4	<1.0	<0.4	<0.2	<0.04	<0.1	<0.005

conditions were obtained. To ensure the accuracy and repeatability of the collected data, all experiments were repeated 3 times, and the average value of the three experiments was used as the follow-up data analysis. The removal percentage ( $R\%$ ), adsorption capacity ( $Q_e$ ), and partition coefficient ( $K_d$ ) were used to evaluate the adsorption performance of Kaolin. The adsorption capacity ( $Q_e$ ) represents the amount of GO adsorbed on the adsorbent per unit weight. The following equation (Eq.1-3) is used to calculate the relevant parameters (Eq.1-3) (Zou et al. 2016).:

$$R = \frac{C_0 - C_e}{C_0} \times 100\% \quad \dots(1)$$

$$Q_e = \frac{(C_0 - C_e) \times V}{m} \quad \dots(2)$$

$$K_d = \frac{Q_e}{C_e} \quad \dots(3)$$

Where  $C_0$  ( $\text{m}\cdot\text{L}^{-1}$ ) is the initial GO concentration of an aqueous solution, and  $C_e$  ( $\text{mg}\cdot\text{L}^{-1}$ ) is the equilibrium GO concentration.  $m$  (g) is the amount of adsorbent and  $V$  (L) is the volume of solution.  $K_d$  is the distribution coefficient.

## RESULTS AND DISCUSSION

### Effect of pH

The pH value of GO solution is an important parameter for adsorption, not only because the distribution of GO in water mainly depends on the pH value of the solution, but also because the surface of the adsorbent can be protonated

or deprotonated. Therefore, the effects of pH on the adsorption capacity, removal rate, and partition coefficient were investigated by adjusting the pH value of the solution. In fact, under other conditions (Adsorbent amount 50 mg,  $C_0 = 60 \text{ mg}\cdot\text{L}^{-1}$ , equilibrium time 6 h,  $T = 303 \text{ K}$ ), the pH value was optimized in the range of 3.0-8.0. The results are shown in Fig. 1. It can be seen from the figure that when  $\text{pH} = 3$ , Kaolin adsorbs more than 75% of GO. On the one hand, it may be that under acidic pH, GO has a strong self-aggregation ability (Konkena & Vasudevan 2012), resulting in a small amount of GO suspended in the solution. On the other hand, GO and Kaolin are an electrostatic attraction at this time, so the interaction ability is strong, the GO in the supernatant is very small and the adsorption rate is very high. The adsorption capacity of GO by Kaolin decreases with the increase of pH in the range of 3-8. When  $\text{pH} = 8$ , the adsorption capacity is almost zero. This may be due to the weakening of electrostatic interaction between Kaolin and GO with the increase of pH value. It should be noted that there is electrostatic repulsion between kaolin and GO in the pH range of 3.0-8.0, so the adsorption in this process may be chemical. That is the hydrogen bond interaction and Lewis acid-base interaction between the oxygen-containing functional groups on the surface of GO and the oxygen-containing groups on the mineral surface (Qi et al. 2014a, He et al. 2019, Mouni et al. 2017, Nandi et al. 2009).

Therefore, it can be concluded that a low pH value is conducive to the adsorption of GO by Kaolin, and alkaline conditions will inhibit the adsorption of GO by Kaolin. It

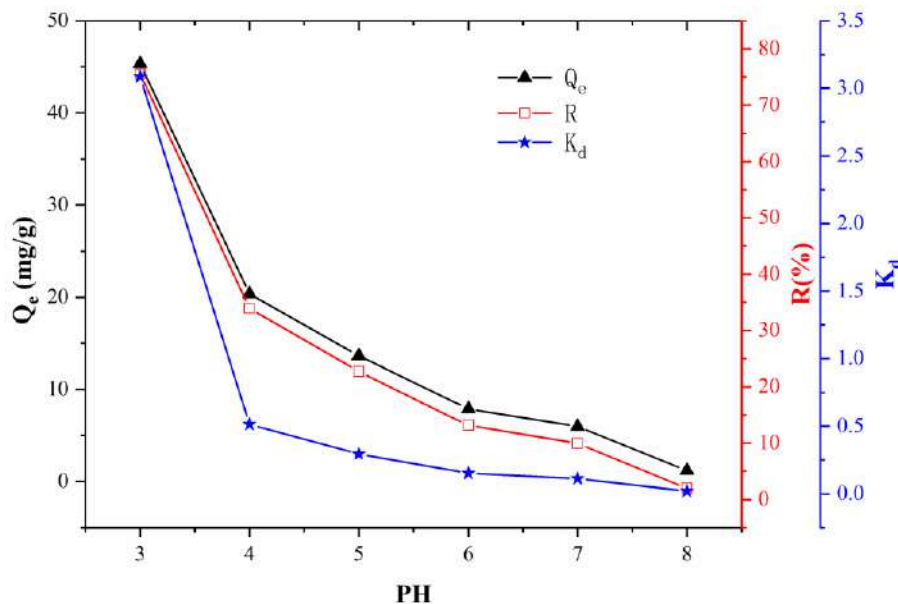


Fig. 1: Removal of GO by Kaolin as a function of pH value.

is suggested that the adsorption process should be carried out at  $\text{pH} = 3$ .

### Effect of Adsorbent Mass

The amount of adsorbent is also one of the important parameters affecting the removal of harmful substances in an aqueous solution. Therefore, the influence of Kaolin contents on adsorption capacity, removal rate, and partition coefficient was investigated by changing the amount of Kaolin. In fact, under other conditions (Adsorbent mass  $\text{pH} = 3$ ,  $C_0 = 60 \text{ mg}\cdot\text{L}^{-1}$ , equilibrium time 6 h,  $T = 303 \text{ K}$ ), the Kaolin content was optimized in the range of 30 mg-70 mg. Fig. 2 shows the effect of Kaolin content on the adsorption capacity, efficiency, and partition coefficient. It can be seen from the figure that the removal rates increase with the increase in Kaolin content. When the Kaolin content is 70 mg, the removal rate is close to 100%. Similarly, the adsorption capacity and distribution coefficient also reach the maximum value. The results show that with the increase in Kaolin content, the adsorption sites of Kaolin and GO increase, which makes Kaolin have high adsorption capacity and can better remove GO from aqueous solution, thus playing an important role in the application of Kaolin to remove GO from aqueous solution.

### Effect of GO Initial Concentration

The initial concentration of GO is also an important parameter affecting the removal of GO by Kaolin. Therefore, the effects of GO initial concentration on adsorption capacity,

removal rate, and partition coefficient were investigated by changing the initial concentration of GO. In fact, under other conditions (Adsorbent mass  $\text{pH} = 3$ , Kaolin content = 70 mg, equilibrium time 6 h,  $T = 303 \text{ K}$ ), the initial GO concentration was optimized in the range of  $20 \text{ mg}\cdot\text{L}^{-1}$ - $100 \text{ mg}\cdot\text{L}^{-1}$ . Fig. 3 shows the effect of GO initial concentration on adsorption capacity, efficiency, and partition coefficient. It can be seen from the figure that with the increase of GO initial concentration, the removal first increases and then decreases. When the GO initial concentration is  $60 \text{ mg}\cdot\text{L}^{-1}$ , the removal rate is close to 100%. The results show that the adsorption sites and electrostatic interaction between Kaolin and GO increase with the increase of GO concentration when the initial GO concentration is  $20 \text{ mg}\cdot\text{L}^{-1}$ - $60 \text{ mg}\cdot\text{L}^{-1}$ . When the initial GO concentration is  $60 \text{ mg}\cdot\text{L}^{-1}$ - $100 \text{ mg}\cdot\text{L}^{-1}$ , the increase in GO concentration inhibits the electrostatic interaction between Kaolin and GO, resulting in a decrease in the GO removal rate (Zou et al. 2016, Wang et al. 2016).

Therefore, when Kaolin is used to remove GO from water solution, the concentration of GO in aqueous solution should be measured first, to achieve the best effect of removing GO by Kaolin.

### SEM and TEM Analysis

Fig. 4 shows SEM (a) and TEM (b) of GO and SEM (c) and TEM (d) of Kaolin /GO. It can be seen that the SEM images of GO are multi-layer lamellar three-dimensional structures, and the SEM images of Kaolin/GO also show lamellar structures.

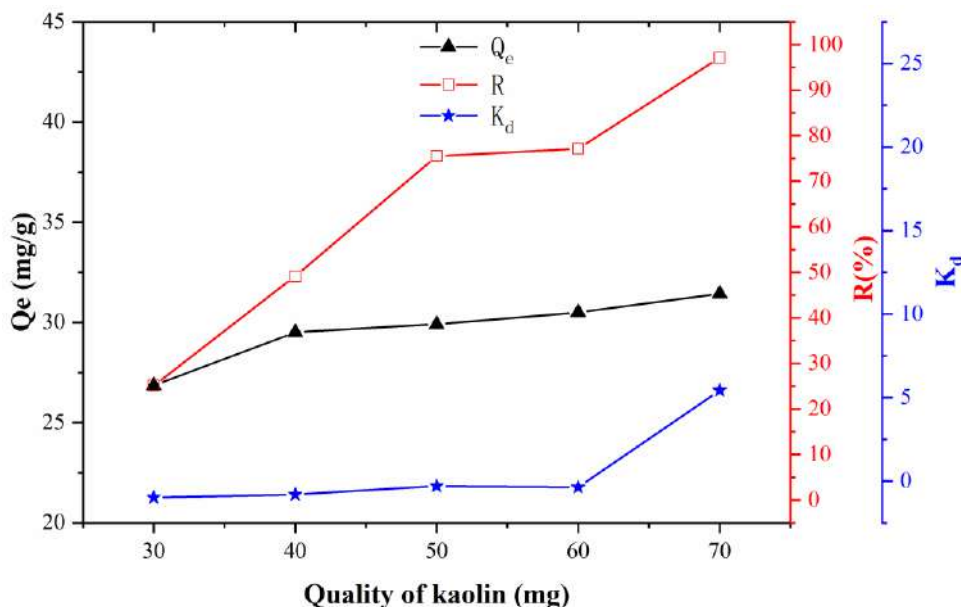


Fig. 2: Removal of GO by Kaolin as a function of Kaolin contents.

This indicates that GO is adsorbed on Kaolin. The comparison between the TEM (b) diagram of GO and the TEM (d) diagram

of Kaolin/GO can also reveal this phenomenon, which proves that Kaolin can remove GO from water solution.

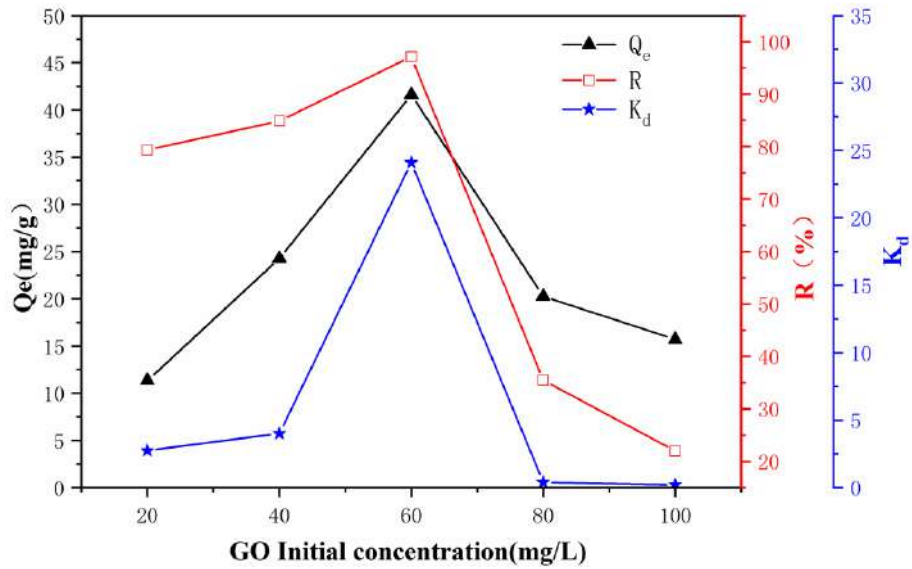


Fig. 3: Removal of GO by Kaolin as a function of GO contents.

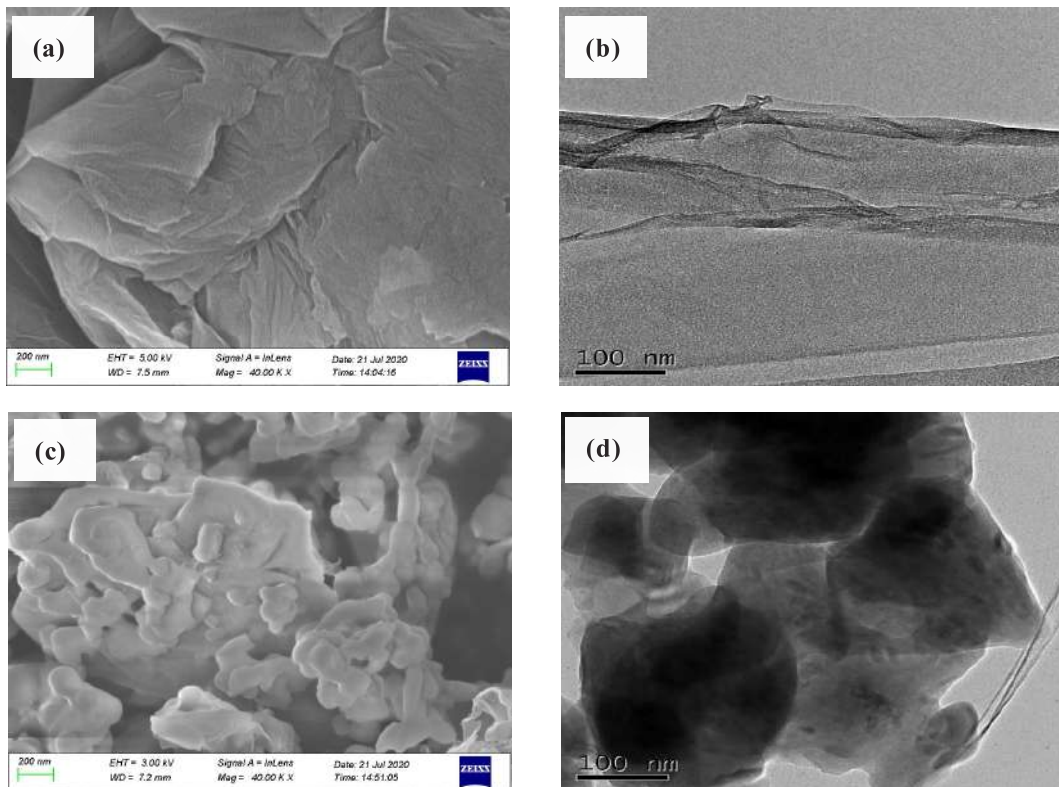


Fig. 4: SEM (a) and TEM (b) of GO, SEM (c) and TEM (d) of Kaolin/GO.

### XRD and FT-IR Analysis

To reveal the adsorption mechanism, GO, Kaolin, and Kaolin/GO materials were characterized by XRD technology, and the results are shown in Fig. 5(a). It can be seen from the figure that the characteristic diffraction peaks of Kaolin/GO and Kaolin are almost the same, which indicates that GO is not accumulated on the surface of Kaolin but wrapped in Kaolin. This is consistent with the results of TEM and SEM of Kaolin/GO.

For the sake of obtaining the effective adsorption functional groups of Kaolin surface before and after GO adsorption, FT-IR analysis was carried out. Fig. 5(b) shows the FT-IR spectra of GO, Kaolin, and Kaolin after adsorption of GO. The main band on FT-IR of Kaolin at  $\sim 3448\text{ cm}^{-1}$  can be attributed to the tensile vibration of O-H, while the frequency band of  $\sim 1635\text{ cm}^{-1}$  can be attributed to the bending vibration of coordination water (Deng & Shi 2015, Mouni et al. 2017). The peaks at  $\sim 1110\text{ cm}^{-1}$  and  $\sim 990\text{ cm}^{-1}$  can be attributed

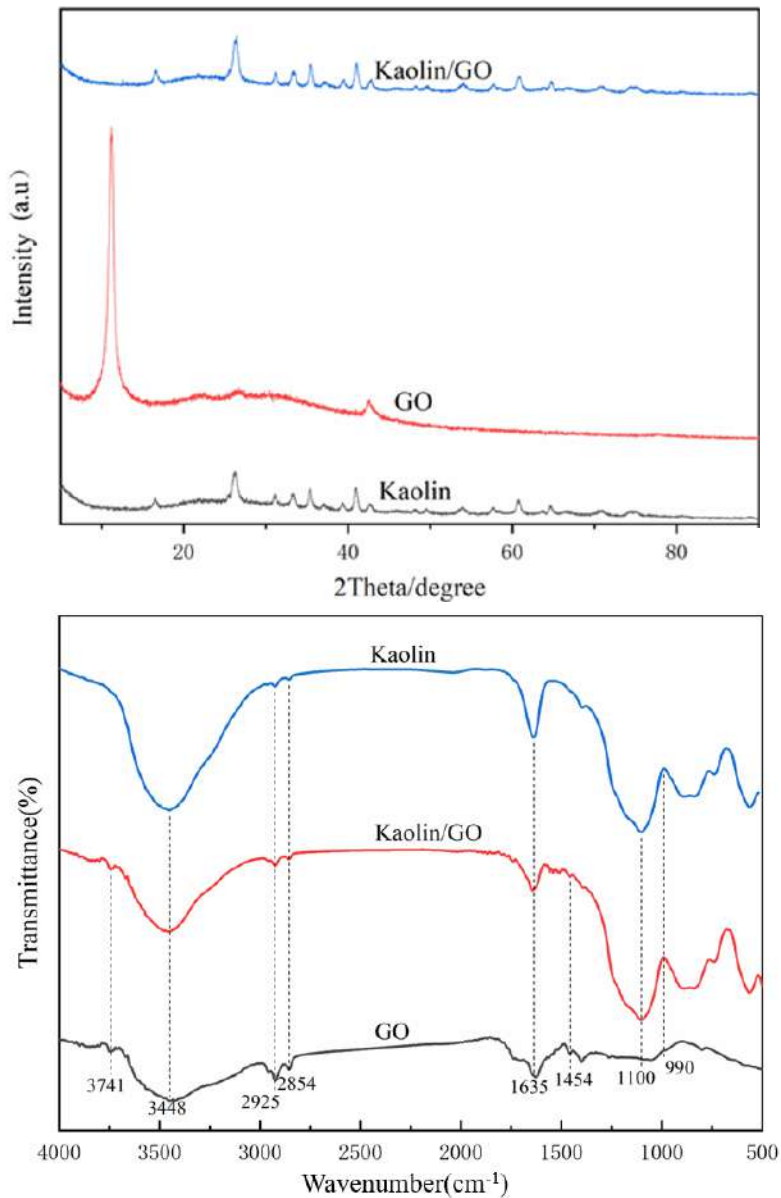


Fig. 5: XRD patterns (a) of GO, Kaolin, Kaolin/GO, FT-IR patterns (b) of GO, Kaolin, Kaolin/GO.



to the tensile vibration of Si-O-Si of Kaolinite (Mouni et al. 2017). The FT-IR spectra of Kaolin after adsorption of GO showed that the functional groups of Kaolin participated in the adsorption of GO. In addition, a new band appears at  $\sim 1484\text{cm}^{-1}$ , which may be due to the (C=C) of GO adsorbed on the Kaolin surface. A new band appears at  $\sim 3741\text{cm}^{-1}$ , which is the same as that of GO.

### XPS and AFM Analysis

To further explore the adsorption mechanism of GO by Kaolin, GO and Kaolin/GO were analyzed by XPS and AFM. The results are shown in Fig. 6 and Fig. 7, respectively. As shown in Fig. 6(a), various strong peaks, such as Al2p, Si2p, N1s, S2p, O1s, and C1s can be observed. According to the high-resolution spectrum of C1s before adsorption of GO, the deconvolution of the C1s spectrum can be divided into three components, about 284.7 eV, 286.7 eV, and 288.5 eV,

respectively, which are assigned to C-C, C-O, and O-C=O groups (Fig. 6(b)) (Littunen et al. 2011, Yu et al. 2012, Zhang et al. 2014). However, after Kaolin adsorbs GO, the intensity and position of C1s peak of Kaolin/GO change. The relative areas of C-C, C-O, and O-C=O assigned to Kaolin/GO decrease significantly, and the peak position of O-C=O changes from 288.5 eV to 288.8 eV. The peak positions of C-C and C-O are almost unchanged (Fig. 6(c)). The relative area and peak position of O-C=O changes obviously, which indicates that the interaction between GO and Kaolin is carried out by O-C=O. From the height of the AFM image and the corresponding morphology, the thickness of GO is 1.02 nm, and the thickness of Kaolin/GO is 2.55 nm, which indicates that the thickness of Kaolin/GO becomes thicker due to the aggregation of GO in Kaolin, which is consistent with TEM results. Based on the above analysis, Kaolin can effectively remove GO through the aggregation of GO in Kaolin.

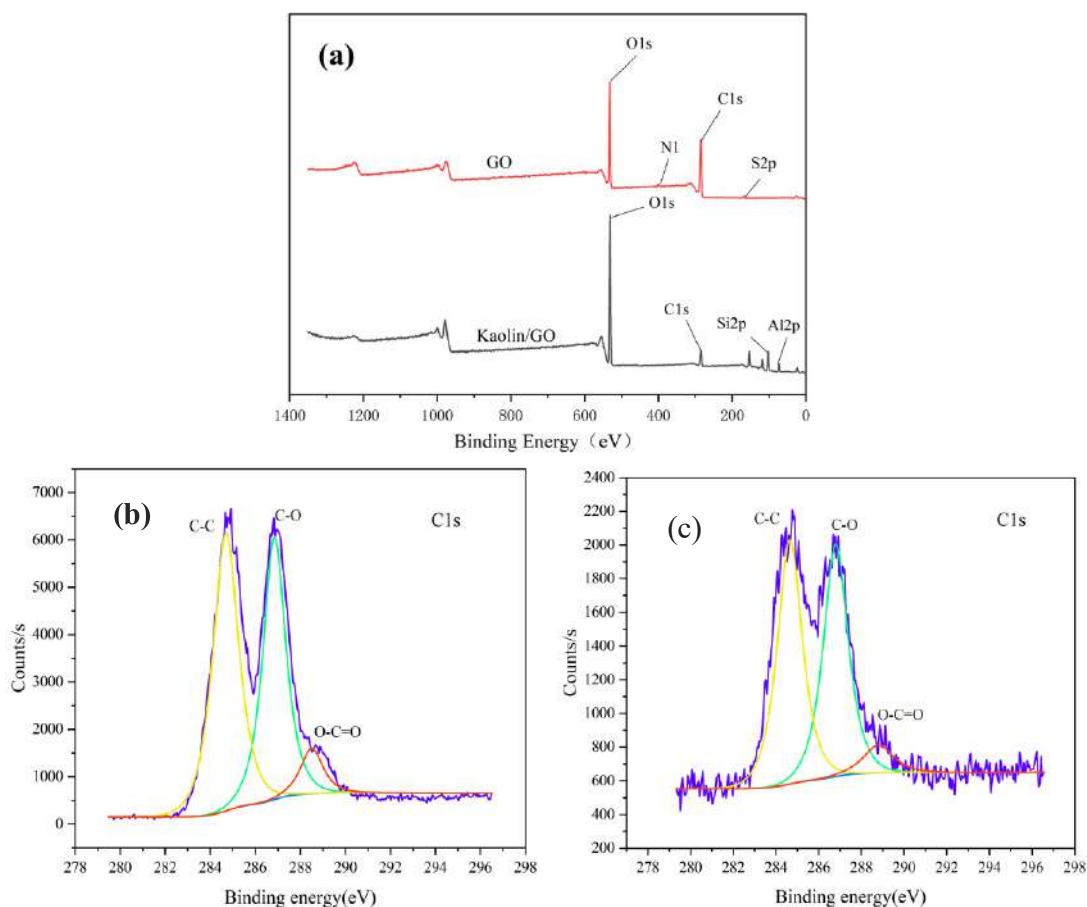


Fig. 6: XPS spectra of Kaolin/GO before and after GO removal (a), the high C1s deconvolution of GO (b), and the high C1s deconvolution of Kaolin/GO (c).

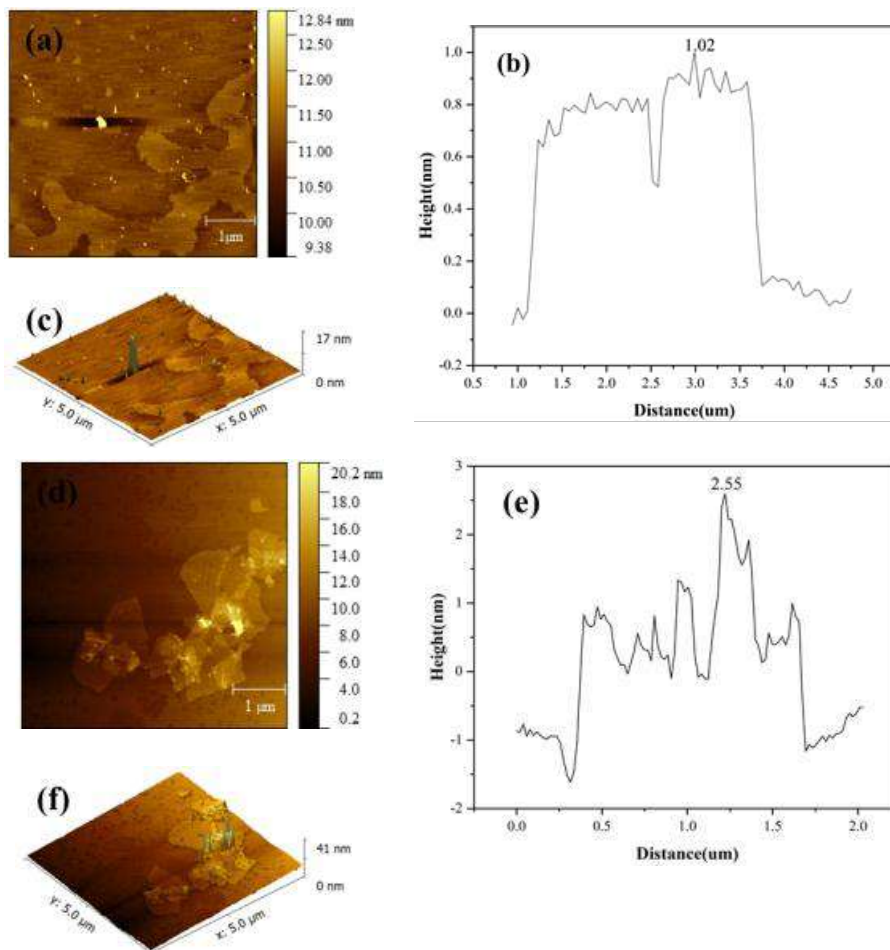


Fig. 7: AFM image and the corresponding height profiles of GO (a) (b) (c) and Kao/GO (d) (e) (f).

## CONCLUSION

This paper studies the kaolin's adsorption performance and mechanism of GO and has obtained some meaningful conclusions: The highest removal rate and adsorption capacity was 97.1%, and 45.3 mg, respectively. The microscopic characterization further confirmed the occurrence of the Human Soil in the GO adsorption process, where the XPS spectrum showed the interaction of GO and kaolin was achieved by the O-C=O key, and kaolin's adsorption of GO was a chemical adsorption process. In summary, kaolin can effectively remove GO in an aqueous solution by simple and rapid chemical adsorption.

## ACKNOWLEDGMENT

This research was funded by the National Natural Science Foundation of China (52179107). Thanks to Weiqing Zhang and Jiahui Gu for assistance with the experiments.

## REFERENCES

- Akhavan, O. and Ghaderi, E. 2010. Toxicity of graphene and graphene oxide nanowalls against bacteria. *ACS Nano*, 4(10): 5731-5736.
- Al-Degs, Y.S., Al-Ghouti, M.A. and Olimat, A.A.M. 2014. Studying competitive sorption behavior of methylene blue and malachite green using multivariate calibration. *Chem. Eng. J.*, 11: 251.
- Awad, F.S., Abouzied, K.M., Abou, E.M., El-Wakil, A.M. and Samy, E.S.M. 2018. Effective removal of mercury(II) from aqueous solutions by chemically modified graphene oxide nanosheets. *Arab. J. Chem.*, 13: 2659-2670.
- Azadian, E., Arjmand, B., Ardehshirylajimi, A., Hosseinzadeh, S. and Khojasteh, A. 2019. Polyvinyl alcohol modified polyvinylidene fluoride raphene oxide scaffold promotes osteogenic differentiation potential of human-induced pluripotent stem cells. *J. Cell. Biochem.*, 121(5-6).
- Bao, T., Dantie, M.M., Wu, K., Wei, X.L., Zhang, Y., Chen, J., Deng, C.X., Jin, J., Yu, Z.M. and Wang, L. 2019. Rectorite-supported nano-Fe<sub>3</sub>O<sub>4</sub> composite materials as a catalyst for P-chlorophenol degradation: Preparation, characterization, and mechanism. *Appl. Clay Sci.*, 176(8): 66-77.
- Baragao, D., Forján, R., Welte, L. and Gallego, J.L.R. 2020. Nanoremediation of As and metals polluted soils by means of graphene oxide nanoparticles. *Sci. Rep.*, 10(1): 54.

- Basaleh, A., Al-Malack, M.H. and Saleh, T.A. 2019. Methylene Blue removal using polyamide-vermiculite nanocomposites: Kinetics, equilibrium and thermodynamic study. *J. Environ. Chem. Eng.*, 7(3): 43.
- Chen, H., Gao, B. and Li, H. 2015. Removal of sulfamethoxazole and ciprofloxacin from aqueous solutions by graphene oxide. *J. Hazard. Mater.*, 282(23): 201-207.
- Chowdhury, I., Duch, M.C., Mansukhani, N.D., Hersam, M.C. and Bouchard, D. 2013. Colloidal properties and stability of graphene oxide nanomaterials in the aquatic environment. *Environ. Sci. Technol.*, 47(12): 130.
- Deng, L. and Shi, Z. 2015. Synthesis and characterization of a novel Mg-Al hydrotalcite-loaded kaolin clay and its adsorption properties for phosphate in an aqueous solution. *J. Alloys Comp.*, 637: 188-196.
- Haouti, R.E., Ouachtak, H., Guerdaoui, A.E., Amedlous, A., Amaterz, E., Haounati, R., Addi, A. A., Akbal, F., Alem, N.E. and Taha, M.L. 2019. Cationic dye adsorption by Na-montmorillonite nano clay: Experimental study combined with a theoretical investigation using DFT-based descriptors and molecular dynamics simulations. *J. Mol. Liq.*, 290: 111139.
- He, G., Wang, C., Cao, J., Fan, L., Zhao, S. and Chai, Y. 2019. Carboxymethyl chitosan-kaolinite composite hydrogel for efficient copper ions trapping. *J. Environ. Chem.*, 16: 541-563.
- Hu, R., Dai, S., Shao, D., Alsaedi, A., Ahmad, B. and Wang, X. 2015. Efficient removal of phenol and aniline from aqueous solutions using graphene oxide/polypyrrole composites. *J. Mol. Liq.*, 203: 80-89.
- Hussain, S.T. and Ali, S.A.K. 2021. Removal leads Pb (II) from wastewater using kaolin clay. *IOP Conf. Series Mater. Sci. Eng.*, 1058(1): 012069.
- layda, D., Duygu, E., Ali and Reza, K. 2016. Graphene oxides for removal of heavy and precious metals from wastewater. *J. Mater. Sci.*, 14: 31.
- Jing, J.H., Wu, H.Y., Shao, Y.W., Qi, X.D. and Wang, Y. 2019. Melamine foam-supported form-stable phase change materials with simultaneous thermal energy storage and shape memory properties for thermal management of electronic devices. *ACS Appl. Mater. Interfaces*, 11(21): 56.
- Konkena, B. and Vasudevan, S. 2012. Understanding the aqueous dispersibility of graphene oxide and reduced graphene oxide through pKa measurements. *J. Phys. Chem. Letts.*, 3(7): 867.
- Kryuchkova, M. and Fakhrollin, R. 2018. Kaolin alleviates graphene oxide toxicity. *Environmental Science & Technology Letters*. 5(5):295-300.
- Li, J., Zhang, S., Chen, C., Zhao, G. and Wang, X. 2012. Removal of Cu(II) and fulvic acid by graphene oxide nanosheets decorated with Fe<sub>3</sub>O<sub>4</sub> nanoparticles. *ACS Appl. Mater. Interfaces*, 4(9): 4991.
- Liao, K.H., Lin, Y.S., Macosko, C.W. and Haynes, C.L. 2011. Cytotoxicity of graphene oxide and graphene in human erythrocytes and skin fibroblasts. *ACS Appl. Mater. Interfaces*, 3(7): 2607-2615.
- Littunen, K., Hippel, U., Johansson, L.S., Sterberg, M., Tammelin, T., Laine, J. and Seppel J. 2011. Free radical graft copolymerization of nanofibrillated cellulose with acrylic monomers. *Carbohydrate Polymers*, 84(3): 1039-1047.
- Mouni, L., Belkhiri, L., Bollinger, J.C., Bouzaza, A., Assadi, A., Tirri, A., Dahmoune, F., Madani K. and Remini, H. 2017. Removal of Methylene Blue from aqueous solutions by adsorption on Kaolin: Kinetic and equilibrium studies. *Appl. Clay Sci.*, 153: 38-45.
- Nandi, B.K., Goswami, A. and Purkait, M.K. 2009. Adsorption characteristics of brilliant green dye on kaolin. *J. Hazard. Mater.*, 161(1): 387-395.
- Nguyen, P. H., Le, Q.T., Pham, T.C.T. and Le, T.T. 2021. Synthesis of glue-free naa zeolite granules from natural kaolin for the adsorption of Pb(II) ions in aqueous solution using a fixed-bed column study. *ACS Omega*, 6(32): 21024-21032.
- Pawar, R.R., Lalmunsiama, G.P., Sawant, S.Y., Shahmoradi, B. and Lee, S.M. 2018. Porous synthetic hectorite clay-alginate composite beads for effective adsorption of methylene blue dye from an aqueous solution. *Int. J. Biol. Macromol.*, 11: 1315.
- Puri, C. and Sumana, G. 2018. Highly effective adsorption of crystal violet dye from contaminated water using graphene oxide intercalated montmorillonite nanocomposite. *Appl. Clay Sci.*, 166(12): 102-112.
- Qi, Z., Zhang, L. and Chen, W. 2014a. Transport of graphene oxide nanoparticles in saturated sandy soil. *Environ. Process Impacts*, 16(10): 2268-2277.
- Qi, Z., Zhang, L., Wang, F., Hou, L. and Chen, W. 2014b. Factors controlling transport of graphene oxide nanoparticles in saturated sand columns. *Environ. Toxicol. Chem.*, 33(5): 998-1004.
- Queiroga, L.N.F., Pereira, M.B.B., Silva, L.S., Silva, F.E.C., Santos, I.M.G., Fonseca, M.G., Georgelin, T. and Jaber, M. 2019. Microwave bentonite silylation for dye removal: Influence of the solvent. *Appl. Clay Sci.*, 168(2): 478-487.
- Vallabani, N.V.S., Mittal, S., Shukla, R.K., Pandey, A.K., Dhakate, S.R., Pasricha, R. and Dhawan, A. 2011. Toxicity of graphene in normal human lung cells (BEAS-2B). *J. Biomed. Nanotechnol.*, 7(1): 106.
- Vimonses, V., Lei, S., Jin, B., Chow, C.W.K. and Saint, C. 2009. Adsorption of congo red by three Australian kaolins. *Appl. Clay Sci.*, 43(3-4): 465-472.
- Wang, C., Luo, H., Zhang, Z., Wu, Y., Zhang, J. and Chen, S. 2014. Removal of As(III) and As(V) from aqueous solutions using nanoscale zero-valent iron-reduced graphite oxide modified composites. *J. Hazard. Mater.*, 268(15): 124-131.
- Wang, J., Wang, X., Tan, L., Chen, Y., Hayat, T., Hu, J., Alsaedi, A., Ahmad, B., Guo, W. and Wang, X. 2016. Performances and mechanisms of Mg/Al and Ca/Al layered double hydroxides for graphene oxide removal from aqueous solution. *Chem. Eng. J.*, 297: 106-115.
- Wiem, H., Nesrine, D., Bel, H., Hadjlaief, M. and Eloussaief, M.B. 2018. Sono-assisted adsorption of Cristal Violet dye onto Tunisian Smectite Clay: Characterization, kinetics, and adsorption isotherms. *Ecotoxicol. Environ. Safety*, 11: 235
- Xing, M., Zhuang, S. and Wang, J. 2019. Efficient removal of Cs(I) from aqueous solution using graphene oxide. *Prog. Nucl. Energy*, 119: 103167.
- Yavuz, O. and Saka, C. 2013. Surface modification with cold plasma application on kaolin and its effects on the adsorption of methylene blue. *Appl. Clay Sci.*, 85(11): 96-102.
- Yu, X., Tong, S., Ge, M., Zuo, J. and Song, W. 2012. One-step synthesis of magnetic composites of cellulose@iron oxide nanoparticles for arsenic removal. *J. Mater. Chem. A*, 3: 959-965
- Zhang, S., Zeng, M., Li, J., Li, J., Xu, J. and Wang, X. 2014. Porous magnetic carbon sheets from biomass as an adsorbent for the fast removal of organic pollutants from aqueous solution. *J. Mater. Chem. A*, 2(12): 4391-4397.
- Zhang, X., Yin, J., Peng, C., Hu, W., Zhu, Z., Li, W., Fan, C. and Huang, Q. 2011. Distribution and biocompatibility studies of graphene oxide in mice after intravenous administration. *Carbon*, 49(3): 986-995.
- Zong, P., Wang, S., Zhao, Y., Wang, H. and He, C. 2013. Synthesis and application of magnetic graphene/iron oxides composite for the removal of U(VI) from aqueous solutions. *Chem. Eng. J.*, 220: 45-52.
- Zou, Y., Wang, X., Ai, Y., Liu, Y., Li, J., Ji, Y. and Wang, X., 2016. Coagulation Behavior of Graphene Oxide on Nanocrystalline Mg/Al Layered Double Hydroxides: Batch Experimental and Theoretical Calculation Study. *Environ. Sci. Technol.*, 50(7): 3658.





# A Study of Nutrient Removal Efficiency from Simulated Agriculture Run-off (SAR) Using Constructed Wetland Technology

Simranjeet Singh\*†, Anubha Kaushik\*\* and Bhoopesh Kumar Sharma\*\*\*

\*Department of Environmental Science, Faculty of Science, Shree Guru Gobind Singh Tricentenary University, Gurugram-122 505, India

\*\*University School of Environment Management, Guru Gobind Singh Indraprastha University, New Delhi-110 078, India

\*\*\*Department of Forensic Science, Faculty of Science, Shree Guru Gobind Singh Tricentenary University, Gurugram- 122 505, India

†Corresponding author: Simranjeet Singh; simranjeet\_fps@sgtuniversity.org

Nat. Env. & Poll. Tech.  
Website: [www.neptjournal.com](http://www.neptjournal.com)

Received: 22-01-2022

Revised: 02-03-2022

Accepted: 11-03-2022

## Key Words:

Constructed wetland  
Nutrient removal  
Simulated agricultural waste  
Hydraulic retention time

## ABSTRACT

In this study, a vertical flow constructed wetland in batch mode was examined for the removal efficiency of simulated agricultural run-off (SAR) using gravel and soil as substrates, planted with *Canna*, *Typha* and *Eichhornia* plant species in single and mixed culture conditions. From this study, it was found that the constructed wetland (CW) planted with *Canna* + *Eichhornia* plant species (mixed) showed maximum removal efficiency of the studied parameters, i.e. phosphates, nitrates and ammonical nitrogen to the tune of 99%, 96% and 98%, respectively of simulated agricultural run-off as compared to other studied CWs. *Canna* and *Typha* macrophytes showed higher biomass and chlorophyll content, indicating better tolerance in the mixed culture CW system. Treatment efficiency improved when longer hydraulic retention times (HRTs) were used. Maximum treatment efficiency was shown by hybrid CW, which included the properties of the horizontal flow (HF) and vertical flow (VF) type CWs.

## INTRODUCTION

In India, the problem of freshwater pollution is raising increasing day by day with domestic sewage and industrial waste discharges being the most critical sources of pollution. Major sources of water pollution include point and non-point sources like discharges from industries and stormwater respectively. Pollution from non-point sources such as agriculture run-off, leaching from waste disposal sites and stormwater is difficult to control, while pollution from point sources can be controlled by different treatment technologies. According to the Ministry of Environment and Forest (2009), the agricultural sector has a predominant impact on water quality. Overuse of chemical pesticides and fertilizers, by farmers due to heavy subsidies, increased per hectare consumption of fertilizers. The higher amount of nutrients applied to crops implies environmental pollution both from runoff (liquid phase) as well as sediment (solid phase) (Zuazo et al. 2004, Divya & Belagali 2012). Removal of nutrients through sediments and runoff water not only declines soil fertility but also causes environmental problems when these nutrients are transported further down the valleys, lakes, and reservoirs (Kin-Che et al. 1997). In India due to low

literacy rate among farmers, makes them non-effective to understand the written instructions on pesticide containers which results in an improper application, over application and lack of training are a couple of examples of different ways of reaching pesticides and fertilizers in rivers and water bodies (Abhilash & Singh 2009). Nonpoint-source pesticide pollution from agricultural areas is widely regarded as one of the greatest causes of contamination of surface waters (Gangbazo et al. 1999, Humenik et al. 1987, Line et al. 1997). Mandal et al. (2012) also studied Runoff, sediment, and nutrient losses from an agricultural field under natural rainfall events in a semi-arid tropical region of India, which contributes to increasing non-point source pollution and the risk of eutrophication in lowland surface water bodies. The average nutrient losses during 2005-2009 were 41.72 kg ha<sup>-1</sup> yr<sup>-1</sup> for total C, 10.2 kg ha<sup>-1</sup> yr<sup>-1</sup> for total N, 1.0 kg ha<sup>-1</sup> yr<sup>-1</sup> for total P, and 20.07 kg ha<sup>-1</sup> yr<sup>-1</sup> for total K. loss of soil 560-1010 kg ha<sup>-1</sup> yr<sup>-1</sup> with 3.9 kg N, 2.1-2.4 kg P and 1.6-10.2 kg K from agricultural soil in a semi-arid region of India was also reported by Mishra et al. (2010). Nitrogenous fertilizers are the main source of NO<sub>3</sub><sup>-</sup> pollution in groundwater and other water bodies (Schepers et al. 1984). A high concentration of nitrate, ranging from 2.8 to



91 mg.L<sup>-1</sup> in water samples collected from hand pumps in the industrial areas of Ludhiana town was also reported by Goyal et al. (1981). Groundwater samples from Haryana and Punjab where fertilizer consumption is highest showed high amounts of nitrate in the groundwater (Lunkad 1994). Several studies also reported higher concentrations of nitrate concentrations in groundwater samples of different districts (Lakshmanam et al. 1986, Singh et al. 1991, Tamta et al. 1992, Handa 1986, Kumar & Singh, 1988). So for the treatment of such type of wastewater advanced technology was needed which is more environment-friendly, low in cost, and maintenance. In the early 1970s constructed wetlands (CWs) were mainly used for the treatment of domestic or municipal sewage (Vymazal et al. 2006). After the 1990s application was expanded to treat different kinds of wastewater including agricultural wastewaters (Zhou et al. 2004), dairy wastewater (Kern & Brettar 2002), and landfill leachate (Bulc 2006). Most of the initial studies referred to the potential of wetlands for the removal of herbicides and some other organic chemicals (Kadlec & Hey 1994, More et al. 2000). Treatment of wastewater in constructed wetland systems includes various biological and biochemical processes. Thus, constructed wetland technology has been found useful in treating wastewaters of various types in an environmentally friendly manner. The present study is proposed to examine the efficiency of different types of constructed wetland systems to treat various organic and inorganic chemicals present in the agricultural run-off, which is very important in the agriculturally predominant state of Haryana.

## MATERIALS AND METHODS

### Experimental Setup and Design

**Batch mode:** Normal washing buckets with a capacity of 15 L and a working volume of 3 L were used in the experiment as CW reactors. The buckets were fitted with rubber tubing, a few centimeters (2") from the bottom, and screw clips were used to close the rubber tubing. Soil and gravel were used as the substrate. The gravels were thoroughly washed with tap water and placed at the bottom of the bucket followed by soil and then gravel again. Macrophytes *Canna*, *Typha*, and *Eichhornia* in single and mixed cultures were used as the wetland plants. Various combinations of the plant species used in variously constructed wetland reactors were C=CW<sub>1</sub>, T=CW<sub>2</sub>, E=CW<sub>3</sub>, C+T=CW<sub>4</sub>, C+E=CW<sub>5</sub>, E+T=CW<sub>6</sub>, and E+C+T=CW<sub>7</sub> where C represents *Canna*, T: *Typha* and E for *Eichhornia*. CW represents the constructed wetland systems and numbering is given to various reactors with different macrophyte combinations. The experimental plants were cleaned with distilled water and then these plants were

acclimatized in reactors containing fresh tap water for 5-7 days under natural environmental conditions. Simulated wastewater was loaded at the surface of the wetland system and collected at fixed time intervals through an outlet of the reactor. Sampling was done every 24 h and the sample was analyzed for various parameters.

**Continuous mode:** CW reactors made of Stainless Steel (60x30x30 cm) were fabricated for use as Horizontal, Vertical and Hybrid subsurface flow Constructed Wetland systems. For Horizontal flow CWs layer of gravel at the inlet and outlet of the reactor was placed, portioning was done with the help of plates of stainless steel, and the middle part of the reactor was filled with soil for planting the macrophytes. In vertical flow CWs, a layer of gravel at the bottom was followed by a layer of soil, and then again gravel layer was placed. The wastewater was fed into the reactor at a required HRT with the help of a peristaltic pump through the inlet. Both soil and gravel were used as substrates in the reactors which had a working volume of 10 L.

### Preparation of Simulated Agricultural Run-off (SAR)

Simulated agricultural runoff was prepared by dissolving Urea, and DAP (Diammonium phosphate) in tap water. The simulated agricultural runoff was characterized for various parameters like pH, orthophosphates, nitrate, and ammonical nitrogen using standard methods (APHA 1995).

### Analytical Methods

Simulated agricultural runoff was analyzed for various parameters such as pH, electrical conductivity (EC), using a pH-EC meter, nitrate-nitrogen (NO<sub>3</sub><sup>-</sup>-N) by colorimetric method using brucine sulphanilic acid, total nitrogen (TN), ammonical nitrogen (NH<sub>4</sub><sup>+</sup>-N) by colorimetric method using Nessler's reagent, phosphate (PO<sub>4</sub><sup>3-</sup>) by molybdenum-blue complex method (APHA 1995). Chlorophyll (a, b and Total) was measured by using Arnon's (1949) method.

## RESULTS AND DISCUSSION

Initial Characteristics of Simulated Agricultural Run-off were Analyzed and given in Table 1.

Table 1: Characteristics of simulated agricultural run-off used in the batch experiment.

Parameter	Parameter value
pH	8.03
Phosphate [mg.L <sup>-1</sup> ]	52.6
Nitrate [mg.L <sup>-1</sup> ]	1.9
Ammonical Nitrogen [mg.L <sup>-1</sup> ]	34.15

**Change in pH of Batch Treated SAR**

During the experiment pH of simulated agricultural runoff changed from alkaline to neutral in all studied Constructed Wetland systems (CWs). A gradual trend of decrease in pH was observed during the 16 days of the experiment (Fig. 1).

**Removal of Nitrates From Batch-Treated SAR**

In the initial 4 days of the experiment, there was a sharp increase in the concentration of nitrate which could be due to the conversion of ammonical nitrogen into nitrate by nitrifying bacteria present in the CW substrate and root zone of the plants.

After 4 days, the concentration of nitrates started declining (Fig. 2) which may be due to the removal mechanisms;

denitrification, storage in the substrate, uptake, and storage in plant biomass in constructed wetland systems (Brix 1993).

Most of the differences in nitrate concentrations in treated run-off from CWs with different types and combinations of plants exceeded the critical difference value (CD = 0.6) showing a significant effect due to plant type present in the CW microcosms (Table 2).

**Change in Ammonical Nitrogen (NH<sub>4</sub><sup>+</sup>-N) Concentration of Batch Treated SAR**

Concentration of ammonical nitrogen was reduced (Fig. 3) to 1.67 mg.L<sup>-1</sup>, 4.77 mg.L<sup>-1</sup>, 6.24 mg.L<sup>-1</sup>, 0.74 mg.L<sup>-1</sup>, 2.64 mg.L<sup>-1</sup>, 3.06 mg.L<sup>-1</sup> and 2.84 mg.L<sup>-1</sup> for CW<sub>1</sub>, CW<sub>2</sub>, CW<sub>3</sub>, CW<sub>4</sub>, CW<sub>5</sub>, CW<sub>6</sub> and CW<sub>7</sub>, respectively, from an initial value

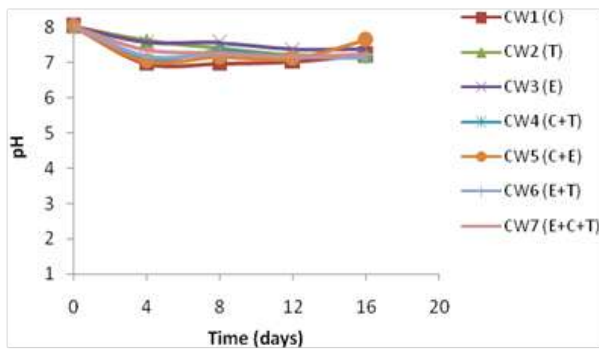


Fig. 1: Change in pH of treated SAR in CWs with different wetland macrophytes.

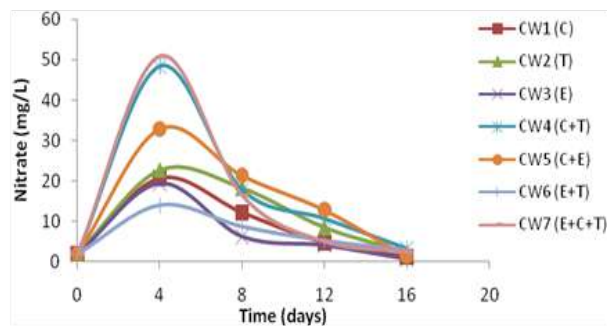


Fig. 2: Change in nitrate concentration of treated SAR in CWs with different wetland macrophytes.

Table 2: Statistical significance of differences in nitrate concentration after 16d batch treatment by *Canna*, *Typha*, and *Eichhornia* in their different combinations in CW microcosms based on Critical Difference (CD= 0.6).

Canna	C- T	C- E	C- CT	C- CE	C- TE	C- CTE	CT- CE	CT- CTE
4	1.9	1.3	27.7	12.1	6.7	30.1	15.6	48.4
8	6	5.9	5.6	9.1	3.5	4.2	3.5	17.8
12	3.76	0.57*	6	8.1	0.53*	0.3*	2.1	10.7
16	1.16	0.41*	2.13	0.13*	1.73	1.33	2	3.3
<i>Typha</i>	T- C	T- E	T- CT	T- CE	T- TE	T- CTE	TE- CT	TE- CTE
4	1.9	3.2	29	15.6	18.8	36.8	34.4	14
8	6	11.9	0.4*	3.1	9.5	1.8	9.1	8.7
12	3.76	4.33	6.57	2.1	7.57	0.23*	5.47	5.23
16	1.16	1.57	2.54	2	1.6	0.4*	0.4*	2.9
<i>Eichhornia</i>	E- C	E- T	E- CT	E- CE	E- TE	E- CTE	ET- CE	EC- CTE
4	1	2.9	29	13.4	5.4	31.4	18.8	32.8
8	5.9	11.9	11.5	15	2.4	10.1	12.6	21.3
12	0.57*	4.33	6.57	8.67	1.1	0.87	7.57	12.8
16	0.41*	1.57	2.54	0.54*	2.14	1.74	1.6	1.3

\*Non-significant (p>0.05)

of 34.15 mg.L<sup>-1</sup>. The highest treatment efficiency (91.8%) was recorded for CW<sub>5</sub> planted with *Canna* and *Eichhornia* plant species in mixed combinations after 16 days of treatment (Table 4). A sharp fall in NH<sub>4</sub><sup>+</sup>-N concentrations in the treated SAR from the beginning suggests the transformation of this form of nitrogen to nitrate, which showed an increase in the beginning.

Most of the comparisons show differences greater than CD, indicating the effects of these different plant combinations to be statistically significant as shown in Table 3.

**Removal of Phosphates from Batch-Treated SAR**

In all the studied CW systems, there was a sharp decrease in the concentration of phosphate right from the beginning of the experiment followed by stabilization with time (Fig. 4). Phosphate concentration reduced from initial 52.64 mg.L<sup>-1</sup>

to 0.53, 0.73, 0.68, 1.13, 0.21, 1.2 and 0.57 mg.L<sup>-1</sup> for CW<sub>1</sub>, CW<sub>2</sub>, CW<sub>3</sub>, CW<sub>4</sub>, CW<sub>5</sub>, CW<sub>6</sub> and CW<sub>7</sub>, respectively showing very rapid and high removal. No significant difference in the removal of phosphate was observed between pairs of constructed wetland microcosms.

Percentage removal efficiency for all the CWs was in the range of 97% to 99% with a maximum in CW<sub>5</sub> as shown in Table 4. Inorganic phosphate in dissolved form can form complexes with ligands and these complexes get bound to the soil/media structure through adsorption and precipitation process. While under aerobic conditions, phosphate forms insoluble complexes with hydrous oxides of aluminum, iron, and calcium (Sakadevan & Bavor 1998).

Based on the above results, it may be concluded that all the CWs planted with single or mixed cultures of wetland macrophytes were quite efficient in the removal of different

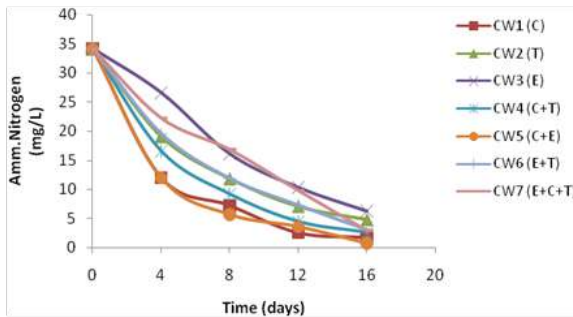


Fig. 3: Change in ammonical nitrogen concentration of treated SAR in CWs with different wetland macrophytes.

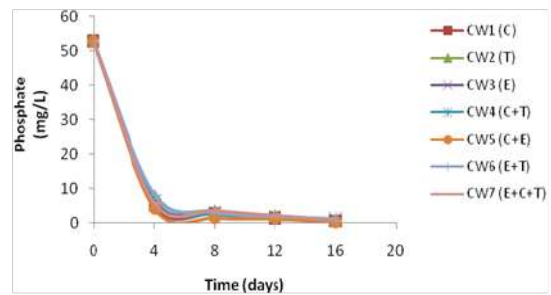


Fig. 4: Change in phosphate concentration of treated SAR in CWs with different wetland macrophytes.

Table 3: Statistical significance of differences in ammonical nitrogen concentration after 16d batch treatment by *Canna*, *Typha* and *Eichhornia* in their different combinations in CW microcosms based on Critical Difference (CD = 0.6).

<i>Canna</i>	C- T	C- E	C- CT	C- CE	C- TE	C- CTE	CT- CE	CT- CTE
4	7.08	14.6	4.62	0.04*	7.58	10.2	4.58	5.58
8	4.63	8.91	2.03	1.49	4.6	9.59	3.52	7.56
12	4.53	7.81	2.01	1.1	4.79	7.22	0.91	5.21
16	3.1	4.57	0.97	0.93	1.39	1.17	1.9	0.2*
<i>Typha</i>	T-C	T- E	T- CT	T- CE	T- TE	T- CTE	TE- CT	TE- CTE
4	7.08	7.52	2.46	7.04	0.5*	3.12	2.96	2.62
8	4.63	4.28	2.6	6.12	0.03*	4.96	2.57	4.99
12	4.53	3.28	2.52	3.43	0.26*	2.69	2.78	2.43
16	3.1	1.47	2.13	4.03	1.71	1.93	0.42*	0.22*
<i>Eichhornia</i>	E-C	E-T	E- CT	E- CE	E- TE	E- CTE	ET- CE	EC- CTE
4	14.6	7.52	9.98	14.56	7.02	4.4	7.54	10.16
8	8.91	4.28	6.88	10.4	4.31	0.68	6.09	11.08
12	7.81	3.28	5.8	6.71	3.02	0.6	3.69	6.12
16	4.57	1.47	3.6	5.5	3.18	3.4	2.32	2.1

\*Non -significant (p>0.05)

Table 4: Nutrient removal efficiency of Constructed Wetland Microcosms (CWMs) with different wetland macrophytes in 16 days' batch treatment.

Parameter	Removal Efficiency (%)						
	CW <sub>1</sub> (C)	CW <sub>2</sub> (T)	CW <sub>3</sub> (E)	CW <sub>4</sub> (C+T)	CW <sub>5</sub> (C+E)	CW <sub>6</sub> (E+T)	CW <sub>7</sub> (E+C+T)
Phosphate	99	99	99	98	99	98	99
Nitrate	94	90	96	93	96	79	95
Ammonical Ni-trogen	95	86	82	92	98	91	92

nutrients within 16d of the treatment period. But CW<sub>5</sub> planted with *Canna* + *Eichhornia* plant species showed maximum removal efficiency as compared to other studied CWs.

A perusal of Table 4 clearly shows very high efficiency (79-99 %) of the CWMs in treating the run-off (SAR) with maximum efficiency being in the case of CW<sub>5</sub> (C+E), which showed 96-98 % removal of the major nutrients (PO<sub>4</sub><sup>3-</sup>, NO<sub>3</sub><sup>-</sup> and NH<sub>4</sub><sup>+</sup>).

**Growth and Tolerance of the Wetland Macrophytes in CWs Treating Simulated Agricultural Run-off (SAR)**

The capacity of the wetland macrophytes to tolerate and grow in the high concentration of nutrients and agrochemicals is important since that is going to decide the overall performance of the planted CWs. Therefore, biomass and chlorophyll content of leaves (Chl a, b and total) of the macrophytes and biomass from all the CWs were determined at the initial (0d) and the termination of the experiment (16d), taking biomass and chlorophyll content as an important index of growth and tolerance, changes in these parameters are shown in Fig. 5.

An increase in the chlorophyll content and relative biomass was observed in single and mono culture *Canna* and *Eichhornia* macrophytes. *Typha* plant in monoculture shows a decline in the relative biomass and chlorophyll content, while in combination with *Eichhornia* macrophyte slight increase in the chlorophyll content and biomass was observed as given in Table 5.

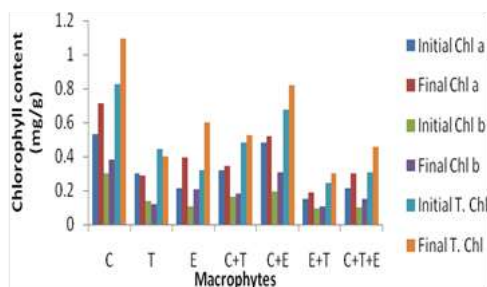


Fig. 5: Change in leaf chlorophyll content of the wetland plants in CWMs treating agricultural run-off.

**Treatment of Simulated Agricultural Runoff (SAR) in Constructed Wetland in Continuous mode at Different Flow Rates**

In this experiment different types of Constructed Wetland systems (CWs) viz. Horizontal flow, Vertical flow and hybrid CW were used with different HRTs (2, 4 & 6 days) at corresponding flow rates of 3.4, 1.7 & 1.1 ml/min., to compare the treatment efficiency of simulated agricultural runoff (SAR). *Canna* (C) and *Eichhornia* (E) (observed best combination plant species from the plant optimization experiment for treatment of SAR in batch mode) in mixed culture conditions were used as the wetland plants, with soil + gravel as a substrate for treatment of the SAR. Characteristics of the SAR are shown in Table 6.

During the experiment pH of the simulated agricultural run-off remained alkaline in all studied constructed wetland systems (CWs), showing minor variations.

**Removal of Phosphate from SAR in HF, VF and Hybrid CW**

Variations in phosphate concentration of the SAR at different HRTs in the Horizontal flow, Vertical flow and Hybrid CW systems are depicted in Fig. 6. At 2d HRT, there was a decline in phosphate concentration from an initial 35.5 mg/L to 18 mg/L, 12.8 mg/L, 11.6 mg/L, 6.4 mg/L, 4.5 mg/L and 3.2 mg/L in the unplanted HF, planted HF, unplanted VF, planted

Table 5: Relative change in biomass of the plants in the CW treating SAR.

Macrophyte	C	T	E	CT	CE	ET	ECT
Relative Bio-mass (g)	142	88	114	147	161	110	138

\*Initial plant weight was taken as 100.

Table 6: Characteristics of SAR.

Parameter	Parameter value
pH	7.64
Phosphate (mg.L <sup>-1</sup> )	35.5
Amm. Nitrogen (mg.L <sup>-1</sup> )	18.3
Total Nitrogen (mg.L <sup>-1</sup> )	15.5

VF, unplanted Hybrid and planted Hybrid CWs, respectively. At 4d HRT, phosphate concentration decreased from 35.5 mg/L to 14.6, 8.26, 7.28, 3.2, 2.1 and 1.4 mg/L in the unplanted HF, planted HF, unplanted VF, planted VF, unplanted Hybrid and planted Hybrid CWs, respectively. At 6d HRT, the concentration of phosphate declined from an initial 35.5 mg/L to 8.03, 5.5, 2.3, 1.9 and 0.4 mg/L in the unplanted HF, planted HF, unplanted VF, planted VF, unplanted Hybrid and planted Hybrid CWs, respectively shown in Fig. 6.

Maximum removal of phosphate (99%) was observed at 6d HRT, in Hybrid CWs followed by 96% and 91% at 4 and 2 days HRT, respectively (Table 7).

Whereas VF CW showed better phosphate removal compared to HF CW for both planted and unplanted reactors. This indicates the good nutrient removal capacity of VF compared to HF. The phosphate removal efficiency of all types of CWs improved when longer HRT was used which

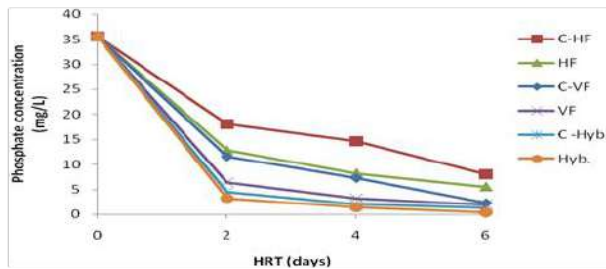


Fig. 6: Change in phosphate concentration of treated SAR in HF, VF and hybrid CWs at different HRTs.

Table 7: Percentage removal of nutrients and pesticides from SAR in HF, VF and Hybrid CWs at different HRTs.

Parameter	HRT (d)	Removal Efficiency (%)					
		C-HF	HF	C-VF	VF	C-Hybrid	Hybrid
Phosphate	2	49	64	67	82	87	91
	4	59	77	80	91	94	96
	6	77	84	93	94	96	99
Ammonical Nitrogen	2	22	27	26	33	40	49
	4	29	43	43	65	55	62
	6	51	62	61	72	74	80
Total Nitrogen	2	10	14	15	17	39	43
	4	28	38	42	55	61	70
	6	51	61	65	70	80	89

HF= Horizontal flow, VF= Vertical flow, Hybrid= Hybrid Constructed Wetland Systems, C= unplanted control

suggests that greater contact times facilitate nutrient removal by CWs (Akratos & Tsihrintzis, 2007).

### Removal of Ammonical Nitrogen

Variations in ammonical nitrogen concentration of the SAR at different HRTs in the Horizontal flow, Vertical flow and Hybrid CW systems are depicted in Fig. 7. At 2d HRT, there was a decline in ammonical nitrogen concentration from an initial 18.3 mg/L to 14.26 mg/L, 13.3 mg/L, 13.5 mg/L, 12.3 mg/L, 11 mg/L and 9.4 mg/L in the unplanted HF, planted HF, unplanted VF, planted VF, unplanted Hybrid and planted Hybrid CWs, respectively.

At 4d HRT, ammonical nitrogen concentration decreased from 18.3 mg/L to 12.9, 10.5, 10.4, 6.4, 8.2 and 7 mg/L in the unplanted HF, planted HF, unplanted VF, planted VF, unplanted Hybrid and planted Hybrid CWs, respectively. At 6d HRT, the concentration of ammonical nitrogen declined from an initial 18.3 mg/L to 9, 6.9, 7.2, 5.16, 4.7 and 3.6 mg/L in the unplanted HF, planted HF, unplanted VF, planted VF, unplanted Hybrid and planted Hybrid CWs, respectively. In this case, also hybrid systems performed best compared to VF and HF. Since, greater removal of ammonical nitrogen indicates the establishment of aerobic conditions in the reactors, it can be deduced that HF CWs probably did not have a sufficient aerobic environment that could facilitate nitrification and hence they showed the least ammonical nitrogen removal. Moreover, it was observed that all the planted reactors showed better removal efficiency than the unplanted ones in their respective flow types. This might be due to the root zone effect which somehow enhanced the nitrification process by the release of oxygen in the rhizosphere (Fan et al. 2012).

### Removal of Total Nitrogen from SAR in HF, VF and Hybrid CW

Change in total nitrogen concentration of SAR at 2d HRT, from an initial 15.5 mg/L to 14 mg/L, 13.4 mg/L, 13.1 mg/L, 12.8 mg/L, 9.4 mg/L and 6.8 mg/L in the unplanted HF,

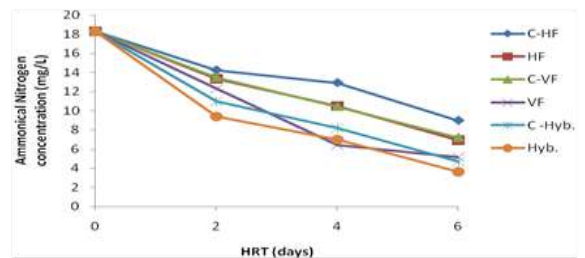


Fig. 7: Change in ammonical nitrogen concentration of treated SAR in HF, VF and hybrid CWs at different HRTs.



planted HF, unplanted VF, planted VF, unplanted Hybrid and planted Hybrid CWs, respectively. At 4d HRT, total nitrogen concentration decreased from 15.5 mg/L to 11.1, 9.6, 8.9, 7, 6.1 and 4.7 mg/L in the unplanted HF, planted HF, unplanted VF, planted VF, unplanted Hybrid and planted Hybrid CWs, respectively. At 6d HRT, concentration of total nitrogen declined from an initial 15.5 mg/L to 7.5, 6, 5.4, 4.6, 3.1 and 1.7 mg/L in the unplanted HF, planted HF, unplanted VF, planted VF, unplanted Hybrid and planted Hybrid CWs, respectively as shown in Fig. 8.

As it is evident from the results that the total nitrogen removal also followed a similar trend to that of removal of ammonical nitrogen. All CW systems showed an appreciable decrease in the concentration of total nitrogen after 6d HRT but planted hybrid CW showed maximum removal efficiency of 89% at 6d, HRT (Table 7). It is therefore considered that all the factors viz. high retention time, presence of vegetation, the microflora of rhizosphere and flow of wastewater in the hybrid system probably played a considerable part in maintaining adequate conditions for nitrification and denitrification which resulted in maximum removal of total nitrogen from wastewater. Arivoli and Mohanraj (2013) also reported that combined nitrification and denitrification along with sedimentation are specific processes for the treatment of nitrogen forms in a vertical flow CWs planted with *Typha angustifolia*.

Vertical flow CW was found to be more efficient than horizontal flow CW in removing various pollutants at different HRTs. Hybrid CW was most efficient for the removal of all pollutants, showing 91-99% removal of phosphate, 49-80% of ammonical nitrogen 43-89% of total nitrogen (Table 4.10). Removal in VF CWs was in the range of 17-94% and that in HF CWs varied from 14-84%. Planted CWs showed greater removal than unplanted CWs in all (HF, VF and Hybrid CWs).

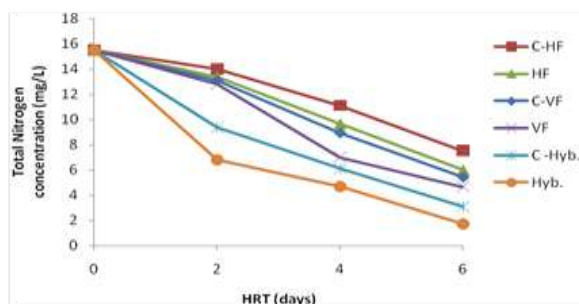


Fig. 8: Change in total nitrogen concentration of treated SAR in HF, VF and Hybrid CWs at different HRTs.

## CONCLUSION

Based on the above results, it may be concluded that CWs planted with *Canna* + *Eichhornia* plant species in mixed cultures were very efficient in treating the nutrients present in agricultural run-off (SAR). *Canna indica* and *Typha latifolia* bi-culture showed 96-98% removal of the major nutrients ( $\text{PO}_4^{3-}$ ,  $\text{NO}_3^-$  and  $\text{NH}_4^+$ ) from simulated agricultural run-off (SAR) along with an increase in the leaf chlorophyll content and relative biomass. Treatment efficiency improved when longer HRTs were used. Hybrid CW (which includes the properties of HF and VF types of CWs) had maximum removal of all nutrients, 91-99% removal of phosphate, 49-80% of ammonical nitrogen 43-89% of total nitrogen.

## ACKNOWLEDGEMENT

The author is grateful for the university resources provided by Guru Jambheshwar University of Science & Technology, Hisar, and Shree Guru Gobind Singh Tricentenary University, Gurugram, Haryana, India. Special thanks are due to the University Grants Commission, New Delhi for granting financial support to one of the authors (SS) under the Maulana Azad National Fellowship (MANF) scheme.

## REFERENCES

- Abhilash, P. and Singh, N. 2009. Pesticide use and application: An Indian scenario. *J. Hazard. Mater.*, 165(1-3): 1-12.
- Akratos, C.S. and Tsihrantzis, V.A. 2007. Effect of temperature, HRT, vegetation, and porous media on removal efficiency of pilot-scale horizontal subsurface flow constructed wetlands. *Ecol. Eng.*, 29 (2): 173-191.
- American Public Health Association (APHA). 1995. Water Pollution Control Federation. American Water Works Association (20th ed.), Standard Methods for the Examination of Water and Wastewater, Washington, DC.
- Arivoli, A. and Mohanraj, R. 2013. Efficacy of *Typha angustifolia*-based vertical flow constructed wetland system in pollutant reduction of domestic wastewater. *Int. J. Environ. Sci.*, 3(5): 1497-1508.
- Arnon, D.I. 1949. Copper enzymes in isolated chloroplasts: Polyphenoloxidase in *Beta vulgaris*. *Plant Physiol.*, 24: 1-15.
- Brix, H. 1993. Wastewater Treatment in Constructed Wetlands: System Design and Treatment Performance. In Moshiri, G.A. (ed), *Constructed Wetlands for Water Quality Improvement*, CRC Press Inc., Boca Raton., pp. 9-22.
- Bulc, T.G. 2006. Long-term performance of a constructed wetland for landfill leachate treatment. *Ecol. Eng.*, 26: 365-374.
- Divya, J. and Belagali S.L. 2012. Impact of chemical fertilizers on water quality in selected agricultural areas of Mysore district, Karnataka, India. *Int. J. Environ. Stud.*, 2(3): 1149-1158.
- Fan, J.L., Liang, S., Zhang, B. and Zhang, Z. 2012. Enhanced organics and nitrogen removal in batch-operated vertical flow constructed wetlands by the combination of intermittent aeration and step feeding strategy. *Environ. Sci. Pollut. Res.*, 20(4): 2448-2455.
- Gangbazo, G.D.C and Bernard, C. 1999. Knowledge acquired on agricultural nonpoint pollution in Quebec—1993–1998: Analysis and perspectives. *Vecteur Environ.*, 32: 36-45.

- Goyal, M.R., Abrol, O.P. and Vohra, A.K. 1981. Pollution of Upper Aquifer in Punjab (India): Quality of Groundwater. Elsevier Scientific Publishing Company, The Netherlands.
- Handa, B.K. 1986. Pollution of groundwater by nitrates in India. *Bhu-Jal News*, 1: 16-19.
- Humenik, F.J., Smolen, M.D. and Dressing, S.A. 1987. Pollution from nonpoint sources. *Environ. Sci. Technol.*, 21: 737-742.
- Kadlec, R.H. and Hey, D.L. 1994. Constructed wetlands for river water quality improvement. *Water Sci. Technol.*, 29: 159-168.
- Kern, J. and Brettar, J. 2002. Nitrogen turnover in a subsurface constructed wetland receiving dairy farm wastewater. In Pries, J. (ed), *Treatment for Water Quality Improvement*, CH2M Hill Canada Limited, Waterloo, Ontario, pp. 15-21.
- Kin-Che, L., Leung Y.F. and Yao, Q. 1997. Nutrient fluxes in the Shenchong Basin, Deqing County, South China. *Catena*, 29: 191-210.
- Kumar, S. and Singh, J. 1988. Pollution of groundwater by nitrates in and around Mahendragarh district, Haryana. *International Seminar on Hydrology, Colloquium on water Resources problems of South Asian Countries*, Andhra University, Visakhapatnam, India, pp. 11-21.
- Lakshmanam, A.R., Rao, T.K. and Viswanathan, S. 1986. Nitrate and fluoride levels in drinking waters in the twin cities of Hyderabad and Secundrabad. *Indian J. Environ. Hlth.*, 28: 39-47.
- Line, D.E., Osmond D.L., Coffey S.W., McLaughlin R.A., Jennings G.D., Gale J.A., and Spooner J. 1997. Nonpoint sources. *Water Environ. Res.*, 69: 844-860.
- Lunkad, S.K. 1994. Rising nitrate levels in groundwater and increasing N-fertilizer consumption. *Bhu-Jal News*, 4: 10.
- Mandal, K. U., Sharma, M.K.L., Prasad, J.V.N.S., Reddy, B.S., Narsimlu, B., Saikia, U.S., Adake, R. V., Yadaiah, P., Masane, R.N., Venkanna, K., Venkatravamma, K., Satyam, B., Raju, B. and Srivastava, N.N. 2012. Nutrient losses by runoff and sediment from an agricultural field in semi-arid tropical India. *Indian J. Dry-land Agri. Res. Dev.*, 27(1): 01-09.
- Ministry of Environment and Forests (MoEF). 2009. *State of Environment Report*. New Delhi.
- Mishra, P.K., Cogle, A.L., Sharma, K.L., Smith, G.D., Rao, K.V., Freebairn, D.M., Subba Reddy, G., King, C., Korwar, G.R., Osman, M. and Venkateswarlu, B. 2010. *Natural Resources Management in Semi-arid Regions: Learning from Farm and Watershed Level Action*. Research of ICAR-ACIAR Collaborative Project, Central Research Institute for Dry-land Agriculture, Hyderabad, 184.
- Moore, M.T., Rodgers, J.H. Jr., Cooper, C.M. and Smith, S. 2000. Constructed wetlands for mitigation of atrazine-associated agricultural runoff. *Environ. Pollut.*, 110: 393-399.
- Sakadevan, K. and Bavor, H.J. 1998. Phosphate adsorption characteristics of soils, slags, and zeolite to be used as substrates in constructed wetland systems. *Water Res.*, 32(2): 393-399.
- Schepers, J.S., Frank, K.D. and Watts, D.G. 1984. Influence of irrigation and nitrogen fertilization on groundwater quality. *Proceedings of the International Union of Geodesy and Geophysics, August 1983, Hamburg, West Germany*, IAHS Publication, Wallingford, UK, pp. 21-32.
- Singh, B.K., Pal, O.P. and Pandey, D.S. 1991. Ground water pollution: A case study around north eastern railway city station, Lucknow, Uttar Pradesh. *Bhu-Jal News*, 6: 46-49.
- Tamta, S.R., Kapoor, S.L. and Goverdhanan, T. 1992. Quality assessment of groundwater in Bangalore district of Karnataka. *Bhu-Jal News*, 7: 58.
- Vymazal, J., Greenway, M., Tonderski, K., Brix, H. and Mander, Ü. 2006. *Constructed Wetlands for Wastewater Treatment Ecological Studies*. In Verhoeven, J.T.A., Beltman, B., Bobbink R. and Whigham, D.F. (Eds.) *Wetlands and Natural Resource Management*, Vol. 190, Springer Berlin Heidelberg, Germany, pp. 46-115.
- Zhou, Q., Zhang, R., Shi, Y., Li, Y., Paing, J. and Picot, B. 2004. Nitrogen and phosphorus removal in subsurface constructed wetland treating agriculture stormwater runoff. In: *Proceedings of the 9th International Conference on Wetland Systems for Water pollution Control*, ASTEE, Cemagref, Lyon, France, pp. 75-82.
- Zuazo, V.H.D., Raya, A.M. and Ruiz, J.A. 2004. Nutrient losses by runoff and sediment from the taluses of orchard terraces *Water Air Soil Pollut.*, 153: 355-373.



# Evaluation of Biodegradation Efficiency of Xylene Pretreated Polyethylene Wastes by Isolated *Lysinibacillus fusiformis*

Arun Kalia and M. S. Dhanya†

Department of Environmental Sciences and Technology, School of Environment and Earth Sciences, Central University of Punjab, Bathinda-151401, India

†Corresponding author: M. S Dhanya; ms.dhanya@cup.edu.in

Nat. Env. & Poll. Tech.  
Website: [www.neptjournal.com](http://www.neptjournal.com)

Received: 01-10-2021

Revised: 02-12-2021

Accepted: 22-12-2021

## Key Words:

Low-density polyethylene  
Xylene  
Pretreatment  
Biodegradation  
*Lysinibacillus fusiformis*

## ABSTRACT

The ability of the bacterial degradation of low-density polyethylene (LDPE) waste by *Lysinibacillus fusiformis* isolated from hydrocarbon-contaminated soil was investigated in the present study. The potential of the bacterial isolate to utilize LDPE waste bags of two different thicknesses in a month as a sole carbon source in mineral salt media was assessed. Further, the effect of pretreatment by xylene on the bacterial degradation of LDPE waste bags (0.5 percent w/v) in 30 days was investigated. The isolated *Lysinibacillus fusiformis* was able to degrade 9.51 percent of LDPE with 30  $\mu$ m thickness but able to degrade only 1.45 percent of LDPE having 50  $\mu$ m thickness. The bacterial biomass was 1.77 times higher on LDPE- 30  $\mu$ m containing media in comparison to LDPE- 50  $\mu$ m. The xylene pretreatment of LDPE wastes enhanced the biodegradation efficiency of isolated *Lysinibacillus fusiformis* to 12.09 and 1.97 percent respectively in 30  $\mu$ m and 50  $\mu$ m thick LDPE bags. The xylene pre-treatment improved the bacterial growth on media with LDPE of both thicknesses. The adherence of bacterium on the surface of LDPE was found more on 50  $\mu$ m thick xylene treated LDPE compared to its untreated LDPE than 30  $\mu$ m thick LDPE films. The xylene pre-treatment of polyethylene waste had an additive effect on the biodegradation of waste LDPE films with a significant effect on thickness.

## INTRODUCTION

The generation and dumping of different types of plastic wastes after consumption into the environment had increased manifold in the present era of expeditious industrialization. The global annual production of plastic is around 400 million tonnes and nearly 8 to 13 million tonnes of plastic wastes are ended with direct ocean dumping (Danso et al. 2019). Out of the total plastics produced, polyethylene and polypropylene are major polymers that comprise 92% of the total production. The natural aging and weathering of plastics from marine dumping or landfilling increased their mobility and were easily incorporated into the food chain, thus adversely affecting the organisms (Sen & Raut 2015). The disposal of plastic wastes in landfills generates hazardous chemicals and in turn, contaminates the groundwater (North & Halden 2013). The microplastics formed from plastic waste had the potential to act as a carrier for the adsorption of recalcitrant hydrophobic toxic chemicals such as polychlorinated biphenyls (de Souza Machado et al. 2018).

The different methods for the management of plastic waste are landfilling, incineration, and recycling, (Peng et al. 2018, Ali et al. 2021). But these conventional degradation methods have their limitations such as the negative impact on

climate, space constraints, effect on soil fertility, and leakage of toxic components in water and soil (Hopewell et al. 2009). The indigenous microbial population present in contaminated habitats holds the key to solving most of the challenges linked with the bioremediation of environmental pollutants (Verma & Jaiswal 2016). The microbes having potential for degrading polyethylene is limited. Many studies are focused on searching for polyethylene degrading microbial strains from diverse habitats like oil spillage, sludge, municipal landfills, and plastic dump sites (Duddu et al. 2015, Soud 2019). The bacterial genera namely *Pseudomonas*, *Bacillus*, *Stenotrophomonas*, *Ralstonia*, *Acinetobacter*, *Streptococcus*, *Rhodococcus*, *Staphylococcus*, *Klebsiella*, and *Streptomyces* are reported for polyethylene degradation (Park & Kim 2019, Shahreza et al. 2019).

The pretreatment of polyethylene including thermal oxidation, UV irradiation, and chemical and mechanical breakdown before the microbial degradation plays an important role in the effective cleanup of these synthetic polymers (Olayan et al. 1996, Raut et al. 2015). The chemical pretreatment increased the availability of the plastic substrate to microorganisms for biodegradation (Balasubramanian et al. 2014, Kundungal et al. 2021). The thickness of dumped polyethylene plastics was in the range of 15-50  $\mu$ m (Tziour-

rou et al. 2021). The present study attempts to investigate the effect of thickness of low-density polyethylene waste bags on the degradation potential of isolated *Lysinibacillus fusiformis* and also the impact of xylene pretreatment on biodegradation.

## MATERIALS AND METHODS

### Bacterium Used in Biodegradation Study

The bacterium *Lysinibacillus fusiformis* used in the present study was previously isolated from the soil contaminated with hydrocarbons collected from areas of coal-fired thermal power facilities in Bathinda, Punjab (Kalia 2015).

### Low-Density Polyethylene Waste Bag Collection

The low-density polyethylene waste bags used in the present study were collected from local dumping sites in Bathinda, Punjab, India. The polyethylene waste bags were sorted based on thickness into two categories namely LDPE- 30  $\mu\text{m}$  and LDPE- 50  $\mu\text{m}$ . The LDPE waste bags having thicknesses of 30  $\mu\text{m}$  and 50  $\mu\text{m}$  were cut into uniform pieces of 1x1  $\text{cm}^2$  dimensions.

### Xylene Treatment of Polyethylene Waste Bags

The LDPE waste bags of 30  $\mu\text{m}$  and 50  $\mu\text{m}$  thickness cut into uniform pieces of 1x1  $\text{cm}^2$  were subjected to xylene treatment by boiling for 15 min. The LDPE waste bags after xylene treatment was subjected to ethanol washing followed by drying in a hot air oven at a temperature of 60°C. The xylene pretreated samples were stored at room temperature and used for evaluating the effect of xylene on biodegradation study by the bacterium (Das & Kumar 2015).

The untreated (control) and xylene-treated waste LDPE films of 30  $\mu\text{m}$  and 50  $\mu\text{m}$  thickness were analyzed by FT-IR spectroscopy (FTIR Bruker, Model: Tensor 27) to detect the changes in surface functional groups on polyethylene in the spectral range of 4000-600  $\text{cm}^{-1}$  (Albertsson et al. 1987, Sudhakar et al. 2008).

### Biodegradation of Waste Polyethylene by *Lysinibacillus fusiformis*

The mineral salt media used in the present biodegradation study contained  $(\text{NH}_4)_2\text{SO}_4$ ,  $\text{K}_2\text{HPO}_4$  and NaCl in 1  $\text{g.L}^{-1}$ ,  $\text{MgSO}_4 \cdot 7\text{H}_2\text{O}$  in 0.5  $\text{g.L}^{-1}$ ,  $\text{CaCl}_2 \cdot 2\text{H}_2\text{O}$  in 0.002  $\text{g.L}^{-1}$ ,  $\text{KH}_2\text{PO}_4$  in 0.2  $\text{g.L}^{-1}$ ,  $\text{ZnSO}_4 \cdot 7\text{H}_2\text{O}$ ,  $\text{MnSO}_4 \cdot \text{H}_2\text{O}$  and  $\text{CuSO}_4 \cdot 5\text{H}_2\text{O}$  in 0.001  $\text{g.L}^{-1}$  with pH maintained at 7 (Das & Kumar 2015).

The degrading efficiency of bacterial isolate *Lysinibacillus fusiformis* was tested by supplementing waste LDPE bags of two thicknesses, 30  $\mu\text{m}$  and 50  $\mu\text{m}$  at 0.5 percent (w/v) in the mineral salt medium as the sole carbon source (Gilan et

al. 2004, Balasubramanian et al. 2014). The biodegradation study of untreated and xylene-treated waste LDPE bags was performed with isolated *Lysinibacillus fusiformis* in a 250 mL Erlenmeyer flask incubated in a rotatory incubator shaker at 30°C and 180 rpm for 30 days. The weight loss of polyethylene bags of two thicknesses from initial weight was used to measure the biodegradation efficiency of *Lysinibacillus fusiformis*.

The waste LDPE samples collected from the culture media after the degradation study was washed with aqueous sodium dodecyl sulfate solution (2% v/v) followed by distilled water washing (Gilan et al. 2004). The weight loss of the films from initial to final weight indicated the degradation as per the formula given below.

$$\text{Biodegradation (\%)} = \frac{\text{Initial weight} - \text{final weight}}{\text{Initial weight}} \times 100$$

### Growth of Isolated *Lysinibacillus Fusiformis* on Low-Density Polyethylene Waste Bags

The bacterial population on the surface of untreated and xylene treated LDPE was estimated from the amount of extractable protein present on the samples. The LDPE samples were collected from the growth medium at 5 days intervals. The samples were boiled for 30 min in 0.5 N NaOH, centrifuged and the supernatant was collected. The protein concentration was determined spectrophotometrically by the Lowry method (Lowry et al. 1951).

### Statistical Analysis

The biodegradation study was conducted in triplicates. The statistical analysis for testing of significance by ANOVA single factor and correlation studies were carried out.

## RESULTS AND DISCUSSION

### Waste Polyethylene Biodegradation Potential of *Lysinibacillus fusiformis*

The *Lysinibacillus fusiformis*, previously isolated from hydrocarbon-contaminated soil was able to grow in the liquid, mineral salt medium enriched with waste LDPE- 30  $\mu\text{m}$  and LDPE- 50  $\mu\text{m}$  films as sole carbon sources without any treatment. The biomass growth was measured in terms of protein content confirming the growth on the surface of both LDPE waste bags (Fig. 2). The 30  $\mu\text{m}$  thick LDPE waste bags had more *Lysinibacillus fusiformis* growth than the 50  $\mu\text{m}$  thick bags. The increase in growth of *Lysinibacillus fusiformis* from incubation was 2.01 and 2.19 times respectively for 30 $\mu\text{m}$  and 50 $\mu\text{m}$  thick LDPE wastes in 5 days. The growth on the 15<sup>th</sup> day on the LDPE 30  $\mu\text{m}$  and LDPE- 50 $\mu\text{m}$  films



were 62 percent and 42 percent higher than on the 10<sup>th</sup> day of incubation. The bacterial proliferation got reduced further and only an 8.16 percent increase in protein concentration was reported from 25 to 30 days period of bacterial growth using untreated LDPE- 30  $\mu\text{m}$  films in vitro. The protein concentration on the 20<sup>th</sup> day was 32 percent higher than on the 15<sup>th</sup> day of incubation. Further, a decrease in the rate of increase in protein concentration and was only a 12 percent increase was noticed in the next five days in 30 days of incubation using waste LDPE- 50  $\mu\text{m}$  films. The thickness of LDPE had a significant effect on bacterial proliferation and the more the thickness, the lower the growth. The LDPE films are hydrophobic in nature and restrict the easy attachment of microbes. A few bacterial strains were able to synthesize biosurfactants with an emulsifying activity that reduced the surface and inter-surface tension to increase the polymer bioavailability (Hassanshahian et al. 2014).

Subsequently, after initial bacterial attachment on the polymer surface, the *Lysinibacillus fusiformis* was able to utilize 1.17 percent of supplied LDPE- 30  $\mu\text{m}$  films in 10 days. But the degradation of LDPE- 50  $\mu\text{m}$  films in 10 days was only 0.55 percent of the incubated concentration. The degradation percentage of *Lysinibacillus fusiformis* was increased by 3.96 times in the next 10 days of incubation in growth media enriched with waste LDPE- 30  $\mu\text{m}$  films in comparison to an increase of 0.62 percent in LDPE- 50  $\mu\text{m}$ . Further increases in degradation percent in 30 days for LDPE- 30  $\mu\text{m}$  and LDPE- 50  $\mu\text{m}$  were 4.38 percent and 0.28 percent respectively.

The bacterial isolate was able to utilize 9.51 percent and 1.44 percent of the untreated waste LDPE- 30  $\mu\text{m}$  and LDPE- 50  $\mu\text{m}$  films in vitro respectively in 30 days (Fig. 3). The bacterial isolate *Lysinibacillus fusiformis* was able to accumulate 1.78 times more protein concentration and 6.58 times more degradation from untreated LDPE- 30  $\mu\text{m}$  films than LDPE- 50  $\mu\text{m}$  films as the sole carbon source. The bacteria with polyethylene degrading capabilities isolated from contaminated environments were also reported by Duddu et al. (2015). The adherence of the bacterial population on the surface of LDPE had a significant effect on the degradation pattern (Montazer et al. 2018). The bacterial strains from hydrocarbon-contaminated sites marked the presence of catabolic genes that encode alkane hydroxylases needed for polyethylene degradation (Gilan et al. 2004, Tanase et al. 2013, Lima et al. 2019).

The comparatively lesser growth and low degradation of LDPE- 50  $\mu\text{m}$  films were due to the higher thickness. The increase in polymer thickness decreased the contact between the surface exposed to the hydrolytic enzyme and microbial attachment, thereby reducing the degradation rate (Yang

et al. 2005). The higher thickness also reduced the oxygen diffusion in the core of the polymer and thereby reduced the degradation rate (Lin & Anseth 2013).

### Effect of Xylene Treatment on Biodegradation of Polyethylene Waste Bags

The waste LDPE- 30  $\mu\text{m}$  and LDPE- 50  $\mu\text{m}$  films were further subjected to xylene treatment. The xylene treatment fragmented the polymer and converted it to powder (Fig. 1). The structural changes in the high-density polyethylene by pretreatment of *p*-xylene were reported by Blackadder & Keniry (1972). The dissolution of LDPE by xylene as a safe pretreatment method was reported by Wong et al. (2014). The solubility of high-density polyethylene and polypropylene in xylene was also studied by Richards (1946) and Arkan et al. (2017).

The structural changes in the polyethylene were analyzed by the FTIR analysis of the powdered polymer after xylene treatment. The FTIR spectra of untreated LDPE films had peaks at 723  $\text{cm}^{-1}$  (C-H), 1086  $\text{cm}^{-1}$  (C-O stretch), 1459  $\text{cm}^{-1}$  ( $\text{CH}_2$  bending) and 2,660  $\text{cm}^{-1}$  (CHO stretch). This was in accordance with the peaks obtained for the IR spectrum of LDPE reported by Das & Kumar (2015). The spectra of LDPE films treated with xylene were shown some different peaks. The FTIR spectra of xylene-treated LDPE- 30  $\mu\text{m}$  (X\_LDPE-30  $\mu\text{m}$ ) film showed peaks at 1484, 2872, and 3426  $\text{cm}^{-1}$ . The powdered LDPE- 50  $\mu\text{m}$  films after xylene treatment (X\_LDPE-50  $\mu\text{m}$ ) had marked peaks at 1375, 1459,

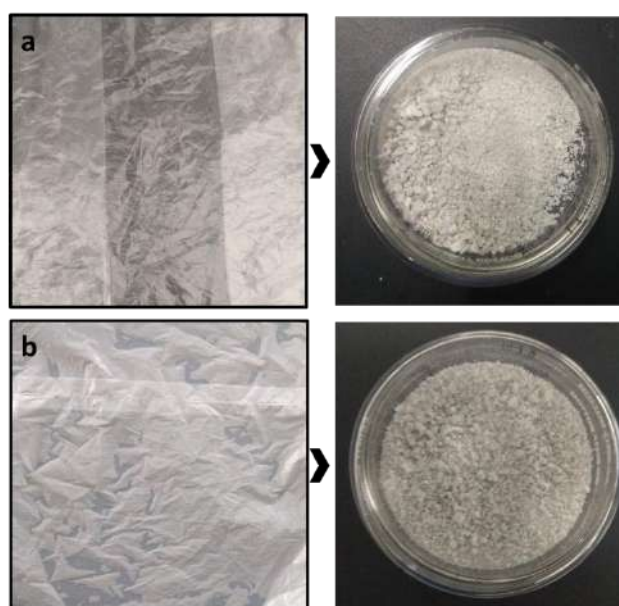


Fig. 1: Waste polyethylene films a) LDPE- 30  $\mu\text{m}$  and b) LDPE- 50  $\mu\text{m}$  before and after treatment with xylene.



2832, 2876, 2959, and 3426  $\text{cm}^{-1}$ . The changes in the peaks value for every functional group and generation of new peaks in xylene-treated LDPE films confirmed the changes in the structure by the treatment of xylene.

The bacterial isolate was able to adhere to the xylene-treated LDPE films supplied in the culture broth. The treatment with xylene improved the growth in both 30  $\mu\text{m}$  and 50  $\mu\text{m}$  thick LDPE wastes. The biomass increase in *Lysinibacillus fusiformis* after xylene treatment was 2.54 and 2.39 times for 30  $\mu\text{m}$  and 50  $\mu\text{m}$  thick LDPE wastes respectively in 5 days. The xylene treatment of waste LDPE- 30  $\mu\text{m}$  and LDPE- 50  $\mu\text{m}$  films increased the biomass growth as evident from extractable protein concentration was 21 percent and 27 percent respectively than the untreated films of LDPE-30  $\mu\text{m}$  and LDPE- 50  $\mu\text{m}$  by *Lysinibacillus fusiformis* in 10 days of incubation (Fig. 2). The percent increase in protein concentration on xylene treated LDPE- 30  $\mu\text{m}$  was 21 percent in 10 days which decreased to 10.78 percent in 30 days in comparison to untreated LDPE- 50  $\mu\text{m}$ . Interestingly the percent increase in protein concentration on xylene treated LDPE- 50  $\mu\text{m}$  was 28 percent in 10 days which increased to 41.5 percent in 30 days in comparison to untreated LDPE- 50  $\mu\text{m}$ .

The biodegradation of xylene treated LDPE-30  $\mu\text{m}$  and LDPE- 50  $\mu\text{m}$  films by *Lysinibacillus fusiformis* were 12.09 percent and 1.97 percent respectively after 30 days of incubation (Fig. 3). The xylene treatment of the waste polyethylene films had an additive effect on biodegradation

as it increased the degradation percentage of LDPE- 30  $\mu\text{m}$  and LDPE- 50  $\mu\text{m}$  films to 27.15 and 36.21 percent than the untreated LDPE films respectively. The xylene treatment of waste LDPE films improved the bacterial biomass (protein concentration) by 10.78 and 41.50 percent than the untreated waste LDPE- 30  $\mu\text{m}$  and LDPE- 50  $\mu\text{m}$  films respectively. The biodegradation of xylene pretreatment of LDPE wastes was highly significant with thickness. The biomass growth was highly correlated with biodegradation of untreated and xylene treated LDPE of 30  $\mu\text{m}$  and 50  $\mu\text{m}$  thickness.

The biofilm formation significantly increases the biodegradation potential of the bacterial isolate (Balasubramanian et al. 2010). The improvements in protein concentration and a weight loss percentage of LDPE- 30  $\mu\text{m}$  and LDPE- 50  $\mu\text{m}$  films were attributed to the structural changes induced by the xylene treatment before incubation with *Lysinibacillus fusiformis*. The dissolution of polyethylene films using xylene fragmented the polymer and resulted in changes in molecular weight distribution and morphology. The pattern of biodegradation of LDPE was similar to the reports of Albertsson (1980) and Das & Kumar (2015).

The pre-treatment helped to increase the availability of LDPE to microorganisms (Cornell et al. 1984, Koutny et al. 2006). The chemical treatments of polyethylene increased the polymer susceptibility for microorganism by inducing functional groups on the polyethylene surface that favors the microbial attachments (Chaudhary & Vijayakumar 2020).

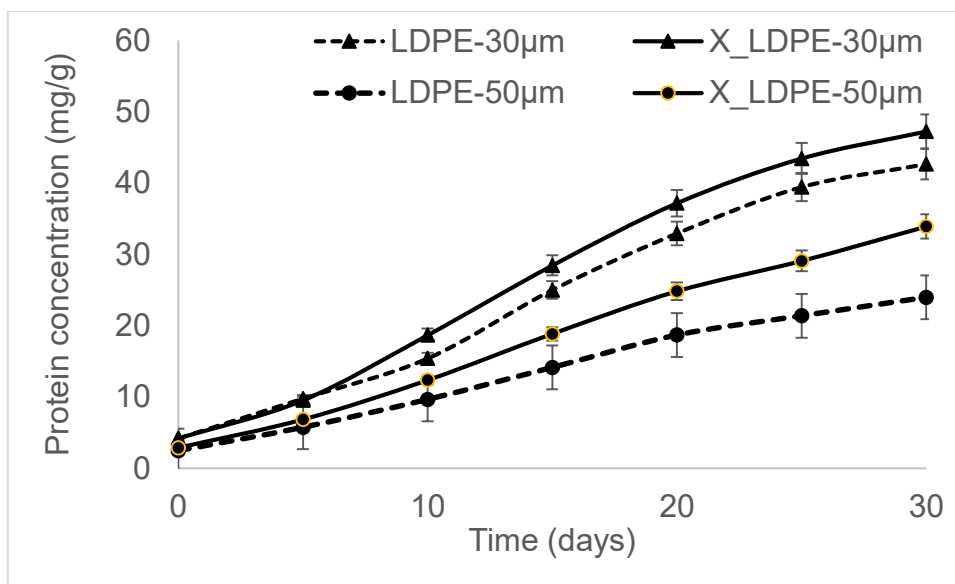


Fig. 2: Effect of xylene treatment on protein concentration in media inoculated with *Lysinibacillus fusiformis* using untreated and xylene pretreated waste LDPE- 30  $\mu\text{m}$  and LDPE- 50  $\mu\text{m}$  films.

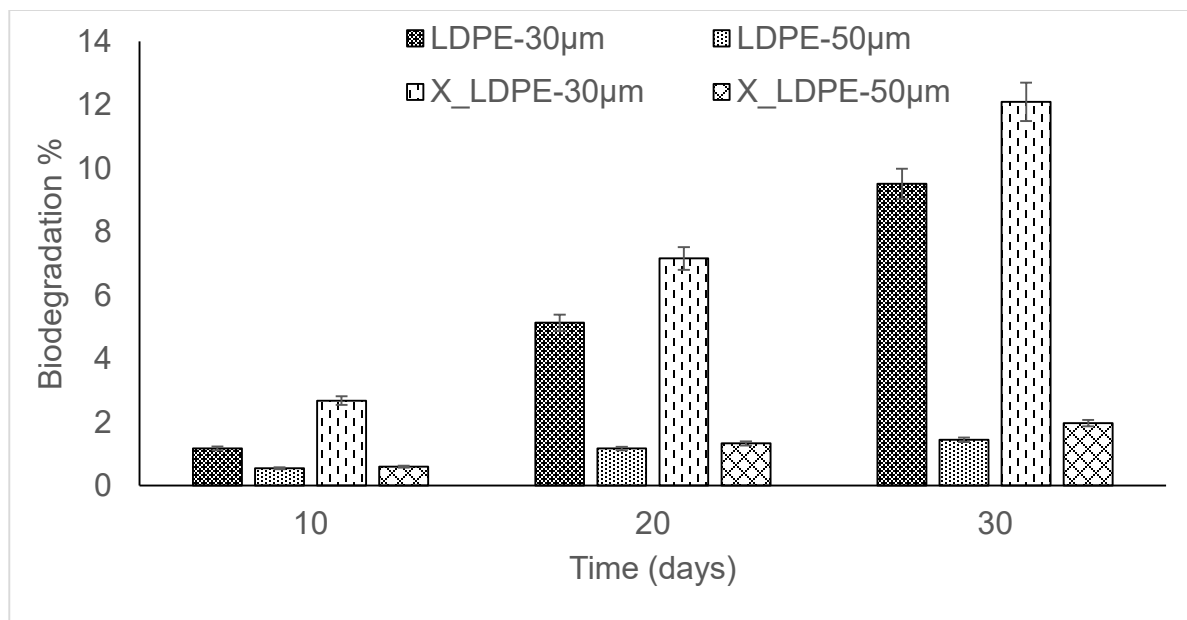


Fig. 3: Comparison of biodegradation efficiency of untreated and xylene treated LDPE- 30 µm and LDPE- 50 µm waste bags after 30 days of incubation with *Lysinibacillus fusiformis*.

## CONCLUSION

The isolated *Lysinibacillus fusiformis* had the potential to degrade the low-density polyethylene. The efficiency of biodegradation varied with the thickness of LDPE. The xylene treatment was found to enhance the biomass growth on the LDPE surface with a faster degradation. The naturally occurring microbial strain with abiotic pretreatment help in the biodegradation of more recalcitrant organic pollutants more efficiently and effectively.

## ACKNOWLEDGEMENT

The authors are thankful to the Central University of Punjab, Bathinda (India) for providing facilities to undertake the present work. The authors especially thank the Central Instrumentation Facility, the Central University of Punjab for FTIR analysis. The first author thanks University Grants Commission for the UGC-JRF.

## REFERENCES

- Albertsson, A.C. 1980. The shape of the biodegradation curve for low and high-density polyethylene in prolonged series of experiments. *Eur. Polym. J.*, 16(154): 623-630.
- Albertsson, A.C., Andersson S.O. and Karlsson, S. 1987. The mechanism of biodegradation of polyethylene. *Polym. Degrad. Stab.*, 18(1): 73-87.
- Ali, S.S., Elsamahy, T., Koutra, E., Kornaros, M., El-Sheekh, M., Abdelkarim, E. and Sun, J. 2021. Degradation of conventional plastic wastes in the environment. A review of the current status of knowledge and future perspectives of disposal. *Sci. Total Environ.*, 771: 144719.

- Arkan, H., Ghassan, H., Kamal, Y., Ghazi Faisal, N. and Farhan, H.S. 2017. Prediction of experimental measurement data for high-density polyethylene and polypropylene solubility in organic solvents. *Chem. Prod. Process Model.*, 12. 10.1515/cppm-2016-0078.
- Balasubramanian, V., Natarajan, K., Hemambika, B., Ramesh, N., Sumathi, C.S., Kottaimuthu, R. and Rajesh Kannan, V. 2010. High-density polyethylene (HDPE)-degrading potential bacteria from the marine ecosystem of the Gulf of Mannar. *India. Lett. Appl. Microbiol.*, 51(2): 205-211.
- Balasubramanian, V., Natarajan, K. and Rajeshkannan, V. 2014. Enhancement of in vitro high-density polyethylene (HDPE) degradation by physical, chemical, and biological treatments. *Environ. Sci. Pollut. Res.*, 21: 12549-12562.
- Blackadder, D.A. and Keniry, J.S. 1972. The morphological consequences of annealing high-density polyethylene in solvents. *J. Appl. Polym. Sci.*, 16(5): 1261-1280.
- Chaudhary, A.K. and Vijayakumar, R.P. 2020. Effect of chemical treatment on biological degradation of high-density polyethylene (HDPE). *Environ. Dev. Sustain.*, 22(2): 1093-1104.
- Cornell, J.H., Kaplan, A.M. and Rogers, M.R. 1984. Biodegradability of photo oxidized polyalkylenes. *J. Appl. Polym. Sci.*, 29: 2581-2597.
- Danso, D., Chow, J. and Streit, W. R. 2019. Plastics: environmental and biotechnological perspectives on microbial degradation. *Appl. Environ. Microbiol.*, 85(19): e01095-19.
- Das, M.P. and Kumar, S. 2015. An approach to low-density polyethylene biodegradation by *Bacillus amyloliquefaciens*, 3 *Biotech.*, 5: 81-86.
- de Souza Machado, A.A., Kloas, W., Zarfl, C., Hempel, S. and Rillig, M.C. 2018. Microplastics as an emerging threat to terrestrial ecosystems. *Glob. Change Biol.*, 24(4): 1405-1416.
- Duddu, M.K., Tripura, K.L., Guntuku, G. and Divya, D.S. 2015. Biodegradation of low-density polyethylene (LDPE) by a new biosurfactant-producing thermophilic *Streptomyces coelicoflavus* NBRC 15399T. *Afr. J. Biotechnol.*, 14(4): 327-340.
- Gilan, I., Hadar, Y., and Sivan, A. 2004. Colonization, biofilm formation, and biodegradation of polyethylene by a strain of *Rhodococcus ruber*. *Appl. Microbiol. Biotechnol.*, 65 (1): 97-104.

- Hassanshahian, M., Zeynalipour, M.S. and Musa, F. H. 2014. Isolation and characterization of crude oil-degrading bacteria from the Persian Gulf (Khorramshahr provenance). *Mar. Pollut. Bull.*, 82(1-2): 39-44.
- Hopewell, J., Dvorak, R. and Kosior, E. 2009. Plastics recycling: Challenges and opportunities. *Philos. Trans. R. Soc. Lond., B, Biol. Sci.*, 364 (1526): 2115-2126.
- Kalia, A. 2015. Polyhydroxyalkanoate Production By Bacteria from Hydrocarbons Contaminated Soil Using Polycyclic Aromatic Hydrocarbons, M. Phil. Thesis, Central University of Punjab, Bathinda, India.
- Koutny, M., Lemaire, J. and Delort, A.M. 2006. Biodegradation of polyethylene films with pro-oxidant additives. *Chemosphere*, 64:1243-1252.
- Kundungal, H., Gangarapu, M., Sarangapani, S., Patchaiyappan, A. and Devipriya, S.P. 2021. Role of pretreatment and evidence for the enhanced biodegradation and mineralization of low-density polyethylene films by greater waxworm. *Environ. Technol.*, 42(5): 717-730.
- Lima, S.D., Oliveira, A.F., Golin, R., Lopes, V.C.P., Caixeta, D.S., Lima, Z.M. and Morais, E.B. 2019. Isolation and characterization of hydrocarbon-degrading bacteria from gas station leaking-contaminated groundwater in the Southern Amazon, Brazil. *Braz. J. Biol. Sci.*, 80: 354-361.
- Lin, C.C. and Anseth, K.S. 2013. The biodegradation of biodegradable polymeric biomaterials. Academic Press, Cambridge MA pp. 716-728.
- Lowry, O.H., Rosebrough, N.J., Farr, A.L. and Randall, R.J. 1951. Protein measurement with the Folin phenol reagent. *J. Biol. Chem.*, 193: 265-275.
- Montazer, Z., Habibi-Najafi, M.B., Mohebbi, M. and Oromiechi, A. 2018. Microbial degradation of UV-pretreated low-density polyethylene films by novel polyethylene-degrading bacteria isolated from plastic-dump soil. *J. Polym. Environ.*, 26(9): 3613-3625.
- North, E.J. and Halden, R.U. 2013. Plastics and environmental health: The road ahead. *Rev. Environ. Health*, 28: 1-8
- Olayan, H.B., Hami, H.S. and Owen, E.D. 1996. Photochemical and thermal crosslinking of polymers. *J. Macromol. Sci. C.*, 36: 671-719.
- Park, S.Y. and Kim, C.G. 2019. Biodegradation of micro-polyethylene particles by bacterial colonization of a mixed microbial consortium isolated from a landfill site. *Chemosphere*, 222: 527-533.
- Peng, R.T., Xia, M.L., Ru, J.K., Huo, Y.X. and Yang, Y. 2018. Microbial degradation of polyurethane plastics. *Chin. J. Biotechnol.*, 34: 1398-1409.
- Raut, S., Raut, S., Sharma, M., Srivastav, C., Adhikari, B. and Sen, S.K. 2015. Enhancing degradation of low-density polyethylene films by *Curvularia lunata* SG1 using particle swarm optimization strategy. *Indian J. Microbiol.*, 55: 258-268.
- Richards, R.B. 1946 The phase equilibria between a crystalline polymer and solvents: The effect of polymer chain length on the solubility and swelling of polythene. *Trans. Faraday Soc.*, 42:10-28.
- Sen, S.K. and Raut, S. 2015. Microbial degradation of low-density polyethylene (LDPE): A review. *J. Environ. Chem. Eng.*, 3: 462-473.
- Shahreza, H., Sepahy, A.A., Hosseini, F. and Nejad, R.K. 2019. Molecular Identification of *Pseudomonas* strains with polyethylene degradation ability from soil and cloning of alkB Gene. *Arch. Pharm. Pract.*, 10(4): 11-19.
- Soud, S.A. 2019. Biodegradation of Polyethylene LDPE plastic waste using locally isolated *Streptomyces sp.* *Int. J. Pharm. Sci. Res.*, 11(4): 1333-1339.
- Sudhakar, M., Doble, M., Murthy, P.S. and Venkatesan, R. 2008. Marine microbe-mediated biodegradation of low- and high-density polyethylenes. *Int. Biodeterior. Biodegrad.*, 61: 203-213.
- Tanase, A.M., Ionescu, R., Chiciudean, I., Vassu, T. and Stoica, I. 2013. Characterization of hydrocarbon-degrading bacterial strains isolated from oil-polluted soil. *Int. Biodeterior. Biodegrad.*, 84: 150-154.
- Tziourrou, P., Kordella, S., Ardali, Y., Papatheodorou, G. and Karapanagioti, H.K. 2021. Microplastics formation is based on the degradation characteristics of beached plastic bags. *Mar. Pollut. Bull.*, 169: 112470.
- Verma, J.P. and Jaiswal, D.K. 2016. Book review: advances in biodegradation and bioremediation of industrial waste. *Front. Microbiol.*, 6: 1555.
- Wong, S.L., Ngadi, N. and Abdullah, T.A.T. 2014. Study on the dissolution of low-density polyethylene (LDPE). *Appl. Mech. Mat.*, 695: 170-173.
- Yang, H.S., Yoon, J.S. and Kim, M.N. 2005. Dependence of biodegradability of plastics in compost on the shape of specimens. *Polym. Degrad. Stabil.*, 780(87): 131-135.



# Approaches in Bioremediation of Dioxins and Dioxin-Like Compounds – A Review on Current and Future Prospects

Priyanka Mary Sebastian and K. V. Bhaskara Rao†

Department of Biomedical Science, School of Biosciences and Technology, Vellore Institute of Technology, Vellore-632 014, Tamil Nadu, India

†Corresponding author: K. V. Bhaskara Rao; [kvbhaskararao@vit.ac.in](mailto:kvbhaskararao@vit.ac.in)

Nat. Env. & Poll. Tech.  
Website: [www.neptjournal.com](http://www.neptjournal.com)

Received: 04-02-2022

Revised: 30-03-2022

Accepted: 07-04-2022

## Key Words:

Bioremediation  
Carcinogenicity  
Microorganisms  
Nanoremediation  
Persistent organic pollutants  
Polychlorinated dioxins  
Toxicity assessment

## ABSTRACT

Waste generation is becoming increasingly prominent in the environmental arena due to the increase in population and living standards of life. Dioxin and Dioxin-related compounds are a set of hazardous chemicals that are ubiquitously distributed. Polychlorinated dioxins are introduced into our surroundings by both spontaneous and induced activities like combustion, incineration of waste, recycling of e-waste, and paper and pesticide manufacturing. They are chloroaromatic compounds that are found to be lethal and possess carcinogenic properties and are one of the primary examples of persistent environmental pollutants (POP). Removal of these compounds from the environment is very challenging due to their recalcitrant nature. An alternative technique is the use of microbial technology which includes the use of bacteria and fungi to detoxify the dioxins that are considered to be a more effective, economical, and environmentally sustainable alternative. Different microbial interactions were studied for their degradation potential. Polychlorinated dibenzo-p-dioxin and furans (PCDD/F) are found to be degraded by bacteria by adopting either aerobic or anaerobic pathways and the details regarding the diversity, distribution, bioremediation potential, metabolic pathway have been analyzed. This review provides an overview of the source of contamination, its potential toxicity assessment, and various bioremediation techniques that are employed are discussed in detail. It also highlights the nanoremediation technique - a promising tool in which nanoparticles are used in the treatment of toxic organic pollutants.

## INTRODUCTION

The environment is highly contaminated by various toxic chemicals due to several anthropogenic and industrial activities that often release organic and inorganic pollutants into the surrounding environment that accumulate as highly toxic pollutants. Any substance uncommonly present in the environment in a higher concentration than the acceptable level that is hardly subjected to biodegradation is termed xenobiotics (Mathew et al. 2017). In the present world scenario, the term dioxin is gaining much importance due to its persistent and toxic characteristics. Dioxins and Dioxin-like compounds (DLC) are chemical compounds that include PCDD/F depicted by the chlorine atom arrangement (Kulkarni et al. 2008) and polychlorinated biphenyls (PCB) that are considered to be persistent organic pollutants. These compounds are found to be highly toxic and possess carcinogenic properties. Once these toxic compounds have been generated, they can pertain to the soil, sediment, and dump yards of E-waste for the distant future. Dioxins possess the potential to sustain in the environment for a longer duration when absorbed onto clay and the organic content of the soil matrix due to its hydrophobic nature (Thi et al. 2019, Srogi 2008).

Dioxin structure consists of two benzene rings linked by an oxygen atom. For PCDD, the aromatic ring is linked by two oxygen atoms and for PCDF, the ring is connected by a carbon bond and oxygen ring. Dioxins have a high melting point and low vapor pressure (Srogi 2008a). Among various categories of dioxin congeners, only 7 out of 75 PCDD congeners, and 10 out of 135 PCDF congeners have dioxin-like toxicity. Their level of toxicity is calculated by the positioning of chlorine atoms (Kulkarni et al. 2008b). Among the dioxin derivatives, the highly toxic compound known is 2,3,7,8-tetrachlorinated dibenzo-p-dioxin (Nguyen et al. 2021) and is labeled as a human carcinogen by the International Agency for Research on Cancer (ICAR) (Srogi 2008b). These chemicals are top-ranked as one of the persistent organic pollutants (POP) often specified as the “Dirty dozen” (Weber et al. 2008). Dioxins are found to possess toxic, carcinogenic, and mutagenic properties (Saibu et al. 2020a). Polychlorinated dibenzo-furan isomers have also been reported in various media like soil, and sediment in many industrialized areas. Fig. 1 depicts the structure of PCDD and PCDF with their possible number of congeners.

## SOURCE, ORIGIN AND TOXICITY OF DIOXINS

PCDD/F are formed through various natural and human activities. Various sources of dioxin contamination are summarized in Fig. 2. Accidental events such as volcanic eruptions, forest fires, and house fires result in dioxin emissions to a limited extent (Kulkarni et al. 2008, Ruokojärvi et al. 2000). Dioxins are unintentionally released as a by-product during various anthropogenic activities which include combustion of chlorinated compounds, incineration of residues from household and production sectors (Mukherjee et al. 2016, Tuppurainen et al. 1998), bleaching of pulp and

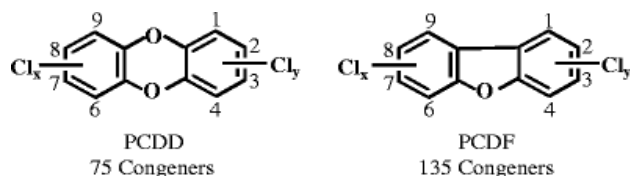


Fig.1: Chemical structure of PCDD and PCDF with their possible congeners (Bunge & Lechner 2009a).

paper mill (Rosenberg et al. 1994, Thacker et al. 2007) metallurgical process (Buekens et al. 2001, Łechtańska et al. 2017), dumping of e-waste (Dai et al. 2020). Burning of PCDD and PCDF are also produced as a micropollutant during the chlorination of Pentachlorophenol (PCP) which was initially used as a wood preservative. Agent Orange – a known herbicide containing dioxin profusely used during the Vietnam war in the 1960s remains a significant environmental threat and greatly affects human beings (Thi et al. 2019). In the Luoi Valley of Vietnam, soil, animal tissue, and human blood were found to contain increased levels of the most toxic dioxin molecule, 2,3,7,8-tetrachlorodibenzo-p-dioxin (TCDD) (Dwernychuk et al. 2002, Thi et al. 2019). Toxic equivalence quantities (TEQs) are used to express the toxicity of dioxin where TCDD is rated as 1 and the fraction of this for other less toxic congeners (Kulkarni et al. 2008d). The concentration of Dioxin-like compounds (DLC) in the environment is determined by the Dioxin toxicity equivalence.

## HEALTH HAZARDS DUE TO DIOXIN-POLLUTED ENVIRONMENT



Fig. 2: Major sources of dioxins in the environment.



Dioxin being inadequately incinerated is released into the soil and aquatic sediment bioaccumulates in the fatty tissues of animals. Humans are exposed to dioxin mainly through food, accounting for more than 90% of dioxin exposure. The lipophilic nature of dioxin is high in the fat of animals and fishes and that results in the presence of dioxin in food and dairy products (Rathoure 2018). Exposure to TCDD is reported to cause epigenetic modification and relative toxicity. Similarly, the experimental data conducted in cell line and animal studies has resulted in a decreased male/female ratio in offspring (Viluksela & Pohjanvirta 2019). The et al. (2020), studied and proved that the perinatal exposure to dioxin subsequently affected the learning ability of children particularly boys. It has also been reported that exposure to dioxin has a detrimental effect on human health which includes simple skin lesions to altered hepatic function, as well as the immune, nervous, and endocrine systems functioning adversely. Dioxin can percolate the blood-brain barrier and attack the nerve cells directly exerting a toxic effect on the central nervous system (Miyazaki et al. 2016).

### IMPORTANCE OF BIOREMEDIATION FOR DIOXIN-CONTAMINATED SOIL

Removal of highly recalcitrant dioxin and dioxin-like compounds from the environment is much demanding. Their persistent nature has become a major global concern. Therefore, remediation of such highly contaminated areas is required. Diverse methods and technologies have been devised and adapted which can be categorized into three broad groups: Physical, chemical, and biological treatments (Binh et al. 2016). Physical and chemical treatments include incineration and thermal desorption method, photolysis, radiolytic treatment using gamma rays, alkaline dehydrochlorination, Fenton treatment, and usage of different oxidants and reductants (Haglund 2007, Hrabák et al. 2016). Although incineration has been an inexpensive technique for maximum destruction of dioxin when compared to other physico-chemical techniques, treating a massive amount of contaminated soils and sediment has its own disadvantages. This paved a way for a biological alternative (Wittich 1998). Biological treatment which includes biodegradation of dioxin-contaminated soil using microbial diversity which is capable of degrading dioxin is given more importance, especially from the ecological and economical point of view (Binh et al. 2016). It is one of the promising alternatives to clean up dioxin-contaminated soil due to its low-cost performance when compared to others. The microbiological approach involves a sustainable and cost-effective treatment for the PCDD/F contaminated soil (Chen et al. 2013). Nam et al. (2008) evaluated the removal of PCDD/F from the fly ash, a

major source of dioxin contamination using a biocatalyst that contains bacterial and fungal consortia capable of degrading dioxins. The above treatment resulted in 68.7% removal of PCDD/F in 21 days.

### MECHANISM AND APPROACHES OF MICROBIAL REMEDIATION OF DIOXINS

Biodegradation utilizes microorganisms to break down the potentially hazardous chemical substances into less/ non-toxic smaller compounds using its metabolic or enzymatic mechanism. The extent of biodegradability greatly relies on the toxicity, the concentration of the contaminants, the type of microorganism involved, and the properties of the contaminated soil. The concentration of the contaminants can be reduced by both aerobic and anaerobic mechanisms. (Kao et al. 2004). The key difference between them is that the aerobic degradation takes place in lower chlorinated congeners while the anaerobic pathway takes place in highly chlorinated congeners (Kulkarni et al. 2008e). The microbial consortium and fungal remediation are also found to be useful in degrading chlorinated DD/F (Chen et al. 2013, Dao et al. 2021). The products of the catabolic reaction should be further mineralized because incomplete degradation of such compounds can result in more toxic metabolites than the primary substrate (Kao et al. 2004).

#### Aerobic Biodegradation of Dioxins

In aerobic conditions, the microorganism involved in degrading the dioxins undergoes an oxidative degradation pathway. The two main pathways in oxidative degradation are lateral and angular dioxygenation. The initial is the addition of two hydroxyl groups into the ring structure using the enzyme dioxygenase; the resultant is transformed into cis-hydrodiols. Both angular and lateral deoxygenation systems are found in species of different phylogenetic groups (Nojiri & Omori 2002, Saibu et al. 2020b)

Bacterial strains possessing the ability to degrade DD and DF were isolated and characterized (Habe et al. 2001). *Sphingomonas wittichii* strain RW1 was the extensively researched organism that can degrade dioxin based on metabolic processes. The organism isolated from the enriched culture was inoculated with the water sample obtained from the Elbe river. The organism underwent angular dehydroxylation and the catechol thus obtained was found to be cleaved by *Sphingomonas wittichii* strain RW1 (Wittich et al. 1992). Saibu et al. (2020a) isolated dioxin degrading bacterial strains from polluted soil. Among 17 strains isolated, two strains displaying better metabolic competencies were selected and the organisms were identified as *Bacillus* sp. SS2 and *Serratia* sp. SSA 1 and the percentage of removal of dibenzofuran

were found to be 93.87% for SS2 and 2,8 – dichlorodibenzo-furans and 2,7 – dichlorodibenzo-p-dioxin it was 86.22% and 82.30% respectively. Other bacterial strains that are found to be capable of DD/DF biodegradation and their congeners belong to *Rhodococcus* and *Terrabacter* (Iida et al. 2002), *Geobacillus* sp. UZO 3 (Suzuki et al. 2016), *Burkholderia cenocepacia* strain 869T2 (Nguyen et al. 2021), and *Pseudomonas mendocina* NSYSU (Lin et al. 2017). Quensen & Matsumura (1983) studied the oxidative degradation of 2,3,7,8 TCDD by *B. megaterium* and *Norcardiopsis* sp. They concluded that the solvent used greatly influences the degree of metabolism. *Janibacter terrae* strain XJ-1 isolated from sediment degraded dibenzofuran aerobically by using them as a sole source of carbon and energy and produced gentisic acid as final products with several metabolites as intermediates (Jin et al. 2006).

### Anaerobic Biodegradation of Dioxins

One of the most favorable techniques for detoxification of highly chlorinated dioxin is reductive dechlorination. Highly chlorinated congeners are difficult to be degraded by aerobic pathways. Such compounds can be successfully degraded by an anaerobic mechanism. The reductive dechlorination process removes the chlorine from the aromatic ring anaerobically. Microorganism uses different molecular strategies to cleave the carbon-halogen bond. In the absence of oxygen, the microbial communities metabolize the organic compound using alternate electron acceptors (dehalorespiration). The absence of the electron acceptor has a direct impact on the degradation of the organic compounds (Bossert et al. 2005). Microbial dehalogenation of the various organic compounds has been observed in organisms from anoxic estuarine and

marine sources (Rodenburg et al. 2017, Vargas et al. 2001). The corresponding fully dechlorinated or partially dechlorinated product is more susceptible to further degradation by both aerobic and anaerobic techniques. Bacteria related to the genus *Dehalococcoides* were found to undergo reductive dechlorination of highly chlorinated dioxins to a much lower chlorinated compound (Bunge & Lechner 2009b). In another study, a microcosm was built to analyze the dechlorination mechanism of sediments contaminated with PCDD/F taken from the historically contaminated site of the Kymijoki River. It was spiked with 1,2,3,4-Tetrachloro dibenzofuran and the result showed that the sediment contained indigenous microorganisms capable of dechlorinating the dioxin (Kuokka et al. 2014).

### Mycoremediation of Dioxins

Degradation of dioxin is found to be carried out by various ligninolytic fungi isolated from soil (Dao et al., 2019). The organisms that are capable of degrading the most complex polymer, lignin, using an extracellular enzyme which includes lignin peroxidase and manganese peroxidase, have the potential to degrade most recalcitrant compounds including polychlorinated dioxins (Field et al. 1993). Furthermore, the fungus has the ability to absorb and biotransform hazardous contaminants. Biodegradation of dioxin by microorganisms was first reported by white-rot fungi *Phanerochaete sortida* YK-624 (Kanan & Samara 2018). Bumpus et al. (1985) evaluated the biodegradation potential of *P. chrysosporium* in degrading the 2,3,7,8-TCDD. Takada et al. (1996) reported that *P. sortida* could degrade highly chlorinated dioxins and furans. Table 1. gives the details of various fungi and their biodegradation ability of various dioxin congeners.

Table 1: Dioxin degrading fungi with their degradation potential of various congeners.

Organism	Compound degraded	Duration	Percentage of degradation	Reference
<i>Rigidoporus</i> sp. FMD21	2,3,7,8- Tetrachlorodibenzo-p-dioxin	50 days	79.9%	(Dao et al. 2021)
<i>Phanerochaete chrysosporium</i> OGC101	2,7- Dichlorodibenzo-p-dioxin	27 days	50 %	(Valli et al. 1992)
<i>P. velutina</i> , <i>Stropharia rugosoannulata</i> , <i>Gymnopilus luteofolius</i>	Polychlorinated dibenzo-p-dioxin/Furan	77 days	67%	(Anasonye et al. 2014)
		70 days	61%	
			69%	
<i>Phlebia brevispora</i>	1,3,6,8- Tetrachlorodibenzo-p-dioxin	90 days	50%	(Kamei et al. 2009)
<i>P. sordida</i> YK-624	Polychlorinated dibenzo-p-dioxin/Furan	14 days	76% 70%	(Takada et al. 1996b)
<i>Pleurotus pulmonarius</i>	Polychlorinated dibenzo-p-dioxin/Furan	72 days	96%	(Kaewlaoyong et al. 2020)
<i>Panellus styticus</i>	2,7- Dichlorodibenzo-p-dioxin	40 days	100 %	(Sato et al. 2002)

### Dioxin Removal by Composting Microorganisms

Compost-mediated bioremediation is a biological process based on combining the feedstock with contaminated soil, where the compost matures, which ultimately results in the degradation of the pollutant (Semple et al. 2001). Co-composting is regarded as one of the efficient methods for the degradation of the recalcitrant compounds into less toxic compounds with the aid of microorganisms (Covino et al. 2016, Mattei et al. 2016). The potential composting relies on various factors like microbial metabolism, moisture content, temperature, pH, nutrients, and the density of bulking agent (Semple et al. 2001). Lin et al. (2018) studied the degradation of dioxin-contaminated soil by a co-composting technique using food waste. The results showed that 70% of PCDD/F was successfully degraded in 49 days with initial TEQ 6048 ng-TEQ/kg was reduced to 1604 ng-TEQ/kg. The author concluded that thermophilic degradation can be used to degrade dioxin. Huang et al. (2019) examined the organisms involved in co-composting and found that after 42 days of composting the degradation was around 75% and the toxic equivalent quantity (TEQ) was reduced from 16.004 ng-TEQ kg<sup>-1</sup> to 1916 ng-TEQ kg<sup>-1</sup> day<sup>-1</sup>. Beesley et al., (2010) state that the use of compost enhances the efficiency of degrading the PAH-contaminated soil by 25%, and their phytotoxicity test ensures that the amendment has increased the shoot length. Narihiro et al. (2010) used a developed fermentor which yielded a 15 – 16% reduction during remediation. Molecular studies revealed three major phylogenetic groups including *Acidaminobacter*, *Dehalococcoides*, and *Rhizobium* were present. Tran et al. (2020) suggested that the biodegradation of dioxin-contaminated sites can be carried out using bacteria obtained from aerobic composting with the removal efficiency of 81% in 35 days. The 16s RNA sequencing indicated that the organism belongs to *Bacilli*, *Actinobacteria*, *Clostridia*, *Gammaproteobacteria*, and *Alphaproteobacteria*. It provides an easy and safe method for remediation of dioxin-contaminated soil.

### DEGRADATION OF DIOXINS IN MICROCOSMS

A microcosm is a miniaturized ecosystem model representing a portion of the natural environment under controlled laboratory conditions, therefore, representing microbial diversity (Cravo-Laureau & Duran 2014, Grenni et al. 2012). Microcosm experiment provides some advantages namely i) simple, cost-effective ii) maintaining replicates easily and manipulating the growth condition for maximum degradation results iii) identifying microbial community present in the natural environment inheriting the ability to degrade the pollutant (Salam et al. 2015). Chen et al. (2013) conducted

an experiment in the PCDD/F contaminated soil to detect the bioremediation potential of various microorganisms by constructing a microcosm. Microbial activity was stimulated in a closed microcosm by adding oxygen and additional nutrients. Nearly 100% and 95-98% reduction was observed in Octachlorodibenzofurans (OCDF) and Heptachlorodibenzofurans (H<sub>p</sub>CDF) respectively after six weeks and no significant reduction in Octachlorodibenzo-p-dioxin (OCDD) within 12 weeks. In the second batch microcosm, the bacterial consortium from the first batch was added to the fresh medium with 50 mg OCDF powder and the degradation efficiency for OCDF was 82.1% and 87.9% for OCDD demonstrating the microbial community present in the microcosm enhanced the degradation of highly chlorinated PCDD/F.

In an experiment conducted by Lin et al. (2017) the biodegradation potential of a novel strain, *Pseudomonas mendocina* NSYSU in OCDF polluted soil was studied through a microcosm under anaerobic conditions. A batch of seven different microcosms was set up. Upon incubation of 64 days, it was observed that 59% of OCDF was degraded in a batch containing the *P. mendocina* NSYSU and sterile soil, a 23% reduction was observed in the batch containing *P. mendocina* NSYSU and unsterile soil, and no reduction was observed in control batch.

### NANOREMEDIATION OF DIOXINS

The concept of accelerating the removal of hazardous environmental contaminants (organic or inorganic pollutants) using a cost-effective treatment process led to the development of nanobioremediation (Cecchin et al. 2017). Nanobioremediation uses a combined effort of nanoremediation with microorganism-mediated biological treatment to clean up the recalcitrant environmental pollutants. In recent times, the use of nanoparticles is gaining greater importance in different fields of research due to their unique physicochemical properties which include a large surface area, the surface modification which ultimately results in increased reactivity, and better remediation performance (Chauhan et al., 2020, Guerra et al. 2018). Zero-valent(ZVI) iron is a widely used nanomaterial to treat sites contaminated with hazardous compounds (Galdames et al. 2020). Kim et al. (2008) evaluated the ZVI potential of nanoparticles in PCDD degradation. The results obtained show that the palladized ZVI shows three times increased dechlorination potential when compared to unpalladized ZVI. Binh et al. (2016) studied the 2,3,7,8- TCDD biodegradation using sequentially enriched microorganisms obtained from dioxin-contaminated soil with Carboxymethylcellulose (CMC) coated NZVI in a sequential anaerobic degradation followed by aerobic treatment. The results showed 58% degradation of the toxic compound.

## CONCLUSION AND FUTURE PROSPECTIVES

The past century has witnessed an uncontrolled growth of industries and rapid urbanization that resulted in the massive contamination of the environment and one among them are dioxins. Their persistence is a global threat and immediate measures are to be taken to reduce their level in the environment. Their structural complexity makes them resistant to degradation. The environment is a niche containing a richness of species which is a reservoir of thousands of diverse microorganisms having various potentials including degradation of hazardous environmental pollutants. The current status of the bioremediation of dioxin shows promising results for biodegradation and detoxification of highly chlorinated dioxins. This review provides an opportunity to study microorganism and their mechanism involved in degrading the pollutant. Different techniques in bioremediation are also discussed in detail. The uncovered part of the study is the isolation of microorganisms from extremes of the environment and conduct of transcriptome, metagenomics, and proteomics studies, and the use of engineered organisms for carrying dioxin metabolizing enzymes for better efficiency of remediation. Further research has to be extended by involving molecular techniques to find a wide range of microorganism that possesses the potential to reduce high levels of dioxin in the soil. The Nanobioremediation technique is an emerging versatile technique that possesses the potential in treating the most toxic environmental pollutant. The use of nanomaterials along with the microorganism has proven to show high efficiency in degrading hazardous pollutants. Therefore, the advancement in the use of nanobioremediation would also promising technique for remediation of environmental challenges.

## REFERENCES

- Anasonye, F., Winquist, E., Kluczek-Turpeinen, B., Räsänen, M., Salonen, K., Steffen, K.T., and Tuomela, M. 2014. Fungal enzyme production and biodegradation of polychlorinated dibenzo-p-dioxins and dibenzofurans in contaminated sawmill soil. *Chemosphere*, 110: 85-90.
- Binh, N.D., Imsapsangworn, C., Kim Oanh, N.T., Parkpian, P., Karstensen, K., Giao, P.H. and DeLaune, R.D. 2016. Sequential anaerobic-aerobic biodegradation of 2, 3, 7, 8-TCDD contaminated soil in the presence of CMC-coated nZVI and surfactant. *Environ. Technol.*, 37(3): 388-398.
- Bossert, I.D., Häggblom, M.M. and Young, L.Y. 2004. Microbial ecology of dehalogenation. In Häggblom, M.M. and Bossert, I.D. (eds), *Dehalogenation*, Springer, Boston, MA, pp. 33-52.
- Buekens, A., Stieglitz, L., Hell, K., Huang, H. and Segers, P. 2001. Dioxins from thermal and metallurgical processes: recent studies for the iron and steel industry. *Chemosphere*, 42(5-7): 729-735.
- Bumpus, J.A., Tien, M., Wright, D. and Aust, S.D. 1985. Oxidation of persistent environmental pollutants by a white rot fungus. *Sci.*, 228(4706): 1434-1436.
- Bunge, M. and Lechner, U. 2009. Anaerobic reductive dehalogenation of polychlorinated dioxins. *Appl. Microbiol. Biotechnol.*, 84(3): 429-444.
- Cecchin, I., Reddy, K.R., Thomé, A., Tessaro, E.F. and Schnaid, F. 2017. Nanobioremediation: Integration of nanoparticles and bioremediation for sustainable remediation of chlorinated organic contaminants in soils. *Int. Biodeter. Biodegr.*, 119: 419-428.
- Chauhan, R., Yadav, H. O. and Sehrawat, N. 2020. Nanobioremediation: A new and a versatile tool for sustainable environmental clean up-Overview. *J. Mater. Environ. Sci.*, 11(4): 564-573.
- Chen, W.Y., Wu, J.H., Lin, Y.Y., Huang, H.J. and Chang, J.E. 2013. Bioremediation potential of soil contaminated with highly substituted polychlorinated dibenzo-p-dioxins and dibenzofurans: Microcosm study and microbial community analysis. *J. Hazard. Mater.*, 261: 351-361.
- Covino, S., Fabianová, T., Křesinová, Z., Čvančarová, M., Burianová, E., Filipová, A. and Cajthaml, T. 2016. Polycyclic aromatic hydrocarbons degradation and microbial community shifts during co-composting of creosote-treated wood. *J. Hazard. Mater.*, 301: 17-26.
- Cravo-Laureau, C. and Duran, R. 2014. Marine coastal sediments microbial hydrocarbon degradation processes: Contribution of experimental ecology in the omics' era. *Front. Microbiol.*, 5: 39.
- Dai, Q., Xu, X., Eskenazi, B., Asante, K.A., Chen, A., Fobil, J. and Huo, X. 2020. Severe dioxin-like compound (DLC) contamination in e-waste recycling areas: An under-recognized threat to local health. *Environ. Int.*, 139: 105731.
- Dao, A. T., Loenen, S. J., Swart, K., Dang, H. T., Brouwer, A. and de Boer, T. E. 2021. Characterization of 2, 3, 7, 8-tetrachlorodibenzo-p-dioxin biodegradation by extracellular lignin-modifying enzymes from ligninolytic fungus. *Chemosphere*, 263, 128280.
- Dao, A.T., Vonck, J., Janssens, T.K., Dang, H.T., Brouwer, A. and de Boer, T.E. 2019. Screening white-rot fungi for bioremediation potential of 2, 3, 7, 8-tetrachlorodibenzo-p-dioxin. *Ind. Crops Prod.*, 128: 153-161.
- Dwernychuk, L.W., Cau, H.D., Hatfield, C.T., Boivin, T.G., Hung, T.M., Dung, P.T. and Thai, N.D. 2002. Dioxin reservoirs in southern Viet Nam: A legacy of Agent Orange. *Chemosphere*, 47(2): 117-137.
- Field, J.A., de Jong, E., Feijoo-Costa, G. and de Bont, J.A. 1993. Screening for ligninolytic fungi applicable to the biodegradation of xenobiotics. *Trends Biotechnol.*, 11(2): 44-49.
- Galdames, A., Ruiz-Rubio, L., Orueta, M., Sánchez-Arzalluz, M. and Vilas-Vilela, J.L. 2020. Zero-valent iron nanoparticles for soil and ground-water remediation. *Int. J. Environ. Res. Public Health*, 17(16): 5817.
- Grenni, P., Falconi, F. and Caracciolo, A. B. 2012. Microcosm experiments for evaluating natural bioremediation of contaminated ecosystems. *Chemical Engineering*, 28(7), e12.
- Guerra, F.D., Attia, M.F., Whitehead, D.C. and Alexis, F. 2018. Nanotechnology for environmental remediation: materials and applications. *Molecules*, 23(7): 1760.
- Habe, H., Chung, J.S., Lee, J.H., Kasuga, K., Yoshida, T., Nojiri, H. and Omori, T. 2001. Degradation of chlorinated dibenzofurans and dibenzo-p-dioxins by two types of bacteria having angular dioxygenases with different features. *Appl. Environ. Microbiol.*, 67(8): 3610-3617.
- Haglund, P. 2007. Methods for treating soils contaminated with polychlorinated dibenzo-p-dioxins, dibenzofurans, and other polychlorinated aromatic compounds. *AMBIO: J. Hum. Environ.*, 36(6): 467-474.
- Iida, T., Mukouzaka, Y., Nakamura, K., Yamaguchi, I. and Kudo, T. 2002. Isolation and characterization of dibenzofuran-degrading actinomycetes: analysis of multiple extradiol dioxygenase genes in dibenzofuran-degrading *Rhodococcus* species. *Biosci. Biotechnol. Biochem.*, 66(7): 1462-1472.
- Jin, S., Zhu, T., Xu, X. and Xu, Y. 2006. Biodegradation of dibenzofuran by *Janibacter terrae* strain XJ-1. *Curr. Microbiol.*, 53(1): 30-36.
- Kaewlaoyong, A., Cheng, C.Y., Lin, C., Chen, J.R., Huang, W.Y. and Sriprom, P. 2020. White rot fungus *Pleurotus pulmonarius* enhanced bioremediation of highly PCDD/F-contaminated field soil via solid state fermentation. *Sci. Tot. Environ.*, 738: 139670.
- Kamei, I., Watanabe, M., Harada, K., Miyahara, T., Suzuki, S., Matsufuji, Y. and Kondo, R. 2009. Influence of soil properties on the biodegrada-



- tion of 1, 3, 6, 8-tetrachlorodibenzo-p-dioxin and fungal treatment of contaminated paddy soil by white rot fungus *Phlebia brevispora*. *Chemosphere*, 75(10): 1294-1300.
- Kanan, S. and Samara, F. 2018. Dioxins and furans: A review from chemical and environmental perspectives. *Trends Environ. Anal. Chem.*, 17: 1-13.
- Kao, C.M., Chai, C.T., Liu, J.K., Yeh, T.Y., Chen, K.F. and Chen, S.C. 2004. Evaluation of natural and enhanced PCP biodegradation at a former pesticide manufacturing plant. *Water Res.*, 38(3): 663-672.
- Kim, J. H., Tratnyek, P.G. and Chang, Y.S. 2008. Rapid dechlorination of polychlorinated dibenzo-p-dioxins by bimetallic and nanosized zerovalent iron. *Environ. Sci. Technol.*, 42(11): 4106-4112.
- Kulkarni, P.S., Crespo, J.G. and Afonso, C.A. 2008. Dioxins sources and current remediation technologies: A Review. *Environ. Int.*, 34(1): 139-153.
- Kuokka, S., Rantalainen, A.L. and Hågglom, M.M. 2014. Anaerobic reductive dechlorination of 1, 2, 3, 4-tetrachlorodibenzofuran in polychlorinated dibenzo-p-dioxin-and dibenzofuran-contaminated sediments of the Kymijoki River, Finland. *Chemosphere*, 98: 58-65.
- Łechtańska, P., Wielgosiński, G., Grochowalski, A., Holtzer, M. and Ćwiągalski, W. 2017. Dioxin emission from some metallurgical processes. *Int. J. Environ. Pollut.*, 61(3-4): 261-277.
- Lin, C., Kaewlaoyong, A., Vu, C.T. and Huang, W.Y. 2017. Treatment of dioxin-contaminated soil by organic waste co-composting system. In *International Conference on Physics and Mechanics of New Materials and Their Applications*, 26 March 2017, Kitakyushi, Japan, Springer, Cham, pp. 619-623.
- Lin, J.L., Chen, S.C., Sung, W.P., Chen, T.Y., Surampalli, R.Y. and Kao, C.M. 2016. Bioremediation of OCDF-contaminated soils by novel bacterial strain. *Appl. Ecol. Env. Res.*, 15: 713-723.
- Mathew, B.B., Singh, H., Biju, V.G. and Krishnamurthy, N.B. 2017. Classification, source, and effect of environmental pollutants and their biodegradation. *J. Environ. Pathol. Toxicol. Oncol.*, 36(1): 55-71.
- Mattei, P., Cincinelli, A., Martellini, T., Natalini, R., Pascale, E. and Renella, G. 2016. Reclamation of river dredged sediments polluted by PAHs by co-composting with green waste. *Sci. Tot. Environ.*, 566: 567-574.
- Miyazaki, W., Fujiwara, Y. and Katoh, T. 2016. The effects of 2, 3, 7, 8-tetrachlorodibenzo-p-dioxin on the development and function of the blood-brain barrier. *Neurotoxicology*, 52: 64-71.
- Mukherjee, A., Debnath, B. and Ghosh, S.K. 2016. A review on technologies of removal of dioxins and furans from incinerator flue gas. *Procedia Environ. Sci.*, 35: 528-540.
- Nguyen, B.A.T., Hsieh, J.L., Lo, S.C., Wang, S.Y., Hung, C.H., Huang, E. and Huang, C.C. 2021. Biodegradation of dioxins by *Burkholderia cenocepacia* strain 869T2: Role of 2-haloacid dehalogenase. *J. Hazard. Mater.*, 401: 123347.
- Nojiri, H. and Omori, T. 2002. Molecular bases of aerobic bacterial degradation of dioxins: involvement of angular dioxygenation. *Biosci. Biotechnol. Biochem.*, 66(10): 2001-2016.
- Quensen, J.F. and Matsumura, F. 1983. Oxidative degradation of 2, 3, 7, 8-tetrachlorodibenzo-p-dioxin by microorganisms. *Environ. Toxicol. Chem. Int. J.*, 2(3): 261-268.
- Rathoure, A.K. 2018. Dioxins source origin and toxicity assessment. *Biodivers. Int. J.*, 2: 310-314.
- Rodenburg, L.A., Dewani, Y., Hågglom, M.M., Kerkhof, L.J. and Fennell, D.E. 2017. Forensic analysis of polychlorinated dibenzo-p-dioxin and furan fingerprints to elucidate dechlorination pathways. *Environ. Sci. Technol.*, 51(18): 10485-10493.
- Rosenberg, C., Kotsas, H., Jäppinen, P., Tornaues, J., Hesso, A. and Vainio, H. 1994. Airborne chlorinated dioxins and furans in a pulp and paper mill. *Chemosphere*, 29(9-11): 1971-1978.
- Ruokojärvi, P., Aatamila, M. and Ruuskanen, J. 2000. Toxic chlorinated and polyaromatic hydrocarbons in simulated house fires. *Chemosphere*, 41(6): 825-828.
- Saibu, S., Adebuseye, S.A. and Oyetibo, G.O. 2020a. Aerobic bacterial transformation and biodegradation of dioxins: a review. *Bioresour. Bioprocess.*, 7(1): 1-21.
- Saibu, S., Adebuseye, S.A., Oyetibo, G.O. and Rodrigues, D.F. 2020. Aerobic degradation of dichlorinated dibenzo-p-dioxin and dichlorinated dibenzofuran by bacteria strains obtained from tropical contaminated soil. *Biodegradation*, 31(1): 123-137.
- Salam, L.B., Ilori, M.O. and Amund, O.O. 2015. Carbazole degradation in the soil microcosm by tropical bacterial strains. *Brazil. J. Microbiol.*, 46(4): 1037-1044.
- Sato, A., Watanabe, T., Watanabe, Y., Harazono, K. and Fukatsu, T. 2002. Screening for basidiomycetous fungi capable of degrading 2, 7-dichlorodibenzo-p-dioxin. *FEMS Microbiol. Lett.*, 213(2): 213-217.
- Semple, K. T., Reid, B. J. and Fermor, T. R. 2001. Impact of composting strategies on the treatment of soils contaminated with organic pollutants. *Environmental pollution*, 112(2), 269-283.
- Srogi, K. 2008. Levels and congener distributions of PCDDs, PCDFs and dioxin-like PCBs in environmental and human samples: A review. *Environ. Chem. Lett.*, 6(1): 1-28.
- Suzuki, Y.M., Nakamura, Y., Otsuka, Y., Suzuki, N., Ohyama, K., Kawakami, T. and Katayama, Y. 2016. 2, 3, 7, 8-tetrachlorodibenzo-p-dioxin (TCDD) degradation by the thermophilic *Geobacillus* sp. UZO 3. *J Environ. Biotechnol.*, 2: 105-108.
- Takada, S., Nakamura, M., Matsueda, T., Kondo, R. and Sakai, K. 1996. Degradation of polychlorinated dibenzo-p-dioxins and polychlorinated dibenzofurans by the white rot fungus *Phanerochaete sordida* YK-624. *Appl. Environ. Microbiol.*, 62(12): 4323-4328.
- Thacker, N.P., Nitnaware, V.C., Das, S.K. and Devotta, S. 2007. Dioxin formation in pulp and paper mills of India. *Environ. Sci. Pollut. Res. Int.*, 14(4), 225-226.
- The, T.P., Ngoc, T.P., Van, T.H., Nishijo, M., Ngoc, N. T., Thi, H. V. and Nishijo, H. 2020. Effects of perinatal dioxin exposure on learning abilities of 8-year-old children in Vietnam. *Int. J. Hyg. Environ. Health*, 223(1), 132-141.
- Thi, T.V.N., Shintani, M., Moriuchi, R., Dohra, H., Loc, N.H. and Kimbara, K. 2019. Isolation and characterization of a moderate thermophilic *Paenibacillus naphthalenovorans* strain 4B1 capable of degrading dibenzofuran from dioxin-contaminated soil in Vietnam. *J. Biosci. Bioeng.*, 128(5): 571-577.
- Tran, H. T., Lin, C., Hoang, H. G., Nguyen, M. T., Kaewlaoyong, A., Cheruiyot, N. K. and Vu, C. T. 2020. Biodegradation of dioxin-contaminated soil via composting: Identification and phylogenetic relationship of bacterial communities. *Environ. Technol. Innov.* 19: 101023.
- Tuppurainen, K., Halonen, I., Ruokojärvi, P., Tarhanen, J. and Ruuskanen, J. 1998. Formation of PCDDs and PCDFs in municipal waste incineration and its inhibition mechanisms: A review. *Chemosphere*, 36(7): 1493-1511.
- Valli, K.H. Wariishi, H.I. and Gold, M.H. 1992. Degradation of 2, 7-dichlorodibenzo-p-dioxin by the lignin-degrading basidiomycete *Phanerochaete chrysosporium*. *J. Bacteriol.*, 174(7): 2131-2137.
- Vargas, C., Fennell, D. and Hågglom, M. 2001. Anaerobic reductive dechlorination of chlorinated dioxins in estuarine sediments. *Appl. Microbiol. Biotechnol.*, 57(5): 786-790.
- Viluksela, M. and Pohjanvirta, R. 2019. Multigenerational and transgenerational effects of dioxins. *Int. J. Mol. Sci.*, 20(12): 2947.
- Weber, S., Tysklind, M. and Gaus, C. 2008. Dioxin-contemporary and future challenges of historical legacies. *Environ. Sci. Pollut. Res. Int.*, 15(2): 96.
- Wittich, R.M. 1998. Degradation of dioxin-like compounds by microorganisms. *Appl. Microbiol. Biotechnol.*, 49(5): 489-499.
- Wittich, R.M., Wilkes, H.E., Sinnwell, V., Francke, W. and Fortnagel, P. 1992. Metabolism of dibenzo-p-dioxin by *Sphingomonas* sp. strain RW1. *Appl. Environ. Microbiol.*, 58(3): 1005-1010.







# Effects of Cadmium on Superoxide Dismutase Activity in Reed Leaves

Haifu Li\*, Chengjiu Guo\*, Fangli Su\* and Lifeng Li\*\*(\*\*\*)<sup>†</sup>

\*College of Water Conservancy, Shenyang Agricultural University/Liaoning Provincial Key Laboratory of Soil Erosion and Ecological Restoration, Shenyang, Liaoning, 110866, China

\*\*College of Science, Shenyang Agricultural University, Shenyang, Liaoning, 110866, China

\*\*\*Liaoning Panjin Wetland Ecosystem National Observation and Research Station, Panjin, Liaoning, 124112, China

<sup>†</sup>Corresponding author: Lifeng Li; syaulhf@syau.edu.cn

## Nat. Env. & Poll. Tech.

Website: [www.neptjournal.com](http://www.neptjournal.com)

Received: 15-08-2021

Revised: 21-10-2021

Accepted: 28-10-2021

### Key Words:

Cadmium, Superoxide dismutase activity, Reed leaves, Reactive oxygen species, Antioxidant enzymes

## ABSTRACT

Industrial polluted water has become an important water source for irrigation in the majority of constructed wetlands or even natural wetlands in China. The shortage of clean water resources has raised concerns about the potential accumulation of heavy metals, such as cadmium. Plants stressed by high levels of cadmium can increase the activity of superoxide dismutase. We have identified a positive correlation between the superoxide dismutase activity and the cadmium content of reed leaves in the wetland. Regression analysis confirmed that the superoxide dismutase activities fit a logistic curve. The logistic model was then applied to describe the superoxide dismutase activity, estimating parameters under different levels of cadmium stress. According to the findings, higher cadmium concentrations would cause the superoxide dismutase activity to increase at a higher intrinsic rate, have a lower environmental capacity  $k$ , and have lower inflection points. The dynamic model predicted an acceptable cadmium concentration of less than  $3\text{mg}\cdot\text{kg}^{-1}$ . At this concentration, reeds could develop and grow satisfactorily in the presence of cadmium. Therefore, the concentration of cadmium in the irrigated water of polluted water in mine sites, papermaking wastewater, or other industrial wastewater should be less than or equal to  $3\text{mg}\cdot\text{kg}^{-1}$  to ensure the normal growth of reeds in related wetlands.

## INTRODUCTION

The rapid development of industry and agriculture has led to a shortage of water resources for irrigation, especially because agricultural practices account for 70% of the total water withdrawn from freshwater resources (Koehler 2008, Xu et al. 2020). Using wastewater for irrigation can thus help in minimizing freshwater use for agriculture. Irrigation with treated wastewater improved plant growth, reduced mold infection rate, and increased the productivity of poor soils (AlMomány et al. 2019). Consequently, treated industrial wastewater has been increasingly used to irrigate wetlands. However, the remaining contaminants present in wastewater can threaten the growth of wetland plants as well as the environment (Qadir et al. 2007). Such heavy metals in polluted water are not prone to microbial or chemical degradation, which may not only lead to the accumulation of metals in soil but also may result in excessive uptake of the contaminants by plants (Dhiman et al. 2020, Khan et al. 2015). Plants uptake metals via roots and transport them into various plant tissues, where their presence triggers physiological, as well as genetic changes (Ahmad et al. 2016).

Superoxide dismutase (SOD) and peroxidases are antioxidant enzymes that protect cells against the damaging effects

of reactive oxygen species. Antioxidant enzymes mainly include superoxide dismutase (SOD), superoxide dismutase (POD), catalase (CAT), ascorbate peroxidase (APX), etc. The SOD is responsible for the disproportionation of excessive production of  $\text{H}_2\text{O}_2$ , and  $\text{O}_2$ . The POD, CAT, and APX are then responsible for decomposing  $\text{H}_2\text{O}_2$  into  $\text{H}_2\text{O}$  and  $\text{O}_2$  (Bowler et al. 1992, Elster 1982). It shows that SOD activity is the first response indicator of plant resistance to stress compared with other antioxidant enzymes, which can indicate the feedback of plants to environmental stress. The environmental factors that influence SOD activities in plants include season changes, illumination, and moisture content. One of the promptest effects, when plant cells are exposed to toxic concentrations of heavy metals, is the production of reactive oxygen species (ROS), the generation of  $\text{O}^{2-}$  leads to the formation of  $\text{H}_2\text{O}_2$  via the action of SOD and in the cell wall class III peroxidases catalyze the oxidation of various substrates (via the peroxidative cycle), which results in cell wall cross-linking and growth arrest (Passardi et al. 2004).

Heavy metal cadmium (Cd) influences antioxidant activity in plants mainly by the production of high levels of reactive oxygen (Assche and Clijsters, 1990). This effect varies with factors such as concentration, duration of

exposure, and plant size (Sun et al. 2009). High levels of Cd increase the activities of SODs and peroxidases, which are thought to serve an antiperoxidative function in reeds (Wang et al. 2002). SOD activity under Cd stress is also influenced by the stage of growth in reeds. An increase in Cd<sup>2+</sup> concentration from 0.2 to 0.6 mmol.L<sup>-1</sup> considerably reduces antioxidant activity in reed seedlings (Di et al. 2007). A concentration of 17.6 μmol.L<sup>-1</sup> significantly increased SOD activity in reed leaves during the heading period (Alfadul and Al-Fredan, 2013). Concentrations up to 100 μmol.L<sup>-1</sup> significantly increased SOD activity in the leaves of broad beans during germination (Issam et al. 2012). A Cd concentration of 10 μmol.L<sup>-1</sup> inhibited growth and increased SOD activity in Arabidopsis seedlings, but a concentration of 1 μmol.L<sup>-1</sup> had no significant effect on SOD activity (Issam et al. 2012). Other studies have shown that excessive nickel stress leads to the peroxidation of the cell wall of basmati rice seedlings, which causes a reduction in the germination rate of rice (Khan et al. 2015). Therefore, determining the tolerable concentration of heavy metals in plants is the key to the application of wastewater irrigation wetlands.

Reeds are the main species in wetlands and can efficiently absorb such pollutants as heavy metals and nutrients from the water imported by the rivers or slope runoff (Ren et al. 2010). In the previous studies of our research group, it was found that the concentration of cadmium treatment, the duration, and the growth period of reeds all have significant effects on SOD and POD activities in reed leaves. Among them, POD activity exhibits a linear change characteristic, which is difficult to indicate the feedback of plants to stress. However, SOD activity presents more complex changes. Therefore, an in-depth study of the kinetic characteristics of SOD activity can analyze the response of plants to external stress and determine the mechanism of cadmium resistance in reeds.

In this study, we experimentally investigated the effects of different Cd concentrations on the activities of SOD in reed leaves. We developed a dynamic model to determine the maximum reaction rates and inflection points of SOD activity at different Cd concentrations. The study aimed to explore the responses of reeds to Cd stress and to provide a theoretical basis and technical support for the wise use of the polluted water in mine sites, papermaking wastewater, or other industrial wastewater to irrigation wetlands and the restoration of degraded wetlands.

## MATERIAL AND METHODS

### Materials

The reeds as the heavy metal hyperaccumulator plant were used in this study to explore the impact of Cd pollution

on plant growth. The experimental material reeds were collected in April 2019 from the core area of the Liaohe estuarine wetland in the city of Panjin, Liaoning Province, China. Ungerminated reed rhizomes with healthy buds were also collected, cut into pieces 30 cm in length, wrapped in soil-laden sacks, and sprinkled with water to keep the roots wet. The plants were taken to the test field at Shenyang Agricultural University and transplanted into experimental buckets. The soil was collected from the Water Conservancy Comprehensive Experimental Site of Shenyang Agricultural University. The soil type was meadow soil, with a pH of 8.47, organic-matter content of 1.12%, and a density of 1.03 g.cm<sup>-3</sup>. The Cd content in the soil was lower than the detection limit by ICP and has not been detected, which showed there was no Cd in the soil.

### Experimental Design

To clarify the effect of different concentrations of Cd stress on the growth of reeds, this study set 6 concentration gradients as C1(1 mg.kg<sup>-1</sup>), C2(2 mg.kg<sup>-1</sup>), C3(3 mg.kg<sup>-1</sup>), C4(4 mg.kg<sup>-1</sup>), C5(5 mg.kg<sup>-1</sup>) and control concentration C0(0 mg.kg<sup>-1</sup>) according to the preliminary soil and wastewater investigation in Fushun West Open-pit Mine. A certain amount of CdCl<sub>2</sub>.2.5H<sub>2</sub>O was mixed into air-dried soil in each barrel based on the set concentration gradient to explore the effect of Cd pollution on the growth of reeds more effectively.

Three replicates were set for each concentration, and the collected reed rhizomes were planted in 18 white steel buckets marked with the corresponding concentration under a ventilated and photo permeable rain shelter. The planting density of reeds was controlled at an average of 10 plants per experimental bucket. The reeds were transplanted into each barrel from the wetland test facility on April 12th, 2019. Tap water was added to the barrels and maintained at a level 5 cm above the soil. The tap water contained no Cd.

Six fully expanded healthy reed leaves were collected randomly from each experimental bucket according to the corresponding concentration markers at the end of each growth stage of reeds. The collected samples were stored in an ice bag and brought back to the laboratory for pretreatment quickly.

The reed's growth stages were divided as follows: germination stage (Mid-April to early May), leaf expansion stage (Mid-May to early June), rapid growth stage (Mid-August-early September), heading stage (Mid-August-early September) and maturation stage (Mid-September-October) according to the growth and development process of reeds under local climate conditions of Shenyang.

### Sample Collection and Processing

**SOD activity:** One gram of fresh leave of reeds in phosphate buffer was ground in a mortar in an ice bath. The homogenate was centrifuged, and enzymes were extracted from the supernatant. Enzymatic activity was determined by the nitroblue tetrazolium (NBT) method, where 50% inhibition of NBT photochemical reduction per unit time is regarded as one unit of activity (Wang et al. 2002).

**Cd content:** Three healthy leaves from each barrel were steamed, dried, crushed (refer to Wang 2005) for information on phytotreatment and decomposition, and placed into three 100 mL plastic bottles individually. The Cd concentrations of the samples were determined by inductively coupled plasma atomic emission spectrometry.

An inductively coupled plasma emission spectrometer (Thermo iCAP 7000 Series) was used to determine the concentrations of Cd in the wastewater and plant samples. A national standardized solution containing 32 metal elements was purchased from a Chinese standard material website.

### Data Processing and Analysis

In a limited environment, the physiological changes in plants follow a logistic pattern (Ding et al. 2009), and its differential form is:

$$\frac{df}{dt} = rf((k - f) / k) \quad \dots(1)$$

In the above formula,  $f(t)$  is the enzyme activity at the time  $t$ , which represents the SOD activity in this study specifically.  $r$  is the intrinsic growth rate, which represents the potential growth capacity,  $k$  is the environmental capacity, which represents the upper limit of enzyme activity.

When  $f(0) = f_0$ , let  $a = \frac{k - f_0}{f_0}$ , which represents the influence of initial conditions on enzyme activity and integrate (1) into an explicit functional form:

$$f(t) = 1 / (1 / k + e^a / k) \cdot e^{-rt} \quad \dots(2)$$

Introduce parameter  $t_m$  instead of  $a$ , let

$$a = rt_m \quad \dots(3)$$

Obtained Bartlett form:

$$f = k / (1 + e^{-r(t-t_m)}) \quad \dots(4)$$

When  $t = t_m$ ,  $f = k/2$ ,  $k/2$  is the maximum sustained activity of the enzyme, and the moment  $t_m$  is the time when the inflection point of the Logistic curve is located. The inflection point is always reached  $f = k/2$ .

## RESULTS AND DISCUSSION

### The Effects of Cd on SOD Activity in Reed Leaves

SOD activity is affected by such factors as illumination, temperature, water content, and the presence of heavy metals. The influence of the different Cd concentrations on SOD activity in reed leaves at the five stages of growth is shown in Fig. 1.

SOD activity in the leaves generally increased with Cd concentration. The variation in SOD activity increased as the plants matured.

In the whole stage of physiological, with levels C0 and C1, the changes in SOD activity were not significant, with levels C2, C3, C4, and C5, SOD activity increased and have a significant difference from the contraposition ( $P < 0.05$ ),

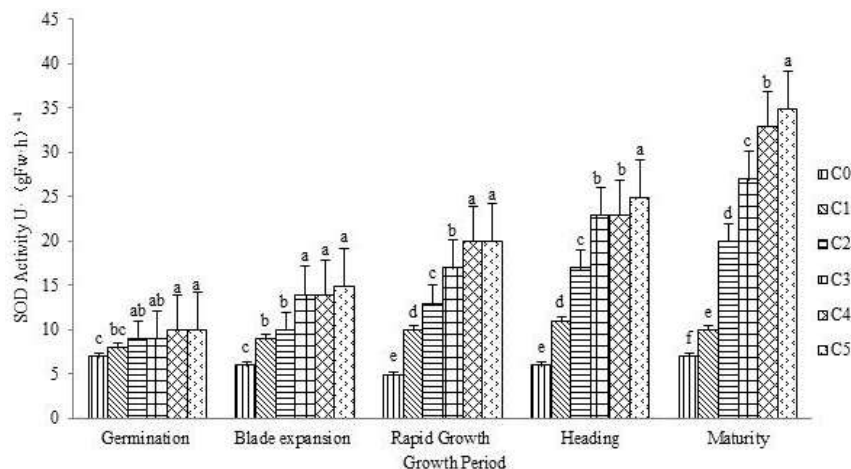


Fig. 1: The influence of Cd contamination on SOD activity in reed leaves. Different letters indicate significant differences. "FW" means fresh weight.

indicating that factors such as illumination did not cause significant changes in SOD activity. The significant changes in SOD activity were thus likely caused by Cd concentration.

Different concentrations of Cd led to significant changes in SOD activity at different stages of growth. The variation in SOD activity was similar at C3, C4, and C5, and SOD activity was higher at maturation than at the heading stage. SOD activity was lowest at germination. The increases in SOD activity were significant at C2 in the rapid-growth, heading, and maturation stages. SOD activity changed little at C0 and C1 in the germination and leaf expansion stages. At C1 and C2, SOD activity tended to first increase and then decrease. Plants under Cd stress typically resort to resistance measures to adapt to adverse environments. If the stress is too large and exceeds the limit of tolerance of the plants, the health of the plants will weaken until death occurs.

### The Kinetic Analysis of SOD Activity in Reed Leaves under Cd Stress

Cd concentration was used as an impact factor and then for trend analysis of the intrinsic rate of increase in SOD activity and carrying capacity. These analyses allowed us to determine the quantitative relationships between Cd concentration and carrying capacity or the intrinsic rate of increase. Regression equations were derived from the logistic curves (Table 1).

The relationship between Cd concentration and carrying capacity is:

$$k = -0.0528x^3 + 7.3488x + 12.4 \quad (R^2=0.972)$$

The relationship between Cd concentration and intrinsic rate of increase is:

$$v_x = -0.0005x^3 + 0.0438x + 0.1229 \quad (R^2=0.991)$$

Applying these values to equation (4), we can derive the dynamic equation of SOD activity under Cd stress:

$$f = \frac{-0.0528x^3 + 7.3488x + 12.4}{1 + e^{(a - (0.0005x^3 + 0.0438x + 0.1229))t}} \quad \dots(5)$$

where  $x$  is Cd concentration (in units),  $t$  is time,  $a$  is a constant representing initial conditions, and  $v_x$  is the intrinsic rate of increase.

Comparing equation (4) with the regression equations (Table 1), we could derive the parameters  $a$ ,  $v_x$ , and  $k$  of SOD activity in reed leaves at different Cd concentrations and then use equation (5) to derive the parameters  $t_m$  and  $k/2$  (Table 2).

Table 2 indicates a positive correlation between Cd concentration and intrinsic rate of increase in SOD activity in reed leaves. In contrast, Cd concentration is negatively correlated with carrying capacity, Michaelis constant, and inflection point. The ability of the reeds to react to Cd stress thus increased as Cd concentrations increased. If concentrations are too high, though, the reaction of the plants to Cd will lower the maximum continuous activity. At a Cd concentration of 5 mg.kg<sup>-1</sup>, the inflection point (7.85) occurred at the end of July when the rate of increase in SOD activity was highest. At a Cd concentration of 4 mg.kg<sup>-1</sup>, the inflection point (8.60) occurred in the middle of August. Reeds are at the heading stage at this time, and the plants' resistance to Cd stress is at its peak. Beyond this point, resistance declines, and biomass and absorption of Cd increase. At concentrations of 3 or 2 mg.kg<sup>-1</sup>, the inflection points were 10.04 or 12.07, respectively, which occurred in October or December. Reeds are mature at this time and are ready

Table 1: Parameters of SOD activity at different concentrations of Cd.

Concentration	Regression equation	Correlation
C5	$Y=1/(1/27.188+e^{2.307/27.188}) * e^{-0.294*t}$	0.994
C4	$Y=1/(1/31.608+e^{2.433/31.608}) * e^{-0.283*t}$	0.984
C3	$Y=1/(1/39.696+e^{2.479/39.696}) * e^{-0.247*t}$	0.977
C2	$Y=1/(1/42.153+e^{2.593/42.153}) * e^{-0.215*t}$	0.987

Table 2: Parameters of SOD activity from regression equations at different Cd concentrations.

Concentration	$a$	The intrinsic rate of increase $v_x$ (maximum rate of increase)	Carrying capacity $k$ (maximum activity)	Michaelis constant $k/2$ (maximum continuous activity)	Inflection point ( $t_m$ )
C5	2.307	0.294	27.188	13.5940	7.8469
C4	2.433	0.283	31.608	15.8040	8.5972
C3	2.479	0.247	39.696	19.8480	10.0364
C2	2.593	0.215	42.153	21.0765	12.065



to be harvested, so Cd will have little impact on biomass. The limiting concentration of Cd on SOD activity is thus 3 mg.kg<sup>-1</sup>. At this concentration, the reeds still respond to Cd, which will have little effect on increases in biomass. Cd is fully absorbed at a time when biomass increases the most and economic benefits are highest.

## CONCLUSIONS

- (1) SOD activity in reed leaves increased as Cd concentrations increased under laboratory conditions. The variation in SOD activity was significant at different concentrations of Cd and different growth stages. Over the entire growth period, SOD activity reacted similarly to Cd concentration. SOD activity at the various growth stages showed the general trend of C5>C4>C3>C2>C1>C0, illustrating that Cd stress favored increases in SOD activity in reed leaves.
- (2) The changes in SOD activity at different Cd concentrations followed a logistic curve. The experimental results indicated that the intrinsic rate of increase rose with increasing Cd concentration, but the variation in carrying capacity decreased, and the inflection point was extended.
- (3) The quantitative relationships between Cd concentration and the intrinsic rate of increase and the carrying capacity of SOD activity in reed leaves were determined. These were expressed as logistic curves to establish the dynamic equation of state for the variation of SOD activity under Cd stress. This equation identified a limiting Cd concentration of 3mg.kg<sup>-1</sup> on SOD activity. At this concentration, reeds can effectively respond to Cd stress and grow satisfactorily. Therefore, the concentration of cadmium in polluted water used to irrigate reed wetland should be less than or equal to 3mg.kg<sup>-1</sup> to ensure the normal growth of wetland plants. The result has an important practical guiding role in the environmental remediation of chromium-polluted mining areas, the purification of papermaking wastewater, and other biological treatment of industrial polluted water bodies.

## ACKNOWLEDGEMENTS

This work was financially supported by the National Key Research and Development Program of China [2017YFC1503105, 2016YFC0500408]; the National Natural Science Foundation of China [31570706, 31670711, 31470710]. The sample and data collection work was supported by the Liaoning Shuangtai Estuary Wetland Ecosystem Research Station.

## REFERENCES

- Ahmad, P., Abdel Latif, A.A., Abd-Allah, E.F., Hashem, A., Sarwat, M., Anjum, N.A. and Guceci, S. 2016. Calcium and potassium supplementation enhanced growth, osmolyte secondary metabolite production, and enzymatic antioxidant machinery in cadmium-exposed chickpea (*Cicer arietinum* L.). *Front. Plant Sci.*, 7: 513.
- Alfadul, S.M.S and Al-Fredan, M.A.A. 2013. Effects of Cd, Cu, Pb, and Zn combinations on *Phragmites australis* metabolism, metal accumulation, and distribution. *Arab. J. Sci. Eng.*, 38(1): 11-19.
- AlMomany, A.M., Arabiat, S. and Fardous, A. 2019. Growth and quality of sweet corn irrigated with treated wastewater to control Fusarium Wilt. *Fresenius Environ. Bull.*, 28(6): 4613-4621.
- Assche, F. and Clijsters, H. 1990. Effects of metals on enzyme activity in plants. *Plant Cell Environ.*, 13(3): 195-206.
- Bowler, C., Montagu, M.V. and Inze, D., 1992. Superoxide dismutase and stress tolerance. *Annu. Rev. Plant. Physiol. Plant. Mol. Biol.*, 43: 83-116.
- Dhiman, J., Prasher, S.O., ElSayed, E., Patel, R., Nzediegwu, C. and Mawof, A. 2020. Use of polyacrylamide superabsorbent polymers and plantain peel biochar to reduce heavy metal mobility and uptake by wastewater-irrigated potato plants. *Trans. ASABE*, 63(1): 11-28.
- Di, H.E., Liu, Y.G., Huang, Y.E., Lian, X.J. and Zhang, W. 2007. Effects of calcium on chlorophyll and antioxidant enzymes in *Phragmites australis* under cadmium stress. *J. Agro-Environ. Sci.*, 26(1): 197-202.
- Ding, L., Li, W., Shi, P., Li, Q., Wang, G.X. and Zheng, L.F. 2009. Effects of water transparency on *Potamogeton crispus* growth and its dynamic model. *Acta Ecol. Sin.*, 29: 92-96.
- Elster, E.F. 1982. Oxygen activation and oxygen toxicity. *Ann. Plant Physiol.*, 33: 73-96.
- Issam, N., Kawther, M., Haythem, M. and Moez, J. 2012. Effects of CaCl<sub>2</sub> pretreatment on antioxidant enzyme and leaf lipid content of faba bean (*Vicia faba* L.) seedlings under cadmium stress. *Plant Growth Regul.*, 68(1): 37-47.
- Khan, A., Khan, S., Khan, M.A., Qamar, Z. and Waqas, M. 2015. The uptake and bioaccumulation of heavy metals by food plants, their effects on plants nutrients, and associated health risk: A review. *Environ. Sci. Pollut Res.*, 22(18): 13772-13799.
- Koehler, A. 2008. Water use in LCA: managing the planet's freshwater resources. *Int. J. Life Cycle Assess.*, 13(6): 451.
- Passardi, F., Penel, C. and Dunand, C. 2004. Performing the paradoxical: How to plant peroxidases modify the cell wall. *Trends in Plant Sci.*, 9(11): 534-540.
- Qadir, M., Sharma, B.R., Bruggeman, A., Choukr-Allah, R. and Karajeh, F. 2007. Non-conventional water resources and opportunities for water augmentation to achieve food security in water-scarce countries. *Agric. Water Manag.*, 87(1): 2-22.
- Ren, J., Tao, L., Yang, Q. and Fang-Ke, Y.U. 2010. Accumulation ability of Cd in water for *Phragmites australis*, *Acorus calamus*, and *Scirpus tabernaemontani*. *J. Agro-Environ. Sci.*, 29(9): 1757-1762.
- Sun, Y.B., Zhou, Q.X., Lin, W., Liu, W.T. and Rui, L. 2009. Characteristics of cadmium tolerance and bioaccumulation of *Bidens pilosa* L. seedlings. *Environ. Sci.*, 30(10): 3028-3035.
- Wang, X. 2005. Comparison of different digestion methods used for the decomposition of plant samples in elemental quantification by using ICP-AES. *Spectrosc. Spectr. Anal.*, 25(4): 563-566.
- Wang, Z.Q., Jiang, X.Y. and Wang, C.H. 2002. Effects of Pb, Cd, and Zn on oxidative stress and antioxidative ability in *Phragmites australis*. *Chin. J. Process Eng.*, 2(6): 558-563.
- Xu, X., Yang, Y., Wang, G., Zhang, S., Cheng, Z., Li, T., Yang, Z., Xian, J., Yang, Y. and Zhou, W. 2020. Removal of heavy metals from industrial sludge with new plant-based washing agents. *Chemosphere*, 246: 125816.





# Estimation of Water Balance Components for the Watershed of Ghataprabha Sub-Basin

Akshata Bandi H.\*† and Nagraj S. Patil\*\*

\*Department of Civil Engineering, SDM College of Engineering, Dharwad-580002, Karnataka, India

\*\*Department of Civil Engineering, Visvesvaraya Technological University, Centre for PG studies, Belgaum, Karnataka, India

†Corresponding author: Akshata Bandi H.; akshatabandi9090@gmail.com

## Nat. Env. & Poll. Tech.

Website: [www.neptjournal.com](http://www.neptjournal.com)

Received: 25-08-2021

Revised: 15-11-2021

Accepted: 19-11-2021

### Key Words:

Calibration

Validation

SWAT model

Watershed

Water balance

## ABSTRACT

Evaluation of hydrological components in the water balance study is important in planning and maintaining a sustainable watershed to understand the hydrology of the river sub-basin/watershed. This study was carried out to estimate the water balance components in the watershed of the Ghataprabha sub-basin using the hydrological model SWAT (Soil and Water Assessment Tool). The river watershed was further delineated into 35 sub-basins comprising 542 hydrological response units (HRUs). A monthly calibration and validation study has been performed. Statistical model performance indicators, coefficient of determination ( $R^2$ ), and Nash & Sutcliffe (1970) efficiency (NSE) were used to correlate the monthly observed discharge data and monthly simulated discharge data.  $R^2$  of 0.75 and NSE of 0.63 for calibration and 0.7 and 0.65 for validation respectively, indicated the satisfactory performance of the model simulation on monthly simulation of flow. Monthly average water balance components (Precipitation, Evapotranspiration, Stream flow, Water yield) were estimated for the watershed.

## INTRODUCTION

The geographical variations, lands use land cover changes, water usage policies and strategies, and climatic variations along with uneven distribution of rainfall with irregular frequency influence the driving mechanism of water resource planning and management, quality and quantity of water body spatially and temporally. The rise in population exerts pressure on the demand for production of more yield, and rising temperature day by day causes an inadequate supply of water for various needs such as irrigation, drinking purposes, domestic usage, manufacturing, and treatment sites. In this respect, it is necessary to quantify the geographical changes and demographical changes spatially and temporally in the study area to understand the hydrology in the watershed to meet the various objectives set to fulfill the need for domestic and commercial purposes and to achieve sustained management of water resource spatially and temporally. The present study made utilization of remotely sensed tools with geographic information system (GIS) techniques for hydrological modeling and water resource assessment with an evaluation of water balance components. Models are classified into three types; empirical, conceptual, and physical models based on the model structure, algorithm, and data availability. Models are also categorized based

on the spatial variability of the catchment area which is lumped, semi-distributed, and distributed. The model has to be chosen based on the objective of the study, data availability, and model simplicity (Sitterson et al. 2014). The physically-based hydrological model considers the land use land cover, topography, and management practices spatially and temporally, thus it makes it easy to interpret the effects of various driving factors on the hydrological system in the study area. SWAT is one such a physically-based continuous time scale, a semi-distributed model which has been widely used as a hydrological model to simulate climate change, surface runoff, sediment transportation, and nutrients loading (Arnold et al. 2012, Moriasi et al. 2007, 2012, Neitsch et al. 2002). Many studies have been performed to estimate the average annual and monthly average flows (Erhui et al. 2016, Rederick et al. 2018 Xu et al. 2013).

One of the studies calibrated and validated the hydrological model SWAT using performance indicators and estimated the average annual water balance components and concluded that there was variation in the soil storage and evapotranspiration caused more loss of water from the watershed (Shawul et al. 2013, Gupta et al. 2020). It was found that 57% of precipitation melted into the lake and it was a major cause of expanding the catchment. Glaciers melt

for lesser evaporation (Adnan et al. 2019). The researcher carried out a water balancing components study using SWAT and SWAT CUP for hydrological simulation in the Tandula (India) reservoir catchment to overcome the lack of water supply for the paddy growth, which boosts the economy of the people in the area since it was known for the cultivation of paddy and covering 86% of the area of the catchment (Jaiswal et al. 2020). Evaluation of snowmelt in the river was one of the great works to estimate the water balance components at mountain glaciers and 25% was lost as evapotranspiration from the river (Dhami et al. 2018). The objectives of the study were to standardize the SWAT model and to estimate the water balance components for the monsoon season in the watershed of the Ghataprabha sub-basin.

## MATERIALS AND METHODS

### Study Area

The sub watershed lies between 15°45' to 16°20' N & 74°0' to 75°5' E in the Ghataprabha basin, India (Fig. 1). Common soil types are gravelly sandy clay loam and clay. The area of the watershed is 4717 km<sup>2</sup>. The average slope is 22°. The climate in the watershed is typical of a semiarid environment. Most of the basin receives monsoon rainfall. Rainfall shows high seasonal variability. The average annual precipitation is 633.07 mm.

### Datasets

The various types of data to be given as input to the model were digital elevation model (DEM), Soil data, land use/

land cover, and weather data like precipitation, temperature, and discharge data. A 32 m DEM tiles were obtained from the Bhuvan website, India. Land use/ land cover data was obtained from the Arc-SWAT website (Indian dataset for SWAT 2012). Soil data (Soil HWSD FAO (worldwide data)) was derived from the Arc-SWAT website (Indian dataset for SWAT 2012). Weather Data includes Precipitation, Temperature, relative humidity, solar radiation, and wind speed data obtained from the Arc-SWAT website. Daily river discharge data from 1990-to 2011 is collected from the water resource information system (WRIS), India.

### Methods

The Soil and Water Assessment Tool (SWAT) was used for hydrological simulation of the flow in the study (Arnold et al. 2012). The model setup involved preparation of data, formation of sub-basin, defining HRUs, analysis of sensitive parameters, calibration, and validation. The river sub-basin was further delineated into 35 sub-basins comprising 542 hydrological response units (HRUs) Using the DEM (Fig. 2(a)). The soil data, land use land cover data, and the meteorological data between 1975 and 2016 were given as input to the model, SWAT model was run to simulate the monthly stream flow from 1990 to 2016. Soil, Land use land cover, and slope maps were prepared (Fig. 2(b), 2(c), 2(d) 2(e)). The simulation period was split as spatially to perform the validation at a different site (Arnold et al. 2012). The calibration period was from 2007 to 2011 for the Lolasure station and the validation period was from 2007–to 2011 for Hudli. The sensitivity of the parameters was tested by using ArcSWAT during the calibration of the model. The calibrated parameters were used during the validation of the model.

The simulated and observed flow were compared and the model performance was evaluated using R<sup>2</sup> and NSE [12].

$$R^2 = \frac{[\sum_i (O_i - \bar{O})(S_i - \bar{S})]^2}{\sum_i (O_i - \bar{O})^2 \sum_i (S_i - \bar{S})^2} \quad \dots(1)$$

$$NSE = 1 - \frac{\sum_i (O - S)_i^2}{\sum_i (O_i - \bar{O})^2} \quad \dots(2)$$

Where O<sub>i</sub> and S<sub>i</sub> are observed flow and simulated flow values in the month i, respectively,  $\bar{O}$  and  $\bar{S}$  are the average values of observed flow and simulated flow respectively. Model performance was accepted as satisfactory if NSE > 0.55 and R<sup>2</sup> > 0.7 for monthly flow and as good if NSE > 0.7 and R<sup>2</sup> > 0.8 (Moriassi et al. 2015).

## RESULTS AND DISCUSSION

The simulated results were compared with observed data as shown in Fig. 3. The simulated flow peaks were not

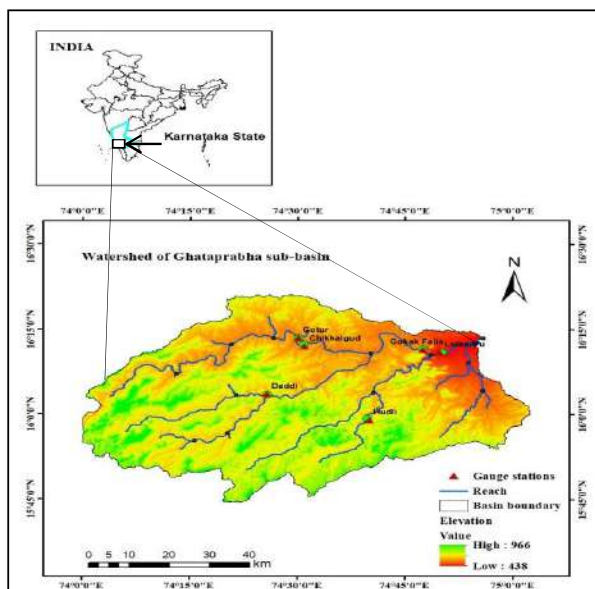


Fig. 1: Study area of the watershed.



properly matching with observed datasets. The value of  $R^2$  for observed and flow-out discharge from the scattered plot is 0.71 (Fig. 4). Comparatively lesser  $R^2$  indicates the scope for model tuning is available to ensure accurate hydrological data for the study area.

Calibration was done for five years starting from -2007 to 2011 to match simulated results with observed data values. The sensitive parameters were identified and adjusted to obtain better calibration (Fig. 5). This is confirmed by knowing the  $R^2$  and NSE values between observed values and simulated results and must be within the allowable limits.

Table 1 shows the adjusted parameters during the calibration of the model.

Table 1: Sensitive parameters and best-fitted values for calibration.

S No.	Sensitive Parameter	Fitted Value	Min. Value	Max. Value
1	CN2	86	35	98
2	SOL_AWC	0.13	0	1
3	ESCO	1	0	1
4	EPCO	0.95	0	1
5	SURLAG	0.5	0.1	24

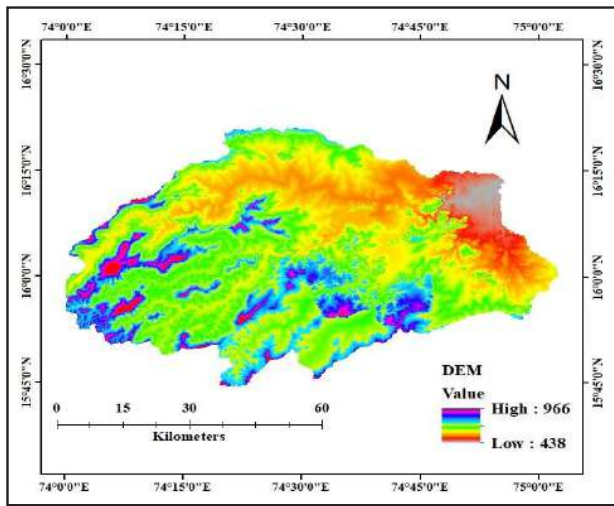


Fig. 2(a): Digital elevation map.

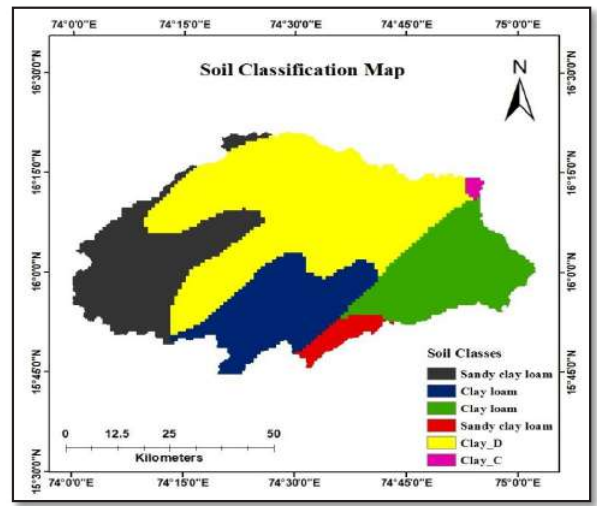


Fig. 2(b): Soil classification map.

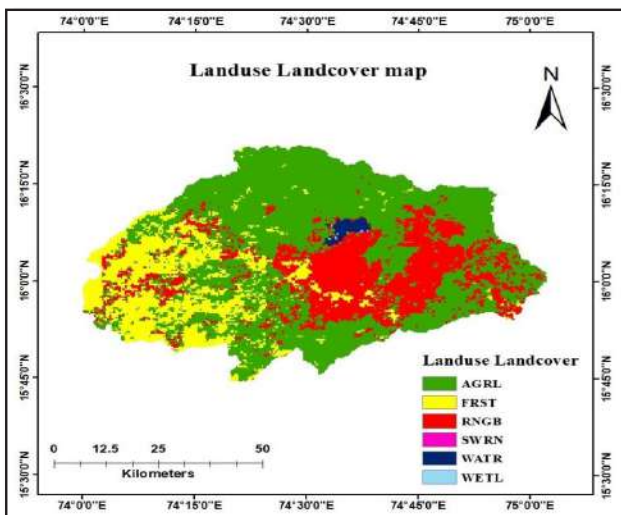


Fig. 2(c): Land use the land cover map.

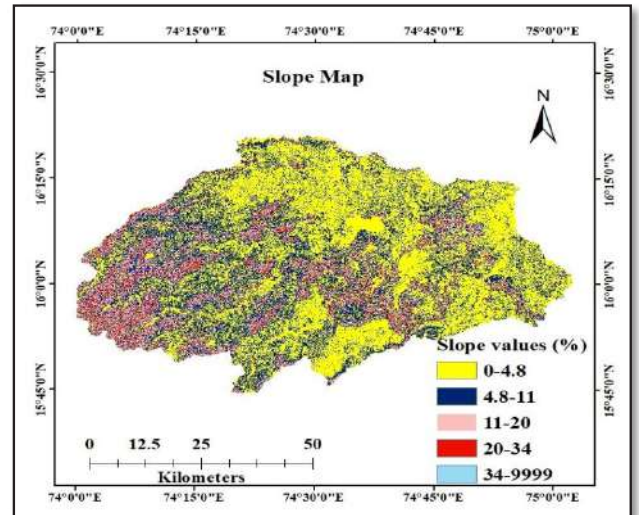


Fig. 2(d): Slope map.



The sensitive parameters were identified during the calibration of a model and adjusted to rate the performance of the model using  $R^2$  and NSE.  $R^2$  of 0.75 (Fig. 6), the NSE of 0.63 for calibration and 0.7 (Figs. 7 & 8), and 0.65 respectively for validation as shown in Table 2, Statistical parameters indicated the satisfactory performance of the model simulation on the flow of monthly time period (Moriassi et al. 2015).

**Water Balance Components**

Variation in the hydrological process of any system contributes to the difference in impoundment of storage in the watershed. Water balance is the driving mechanism for these variations to take place in the study area. SWAT model was simulated again after the calibration and validation to ensure the best simulation available to carry out the water balance study. The SWAT output file provided the monthly average of various water balance components. The comparison study of various hydrological components such as precipitation, evapotranspiration, stream flow, and water yield for the monsoon season is represented graphically (Fig. 9). Estimated water

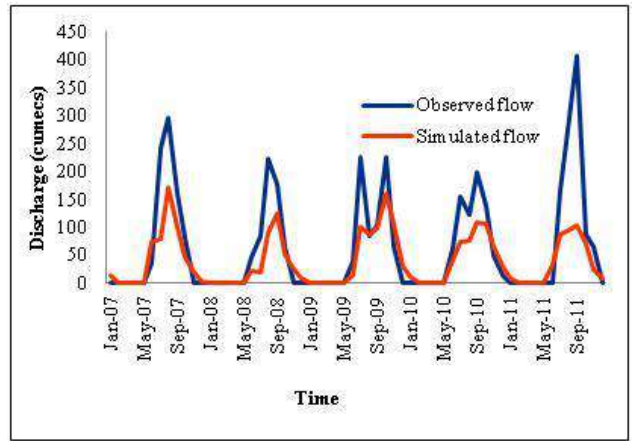


Fig. 3: Comparison of observed flow with the simulated flow before calibration.

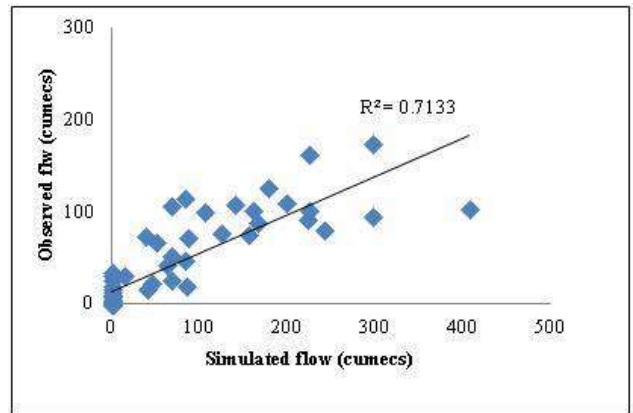


Fig. 4: Scatter plot of simulated versus observed flow before calibration.

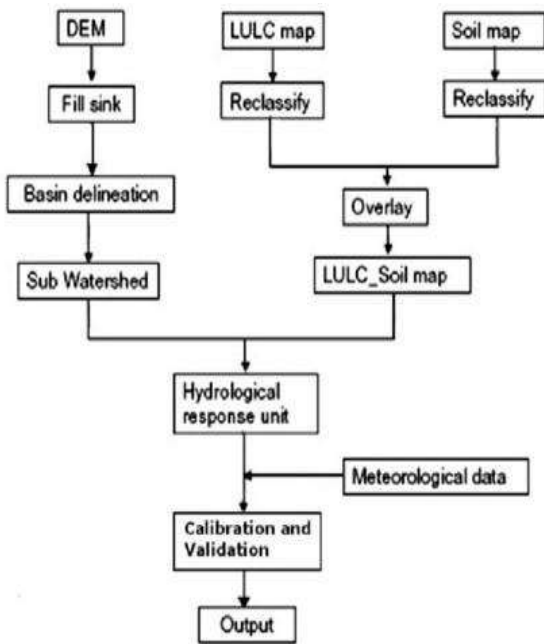


Fig. 2(e): Flowchart of SWAT methodology.

Table 2: Performance ratings of model.

S.No	Model	$R^2$	NSE
1	Calibration	0.75	0.63
2	Validation	0.7	0.65

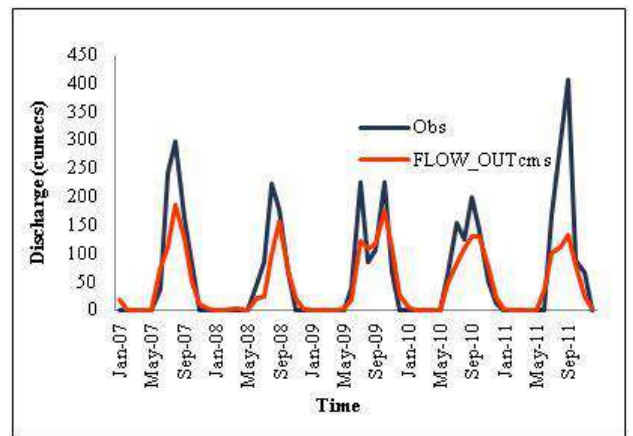


Fig. 5: Comparison of observed flow with the simulated flow after calibration.

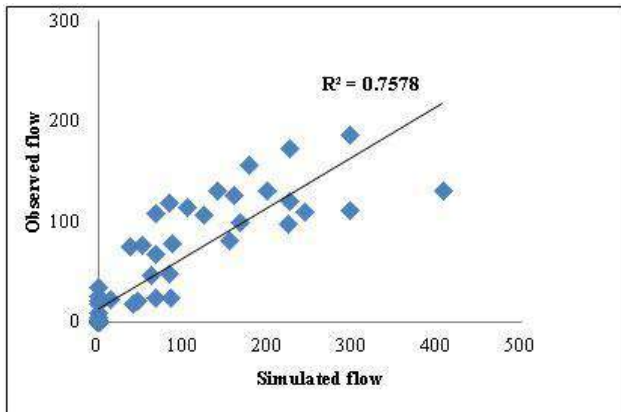


Fig. 6: Scatter plot of simulated versus observed flow after calibration.

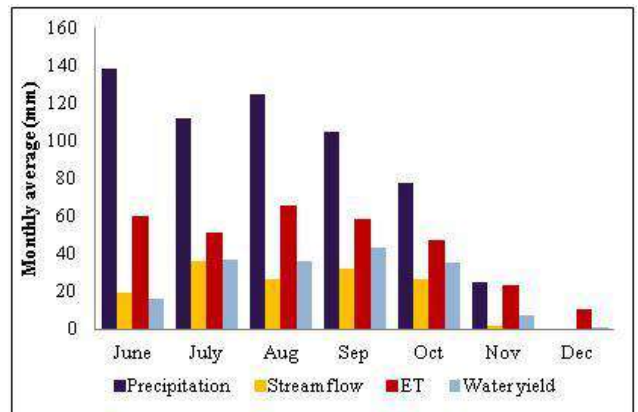


Fig. 9: Monthly average of Stream flow, Precipitation, and Evapotranspiration, water yield for the watershed.

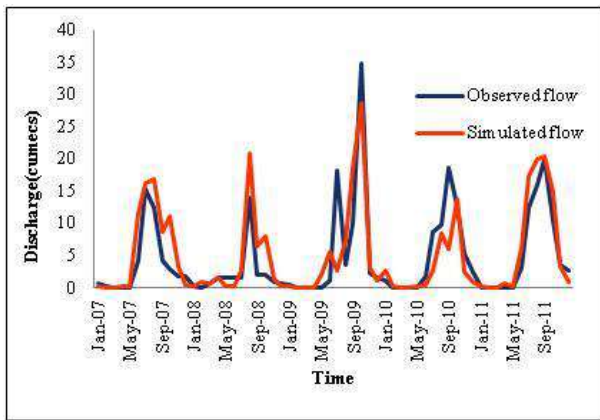


Fig. 7: Comparison of observed flow with the simulated flow for Hudli station.

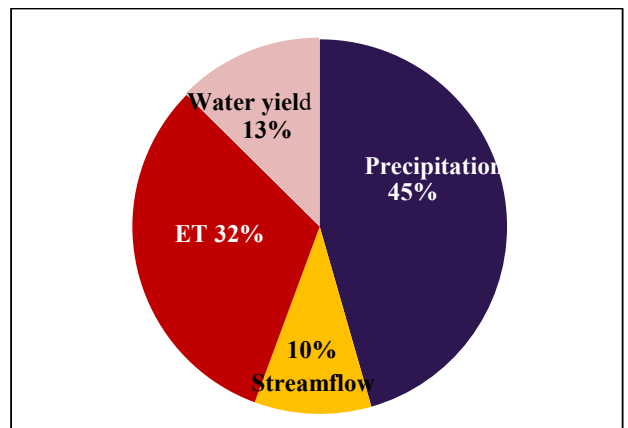


Fig. 10: Contribution of monthly average stream flow, precipitation evapotranspiration, and water yield for the watershed in percentage.

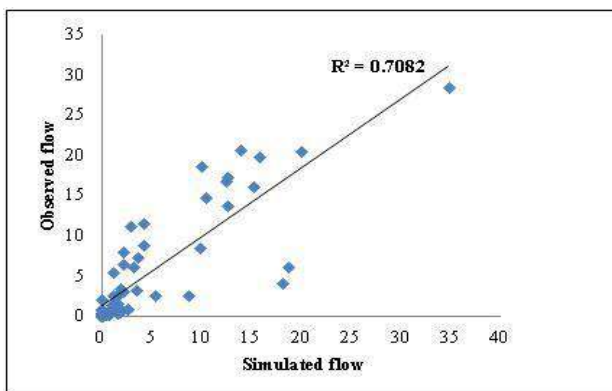


Fig. 8: Scatter plot of simulated versus observed flow after validation.

balance components accounted for 53% of precipitation, 10% of evapotranspiration, 32% of stream flow, and 13% of water yield (Fig. 10).

**CONCLUSION**

The model was calibrated and validated. The calibration and validation of the model for the study area were done with reference to observed data obtained from WRIS, CWC, and the Government of India. The calibration was carried out for the year 2007- 2011 for Lolasuru station and the period from 2007-to 2011 was used to validate the process for Hudli station. The model was also simulated with only default parameters, and it showed satisfactory results before calibration. Still toning of the model was available to ensure the best simulation to carry out the water balance study. During calibration, it was found that CN2, SOL\_AWC, ESCO, EPCO, and SURLAG were the most sensitive parameters in the study area. With the default parameters, the results were found to be reasonable, and they improved after calibration,

the  $R^2$  and NSE values for calibration were 0.75 and 0.63 and for validation, it was 0.7 and 0.65 which indicates that The model's performance was satisfactory. Further water balance components study was done. The monthly average contribution of precipitation was 53% causing the stream flow of 10%, with the loss of water due to evapotranspiration was 32% and water yield was accounted for 13% through the estimation of mean monthly stream flow. The result showed that there was more loss of water due to evapotranspiration due to rising temperature. It also means that there was enough water accumulation in the area due to the precipitation. To avoid more evapotranspiration losses, the best watershed management practices can be installed to store this water as groundwater storage through infiltration. The study of the water balance components helps in accounting for inflow and outflow of water, estimating the proper water supply, also estimates the future supply for the agricultural, commercial, or domestic purposes, and in the assessment of the hydrological study.

## REFERENCES

- Adnan, A., Kang, S., Zhang, G., Saifullah, M., Muhammad N.A. and Ali, A.F. 2019. Simulation and analysis of the water balance of the Nam Co lake using the SWAT model. *Water*, 11: 1383.
- Arnold, J.G., Moriasi, D.N., Gassman, P.W., Abbaspour, K.C., White, M.J., Srinivasan, R. and Kannan, N. 2012. SWAT: Model use, calibration, and validation. *Trans. ASABE*, 55(4): 1491-1508,
- Dhami, B., Sushil, K., Himanshu, Pandey, A. and Gautam, A. 2018. Evaluation of the SWAT model for water balance study of a mountainous snow-fed river basin of Nepal. *Nature Environ. Earth Sci.*, 77: 21.
- Erhui, L., Xingmin, M., Guangju, Z., Peng, G. and Wenyi S. 2016. Effects of check dams on runoff and sediment load in a semi-arid river basin of the Yellow River. *Stoch. Environ. Res. Risk Assess.*, 6: 11-21.
- Gupta, A., Sushil K., Himanshu, Gupta, S. and Ronald S. 2020. Evaluation of the SWAT Model for Analysing the Water Balance Components for the Upper Sabarmati Basin: *Advances in Water Resources Engineering and Management*. Springer Nature Singapore Pte Ltd, Singapore.
- Jaiswal, R.K., Yadav, R., Kumar A., Lohani, T. H. and Yadav, S. 2020. Water balance modeling of Tandula (India) reservoir catchment using SWAT. *Saudi Soc. Geosci.*, 13: 148.
- Moriasi, D., Arnold, J., Van Liew, M., Bingner, R., Harmel, R. and Veith, T. 2007. Model evaluation guidelines for systematic quantification of accuracy in watershed simulations. *Trans. ASABE*, 50(3): 885-900.
- Moriasi, D., Wilson, B., Douglas-Mankin, K., Arnold, J. and Gowda, P. 2012. Hydrologic and water quality models: Use, calibration, and validation. *Trans. ASABE*, 55(4): 1241-1247.
- Moriasi, D.N., Gitau, M.W., Pai, N. and Daggupati, P. 2015. Hydrologic and water quality models: performance measures and evaluation criteria. *Trans. ASABE*, 58(6): 1763-1785.
- Nash, J.E. and Sutcliffe, J. E. 1970. River flow forecasting through conceptual models: Part I. A discussion of principles. *J. Hydrol.*, 10(3): 282-290.
- Neitsch, S.L., Arnold, J.G. Kiniry, J.R., Srinivasan, R. and Williams, J.R. 2002. *Soil and Water Assessment Tool, User Manual, Version 2000*.
- Rederick, A. and Jha, M. K. 2018. Estimation of Water Balance and Water Yield in the Reedy Fork-Buffalo Creek Watershed in North Carolina using SWAT. *SWAT. Int. Soil Water Conserv. Res.*, 6339(17): 30241-30251.
- Shawul, A. A., Alamirew, T. and Dinka, M. O. 2013. Calibration and validation of SWAT model and estimation of water balance components of Shaya mountainous watershed, Southeastern Ethiopia. *Hydrol. Earth Syst. Sci. Discuss.*, 10: 13955-13978.
- Sitterson, J., Knightes, C., Parmar, R., Wolfe, K., Muche, M. and Brian A. 2014. *An Overview of Rainfall-Runoff Model Types*. EPA/600/R-14/152.
- Tripathi, M.P., Raghuvanshi, N.S. and Rao, G.P. 2006. Effect of the watershed subdivision on simulation of water balance components. *Hydrol. Process.*, 20: 1137-1156.
- Xu, Y.D., Fu, B.J. and He, C.S. 2013. Assessing the hydrological effect of the check dams in the Loess Plateau, China by model simulations. *Hydrol. Earth Syst. Sci.*, 17: 2185-2193.



# Changes in Carbon, Nitrogen and Phosphorus Stoichiometry of Leaf-Litter-Soil in Differently Stands Under 'Plain Afforestation Program' in China

Jie Li\*†, Da Yao\*\*, Zhongyu Shi\* and Kaiyu Song\*

\*College of Landscape Architecture, Shangqiu University, Shangqiu 476000, China

\*\*Shangqiu Institute of Technology, Shangqiu 476000, China

†Corresponding author: Jie Li; 14034@sqxy.edu.cn

Nat. Env. & Poll. Tech.  
Website: [www.neptjournal.com](http://www.neptjournal.com)

Received: 11-08-2021

Revised: 29-10-2021

Accepted: 18-11-2021

## Key Words:

Plain afforestation

Soil

Ecological stoichiometry

Typical forests

## ABSTRACT

Changes in land use might affect the combined C, N, and P stoichiometry in soil. The Plain Afforestation Program, which converts low-yield croplands or abandoned lands into forest, shrub, and/or grassland, was a famous land reforestation project in Beijing. To clarify the spatial distribution, stoichiometric characteristics, and controlling factors of carbon (C), nitrogen (N), and phosphorus (P), four typical Plain Afforestation forests including *Robinia pseudoacacia*, *Pinus tabuliformis*, *Ailanthus altissima*, and *Salix matsudana* plantations were selected in Yongding River plain afforestation area, Beijing. Leaf, litter, and soil C, N, and P concentrations and their stoichiometric relationships were analyzed. The results showed that the concentrations of N and P in the four plantations were in order of *R. pseudoacacia* > *A. altissima* > *S. matsudana* > *P. tabuliformis* in leaf and litter. Compared with leaves, the concentrations of C for *P. tabuliformis* were highest. The concentrations of N and P, as well as N:P for *R. pseudoacacia* plantation, were significantly higher than those for the other plantations. C and N concentrations were the highest in surface soil (0-10 cm), and C:N and C:P both demonstrated the trend of litter > soil in the plantations with the exception of *S. matsudana*. The total N concentration of leaf was positively correlated with that of litter in the four plantations. Overall, our findings suggested the growth of *R. pseudoacacia*, *P. tabuliformis*, and *S. matsudana* was mainly restricted by P, while that of *A. altissima* was constrained by N. In addition, it is a feasible method that uses nitrogen fertilizer when tending the artificial forest in the plain area.

## INTRODUCTION

Stoichiometry is a science that studies the balance of multiple chemical substances in biological systems and ecological processes in the context of ecology (Drenovsky et al. 2019). Elser et al. (2007) have extensively explored the causes and consequences of these constraints under the terminology of ecological stoichiometry. The study of the Stoichiometry measurement ratio of vegetation carbon (C), nitrogen (N), phosphorus (P), and the level of community nutrient supply can reveal the relationship between nutrient supply characteristics and vegetation development in various regions (Agren 2004). The ratio of nitrogen and phosphorus is a very important indicator of the absorption ability of N and P elements by plants (Cleveland & Liptzin 2007). There is considerable empirical evidence that the change of C, N, and P in the soil can feed back the effectiveness of soil nutrients, and the change of C, N, and P in leaf also affects soil nutrients (Elser et al. 2003, Güsewell et al. 2006, Brant et al. 2015). Ecological stoichiometry has provided an integrative solution to measure changes in C, N, and P within a plant at a time (Makino et al. 2003). Changes in C:N and C:P influence C

fixation and exhaustion in diverse ecosystems, thus making both ratios important indices to assess N or P use efficiency. Previous research has highlighted a diverse set of geochemical and ecological factors that can influence the identity and nature of C:N:P stoichiometry in particular ecosystems (Tessier & Raynal 2003). It is reasonable that the ratios of nutrients in the plant tend to be constant finally in a specific situation and may vary as the environment changes (Fanin et al. 2013). In monoculture plantation environments, stand age is key because of nutrient transformations from leaves, litter, and soil over time scales of 10-20 years. At present, most knowledge about the change in the ecological stoichiometry of elements is derived from studies across space, while only a few are touched. Many studies demonstrated the interactions between the season, vegetation type, and structure (See et al. 2015). Soil nitrogen affects phosphorus recycling: foliar resorption and plant-soil feedbacks in a northern hardwood forest. Ecology 96: 2488-2498), and soil properties affect microbial nutrient immobilization under a Mediterranean-type climate to influence the biogeochemical cycles for C, N, and P in Mediterranean forest ecosystems (Wright et al. 2010). To date, studies on the soil C, N, and P stoichiometry at different



scales are lacking, and information about their influences on the global or regional scale is scarce, particularly in China.

In China, widespread ecological degradation has constrained sustainable socio-economic development in recent decades, particularly before the end of the 20th century (Fu et al. 2002). Since the 1950s (Uchida et al. 2009, Zhao et al. 2014), the Chinese government has made great efforts to afforestation and restore ecosystems (Chang et al. 2011, Bui & Henderson 2013). More than 9.27 million ha of cropland and abandoned land have been afforested in China through the “Plain Afforestation Program” (PAP). The afforestation area in the afforestation Plain of north China lacks available phosphorus, and the rapid development of industrialization and urbanization in this area leads to the phenomenon of high nitrogen deposition (Lü 2012, Cui et al. 2015). The status and ratio characteristics of nitrogen and phosphorus in vegetation and soil need to be further studied. Although the initial goal of the PAP was to control soil erosion, the program strongly affects the C, N, and P cycling in soil. However, few studies have reported the soil C, N, and P stoichiometries under PAP. To clarify the spatial distribution, stoichiometric characteristics, and controlling factors of carbon (C), nitrogen (N), and phosphorus (P), four typical forests including *Robinia pseudoacacia* (*R. pseudoacacia*), *Pinus tabulaeformis* (*P. tabulaeformis*), *Ailanthus altissima* (*A. altissima*), and *Salix matsudana* (*S. matsudana*) plantations were selected in Yongding River plain afforestation area, Beijing. This study aims to accomplish the following: a) illustrate the distribution of the soil C:N, C:P, N:P values under the PAP; b) establish the changes in the soil C:N, C:P, N:P values after the change in land use; and c) study the factors driving the changes in the C:N, C:P, N:P ratios.

## MATERIALS AND METHODS

### Study Area

The study area is located in Beijing (39°30'13.99" N, 116°15'26.54" E). It features 30–45 m above sea level. The climate of this area belongs to a warm temperate semi-arid continental monsoon climate. The annual average temperature is 11.5°C, the precipitation is 568.9 mm, the rainfall is mainly concentrated in July and September, and the annual average humidity is 63%–68%. Before the

implementation of the plain forest construction, the study area was the sand wasteland, the lotus root land of potholes, and the land for conversion of farmland to forest. Its own land force is relatively weak compared with the natural forest, mainly distributed in light loamy brown tide soil and sandy loam soil, and the pH value is 8.8–9.1. The forests are all same age(6a), including *R. pseudoacacia*, *P. tabulaeformis*, *A. altissima*, *S. matsudana*, *Ginkgo biloba*, *Acer truncatum*, and *Ulmus pumila* (Table 1).

### Plant Sampling

Each tree in the selected quadrat was measured to measure the altitude, longitude, latitude, soil thickness, planting density, average tree height, and average crown in August 2019. Three standard trees were randomly selected in each standard quadrat. Each standard tree was collected from four directions of the upper, middle, and lower three levels of the crown with a high branch as a sample, the mature leaves with healthy growth were used. According to the five-point method of plum blossom, a representative 100 cm × 100 cm litter quadrat is set under each quadrat to collect litter. At the end of September, two layers of soil (0–30 cm due to the shallow soil layer in the study area) are collected at the place where litter samples are collected). After the soil sample is fully mixed, the soil sample of the afforestation site is collected outside the afforestation area according to the same method.

### Measurement and Calculation

The litter in the samples was harvested using the harvest method, weighed after being mixed, marked for drying in an oven at 8°C, and the leaves and litter were crushed by a plant crusher. The mixed soil sample of topsoil (0–10 cm) was taken from the sample of litter using the soil drilling method. After the soil sample was air-dried, stones, roots, and other impurities were removed, and ground using a 0.16 mm mesh screen. Organic C was measured by the potassium dichromate / sulphuric acid mixture titration method. Total N was measured by using the semi-micro Kjeldahl method with a Kjeldahl Auto-analyser (KDN-102C, Shanghai, China). Total P was measured by using the HNO<sub>3</sub> digest-Mo-Sb antispotrophotography method with a spectrophotometer (UV-2102 PCS, Shanghai, China) (Table 2). The ecological

Table 1: Basic status of sampling sites.

Plantation type	Altitude [m]	Average DBH [cm]	Average tree height [m]	Canopy density
<i>R. pseudoacacia</i>	40	13.6	5.8	0.78
<i>A. altissima</i>	41	13.3	6.9	0.85
<i>P. tabulaeformis</i>	38	11.1	5.1	0.65
<i>S. matsudana</i>	36	17.1	11.1	0.80



stoichiometric ratios of C, N, and P were calculated as organic C vs. total N (C:N), organic C vs total P (C:P), and total N vs. total P (N:P).

### Statistical Analysis

Excel 2016 was used for mapping, SPSS 19.0 was used for one-way variance analysis and Pearson correlation analysis, Duncan's test method was used for LSD multiple comparisons of relevant indexes, and the differences in stoichiometric ratios among stands and between cuts were analyzed using One-Way ANOVAs. Where there were no significant effects, the average was compared using a One-Way ANOVA. and  $P = 0.05$  was used as the benchmark for a significant difference.

## RESULTS

### Contents and Stoichiometric Ratio of C, N, and P in Leaves of Different Forests

Fig. 1 shows that the content of C in leaves of *R. pseudoacacia*, *P. tabulaeformis*, *A. altissima*, and *S. matsudana* forest were 354.19, 331.67, 393.23, and 411.21  $\text{g.kg}^{-1}$ , respectively. The leaf N content of *R. pseudoacacia* forest, *Ailanthus altissima* forest, *P. tabulaeformis* forest, and *S. matsudana* forest showed the change of *R. pseudoacacia* forest (22.82  $\text{g.kg}^{-1}$ ) > *Ailanthus altissima* forest (17.24  $\text{g.kg}^{-1}$ ) > *S. matsudana* forest (16.97  $\text{g.kg}^{-1}$ ) > *P. tabulaeformis* forest (11.3  $\text{g.kg}^{-1}$ ). The leaf P content was the highest in *A. altissima* forest (1.61  $\text{g.kg}^{-1}$ ), and the lowest in *P. tabulaeformis* forest (0.76  $\text{g.kg}^{-1}$ ).

### Contents and Stoichiometric Ratio of C, N, and P in Litters of Different Forests

The highest litter C content was 427.11  $\text{g.kg}^{-1}$ , and the highest litter N content was 20.12  $\text{g.kg}^{-1}$ , followed by *A. altissima* forest (15.91  $\text{g.kg}^{-1}$ ), *S. matsudana* forest (13.88  $\text{g.kg}^{-1}$ ), *P. tabulaeformis* forest (7.24  $\text{g.kg}^{-1}$ ), and the lowest litter P content was 1.51  $\text{g.kg}^{-1}$ , 1.13  $\text{g.kg}^{-1}$ , 0.89  $\text{g.kg}^{-1}$ , and 0.40  $\text{g.kg}^{-1}$ . The litter C: P and C: N of the four industrial forests in the study area were all in the form of *P. tabulaeformis* forest, *S. matsudana* forest, *A. altissima* forest, and

*R. pseudoacacia* forest, and the difference between them was significant are shown in Fig. 1 ( $P < 0.05$ ). Compared with the *Robinia* forest with the lowest metering ratio, the C: P of the highest *P. tabulaeformis* forest was 41.2% higher and the C: N was 32.7% higher. N: P was significantly higher in the *R. pseudoacacia* forest (14.14) than in other forest types.

### Contents and Stoichiometric Ratio of C, N and P in the Soil of Different Forests

The soil C content of the artificial forest in the study area showed that *R. pseudoacacia* (15.23  $\text{g.kg}^{-1}$ ) > *A. altissima* (11.04  $\text{g.kg}^{-1}$ ) > *S. matsudana* (8.21  $\text{g.kg}^{-1}$ ) > *P. tabulaeformis* forest (7.33  $\text{g.kg}^{-1}$ ), and the difference between the two was significant ( $P < 0.05$ ) (Fig. 1). The content of soil N was 0.79, 0.68, 0.57 and 0.67  $\text{g.kg}^{-1}$  in *R. pseudoacacia* forest, *A. altissima* forest, *S. matsudana* forest, and *P. tabulaeformis* forest, with significant difference ( $P < 0.05$ ). The highest soil P content was *S. matsudana* forest (0.77  $\text{g.kg}^{-1}$ ), followed by *Ailanthus altissima* forest (0.74  $\text{g.kg}^{-1}$ ), significantly higher than *Robinia pseudoacacia* forest and *Pinus tabulaeformis* forest. The average C:N value of the soil was 13.73, and there was a significant difference between the two trees ( $P < 0.05$ ). The C: P value showed that *R. pseudoacacia* forest > *A. altissima* forest > *P. tabulaeformis* forest > *S. matsudana* forest, and there was a significant difference between *P. tabulaeformis* forest and *Robinia pseudoacacia* forest ( $P < 0.05$ ). The N: P value of soil showed that *P. tabulaeformis* forest > *R. pseudoacacia* forest > *S. psammophila* forest > *A. altissima* forest. There was a significant difference between *P. tabulaeformis* forest, *R. pseudoacacia* forest, and *S. psammophila* forest. The results of the stoichiometric ratio of soil in different depths of the same stand show that (Fig. 2), with the increase of soil depth, the content of C and N gradually decreases, the content of P does not change significantly, and the content of all elements in the soil without afforestation is the smallest, which shows that afforestation has an obvious effect on the improvement of the regional land force.

Table 2: Soil properties of the 0-10 cm layer of three different shrub sample plots.

Plantation type	SOC content [ $\text{g.kg}^{-1}$ ]	TN content [ $\text{g.kg}^{-1}$ ]	TP content [ $\text{g.kg}^{-1}$ ]	AN content [ $\text{mg.kg}^{-1}$ ]	AP content [ $\text{mg.kg}^{-1}$ ]
<i>R. pseudoacacia</i>	37.57 ± 10.03a	1.72 ± 0.58a	1.09 ± 0.05a	214.93 ± 31.68a	47.51 ± 17.73a
<i>A. altissima</i>	23.14 ± 7.15a	1.53 ± 0.52a	1.64 ± 0.02a	113.87 ± 40.01a	29.41 ± 20.83a
<i>P. tabulaeformis</i>	31.12 ± 4.16a	2.15 ± 0.52b	1.12 ± 0.04a	201 ± 42.58b	37.51 ± 11.61a
<i>S. matsudana</i>	22.92 ± 4.06a	1.95 ± 0.52a	1.07 ± 0.03a	101 ± 32.18a	24.11 ± 14.53a

Note: SOC, soil organic carbon; TN, total nitrogen; TP, total phosphorus; AN, alkali-hydrolyzable nitrogen; AP, available phosphorus. Different lowercase letters in the same column indicate significant differences at the  $P < 0.05$  level. The same is below.

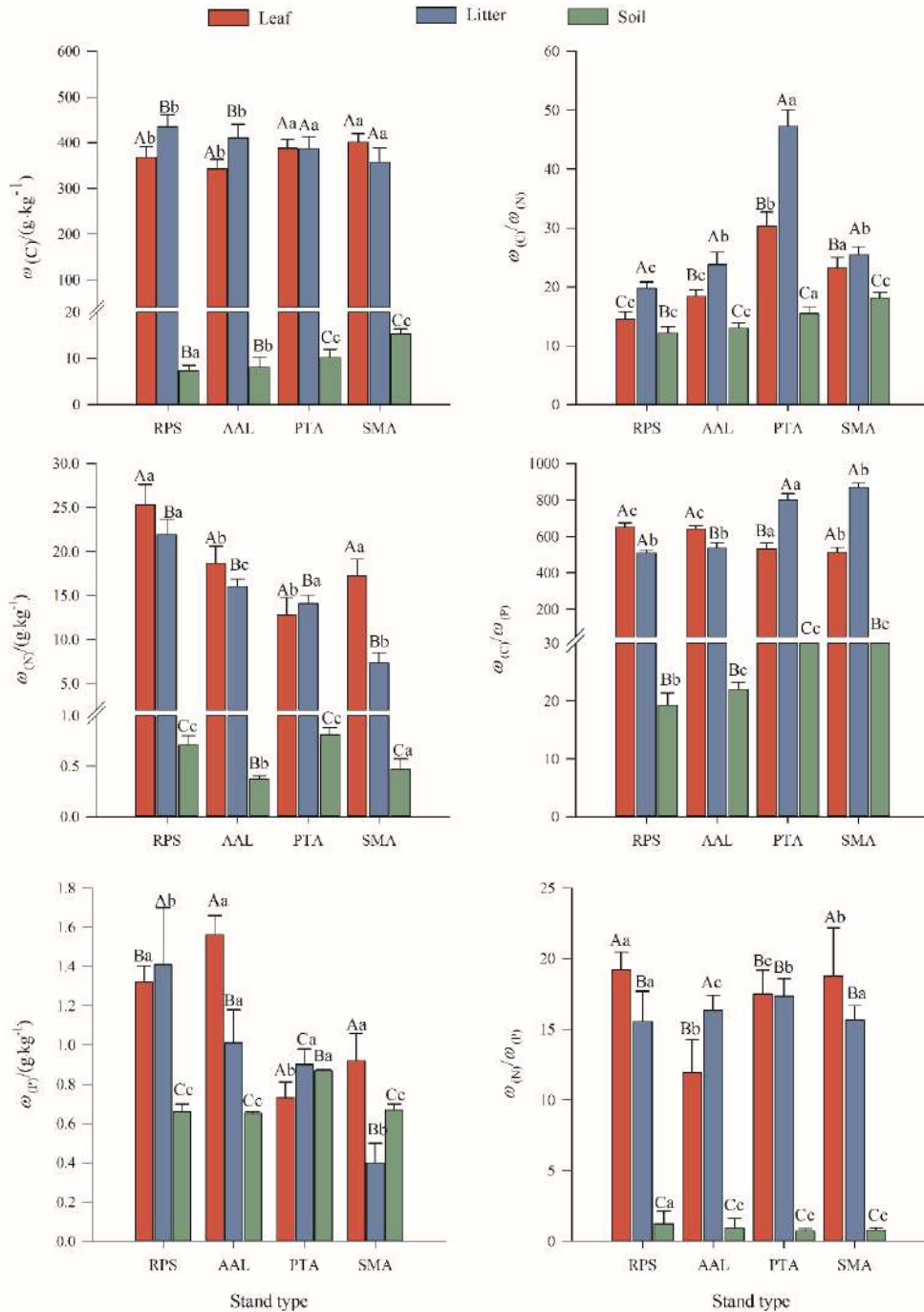


Fig. 1: Distribution characteristics of Carbon, nitrogen, phosphorus contents, C: N, C: P, and N: P of different components in the plantations.

Note: RPS, PTA, AAL, and SMA respectively represent *Robinia pseudoacacia*, *Pinus tabuliformis*, *Ailanthus altissima*, and *Salix matsudana*, Different small letters in the same component meant significant differences among different species, and different capital letters in the same species meant significant difference among different components at 0.05 level.

## Correlation Analysis of the Content and Ratios of C, N and P

Pearson correlation analysis on nutrient concentration and stoichiometric characteristics of leaf litter soil showed that the correlation was close between C, N, and P of three broad-leaved trees (Table 3), N value of *R. pseudoacacia* was a significantly positive correlation between leaf and litter ( $P < 0.05$ ), N value of *A. altissima* forest and *S. matsudana* forest was a significantly positive correlation between soil and litter ( $P < 0.05$ ). As shown in Table 4, N: P of *R. pseudoacacia* and P of *A. altissima* have a significant negative correlation between litter and soil, N and P content of *R. pseudoacacia* leaves and litter has a significant correlation, C, N, P and the stoichiometric characteristic ratio of *P. tabulaeformis* have no significant correlation between leaves and litter, leaves and soil, litter and soil. On the whole, N content was positively correlated between leaves and litter, and the ratios of C:N, C:P, and N: P in the litter layer were not significantly correlated with the ratios of C:N, C:P and N:P in the soil layer. In this study, soil C: N, C: P, and N: P had a very significant correlation with the content of SOC and TN ( $P < 0.01$ ) (Table 5), which indicated that the content of SOC and TN was a factor affecting the stoichiometric ratio of C, N, and P, and there was a coupling among C:N, C:P, and N:P.

## DISCUSSION

### Changes of C:N, C:P, and N:P in the Leaf-Litter-Soil in Differently Stands

C, N and P are essential nutrients for plant growth and development, and their contents can affect plant growth (Güsewell 2004). In this study, *P. tabulaeformis* forest and *S. matsudana* forest are significantly higher than *R. pseudoacacia* forest and *A. altissima* forest. The results show that the average C content of each organ of the coniferous tree is 1.6% - 3.4% higher than that of a broad-leaved tree (Ma et al. 2002). The results of this study are consistent with that of this study. The N content of *R. pseudoacacia* is rich because of its biological characteristics of nitrogen fixation. In addition, the N and P content of *R. pseudoacacia* leaves and litter are also higher than that of *Pinus tabulaeformis*. The content of N and P in leaves showed a significant positive correlation, which was affected by their own properties and biological characteristics of tree species, indicating that there was a coupling between N and P of different tree species (Elser et al. 2003). Plants absorbed the nutrient elements needed for their growth from the soil and synthesized organic compounds continuously through the photosynthesis of leaves, and the leaves withered to the ground in the form of litter after completing

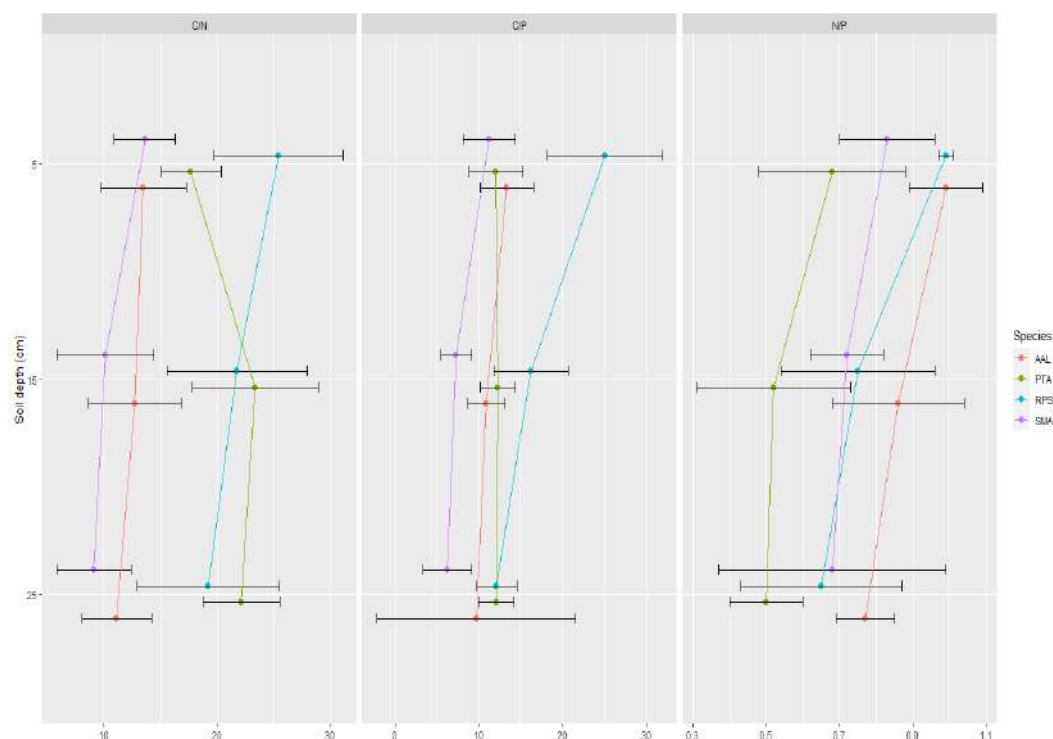


Fig. 2: C, N, P stoichiometric ratio at the different soil depths in the various stand types.

Table 3: Correlation coefficients between C, N, and P of different forests.

Element	Composition	RPS	AAL	PTA	SMA	Overall
C	Leaf and litter	0.53	-0.14	0.46	-0.56	-0.31
	Leaf and soil	0.22	0.22	0.51	0.68	0.47
	Litter and soil	0.57	0.16	-0.21	-0.47	0.14
N	Leaf and litter	0.87*	0.68	0.57	0.13	0.76**
	Leaf and soil	0.42	0.13	0.69	0.32	0.29
	Litter and soil	0.56	0.79*	0.38	0.59*	0.39
P	Leaf and litter	0.79*	0.17	0.59	-0.31	0.22
	Leaf and soil	-0.23	0.32	0.41	0.68	0.38
	Litter and soil	-0.69	-0.69	-0.23	0.44	-0.45

Note: \* indicates significantly related,  $P < 0.05$ ; \*\*indicates highly significantly related,  $P < 0.01$ .

Table 4: Correlation coefficients between the stoichiometric ratio of C, N, and P of different forests.

Element	Composition	RPS	AAL	PTA	SMA	Overall
C:N	Leaf and litter	0.89**	0.57	0.55	-0.63	0.11
	Leaf and soil	0.73**	0.46	-0.61*	-0.52	0.29
	Litter and soil	0.56	0.31	0.44	0.63	0.34
C:P	Leaf and litter	0.49	-0.16	-0.72	0.81*	0.27
	Leaf and soil	0.52	0.15	0.68	0.62	0.55
	Litter and soil	0.66	0.19	0.56	0.53	0.61
N:P	Leaf and litter	0.47	0.34	0.45	-0.18	0.33
	Leaf and soil	-0.60	0.44	0.72	-0.38	0.38
	Litter and soil	-0.59*	0.31	-0.17	0.45	-0.58

Note: \* indicates significantly related,  $P < 0.05$ ; \*\*indicates highly significantly related,  $P < 0.01$ .

the biological life cycle (Koerselman & Meuleman 1996, Clinton et al. 2002).

In this study, the content of litter C, N, and P in *R. pseudoacacia* forest was the highest, while that in *P. tabulaeformis* forest was the lowest, which was consistent with the content of N and P in leaves. The correlation analysis showed that there was a significant positive correlation between the content of litter N and P in leaves, and there were significant differences in the release patterns of P elements in different tree species (Huang et al. 2007). In addition, N: P ratio of litter in *Ailanthus altissima* plantation was the lowest among the four tree species, which might be beneficial to nutrient storage due to its small leaf type and easy decomposition and return to the soil (Knecht 2004). The average content of N and P in the plain plantation soil in the study area is lower than the national average content of 1.88 g.kg<sup>-1</sup> and 0.78 g.kg<sup>-1</sup> (Ren et al. 2018), which is generally in the lack of total nitrogen, which is consistent with the research results of Zheng et al. (2018). The lowest value of *Pinus tabulae-*

*formis* is 0.47 g.kg<sup>-1</sup>, which indicates that the ability of soil nutrient storage is poor, which is related to the characteristics of coniferous tree species of *P. tabulaeformis*. Because the leaf life of the evergreen coniferous forest is longer than that of the deciduous broad-leaved forest, the amount of leaf litter is less in the same years, and the acid environment formed by the decomposition of coniferous litter will inhibit the activity of soil microorganisms, which is not conducive to soil N, P accumulation (Bao et al. 2018). Soil C and N contents of different types of forests decrease with the increase of soil depth, and the content of 0-10 cm in the soil surface is the highest, showing the phenomenon of "surface accumulation", which is related to the high microbial activity in the soil surface (Su et al. 2016), and the nutrients returned by litter are mainly concentrated in the surface soil. As Fig. 3 shows, C:N is higher than the Chinese forest soil average, and C:P and N:P are lower than the Chinese average, which further verifies the lack of soil phosphorus, indicating that the content of soil SOC and TN is the factor affecting the stoichiometric

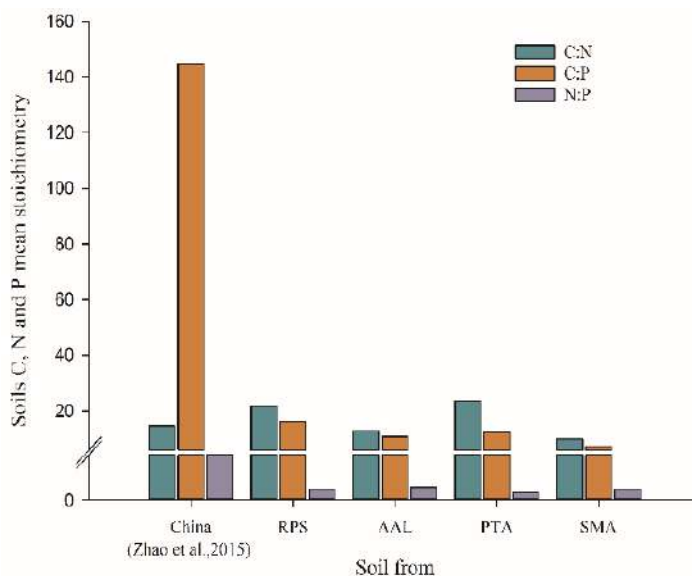


Fig. 3: Soils C, N, and P stoichiometry for this study compared with Chinese forest soil average (reference Zhao et al. 2015) level.

ratio of soil C, N, and P. There is no correlation between the stoichiometric ratio of the litter layer and the stoichiometric ratio of the soil layer, which indicates that simply increasing the quantity and quality of litter does not necessarily improve the soil nutrients, so it is very important to change the quality of litter layer in forest management.

### Correlations of Stoichiometric Ratios with Concentrations or Ratios of C, N, and P

In this study, N: P of different components of *R. pseudo-acacia* forest is the largest of four tree species, in which

N: P of leaves and litter is significantly higher than that of soil, C: N and C: P of *R. pseudoacacia*, *A. altissima*, and *P. tabulaeformis* litter are higher than that of leaves. Plants absorb N and P from the soil and re-absorb N and P through the nutrient reabsorption process before leaves fall. In this study, we found that the total N content of plantation was a significantly positive correlation between leaves and litter, which indicated that plants fixed organic matter by photosynthesis and returned nutrient elements to the soil in the form of litter after completing their life cycle (Hobbie 1992, Liu et al. 2010, Sardans et al. 2011). As an important physiological

Table 5: Multi-Factor Analysis of Variance between its stoichiometric ratio and soil factors.

Species	Variables	pH	MC	SOC	TN	TP
RPS	Soil C:N	0.14	0.10	0.63	-0.78**	0.40
	Soil C:P	0.27	0.08	0.72*	0.49	0.51
	Soil N:P	0.22	0.11	0.53	0.53	0.63*
AAL	Soil C:N	0.31	0.24	0.74*	-0.55*	0.24
	Soil C:P	0.25	0.21	0.69	0.43	0.54
	Soil N:P	0.24	0.24	0.58	0.83	0.51
PTA	Soil C:N	0.27	0.19	0.81**	-0.61**	0.22
	Soil C:P	0.32	0.22	0.74*	0.37	0.62
	Soil N:P	0.64	0.17	0.46	0.75	0.48
SMA	Soil C:N	0.13	0.31	0.66*	0.12	0.17
	Soil C:P	0.35	0.24	0.71	0.44	0.31
	Soil N:P	0.33	0.16	0.69	0.57*	0.58

Notes: \* indicates significantly related,  $P < 0.05$ ; \*\* indicates highly significantly related,  $P < 0.01$ . MC, Moisture content; SOC, soil organic carbon; TN, total nitrogen; TP, total phosphorus; AN, alkali-hydrolyzable.



index, C: N and C: P can reflect the growth rate of plants. Generally speaking, the plant growth rate characterized by low C: N and C: P is faster (Elser et al. 2003). Generally, the higher the C: N ratio, the slower the mineralization of soil organic matter. On the other hand, the ratio can be used to estimate the balance of soil C and N nutrition (Van de Waal et al. 2010). The C: N and C: P values of the leaves of *P. tabulaeformis* are higher than those of other tree species, indicating that the growth rate of *P. tabulaeformis* is lower. *P. tabulaeformis* is suitable for an acid and neutral soil environment, but if there is a lot of construction waste in the soil, not excluding the lime component will have a bad impact on *Pinus tabulaeformis*. According to the judgment standard that when N:P > 16 represents the P limit, N:P < 14 represents the N limit (Tessier et al. 2003), the growth of *R. pseudoacacia*, *P. tabulaeformis*, and *S. mandshurica* plantation in this study is limited by P, and the growth of *A. altissima* is limited by N. As an evergreen coniferous forest plant, *P. tabulaeformis* has poor decomposition capacity of plant residues and different root distribution characteristics from other broad-leaved trees (Liu et al. 2010), so the correlation between leaves and litter of *P. tabulaeformis* and soil nutrient elements is relatively small. In addition, the number of dead branches and leaves of conifers is relatively small, decomposition is slow, and the return of nutrient elements to the soil is less (An et al. 2010, Tian et al. 2010). The coordination of stoichiometry among index variables of different components can facilitate the interpretation of the coupling process among nutrients.

## CONCLUSIONS

The cycle of C, N, and P in a forest ecosystem is the mutual transformation among plants, litter, and soil, which indicates that there is mutual transportation and transfer of N and P between leaves, litter, and soil in a plantation ecosystem. Although C, N, and P stoichiometry have proved useful in studies of nutrient limitation, our objective is to better understand nutrient controlling factors of plant-soil interaction and reveal interactions of N and P to provide insight and theoretical fundamentals for forest environmental governance. Based on the study, the following conclusions may be drawn:

1. The N content in leaves, litter, and soil of *R. pseudoacacia* forest is significantly higher than that of the other three tree species. In contrast, *R. pseudoacacia* is the most suitable tree species for afforestation in the Beijing plain. The C, N content and stoichiometric ratio of plantation soil (0-10 cm) the highest, and their significant difference decreases with the increase of soil depth. There is no significant correlation between litter and soil stoichiometric ratio.
2. In terms of nutrient limitation, since one nutrient that is

more stable and less sensitive to environmental gradients would be more easily a limiting factor to plant growth, the growth of *R. pseudoacacia* forest, *P. tabulaeformis* forest, and *S. matsudana* forest is limited by P, while that of *A. altissima* forest is limited by N.

3. To ensure that the artificial forest can play its ecological function, we should pay attention to the use of nitrogen fertilizer when tending the artificial forest in the plain area. First, combine the nutrient concentration and stoichiometry ratio of the leaves of each tree species to analyze, with the help of long-term monitoring, to reveal the influence of tree species on the soil nutrient and the dynamic transformation of nutrients between the soil litter leaves under the forest in the plain area. Second, ensure the healthy growth of ecological trees in the plain, increase the return of soil organic matter, and promote nutrient cycling. Third, strengthen the supervision of plain ecological forest land, prohibit dumping and stacking construction and domestic garbage in the forest land, and prevent the variation of soil structure, texture, and chemical properties. Finally, we should consider reducing "clearing forest", pay attention to the protection of the dead branches and leaves of forest land to return the soil and undergrowth vegetation, and increase the accumulation of litter properly, which is conducive to the accumulation of C and N.

## ACKNOWLEDGMENTS

The authors gratefully acknowledge the reviewers and editors who contributed to this article. This research was funded by the Reform Project of New Agricultural Science Research and Practice of Henan Province in 2020, grant number 2020JGLX152.

## REFERENCES

- Agren, G. 2007. The C:N:P stoichiometry of autotrophs-theory and observations. *Ecol. Lett.*, 20: 7.
- An, Y., Wan, S. and Zhou, X. 2010. Plant nitrogen concentration, use efficiency, and contents in a tallgrass prairie ecosystem under experimental warming. *Glob. Change Biol.*, 11(10): 1733-1744.
- Bao, Y., Ying, G. and Xiao, M. 2018. Relationships between carbon and nitrogen contents and enzyme activities in the soil of three typical subtropical forests in China. *Chin. J. Plant Ecol.*, 42(4): 508-516.
- Brant, A.N. and Chen, H.Y.H. 2015. Patterns and mechanisms of nutrient resorption in plants. *Crit. Rev. Plant Sci.*, 34: 471-486.
- Bui, E.N. and Henderson, E.N. 2013. C:N:P stoichiometry in Australian soils with respect to vegetation and environmental factors. *Plant Soil*, 373: 553-568.
- Chang, R.Y., Fu, B.J., Liu, G.H. and Liu, S.G. 2011. Soil carbon sequestration potential for the "Grain for Green" project in Loess Plateau, China. *Environ Manage.*, 48: 1158-1172.
- Cleveland, C.C. and Liptzin, D. 2007. C:N:P stoichiometry in soil: Is there a "Redfield ratio" for the microbial biomass? *Biogeochemistry*, 85: 235-252.

- Clinton, P.W., Allen, R.B. and Davis, M.R. 2002. Nitrogen storage and availability during stand development in a New Zealand *Nothofagus* forest. *Can. J. For. Res.*, 32: 344-352.
- Cui, Y.P., Liu, J.Y. and Qin, Y.C. 2015. The impact of urban sprawl on heat island intensity in Beijing [J]. *Chin. J. Ecol.*, 34(12): 3485-3492.
- Drenovsky, R.E., Pietrasiak, N., Short, T.H. and Silva, T. 2019. Global temporal patterns in plant nutrient resorption plasticity. *Glob. Ecol. Biogeogr.*, 28: 728-743.
- Elser, J.J., Acharya, K., Kyle, M., Cotner, J., Makino, W. and Markow, T. 2003. Growth rate-stoichiometry couplings in diverse biota. *Ecol. Lett.*, 10: 936-943.
- Elser, J.J., Bracken, M.E.S. and Cleland, E.E. 2007. Global analysis of nitrogen and phosphorus limitation of primary producers in freshwater, marine, and terrestrial ecosystems. *Ecol. Lett.*, 10(12): 1135-1142.
- Fanin, N., Fromin, N. and Buatots, B. 2013. An experimental test of the hypothesis of non-homeostatic consumer stoichiometry in a plant litter-microbe system. *Ecol. Lett.*, 16(6): 764-772.
- Fu, B.J., Chen, L.D., Qiu, Y., Wang, J. and Meng, Q.H. 2002. *Land Use Structure and Ecological Processes in the Losses Hilly Area*. Chinese Commercial Press, Beijing.
- Güsewell, S. and Verhoeven, J.T.A. 2006. Litter N:P ratios indicate whether N or P limits the decomposability of graminoid leaf litter. *Plant Soil*, 287: 131-143.
- Hobbie, S. 1992. Effect of plant species on nutrient cycling. *Trends Ecol. Evol.*, 7: 336-339.
- Huang, J., Wang, X. and Yan, E. 2007. Leaf nutrient concentration, nutrient resorption, and litter decomposition in an evergreen broad-leaved forest in eastern China. *For. Ecol. Manage.*, 239(1): 150-158.
- Koerselman, W. and Meuleman, A.F.M. 1996. The vegetation N: P ratio: A new tool to detect the nature of nutrient limitation. *J. Appl. Ecol.*, 33(6): 1441-1450.
- Liu, X.Z., Zhou, G.Y. and Zhang D.Q. 2010. N and P stoichiometry of plant and soil in lower subtropical forest successional series in southern China. *Catena*, 34 (1): 64-71.
- Lü, Y.H. 2012. A policy-driven large-scale ecological restoration: Quantifying ecosystem services changes in the Loess Plateau of China. *PLoS One*, 7: e31782.
- Ma, Q.Y., Chen, X.L. and Wang, J. 2002. Carbon content rate in constructive species of main forest types in northern China[J]. *J. Beij. Forest. Univ.*, 24(5): 96-100.
- Makino, W., Cotner, J.B., Sterner, R.W. and Elser, J.J. 2003. Are bacteria more like plants or animals? Growth rate and resource dependence of bacterial C:N:P stoichiometry. *Func. Ecol.*, 17: 121-130.
- Ren, Y., Gao, G.L. and Ding, G.D. 2018. Stoichiometric characteristics of nitrogen and phosphorus in the leaf-litter-soil system of *Pinus sylvestris* var. *Mongolica* plantations. *Chin. J. Appl. Ecol.*, 30(3): 743-750.
- Sardans, J., Rivas-ubach, A. and Penuelas, J. 2011. Factors affecting nutrient concentration and stoichiometry of forest trees in Catalonia (NE Spain). *For. Ecol. Manag.*, 262(11): 2024-2034.
- See, C.R., Yanai, R.D., Fisk, M.C., Vadeboncoeur, M.A., Quintero, B.A. and Fahey, T.J. 2015. Soil nitrogen affects phosphorus recycling: foliar resorption and plant-soil feedbacks in a northern hardwood forest. *Ecology*, 96: 2488-2498.
- Su, H.J., Wu, Y. and Xie, P. 2016. Effects of taxonomy, sediment, and water column on C:N:P stoichiometry of submerged macrophytes in Yangtze floodplain shallow lakes, China. *Environ. Sci. Pollut. Res.*, 23(22): 577-585.
- Tessier, J.T. and Reynal D.J., 2003. Use of nitrogen to phosphorus ratios in plant tissue as an indicator of nutrient limitation and nitrogen saturation. *J. Appl. Ecol.*, 40: 523-534.
- Tian, H.Q., Chen, G.S., Zhang, C., Melillo, J.M. and Hall, C.A.S. 2010. Pattern and variation of C:N:P ratios in China's soils: a synthesis of observational data. *Biogeochem.*, 98: 139-151.
- Uchida, E., Rozelle, S. and Xu, J. 2009. Conservation payments, liquidity constraints, and off-farm labor: impact of the Grain-for-Green Program on rural households in China. *Am. J. Agr. Econ.*, 91, 70-86.
- Van de Waal, D.B., Verschoor, A.M. and Verspagen, J.M.H. 2010. Climate-driven changes in the ecological stoichiometry of aquatic ecosystems. *Front. Ecol. Environ.*, 8(3): 145-152.
- Wright, I.J., Reich, P.B. and Cornelissen, J.H.C. 2010. Assessing the generality of global leaf trait relationships. *New Phytol.*, 166(2): 485-496.
- Zhao, F.Z., Han, X.H., Yang, G.H., Feng, Y.Z. and Ren, G.X. 2014. Soil structure and carbon distribution in the subsoil are affected by vegetation restoration. *Plant Soil Environ.*, 60: 21-26.
- Zheng, Y. L., Wang, H.Y. and Xie, Y. L. 2018. Effect of tree species on soil fertility quality in plain afforestation area, Beijing. *Sci. Soil Water Conserv.*, 16(06): 89-98.





# Application of Material Flow Analysis to Municipal Solid Waste in Urban Areas in Developing Countries and Possible Solutions Under Circular Economic Framework

N. A. Hemali† and A. A. P. De Alwis

Department of Chemical & Process Engineering, University of Moratuwa, Sri Lanka

†Corresponding author: N. A. Hemali; arosha.hemali@gmail.com

Nat. Env. & Poll. Tech.  
Website: [www.neptjournal.com](http://www.neptjournal.com)

Received: 07-10-2021

Revised: 13-12-2021

Accepted: 19-12-2021

## Key Words:

Material flow analysis  
Municipal solid waste  
Material circularity

## ABSTRACT

The understanding waste flow of a country is important to identify the main problems associated with waste management and identify opportunities in material flow management. A tool such as material flow analysis (MFA) is a widely used method in waste management studies, to provide a comprehensive analysis of material movements, support for material characterization analysis to identify the severity of a problem, identify the real root cause, and propose suitable management methods. This paper presents an application of MFA for municipal solid waste (MSW) management in Western provinces in Sri Lanka. The outcome includes the identification, and quantification of the main input and output flows of the system in the present context, from waste generation, collection, unaccounted and unidentified flows, material recovery, and final disposal of MSW. Results are evaluated under treatment mechanisms of Recycling, Reusing, and repurposing the materials.

Overall results show per capita per day of waste generation in Sri Lanka stood at 0.43 kg, whereas, the Western province represents that 0.56 kg due to the high population area with the highest rate of urbanization. However, the global average per capita per day of waste generation stood at 2.22 kg. The material and energy recovery represent 31% and 33% respectively in the study area from total collected waste. 36% of the material finally ended up in open dumpsites even after collection. Further research needs to be done on material and energy recovery potential identification in dumping waste, as this can convert to valuable results with proper management practices with available resources.

## INTRODUCTION

Rapid economic growth, urbanization, and increasing population have caused (material-intensive) resource consumption to increase, and the consequent release of large amounts of waste to the environment. The current waste and resource management system lack a holistic approach that covers the entire chain of product design, raw material extraction, production, consumption, recycling, and waste management.

In 2018, it was estimated that MSW generation is expected to grow 3.4bn Mt by 2050 given the way things are handled at present. By 2050, the amount of waste generated in developing countries will see a threefold increase (Kaza et al. 2018). Asia and the Pacific region will generate most of the world's waste- a considerable 23%. In developing nations, food and green waste amount to more than 50%. Recyclables such as paper, cardboard, plastic, metal, and glass make up a substantial fraction of waste streams, ranging from 16% in developing countries to about 50% in developed countries.

In Sri Lanka, more than 60 % of municipal solid waste is a bio-degradable organic material and the rest is non-bio-degradable materials (Visvanathan et al. 2006). There is no proper segregation of waste at the household level before disposal (Warunasinghe & Yapa 2016). Also highlighted, there is a vital need to have in place an integrated solid waste management system in the country (Bandara 2011)

## PAST STUDIES

The composition of MSW includes food waste, paper, biomass, glass, metals, plastics, rubbers, and textiles. (Ashani et al. 2020). The technologies discussed include Recycling (Ragaert et al. 2017), Composting (Bekchanov & Mirzabaev 2018), pyrolysis (Lu et al. 2020), Refused Derived Fuel (RDF) for co-fueling, and Waste to Energy (WTE) (Anoop et al. 2016), which are practicing for Municipal Solid Waste management.

The technologies are categorized into material recovery (Recycling, Composting & Pyrolysis), and energy recovery (RDF, and WTE). The technology mentioned

is discussed accordingly with its pros and cons being highlighted.

Recycling is the process of converting waste materials into new materials and objects in a mechanical process or chemical process (Ragaert et al. 2017). The recyclability of a material depends on its ability to reacquire the properties it had in its original state. This can apply to main material types such as plastic, metal, glass, rubber, and compostable bio-degradable materials.

Pyrolysis is the thermal process in the absence of oxygen that breakdowns the long chain of polymer molecules into smaller, less complex molecules at a temperature higher than 400°C, with oil, gas, and char as the main products (Lu et al. 2020).

MSW which are received as mixed form can be diverted to RDF this can substitute alternative fuel in the WTE process or thermal intense processes such as cement and glass manufacturing. It is recommended to separate biological waste at the source to lower moisture and ash content and increase heating value for potential fuel production from waste (Arina et al. 2020).

Materials flow analysis (MFA) has been extensively applied for environmental research, particularly in waste management to identify material chain composition and the stages of the supply chain. In previous studies, many articles were found in other countries on MFA for quantifying the material flow and accumulation of tire waste in Thailand, (Jacob et al. 2014), analytics to make decisions on waste management policy (Allesch & Brunner 2015), as the MFA for assessing solid waste management in Germany (Hartlieb et al. 2005), MFA to evolve the waste management solution in Oahu, Hawaii (Matthew & Marian 2009), derived the results of a municipal solid waste management planning based on an extensive utilization of material and substance flow analysis (Arena & Gregorioa 2014), MFA is used to assess the current status of MSW management system in Lahore, Pakistan (Masood et al. 2014), MFA to draw plastic flow in Austria and Poland for presenting plastic waste management (Bogucka et al. 2008), MFA to assess the amount of plastic materials flow and stock in Serbia (Vujić, 2010). Similarly, there is a study on using the MFA method as a tool to monitor the flow and stock of Thailand, whereas the work is aimed to deploy planning on plastic waste management (Chanchampee 2010). Most of the past studies supported policymakers in waste management. However, there was no study using MFA for MSW which supports policymakers in Sri Lanka to identify the application of results of MFA for integrated material and energy recovery technologies.

## RESEARCH OBJECTIVE

At present, the responsibility to manage the MSW falls under

the purview of the local government network constitutes 24 Municipal Councils, 41 Urban Councils, and 276 Divisional Councils in the country. However, different local government bodies follow different waste management activities based on their capabilities instead of having an integrated waste management system throughout the country. Hence, to establish an integrated waste management system, a proper evaluation of the waste material flow is essential. Based on the material categorization waste management technologies can be defined.

Given this context, this study focuses on the waste generation volumes, characterization, waste management, and waste material recovery potential in the municipal solid waste in Western Province in Sri Lanka. The research results will facilitate the identification of the potential in terms of waste management solutions for mismanaged waste. Simulation of possible material and energy recovery options are presented under the study based on the Circular Economic framework. Further, the study will promote material recovery options and contribute to future research in terms of finding solutions for mismanaged waste in the household waste material chain. The study area records 25 open dumping sites and the dumped waste is collected through a channel operated by local authorities, which is the key institutional setup to handle waste in Sri Lanka. The authors aim to identify potential material recovery and energy recovery which are currently in these sites. The results are expected to be useful for the authorities who are involved in policymaking on waste management, to careful planning on the waste management policy framework.

## MATERIALS AND METHODS

### Study Area

Sri Lanka's Western Province (WP) which has a population of 5.8 million (amounts to 27% of the country's entire population) was selected as the pilot study area as per

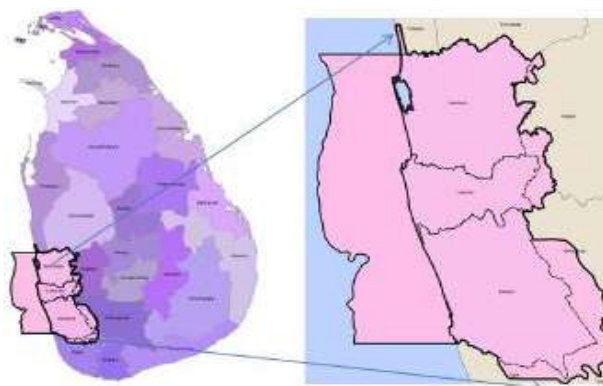


Fig. 1: Western Province, Sri Lanka.



Fig. 1. The Western Province constitutes about 6 % of the land area in Sri Lanka and accommodates the highest population among the other provinces. It produces more than 39% of the total GDP of Sri Lanka thereby making a significant contribution to the national economy (Central Bank of Sri Lanka (CBSL) 2019). The dense population coupled with rapid development in this area had led to a considerable increase in the generation of MSW.

The waste generation in Sri Lanka has increased from around 6,400 tons per day in 1999 to 10,768 tons per day in 2021 due to population increase, economic growth, and the end of the civil war (Ministry of Environment (MOE) Sri Lanka 2021). Among the nine provinces in the country, the generation amount of the Western Province is the largest, accounting for 40% of the total waste generation while that of other provinces contributes to 60% of total generation.

**Material Flow Analysis (MFA)**

The study uses Material Flow Analysis (MFA) to identify the waste material chain from the household level to final disposal in the pilot area. MFA is an analytical method to quantify flows and stocks of materials or substances in a well-defined system (Hunt et al. 2014). This is based on the law of mass conservation. and is the widely used methodology in waste material flow analysis in most of the research (Allesch & Brunner 2015, Gehrman et al. 2017). It has been widely applied for environmental education, particularly in waste management as analytics to make decisions on various issues related to waste-related analysis.

The mass that enters a system must, by conservation of mass, either leave the system or accumulate within the system. Mathematically, the mass balance for a system is as follows in equation 1;

$$\sum_{k_I} \dot{m}_{input} = \sum_{k_O} \dot{m}_{output} + \dot{m}_{storage} \quad \dots(1)$$

where the number of the system flow is denoted by k, I, and O are input and output and denotes flow or flux. In general,  $\dot{m}_{storage}$ , or stock is calculated by the difference in input and output from the overall system. In this research, a material balance approach was adopted as the main methodology to investigate the stocks and flows of waste generation (Brunner et al. 2017). The basic mass balancing principle is applied.

**Calculation of Waste Recovery Percentage**

This study applies the principles of circular economy to assess the waste material recovery factor. A circular economy is an economic system aimed at eliminating waste while continuously regenerating resources (Tamine et al. 2020). Progress toward a circular economy should include not only

responsible use of natural resources but also enabling reuse, repurposing, recycling, and recovery of the value-locked materials traditionally viewed as waste (Bouton et al. 2016).

The waste recycling factor was developed using the following equation 4 supported with material flow structure as per fig. 2:

$$\sum_a^n [CaR(P + T + Pl + R + M + G) + CaCoCm + CmaCm - Bua - Bra - Da - Oo - CaL] \quad \dots(2)$$

Where a is the total MSW generation at the area an (area can be a province) in tons per day.

Ca- MSW collection percentage by local authorities

R- MSW recyclable volume percentage out of the collection  
Co- Compostable material percentage out of collected volumes by local authorities.

P, T, Pl, R, M, G, Cm are the percentage of recyclable volumes percentages in Paper, Textile, Plastic, Rubber, Metal, and Glass. and compostable material respectively at the waste yard.

Bua, Bra, Da, Oo L represents the Burn, Burry, Open dump & landfill respectively

To identify the total recyclable material percentage out of the whole MSW generation.

Where total MSW generation

$$\sum_a^n [a + \dots + n] \quad \dots(3)$$

Therefore, the portion of the recyclable volume is given by:

$$\text{Equation (2)/Equation (3)} \quad \dots(4)$$

**Data Collection Procedure**

The system boundary identified for the study includes the

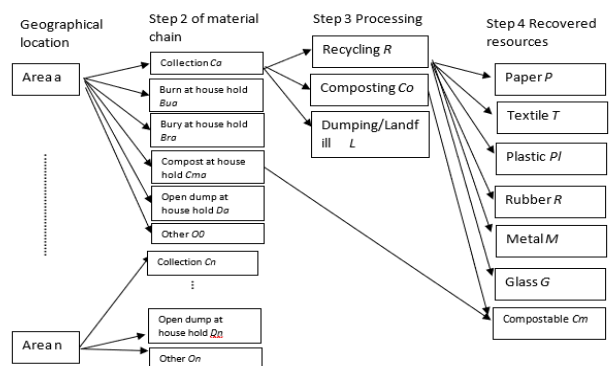


Fig. 2: Material flow structure.

household waste generation point to final disposal as per Fig. 2. The required data for analysis was obtained through the identification of municipal solid waste generation and waste management practices as well as types and quantity of wastes and disposal methods.

The generated waste materials in the study area were characterized. Furthermore, the required information to study the composition and management status of waste was obtained through published surveys, questionnaires, interviews, and feedback from local authorities as per the framework in Fig. 3. Author's survey data used for Western Province.

## RESULTS AND DISCUSSION

### Materials Follow the Analysis of Waste Generation, Collection, And Primary Treatment.

Fig. 4 shows the WP household level waste generation and primary disposal methods. The waste material flow was analyzed to identify material composition at different points of the material chain. Step 1 of Fig. 4 represents the disposal methods at the household level. 58% of the total waste generation gets collected by the local authority waste collection channel. 38% is identified as a burn or burry at the household level where the results of the study highlight the need for further research on unaccounted and unidentified material composition under burry and burn.

Overall results of the study show per capita waste generation of WP represents 0.56 kg per day whereas in Sri Lanka stood at 0.43 kg per day. Also, it is stated that the pattern of waste generation in different countries in the same continent or different provinces/states in the same country is not the same (Adeleke et al. 2020). There is a direct relationship between population and urbanization to waste generation (The World Bank n.d) reflects in the data for the study scope. Another study done for Indonesia shows the direct relationship between waste generation to population (Supangkat & Herdiansyah 2020). However, as per the literature, various

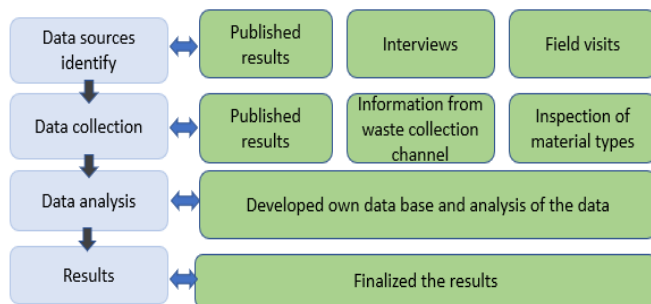


Fig. 3: Methodological framework for data identification, collection and analysis.

models have been developed to predict waste generation using input variables such as population (Liu & Yu 2007, Oumarou et al. 2012), income level (Thanh 2010, Liu & Yu 2007), and education (Keser et al. 2012).

The dense population coupled with rapid development in this area had led to a considerable increase in the generation of municipal solid waste. Therefore, the main waste management system requirement is essential for WP.

The collection mainly happens in the western province, being the key economic hub of the country. At present, the responsibility to collect municipal solid waste falls under the purview of the local government network under the ministry of Local government and provincial councils.

However, different local government bodies follow different waste management activities based on their capabilities instead of having an integrated waste management system throughout the country.

### Primary Waste Streams and Treatment Methods

In the results of the study presented in Table 1, each waste category in the selected location was prioritized by arranging them in descending order of magnitude. A Pareto chart is used for preliminary identification of the most significant waste streams. The outcome of the analysis is given in Table 1 presenting the results following the application of the Pareto principle. Fig 5 shows the waste generation in the study location (WP). The total waste generation accounted for 3248 tons per day, of which 1881 tons per day (58%) is collected by the collection channel.

The wastes stream quantities in the surveyed area were evaluated during the study. Biodegradable waste from kitch-

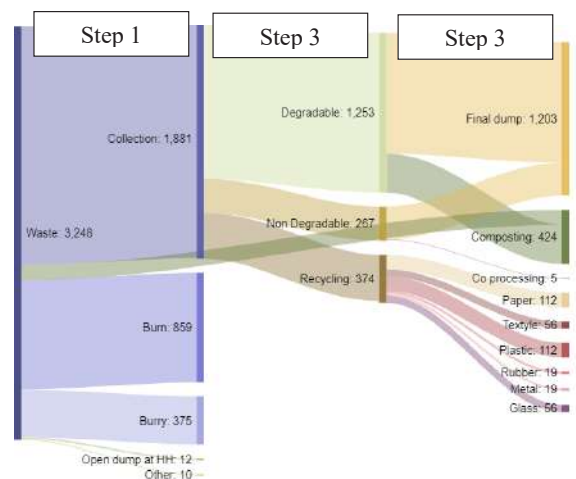


Fig. 4: Waste generation at house hold level in Western Province, Sri Lanka.

en waste accounted 52.5 % of the total wastes collected, followed by biodegradable grass and wood (14.1%), paper (13.6%), plastic (10.5%), textile (4.3%), stones & ceramic (2.3%), glass (1.2%), metal (0.7%) rubber (0.6%) and other mixed waste (0.3%). The remaining wastes constituted less than 5% of the total waste. The accuracy of results could be affected due to challenges with various data collection points of local authorities. The data in this instance is the associates with a visual inspection and judgmental understanding of the waste categories in the collection channel.

M1, M2, M3, M4, M5, and M6: represent material recovery methods whereas E1, and E2: represent energy recovery methods in Fig.5.

- Where M1- Composting
- M2- Recycling paper
- M3- Recycling Plastic
- M4- Recycling Glass

Table 1: Types of waste collection in Western Province, Sri Lanka.

Type of waste	Volume tons per day
Bio-degradable kitchen waste	987.5
Bio-degradable Grass and wood	265.2
Paper	255.8
Plastic	197.5
Textile	80.9
Stones & Ceramic	43.3
Glass	22.6
Metal	13.2
Rubber	11.3
Other	3.8

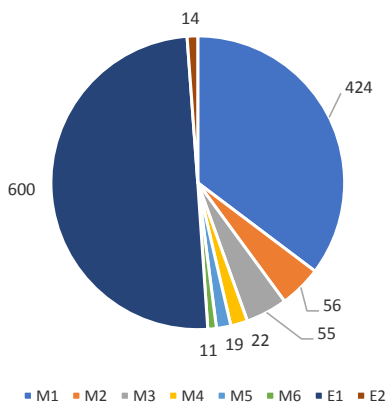


Fig. 5: Waste treatments (tons per day) of Western province, Sri Lanka.

- M5- Recycling Metal
- M6- Recycling Rubber/Pyrolysis
- E1- Waste to Energy (WTE)
- E2- RDF for Co-processing

As per Fig. 6, WTE represents 600 tons per day volume followed by 424 tons per day of composting, 56 tons per day of paper recycling, 55 tons per day of plastic recycling, 22 tons per day of glass recycling, 19 tons per day of metal recycling, 14 tons per day of RDF for co-processing and 11 tons per day of rubber pyrolysis under material recovery and energy recovery techniques. However, 19 tons per day of sanitary landfilling and 660 tons per day of open dumping at waste yards happen in the study areas which are not considered superior solutions for MSW management under the circular economic framework.

**Analysis of Waste Circulation Factor In Terms Of Material Or Energy Recovery**

Recovery can be categorized under material and energy recoveries. Composting, Recycling, and Pyrolysis (Lu et al. 2020) technologies consider material recovery techniques whereas Waste to Energy and RDF for Co-processing are considered energy recovery techniques (Arian et al. 2020). As per equation 4 of waste recovery percentage calculation, the following results were analyzed under material and energy recovery out of total waste collection and generation as per the results shown in Fig. 6 and 7.

**Material & Energy Recovery Out Of The Total Waste Material Collection**

As per Fig. 6, Material recovery technologies are considered based on waste material processed through Recycling, Composting & Pyrolyzing (Tang et al. 2020.). In WP material

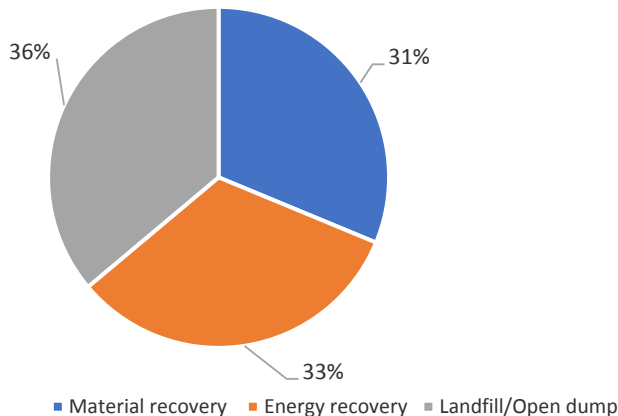


Fig. 6: Material & Energy recovery out of total MSW collection.

recovery is 31% in terms of Recycling of paper, plastic, glass, and metal, followed by composting for biodegradable waste and pyrolysis for rubber waste. 33% of the material disposed of under energy recovery techniques in terms of WTE via generation of electricity and RDF via co fueling for thermal intense industries such as cement production.

### Material and Energy Recovery Out Of Total Waste Generation

As per Fig. 7, 42% of the total waste generation is burned or burry at the household level causing environmental impacts on society. Common waste management practices found included open burning, burying, reusing, disposing of MSW in backyard pit, mixed waste disposal in the backyard, selling, and recycling. Most rural households in the world are still using traditional methods of managing waste, even though recommended waste management practices such as reusing and recycling were found in some households (Nxumalo et al. 2020).

### Waste Treatment Mechanisms

The following options are identified as the most common waste disposal methods used in the study area.

- Option 1: Composting
- Option 2: Recycling (Based on material type)
- Option 3: Pyrolysis
- Option 4: Waste to Energy
- Option 5: RDF for Co-processing
- Option 6: Sanitary landfilling
- Option 7: Open dumping

The proportions of primary waste disposal methods were calculated and are shown in Fig. 8.

### Waste composting

Of the total waste generation in the WP, 13% recovery is reported at waste composting (424 tons per day). There

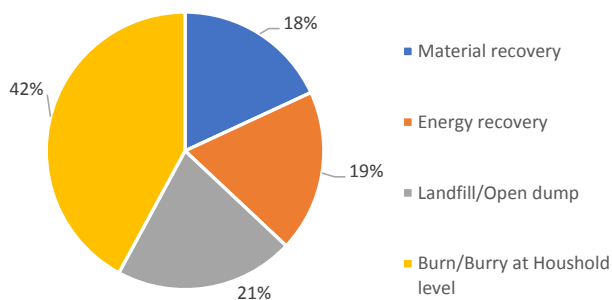


Fig 7: Material & Energy recovery out of total MSW generation.

is a potential to improve compostable volume in the area. Composting is a win-win option for reducing environmental pollution derived from the open dumping of waste and recovering nutrients essential for producing fertilizers (Bekchanov & Mirzabaev 2018).

The national strategy on waste management aims to redirect 19% of the organic waste generation into composting (Bekchanov & Mirzabaev 2018). This is amounting to 7% of total waste generation. In 2008 government introduced the Pilisaru program which aimed to establish composting plants throughout the country and currently there is 119 such plant in the county as to the ministry of environment. However, the efficiency of these plants is not up to the slandered.

There is a potential to improve compostable volume in the whole country being an agricultural-based society dominated in the rural areas, especially in Central, Southern, Northern, North Central, Sabaragamuwa, and Uva provinces. WP is the least agricultural-based area and represents less composting volumes than MSW. Composting is the second preferred method of solid waste management, mainly due to the high percentage of organic material in the waste composition.

### Waste recycling and repurposing

The study represents that recycling and composting are the main recovery methods adopted in the country for proper waste management even though recycling is not significant in volume. Material category wise paper, plastic, glass, metal, and rubber are considered potential recycling materials. However, the majority of the waste ends up at open dumps that need to be further evaluated for possible recyclable and repurposed materials. This is not under the scope of the study.

Most developed countries use Clean Material Recovery Facilities where clean sources segregated dry materials

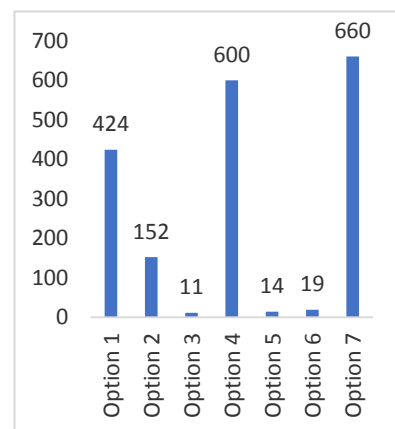


Fig. 8: The treatment methods of the primary waste streams (tons per day) in Western Province, Sri Lanka in Western Province, Sri Lanka.

are used. Source segregation is the less expensive method compared to treating mixed waste. Mostly in developing countries mixed waste is used for Dirty Material Recovery Facilities with the high cost involved during the processing stage. Hence most of the recovery and recycling techniques are not economical in developing countries, therefore less volume is diverted for recycling methods (Kaza et al. 2018).

Recent developments in the producer responsibility (PRO) model for post-consumer waste is supporting to increase in the recycling materials in the study area. The current recycle volume is 152 t per day.

**Waste Pyrolysis**

There are five pyrolysis plants in the country with an equal capacity of 10 t input per batch. Only one plant is in the study areas. However, 60% of the waste rubber generated from MSW in the sturdy area gets disposed of via all five plants. Apart from that industrial rubber waste is recycled through rubber industries which are out of the scope of the study. 11 tons per day of rubber volume is circulated back to the system in the study area.

However, there are other researches on energy-effective pyrolysis process with the lowest possible carbon footprint to realize the recycling of organic wastes, the generation of renewable energy, and the release of minimal quantities of greenhouse gas and pollutants from MSW treatments in the world (Lu et al. 2020)

**Waste to Energy**

Due to economic and industrial growth, the country needs more electric power. Therefore, reducing the volume of waste and at the same time generation of power out of it can be achieved by municipal waste to energy plants. There is one waste to energy (WTE) plant in the country, establish within the sturdy areas in 2021 with the capacity of disposing of 600 tons MSW volume disposal per day (this is further referred to in Fig 5). WTE is a widely practiced technology for MSW management in most developed countries, Environmental Protection Agency has stated that WTE technologies are clean reliable sources of renewable energy with less environmental impact than any other source of energy (Anoop et al. 2016).

The main drawback of WTE plants is pollutant emissions in general and in WP Sri Lanka W2E plants face a problem of final disposal of bottom ashes which is coming out of the system. but the plant is still not in full operation. In this study, however, energy waste is not considered a material recovery option. Meanwhile, incineration and landfilling are not considered the recovery option. Another study stated that recycling has high industrial potential and complementary

pathways for closing the loop on most of the waste categories and is vastly preferable to energy recovery and landfilling (Ragaert et al. 2017).

**RDF for Co-processing**

RDF is organic matter containing a high calorific fraction of processed MSW (paper, plastic, textiles, wood, rubber, and others) compatible with conventional fossil fuels or biomass with respect to calorific value. The use of RDF as a source of energy is an integral part of waste management and it is regulated by EU regulations (EU Parliament Directive 2008/98/EC on waste). RDF is becoming more and more attractive as an energy source as the necessity to increase the proportion of alternative energy use is becoming harder (Porshnov et al. 2018)

14 tons per day of volume is co-processed from the study area. There is a possibility to increase this volume further with proper waste segregation at the source.

**Sanitary Land Filling**

One small-scale landfill is operating in the study area with a capacity of 19 tons per day. The majority of MSW in the respective local authority area is disposed of in a landfill. There is a large-scale project to develop the divert large volumes to sanitary landfill situated over 100 km from the study area for disposal waste generation in a high populated area under study scope. However, this is currently not functioning.

**Waste Burning and Burying at the Household Level (HH)**

The results of the study highlight the need for further research on unaccounted and unidentified material flows involved in household-level burying and burning. This causes more harm to the environment and human beings.

Table 2: Waste composting percentages (as a percentage of total waste generation of the province).

Province	Composting % of total waste generation
Western	13.05%
Central	12.68%
North- Western	5.67%
Southern	18.17%
Northern	10.50%
Eastern	2.31%
North Central	7.36%
Sabaragamuwa	9.71%
Uva	14.51%



Common waste management practices found included open burning, burying, reusing, disposing of plastics in backyard pit, mixed waste disposal in the backyard, selling, and recycling. Most rural households in the world are still using traditional methods of managing waste, even though recommended waste management practices such as reusing and recycling were found in some households (Nxumalo et al. 2020).

Study results show that the most of waste is burnt at the household level in North Central, North Western, Northern, Southern, Uva, and Sabaragamuwa as per Table 3. This may lead to inadequate waste collection and a lack of awareness by the local authorities to the public.

## CONCLUSION

Municipal Solid Waste is the largest waste volume generation source in the country. However, this material has a huge potential in terms of waste recycling and reuse. An analysis of scientific literature discloses that the majority of municipal solid waste is burned or buried. Therefore, this study reflects on the importance of research in unaccounted and unidentified material flows involved in household-level burying and burning. Moreover, given that a large portion of collected waste is directed to open dumps, further study is required to evaluate the recycling potential of this element of waste.

A major factor that influences the rate of generated waste per year and the percentage composition of each physical waste stream is the socio-economic level. Moreover, the organic stream of the waste and the rate of recycling volumes depends largely on the income levels of the society.

Overall results show per capita per day of waste generation in Sri Lanka stood at 0.43kg, whereas, the Western

Table 3: Waste burning and burying percentages out of total generation in respective provinces.

Province	Waste burning % of the total waste generation of the respective province	Waste burying % of the total waste generation of the respective province
Western	27.16%	11.85%
Central	42.84%	26.73%
North- Western	61.26%	25.66%
Southern	48.63%	51.23%
Northern	56.98%	19.12%
Eastern	38.55%	20.22%
North Central	66.43%	20.45%
Sabaragamuwa	43.20%	39.72%
Uva	48.43%	28.58%

province represents that 0.56 kg due to the high population area with the highest rate of urbanization. However, the global average per capita per day of waste generation stood at 2.22 kg (USEPA 2021). The material and energy recovery represent 31% and 33% respectively in the study area from total collected waste. 36% of the material finally ended up in open dumpsites even after collection. Further research needs to be done on material and energy recovery potential identification in dumping waste, as this can convert to valuable results with proper management practices with available resources.

## REFERENCES

- Adeleke, O.A., Akinlabi, S.A., Jen, T.C. and Dunmade, I. 2020. An overview of factors affecting the rate of generation and physical composition of municipal solid waste. *Int. Conf. Eng. Sustain. Worl*, 12: 96 <https://doi.org/10.1088/1757-899X/1107/1/012096>.
- Allesch, A. and Brunner, P.H. 2015. Material flow analysis as a decision support tool for waste management: A literature review. *J. Ind. Ecol.*, 19(5): 753-764.
- Arena, U. and Gregorio, F. 2014. A waste management planning based on substance flow analysis. *Resources, Conservation and Recycling*, 85(2014): 54-66.
- Arina, D., Bendere, R., Benafas, G., Kalnacs, J. and Kriipsalu, M. 2020. Characterization of refuse-derived fuel production from municipal solid waste: The case studies in Latvia and Lithuania. *Environ. Climate Technol.*, 24(3): 112-118. <https://doi.org/10.2478/rtuct-2020-0090>
- Anoop, K.G, Naveen, K.A. and Gangadhara, S.B. 2016. A review of recovery of energy from waste. *Int. J. Eng. Res.*, 5(6): 1129-1254. <https://doi.org/10.17950/ijer/v5i6/004>
- Ashani, P.N., Shafiei, M. and Karimi, K. 2020. Biobutanol production from municipal solid waste: Technical and economic analysis. *Bioresour. Technol.*, 308: 123267.
- Bandara, N.J.G.J. 2011. Municipal solid waste management: The Sri Lankan case. *Proc. Int. For. Environ. Symp.*, 11: 12-15.
- Bekchanov, M. and Mirzabaev A. 2018. Circular economy of composting in Sri Lanka: Opportunities and challenges for reducing waste-related pollution and improving soil health. *J. Clean. Prod.*, 202: 1107-1119. <https://doi.org/10.1016/j.jclepro.2018.08.186>
- Brunner, P.H. and Rechberger, H. 2017. Material flow analysis. *Book Rev. Pract. Handbook of Mater. Flow Anal.*, 9(5): 337-338.
- Bogucka, R., Kosinska, I. and Brunner, P. 2008. Setting priorities in plastic waste management: Lessons learned from material flow analysis in Austria and Poland. *Polimery*, 8: 55-59.
- Bouton, S. 2016. *The Circular Economy Moving from Theory to Practice*. McKinsey Center for Business and Environment.
- Central Bank of Sri Lanka. 2019. Provincial Gross Domestic production 2019. <https://www.cbsl.gov.lk/en/news/provincial-gross-domestic-product-2019>
- Chan Champee, P. 2010. *Methods for Evaluation of Waste Management in Thailand in Consideration of Policy, Environmental Impact and Economics*. Doctoral Thesis Technische Universität Berlin, Fakultät III – Prozesswissenschaften.
- Gehrmann, H., Hiebel, H. and Simon, F. 2017. Methods for the evaluation of waste treatment processes. *Waste Manag.*, 17: 11-23.
- Hartlieb, N., Bräutigam, K.R., Achternbosch, M., Kupsch, C. and Sardeemann, G. 2005. Use of material flow analysis for assessing solid waste management: In Germany regarding sustainable solutions. *Ecosyst. Sustain. Develop.*, 81: 723-733.
- Hunt, D., Leach, J., Lee, S., Bouch, C., Braithwaite, P. and Rogers, C. 2014. *Material Flow Analysis (MFA) for Liveable Cities*. The 4th World Sustainability Forum, 010.

- Jacob, P., Kashyap, P., Suparat, T. and Visvanathan, C. 2014. Dealing with emerging waste streams: Used tire assessment in Thailand using material flow analysis, *Waste Manag. Res.*, 32(9): 918-926.
- Kaza, S., Lisa, Y., Tata, P.B. and Woerden, F. V. 2018. What a Waste 2.0: A Global Snapshot of Solid Waste Management to 2050. Urban Development Series., World Bank, Washington, DC. <https://doi.org/10.1596/978-1-4648-1329-0>
- Keser, S., Duzgun, S. and Aksoy, A. 2012. Application of spatial and non-spatial data analysis in the determination of the factors that impact municipal solid waste generation rates in Turkey. *Waste Management*, 32(3): 359-371.
- Kolekar, K.A., Hazra, T. and Chakrabarty, S. N. 2016. A review on prediction of municipal solid waste generation models. *Procedia Environ. Sci.*, 5: 238-244.
- Laurenti, R., Singh, J. and Frostell, B. 2014. Progress and challenges to the global waste management system, *Waste Manage.*, 4: 20-25.
- Liu, G. and Yu, J. 2007. Gray correction analysis and prediction model of living refuse generation in Shanghai city. *Waste Manage.*, 27(3): 345-351.
- Lu, J.S., Chang, Y., Poon, C.S. and Lee, D.J. 2020. Slow pyrolysis of municipal solid waste (MSW): A review. *Bioresour. Technol.*, 23: 615. <https://doi.org/10.1016/j.biortech.2020.123615>
- Masood, M., Barlow, C.Y. and Wilson, D.C. 2014. An assessment of the current municipal solid waste management system in Lahore, Pakistan, *Waste Manag. Res.*, 32(9): 834-847
- Matthew, J.E. and Marian, R.C. 2009. Using material flow analysis to illuminate long-term waste management solutions in Oahu, Hawaii. *J. Industr. Ecol.*, 3(5): 758-774
- Ministry of Environment Sri Lanka (MOE) 2021. National action plan on plastic waste management 2021-2030.
- Nxumalo, S.M, Mabaso, S.D., Mamba, S.F. and Singwane, S.S. 2020. Plastic waste management practices in the rural areas of Eswathini. *Social Sci. Human. Open*, 2(1): 2590-2911 <https://doi.org/10.1016/j.sso.2020.100066>
- Oumarou, M.B., Dauda, M., Abdulrahim, A.T. and Abubakar, A.B. 2012. Characterization and generation of municipal solid waste in north central, Nigeria. *Int. J. Modern Eng. Res.*, 2(5): 3669-3672.
- Porshnov, D., Ozols, V., Ansone-Bertina, L., Burlakovs, J. and Klavins, M. 2018. Thermal decomposition study of major refuse derived fuel components. *Energy Procedia*, 147: 48-53.
- Ragaert, K., Delva, L. and Geem, K.V. 2017. Mechanical and chemical recycling of solid plastic waste. *Waste Manag.*, 7: 44 <http://doi.org/10.1016/j.wasman.2017.07.044>
- Supangkat, S. and Herdiansyah, H. 2020. Analysis correlation of municipal solid waste generation and population: an environmental perspective. *Int. Conf. Sci. Energy*. 519: 012056. <https://doi.org/10.1088/1755-1315/519/1/012056>.
- Tamine, I. 2020. The integration of recycling cooperatives in the formal management of municipal solid waste is a strategy for the circular economy. *Sustainability*, 12(24): 10513.
- Tang, F., Yu, Z., Li, Y., Chen, L. and Ma, X. 2020. Catalytic co-pyrolysis behaviors, product characteristics, and kinetics of rural solid waste and *Chlorella vulgaris*. *Bioresour. Technol.*, 299: 122636.
- Thanh, N.P., Matsui, Y. and Fujiwara, T. 2010. Household solid waste generation and characteristics in a Mekong Delta city, Vietnam. *J. Environ. Manag.*, 91(11): 2307-2321.
- The World Bank. n.d. Solid Waste Management. Retrieved on July 25, 2021, from <https://www.worldbank.org/en/topic/urbandevelopment/brief/solid-waste-management>
- The United States Environmental Protection Agency (USEPA). 2021. Facts and Figures about Materials, Waste, and Recycling. Retrieved from <https://www.epa.gov/facts-and-figures-about-materials-waste-and-recycling/national-overview-facts-and-figures-materials> viewed on 24th July 2021.
- Visvanathan, C., Glawe, U. and Luang, K. 2006. Domestic solid waste management in South Asian Countries: A comparative analysis. *Solid Waste Gener.*, 4(1): 1-14.
- Vujić, G.V. 2010. Assessment of plastic flows and stocks in Serbia using material flow. *Thermal Sci.*, 14: 89-95.
- Warunasinghe, W.A.A. and Yapa, P.I. 2016. A survey on household solid waste management (SWM) with special reference to a peri-urban area (Kottawa) in Colombo. *Procedia Food Sci.*, 6(0): 257-260.





# The Impact of Textile and Clothing Export on Environmental Quality in Bangladesh: An ARDL Bound Test Approach

Mahmuda Akter Khuky<sup>†</sup>, Law Siong Hook, Lee Chin and Mohd Yusof Bin Saari

School of Business and Economics, Universiti Putra Malaysia, 43400, Serdang, Selangor, Malaysia

<sup>†</sup>Corresponding author: Mahmuda Akter Khuky; mahmudaakterkhuky@gmail.com

Nat. Env. & Poll. Tech.  
Website: [www.neptjournal.com](http://www.neptjournal.com)

Received: 08-10-2021

Revised: 02-12-2021

Accepted: 20-12-2021

## Key Words:

Textile & Clothing

CO<sub>2</sub> emissions

Ecological footprint

ARDL

## ABSTRACT

The purpose of the study is to investigate the impact of Textile and clothing (T&C) exports on environmental quality in Bangladesh's economy. The fact that Bangladesh's clothing industry is one of the biggest T & C exporters in the world, justifies the importance of environmental evaluation in the case of Bangladesh's T&C. In this regard, this study has used the yearly time series data of T&C sector exports, CO<sub>2</sub> per capita, and ecological footprint per capita (EF) as a measure of environmental quality measurement from 1983 to 2019. The empirical investigation is carried out by applying the Autoregressive distribution lag model (ARDL) method. The findings of the study have identified the significant impact of the T&C industry on the environment of Bangladesh. The empirical findings demonstrate that T&C exports have made a significant positive contribution to environmental degradation in Bangladesh (both CO<sub>2</sub> and EF). The study recommended that policymakers can introduce environmentally friendly ways of production. To reduce carbon dioxide emissions, one should start a cleaner production while taking energy consumption and economic growth into account. Hence, the policy focuses on improving various aspects of production, especially green manufacturing to mitigate the adverse effect of the industry on the environment.

## INTRODUCTION

At present, the environmental quality is facing deterioration. The greenhouse gas (GHG) emissions are the major reason for the continuous environmental degradation. Mainly, due to the numerous industrial activities, a large amount of GHG emissions reach the atmosphere. The increased production scales and the role of advancements in industrialization in the current time are resulting in an increased amount of GHG discharge in the environment (Akter et al. 2017).

Precisely, the manufacturing process involved in the textile industry and the finishing results are responsible for the augmented greenhouse gas emissions. In this regard, It is stated that the textile sector contributes 1 ton of carbon from the entire 19.8 tons of carbon emission in the atmosphere. The textile industry is heavily dependent on a fossil-based energy source, resulting in carbon dioxide emission that ultimately constitutes a major part of greenhouse gasses (Heo et al. 2019).

Textile industries cause both direct and indirect effects on environmental degradation. The burning of fossil fuels involved in the manufacturing process of textiles generates direct GHG in the atmosphere. The textile industry indirectly increases harmful emissions because it uses more electricity along its whole supply chain. Numerous studies on the textile

industry have revealed that higher energy use has resulted in higher CO<sub>2</sub> emissions and consequently adverse environmental impacts (Huang et al. 2017a). Even though, the existing literature is unable to explore the conclusive role of the textile industry in causing environmental damage. Very few empirical investigations are done to examine the impact of textile export on CO<sub>2</sub> emissions. In response to this, the current study is motivated to examine the role of textile manufacturing on CO<sub>2</sub> emissions. Precisely, the objective of the current study is to empirically examine the T & C export on environmental degradation of Bangladesh. Many studies elaborated that developing countries are mostly responsible for environmental degradation due to their main focus on self-survival and economic growth. Hence, the current study is novel for evaluating the textile-environment link in the context of Bangladesh's textile industry. The novelty of the current study would be able to identify how the textile industry can threaten or hurt environmental stability.

Furthermore, the findings of the current study will provide some policy suggestions to the government in identifying the threats that can result from the expansion of the textile industry in Bangladesh. Moreover, the findings will allow the policymaker to impose ecologically beneficial industrial practices in the textile sector by reducing the use of fossil-based energy and finding environmentally friendly alternatives to green

energy sources. The findings may have policy ramifications for the government in identifying the genuine potential of the textile industry in the country's growth process, as well as being beneficial to environmental issues.

The remainder of the paper is given below. The next section will provide a review of available research to define the predicted relationship between the variables of interest. A brief description of the methodology is provided in section three. The study's findings are provided and discussed in section four. Finally, part five brings the study to a conclusion with suggestions and policy implications.

## PAST STUDIES

Sustainable development is based on environmentally sound economic growth principles. The familiar setting is relevant in this context. According to Kuznets theory, economic growth and improvements have a detrimental impact on environmental quality, but after a nation reaches a particular income level, the increase in wealth has a positive impact on the environment. In this context, various studies looked at how the textile sector operates, how its carbon footprint is increasing, and how dependent it is on energy. It has been condemned that the textile industry is one of the world's worst polluter offenders. As one of the most energy and carbon-intensive industries, the textile industry uses large amounts of chemicals, water, and fossil fuels in its manufacturing process, producing pollution from the soil, sound, water, and air. Different effective government policies should be implemented to solve the problems of energy and environmental pollution. The production of textiles must be controlled strictly (Huisingh et al. 2015).

Similarly, numerous studies aim at studying the role of carbon dioxide in the textile industry. Wang et al. (2011) looked at the contribution and sources of carbon dioxide emissions in the Chinese textile sector. According to the study, the expansion of China's textile industry is the primary driver of increased greenhouse gas emissions. In terms of Bangladesh's textile industry is the world's second-largest T & C exporter after China.

Bangladesh is a South Asian country and its economy is rapidly growing. The garment industry is one of Bangladesh's promising industries. The garment industry is the backbone of the economy of Bangladesh. It is the second-largest exporter of textile products in the world after China. Rapid growth in the textile industry, also called garment and industry significantly strengthened the economy. It is the second biggest garment industry in the world and the export of Bangladesh is mostly dominated by the textile industry. In the fiscal year 2018-19, the total value of the T & C export of Bangladesh to the world was approximately US\$ 34 billion out of its total export of US\$ 40 billion which is almost 84% of the total export value (BGMEA 2020). Bangladesh textile industries cause a range of environmental problems, mostly the pollution of water resources (Ahmed & Tareq 2008).

Fig. 1 clearly shows an upward increase in T & C export as well as the CO<sub>2</sub> emission at the same time. The increase in garment export is good for the country and has a big role in economic development but the sharp increase in carbon emissions is also very noticeable. The carbon emissions of Bangladesh have increased more than ten times in 2019 compared to 1983. While carbon emission was 8236 metric tons in 1983, it increased to 93761 metric tons in 2019. Trade-related carbon dioxide (CO<sub>2</sub>) emissions are measured

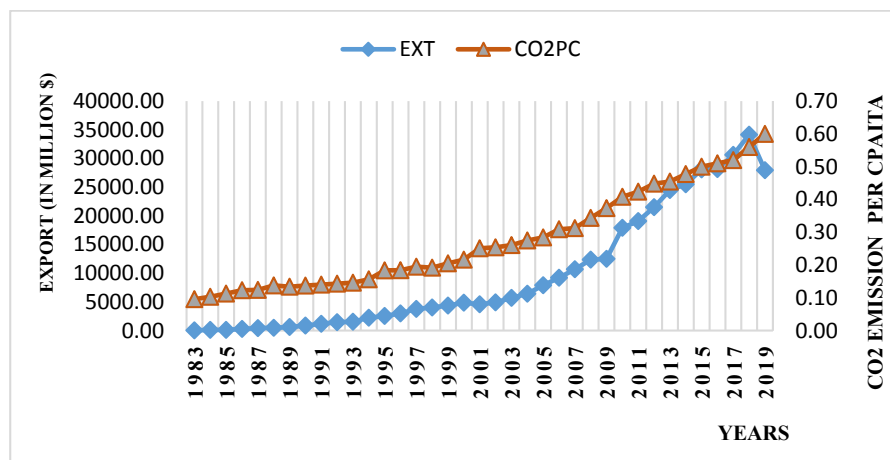


Fig. 1: Bangladesh's total CO<sub>2</sub> emission and RMG export.

(Source: World Bank and BGMEA 2019)



as whether the emissions are exported or imported as the percentage of domestic production emissions. It is evident from Fig. 2 that the RMG export and the ecological footprint are increasing simultaneously after the year 2007 and onward.

Lin & Ahmad (2017) studied the causes which increased power-related CO<sub>2</sub> emissions in the textile industry from 1990 to 2014 in the Pakistani textile sector. The study found that the country’s growing population is a major contributor to rising carbon emissions. Furthermore, the findings revealed that economic growth is a key factor in accelerating environmental deterioration in Pakistan’s textile sector. The relation between environmental quality and Taiwan textiles was studied Hong et al. (2010). The research examined the outcomes of 303 companies in terms of energy conservation, and the author observed that taking energy-saving measures in the workplace helped reduce the textile industry’s carbon emissions to 143,669 tonnes, which might enhance the environment in Taiwan. A similar analysis of recycling measures in the textile business and their possible impact on environmental deterioration was also undertaken in the textile industry in Sweden by Zamani et al. (2015). The results showed that burning had negative environmental impacts and significantly added to the degradation of the atmosphere. Even after that, the literature did not successfully identify the textile industry’s conclusive role in environmental causes damage because very few investigations have been carried out on the exclusive effects of production or empirically analyzed CO<sub>2</sub> emission textile manufacture.

**DATA AND METHODOLOGY**

The total T & C export yearly data was collected from the Bangladesh Garments Manufacturer and Exporter Association (BGMEA). The remaining data was obtained from the World Development Indicator (WDI 2019). Table 1 shows the descriptions of all variables and their sources. The present study adopts Autoregressive Distributed Lag (ARDL) with

Bounds testing. This study uses annual data starting from 1983 to 2019 for Bangladesh.

To estimate the ARDL model, at first, we check the stationarity of all the variables by employing some conventional unit root tests, such as Augmented Dickey-Fuller (ADF) test (ADF 1979) and Phillips-Perron (PP) test (Perron 1990). We check the cointegration among the variables by using the bounds test developed by Pesaran et al. (2001). To confirm the cointegration: the null hypothesis  $H_0: \beta_0 = \beta_1 = \beta_2 = \beta_3 = \beta_4 = \beta_5 = \beta_6 = 0$  which indicated that there is no cointegration against alternate  $H_1: \beta_0 \neq \beta_1 \neq \beta_2 \neq \beta_3 \neq \beta_4 \neq \beta_5 \neq \beta_6 \neq 0$  which indicated there is cointegration among the variables.

Pesaran et al. (2001) suggested that when the value of the F-test is larger than the upper bound critical value, the null hypothesis of no cointegration will be rejected which tells the existence of the long-term relationship. Alternatively, if the estimated value of the F-test is below the critical value it means there is no long-run relationship (Pesaran & Pesaran 1997).

**ESTIMATED MODELS**

Following the studies by Mrabet & Alsamara (2017) and Altıntaş & Kassouri (2020), the general form of our empirical model used in this study is as follows:

$$ED = f(EX, GDP, GDP^2, FD, EU) \dots(1)$$

Where, *ED* refers to indicators of environmental degradation which is captured in our paper by per capita carbon emissions (CO<sub>2</sub>) and per capita ecological footprint (EF). To provide further insights we used these two proxies of environmental degradation. We estimated separate models for both proxies. By taking the natural logarithmic forms of all variables, we can specify the models we used in this paper. Since this paper compares two different indicators for environmental degradation, the empirical analysis will estimate two different specifications derived from equation (1): the first specification uses CO<sub>2</sub> emissions, whereas the

Table 1: Summary of variable and data sources.

Variables	Description	Sources
Carbon emission per capita (LnCO <sub>2</sub> )	CO <sub>2</sub> Emission measured in per capita metric tons	World Bank
Ecological footprint of consumption (LnEF)	It is measured in global hectares per capita	Global Footprint Network
T & C Export (LnEx)	T & C export in current US\$	Bangladesh Garments Manufacturer and Exporter Association (BGMEA)
Economic growth (LGDP)	Per capita GDP measured in constant 2010 US \$	World Bank
Square term of GDP (LGDP <sup>2</sup> )	Square term of GDP to check the nonlinear relationship	World Bank
Energy consumption (LnEU)	Energy consumption per capita kg of oil equivalent	World Bank
Financial development (LnFD)	Domestic credit to the private sector (% of GDP)	World Bank

second one uses the ecological footprint (EF) as an indicator for the environmental degradation.

$$\ln CO_2_t = \alpha_0 + \alpha_1 \ln EX_t + \alpha_2 \ln GDP_t + \alpha_3 \ln GDP_t^2 + \alpha_4 \ln FD_t + \alpha_5 \ln EU_t + \epsilon_t \quad \dots(2)$$

$$\ln EF_t = \beta_0 + \beta_1 \ln EX_t + \beta_2 \ln GDP_t + \beta_3 \ln GDP_t^2 + \beta_4 \ln FD_t + \beta_5 \ln EU_t + \epsilon \quad \dots(3)$$

To check the long-term linear relationship amongst the selected variables, therefore, the model specification is designed on ARDL Bound approach following Pesaran & Shin (1998) and Pesaran et al. (2001). To check the impact of T & C export on carbon emission proxy in Bangladesh, we perform the following econometric model:

$$\Delta \ln CO_2_t = \beta_0 + \beta_1 \ln CO_{2,t-1} + \beta_2 \ln EX_{t-1} + \beta_3 \ln GDP_{t-1} + \beta_4 \ln GDP_{t-1}^2 + \beta_5 \ln EU_{t-1} + \beta_6 \ln FD_{t-1} + \sum_{i=1}^r \varphi_i \Delta \ln CO_{2,t-i} + \sum_{i=1}^r \pi_i \Delta \ln EX_{t-i} + \sum_{i=1}^r \tau_i \Delta \ln GDP_{t-i} + \sum_{i=1}^r \delta_i \Delta \ln GDP_{t-i}^2 + \sum_{i=1}^r \gamma_i \Delta \ln EU_{t-i} + \sum_{i=1}^r \Omega_i \Delta \ln FD_{t-i} + \epsilon_t \quad \dots(4)$$

Taking the ecological footprint (EF) proxy to examine the impact of T & C export on the environment the following model is estimated:

$$\ln EF_t = \beta_0 + \beta_1 \ln EF_{t-1} + \beta_2 \ln EX_{t-1} + \beta_3 \ln GDP_{t-1} + \beta_4 \ln GDP_{t-1}^2 + \beta_5 \ln EU_{t-1} + \beta_6 \ln FD_{t-1} + \sum_{i=1}^r \varphi_i \Delta \ln EF_{t-i} + \sum_{i=1}^r \pi_i \Delta \ln EX_{t-i} + \sum_{i=1}^r \tau_i \Delta \ln GDP_{t-i} + \sum_{i=1}^r \delta_i \Delta \ln GDP_{t-i}^2 + \sum_{i=1}^r \gamma_i \Delta \ln EU_{t-i} + \sum_{i=1}^r \Omega_i \Delta \ln FD_{t-i} + \epsilon_t \quad \dots(5)$$

Where *ln* is the natural logarithm, T= 1,2,..., T for time period that takes the years from 1983 to 2019. Concurrently, to determine the short-run relationships of the variables, this study applied the error correction model and the short-term models for both carbon emission and ecological footprint in models (4) and model (5) as follows:

$$\Delta \ln CO_2_t = \beta_0 + \beta_1 \ln CO_{2,t-1} + \beta_2 \ln EX_{t-1} + \beta_3 \ln GDP_{t-1} + \beta_4 \ln GDP_{t-1}^2 + \beta_5 \ln EU_{t-1} + \beta_6 \ln FD_{t-1} + \sum_{i=1}^r \varphi_i \Delta \ln CO_{2,t-i} + \sum_{i=1}^r \pi_i \Delta \ln EX_{t-i} + \sum_{i=1}^r \tau_i \Delta \ln GDP_{t-i} + \sum_{i=1}^r \delta_i \Delta \ln GDP_{t-i}^2 + \sum_{i=1}^r \gamma_i \Delta \ln EU_{t-i} + \sum_{i=1}^r \Omega_i \Delta \ln FD_{t-i} + \theta ECT_{t-i} + \epsilon_t \quad \dots(6)$$

$$\Delta \ln EF_t = \beta_0 + \beta_1 \ln EF_{t-1} + \beta_2 \ln EX_{t-1} + \beta_3 \ln GDP_{t-1} + \beta_4 \ln GDP_{t-1}^2 + \beta_5 \ln EU_{t-1} + \beta_6 \ln FD_{t-1} + \sum_{i=1}^r \varphi_i \Delta \ln EF_{t-i} + \sum_{i=1}^r \pi_i \Delta \ln EX_{t-i} + \sum_{i=1}^r \tau_i \Delta \ln GDP_{t-i} + \sum_{i=1}^r \delta_i \Delta \ln GDP_{t-i}^2 + \sum_{i=1}^r \gamma_i \Delta \ln EU_{t-i} + \sum_{i=1}^r \Omega_i \Delta \ln FD_{t-i} + \theta ECT_{t-i} + \epsilon_t \quad \dots(7)$$

Where  $\theta$  is the measure of the speed of adjustment of how quickly variables return to their long-term equilibrium following a short-term shock, and ECT is an error correction term.

The descriptive statistics and correlation are shown in Table 2 and Table 3 in Appendix. The results of unit root test ADF and PP confirm all variables are stationary either at levels or in first differencing. The results are shown in Table 3. Our empirical results for all tests are found stationary at level I(0) or level one I(1) and similar results are obtained for all three tests. Thus, we find that none of the variables is integrated into order two. We estimate two types of environmental quality measurements separately. In model (1) the dependent variable environmental quality is proxied by the carbon emission per capita (CO<sub>2</sub>), while it is proxied by the ecological footprint (EF) in model 2. Both models are estimated with an unrestricted constant and restricted trend. The results of the ARDL bounds F-test are displayed in Table 5. We find that the F-statistics for both models are greater than the upper bound critical values (I(1) at a 5% significant level. Hence, we conclude the presence of a cointegration relationship among the various variables for both models under consideration.

Before we estimate the short and long-term coefficients, it is important to check for the validity of the estimated models by performing a series of diagnostic tests, such as the normality tests, the serial correlation tests, and the tests of the absence of heteroscedasticity of the error term. The findings of diagnostic tests are presented in Table 6. They indicate that the error terms are normally distributed, not correlated, and not heteroscedastic as all p-values are higher than 5%. Thus, both models pass the diagnostic tests. Besides, the

Table 2: Descriptive statistics.

	CO <sub>2</sub>	EF	EXT	GDP	EU	FD
Mean	0.278233	0.491924	9828.257	635.3309	162.0121	27.04676
Median	0.250765	0.466320	4859.830	541.2917	153.5601	24.17959
Maximum	0.600000	0.603059	34133.27	1287.822	229.2464	47.58330
Minimum	0.095610	0.409406	31.57000	378.0920	107.6725	9.034444
Std. Dev.	0.149971	0.066260	10644.79	258.0097	42.95986	12.34052
Skewness	0.611013	0.605627	0.949620	1.008287	0.396944	0.353714
Kurtosis	2.068077	1.827289	2.441163	2.916355	1.677778	1.658397
Observations	37	37	37	37	37	37

Note: Number of observations 37. The figures represent the raw data.

results of CUSUM and CUSUMQ came out stable. Figures (2) and (3) are shown in appendix 1.

Now, finally, we turn to present the results of the estimation of the error correction models in Tables 7 and 8 respectively. The next step of the estimation is to examine the long and short-run impact of T & C export, real GDP per capita, energy use per capita, and financial development on environmental degradation using the ARDL method. In the case of the first specification (CO<sub>2</sub> model), the results show that the long-run coefficients are found statistically significant. In specific, the export of T & C exports has a positive and significant impact on CO<sub>2</sub> emissions. The results show that a 1% increase in export of T & C increases CO<sub>2</sub> emissions by 0.0468%. The real GDP per capita and the per capita real GDP squared have a positive and negative impact on CO<sub>2</sub> emission, respectively. The result of this indicates that the relationship between CO<sub>2</sub> emission and real GDP per capita is inverted U-shaped which means the EKC hypothesis is valid for Bangladesh when using CO<sub>2</sub> as an indicator of environmental degradation. This result is according to the

EKC curve theory, which implies in the long run, the increase in economic growth will be responsible for reducing the CO<sub>2</sub> emission. Our finding is consistent with many previous studies, in which an inverted U-shaped curve has also been found between economic growth and CO<sub>2</sub> emissions. All these studies have found an important role in enhancing the environmental quality of different countries by increasing economic growth. The results of the study imply, however, that increases in the actual income level stimulate carbon emissions to some degree, and then mitigate Bangladesh's pollution (Shahbaz et al. 2014, Kasman & Duman, 2015).

Moreover, energy use has a long-run positive and significant impact on CO<sub>2</sub> emissions. The result shows that a 1% increase in energy use increases CO<sub>2</sub> emission by 0.76%. This long-run positive impact is expected as Bangladesh's textile industry is heavily dependent on non-renewable energy sources like fuel oil, coal oil, and natural gas. An increase in energy consumption also leads to an increase in CO<sub>2</sub> emission in long run. The financial development variable has a positive and statistically significant impact on CO<sub>2</sub>

Table 3: Pair-wise correlations.

	LNCO <sub>2</sub>	LNEF	LNEXT	LNEU	LNFD	LNGDP
LNCO <sub>2</sub>	1					
LNEF	0.910002	1				
LNEXT	0.947077	0.765357	1			
LNEU	0.992438	0.92605	0.930614	1		
LNFD	0.991401	0.882139	0.962913	0.985764	1	
LNGDP	0.978909	0.945569	0.889327	0.976515	0.952779	1

Note: Correlation analysis of the variables shown represents their natural logarithmic values.

Table 4: Unit root tests.

VARIABLES	AUGMENTED DICKEY-FULLER TEST (ADF)		PHILLIPS PERRON TEST (PP)		Order of Integration
	Level	1 <sup>st</sup> Difference	Level	1 <sup>st</sup> Difference	
LCO <sub>2</sub> PC	3.8407 (1.0000) -0.0596 (0.9937)	-4.1592 (0.0025)*** -6.0575 (0.0001)***	7.1920 (1.0000) 1.3037 (0.9999)	-4.0956 (0.0030)*** -7.8937 (0.0000)***	I(1)
LEF	1.0775 (0.9965) -1.3894 (0.8455)	-4.7468 (0.0006)*** -5.4666 (0.0005)***	0.8214 (0.9929) -1.3895 (0.8454)	-4.8275 (0.0005)*** -5.4650 (0.0005)***	I(1)
LEXT	1.8562 (0.9996) -4.2223 (0.0126)**	-3.7456 (0.0090)*** -4.0362 (0.0195)**	0.6259 (0.9885) -1.6420 (0.7558)	-5.5069 (0.0001)*** -5.9240 (0.0001)***	I(1)
LRGDP	11.707 (1.0000) 5.4086 (1.0000)	-0.9385 (0.7638) -2.6394 (0.0002)***	10.6692 (1.0000) 4.8174 (1.0000)	-0.4172 (0.8953) -2.5012 (0.0012)***	I(1)
LEU	0.3113 (0.9757) -1.8256 (0.6713)	-2.7478 (0.0766)* -2.6126 (0.2774)	0.1861 (0.9679) -1.9450 (0.6105)	-5.8045 (0.0000)*** -5.7763 (0.0002)***	I(1)
LFDP	-1.9497 (0.3068) -3.9104 (0.0218)**	-7.7154 (0.0000)*** -7.5865 (0.0000)***	-2.1787 (0.2171) -3.9104 (0.0218)**	-13.4098 (0.0000)*** -14.2603 (0.0000)***	I(1)

Note: (\*)Significant at the 10%; (\*\*)Significant at the 5%; (\*\*\*) Significant at the 1% and P-value are below the coefficient values in parantheses.

emissions in the long run. This result reveals that an increase of 1% in financial development will cause a 0.49% increase in CO<sub>2</sub> emission in Bangladesh. A possible reason is that the share of capital used by the financial activities will promote the economic activity, export, and production of Bangladesh which contributes to environmental degradation in the future. This indicates the development of the financial sector could stimulate the demand for energy consumption and expansion of the production scale, which increases carbon emissions from Bangladesh's perspective. A similar result was found for Bangladesh by Hossain & Hasanuzzaman (2012) for Malaysia but this study is different from the results of Mrabet & Alsamara (2017).

Table 8 also provides the short-run results for the first specification of the CO<sub>2</sub> model which are the results of error correction representation. The T & C export is increasing the carbon emission in the short-run but this result becomes significant in long-run estimation. It means the garment and production are responsible for environmental degradation in the short run. The (DRGDP) coefficient is positive which means economic growth causes carbon emissions in the short run for Bangladesh. The (DRGDP2) coefficient is negative

and non-significant for the short run. This result indicates the EKC hypothesis is not valid in the short run. On the other hand, the energy consumption (DEU) coefficient is positive and non-significant for the short run but in long run, we found a similar relationship with a significant value. The financial development (DFD), the positive and significant results will increase carbon emissions by 0.356 percent with a 1% increase in financial development. The same result is also found for (LFD) in a long-term estimate. The error correction term is correctly signed and significant with a negative value of 0.80 percent to validate earlier results of the long-run relationship among variables in model 1a. It suggests a high speed of adjustment of the dependent variable to equilibrium. This result supports the long-run relationship between the selected variables and indicates that any adjustment in CO<sub>2</sub> emissions from the short run towards long-run equilibrium will occur by 0.8% every year.

In the case of the second specification (EF model), the long-run estimated coefficients are found statistically significant except for GDP and GDP<sup>2</sup>. In the context of per capita real GDP and per capita real GDP squared have positive and negative impacts on EF respectively, but because the

Table 5: Results of ARDL Bounds test.

<b>Carbon emission Model (Model 1)</b>			
	Lower bound	Upper bound	Significance levels (%)
F= 8.101470	2.08	3	10
K=5	2.39	3.38	5
	3.06	4.15	1
<b>Ecological footprint Model (Model 2)</b>			
F= 4.886144	2.49	3.38	10
K=5	2.81	3.76	5
	3.5	4.63	1

Note: k is the number of regressors. The model selection method is the Akaike info criteria (AIC).

Table 6: Results of diagnostic tests.

		Carbon emission Model	Ecological footprint Model
		Model 1	Model 2
Normality test	Jarque-Bera (p-value)	0.46 (0.79)	0.34 (0.84)
Breusch-Godfrey Serial correlation LM test	F-stat. (p-value)	1.53 (0.23)	1.04 (0.59)
Breusch-Pagan-Godfrey Heteroscedasticity	F-stat (p-value)	5.01 (0.75)	3.7 (0.80)
CUSUM		stable	stable
CUSUMQ		stable	stable

Note: Figures in parenthesis show p-values

GDP squared value is insignificant, we can conclude there is the absence of the EKC hypothesis. In other words, the existence of an inverted U-shaped nexus is missing when considering the ecological footprint as a proxy of environmental degradation in Bangladesh. However, this finding is opposite to the result of model 1 where we used CO<sub>2</sub>PC as a proxy for environmental degradation. This result is in line with Al-Mulali et al. (2015) who investigated the EKC hypothesis for different income groups and countries by using ecological footprint (EFP) measures. This result implies that the EKC hypothesis was not confirmed in Bangladesh. This result indicates in the long run it is expected Bangladesh relies on the production and the exports of T & C products to sustain its economic growth. This will create an increasing

volume of polluted goods. Moreover, this result shows that the connection between revenue and pollution does not reach the point at which the relation between the two components is negative.

The other explanatory variables have similar effects on the ecological footprint. The T & C export has a significant effect on the ecological footprint by 1% increase in export will increase the ecological footprint by 0.0132%. This result is in line with Kurniawan et al. (2018). They discovered that trade is responsible for increasing environmental degradation (ecological footprint).

Energy use has a significant and positive impact on the environmental footprint, which will increase the environmen-

Table 7: Long-Run estimates.

Variables	Carbon emission Model	Ecological footprint Model
	Model 1 Coefficient (p-value)	Model 2 Coefficient (p-value)
LEX	0.0468** (0.0084)	0.0132** (0.0744)
LGDP	6.6948** (0.0048)	13.1869** (0.0115)
LGDP <sup>2</sup>	-0.4123** (0.0115)	-0.8048 (0.1229)
LEU	0.7658** (0.0360)	0.8727** (0.0546)
LFD	0.4938** (0.0021)	0.4825** (0.0323)
Constant	-16.554** (0.0023)	-30.919** (0.0081)

Note: (\*) Significant at the 10%; (\*\*)Significant at the 5%; (\*\*\*) Significant at the 1%; the values between parentheses are p-values.

Table 8: Short-Run estimates.

Variables	Carbon emission Model	Ecological footprint Model
	Model 1 Coefficient (p-value)	Model 2 Coefficient (p-value)
D(EX)	0.0183 (0.5018)	-0.0474 (0.1170)
D(EX(-1))		0.0511 (0.0186)
D(GDP)	16.691 (0.2274)	32.563** (0.0080)
D(GDP(-1))		-0.3889 (0.9755)
D(GDP <sup>2</sup> )	-1.4279 (0.2030)	-2.4822** (0.0112)
D(GDP <sup>2</sup> (-1))		-0.0568 (0.9565)
D(EU)	0.3380 (0.1523)	-0.5444** (0.0118)
D(EU(-1))		0.1339 (0.4529)
D(FD)	0.3565**(0.0012)	0.1288 (0.1067)
D(FD(-1))		0.0070 (0.9175)
ECT(-1)	-0.8080**(0.0014)	-0.6205**(0.0007)
R-squared	0.7610	0.643
Adjusted R-squared	0.6615	0.472
Durbin-Watson	1.748	2.118

Note: (\*)Significant at the 10%; (\*\*)Significant at the 5%; (\*\*\*) Significant at 1%; the values between parentheses are p-values.



tal footprint by 0.87 percent 1 percent. The use of energy, therefore, increases Bangladesh's environmental degradation. This study is consistent with a previous study by Destek & Sarkodie (2019) that explored the effect of the use of energy on the ecological footprint and the main variables which degrade the environment, taking 11 industrialized countries as samples and consumption of food energy. Furthermore, Nathaniel & Khan (2020) also found a similar result about the impact of energy consumption on the ecological footprint (EF) of Indonesia. Additionally, this finding is consistent with the result on the relationship between energy use and the CO<sub>2</sub> emission model. This finding is complemented by those who found the impact of energy consumption to be a significant factor in extended environmental degradation. For example, Huang et al. (2017b) identified the key cause of the Chinese garment industry's increased emissions of coal.

Financial development has a positive and significant impact on the ecological footprint, this means that when financial development increases by 1% in Bangladesh, it stimulates the ecological footprint by 0.4825%. Therefore, financial development is attached to negative environmental consequences as it creates more damage to the ecological system. This result confirms that financial development promotes economic activity, which in turn increases the global human demands on nature and contributes to environmental degradation. In addition, these findings are in line with several earlier studies, for example, Al-Mulali et al. (2015) have examined the link between financial development and carbon emissions in European-focused countries, founding that financial development can increase long-term carbon emissions.

Table 8, also reports the short-term result for the specification of taking ecological footprint (EF) proxy. The T & C export is found to increase the environmental quality in the short run but the effect becomes positive and significant with the value of 0.05% in 1st lag (D(EX(-1)), justifying that the T & C industry reduces the environmental quality of Bangladesh. The coefficient of (DGDP) shows positive and significant but it becomes negative and insignificant in the first lag. The coefficient of D(GDP2) is negative and significant with a value of 2.48% but after taking one lag the coefficient becomes insignificant with a value of 0.056%. The energy consumption (DEU) has a sign with a negative value of 0.544% at a 5% significant level. Whereas, the change of EU with 1 year lagged effect D(EU(-1)) has a positive and insignificant effect on the ecological footprint of Bangladesh. The change in financial development has a positive coefficient in both D(FD) and D(FD(-1)) and the value is insignificant in the short run but eventually, in the long run, the value becomes significant. This means finan-

cial development is responsible for reducing the ecological footprint of Bangladesh. In model 2a, the error correction term is correctly signed and significant with a negative value of 0.62 percent to validate earlier results of the long-run relationship among variables. It suggests the high speed of adjustment (62%) of the dependent variable to equilibrium as shown in model 2a.

## CONCLUSION AND POLICY IMPLICATIONS

Bangladesh's largest manufacturing industry is textile production. The expansion of this sector, as well as other small and medium-sized businesses, has unquestionably benefited national economic development; yet, there are also environmental issues. The objective of this study is to investigate the impact of T & C export, per capita real GDP, energy use, and financial development on environmental degradation in the case of Bangladesh over the period of 1983-2019, by employing the ARDL approach. To this end, we compare the results of two alternative environment indicators: CO<sub>2</sub> emissions and EF. The CO<sub>2</sub> emissions represent only a small share of total environmental degradation, whereas the EF is considered a more comprehensive measure of environmental damage. The current climate condition of Bangladesh is declining due to the numerous industrial activities. In specific, fabrics are considered to create atmospheric pollution and the increased number of T & C manufacturing augmented GHG emissions. The findings confirmed that the effect of T & C export on the environment is positive and significant for both measures of the environment (CO<sub>2</sub> emission and EF). This result is consistent with Hasseb et al.'s (2020) study where they found T & C industries positively contribute to the CO<sub>2</sub> emissions in China, Indonesia, Pakistan, and India.

The long-run estimation result indicates a positive and significant effect of per capita real GDP emission and a negative impact of per capita real GDP squared on the CO<sub>2</sub> emissions. This result is in line with Al-Mulali et al. (2015) who investigated the EKC hypothesis for different income groups and countries by using ecological footprint (EFP) measures. In their study, they found that the EKC hypothesis is missing for lower-middle-income and upper-middle-income countries. Similar signs of GDP and GDP squared on EFP. However, the values are significant for the CO<sub>2</sub> emission measure but not significant for EFP. Thus, we can conclude that the EKC hypothesis is supported when we use CO<sub>2</sub> emission but using EFP did not support the EKC hypothesis. Similar results were also reported by Jorgenson et al. (2017) and Ghazali & Ali (2019); Imamoglu (2018) for Turkey & Mrabet & Alsamara (2017) for Qatar. All these studies confirmed the non-existence of the EKC phenomena while taking the ecological footprint as a proxy. Mrabet et al.

(2017), used ecological footprint and found in their long-term estimates show that the environmental quality of economic growth is degraded by increasing the ecological footprint for Qatar. This result indicates in the long run it is expected Bangladesh relies on the production and the exports of T&C products to sustain its economic growth. This will create an increasing volume of polluted goods. The rest of the variables were found similar in both measures.

Energy consumption is found to significantly affect the environment of Bangladesh. In both proxies, energy consumption is found to have a significant and positive impact on the environment both short-term and long-run. The policymakers need to explore alternative modes of energy consumption (green energy) to reduce the continuous environmental degradation in Bangladesh. It is also recommended Bangladesh prioritize energy efficiency projects to improve energy saving and enhance the role of renewable energy in reducing the ecological footprint arising from the consumption of energy mostly oil, and fossil fuels. In addition, policymakers need to urgently up their investments in renewable sources (like wind, solar, tides, bioenergy, etc.) because renewable sources are clean and low in emissions. Moreover, trade-related actions and strategies to increase environmental protection is needed to initiate because T & C export increases the ecological footprints of Bangladesh. The adoption of suitable trade openness policies is a further policy alternative emissions of dioxide and thus environmental improvement which will help to reduce carbon levels quality. Bangladesh needs to take steps in energy conservation and environmental protection policies to curb CO<sub>2</sub> emissions and find out alternative and green sources of energy. Technological improvement through research and development is necessary in this regard.

The result of this study concluded that financial development led to an increase in environmental degradation.

Financial development is another factor that has become more important recently. Various studies focused on including this factor in EKC estimates. The government, banks, and other institutions should participate in projects or activities that acknowledge the significance and adopt a code of good practice in Bangladesh in environmental matters. In the future, Bangladesh can employ carbon intensity in the financial embodied of government policy. The current study suggests that the regulators adopt some policies that promote environmental protection for the textile industry. Green technology must also be promoted in T&C sector processing in Bangladesh. In addition, this study suggests that government and policymakers increase investments in textile and focus on research and development to promote eco-friendly technologies related to the textile sector production and distribution. In addition, carbon tariffs have to be introduced to discourage the emission of greenhouse energy to reduce adversity environmental pollution. Furthermore, the cooperation of many stakeholders should be encouraged to raise the environmental awareness of staff, directors, retailers, manufacturers, and traders so that Bangladesh can get continuous benefit from the textile sector's growth as well as environmental sustainability. The current study is limited to recognizing the overall effect of garments and production on environmental degradation, which is useful in determining the garment industry's overall impact on CO<sub>2</sub> discharge, however, future studies can be recommended to augment the textile-environment nexus with a detailed examination of garment process, such as spinning, weaving, dyeing, wetting, printing and so on.

## REFERENCES

- Ahmed, T. and Tareq, S.M. 2008. Textile Industries in Bangladesh: A Rising Environmental Degradation Down the Drains. <https://www.textiletoday.com.bd/textile-industries-in-bangladesh-a-rising-environmental-degradation/>.

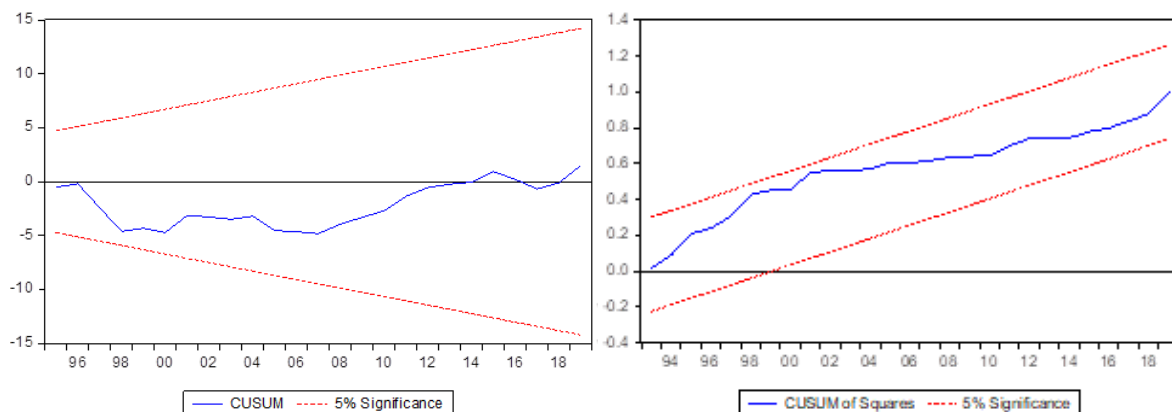


Fig. 2: CUSUM and CUSUMQ (CO<sub>2</sub>PC model)

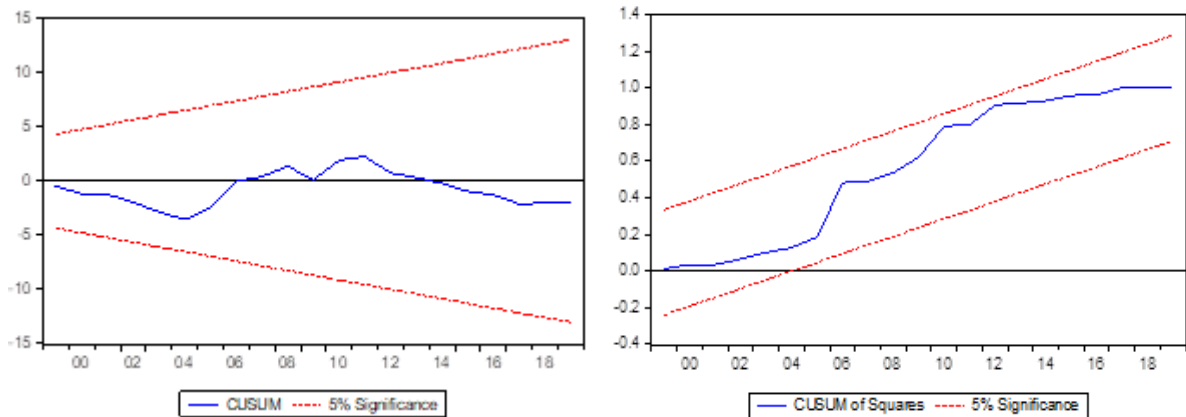


Fig. 3: CUSUM and CUSUMQ (EF model).

- Akter, S., Baig, S.F., Saif, S., Mahmood, A. and Ahmad, S.R. 2017. The five-year carbon footprint of the textile industry: A podium to incorporate sustainability. *Nature Environ. Pollut. Technol.*, 16(1): 125.
- Al-Mulali, U., Saboori, B. and Ozturk, I. 2015. Investigating the environmental Kuznets curve hypothesis in Vietnam. *Energy Policy*, 76: 123-131.
- Altinta, H. and Kassouri, Y. 2020. Is the environmental Kuznets Curve in Europe related to the per-capita ecological footprint or CO<sub>2</sub> emissions? *Ecol. Indic.*, 113: 106187.
- BGMEA. 2020. Retrieved from BGMEA: <http://www.bgmea.com.bd/>.
- Destek, M.A. and Sarkodie, S.A. 2019. Investigation of environmental Kuznets curve for ecological footprint: the role of energy and financial development. *Sci.Total Environ.*, 650: 2483-2489.
- Dickey, D.A. and Fuller, W.A., 1979. Distribution of the estimators for autoregressive time series with a unit root. *Journal of the American statistical association*, 74(366a): 427-431.
- Ghazali, A. and Ali, G. 2019. Investigation of key contributors of CO<sub>2</sub> emissions in extended STIRPAT model for newly industrialized countries: A dynamic common correlated estimator (DCCE) approach. *Energy Rep.*, 5: 242-252.
- Heo, J.N., Kim, J., Do, J.Y., Park, N.K. and Kang, M. 2020. Self-assembled electron-rich interface in defected ZnO: rGO-Cu: Cu<sub>2</sub>O, and effective visible light-induced carbon dioxide photoreduction". *Appl.Catal. B Environ.*, 266: 118648.
- Hong, G.B., Su, T.L., Lee, J.D., Hsu, T.C. and Chen, H.W. 2010. Energy conservation potential in the Taiwanese textile industry. *Energy Policy*, 38(11): 7048-7053.
- Hossain, A.K. and Hasanuzzaman, S. 2012. The Impact of Energy Consumption, Urbanization, Financial Development, and Trade Openness on the Environment in Bangladesh: An ARDL Bound Test Approach. Shahjalal University of Science & Technology, Sylhet, Bangladesh.
- Huang, B., Zhao, J., Geng, Y., Tian, Y. and Jiang, P. 2017a. Energy-related GHG emissions of the textile industry in China. *Resour. Conserv. Recycl.*, 119: 69-77.
- Huang, M., Cui, G., Melgosa, M., Garcia, P.A., Liu, H., Liu, Y. and Luo, M.R. 2017b. Color harmony in two piece garments. *Color Res. Appl.*, 42(4): 498-511.
- Huisingh, D., Zhang, Z., Moore, J.C., Qiao, Q. and Li, Q. 2015. Recent advances in carbon emissions reduction: Policies, technologies, monitoring, assessment, and modeling. *J. Clean. Prod.*, 103: 1-12.
- Imamoglu, H. 2018. Is informal economic activity a determinant of environmental quality? *Environ. Sci. Pollut. Res.*, 25(29): 29078-29088.
- Jorgenson, A., Schor, J. and Huang, X. 2017. Income inequality and carbon emissions in the United States: a state-level analysis, 1997-2012. *Ecol. Eco.*, 134: 40-48.
- Kasman, A. and Duman, Y.S. 2015. CO<sub>2</sub> emissions, economic growth, energy consumption, trade and urbanization in new EU member and candidate countries: a panel data analysis. *Eco.Model.*, 44: 97-103.
- Kurniawan, R., Sugiawan, Y. and Managi, S. 2018. Cleaner energy conversion and household emission decomposition analysis in Indonesia. *J. Clean. Prod.*, 201: 334-342.
- Lin, B. and Ahmad, I. 2017. Analysis of energy-related carbon dioxide emission and reduction potential in Pakistan. *J. Clean. Prod.*, 143: 278-287.
- Mrabet, Z. and Alsamara, M. 2017. Testing the Kuznets Curve hypothesis for Qatar: A comparison between carbon dioxide and ecological footprint. *Renew. Sustain. Energy Rev.*, 70: 1366-1375.
- Nathaniel, S. and Khan, S.A.R. 2020. The nexus between urbanization, renewable energy, trade, and ecological footprint in ASEAN countries. *J. Clean. Prod.*, 272: 122709.
- Perron, P. 1990. Testing for a unit root in a time series with a changing mean. *Journal of Business & Economic Statistics*, 8(2): 153-162.
- Pesaran, H.H. and Shin, Y. 1998. Generalized impulse response analysis in linear multivariate models. *Economics letters*, 58(1): 17-29.
- Pesaran, M.H. and Pesaran, B. 1997. Working with microfit 4.0. *Camfit Data Ltd, Cambridge*
- Pesaran, M.H., Shin, Y. and Smith, R.J. 2001. Bounds testing approaches to the analysis of level relationships. *Journal of applied econometrics*, 16(3): 289-326.
- Shahbaz, M., Sbia, R., Hamdi, H. and Ozturk, I. 2014. Economic growth, electricity consumption, urbanization and environmental degradation relationship in United Arab Emirates. *Ecological Indicators*, 45: 622-631.
- Wang, L., Zhang, X., Li, B., Sun, P., Yang, J., Xu, H. and Liu, Y. 2011. Superhydrophobic and ultraviolet-blocking cotton textiles. *ACS applied materials & interfaces*, 3(4): 1277-1281.
- World Development Indicator (WDI), World Bank 2020 <https://databank.worldbank.org/data/reports.aspx?source=worlddevelopment-indicators>.
- Zamani, B., Svanström, M., Peters, G. and Rydberg, T. 2015. A carbon footprint of textile recycling: A case study in Sweden. *Journal of industrial ecology*, 19(4): 676-687.



# Salinity Prediction at the Bhairab River in the South-Western Part of Bangladesh Using Artificial Neural Network

Khan Md. Rabbani Rasha†

Department of Civil Engineering, Khulna University of Engineering and Technology, Khulna-9203, Bangladesh

†Corresponding author: Khan Md. Rabbani Rasha; rabbanirashakhan@gmail.com

Nat. Env. & Poll. Tech.  
Website: [www.neptjournal.com](http://www.neptjournal.com)

Received: 20-10-2021

Revised: 16-12-2021

Accepted: 23-12-2021

## Key Words:

Salinity  
Water quality  
Artificial neural network  
Bhairab river  
Correlation

## ABSTRACT

Salinity is a significant ecological element that influences the kind of creatures that reside in a water body. Salinity also determines the types of plants that will grow in a water body or on land that is fed by a water body. Three models were generated using an artificial neural network to estimate the salinity concentrations in the Bhairab River. Different combinations of variables were used to train the model using sample values of temperature, pH, turbidity, electrical conductivity (EC), color, total dissolved solids (TDS), total solids (TS), and suspended solids (SS). The performance of the models was determined using the statistical mechanism root mean square error (RMSE), coefficient of correlation (R), and determination coefficient (DC). ANN-2 model had the best performance which had the input variables electrical conductivity (EC), total dissolved solids (TDS), and total solids (TS). These three input variables were highly correlated with salinity. The correlation between the observed and the predicted values was also very high, the coefficient of correlation is 0.98 in validation. The RMSE value was very low for the model training and the value reduced even more after validation to 0.58.

## INTRODUCTION

Khulna is the commercial and port city of Bangladesh, situated in the country's southwest. Nonetheless, the region is surrounded by a lot of industries for geographical, cultural, social, and financial purposes. The water supply system in Khulna is entirely reliant on groundwater. Drinking water is not available in the Khulna region due to high salinity and iron levels. Due to the clayey soil, deep boring is needed to obtain drinking water. Since the upper aquifer is salt water, Khulna's water supply scheme is entirely reliant on groundwater sources. The WHO's (World Health Organization) norm threshold for water quality is used as a benchmark. Clean drinking water is a prerequisite for good health.

The Bhairab, which is thought to be older than its parent river, the Jalangi, splits from it at Bhagwangola (Vidhan Sabha constituency) in Murshidabad district, a few miles north of Karimpur near Akheriganj (in West Bengal). This river has been virtually dead for a long time, with its intake from the Jalangi having silted up. The stagnancy of its water is blamed in large part for the poor environment of Meherpur, which lies on its banks. The Khulna-Ichamati and the Kobadak are the two major branches of the Bhairab River. Bangladesh and India are separated by the Khulna-Ichamati River. The cities of Khulna and Jessore are located on the river's side. The river affected the growth of their settlements

and culture. The Bhairab and Atai rivers combine to form the Rupsa River, which flows into the Pasur River.

The cumulative concentration of dissolved inorganic ions in water or soil is referred to as salinity (Williams & Sherwood 1994). The ionic activity of a solution can also be expressed in terms of its ability to transmit electrical current (electrical conductivity (EC), measured in Siemens per meter). As a result, EC is commonly used to determine salinity, and the relationship between the two is dependent on water temperature. The following are the salt content classifications for surface waters (Battaglia 1958): freshwater  $< 0.5 \text{ g.L}^{-1}$ ; oligohaline  $0.5\text{-}4.0 \text{ g.L}^{-1}$ ; mesohaline water  $5\text{-}18 \text{ g.L}^{-1}$ ; polyhaline water  $18\text{-}30 \text{ g.L}^{-1}$ ; euhaline water  $30\text{-}40 \text{ g.L}^{-1}$ ; hyperhaline water  $> 40 \text{ g.L}^{-1}$  (Cañedo-Argüelles et al. 2013). Salinity and the proportions of the above ions come from three places in the absence of anthropogenic factors. (1) Catchment weathering is influenced by both the geology of the catchment and the amount of precipitation. (2) Sea water, though this is a major source of salts only in coastal areas. (3) As a result of seawater evaporation, small quantities of salts dissolve in rainwater. This third source of salt may be a major source of salt in land areas far from the sea (Herczeg et al. 2001). Because of the underlying geology and high evaporation in semiarid and arid areas, rivers and streams are frequently naturally saline; however, irrigation agriculture is one of the major causes of secondary, or anthropogenic, salinization.



One of the main causes of secondary salinization has been identified as irrigation and rising groundwater tables, especially in arid and semi-arid regions of the world where crop production consumes large amounts of water. Salt concentrates and soil water becomes more acidic as crops consume just a fraction of the salt in irrigation water (Maryoung et al. 2014). These salts can be leached out and end up in the river as a result of run-off. Furthermore, irrigation, which is primarily formed in flat geomorphological bottom areas (arid landscape natural salt sinks), triggers the mobilization of vast fossil salt storages dating from the soil's past marine or otherwise saline geological history (Smedema & Shiaty 2002). As a result, irrigation has been blamed for the salinization of many streams, including the Amu Darya and Syr Darya Rivers in Central Asia (Létolle & Chesterikoff 1999, Crosa et al. 2006). South Africa's Breede River (Scherman et al. 2003), Spain's Ebro River (Isidoro et al. 2006), and Turkey's Great Menderes River (Koç 2008). A large portion of groundwater in Australia is saline due to the climatic and geomorphological features of the landscape (Blinn et al. 2004).

As a result, salinization has been identified as one of the most serious stressors facing freshwater habitats worldwide (Douglas 2017). Furthermore, salinization is one of the top 15 causes of stream impairment in the United States, ranking alongside pesticide input (Watershed Assessment, Tracking & Environmental Results 2012). In an Australian survey of river managers, salinity was ranked among the top three most significant environmental pollutants.

Pumping groundwater to bring the level down, then reusing wastewater or rather discharging it into local rivers, wetlands or streams is perhaps the most feasible alternative for controlling salinization (G.o. 1988). Unfortunately, there is a scarcity of scientific evidence to determine the biological consequences of these saline wastewater discharge systems (Brock & Hammer 1987).

An Artificial Neural Network (ANN) is a computational tool inspired by biological organisms' brains and nervous systems. ANNs are mathematical models that are highly idealized representations of our current knowledge of complex systems. The capacity of neural networks to learn is one of their characteristics. A neural network is not configured similar to a traditional computer program; instead, it resembles provided with instances of processes, insights, theories, or any other type of data that it must comprehend. Through the learning (also known as training) phase, the neural network arranges itself to generate an intrinsic collection of characteristics that it utilizes to recognize data. ANNs can handle inaccurate or partial data, provide estimations, and are less susceptible to anomalies than traditional techniques. They

are pretty similar, which means that their numerous independent processes may be performed at the same time. The ANN's massively parallel processing architecture allows it to efficiently handle complex computations, making it the leading method for high-speed data processing today (Sarkar & Pandey 2015). These characteristics make ANNs ideal tools for dealing with a variety of water modeling issues. But the number of applications for ANNs is growing, and it has recently been effective in predicting various water-related problems (Daniell 1991).

## ARTIFICIAL NEURAL NETWORK (ANN)

### Framework of ANN

An artificial neural network (ANN) is a computational device made up of a highly interconnected group of basic information processing elements called units, which are similar to neurons. The neuron receives input from sources and generates output in accordance with a non-linear mechanism that is predetermined. The interconnection of several neurons in a known configuration creates an ANN model.

The training step creates the link between neurons using known inputs and outputs and shows them in a logical sequence to the ANN. An error convergence approach is used to generate the appropriate power given a known input of data to adjust the intensity of these interconnections.

The feed-forward error backpropagation algorithm is used for ANN training in this analysis (Rumelhart et al. 1986). The ANN network utilized in this research is represented in Fig. 1. The input, the covert, and the output layers are the three fundamental layers or tiers of information systems. Each of these levels comprises the processing units of neural network nodes. The neural weight is the relation of nodes in various layers (Daniell 1991).

### Training and Validation of ANN

Neural networks learn by analyzing instances with a given "input" and "end," resulting in probability-weighted connections between the two that are stored in the net's data structure. When training a neural network from a given example, the difference between the network's processed output and a target output is generally determined. This is the error. Using this error value and a learning rule, the network then modifies its weighted associations. With each modification, the neural network can provide output that becomes closer and closer to the desired output. After a sufficient number of these adjustments have been made, the training may be ended based on certain circumstances.

This is referred to as supervised learning. The number of input nodes, output nodes, and hidden layer nodes varies



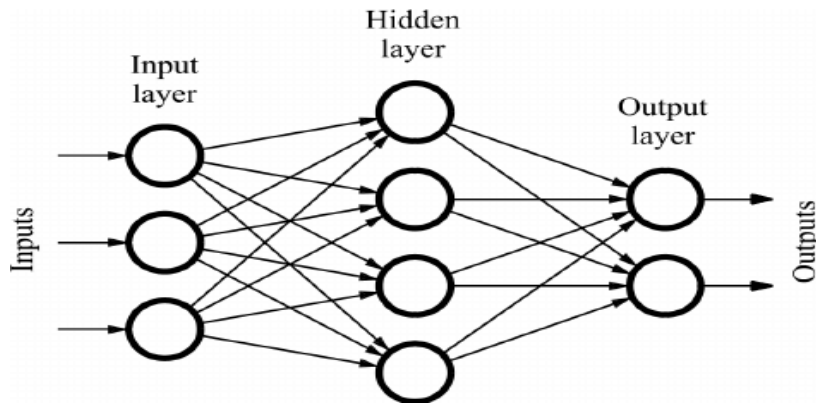


Fig. 1: A multi-layer feed-forward Artificial Neural Network model's layout.

according to the task at hand. If the hidden layer has a small number of nodes, the network will not have enough degrees of freedom to appropriately learn the process. If the number is excessively huge, the training process may take a lengthy time, and the network may over-fit the data in some situations (Sarkar & Pandey 2015).

After training is finished, the ANN's output is verified. Depending on the outcome, the ANN will either need to be retrained or will be able to serve its original function.

### Performance Assessment of ANN Model

A wide variety of statistical parameters are available to evaluate the suitability of any particular model. The root mean square error (RMSE), coefficient of correlation (R), and determination coefficient (DC) are the success assessment statistics used in this study for ANN preparation. The following equations were used to calculate these parameters.

$$\text{RMSE} = \sqrt{\frac{\sum_{i=1}^n (Q_i - q_i)^2}{n}} \quad \dots (1)$$

$$R = \frac{\sum_{i=1}^n (Q_i - \bar{Q})(q_i - \bar{q})}{\sqrt{\sum_{i=1}^n (Q_i - \bar{Q})^2 (q_i - \bar{q})^2}} \quad \dots (2)$$

$$\text{DC} = \frac{\sum_{i=1}^n (Q_i - \bar{Q})^2 - \sum_{i=1}^n (Q_i - \bar{Q})(q_i - \bar{q})}{\sqrt{\sum_{i=1}^n (Q_i - \bar{Q})^2}} \quad \dots (3)$$

Where,  $\bar{Q} = \frac{1}{n} \sum_{i=1}^n Q_i$ ,  $\bar{q} = \frac{1}{n} \sum_{i=1}^n q_i$ ,  $Q =$  observed,  $q =$  calculated

## MATERIALS AND METHODS

### Study Area and Data Collection

The Bhairab River was chosen for determining various water quality parameters and determining whether the river water is appropriate for drinking according to WHO standard permissible limits (World Health Organization). These criteria aid in determining the impurity level of river water, characterizing temporal data variations in water quality, and identifying various trends in data analysis based on tidal conditions, day-to-day differences, and seasonal changes over the course of a year. By measuring the appropriate parameters, it may be possible to understand the impact of seasonal precipitation, surface run-off, and other natural changes in river water parameters. The Bhairab river serves as a natural water source in the Khulna area, carrying away industrial polluted water. This data was collected from an undergraduate thesis study at Khulna University of Engineering and Technology (Chowdhury & Hamidul Bari 2020). Nine water quality parameters were considered for the completion of this study - temperature, pH, turbidity, electrical conductivity (EC), color, salinity, total dissolved solids (TDS), total solids (TS), and suspended solids (SS). Salinity is a major component when you consider the quality of water, especially drinking water. The information demonstrates that the salinity level is far beyond the WHO guideline's normal threshold. A total of 126 samples of data were available.

## RESULTS AND DISCUSSION

Standardization of input data is a crucial phase in the data processing process before implementing ANN. The ANN model was used to standardize the input data for a target variable in this analysis. The available data is split into two

sections when estimating the parameters of an ANN model. The first is for calibrating the model, and another is for validating it. This is called a “split-sample” test. The number of parameters to be estimated determines the duration of calibration data. The rule of thumb is to use half to two-thirds of the data for training and the rest for testing. Other than salinity itself, the rest of the eight of the nine parameters were used for training and validation to predict salinity.

Various parameter combinations were used in the development of the ANN model: (a) Datasets of temperature, pH, color, turbidity, suspended solids (SS) (b) Dataset of electrical conductivity (EC), total solids (TS), total dissolved solids (TDS) (c) Datasets of temperature, pH, turbidity, electrical conductivity (EC), color, total dissolved solids (TDS), total solids (TS), suspended solids (SS). For the analysis, the ANN model had 5 input variables, 3 input variables, and 8 input variables for the case (a), (b), and (c) respectively. The training of the ANN model epoch had 1000 cycles. A three-layer standard network was used.

Table 1 compares the accuracy of various ANN models for salinity estimation based on RMSE, correlation coefficient, and determination coefficient. It shows that the RMSE, R, and DC values for all built models during calibration range from 0.78 to 2.41, 0.6 to 0.97, and 0.34 to 0.94, respectively. During model validation, the values

of RMSE, R, and DC range from 0.58 to 2.55, 0.53 to 0.98, and 0.28 to 0.96, respectively. Three types of ANN models have been built with different combinations of variables, as discussed in the previous sections. The three ANN models have distinct results. The ANN2 model had the best performance, with RMSE, R, and DC values of 0.78, 0.97, and 0.94 during calibration and 0.58, 0.98, and 0.96 during validation. ANN-2 model has the best performance which has 3 input variables electrical conductivity (EC), total solids (TS), and total dissolved solids (TDS). These three input parameters are highly correlated with salinity so these variables are the optimum variables to correctly measure salinity. ANN-1 model had 5 input parameters pH, color, temperature, turbidity, and suspended solids (SS) which are loosely correlated with the values of salinity so, the model found it tough to find out the values of salinity. Because there are fewer input variables, the performance is significantly reduced when compared to ANN-2. These input variables are unable to identify the underlying physical mechanism. There are many input parameters for the ANN-3 model, which combines all of the parameters, including temperature, pH, turbidity, electrical conductivity (EC), colour, total dissolved solids (TDS), total solids (TS), and suspended solids (SS). These input parameters include both parameters that are highly and weakly correlated with

Table 1: Comparative performance of ANN models.

ANN Model	Training			Validation		
	RMSE	R	DC	RMSE	R	DC
ANN-1	2.39	0.61	0.36	2.51	0.55	0.3
ANN-2	0.78	0.97	0.94	0.58	0.98	0.96
ANN-3	2.41	0.6	0.34	2.55	0.53	0.28

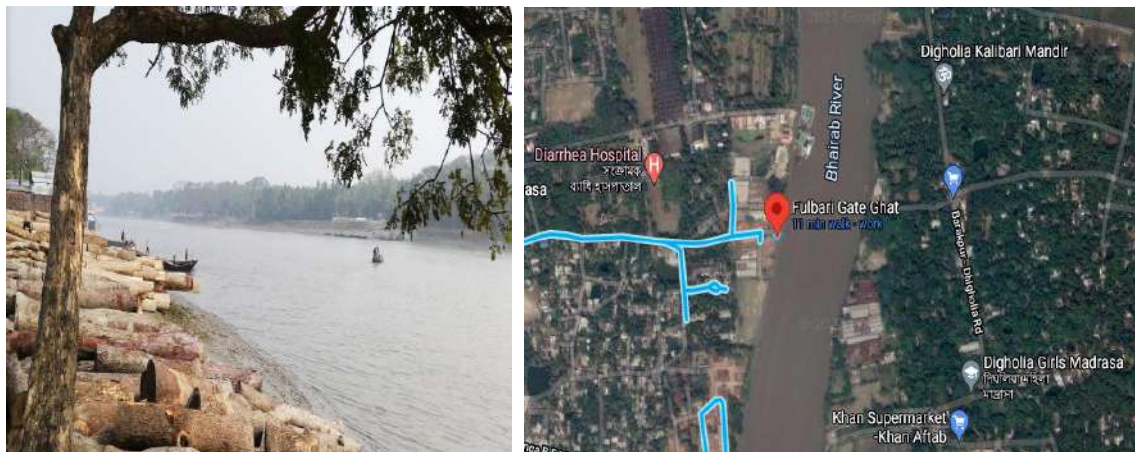


Fig. 2: Sample collection area of the Bhairab River.

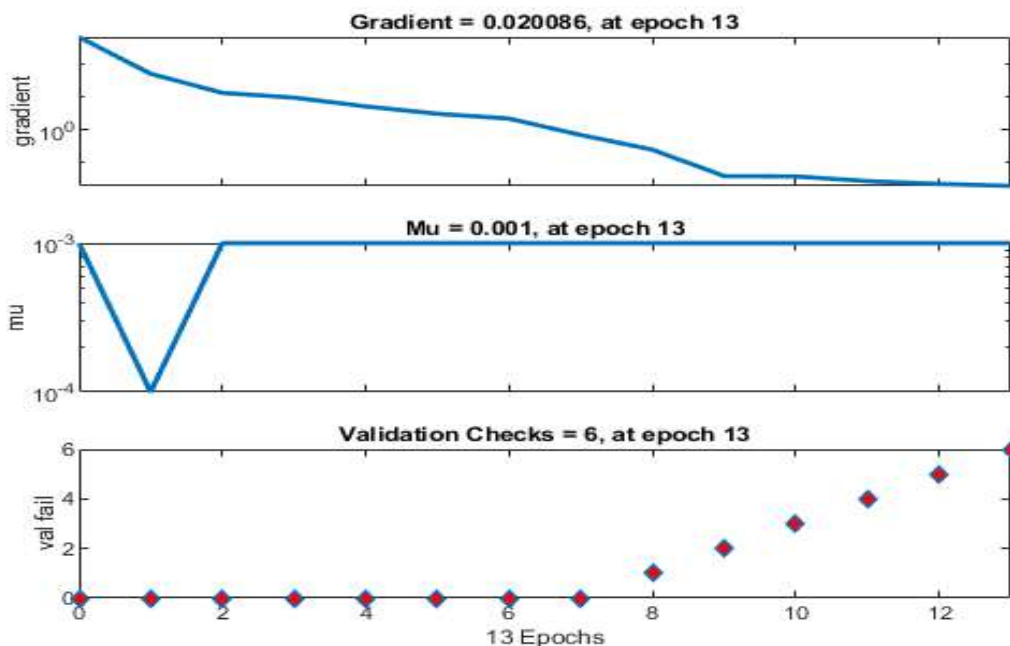
salinity. So, this makes the model more convoluted and may lead to the model overfitting the training data, resulting in bad forecasts (Tokar & Johnson 1999). As a result, it is critical to employ the optimum number of input variables when developing an ANN model, and the findings of this study show that 3 input variables that are highly correlated to salinity, as used in ANN-2, are optimal for salinity simulation at Bhairab river. Fig. 1 shows the graphical results of the top performing ANN, ANN-2, in the form of gradient values, and regression plots, demonstrating a good relationship between the observed and predicted salinity using the ANN approach.

With regard to the unknown weights and biases, the gradient is the gradient of the error function's square (Error = Known target - Variable output). Typically, the training goal is to minimize the sum of squared errors by utilizing the steepest descent technique to optimize the choice of weights and biases. A dynamic component is included to control the descent rate in order to stop the search value from going backward or forward before stopping close enough to it. The gradient value in an artificial neural network tends to be zero and in the 0-1 value range. As shown in Fig. 3, the gradient value during training for the ANN-2 model is close to 0.02, which is well within the acceptable range. The model is doing very well in the regression part where it achieves more than 90 percent accuracy in all categories. In training, the model predicted the values of salinity very accurately.

When the model is validated using Fig. 4, the gradient value is close to 0.01, which is well within the permitted range and has decreased since the training, indicating that the model has been properly trained and that the error has decreased. The hidden layers were thoroughly checked and from trial and error, the right number of hidden layers were applied to reduce the model from overfitting. It can be observed from the regression and prediction section that the ANN-2 model predicts the salinity values much more accurately than during training, indicating a very accurate model.

## CONCLUSION

Water quality modeling using artificial neural networks is hardly used in Bangladesh. Measuring water quality parameters throughout the year or in a very specific time continuously is a very tough and long process. Using an artificial neural network this predictive model could save time and ease the process. Of the model that was created to predict salinity ANN-2 model had the most efficient result. For identifying the performance of the model, the values of RMSE, R, and DC were very helpful. These values presented that the ANN-2 model had highly correlated input parameters that were very good at predicting the salinity values. The quality of the input data and the number of hidden layers used were paramount to better the accuracy of the model.



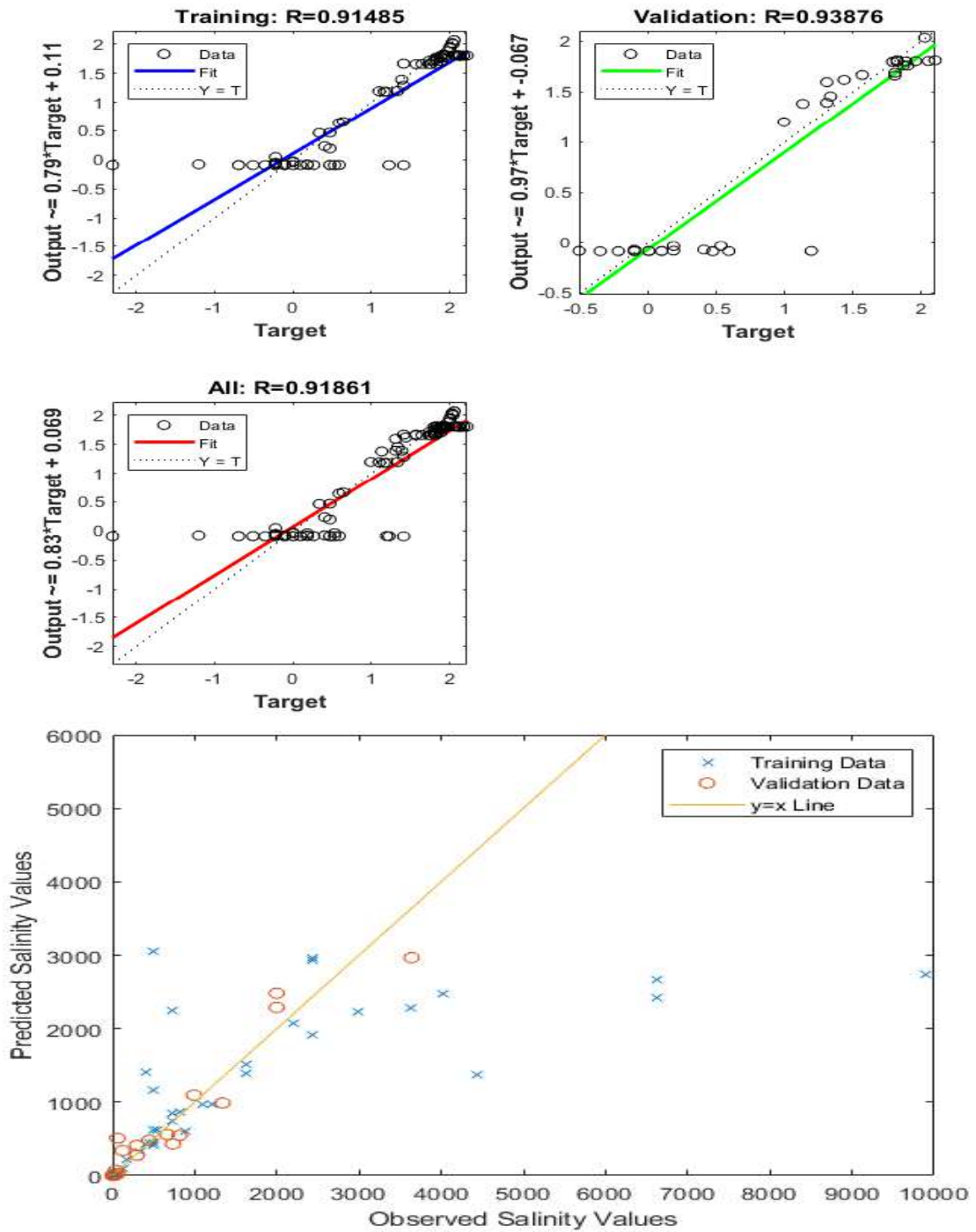
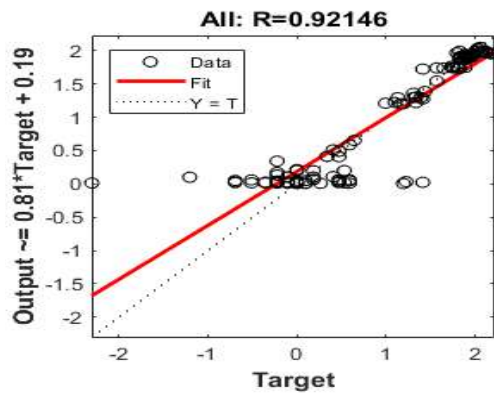
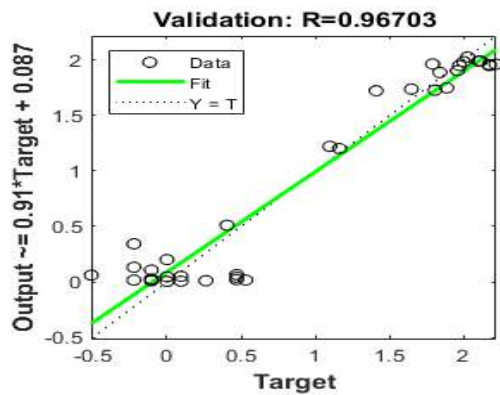
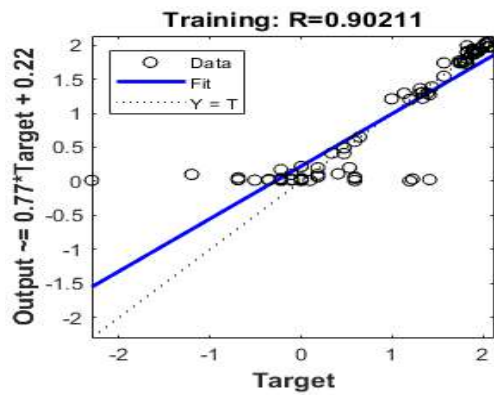
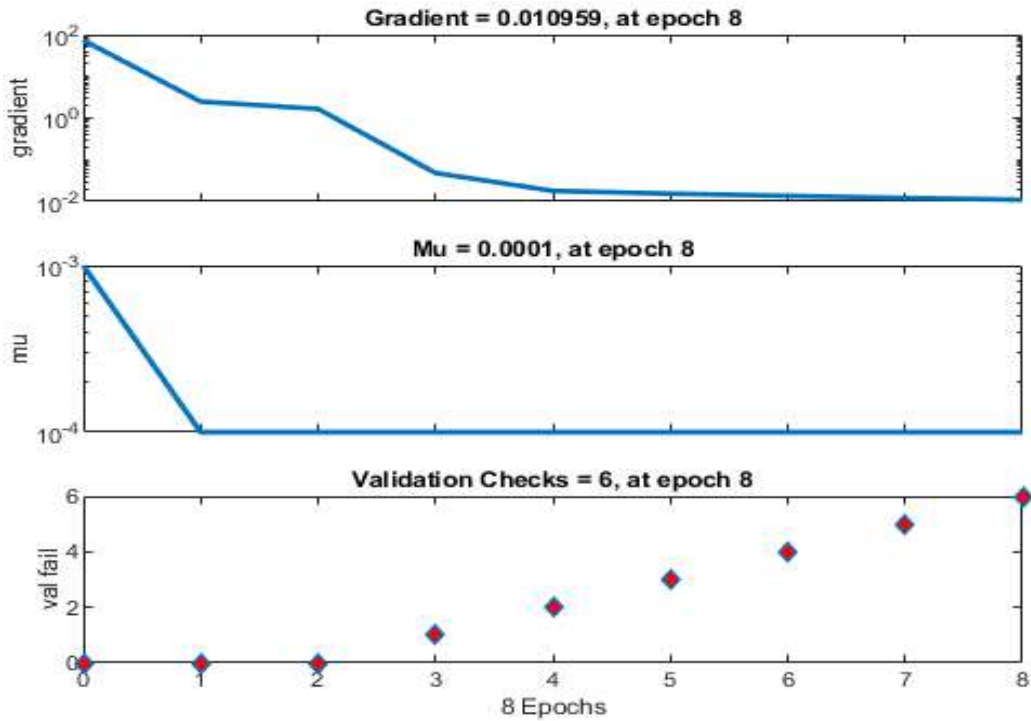


Fig. 3: Gradient values, regression, and predicted values of salinity in the training of the ANN-2 model.





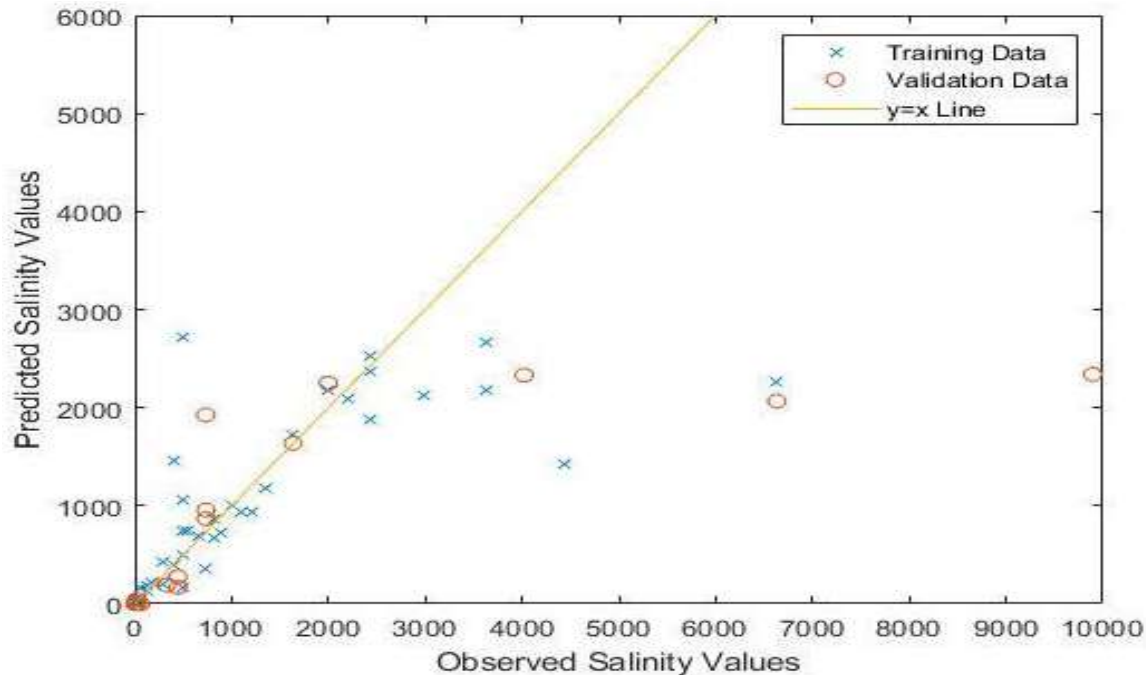


Fig. 4: Gradient values, regression, and predicted values of salinity in the validation of the ANN-2 model.

## REFERENCES

- Battaglia, B. 1958. Symposium on the classification of brackish waters. *Oikos*, 9(2): 311.
- Blinn, D., Halse, S., Pinder, A. and Shiel, R. 2004. Diatom and micro-invertebrate communities and environmental determinants in the western Australian wheat belt: A response to salinization. *Hydrobiologia*, 528(1-3): 229-248.
- Brock, M.A. and Hammer, U.T. 1987. Saline lake ecosystems of the world. *J. Ecol.*, 75(2): 580.
- Cañedo-Argüelles, M., Kefford, B.J., Piscart, C., Prat, N., Schäfer, R.B. and Schulz, C.J. 2013. Salinisation of rivers: An urgent ecological issue. *Environ. Pollut.*, 173: 157-167.
- Chowdhury, D. and Hamidul Bari, Q. 2020. Seasonal Variation of Water Quality Parameters in Bhairab River. *Khulna University of Engineering & Technology, Khulna*.
- Crosa, G., Froebrich, J., Nikolayenko, V., Stefani, F., Galli, P. and Calamari, D. 2006. Spatial and seasonal variations in the water quality of the Amu Darya River (Central Asia). *Water Res.*, 40(11): 2237-2245.
- Daniell, T.M. 1991. Neural networks. Applications in hydrology and water resources engineering. *Natl. Conf. Publ. Inst. Eng. Aust.*, 3: 797-802.
- Douglas, I. 2017. Ecosystems and human well-being. In: *Encycl. Anthr.*, 1-5: 185-197.
- G.o. 1988. Salt action, joint action: Victoria's strategy for managing land and water salinity. T2-A2.
- Herczeg, A.L., Dogramaci, S.S. and Leaney, F.W.J. 2001. Origin of dissolved salts in a large, semi-arid groundwater system: Murray Basin, Australia. *Mar. Freshw. Res.*, 52(1): 41-52.
- Isidoro, D., Quílez, D. and Aragüés, R. 2006. Environmental impact of irrigation in La Violada District (Spain). *J. Environ. Qual.*, 35(3): 766-775.
- Koç, C. 2008. The environmental effects of salinity load in Great Menderes Basin irrigation schemes. *Environ. Monit. Assess.*, 146(1-3): 479-489.
- Létolle, R. and Chesterikoff, A. 1999. The salinity of surface waters in the Aral sea region. *Int. J. Salt Lake Res.*, 8(4): 293-306.
- Maryoung, L.A., Lavado, R. and Schlenk, D. 2014. Impacts of hypersaline acclimation on the acute toxicity of the organophosphate chlorpyrifos to salmonids. *Aquat. Toxicol.*, 152: 284-290.
- Rumelhart, D.E., Hinton, G.E. and Williams, R.J. 1986. Learning representations by back-propagating errors. *Nature*, 323(6088): 533-536.
- Sarkar, A. and Pandey, P. 2015. River Water Quality Modelling Using Artificial Neural Network Technique. *Aquat. Procedia.*, 4: 1070-1077.
- Scherman, P.A., Muller, W.J. and Palmer, C.G. 2003. Links between ecotoxicology, biomonitoring, and water chemistry in the integration of water quality into environmental flow assessments. *River Res. Appl.*, 19(5-6): 483-493.
- Smedema, L.K. and Shiati, K. 2002. Irrigation and salinity: A perspective review of the salinity hazards of irrigation development in the arid zone. *Irrig. Drain Syst.*, 16(2): 161-174.
- Tokar, A.S. and Johnson, P.A. 1999. Rainfall-runoff modeling using artificial neural networks. *J. Hydrol. Eng.*, 4(3): 232-239.
- Watershed Assessment, Tracking & Environmental Results. 2012. <https://www.epa.gov/waterdata/waters-watershed-assessment-tracking-environmental-results-system>
- Williams, W.D. and Sherwood, J.E. 1994. Definition and measurement of salinity in salt lakes. *Int. J. Salt Lake Res.*, 3(1): 53-63.



# Perspectives for the Use of Hydrogen Energy in European Countries

Vyacheslav M. Krayev\*, Alexey I. Tikhonov\*† and Irina Kuzmina-Merlino\*\*

\*Department of Human Resource Management, Moscow Aviation Institute (National Research University), 125993 Volokolamskoe Highway 4, Moscow, Russian Federation

\*\*Department of Economics, Transport and Telecommunication Institute, Lomonosov Street 1, Riga, Latvia, LV-1019, Riga, Latvia

†Corresponding author: Alexey I. Tikhonov; tikhonovmai@mail.ru

Nat. Env. & Poll. Tech.  
Website: [www.neptjournal.com](http://www.neptjournal.com)

Received: 24-01-2022

Revised: 08-03-2022

Accepted: 10-03-2022

## Key Words:

Ecology  
Hydrogen energy  
Renewable energy sources  
Low-carbon economy  
Energy strategy

## ABSTRACT

The most actual environmental problems in the XXI century are the following: global warming due to greenhouse gas emissions, energy production at coal, oil and power plants, air pollution, water pollution and waste recycling. Other environmental problems can be added to this short list, but the authors solve a specific task of promoting the idea of a promising “green” energy that will help humanity in conservation and development. European Union (EU) countries are planning to solve the main environmental challenges for the transition to low-carbon electricity by 2050. In many countries in the world every year there are more and more supporters of reducing emissions of carbon dioxide CO<sub>2</sub>, nitrogen oxides NO and NO<sub>2</sub> and other greenhouse gases into the atmosphere. In recent years, EU has been consistently pursuing its own policy in the field of environmental protection, carrying out large-scale environmental measures. In Germany, United Kingdom (UK) and other European countries, a number of environmental initiatives are already gaining the status of state policy, which is being formalized in laws and regulations. Russian Federation acts on the world market as a leading country that produces and supplies significant energy resources not only to Europe, but also to many countries in the Asia-Pacific region. It is clear that the competitive stability of Russian energy companies significantly depends on the situation on the world energy market, but with the right strategy, Russia can actively influence the state of the entire energy market. With a confident leadership position, provided with significant natural, technological and human resources, Russian Federation has undeniable advantages over other energy-producing countries. It is Russia that can become the main supplier of clean energy for all other countries of the world, where tougher environmental requirements for energy generation are being cultivated. The authors of the study are considering the possibility of producing environmentally friendly hydrogen in Russia based on renewable energy sources (RES). The performed analysis shows the undeniable advantages of Russia in the export of hydrogen to other European countries.

## INTRODUCTION

Despite the ongoing economic sanctions policy on the part of some states of the world, Russia remains a reliable and stable energy partner for most European countries. For all countries of the EU, there are uniform coordinated documents at the interstate level. Active work is constantly being carried out to unify and improve environmental requirements in the field of energy for all EU member states, which is reflected in a number of regulatory documents. In 2005, the “Energy Policy of EU” was approved. It is aimed at achieving three main goals, which are outlined in the “Energy Strategy of EU”:

1. Ensuring reliable and safe power supply;
2. Creation of a competitive environment for energy suppliers to ensure affordable prices for energy resources;
3. Ensuring stable consumption of energy resources by increasing energy efficiency and reducing greenhouse

gas emissions, reducing environmental pollution and dependence on the type of fuel (Isaeva 2019).

Currently, half of the energy needs of EU member states are met by external suppliers. In the future, this proportion may increase to 2/3 (Kaveshnikov 2014, Zuev 2007). EU countries are planning in the future to most effectively apply the principle according to which it is the “polluter” who pays. Each supplier of any resource will be considered a violator of the environment: raw materials, energy carriers or end product. Penalties provide for mandatory financial compensation for any environmental pollution. The amount of such financial compensation will depend on the degree of environmental friendliness of production processes.

It is considered to be free from such compensation, some ideal processes using RES. RES include those energy sources, the natural renewal of which occurs quickly enough for them in the short term. The most common RES are the

following types of energy: solar, hydraulic, geothermal, wind and biomass. When using RES, energy is generated through natural processes, while environmental pollution occurs on a minimal scale. It should be noted that environmental pollution can be minimal, but not equal to zero. This is explained by the fact that the creation of a technological process of energy conversion requires significant infrastructure and special equipment, the creation of which causes certain damage to the environment.

The existing strong dependence of the economies of many EU countries on non-RES has led to attempts to change the accepted classification of RES in order to include other sources in this list. An example is the nuclear power industry, where there are no massive harmful emissions of such non-environmentally friendly gases as CO<sub>2</sub>, nitrogen oxides NO and NO<sub>2</sub>, etc. However, it can hardly be considered that fuel for nuclear power plants, formally, is a renewable type in real time human.

It should be noted that new processes in the field of regulation of energy resources impose special requirements on energy resources exported to European countries, for example, natural gas. Russian energy companies supply about 42% of all natural gas to European countries. It consists mainly of methane, although it is a non-RES source, nevertheless, it belongs to the most environmentally friendly form of energy due to the low CO<sub>2</sub> emissions during its production and combustion. The authors predict that the practical implementation of the “EU Energy Strategy” to reduce carbon emissions may, in the future, significantly reduce the level of natural gas supplies from Russia to Europe, or reduce profitability for Russian suppliers due to the implementation of the “polluter pays” principle. Another powerful factor in the implementation of the newest hydrogen strategy in Russia is the unique natural opportunities of the largest country in the world to obtain energy using RES.

## PAST STUDIES

The authors of the study (Kaveshnikov 2014) review European energy policy and point out the significant cost of new reforms in the energy sector. Only a few European countries are relatively energy independent from external energy suppliers. Economically leading countries consume several times more energy than they produce energy themselves, and over time, this disproportion is increasing more and more. It is also necessary to note purely national differences in various sources of energy generation. For example, Germany is the leader among EU countries in the production of electricity from coal-fired power plants, and France is the leader in nuclear power plants.

As we know, the most environmentally friendly is the production of energy based on the oxidation of hydrogen, because as a result of a chemical reaction, the product of hydrogen combustion is water. The topic of hydrogen energy has found its place in the “Energy Strategy of EU”, in which the countries of Western Europe have formed an environmental strategy for their development until 2050 (Gurkov 2014). “Action Plan for the Development of Hydrogen Energy in the Russian Federation until 2024” contains a roadmap that indicates that hydrogen can be used for the accumulation, storage and delivery of energy. Russian power engineers consider hydrogen as a promising energy carrier and a tool for solving new challenges to develop a low-carbon economy and reduce the anthropogenic impact on the climate. The uniqueness of hydrogen fuel lies not only in the complete absence of harmful emissions but also in its high calorific value. Another indisputable advantage is the technologically simple method of transporting hydrogen gas. “Action Plan for the Development of Hydrogen Energy” adopted in Russia was carefully and long prepared by leading power engineers and economists because they have been dealing with the problem of “decarbonization” for many years, said A. Belousov, First Deputy Prime Minister of the Russian Federation (Belousov 2021). He also noted that for the transportation of pure hydrogen, and as a part of a complex mixture, modern energy transport infrastructure can be used, for example, the new main gas pipeline from Russia to Germany through the Baltic Sea, Nord Stream 2 (Belousov 2021).

Currently, the cheapest way to produce hydrogen is the traditional method of steam reforming of methane, although it cannot be called environmentally friendly (Kraev 2020). Electrolysis is considered an alternative way to produce hydrogen, but it still cannot compete with the steam reforming of methane due to the significantly high cost, which is determined by the cost of electricity for this technology. Previous studies carried out by the authors comparing different methods of hydrogen production led to the conclusion that hydrogen produced using RES will be more than ten times more expensive than hydrogen produced by steam reforming from methane (Kraev 2020). So, existing RES do not allow the production of cost-competitive hydrogen. The Government of the Russian Federation is considering a modern technology of water electrolysis based on a nuclear power plant and a hydroelectric power plant, which will ensure the competitiveness of hydrogen produced by water electrolysis. Such a decision is justified and will allow minimizing daily fluctuations in the load of nuclear power plants due to the consumption of electricity for hydrogen production.

Not only in Russia, but also in other European countries, they show great interest in promising technologies for the

production of hydrogen. Avacon AG, a regional energy company from Germany, is already working on adapting the existing gas infrastructure to the practical use of hydrogen. Experimental studies are carried out on the existing gas distribution system of the city of Genthin (Saxony-Anhalt). The purpose of the measures is to increase the specific share of hydrogen in the main natural gas, which is supplied to German cities. To improve the environmental friendliness of energy systems, they began to replace up to 1/5 of the natural gas with hydrogen, although previously it was allowed to replace no more than 1/10. Stephan Tenge, one of the heads of Avacon AG, believes that since environmentally friendly “green” gas will play an increasingly important role in the future, it is necessary to re-equip the gas distribution network now so that it is adapted to receive the highest possible share of hydrogen.

## METHODOLOGY

The study conducted by the authors is based on various methods of theoretical and scientific-practical study of environmental and economic approaches in obtaining promising types of fuel to meet the needs of the population. The work uses elements of functional cost analysis, methods of generalization, synthesis and abstraction. The research methodology included an economic analysis of data on various types of fuel used in modern energy. The authors used complex systems of methods in the field of management, which are used by Russian and foreign experts in the field of energy efficiency and ecology. In addition to theoretical ones, specific scientific and practical methods of socio-economic research are actively used in research work, primarily the analysis of documentary sources and the method of statistical analysis of statistical information. Information sources used in scientific work include documentary and statistical materials, special literature on the research topic and media materials.

## RESULTS

The authors in their studies conducted an organizational and economic analysis of the feasibility of using hydrogen as a fuel in the aviation industry and noted that the first cargo transportation on hydrogen could be carried out as early in 2024 (Aslanov 2021). Our results showed a certain limitation of the use of hydrogen in aviation transport due to its specific physical properties, namely, very low density. For example, 1 m<sup>3</sup> of liquid hydrogen has a weight of 70 kg, while the density of liquefied natural gas ranges from 430 to 520 kg/m<sup>3</sup>, and the specific gravity of kerosene is 780-850 kg/m<sup>3</sup>. The use of aviation fuels with low density will require a significant increase in the volume of fuel tanks and a reduction in the usable volume on board the aircraft. However, for road and

rail ground transport and stationary power plants, the use of hydrogen fuel is extremely promising.

After analyzing the energy plans of a number of European states, the authors believe that in the near future the demand for hydrogen in the developed countries of the world will grow by dozens, and perhaps even hundreds of times. Consulting firm Aurora Energy Research conducted in 2020 its study “Hydrogen for a net zero GB: an integrated energy market perspective” which notes that while it focuses on the UK, its results apply to other countries, including developing nations. The report says that the total capacity of electrolysis hydrogen projects to be completed by 2040 is a thousand times greater than all the electrolysis facilities currently operating in the world. The final power should be an impressive value of 213.5 GW. The report also presented a functional cost analysis of the process of hydrogen production by electrolysis and concluded that it is possible to reduce the cost of hydrogen in the future to below 2.5 Euro/kg. Analysts at Aurora Energy Research predict in their optimistic scenario a hydrogen price cap of 2 - 2.5 Euro/kg.

One of the world leaders in the energy sector, Shell, with the financial support of the EU, began construction in Germany in 2020 of the world’s largest hydrogen production plant using water electrolysis. Until now, hydrogen at this enterprise was obtained only from natural gas. The volume of production will be 1.3 kilotons of hydrogen per year.

According to Bloomberg NEF experts, clean hydrogen could be used in the coming decades to cut up to 1/3 of global greenhouse gas emissions from fossil fuels and industry. At the same time, we are talking about acceptable costs in the transition to a new type of energy. This requires that at the level of the governments of the countries of the world, appropriate measures are taken to help expand the scale of modern technologies and reduce costs. The report notes the possibility of producing hydrogen in many countries before 2050, making it competitive with current natural gas prices in Brazil, China, India, Germany and Scandinavian countries on an energy equivalent basis. Experts from the Industrial Decarbonization department believe that hydrogen has sufficient potential to become a promising new fuel for the economy. In the coming years, it can be produced at a competitive price, stored underground for several months if necessary, and then transported through pipes. Bloomberg NEF analytical report on hydrogen price forecasts in various countries of the world provides the cost of producing sustainable “green” hydrogen, i.e. produced with the help of RES until 2050 (Table 1). We pay attention to the fact that hydrogen in European countries will not be the cheapest fuel: in Poland, 1 kg of hydrogen will cost 2.5 Euros, in Germany it will cost 2.25 Euros and in France, it will cost 2 Euros.



The cost of produced hydrogen depends significantly on the technology of its production. For example, hydrogen produced by electrolysis from solar and wind energy costs 5 to 10 times more than “conversion” hydrogen produced from natural gas. However, the cost of hydrogen depends on the energy source. For example, the price of “green” hydrogen from the energy of a nuclear power plant is 2 times cheaper than that from solar energy.

The cost of hydrogen, of course, depends on the producing country and the prices for energy carriers/raw materials in it. In Russia, hydrogen produced from methane costs about 1.1-1.6 Euro/kg, in the countries of the Middle East its cost drops to 0.9 Euro/kg, and in Europe, it reaches 2.23 Euro/kg. From an energy point of view, the thermal value of 1 kg of hydrogen is 2.5 times higher than that of methane or gasoline. It should be noted that the cost of hydrogen production in Russia is projected at the level of 1.5 Euro/kg if we use averaged data on the cost of electricity for hydrogen production in the calculations. A more detailed study of various energy sources and functional cost analysis confirm that the above data for Russia are approximate and do not reflect the real cost of electricity, and therefore do not demonstrate all the possibilities of the Russian energy sector.

We calculate in more detail the cost of electricity generation, as the main source of energy for the production of environmentally friendly hydrogen. The analysis below is based on official data on the cost of electricity, approved by the Federal Antimonopoly Service of the Russian Federation. The normative document under consideration contains selling wholesale prices for electricity for each electric power generation facility in Russia. We carry out a cost analysis in segmentation by types of generating processes: thermal, nuclear and hydropower plants. The significant difference in the cost of electricity depending on the type of power plant is impressive. The most expensive electricity is generated at the condenser-type thermal power plant, where the tariff rate for

electricity per 1 kWh will be in the range of 0.01-0.02 Euro. The energy produced at nuclear power plants (NPP) is cheaper: 0.003-0.004 Euro/(kWh). An additional effect is a new possibility of obtaining hydrogen to reduce daily fluctuations in the power of a nuclear power plant, i.e. elimination of an inefficient unloading mode (Aminov & Bairamov 2016; Fateev et al. 2018). However, in Russia, there are even cheaper sources of electricity. Their presence is associated with the unique natural features of a large Russian territory. We are talking about hydroelectric power plants (HPP). According to the order of the Federal Antimonopoly Service of the Russian Federation, the cost of electricity generation at hydroelectric power plants will be 0.0002-0.0004 Euro/(kWh) (Fig. 1).

Based on the data on the cost of electricity generation, we can say with confidence that hydropower has an undeniable advantage over other types. Another undoubted advantage of hydroelectric power plants is that they belong to truly RES, in contrast to nuclear and thermal energy.

The authors (Sinyak & Petrov 2008) analyzed the costs of hydrogen production and concluded that the electrolytic technology for hydrogen production would require about 60 kWh of electricity per 1 kg. We consider how much it costs to produce 1 kg of gaseous hydrogen by electrolysis when generating electricity using various technologies (Table 2). It should be noted that a change in the cost of hydrocarbon fuels can significantly affect the cost of electricity generated by thermal power plants, while electricity produced by nuclear power plants and hydroelectric power plants practically does not depend on the global price situation in fuel markets.

As mentioned previously, thermal energy-producing companies or private households will be the main consumers of hydrogen. We then take into account the price of thermal energy generated by various technologies. The findings of estimating the cost of 1 MJ of thermal energy produced by gaseous fuel burning are shown in Table 3. Please note that these calculations are of an estimated nature and do not take

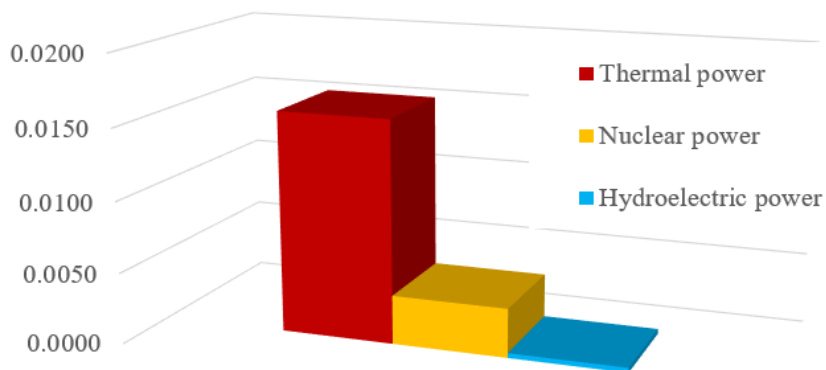


Fig. 1: Electrical power generation price in Russia for 1 kWh, Euro.



into account capital investments in generation facilities, as well as transportation costs.

The estimated calculation given in Table 3 shows the undeniable advantage of hydroelectric power plants as a way to generate electricity for hydrogen production. It is fascinating to compare the costs of thermal energy produced from pure hydrogen and its mixing with natural gas, which is the primary energy source in the majority of European nations right now. The cost of the thermal energy received will be lower than the cost of thermal energy produced by burning natural gas with an equal mixture of hydrogen produced by electrolysis at hydroelectric power plants (50%) and natural gas (50%) (Fig. 2).

## DISCUSSION

With a more accurate calculation, it is required to take into account the depreciation costs for electrolysis plants in the cost of the received energy (Sinyak & Petrov 2008). Within the framework of this research work, the authors do not talk about the process of gas transportation from the place of its production to the place of its consumption. Hydrogen can be transported in its gaseous or liquid state. The fundamental difference for determining costs lies in the significantly low temperature of liquid hydrogen: below 2600°C at atmospheric pressure, which is technically very difficult and expensive to make for mass consumption. By increasing the pressure in the line to 10 bar, we can slightly increase the boiling point by 100°C. By the way, the process of gas liquefaction is very energy-intensive and will require up to 1/3 of the growth in the cost of hydrogen (Kraev et al. 2018). When transporting

liquid hydrogen, it will be necessary to additionally provide high-level thermal insulation for pipelines (Krenn & Desenberg 2020). Pumping liquid hydrogen will also require more additional energy to provide a cryogenic temperature level in the elements of pumping equipment. In the aggregate of the difficulties associated with the transportation of the liquid phase of hydrogen, this type of transportation at the level of modern technologies for industrial volumes of hydrogen production seems unacceptable.

The most optimal alternative to pipeline transportation of liquid hydrogen is its pumping in a gaseous state. Alternatively, the existing natural gas pipeline infrastructure in the world can be used (Belousov 2021). Modern gas pipelines, such as the Nord Stream, make it possible to transport any gas at high pressures up to 200 bar over remote distances of several thousand kilometers. Taking into account the significant differences in the physical properties of hydrogen and methane, as the main component of natural gas, the task of adapting compressor stations for pumping gaseous hydrogen may arise. The fact is that hydrogen is a gas with a low density (0.09 kg/m<sup>3</sup>), and for comparison, the density of methane is an order of magnitude higher: 0.7 kg/m<sup>3</sup>. With the existing high level of technological development, this problem is easily solved by certain engineering and technical methods. However, when transporting a gaseous mixture of natural gas and hydrogen in a ratio of 4:1, the change in the density of the mixture is not critical, and it is possible to use the existing gas transmission infrastructure in Europe.

## CONCLUSION

The research project takes into account a new strategic focus on environmentally friendly hydrogen energy among several top European nations. Based on RES and the current gas transportation infrastructure, Russia has a unique chance to create the most promising and environmentally friendly hydrogen fuel for the export of gaseous hydrogen to EU nations. According to estimated calculations made by the authors, electrolytic hydrogen produced using existing hydroelectric power plants provides a significant (more than ten times) cost advantage. The environmental situation is improved at

Table 1: Producing green hydrogen prices in the countries of the world by 2050.

Country	Hydrogen price, Euro/kg
Japan	2.75
Poland	2.5
Germany	2.25
France	2
Argentina	1.5
Canada	1.5
Russia	1.5
Australia	1.25
Brazil	1.25
Chile	1.25
China	1.25
India	1.25
Morocco	1.25

Table 2: Comparison of hydrogen production cost depending on the method of generating electricity.

Generation source	Cost of 1 kWh of electricity, Euro	Cost of 1 kg of hydrogen, Euro
Thermal power	0.01 - 0.02	0.60 – 1.25
Nuclear power	0.003 – 0.004	0.18 – 0.22
Hydroelectric power	0.0002 – 0.0004	0.015 – 0.025

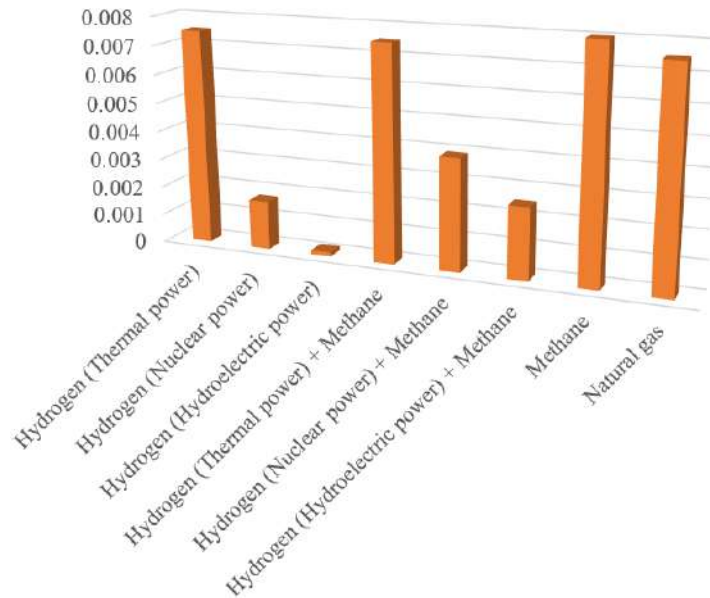


Fig. 2: Cost of generating 1 MJ of thermal electricity depending on the type of gas generation, Euro.

Table 3: Comparison of the cost of thermal energy depending on energy production technologies.

Energy carrier		Specific heat of combustion of gaseous fuel, MJ/kg	Cost of producing 1 kg of gaseous fuel, Euro	Cost of 1 MJ of thermal energy when burning gas, Euro
Hydrogen	Thermal power	120	0.60 – 1.25	0.005 – 0.01
	Nuclear power		0.18 – 0.22	0.0015 – 0.0019
	Hydroelectric power		0.015 – 0.025	0.0001 – 0.0002
Hydrogen + Methane (50% H <sub>2</sub> and 50% CH <sub>4</sub> by mass)	Thermal power		0.50 – 0.90	0.006 – 0.009
	Nuclear power	85	0.30 – 0.35	0.0038 – 0.004
	Hydroelectric power		0.24 – 0.25	0.0029 – 0.003
Methane		50	0.45	0.008
Natural gas		45	0.40	0.0075

the same time as the basic requirements for the production of “green” hydrogen using RES are met.

## REFERENCES

- Aminov, R.Z. and Bairamov, A.N. 2016. Evaluation of the efficiency of hydrogen production based on off-peak electricity from nuclear power plants. *Int. Scient. J. Alt. Energy and Ecol. (ISJAEE)*, 5: 59-70.
- Aslanov, A. 2021. Unsteady effects in cryogenic fuel pipelines of perspective aviation jet engines. *J. of Int. Acad. of Refr.*, 1: 3-11.
- Belousov, A.R. 2021. On the general approaches of the Russian Federation to the process of decarbonization of the economy. *Kommersant*, 189: 2
- Fateev, V.N., Alekseeva, O.K., Korobtsev, S.V., Seregina, E.A., Fateeva, T.V., Grigoriev, A.S. and Aliev, A.Sh. 2018. Problems of accumulation and storage of hydrogen. *Chem. Probl.*, 4(16): 453-483.
- Gurkov, A. 2014. From the wind and the sun will make “green hydrogen” for cars. *Autogas filling complex + Alternative fuel*, 9(90): 46-47.
- Isaeva, E.A. 2019. The evolution of the energy policy of the European Union. *Innov. and invest.*, 9: 113-120.
- Kaveshnikov, N. Yu. 2014. The policy of the European Union in the field of energy saving. *Bull. of MGIMO Un.*, 4(37): 109-115.
- Krayev, V. M. 2020. Economic efficiency of the use of cryogenic fuels in aviation. *Moscow Ec. J.*, 11: 699-712.
- Krayev, V.M., Tikhonov, A.I. and Novikov, S.V. 2018. Economic conversion in the aviation industry. *Russ. Eng. Res.*, 38(4): 330-333.
- Krenn, A. and Desenberg, D. 2020. Return to service of a liquid hydrogen storage sphere. *IOP Conf. Ser.: Mater. Science and Eng.*, 755(1): 012023.
- Sinyak, Y.V. and Petrov, V.Y. 2008. Predictive estimates of the cost of hydrogen in the conditions of its centralized production. *Forec. Probl.*, 3(108): 35-46
- Zuev, V. N. 2007. Formation of the EU energy policy. *Bull. of Int. Org. (ed), Science, New Econ.*, 2(1): 53-62.



# How Livestock and Industrial Energy Affect Indonesia's Surface Temperature

N. P. A. Widjanarko and A. P. Siregar†

Department of Agricultural Socio-economics, Faculty of Agriculture, Universitas Gadjah Mada (UGM), Yogyakarta Special Region, Indonesia

†Corresponding author: Abi Pratiwa Siregar; [abipratiwasiregar@ugm.ac.id](mailto:abipratiwasiregar@ugm.ac.id)

Nat. Env. & Poll. Tech.  
Website: [www.neptjournal.com](http://www.neptjournal.com)

Received: 28-04-2022

Revised: 27-05-2022

Accepted: 30-05-2022

## Key Words:

Livestock  
Industrial energy consumption  
Renewable energy  
Surface temperature

## ABSTRACT

As part of the agricultural sector, livestock is a source of food for Indonesia and consumers abroad. Therefore, the demand for livestock commodities tends to increase, aligning with the positive growth of the population. Additionally, as part of their efforts to promote higher consumption, one of the attempts made by producers and the government as policymakers is to encourage an increase in the livestock population from time to time. On the other hand, the industrial sector that engages in processing likewise continues to expand to improve products downstream. However, the increase in the number of livestock and industries can contribute to the rise in emissions that impact environmental conditions. In this study, the environmental situation referred to is temperature variations. Moreover, this research aims to determine the impact of livestock population and energy consumption in the industrial sector on temperature changes. The method used in this research is explanatory. The data sources used for multiple linear regression analysis came from the World Bank, Indonesia's Central Bureau of Statistics (BPS), and the Ministry of Energy and Mineral Resources. The analysis reveals that large and small livestock, as well as energy use in the industrial sector are factors that have an impact on Indonesia's temperature. Large and small livestock cause an increase in temperature due to the large number of emissions produced by enteric fermentation and excretion. Meanwhile, the rise in energy consumption is inversely proportional to changes in temperature. This condition occurred because of the higher proportion of renewable energy in total energy consumption.

## INTRODUCTION

The increase in population needs to be followed by the rise in the food supply. Livestock is a business field that produces commodities to fulfill basic needs. According to Van Kernebeek et al. (2016), Claeys et al. (2014), and Bernacka (2011), the products produced by the livestock sector are not only for consumption but also for the production of protein, minerals, and vitamins. Furthermore, based on the Directorate General of Livestock and Animal Health (2019) publication, the demand for eggs, poultry meat, large and small livestock meat, and milk in Indonesia has increased by around 3.5%, 9.3%, 18.7%, and 0.3% per year, respectively. The increase was not only in raw materials but also in processed products, such as dried meat, canned meat, and sausage.

Even though it helps the community achieve its fundamental needs, the increasing cattle population has a negative impact on the environment. According to Seidavi et al. (2019), poultry (free-range chicken, laying hen, and broiler) contributes to increased exhaust gases released into the air. The gas produced is generated from the respiration process in the form of carbon dioxide and manure in

methane. The highest comes from the excretion process in the form of nitrous oxide and ammonia. These gases contribute about 0.64% of agricultural emissions and lead to warmer temperatures. Like poultry, large and small livestock processes also contribute to exhaust gases that make the temperature warmer.

Moreover, Zervas & Tsiplakou (2012) along with Seidavi et al. (2019) explained that large and small livestock release greenhouse emissions from four processes such as respiratory (carbon dioxide), excretion (nitrous oxide and ammonia), enteric fermentation (methane), and manure storage (methane). In addition, Mandal et al. (2013) described that large and small livestock emitted higher emissions than poultry because livestock experienced enteric fermentation. This process releases higher methane than from manure management process. Furthermore, Swain et al. (2016) described that large and small livestock emitted gas from enteric fermentation, and manure is 23 times higher in a potentially degraded environment than from respiratory. These gases relatively increase the temperature higher than in the previous period.

In addition to meeting the community's needs, the government should always strive for the smoothness and

acceleration of production and service activities. One form of this effort is to encourage the enhanced performance of the industrial sector. According to the Ministry of Industry (2010), this sector contributes approximately 26.4% of Indonesia's GDP. The BPS publication (2022a) stated the number of industries in this sector grew by 2.45% per year. Along with increasing awareness of environmental sustainability, the government also encourages business actors in the industrial sector to increase the renewable energy mix to total energy consumption.

In terms of GDP and emissions from energy use, the industrial sector contributes significantly. Juntueng et al. (2012) explained that the industrial sector contributes to emissions from energy usage, such as electricity usage and fuel combustion process. Furthermore, Punyawadee (2010) discovered that energy usage of the industry has a positive impact on economic growth. However, increasing energy consumption will negatively impact the environment through the emissions spread to the air. Additionally, Sharvini et al. (2018) and Hidayatno et al. (2019) described that non-renewable energy used in the industrial sector emits carbon dioxide, increasing the temperature. These studies also draw attention to the government of Indonesia's initiatives to decrease non-renewable energy use and increase the use of renewable energy, which is more environmentally friendly and safe for the environment.

Studies on emission generally involve manure (Nugrahaeningtyas et al. 2018), enteric fermentation (Thakuri et al. 2020), and feces or urine (Seidavi et al. 2019). In other words, studies on the relationship between livestock population and energy use are still rare. In fact, in developing countries, especially Indonesia, these two variables play a strategic role. To meet the basic needs of Indonesian citizens as well as to produce goods for export, the population of livestock will therefore continue to grow. Additionally, as one of the tools for economic development, the industrial sector's energy consumption will undoubtedly continue to rise periodically.

This study aims to determine which factors can affect the surface temperature change in Indonesia. We use large and small livestock, poultry population, and industry sectors' energy consumption as independent variables to investigate the range of dependent variable values.

## MATERIALS AND METHODS

### Research Method

This research uses an explanatory approach to investigate the phenomena that occur among the variables involved and prepare recommendations for the future. The type of data

used in this study is quantitative and statistical tests are used to assess the validity of the relationship between exogenous and endogenous variables (Sue & Ritter 2012).

### Data Source

The data for this study is accessed from the World Bank, Indonesia's Central Bureau of Statistics (BPS), and the Ministry of Energy and Mineral Resources. Temperature data has been accessed from the World Bank (World Bank 2022a). The information accessed from BPS consists of the number of free-range chickens (BPS 2022b), laying hens (BPS 2022c), broilers (BPS 2022d), horses (BPS 2022e), beef cattle (BPS 2022f), dairy cattle (BPS 2022g), buffalo (BPS 2022h) and goat (BPS 2022i). Furthermore, the data obtained from the Ministry of Energy and Mineral Resources (2016, 2020) is energy use in the industrial sector. Moreover, the data interval used in this study is from the period 2000 to 2018.

### Data Analysis

The data analysis used to estimate the determinants of temperature changes in Indonesia is multiple regression using the Ordinary Least Squares (OLS) (1). OLS is used because the data is normally distributed, and applicable with a relatively small observation size (Ahmad et al. 2021). The dependent variable in this study is the surface air temperature of Indonesia ( $^{\circ}\text{C}$ ) (World Bank 2022b). Meanwhile, the independent variables consist of the number of poultry, large and small livestock (Directorate General of Livestock and Animal Health 2021), and the use of energy in the industrial sector (both from fossil fuels and biomass) measured in barrels of oil equivalent (BOE) units (Ministry of Energy and Mineral Resources 2020)

$$Y = \beta_0 + \beta_1 X_1 + \beta_2 X_2 + \beta_3 X_3 + \varepsilon \quad \dots(1)$$

Where; Y = temperature;  $\beta_0$  = intercept;  $\beta_1$ - $\beta_3$  = coefficient of independent variable;  $X_1$  = number of poultry (free-range chicken + laying hen + broiler);  $X_2$  = large and small livestock (horse + beef cattle + dairy cattle + buffalo + goat);  $X_3$  = industrial sector's energy consumption;  $\varepsilon$  = error term.

## RESULTS AND DISCUSSION

### Temperature

The average annual temperature in Indonesia from 2000 to 2018 was 26.16  $^{\circ}\text{C}$ , ranging from 25.9  $^{\circ}\text{C}$  to 26.4  $^{\circ}\text{C}$  (Fig. 1). The temperature in Indonesia tended to decrease between 2000 and 2008, then increase after that. According to Komariah et al. (2015), the increase or decrease in temperature cannot be separated from the area covered by clouds. Therefore, the larger/smaller the range of cloud cover, the

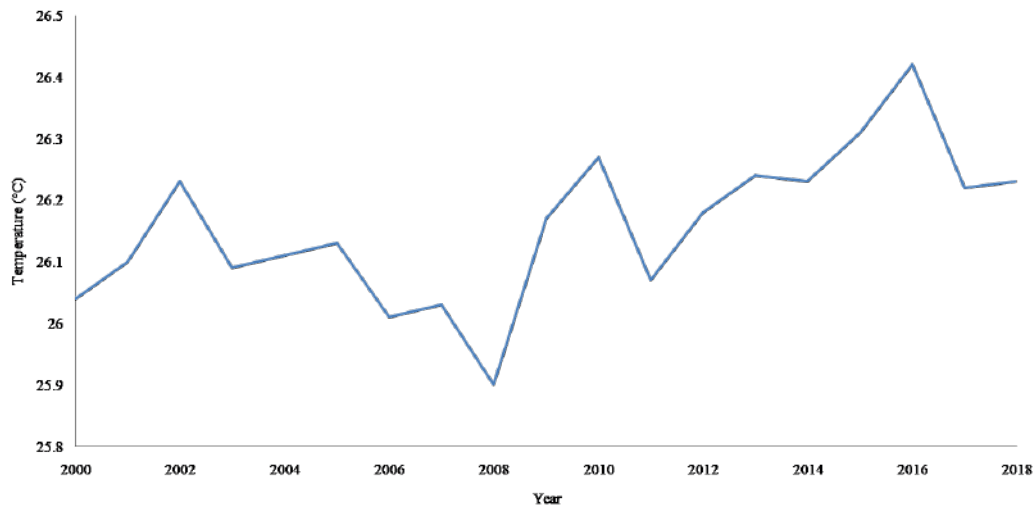


Fig.1: Indonesia's temperature in °C from 2000 to 2018.  
(Source: World Bank 2022a)

temperature will tend to decrease/increase. This change is caused by the decreasing/increasing intensity of solar radiation pushing more/less water vapor carried to the clouds and then advancing/decreasing the probability of rain.

Furthermore, according to Megahed & Srikantaswamy (2020), a decrease in temperature can cause relative humidity to increase. Both of these phenomena can increase the chance of rain. In contrast to the incidence of increasing temperature, Cianconi et al. (2020) stated that an increase in temperature could cause a decrease in humidity and evapotranspiration and later cause dryness.

### Free-Range Chicken

Free-range chicken is a general term for non-race chicken in Indonesia. From 2000 to 2018, the average population was 274,794,566 units (Fig. 2), increasing by almost 0.90% annually. According to the Ministry of Agriculture (2008), Java Island is the area with the highest number of free-range chickens in Indonesia. Therefore, as the population of this area declines, it immediately affects the national decrease in the total number of free-range chickens. When this incidence took place in 2007, the amount of this livestock in the Java Island region had fallen by 14.29%. As a result, there was a nationwide decline in that year of up to 6.47%. In addition, mortality instances caused a fall in the number of chickens that year, which meant that more free-range chickens died than in previous years. According to Nova et al. (2012), the increase in mortality was caused by the culling of free-range chickens due to the reappearance of bird flu cases in Indonesia in 2007.

In general, the part of free-range chicken consumed is eggs and meat. Therefore, another benefit of this

livestock is a saving instrument for farming households. This condition happens because the selling price is relatively higher than other types of chicken (Kalangi et al. 2020).

### Laying Hen

Laying hen is a common term for a female, grown chicken that is kept primarily for laying eggs, and whose eggs are mainly consumed by the Indonesian people compared to other types of poultry. According to the Directorate General of Livestock and Animal Health (2019) data, per capita consumption per year for laying hen eggs increases by approximately 3.65% per year. Furthermore, this institution reports that in 2017 the demand for laying hen eggs was relatively higher than in other periods, around 6.635%. Based on Astaman et al. (2020) study, the increase in demand occurred due to the decline in egg prices. This condition is in line with the Directorate General of Livestock and Animal Health (2019) data, which stated a decrease in egg prices by IDR 617, tended to increase egg prices in the previous period. Responding to this positive trend, these livestock producers are trying to increase the population to meet consumer needs and increase market penetration. The laying hen population, which tends to rise annually, is a good indicator of this effort (Fig. 3).

### Broiler

Indonesia has various types of chickens, and broilers are the country's most abundant type of chicken. This fact is inseparable from the preferences of people who tend to choose broilers over other types of chicken because of the relatively lower costs and comparably larger portions of meat. Based



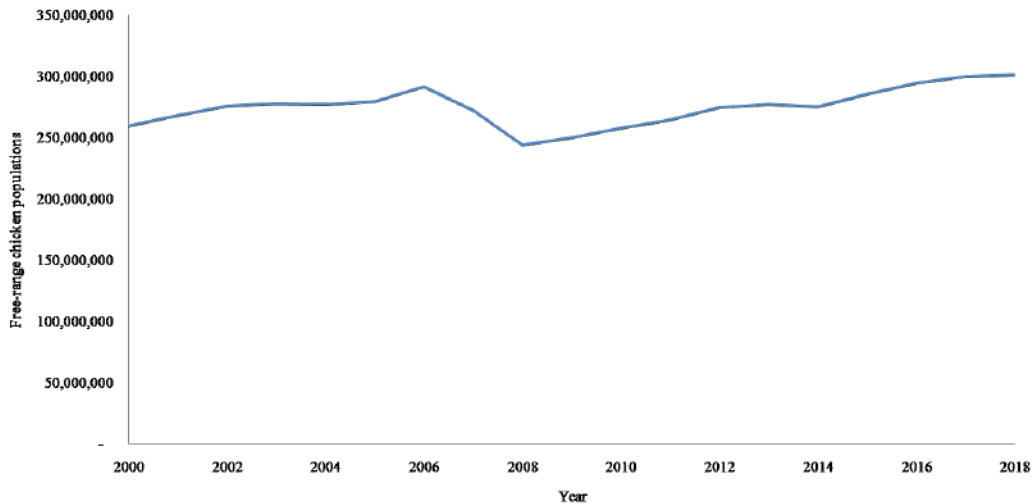


Fig. 2: Free-range chicken populations from 2000 to 2018.  
(Source: BPS 2022a)

on Fig. 4, the broiler population continues to increase from time to time, increasing 11.67% per year.

## Horse

East Nusa Tenggara, West Nusa Tenggara and South Sulawesi are the top three provinces with the largest horse populations in Indonesia (BPS 2022d). In these three regions and other provinces in Indonesia, horses are used for various purposes, including labor, transportation, sports, recreation, and consumption (Sihita et al. 2018). According to Kadir (2011), horse meat has advantages over beef, namely the relatively lower fat content. Furthermore, according to Ginting et al. (2019), another product from horses (horse milk) has good

ingredients for treating several diseases, namely asthma, hypertension, and diabetes. Furthermore, the number of horses from 2000 to 2018 has consistently been above 300,000 heads (Fig. 5). However, there has been a downward trend in the last eighteen years. High demand for horse meat compared to supply and poor rearing practices are two factors in the declining horse population.

## Beef Cattle

According to Akinsulu et al. (2019), the consumption of beef cattle increases when the number of household members increases (Fig. 6). In addition, higher income and education level have a positive effect on the amount of beef consumed.

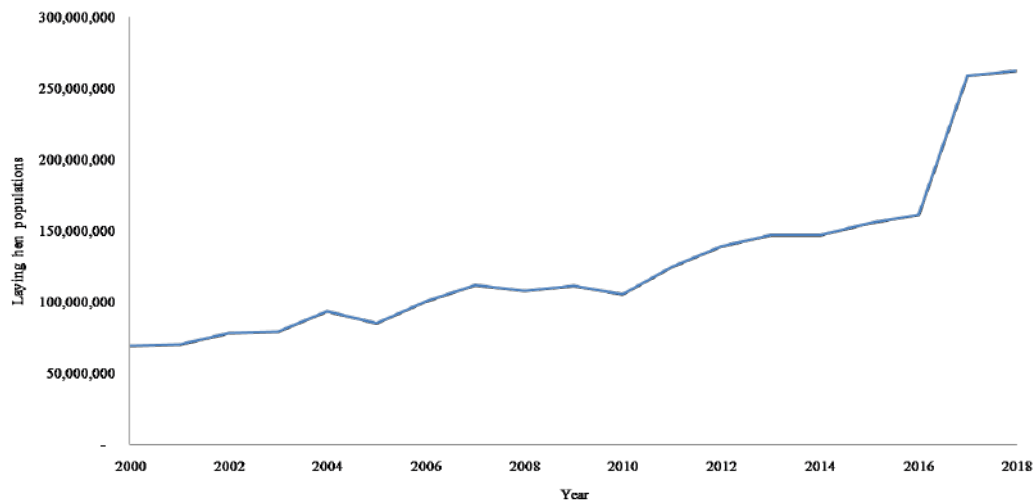


Fig. 3: Laying hen populations from 2000 to 2018.  
(Source: BPS 2022b)

As one of the largest countries in the world, Indonesia has experienced an increase in population, economic growth, and an improving level of education from time to time. Thus, the number of beef cattle needed to meet beef consumption is also increasing. Based on this, cattle farmers look for more livestock to take advantage of opportunities to meet consumer demand.

**Dairy Cattle**

The main product of dairy cows is milk. Based on data from the Directorate General of Livestock and Animal Health

(2021), the consumption level of cow’s milk by the Indonesian people is around 16.27 kg per year. Therefore, with the existing population, the need for this product reaches 4.3 million tons per year. However, based on Fig. 7, there was a population decline of 167,674 units from 2012-2013. This decline impacts domestic cow’s milk production, which is increasingly declining and encouraging more imports. On this basis, the government issued the Blue Print for Indonesian Dairy 2013-2025. Through this roadmap, it is hoped that the national demand for cow’s milk can be dominated (>50%) by domestic producers. One of the efforts to achieve this target is

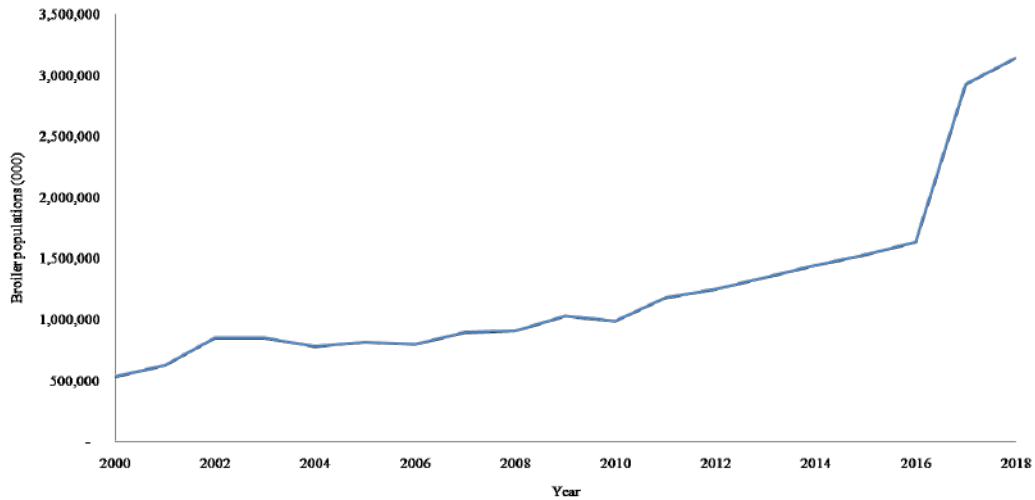


Fig. 4: Broiler populations from 2000 to 2018. (Source: BPS 2022c)

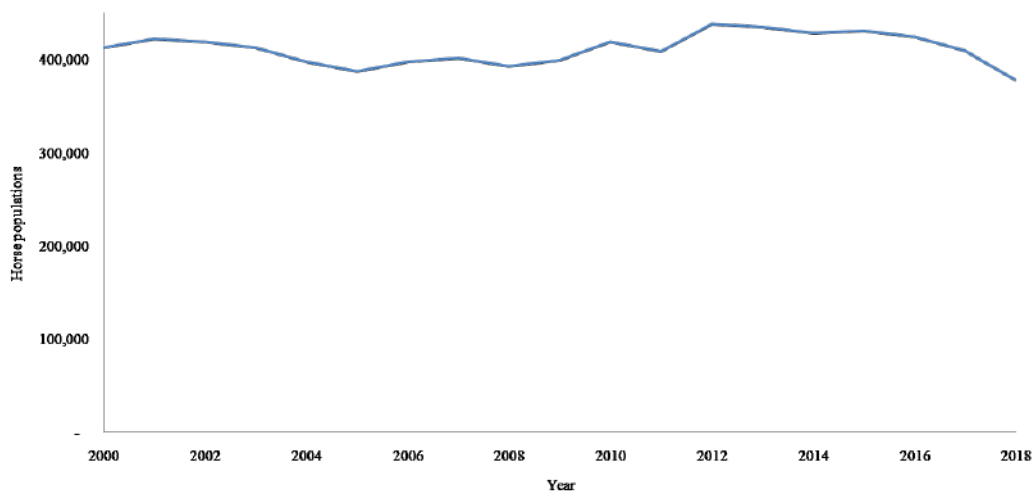


Fig. 5: Horse populations from 2000 to 2018. (Source: BPS 2022d)

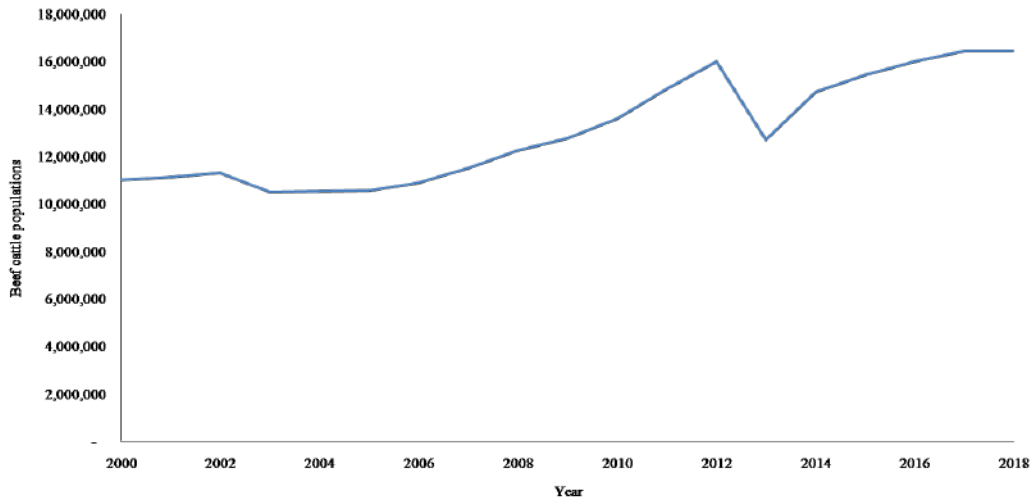


Fig. 6: Beef cattle populations from 2000 to 2018. (Source: BPS 2022e)

to increase the dairy cattle population sustainably. The trend of the dairy cattle population, which has increased annually since 2013, provides evidence of this industry.

**Buffalo**

Buffalo is one of the ruminant animals kept by many people in Indonesia, especially farmers. This livestock is used to assist producers in ploughing the land. Based on the study of Amin et al. (2016), buffalo are relatively common in the central part of Indonesia, such as West Nusa Tenggara, Bali, and Sulawesi. However, Amin et al. (2016) explained that from

2003 to 2011, there was a decline in the buffalo population (Fig. 8). These findings align with this study. In the last 18 years, there has been a decline in the buffalo population by around 4.31% per year. This decline is thought to be caused by poor livestock cultivation, namely breeding the closely linked gene of buffalo.

**Goat**

The goat population in Indonesia tends to increase from time to time. This increase is inseparable from the role of goats as a source of protein for the Indonesian people and the tradition

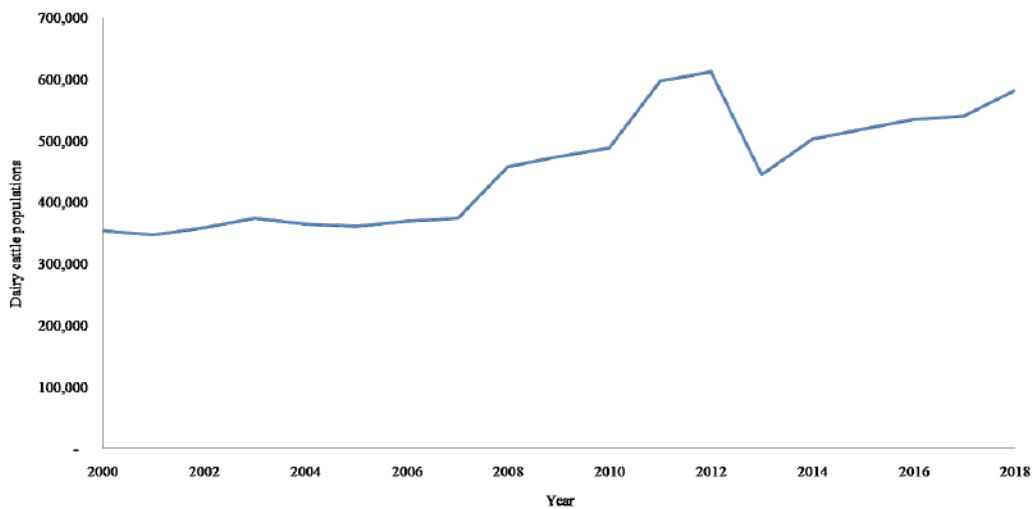


Fig. 7: Dairy cattle populations from 2000 to 2018. Source: BPS 2022f.

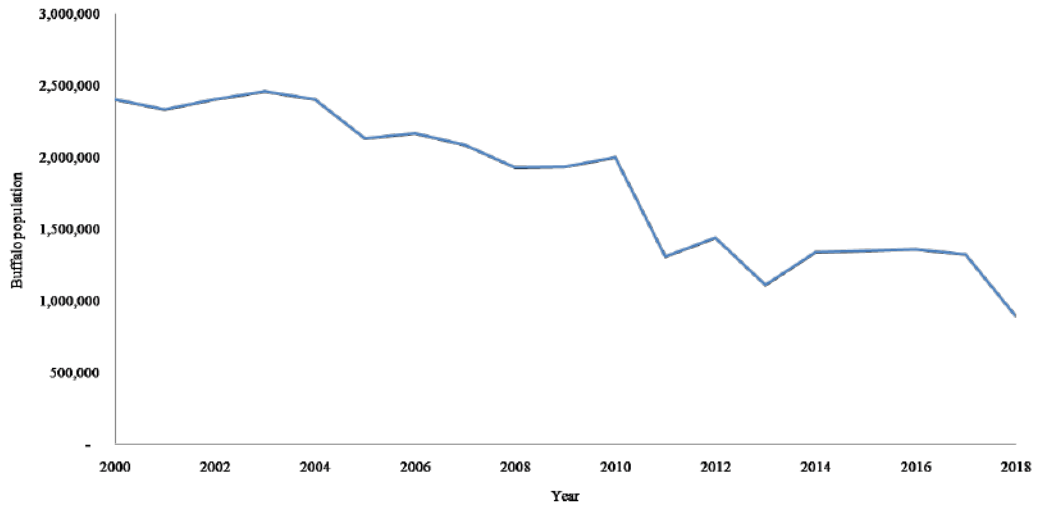


Fig. 8: Buffalo populations from 2000 to 2018. (Source: BPS 2022g)

of some people in this country who use goats as sacrificial animals (Murray-Prior et al. 2010). Furthermore, from the agricultural side, goat manure is used as a combination of organic fertilizers to meet plants’ nutrient needs (Kurniawati et al. 2021). On this basis, goat breeders continue to seek to increase the number of livestock to increase income through meeting community needs.

**Industrial Sector Energy Consumption**

The industrial sector plays a strategic role in contributing to Indonesia’s GDP. Therefore, efforts are made to improve

the quality and quantity levels in this economic sector. Additionally, the industrial sector has a direct impact on energy usage to support its activities. From 2000 to 2018 (Fig. 10), the amount of energy used for this sector fluctuated with an upward trend. The increase is around 1.94% per year. Furthermore, the increase or decrease is caused by the number of industries, which tends to change every year.

**Effect of Livestock Population and Industrial Energy Consumption on Temperature**

Large and small livestock contribute to air emissions through

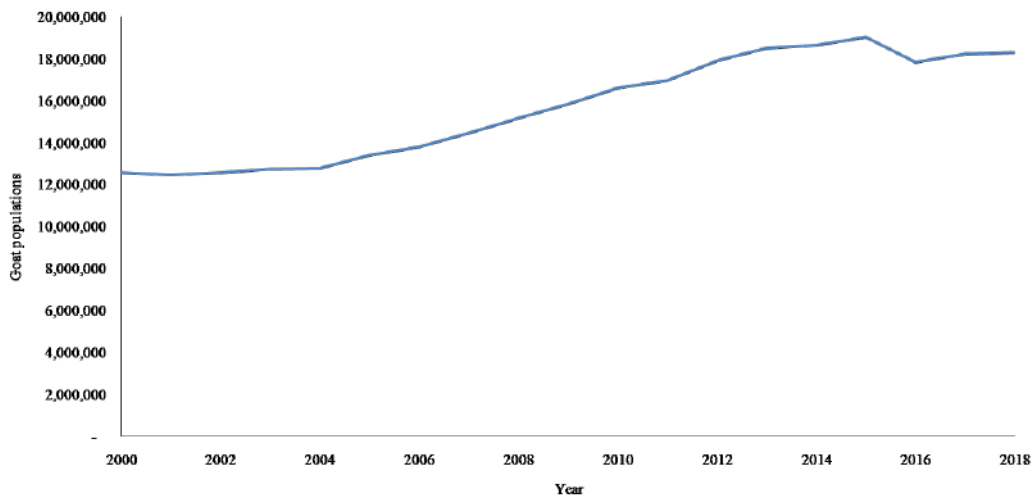


Fig. 9: Goat populations from 2000 to 2018. (Source: BPS 2022h)

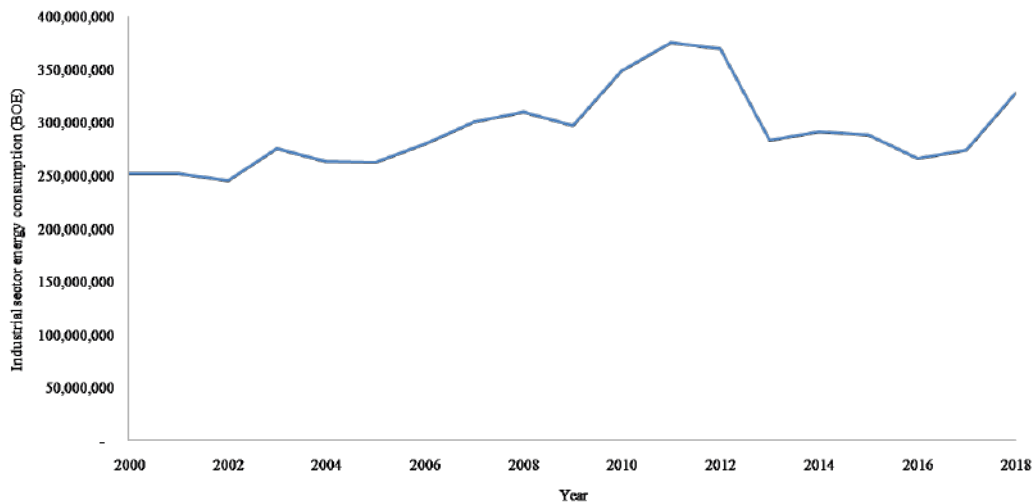


Fig. 10: Industrial sector energy consumption from 2000 to 2018. (Source: Ministry of Energy and Mineral Resources 2016, 2020)

enteric fermentation and excretion. Enteric fermentation occurs in the digestive tract of ruminant animals, known as the rumen. When the feed enters the digestive tract of ruminants, it produces gas in the form of carbon dioxide. Methane is produced when the gas reacts in the rumen with hydrogen gas and microbes (Thakuri et al. 2020). According to Gibbs et al. (2001), methane from enteric fermentation is released as a gas, either on exhalation (respiration) or flatulence. Furthermore, the process of excreting or removing waste from the body of ruminants and other large livestock, as well as small livestock is in the form of feces and urine (Dong et al. 2014). Ammonia and nitrous oxide, two volatile gases, are present in both types of contaminants. Ammonia gas is produced from the reaction between microbial enzymes in the feces and urea in the urine. This process can continue until ammonia is oxidized and turns into nitrate and nitrous oxide during nitrification (Cobellis et al. 2016, Wang et al. 2017).

Increasing the population of large and small livestock by 1 unit will lead to an increase in temperature of around  $0.00000319^{\circ}\text{C}$  (Table 1). This finding is in line with a study from Lynch (2019), who stated that livestock, dominated by large and small livestock, became the largest methane contributor through enteric fermentation. On the other hand, Nugrahaeningtyas et al. (2018) explained that emissions from the excretion of large and small livestock are relatively higher than different types of livestock. This rather large share occurs because the consumption of feed by these animals is increasingly intense than that of poultry.

In detail, Santiago-Juarez et al. (2016) and Zhuang et al. (2020) explained how the increasing livestock population

leads to an increase in temperature: enteric fermentation and excretion produce exhaust gas in the form of methane. Additionally, excretory products are used as manure-making basic materials. Thus, the manure processing cycle also produces exhaust gases that are released into the air. This condition happens because there is an accumulation of around  $7,222.1 \text{ g CO}_2\text{-eq}$  in the processing cycle. Therefore, the more significant emission has a positive effect on the increase in temperature in Indonesia.

Furthermore, the energy consumption variable affects the dependent variable differently (Table 1). Increasing energy consumption by the industrial sector negatively impacts the increase in temperature. In Indonesia, the energy used by the industrial sector consists of non-renewable and renewable, such as coal, oil, gas, and biomass crop residue (rice, sugar, palm oil, and coconut) (ADB 2020). Over time, especially since 2002, the government has encouraged the use of more environmentally friendly energy than non-renewable energy. This effort is realized through Ministerial Decree No. 1122 K/30/MEM/2002 about Distributed Small Power Generation.

Empirically, a one-unit increase in energy use for the industrial sector will reduce the temperature by about  $0.000000184^{\circ}\text{C}$  (Table 1). Because the industrial sector uses less energy and creates less carbon dioxide, the temperature decreases. The increased biomass composition is what causes the reduction in emissions, and this kind of resource is relatively eco-friendly. This finding supports the results of Gyamfi et al. (2021) who concluded that the use of energy involving biomass could reduce pollution from carbon dioxide gas.



Table 1: Regression results.

Variables	Coefficient	Standard Error	P-value
C	2.57E+01	0.19E+00	0.0000
Poultry	-3.64E-11	4.31E-11	0.4125
Large and small livestock	3.19E-08	9.12E-09	0.0032
Industrial sector's energy consumption	-1.84E-09	6.70E-10	0.0151
Adjusted R-square	0.50E+00		
F-statistics	7.10E+00		0.003414

Source: Secondary data analysis

## CONCLUSION

Livestock populations and energy consumption in the industrial sector tend to increase continuously to fulfill the community's demand. Empirically, large and small livestock, as well as the energy usage from the group of particular firms affect the temperatures inversely. The positive growth of the cattle, buffalo, horse and goat population encourages a warmer climate. This condition is caused by attention to waste gas management that has not been maximized and is oriented towards environmental sustainability. Based on this study, it is hoped that stakeholders in livestock farming will focus on economic and social aspects and the environment. On the contrary, higher energy consumption negatively impacts the temperature. Thus, the government's efforts to encourage business actors to increase the percentage of environmentally friendly energy for the production process need to be continuously stimulated and evaluated from time to time.

## REFERENCES

- Asian Development Bank (ADB). 2020. Indonesia Energy Sector Assessment, Strategy, and Road Map Update. Report Dec. 2020, Asian Development Bank, Philippines, pp. 1-40. <https://doi.org/10.22617/TCS200429>.
- Ahmad, I., Dar, M.A., Fenta, A., Halefom, A., Nega, H., Andualem, T.G. and Teshome, A. 2021. The spatial configuration of groundwater potential zones using the OLS regression method. *J. Afr. Earth Sci.*, 177: 1-9.
- Akinsulu, A.A., Ajijola, S., Odetola, S.K. and Awoyemi, D.O. 2019. Factors influencing meat consumption in Ijebu-North local government area of Ogun States, Nigeria. *J. Mark. Consum. Res.*, 52: 10-16.
- Amin, M., Suarsini, E., Azmi, I. and Gofur, A. 2016. Phylogenetic analysis of local endemic buffalo (*Bubalus bubalis*) based on cytochrome B gene in central Indonesia. *J. Technol.*, 78(5): 393-397.
- Astaman, P., Siregar, A.R. and Nurbayani, S.U. 2020. Analysis effect the price of the demand for chicken eggs in Biringkanaya district. *IOP Conf. Ser. Earth Environ. Sci.*, 473: 1-6.
- Bernacka, H. 2011. Health-promoting properties of goat milk. *Med. Water*, 67(8): 507-511.
- BPS. 2022a. The Number of Big and Medium Industrial Processes, Java and Outside Java. Online: <https://www.bps.go.id/indicator/9/732/1/jumlah-industri-pengolahan-besar-dan-sedang-jawa-dan-luar-jawa.html> (accessed on 18 March 2022).
- BPS. 2022b. Free-Range Chicken Population By Province. Online: <https://www.bps.go.id/indicator/24/476/1/populasi-ayam-buras-menurut-provinsi-.html> (accessed on 18 March 2022).
- BPS. 2022c. Laying Hen Population By Province. Online: <https://www.bps.go.id/indicator/24/477/1/populasi-ayam-ras-petelur-menurut-provinsi.html> (accessed on 18 March 2022).
- BPS. 2022d. Broiler Population By Province. Online: <https://www.bps.go.id/indicator/24/478/1/populasi-ayam-ras-pedaging-menurut-provinsi.html> (accessed on 18 March 2022).
- BPS. 2022e. Horse Population By Province. Online: <https://www.bps.go.id/indicator/24/475/1/populasi-kuda-menurut-provinsi.html> (accessed on 18 March 2022).
- BPS. 2022f. Beef Cattle Population By Province. Online: <https://www.bps.go.id/indicator/24/469/1/populasi-sapi-potong-menurut-provinsi.html> (accessed on 18 March 2022).
- BPS. 2022g. Dairy Cattle Population By Province. Online: <https://www.bps.go.id/indicator/24/470/1/populasi-sapi-perah-menurut-provinsi.html> (accessed on 18 March 2022).
- BPS. 2022h. Buffalo Population By Province. Online: <https://www.bps.go.id/indicator/24/471/1/populasi-kerbau-menurut-provinsi.html> (accessed on 18 March 2022).
- BPS. 2022i. Goat Population By Province. Online: <https://www.bps.go.id/indicator/24/472/1/populasi-kambing-menurut-provinsi.html> (accessed on 18 March 2022).
- Cianconi, P., Betrò, S. and Janiri, L. 2020. The impact of climate change on mental health: A systematic descriptive review. *Front. Psych.*, 11(74): 1-15.
- Claeys, W.L., Verrae, C., Cardoen, S., De Block, J., Huyghebaert, A., Raes, K., Dewettinck, K. and Herman, L. 2014. Consumption of raw or heated milk from different species: An evaluation of the nutritional and potential health benefits. *Food Control*, 42: 188-201.
- Cobellis, G., Trabalza-Marinucci, M. and Yu, Z. 2016. Critical evaluation of essential oils as rumen modifiers in ruminant nutrition: A review. *Sci. Total Environ.*, 46: 556-568.
- Directorate General of Livestock and Animal Health. 2019. Livestock and Animal Health Statistics. Ministry of Agriculture, Indonesia.
- Directorate General of Livestock and Animal Health. 2021. Ministry of Agriculture Committed to Developed Domestic Fresh Milk Production. Online: <http://ditjenpkh.pertanian.go.id/kementan-berkomitmen-kembangkan-produksi-susu-segar-dalam-negeri#:~:text=> (accessed on 4 April 2022).
- Dong, R.L., Zhao, G.Y., Chai, L.L. and Beauchemin, K.A. 2014. Prediction of urinary and fecal nitrogen excretion by beef cattle. *J. Anim. Sci.*, 92: 4669-4681.
- Gibbs, M. J., Conneely, D., Johnson, D., Lasse, K. R. and Ulyatt, M. J. 2001. CH<sub>4</sub> Emissions from Enteric Fermentation in Austria. Working Paper Intergovernmental Panel on Climate Change.

- Ginting, S.L., Hamdan, M., Henuk, Y.L., Mirwandhono, R.E. and Wahyuni, T.H. 2019. Reproductive and morphological performances of stallions in District of Karo, North Sumatera, Indonesia. *IOP Conf. Ser. Earth Environ. Sci.*, 260: 1-7.
- Gyamfi, B.A., Ozturk, I., Bein, M.A. and Bekun, F.V. 2021. An investigation into the anthropogenic effect of biomass energy utilization and economic sustainability on environmental degradation in E7 economies. *Biofuels Bioprod. Bioref.*, 15: 840-851.
- Hidayatno, A., Destyanto, A.R., and Noor, S.T. 2019. Conceptualizing carbon emissions from energy utilization in Indonesia's industrial sector. *Energy Procedia*, 156: 139-143.
- Juntueng, S., Chiarakorn, S. and Towprayoon, S. 2012. CO<sub>2</sub> intensity and energy intensity of iron and steel production in Thailand. *Environ. Nat. Resour. J.*, 10(2): 50-57.
- Kadir, S. 2011. Consumer preference for processed meat the horse in Makassar. *Agribisnis*, 10(3): 81-97.
- Kalangi, J. K. J., Rintjap, A. K. and Lainawa, J. 2020. The cooperative farming concept as a business development strategy model of native chickens in Province North Sulawesi Indonesia. *IOP Conf. Ser. Earth Environ. Sci.*, 478: 1-7.
- Komariah, S.M., Sumani, D.W.S., Yoshiyama, K. and Rachmadiyanto, A.N. 2015. The Impacts of Decreasing Paddy Field Area on Local Climate in Central Java, Indonesia. Working Paper Air, Soil, and Water Research Data Center and Agriculture Information.
- Kurniawati, A., Windriyati, R.D.H., Wulansari, N. K., Toth, G. and Toth, Z. 2021. Alternatives for circular bioeconomy in organic farming under excessive nutrients (goat manure arbuscular mycorrhizal fungi): A case study in Indonesia. *Sustainability*, 13: 1-11.
- Lynch, J. 2019. Availability of disaggregated greenhouse gas emissions from beef cattle production: A systematic review. *Environ. Impact Assess. Rev.*, 76: 69-78.
- Mandal, R.A., Dutta, I.C., Jha, P.K., Bir, S., Yadav, B.K. and Kafle, R.R. 2013. CO<sub>2</sub> and CH<sub>4</sub> emission from domestic fuel and livestock keeping in Tarai and Bhawal in Nepal: A household-level analysis. *Environ. Nat. Resour. J.*, 11(1): 1-11.
- Megahed, A.S.H. and Srikantaswamy, S. 2020 Study of the indicators of climate change in Mysore District, Karnataka, India. *Atmos. Clim. Sci.*, 10: 159-167.
- Ministry of Agriculture. 2008. Outlook of Livestock Commodity. Data Center and Agriculture Information, Ministry of Agriculture, Jakarta, Indonesia.
- Ministry of Energy and Mineral Resources. 2016. Handbook of Energy & Economic Statistics of Indonesia. Ministry of Energy and Mineral Resources, Jakarta, Indonesia.
- Ministry of Energy and Mineral Resources. 2020. Handbook of Energy & Economic Statistics of Indonesia. Ministry of Energy and Mineral Resources.
- Ministry of Industry. 2010. Industry for A Better Life. Ministry of Industry, Jakarta, Indonesia
- Murray-Prior, R., Natsir, A., Asja, M. A., Nasrullah, Yusmasari, N.A. and Murray, P. 2010. Goat Meat Consumption in Makassar, Sulawesi: Important for Religious and Cultural Ceremonies, But Many Consider It a Health Risk. The 5<sup>th</sup> International Seminar on Tropical Animal Production, Faculty of Animal Science, Universitas Gadjah Mada, 19-22 December 2010, Yogyakarta, Indonesia, pp. 733-740.
- Nova, T. D., Heryandi, Y. and Setiawan, R. 2012. The Application of Biosecurity and Spread Viruses Detection of Avian Influenza in 3 and 4 Chicken Farm sector in Padang City. Proceedings of the 1<sup>st</sup> Poultry International Seminar, 30-31 August 2012, Padang, Indonesia.
- Nugrahaeningtyas, E., Baek, C.Y., Jeon, J.H., Jo, H.J. and Park, K.H. 2018. Greenhouse gas emission intensities for the livestock sector in Indonesia, based on the national specific data. *Sustainability*, 10: 1-15.
- Punyawadee, V. 2010. Management of energy demand in Thailand. *Environ. Nat. Resour. J.*, 8(1): 44-53.
- Santiago-Juarez, B., Moraes, L.E., Appuhamy, J.A.D.R.N., Pellikaan, W.F., Casper, D.P., Tricarico, J. and Kebreab, E. 2016. Prediction and evaluation of enteric methane emissions from lactating dairy cows using different levels of covariate information. *Anim. Prod. Sci.*, 5: 557-564.
- Seidavi, A.R., Zaker-Esteghamati, H. and Scanes, C.G. 2019. Present and potential impacts of waste from poultry production on the environment. *World Poultr. Sci. J.*, 75: 29-42.
- Sharvini, S.R., Noor, Z.Z., Chong, C.S., Stringer, L.C. and Yusuf, R.O. 2018. Energy consumption trends and their linkages with renewable energy policies in East and Southeast Asian countries: Challenges and opportunities. *Sustain. Environ. Res.*, 28: 257-266.
- Sihite, I., Kadersih, S. and Dwatmadji, K. 2018. Analysis of factors affecting consumption of horse meat in households in Doloksanggul District, Humbang Hasundutan District, North Sumatra. *J. Sain Peternak. Indones.*, 13(3) : 303-309.
- Sue, V.M., and Ritter, L.A. 2012. Conducting Online Surveys. Second edition. California State University, California.
- Swain, P.S., Dominic, G., Bhakthavatsalam, K.V.S. and Terhuja, M. 2016. Impact of ruminants on global warming: Indian and global context. In: Nautiyal S, Schaldach R, Raju K, Kaechele H, Pritchard B, Rao K, editors. *Climate Change Challenge (3C) and Social-Economic-Ecological Interface-Building*, Denmark.
- Thakuri, S., Baskota, P., Khatri, S.B., Dhakal, A., Chaudhary, P., Rijal, K. and Byanju, R.M. 2020. Methane emission factors and carbon fluxes from enteric fermentation in cattle of Nepal Himalaya. *Sci. Total Environ.*, 746: 1-15.
- Van Kernebeek, H.R.J., Oosting, S.J., Van Ittersum, M.K., Bikker, P. and De Boer, I.J.M. 2016. Saving land to feed a growing population: Consequences for consumption of crop and livestock products. *Int. J. Life Cycle Assess.*, 21: 677-687.
- Wang, Y., Sun, J. and Lin, H. Environmental pollution of livestock and poultry raising in rural areas control measures: Taking Hebei Province in China as an example. *Nature Environ. Pollut. Technol.*, 16: 849-855.
- World Bank. 2022a. Download Data. Online: <https://climateknowledge-portal.worldbank.org/download-data> (accessed on 18 March 2022).
- World Bank. 2022b. Glossary of Terms and Definitions. *Climate Change and Knowledge Portal*, Washington D.C., USA.
- Zervas, G. and Tsiplakou, E. 2012. An assessment of GHG emissions from small ruminants in comparison with GHG emissions from large ruminants and monogastric livestock. *Atmos. Environ.*, 49: 13-23.
- Zhuang, M., Shan, N., Wang, Y., Caro, D., Fleming, R.M. and Wang, L. 2020. Different characteristics of greenhouse gases and ammonia emissions from conventional stored dairy cattle and swine manure in China. *Sci. Total Environ.*, 722: 1-8.



# Response and Environmental Adaptation of Plant Community to Periodic Flooding in the Riparian Zone of Three Gorges Reservoir, China

Guanhua Zhang<sup>\*(\*\*)</sup>†, Baoyang Sun<sup>\*(\*\*)</sup>, Feipeng Ren<sup>\*(\*\*)</sup> and Hao Li<sup>\*(\*\*)</sup>

\*Soil and Water Conservation Department, Changjiang River Scientific Research Institute, Wuhan 430010, China

\*\*Research Center on Mountain Torrent & Geologic Disaster Prevention of Ministry of Water Resources, Wuhan 430010, China

†Corresponding author: Guanhua Zhang; [zgh83113@126.com](mailto:zgh83113@126.com)

Nat. Env. & Poll. Tech.  
Website: [www.neptjournal.com](http://www.neptjournal.com)

Received: 20-08-2021

Revised: 24-09-2021

Accepted: 26-10-2021

## Key Words:

Riparian zone  
Periodic flooding  
Drought stress  
Plant functional traits  
Response and adaptation

## ABSTRACT

The plant is an important component of the riparian ecosystem, which could reflect both the environmental and functional characteristics of the riparian zone. Studies on species composition, diversity, community structure, distribution pattern, and adaptation strategies of plant communities in the riparian zone of the Three Gorges Reservoir (TGR) will help to explore the maintaining mechanism of the plant communities' ecological function under severe water-level fluctuation. The paper reviewed the plant community characteristics, functional traits as well as their eco-physiological responses and environmental adaptations in this special ecological zone. Based on this, future research orientations in this field were also prospected, which may focus on the maintenance mechanism of the plant community, suitable plants selection and their adaptation mechanism, the relationship between plant functional traits and ecosystem functions, plant niche in the riparian zone, and the connectivity of riparian zone to the surrounding environment. The results can promote the correlational research on plant communities in the riparian zone and deepen the understanding of ecosystem services the riparian ecotone provides.

## INTRODUCTION

Riparian zones are typical aquatic-terrestrial ecotones formed by the water-level periodic fluctuation of reservoir operation that could provide multiple ecological functions, such as stabilizing reservoir bank, purifying water quality, conserving biodiversity, beautifying the landscape, and ensuring reservoir system health (Zhu et al. 2020). The construction and operation of the Three Gorges Reservoir (TGR) of China, the largest hydropower dam in the world, has created a unique riparian zone with an area of 350 km<sup>2</sup> along the mainstream of the Yangtze River and its tributary due to anti-seasonal water-level fluctuation (i.e., water levels of 145 m in summer and 175 m in winter; Fig. 1) (Ye et al. 2017, Zhu et al. 2020). However, it also poses a significant impact on the ecosystem, land surface processes, and social economy in the reservoir area. In particular, the ecological degradation in the riparian zone has attracted widespread attention, and many studies have been conducted to explore the impacts of the TGR on landscape patterns (Wu et al. 2017, Chen et al. 2018), variations of vegetation distribution, and diversity (Hu et al. 2018, Zhu et al. 2019), as well as the spatial-temporal characteristics of the plant-soil system (Ye et al. 2020, Liu et al. 2021). Though these studies have

elucidated the changes in the eco-hydrological environment since the reservoir impoundment, the dynamic characteristics and maintaining mechanism of the plant community function derived from the hydrological regime in the riparian zone of the reservoir are still unclear. Additionally, the response mechanism of plant communities in terms of functional traits or physiological ecology and their environmental adaptation to periodic flooding and drought stress (alternate wetting-drying conditions) at different altitudes have not been fully understood.

## STATE OF THE ART

Plants are the important components of the riparian ecosystem, which could reflect both the environmental and functional characteristics of the riparian zone. Repeated submersion and exposure could greatly reduce the original vegetation and new plant communities gradually formed. Currently, research on plant communities in the riparian zone mainly concerns species composition and diversity (Zhang et al. 2016), community structure and its dynamics (Lei et al. 2015), physiological characteristics of dominant species (Ai 2013), plant ecological stoichiometry (Du et al. 2014), flooding-tolerant plants selection (Fan et al. 2015),

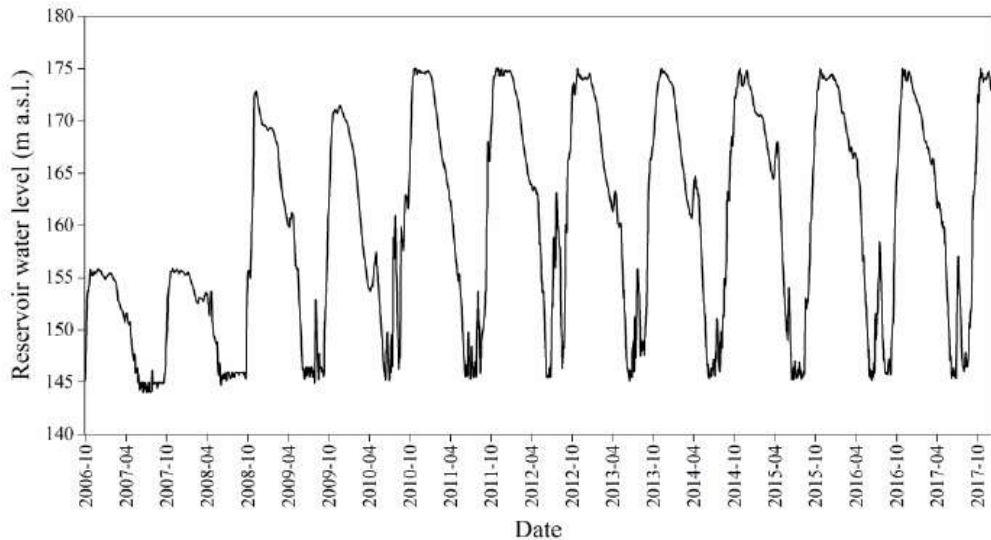


Fig. 1: Water-level fluctuation of the Three Gorges Reservoir during 2006-2017 (Data source: Zhang 2020).

the limiting factors and modes of vegetation restoration (Guo et al. 2012), and plant functional traits (Budelsky & Galatowitsch 2004).

### Plant Community Composition and Species Diversity

Wang et al. (2011a) showed that plants in the riparian zone of the TGR were mainly distributed in the high-altitude localities with gentle slopes and fine texture. Species diversity and proportion of annual plants increased with elevation, and the plant composition was consistent with spatial variations of flooding disturbance intensity. Long-term winter submersion, dramatic water-level fluctuation, and high-temperature summer drought in the water-falling season are the driving factors of vegetation composition in this riparian zone. Zhang

et al. (2016) found that since the experimental impoundment of the TGR in 2006, a large number of plant communities in the inundated area have disappeared, forming permanent waters and environmentally adaptable plant communities. Before impoundment, there were 769 species of vascular plants (belonging to 400 genera in 121 families) with annual herbs, perennial herbs, and shrubs being the dominant life forms; after impoundment, the vascular plants decreased to about 300 species, among which the proportion of annual herbs increased from 26.4% to 45.5%, perennial herbs decreased from 44.4% to 32.5%, and woody plants (arbors and shrubs) decreased from 23.7% to 15.2%, indicating that shrubs were no longer the dominant life form (Fig. 2). Actually, the existing vegetation types in the riparian zone of

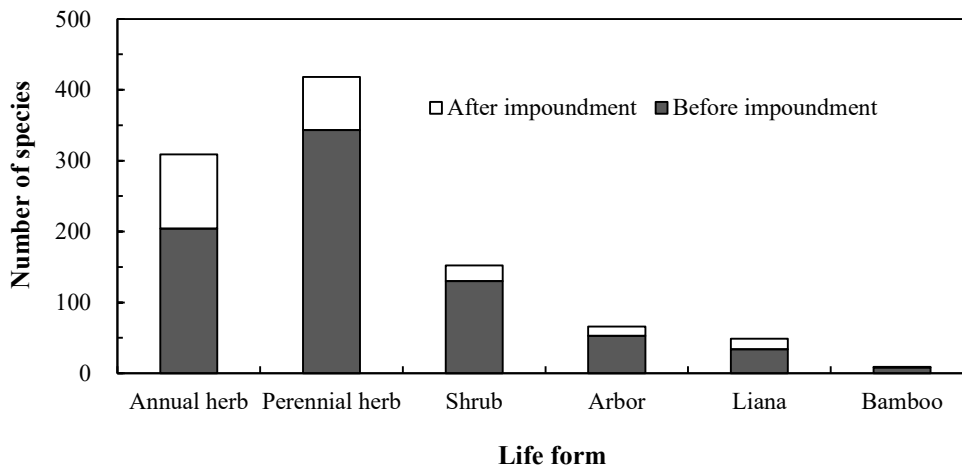


Fig. 2: Life form of vascular plants in the inundated area of the TGR before and after the reservoir impoundment (Data source: Zhang et al. 2016).

the TGR were predominantly annual and perennial herbs and the species diversity showed a “single peak” pattern along with the elevation, with the medium elevation (155-165 m) being the highest species diversity (Guo et al. 2019). Under the influence of repeated periodic water-level fluctuation, herbaceous plants (including annuals and perennials) would replace arbors, shrubs, lianas, and other life forms, which is an inevitable trend of the composition change in plant life forms in the riparian zone of the TGR.

### Plant Ecological Stoichiometry

Ecological stoichiometric theory unifies ecology with elemental ratios and stoichiometric invariance that studies energy balance and multiple chemical elements (principally C, N, and P) balance in biological systems (Zhang et al. 2019). Plants generally adjust their element content and ratio for adapting to the ambient environmental changes. In the riparian zone of the TGR, the characteristics of plant communities and suitable plant selection are the most discussed topics. However, there are few studies regarding plant characteristics from the perspective of elements or ecological stoichiometry. Laboratory fertilization experiments revealed that plant growth in the riparian zone of the TGR was restricted by N, and N and P addition could relieve this restriction effect (Mi et al. 2016).

### Suitable Propagules and Seed Selection

It is generally acknowledged that there are two ways for vegetation restoration, one is artificial construction like propagules planting or seed sowing; another is seed bank transplantation (Li et al. 2010a). The riparian zone of the TGR is characterized by high water-level drop, long duration, anti-seasonal and irregular flooding, with the flooding time of 150 m elevation (145-155 m) being about 8~10 months,

160 m (155-165 m) about 6~7 months, and 170 m (165-175 m) about 2~4 months (Fig. 3). According to these characteristics, Huang et al. (2013) divided the riparian zone into lower (146-156 m), middle (156-173 m) and upper (173-176 m) parts, and suggested that different measures should be taken for different parts to ensure both ecological benefits and landscape effects. The key to vegetation restoration in the riparian zone of the TGR is to select the species (propagules and seeds) that could tolerate the above-mentioned adverse stresses.

Artificial selection of adaptable plants could not only provide technical support for the construction of stable plant communities and ecological restoration but also enrich the species diversity. In recent years, many scholars have screened out a variety of adaptable species via actual or simulated flooding tests, the perennial herbaceous plants mainly included *Cynodon dactylon* (Liu & Liu 2005), *Paspalum paspaloides*, *Cyperus rotundus*, *Alternanthera philoxeroides* (Fan et al. 2015), *Iris pseudacorus* (Wang et al. 2008), and *Arundinella anomala* (Ye & Zeng 2013); the perennial woody plants mainly included *Chinese maple poplar*, *Vitex negundo* (Lu et al. 2010), *Ascendens mucronatum* (Yin et al. 2014), *Taxodium ascendens Brongn* (Li et al. 2011), etc. Liu et al. (2005) conducted plant adaptability tests in the field waters of the Yangtze River under limiting conditions, and the results displayed that *Cynodon dactylon* had strong adaptability and could survive such conditions as the flooding depth of 0-25 m. Ma et al. (2009) screened out two species (*Cynodon dactylon* and *Ficus tikoua*) with strong adaptability through in situ and simulated flooding experiments. Chen et al. (2008) found that short-term simulated flooding (10, 20, and 30 d) had no obvious negative effects on the survival rate and physiological activities of the annual herb *Polygonum hydropiper*. Wang et al. (2008) indicated that

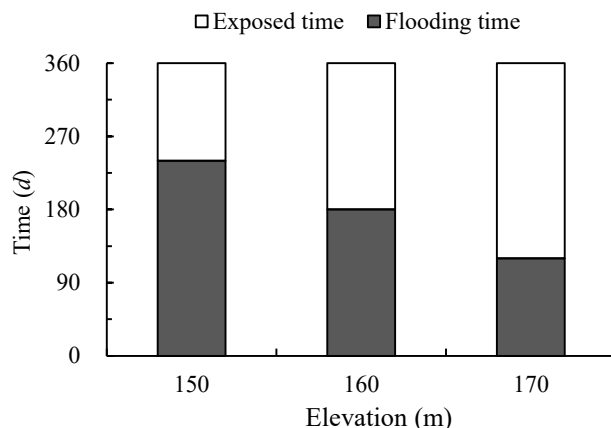


Fig. 3: The flooding time and exposure time of the water-level-fluctuation zone of the TGR (Data source: You et al. 2017).



*Vetiveria zizanioides*, *Acorus calamus*, and *Alternanthera philoxeroides* still had extremely high survival rates after long-term flooding. Some common annual herbs in the riparian zone of the TGR have a very low flooding tolerance and lost their germination ability after being flooded, for instance, *Humulus scandens*, *Bidens pilosa*, and *Cyperus nipponicus* (Wang et al. 2011b).

### Vegetation Collocation Mode

It is commonly recognized that adaptable species were selected according to the flooding duration and depth at different elevations in the riparian zone (Du et al. 2012). Li et al. (2017) proposed that the collocation modes of “arbor-shrub-grass-lianas” for 177-170 m, “shrub-grass-lianas” for 170-160 m, and “grass-lianas” for 160-145 m should be adopted for different elevations in the riparian zone. Du et al. (2012) stated that in the ecological barrier area, plants with strong decontamination ability like *Cynodon dactylon*, *Acorus calamus*, and *Arundo donax* Linn. should also be collocated. Summarily, the adaptable species collocation in the riparian zone primarily focused on the following aspects: 1) Ecological benefits. Through the collocation of “arbor-shrub-grass-lianas”, the vegetation coverage during the land-forming stage of the riparian zone could be guaranteed, and soil erosion could also be prevented; 2) Landscape effect. Species with landscape effect are used in the elevation of 170-177 m; 3) Economic benefits. In the upper part of the riparian zone with a longer land-forming period and the ecological barrier area, the combination of aquatic flowers and plants, forage grass, fruit trees, and mulberry could not only meet the pollution intercepting effect but also have certain economic benefits.

### Plant Functional Traits and Their Environmental Adaptability in The Riparian Zone

Plant functional traits play an indicative role in the ecosystem's functional changes. Nowadays, it has become an important hotspot of ecological research, especially ecological function research under varying environments (Meng et al. 2007, Feng et al. 2008). Studies showed that the plant functional traits in the riparian zone of the TGR exhibited homogeneity at the watershed scale; the specific root length had a high variability and the main stem mass had a low variability (Hou 2019). Plants mostly suffer stress under the harsh environmental conditions of the riparian zone; the high variability of specific root length thus denotes the sensitivity of plants to different habitats (Hou 2019). Moreover, plants behave with different functional traits for different flooding gradients, with plant total length, main stem dry matter, and chlorophyll content increasing

along with the elevation. While root length/plant total length and leaf water content decreased with elevation, both stem water content and leaf thickness firstly increased and then decreased (Hou 2019). With the progress of elevation, high-temperature summer drought became a new limiting factor, and plants adapted to the adverse stress by enhancing tissue construction investment at the elevation of 170-175 m.

Due to the differences in plant functional traits, different plant species will choose different environmental adaptive strategies to occupy the appropriate ecological niche. Gramineous plants generally have a strong tillering ability, and their greater specific root length could make water and nutrients absorption and cycle more effectively thereby improving the growth rate and occupying an ecological niche even in the lower part (with a short initial exposure time) of the riparian zone. This kind of environmental adaptive strategy can also be suitable for other ecological environments, which is the reason why most gramineous plants are widely distributed in the world. Hygrophyte plants generally live near the water with runty bodies and undeveloped mechanical tissue and maintain the plant erect through high water content. The species of slow-growing and distributed in resources-limited habitats usually have relatively small specific leaf areas (Brown et al. 1999), while plants with larger specific leaf areas have a stronger ability to maintain nutrients (Pan et al. 2009). The specific leaf area and main stem dry matter of herbaceous plants in Compositae and Malvaceae families are significantly higher than those of other species, as ascribed to the environmental and phylogenetic effects that need to not only complete the life history in a short time but to increase the investment in mechanical tissue construction to resist the high-temperature summer drought.

### Eco-Physiological Responses and Adaptation Strategies of Plant Communities to Alternate Drying-Wetting Environments

#### Eco-physiological Responses

The anti-seasonal water-level fluctuation may induce changes in the eco-physiological adaptability of the original plants in the riparian zone, and meanwhile, the adaptable plants are required to have high water and drought tolerance. Changes in plant eco-physiological adaptability mainly behave as substance metabolism and photosynthetic physiology.

#### Metabolic Response

Alternate wetting-drying stress in the riparian zone would directly affect the physiological and biochemical characteristics of plant roots and indirectly affect the physiological and biochemical processes of aboveground parts (Vartapetian

& Jackson 1997). Under alternate wetting-drying stress in the riparian zone of the TGR, the accumulation of hydroxyl radicals, hydrogen peroxide, and oxygen radicals in roots resulted in membrane lipid peroxidation reaction, and DNA, macromolecular protein, and membrane structure were damaged. Plant roots could produce a large amount of malic acid and shikimic acid, which could prevent the accumulation of root biomass to adapt to the flooding environment (Ai 2013). Plants could adapt to the mild drought and saturated environment by maintaining their metabolism and growth at the same level as conventional growth. Besides, through the adaptive changes of metabolic pathways, plants could also reduce or eliminate the production of toxic substances and promote the production of metabolic substances that are resistant to adverse conditions (Zhong 1998). Malondialdehyde is one of the products of lipid peroxidation reaction, which can reflect the degree of oxidative damage. Malondialdehyde itself can also make the cell membrane function disorder, thus further damaging the biofilm function (McCord & Fridovich 1969). To control reactive oxygen species (ROS) levels under adverse stress, plants activate some small molecular antioxidants and protective enzyme systems to remove or balance ROS production (Hegedus et al. 2001). Therefore, under the flooding conditions of the riparian zone of the TGR, elucidating changes in malondialdehyde, free proline, protective enzymes, and electrolyte characteristics in plants could provide insight into the physiological and biochemical adaptation mechanism of plants.

### Photosynthetic Physio-Response

The effects of flooding stress on photosynthetic physiology and biochemistry of plants in the riparian zone can be reflected by the changes in photosynthetic gas exchange parameters such as chlorophyll, photosynthetic rate, transpiration rate, stomatal conductance, intercellular CO<sub>2</sub> concentration, light energy utilization rate, and internal water use efficiency. Luo et al. (2007, 2008) explored whether the physiological characteristics of several common terrestrial plants would be substantially affected by flooding from the aspects of plant photosynthesis, chlorophyll fluorescence, and underwater photosynthetic capacity. They found that the effect of flooding on the maximum photochemical efficiency of *Salix variegata* was less than that of *Arundinella anomala* with the underwater photosynthetic capacity of both species being significantly higher than that of typical terrestrial plants, and these two plants still had the underwater photosynthetic capacity even experiencing long-term flooding. In addition, Li et al. (2010b) simulated the water variation characteristics and designed four treatments (groups): normal growth water condition (NG), light drought stress (LD), soil water saturation

(SW), and flooding stress (FS). The results revealed that the mean photosynthetic rate and stomatal conductance in the LD group were significantly lower than in NG, whereas the mean photosynthetic rate and stomatal conductance in SW and FS groups were significantly higher than in NG; photosynthetic pigment content in the FS group was always at the lowest level, which was affected obviously and showed lower light energy use efficiency, CO<sub>2</sub> use efficiency and net photosynthetic rate. On the contrary, the light energy use efficiency, CO<sub>2</sub> use efficiency, and net photosynthetic rate of the SW group were not significantly affected.

### ADAPTATION STRATEGIES

Environmental variations considerably influenced seed germination, seedling construction as well as plant growth and development (Yamaguchi-Shinozaki & Shinozaki 2006). Plants can transfer extracellular signals to intracellular signals, and cope with environmental changes via a series of regulations from molecular to plant level. For example, plants can sense the light change through different types of photoreceptors, and then regulate different developmental stages, sense water stress, induce related gene expression, stimulate root growth downward, etc.; low-temperature stress induces the reorganization of the cytoskeleton to maintain the cell morphology and structure and meanwhile accumulates lots of compatible small molecule metabolites to enhance the water retention ability of cells (Zhang et al. 2009).

#### Plants adapt to flooding stress mainly through the following three strategies:

“Escape” by morphological anatomy structure as well as physiological and biochemical adjustment. Flooding creates a hypoxic environment, plants can better adapt to environmental changes through morphological structure, physiological and biochemical “escape”, such as the formation of adventitious roots, aerenchyma, stem elongation, antioxidant enzyme activity, and energy metabolism regulation to enhance plant tolerance to flooding (Ahmed et al. 2013).

“Silence” by inhibiting adventitious roots, aerenchyma, and stem elongation to reduce the consumption of energy storage material. In contrast to the “escape” strategy with high energy investment, the energy metabolic rate of the “silence” strategy was significantly lower (Bailey-Serres & Voesenek 2010). Through the “silence” strategy, plants can not only reduce the energy storage consumption, such as inhibiting plant growth, elongation of internode or stem, adventitious root generation, etc., but also maintain the minimum oxygen consumption of plants, to tolerate long-term flooding stress (Bailey-Serres & Voesenek 2010).

Accumulating large amounts of non-structural carbohydrates enhances the tolerance to flooding stress and maintains the plants' survival (Palacio et al. 2014). Herbaceous plants can store photo contract products in their stems to resist long-term adverse environmental effects (Slewinski 2012). However, plants tended to transfer photo contact products from damaged and non-damaged tissues to roots and stems when facing periodic environmental stress. For this, some scholars have proposed that under periodic environmental stress, there may be a mixed tolerance strategy to deal with the relationship between photo contract product storage and plant survival and growth.

## CONCLUSION AND FUTURE DIRECTIONS

In conclusion, since the impoundment of the TGR, many achievements have been made in the characteristics of plant communities in the riparian zone and their responses and adaptation to flooding stress, which have laid an important foundation for understanding the ecological function maintenance mechanism of plant communities in this particular riparian ecotone. However, there are still many unanswered questions to be further explored.

Over the past decade, many scholars have conducted a series of explorations on ecological restoration of the TGR from theory to practice, which not only enriched the species and seed banks suitable for artificial construction but also theoretically explored the flooding tolerance mechanism of suitable species. However, the effects of periodic flooding on the physiological and ecological characteristics of adaptable plants are still poorly understood, such as whether adaptive evolution of suitable plants occurs. After many years of natural restoration, there is also a lack of large-scale understanding of the ecological environment and the changes in seed banks in the reservoir area. Moreover, whether the water-level scheduling scheme has a positive effect on the seed dispersal in the riparian zone, and thus is conducive to the population dispersal of adaptable species.

The selection of suitable plants is the basis of vegetation restoration and construction in the riparian zone. However, the simulated flooding experiment is predominantly applied during the selection process, and more attention is paid to the measurement of flooding-tolerance ability, few were given to the drought-tolerance of plants in the summer. The simulation experiment is beneficial to the study of mechanisms, but it also has obvious shortcomings. First, the water environment, light conditions at different water depths, soil structure, and site climate cannot completely simulate the natural conditions in the riparian zone. Second, the experimental period is relatively short, and the research results may not apply to the field circumstance. Therefore, the simulation experiment

only provides limited life information of suitable plants, and the selected flooding-tolerant plants can only be used for vegetation construction after being verified in the field under the alternate drying-wetting environment.

Plant functional traits define the ability of plants to grow, reproduce and survive in a specific environment, which may be related to the effects of plants on environmental changes and disturbances, as well as the responses of plants to biochemical cycles and disturbances. Future studies on the relationship between plant functional traits and ecosystem functions should focus on the relationship between above- and below-ground plant traits and their effects on ecosystem functions, ecosystem functional diversity, ecosystem functions at different temporal and spatial scales, and global changes.

Strengthen the research of plant niche in the riparian zone. Niche quantitatively reflects the interaction between species and habitats. The study of species' niches is beneficial to understand interspecific relationships, biodiversity, community structure and dynamic succession, population evolution, the relationship between organisms and the environment, etc. It is also an effective means for vegetation restoration and community construction in the riparian zone.

Strengthen the research on the connectivity between the riparian zone and the ambient environment, such as under the combined effects of biotic and abiotic factors of the aquatic-terrestrial ecosystem, water-level fluctuation characteristics, vegetation succession trend, community change characteristics, and ecological environment changes. The research on the interaction mechanism of each factor should also be strengthened.

## ACKNOWLEDGEMENTS

This research is financially supported by the Fundamental Research Funds for Central Public Welfare Research Institutes (Grant No. CKSF2021487/TB) and the National Natural Science Foundation of China (Grant No. 41877082, 42107352).

## REFERENCES

- Ahmed, F., Rafii, M.Y., Ismail, M.R., Rahim, H.A., Asfaliza, R. and Latif, M.A. 2013. Waterlogging tolerance of crops: Breeding, mechanism of tolerance, molecular approaches, and prospects. *Biomed Res. Int.*, 2013(1): 963525.
- Ai, L. 2013. Physiological and Ecological responses of *Salix rosthornii* to Alternating Flooding and Drought Conditions of Three Gorges water-level fluctuating zone. Nanjing Forestry University, Xuanwu, China.
- Bailey-Serres, J. and Voesenek, L.A. 2010. Life in the balance: a signaling network controlling survival of flooding. *Curr. Opin. Plant Biol.*, 13(5): 489-494.
- Brown, J.H., West, G.B. and Enquist, B.J. 1999. A general model for the structure and allometry of plant vascular systems. *Nature*, 400(6745): 664-667.

- Budelsky, R.A. and Galatowitsch, S.M. 2004. Establishment of *Carex stricta* Lam. seedlings in experimental wetlands with implications for restoration. *Plant Ecol.*, 175(1): 91-105.
- Chen, C., Ma, M., Wu, S., Jia, J. and Wang, Y. 2018. Complex effects of landscape, habitat, and reservoir operation on riparian vegetation across multiple scales in a human-dominated landscape. *Ecol. Indic.*, 94: 482-490.
- Chen, F., Li, Y. and Qie, G. 2008. The ecophysiological response of *Polygonum hydropiper* plants to simulated flooding. *Ecol. Environ.*, 17(3): 1096-1099.
- Du, L., Fang, F., Guo, J., Fu, C., Li, Z. and Bao, Z. 2012. Ecological planning and protection of urban water-level-fluctuation zone in the Three Gorges Reservoir. *Res. Environ. Yangtze Basin*, 21(6): 726-731.
- Du, L., Fang, F., Guo, J., Gao, H., Wang, C. and Li, Z. 2014. Characteristics of carbon, nitrogen, and phosphorus release from dominant herbaceous plants in the water-level fluctuation zone of the Three Gorges Reservoir. *Res. Environ. Sci.*, 27(9): 1024-1031.
- Fan, D., Xiong, G., Zhang, A., Liu, X., Xie, Z. and Li, Z. 2015. Effect of water-level regulation on species selection for ecological restoration practice in the water-level fluctuation zone of Three Gorges Reservoir. *Chin. J. Plant Ecol.*, 39(4): 416-432.
- Feng, Q., Shi, Z. and Dong, L. 2008. Response of plant functional traits to the environment and its application. *Sci. Silvae Sin.*, 44(4): 125-131.
- Guo, J., Huang, X., Zhang, B., Fang, F. and Fu, C. 2012. Distribution characteristics of organic matter and total nitrogen in the soils of a water-level-fluctuation zone of the Three Gorges Reservoir area. *J. Lake Sci.*, 24(2): 213-219.
- Guo, Y., Yang, S., Shen, Y., Xiao, W. and Cheng, R. 2019. Study on the natural distribution characteristics and community species diversity of existing plants in the Three Gorges Reservoir. *Acta Ecol. Sin.*, 39(12): 4255-4265.
- Hegedus, A., Erdei, S. and Horvath, G. 2001. Comparative studies of H<sub>2</sub>O<sub>2</sub> detoxifying enzymes in green and greening barley seedlings under cadmium stress. *Plant Sci.*, 160: 1085-1093.
- Hou, C. 2019. Study on Plant Functional Traits and Their Environmental Adaptation in the Hydro-Fluctuation Belt of the Three Gorges Reservoir. Chongqing Normal University, Chongqing, China.
- Hu, J., Xie, Y., Tang, Y., Li, F. and Zou, Y. 2018. Changes in vegetation distribution in the east Dongting Lake after the operation of the Three Gorges Dam, China. *Front. Plant Sci.*, 9: 582.
- Huang, S., Ma, L., Fang, W., Liu, Y. and Chen, X. 2013. Study on the reconstruction and ecological restoration techniques of vegetation in the hydro-fluctuation belt of the Three Gorge Reservoir. *J. Southwest Forest. Coll.*, 33(3): 74-78.
- Lei, B., Wang, Y., You, Y., Zhang, S. and Yang, C. 2015. Diversity and structure of herbaceous plant community in the typical water-level-fluctuation zone with different spacing elevations in Three Gorges Reservoir. *J. Lake Sci.*, 26(4): 600-606.
- Li, C., Wei, H., Lv, Q. and Zhang, Y. 2010a. Effects of different water treatments on growth and contents of secondary metabolites in roots of slash pine (*Pinus elliottii* Engelm.) seedlings. *Acta Ecologica Sinica*, 30(22): 6154-6162.
- Li, C., Zhou, Q., Wang, D. and Gu, X. 2011. Effects of flooding on the growth and physiological and biochemical characteristics of *Taxodium ascendens* Brongn and *Sapium sebiferum* (Linn.) Roxb seedlings in the Three Gorges reservoir area. *J. Southwest Agric. Univ., Nat. Sci.*, 33(10): 46-50.
- Li, L., Liao, J., Jiang, M., Huang, H. and He, D. 2010b. Effects of dry storage and water submersion on seed germination of 21 herbaceous species indigenous to the Three Gorges Reservoir region. *J. Wuhan Bot. Res.*, 28(1): 99-104.
- Li, X., Gao F, Liu, Z., Zhang, L., Hao, Y., Guo, Y. and Liu, Y. 2017. A suitable contour planted geotechnical pattern for middle and steep soil slope in water-level fluctuation zone of Three Gorges Reservoir. *Bull. Soil Water Conserv.*, 37(5): 266-269.
- Liu, Y. and Liu, Z. 2005. Adaptability test of *Cynodon dactylon* (L.) in the riparian zone of the Three Gorges Reservoir under extreme conditions. *J. Southwest Agric. Univ. Nat. Sci.*, 27(5): 661-663.
- Liu, Y., Ma, M., Ran, Y., Yi, X., Wu, S. and Huang, P. 2021. Disentangling the effects of edaphic and vegetational properties on soil aggregate stability in riparian zones along a gradient of flooding stress. *Geoderma*, 385: 114883.
- Lu, Z., Li, L., Huang, H., Tao, M., Zhang, Q. and Jiang, M. 2010. Preliminary effects of impounding on vegetation in drawdown zone of the Three Gorges Reservoir region. *J. Wuhan Bot. Res.*, 28(3): 303-314.
- Luo, F., Zeng, B., Chen, T., Ye, X. and Liu, D. 2007. Response to simulated flooding of photosynthesis and growth of riparian plant *Salix Variegata* in the Three Gorges Reservoir region of China. *J. Plant Ecol.*, 31(5): 910-918.
- Luo, F., Zeng, B., Ye, X., Chen, T. and Liu, D. 2008. Underwater photosynthesis of the riparian plants' *Salix variegata* Franch. and *Arundinella anomala* Steud. in the Three Gorges reservoir region as affected by simulated flooding. *Acta Ecol. Sin.*, 28(5): 1964-1970.
- Ma, L., Tang, Y., Zhang, M., Teng, Y., Liu, D. and Zhao, J. 2009. Evaluation of adaptability of plants in water-fluctuation-zone of the Three Gorges Reservoir. *Acta Ecol. Sin.*, 29(4): 1885-1892.
- Mccord, J.M. and Fridovich, I. 1969. Superoxide dismutase: An enzymic function for erythrocyte (Hemocaprein). *J. Biol. Chem.*, 224(2): 6049-6055.
- Meng, T., Ni, J. and Wang, G. 2007. Plant functional traits, environments, and ecosystem function. *J. Plant Ecol.*, 31(1): 150-165.
- Mi, W., Zou, Y., Li, M., Chen, M. and Dong, F. 2016. Nitrogen and phosphorus stoichiometry characteristics of typical herb plants in the water-fluctuation-zone of Three Gorges Reservoir. *J. Lake Sci.*, 28(4): 802-811.
- Palacio, S., Hoch, G., Sala, A. and Millard, P. 2014. Does carbon storage limit tree growth? *New Phytol.*, 201(4): 1096-1100.
- Pan, H., Li, M., Cai X., Wu, J., Du, Z. and Liu, X. 2009. Responses of growth and ecophysiology of plants to altitude. *Ecol. Environ. Sci.*, 18(2): 722-723.
- Slewinski, T.L. 2012. Non-structural carbohydrate partitioning in grass stems: a target to increase yield stability, stress tolerance, and biofuel production. *J. Exper. Bot.*, 63(13): 4647-4670.
- Vartapetian, B.B. and Jackson, M.B. 1997. Plant adaptation to anaerobic stress. *Annals Bot.*, 79: 3-20.
- Wang, H., Zeng, B., Li, Y., Qiao, P., Ye, X. and Luo, F. 2008. Effects of long-term submergence on survival and recovery growth of four riparian plant species in Three Gorges Reservoir region, China. *J. Plant Ecol.*, 32(5): 977-984.
- Wang, J., Zhu, B. and Wang, T. 2011. Characteristics of restoration of natural herbaceous vegetation of typical water-level fluctuation zone after flooding in the Three Gorges Reservoir Area. *Res. Environ. Yangtze Basin*, 20(5): 603-610.
- Wang, Q., Yuan, X., Liu, H., Zhang, Y., Chen, Z. and Li, B. 2011. Effect of Initial Impoundment on the Vegetation and Species Diversity in Water-level Fluctuation Zone of the Three Gorges Reservoir. *J. Nat. Res.*, 26(10): 1680-1693.
- Wu, H., Zeng, G., Liang, J., Chen, J., Xu, J., Dai, J., Sang, L., Li, X. and Ye, S. 2017. Responses of landscape pattern of China's two largest freshwater lakes to early dry season after the impoundment of Three-Gorges Dam. *Int. J. Appl. Earth OBS.*, 56: 36-43.
- Yamaguchi-Shinozaki, K. and Shinozaki, K. 2006. Transcriptional regulatory networks in cellular responses and tolerance to dehydration and cold stresses. *Annual Rev. Plant Biol.*, 57(57): 781.
- Ye, C., Butler, O. M., Chen, C., Liu, W., Du, M. and Zhang, Q. 2020. Shifts in characteristics of the plant-soil system are associated with flooding and revegetation in the riparian zone of Three Gorges Reservoir, China. *Geoderma*, 361: 114015.
- Ye, C., Chen, C., Du, M., Liu, W. and Zhang, Q. 2017. Revegetation affects soil denitrifying communities in a riparian ecotone. *Ecol. Eng.*, 103: 256-263.



- Ye, X. and Zeng, B. 2013. Survival and carbohydrate storage in two tolerant plant species exposed to prolonged flooding in the Three Gorges Reservoir region. *Acta Hydrobiol. Sin.*, 37(3): 450-457.
- Yin, Y., Hua, J., Han, L., Wu, Xiao. and Qi, X. 2014. A trial on the silviculture of *Taxodium hybrid* 'Zhonshanshan118' planted in the hydro-fluctuation belt of the Three Gorges Reservoir within the Wanzhou district area of Chongqing City. *China Forest. Sci. Technol.*, 28(2): 110-114.
- You, Y., Yang, C., Lei, B., Zhang, S., Wang, Y. and Liu, J. 2017. Effect of water level regulation on vegetation characteristics in the water-level fluctuation zone of the Three Gorges Reservoir. *Chin. J. Appl. Environ. Biol.*, 23 (6): 1103-1109.
- Zhang, A., Xiong, G., Fan, D. and Xie, Z. 2016. Effects of damming on plant diversity in the inundated and riparian zones of the Three Gorges Reservoir Area, China. *Chin. J. Ecol.*, 35(9): 2505-2518.
- Zhang, C., Fang, J., Tian, Y. and Lu, X. 2009. The response mechanism of plants to cold stress. *Plant Physiol. Comm.*, 45(7): 721-726.
- Zhang, J., Ai, Z., Liang, C., Wang, G., Liu, G. and Xue, S. 2019. How microbes cope with short-term N addition in a *Pinus tabulaeformis* forest ecological stoichiometry. *Geoderma*, 337: 630-640.
- Zhang, S. 2020. Soil structure changes and the response mechanism of soil shear strength in the water-level fluctuation zone of the Three Gorges. Institute of Mountain Hazards and Environment, Chinese Academy of Sciences, Chengdu.
- Zhong, Z. 1998. Study on the evergreen broadleaf forest ecosystem. Chongqing: Southwest China Normal University Press.
- Zhu, K.W., Chen, Y.C., Zhang, S., Lei, B., Yang, Z.M. and Huang, L. 2020. Vegetation of the water-level fluctuation zone in the Three Gorges Reservoir at the initial impoundment stage. *Glob. Ecol. Conserv.*, 21: e00866.
- Zhu, Z., Chen, Z., Li, L. and Shao, Y. 2020. Response of dominant plant species to periodic flooding in the riparian zone of the Three Gorges Reservoir (TGR), China. *Sci. Total Environ.*, 747: 141101.





# Strength Characteristics of Cement-Modified Iron Tailings and Their Adsorption on Graphene Oxide

Ping Jiang<sup>\*(\*\*)</sup>†, Xuhui Zhou<sup>\*\*</sup>, Jiandong Yang<sup>\*\*</sup> and Lin Zhou<sup>\*\*</sup>

\*School of Transportation, Southeast University, Nanjing, Jiangsu 211189, China

\*\*School of Civil Engineering, Shaoxing University, Shaoxing, Zhejiang 312000, China

†Corresponding author: Ping Jiang; jiangping@usx.edu.cn

Nat. Env. & Poll. Tech.  
Website: [www.neptjournal.com](http://www.neptjournal.com)

Received: 18-10-2021  
Revised: 05-12-2021  
Accepted: 23-12-2021

## Key Words:

Cement-modified iron tailings  
Graphene oxide  
Mechanical properties  
Adsorption characteristics  
Micro mechanism

## ABSTRACT

To explore the mechanical properties of cement-modified iron tailings (CIT) and its adsorption on graphene oxide (GO), the unconfined compressive strength (UCS) tests of CIT with 10% cement were carried out for 7 and 28 days. CIT adsorption of GO was carried out under the conditions of different pH, CIT dosage, and GO initial concentration. The micro characterization of CIT adsorption of GO was carried out by SEM, TEM, AFM, EDS, FT-IR, XRD, and XPS. The results show that: (1) the CIT strength of 28 d curing age is 1202 kPa is twice of 7 d. (2) At the same pH, the GO adsorption effect of CIT at 7 days curing age was better than that at 28 days. When pH is 6, CIT content is 50 mg, and GO initial concentration is 100 mg.L<sup>-1</sup>, CIT has the best adsorption effect on the GO, and the removal rate reached 93.5%. (3) Through microscopic characterization, it can be concluded that the bound water in the CIT structure and the asymmetric stretching vibration of the O-H bond in hydrated calcium silicate (C-S-H) are the main factors affecting the adsorption of GO. The above research results show that CIT not only has good strength properties but also has good adsorption properties for GO. CIT is a potential environmental treatment material.

## INTRODUCTION

Graphene is a new material that consists of carbon atoms stacked in a single hexagonal honeycomb, formed by an sp<sup>2</sup> hybrid connection. It is widely used in the research of various materials because it has been found that graphene has ultra-high-strength, good toughness, light transmittance, and excellent carrier mobility. With the continuous progress of production technology, a large number of wastes containing graphene derivatives will enter the soil, air, and water. Many studies show that graphene derivatives have an impact on the environment and biological toxicity. Guan et al. (2014) used MTT colorimetry to detect the effect of silk fibroin graphene oxide composite membrane on the relative proliferation rate (RGR) of mouse cells. The results showed that the concentration of graphene oxide (GO) increased and the cytotoxicity increased, but when the concentration of GO was lower than 1 wt%, there was no obvious cytotoxicity. Schinwald et al. (2016) and Qiao et al. (2013) have studied and proved the toxicity of GO to the human body. Graphene will deposit in alveoli when entering the human lungs. In addition, graphene also has genetic material toxicity and will seriously damage DNA (Jia 2019, Li et al. 2016, 2018).

Therefore, the effective treatment of toxic pollution of GO aqueous solution is an important research topic at

present. At present, the main methods of sewage treatment include the adsorption method, ion exchange method, extraction method, and membrane analysis method (Liu & Wang 2003, Luo et al. 2019). The commonly used sewage treatment method is the adsorption method, which uses the porosity and other characteristics of the adsorbent to adsorb one or several pollutants in sewage, recover or remove these pollutants, to purify sewage (Zhao et al. 2015, Sun et al. 2017, Tang et al. 2016, Yoon et al. 2016). Luan and Tang (1993) measured that the specific surface area of tailings is 30 m<sup>2</sup>.g<sup>-1</sup>~40 m<sup>2</sup>.g<sup>-1</sup>. By comparing the performance of tailing sand in adsorbing Cu<sup>2+</sup>, Pb<sup>2+</sup>, and Cd<sup>2+</sup>, the results show that tailing sand has a strong adsorption capacity for heavy metal ions, especially when the pH is above 5.

Finding an adsorbent material with high economic benefits has always been an important goal of water pollution control. In the world, the stock of metal tailings is very huge, of which iron tailings account for the vast majority (Bing et al. 2018). The resource application of iron tailings is an effective way to reduce the stock of tailings. Due to the single-particle size and low strength of iron tailings, it is difficult to be directly applied. It can be modified with cement to improve its mechanical properties. Therefore, this test first studies the strength characteristics of cement-modified iron tailings (CIT) and uses the CIT after hydration reaction to

adsorb GO aqueous solution to study the performance of cement iron tailings in removing GO from aqueous solution to achieve the purpose of sustainable development of ecological environment.

## MATERIALS AND METHODS

### Materials

Added 10% cement into iron tailings to obtain CIT samples. Conducted unconfined compressive strength test after curing for 7 and 28 days. Ground the tested CIT sample to powder state as adsorbent for adsorbing GO. The adsorbate was a GO aqueous solution, the manufacturer was Suzhou Tang Feng Technology Co., Ltd. in China, and its concentration was 2 mg.mL<sup>-1</sup>. The adsorption test process under different acid-base environmental conditions was as follows: first sucked 3 mL GO solution with a pipette and put it into the reagent bottle, then added 47 mL deionized water with a resistivity of 18 MΩ•cm to the reagent bottle, adjust the pH value with NaOH and HCl solution with a concentration of 0.1 mol.L<sup>-1</sup>, weighed the ground CIT with a high-precision electronic scale as the adsorbent, and then put the reagent bottle into the ultrasonic instrument for 30 min, Then put the oscillator into oscillation for 1 h, set the speed to 240 rpm and the temperature to 30°C, and finally put it into the incubator for 12 h. The incubator was set to 30°C, that is, T = 303 K.

### Batch Experiments

The mechanical test mainly used the full-automatic unconfined compression tester of Nanjing TKA Co., Ltd. in China. Scanning electron microscopy (SEM, JSM-6360LV), energy-dispersive X-ray spectroscopy (EDX), transmission electron microscopy (TEM, JEM-2100F), atomic force microscopy (AFM, SPA400), X-ray diffractometer (XRD, Empyrean), X-ray photoelectron spectroscopy (XPS, Thermo ESCALAB 250xi) and Fourier infrared spectroscopy (FT-IR, Nexus) were mainly used for microscopic characterization. Among them, SEM, TEM, and AFM were used to characterize the micromorphology of the material, EDS was used to analyze the surface composition, XRD was used to analyze the phase of the adsorbed material, XPS was used to analyze the information of the element composition and content, chemical state, molecular structure and chemical bond of the compound, and FT-IR was used to determine the chemical composition of the adsorbed crystal through the absorption peak of the functional group of the infrared spectrum.

Sucked 1 mL supernatant of GO aqueous solution adsorbed by CIT after standing, transferred it into the test tube, added deionized water to the 25 mL scale mark, and then shook it evenly. The remaining GO concentration in

the supernatant aqueous solution was analyzed by UV-Vis spectrophotometer at the wavelength of 210 nm. To ensure the test accuracy, each data was tested three times, and the relative error was within 5%. The following three formulas were used to calculate the removal rate  $R$ , adsorption capacity  $Q_e$ , and distribution coefficient  $K_d$ .

$$R = \frac{C_0 - C_e}{C_0} \times 100\% \quad \dots(1)$$

$$Q_e = \frac{(C_0 - C_e) \times V}{m} \quad \dots(2)$$

$$K_d = \frac{Q_e}{C_e} \quad \dots(3)$$

Where,  $C_0$  is the initial concentration (mg.L<sup>-1</sup>),  $C_e$  is the equilibrium concentration (mg.L<sup>-1</sup>),  $V$  is the volume of GO aqueous solution (L), and  $m$  is the mass of adsorbent (mg).

## RESULTS AND DISCUSSION

### Mechanical Properties of CIT

The stress-strain curves of 7 d and 28 d CIT can be obtained through an unconfined compressive strength test, as shown in Fig. 1.

It can be seen from Fig. 1 that the stress-strain curve of CIT was a softening curve, that is, with the increase of strain, the stress first increases, reached the peak, and the stress gradually decreased with the increase of strain, and finally tended to be stable. From the curve, the unconfined compressive strength of CIT after curing for 7 d and 28 d was 614 kPa and 1202 kPa, respectively, indicating that adding cement to iron tailings can effectively improve its mechanical properties, and the strength of CIT increases by about twice when the curing age increases from 7 d to 28 d. This is because calcium silicate hydrate (C-S-H) gel produced by the hydration of cement can reinforce iron tailings. The

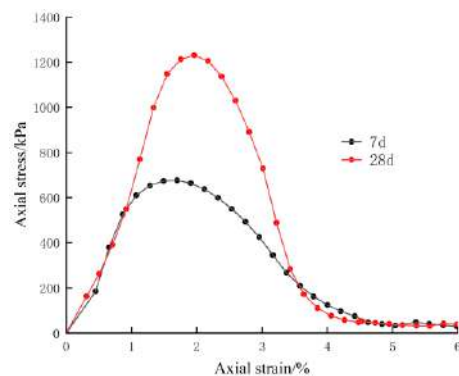


Fig. 1: CIT unconfined compressive strength.

cement hydration reaction in CIT for 7 d was not complete, resulting in less C-S-H, which cannot fully reinforce the iron tailings. However, the cement hydration reaction continued after 7 days, and it is not completed until 28 days, resulting in more C-S-H and a better reinforcement effect on iron tailings, which was reflected in the increase of unconfined compressive strength. By testing the zeta potential of CIT at 7 d and 28 d, the potential was -16 mV and -10 mV, respectively, indicating that the bound water in CIT decreased and the microstructure was more stable from 7 d to 28 d.

### Adsorption Performance OF CIT ON GO

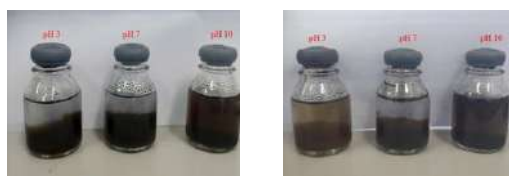
**Effect of pH on GO adsorption:** Firstly, the performance of GO aqueous solution adsorbed by 7 d CIT and 28 d CIT was compared, and the pH was set as 3, 7, and 10. Fig. 2 shows the adsorption capacity, adsorption rate, and partition coefficient of GO removed by CIT at 7 and 28 days. Both have the most obvious adsorption effect at pH 7, and the adsorption effect of 7 d CIT is better than that of 28 d CIT. The main reason may be that, on the one hand, the cement hydration reaction in 7 d CIT has not been completely completed. Due to its large surface area and a large number of epoxy functional groups on the lamella, GO will form a recombinant flocculation structure in the unreacted CIT, resulting in a low GO content in the supernatant (Wang 2017). On the other hand, the hydration reaction of CIT after 28 d is complete. The hydrated calcium silicate (C-S-H) gel produced by cement hydration completely solidified the iron tailings, resulting in the reduction of the iron tailings contacting with GO solution, resulting in the weakening of its adsorption effect on GO. At the same time, this phenomenon is also reflected in the change of solution after adsorption. It can also be seen from the comparison of (a) and (b) in Fig. 3 that the supernatant after CIT adsorption for 7 days is relatively clear.

To further study the adsorption effect of CIT on GO at the curing age of 7 days, the adsorption effect of CIT at different

pH (3-10) was discussed. The CIT content was controlled to 50 mg. Fig. 4 shows the adsorption capacity, adsorption rate, and distribution coefficient of CIT on GO at different pH.

It can be seen from Fig. 4 that the adsorption capacity  $Q_e$  and removal rate  $R$  of GO removed by CIT first increase slowly with the increase of pH value, and then decrease rapidly when pH is 8, indicating that it is not conducive to CIT to adsorb GO in aqueous solution in an alkaline environment. It can be seen from the partition coefficient  $K_d$  that the adsorption effect is the best when pH is 6. At this time, the adsorption capacity  $Q_e$  is 114.9 mg.g<sup>-1</sup>, the removal rate  $R$  is 95.8%, and the partition coefficient  $K_d$  is 22.6. The corresponding solution test picture after adsorption is shown in Fig. 5, which is completely consistent with the trend of the test data. The clarity of the solution is obviously layered in the acidic environment, there are more and more clear aqueous solutions in the upper part, and the clarity of the solution gradually becomes better, which indicates that the adsorption effect of CIT is better. However, in an alkaline environment, the solution after CIT adsorbs GO becomes more and more turbid, there is no obvious stratification, and the upper aqueous solution is less and less, which indicates that CIT adsorbs GO better in an acidic environment.

**Effect of CIT content on GO adsorption:** Fig. 6 shows the adsorption capacity, adsorption rate, and distribution coefficient of GO under different CIT contents. Among them, pH = 6,  $C_0 = 120 \text{ mg.L}^{-1}$ , equilibrium time is 12 h,  $T = 303 \text{ K}$ , CIT is 30 mg, 40 mg, 50 mg, 60 mg and 70 mg.



(a) CIT with 7d curing time (b) CIT with 28d curing time

Fig. 3: Adsorption effect at different ages.

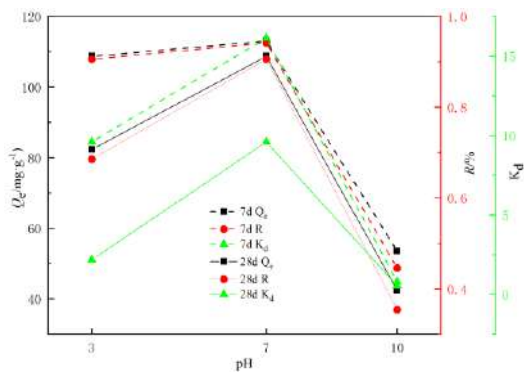


Fig. 2: Effect of pH on GO adsorption by CIT at different ages.

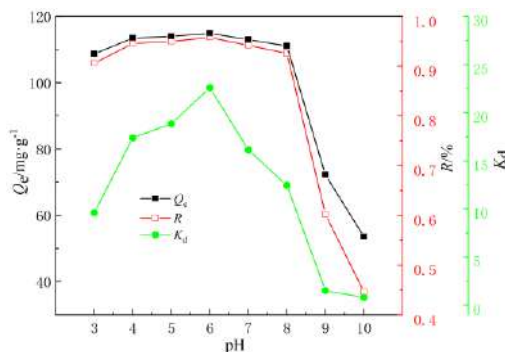


Fig. 4: Effect of pH on GO adsorption by CIT at 7-day.

It can be seen from Fig. 6 that with the increase of CIT content, the adsorption capacity of CIT on GO continues to decrease, which is due to the decrease of steric hindrance and increase of molecular weight when CIT is excessive, and the adsorption capacity of GO on the surface of CIT particles decreases (Yi et al. 2012). However, the adsorption rate and partition coefficient of GO increased with the increase of CIT content, reaching the maximum when CIT content is 50 mg. When CIT continues to increase, the adsorption rate and partition coefficient will decrease with the adsorption capacity. This shows that we should reasonably select high adsorption capacity (low adsorbent consumption) or high adsorption rate according to the actual situation. In this study, 50 mg CIT was used for the follow-up test. The solution image after adsorption also shows this law, as shown in Fig. 7. The solution is the most turbid when CIT is 30 mg, and the upper separator is the clearest when CIT is 50 mg.

**Effect of initial concentration of GO on GO adsorption:**

When the initial concentrations of GO were 80 mg.L<sup>-1</sup>, 100 mg.L<sup>-1</sup>, 120 mg.L<sup>-1</sup>, 140 mg.L<sup>-1</sup>, and 160 mg.L<sup>-1</sup>, CIT had a better adsorption effect on GO. Fig. 8 shows that the adsorption capacity is affected by the initial concentration of GO.

It can be clearly seen from Fig. 8 that with the increase of GO concentration, the adsorption capacity of CIT to GO gradually increases, but the adsorption rate *R* and partition coefficient *K<sub>d</sub>* increase first and then decreases with the increase of the initial concentration of GO. When the initial concentration is 100 mg.L<sup>-1</sup>, it reaches the maximum val-

ue, which is *R*=93.5% *K<sub>d</sub>*=14.3. This shows that when the initial concentration of GO is 80-100 mg.L<sup>-1</sup>, increasing the concentration of GO can increase the adsorption point of CIT and enhance the electrostatic effect, which is reflected in the improvement of the adsorption rate of CIT to GO. When the GO concentration exceeds 100 mg.L<sup>-1</sup>, the increase of the initial GO concentration will inhibit the electrostatic interaction between CIT and GO, resulting in the decline of the adsorption performance of CIT to GO. Fig. 9 shows the solution image of CIT after adsorption of GO under different



Fig. 7: Experimental pictures of the influence of CIT dosage on adsorption.



Fig. 5: Experimental picture of pH adsorbing GO to CIT at 7 days.

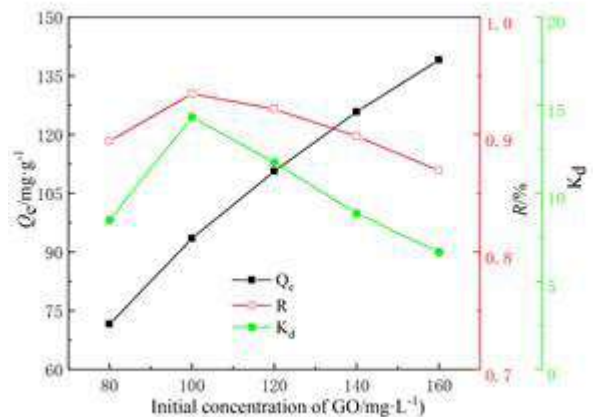


Fig. 8: Experimental pictures of the influence of CIT dosage on adsorption.

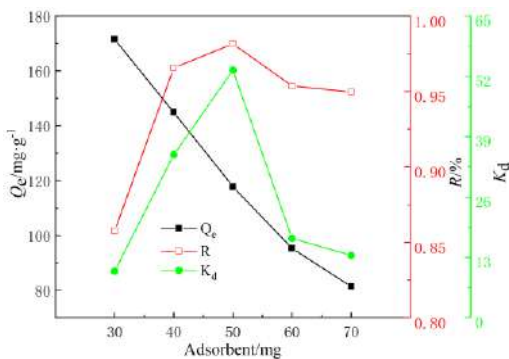


Fig. 6: Effect of CIT dosage on adsorption of GO.

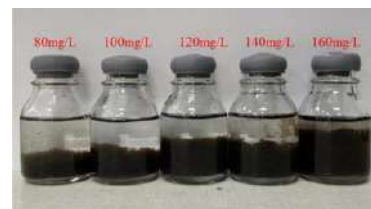


Fig. 9: Experimental pictures of the influence of CIT dosage on adsorption.



initial GO concentrations. It can be seen from Fig. 9 that CIT has high adsorption when the initial GO concentration is low. When the initial GO concentration is  $100 \text{ mg}\cdot\text{L}^{-1}$ , the solution stratification is the clearest and the upper separation is the clearest.

### Microscopic Characterization

To analyze the adsorption mechanism of CIT adsorbed GO, extracted the substance (CITGO) after CIT adsorbed GO, poured out the supernatant of the solution after CIT adsorbed GO, transferred the remaining suspension into a 10 mL polyethylene centrifuge tube with a pipette, and centrifuged it in a high-speed centrifuge (Shanghai Lichen Bangxi Instrument Technology Co., Ltd., L0-LX-HL210D) for solid-liquid two-phase separation. The centrifugation speed was set to 6000 rpm and the time was set to 2 minutes. After repeated centrifugation many times, it was put into a freeze dryer (Shanghai Yuming Instrument Co., Ltd., LGJ-10A) for freeze drying to obtain dry CITGO. The dried CITGO was characterized by SEM, TEM, EDS, FT-IR, XRD, XPS, and AFM to fully reveal the mechanism of CIT adsorbing GO from the changes of morphology, elements, crystals, and functional groups.

### SEM and TEM

The SEM and TEM diagrams of GO, CIT, and CITGO are shown in Fig. 10. It can be clearly seen from Fig. 10 that GO is a typical two-dimensional material, characterized by smooth and relatively uniform flake structure (Fig. 10 (a)),

while CIT in Fig. 10 (b) can see an obvious fast structure, which is formed by the formation of C-S-H gel after cement hydration reaction with iron tailings. In CITGO formed by CIT adsorbing GO, it can still be seen that it is similar to the CIT block structure in Fig. 10 (b), but its surface is smoother than that of CIT, which may be caused by the adsorption of GO with a smooth surface on CIT. This conjecture is proved in the TEM diagram of CITGO. From Fig. 10 (d), it can be seen that GO is like an open layer of tulle, and this layer of tulle in contact with CIT, is attached to CIT crystal particles (Fig. 10 (e)). Therefore, the observation of SEM and TEM test images showed that GO is adsorbed on the CIT surface. However, the surface of CITGO is not completely covered by GO. By comparing Fig. 10(b) and Fig. 10(c), Fig. 10(d), and Fig. 10(e), it can be found that some CIT is exposed, which reflects that the surface of CITGO may be a mixture of CIT and GO.

### EDS, FT-IR and XRD

Fig. 11 shows EDS diagrams of GO, CIT, and CITGO, respectively. It can be seen from Fig. 11 that the main elements of CIT and CITGO are C, O, Mg, Al, Si, and Fe. In addition, the increase of the C element indicates the adsorption of GO on CIT, which indicates that CIT is the main surface of CITGO, which is consistent with the experimental structure of SEM and TEM. CITGO is a mixture of CIT and GO. To further verify this conjecture, GO, CIT and CITGO were characterized by FT-IR and XRD. The characterized test structure is shown in Fig. 12 and Fig. 13.

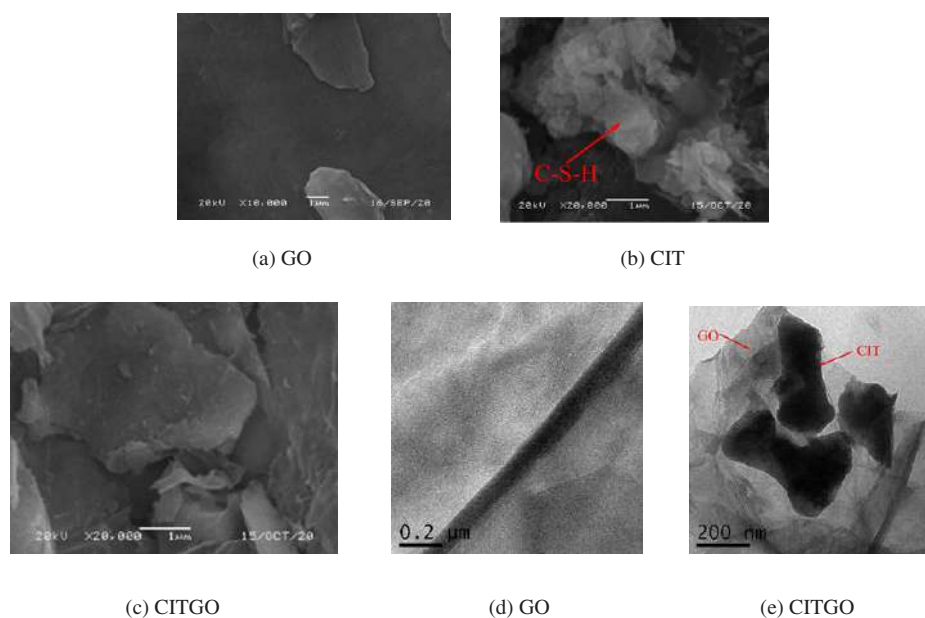


Fig. 10: SEM images of GO(a), CIT(b), and CITGO(c), TEM images of GO(d) and CITGO (e).



It can be seen from Fig. 12 that there is little difference between the spectra of GO, CIT, and CITGO, and the spectra between CIT and CITGO are the most similar. Among them,  $1600\text{ cm}^{-1} \sim 1650\text{ cm}^{-1}$  is the characteristic absorption peak of C-S-H, and the wave peak is slightly stronger under acidic environmental conditions, so the higher the degree of polymerization is. It can be seen from Fig. 13 that the adsorption of GO under acidic conditions increases the oxygen-containing functional groups of CIT materials because the GO surface contains a large number of oxygen-containing functional groups.  $3419\text{ cm}^{-1}$  is the stretching vibration absorption peak of the O-H bond, which is caused by the combined water in the CIT structure and the asymmetric stretching vibration of -OH in hydrated calcium silicate (Chen et al. 2019). In the XRD test results, there are also results similar to those

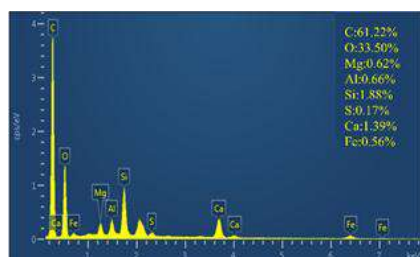
of EDX and FT-IR. Among the spectra of GO, CIT, and CITGO, CIT and CITGO are the most similar, but there are also characteristic peaks of GO. Combined with the SEM and TEM test results, it shows that the surface of CITGO is a hybrid composition of CIT and GO, but the characteristics of CIT play a major role.

### Analysis of XPS and AFM

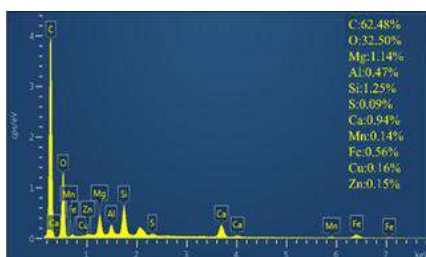
To provide more detailed information on CIT adsorption and GO adsorption mechanism, CIT and CITGO spectra before and after adsorption were analyzed by XPS, as shown in Fig. 14.

It can be found from Fig. 14 that O1s and C1s peaks appear at 530.97 eV and 283.97 eV, O1s and C1s peaks of CITGO are significantly stronger than GO, and N1s, Ca2p, and Si2p peaks also appear in crystal CITGO after adsorption. In addition, it can be observed that C1s are significantly enhanced after adsorption, indicating that CIT has a strong adsorption effect on GO. The high deconvolution of the C1s spectra of GO and CITGO before and after adsorption is shown in Fig. 14 (b). The C1s spectrum can be decomposed into four components at about 284.47 eV, 285.97 eV, and 289.32 eV, corresponding to C-C, C-O, and O-C=O structures respectively. When CIT adsorbs GO, the corresponding peak area increases greatly, indicating that some interactions have taken place between C-C, C-O, and O-C=O. Based on the above analysis, CIT can effectively adsorb GO. To some extent, SEM and TEM analyze the morphology of CITGO adsorbed by CIT on a two-dimensional scale. To further analyze the morphology of CITGO, the morphology of CITGO is analyzed on a three-dimensional scale by AFM, as shown in Fig. 15.

It can be seen from Fig. 15(a) that the maximum thickness of GO is about 1.19 nm, and from Fig. 15(b), the maximum thickness of the CITGO compound is about 17.51 nm, and the other peak is 16.81 nm. Compared with GO before adsorp-



(a) CIT



(b) CITGO

Fig. 11: EDS diagram of adsorption in different environments.

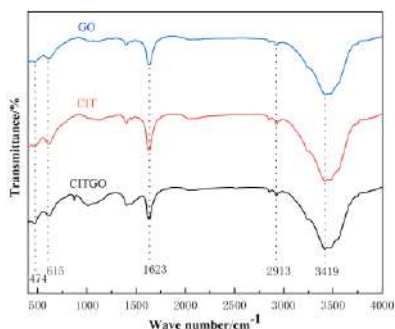


Fig. 12: FTIR diagram before and after adsorption in different environments.

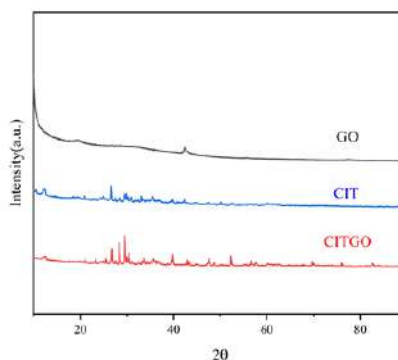


Fig. 13: Diffraction patterns before and after adsorption in different environments.

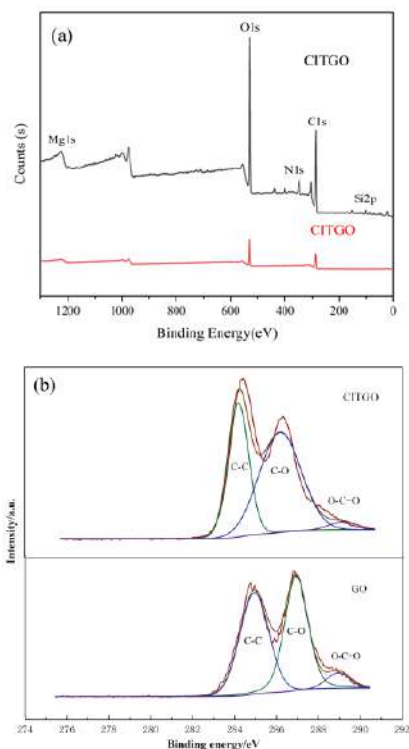


Fig. 14: XPS diagram before and after adsorption in different environments.

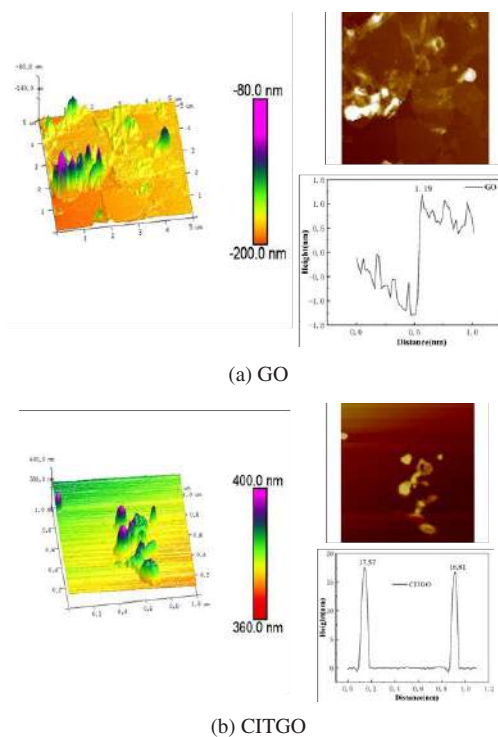


Fig. 15: AFM diagram before and after adsorption in different environments.

tion, the height of CITGO after CIT adsorbs GO increases significantly, and the surface becomes rougher, with different heights, showing double peaks. Combined with SEM, TEM, and two-dimensional images, the effective adsorption of CIT on GO is more fully explained.

## CONCLUSION

CIT was obtained by strengthening iron tailings with cement, and the mechanical properties and GO adsorption capacity of CIT were studied. The main conclusions are as follows:

- (1) Cement has a good reinforcement effect on iron tailings. The hydration reaction of cement is the main reason for strengthening iron tailings. The generated C-S-H can cement iron tailings, to improve the unconfined compressive strength of CIT, and this effect becomes more and more obvious with the increase of age because the longer the age, the more complete the hydration reaction of cement and the more C-S-H, which is reflected in the higher unconfined compressive strength of CIT.
- (2) CIT at the age of 7 days had good adsorption performance for GO. When pH is 6, CIT content is 50 mg, and GO initial concentration is 100 mg.L<sup>-1</sup>, CIT has the best adsorption effect on GO, and its adsorption rate is 93.5%. The adsorbed product CITGO was characterized by SEM, TEM, EDX, FT-IR, XRD, XPS, and AFM. It was found that GO was distributed on the surface of CIT, but the characteristics of CIT were significantly stronger than GO.
- (3) With the increase of curing age, the zeta potential of CIT decreases, the bound water decreases, and the C-S-H products increase, resulting in asymmetric stretching vibration between the bound water and the O-H bond in C-S-H, weakening the relationship between the O-H bond and the oxygen-containing functional groups in GO, thus affecting the adsorption of CIT on GO.

## REFERENCES

- Chen, Y., Wu, Qi, Xiao, H., Xie, Y. and Wang, M. 2019. Formula optimization and mechanism of preparing geopolymers based on iron tailings and Metakaolin. *Metal Mine*, (04): 199-203.
- Guan, S., Wu, F. and Zhao, B. 2014. MTT assay for detection of the cytotoxicity of graphene oxide. *China Mod. Doc.*, 52(17): 18-20.
- Jia, P. 2019. The Toxicological Mechanism of Graphene and Graphene Oxide. Chinese Academy of Sciences (Chongqing Institute of Green Intelligent Technology), Chongqing.
- Li, B., Zhao, Z., Tang, B., Li, H., Cheng, H. and Ma, Z. 2018. Comprehensive utilization of iron tailings in China. *IOP Conf. Series Earth Environ. Sci.*, 199(4): 042005.
- Li, T., Zhang, C., Shen, D. and Yuan, Y. 2016. Research progress on biological toxicity of graphene and graphene oxide. *J. Nanjing Univ. Nat. Sci.*, 52(02): 235-243.

- Liu, F. and Wang, P. 2003. Modern water treatment methods and materials. China Environ. Sci. Press.
- Luan, Z. and Tang, H. 1993. II. Adsorption of heavy metals by tailings sand. Environ. Chem., (05): 356-364.
- Luo, H., Zhou, J., Zhang, Y., Hu, H., Huang, Z. and Shen, F. 2019. Preparation of graphene oxide and its adsorption properties for rhodamine B. New Chem. Mater., 47(01): 172-176.
- Qiao, Y., An, J. and Ma, L. 2013. Single-cell array-based assay for in vitro genotoxicity study of nanomaterials. Anal. Chem., 85(8): 4107-4112.
- Schinwald, A., Murphy, F.A., Jones, A., MacNee, W. and Donaldson, K. 2012. Graphene-based nanoplatelets: A new risk to the respiratory system as a consequence of their unusual aerodynamic properties. ACS Nano, 6(1): 736-746.
- Sun, S., Sheng, Y., Sun, Q., Zheng, M., Li, Z. and Sun, X. 2017. Study on treatment of sludge thermal drying steam by activated carbon adsorption. Environ. Sci. Technol., 40(3): 650-658.
- Tang, C., Chen, H., Ye, X. and Liu, M. 2016. Research progress on the removal of iron and manganese from groundwater by adsorption. J. Yangtze River Sci. Res. Instit., 33(6): 18-23.
- Wang, J. 2017. Study of Graphene Oxide on Properties of Cement and Its Mechanism. Beijing University of Civil Engineering and Architecture, Beijing.
- Yi, C., Tang, Q., Huang, X. and Qiu, X. 2012. Adsorption behavior of polycarboxylate superplasticizer on the surface of cement particles. Ciese J., (08): 2460-2468.
- Yoon, Y., Park, W., Kyu, H., TaeMun, Y. and Dae, H. 2016. Comparative evaluation of magnetite-graphene oxide and magnetite-reduced graphene oxide composite for As (III) and As (V) removal. J. Hazard. Mater., 304: 196-204.
- Zhao, Y., Hu, H. and Zhang, Qi. 2015. Treatment of chromium wastewater by steel slag. Appl. Chem. Ind., 044(8): 1496-1498, 1502.

... Continued from inner front cover

- The text of the manuscript should run into **Abstract, Introduction, Materials & Methods, Results, Discussion, Acknowledgement** (if any) and **References** or other suitable headings in case of reviews and theoretically oriented papers. However, short communication can be submitted in running with **Abstract and References**. The references should be in full with the title of the paper.
- The figures should preferably be made on a computer with high resolution and should be capable of withstanding a reasonable reduction with the legends provided separately outside the figures. Photographs may be black and white or colour.
- Tables should be typed separately bearing a short title, preferably in vertical form. They should be of a size, which could easily be accommodated in the page of the Journal.
- References in the text should be cited by the authors' surname and year. In case of more than one reference of the same author in the same year, add suffix a,b,c,.... to the year. For example: (Thomas 1969, Mass 1973a, 1973b, Madony et al. 1990, Abasi & Soni 1991).

### List of References

The references cited in the text should be arranged alphabetically by authors' surname in the following manner: (Note: The titles of the papers should be in running 'sentence case', while the titles of the books, reports, theses, journals, etc. should be in 'title case' with all words starting with CAPITAL letter.)

- Dutta, A. and Chaudhury, M. 1991. Removal of arsenic from groundwater by lime softening with powdered coal additive. *J. Water Supply Res. Techno. Aqua.*, 40(1) : 25-29.
- Hammer, D.A. (ed.) 1989. *Constructed Wetlands for Wastewater Treatment-Municipal, Industrial and Agricultural*. Lewis Publishers Inc., pp. 831.
- Haynes, R. J. 1986. Surface mining and wetland reclamation. In: Harper, J. and Plass, B. (eds.) *New Horizons for Mined Land Reclamation*. Proceedings of a National Meeting of the American Society for Surface Reclamation, Princeton, W.V.

### Submission of Papers

- The paper can be submitted by e-mail as an attachment in a single WORD file at **contact@neptjournal.com**
- The paper can also be submitted online in a single WORD file through the **online submission portal** of journal's website: **www.neptjournal.com**

### Attention

1. Any change in the authors' affiliation may please be notified at the earliest.
2. Please make all the correspondence by e-mail, and authors should always quote the manuscript number.

**Note:** In order to speed up the publication, authors are requested to correct the galley proof immediately after receipt. The galley proof must be checked with utmost care, as publishers owe no responsibility for mistakes. The papers will be put on priority for publication only after receiving the processing and publication charges.



# Nature Environment and Pollution Technology

**(Abbreviation: Nat. Env. Poll. Tech.)**

**(An International Quarterly Scientific Journal)**

Published by



**Technoscience Publications**

A-504, Bliss Avenue, Opp. SKP Campus  
Balewadi, Pune-411 045, Maharashtra, India

In association with

**Technoscience Knowledge Communications**

Mira Road, Mumbai, India

For further details of the Journal, please visit the website. All the papers published on a particular subject/topic or by any particular author in the journal can be searched and accessed by typing a keyword or name of the author in the 'Search' option on the Home page of the website. All the papers containing that keyword or author will be shown on the home page from where they can be directly downloaded.

**[www.neptjournal.com](http://www.neptjournal.com)**

©**Technoscience Publications:** The consent is hereby given that the copies of the articles published in this Journal can be made only for purely personal or internal use. The consent does not include copying for general distribution or sale of reprints.

Published for Proprietor, Printer and Publisher: Mrs. T. P. Goel, A-504, Bliss Avenue, Balewadi, Pune, Maharashtra, India; Editors: Dr. P. K. Goel (Chief Editor) and Prof. K. P. Sharma